



Synthetic Edge and SOL Diagnostics: A Bridge between Experiments and Theory

Nielsen, Anders Henry; Naulin, Volker; Rasmussen, Jens Juul; Olsen, J.; Thrysøe, Alexander Simon; Eich, T.; Pokol, G. I.; Asztalos, O.; Coelho, R.; Réfy, D. I.; Tál, B.; Hu, G. H.; Ning, Y.

Published in:

27th IAEA Fusion Energy Conference Programme and Abstracts

Publication date:

2018

Document Version

Publisher's PDF, also known as Version of record

[Link back to DTU Orbit](#)

Citation (APA):

Nielsen, A. H., Naulin, V., Rasmussen, J. J., Olsen, J., Thrysøe, A. S., Eich, T., ... Ning, Y. (2018). Synthetic Edge and SOL Diagnostics: A Bridge between Experiments and Theory. In 27th IAEA Fusion Energy Conference Programme and Abstracts (pp. 529-529). [4] International Atomic Energy Agency.

General rights

Copyright and moral rights for the publications made accessible in the public portal are retained by the authors and/or other copyright owners and it is a condition of accessing publications that users recognise and abide by the legal requirements associated with these rights.

- Users may download and print one copy of any publication from the public portal for the purpose of private study or research.
- You may not further distribute the material or use it for any profit-making activity or commercial gain
- You may freely distribute the URL identifying the publication in the public portal

If you believe that this document breaches copyright please contact us providing details, and we will remove access to the work immediately and investigate your claim.



FEC 2018

27TH IAEA FUSION ENERGY CONFERENCE

22–27 October 2018
Ahmedabad, India

Programme and Abstracts

Organized by the



IAEA

International Atomic Energy Agency

Hosted by the Government of India
through the



Institute for Plasma Research



CN-258
www.iaea.org/meetings

Organized by the:



IAEA

International Atomic Energy Agency

Atoms for Peace

Hosted by the Government of India through the
Institute for Plasma Research (IPR), Bhat, Gandhinagar, India



and the
Department of Atomic Energy, Mumbai 400 001, India



27th IAEA

Fusion Energy Conference

22–27 October 2018 Ahmedabad, India

Programme & Book of Abstracts

**Scan relevant QR to download the
“IAEA conferences and meetings” application.**



QR for Android



QR for iPhone

Mobile Conference App for smartphones and tablets

The IAEA Conferences and Meetings App provides a one-stop access to information on the Conference and exhibitions. The app also allows users to put together their own personalized schedule of events. Via this app participants will be able to view contributed papers and the latest conference programme, message other participants, and view PowerPoint presentations released after the event. Participants will receive an email inviting them to register for the app approximately one week before the conference.

For iPhone or iPad users, get your free download through the [Apple iTunes Store](#); those with Android devices can visit the [Google Play Store](#).

Once installed and running, search and download the FEC-2018 conference. The application provides a digital, mobile copy of the conference agenda and timetables, venue information, social network updates, and more.

Colophon

This book has been assembled from the abstract sources submitted by the contributing authors via the [Indico](#) conference management platform. Layout, editing, and typesetting of the book, including customized \TeX & \LaTeX macros, was done by Paul Knowles, LogrusData, Toronto, Canada. The font is TeX Gyre Pagella, a decendent of Hermann Zapf’s Palatino.

This book is PDF hyperlinked: activating coloured text will, in general, move you throughout the book.

Introduction

The International Atomic Energy Agency (IAEA) fosters the exchange of scientific and technical results in nuclear fusion research and development through its series of Fusion Energy Conferences. The 27th IAEA Fusion Energy Conference (FEC 2018) aims to provide a forum for the discussion of key physics and technology issues as well as innovative concepts of direct relevance to the use of nuclear fusion as a source of energy.

With a number of next-step fusion devices currently being implemented —such as the International Thermonuclear Experimental Reactor (ITER) in Cadarache, France, and the Wendelstein 7-X stellarator in Greifswald, Germany— and in view of the concomitant need to demonstrate the technological feasibility of fusion power plants as well as the economic viability of this method of energy production, the fusion community is now facing new challenges. The way these challenges are addressed will dictate research orientations in the present and coming decades.

The scientific scope of FEC 2018 is, therefore, intended to reflect the priorities of this new era in fusion energy research. The conference aims to serve as a platform for sharing the results of research and development efforts in both national and international fusion experiments that have been shaped by these new priorities, and to thereby help in pinpointing worldwide advances in fusion theory, experiments, technology, engineering, safety and socio-economics. Furthermore, the conference will also set these results against the backdrop of the requirements for a net energy producing fusion device and a fusion power plant in general, and will thus help in defining the way forward.

With the participation of international organizations such as the ITER Organization and the European Atomic Energy Community (Euratom), as well as the collaboration of more than forty countries and several research institutes, including those working on smaller plasma devices, it is expected that this conference will, as in the past, serve to identify possibilities and means for continuous and effective international collaboration in this area.

The [27th IAEA Fusion Energy Conference](#) is being organized by the [IAEA](#) in cooperation with Department of Atomic Energy, Government of India and the [Institute for Plasma Research](#) at the Mahatma Mandir, Gandhinagar (Ahmedabad) Gujarat, India. Previous conferences in this series were held in [Salzburg \(1961\)](#), [Culham \(1965\)](#), [Novosibirsk \(1968\)](#), [Madison \(1971\)](#), [Tokyo \(1974\)](#), [Berchtesgaden \(1976\)](#), [Innsbruck \(1978\)](#), [Brussels \(1980\)](#), [Baltimore \(1982\)](#), [London \(1984\)](#), [Kyoto \(1986\)](#), [Nice \(1988\)](#), [Washington DC \(1990\)](#), [Würzburg \(1992\)](#), [Seville \(1994\)](#), [Montreal \(1996\)](#), [Yokohama \(1998\)](#), [Sorrento \(2000\)](#), [Lyon \(2002\)](#), [Vilamoura \(2004\)](#), [Chengdu \(2006\)](#), [Geneva \(2008\)](#), [Daejeon \(2010\)](#), [San Diego \(2012\)](#), [St. Petersburg \(2014\)](#), and [Kyoto \(2016\)](#).

	Name	Country/International Organization
Chair:	Boris V. Kuteev	Russian Federation
Vice Chair:	Elizabeth Surrey	EU
	Alain Becoulet	EU
	Richard BATTERY	USA
Choong-Seock (CS) Chang		USA
	Shishir Deshpande	India
	Joydeep Ghosh	India
	Carlos Hidalgo	EU
	Matthew Hole	Australia
Yong Seok Hwang		Republic of Korea
	Shunsuke Ide	Japan
	Victor Ilgisonis	Russian Federation
	Takashi Inoue	Japan
	Sylvie Jacquemot	EU
	Frank Jenko	EU
	Yasuaki Kishimoto	Japan
	Sergey Lebedev	Russian Federation
	Ray Leeper	USA
Guangnan Luo		China
	John Mandrekas	USA
	Darren McDonald	EU
Tomohiro Morisaki		Japan
Hyeon K. Park		Republic of Korea
	Simon Pinches	ITER
Yasuhiko Sentoku		Japan
	Ivan Vargas-Blanco	Costa Rica
	Anne White	USA
	Min Xu	China

Conference Secretariat

IAEA Scientific Secretaries:

Mr Danas Ridikas

Ms Sehila M. González de Vicente

IAEA Scientific Support:

Mr Matteo Barbarino

Physics Section

Division of Physical and Chemical Sciences

Department of Nuclear Science and Applications

International Atomic Energy Agency

Vienna International Centre, PO Box 100

1400 Vienna, Austria

tel: +43 1 2600 21751 (Ridakas)

tel: +43 1 2600 21753 (González)

Fusion-Physics@iaea.org

IAEA Administration and Organization:

Ms Martina Khaelss

Ref.: CN-258

Division of Conference and Document Services

International Atomic Energy Agency

Vienna International Centre, PO Box 100

1400 Vienna, Austria

tel: +43 1 2600 21315

fax: +43 1 26007

M.Khaelss@iaea.org

Local Organization

Host Government Officials:

Mr Shashank Chaturvedi

Institute for Plasma Research

Near Indira Bridge, Bhat

Gandhinagar

Gujarat 382428

India

tel: +91 79 2396 2000

fax: +91 79 2396 2277

fec2018@ipr.res.in

Mr Daniel Raju

Institute for Plasma Research

Near Indira Bridge, Bhat

Gandhinagar

Gujarat 382428

India

tel: +91 79 2396 2000

fax: +91 79 2396 2277

fec2018@ipr.res.in

Presentation and Abstract Book

This book contains all abstracts accepted for the conference. Abstracts have been edited for style uniformity. The views expressed remain the responsibility of the named authors. No responsibility is held by the organizers for any material reproduced, or linked, in this book.

IAEA Publications

All IAEA publications may be ordered from the
Sales and Promotion Unit,
International Atomic Energy Agency,
P.O. Box 100, A-1400 Vienna, Austria
Fax: +43 1 2600-29302

sales.publications@iaea.org

www.iaea.org/Publications/index.html

Conference Material

Contributed papers will be published electronically on the [IAEA Fusion Portal](#) under the FEC dedicated webpage as a part of the FEC material.

International Nuclear Information System (INIS)

Contributed papers will be published electronically in the INIS repository ([IAEA-CN-258](#)).

Nuclear Fusion Journal

Participants have been invited to submit their paper for possible publication in the IAEA journal, [Nuclear Fusion](#). If your institution does not have access to the journal, pdfs of these FEC derived articles can be requested from nf@iaea.org.

Participation in an IAEA Scientific Meeting

Governments of Member States and those organizations whose activities are relevant to the meeting subject matter are invited to designate participants in the IAEA scientific conferences and symposia. In addition, the IAEA itself may invite a limited number of scientists as invited speakers. Only participants designated or invited in this way are entitled to present papers and take part in the discussions.

Representatives of the press, radio, television or other information media and members of the public, the latter as “observers”, may also be authorized to attend, but without the right to take part in the proceedings.

Scientists interested in participating in any of the IAEA meetings should request information from the Government authorities of their own countries, in most cases the Ministry of Foreign Affairs or national atomic energy authority.

Working Language & Resolutions

Working Language: English. No simultaneous translation will be provided.

Resolutions: No resolutions may be submitted for consideration on any subject; no votes will be taken.

Satellite Meetings

Satellite meetings can be held. Meeting rooms and times can be reserved via the [conference website](#).

Information for Participants

The [conference website](#) contains links to many helpful guides. Notably, the [Indico](#) conference system is used for all correspondence concerning contributions.

This book contains all abstracts accepted by the FEC programme committee. Note that abstracts have been edited for style uniformity.

Overview of Contributions (as of October 16, 2018)

- 4 Keynote presentations
- 24 Overview talks with posters
- 78 Regular talks
- 17 Rapporteured papers
- 11 Overview poster presentations
- 518 Regular poster presentations
- Post deadline talks
- Post deadline poster presentations
- 5 Summary talks

Overview posters will be exhibited during the entire conference. All oral presentations will also be displayed as posters according to the programme.

The duration of oral presentations indicated in the programme already includes discussion time. Speakers are requested to make available the following times for discussions:

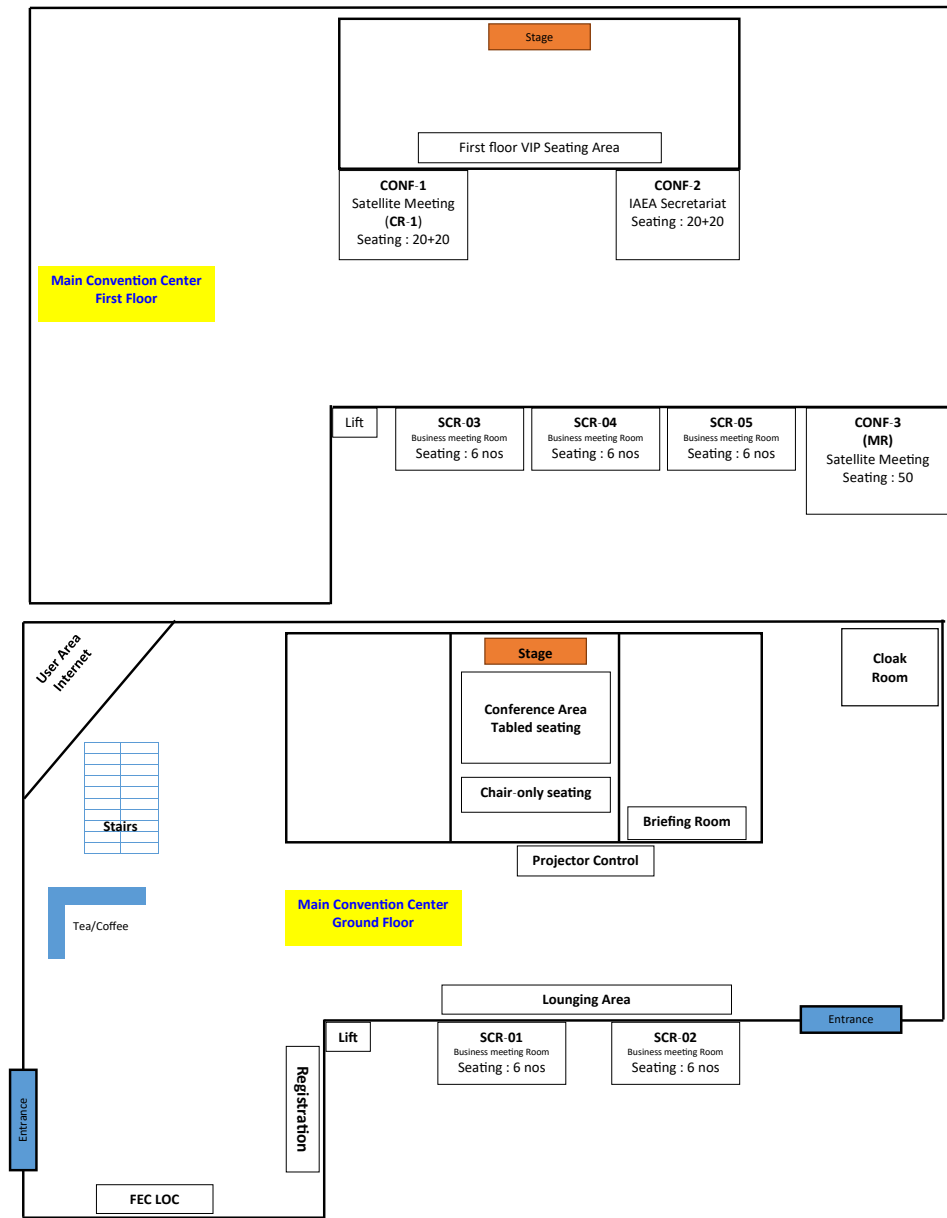
- 4' for overview presentation (total 25')
- 3' for regular oral presentation (total 20')

Rapporteur papers are identified by the letter "a" after the paper number. Rapporteured papers are identified by the letters "b" or "c" after the paper number.

Explanation of Abbreviations

- O** Opening
- S** Summary
- OV** Overviews
- OVP** Overview Posters
- EX** Magnetic Confinement Experiments
- TH** Magnetic Confinement Theory and Modelling
- For both **EX** and **TH**, subdivisions are:
 - C:** *Confinement*
 - D:** *Plasma-material interactions; divertors; limiters; scrape-off layer (SOL)*
 - S:** *Stability*
 - W:** *Wave-plasma interactions; current drive; heating; energetic particles*
- FIP** Fusion Engineering, Integration and Power Plant Design
- FNS** Fusion Nuclear Physics and Technology
- ICC** Innovative Confinement Concepts
- IFE** Inertial Fusion Experiments and Theory
- MPT** Materials Physics and Technology
- PD** Post-Deadline Contributions
- PPC** Plasma Overall Performance and Control
- SEE** Safety, Environmental and Economic Aspects of Fusion

Mahatma Mandir
Gandhinagar (Ahmedabad) Gujarat
India



Day Date	Monday Oct. 22, 2018		Tuesday Oct. 23, 2018		Wednesday Oct. 24, 2018		Thursday Oct. 25, 2018		Friday Oct. 26, 2018		Saturday Oct. 27, 2018
08:30 — 10:15	<i>O/1</i>		<i>OV/3</i>	<i>P1</i>	<i>IFE/1</i>	<i>P3</i>	<i>EX/5, PPC/1, TH/3</i>	<i>P5</i>	<i>EX/7-TH/5</i>	<i>P7</i>	<i>EX/10-TH/8</i>
	Opening —&— Keynote		Overview: Magnetic Fusion	Posters	Inertial Fusion	Posters	Integrated Modelling & Transport	Posters	Active ELM Control	Posters	Transport
	p. 10		p. 14	p. 15	p. 26	p. 27	p. 38	p. 39	p. 49	p. 50	p. 65
Coffee Break: 10:15 — 10:45											
10:45 — 12:30	<i>OV/1</i>		<i>EX/1-TH/1</i>	<i>P1</i>	<i>EX/2</i>	<i>P3</i>	<i>EX/6-TH/4</i>	<i>P5</i>	<i>MPT/2, FNS/1, SEE/2</i>	<i>P7</i>	<i>EX/11, SEE/3, PD</i>
	Overview: Magnetic Fusion		Energetic Particles	Posters	Pedestal & ELM Optimization	Posters	Runaways & Disruption Mitigation	Posters	Materials, Fu- sion Nuclear Science, Envi- ronmental	Posters	Stability, Environmental & PD
	p. 10		p. 14	p. 15	p. 26	p. 27	p. 38	p. 39	p. 49	p. 50	p. 65
Lunch: 12:30 — 14:00											
14:00 — 16:10	<i>OV/2</i>	<i>OVP</i>	<i>OV/4</i>	<i>P2</i>	<i>EX/3</i>	<i>P4</i>	<i>FIP/2, MPT/1, SEE/1</i>	<i>P6</i>	<i>EX/8, PPC/2, TH/6</i>	<i>P8</i>	<i>S/1</i>
	Overview: Magnetic Fusion	Posters	Overview: Magnetic Fusion	Posters	Plasma Performance & Control	Posters	In Vessel Components & Plasma Interface	Posters	Heating, Current Drive & Steady State	Posters	Summary (14:00 – 16:00)
	p. 10	p. 12	p. 21	p. 22	p. 33	p. 34	p. 42	p. 43	p. 57	p. 58	p. 66
Coffee Break: 16:10 — 16:40											
16:40 — 18:45	<i>FIP/1</i>	<i>OVP</i>	<i>OV/5</i>	<i>P2</i>	<i>EX/4-TH/2</i>	<i>P4</i>	<i>FIP/3</i>	<i>P6</i>	<i>EX/9-TH/7</i>	<i>P8</i>	<i>S/2</i>
	ITER Technology	Posters	Overview: Magnetic Fusion	Posters	H-Mode & Pedestal	Posters	DEMO & Advance Technology	Posters	Divertor & Exhaust Physics	Posters	Summary (16:30 – 18:00)
	p. 11	p. 12	p. 21	p. 22	p. 33	p. 34	p. 43	p. 43	p. 57	p. 58	p. 66
19:30 — 22:00	Reception		Nuclear Fusion Board Meeting		Banquet						

08:00 – 16:00: Conference Registration**O/1****Opening Plenary**

Chair: Shashank Chaturvedi (India)

*Main Hall***(08:30 – 10:15)**

Time Id	Presenter		Title
08:30 O/1-1		India	Traditional Lighting of the Lamp
08:35 O/1-2	M. Venkatesh	IAEA	Opening Address
08:45 O/1-3	Host Country Representative	India	Welcome Address
09:00 O/1-4	R. B. Grover	India	Importance of Energy and the Role of Nuclear Energy in India's Energy Mix
09:15 O/1-5	S. P. Deshpande	India	India's Quest for Fusion Energy & Road to ITER
09:30 O/1-6	P. A. Child	EC	EU R&D Energy Policy and the Role of Fusion Research
09:50 O/1-7	N. K. Prinja	UK	Fusion is our Future: Readiness of the Fusion Technology and the 4th Industrial Revolution

OV/1**Overviews 1: Magnetic Fusion**

Chair: Sen Abhijit (India)

*Main Hall***(10:45 – 12:30)**

Time Id	Presenter		Title
10:45 OV/1-1	A. K. Chakraborty	India	Progress of ITER-India Activities for ITER Deliverables: Challenges and Mitigation Measures
11:10 OV/1-2	B. Bigot	ITER	Progress Toward ITER's First Plasma
11:35 OV/1-3	E. Joffrin	France	Overview of the JET Preparation for Deuterium-Tritium Operation
12:00 OV/1-4	C. C. Petty	USA	DIII-D Research Towards Establishing the Scientific Basis for Future Fusion Reactors

OV/2**Overviews 2: Magnetic Fusion**

Chair: Yasuhiko Takeiri (Japan)

*Main Hall***(14:00 – 16:10)**

Time Id	Presenter		Title
14:00 OV/2-1	H. Meyer	UK	Overview of Physics Studies on ASDEX-Upgrade
14:25 OV/2-2	B. N. Wan	China, P. R.	Recent Advances in EAST Physics Experiments in Support of Steady-State Operation for ITER and CFETR

Continued...

OV/2 continued...

Time Id	Presenter		Title
14:50 OV/2-3	H. K. Park	Korea, Rep. of	Overview of the KSTAR Research Progress and Future Plan Toward ITER and K-DEMO
15:15 OV/2-4	E. S. Marmar	USA	Overview of Research Results from the Alcator C-Mod Tokamak
15:40 OV/2-5	J. L. Kline	USA	Progress of Indirect Drive Inertial Confinement Fusion in the USA

FIP/1

Fusion Engineering, Integration and Power Plant Design: ITER Technology

Chair: Rajesh Maingi (USA)

Main Hall

(16:40 – 18:45)

Time Id	Presenter		Title
16:40 FIP/1-1	M. Nakahira	Japan	Completion of the First TF Coil Structure of ITER
17:00 FIP/1-2Ra	Y. Oda	Japan	Completion of 1st ITER Gyrotron Manufacturing and 1 MW Test Result
FIP/1-2Rb			Outcome of R&D Programme for ITER ICRF Power Source System
FIP/1-2Rc			Recent Progress in the Development of the European 1 MW, 170 GHz CW Gyrotron for ITER
17:20 FIP/1-3Ra	J. Joshi	India	Technologies for Realization of Large Size RF Sources for –ve Neutral Beam Systems for ITER: Challenges, Experience and Path Ahead
FIP/1-3Rb			Progress in the ITER Neutral Beam Test Facility
FIP/1-3Rc			Demonstration of 1 MV Vacuum Insulation for the Vacuum Insulated Beam Source in the ITER NB System
17:40 FIP/1-4	A. Litnovsky	Germany	Diagnostic Mirrors for ITER: Research in a Frame of International Tokamak Physics Activity
18:00 FIP/1-5	E. E. Mukhin	Russian Fed.	Integration of Thomson Scattering and Laser-Induced Fluorescence in ITER Divertor: Engineering and Performance Analysis
18:20 FIP/1-6	X. Wang	China, P. R.	Current Design and R&D Progress of CN HCCB TBS

OVP

Overview Posters

Main Hall

(14:00 – 18:45)

Id	Presenter		Title
OV/1-1	A. K. Chakraborty	India	Progress of ITER-India Activities for ITER Deliverables: Challenges and Mitigation Measures
OV/1-2	B. Bigot	ITER	Progress Toward ITER's First Plasma
OV/1-3	E. Joffrin	France	Overview of the JET Preparation for Deuterium-Tritium Operation
OV/1-4	C. C. Petty	USA	DIII-D Research Towards Establishing the Scientific Basis for Future Fusion Reactors
OV/2-1	H. Meyer	UK	Overview of Physics Studies on ASDEX-Upgrade
OV/2-2	B. N. Wan	China, P. R.	Recent Advances in EAST Physics Experiments in Support of Steady-State Operation for ITER and CFETR
OV/2-3	H. K. Park	Korea, Rep. of	Overview of the KSTAR Research Progress and Future Plan Toward ITER and K-DEMO
OV/2-4	E. S. Marmor	USA	Overview of Research Results from the Alcator C-Mod Tokamak
OV/2-5	J. L. Kline	USA	Progress of Indirect Drive Inertial Confinement Fusion in the USA
OV/3-1	P. Barabaschi	F4E	Progress of JT-60SA Project
OV/3-2	G. Zhuang	China, P. R.	Progress of the CFETR Design
OV/3-3	M. Sugimoto	Japan	Overview of the Validation Activities of IFMIF/EVEDA: LIPAc, the Linear IFMIF Prototype Accelerator and LiFus6, the Lithium Corrosion Induced Facility
OV/3-4	H. Tanigawa	Japan	The Strategy of Fusion DEMO In-Vessel Structural Material Development
OV/4-1	T. Klinger	Germany	Overview of First Wendelstein 7-X High-Performance Operation with Island Divertor
OV/4-2	T. Morisaki	Japan	Overview of the First Deuterium Experiment in LHD
OV/4-3	E. Ascasibar	Spain	Overview of TJ-II Stellarator Results
OV/4-4	S. Pamela	UK	ELM and ELM-control Simulations
OV/4-5	E. J. Strait	USA	Experiments in Disruption Avoidance for ITER Using Passive and Active Control
OV/5-1	M. Xu	China, P. R.	Overview of HL-2A Recent Experiments
OV/5-2	S. Coda	Switzerland	Physics Research on the TCV Tokamak Facility: From Conventional to Alternative Scenarios and Beyond

Continued...

OVP *continued...*

Id	Presenter	Title
OV/5-3	R. L. Tanna	India Overview of Operation and Experiments in the ADITYA-U Tokamak
OV/5-4	N. N. Bakharev	Russian Fed. Tokamak Research in Ioffe Institute
OV/5-5Ra	J. E. Menard	USA NSTX-U Theory and Modelling Results
OV/5-5Rb	J. R. Harrison	UK Overview of New MAST Physics in Anticipation of First Results from MAST Upgrade
OV/P-1	G. Pucella	Italy Overview of the FTU Results
OV/P-2	B. P. Radha	USA Overview and Status of Direct-Drive Inertial Confinement Fusion in the United States
OV/P-3	M. Komm	Czech Republic ITER-Relevant Research on the COMPASS Tokamak
OV/P-4	T. A. Carter	USA Advances in Fusion-Relevant Physics on the Large Plasma Device
OV/P-5	N. C. Wang	China, P. R. Overview of the Recent Experimental Research on the J-TEXT Tokamak
OV/P-6	J. E. Menard	USA Fusion Energy Development Applications Utilizing the Spherical Tokamak and Associated Research Needs and Tools
OV/P-7	M. Kakati	India Design, Development and Recent Experiments at the CIRCLE-PSI Device
OV/P-8	W. Liu	China, P. R. Overview of Diagnostics Upgrade and Experiment Progress on KTX
OV/P-11	H. Gota	USA Formation of Hot, Stable, Long-Lived Field-Reversed Configuration Plasmas on the C-2W Device
OV/P-12	S. M. Belsare	India Activity of Indian High Heat Flux Test Facility

19:30 – 22:00: Welcome Reception

Tue

OV/3

Overviews 3: Magnetic Fusion

Chair: Liu Yong (P. R. China) Main Hall (08:30 – 10:15)

Time Id	Presenter		Title
08:30 OV/3-1	P. Barabaschi	F4E	Progress of JT-60SA Project
08:55 OV/3-2	G. Zhuang	China, P. R.	Progress of the CFETR Design
09:20 OV/3-3	M. Sugimoto	Japan	Overview of the Validation Activities of IFMIF/EVEDA: LIPAc, the Linear IFMIF Prototype Accelerator and LiFus6, the Lithium Corrosion Induced Facility
09:45 OV/3-4	H. Tanigawa	Japan	The Strategy of Fusion DEMO In-Vessel Structural Material Development

EX/1 and TH/1

Energetic Particles

Chair: Simon Pinches (ITER) Main Hall (10:45 – 12:30)

Time Id	Presenter		Title
10:45 EX/1-1	P. Lauber	Germany	Strongly Nonlinear Energetic Particle Dynamics in ASDEX-Upgrade Scenarios with Core Impurity Accumulation
11:05 TH/1-1	W. Shen	China, P. R.	Simulations of Energetic Particle Driven Instabilities and Fast Particle Redistribution in EAST Tokamak
11:25 EX/1-2	M. Podestà	USA	Reduced Energetic Particle Transport Models Enable Comprehensive Time-Dependent Tokamak Simulations
11:45 TH/1-2	Y. Todo	Japan	Critical Fast Ion Distribution in Phase Space for the Synchronized Sudden Growth of Multiple Alfvén Eigenmodes and the Global Transport of Fast Ions
12:05 EX/1-3Ra	S. Yamamoto	Japan	Impact of ECH/ECCD on Fast-Ion-Driven MHD Instabilities in Helical Plasmas
EX/1-3Rb			Excitation Mechanism of the Energetic Particle Driven Resistive Interchange Mode and Strategy to Control the Mode in Large Helical Device

P1

Posters 1

Main Hall

(08:30 – 12:30)

Tue

Id	Presenter		Title
FIP/1-1	M. Nakahira	Japan	Completion of the First TF Coil Structure of ITER
FIP/1-2Ra	Y. Oda	Japan	Completion of 1st ITER Gyrotron Manufacturing and 1 MW Test Result
FIP/1-2Rb	R. G. Trivedi	India	Outcome of R&D Programme for ITER ICRF Power Source System
FIP/1-2Rc	G. Gantenbein	Germany	Recent Progress in the Development of the European 1 MW, 170 GHz CW Gyrotron for ITER
FIP/1-3Ra	J. Joshi	India	Technologies for Realization of Large Size RF Sources for –ve Neutral Beam Systems for ITER: Challenges, Experience and Path Ahead
FIP/1-3Rb	V. Toigo	Italy	Progress in the ITER Neutral Beam Test Facility
FIP/1-3Rc	A. Kojima	Japan	Demonstration of 1 MV Vacuum Insulation for the Vacuum Insulated Beam Source in the ITER NB System
FIP/1-4	A. Litnovsky	Germany	Diagnostic Mirrors for ITER: Research in a Frame of International Tokamak Physics Activity
FIP/1-5	E. E. Mukhin	Russian Fed.	Integration of Thomson Scattering and Laser-Induced Fluorescence in ITER Divertor: Engineering and Performance Analysis
FIP/1-6	X. Wang	China, P. R.	Current Design and R&D Progress of CN HCCB TBS
EX/P1-1	M. Komm	Czech Republic	Divertor Impurity Seeding Experiments at the COMPASS Tokamak
EX/P1-2	M. J. Hole	Portugal	Experimental Studies of Pressure and Plasma Current Profiles for Equilibria Calculations During AC Transition in the ISTTOK Tokamak
EX/P1-3	D. Frigione	Italy	Impact of Neon Injection on Electron Density Peaking in JET Hybrid Plasmas
EX/P1-4	H. Weisen	Switzerland	Isotope Dependence of Confinement in JET Deuterium and Hydrogen Plasmas
EX/P1-5	H.-T. Kim	UK	High Fusion Performance at High T_i/T_e in JET-ILW Baseline Plasmas with High NBI Heating Power and Low Gas Puffing

Continued...

P1 *continued...*

Tue

Id	Presenter		Title
EX/P1-6	B. P. Duval	Switzerland	Singlet Breakdown Optimization to a Doublet Plasma Configuration on the TCV Tokamak
EX/P1-9	T. Estrada	Spain	Turbulence and Radial Electric Field Asymmetries Measured at TJ-II Plasmas
EX/P1-11	E. Sánchez	Spain	Validation of Global Gyrokinetic Simulations in Stellarator Configurations
EX/P1-12	A. Vertkov	Russian Fed.	The Concept of Lithium Based Plasma Facing Elements for Steady State Fusion Tokamak-Reactor and its Experimental Validation
EX/P1-14	D. Borodin	Germany	Extrapolation of Be Erosion Modelling from JET and PISCES-B to ITER
EX/P1-15	M. Mayer	Germany	Erosion and Deposition in the JET Divertor During the ITER-Like Wall Campaigns
EX/P1-16	G. De Tommasi	Italy	The Impact of Poloidal Flux Expansion on JET Divertor Radiation Performance
EX/P1-17	S. Jachmich	Sweden	First Mirror Test in JET for ITER: Complete Overview After Three Campaigns in JET with ITER-Like Wall
EX/P1-18	I. E. Garkusha	Ukraine	Influence of Magnetic Field on Plasma Energy Transfer to Material Surfaces in ELM Simulation Experiments with QSPA-M
EX/P1-19	C. Theiler	Switzerland	SOL Transport and Detachment in Alternative Divertor Configurations in TCV L- and H-Mode Plasmas
EX/P1-20	C. Hidalgo	Spain	On the Role of Radial Electric Fields on Turbulence Spreading in the Plasma Boundary of Fusion Devices
EX/P1-21	I. Furno	Switzerland	Basic Studies of the Interaction of Blobs with Suprathermal Ions and Millimetre-Wave Beams in the TORPEX Device
EX/P1-22	C. Sozzi	Italy	Early Identification of Disruption Paths for Prevention and Avoidance
EX/P1-23	S. Jachmich	Germany	Minimizing Power Load Asymmetries During Disruption Mitigation at JET
EX/P1-24	S. N. Gerasimov	UK	Overview of Disruptions with JET-ILW
EX/P1-25	M. Kong	Switzerland	Control of NTMs and Integrated Multiactuator Control on TCV
EX/P1-26	O. Ficker	Czech Republic	Runaway Electron Beam Stability and Decay in COMPASS
EX/P1-28	S. E. Sharapov	UK	Plasma and Diagnostics Preparation for α -Particle Studies in JET DT

Continued...

P1 *continued...*

Id	Presenter		Title
EX/P1-29	C. C. Klepper	USA	Subdivertor Fuel Isotopic Content Detection Limit for JET and Impact on the Control of ICRH for JET-ILW and JET-DT Operation
EX/P1-30	C. Piron	Italy	Extension of the Operating Space of High- β_N Fully Noninductive Scenarios on TCV Using Neutral Beam Injection
EX/P1-31	V. Huber	Germany	The Software and Hardware Architecture of the Real-Time Protection of In-Vessel Components in JET-ILW
TH/P1-1	M. Drevlak	Germany	New Results in Stellarator Optimization
TH/P1-2	N. Kasuya	Japan	Numerical Diagnostic to Investigate Poloidal Asymmetry in Three-Dimensional Magnetic Configurations
TH/P1-3	S. Satake	Japan	Effect of Magnetic Shear and the Finite Banana-Orbit Width on the Neoclassical Toroidal Viscosity in Perturbed Tokamaks
TH/P1-4	L. E. Sugiyama	USA	Steady States for Nonaxisymmetric Rotating Toroidal Plasmas
TH/P1-5	F. Schluck	Germany	Plasma-Surface Related 3D Modelling Results for Wendelstein 7-X and EAST
TH/P1-6	D. Schwörer	Germany	Influence of Neutral-Plasma Interactions on 3D Scrape-Off Layer Filaments
TH/P1-7	L. Li	China, P. R.	Comparative Modelling of Plasma Boundary Corrugation due to the Application of 3D Fields with ELM Control Coils in Various ITER Scenarios
TH/P1-8	B. C. Lyons	USA	Predict-First Analysis and Experimental Validation of MHD Equilibrium, Stability, and Plasma Response to 3D Magnetic Perturbations
FIP/P1-1	L. R. Baylor	USA	Shattered Pellet Injection Technology Design and Characterization for Disruption Mitigation Experiments
FIP/P1-2	S. Simrock	ITER	Automated Testing of ITER Diagnostics Scientific Instrumentation
FIP/P1-3	Z. Wang	USA	Hollow Pellets for Magnetic Fusion
FIP/P1-4	J. Smith	USA	Recent Progress on the Production and Testing of the ITER Central Solenoid Modules
FIP/P1-5	A. G. Razdobarin	Russian Fed.	Dielectric Windows as Front-End Diagnostic Elements in ITER
FIP/P1-7	M. Tanaka	Japan	Exhaust Behaviour and Mass Balance of Tritium in Large Helical Device

Continued...

Tue

P1 *continued...*

Tue

Id	Presenter		Title
FIP/P1-8	T. Kobayashi	Japan	Progress in Development and Fabrication of the JT-60SA ECH/CD System
FIP/P1-9	A. K. Verma	India	Preliminary Pipe Stress Analysis of High Pressure, High Temperature Experimental Helium Cooling System
FIP/P1-10	H. Tobari	Japan	Completion of DC 1 MV Power Supply System for ITER Neutral Beam Test Facility
FIP/P1-11	K. Kajiwara	Japan	Improvement of ITER Equatorial EC Launcher Design for Poloidal Steering Compatibility
FIP/P1-12	A. Y. Dnestrovsky	Russian Fed.	Integrated Modelling of Core and Divertor Plasmas for DEMO-FNS Hybrid Facility
FIP/P1-13	A. Kasugai	Japan	RFQ Commissioning of Linear IFMIF Prototype Accelerator (LIPAc)
FIP/P1-14	R. Imazawa	Japan	Development of the Far-Infrared Laser Polarimetry for Current Profile Measurement on ITER
FIP/P1-15	D. L. Brower	USA	Overview of ITPA R&D Activities in Support of ITER Diagnostics
FIP/P1-16	S. Clement-Lorenzo	F4E	Verification Tests for Remote Participation at ITER REC
FIP/P1-17	E. Gaio	Italy	Consorzio RFX Contribution to the JT-60SA Project in the Frame of the Broader Approach Agreement
FIP/P1-18	T. Schwarz-Selinger	Germany	The Influence of Displacement Damage and Helium on Deuterium Transport and Retention in Tungsten
FIP/P1-19	N. Bairagi	India	Experimental Measurements of Cryogenic Heat Loads on SST-1 Helium Cryogenic Plant
FIP/P1-20	R. Bright	India	Thermo-Mechanical Experiments On Lithium Titanate Pebble Bed
FIP/P1-21	K. Patel	India	The Operation, Control, Data Acquisition System of ASDEX Pressure Gauge for Neutral Pressure
FIP/P1-22	E. A. Tolman	USA	Conceptual Design Study for Heat Exhaust Management in the ARC Fusion Pilot Plant
FIP/P1-24	P. Chaudhuri	India	Progress on Lithium Ceramic Breeder Materials Development, Characterization and R&D Activities in IPR
FIP/P1-25	R. Sugandhi	India	Machine Control System for Large Volume Plasma Device: Current Status and Future Directions

Continued...

P1 *continued...*

Id	Presenter		Title
FIP/P1-26	V. N. Muvvala	India	Application of Finite Element Techniques in Simulation of Mechanical Design and Performance Assessment of Different Components of a Neutral Beam Systems
FIP/P1-27	I. Kodeli	Slovenia	TRIGA Integral Activation of Mn Foils, Li ₂ O and LiF as Potential Tritium Production Monitors for Fusion Applications
FIP/P1-28	R. Anand	India	Seismic Analysis of High Power Amplifier in ITER ICRF Range
FIP/P1-29	P. V. Subhash	India	ACTYS Code System: Towards Next Generation Nuclear Activation Codes for Fusion Reactors
FIP/P1-31	A. K. Tyagi	India	Deuterium Depth Profile Measurement in Pre- and Postirradiated Tungsten
FIP/P1-32	R. Kumar	India	Development of a High-Temperature Blackbody Source for ITER ECE Diagnostic
FIP/P1-33	G. L. Vyas	India	Alignment and Calibration Schemes for ITER CXRS-Pedestal Diagnostic
FIP/P1-34	S. Varshney	India	Thermal Analysis of Protection Important Components of ITER XRCS-Survey Diagnostic System
FIP/P1-35	S. Jha	India	Preliminary Design of IN-DA Diagnostic Plant Instrumentation & Control
FIP/P1-36	S. Kumar	India	Design Validation of ITER XRCS Survey Spectrometer with Nuclear Code RCC-MR
FIP/P1-37	M. Manuelraj	India	In-Vessel Inspection System: Design Progress of High Vacuum and Temperature Compatible Remote Handling for Fusion Purposes
FIP/P1-38	L. Cai	China, P. R.	Preliminary Development on a Conceptual First Wall for DEMO
FIP/P1-39	N. P. Singh	India	Installation and Initial Run of 96 kV 7.2 MW Acceleration Grid Power Supplies
FIP/P1-40	M. J. Singh	India	R&D Status of Indian Test Facility for ITER DNB Characterization
FIP/P1-41	H. Tyagi	India	Design and Development of Safety Control System of Indian Test Facility (IN-TF) for ITER DNB
FIP/P1-42	A. Maheshwari	India	Study of Corrosion Properties ITER In-Wall Shield (IWS) Fasteners and Structural Integrity of IWS

Continued...

Tue

P1 *continued...*

Tue

Id	Presenter		Title
FIP/P1-43	D. Aggarwal	India	Nuclear Performance Analysis and Optimization Study of Indian Solid Breeder Blanket for DEMO
FIP/P1-44	K. K. Gotewal	India	Design and Development of the Articulated Robotic Inspection Arm (ARIA) for Fusion Machine
FIP/P1-45	K. M. Patel	India	Baking System of ADITYA Upgrade Tokamak
FIP/P1-46	S. Muralidhara	India	Dynamic Simulation of Loss of Insulation Vacuum Event for ITER Cryodistribution System
FIP/P1-47	P. Dutta	India	Visual Servo of Tokamak Relevant Remote Handling Systems Using Neural Network Architecture
FIP/P1-50	S. V. Rogozhkin	Russian Fed.	The Influence of Fe-Ion Irradiation on the Microstructure of Reduced Activation Ferritic-Martensitic Steel Eurofer 97
FIP/P1-51	J. E. Menard	USA	Electromagnetic Particle Injector (EPI) as a Fast Time Response Disruption Mitigation Concept
FIP/P1-52	H. B. Pandya	India	Preliminary Results of Prototype Martin-Puplett Interferometer and Transmission Line Developed for ITER ECE Diagnostic
FIP/P1-53	J. Rapp	USA	Performance of the Plasma Source and Heating Concept for the Prototype-Material Plasma Exposure Experiment (Proto-MPEX)
FIP/P1-54	K. Ikeda	Japan	Exploring Deuterium Beam Operation and Behaviour of Coextracted Electron in Negative-Ion-Based Neutral Beam Injector
FIP/P1-55	D. Sharma	India	Thermal-Hydraulics and Structural Analyses of LLCB TBM Set
FIP/P1-56	T. Kariya	Japan	Development of High Power Gyrotrons for Advanced Fusion Devices and DEMO
FIP/P1-57	R. N. Panchal	India	Performance Evaluation of 1.3 kW at 4.5 K Helium Refrigerator/Liquefier (HRL) at IPR
FIP/P1-58	G. Vadolia	India	Survey on Hot Isostatic Pressing Technique for Development of Tokamak Components
FIP/P1-59	A. D. Mankani	India	Design and Development of 500 kV, 100 mA DC High Voltage Power Supply for Particle Accelerators at IPR

OV/4

Chair: Michael Zarnstorff (USA)

Overviews 4: Magnetic Fusion

Main Hall

(14:00 – 16:10)

Time Id	Presenter		Title
14:00 OV/4-1	T. Klinger	Germany	Overview of First Wendelstein 7-X High-Performance Operation with Island Divertor
14:25 OV/4-2	T. Morisaki	Japan	Overview of the First Deuterium Experiment in LHD
14:50 OV/4-3	E. Ascasíbar	Spain	Overview of TJ-II Stellarator Results
15:15 OV/4-4	S. Pamela	UK	ELM and ELM-control Simulations
15:40 OV/4-5	E. J. Strait	USA	Experiments in Disruption Avoidance for ITER Using Passive and Active Control

OV/5

Chair: Hyeon Park (Korea, Rep. of)

Overviews 5: Magnetic Fusion

Main Hall

(16:40 – 18:45)

Time Id	Presenter		Title
16:40 OV/5-1	M. Xu	China, P. R.	Overview of HL-2A Recent Experiments
17:05 OV/5-2	S. Coda	Switzerland	Physics Research on the TCV Tokamak Facility: From Conventional to Alternative Scenarios and Beyond
17:30 OV/5-3	R. L. Tanna	India	Overview of Operation and Experiments in the ADITYA-U Tokamak
17:55 OV/5-4	N. N. Bakharev	Russian Fed.	Tokamak Research in Ioffe Institute
18:20 OV/5-5Ra	J. E. Menard	USA	Overview of Recent Progress in Understanding NSTX and NSTX-U Plasmas
OV/5-5Rb			Overview of New MAST Physics in Anticipation of First Results from MAST Upgrade

Tue

P2		Posters 2	
		Main Hall	(14:00 – 18:45)
Id		Presenter	Title
EX/1-1	P. Lauber	Germany	Strongly Nonlinear Energetic Particle Dynamics in ASDEX-Upgrade Scenarios with Core Impurity Accumulation
EX/1-2	M. Podestà	USA	Reduced Energetic Particle Transport Models Enable Comprehensive Time-Dependent Tokamak Simulations
EX/1-3Ra	S. Yamamoto	Japan	Impact of ECH/ECCD on Fast-Ion-Driven MHD Instabilities in Helical Plasmas
EX/1-3Rb	S. Ohdachi	Japan	Excitation Mechanism of the Energetic Particle Driven Resistive Interchange Mode and Strategy to Control the Mode in Large Helical Device
TH/1-1	W. Shen	China, P. R.	Simulations of Energetic Particle Driven Instabilities and Fast Particle Redistribution in EAST Tokamak
TH/1-2	Y. Todo	Japan	Critical Fast Ion Distribution in Phase Space for the Synchronized Sudden Growth of Multiple Alfvén Eigenmodes and the Global Transport of Fast Ions
EX/P2-1	D. F. Kong	China, P. R.	$E_r \times B$ Shear Effect on Cross Phase Mitigates ELM at High Collisionality
EX/P2-3	L. Zhang	China, P. R.	Tungsten Control in NBI-Dominant H-Mode Discharges in EAST Tokamak
EX/P2-4	G. S. Xu	China, P. R.	A Promising Grassy ELM Regime for High-Performance Steady-State Operations with Metal Wall in EAST and CFETR
EX/P2-5	M. Sharma	India	Leak Width in a Multicusp Field Configuration: A Revisit with a Versatile Experimental Device
EX/P2-6	U. Kumar	India	Effect of the Controlled Density Gradient on Equilibrium and Confinement in a Simple Toroidal Device with Two Plasma Sources
EX/P2-7	M. Kumar	India	Imaging of SST-1 Plasma with LHCD Power
EX/P2-8	L. Wang	China, P. R.	Advances in Plasma-Wall Interaction Control for H-Mode Operation over 100 s with ITER-like Tungsten Divertor on EAST
EX/P2-9	J. Pramanik	India	Characterization of Particle Growth and Enhancement of Sputtering Yields in a Cogenerated Dusty Plasma

Continued...

P2 *continued...*

Id	Presenter		Title
EX/P2-10	P. Sharma	India	A Transmission Electron Microscopy Investigation of Defects Induced in Tungsten Foils by Au and B Ion Irradiation
EX/P2-11	M. Himabindu	India	Modelling Studies of X-Divertor Configuration on SST-1 Tokamak Using SOLPS5.1
EX/P2-12	P. J. Sun	China, P. R.	Experimental Study of Multiscale Interaction between (Intermediate, Small)-Scale Microturbulence and MHD Modes in EAST Plasmas
EX/P2-13	M. P. Bhuva	India	Effect of Cathode Geometry on Magnetically Coupled Hollow Cathode Plasma Source
EX/P2-14	L. Xu	China, P. R.	Kink Mode Study in EAST High- β_P Plasma
EX/P2-15	J. Huang	China, P. R.	Fast-Ion Studies in High Performance Fully Noninductive Discharges on EAST
EX/P2-16	A. Ekedahl	France	Progress Towards Development of Long Pulse ITER Operation through RF Heated H-Mode Experiments on EAST and HL-2A
EX/P2-17	C. Mallick	India	Observations of Plasma Stimulated Electrostatic Sideband Emission and Harmonic Distortion: Evidence of Overdense Plasma Generation Inside a Microwave Discharge Ion Source
EX/P2-18	S. Das	India	Radial Characteristics of a Magnetized Plasma Column
EX/P2-20	P. Srivastav	India	Investigations on Temperature Fluctuations and Energy Transport in ETG Dominated Large Laboratory Plasma
EX/P2-22	D. Rathi	India	Preliminary Results of Wall Conditioning Experiments Using High Power ICRH System on SST-1 at Different Toroidal Magnetic Fields
EX/P2-23	L. Soto	Chile	Recent Finding in Fusion Studies Using Table Top and Miniaturized Dense Plasma Focus Devices Operating from Hundred Joules to less than One Joule
EX/P2-26	D. Moreau	France	Model-Predictive Kinetic Control for Steady State Plasma Operation Scenarios on EAST
EX/P2-27	J. Prompting	Thailand	Simulation Study of Heat Transport with On-Off Axis ICRH in Thailand Tokamak Using BALDUR Code
TH/P2-1	D. Zarzoso	France	Transport Induced by Energetic Geodesic Acoustic Modes

Continued...

Tue

P2 *continued...*

Tue

Id	Presenter		Title
TH/P2-2	U. Maurya	India	Burning Plasma Simulation with α -Particle Heating
TH/P2-3	H. He	China, P. R.	Simulation of Toroidicity-Induced Alfvén Eigenmode Excited by Energetic Ions in HL-2A Tokamak Plasmas
TH/P2-4	R. Kleiber	Germany	Global Gyrokinetic Multimodel Simulations of ITG and Alfvénic Modes for Tokamaks and the First Operational Phase of Wendelstein 7-X
TH/P2-5	P. Garcia-Martinez	Argentina	Reconstruction of MHD Modes for Energetic Particle Dynamics Studies in Toroidal Equilibria with Arbitrary q Profiles
TH/P2-6	Z. Qiu	China, P. R.	Nonlinear Decay and Plasma Heating by Toroidal Alfvén Eigenmodes
TH/P2-7	Y. Hou	China, P. R.	Analysis of Energetic Particle Driven Toroidal Alfvén Eigenmodes in CFETR Baseline Scenario
TH/P2-8	A. Snicker	Finland	The Combined Effect of Neoclassical Tearing Modes and ELM Control Coils on Fast-Ions: Validation in AUG and Extrapolation for ITER
TH/P2-9	A. Biancalani	Germany	Self-Consistent Gyrokinetic Description of the Interaction between Alfvén Modes and Turbulence
TH/P2-10	G. Vlad	Italy	Comparison of Energetic Particle Radial Transport between Single- n and Multiple- n Simulations of Alfvénic Modes
TH/P2-11	H. Wang	Japan	Simulations of Two Types of Energetic Particle Driven Geodesic Acoustic Modes and the Energy Channelling in the Large Helical Device Plasmas
TH/P2-12	R. Seki	Japan	Comprehensive Magnetohydrodynamic Hybrid Simulations of Fast Ion Losses due to the Fast Ion Driven Instabilities in the Large Helical Device
TH/P2-14	J. P. Graves	Switzerland	Advanced Energetic Ion and Impurity Ion Physics in 2D and 3D Magnetically Confined Plasmas
TH/P2-15	Y. V. Yakovenko	Ukraine	Simulations of the Sawtooth-Induced Redistribution of Fast Ions in JET and ITER
TH/P2-16	E. V. Belova	USA	Numerical Simulations of GAE Stabilization in NSTX-U

Continued...

P2 *continued...*

Id		Presenter	Title	
TH/P2-17	Z. Lin	USA	Verification and Validation of Integrated Simulation of Energetic Particles in Toroidal Plasmas	

Tue

Wed

IFE/1

Inertial Fusion Experiments & Theory

Chair: Sylvie Jacquemot (France)

Main Hall

(08:30 – 10:15)

Time Id	Presenter		Title
08:30 IFE/1-1	Y. Arikawa	Japan	Two-Colour Mixed Petawatt Laser Designed for Fast Ignition Experiment
08:50 IFE/1-2	S. Fujioka	Japan	Production of keV-Temperature Plasma Core with Magnetized Fast Isochoric Heating
09:10 IFE/1-3	R. J. Leeper	USA	Liquid DT Layer Approach to Inertial Confinement Fusion
09:30 IFE/1-4	J. M. Perlado	Spain	Thermo-Mechanical and Atomistic Assessment of First Wall and Optics in Nonprotective Chamber in Inertial Fusion Energy
09:50 IFE/1-5	A. Iwamoto	Japan	Demonstrations of Foam Shell and Infrared Heating Methods for FIREX Targets

EX/2

Pedestal & ELM Optimization

Chair: Richard Buttery (USA)

Main Hall

(10:45 – 12:30)

Time Id	Presenter		Title
10:45 EX/2-1	E. de la Luna	Spain	Impact of ELM Control in JET Experiments on H-Mode Terminations with/without Current Ramp-Down and Implications for ITER
11:05 EX/2-2	D. R. Ernst	USA	Viability of Wide Pedestal QH-Mode for Burning Plasma Operation
11:25 EX/2-3	T. Happel	Germany	Advances in the Understanding of the I-Mode Confinement Regime: Access, Stationarity, Edge/SOL Transport and Divertor Impact
11:45 EX/2-4	P. B. Snyder	USA	High Fusion Performance in Super H-Mode Experiments on Alcator C-Mod and DIII-D
12:05 EX/2-5	B. Labit	Switzerland	Plasma Shape and Fuelling Dependence on the Small ELM Regime in TCV and AUG

P3

Posters 3

Main Hall

(08:30 – 12:30)

Id	Presenter		Title
EX/P3-1	M. Yoshikawa	Japan	Fluctuation Suppression by the Potential Formation in GAMMA 10/PDX Plasma
EX/P3-2	T. Minami	Japan	Effect of Magnetic Field Structure on Electron Internal Transport Barrier and its Role for the Barrier Formation in Heliotron J
EX/P3-3	S. Ohshima	Japan	The Configuration Dependence of Isotope Effects on Turbulence System in Heliotron J
EX/P3-4	K. Kamiya	Japan	Multiple Turbulent Plasma States in the H-Mode Transition on JT-60U
EX/P3-5	H. Yamada	Japan	Characterization of Isotope Effect on Confinement of Dimensionally Similar NBI-Heated Plasmas in LHD
EX/P3-6	K. Tanaka	Japan	Isotope Effects on Confinement and Turbulence in ECRH Plasma of LHD
EX/P3-7	T. Tokuzawa	Japan	Rapid Radial Propagation of Momentum Change and Flow Oscillation Associated with a Pellet Injection
EX/P3-8	M. Nishiura	Japan	Experimental Analysis of Self-Organized Structure and Transport on Magnetospheric Plasma Device RT-1
EX/P3-9	N. Ezumi	Japan	Synergistic Effect of Impurity and Hydrogen Gas Puffs on Plasma Detachment in the GAMMA 10/PDX Tandem Mirror
EX/P3-10	M. Kobayashi	Japan	Core Transport Improvement in Stable Detachment with RMP Application to the Edge Stochastic Layer of LHD
EX/P3-11	T. Oishi	Japan	Effect of Deuterium Plasmas on Carbon Impurity Transport in the Edge Stochastic Magnetic Field Layer of Large Helical Device
EX/P3-12	K. Hanada	Japan	Particle Balance Investigation with the Combination of Rate Equations of Hydrogen State and Hydrogen Barrier Model in Long Duration Discharges on All-Metal PFW QUEST
EX/P3-13	Y. H. Ding	China, P. R.	Recent Progresses on the RMP Researches Towards Active Control of Tearing Mode in the J-TEXT Tokamak
EX/P3-14	Y. Suzuki	Japan	Investigation of Magnetic Topology on Spontaneous Transition Phenomena for High- β Plasma of Large Helical Device

Continued...

Wed

P3 *continued...*

Wed	Id		Presenter	Title
	EX/P3-15	K. Y. Watanabe	Japan	Dependence of RMP Penetration Threshold on Plasma Parameters and Ion Species in Helical Plasmas
	EX/P3-16	Y. Takemura	Japan	Study of Locking Mechanism of Locked-Mode-Like Instability in Helical Plasmas
	EX/P3-17	M. Nagata	Japan	Experimental Studies of Plasmoid Reconnection for Closed Flux Current Generated by Coaxial Helicity Injection on HIST
	EX/P3-19	H. Tanaka	Japan	Electron Bernstein Wave Heating and Current Drive with Multielectron Cyclotron Resonances During Noninductive Start-Up on LATE
	EX/P3-20	K. Ogawa	Japan	Energetic-Ion Confinement Studies by Using Comprehensive Neutron Diagnostics in the Large Helical Device
	EX/P3-21	H. Idei	Japan	Fully Noninductive 2nd Harmonic Electron Cyclotron Current Ramp-Up with Focussed Polarized Beams in the QUEST Spherical Tokamak
	EX/P3-22	H. Tanabe	Japan	Investigation of Fine Structure Formation of Guide Field Reconnection During Merging Plasma Startup of Spherical Tokamak in TS-3U
	EX/P3-23	A. Ejiri	Japan	Plasma Current Generation and Ramp-Up by the Lower Hybrid Wave Using Outboard-Launch and Top-Launch Antennas on the TST-2 Spherical Tokamak
	EX/P3-24	Y. Ono	Japan	Scaling Study of Reconnection/Merging Heating of Spherical Tokamak Plasmas for Direct Access to Burning Plasma
	EX/P3-25	T. Wakatsuki	Japan	Safety Factor Profile Control with Reduced CS Flux Consumption During Plasma Current Ramp-Up Phase Using Reinforcement Learning Technique
	EX/P3-26	G. De Tommasi	Italy	2D and 3D Modelling of JT-60SA for Disruptions and Plasma Start-Up
	EX/P3-27	G. Motojima	Japan	New Approach to the Control of Particle Recycling Using Divertor Pumping in LHD

Continued...

P3 *continued...*

Id	Presenter	Title
FIP/P3-1	F. Bedoya	USA Surface Characterization of Li Coatings and their Interaction with Plasmas for Fusion Applications via Ion Beam Analysis Techniques
FIP/P3-2	K. Gi	Japan Contribution of Fusion Energy to Low-Carbon Development under the Paris Agreement and Accompanying Uncertainties
FIP/P3-3	H. Noto	Japan Dispersion Strengthened Copper Alloys Produced by Mechanical Alloying and Hot Isostatic Pressing for Divertor Application
FIP/P3-4	M. Kobayashi	Japan Neutron Flux Distributions in the LHD Torus Hall Evaluated by an Imaging Plate Technique in the First Campaign of Deuterium Plasma Experiment
FIP/P3-5	P. Kanth	India A Multiparameter Optimization Technique Considering Temporal and Spatial Variation in Nuclear Response of Materials in Fusion Devices
FIP/P3-6	K. Ochiai	Japan Design Progress of Advanced Fusion Neutron Source for JA/DEMO Fusion Reactor
FIP/P3-7	G. Stankunas	Lithuania Neutronic Analysis of IFMIF-DONES Test Cell Cooling System
FIP/P3-8	C. Day	Germany The DEMO Fuel Cycle: Novel Technologies for Tritium Inventory Reduction
FIP/P3-9	Ž. Štancar	Slovenia Multiphysics Approach to Plasma Neutron Source Modelling at the Tokamak JET
FIP/P3-10	S. P. Smith	USA The Potential for Retention of Spin Polarization to Raise Fusion Reactivity
FIP/P3-12	A. Abhishek	India Artificial Neural Network for Yield Strength Prediction of Irradiated RAFM Steels
FIP/P3-14	R. Joshi	India Modification in LHCD DAC System to Incorporate Measurement of RF Power
FIP/P3-15	S. S. Mukherjee	India Thermal Performance Analysis of Al_2O_3 -Water Nanofluid as a Coolant in Nuclear Applications
FIP/P3-16	A. Arumugam	India RGA Analysis and Surface Analysis of SST-1 Graphite Tiles in High Temperature Vacuum Baking
FIP/P3-18	K. P. Singh	India Studies on High Temperature Vacuum Brazing of Tungsten to Tungsten Alloy Materials for DEMO Divertor Application

Continued...

P3 *continued...*

Id	Presenter		Title
FIP/P3-19	M. Sugimoto	France	Deuteron Beam Commissioning of the Linear IFMIF Prototype Accelerator Source and LEBT
FIP/P3-20	D. Panayotov	EC	Overview of the Methods Developed for Fission Plants Safety Relevant to the Safety of Fusion Facilities
FIP/P3-23	A. S. Arakcheev	Russian Fed.	Status of Studies of Pulsed Heat Load Influence on Tungsten at BETA Facility and Station of SR Scattering "Plasma" in BINP
FIP/P3-25	M. Coleman	UK	Global Supply of Tritium for Fusion R&D
FIP/P3-26	J. M. Park	USA	The Advanced Tokamak Path to a Compact Net Electric Pilot Plant
FIP/P3-27	S. Shah	India	Neutron Irradiation Impact on ITER Grade Insulating Material
FIP/P3-28	S. Tiwari	India	Conceptual Design of Neutron Activation System for IN-LLCB TBM
FIP/P3-29	M. Rajput	India	Energy Differential and Displacement Damage Cross Section of DT Neutron Induced Reactions on Fusion Reactor Materials (Fe, Cr & W)
FIP/P3-30	A. Patel	India	Application of ANSYS FLUENT MHD Code for Liquid Metal MHD Studies
FIP/P3-31	S. G. Khambholja	India	Structural and Vibrational Properties of Lead-Lithium Alloys: A First Principles Study
FIP/P3-32	K. S. Bhatt	India	Structural Analysis for Strength and Fatigue Life of Half Coupling Weldment for Large Cooling Water Pipes
FIP/P3-33	S. S. Vala	India	Performance of 14-MeV Neutron Generator at IPR
FIP/P3-34	D. Dubey	India	Tritium Handling and Recovery System for Accelerator Based 14-MeV Neutron Generator
FIP/P3-34	V. Shukla	India	Extent of Tritium Contamination of Helium Circuit in a Fusion Reactor: Probable Scenarios
FIP/P3-36	E. Pajuste	Latvia	Novel Method for Determination of Tritium Depth Profiles in Metallic Samples
FIP/P3-38	P. Chakraborty	India	Effect of Magnetic Field on the Corrosion Behaviour of Indian RAFMS in Liquid PbLi
FIP/P3-39	P. A. Rayjada	India	Er ₂ O ₃ Coating by Multilayer Metallic Sputtering and Intermediate Oxidation Approach

Continued...

P3 *continued...*

Id	Presenter	Title
FIP/P3-40	J. Jiang	China, P. R. Development of HINEG and its Experimental Campaigns
FIP/P3-41	V. M. Chernov	Russian Fed. Radiation Properties of the Metal Structural Materials during Low-Temperature Damaging Irradiation
FIP/P3-42	C. S. Sasmal	India Effect of Simulated Postweld Heat Treatment on the Microstructure and Mechanical Properties of IN-RAFM Steel Ion Irradiation Induced Modifications in Tungsten Foils
FIP/P3-44	A. Attri	India Tungsten Fuzz Formation on the Nitrided Tungsten Surface
FIP/P3-45	T. Tulenbergenov	Kazakhstan Neutronics Experiment for Design Validation of Indian TBM Shield Module
FIP/P3-46	H. L. Swami	India Study on Production and Extraction of Negative Ion Impurity Ions in a Caesiated Negative Ion Source
FIP/P3-47	A. Patel	India 3 MW Dual-Output High Voltage Power Supply Operation: Results for Accuracy, Stability and Protection Test
FIP/P3-48	A. J. Deka	India Evaluation of Beam Properties of a Negative Hydrogen Source by Doppler Shift Spectroscopy
FIP/P3-49	S. S. Mukherjee	India Thermohydraulic Analysis of Forced Flow Helium Cooled Cryopanel of Cryopump Using Venecia Code
FIP/P3-50	J. S. Mishra	India Pellet Fuelling Prospects and Injector System for ADITYA-U Tokamak
FIP/P3-51	P. Bhatt	India Performance of Transmission Line System at 42.0 ± 0.2 GHz for an Indigenous Gyrotron System
FIP/P3-52	Y. M. Jain	India Development and Qualification of Passive Active Multijunction (PAM) Launcher for LHCD System of ADITYA-Upgrade Tokamak
FIP/P3-53	R. Gangradey	India Effect of Sorbent Selection and Geometrical Arrangement of Cryopanel on Pumping Speed of Cryopump
FIP/P3-54	L. Hao	China, P. R. Advanced Capabilities of Multifunctional Calculation Programme SuperMC3.2 for Complex Nuclear System

Continued...

Wed

Wed

P3 <i>continued...</i>			
Id Presenter		Title	
FIP/P3-56	M. R. Jana	India	Development of Technology for Fabrication of Prototype Ion Extraction Grid for Fusion Research
FIP/P3-57	S. S. Chauhan	India	Development of RF Based Capacitively-Coupled Plasma System for Deposition of Tungsten Nanolayers on Graphite
FIP/P3-58	R. Kumar	India	Real-Time Feedback Control System for Plasma Position Stabilization in ADITYA-U Tokamak
FIP/P3-62	A. Patel	India	Design and Simulation Studies of Calorimetric Dummy Load for Gyrotron System
FIP/P3-63	S. P. Gerhardt	USA	Overview of the NSTX-U Recovery Project Physics and Engineering Design
FIP/P3-64	K. A. Jadeja	India	Novel Approach of Pulsed-Glow Discharge Wall Conditioning in ADITYA Upgrade Tokamak
FIP/P3-65	C. Walters	UK	New Fusion Facilities at UKAEA: FTF and H3AT
FIP/P3-66	J. Yagi	Japan	A Concept of Self-Cooled Breeding Blanket with Advanced Molten Salt FLiNaK for High-Efficiency and Long-Life Operation

EX/3

Plasma Performance & Control

Chair: Evgenii Gusakov (Russian Fed.)

Main Hall

(14:00 – 16:10)

Time Id	Presenter		Title
14:00 EX/3-1	X. Z. Gong	China, P. R.	Integrated Operation of Steady-State Long Pulse H-Mode in EAST
14:20 EX/3-2	N. Vianello	Italy	Developing Steady State ELM-Absent H-Mode Scenarios with Advanced Divertor Configuration in EAST Tokamak
14:40 EX/3-3	F. Turco	USA	Integration of the High-N Hybrid Scenario to a High Performance Pedestal, Stable Zero Torque Operation and a Divertor Solution
15:00 EX/3-4	C. Giroud	UK	Optimization of JET-DT and ITER Operation by Developing an Understanding of the Role of Low-Z Impurity on the H-Mode Pedestal
15:20 EX/3-5	G. Fuchert	Germany	Increasing the Density in W7-X: Benefits and Limitations
15:40 EX/3-6	L. Garzotti	UK	Scenario Development for DT Operation at JET

EX/4 and TH/2

H-Mode & Pedestal

Chair: Saskia Mordijck (USA)

Main Hall

(16:40 – 18:45)

Time Id	Presenter		Title
16:40 TH/2-1	S.-H. Ku	USA	A Gyrokinetic Discovery of Fast L-H Bifurcation Physics in a Realistic, Diverted, Tokamak Edge Geometry
17:00 EX/4-1	J. C. Hillesheim	UK	Implications of JET-ILW L-H Transition Studies for ITER
17:20 EX/4-2	L. Schmitz	USA	L-H Transition Trigger Physics in ITER-Similar Plasmas with and without Applied $n = 3$ Magnetic Perturbations
17:40 TH/2-2	M. T. Kotschenreuther	USA	Gyrokinetic Analysis and Simulations of Pedestals
18:00 EX/4-3	J. T. McClenaghan	USA	Transport Barriers in DIII-D High- β_p Plasmas and Development of Candidate Steady State Scenarios for ITER
18:20 EX/4-4	T. Tala	Finland	Core Density Peaking Experiments in JET, DIII-D and C-Mod in Various Operational Scenarios Driven by Fuelling or Transport

P4

Posters 4

Main Hall

(14:00 – 18:45)

Wed

Id	Presenter		Title
EX/2-1	E. de la Luna	Spain	Impact of ELM Control in JET Experiments on H-Mode Terminations with/without Current Ramp-Down and Implications for ITER
EX/2-2	D. R. Ernst	USA	Viability of Wide Pedestal QH-Mode for Burning Plasma Operation
EX/2-3	T. Happel	Germany	Advances in the Understanding of the I-Mode Confinement Regime: Access, Stationarity, Edge/SOL Transport and Divertor Impact
EX/2-4	P. B. Snyder	USA	High Fusion Performance in Super H-Mode Experiments on Alcator C-Mod and DIII-D
EX/2-5	B. Labit	Switzerland	Plasma Shape and Fuelling Dependence on the Small ELM Regime in TCV and AUG
IFE/1-1	Y. Arikawa	Japan	Two-Colour Mixed Petawatt Laser Designed for Fast Ignition Experiment
IFE/1-2	S. Fujioka	Japan	Production of keV-Temperature Plasma Core with Magnetized Fast Isochoric Heating
IFE/1-3	R. J. Leeper	USA	Liquid DT Layer Approach to Inertial Confinement Fusion
IFE/1-4	J. M. Perlado	Spain	Thermo-Mechanical and Atomistic Assessment of First Wall and Optics in Nonprotective Chamber in Inertial Fusion Energy
IFE/1-5	A. Iwamoto	Japan	Demonstrations of Foam Shell and Infrared Heating Methods for FIREX Targets
EX/P4-1	A. Sinha	India	Broadband Characterization of High Temperature Blackbody Source with Fourier Transform Michelson Interferometer for ECE Measurements
EX/P4-2	U. C. Nagora	India	Design and Development of 140 GHz D-Band Phase-Locked Heterodyne Interferometer System for Real-Time Density Measurement
EX/P4-3	S. Patel	India	Study of Iron Impurity Behaviour Using VUV Spectroscopy in ADITYA and ADITYA-U Tokamak
EX/P4-4	S. Banerjee	India	Runaway Electron (RE) Mitigation Using Supersonic Molecular Beam Injection in the ADITYA-U Tokamak

Continued...

P4 continued...

Id	Presenter		Title
EX/P4-5	M. B. Chowdhuri	India	Neon Gas Seeded Radiative Improved Mode in ADITYA-U Tokamak
EX/P4-6	R. Manchanda	India	Impurity Screening in High Density ADITYA Tokamak Plasmas
EX/P4-7	K. Tahiliani	India	Radiation Power Loss Study During Gas Puff Induced Disruptions in ADITYA-U Tokamak
EX/P4-9	K. Shah	India	Observations of Intrinsic Toroidal Rotation Using X-Ray Crystal Spectrometer in ADITYA-U Tokamak
EX/P4-10	G. Shukla	India	Controlling Plasma Rotation Using Periodic Gas-Puff in ADITYA-U Tokamak
EX/P4-11	L. T. Lachhvani	India	Effect of Externally Applied Radial Electric Field (Biased-Electrode) on Geodesic Acoustic Modes in SINP Tokamak
EX/P4-12	S. Akkireddy	India	Application of TEM to Study the Changes in Subsurface Defects in Tungsten Samples as a Function of Annealing Temperature
EX/P4-13	N. Yadav	India	Effect of Multiple Periodic Gas Puff on Neutral Temperature in ADITYA-U Tokamak
EX/P4-14	P. Pandit	India	Design of a NIR Spectrometer for ADITYA-U Tokamak and Initial Results
EX/P4-15	S. Mishra	India	Mass Dependent Impurity Transport Study in ADITYA Tokamak
EX/P4-16	A. Kanik	India	Plasma Potential Measurements in the Edge Region of ADITYA-U Tokamak Using Reciprocating Laser Heated Emissive Probes
EX/P4-17	T. Macwan	India	Edge Current Density Profile Measurement Using an Array of Miniature Magnetic Probes in ADITYA-U Tokamak
EX/P4-18	J. V. Raval	India	Development of Multipurpose Soft X-Ray Tomography System for ADITYA-U
EX/P4-19	J. J. U. Buch	India	Ka-Band Reflectometer System for Measuring Radial Electron Density Profile at IPR
EX/P4-20	J. K. Joshi	India	Experimental Investigation of Power Coupling by RF Antenna into Plasmas in Presence of Magnetized Ions

Continued...

P4 *continued...*

Id	Presenter		Title
EX/P4-21	S. N. Pandya	India	A Diagnostic Approach for the Detection of Spatially Distributed Low Energy Confined Runaway Electrons in the ADITYA-U Tokamak by Means of Synchrotron Emission Imaging in the Sub-Millimetre Wavelength Band
EX/P4-22	J. Kumar	India	Design and Testing of X-Mode Reflectometry System for Coupling Studies of Lower Hybrid Waves in ADITYA-U Tokamak
EX/P4-23	S. Aggarwal	India	Design and Development of Passive Charge Exchange Neutral Particle Analyser for ADITYA-U Tokamak
EX/P4-24	L. M. Awasthi	India	Excitation of Electron Temperature Gradient (ETG) Turbulence and Effect on Plasma Transport in LVPD
EX/P4-25	K. Ajay	India	ADITYA Experimental Results of Core Ion Temperature Measurements on ADITYA Tokamak Using Four Channel Neutral Particle Analyser
EX/P4-26	P. K. Srivastava	India	Chord Average Density Measurement Using Microwave Interferometry in LVPD
EX/P4-27	A. K. Sanyasi	India	Investigations on Growth of Quasi-Longitudinal (QL) Whistlers with Energy Scaling of Energetic Electrons in LVPD
EX/P4-28	K. K. Mishra	India	Fast Wave Induced ICRF Plasma Expansion in ADITYA Torus
EX/P4-29	N. Patel	India	Gas Fuelling Control System of ADITYA Tokamak
EX/P4-30	R. Rajpal	India	Integrated System Electronics and Instrumentation; Operation and Diagnostic for ADITYA-U Tokamak
EX/P4-31	S. Aich	India	Plasma Column Position Measurements Using Magnetic Diagnostics in ADITYA-U Tokamak
IFE/P4-1	G. M. Elaragi	Egypt	Experimental Discharge Characterization of IEC Plasma Device
IFE/P4-4	H. Hora	Australia	H- ¹¹ B Fusion Reactor with Extreme Laser Pulses for Non-LTE Ignition
IFE/P4-6	Y. Mori	Japan	Development of Shell Injection System for the Future IFE Power Plant

Continued...

P4 *continued...*

Id	Presenter	Title
IFE/P4-7	B. V. Kuteev	Russian Fed. Mechanical Mockup of IFE Reactor Intended for the Development of Cryogenic Targets Mass Production and Rep-Rate Delivery into the Reaction Chamber
IFE/P4-8	N. Iwata	Japan Electron Acceleration in Dense Plasmas Heated by Picosecond Relativistic Laser
IFE/P4-9	H. Nagatomo	Japan Target Design Study of Fast Ignition for Ignition and Burning Experiments
IFE/P4-10	T. Watari	Japan Progress of a DPSSL Based R&D Facility TERU for IFE Technology and Industrial Applications
IFE/P4-13	K. F. Al-Shboul	Jordan Interpenetration and Stagnation in Collapsing Plasmas
TH/P4-1	A. K. Singh	India Analysis of Electron Cyclotron Wave Assisted Plasma Start-Up in SST-1
TH/P4-2	T. Y. Xia	China, P. R. Simulations on the Particle and Heat Fluxes for the RF Heating H-Mode on EAST
TH/P4-5	T. Kurki-Suonio	Finland Beam Ion Performance and Power Loads in the ITER Prefusion Power Operating Scenarios (PFPO) with Reduced Field and Current
TH/P4-6	P. Aleynikov	Germany ECRH and Mode Conversion in Overdense W7-X Plasmas
TH/P4-7	A. Kuley	India Global PIC Simulation of RF Waves in Toroidal Geometry
TH/P4-8	J. K. Atul	India Mode Converted Electrostatic Nonlinear Ion-Ion Hybrid Mode in Tokamak Plasma
TH/P4-9	S. Usami	Japan Particle Simulation Studies on Ion Effective Heating through Merging Plasmas
TH/P4-10	E. Z. Gusakov	Russian Fed. Anomalous Absorption and Emission in ECRH Experiments due to Parametric Excitation of Localized UH Waves
TH/P4-11	P. V. Minashin	Russian Fed. Modelling of Electron Cyclotron Resonance Heating and Current Drive in the T-15-MD Tokamak with GENRAY and CQL3D Codes
TH/P4-12	A. K. Ram	USA Theoretical and Computational Studies on the Scattering of Radiofrequency Waves by Fluctuations
TH/P4-13	N. Bertelli	USA The Impact of the Hydrogen Species on the HHFW Performance with Possible New NSTX-U Scenarios

EX/5, PPC/1, TH/3

Chair: Baonian Wan (P. R. China)

Integrated Modelling & Transport

Main Hall

(08:30 – 10:15)

Time Id	Presenter		Title
08:30 TH/3-1	J. Garcia	France	First Principles and Integrated Modelling Achievements Towards Trustful Fusion Power Predictions for JET and ITER
08:50 EX/5-1	K. Nagaoka	Japan	Transport Characteristics of Deuterium and Hydrogen Plasmas with Ion Internal Transport Barrier in LHD
09:10 TH/3-2	F. J. Casson	UK	Predictive Multichannel Flux-Driven Modelling to Optimize ICRH Tungsten Control in JET
09:30 PPC/1-1	N. Hayashi	Japan	Predictive Integrated Modelling of Plasmas and their Operation Scenarios towards Exploitation of JT-60SA Experiment
09:50 EX/5-2	C. Chrystal	USA	Predicting the Toroidal Rotation Profile for ITER

EX/6 and TH/4

Chair: Yeong-Kook Oh (Korea, Rep. of)

Runaways & Disruption Mitigation

Main Hall

(10:45 – 12:30)

Time Id	Presenter		Title
10:45 EX/6-1	C. Paz-Soldan	USA	Advances in Runaway Electron Control and Model Validation for ITER
11:05 TH/4-1	J. R. Martín Solís	Spain	Runaway Electron Mitigation in ITER Disruptions by Injection of High- <i>Z</i> Impurities
11:25 TH/4-2	A. Matsuyama	Japan	Self-Consistent Runaway Beam Formation in 3D Magnetic Fields During Radiation-Driven Disruptions
11:45 TH/4-3	L. Carbajal	USA	Pitch Angle Dynamics and Synchrotron Emission of Runaway Electrons in Quiescent and Disrupted DIII-D Plasmas
12:05 TH/4-4	H. Strauss	USA	Asymmetric Wall Force Reduction in ITER and JET Disruptions

P5

Posters 5

Main Hall

(08:30 – 12:30)

Id	Presenter		Title
EX/3-1	X. Gong	China, P. R.	Integrated Operation of Steady-State Long Pulse H-Mode in EAST
EX/3-2	G. Calabrò	Italy	Developing Steady State ELM-Absent H-Mode Scenarios with Advanced Divertor Configuration in EAST Tokamak
EX/3-3	F. Turco	USA	Integration of the High-N Hybrid Scenario to a High Performance Pedestal, Stable Zero Torque Operation and a Divertor Solution
EX/3-4	C. Giroud	UK	Optimization of JET-DT and ITER Operation by Developing an Understanding of the Role of Low-Z Impurity on the H-Mode Pedestal
EX/3-5	G. Fuchert	Germany	Increasing the Density in W7-X: Benefits and Limitations
EX/3-6	L. Garzotti	UK	Scenario Development for DT Operation at JET
EX/4-1	J. C. Hillesheim	UK	Implications of JET-ILW L-H Transition Studies for ITER
EX/4-2	L. Schmitz	USA	L-H Transition Trigger Physics in ITER-Similar Plasmas with and without Applied $n = 3$ Magnetic Perturbations
EX/4-3	J. T. McClenaghan	USA	Transport Barriers in DIII-D High- β_p Plasmas and Development of Candidate Steady State Scenarios for ITER
EX/4-4	T. Tala	Finland	Core Density Peaking Experiments in JET, DIII-D and C-Mod in Various Operational Scenarios Driven by Fuelling or Transport
TH/2-1	S.-H. Ku	USA	A Gyrokinetic Discovery of Fast L-H Bifurcation Physics in a Realistic, Diverted, Tokamak Edge Geometry
TH/2-2	M. T. Kotschenreuther	USA	Gyrokinetic Analysis and Simulations of Pedestals
EX/P5-2	G. S. Kurskiev	Russian Fed.	Thermal Energy Confinement at the Globus-M Spherical Tokamak
EX/P5-3	W. Z. Zhong	China, P. R.	Plasma Confinement and Pedestal Dynamics Responses to Impurity Seeding in HL-2A H-Mode Plasmas
EX/P5-4	M. Jiang	China, P. R.	Localized Modulation of Turbulence by Magnetic Islands on HL-2A Tokamak
EX/P5-6	J. Cheng	China, P. R.	Pedestal Dynamics in Inter-ELM Phase on HL-2A Tokamak

Continued...

P5 *continued...*

Id	Presenter	Title	
EX/P5-8	Y. P. Zhang	China, P. R.	Effect of LBO-Seeded Impurity on ELMs in the HL-2A Tokamak
EX/P5-9	W. Mao	China, P. R.	Characteristics of Electromagnetic Turbulence on KTX Experiment Device
EX/P5-10	A. V. Melnikov	Russian Fed.	Electric Potential and Turbulence in OH and ECRH Low-Density Plasmas
EX/P5-13	L. N. Khimchenko	Russian Fed.	Ecton Mechanism of Energy Load on ITER-Grade Tungsten Limiter T-10 Tokamak and Forecast for ITER
EX/P5-15	X. Q. Ji	China, P. R.	Nonlinear Evolution of Multihelicity Neoclassical Tearing Modes in HL-2A Low Rotation Plasmas
EX/P5-16	D. V. Ryzhakov	Russian Fed.	Peculiar Properties of Disruptions on T-10 Tokamak at Different Edge Safety Factor Values
EX/P5-19	P. W. Shi	China, P. R.	Energetic-Ion Driven Toroidal and Global Alfvén Eigenmodes on HL-2A
EX/P5-20	W. Chen	China, P. R.	Suppression and Destabilization of Ion Fishbone Activities on HL-2A
EX/P5-21	M. R. Nurgaliev	Russian Fed.	Influence of Electron Cyclotron Resonance Heating on Ion Heat Conductivity in T-10 Plasma
EX/P5-23	Y. Xu	China, P. R.	Physics and Engineering Design for Chinese First Quasi-Axisymmetric Stellarator(CFQS)
EX/P5-25	V. V. Prikhodko	Russian Fed.	Stability and Confinement Studies in the Gas Dynamic Trap
EX/P5-26	A. V. Burdakov	Russian Fed.	Plasma Transport in Linear and Helical Multiple-Mirror Systems
EX/P5-27	L. W. Yan	China, P. R.	Real-Time Control System of Neoclassical Tearing Modes in the HL-2A Tokamak
EX/P5-28	Y. Liu	China, P. R.	Development of the $q = 1$ Advanced Tokamak Scenarios in HL-2A
EX/P5-30	X. M. Song	China, P. R.	First Plasma Scenario Development for HL-2M
TH/P5-1	C. A. Bowie	Australia	Sandpile Modelling of Pellet Pacing in Fusion Plasmas
TH/P5-3	R. Mukherjee	India	Numerical Relaxation of a 3D MHD Taylor–Woltjer State Subject to Abrupt Expansion
TH/P5-4	D. Sharma	India	ADITYA Up-Gradation Equilibrium Study
TH/P5-5	T. Moritaka	Japan	Gyrokinetic Modelling with an Extended Magnetic Equilibrium Including the Edge Region of Large Helical Device

Continued...

P5 *continued...*

Id	Presenter		Title
TH/P5-6	J. Kim	Korea, Rep. of	Effects of Magnetic Perturbations on Magnetic Field Stochasticity During Edge Pedestal Collapse
TH/P5-7	Z. Lin	USA	Roles of RMP-Induced Changes of Radial Electric Fields in ELM Suppression
TH/P5-8	L. E. Sugiyama	USA	Endogenous Magnetic Reconnection and Associated Processes of Relevance to Fusion Burning Plasmas
TH/P5-9	R. Hager	USA	Gyrokinetic-MHD Coupled Simulation of RMP Plasma Interaction Reproduces Density Pump-Out Seen in the Tokamak Edge
TH/P5-10	F. M. Poli	USA	Effects of Microtearing Modes on the Evolution of Electron Temperature Profiles in High Collisionality NSTX Discharges
TH/P5-11	Y. Patil	India	Electromagnetic Analysis of APPEL Linear Device Magnets
TH/P5-12	M. J. Hole	Australia	The Effect of Pressure Anisotropy on Ballooning Modes in Tokamak Plasmas
TH/P5-13	G. Z. Hao	China, P. R.	Centrifugal Force Driven Low Frequency Modes in Spherical Tokamak
TH/P5-18	F. Liu	France	Nonlinear MHD Simulations of Quiescent H-Mode in ASDEX-Upgrade and ITER
TH/P5-19	S. Günter	Germany	NTM Excitation by Sawtooth Crashes and the Suppression of Their Onset by Resonant Magnetic Perturbation
TH/P5-21	D. Chandra	India	Simulation of the Internal Kink Mode in Visco-Resistive Regimes
TH/P5-22	P. Zanca	Italy	A Power-Balance Model of Density Limit in Fusion Plasmas
TH/P5-23	L. Pigatto	Italy	Resistive Wall Mode Physics and Control Challenges in JT-60SA High- β_N Scenarios
TH/P5-24	S. Inoue	Japan	Nonlinear Dynamics of Tearing Mode Driven by Static and Rotating External 3D Fields
TH/P5-25	M. Sato	Japan	Ion Kinetic Effects on MHD Instabilities in High- β LHD Plasmas
TH/P5-26	G. Y. Park	Korea, Rep. of	Comparative Simulations of the Plasma Response to RMPs During ELM-Crash Mitigated and Suppressed Phases in KSTAR
TH/P5-27	R. Coelho	Portugal	Plasma Equilibrium Reconstruction of JET Discharges Using the IMAS Modelling Infrastructure

Continued...

Thu

Thu

P5 <i>continued...</i>			
Id		Presenter	Title
TH/P5-28	D. López-Bruna	Spain	Nonlinearly Saturated Ideal Magnetohydrodynamic Equilibrium States with Periodicity-Breaking in Stellarators
TH/P5-30	Y. Liu	USA	Role of NTV Particle Flux in Density Pumpout during ELM Control by RMP
TH/P5-31	L. J. Zheng	USA	Negative Triangularity Effects on Tokamak MHD Stability
TH/P5-32	A. Reiman	USA	Equilibrium Pressure-Driven Current in the Presence of a Small Magnetic Island: Singular Behaviour and Symmetry Effects
TH/P5-33	C. Ribeiro	Brazil	Advances on the High Field Ultralow Aspect Ratio Tokamak

FIP/2, MPT/1, SEE/1		In Vessel Components & Plasma Interface	
Chair: Yogesh Saxena (India)		Main Hall	(14:00 – 16:10)
Time Id	Presenter	Title	
14:00 SEE/1-1	C. Grisolia	France	Tritiated Dust: The Impact on Tokamak Operation
14:20 FIP/2-1	J. Chen	China, P. R.	Progress in Developing ITER and DEMO First Wall Technologies at SWIP
14:40 FIP/2-2	T. R. Barrett	UK	Technologies for Plasma-Facing Wall Protection in EU DEMO
15:00 FIP/2-3	R. Lunsford	USA	Active Conditioning of ASDEX-Upgrade Tungsten PFCs through Boron Particulate Injection
15:20 FIP/2-4	D. Iglesias	UK	Advances in Predictive Thermo-Mechanical Modelling for the JET Divertor Experimental Interpretation, Improved Protection, and Reliable Operation
15:40 MPT/1-1	A. Kreter	Germany	Influence of Plasma Impurities on the Fuel Retention in Tungsten

FIP/3

DEMO & Advance Technology

Chair: Guang-Nan Luo (P. R. China)

Main Hall

(16:40 – 18:45)

Time Id	Presenter		Title
16:40 FIP/3-1	G. Federici	Germany	Overview of the DEMO Design-Staged Approach in Europe
17:00 FIP/3-2	Y. Sakamoto	Japan	Development of Physics and Engineering Designs for Japan's DEMO Concept
17:20 FIP/3-3	G. M. Wallace	USA	Novel Radiofrequency Current Drive Systems for Fusion Plasma Sustainment on DIII-D
17:40 FIP/3-4	M. Kikuchi	Japan	Impact of High Field & High Confinement on L-Mode-Edge Negative Triangularity Tokamak (NTT) Reactor
18:00 FIP/3-5Ra	R. Maingi	USA	Amelioration of Plasma-Material Interactions and Improvement of Plasma Performance with a Flowing Liquid Li Limiter and Li Conditioning on EAST
FIP/3-5Rb			Experiments on FTU with a Liquid Tin Limiter
18:20 FIP/3-6	R. J. Goldston	USA	Development of a Lithium Vapour Box Divertor for Controlled Plasma Detachment

P6

Posters 6

Main Hall

(14:00 – 18:45)

Id	Presenter		Title
EX/5-1	K. Nagaoka	Japan	Transport Characteristics of Deuterium and Hydrogen Plasmas with Ion Internal Transport Barrier in LHD
EX/5-2	C. Chrystal	USA	Predicting the Toroidal Rotation Profile for ITER
EX/6-1	C. Paz-Soldan	USA	Advances in Runaway Electron Control and Model Validation for ITER
PPC/1-1	N. Hayashi	Japan	Predictive Integrated Modelling of Plasmas and their Operation Scenarios towards Exploitation of JT-60SA Experiment
TH/3-1	J. Garcia	France	First Principles and Integrated Modelling Achievements Towards Trustful Fusion Power Predictions for JET and ITER
TH/3-2	F. J. Casson	UK	Predictive Multichannel Flux-Driven Modelling to Optimize ICRH Tungsten Control in JET

Continued...

P6 *continued...*

Id	Presenter		Title
TH/4-1	J. R. Martín Solís	Spain	Runaway Electron Mitigation in ITER Disruptions by Injection of High-Z Impurities
TH/4-2	A. Matsuyama	Japan	Self-Consistent Runaway Beam Formation in 3D Magnetic Fields During Radiation-Driven Disruptions
TH/4-3	L. Carbajal	USA	Pitch Angle Dynamics and Synchrotron Emission of Runaway Electrons in Quiescent and Disrupted DIII-D Plasmas
TH/4-4	H. Strauss	USA	Asymmetric Wall Force Reduction in ITER and JET Disruptions
EX/P6-1	J. S. deGrassie	USA	DIII-D Shaping Demonstrates Correlation of Intrinsic Momentum with Energy
EX/P6-2	A. Diallo	USA	ELMs Onset Triggered by Mode Coupling Near Rational Surfaces in the Pedestal
EX/P6-3	B. A. Grierson	USA	Rotation Profile Hollowing in DIII-D Low-Torque Electron-Heated H-Mode Plasmas
EX/P6-4	F. M. Laggner	USA	The Universality of Inter-ELM Pedestal Fluctuations in AUG and DIII-D: Impacting the Edge Profile Structure by Clamping of the Gradients
EX/P6-5	S. Mordijck	USA	Particle Transport from the Bottom Up
EX/P6-6	M. E. Austin	USA	High Confinement in Negative Triangularity Discharges in DIII-D
EX/P6-8	L. F. Delgado-Aparicio	USA	Rotation-Induced Electrostatic-Potentials and Density Asymmetries in NSTX
EX/P6-9	M. V. Umansky	USA	Extending the Boundary Heat Flux Width Database to 1.3 Tesla Poloidal Magnetic Field in the Alcator C-Mod Tokamak
EX/P6-10	H. Y. Guo	USA	Development and First Experimental Tests of a Small Angle Slot Divertor on DIII-D
EX/P6-11	T. W. Petrie	USA	High Performance Double-Null Plasmas Under Radiating Divertor and Mantle Scenarios on DIII-D
EX/P6-12	A. W. Leonard	USA	Parallel Energy Transport in Detached DIII-D Divertor Plasmas
EX/P6-13	T. Abrams	USA	Inter vs. Intra-ELM Tungsten Erosion and Transport from the Divertor in DIII-D
EX/P6-14	M. E. Fenstermacher	USA	High-Performance H-Mode Discharges The Effect of RMP ELM Control for ITER on Pedestal Pressure Compared to EPED No-RMP Predictions

Continued...

P6 continued...

Id	Presenter		Title
EX/P6-15	A. G. McLean	USA	Quantification of Radiating Species in the DIII-D Divertor in the Transition to Detachment Using Extreme Ultraviolet Spectroscopy
EX/P6-16	E. A. Unterberg	USA	Measurements of High-Z Divertor Impurity Sourcing and Divertor Leakage Using Isotopic Tungsten Tracer Sources in DIII-D
EX/P6-17	D. M. Orlov	USA	Favourable Impact of RMP ELM Suppression on Divertor Heat Fluxes at ITER-like Conditions
EX/P6-18	E. T. Hinson	USA	Enhancement of Helium Exhaust During Suppression of Edge Localized Modes by Resonant Magnetic Perturbation Fields at DIII-D
EX/P6-19	T. M. Wilks	USA	Access Requirements for Stationary ELM-Suppressed Pedestals in DIII-D and C-Mod Plasmas
EX/P6-20	R. S. Granetz	USA	Machine Learning for Disruption Warning on Alcator C-Mod, DIII-D, and EAST Tokamaks
EX/P6-21	J. L. Barr	USA	Fast ITER-Relevant Low-Disruptivity Ramp-Downs in DIII-D and EAST
EX/P6-22	N. W. Eidietis	USA	Implementing a Finite-State Off-Normal and Fault Response System for Robust Disruption Avoidance in Tokamaks
EX/P6-23	J. Herfindal	USA	Injection of Multiple Shattered Pellets for Disruption Mitigation in DIII-D
EX/P6-24	M. W. Shafer	USA	Observation of Multiple Helicity Mode-Resonant Locking Leading to a Disruption on DIII-D
EX/P6-25	M. Okabayashi	USA	Critical Processes of Tearing Mode Entrainment in the Presence of a Static Error Field
EX/P6-26	S. A. Sabbagh	USA	Disruption Event Characterization and Forecasting in Tokamaks
EX/P6-28	S. G. Baek	USA	Observation of Efficient Lower Hybrid Current Drive at High Density on Alcator C-Mod
EX/P6-29	K. E. Thome	USA	High-Frequency Energetic Particle Driven Instabilities and their Implications for Burning Plasmas
EX/P6-30	B. Van Compernelle	USA	Fast Wave Experiments in LAPD in Support of Fusion

Continued...

P6 *continued...*

Id	Presenter		Title
EX/P6-32	M. Podestà	USA	Global Alfvén Eigenmode Stability Dependence on Fast-Ion Distribution Function
EX/P6-33	D. Kim	USA	Investigation of Fast Particle Redistribution Induced by Sawtooth Instability in NSTX-U
EX/P6-34	M. W. Bongard	USA	Advancing Local Helicity Injection for Nonsolenoidal Tokamak Startup
EX/P6-36	C. B. Forest	USA	Development of a High-Flux Fusion Neutron Source Using Recent Advances in Technology
EX/P6-37	Z. Lin	USA	First Simulations of Turbulent Transport in the Field-Reversed Configuration
EX/P6-38	B. A. Grierson	USA	Dynamic Neutral Beam Injection as a Mechanism for Plasma Control and an Actuator for Instability Drive
EX/P6-39	E. Schuster	USA	Physics-Model-Based Real-Time Optimization for the Development of Steady-State Scenarios at DIII-D
EX/P6-40	N. M. Ferraro	USA	Error Field Impact on Mode Locking and Divertor Heat Flux in NSTX-U
TH/P6-1	G. Q. Li	China, P. R.	Transport Simulation of EAST Long Pulse Discharge and High- β_N Discharge with Integrated Modelling
TH/P6-4	L. Wang	China, P. R.	Theory of Turbulence Driven Intrinsic Rotation and Current
TH/P6-5	T. Görler	Germany	En Route to High-Performance Discharges: Insights and Guidance from High-Realism Gyrokinetics
TH/P6-6	A. Bhattacharya	India	Application of the Semi-Implicit Numerical Method on the Radial Impurity Transport Equation and Determination of O^{4+} Emissivity with Two Separate PEC Databases
TH/P6-7	S. D. Pinches	ITER	Progress in the ITER Integrated Modelling Programme and the ITER Scenario Database
TH/P6-8	M. Nunami	Japan	Kinetic Simulation Studies on Multi-Ion-Species Plasma Transport in Helical Systems
TH/P6-9	E. Narita	Japan	Gyrokinetic Modelling of Turbulent Particle Fluxes towards Efficient Predictions of Density Profiles

Continued...

P6 *continued...*

Id	Presenter		Title
TH/P6-10	L. Qi	Korea, Rep. of	Nonlinear Gyrokinetic Analysis of Linear Ohmic Confinement to Saturated Ohmic Confinement Transition
TH/P6-12	D. López-Bruna	Spain	Flux-Surface Averaged Radial Transport in Toroidal Plasmas with Magnetic Islands
TH/P6-13	S. Buller	Sweden	Transport of Collisional Impurities with Flux-Surface Density Variation in Stellarator Plasmas
TH/P6-14	P. Strand	Sweden	Towards a Predictive Modelling Capacity for DT Plasmas: European Transport Simulator (ETS) Verification and Validation
TH/P6-15	B. Chatthong	Thailand	Ion and Electron Temperature Predictions Based on Thailand Tokamak Plasmas Using CRONOS Code
TH/P6-16	O. Meneghini	USA	Neural-Network Accelerated Coupled Core-Pedestal Simulations with Self-Consistent Transport of Impurities
TH/P6-17	W. X. Wang	USA	Self-Driven Current Generation in Turbulent Fusion Plasmas
TH/P6-19	P. W. Terry	USA	Scalings of Ion Temperature Gradient Turbulence and Transport
TH/P6-20	C.-S. Chang	USA	Total- f Gyrokinetic Turbulent-Neoclassical Simulation of Global Impurity Transport and its Effect on the Main-Plasma Confinement
TH/P6-21	M. D. J. Cole	USA	Confinement in Stellarators with the Global Gyrokinetic Code XGC
TH/P6-22	Z. H. Wang	China, P. R.	Physics of Fast Component of Deuterium Gas Jet Injection in Magnetized Plasmas
TH/P6-23	N. K. Bisai	India	Dynamics of Neon Ions after Neon Gas Seeding and Puffing into Tokamak Plasma
TH/P6-24	G. Telesca	Poland	Numerical Simulation of High Neutron Rate JET-ILW DD Pulses in View of Extension to DT Experiments
TH/P6-25	S. Sangaroon	Thailand	Parametric Study of the Impurity Profile in the Thailand Tokamak
TH/P6-26	S. Nowak	Italy	Analysis and Modelling of NTMs Dynamics in JET Discharges Using the European Transport Simulator (ETS) and Integrated Modelling Tools

Continued...

Thu

P6 *continued...*

Thu

Id		Presenter	Title	
TH/P6-28	D. Mandal	India	Study of Evolution of Trapped Particle Undamped Coherent Structures: An Important Agent in Intermittent Plasma Turbulence and Anomalous Transport	
TH/P6-29	H. Yamaguchi	Japan	Simulation Study of Electrostatic Potential Generated by NBI and its Effect on the Neoclassical Transport of Carbon Impurity Ions in LHD	
TH/P6-30	J. J. Martinell	Mexico	Weak Turbulence Transport with Background Flows Using Mapping Techniques Including Finite Larmor Radius Effects	

EX/7 and TH/5**Active ELM Control**

Chair: Annika Ekedahl (France)

*Main Hall***(08:30 – 10:15)**

Time Id	Presenter		Title
08:30 EX/7-1	Y. In	Korea, Rep. of	Test of the ITER-Like RMP Configurations for ELM-Crash-Suppression on KSTAR
08:50 EX/7-2	Y. Sun	China, P. R.	Dynamic ELM and Divertor Control Using Mixed Toroidal Harmonic Resonant Magnetic Perturbations in DIII-D and EAST
09:10 EX/7-3	W. Suttrop	Germany	Experimental Conditions for Suppressing Edge Localized Modes by Magnetic Perturbations in ASDEX-Upgrade
09:30 EX/7-4	G. L. Xiao	China, P. R.	ELM Control Physics with Impurity Seeding and LHCD in the HL-2A Tokamak
09:50 TH/5-1	D. Chandra	India	A Nonlinear 2-Fluid Study of the Effect of Pellet Injection on ELM Dynamics

MPT/2, FNS/1, SEE/2**Materials, FNS, Environmental**

Chair: Viacheslav Chernov (Russian Fed.)

*Main Hall***(10:45 – 12:30)**

Time Id	Presenter		Title
10:45 MPT/2-1	T. Nagasaka	Japan	High-Temperature Creep Properties of NIFS-HEAT-2 High-Purity Low-Activation Vanadium Alloy
11:05 MPT/2-2	R. Ding	China, P. R.	Model Validation on EAST and DIII-D Experiments towards Understanding of High-Z Material Erosion and Migration in a Mixed Materials Environment
11:25 MPT/2-3	P. N. Maya	India	Evaluation of Tungsten as Divertor Plasma-Facing Material: Results from Ion Irradiation Experiments and Computer Simulations
11:45 MPT/2-4	A. Ibarra	Spain	The European Approach to the Fusion-Like Neutron Source: The IFMIF-DONES Project
12:05 SEE/2-1	M. R. Gilbert	UK	Waste Implications from Minor Impurities in European DEMO Materials

P7		Posters 7	
		Main Hall	(08:30 – 12:30)
Id	Presenter	Title	
FIP/2-1	J. Chen	China, P. R.	Progress in Developing ITER and DEMO First Wall Technologies at SWIP
FIP/2-2	T. R. Barrett	UK	Technologies for Plasma-Facing Wall Protection in EU DEMO
FIP/2-3	R. Lunsford	USA	Active Conditioning of ASDEX-Upgrade Tungsten PFCs through Boron Particulate Injection
FIP/2-4	D. Iglesias	UK	Advances in Predictive Thermo-Mechanical Modelling for the JET Divertor Experimental Interpretation, Improved Protection, and Reliable Operation
FIP/3-1	G. Federici	Germany	Overview of the DEMO Design-Staged Approach in Europe
FIP/3-2	Y. Sakamoto	Japan	Development of Physics and Engineering Designs for Japan's DEMO Concept
FIP/P8-9	G. M. Wallace	USA	Novel Radiofrequency Current Drive Systems for Fusion Plasma Sustainment on DIII-D
FIP/3-4	M. Kikuchi	Japan	Impact of High Field & High Confinement on L-Mode-Edge Negative Triangularity Tokamak (NTT) Reactor
FIP/3-5Ra	R. Maingi	USA	Amelioration of Plasma-Material Interactions and Improvement of Plasma Performance with a Flowing Liquid Li Limiter and Li Conditioning on EAST
FIP/3-5Rb	G. Mazzitelli	Italy	Experiments on FTU with a Liquid Tin Limiter
FIP/3-6	R. J. Goldston	USA	Development of a Lithium Vapour Box Divertor for Controlled Plasma Detachment
MPT/1-1	A. Kreter	Germany	Influence of Plasma Impurities on the Fuel Retention in Tungsten
MPT/2-1	T. Nagasaka	Japan	High-Temperature Creep Properties of NIFS-HEAT-2 High-Purity Low-Activation Vanadium Alloy
MPT/2-2	R. Ding	China, P. R.	Model Validation on EAST and DIII-D Experiments towards Understanding of High-Z Material Erosion and Migration in a Mixed Materials Environment

Continued...

P7 *continued...*

Id	Presenter	Title
MPT/2-3	P. N. Maya	India Evaluation of Tungsten as Divertor Plasma-Facing Material: Results from Ion Irradiation Experiments and Computer Simulations
MPT/2-4	A. Ibarra	Spain The European Approach to the Fusion-Like Neutron Source: The IFMIF-DONES Project
SEE/1-1	C. Grisolia	France Tritiated Dust: Their Impact on Tokamak Operation
SEE/2-1	M. R. Gilbert	UK Waste Implications from Minor Impurities in European DEMO Materials
SEE/3-1Ra	S. Konishi	Japan Future Possibility of Carbon Sequestration by Biomass-Fusion Hybrid Systems
SEE/3-1Rb	S. Takeda	Japan Economic Performance of Fusion Power Plant on Future Deregulated Electricity Market
SEE/3-1Rc	H. Nam	Japan Techno-Economic Analysis of Biodiesel and Hydrogen Production via Fusion-Biomass Hybrid Model
EX/P7-1	G. Verdoolaege	Belgium First Analysis of the Updated ITPA Global H-Mode Confinement Database
EX/P7-3	J. Jo	Korea, Rep. of Time Resolved Triton Burnup Measurements Using the Scintillating Fibre Detector on KSTAR
EX/P7-4	S. G. Lee	Korea, Rep. of Intrinsic Toroidal Rotation for Ohmic L-Mode Plasmas in KSTAR
EX/P7-5	S.-W. Yoon	Korea, Rep. of The Effect of Electron Cyclotron Heating on Thermal and Fast-Ions Transport in High- β -Poloidal Discharges at KSTAR
EX/P7-7	J.-S. Park	Korea, Rep. of Characteristics of Asymmetric (Low-Field-Side and High-Field Side) Divertor Detachment in KSTAR L-Mode Plasmas
EX/P7-8	J. J. Jang	Korea, Rep. of ELM Suppression and Internal Transport Barrier Formation by Krypton Seeding in KSTAR Plasmas
EX/P7-9	I. Song	Korea, Rep. of Experimental Observation and Modelling of High- Z Impurity Transport by Tungsten Powder Injection in KSTAR Plasmas
EX/P7-10	S.-H. Hong	Korea, Rep. of Observation of Heat Load on the Castellated Tungsten Block by Back-Scattered Particles from Intentionally Misaligned Protruding Edge

Continued...

P7 <i>continued...</i>			
Id		Presenter	Title
EX/P7-11	C. Xiao	Canada	Effects of Lithium Coating of Chamber Wall on the STOR-M Tokamak Discharges
EX/P7-12	M. Lehnen	ITER	R&D for Reliable Disruption Mitigation in ITER
EX/P7-13	J. Lee	Korea, Rep. of	Bifurcation of Perpendicular Rotation and Field Penetration at the Transition to RMP-Induced ELM-Crash Suppression
EX/P7-14	J. Kim	Korea, Rep. of	Evolution of Locked Mode Under the Existence of Nonaxisymmetric Fields in KSTAR
EX/P7-15	Y. M. Jeon	Korea, Rep. of	Experimental Observations of the Plasma Shape Effect on the RMP-ELM Coupling for Optimization of the KSTAR ELM-Crash Control
EX/P7-16	Y.-S. Park	USA	Stability, Transport, and Active MHD Mode Control Analysis of KSTAR High Performance Plasmas Supporting Disruption Avoidance
EX/P7-17	M. Inomoto	Japan	Effects of Reconnection Downstream Conditions on Electron Parallel Acceleration during Merging Start-Up of Spherical Tokamak
EX/P7-18	V. I. Vargas-Blanco	Costa Rica	Conversion of Electrostatic Bernstein Waves in the SCR-1 Stellarator Using a Full Wave Code
EX/P7-19	S.-H. Kim	Korea, Rep. of	Power Coupling of Lower Hybrid Fast Wave in VEST
EX/P7-20	T. Asai	Japan	Collisional Merging of a Field-Reversed Configuration in the FAT-CM Device
EX/P7-21	H. Y. Lee	Korea, Rep. of	Solenoid-Free Start-Up Utilizing Outer PF Coils with the Help of EBW Preionization and Change of External Inductance in VEST
EX/P7-22	J.-H. Yang	Korea, Rep. of	Internal Structure of MHD Fluctuations for Various Current Density Profiles during Current Rise Phase of Ohmic Discharge in VEST
EX/P7-23	A. Loarte	ITER	Advances in Modelling of Plasma Pedestal Behaviour and ELM Control in ITER Reference Plasma Scenarios
EX/P7-24	H. Anand	ITER	Implementation of 3D Effects of the ITER Plasma-Facing Components in a 2D Real-Time Model-Based Approach for Wall Heat Flux Control on ITER

Continued...

P7 *continued...*

Id	Presenter	Title
EX/P7-25	F. Köchl	UK Optimizing the ITER 15 MA DT Baseline Scenario by Exploiting a Self-Consistent Free-Boundary Core-Edge-SOL Workflow in IMAS
EX/P7-26	E. Schuster	USA Robust Burn Control in ITER Under Deuterium-Tritium Concentration Variations in the Fuelling Lines
EX/P7-27	F. M. Poli	USA The ITER Plasma Current Termination Phase: Physics Constraints on Control
FIP/P7-1	M. Siccino	Germany Development of a Plasma Scenario for the EU-DEMO: Current Activities and Perspectives
FIP/P7-2	H. Lux	Germany Implications of Uncertainties on the European DEMO Design
FIP/P7-3	S. S. Ananyev	Russian Fed. Development of DEMO-FNS Fuelling Systems and Modelling Hydrogen Isotopes Distribution via "FC-FNS" Simulation Code
FIP/P7-4	Y. Takase	Japan Development of Capacitively-Coupled Comb-Line Antennas for Current Drive in Tokamaks
FIP/P7-5	L. Zani	France Progresses at CEA on EU DEMO Reactor Cryomagnetic System Design Activities and Associated R&D
FIP/P7-6	B. K. Yadav	India Design Optimization of Helium Cooling Systems for Indian LLCB TBM
FIP/P7-7	Y. S. Shpanskiy	Russian Fed. Progress in Design of DEMO-FNS Hybrid Facility
FIP/P7-8	V. L. Tanna	India SST-1 Cryogenic Requirements and the Way Forward
FIP/P7-9	U. Prasad	India Thermal-Hydraulic Characteristics Study of Superconducting Magnets of SST-1
FIP/P7-10	G. Mahesuria	India Pump Characterization of 80 K Liquid Nitrogen Booster System for SST-1
FIP/P7-12	G. Gantenbein	Germany Overview of Recent Gyrotron R&D towards DEMO within EUROfusion Work Package Heating and Current Drive
FIP/P7-13	L. Savoldi	Italy Assessment and Optimization of the Cavity Thermal Performance for the European Continuous Wave Gyrotrons
FIP/P7-14	A. Garg	India Operational Results and Troubleshooting in Current Feeder System for SST-1
FIP/P7-15	D. B. Gin	Russian Fed. Recent Progress in Developing Gamma Spectrometer in ITER

Continued...

Fri

P7 *continued...*

Id	Presenter		Title
FIP/P7-16	R. Sugandhi	India	Timing and Synchronization for Integrated Operation of Large Volume Plasma Device
FIP/P7-17	V. G. Devi	India	Design and Thermal Fluid Structure Interaction Analysis of Liquid Nitrogen Cryostat of Cryogenic Molecular Sieve Bed Adsorber for Hydrogen Isotopes Removal System
FIP/P7-19	S. Dutta	India	Error Field Experiment and Analysis in SST-1
FIP/P7-20	D. Christian	India	Maintenance Experience of 315 kW Electrical Motor of Helium Screw Compressor in 1.3 kW Helium Liquefier
FIP/P7-21	A. Tomar	India	Thermo-Structural and Heat Load Analysis of SST-1 Superconducting Coils
FIP/P7-22	A. Shrivastava	India	Thermal Diffusivity Measurement of Functional & Structural Materials for Fusion Blanket Application
FIP/P7-24	N. Rastogi	India	Development of a Prototype Collaborative Robot for Fusion Remote Handling Applications
FIP/P7-25	B. R. Doshi	India	Design of the TF/PF Bus Bar Layout and its Connections with Current Feeder System of SST-1 Tokamak
FIP/P7-26	S. Roy	India	Preventive Measures to Avoid Electrical Arcing Incidences in SST-1 PF Current Leads
FIP/P7-27	H. Chen	China, P. R.	Model Development and Electromagnetic Analysis of Vertical Displacement Event for CFETR Helium Cooled Solid Blanket
FIP/P7-28	P. Prajapati	India	Key Considerations in the Power Extraction from Fusion Reactors
FIP/P7-29	D. Chen	China, P. R.	Development and Experiment of PbLi Facilities for Fusion Nuclear Technology
FIP/P7-30	J. Mora-Meléndez	Costa Rica	Implementation of the Spherical Tokamak MEDUSA-CR: Stage 1
FIP/P7-33	O. Crofts	UK	Early Definition of the Maintenance Plan Is Essential to Achieve an Economic EU DEMO
FIP/P7-34	V. B. Minaev	Russian Fed.	The Influence of Toroidal Magnetic Field Growth on Plasma Performance in the Spherical Tokamak Globus-M/-M2
FIP/P7-35	K. Kizu	Japan	Progress in Design and Fabrication of Current and Helium Feeding System for JT-60SA Superconducting Coils

Continued...

P7 continued...

Id	Presenter		Title
FIP/P7-36	S. Binwal	India	Noninvasive Plasma Density Measurement in a 13.56 MHz Magnetized Capacitive Coupled RF Discharge
FIP/P7-37	Y. Shibama	Japan	Advanced Assembly Technology of the Superconducting Coils in JT-60SA Tokamak
FIP/P7-38	T. Brown	USA	A Toroidal Confinement Facility Study and Eventual Experimental Device to Investigate a Range of Liquid Metal Divertor and First-Wall Concepts
FIP/P7-39	T. Goto	Japan	Conceptual Design of a Compact Helical Fusion Reactor FFHR-c1 for the Early Demonstration of a Year-Long Electric Power Generation
FIP/P7-40	V. Antoni	Italy	Negative Ion Beam Source Physics as a Complex System: Identification of Main Processes and Key Interdependence
FIP/P7-42	J. Figueiredo	Portugal	JET Upgraded Diagnostic Capabilities and Scientific Exploitation in Support of Deuterium-Tritium Operation
TH/P7-1	D. Zarzoso	France	Poloidal Flows, Asymmetries and Multiscale Organization in Interplaying Core-Edge-SOL Turbulent Plasmas
TH/P7-2	R. J. Buttery	USA	Integrated Modelling of Core, Edge Pedestal and Scrape-Off-Layer for High- β_N Steady-State Scenarios on DIII-D
TH/P7-3	M. Y. Ye	China, P. R.	Simulation Study of the Impurity Radiation in the Quasi-Snowflake Divertor with Ne Seeding for CFETR
TH/P7-4	A. H. Nielsen	Denmark	Synthetic Edge and SOL Diagnostics: A Bridge between Experiments and Theory
TH/P7-5	M. Wischmeier	Germany	The Physics Basis for a Solution to the Power and Particle Exhaust Problem of a Next Step Device
TH/P7-6	D. Sharma	India	The Scrape-Off Layer Plasma Transport Physics Simulation Activity for Indian Tokamaks ADITYA and SST-1
TH/P7-7	V. Pericoli Ridolfini	India	Comparative Analysis of the SOL Properties for the Various Magnetic Configurations Proposed for the DEMO Divertor
TH/P7-8	N. Shukla	India	Electron Impact Excitation of W^{40+} to W^{43+} Ions: Cross Section and Polarization

Continued...

P7 *continued...*

Id	Presenter		Title
TH/P7-9	B. P. Sahoo	India	Plasma Transport in Toroidally Discontinuous Limiter Generated 3D SOL Configurations of ADITYA Tokamak
TH/P7-10	R. Zanino	Italy	Self-Consistent Modelling of a Liquid Metal Pool-Type Divertor
TH/P7-11	S. Togo	Japan	SOL/Divertor Plasma Simulation of Diverging Magnetic Field Configurations for Advanced Divertors
TH/P7-12	H. Hasegawa	Japan	Ion Inertial Effects on 3D Filament Dynamics
TH/P7-13	R. Khanal	Nepal	Velocity Profile and Modulation Frequency of Ions in a Magnetized Plasma Sheath Using Kinetic Trajectory Simulation Method
TH/P7-15	J. P. S. Bizarro	Portugal	Exact Conservative Solutions of Fluid Models for the Scrape-Off Layer as the Ancestors of Blobs?
TH/P7-17	I. B. Kupriyanov	Russian Fed.	Simulation of Beryllium Erosion and Surface Damage Under ITER-Like Transient Plasma Heat Loads
TH/P7-18	H. Reimerdes	Switzerland	Assessment of Alternative Divertor Configurations as an Exhaust Solution for DEMO
TH/P7-20	M. Wigram	UK	Performance Assessment of Tightly-Baffled Long-Leg Divertor Geometries in the ARC Reactor Concept
TH/P7-21	X. Q. Xu	USA	Simulations of Tokamak Boundary Plasma Turbulent Transport
TH/P7-22	C.-S. Chang	USA	Wide Divertor Heat-Flux Width in ITER from Self-Organization between the Neoclassical and Turbulent Transports across the Separatrix Surface
TH/P7-23	A. Hakim	USA	Continuum Gyrokinetic Simulations of NSTX SOL Turbulence with Sheath-Limited Model Geometries
TH/P7-24	M. A. Dorf	USA	Simulation of Cross-Separatrix Edge Plasma Transport with the Continuum Gyrokinetic Code COGENT
TH/P7-25	J. M. Canik	USA	Multiphysics Modelling of the Long-Term Evolution of Plasma-Exposed Surfaces
TH/P7-26	R. M. Churchill	USA	Pressure Balance in a Low Collisionality Tokamak Scrape-Off Layer

EX/8, PPC/2, TH/6**Heating, Current Drive & Steady State**

Chair: Kenkichi Ushigusa (Japan)

Main Hall

(14:00 – 16:10)

Time Id	Presenter		Title
14:00 TH/6-1	M. Schneider	France	Modelling Third Field Operation in the ITER Prefusion Power Operation Phase
14:20 TH/6-2	E. M. Bass	USA	Predictions of α -Particle and Neutral-Beam Heating and Transport in ITER Scenarios
14:40 PPC/2-1	T. C. Luce	ITER	Exploring an Alternate Approach to $Q = 10$ in ITER
15:00 TH/6-3	M. Weiland	Germany	Real-Time Simulation of the NBI Fast-Ion Distribution
15:20 EX/8-1	Y. O. Kazakov	Belgium	Recent Advances in ICRF Heating of Mixture Plasmas: Survey of JET and AUG Experiments and Extrapolation to JET-DT and ITER
15:40 EX/8-2	G. M. Wallace	USA	Experimental Evidence of Lower Hybrid Wave Scattering in Alcator C-Mod Due to Scrape Off Layer Density Fluctuations

EX/9 and TH/7**Divertor & Exhaust Physics**

Chair: Choong-Seok Chang (USA)

Main Hall

(16:40 – 18:45)

Time Id	Presenter		Title
16:40 EX/9-1	T. Sunn Pedersen	Germany	First Divertor Physics Studies in Wendelstein 7-X
17:00 EX/9-2	F. Effenberg	USA	Demonstration of Power Exhaust Control by Impurity Seeding in the Island Divertor at Wendelstein 7-X
17:20 EX/9-3	A. E. Järvinen	USA	Progress in DIII-D Towards Validating Divertor Power Exhaust Predictions
17:40 TH/7-1	F. Militello	UK	Predicting Scrape-Off Layer Profiles and Filamentary Transport for Reactor Relevant Devices
18:00 TH/7-2	M. V. Umansky	USA	Study of Passively Stable, Fully-Detached Divertor Plasma Regimes Attained in Innovative Long-Legged Divertor Configurations
18:20 EX/9-4	S. Brezinsek	Germany	Erosion, Screening, and Migration of Tungsten in JET Equipped with Tungsten Divertor

P8		Posters 8	
		Main Hall	(14:00 – 18:45)
Id		Presenter	Title
EX/7-1	Y. In	Korea, Rep. of	Test of the ITER-Like RMP Configurations for ELM-Crash-Suppression on KSTAR
EX/7-2	Y. Sun	China, P. R.	Dynamic ELM and Divertor Control Using Mixed Toroidal Harmonic Resonant
EX/7-3	W. Suttrop	Germany	Magnetic Perturbations in DIII-D and EAST Experimental Conditions for Suppressing Edge Localized Modes by Magnetic Perturbations in ASDEX-Upgrade
EX/7-4	G. L. Xiao	China, P. R.	ELM Control Physics with Impurity Seeding and LHCD in the HL-2A Tokamak
EX/8-1	Y. O. Kazakov	Belgium	Recent Advances in ICRF Heating of Mixture Plasmas: Survey of JET and AUG Experiments and Extrapolation to JET-DT and ITER
EX/8-2	G. M. Wallace	USA	Experimental Evidence of Lower Hybrid Wave Scattering in Alcator C-Mod Due to Scrape Off Layer Density Fluctuations
EX/9-1	T. Sunn Pedersen	Germany	First Divertor Physics Studies in Wendelstein 7-X
EX/9-2	F. Effenberg	USA	Demonstration of Power Exhaust Control by Impurity Seeding in the Island Divertor at Wendelstein 7-X
EX/9-3	A. E. Järvinen	USA	Progress in DIII-D Towards Validating Divertor Power Exhaust Predictions
EX/9-4	S. Brezinsek	Germany	Erosion, Screening, and Migration of Tungsten in JET Equipped with Tungsten Divertor
EX/10-1	K. Ida	Japan	Isotope Effect on Impurity and Bulk Ion Particle Transport in the Large Helical Device
EX/10-2	V. A. Vershkov	Russian Fed.	3D Structure of Density Fluctuations in T-10 Tokamak and New Approach for Current Profile Estimation
EX/10-3	P. Rodriguez-Fernandez	USA	Explaining Cold-Pulse Dynamics in Tokamak Plasmas Using Local Turbulent Transport Models
EX/11-1	H. Raj	India	Origin of Harmonics of Drift Tearing Mode in ADITYA Tokamak
EX/11-2	M. J. Choi	Korea, Rep. of	Effect of Multiscale Interaction between an $m/n = 2/1$ Mode and Microinstabilities on Transport of KSTAR Plasmas

Continued...

P8 *continued...*

Id	Presenter		Title
PPC/2-1	T. C. Luce	ITER	Exploring an Alternate Approach to $Q = 10$ in ITER
TH/5-1	D. Chandra	India	A Nonlinear 2-Fluid Study of the Effect of Pellet Injection on ELM Dynamics
TH/6-1	M. Schneider	ITER	Modelling Third Field Operation in the ITER Prefusion Power Operation Phase
TH/6-2	E. M. Bass	USA	Predictions of α -Particle and Neutral-Beam Heating and Transport in ITER Scenarios
TH/6-3	M. Weiland	Germany	Real-Time Simulation of the NBI Fast-Ion Distribution
TH/7-1	F. Militello	UK	Predicting Scrape-Off Layer Profiles and Filamentary Transport for Reactor Relevant Devices
TH/7-2	M. V. Umansky	USA	Study of Passively Stable, Fully-Detached Divertor Plasma Regimes Attained in Innovative Long-Legged Divertor Configurations
TH/8-1	J.-M. Kwon	Korea, Rep. of	Gyrokinetic XGC1 Simulation Study of Magnetic Island Effects on Neoclassical and Turbulence Physics in a KSTAR Plasma
TH/8-2	A. B. Altukhov	Russian Fed.	Benchmarking of Full- f Global Gyrokinetic Modelling Results against the FT-2 Tokamak Doppler Reflectometry Data Using Synthetic Diagnostics
EX/P8-1	A. Kappatou	Germany	Energy Confinement and Performance of Pure Helium Plasmas and Helium Seeded Deuterium Plasmas
EX/P8-2	M. G. Dunne	Germany	Impact of Impurity Seeding on Pedestal Structure in ASDEX-Upgrade and Alcator C-Mod
EX/P8-3	F. Ryter	Germany	Heat Transport Driven by the ITG and TEM Instabilities in the ASDEX-Upgrade Tokamak
EX/P8-4	T. Pütterich	Germany	The ITER Baseline Scenario Investigated at ASDEX-Upgrade
EX/P8-5	E. Viezzer	Spain	ELM-Induced Energy and Momentum Transport in ASDEX-Upgrade
EX/P8-6	L. Marrelli	Italy	From RFX-Mod to RFX-Mod2: Perspectives of the Reversed Field Pinch Configuration
EX/P8-7	R. Cavazzana	Italy	Challenges and Solutions in the Design of RFX-Mod2, a Multiconfiguration Magnetic Confinement Experimental Device

Continued...

P8 *continued...*

Id	Presenter		Title
EX/P8-8	S. A. Bozhenkov	Germany	High Density and High Performance Operation with Pellet Injection in W7-X
EX/P8-9	O. Grulke	Germany	Plasma Dynamics and Transport Studies in Wendelstein 7-X
EX/P8-11	C. Silva	Portugal	IST Contributions to the ASDEX-Upgrade Edge and Divertor Physics Using Microwave Reflectometry
EX/P8-12	B. A. Unterberg	Germany	Characterization of Advanced Concepts for First Wall Materials by Plasma Exposure in the Linear Plasma Device PSI-2
EX/P8-13	N. Vianello	Italy	SOL Transport and Filamentary Dynamics in High Density Tokamak Regimes
EX/P8-14	P. Zanca	Italy	Helical Plasma-Wall Interaction in the RFX-Mod: Effects of High- n Mode Locking
EX/P8-15	S. C. Liu	Germany	The Effects of Magnetic Topology on the SOL Island Structure and Turbulence Transport in the First Divertor Plasma Operation of W7-X
EX/P8-16	M. W. Jakubowski	Germany	3D Heat and Particle Fluxes in Wendelstein 7-X
EX/P8-17	R. Brakel	Germany	Strategy and Optimization of Wall Conditioning at the Wendelstein 7-X Stellarator
EX/P8-18	C. Killer	Germany	Characterization of the W7-X Scrape-Off Layer Using the Multipurpose Manipulator
EX/P8-19	J. D. Lore	USA	Measurement and Modelling of Magnetic Configurations to Mimic Overload Scenarios in the W7-X Stellarator
EX/P8-20	M. Willensdorfer	Germany	Impact of the 3D Geometry from Nonaxisymmetric Magnetic Perturbations on the Local Edge Stability in ASDEX-Upgrade
EX/P8-21	V. Igochine	Germany	Seeding of Tearing Modes by Internal Crash Events in ASDEX-Upgrade and DIII-D Tokamaks
EX/P8-22	L. Frassinetti	Sweden	Role of the Pressure Position on the Pedestal Stability in AUG, JET-ILW and TCV in Deuterium and Hydrogen Plasmas and Implications for ITER
EX/P8-23	J.-M. Noterdaeme	Germany	Ion Cyclotron Range of Frequency Power: Progress in Operation and Understanding for Experiments with Metallic Walls

Continued...

P8 *continued...*

Id	Presenter	Title
EX/P8-24	B. Geiger	Germany Fast-Ion Confinement in Low Collisionality Discharges at ASDEX-Upgrade and TCV
EX/P8-25	D. Rittich	Germany Quantification of Neutral Beam Driven Current and the Effect of Radial Fast-Ion Transport in ASDEX-Upgrade
EX/P8-26	J. Galdon-Quiroga	Spain Impact of an Edge Resonant Transport Layer on Fast-Ion Confinement in the ASDEX-Upgrade Tokamak
EX/P8-27	J. Ongena	Belgium Preparing the ICRH System for the Wendelstein 7-X Stellarator
EX/P8-28	H. P. Laqua	Germany On a Path to Steady-State High-Performance Operation in W7-X: Heating, Current Drive and Fuelling Experiments with High Power ECRH
EX/P8-29	R. Majeski	USA The LTX- β Research Programme and First Results
EX/P8-30	A. Dinklage	Germany Plasma Termination by Excess Fuel and Impurities in TJ-II, LHD and W7-X
FIP/P8-1	R. Patel	India Installation and Commissioning of 80 K Liquid Nitrogen Booster System
FIP/P8-2	R. C. O'Neill	USA High Power Helicon Antenna Design for DIII-D
FIP/P8-3	C. K. Gupta	India Implementation of Synchronous Reference Frame Theory Based Shunt Active Power Filter Using DSP Controller
FIP/P8-4	J. Patel	India Operation and Control of 42 GHz Gyrotron System in ECRH
FIP/P8-5	K. Mohan	India Design and Development of Control Grid Power Supply for RF Amplifier
FIP/P8-6	A. Fasoli	Switzerland TCV Heating and Divertor Upgrades
FIP/P8-7	J. Kumar	India Design and Simulation of Circular Waveguide Elbows Applicable in High Power Microwave Coupling to Plasma
FIP/P8-8	M. Patel	India Development of Solid State Power Amplifier for ICH & CD RF Source
FIP/P8-9	R. Kumar	India RT Amplitude Control Loop: Testing of R&D ICRF Source at High Power
FIP/P8-10	J. C. Patel	India Mechanical Engineering Aspects for Overhauling of Helium Compressor and Heavy Duty Electrical Motors of 1.3 kW Helium Refrigerator/Liquefier System
FIP/P8-11	R. Ragona	Belgium A Travelling Wave Array System as Solution for the ICRF Heating of DEMO

Continued...

P8 *continued...*

Id	Presenter	Title
FIP/P8-12	R. Sharma	India Development of Indigenous Electrical Insulation Breaks for Superconducting Magnets of Fusion Devices
FIP/P8-13	P. Y. Li	China, P. R. Recent Progress of ITER Magnet Supports Package in SWIP
FIP/P8-14	U. Fischer	Germany Nuclear Design Issues of a Stellarator Fusion Power Plant with Breeder Blanket in Comparison to Tokamaks
FIP/P8-15	M. Ghate	India Numerical Investigations towards Manufacturing of High Current Carrying Superconducting CICC
FIP/P8-16	A. Jha	India Development of Wideband Amplifier in ITER ICRF Range
FIP/P8-17	M. Bandyopadhyay	India Development of Various Diagnostics for NNBI Programme in IPR
FIP/P8-18	R. K. Buddu	India Studies of Ultrasonic and Phased Array Inspection NDT Techniques on High Thick SS-316L Welded Joint Mock-Ups of Fusion Reactor Components Fabrication Applications
FIP/P8-19	R. Bahl	India Simulation Studies for Optimization of 60 MHz Rod-Type Radiofrequency Quadrupole Accelerator Design at IPR
FIP/P8-20	H. K. Patel	India Manufacturing Technologies for UHV Compatible 10 MW/m ² High Heat Flux Components for Application in Fusion Devices
FIP/P8-22	T. K. Sharma	India Development and Validation of Cryostat Finite Element Model with Unique FE Method
FIP/P8-23	A. Patel	India Characterization of Argon Plasma in a Multiline Cusp Magnetic Field: Towards a Favourable Source for NBI System
FIP/P8-24	Z. Shaikh	India A Versatile Multicusp Plasma Device for Confining Contact Ionized Alkali Ions: Source for the Experimental Studies
FIP/P8-25	M. Sharma	India Evolution and Implementation of Lossless Data Acquisition for Steady State Tokamak
FIP/P8-26	B. K. Shukla	India Technology Developments for ECRH System
FIP/P8-29	B. Chektybayev	Kazakhstan Concept of a New Approach in Thermographic Measurements for Plasma-Wall Interaction Studies on KTM Tokamak

Continued...

P8 *continued...*

Id	Presenter		Title
TH/P8-1	K. Hallatschek	Germany	Highly Collisional Two-Fluid and Gyrokinetic Simulations of Tokamak Edge Turbulence and the Transition between Kinetic and Fluid Regime
TH/P8-2	A. Y. Aydemir	Korea, Rep. of	Effect of Poloidal Density Asymmetries on Shear Flows and Radial Electric Field at the Plasma Edge
TH/P8-3	R. Singh	Korea, Rep. of	Multiscale Interaction between Ballooning Mode and Electron-Scale Turbulence and the Mesoscale Structure Formation in the Edge Pedestal
TH/P8-4	J. Kim	Korea, Rep. of	Correlation Analysis Based Magnetic Kubo Number Estimation during Pedestal Collapse in BOUT++ Simulation
TH/P8-5	R. Dey	India	Studies of the Gas Puff Effect on Edge Plasma of ADITYA Tokamak Using Coupled DEGAS2-UEDGE Code
TH/P8-6	A. Wisitsorasak	Thailand	Predictive Simulations of Core-Edge Plasma for Tokamak Plasma Using BALDUR Code
TH/P8-7	J. Chowdhury	USA	Gyrokinetic Neoclassical Study of the Effect of the X-Point Height on $E \times B$ Flow Structure in an H-Mode Edge Plasma
TH/P8-8	V. K. Bandaru	Germany	Nonlinear Interaction of Runaway Electrons with Resistive MHD Modes in an ITER VDE
TH/P8-9	I. Bandyopadhyay	India	Simulations of Plasma Disruptions in ITER due to Material Ingress
TH/P8-10	N. M. Ferraro	USA	Nonlinear 3D Simulations of Vertical Displacement Events in Tokamaks
TH/P8-12	G. Q. Dong	China, P. R.	Nonlinear Interplay between Edge Localized Infernal Mode and Plasma Flow
TH/P8-13	Y. Li	China, P. R.	Nonlinear Turbulent Parallel Momentum Transport due to Blobs
TH/P8-14	Y. Peysson	France	Modelling Runaway Electrons Dynamics in Tokamak Plasmas: Progresses and Challenges
TH/P8-15	G. I. Pokol	Hungary	Runaway Electron Modelling in the ETS Self-Consistent Core Transport Simulator
TH/P8-16	C. Liu	USA	Energy Loss and Pitch Angle Scattering of Runaway Electrons due to Kinetic Instabilities
TH/P8-17	D. A. Spong	USA	Interactions of Runaway Electrons with Alfvén and Whistler Waves

Continued...

Fri

P8 *continued...*

Id		Presenter		Title
TH/P8-18		R. W. Harvey	USA	Time-Dependent Runaway Simulations: Ampère–Faraday Equations Implemented in CQL3D
TH/P8-19		D. del-Castillo-Negrete	USA	Integrated Simulation of Runaway Electrons: A Backward Monte Carlo Approach for a Fluid-Kinetic Self-Consistent Coupling

EX/10 and TH/8

Transport

Chair: Yasuaki Kishimoto (Japan)

Main Hall

(08:30 – 10:15)

Time Id	Presenter		Title
08:30 EX/10-1	K. Ida	Japan	Isotope Effect on Impurity and Bulk Ion Particle Transport in the Large Helical Device
08:50 EX/10-2	V. A. Vershkov	Russian Fed.	3D Structure of Density Fluctuations in T-10 Tokamak and New Approach for Current Profile Estimation
09:10 TH/8-1	J.-M. Kwon	Korea, Rep. of	Gyrokinetic XGC1 Simulation Study of Magnetic Island Effects on Neoclassical and Turbulence Physics in a KSTAR Plasma
09:30 EX/10-3	P. Rodriguez-Fernandez	USA	Explaining Cold-Pulse Dynamics in Tokamak Plasmas Using Local Turbulent Transport Models
09:50 TH/8-2	A. B. Altukhov	Russian Fed.	Benchmarking of Full- f Global Gyrokinetic Modelling Results against the FT-2 Tokamak Doppler Reflectometry Data Using Synthetic Diagnostics

EX/11, SEE/3, PD

Stability, Environmental, and PD

Chair: Matthew Hole (Australia)

Main Hall

(10:45 – 12:30)

Time Id	Presenter		Title
10:45 EX/11-1	H. Raj	India	Origin of Harmonics of Drift Tearing Mode in ADITYA Tokamak
11:05 EX/11-2	M. J. Choi	Korea, Rep. of	Effect of Multiscale Interaction between an $m/n = 2/1$ Mode and Microinstabilities on Transport of KSTAR Plasmas
11:25 SEE/3-1Ra	S. Konishi	Japan	Future Possibility of Carbon Sequestration by Biomass-Fusion Hybrid Systems
SEE/3-1Rb			Economic Performance of Fusion Power Plant on Future Deregulated Electricity Market
SEE/3-1Rc			Techno-Economic Analysis of Biodiesel and Hydrogen Production via Fusion-Biomass Hybrid Model
11:45 PD/1-1	TBA	—	Post Deadline Oral #1
12:05 PD/1-2	TBA	—	Post Deadline Oral #2

Sat

S/1		Summary 1	
Chair: Elizabeth Surrey (UK)		Main Hall	(14:00 – 16:00)
Time Id	Presenter	Title	
14:00 S/1-NF	R. Hawryluk	IAEA	The Nuclear Fusion Prize
	S. J. Le Masurier	IAEA	
14:30 S/1-1	D. J. Campbell	ITER	Summary EXC, EXS & PPC
15:00 S/1-2	K. Ida	Japan	Summary EXD, EXW & ICC
15:30 S/1-3	R. Galvao	Brazil	Summary Magnetic Confinement Theory

Sat	S/2		Summary 2	
	Chair: Boris Kuteev (Russian Fed.)		Main Hall	(16:30 – 18:00)
	Time Id	Presenter	Title	
	16:30 S/2-1	B. P. Radha	USA	Summary Inertial Fusion Experiments and Theory
	17:00 S/2-2	T. Inoue	Japan	Summary FIP, FNS, MPT & SEE
	17:30 S/2-3	IAEA Representative	IAEA	Closing Address
	17:50 S/2-4	Host Country Representative	India	Conference Closing

Contents

Introduction	1
Programme Committee	2
Conference Secretariat	3
Overview of Contributions	6
Explanation of Abbreviations	6
Timetable	9
Monday 22 October 2018	10
Tuesday 23 October 2018	14
Wednesday 24 October 2018	26
Thursday 25 October 2018	38
Friday 26 October 2018	49
Saturday 27 October 2018	65
 Abstracts	 115
O/1: Opening Plenary	115
O/1-4 R. B. Grover, Importance of Energy and the Role of Nuclear Energy in India's Energy Mix	116
O/1-5 S. P. Deshpande, India's Quest for Fusion Energy & Road to ITER	117
O/1-6 P. A. Child, EU R&D Energy Policy and the Role of Fusion Research	119
O/1-7 N. K. Prinja, Fusion is our Future: Readiness of the Fusion Technology and the 4th Industrial Revolution	120
OV: Overviews	121
OV/1-1 A. K. Chakraborty, <i>et al.</i>, Progress of ITER-India Activities for ITER Deliverables: Chal- lenges and Mitigation Measures	122
OV/1-2 B. Bigot, Progress Toward ITER's First Plasma	123
OV/1-3 E. Joffrin, Overview of the JET Preparation for Deuterium-Tritium Op- eration	124

OV/1-4	C. C. Petty, DIII-D Research Towards Establishing the Scientific Basis for Future Fusion Reactors	125
OV/2-1	H. Meyer, Overview of Physics Studies on ASDEX-Upgrade	126
OV/2-2	B. N. Wan, et al., Recent Advances in EAST Physics Experiments in Support of Steady-State Operation for ITER and CFETR	127
OV/2-3	H. K. Park, et al., Overview of the KSTAR Research Progress and Future Plan Toward ITER and K-DEMO	128
OV/2-4	E. S. Marmar, Overview of Research Results from the Alcator C-Mod Toka- mak	130
OV/2-5	J. L. Kline, et al., Progress of Indirect Drive Inertial Confinement Fusion in the USA	131
OV/3-1	P. Barabaschi, et al., Progress of JT-60SA Project	133
OV/3-2	G. Zhuang, et al., Progress of the CFETR Design	134
OV/3-3	M. Sugimoto, et al., Overview of the Validation Activities of IFMIF/EVEDA: LI- Pac, the Linear IFMIF Prototype Accelerator and LiFus6, the Lithium Corrosion Induced Facility	135
OV/3-4	H. Tanigawa, et al., The Strategy of Fusion DEMO In-Vessel Structural Material Development	136
OV/4-1	T. Klinger, Overview of First Wendelstein 7-X High-Performance Oper- ation with Island Divertor	137
OV/4-2	T. Morisaki, Overview of the First Deuterium Experiment in LHD	138
OV/4-3	E. Ascasíbar, Overview of TJ-II Stellarator Results	139
OV/4-4	S. Pamela, et al., ELM and ELM-control Simulations	140
OV/4-5	E. J. Strait, et al., Experiments in Disruption Avoidance for ITER Using Passive and Active Control	141
OV/5-1	M. Xu, Overview of HL-2A Recent Experiments	142

OV/5-2	S. Coda, Physics Research on the TCV Tokamak Facility: From Con- ventional to Alternative Scenarios and Beyond	143
OV/5-3	R. L. Tanna, et al., Overview of Operation and Experiments in the ADITYA-U Tokamak	144
OV/5-4	N. N. Bakharev, et al., Tokamak Research in Ioffe Institute	145
OV/5-5Ra	S. M. Kaye, et al., Overview of Recent Progress in Understanding NSTX and NSTX-U Plasmas	146
OV/5-5Rb	J. R. Harrison, Overview of New MAST Physics in Anticipation of First Results from MAST Upgrade	147
OV/P-1	G. Pucella, Overview of the FTU Results	148
OV/P-2	B. P. Radha, Overview and Status of Direct-Drive Inertial Confinement Fusion in the United States	149
OV/P-3	R. Panek, et al., ITER-Relevant Research on the COMPASS Tokamak	150
OV/P-4	T. A. Carter, et al., Advances in Fusion-Relevant Physics on the Large Plasma Device	151
OV/P-5	N. C. Wang, et al., Overview of the Recent Experimental Research on the J-TEXT Tokamak	152
OV/P-6	J. E. Menard, et al., Fusion Energy Development Applications Utilizing the Spher- ical Tokamak and Associated Research Needs and Tools . .	153
OV/P-7	M. Kakati, et al., Design, Development and Recent Experiments at the CIRCLE- PSI Device	154
OV/P-8	W. Liu, et al., Overview of Diagnostics Upgrade and Experiment Progress on KTX	155
OV/P-11	H. Gota, et al., Formation of Hot, Stable, Long-Lived Field-Reversed Con- figuration Plasmas on the C-2W Device	156
OV/P-12	S. M. Belsare, et al., Activity of Indian High Heat Flux Test Facility	157

EX: Magnetic Confinement Experiments	159
EX/1-1 P. Lauber, <i>et al.</i>, Strongly Nonlinear Energetic Particle Dynamics in ASDEX- Upgrade Scenarios with Core Impurity Accumulation	160
EX/1-2 M. Podestà, <i>et al.</i>, Reduced Energetic Particle Transport Models Enable Com- prehensive Time-Dependent Tokamak Simulations	161
EX/1-3Ra S. Yamamoto, <i>et al.</i>, Impact of ECH/ECCD on Fast-Ion-Driven MHD Instabilities in Helical Plasmas	162
EX/1-3Rb S. Ohdachi, <i>et al.</i>, Excitation Mechanism of the Energetic Particle Driven Resis- tive Interchange Mode and Strategy to Control the Mode in Large Helical Device	163
EX/2-1 E. de la Luna, <i>et al.</i>, Impact of ELM Control in JET Experiments on H-Mode Ter- minations with/without Current Ramp-Down and Implica- tions for ITER	164
EX/2-2 D. R. Ernst, <i>et al.</i>, Viability of Wide Pedestal QH-Mode for Burning Plasma Operation	165
EX/2-3 T. Happel, <i>et al.</i>, Advances in the Understanding of the I-Mode Confinement Regime: Access, Stationarity, Edge/SOL Transport and Di- vertor Impact	166
EX/2-4 P. B. Snyder, <i>et al.</i>, High Fusion Performance in Super H-Mode Experiments on Alcator C-Mod and DIII-D	167
EX/2-5 B. Labit, <i>et al.</i>, Plasma Shape and Fuelling Dependence on the Small ELM Regime in TCV and AUG	168
EX/3-1 X. Z. Gong, <i>et al.</i>, Integrated Operation of Steady-State Long Pulse H-Mode in EAST	169
EX/3-2 G. Calabrò, <i>et al.</i>, Developing Steady State ELM-Absent H-Mode Scenarios with Advanced Divertor Configuration in EAST Tokamak .	170
EX/3-3 F. Turco, <i>et al.</i>, Integration of the High-N Hybrid Scenario to a High Perfor- mance Pedestal, Stable Zero Torque Operation and a Divertor Solution	171

EX/3-4	C. Giroud, <i>et al.</i>,	Optimization of JET-DT and ITER Operation by Developing an Understanding of the Role of Low-Z Impurity on the H-Mode Pedestal	172
EX/3-5	G. Fuchert, <i>et al.</i>,	Increasing the Density in W7-X: Benefits and Limitations . .	173
EX/3-6	L. Garzotti, <i>et al.</i>,	Scenario Development for DT Operation at JET	174
EX/4-1	J. C. Hillesheim, <i>et al.</i>,	Implications of JET-ILW L-H Transition Studies for ITER . .	175
EX/4-2	L. Schmitz, <i>et al.</i>,	L-H Transition Trigger Physics in ITER-Similar Plasmas with and without Applied $n = 3$ Magnetic Perturbations	177
EX/4-3	J. T. McClenaghan, <i>et al.</i>,	Transport Barriers in DIII-D High- β_p Plasmas and Development of Candidate Steady State Scenarios for ITER	178
EX/4-4	T. Tala, <i>et al.</i>,	Core Density Peaking Experiments in JET, DIII-D and C-Mod in Various Operational Scenarios Driven by Fuelling or Transport	179
EX/5-1	K. Nagaoka, <i>et al.</i>,	Transport Characteristics of Deuterium and Hydrogen Plasmas with Ion Internal Transport Barrier in LHD	181
EX/5-2	C. Chrystal, <i>et al.</i>,	Predicting the Toroidal Rotation Profile for ITER	182
EX/6-1	C. Paz-Soldan, <i>et al.</i>,	Advances in Runaway Electron Control and Model Validation for ITER	183
EX/7-1	Y. In, <i>et al.</i>,	Test of the ITER-Like RMP Configurations for ELM-Crash-Suppression on KSTAR	184
EX/7-2	Y. Sun, <i>et al.</i>,	Dynamic ELM and Divertor Control Using Mixed Toroidal Harmonic Resonant Magnetic Perturbations in DIII-D and EAST	185
EX/7-3	W. Suttrop, <i>et al.</i>,	Experimental Conditions for Suppressing Edge Localized Modes by Magnetic Perturbations in ASDEX-Upgrade . . .	186
EX/7-4	G. L. Xiao, <i>et al.</i>,	ELM Control Physics with Impurity Seeding and LHCD in the HL-2A Tokamak	187

EX/8-1	Y. O. Kazakov, Recent Advances in ICRF Heating of Mixture Plasmas: Survey of JET and AUG Experiments and Extrapolation to JET-DT and ITER	188
EX/8-2	E. H. Martin, et al., Experimental Evidence of Lower Hybrid Wave Scattering in Alcator C-Mod Due to Scrape Off Layer Density Fluctuations	189
EX/9-1	T. Sunn Pedersen, First Divertor Physics Studies in Wendelstein 7-X	190
EX/9-2	F. Effenberg, et al., Demonstration of Power Exhaust Control by Impurity Seeding in the Island Divertor at Wendelstein 7-X	191
EX/9-3	A. E. Järvinen, et al., Progress in DIII-D Towards Validating Divertor Power Exhaust Predictions	192
EX/9-4	S. Brezinsek, et al., Erosion, Screening, and Migration of Tungsten in JET Equipped with Tungsten Divertor	193
EX/10-1	K. Ida, et al., Isotope Effect on Impurity and Bulk Ion Particle Transport in the Large Helical Device	194
EX/10-2	V. A. Vershkov, et al., 3D Structure of Density Fluctuations in T-10 Tokamak and New Approach for Current Profile Estimation	195
EX/10-3	P. Rodriguez-Fernandez, et al., Explaining Cold-Pulse Dynamics in Tokamak Plasmas Using Local Turbulent Transport Models	196
EX/11-1	H. Raj, et al., Origin of Harmonics of Drift Tearing Mode in ADITYA Tokamak	197
EX/11-2	M. J. Choi, et al., Effect of Multiscale Interaction between an $m/n = 2/1$ Mode and Microinstabilities on Transport of KSTAR Plasmas . . .	198
EX/P1-1	M. Komm, et al., Divertor Impurity Seeding Experiments at the COMPASS Tokamak	199
EX/P1-2	A. Malaquias, et al., Experimental Studies of Pressure and Plasma Current Profiles for Equilibria Calculations During AC Transition in the ISTOK Tokamak	200
EX/P1-3	D. Frigione, et al., Impact of Neon Injection on Electron Density Peaking in JET Hybrid Plasmas	201

EX/P1-4	H. Weisen, <i>et al.</i>,	Isotope Dependence of Confinement in JET Deuterium and Hydrogen Plasmas	202
EX/P1-5	H.-T. Kim, <i>et al.</i>,	High Fusion Performance at High T_i/T_e in JET-ILW Baseline Plasmas with High NBI Heating Power and Low Gas Puffing	203
EX/P1-6	B. P. Duval, <i>et al.</i>,	Singlet Breakdown Optimization to a Doublet Plasma Configuration on the TCV Tokamak	204
EX/P1-9	T. Estrada, <i>et al.</i>,	Turbulence and Radial Electric Field Asymmetries Measured at TJ-II Plasmas	205
EX/P1-11	E. Sánchez, <i>et al.</i>,	Validation of Global Gyrokinetic Simulations in Stellarator Configurations	206
EX/P1-12	A. Vertkov, <i>et al.</i>,	The Concept of Lithium Based Plasma Facing Elements for Steady State Fusion Tokamak-Reactor and its Experimental Validation	207
EX/P1-14	D. Borodin, <i>et al.</i>,	Extrapolation of Be Erosion Modelling from JET and PISCES-B to ITER	208
EX/P1-15	M. Mayer, <i>et al.</i>,	Erosion and Deposition in the JET Divertor During the ITER-Like Wall Campaigns	209
EX/P1-16	B. Viola, <i>et al.</i>,	The Impact of Poloidal Flux Expansion on JET Divertor Radiation Performance	210
EX/P1-17	M. Rubel, <i>et al.</i>,	First Mirror Test in JET for ITER: Complete Overview After Three Campaigns in JET with ITER-Like Wall	211
EX/P1-18	I. E. Garkusha, <i>et al.</i>,	Influence of Magnetic Field on Plasma Energy Transfer to Material Surfaces in ELM Simulation Experiments with QSPA-M212	
EX/P1-19	C. Theiler, <i>et al.</i>,	SOL Transport and Detachment in Alternative Divertor Configurations in TCV L- and H-Mode Plasmas	213
EX/P1-20	G. Grenfell, <i>et al.</i>,	On the Role of Radial Electric Fields on Turbulence Spreading in the Plasma Boundary of Fusion Devices	214
EX/P1-21	I. Furno, <i>et al.</i>,	Basic Studies of the Interaction of Blobs with Suprathermal Ions and Millimetre-Wave Beams in the TORPEX Device . .	215

EX/P1-22	C. Sozzi, <i>et al.</i>, Early Identification of Disruption Paths for Prevention and Avoidance	216
EX/P1-23	S. Jachmich, <i>et al.</i>, Minimizing Power Load Asymmetries During Disruption Mitigation at JET	218
EX/P1-24	S. N. Gerasimov, <i>et al.</i>, Overview of Disruptions with JET-ILW	219
EX/P1-25	M. Kong, <i>et al.</i>, Control of NTMs and Integrated Multiactuator Control on TCV	220
EX/P1-26	O. Ficker, <i>et al.</i>, Runaway Electron Beam Stability and Decay in COMPASS	221
EX/P1-28	S. E. Sharapov, <i>et al.</i>, Plasma and Diagnostics Preparation for α -Particle Studies in JET DT	222
EX/P1-29	C. C. Klepper, <i>et al.</i>, Subdivertor Fuel Isotopic Content Detection Limit for JET and Impact on the Control of ICRH for JET-ILW and JET-DT Operation	223
EX/P1-30	C. Piron, <i>et al.</i>, Extension of the Operating Space of High- β_N Fully Noninductive Scenarios on TCV Using Neutral Beam Injection	224
EX/P1-31	V. Huber, <i>et al.</i>, The Software and Hardware Architecture of the Real-Time Protection of In-Vessel Components in JET-ILW	225
EX/P2-1	D. F. Kong, <i>et al.</i>, $E_r \times B$ Shear Effect on Cross Phase Mitigates ELM at High Collisionality	226
EX/P2-3	L. Zhang, <i>et al.</i>, Tungsten Control in NBI-Dominant H-Mode Discharges in EAST Tokamak	227
EX/P2-4	G. S. Xu, <i>et al.</i>, A Promising Grassy ELM Regime for High-Performance Steady-State Operations with Metal Wall in EAST and CFETR228	
EX/P2-5	M. Sharma, <i>et al.</i>, Leak Width in a Multicusp Field Configuration: A Revisit with a Versatile Experimental Device	229
EX/P2-6	U. Kumar, <i>et al.</i>, Effect of the Controlled Density Gradient on Equilibrium and Confinement in a Simple Toroidal Device with Two Plasma Sources	230

EX/P2-7	M. Kumar, <i>et al.</i>, Imaging of SST-1 Plasma with LHCD Power	231
EX/P2-8	L. Wang, <i>et al.</i>, Advances in Plasma-Wall Interaction Control for H-Mode Operation over 100 s with ITER-like Tungsten Divertor on EAST	232
EX/P2-9	J. Pramanik, <i>et al.</i>, Characterization of Particle Growth and Enhancement of Sputtering Yields in a Cogenerated Dusty Plasma	233
EX/P2-10	P. Sharma, <i>et al.</i>, A Transmission Electron Microscopy Investigation of Defects Induced in Tungsten Foils by Au and B Ion Irradiation	234
EX/P2-11	M. Himabindu, <i>et al.</i>, Modelling Studies of X-Divertor Configuration on SST-1 Toka- mak Using SOLPS5.1	235
EX/P2-12	P. J. Sun, <i>et al.</i>, Experimental Study of Multiscale Interaction between (In- termediate, Small)-Scale Microturbulence and MHD Modes in EAST Plasmas	236
EX/P2-13	M. P. Bhuva, <i>et al.</i>, Effect of Cathode Geometry on Magnetically Coupled Hol- low Cathode Plasma Source	237
EX/P2-14	L. Xu, <i>et al.</i>, Kink Mode Study in EAST High- β_P Plasma	238
EX/P2-15	J. Huang, <i>et al.</i>, Fast-Ion Studies in High Performance Fully Noninductive Discharges on EAST	239
EX/P2-16	A. Ekedahl, <i>et al.</i>, Progress Towards Development of Long Pulse ITER Opera- tion through RF Heated H-Mode Experiments on EAST and HL-2A	240
EX/P2-17	C. Mallick, <i>et al.</i>, Observations of Plasma Stimulated Electrostatic Sideband Emission and Harmonic Distortion: Evidence of Overdense Plasma Generation Inside a Microwave Discharge Ion Source	241
EX/P2-18	S. Das, <i>et al.</i>, Radial Characteristics of a Magnetized Plasma Column	242
EX/P2-20	P. Srivastav, <i>et al.</i>, Investigations on Temperature Fluctuations and Energy Trans- port in ETG Dominated Large Laboratory Plasma	243

EX/P2-22	D. Rathi, <i>et al.</i>, Preliminary Results of Wall Conditioning Experiments Using High Power ICRH System on SST-1 at Different Toroidal Magnetic Fields	244
EX/P2-23	L. Soto, <i>et al.</i>, Recent Finding in Fusion Studies Using Table Top and Minia- turized Dense Plasma Focus Devices Operating from Hun- dred Joules to less than One Joule	245
EX/P2-26	D. Moreau, <i>et al.</i>, Model-Predictive Kinetic Control for Steady State Plasma Operation Scenarios on EAST	246
EX/P2-27	J. Prompting, <i>et al.</i>, Simulation Study of Heat Transport with On-Off Axis ICRH in Thailand Tokamak Using BALDUR Code	247
EX/P3-1	M. Yoshikawa, <i>et al.</i>, Fluctuation Suppression by the Potential Formation in GAMMA 10/PDX Plasma	248
EX/P3-2	T. Minami, <i>et al.</i>, Effect of Magnetic Field Structure on Electron Internal Trans- port Barrier and its Role for the Barrier Formation in Heliotron J	249
EX/P3-3	S. Ohshima, <i>et al.</i>, The Configuration Dependence of Isotope Effects on Turbu- lence System in Heliotron J	250
EX/P3-4	K. Kamiya, <i>et al.</i>, Multiple Turbulent Plasma States in the H-Mode Transition on JT-60U	251
EX/P3-5	H. Yamada, <i>et al.</i>, Characterization of Isotope Effect on Confinement of Dimen- sionally Similar NBI-Heated Plasmas in LHD	252
EX/P3-6	K. Tanaka, <i>et al.</i>, Isotope Effects on Confinement and Turbulence in ECRH Plasma of LHD	253
EX/P3-7	T. Tokuzawa, <i>et al.</i>, Rapid Radial Propagation of Momentum Change and Flow Oscillation Associated with a Pellet Injection	254
EX/P3-8	M. Nishiura, <i>et al.</i>, Experimental Analysis of Self-Organized Structure and Trans- port on Magnetospheric Plasma Device RT-1	255
EX/P3-9	N. Ezumi, <i>et al.</i>, Synergistic Effect of Impurity and Hydrogen Gas Puffs on Plasma Detachment in the GAMMA 10/PDX Tandem Mirror	256

EX/P3-10	M. Kobayashi, <i>et al.</i>, Core Transport Improvement in Stable Detachment with RMP Application to the Edge Stochastic Layer of LHD . . .	257
EX/P3-11	T. Oishi, <i>et al.</i>, Effect of Deuterium Plasmas on Carbon Impurity Transport in the Edge Stochastic Magnetic Field Layer of Large Helical Device	258
EX/P3-12	K. Hanada, <i>et al.</i>, Particle Balance Investigation with the Combination of Rate Equations of Hydrogen State and Hydrogen Barrier Model in Long Duration Discharges on All-Metal PFW QUEST . .	259
EX/P3-13	Y. H. Ding, <i>et al.</i>, Recent Progresses on the RMP Researches Towards Active Control of Tearing Mode in the J-TEXT Tokamak	260
EX/P3-14	Y. Suzuki, <i>et al.</i>, Investigation of Magnetic Topology on Spontaneous Transition Phenomena for High- β Plasma of Large Helical Device	261
EX/P3-15	K. Y. Watanabe, <i>et al.</i>, Dependence of RMP Penetration Threshold on Plasma Pa- rameters and Ion Species in Helical Plasmas	262
EX/P3-16	Y. Takemura, <i>et al.</i>, Study of Locking Mechanism of Locked-Mode-Like Instabil- ity in Helical Plasmas	263
EX/P3-17	M. Nagata, <i>et al.</i>, Experimental Studies of Plasmoid Reconnection for Closed Flux Current Generated by Coaxial Helicity Injection on HIST264	
EX/P3-19	H. Tanaka, <i>et al.</i>, Electron Bernstein Wave Heating and Current Drive with Multielectron Cyclotron Resonances During Noninductive Start-Up on LATE	265
EX/P3-20	K. Ogawa, <i>et al.</i>, Energetic-Ion Confinement Studies by Using Comprehensive Neutron Diagnostics in the Large Helical Device	266
EX/P3-21	H. Idei, <i>et al.</i>, Fully Noninductive 2nd Harmonic Electron Cyclotron Cur- rent Ramp-Up with Focussed Polarized Beams in the QUEST Spherical Tokamak	267
EX/P3-22	H. Tanabe, <i>et al.</i>, Investigation of Fine Structure Formation of Guide Field Reconnection During Merging Plasma Startup of Spherical Tokamak in TS-3U	268

EX/P3-23	A. Ejiri, <i>et al.</i>, Plasma Current Generation and Ramp-Up by the Lower Hybrid Wave Using Outboard-Launch and Top-Launch Antennas on the TST-2 Spherical Tokamak	269
EX/P3-24	Y. Ono, <i>et al.</i>, Scaling Study of Reconnection/Merging Heating of Spherical Tokamak Plasmas for Direct Access to Burning Plasma	270
EX/P3-25	T. Wakatsuki, <i>et al.</i>, Safety Factor Profile Control with Reduced CS Flux Consumption During Plasma Current Ramp-Up Phase Using Reinforcement Learning Technique	271
EX/P3-26	G. De Tommasi, <i>et al.</i>, 2D and 3D Modelling of JT-60SA for Disruptions and Plasma Start-Up	272
EX/P3-27	G. Motojima, <i>et al.</i>, New Approach to the Control of Particle Recycling Using Divertor Pumping in LHD	273
EX/P4-1	A. Sinha, <i>et al.</i>, Broadband Characterization of High Temperature Blackbody Source with Fourier Transform Michelson Interferometer for ECE Measurements	274
EX/P4-2	U. C. Nagora, <i>et al.</i>, Design and Development of 140 GHz D-Band Phase-Locked Heterodyne Interferometer System for Real-Time Density Measurement	275
EX/P4-3	S. Patel, <i>et al.</i>, Study of Iron Impurity Behaviour Using VUV Spectroscopy in ADITYA and ADITYA-U Tokamak	276
EX/P4-4	S. Banerjee, <i>et al.</i>, Runaway Electron (RE) Mitigation Using Supersonic Molecular Beam Injection in the ADITYA-U Tokamak	277
EX/P4-5	M. B. Chowdhuri, <i>et al.</i>, Neon Gas Seeded Radiative Improved Mode in ADITYA-U Tokamak	278
EX/P4-6	R. Manchanda, <i>et al.</i>, Impurity Screening in High Density ADITYA Tokamak Plasmas	279
EX/P4-7	K. Tahiriani, <i>et al.</i>, Radiation Power Loss Study During Gas Puff Induced Disruptions in ADITYA-U Tokamak	280
EX/P4-9	K. Shah, <i>et al.</i>, Observations of Intrinsic Toroidal Rotation Using X-Ray Crystal Spectrometer in ADITYA-U Tokamak	281

EX/P4-10	G. Shukla, <i>et al.</i>, Controlling Plasma Rotation Using Periodic Gas-Puff in ADITYA-U Tokamak	282
EX/P4-11	L. T. Lachhvani, <i>et al.</i>, Effect of Externally Applied Radial Electric Field (Biased-Electrode) on Geodesic Acoustic Modes in SINP Tokamak	283
EX/P4-12	S. Akkireddy, <i>et al.</i>, Application of TEM to Study the Changes in Subsurface Defects in Tungsten Samples as a Function of Annealing Temperature	284
EX/P4-13	N. Yadav, <i>et al.</i>, Effect of Multiple Periodic Gas Puff on Neutral Temperature in ADITYA-U Tokamak	285
EX/P4-14	P. Pandit, <i>et al.</i>, Design of a NIR Spectrometer for ADITYA-U Tokamak and Initial Results	286
EX/P4-15	S. Mishra, <i>et al.</i>, Mass Dependent Impurity Transport Study in ADITYA Tokamak	287
EX/P4-16	A. Kanik, <i>et al.</i>, Plasma Potential Measurements in the Edge Region of ADITYA-U Tokamak Using Reciprocating Laser Heated Emissive Probes	288
EX/P4-17	T. Macwan, <i>et al.</i>, Edge Current Density Profile Measurement Using an Array of Miniature Magnetic Probes in ADITYA-U Tokamak	289
EX/P4-18	J. V. Raval, <i>et al.</i>, Development of Multipurpose Soft X-Ray Tomography System for ADITYA-U	290
EX/P4-19	J. J. U. Buch, <i>et al.</i>, Ka-Band Reflectometer System for Measuring Radial Electron Density Profile at IPR	291
EX/P4-20	J. K. Joshi, <i>et al.</i>, Experimental Investigation of Power Coupling by RF Antenna into Plasmas in Presence of Magnetized Ions	292
EX/P4-21	S. P. Pandya, <i>et al.</i>, A Diagnostic Approach for the Detection of Spatially Distributed Low Energy Confined Runaway Electrons in the ADITYA-U Tokamak by Means of Synchrotron Emission Imaging in the Sub-Millimetre Wavelength Band	293
EX/P4-22	J. Kumar, <i>et al.</i>, Design and Testing of X-Mode Reflectometry System for Coupling Studies of Lower Hybrid Waves in ADITYA-U Tokamak	294

EX/P4-23	S. Aggarwal, <i>et al.</i>, Design and Development of Passive Charge Exchange Neu- tral Particle Analyser for ADITYA-U Tokamak	295
EX/P4-24	L. M. Awasthi, <i>et al.</i>, Excitation of Electron Temperature Gradient (ETG) Turbu- lence and Effect on Plasma Transport in LVPD	296
EX/P4-25	K. Ajay, <i>et al.</i>, ADITYA Experimental Results of Core Ion Temperature Mea- surements on ADITYA Tokamak Using Four Channel Neu- tral Particle Analyser	297
EX/P4-26	P. K. Srivastava, <i>et al.</i>, Chord Average Density Measurement Using Microwave In- terferometry in LVPD	298
EX/P4-27	A. K. Sanyasi, <i>et al.</i>, Investigations on Growth of Quasi-Longitudinal (QL) Whistlers with Energy Scaling of Energetic Electrons in LVPD	299
EX/P4-28	K. K. Mishra, <i>et al.</i>, Fast Wave Induced ICRF Plasma Expansion in ADITYA Torus300	
EX/P4-29	N. Patel, <i>et al.</i>, Gas Fuelling Control System of ADITYA Tokamak	301
EX/P4-30	R. Rajpal, <i>et al.</i>, Integrated System Electronics and Instrumentation; Opera- tion and Diagnostic for ADITYA-U Tokamak	302
EX/P4-31	S. Aich, <i>et al.</i>, Plasma Column Position Measurements Using Magnetic Di- agnostics in ADITYA-U Tokamak	303
EX/P5-2	G. S. Kurskiev, <i>et al.</i>, Thermal Energy Confinement at the Globus-M Spherical Tokamak	304
EX/P5-3	W. Z. Zhong, <i>et al.</i>, Plasma Confinement and Pedestal Dynamics Responses to Impurity Seeding in HL-2A H-Mode Plasmas	305
EX/P5-4	M. Jiang, <i>et al.</i>, Localized Modulation of Turbulence by Magnetic Islands on HL-2A Tokamak	306
EX/P5-6	J. Cheng, <i>et al.</i>, Pedestal Dynamics in Inter-ELM Phase on HL-2A Tokamak	307
EX/P5-8	Y. P. Zhang, <i>et al.</i>, Effect of LBO-Seeded Impurity on ELMs in the HL-2A Tokamak	308
EX/P5-9	W. Mao, <i>et al.</i>, Characteristics of Electromagnetic Turbulence on KTX Ex- periment Device	309

EX/P5-10	A. V. Melnikov, <i>et al.</i>, Electric Potential and Turbulence in OH and ECRH Low-Density Plasmas	310
EX/P5-13	L. N. Khimchenko, <i>et al.</i>, Ecton Mechanism of Energy Load on ITER-Grade Tungsten Limiter T-10 Tokamak and Forecast for ITER	311
EX/P5-15	X. Q. Ji, <i>et al.</i>, Nonlinear Evolution of Multihelicity Neoclassical Tearing Modes in HL-2A Low Rotation Plasmas	312
EX/P5-16	D. V. Ryzhakov, <i>et al.</i>, Peculiar Properties of Disruptions on T-10 Tokamak at Different Edge Safety Factor Values	313
EX/P5-19	P. W. Shi, <i>et al.</i>, Energetic-Ion Driven Toroidal and Global Alfvén Eigenmodes on HL-2A	314
EX/P5-20	W. Chen, <i>et al.</i>, Suppression and Destabilization of Ion Fishbone Activities on HL-2A	315
EX/P5-21	M. R. Nurgaliev, <i>et al.</i>, Influence of Electron Cyclotron Resonance Heating on Ion Heat Conductivity in T-10 Plasma	316
EX/P5-23	Y. Xu, <i>et al.</i>, Physics and Engineering Design for Chinese First Quasi-Axisymmetric Stellarator(CFQS)	317
EX/P5-25	V. V. Prikhodko, <i>et al.</i>, Stability and Confinement Studies in the Gas Dynamic Trap	318
EX/P5-26	A. V. Burdakov, <i>et al.</i>, Plasma Transport in Linear and Helical Multiple-Mirror Systems	319
EX/P5-27	L. W. Yan, <i>et al.</i>, Real-Time Control System of Neoclassical Tearing Modes in the HL-2A Tokamak	320
EX/P5-28	Y. Liu, <i>et al.</i>, Development of the $q = 1$ Advanced Tokamak Scenarios in HL-2A	321
EX/P5-30	X. M. Song, <i>et al.</i>, First Plasma Scenario Development for HL-2M	322
EX/P6-1	J. S. deGrassie, <i>et al.</i>, DIII-D Shaping Demonstrates Correlation of Intrinsic Momentum with Energy	323
EX/P6-2	A. Diallo, <i>et al.</i>, ELMs Onset Triggered by Mode Coupling Near Rational Surfaces in the Pedestal	324

EX/P6-3	B. A. Grierson, <i>et al.</i>, Rotation Profile Hollowing in DIII-D Low-Torque Electron-Heated H-Mode Plasmas	325
EX/P6-4	F. M. Laggner, <i>et al.</i>, The Universality of Inter-ELM Pedestal Fluctuations in AUG and DIII-D: Impacting the Edge Profile Structure by Clamping of the Gradients	326
EX/P6-5	S. Mordijck, <i>et al.</i>, Particle Transport from the Bottom Up	327
EX/P6-6	M. E. Austin, <i>et al.</i>, High Confinement in Negative Triangularity Discharges in DIII-D	328
EX/P6-8	L. F. Delgado-Aparicio, <i>et al.</i>, Rotation-Induced Electrostatic-Potentials and Density Asymmetries in NSTX	329
EX/P6-9	D. Brunner, <i>et al.</i>, Extending the Boundary Heat Flux Width Database to 1.3 Tesla Poloidal Magnetic Field in the Alcator C-Mod Tokamak	330
EX/P6-10	H. Y. Guo, <i>et al.</i>, Development and First Experimental Tests of a Small Angle Slot Divertor on DIII-D	331
EX/P6-11	T. W. Petrie, <i>et al.</i>, High Performance Double-Null Plasmas Under Radiating Divertor and Mantle Scenarios on DIII-D	332
EX/P6-12	A. W. Leonard, <i>et al.</i>, Parallel Energy Transport in Detached DIII-D Divertor Plasmas	333
EX/P6-13	T. Abrams, <i>et al.</i>, Inter vs. Intra-ELM Tungsten Erosion and Transport from the Divertor in DIII-D High-Performance H-Mode Discharges	334
EX/P6-14	M. E. Fenstermacher, <i>et al.</i>, The Effect of RMP ELM Control for ITER on Pedestal Pressure Compared to EPED No-RMP Predictions	335
EX/P6-15	A. G. McLean, <i>et al.</i>, Quantification of Radiating Species in the DIII-D Divertor in the Transition to Detachment Using Extreme Ultraviolet Spectroscopy	336
EX/P6-16	E. A. Unterberg, <i>et al.</i>, Measurements of High-Z Divertor Impurity Sourcing and Divertor Leakage Using Isotopic Tungsten Tracer Sources in DIII-D	337
EX/P6-17	D. M. Orlov, <i>et al.</i>, Favourable Impact of RMP ELM Suppression on Divertor Heat Fluxes at ITER-like Conditions	338

EX/P6-18	E. T. Hinson, <i>et al.</i>, Enhancement of Helium Exhaust During Suppression of Edge Localized Modes by Resonant Magnetic Perturbation Fields at DIII-D	339
EX/P6-19	T. M. Wilks, <i>et al.</i>, Access Requirements for Stationary ELM-Suppressed Pedestals in DIII-D and C-Mod Plasmas	340
EX/P6-20	R. S. Granetz, <i>et al.</i>, Machine Learning for Disruption Warning on Alcator C- Mod, DIII-D, and EAST Tokamaks	341
EX/P6-21	J. L. Barr, <i>et al.</i>, Fast ITER-Relevant Low-Disruptivity Ramp-Downs in DIII-D and EAST	342
EX/P6-22	N. W. Eidietis, <i>et al.</i>, Implementing a Finite-State Off-Normal and Fault Response System for Robust Disruption Avoidance in Tokamaks	343
EX/P6-23	J. Herfindal, <i>et al.</i>, Injection of Multiple Shattered Pellets for Disruption Mitiga- tion in DIII-D	344
EX/P6-24	M. W. Shafer, <i>et al.</i>, Observation of Multiple Helicity Mode-Resonant Locking Leading to a Disruption on DIII-D	345
EX/P6-25	M. Okabayashi, <i>et al.</i>, Critical Processes of Tearing Mode Entrainment in the Pres- ence of a Static Error Field	346
EX/P6-26	S. A. Sabbagh, <i>et al.</i>, Disruption Event Characterization and Forecasting in Toka- maks	347
EX/P6-28	S. G. Baek, <i>et al.</i>, Observation of Efficient Lower Hybrid Current Drive at High Density on Alcator C-Mod	348
EX/P6-29	K. E. Thome, <i>et al.</i>, High-Frequency Energetic Particle Driven Instabilities and their Implications for Burning Plasmas	349
EX/P6-30	B. Van Compernelle, <i>et al.</i>, Fast Wave Experiments in LAPD in Support of Fusion	350
EX/P6-32	E. D. Fredrickson, <i>et al.</i>, Global Alfvén Eigenmode Stability Dependence on Fast-Ion Distribution Function	351
EX/P6-33	D. Kim, <i>et al.</i>, Investigation of Fast Particle Redistribution Induced by Saw- tooth Instability in NSTX-U	352

EX/P6-34	M. W. Bongard, <i>et al.</i>, Advancing Local Helicity Injection for Nonsolenoidal Tokamak Startup	353
EX/P6-36	C. B. Forest, <i>et al.</i>, Development of a High-Flux Fusion Neutron Source Using Recent Advances in Technology	354
EX/P6-37	C. K. Lau, <i>et al.</i>, First Simulations of Turbulent Transport in the Field-Reversed Configuration	355
EX/P6-38	M. D. Boyer, <i>et al.</i>, Dynamic Neutral Beam Injection as a Mechanism for Plasma Control and an Actuator for Instability Drive	356
EX/P6-39	E. Schuster, <i>et al.</i>, Physics-Model-Based Real-Time Optimization for the Development of Steady-State Scenarios at DIII-D	357
EX/P6-40	N. M. Ferraro, <i>et al.</i>, Error Field Impact on Mode Locking and Divertor Heat Flux in NSTX-U	358
EX/P7-1	G. Verdoolaege, <i>et al.</i>, First Analysis of the Updated ITPA Global H-Mode Confinement Database	359
EX/P7-3	J. Jo, <i>et al.</i>, Time Resolved Triton Burnup Measurements Using the Scintillating Fibre Detector on KSTAR	360
EX/P7-4	S. G. Lee, <i>et al.</i>, Intrinsic Toroidal Rotation for Ohmic L-Mode Plasmas in KSTAR	361
EX/P7-5	S.-W. Yoon, <i>et al.</i>, The Effect of Electron Cyclotron Heating on Thermal and Fast-Ions Transport in High- β -Poloidal Discharges at KSTAR	362
EX/P7-7	J.-S. Park, <i>et al.</i>, Characteristics of Asymmetric (Low-Field-Side and High-Field Side) Divertor Detachment in KSTAR L-Mode Plasmas	363
EX/P7-8	J. J. Jang, <i>et al.</i>, ELM Suppression and Internal Transport Barrier Formation by Krypton Seeding in KSTAR Plasmas	364
EX/P7-9	I. Song, <i>et al.</i>, Experimental Observation and Modelling of High-Z Impurity Transport by Tungsten Powder Injection in KSTAR Plasmas	365
EX/P7-10	S.-H. Hong, <i>et al.</i>, Observation of Heat Load on the Castellated Tungsten Block by Back-Scattered Particles from Intentionally Misaligned Protruding Edge	366

EX/P7-11	C. Xiao, <i>et al.</i>, Effects of Lithium Coating of Chamber Wall on the STOR-M Tokamak Discharges	367
EX/P7-12	M. Lehnen, <i>et al.</i>, R&D for Reliable Disruption Mitigation in ITER	368
EX/P7-13	J. Lee, <i>et al.</i>, Bifurcation of Perpendicular Rotation and Field Penetration at the Transition to RMP-Induced ELM-Crash Suppression .	369
EX/P7-14	J. Kim, <i>et al.</i>, Evolution of Locked Mode Under the Existence of Nonaxisymmetric Fields in KSTAR	370
EX/P7-15	Y. M. Jeon, <i>et al.</i>, Experimental Observations of the Plasma Shape Effect on the RMP-ELM Coupling for Optimization of the KSTAR ELM-Crash Control	371
EX/P7-16	Y.-S. Park, <i>et al.</i>, Stability, Transport, and Active MHD Mode Control Analysis of KSTAR High Performance Plasmas Supporting Disruption Avoidance	372
EX/P7-17	M. Inomoto, <i>et al.</i>, Effects of Reconnection Downstream Conditions on Electron Parallel Acceleration during Merging Start-Up of Spherical Tokamak	373
EX/P7-18	V. I. Vargas-Blanco, <i>et al.</i>, Conversion of Electrostatic Bernstein Waves in the SCR-1 Stellarator Using a Full Wave Code	374
EX/P7-19	S.-H. Kim, <i>et al.</i>, Power Coupling of Lower Hybrid Fast Wave in VEST	375
EX/P7-20	T. Asai, <i>et al.</i>, Collisional Merging of a Field-Reversed Configuration in the FAT-CM Device	376
EX/P7-21	H. Y. Lee, <i>et al.</i>, Solenoid-Free Start-Up Utilizing Outer PF Coils with the Help of EBW Preionization and Change of External Inductance in VEST	377
EX/P7-22	J.-H. Yang, <i>et al.</i>, Internal Structure of MHD Fluctuations for Various Current Density Profiles during Current Rise Phase of Ohmic Discharge in VEST	378
EX/P7-23	A. Loarte, <i>et al.</i>, Advances in Modelling of Plasma Pedestal Behaviour and ELM Control in ITER Reference Plasma Scenarios	379

EX/P7-24	H. Anand, <i>et al.</i>, Implementation of 3D Effects of the ITER Plasma-Facing Components in a 2D Real-Time Model-Based Approach for Wall Heat Flux Control on ITER	380
EX/P7-25	F. Köchl, <i>et al.</i>, Optimizing the ITER 15 MA DT Baseline Scenario by Ex- ploiting a Self-Consistent Free-Boundary Core-Edge-SOL Workflow in IMAS	381
EX/P7-26	A. Pajares, <i>et al.</i>, Robust Burn Control in ITER Under Deuterium-Tritium Con- centration Variations in the Fuelling Lines	382
EX/P7-27	F. M. Poli, <i>et al.</i>, The ITER Plasma Current Termination Phase: Physics Con- straints on Control	383
EX/P8-1	A. Kappatou, <i>et al.</i>, Energy Confinement and Performance of Pure Helium Plas- mas and Helium Seeded Deuterium Plasmas	384
EX/P8-2	M. G. Dunne, <i>et al.</i>, Impact of Impurity Seeding on Pedestal Structure in ASDEX- Upgrade and Alcator C-Mod	386
EX/P8-3	F. Ryter, <i>et al.</i>, Heat Transport Driven by the ITG and TEM Instabilities in the ASDEX-Upgrade Tokamak	387
EX/P8-4	T. Pütterich, <i>et al.</i>, The ITER Baseline Scenario Investigated at ASDEX-Upgrade	388
EX/P8-5	E. Viezzer, <i>et al.</i>, ELM-Induced Energy and Momentum Transport in ASDEX- Upgrade	389
EX/P8-6	L. Marrelli, From RFX-Mod to RFX-Mod2: Perspectives of the Reversed Field Pinch Configuration	390
EX/P8-7	R. Cavazzana, Challenges and Solutions in the Design of RFX-Mod2, a Mul- ticonfiguration Magnetic Confinement Experimental Device	391
EX/P8-8	S. A. Bozhnikov, <i>et al.</i>, High Density and High Performance Operation with Pellet Injection in W7-X	392
EX/P8-9	O. Grulke, Plasma Dynamics and Transport Studies in Wendelstein 7-X	393
EX/P8-11	C. Silva, <i>et al.</i>, IST Contributions to the ASDEX-Upgrade Edge and Divertor Physics Using Microwave Reflectometry	394

EX/P8-12	B. A. Unterberg, <i>et al.</i>, Characterization of Advanced Concepts for First Wall Materials by Plasma Exposure in the Linear Plasma Device PSI-2	395
EX/P8-13	N. Vianello, <i>et al.</i>, SOL Transport and Filamentary Dynamics in High Density Tokamak Regimes	396
EX/P8-14	P. Scarin, <i>et al.</i>, Helical Plasma-Wall Interaction in the RFX-Mod: Effects of High- n Mode Locking	398
EX/P8-15	S. C. Liu, <i>et al.</i>, The Effects of Magnetic Topology on the SOL Island Structure and Turbulence Transport in the First Divertor Plasma Operation of W7-X	399
EX/P8-16	M. W. Jakubowski, <i>et al.</i>, 3D Heat and Particle Fluxes in Wendelstein 7-X	400
EX/P8-17	R. Brakel, <i>et al.</i>, Strategy and Optimization of Wall Conditioning at the Wendelstein 7-X Stellarator	401
EX/P8-18	C. Killer, <i>et al.</i>, Characterization of the W7-X Scrape-Off Layer Using the Multipurpose Manipulator	402
EX/P8-19	J. D. Lore, <i>et al.</i>, Measurement and Modelling of Magnetic Configurations to Mimic Overload Scenarios in the W7-X Stellarator	403
EX/P8-20	M. Willensdorfer, <i>et al.</i>, Impact of the 3D Geometry from Nonaxisymmetric Magnetic Perturbations on the Local Edge Stability in ASDEX-Upgrade	404
EX/P8-21	V. Igochine, <i>et al.</i>, Seeding of Tearing Modes by Internal Crash Events in ASDEX-Upgrade and DIII-D Tokamaks	405
EX/P8-22	L. Frassinetti, <i>et al.</i>, Role of the Pressure Position on the Pedestal Stability in AUG, JET-ILW and TCV in Deuterium and Hydrogen Plasmas and Implications for ITER	406
EX/P8-23	J.-M. Noterdaeme, <i>et al.</i>, Ion Cyclotron Range of Frequency Power: Progress in Operation and Understanding for Experiments with Metallic Walls	407
EX/P8-24	B. Geiger, <i>et al.</i>, Fast-Ion Confinement in Low Collisionality Discharges at ASDEX-Upgrade and TCV	409

EX/P8-25	D. Rittich, <i>et al.</i>, Quantification of Neutral Beam Driven Current and the Effect of Radial Fast-Ion Transport in ASDEX-Upgrade	410
EX/P8-26	J. Galdon-Quiroga, <i>et al.</i>, Impact of an Edge Resonant Transport Layer on Fast-Ion Confinement in the ASDEX-Upgrade Tokamak	411
EX/P8-27	J. Ongena, <i>et al.</i>, Preparing the ICRH System for the Wendelstein 7-X Stellarator	413
EX/P8-28	H. P. Laqua, <i>et al.</i>, On a Path to Steady-State High-Performance Operation in W7-X: Heating, Current Drive and Fuelling Experiments with High Power ECRH	414
EX/P8-29	R. Majeski, <i>et al.</i>, The LTX- β Research Programme and First Results	415
EX/P8-30	A. Dinklage, <i>et al.</i>, Plasma Termination by Excess Fuel and Impurities in TJ-II, LHD and W7-X	416
TH:	Magnetic Confinement Theory and Modelling	417
TH/1-1	W. Shen, <i>et al.</i>, Simulations of Energetic Particle Driven Instabilities and Fast Particle Redistribution in EAST Tokamak	418
TH/1-2	Y. Todo, Critical Fast Ion Distribution in Phase Space for the Synchronized Sudden Growth of Multiple Alfvén Eigenmodes and the Global Transport of Fast Ions	419
TH/2-1	S.-H. Ku, <i>et al.</i>, A Gyrokinetic Discovery of Fast L-H Bifurcation Physics in a Realistic, Diverted, Tokamak Edge Geometry	420
TH/2-2	M. T. Kotschenreuther, <i>et al.</i>, Gyrokinetic Analysis and Simulations of Pedestals	421
TH/3-1	J. Garcia, <i>et al.</i>, First Principles and Integrated Modelling Achievements Towards Trustful Fusion Power Predictions for JET and ITER	422
TH/3-2	F. J. Casson, <i>et al.</i>, Predictive Multichannel Flux-Driven Modelling to Optimize ICRH Tungsten Control in JET	423
TH/4-1	J. R. Martín Solís, <i>et al.</i>, Runaway Electron Mitigation in ITER Disruptions by Injection of High-Z Impurities	425
TH/4-2	A. Matsuyama, <i>et al.</i>, Self-Consistent Runaway Beam Formation in 3D Magnetic Fields During Radiation-Driven Disruptions	426

TH/4-3	L. Carbajal, <i>et al.</i>,	
	Pitch Angle Dynamics and Synchrotron Emission of Run-	
	away Electrons in Quiescent and Disrupted DIII-D Plasmas	427
TH/4-4	H. Strauss, <i>et al.</i>,	
	Asymmetric Wall Force Reduction in ITER and JET Disruptions	428
TH/5-1	D. Chandra, <i>et al.</i>,	
	A Nonlinear 2-Fluid Study of the Effect of Pellet Injection on	
	ELM Dynamics	429
TH/6-1	M. Schneider, <i>et al.</i>,	
	Modelling Third Field Operation in the ITER Prefusion Power	
	Operation Phase	430
TH/6-2	E. M. Bass, <i>et al.</i>,	
	Predictions of α -Particle and Neutral-Beam Heating and	
	Transport in ITER Scenarios	432
TH/6-3	M. Weiland, <i>et al.</i>,	
	Real-Time Simulation of the NBI Fast-Ion Distribution	433
TH/7-1	F. Militello, <i>et al.</i>,	
	Predicting Scrape-Off Layer Profiles and Filamentary Trans-	
	port for Reactor Relevant Devices	434
TH/7-2	M. V. Umansky, <i>et al.</i>,	
	Study of Passively Stable, Fully-Detached Divertor Plasma	
	Regimes Attained in Innovative Long-Legged Divertor Con-	
	figurations	435
TH/8-1	J.-M. Kwon, <i>et al.</i>,	
	Gyrokinetic XGC1 Simulation Study of Magnetic Island Ef-	
	fects on Neoclassical and Turbulence Physics in a KSTAR	
	Plasma	436
TH/8-2	A. B. Altukhov, <i>et al.</i>,	
	Benchmarking of Full- f Global Gyrokinetic Modelling Re-	
	sults against the FT-2 Tokamak Doppler Reflectometry Data	
	Using Synthetic Diagnostics	437
TH/P1-1	M. Drevlak, <i>et al.</i>,	
	New Results in Stellarator Optimization	438
TH/P1-2	N. Kasuya, <i>et al.</i>,	
	Numerical Diagnostic to Investigate Poloidal Asymmetry in	
	Three-Dimensional Magnetic Configurations	439
TH/P1-3	S. Satake, <i>et al.</i>,	
	Effect of Magnetic Shear and the Finite Banana-Orbit Width	
	on the Neoclassical Toroidal Viscosity in Perturbed Tokamaks	440
TH/P1-4	L. E. Sugiyama,	
	Steady States for Nonaxisymmetric Rotating Toroidal Plasmas	441

TH/P1-5	F. Schluck, <i>et al.</i>, Plasma-Surface Related 3D Modelling Results for Wendel- stein 7-X and EAST	442
TH/P1-6	D. Schwörer, <i>et al.</i>, Influence of Neutral-Plasma Interactions on 3D Scrape-Off Layer Filaments	443
TH/P1-7	L. Li, <i>et al.</i>, Comparative Modelling of Plasma Boundary Corrugation due to the Application of 3D Fields with ELM Control Coils in Various ITER Scenarios	444
TH/P1-8	B. C. Lyons, <i>et al.</i>, Predict-First Analysis and Experimental Validation of MHD Equilibrium, Stability, and Plasma Response to 3D Magnetic Perturbations	445
TH/P2-1	D. Zarzoso, <i>et al.</i>, Transport Induced by Energetic Geodesic Acoustic Modes	446
TH/P2-2	U. Maurya, <i>et al.</i>, Burning Plasma Simulation with α -Particle Heating	447
TH/P2-3	H. He, <i>et al.</i>, Simulation of Toroidicity-Induced Alfvén Eigenmode Ex- cited by Energetic Ions in HL-2A Tokamak Plasmas	448
TH/P2-4	R. Kleiber, <i>et al.</i>, Global Gyrokinetic Multimodel Simulations of ITG and Alfvénic Modes for Tokamaks and the First Operational Phase of Wen- delstein 7-X	449
TH/P2-5	P. Garcia-Martinez, <i>et al.</i>, Reconstruction of MHD Modes for Energetic Particle Dy- namics Studies in Toroidal Equilibria with Arbitrary q Profiles	450
TH/P2-6	Z. Qiu, <i>et al.</i>, Nonlinear Decay and Plasma Heating by Toroidal Alfvén Eigenmodes	451
TH/P2-7	Y. Hou, <i>et al.</i>, Analysis of Energetic Particle Driven Toroidal Alfvén Eigen- modes in CFETR Baseline Scenario	452
TH/P2-8	A. Snicker, <i>et al.</i>, The Combined Effect of Neoclassical Tearing Modes and ELM Control Coils on Fast-Ions: Validation in AUG and Extrapolation for ITER	453
TH/P2-9	A. Biancalani, <i>et al.</i>, Self-Consistent Gyrokinetic Description of the Interaction between Alfvén Modes and Turbulence	454

TH/P2-10	G. Vlad, <i>et al.</i>, Comparison of Energetic Particle Radial Transport between Single- n and Multiple- n Simulations of Alfvénic Modes . . .	455
TH/P2-11	H. Wang, <i>et al.</i>, Simulations of Two Types of Energetic Particle Driven Geodesic Acoustic Modes and the Energy Channelling in the Large Helical Device Plasmas	456
TH/P2-12	R. Seki, <i>et al.</i>, Comprehensive Magnetohydrodynamic Hybrid Simulations of Fast Ion Losses due to the Fast Ion Driven Instabilities in the Large Helical Device	457
TH/P2-14	J. P. Graves, <i>et al.</i>, Advanced Energetic Ion and Impurity Ion Physics in 2D and 3D Magnetically Confined Plasmas	458
TH/P2-15	Y. V. Yakovenko, <i>et al.</i>, Simulations of the Sawtooth-Induced Redistribution of Fast Ions in JET and ITER	459
TH/P2-16	E. V. Belova, <i>et al.</i>, Numerical Simulations of GAE Stabilization in NSTX-U . . .	460
TH/P2-17	Z. Lin, <i>et al.</i>, Verification and Validation of Integrated Simulation of Ener- getic Particles in Toroidal Plasmas	461
TH/P4-1	A. K. Singh, <i>et al.</i>, Analysis of Electron Cyclotron Wave Assisted Plasma Start- Up in SST-1	462
TH/P4-2	T. Y. Xia, <i>et al.</i>, Simulations on the Particle and Heat Fluxes for the RF Heat- ing H-Mode on EAST	463
TH/P4-5	T. Kurki-Suonio, <i>et al.</i>, Beam Ion Performance and Power Loads in the ITER Prefu- sion Power Operating Scenarios (PFPO) with Reduced Field and Current	464
TH/P4-6	P. Aleynikov, <i>et al.</i>, ECRH and Mode Conversion in Overdense W7-X Plasmas .	465
TH/P4-7	A. Kuley, <i>et al.</i>, Global PIC Simulation of RF Waves in Toroidal Geometry .	466
TH/P4-8	J. K. Atul, <i>et al.</i>, Mode Converted Electrostatic Nonlinear Ion-Ion Hybrid Mode in Tokamak Plasma	467
TH/P4-9	S. Usami, <i>et al.</i>, Particle Simulation Studies on Ion Effective Heating through Merging Plasmas	468

TH/P4-10	E. Z. Gusakov, <i>et al.</i>, Anomalous Absorption and Emission in ECRH Experiments due to Parametric Excitation of Localized UH Waves	469
TH/P4-11	P. V. Minashin, <i>et al.</i>, Modelling of Electron Cyclotron Resonance Heating and Current Drive in the T-15-MD Tokamak with GENRAY and CQL3D Codes	470
TH/P4-12	A. K. Ram, <i>et al.</i>, Theoretical and Computational Studies on the Scattering of Radiofrequency Waves by Fluctuations	471
TH/P4-13	N. Bertelli, <i>et al.</i>, The Impact of the Hydrogen Species on the HHFW Perfor- mance with Possible New NSTX-U Scenarios	472
TH/P5-1	C. A. Bowie, <i>et al.</i>, Sandpile Modelling of Pellet Pacing in Fusion Plasmas	473
TH/P5-3	R. Mukherjee, <i>et al.</i>, Numerical Relaxation of a 3D MHD Taylor-Woltjer State Subject to Abrupt Expansion	474
TH/P5-4	D. Sharma, <i>et al.</i>, ADITYA Up-Gradation Equilibrium Study	475
TH/P5-5	T. Moritaka, <i>et al.</i>, Gyrokinetic Modelling with an Extended Magnetic Equilib- rium Including the Edge Region of Large Helical Device . . .	476
TH/P5-6	J. Kim, <i>et al.</i>, Effects of Magnetic Perturbations on Magnetic Field Stochas- tication During Edge Pedestal Collapse	477
TH/P5-7	L. Shi, <i>et al.</i>, Roles of RMP-Induced Changes of Radial Electric Fields in ELM Suppression	478
TH/P5-8	B. Coppi, <i>et al.</i>, Endogenous Magnetic Reconnection and Associated Pro- cesses of Relevance to Fusion Burning Plasmas	479
TH/P5-9	R. Hager, <i>et al.</i>, Gyrokinetic-MHD Coupled Simulation of RMP Plasma Inter- action Reproduces Density Pump-Out Seen in the Tokamak Edge	480
TH/P5-10	T. Rafiq, <i>et al.</i>, Effects of Microtearing Modes on the Evolution of Electron Temperature Profiles in High Collisionality NSTX Discharges	481
TH/P5-11	Y. Patil, <i>et al.</i>, Electromagnetic Analysis of APPEL Linear Device Magnets	482

TH/P5-12	M. J. Hole, <i>et al.</i>, The Effect of Pressure Anisotropy on Ballooning Modes in Tokamak Plasmas	483
TH/P5-13	G. Z. Hao, <i>et al.</i>, Centrifugal Force Driven Low Frequency Modes in Spherical Tokamak	484
TH/P5-18	F. Liu, <i>et al.</i>, Nonlinear MHD Simulations of Quiescent H-Mode in ASDEX-Upgrade and ITER	485
TH/P5-19	Q. Yu, <i>et al.</i>, NTM Excitation by Sawtooth Crashes and the Suppression of Their Onset by Resonant Magnetic Perturbation	486
TH/P5-21	D. Chandra, <i>et al.</i>, Simulation of the Internal Kink Mode in Visco-Resistive Regimes	487
TH/P5-22	P. Zanca, <i>et al.</i>, A Power-Balance Model of Density Limit in Fusion Plasmas	488
TH/P5-23	L. Pigatto, <i>et al.</i>, Resistive Wall Mode Physics and Control Challenges in JT-60SA High- β_N Scenarios	489
TH/P5-24	S. Inoue, <i>et al.</i>, Nonlinear Dynamics of Tearing Mode Driven by Static and Rotating External 3D Fields	490
TH/P5-25	M. Sato, <i>et al.</i>, Ion Kinetic Effects on MHD Instabilities in High- β LHD Plasmas	491
TH/P5-26	G. Y. Park, <i>et al.</i>, Comparative Simulations of the Plasma Response to RMPs During ELM-Crash Mitigated and Suppressed Phases in KSTAR	492
TH/P5-27	R. Coelho, <i>et al.</i>, Plasma Equilibrium Reconstruction of JET Discharges Using the IMAS Modelling Infrastructure	493
TH/P5-28	W. A. Cooper, <i>et al.</i>, Nonlinearly Saturated Ideal Magnetohydrodynamic Equilibrium States with Periodicity-Breaking in Stellarators	494
TH/P5-30	Y. Liu, <i>et al.</i>, Role of NTV Particle Flux in Density Pumpout during ELM Control by RMP	495
TH/P5-31	L. J. Zheng, <i>et al.</i>, Negative Triangularity Effects on Tokamak MHD Stability	496

TH/P5-32	A. Reiman, <i>et al.</i>, Equilibrium Pressure-Driven Current in the Presence of a Small Magnetic Island: Singular Behaviour and Symmetry Effects	497
TH/P5-33	C. Ribeiro, Advances on the High Field Ultralow Aspect Ratio Tokamak	498
TH/P6-1	G. Q. Li, <i>et al.</i>, Transport Simulation of EAST Long Pulse Discharge and High- β_N Discharge with Integrated Modelling	499
TH/P6-4	L. Wang, <i>et al.</i>, Theory of Turbulence Driven Intrinsic Rotation and Current	500
TH/P6-5	T. Görler, <i>et al.</i>, En Route to High-Performance Discharges: Insights and Guidance from High-Realism Gyrokinetics	501
TH/P6-6	A. Bhattacharya, <i>et al.</i>, Application of the Semi-Implicit Numerical Method on the Radial Impurity Transport Equation and Determination of O^{4+} Emissivity with Two Separate PEC Databases	503
TH/P6-7	S. D. Pinches, <i>et al.</i>, Progress in the ITER Integrated Modelling Programme and the ITER Scenario Database	504
TH/P6-8	M. Nunami, <i>et al.</i>, Kinetic Simulation Studies on Multi-Ion-Species Plasma Trans- port in Helical Systems	505
TH/P6-9	E. Narita, <i>et al.</i>, Gyrokinetic Modelling of Turbulent Particle Fluxes towards Efficient Predictions of Density Profiles	506
TH/P6-10	L. Qi, <i>et al.</i>, Nonlinear Gyrokinetic Analysis of Linear Ohmic Confine- ment to Saturated Ohmic Confinement Transition	507
TH/P6-12	D. López-Bruna, <i>et al.</i>, Flux-Surface Averaged Radial Transport in Toroidal Plasmas with Magnetic Islands	508
TH/P6-13	S. Buller, <i>et al.</i>, Transport of Collisional Impurities with Flux-Surface Density Variation in Stellarator Plasmas	509
TH/P6-14	P. Strand, <i>et al.</i>, Towards a Predictive Modelling Capacity for DT Plasmas: European Transport Simulator (ETS) Verification and Vali- dation	510
TH/P6-15	B. Chatthong, <i>et al.</i>, Ion and Electron Temperature Predictions Based on Thailand Tokamak Plasmas Using CRONOS Code	511

TH/P6-16	O. Meneghini, <i>et al.</i>, Neural-Network Accelerated Coupled Core-Pedestal Simulations with Self-Consistent Transport of Impurities	512
TH/P6-17	W. X. Wang, <i>et al.</i>, Self-Driven Current Generation in Turbulent Fusion Plasmas	513
TH/P6-19	P. W. Terry, <i>et al.</i>, Scalings of Ion Temperature Gradient Turbulence and Transport	514
TH/P6-20	J. Dominski, <i>et al.</i>, Total- <i>f</i> Gyrokinetic Turbulent-Neoclassical Simulation of Global Impurity Transport and its Effect on the Main-Plasma Confinement	515
TH/P6-21	M. D. J. Cole, <i>et al.</i>, Confinement in Stellarators with the Global Gyrokinetic Code XGC	516
TH/P6-22	Z. H. Wang, <i>et al.</i>, Physics of Fast Component of Deuterium Gas Jet Injection in Magnetized Plasmas	517
TH/P6-23	N. K. Bisai, <i>et al.</i>, Dynamics of Neon Ions after Neon Gas Seeding and Puffing into Tokamak Plasma	518
TH/P6-24	G. Telesca, <i>et al.</i>, Numerical Simulation of High Neutron Rate JET-ILW DD Pulses in View of Extension to DT Experiments	519
TH/P6-25	S. Sangaroon, <i>et al.</i>, Parametric Study of the Impurity Profile in the Thailand Tokamak	520
TH/P6-26	S. Nowak, <i>et al.</i>, Analysis and Modelling of NTMs Dynamics in JET Discharges Using the European Transport Simulator (ETS) and Integrated Modelling Tools	521
TH/P6-28	D. Mandal, <i>et al.</i>, Study of Evolution of Trapped Particle Undamped Coherent Structures: An Important Agent in Intermittent Plasma Turbulence and Anomalous Transport	523
TH/P6-29	H. Yamaguchi, <i>et al.</i>, Simulation Study of Electrostatic Potential Generated by NBI and its Effect on the Neoclassical Transport of Carbon Impurity Ions in LHD	524
TH/P6-30	J. J. Martinell, <i>et al.</i>, Weak Turbulence Transport with Background Flows Using Mapping Techniques Including Finite Larmor Radius Effects	525

TH/P7-1	G. Dif-Pradalier, <i>et al.</i>, Poloidal Flows, Asymmetries and Multiscale Organization in Interplaying Core-Edge-SOL Turbulent Plasmas	526
TH/P7-2	R. J. Buttery, <i>et al.</i>, Integrated Modelling of Core, Edge Pedestal and Scrape-Off- Layer for High- β_N Steady-State Scenarios on DIII-D	527
TH/P7-3	M. Y. Ye, <i>et al.</i>, Simulation Study of the Impurity Radiation in the Quasi- Snowflake Divertor with Ne Seeding for CFETR	528
TH/P7-4	A. H. Nielsen, <i>et al.</i>, Synthetic Edge and SOL Diagnostics: A Bridge between Experiments and Theory	529
TH/P7-5	M. Wischmeier, The Physics Basis for a Solution to the Power and Particle Exhaust Problem of a Next Step Device	530
TH/P7-6	D. Sharma, <i>et al.</i>, The Scrape-Off Layer Plasma Transport Physics Simulation Activity for Indian Tokamaks ADITYA and SST-1	531
TH/P7-7	V. Pericoli Ridolfini, <i>et al.</i>, Comparative Analysis of the SOL Properties for the Various Magnetic Configurations Proposed for the DEMO Divertor	532
TH/P7-8	N. Shukla, <i>et al.</i>, Electron Impact Excitation of W^{40+} to W^{43+} Ions: Cross Section and Polarization	533
TH/P7-9	B. P. Sahoo, <i>et al.</i>, Plasma Transport in Toroidally Discontinuous Limiter Gen- erated 3D SOL Configurations of ADITYA Tokamak	534
TH/P7-10	R. Zanino, <i>et al.</i>, Self-Consistent Modelling of a Liquid Metal Pool-Type Divertor	535
TH/P7-11	S. Togo, <i>et al.</i>, SOL/Divertor Plasma Simulation of Diverging Magnetic Field Configurations for Advanced Divertors	536
TH/P7-12	H. Hasegawa, <i>et al.</i>, Ion Inertial Effects on 3D Filament Dynamics	537
TH/P7-13	R. Khanal, <i>et al.</i>, Velocity Profile and Modulation Frequency of Ions in a Mag- netized Plasma Sheath Using Kinetic Trajectory Simulation Method	538
TH/P7-15	J. P. S. Bizarro, <i>et al.</i>, Exact Conservative Solutions of Fluid Models for the Scrape- Off Layer as the Ancestors of Blobs?	539

TH/P7-17	I. B. Kupriyanov, <i>et al.</i>, Simulation of Beryllium Erosion and Surface Damage Under ITER-Like Transient Plasma Heat Loads	540
TH/P7-18	H. Reimerdes, <i>et al.</i>, Assessment of Alternative Divertor Configurations as an Exhaust Solution for DEMO	541
TH/P7-20	M. Wigram, <i>et al.</i>, Performance Assessment of Tightly-Baffled Long-Leg Diver- tor Geometries in the ARC Reactor Concept	542
TH/P7-21	X. Q. Xu, <i>et al.</i>, Simulations of Tokamak Boundary Plasma Turbulent Transport	543
TH/P7-22	C.-S. Chang, <i>et al.</i>, Wide Divertor Heat-Flux Width in ITER from Self-Organization between the Neoclassical and Turbulent Transports across the Separatrix Surface	544
TH/P7-23	A. Hakim, <i>et al.</i>, Continuum Gyrokinetic Simulations of NSTX SOL Turbu- lence with Sheath-Limited Model Geometries	545
TH/P7-24	M. A. Dorf, <i>et al.</i>, Simulation of Cross-Separatrix Edge Plasma Transport with the Continuum Gyrokinetic Code COGENT	546
TH/P7-25	J. M. Canik, <i>et al.</i>, Multiphysics Modelling of the Long-Term Evolution of Plasma- Exposed Surfaces	547
TH/P7-26	R. M. Churchill, <i>et al.</i>, Pressure Balance in a Low Collisionality Tokamak Scrape-Off Layer	548
TH/P8-1	K. Hallatschek, Highly Collisional Two-Fluid and Gyrokinetic Simulations of Tokamak Edge Turbulence and the Transition between Kinetic and Fluid Regime	549
TH/P8-2	A. Y. Aydemir, <i>et al.</i>, Effect of Poloidal Density Asymmetries on Shear Flows and Radial Electric Field at the Plasma Edge	550
TH/P8-3	R. Singh, <i>et al.</i>, Multiscale Interaction between Ballooning Mode and Electron- Scale Turbulence and the Mesoscale Structure Formation in the Edge Pedestal	551
TH/P8-4	J. Kim, <i>et al.</i>, Correlation Analysis Based Magnetic Kubo Number Estima- tion during Pedestal Collapse in BOUT++ Simulation . . .	552

TH/P8-5	R. Dey, <i>et al.</i>, Studies of the Gas Puff Effect on Edge Plasma of ADITYA Tokamak Using Coupled DEGAS2-UEDGE Code	553
TH/P8-6	A. Wisitsorasak, <i>et al.</i>, Predictive Simulations of Core-Edge Plasma for Tokamak Plasma Using BALDUR Code	554
TH/P8-7	J. Chowdhury, <i>et al.</i>, Gyrokinetic Neoclassical Study of the Effect of the X-Point Height on $E \times B$ Flow Structure in an H-Mode Edge Plasma	555
TH/P8-8	V. K. Bandaru, <i>et al.</i>, Nonlinear Interaction of Runaway Electrons with Resistive MHD Modes in an ITER VDE	556
TH/P8-9	I. Bandyopadhyay, <i>et al.</i>, Simulations of Plasma Disruptions in ITER due to Material Ingress	557
TH/P8-10	I. Krebs, <i>et al.</i>, Nonlinear 3D Simulations of Vertical Displacement Events in Tokamaks	558
TH/P8-12	G. Q. Dong, <i>et al.</i>, Nonlinear Interplay between Edge Localized Infernal Mode and Plasma Flow	559
TH/P8-13	Y. Li, <i>et al.</i>, Nonlinear Turbulent Parallel Momentum Transport due to Blobs	560
TH/P8-14	Y. Peysson, <i>et al.</i>, Modelling Runaway Electrons Dynamics in Tokamak Plas- mas: Progresses and Challenges	561
TH/P8-15	G. I. Pokol, <i>et al.</i>, Runaway Electron Modelling in the ETS Self-Consistent Core Transport Simulator	562
TH/P8-16	C. Liu, <i>et al.</i>, Energy Loss and Pitch Angle Scattering of Runaway Elec- trons due to Kinetic Instabilities	563
TH/P8-17	D. A. Spong, <i>et al.</i>, Interactions of Runaway Electrons with Alfvén and Whistler Waves	564
TH/P8-18	R. W. Harvey, <i>et al.</i>, Time-Dependent Runaway Simulations: Ampère–Faraday Equations Implemented in CQL3D	565
TH/P8-19	D. del-Castillo-Negrete, <i>et al.</i>, Integrated Simulation of Runaway Electrons: A Backward Monte Carlo Approach for a Fluid-Kinetic Self-Consistent Coupling	566

FIP: Fusion Engineering, Integration and Power Plant Design	567
FIP/1-1 M. Nakahira, <i>et al.</i>,	
Completion of the First TF Coil Structure of ITER	568
FIP/1-2Ra Y. Oda, <i>et al.</i>,	
Completion of 1st ITER Gyrotron Manufacturing and 1 MW	
Test Result	569
FIP/1-2Rb R. G. Trivedi, <i>et al.</i>,	
Outcome of R&D Programme for ITER ICRF Power Source	
System	570
FIP/1-2Rc G. Gantenbein, <i>et al.</i>,	
Recent Progress in the Development of the European 1 MW,	
170 GHz CW Gyrotron for ITER	571
FIP/1-3Ra J. Joshi, <i>et al.</i>,	
Technologies for Realization of Large Size RF Sources for	
–ve Neutral Beam Systems for ITER: Challenges, Experience	
and Path Ahead	572
FIP/1-3Rb V. Toigo, <i>et al.</i>,	
Progress in the ITER Neutral Beam Test Facility	573
FIP/1-3Rc A. Kojima, <i>et al.</i>,	
Demonstration of 1 MV Vacuum Insulation for the Vacuum	
Insulated Beam Source in the ITER NB System	574
FIP/1-4 A. Litnovsky, <i>et al.</i>,	
Diagnostic Mirrors for ITER: Research in a Frame of Interna-	
tional Tokamak Physics Activity	575
FIP/1-5 E. E. Mukhin, <i>et al.</i>,	
Integration of Thomson Scattering and Laser-Induced Flu-	
orescence in ITER Divertor: Engineering and Performance	
Analysis	576
FIP/1-6 X. Wang, <i>et al.</i>,	
Current Design and R&D Progress of CN HCCB TBS	577
FIP/2-1 J. Chen, <i>et al.</i>,	
Progress in Developing ITER and DEMO First Wall Tech-	
nologies at SWIP	578
FIP/2-2 T. R. Barrett, <i>et al.</i>,	
Technologies for Plasma-Facing Wall Protection in EU DEMO	579
FIP/2-3 R. Lunsford, <i>et al.</i>,	
Active Conditioning of ASDEX-Upgrade Tungsten PFCs through	
Boron Particulate Injection	580
FIP/2-4 D. Iglesias, <i>et al.</i>,	
Advances in Predictive Thermo-Mechanical Modelling for	
the JET Divertor Experimental Interpretation, Improved Pro-	
tection, and Reliable Operation	581

FIP/3-1	G. Federici, <i>et al.</i>,	
	Overview of the DEMO Design-Staged Approach in Europe	583
FIP/3-2	Y. Sakamoto,	
	Development of Physics and Engineering Designs for Japan's DEMO Concept	584
FIP/3-3	G. M. Wallace, <i>et al.</i>,	
	Novel Radiofrequency Current Drive Systems for Fusion Plasma Sustainment on DIII-D	585
FIP/3-4	M. Kikuchi, <i>et al.</i>,	
	Impact of High Field & High Confinement on L-Mode-Edge Negative Triangularity Tokamak (NTT) Reactor	586
FIP/3-5Ra	R. Maingi, <i>et al.</i>,	
	Amelioration of Plasma-Material Interactions and Improve- ment of Plasma Performance with a Flowing Liquid Li Lim- iter and Li Conditioning on EAST	587
FIP/3-5Rb	G. Mazzitelli, <i>et al.</i>,	
	Experiments on FTU with a Liquid Tin Limiter	588
FIP/3-6	R. J. Goldston, <i>et al.</i>,	
	Development of a Lithium Vapour Box Divertor for Con- trolled Plasma Detachment	589
FIP/P1-1	L. R. Baylor, <i>et al.</i>,	
	Shattered Pellet Injection Technology Design and Character- ization for Disruption Mitigation Experiments	590
FIP/P1-2	S. Simrock, <i>et al.</i>,	
	Automated Testing of ITER Diagnostics Scientific Instrumen- tation	591
FIP/P1-3	Z. Wang, <i>et al.</i>,	
	Hollow Pellets for Magnetic Fusion	592
FIP/P1-4	J. Smith, <i>et al.</i>,	
	Recent Progress on the Production and Testing of the ITER Central Solenoid Modules	593
FIP/P1-5	A. G. Razdobarin, <i>et al.</i>,	
	Dielectric Windows as Front-End Diagnostic Elements in ITER	594
FIP/P1-7	M. Tanaka, <i>et al.</i>,	
	Exhaust Behaviour and Mass Balance of Tritium in Large Helical Device	595
FIP/P1-8	T. Kobayashi, <i>et al.</i>,	
	Progress in Development and Fabrication of the JT-60SA ECH/CD System	596
FIP/P1-9	A. K. Verma, <i>et al.</i>,	
	Preliminary Pipe Stress Analysis of High Pressure, High Temperature Experimental Helium Cooling System	597

FIP/P1-10	H. Tobar <i>i, et al.</i> , Completion of DC 1 MV Power Supply System for ITER Neutral Beam Test Facility	598
FIP/P1-11	K. Kajiwara <i>, et al.</i> , Improvement of ITER Equatorial EC Launcher Design for Poloidal Steering Compatibility	599
FIP/P1-12	A. Y. Dnestrovsky <i>, et al.</i> , Integrated Modelling of Core and Divertor Plasmas for DEMO- FNS Hybrid Facility	600
FIP/P1-13	A. Kasugai <i>, et al.</i> , RFQ Commissioning of Linear IFMIF Prototype Accelerator (LIPAc)	601
FIP/P1-14	R. Imazawa <i>, et al.</i> , Development of the Far-Infrared Laser Polarimetry for Cur- rent Profile Measurement on ITER	602
FIP/P1-15	D. L. Brower <i>, et al.</i> , Overview of ITPA R&D Activities in Support of ITER Diag- nostics	603
FIP/P1-16	S. Clement-Lorenzo <i>, et al.</i> , Verification Tests for Remote Participation at ITER REC . . .	604
FIP/P1-17	E. Gaio <i>, et al.</i> , Consorzio RFX Contribution to the JT-60SA Project in the Frame of the Broader Approach Agreement	605
FIP/P1-18	T. Schwarz-Selinger <i>, et al.</i> , The Influence of Displacement Damage and Helium on Deu- terium Transport and Retention in Tungsten	606
FIP/P1-19	N. Bairagi <i>, et al.</i> , Experimental Measurements of Cryogenic Heat Loads on SST-1 Helium Cryogenic Plant	607
FIP/P1-20	R. Bright <i>, et al.</i> , Thermo-Mechanical Experiments On Lithium Titanate Peb- ble Bed	608
FIP/P1-21	K. Patel <i>, et al.</i> , The Operation, Control, Data Acquisition System of ASDEX Pressure Gauge for Neutral Pressure	609
FIP/P1-22	E. A. Tolman <i>, et al.</i> , Conceptual Design Study for Heat Exhaust Management in the ARC Fusion Pilot Plant	610
FIP/P1-24	P. Chaudhuri <i>, et al.</i> , Progress on Lithium Ceramic Breeder Materials Develop- ment, Characterization and R&D Activities in IPR	611

FIP/P1-25	R. Sugandhi, <i>et al.</i>, Machine Control System for Large Volume Plasma Device: Current Status and Future Directions	612
FIP/P1-26	V. N. Muvvala, <i>et al.</i>, Application of Finite Element Techniques in Simulation of Mechanical Design and Performance Assessment of Different Components of a Neutral Beam Systems	613
FIP/P1-27	I. Kodeli, <i>et al.</i>, TRIGA Integral Activation of Mn Foils, Li ₂ O and LiF as Po- tential Tritium Production Monitors for Fusion Applications	614
FIP/P1-28	R. Anand, <i>et al.</i>, Seismic Analysis of High Power Amplifier in ITER ICRF Range	615
FIP/P1-29	P. V. Subhash, <i>et al.</i>, ACTYS Code System: Towards Next Generation Nuclear Activation Codes for Fusion Reactors	616
FIP/P1-31	A. K. Tyagi, <i>et al.</i>, Deuterium Depth Profile Measurement in Pre- and Postirra- diated Tungsten	617
FIP/P1-32	R. Kumar, <i>et al.</i>, Development of a High-Temperature Blackbody Source for ITER ECE Diagnostic	618
FIP/P1-33	G. L. Vyas, <i>et al.</i>, Alignment and Calibration Schemes for ITER CXRS-Pedestal Diagnostic	619
FIP/P1-34	S. Varshney, <i>et al.</i>, Thermal Analysis of Protection Important Components of ITER XRCS-Survey Diagnostic System	620
FIP/P1-35	S. Jha, <i>et al.</i>, Preliminary Design of IN-DA Diagnostic Plant Instrumenta- tion & Control	621
FIP/P1-36	S. Kumar, <i>et al.</i>, Design Validation of ITER XRCS Survey Spectrometer with Nuclear Code RCC-MR	622
FIP/P1-37	M. Manuelraj, <i>et al.</i>, In-Vessel Inspection System: Design Progress of High Vac- uum and Temperature Compatible Remote Handling for Fusion Purposes	623
FIP/P1-38	L. Cai, <i>et al.</i>, Preliminary Development on a Conceptual First Wall for DEMO	624
FIP/P1-39	N. P. Singh, <i>et al.</i>, Installation and Initial Run of 96 kV 7.2 MW Acceleration Grid Power Supplies	625

FIP/P1-40	M. J. Singh, <i>et al.</i>, R&D Status of Indian Test Facility for ITER DNB Characteri- zation	626
FIP/P1-41	H. Tyagi, <i>et al.</i>, Design and Development of Safety Control System of Indian Test Facility (IN-TF) for ITER DNB	627
FIP/P1-42	A. Maheshwari, <i>et al.</i>, Study of Corrosion Properties ITER In-Wall Shield (IWS) Fasteners and Structural Integrity of IWS	628
FIP/P1-43	D. Aggarwal, <i>et al.</i>, Nuclear Performance Analysis and Optimization Study of Indian Solid Breeder Blanket for DEMO	629
FIP/P1-44	K. K. Gotewal, <i>et al.</i>, Design and Development of the Articulated Robotic Inspec- tion Arm (ARIA) for Fusion Machine	630
FIP/P1-45	K. M. Patel, <i>et al.</i>, Baking System of ADITYA Upgrade Tokamak	631
FIP/P1-46	S. Muralidhara, <i>et al.</i>, Dynamic Simulation of Loss of Insulation Vacuum Event for ITER Cryodistribution System	632
FIP/P1-47	P. Dutta, <i>et al.</i>, Visual Servo of Tokamak Relevant Remote Handling Systems Using Neural Network Architecture	633
FIP/P1-50	S. V. Rogozhkin, <i>et al.</i>, The Influence of Fe-Ion Irradiation on the Microstructure of Reduced Activation Ferritic-Martensitic Steel Eurofer 97 . . .	634
FIP/P1-51	R. Raman, <i>et al.</i>, Electromagnetic Particle Injector (EPI) as a Fast Time Re- sponse Disruption Mitigation Concept	635
FIP/P1-52	H. B. Pandya, <i>et al.</i>, Preliminary Results of Prototype Martin-Puplett Interferom- eter and Transmission Line Developed for ITER ECE Diag- nostic	636
FIP/P1-53	J. Rapp, <i>et al.</i>, Performance of the Plasma Source and Heating Concept for the Prototype-Material Plasma Exposure Experiment (Proto- MPEX)	637
FIP/P1-54	K. Ikeda, Exploring Deuterium Beam Operation and Behaviour of Co- extracted Electron in Negative-Ion-Based Neutral Beam Injector	638
FIP/P1-55	D. Sharma, <i>et al.</i>, Thermal-Hydraulics and Structural Analyses of LLCB TBM Set	639

FIP/P1-56	T. Kariya, <i>et al.</i>,	
	Development of High Power Gyrotrons for Advanced Fusion	
	Devices and DEMO	640
FIP/P1-57	R. N. Panchal, <i>et al.</i>,	
	Performance Evaluation of 1.3 kW at 4.5 K Helium Refriger-	
	ator/Liquefier (HRL) at IPR	641
FIP/P1-58	G. Vadolia, <i>et al.</i>,	
	Survey on Hot Isostatic Pressing Technique for Development	
	of Tokamak Components	642
FIP/P1-59	A. D. Mankani, <i>et al.</i>,	
	Design and Development of 500 kV, 100 mA DC High Voltage	
	Power Supply for Particle Accelerators at IPR	643
FIP/P3-1	F. Bedoya, <i>et al.</i>,	
	Surface Characterization of Li Coatings and their Interaction	
	with Plasmas for Fusion Applications via Ion Beam Analysis	
	Techniques	644
FIP/P3-2	K. Gi, <i>et al.</i>,	
	Contribution of Fusion Energy to Low-Carbon Development	
	under the Paris Agreement and Accompanying Uncertainties	645
FIP/P3-3	H. Noto, <i>et al.</i>,	
	Dispersion Strengthened Copper Alloys Produced by Me-	
	chanical Alloying and Hot Isostatic Pressing for Divertor	
	Application	646
FIP/P3-4	M. Kobayashi, <i>et al.</i>,	
	Neutron Flux Distributions in the LHD Torus Hall Evaluated	
	by an Imaging Plate Technique in the First Campaign of	
	Deuterium Plasma Experiment	647
FIP/P3-5	P. Kanth, <i>et al.</i>,	
	A Multiparameter Optimization Technique Considering Tem-	
	poral and Spatial Variation in Nuclear Response of Materials	
	in Fusion Devices	648
FIP/P3-6	K. Ochiai, <i>et al.</i>,	
	Design Progress of Advanced Fusion Neutron Source for	
	JA/DEMO Fusion Reactor	649
FIP/P3-7	G. Stankunas, <i>et al.</i>,	
	Neutronic Analysis of IFMIF-DONES Test Cell Cooling System	650
FIP/P3-8	C. Day, <i>et al.</i>,	
	The DEMO Fuel Cycle: Novel Technologies for Tritium In-	
	ventory Reduction	651
FIP/P3-9	Ž. Štancar, <i>et al.</i>,	
	Multiphysics Approach to Plasma Neutron Source Mod-	
	elling at the Tokamak JET	652

FIP/P3-10	S. P. Smith, <i>et al.</i>, The Potential for Retention of Spin Polarization to Raise Fusion Reactivity	653
FIP/P3-12	A. Abhishek, <i>et al.</i>, Artificial Neural Network for Yield Strength Prediction of Irradiated RAFM Steels	654
FIP/P3-14	R. Joshi, <i>et al.</i>, Modification in LHCD DAC System to Incorporate Measurement of RF Power	655
FIP/P3-15	S. S. Mukherjee, <i>et al.</i>, Thermal Performance Analysis of Al ₂ O ₃ –Water Nanofluid as a Coolant in Nuclear Applications	656
FIP/P3-16	A. Arumugam, <i>et al.</i>, RGA Analysis and Surface Analysis of SST-1 Graphite Tiles in High Temperature Vacuum Baking	657
FIP/P3-18	K. P. Singh, <i>et al.</i>, Studies on High Temperature Vacuum Brazing of Tungsten to Tungsten Alloy Materials for DEMO Divertor Application	658
FIP/P3-19	N. Chauvin, <i>et al.</i>, Deuteron Beam Commissioning of the Linear IFMIF Prototype Accelerator Source and LEBT	659
FIP/P3-20	D. Panayotov, Overview of the Methods Developed for Fission Plants Safety Relevant to the Safety of Fusion Facilities	660
FIP/P3-23	A. S. Arakcheev, <i>et al.</i>, Status of Studies of Pulsed Heat Load Influence on Tungsten at BETA Facility and Station of SR Scattering “Plasma” in BINP661	661
FIP/P3-25	M. Coleman, <i>et al.</i>, Global Supply of Tritium for Fusion R&D	662
FIP/P3-26	J. M. Park, <i>et al.</i>, The Advanced Tokamak Path to a Compact Net Electric Pilot Plant	663
FIP/P3-27	S. Shah, <i>et al.</i>, Neutron Irradiation Impact on ITER Grade Insulating Material	664
FIP/P3-28	S. Tiwari, <i>et al.</i>, Conceptual Design of Neutron Activation System for IN-LLCB TBM	665
FIP/P3-29	M. Rajput, <i>et al.</i>, Energy Differential and Displacement Damage Cross Section of DT Neutron Induced Reactions on Fusion Reactor Materials (Fe, Cr & W)	666

FIP/P3-30	A. Patel, <i>et al.</i>, Application of ANSYS FLUENT MHD Code for Liquid Metal MHD Studies	667
FIP/P3-31	S. G. Khambholja, <i>et al.</i>, Structural and Vibrational Properties of Lead-Lithium Al- loys: A First Principles Study	668
FIP/P3-32	K. S. Bhatt, <i>et al.</i>, Structural Analysis for Strength and Fatigue Life of Half Coupling Weldment for Large Cooling Water Pipes	669
FIP/P3-33	S. S. Vala, <i>et al.</i>, Performance of 14-MeV Neutron Generator at IPR	670
FIP/P3-34	D. Dubey, <i>et al.</i>, Tritium Handling and Recovery System for Accelerator Based 14-MeV Neutron Generator	671
FIP/P3-34	V. Shukla, <i>et al.</i>, Extent of Tritium Contamination of Helium Circuit in a Fu- sion Reactor: Probable Scenarios	672
FIP/P3-36	E. Pajuste, <i>et al.</i>, Novel Method for Determination of Tritium Depth Profiles in Metallic Samples	673
FIP/P3-38	P. Chakraborty, <i>et al.</i>, Effect of Magnetic Field on the Corrosion Behaviour of Indian RAFMS in Liquid PbLi	674
FIP/P3-39	P. A. Rayjada, <i>et al.</i>, Er ₂ O ₃ Coating by Multilayer Metallic Sputtering and Inter- mediate Oxidation Approach	675
FIP/P3-40	Y. Wu, <i>et al.</i>, Development of HINEG and its Experimental Campaigns	676
FIP/P3-41	V. M. Chernov, Radiation Properties of the Metal Structural Materials during Low-Temperature Damaging Irradiation	677
FIP/P3-42	C. S. Sasmal, <i>et al.</i>, Effect of Simulated Postweld Heat Treatment on the Mi- crostructure and Mechanical Properties of IN-RAFM Steel	678
FIP/P3-44	A. Attri, <i>et al.</i>, Ion Irradiation Induced Modifications in Tungsten Foils	679
FIP/P3-45	A. Miniyazov, <i>et al.</i>, Tungsten Fuzz Formation on the Nitrided Tungsten Surface	680
FIP/P3-46	H. L. Swami, <i>et al.</i>, Neutronics Experiment for Design Validation of Indian TBM Shield Module	681

FIP/P3-47	P. Bharathi, <i>et al.</i>, Study on Production and Extraction of Negative Ion Impurity Ions in a Caesiated Negative Ion Source	682
FIP/P3-48	A. Patel, <i>et al.</i>, 3 MW Dual-Output High Voltage Power Supply Operation: Results for Accuracy, Stability and Protection Test	683
FIP/P3-49	A. J. Deka, <i>et al.</i>, Evaluation of Beam Properties of a Negative Hydrogen Source by Doppler Shift Spectroscopy	684
FIP/P3-50	S. S. Mukherjee, <i>et al.</i>, Thermohydraulic Analysis of Forced Flow Helium Cooled Cryopanel of Cryopump Using Venecia Code	685
FIP/P3-51	J. S. Mishra, <i>et al.</i>, Pellet Fuelling Prospects and Injector System for ADITYA-U Tokamak	686
FIP/P3-52	P. Bhatt, <i>et al.</i>, Performance of Transmission Line System at 42.0 ± 0.2 GHz for an Indigenous Gyrotron System	687
FIP/P3-53	Y. M. Jain, <i>et al.</i>, Development and Qualification of Passive Active Multijunc- tion (PAM) Launcher for LHCD System of ADITYA-Upgrade Tokamak	688
FIP/P3-54	R. Gangradey, <i>et al.</i>, Effect of Sorbent Selection and Geometrical Arrangement of Cryopanel on Pumping Speed of Cryopump	689
FIP/P3-55	L. Hu, <i>et al.</i>, Advanced Capabilities of Multifunctional Calculation Pro- gramme SuperMC3.2 for Complex Nuclear System	690
FIP/P3-56	M. R. Jana, <i>et al.</i>, Development of Technology for Fabrication of Prototype Ion Extraction Grid for Fusion Research	691
FIP/P3-57	S. S. Chauhan, <i>et al.</i>, Development of RF Based Capacitively-Coupled Plasma Sys- tem for Deposition of Tungsten Nanolayers on Graphite	692
FIP/P3-58	R. Kumar, <i>et al.</i>, Real-Time Feedback Control System for Plasma Position Sta- bilization in ADITYA-U Tokamak	693
FIP/P3-62	A. Patel, <i>et al.</i>, Design and Simulation Studies of Calorimetric Dummy Load for Gyrotron System	694
FIP/P3-63	S. P. Gerhardt, <i>et al.</i>, Overview of the NSTX-U Recovery Project Physics and Engi- neering Design	695

FIP/P3-64	K. A. Jadeja, <i>et al.</i>, Novel Approach of Pulsed-Glow Discharge Wall Condition- ing in ADITYA Upgrade Tokamak	696
FIP/P3-65	E. Surrey, <i>et al.</i>, New Fusion Facilities at UKAEA: FTF and H3AT	697
FIP/P3-66	J. Yagi, <i>et al.</i>, A Concept of Self-Cooled Breeding Blanket with Advanced Molten Salt FLiNaK for High-Efficiency and Long-Life Oper- ation	698
FIP/P7-1	M. Siccino, <i>et al.</i>, Development of a Plasma Scenario for the EU-DEMO: Cur- rent Activities and Perspectives	699
FIP/P7-2	H. Lux, <i>et al.</i>, Implications of Uncertainties on the European DEMO Design	700
FIP/P7-3	S. S. Ananyev, <i>et al.</i>, Development of DEMO-FNS Fuelling Systems and Mod- elling Hydrogen Isotopes Distribution via "FC-FNS" Simu- lation Code	701
FIP/P7-4	Y. Takase, <i>et al.</i>, Development of Capacitively-Coupled Comb-Line Antennas for Current Drive in Tokamaks	702
FIP/P7-5	L. Zani, <i>et al.</i>, Progresses at CEA on EU DEMO Reactor Cryomagnetic Sys- tem Design Activities and Associated R&D	703
FIP/P7-6	B. K. Yadav, <i>et al.</i>, Design Optimization of Helium Cooling Systems for Indian LLCB TBM	704
FIP/P7-7	Y. S. Shpanskiy, Progress in Design of DEMO-FNS Hybrid Facility	705
FIP/P7-8	V. L. Tanna, <i>et al.</i>, SST-1 Cryogenic Requirements and the Way Forward	706
FIP/P7-9	U. Prasad, <i>et al.</i>, Thermal-Hydraulic Characteristics Study of Superconduct- ing Magnets of SST-1	707
FIP/P7-10	G. Mahesuria, <i>et al.</i>, Pump Characterization of 80 K Liquid Nitrogen Booster Sys- tem for SST-1	708
FIP/P7-12	K. A. Avramidis, <i>et al.</i>, Overview of Recent Gyrotron R&D towards DEMO within EUROfusion Work Package Heating and Current Drive	709
FIP/P7-13	L. Savoldi, <i>et al.</i>, Assessment and Optimization of the Cavity Thermal Perfor- mance for the European Continuous Wave Gyrotrons	710

FIP/P7-14	A. Garg, et al., Operational Results and Troubleshooting in Current Feeder System for SST-1	711
FIP/P7-15	D. B. Gin, et al., Recent Progress in Developing Gamma Spectrometer in ITER	712
FIP/P7-16	R. Sugandhi, et al., Timing and Synchronization for Integrated Operation of Large Volume Plasma Device	713
FIP/P7-17	V. G. Devi, et al., Design and Thermal Fluid Structure Interaction Analysis of Liquid Nitrogen Cryostat of Cryogenic Molecular Sieve Bed Adsorber for Hydrogen Isotopes Removal System	714
FIP/P7-19	S. Dutta, et al., Error Field Experiment and Analysis in SST-1	715
FIP/P7-20	D. Christian, et al., Maintenance Experience of 315 kW Electrical Motor of He- lium Screw Compressor in 1.3 kW Helium Liquefier	716
FIP/P7-21	A. Tomar, et al., Thermo-Structural and Heat Load Analysis of SST-1 Super- conducting Coils	717
FIP/P7-22	A. Shrivastava, et al., Thermal Diffusivity Measurement of Functional & Structural Materials for Fusion Blanket Application	718
FIP/P7-24	N. Rastogi, et al., Development of a Prototype Collaborative Robot for Fusion Remote Handling Applications	719
FIP/P7-25	B. R. Doshi, et al., Design of the TF/PF Bus Bar Layout and its Connections with Current Feeder System of SST-1 Tokamak	720
FIP/P7-26	S. Roy, et al., Preventive Measures to Avoid Electrical Arcing Incidences in SST-1 PF Current Leads	721
FIP/P7-27	H. Chen, et al., Model Development and Electromagnetic Analysis of Ver- tical Displacement Event for CFETR Helium Cooled Solid Blanket	722
FIP/P7-28	P. Prajapati, et al., Key Considerations in the Power Extraction from Fusion Reactors	723
FIP/P7-29	Q. Huang, et al., Development and Experiment of PbLi Facilities for Fusion Nuclear Technology	724

FIP/P7-30	J. Mora-Meléndez, <i>et al.</i>, Implementation of the Spherical Tokamak MEDUSA-CR: Stage 1	725
FIP/P7-33	O. Crofts, <i>et al.</i>, Early Definition of the Maintenance Plan Is Essential to Achieve an Economic EU DEMO	726
FIP/P7-34	V. B. Minaev, <i>et al.</i>, The Influence of Toroidal Magnetic Field Growth on Plasma Performance in the Spherical Tokamak Globus-M/-M2 . . .	727
FIP/P7-35	K. Kizu, <i>et al.</i>, Progress in Design and Fabrication of Current and Helium Feeding System for JT-60SA Superconducting Coils	728
FIP/P7-36	S. Binwal, <i>et al.</i>, Noninvasive Plasma Density Measurement in a 13.56 MHz Magnetized Capacitive Coupled RF Discharge	729
FIP/P7-37	Y. Shibama, <i>et al.</i>, Advanced Assembly Technology of the Superconducting Coils in JT-60SA Tokamak	730
FIP/P7-38	T. Brown, <i>et al.</i>, A Toroidal Confinement Facility Study and Eventual Experi- mental Device to Investigate a Range of Liquid Metal Diver- tor and First-Wall Concepts	731
FIP/P7-39	T. Goto, <i>et al.</i>, Conceptual Design of a Compact Helical Fusion Reactor FFHR-c1 for the Early Demonstration of a Year-Long Electric Power Generation	732
FIP/P7-40	V. Antoni, <i>et al.</i>, Negative Ion Beam Source Physics as a Complex System: Identification of Main Processes and Key Interdependence .	733
FIP/P7-42	J. Figueiredo, <i>et al.</i>, JET Upgraded Diagnostic Capabilities and Scientific Exploita- tion in Support of Deuterium-Tritium Operation	734
FIP/P8-1	R. Patel, <i>et al.</i>, Installation and Commissioning of 80 K Liquid Nitrogen Booster System	735
FIP/P8-2	R. C. O'Neill, <i>et al.</i>, High Power Helicon Antenna Design for DIII-D	736
FIP/P8-3	C. K. Gupta, <i>et al.</i>, Implementation of Synchronous Reference Frame Theory Based Shunt Active Power Filter Using DSP Controller . . .	737
FIP/P8-4	J. Patel, <i>et al.</i>, Operation and Control of 42 GHz Gyrotron System in ECRH	738

FIP/P8-5	K. Mohan, et al., Design and Development of Control Grid Power Supply for RF Amplifier	739
FIP/P8-6	A. Fasoli, TCV Heating and Divertor Upgrades	740
FIP/P8-7	J. Kumar, et al., Design and Simulation of Circular Waveguide Elbows Ap- plicable in High Power Microwave Coupling to Plasma . . .	741
FIP/P8-8	M. Patel, et al., Development of Solid State Power Amplifier for ICH & CD RF Source	742
FIP/P8-9	R. Kumar, et al., RT Amplitude Control Loop: Testing of R&D ICRF Source at High Power	743
FIP/P8-10	J. C. Patel, et al., Mechanical Engineering Aspects for Overhauling of Helium Compressor and Heavy Duty Electrical Motors of 1.3 kW Helium Refrigerator/Liquefier System	744
FIP/P8-11	R. Ragona, et al., A Travelling Wave Array System as Solution for the ICRF Heating of DEMO	745
FIP/P8-12	R. Sharma, et al., Development of Indigenous Electrical Insulation Breaks for Superconducting Magnets of Fusion Devices	746
FIP/P8-13	P. Y. Li, et al., Recent Progress of ITER Magnet Supports Package in SWIP	747
FIP/P8-14	U. Fischer, et al., Nuclear Design Issues of a Stellarator Fusion Power Plant with Breeder Blanket in Comparison to Tokamaks	748
FIP/P8-15	M. Ghate, et al., Numerical Investigations towards Manufacturing of High Current Carrying Superconducting CICC	749
FIP/P8-16	A. Jha, et al., Development of Wideband Amplifier in ITER ICRF Range .	750
FIP/P8-17	M. Bandyopadhyay, et al., Development of Various Diagnostics for NNBI Programme in IPR	751
FIP/P8-18	R. K. Buddu, et al., Studies of Ultrasonic and Phased Array Inspection NDT Tech- niques on High Thick SS-316L Welded Joint Mock-Ups of Fusion Reactor Components Fabrication Applications	752

FIP/P8-19	R. Bahl, Simulation Studies for Optimization of 60 MHz Rod-Type Radiofrequency Quadrupole Accelerator Design at IPR . . .	753
FIP/P8-20	H. K. Patel, et al., Manufacturing Technologies for UHV Compatible 10 MW/m ² High Heat Flux Components for Application in Fusion Devices	754
FIP/P8-22	T. K. Sharma, et al., Development and Validation of Cryostat Finite Element Model with Unique FE Method	755
FIP/P8-23	A. Patel, et al., Characterization of Argon Plasma in a Multiline Cusp Mag- netic Field: Towards a Favourable Source for NBI System . .	756
FIP/P8-24	Z. Shaikh, et al., A Versatile Multicusp Plasma Device for Confining Contact Ionized Alkali Ions: Source for the Experimental Studies . .	757
FIP/P8-25	M. Sharma, et al., Evolution and Implementation of Lossless Data Acquisition for Steady State Tokamak	758
FIP/P8-26	B. K. Shukla, et al., Technology Developments for ECRH System	759
FIP/P8-29	B. Chektybayev, et al., Concept of a New Approach in Thermographic Measure- ments for Plasma-Wall Interaction Studies on KTM Tokamak	760
IFE: Inertial Fusion Experiments and Theory		761
IFE/1-1	Y. Arikawa, et al., Two-Colour Mixed Petawatt Laser Designed for Fast Ignition Experiment	762
IFE/1-2	S. Fujioka, et al., Production of keV-Temperature Plasma Core with Magne- tized Fast Isochoric Heating	763
IFE/1-3	R. E. Olson, et al., Liquid DT Layer Approach to Inertial Confinement Fusion .	765
IFE/1-4	J. M. Perlado, et al., Thermo-Mechanical and Atomistic Assessment of First Wall and Optics in Nonprotective Chamber in Inertial Fusion Energy	766
IFE/1-5	A. Iwamoto, et al., Demonstrations of Foam Shell and Infrared Heating Methods for FIREX Targets	767
IFE/P4-1	G. M. Elaragi, Experimental Discharge Characterization of IEC Plasma Device	768

IFE/P4-4	H. Hora, <i>et al.</i>, H- ¹¹ B Fusion Reactor with Extreme Laser Pulses for Non-LTE Ignition	769
IFE/P4-6	Y. Mori, <i>et al.</i>, Development of Shell Injection System for the Future IFE Power Plant	770
IFE/P4-7	E. R. Koresheva, <i>et al.</i>, Mechanical Mockup of IFE Reactor Intended for the Development of Cryogenic Targets Mass Production and Rep-Rate Delivery into the Reaction Chamber	771
IFE/P4-8	N. Iwata, <i>et al.</i>, Electron Acceleration in Dense Plasmas Heated by Picosecond Relativistic Laser	772
IFE/P4-9	H. Nagatomo, <i>et al.</i>, Target Design Study of Fast Ignition for Ignition and Burning Experiments	773
IFE/P4-10	T. Watari, <i>et al.</i>, Progress of a DPSSL Based R&D Facility TERU for IFE Technology and Industrial Applications	774
IFE/P4-13	K. F. Al-Shboul, Interpenetration and Stagnation in Collapsing Plasmas . . .	775
MPT:	Materials Physics and Technology	777
MPT/1-1	A. Kreter, <i>et al.</i>, Influence of Plasma Impurities on the Fuel Retention in Tungsten	778
MPT/2-1	T. Nagasaka, <i>et al.</i>, High-Temperature Creep Properties of NIFS-HEAT-2 High-Purity Low-Activation Vanadium Alloy	779
MPT/2-2	R. Ding, <i>et al.</i>, Model Validation on EAST and DIII-D Experiments towards Understanding of High-Z Material Erosion and Migration in a Mixed Materials Environment	780
MPT/2-3	P. N. Maya, <i>et al.</i>, Evaluation of Tungsten as Divertor Plasma-Facing Material: Results from Ion Irradiation Experiments and Computer Simulations	781
MPT/2-4	A. Ibarra, <i>et al.</i>, The European Approach to the Fusion-Like Neutron Source: The IFMIF-DONES Project	782

PPC: Plasma Overall Performance and Control 783

 PPC/1-1 **N. Hayashi, et al.,**
 Predictive Integrated Modelling of Plasmas and their Operation
 Scenarios towards Exploitation of JT-60SA Experiment . 784

 PPC/2-1 **T. C. Luce, et al.,**
 Exploring an Alternate Approach to $Q = 10$ in ITER 785

SEE: Safety, Environmental and Economic Aspects of Fusion 787

 SEE/1-1 **C. Grisolia, et al.,**
 Tritiated Dust: The Impact on Tokamak Operation 788

 SEE/2-1 **M. R. Gilbert, et al.,**
 Waste Implications from Minor Impurities in European DEMO
 Materials 789

 SEE/3-1Ra **S. Konishi, et al.,**
 Future Possibility of Carbon Sequestration by Biomass-Fusion
 Hybrid Systems 790

 SEE/3-1Rb **S. Takeda, et al.,**
 Economic Performance of Fusion Power Plant on Future
 Deregulated Electricity Market 791

 SEE/3-1Rc **H. Nam, et al.,**
 Techno-Economic Analysis of Biodiesel and Hydrogen Pro-
 duction via Fusion-Biomass Hybrid Model 792

Indexes 793

O/1: Opening Plenary

O/1

Importance of Energy and the Role of Nuclear Energy in India's Energy Mix

R. B. Grover¹

¹*Homi Bhabha National Institute (HBNI), Anushakti Nagar, Mumbai 400094, India*

Corresponding Author: R. B. Grover, <http://www.hbni.ac.in/faculty/director.htm>

For the past ten years, cumulative average growth rate for electricity generation in India has been close to 6%. During the year 2016–17, total electricity generation was about 1430 billion kW-hour (= 1430 TW-hour). It will be more than 1500 TW-hour in 2017–18. Considering the rate of economic growth, linkage between economic growth and electricity requirements, increasing urbanization and current low per-capita electricity availability, electricity generation in India is likely to exceed 8000 TW-hour by the middle of this century. Environmental sustainability enjoins on India to generate a significant fraction of the total generation by low-carbon technologies, that is nuclear, hydro, solar and wind. Considering that the total potential of hydro, solar and wind is only about one-fourth of the projected electricity requirements, nuclear must play a dominant role.

The talk will explain near- and medium-term plans to accelerate growth in installed nuclear capacity, and provide a glimpse of ongoing research and development aimed at directing growth in installed capacity in the long-term.

India's Quest for Fusion Energy & Road to ITER

S. P. Deshpande¹

¹*International Thermonuclear Experimental Reactor (ITER), India Centre, Gujarat, India*

Corresponding Author: S. P. Deshpande, Shishir.Deshpande@iter-india.org

Recognizing the limitations of currently available resources, India's quest for new energy sources is common for all nations, which are in a state of rapid growth and aspire to seek a respectable place on the global canvas of peaceful and sustainable co-existence. Lack of adequate energy denies opportunity to lead a developed and precludes realization of human potential into what it could have been. The global impact can be gauged from the fact that among the 17 Sustainable Development Goals, spelt out after an extensive study by the UN, the 7th goal is 'affordable and clean energy'. Today or in very near future — the whole world is or will be in a situation that will require every conceivable energy source to be tapped, improved in efficiency, made cost-effective and be equipped with a method to mitigate any adverse impact on the environment.

In spite of India's taking significant steps towards tapping every bit of both conventional and renewable energy sources, the demand is much higher than what is currently available and is still growing. If one takes a grand challenge of bringing parity with the world-average for the per capita consumption, the capacity has to be trebled! How fast can one add ~ 400 GW? No matter what we do and however staggering this figure is, there is no going back from this target. So, an equally challenging problem that emerges is how do we manage to grow on sub-optimal energy supply in the interim period. Techniques to reduce energy consumption by increasing efficiency of various processes need to be developed. For this one needs new tools, materials and research-infrastructure to innovate, improvise and harness the benefits of improvement on a mass-scale. Scales matter; even a tiny saving/improvement for a nation with billion people is quite impactful.

Advanced technologies like fusion hold the promise but have been traditionally considered too far away for any serious investment so far. The "fear factor" of failure can be overpowering for policy makers. However, it is time to turn it around and ask ourselves: What difference will it make if fusion reactor works as desired? Well, it will make a tremendous difference. It deserves a try, just for that hope we have. The ITER Project is a collective expression of this global quest for energy in the form of the largest scientific endeavour involving more than half of the world population. The task however, is complex and embeds challenges of extreme kind. But fusion research is also all about innovative ways and can continue to provide the world with spin-offs while it graduates from hydrogen plasma to DT and from there on to power-reactors.

Continued...

India has come a long way in both fusion-science and technology via its well-conceived indigenous as well as collaborative measures. India's journey began in 1982 and it has grown in several areas of plasma and fusion research. A number of developments has taken place: tokamaks with copper-coils (ADITYA) and with superconducting coils (SST-1) have been built indigenously in the Institute for Plasma Research, Gandhinagar. The scientists have gained enormous experience in plasma operations of these tokamaks as well as in SINP-tokamak, which is located in the Saha Institute of Nuclear Physics, Kolkata. Now, an upgraded ADITYA-U is in place capable of experiments with shaped plasma. A host of auxiliary technologies have been developed and tested with the test-beds created in-house.

India needs to sustain the momentum of its fusion research to be able to reap the benefits from participation in ITER and to quickly channelize the success of ITER in its vision. The ITER participation has been followed in India with the blanket and the divertor technology development initiatives. Industrial applications of the plasma have come off age and last but not the least, the human resource development has taken place with a strong academic back-bone. In this talk, the above-mentioned developments are overviewed and an outline of the future plan — and how it blends with ITER participation is also presented.

EU R&D Energy Policy and the Role of Fusion Research

P. A. Child¹

¹*Deputy Director-General, European Commission, Brussels, Belgium*

Corresponding Author: P. A. Child, ec.europa.eu/info/persons/deputy-director-general-patrick-child_en

Research and Innovation contributes to several of the ten priorities of the European Commission for 2015–19. The EU’s energy research policy contributes, in particular, to provide its citizens and businesses with secure and affordable energy, while also addressing the causes of climate change. The next Research and Innovation Programme, covering the period 2021–2027, will build on the success of the current Programme (Horizon 2020) under the guiding principle of “evolution, not revolution”. Intensified international cooperation under the next Programme will ensure that European researchers and innovators have access to and benefit from the world’s best talent, expertise and resources. This will, inter alia, enhance the supply and demand of innovative solutions and promote reciprocal international research partnerships. In the area of Fusion Research the implementation of the “Roadmap to the Realization of Fusion Energy” will continue to be the priority focus, with a strong and continued support for the construction of ITER and a significant research effort to prepare for DEMO.

Fusion is our Future: Readiness of the Fusion Technology and the 4th Industrial Revolution

N. K. Prinja¹

¹*AMEC Foster Wheeler, Booths Park, Knutsford, Cheshire, WA16 8QZ, United Kingdom*

Corresponding Author: N. K. Prinja, nawal.prinja@amec.com

The time and cost of further increasing the overall readiness level of fusion energy, which requires testing materials under extreme environment, data collection, analysis and new designs, can be significantly reduced with the advent of the fourth industrial revolution. The fourth industrial revolution is on its way. Known as Industry 4.0, it represents the current trend to use automation and data exchange technologies that include cyber-physical systems, the Internet of things, cloud computing and cognitive computing. These technologies are rapidly being developed to perform industry activities. Components of future fusion reactors are expected to be designed and manufactured by using advanced simulation technologies and advanced manufacturing methods. The costs will be further reduced as there will be increased harmonization of codes and standards. IAEA have already taken steps to ensure that the design rules are harmonized before the technology is commercialized. In case of the fission technology there was commercialization before harmonization but for fusion technology it will be harmonization before commercialization.

OV: Overviews

Progress of ITER-India Activities for ITER Deliverables: Challenges and Mitigation Measures

A. K. Chakraborty^{1,2}, U. K. Baruah^{1,2}, A. Mukherjee^{1,2}, S. L. Rao^{1,2}, V. Kumar^{1,2,3},
A. Kumar^{1,2}, G. Gupta^{1,2}, H. Vaghela^{1,2}, H. A. Pathak¹, H. B. Pandya^{1,2},
I. Bandyopadhyay^{1,2,3}, and S. P. Deshpande^{1,2,3}

¹International Thermonuclear Experimental Reactor (ITER), India Centre, Gujarat, India

²Institute for Plasma Research (IPR), Bhat, Gandhinagar, India

³Homi Bhabha National Institute (HBNI), Anushakti Nagar, Mumbai 400094, India

Corresponding Author: A. K. Chakraborty, arunkc@iter-india.org

The responsibilities of ITER-India include a mix of precision, heavy, R&D intensive and interface intensive systems, under built-to-print and functional systems category. In several systems, components fall under the category of first of its kind or of the largest kind. The uniqueness of specifications lead to a challenging situation—namely that neither the existing labs or potential suppliers have ever done or encountered such scale-up (neither in size/volume, capacity, precision, etc.) and do not have even the R&D infrastructure to match the requirements. Under a graded approach a full-scale prototype or at an appropriate scale needs to be developed apart from the testing infrastructure.

Facilities have been established to demonstrate the integrated and functional performance in the first-of-its-kind and R&D intense systems, as a risk mitigation strategy.

These include, for IC system, an extension of the successful prototype results to demonstrate the production of 2.5 MW in a double chain configuration with a combiner at the output. For neutral beams, development of the ion source to realize the stringent parameter space for DNB and development of special technologies, involving special copper alloy Cu-Cr-Zr and special manufacturing technologies, involving high precision of $> 50 \mu\text{m}$ over $\sim 1 \text{ m}$, as the first of its kind. Additionally, development of SIC compliant isolators and ultimately, setting up of a test facility with an unique attribute to test for the beam transmission. Setting up of a special cryogenic test facility to test the performance, against the designed performance for the 4 K, 50 K and 80 K Helium lines with multiprocess pipes. Development of a SIC compliant 140 kV class feed-through to feed 100 kV for the DNB High voltage power supplies.

It is demonstrated that engineering efforts invested at the stage of prototyping have led to a significantly reduced effort in resolving technical issues encountered at the production stage and manifests as a primary risk mitigation strategy in the management of ITER-India procurement.

The paper presents the technical achievements and the overall status with an emphasis on the special developments for the first of its kind components to meet the challenging specifications.

Progress Toward ITER's First Plasma

B. Bigot¹

¹*International Thermonuclear Experimental Reactor (ITER),
Cadarache Centre, 13108 St. Paul lez Durance, France*

Corresponding Author: B. Bigot, bernard.bigot@iter.org

ITER reached 50% completion of the work required to achieve first plasma (FP) in November 2017. Progress has been made on ITER infrastructure since the 2016 FEC, most visibly the construction of many key buildings. The tokamak assembly building and the tokamak bioshield have been completed. The tokamak building will be ready for equipment in 2020. The cryogenic plant and the magnet power supply buildings are complete, and these systems begin commissioning in 2019. The power conversion and distribution area is complete and the component cooling water system building has started construction. Commissioning of these systems starts in 2018. Thus, the physical plant is moving rapidly toward completion, and key systems are entering the commissioning phase. Equally impressive is progress toward manufacturing components of the ITER tokamak. The base and lower cylinder of the cryostat have been assembled on the ITER site. The first of the six modules of the central solenoid has been wound, and three of the six poloidal field coils are presently being wound. The first winding pack of the toroidal field magnets is complete, as is the first casing, which has been verified to meet the high tolerances required (< 0.5 mm). The first complete set of parts comprising a vacuum vessel sector has been fabricated and demonstrated to meet strict tolerances (< 1 mm). Therefore, the major components of the tokamak have passed into the fabrication phase. The heating and current drive systems (NB, ECH and ICH) are also in the final design phase. The sequence of ITER operation from first plasma to the achievement of the $Q = 10$ and $Q = 5$ project goals has been consolidated in a staged approach. This is a stepwise installation of components and ancillary systems, with all systems installed before the start of the FPO operational phase. The ITER research plan has been revised in 2017 to be consistent with the systems available in each phase. Physics R&D focusses on the disruption mitigation system, design of the ITER tungsten divertor, and modelling of ITER plasma scenarios. An international task force has been established to coordinate R&D on disruption mitigation. Modelling concentrates on the initial phases of the research plan and on the $Q = 10$ scenario, especially plasma termination. The focus is on scenarios that access the H-mode regime in the PFPO-1 and PFPO-2 phases.

Overview of the JET Preparation for Deuterium-Tritium Operation

E. Joffrin¹

The JET Contributors

¹*EUROfusion/JET, Culham Science Centre, Abingdon, Oxfordshire, OX14 3DB, UK*

Corresponding Author: E. Joffrin, emmanuel.joffrin@jet.efda.org

Europe has elaborated a roadmap to the realization of fusion energy in which “ITER is the key facility and its success is the most important overarching objective of the programme”. We review the contribution of the recent JET experiments with the ITER first wall materials mix, and, the underlying physics understanding to mitigate the scientific risks identified in the ITER research plan. Indeed, together with the ITER scenario development, a strong focus on JET is pursued for addressing ITER needs and developing a sound physics basis for the extrapolation through first principle and integrated modelling: plasma wall interaction, disruption mitigation (installation of a third mitigation valve), H-mode access, W-control with higher electron heating (ICRH ITER-like antenna reinstated), pellet ELMs pacing with the optimized vertical high field side track. The JET ITER-Like Wall experiment provides an insight in the coupling between tokamak-plasma operation and plasma-surface interaction in the unique Be/W material environment and acts as test-bed to verify models and modelling tools for ITER. Disruptions are considered as the highest programmatic risk in the ITER research plan and experimental and modelling effort in Europe and JET are reviewed. High spatial resolution Doppler backscattering measurements have revealed novel insights into the development of the edge transport barrier. The operational constraints of a metal wall can prevent reaching plasma energy confinement required for $Q_{DT} = 10$ on ITER. Progress on JET to mitigate this risk is reported aiming at maximizing the core and pedestal performance in stationary condition with the W divertor constrain. The measured DD neutron fluence and γ dose rates have been successfully compared with simulations performed with the codes used for ITER nuclear safety analyses. Finally, the benefit to further use JET beyond 2020 to train the international ITER team with an upgrade tungsten divertor and with the ITER control tools will be discussed.

This work has been carried out within the framework of the EUROfusion Consortium and has received funding from the Euratom research and training programme 2014–2018 under grant agreement No. 633053. The views and opinions expressed herein do not necessarily reflect those of the European Commission.

DIII-D Research Towards Establishing the Scientific Basis for Future Fusion Reactors

C. C. Petty¹

The DIII-D Team

¹*General Atomics, San Diego, CA 92186, USA*

Corresponding Author: C. C. Petty, petty@fusion.gat.com

DIII-D research is addressing critical challenges in preparation for ITER and the next generation of fusion devices through a focus on scientific investigation of plasma physics fundamentals, integration of disparate core and boundary plasma physics, and development of attractive scenarios. Fundamental studies show that including the energetic particle “kick” model in transport codes dramatically improves agreement with the measured beam ion profile during strong Alfvénic activity, while dimensionless parameter scaling studies of intrinsic rotation lead to a predicted ITER rotation profile with significant turbulence stabilization. Hard X-ray spectra measurements show that anomalous dissipation of runaway electron (RE) beams is strongest for low energy RE populations, likely due to interactions between the low energy RE population and RE-driven kinetic instabilities. Core-boundary integration studies show that the small angle slot divertor achieves detachment at lower density and extends plasma cooling across the divertor target plate, which is essential for controlling heat flux and erosion. A rotating $n = 2$ RMP combined with a stationary $n = 3$ RMP has demonstrated access to ELM suppression with lower 3D field strength, while at the same time dynamically controlling the divertor heat and particle flux. Other edge studies show that the higher L-H power threshold with RMP fields is potentially due to both 3D density gradient modifications and changes in $E \times B$ shear layer topology. Super H-mode experiments in the presence of ELMs have achieved near-record pedestal pressures and record stored energies for the present DIII-D configuration with $\beta_{N,ped} \approx 1.3$, $H_{98}(y, 2) \approx 1.6\text{--}2.4$ and $I_p \leq 2.0$ MA. In scenario work, the ITER baseline $Q = 10$ scenario has been advanced by adjusting the early current density profile evolution to obtain reproducibly stable operation with ≈ 0 external torque and without $n = 1$ tearing modes. In the wide pedestal QH-mode regime that exhibits improved performance, the startup counter torque has been eliminated so that the entire discharge uses ≈ 0 applied torque and the operating space is more ITER-relevant. Finally, the high- β_p scenario with large-radius ITB has been extended to $I_p \sim 1$ MA ($q_{95} \sim 6$) with high confinement $H_{98}(y, 2) \sim 1.6$ from both Shafranov shift and negative magnetic shear.

Work supported by the U.S. Department of Energy under DE-FC02-04ER54698.

Overview of Physics Studies on ASDEX-Upgrade

H. Meyer¹

The ASDEX-Upgrade Team and EUROfusion-MST1 Team

¹United Kingdom Atomic Energy Authority, Culham Science Centre, Abingdon, UK

Corresponding Author: H. Meyer, hendrik.meyer@ukaea.uk

The ASDEX-Upgrade (AUG) programme, jointly run with the EUROfusion MST1 task force, continues to enhance significantly the physics base of ITER and DEMO. Here, the full tungsten wall is a key asset for extrapolating to future devices. The high overall heating power and flexible heating mix and comprehensive diagnostic set allows studies ranging from mimicking the scrape-off-layer (SOL) and divertor conditions of ITER and DEMO at high density to fully noninductive operation ($q_{95} = 5.5$, $\beta_N \leq 2.8$) at low density. Higher ECRH heating power ≤ 8 MW, new diagnostics and improved analysis techniques have enhanced the capabilities of AUG. Stable high-density H-modes with $P_{\text{sep}}/R \leq 11$ MW/m with fully detached strike-points have been demonstrated. The ballooning instability close to the separatrix has been identified as a potential cause leading to the H-mode density limit. Density limit disruptions have been successfully avoided using a path-oriented approach to disruption handling and progress has been made in understanding the dissipation and avoidance of runaway electron beams. ELM suppression with resonant magnetic perturbations (RMP) is now routinely achieved reaching $H_{\text{H98}(y,2)} \leq 1.1$ giving new insight into the field penetration physics, in particular with respect to plasma flows. Modelling agrees well with plasma response measurements and a helically localized ballooning structure observed prior to the ELM is evidence for the changed edge stability due to the RMP. Fast measurements of T_i and E_r show that the dominantly neoclassical character of E_r holds through the ELM recovery. Good agreement of 3D nonlinear MHD modelling with measured ELM crash dynamics is achieved. As type-I ELMs (even mitigated) are likely not a viable operational regime in DEMO studies of no ELM regimes have been extended. Stable I-modes up to $n/n_{\text{GW}} \leq 0.7$ have been characterized using β feedback. Despite the sub-Alfvénic beam energy, nonlinear energetic particle modes have been observed allowing modelling comparisons under burning plasma conditions. First measurements of the eddy tilt angle of n_e fluctuations using correlation Doppler reflectometry as well as the radial correlation and cross-phase angles of T_e fluctuations have been achieved, showing good agreement with gyrokinetic simulations. Dedicated matches of H, D and He discharges (core/edge) highlight important isotope physics.

Recent Advances in EAST Physics Experiments in Support of Steady-State Operation for ITER and CFETR

B. N. Wan¹, Y. Liang^{1,2}, X. Z. Gong¹, N. Xiang¹, G. S. Xu¹, Y. Sun¹, L. Wang¹, J. P. Qian¹, H. Q. Liu¹, L. Zeng¹, L. Zhang¹, X. J. Zhang¹, B. J. Ding¹, Q. Zang¹, B. Lyu¹, M. H. Li¹, F. Ding¹, S. Y. Ding¹, H. F. Du¹, Z. P. Luo¹, J. Huang¹, T. Zhang¹, Y. Zhang¹, G. Q. Li¹, and T. Y. Xia¹

The EAST Team

¹*Institute of Plasma Physics, Chinese Academy of Sciences, Hefei, Anhui, People's Republic of China*

²*Forschungszentrum Jülich, Jülich, Germany*

Corresponding Author: B. N. Wan, bnwan@ipp.ac.cn

Significant progress in the development of plasma control mechanism and understanding the related physics for steady-state advanced high-performance H-mode plasmas have been achieved on EAST since the last IAEA FEC in 2016. First demonstration of > 100 s time scale long-pulse steady-state scenario with a good plasma performance ($H_{98}(y, 2) \sim 1.1$) and a good control of impurity and heat exhaust with the tungsten divertor has been successfully achieved on EAST using the pure RF power heating and current drive. The synergy effect between the ECH and two LHW systems (2.45 GHz and 4.6 GHz) on EAST has been investigated for enhanced current driven and improved confinement quality. ELM suppression using the $n = 1$ and 2 RMPs has been achieved in EAST and applied for development of the long-pulse H-mode scenario. Reduction of the peak heat flux on the divertor was demonstrated either in a QSF configuration or using the active radiation feedback control. A fully noninductive steady-state QSF plasma with a duration of 21 s has been obtained with a reduced factor of 2.5 on the outer divertor target. Divertor particle and heat flux control using a low n rotating RMP field has been confirmed. Suppression of the W sputtering has been achieved by lowering the edge medium- Z impurity content (C, O, etc) and forming a mixture deposition on the surface of divertor target after the application of lithium wall conditioning. Disruption mitigation experiments have been studied on EAST with the application of the massive gas injection of helium or argon on the termination of initial stable target plasmas. A further increase in the total heating power and improvement of the plasma confinement are expected when using a 0D model prediction for high bootstrap fraction ($f_{bs} \sim 50\%$) regime. Preliminary 1.5D simulations suggest that the on-axis ECRH will enhance the deposition of LHW power in the core region, which is beneficial to the effective core heating of the plasma. A new designed lower ITER-like tungsten divertor with active water-cooling is reported. With this upgrade, EAST will be capable of accessing the high-triangularity small-ELM H-mode regimes and also performing with target plasma in an advanced X-divertor configuration with assistance from two new water-cooled internal PF coils in support of steady-state operation for ITER and CFETR.

Overview of the KSTAR Research Progress and Future Plan Toward ITER and K-DEMO

H. K. Park¹, M. J. Choi², S. H. Hong², Y. In¹, Y. M. Jeon², W. H. Ko², J. G. Kwak²,
J. M. Kwon², Y. U. Nam², Y.-K. Oh², B. H. Park², S. J. Wang², S. W. Yoon², J.-W. Ahn³,
C.-S. Chang⁴, W. H. Choe⁵, Y. Chu², J. Chung², D. A. Humphreys⁶, S. H. Han², J. H. Kim²,
J. S. Ko², A. Loarte⁷, J. H. Lee², K. C. Lee², W. Lee², D. Mueller⁴, Y.-S. Na⁸, Y. B. Nam⁷,
K. R. Park², J. K. Park⁴, Y. S. Park⁹, R. A. Pitts⁷, S. A. Sabbagh⁹, and G. S. Yun¹⁰

The KSTAR Team

¹Ulsan National Institute of Science and Technology (UNIST), Ulsan, Republic of Korea

²National Fusion Research Institute (NFRI), Daejeon, Republic of Korea

³Oak Ridge National Laboratory (ORNL), Oak Ridge, TN 37831, USA

⁴Princeton Plasma Physics Laboratory (PPPL), Princeton, NJ 08540, USA

⁵Korea Advanced Institute of Science and Technology (KAIST), Daejeon, Republic of Korea

⁶General Atomics, San Diego, CA 92186, USA

⁷International Thermonuclear Experimental Reactor (ITER),

Cadarache Centre, 13108 St. Paul lez Durance, France

⁸Seoul National University, Seoul, Republic of Korea

⁹Columbia University, New York, NY 10027, USA

¹⁰Pohang University of Science and Technology (POSTECH), Pohang, Gyeongbuk 790-784, Republic of Korea

Corresponding Author: H. K. Park, hyeonpark@unist.ac.kr

The KSTAR research efforts have been focussed on expansion of the KSTAR operating space for ITER and K-DEMO[1], validation of critical physics and search of new physics. The operating regimes are high- β_p (up to ~ 2.8) noninductive long pulse up to ~ 8 s, high- β_N up to ~ 4.3 , and elongation $\kappa \sim 2.16$ and a long H-mode discharge over a minute. An improved underlying physics of resonant and nonresonant magnetic perturbation (RMP and NRMP) with the IVCC coils resulted in a long pulse edge localized mode (ELM)-crash suppressed H-mode discharge (~ 34 s) [2]. The ELM-crash suppression dependence on critical physical parameters, such as q_{95} , δ , and ν^* was extensively investigated. Identification of the role of turbulence induced by RMPs in suppression of the ELMs identified the turbulence flow ($\omega_{(\perp e)}$) physics during the RMP ramp up and down periods [3]. The study of L-H transition threshold power (P_{th}) dependence on the nonaxisymmetric field found that the P_{th} is significantly affected by RMPs while NRMP components had no influence on P_{th} [4]. New physics of interaction between the macroscopic fluctuation ($m/n = 2/1$ island) and microturbulences [5] and validation of q_0 issue in sawtooth instability has been explored [6]. Also the misaligned RMP configurations are used to test the divertor heat flux dispersal [6]. A major upgrade plan in KSTAR will be initiated near 2021 for stable higher β long pulse operation. Emphasis will be placed on a new actively cooled tungsten divertor possibly with new first wall materials and current drive (LHCD/Helicon). For the search of metal wall materials in the KSTAR upgrade plan, test of specially designed castellated tungsten block tiles of various shapes [7], impurity transport physics experiments via injection of trace Ar and Kr gases and tungsten dust were performed.

Continued...

This work is supported by the KSTAR research project funded by Korea Ministry of Science, ICT and Future Planning.

References

- [1] Y. K. Oh *et al.*, Fusion Eng. Des., **84**, 344 (2009).
- [2] Y. In *et al.*, Nucl. Fus., **55**, 043004 (2015).
- [3] J. Lee *et al.*, Phys. Rev. Lett., **117**, (7), 075001 (2016), J. Lee *et al.*, *ibid* (2018).
- [4] W. H. Ko *et al.*, APS bulletin (2017).
- [5] J. M. Kwon *et al.*, *ibid* (2018), M. J. Choi *et al.*, Nucl. Fus., **57**, 126058 (2017).
- [6] Y. In *et al.*, *ibid* (2018).
- [7] S. H. Hong *et al.*, *ibid* (2018).

Overview of Research Results from the Alcator C-Mod Tokamak

E. S. Marmar¹

The Alcator C-Mod Team

¹*Massachusetts Institute of Technology (MIT), Cambridge, MA 02139, USA*

Corresponding Author: E. S. Marmar, marmar@psfc.mit.edu

Alcator C-Mod has been the only divertor tokamak in the world capable of operating at magnetic fields up to 8 T, equalling and exceeding that planned for ITER. Because of its relatively compact size, C-Mod accesses regimes of extreme edge power density (1 MW/m² average through the surface of the plasma. H-modes on C-Mod have achieved world-record tokamak volume-average and pedestal plasma pressures ($\langle P \rangle$ above 0.2 MPa, $P_{\text{ped}} \sim 80$ kPa). The highest pedestals are obtained by accessing the super H-mode regime predicted by EPED enabling C-Mod to demonstrate P_{ped} at 90% of the ITER target. Data from a multimachine database shows that the boundary heat flux width scales inversely with B_{θ} , independent of machine size. The most recent data have extended this scaling to $B_{\theta} = 1.3$ T, beyond that envisioned for ITER, and the $1/B_{\theta}$ scaling persists. Based on these results, it is clear that power handling in reactors will be an even bigger challenge than in ITER, arguing for the urgent need for one or more dedicated divertor test tokamaks (DTT). Laser blow-off induced cold-pulses, an enigmatic transient phenomenon that has challenged the standard local-transport paradigm, has been explained by a new local turbulent transport model. Results from the TRANSP power balance code, coupled to the quasi-linear transport model TGLF-SAT1, with a new saturation rule that came about from cross-scale coupling physics, and that captures the nonlinear upshift of the critical gradient, are shown to describe the cold-pulse, including the existence of core temperature inversions at low density and disappearance at high density. A random forests machine learning algorithm has been trained on thousands of C-Mod discharges to detect disruption events. Disruption evolution time scales on C-Mod are relatively short, and this approach gives reliable warning no more than a few ms before disruption. Warning time-scales on larger plasmas are generally longer, good news for reactor applications. Steady-state tokamak reactors will need high bootstrap fraction, supplemented by RF current drive. Lower hybrid current drive is among the most efficient noninductive techniques. Recent modelling indicates that moving the launch point to the high field side can have many benefits, including accessibility at lower n_{\parallel} for higher efficiency.

Progress of Indirect Drive Inertial Confinement Fusion in the USA

J. L. Kline¹, S. H. Batha¹, L. R. Benedetti², D. Bennett², S. Bhandarkar², L. F. Berzak-Hopkines², J. Biener², M. M. Biener², R. Bionta², E. Bond², D. Bradley², P. A. Bradley¹, T. Braun², D. A. Callahan², J. Caggiano², T. Cardenas², C. Cerijan², B. Cagadas², D. Clark², C. Castro², W. S. Daughton¹, E. L. Dewald², T. Döppner², L. Divol², E. S. Dodd¹, R. Dylla-Spears², M. Eckart², D. Edgell³, M. Farrell⁴, J. Field², F. Fierro¹, D. N. Fittinghoff², M. Gatu-Johnson⁵, S. Johnson², G. Grim², N. Guler¹, S. Haan², B. M. Haines¹, C. E. Hamilton¹, A. V. Hamza², E. P. Hartouni², R. Hatarik², K. Hernderson¹, H. W. Herrmann¹, D. Hinkel², D. D. Ho², M. Hohenburger², D. Hoover⁴, H. Huang⁴, M. L. Hoppe⁴, O. A. Hurricane², N. Izumi², O. S. Jones², S. Khan², B. J. Kozioziemski², C. Kong², J. Kroll², G. A. Kyrala², R. J. Leeper², S. LePape², E. Loomis¹, T. Ma², A. J. Mackinnon², A. G. MacPhee², S. MacLaren², L. Masse², J. McNaney², N. B. Meezan², J. F. Merrill¹, E. C. Merritt¹, J. L. Milovich², D. S. Montgomery¹, J. Moody², A. Nikroo², J. Oertel¹, R. E. Olson¹, A. Pak², S. Palaniyappan¹, P. Patel², B. M. Patterson¹, T. S. Perry¹, R. R. Peterson¹, E. Piceno², J. E. Ralph², R. B. Randolph¹, N. Rice⁴, H. F. Robey², J. S. Ross², J. R. Rygg³, M. R. Sacks¹, J. Sauppe¹, J. Salmonson², D. Sayre², J. D. Sater², M. Schneider², M. Schoff⁴, D. W. Schmidt¹, S. Sepke², R. Seugling², R. C. Shah³, M. Stadermann², W. Stoeffl², D. J. Strozzi², R. Tipton², C. Thomas², R. P. J. Town², P. L. Volegov¹, C. Walters², M. Wang², C. Wilde¹, C. Wilson¹, E. Woerner², C. Yeamans², S. A. Yi¹, B. Yoxall², A. B. Zylstra¹, J. Kilkenny⁴, O. L. Landen², W. W. Hsing², and M. J. Edwards²

¹Los Alamos National Laboratory (LANL), Los Alamos, NM 87545, USA

²Lawrence Livermore National Laboratory (LLNL), Livermore, CA 94550, USA

³Laboratory for Laser Energetics, University of Rochester, Rochester, NY 14623, USA

⁴General Atomics, San Diego, CA 92186, USA

⁵Massachusetts Institute of Technology (MIT), Cambridge, MA 02139, USA

Corresponding Author: J. L. Kline, jkline@lanl.gov

Indirect drive converts high power laser into X-rays using small high-*Z* cavities called hohlraums. X-rays generated at the hohlraum walls drive a capsule filled with DT fusion fuel. Recent experiments have produced fusion yields exceeding 50 kJ where alpha heating provides $\sim 3\times$ increase in yield over *P dV* work. Comparison of the results to the common Lawson criterion suggests the current implosions performance is $\sim 30\%$ from conditions expected to initiate thermonuclear gain. Improvements to close the gap on the last $\sim 30\%$ are challenging requiring optimization of the target/implosions and the laser to extract maximum energy. The US programme has a three-pronged approach to maximize target performance each closing some portion of the gap. The first item is optimizing the hohlraum to couple more energy to the capsule while maintaining symmetry control. Novel hohlraum designs are being pursued that enable larger capsule to be driven symmetrically to both reduce 3D effects and increase energy coupled to the capsule.

Continued...

The second issue being addressed is capsule stability. Seeding of instabilities by the hardware used to mount the capsule and fill it with DT fuel remains a concern. Work such reducing the impact of the DT fill tubes and novel capsule mounts such as three sets of two single wire stands forming a cage, as opposed to the thin membranes currently used, are being pursued to reduce the effect of mix on the capsule implosions. There is also growing evidence native capsule seeds such as microstructure may be playing a role on limiting capsule performance and dedicated experiments are being developed to better understand the phenomenon. The last area of emphasis is the laser. As technology progresses and understanding of laser damage/mitigation advances, increasing the laser energy to as much as 2.6 MJ at 351 nm and increasing the laser power to 600 TW seems possible. This would increase the amount of energy available to couple to the capsule and allow larger capsules potentially increasing the hot spot pressure and confinement time. The combination of each of these focus areas have the potential to produce conditions to initiate thermonuclear ignition. The current understanding, status, and plans for near term research in each of these areas will be presented in the context of what is believed to be needed to obtain burning plasmas on NIF.

Progress of JT-60SA Project

P. Barabaschi¹, Y. Kamada², and H. Shirai²

The JT-60SA Team

¹JT-60SA, Fusion for Energy, Boltzmannstrasse 2, Garching, 85748, Germany

²JT-60SA, QST, 801-1 Mukoyama, Naka, Ibaraki, 311-0193 Japan

Corresponding Author: P. Barabaschi, pietro.barabaschi@f4e.europa.eu

The JT-60SA project was initiated in June 2007 under the framework of the broader approach (BA) agreement and Japanese national fusion programme for an early realization of fusion energy by conducting supportive and complementary work for the ITER project towards supporting the basis for DEMO. In 2009, after a complex start-up phase due to the necessity to carry out a re-baselining effort to fit in the original budget while aiming to retain the machine mission, performance, and experimental flexibility, the detailed design of the project could start immediately followed by the start of manufacturing of the long-lead items. Components and systems of JT-60SA are procured by the implementing agencies (IAs): Fusion for Energy in EU and QST (previously JAEA) in Japan. With the project now in an advanced implementation stage, the early defined approach for its implementation has proven to be successful and hence continues to be employed. This is underpinned by the very close collaboration between QST in Japan, F4E in Europe, and all other European stakeholders: the EU Voluntary Contributors (EU-VCs) and EUROfusion. The employed management model follows the early establishment of a single integrated project team (IPT) that operates in accordance to an agreed common quality management system, defining resources and processes crossing the lines between organizations. For JT-60SA the same management model strategy is planned also for the period beyond 2020, that is when the facility will be jointly operated and enhanced by the EU and JA. The paper will overview the progress of the manufacturing and assembly of the JT-60SA machine, the outlook towards first plasma, and progress in preparing for the scientific exploitation of JT-60SA following this milestone.

OV

Progress of the CFETR Design

G. Zhuang¹, V. S. Chan^{1,2}, J. Li³, and Y. X. Wan^{1,3}

The CFETR Team

¹University of Science and Technology of China, Hefei, Anhui, People's Republic of China

²General Atomics, San Diego, CA 92186, USA

³Institute of Plasma Physics, Chinese Academy of Sciences, Hefei, Anhui, People's Republic of China

Corresponding Author: G. Zhuang, gezhuang@ustc.edu.cn

The Chinese Fusion Engineering Test Reactor (CFETR), complementing ITER, is aiming to demonstrate fusion energy production up to 200 MW initially and to eventually reach DEMO relevant power level, to manifest high duty factor of 0.3–0.5, and to pursue tritium self-sufficiency with tritium breeding ratio (TBR) >1 . The key challenge to meet the missions of the CFETR is to run the machine in steady state and high duty factor. Recently, a self-consistent steady-state scenario for CFETR with fully sustained noninductive current drive is developed using a multidimensional code suite with physics-based models. In addition, results from the experimental validation conducted by a recent EAST steady-state experiment with off-axis current drive enhance confidence in the performance prediction from the integrated modelling. Finally, a fully noninductive reverse-shear scenario scaled to $R = 6.7$ m, $\beta_N \sim 3$, $H_{98} \sim 1.5$ and $f_{BS} \sim 0.75$ with the performance that meets the high gain CFETR mission is demonstrated. The scenario presents a self-consistent solution for the CFETR transport, equilibrium and pedestal dynamics.

At present, the CFETR physics design focusses on optimization of the third evolution CFETR ($R = 7$ m, $a = 2$ m, $\kappa = 2$, $B_t = 6.5$ – 7 T, $I_p = 13$ MA) consistent with steady-state or hybrid mode and a radiative divertor. Listed below are the main tasks we needed to tackle in the near-term, e.g., to demonstrate compatibility with the alpha particle stability and transport, and to quantify the tritium burn-up rate during the steady-state burning plasma phase in order to find a solution to meet the central fuelling requirement, and so on. The details will be given in this meeting.

Overview of the Validation Activities of IFMIF/EVEDA: LIPAc, the Linear IFMIF Prototype Accelerator and LiFus6, the Lithium Corrosion Induced Facility

M. Sugimoto¹, P. Cara², A. Kasugai¹, R. Heidinger², K. Sakamoto¹, J. Knaster³, P. Abbon⁴, T. Akagi¹, L. Antoniazzi⁵, N. Bazin⁴, L. Bellan⁵, P.-Y. Beauvais², B. Bolzon⁴, D. Bortolato⁵, N. Chauvin⁴, S. Chel⁴, M. Comunian⁵, H. Dzitzko², T. Ebisawa¹, E. Fagotti⁵, D. Gex², R. Gobin⁴, F. Grespan⁵, Y. Hirata¹, R. Ichimiya¹, D. Jimenez-Rey⁶, A. Jokinen³, I. Kirpichev⁶, K. Kondo¹, S. Maebara¹, A. Marqueta², J. Marroncle⁴, P. Mendez⁶, J. Molla⁶, C. de la Morena⁵, M. Montis⁵, I. Moya³, A. Palmieri⁵, A. Pisent⁵, G. Phillips², I. Podadera⁶, G. Pruneri³, D. Regidor⁶, B. Renard⁴, F. Scantamburlo³, T. Shinya¹, M. Weber³, P. Favuzza⁷, G. Micciché⁷, and A. Aiello⁷

¹National Institutes for Quantum and Radiological Science and Technology (QST), Rokkasho Fusion Institute, Rokkasho-mura, Aomori, Japan

²Fusion for Energy (F4E), Boltzmannstrasse 2, Garching, 85748, Germany

³IFMIF/EVEDA ILIC Unit, Rokkasho, Japan

⁴Commissariat à l'énergie atomique (CEA/Saclay), 91191 Gif-sur-Yvette, France

⁵Istituto Nazionale di Fisica Nucleare (INFN), Laboratori Nazionali di Legnaro, Legnaro, Italy

⁶Centro de Investigaciones Energéticas, Medioambientales y Tecnológicas (CIEMAT), Madrid, Spain

⁷ENEA/Brasimone, Camugnano BO, Italy

Corresponding Author: M. Sugimoto, sugimoto.masayoshi@qst.go.jp

In this report, the latest results of the validation activities of the IFMIF/EVEDA project under the Broader Approach agreement are overviewed. For the linear IFMIF prototype accelerator (LIPAc) to demonstrate the 9 MeV/125 mA D⁺ beam acceleration, the beam qualification study of the injector was completed with the emittance of 0.16 π mm mrad smaller than required 0.3 π mm mrad, and the maximum vane voltage in the RFQ cavity was achieved at 143 kV exceeding the required 132 kV. These components and other subsystems of LIPAc are ready to inject the beam to RFQ to provide the 5 MeV D⁺ beam. The superconducting RF linac necessary for the 9 MeV D⁺ beam is close to the end of manufacturing phase to start its final assembly in Rokkasho. For the liquid lithium loop activities, 4000 hours lithium corrosion test of the reduced activation ferritic-martensitic steels using the LiFus6 were completed and verified that the corrosion rate can be kept under control and well below the requirement of 1 $\mu\text{m}/\text{y}$, after achieving a good purity of lithium, < 30 ppm N.

The Strategy of Fusion DEMO In-Vessel Structural Material Development

H. Tanigawa¹, E. Diegele², Y. Katoh³, T. Nozawa¹, T. Hirose¹, M. Gorley⁴, H. Sakasegawa¹,
E. Gaganidze⁵, J. Aktaa⁵, and G. Pintsuk⁶

¹National Institutes for Quantum and Radiological Science and Technology (QST),
Rokkasho Fusion Institute, Rokkasho-mura, Aomori, Japan

²EUROfusion Programme Management Unit Garching, Boltzmannstraße 2, 85748 Garching Germany

³Oak Ridge National Laboratory (ORNL), Oak Ridge, TN 37831, USA

⁴United Kingdom Atomic Energy Authority, Culham Science Centre, Abingdon, UK

⁵Karlsruhe Institute of Technology (KIT), Karlsruhe, Germany

⁶Forschungszentrum Jülich, Jülich, Germany

Corresponding Author: H. Tanigawa, tanigawa.hiroyasu@qst.go.jp

The structural material development for the breeding blanket in a future fusion reactor is regarded as the most challenging technical issue due to the significance of 14 MeV DT fusion neutron irradiation that induces high displacement damage with a significant amount of the transmutation formed gas elements such as helium and hydrogen.

The strategy of fusion in-vessel structural material development toward fusion DEMO is addressed with special emphasis on the current status and the limitations due to the reliability of data. A major issue in developing and validating structural materials for a fusion DEMO reactor are missing facilities where materials can be tested under the real in-vessel conditions of deuterium-tritium (DT) fusion. Ideally, neutron irradiation induced changes are expected to be negligible or “minor”. The reality is, however, that irradiation effects are neither “negligible” nor “minor”. Thus, it is essential to define the negligible and maximum level of irradiation-induced changes which could be incorporated into safety factors that are defined “empirically”, and the most significant technical challenges are to develop and qualify materials based on the knowledge and data acquired in experiments not performed under “real” fusion environment but in fission neutron irradiation and various simulation irradiation experiments, and to develop and verify a framework of DEMO reactor design criteria for in-vessel components (DDC-IC).

Here we propose a new strategy based on probabilistic approaches, where the probability of failure is calculated based on the probability density function of postulated load distribution and material property distribution, as a part of the design methodology in order to mitigate the uncertainties caused by multiple sources. It is essential to conduct statistical analyses on material property data to make the data applicable to the probability based design method. Consequently, the vast amount of fission neutron irradiation data which fulfil the statistical requirements should be developed up to some critical irradiation dose levels at which the irradiation effects caused by fusion neutron spectra are expected to become very different from fission data.

Overview of First Wendelstein 7-X High-Performance Operation with Island Divertor

T. Klinger¹

The W7-X Team

¹Max-Planck-Institut für Plasmaphysik, Greifswald, Germany

Corresponding Author: T. Klinger, thomas.klinger@ipp.mpg.de

The optimized superconducting stellarator device Wendelstein 7-X restarted operation after the assembly of a graphite heat shield and an inertially cooled island divertor. This paper reports on results from the first high-performance plasma operation. Plasma densities of $1\text{--}4 \times 10^{19}/\text{m}^3$ with electron temperature 5–10 keV were routinely achieved with hydrogen gas fuelling, eventually terminated by a radiative collapse. Up to $1.4 \times 10^{20}/\text{m}^3$ plasma density was reached with repetitive hydrogen pellet injection. Here, the ions are indirectly heated, and at a density of $8 \times 10^{19}/\text{m}^3$ temperatures $T_e \simeq T_i = 3.4$ keV were accomplished, which corresponds to $nT\tau_E = 6.4 \times 10^{19}$ keV s/m³ with peak diamagnetic energy 1.1 MJ. Stable 25 s long-pulse helium discharges with 2–3 MW ECRH power and up to 75 MJ injected energy were created routinely for equilibrium and divertor load studies, with plasma densities around $5 \times 10^{19}/\text{m}^3$ and 5 keV electron temperature. The divertor heat loads remained far below the limits. The O/C impurity concentration ratio has decreased in comparison to the previous limiter operation and no intrinsic impurity accumulation along with high edge radiation were observed in stationary plasmas. During pellet-fuelled hydrogen discharges, full detachment was observed with divertor target heat flux reduction by more than $\times 10$. Both X2 and O2 mode ECRH schemes were applied and electron cyclotron current drive (ECCD) experiments were conducted. During co-ECCD injection experiments with axial currents up to 13 kA, frequent fast crashes were observed mainly in the core electron temperature, suggesting a fast magnetic reconnection mechanism. The radial electric field measured with (Doppler) and correlation reflectometry changes sign at the plasma edge from $+10 \dots +20$ kV/m to $-10 \dots -5$ kV/m, fairly independent of discharge parameters and heating power. Edge and scrape-off layer turbulence was measured with both Langmuir probes and reflectometer diagnostics. Core turbulence was measured with a phase contrast imaging diagnostic and different levels of broad band turbulence as well as coherent Alfvén mode activity were observed.

OV

Overview of the First Deuterium Experiment in LHD

T. Morisaki^{1,2}

The LHD Experiment Group

¹*National Institute for Fusion Science (NIFS), Toki, Gifu, Japan*

²*Department of Fusion Science, Graduate University for Advanced Studies (SOKENDAI), Toki, Gifu, Japan*

Corresponding Author: T. Morisaki, morisaki@nifs.ac.jp

In the first deuterium (D) experiment, LHD established one of the most important milestones towards the realization of the helical fusion reactor, ion temperature $T_i \sim 10$ keV. This is the highest record among stellarator/heliotron devices. Clear reduction of the ion thermal diffusivity in both core and edge regions in D discharge from hydrogen (H) was identified, indicating the effect of the isotope mass. This experimental result was supported by the initial results from gyrokinetic simulations including multispecies of ion. By measuring the neutron flux from D plasma, energetic particle (EP) behaviour trapped in the helical ripple could directly be estimated, which is quite important for heliotron devices, because demonstration of the EP confinement is essential to realize the burning condition. Precise measurement of the tritium exhaust demonstrated the tritium mass balance including the evacuation system.

Overview of TJ-II Stellarator Results

E. Ascasíbar¹

The TJ-II Team

¹*Centro de Investigaciones Energéticas, Medioambientales y Tecnológicas (CIEMAT), Madrid, Spain*

Corresponding Author: E. Ascasíbar, enrique.ascasibar@ciemat.es

The flexibility of TJ-II together with its unique plasma diagnostics makes it an ideal laboratory to study the relationship between magnetic topology, electric fields, transport and model validation.

Zonal flows and heat transport: HIBP measurements of zonal electrostatic potential relaxation are consistent with EUTERPE gyrokinetic (GK) simulations. The width of the oscillating zonal flow (ZF) radial electric field (E_r) structures depends on its frequency. Additional GK simulations predict the localization of density fluctuations, in line with Doppler reflectometry (DR) measurements. Transfer entropy technique-based analyses shows that transport is not smooth and continuous but rather occurs in a stepwise fashion.

Impurity and particle dynamics: Neoclassical (NC) theory results show how a negative E_r field can coexist with an outward impurity flux. Flux-surface variations of electrostatic potential can have a significant impact on high- Z impurity radial fluxes. Probe measurements of plasma potential asymmetries on magnetic flux surfaces and DR measurements of poloidal asymmetries in E_r fields, are consistent with NC simulations. Plasma core fuelling experiments with pellets show that the radial redistribution of particles can be understood qualitatively from NC predictions. Thermal neutrals react to low frequency plasma fluctuations.

NC and turbulent transport: Zero frequency E_r fields as well as low frequency ZF-like global oscillations have been identified during the low to high (L-H) transition in H and D plasmas. No evidence of the isotope effect was observed in the L-H transition.

Power-exhaust physics: The TJ-II programme on liquid metals address fundamental issues such as the self-screening effect driven by liquid lithium evaporation and the tritium inventory control.

Stellarator optimization: Explicit expressions for the radial NC fluxes have been calculated in low collisionality regimes and have been included in a numerical code to deal with magnetic configurations close to omnigenity. The relaxation of the constraint of periodicity imposed by the external confining magnetic field coils in a Helias configuration produces weak periodicity-breaking deformations of the plasma. The conditions of quasi-isodynamicity are not significantly altered by the periodicity-breaking distortions.

OV

ELM and ELM-control Simulations

S. Pamela¹, N. Aiba², H. Urano³, G. T. A. Huijsmans^{4,5}, J. Garcia⁵, S. Smith¹, S. Futatani⁶,
M. Hölzl⁷, and E. de la Luna⁸

¹*Culham Centre for Fusion Energy (CCFE), Culham Science Centre, Abingdon, UK*

²*National Institutes for Quantum and Radiological Science and Technology (QST),
Rokkasho Fusion Institute, Rokkasho-mura, Aomori, Japan*

³*National Institutes for Quantum and Radiological Science and Technology (QST),
Naka Fusion Institute, Naka-shi, Ibaraki-ken, Japan*

⁴*Eindhoven University of Technology, Eindhoven, Netherlands*

⁵*Institut de Recherche sur la Fusion par confinement Magnétique (IRFM),
Commissariat à l'énergie atomique (CEA/Cadarache), 13108 St. Paul lez Durance, France*

⁶*Universitat Politècnica de Catalunya (UPC), Barcelona, Spain*

⁷*Max-Planck-Institut für Plasmaphysik, Garching, Germany*

⁸*Centro de Investigaciones Energéticas, Medioambientales y Tecnológicas (CIEMAT), Madrid, Spain*

Corresponding Author: S. Pamela, stanislas.pamela@ukaea.uk

Future devices like JT-60SA, ITER and DEMO require quantitative predictions of pedestal density and temperature levels, as well as divertor heat fluxes, to improve global confinement capabilities while preventing divertor erosion/melting in the planning of future experiments. Such predictions can be obtained from nonlinear MHD codes like JOEKE, for which systematic validation against current experiments is necessary. In this paper, we show the validation of ELM simulations with JOEKE using quantitative comparison against JT-60U experiments. Note this is the first JOEKE validation of ELM simulations at exact Spitzer resistivity. In addition, we demonstrate the essential importance of the separatrix position, required for a successful agreement with experimental data. On the basis of this validation, we propose estimates of ELM size, ELM-induced divertor heat-fluxes, and pre-ELM pedestal pressure, for future JT-60SA scenarios.

Experiments in Disruption Avoidance for ITER Using Passive and Active Control

E. J. Strait¹, J. L. Barr¹, J. W. Berkery², W. Choi², M. Clement², N. W. Eidietis¹, R. S. Granetz³, J. M. Hanson¹, C. T. Holcomb⁴, D. A. Humphreys¹, J. Kates-Harbeck⁵, K. Kornee⁶, E. Kolemen⁷, R. J. La Haye¹, M. Lancot¹, Y. Q. Liu¹, N. Logan⁷, T. C. Luce¹, S. Munaretto¹, C. E. Myers⁷, M. Okabayashi⁷, J.-K. Park⁷, C. Paz-Soldan¹, F. M. Poli⁷, C. Rea³, S. A. Sabbagh², N. P. Taylor¹, F. Turco², A. Turnbull¹, Z. R. Wang⁷, and A. Welande¹

¹General Atomics, San Diego, CA 92186, USA

²Columbia University, New York, NY 10027, USA

³Massachusetts Institute of Technology (MIT), Cambridge, MA 02139, USA

⁴Lawrence Livermore National Laboratory (LLNL), Livermore, CA 94550, USA

⁵Department of Physics, Harvard University, Cambridge, MA 02138, USA

⁶Eindhoven University of Technology, Eindhoven, Netherlands

⁷Princeton Plasma Physics Laboratory (PPPL), Princeton, NJ 08540, USA

Corresponding Author: E. J. Strait, strait@fusion.gat.com

Key plasma physics and real-time control elements needed for robustly stable operation of high fusion power discharges in ITER have been demonstrated in US fusion research. Optimization of the current density profile has enabled passively stable operation without $n = 1$ tearing modes in discharges simulating ITER's baseline scenario with zero external torque. Stable rampdown of the discharge has been achieved with ITER-like scaled current ramp rates, while maintaining an X-point configuration. Significant advances have been made toward real-time prediction of disruptions: machine learning techniques for prediction of disruptions have achieved 90% accuracy in offline analysis, and direct probing of ideal and resistive plasma stability using 3D magnetic perturbations has shown a rising plasma response before the onset of a tearing mode. Active stability control contributes to prevention of disruptions, including direct stabilization of resistive-wall kink modes in high- β discharges, forced rotation of magnetic islands to prevent wall locking, and localized heating/current drive to shrink the islands. These elements are being integrated into stable operating scenarios and a new event-handling system for off-normal events in order to develop the physics basis and techniques for robust control in ITER.

Work supported by the U.S. Department of Energy under DE-SC0008520, DE-FC02-04-ER54698, DE-SC0016372, DE-FG02-04ER54761, DE-AC52-07NA27344, DE-SC0015878, DE-SC0014264, DE-FG02-99ER54524, DE-FOA-0001498, DE-AC02-09CH11466, DE-FC02-99ER-54512, DE-SC0010720, DE-SC0010492, and the U.S. Department of Energy Computational Science Graduate Fellowship, and by the EUROfusion Consortium with funding through FuseNet from the Euratom research and training programme 2014–2018 under Grant Agreement No. 633053. The views and opinions expressed herein do not necessarily reflect those of the European Commission.

Overview of HL-2A Recent Experiments

M. Xu¹

The HL-2A Team

¹*Southwestern Institute of Physics, Chengdu, Sichuan, People's Republic of China*

Corresponding Author: M. Xu, minxu@swip.ac.cn

Experiments on the HL-2A tokamak have been aimed at physics issues involved in advanced tokamaks and ITER since the last IAEA FEC. In particular, significant progresses have been made in the following areas: techniques and physics of ELM control, energetic-particle physics, MHD, disruption, multiscale interactions, physics of advanced tokamak scenario, edge turbulence. Regarding to techniques and physics of ELM control, intensive experiments for controlling ELMs have been performed in HL-2A with several tools, including RMP, LHCD, LBO-seeded impurities (Al, Fe, W) and impurity SMBI (Ar, Ne). The observed ELM mitigation with pedestal turbulence enhancement and radial spectral shift due to the pedestal velocity shear reduction can be qualitatively simulated by a turbulent heat transport model. Toroidal Alfvén eigenmodes (TAE) driven by energetic-ion had been observed on HL-2A. Progress has been made in understanding the physics of instabilities that may interacts with turbulence causing strong influence on cross-field transport and in developing strategies to control them, including neo-classical tearing modes and core-localized Alfvén eigenmodes. The stabilization of $m/n = 1/1$ ion fishbone activities by ECRH were found on HL-2A. The experimental results confirmed the stabilization of $m/n = 1/1$ fishbone depends not only on the injected power but also on the radial deposition location of ECRH. Disruption mitigation experiments with a new fast SMBI gas injection system have been recently performed. In HL-2A, advanced tokamak scenario with central q close to 1 was achieved. Auxiliary heating (mainly NBI) during the current rise phase was used, creating ITBs with a weak magnetic shear in the plasma centre. In ITB plasmas with weak magnetic shear, kinetic electromagnetic instabilities were confirmed and investigated. For the study of edge turbulence and flows, a signature of incoherent phase slips was evidenced by the study on the interaction between $E \times B$ shear and cross phase between radial velocity perturbation and poloidal velocity perturbation. In the pedestal region, the dynamics of the plasma flows, turbulence and pedestal formation across the L-I-H transition were studied by Doppler reflectometry. The electromagnetic character of filamentary structure was measured in the scrape off layer of HL-2A for the first time.

Physics Research on the TCV Tokamak Facility: From Conventional to Alternative Scenarios and Beyond

S. Coda¹

The TCV Team and The EUROfusion MST1 Team

¹*Swiss Plasma Center (SPC), École polytechnique fédérale de Lausanne (EPFL), 1015 Lausanne, Switzerland*

Corresponding Author: S. Coda, stefano.coda@epfl.ch

The research programme of the TCV tokamak ranges from conventional to advanced tokamak scenarios and advanced divertor configurations, to exotic plasmas driven by theoretical insight, exploiting the device's unique shaping capabilities. The facility is operated intensively both domestically and with EUROfusion support. The new 1 MW NBI has expanded the parameter range, now encompassing ELMy H-modes in an ITER-like shape, stationary noninductive discharges sustained by ECCD and NBCD, and negative-triangularity diverted plasmas.

Disruption avoidance by real-time locked mode prevention or unlocking with ECRH was thoroughly documented, using magnetic and radiation triggers. Runaway generation with high- Z noble gas injection and runaway dissipation by subsequent Ne or Ar injection were studied for model validation.

Turbulence is reduced in the core at negative triangularity, consistent with increased confinement and in accord with global gyrokinetic simulations. The GAM, possibly coupled with avalanche events, has been linked with particle flow to the wall in diverted plasmas.

In H-mode, the pedestal pressure and plasma stored energy are insensitive to fuelling, whereas nitrogen seeding moves the pedestal outwards and increases the stored energy. High fuelling at high triangularity (0.54) is key to accessing the attractive small-ELM (type-II) regime.

Detachment, SOL transport, and turbulence were studied in L- and H-mode in both standard and alternative configurations (snowflake, super-X, and beyond). The L-H transition threshold is independent of the divertor topology. In the attached L-mode phase, an increase in flux expansion or divertor leg length reduces the power exhausted at the outer strike point and increases radiation. The detachment process is caused by power "starvation" reducing the ionization source, with volume recombination playing only a minor role. The SOL density shoulder observed at high collisionality is correlated with increased blob size.

A doublet plasma, featuring an internal X-point, was achieved successfully, if only transiently, and a transport barrier was observed in the mantle just outside the internal separatrix. In the near future variable-configuration baffles and cryopumping will be introduced to investigate the effect of divertor closure on exhaust and performance, and 2 MW ECRH and 1 MW NBI heating will be added.

Overview of Operation and Experiments in the ADITYA-U Tokamak

R. L. Tanna¹, J. Ghosh^{1,2}, H. Raj^{1,2}, R. Kumar¹, S. Aich^{1,2}, T. Macwan^{1,2}, D. Kumawat¹, K. A. Jadeja¹, K. M. Patel¹, M. B. Kalal¹, D. S. Varia¹, D. H. Sadharakiya¹, S. B. Bhatt¹, K. Sathyanarayana¹, B. K. Shukla¹, P. K. Chattopadhyay^{1,2}, M. N. Makwana¹, K. S. Shah¹, S. Gupta¹, V. Ranjan¹, V. Balakrishnan¹, C. N. Gupta¹, V. K. Panchal¹, E. V. Praveenlal¹, B. Arambhadiya¹, M. Shah¹, V. D. Raulji¹, M. B. Chowdhuri¹, S. Banerjee¹, R. Manchanda¹, D. Raju¹, P. K. Atrey¹, S. K. Pathak^{1,2}, U. C. Nagora¹, J. V. Raval¹, Y. S. Joisa¹, M. Kumar¹, K. Tahiliani¹, S. K. Jha¹, M. V. Gopalakrishna¹, J. Thomas¹, A. Kumar¹, and S. N. Pandya¹

¹*Institute for Plasma Research (IPR), Bhat, Gandhinagar, India*

²*Homi Bhabha National Institute (HBNI), Anushakti Nagar, Mumbai 400094, India*

Corresponding Author: R. L. Tanna, rtan.ipr@gmail.com

Ohmically heated circular limiter tokamak, ADITYA has been upgraded to a tokamak named ADITYA Upgrade (ADITYA-U) having open divertor configuration with divertor plates. Experiment research in ADITYA-U ($R_0 = 75$ cm, $a = 25$ cm) has made significant progress, since the last FEC in 2016. After successful commissioning of ADITYA-U, the phase-I plasma operations have been conducted from December 2016, with graphite toroidal belt limiter. Filament preionization assisted purely Ohmic discharges with circular plasma have been obtained. Hydrogen gas breakdown has been obtained in each of ~ 700 discharges without a single failure. Repeatable plasma discharges of plasma current ~ 80 kA–95 kA, duration ~ 80 –100 ms with toroidal magnetic field B_ϕ (max.) ~ 1 T and chord-averaged electron density $\sim 2.5 \times 10^{19}/\text{m}^3$ has been achieved. Later, the discharge duration has been enhanced up to ~ 180 ms with the application of negative converter along with better wall conditioning, achieved by implementing the glow discharge cleaning (GDC) with Ar: H₂, He:H₂ gas mixture and with intense short plasma pulses in ECR produced plasma background. Being a medium sized tokamak, runaway electron generation, transport and mitigation experiments have always been one of the prime focus of ADITYA-U. MHD activities and density enhancement with H₂ gas puffing has also studied. The phase-I operation was successfully completed in March 2017.

The phase-II operation preparation in ADITYA-U includes, calibration of magnetic diagnostics followed by commissioning of major diagnostics and installation of baking systems. After repeated cycles of baking the vacuum vessel up to $\sim 130^\circ\text{C}$, the ADITYA-U phase-II operations have been resumed from February 2018 and are continuing in order to achieve plasma parameters close to the design parameters of circular limiter plasmas using real-time plasma position control. Several experiments, including the fuelling with supersonic molecular beam injection, H₂ gas puffing for runaway control during current flat-top and disruptions, Neon gas puff assisted radiative improved confinement and the experiments related to plasma shaping is undergoing. The complete upgradation including dismantling of ADITYA and reassembling of ADITYA-U along with experimental results of phase-I and phase-II operations from ADITYA-U and overall progress will be discussed in this paper.

Tokamak Research in Ioffe Institute

N. N. Bakharev¹, A. B. Altukhov¹, L. G. Askinazi¹, N. A. Babinov¹, A. N. Bazhenov¹,
A. A. Belokurov¹, E. N. Bondarchuk², I. M. Bukreev¹, V. V. Bulanin³, Al. P. Chernakov⁴,
F. V. Chernyshev¹, L. A. Esipov¹, D. B. Gin¹, A. V. Gorbunov⁵, A. D. Gurchenko¹,
V. K. Gusev¹, E. Z. Gusakov¹, M. A. Irzak¹, A. A. Kavin², N. A. Khromov¹, E. O. Kiselev¹,
T. P. Kiviniemi⁶, V. A. Kornev¹, A. N. Koval¹, S. V. Krikunov¹, O. L. Krutkin¹,
G. S. Kurskiev¹, S. V. Lebedev¹, S. Leerink⁶, A. D. Melnik¹, V. B. Minaev¹, A. B. Mineev²,
I. V. Miroshnikov¹, E. E. Mukhin¹, A. N. Novokhatsky¹, P. Niskala⁶, K. Y. Oshuev¹,
M. I. Patrov¹, A. V. Petrov³, Y. V. Petrov¹, A. Y. Popov¹, A. G. Razdobarin¹,
D. V. Razumenko¹, N. V. Sakharov¹, D. S. Samsonov¹, A. N. Saveliev¹, P. B. Shchegolev¹,
A. E. Shevelev¹, A. D. Sladkomedova¹, A. I. Smirnov¹, V. V. Solokha¹, V. A. Solovei¹,
A. Y. Telnova¹, V. A. Tokarev¹, S. Y. Tolstyakov¹, A. S. Tukachinsky¹, V. I. Varfolomeev¹,
A. Y. Yashin³, E. G. Zhilin⁷, and N. A. Zhubr¹

¹Ioffe Institute, St. Petersburg, Russian Federation

²D. V. Efremov Institute of Electrophysical Apparatus (JSC–NIIEFA), St. Petersburg, Russian Federation

³St. Petersburg State Polytechnical University, St. Petersburg, Russian Federation

⁴Spectral-Tech ZAO, St. Petersburg, Russian Federation

⁵National Research Centre “Kurchatov Institute”, Moscow, Russian Federation

⁶Aalto University, Espoo, Finland

⁷Ioffe Fusion Technology Ltd., St. Petersburg, Russian Federation

Corresponding Author: N. N. Bakharev, bakharev@mail.ioffe.ru

Research of various aspects of tokamak physics is conducted on small tokamaks at Ioffe Institute in a wide range of experimental conditions: $R/a = 1.6$, $B_t = 0.5(1.0)$ T, $I_p = 250(500)$ kA — Globus-M(M2); $R/a = 2.4$, $B_t = 1.0$ T, $I_p = 150$ kA — TUMAN-3M; $R/a = 7.0$, $B_t = 3.0$ T, $I_p = 25$ kA — FT-2 tokamaks. Results obtained in final Globus-M experimental campaign (before upgrade shutdown) with the 25% toroidal magnetic field and plasma current increase up to 0.5 T and 250 kA respectively are presented. In these experiments an overall improvement in plasma performance was observed. Energy confinement time study was performed in both OH and NBI heated H-mode plasma. Strong τ_E dependence on both I_p and B_t was observed, while the dependence on density and absorbed power was similar to the conventional H-mode scaling $IPB_{98}(y, 2)$. The lifetime of modes with ITB reached a few confinement times before the $q = 1$ resonant surface appeared in the plasma. Plasma confinement was also studied in the compact TUMAN-3M tokamak. No noticeable isotope effect in particle confinement in hydrogen and deuterium ohmic L-mode was observed. On the contrary, in the ohmic H-mode particle confinement was approximately 1.5 times higher in deuterium than in hydrogen. Study of TAEs on Globus-M was performed at increased magnetic field. The mode character and influence on the fast ions changed with the increase of the B_t and I_p . At TUMAN-3M ion cyclotron emission in OH and NBI heated discharges was studied. Application of the NBI revealed central location of ICE, excitation by sub-Alfvénic beam ions and fine structure of the emission spectral lines. New diagnostics, designed for Globus-M2, were installed and tested on Globus-M. At the FT-2 tokamak, the ELMFIRE global gyrokinetic modelling of the OH discharge is compared to the experimental data using the specially developed fast linear version of the X-mode DR synthetic diagnostics. The anomalous absorption of the pump wave in the ECRH experiments due to the parametric excitation of trapped UH waves in the vicinity of the density or magnetic field profile local maximum is considered.

Overview of New MAST Physics in Anticipation of First Results from MAST Upgrade

J. R. Harrison^{1,2}

Rapporteured by: J. E. Menard

¹*Culham Centre for Fusion Energy (CCFE), Culham Science Centre, Abingdon, UK*

²*On Behalf of the MAST Upgrade and EUROfusion MST1 Teams*

Corresponding Author: J. R. Harrison, james.harrison@ukaea.uk

MAST Upgrade will operate in 2018 with unique capabilities to explore plasma exhaust and alternative divertor configurations to address this key issue for DEMO.

Modelling of the interaction between filaments with BOUT++ indicates filaments separated by more than $5\times$ their width move independently, and their velocity is slightly perturbed by if their separation is 1 width, suggesting radial density profiles can be modelled as the superposition of filaments. Secondary filaments on MAST are found up to 1 ms after type-I ELMs that correlate with plasma interaction with surfaces near the X-point. A quiescent region devoid of filaments near the X-point has been routinely observed, extending from the separatrix to a normalized flux of 1.02. Counter-streaming flows of doubly ionized carbon along field lines, generated by localized gas puffing, have been observed and reproduced in EMC3-EIRENE simulations. MAST-U will be an excellent facility for understanding detachment onset and control in closed divertors. SOLPS modelling predicts the upstream density needed to reach detachment will be over $2\times$ lower in the Super-X configuration compared with the conventional divertor due to increased total magnetic flux expansion. Analytic modelling predicts detachment control in a Super-X is more amenable to external control.

Detailed measurements of transport through the edge have been made in MAST L-mode plasmas to characterize a geodesic acoustic mode 2 cm from the separatrix. Interpretation of plasma potential profile measurements using ball-pen probes have been improved through kinetic modelling, showing that electrons polarize the material around the probe, leading to $E \times B$ drifts of ions to the probe. Measurements of the effects of sawteeth on fast ion confinement on MAST indicate that passing and trapped particles are equally redistributed by the sawtooth crash. There is no apparent energy threshold for redistribution, indicating redistribution due to a mechanism resonant with the $m = 1$ perturbation.

Gyrokinetic simulations of ETG turbulence in MAST are in close agreement with the measured collisionality dependence of the energy confinement time. Beam emission spectroscopy measurements show that flow shear leads to eddy tilting in up-down symmetric plasmas and skewed density fluctuations. First results from MAST Upgrade operations will be presented.

Overview of the FTU Results

G. Pucella¹

The FTU Team

¹ENEA C. R. Frascati, Dipartimento FSN, Frascati, Italy

Corresponding Author: G. Pucella, gianluca.pucella@enea.it

Since the 2016 IAEA FEC Conference, FTU operations have been mainly devoted to experiments on runaway electrons and investigations about a tin liquid limiter; other experiments have involved elongated plasmas and dust studies. The tearing mode onset in the high density regime has been studied by means of the linear resistive code MARS and the highly collisional regimes have been investigated. New diagnostics, such as a runaway electron imaging spectroscopy system for in-flight runaways studies and a triple Cherenkov probe for the measurement of escaping electrons, have been successfully installed and tested, and new capabilities of the collective Thomson scattering and the laser induced breakdown spectroscopy diagnostics have been explored.

Overview and Status of Direct-Drive Inertial Confinement Fusion in the United States

B. P. Radha¹

¹Laboratory for Laser Energetics, University of Rochester, Rochester, NY 14623, USA

Corresponding Author: B. P. Radha, rbah@lle.rochester.edu

Direct-drive (DD) inertial confinement fusion (ICF) offers a potential path for high yield and ignition. Two approaches—laser direct drive (LDD), being pursued primarily at the OMEGA laser and the National Ignition Facility (NIF), and magnetized liner inertial fusion (MagLIF), being pursued primarily at the Sandia National Laboratories, will be discussed in this talk. In LDD nominally identical laser beams are used to drive an imploding cryogenic shell on OMEGA to obtain high pressures and temperatures in a hot spot surrounded by a cold fuel. The goal is to obtain ignition-relevant hot-spot pressures in OMEGA-scale cryogenic deuterium-tritium layered implosions. Hot-spot pressures up to 56 ± 7 Gbar have been demonstrated in these implosion experiments. In addition, recent implosion results when scaled to NIF energies are predicted to produce fusion yields approaching 300 kJ. Experiments on the NIF are additionally used to address the MegaJoule-scale physics such as laser coupling and preheat from energetic electrons. In the MagLIF approach, a 1 kJ, 1 TW laser pulse is used to preheat the plasma just as the 16 MA current begins to quasi-adiabatically compress the premagnetized deuterium. Promising ion temperatures (~ 3 keV) and neutron yields (5×10^{12} DD neutrons) have been obtained with MagLIF experiments at relatively low implosion speeds of $\sim 7 \times 10^6$ cm/s, indicating successful magnetic flux compression and decreased thermal conductivity losses required for ignition. Ignition remains a challenge for both the direct-drive approaches, including improving understanding of the plasma conditions, controlling nonuniformity, improving laser coupling, and developing enhanced diagnostics. The motivation, challenges, and status of direct-drive research in the United States is presented in this talk.

This material is based upon work supported by the U.S. Department of Energy National Nuclear Security Administration under Award Number DE-NA0001944, the University of Rochester, and the New York State Energy Research and Development Authority. The support of U.S. Department of Energy does not constitute an endorsement by U.S. Department of Energy of the views expressed in this article.

ITER-Relevant Research on the COMPASS Tokamak

R. Panek¹, M. Hron¹, **M. Komm**¹, J. Adamek¹, P. Bilkova¹, O. Bogar¹, P. Bohm¹, J. Cavalier¹, R. Dejarnac¹, M. Dimitrova¹, O. Ficker¹, O. Grover^{1,2}, P. Hacek^{1,2}, J. Havlicek¹, A. Havranek^{1,3}, J. Horacek¹, M. Imrisek^{1,2}, K. Kovarik¹, J. Krbec^{1,3}, L. Kripner^{1,2}, E. Macusova¹, T. Markovic^{1,2}, K. Mitosinkova^{1,2}, J. Mlynář¹, D. Naydenkova¹, P. Pavlo¹, M. Peterka^{1,2}, A. Podolnik^{1,2}, J. Seidl¹, J. Stockel¹, M. Tomes^{1,2}, J. Urban¹, M. Varavin¹, J. Varju¹, P. Vondracek^{1,2}, V. Weinzettl¹, J. Zajac¹, and F. Zacek¹

The EUROfusion MST1 Team

¹*Institute of Plasma Physics AS CR v.v.i., Prague, Czech Republic*

²*Faculty of Mathematics and Physics, Charles University, V Holešovičkách 2, Prague, Czech Republic*

³*FNSPE, Czech Technical University in Prague, Břehová 7, Czech Republic*

Corresponding Author: R. Panek, panek@ipp.cas.cz

In the years 2016–17 the research on the COMPASS tokamak was focussed on support of solution of the key challenges for the design and operation of ITER and next-step devices. This included mainly installations and upgrades of state-of-art edge plasma diagnostics, such as the new divertor probe array and the high resolution Thomson scattering. Strong emphasis was placed on development of relevant scenarios: discharges with impurity seeding at different locations in the divertor were focussed on accessing partially detached plasmas. It was demonstrated that such regime can be achieved, when nitrogen is injected at the outer target, although drop of upstream pressure was also observed.

Measurements of peak ELM energy densities in the divertor complemented the existing scaling by Eich *et al.*, and confirmed the validity of the proposed model. The same set of probes mounted on the horizontal reciprocating manipulator allowed upstream measurements of power decay length during ELMs. It was observed that the power decay length exhibits a significant broadening (factor of 4) compared to the inter-ELM value.

Dedicated campaigns were focussed on experiments with runaway electrons (RE), studying the role of different gases (Ar, Ne, D) on the generation and mitigation of the RE beam. It appeared that an intensive injection of D may significantly slow down the current decay of RE beams triggered by Ar or Ne injection in the discharge phase with practically zero external loop voltage.

On request of the ITER Organization, a unique system of COMPASS high-field-side (HFS) resonant magnetic perturbation (RMP) coils was used to study the effects of error fields (EF) originating from misalignment or inclination of central solenoid on the plasma performance like L-H transition, H-mode performance degradation, locked modes, etc. The experimental observations are compared to predictions of the ideal MHD code IPEC. This study is being carried out in collaboration with ITER Organization and Princeton Plasma Physics Laboratory, USA.

In all the aforementioned fields, a significant progress under the joint EUROfusion effort has been achieved in 2016–17 and the results complemented and broadened the existing databases.

Advances in Fusion-Relevant Physics on the Large Plasma Device

T. A. Carter¹, B. Van Compernelle¹, M. J. Poulos¹, G. Morales¹, G. Rossi¹, M. J. Pueschel², S.-W. Tsao², P. W. Terry³, R. J. Perkins⁴, W. Gekelman¹, P. Pribyl¹, S. K. P. Tripathi¹, and S. Vincena¹

¹University of California Los Angeles, CA 90095, USA

²University of Texas at Austin, Austin, TX 78712, USA

³University of Wisconsin-Madison, Madison, WI 53706, USA

⁴Princeton Plasma Physics Laboratory (PPPL), Princeton, NJ 08540, USA

Corresponding Author: T. A. Carter, tcarter@physics.ucla.edu

Studies of turbulence and transport in the Large Plasma Device (LAPD) have: documented the role of drift-Alfvén waves and flows in avalanche events; revealed a new instability in the edge of increased- β plasmas; and demonstrated an interaction between ICRF waves and edge turbulence, leading to strong modulation of the former and enhancement of the latter. Intermittent collapses of the plasma pressure profile (avalanches) are observed with off-axis heating in LAPD and are associated with unstable drift-Alfvén waves. Flows play a critical role in the dynamics, in particular in the onset of the drift-Alfvén waves and avalanches through the interplay of the stabilizing flow shear and the destabilizing pressure gradient. Active control of the flows is obtained using biasing; this leads to control over the size and frequency of avalanches. With controlled flows, a regime is found in which avalanches are absent. Strongly electromagnetic turbulence, identified as being due to a new instability, the gradient-driven drift coupling instability (GDC), is observed in the edge of increased- β plasmas in LAPD. As the plasma β is increased (up to 15%), magnetic fluctuations are observed to increase substantially, with $\delta B/B \sim 1\%$ at the highest β , while density fluctuations decrease slightly. Parallel magnetic fluctuations are observed to be dominant at the highest β , with $\delta B_{\parallel}/\delta B_{\perp} \sim 2$.

Comparisons of the experimental data with linear and nonlinear GENE simulations of the GDC yield good qualitative and quantitative agreement. An experimental campaign on the physics of ICRF waves on LAPD has established a correlation between strong modulation of core coupled fast waves and edge density fluctuations, both of which increase with antenna power. Strong low-frequency modulation of coupled fast wave power is observed via direct measurement of the core RF waves with magnetic probes. This modulation is well correlated with low-frequency edge density fluctuations associated with drift waves (measured with Langmuir probes). The amplitude of the RF modulation and the amplitude of edge density fluctuations in the drift wave frequency range both grow with increasing RF power, suggesting some nonlinear coupling between the edge drift waves and large amplitude fast waves in the core region.

Overview of the Recent Experimental Research on the J-TEXT Tokamak

N. C. Wang¹, Y. Liang^{1,2,3}, N. C. Wang¹, Z. Y. Chen¹, Y. H. Ding¹, L. Wang¹, Z. P. Chen¹, Z. J. Yang¹, Z. F. Cheng¹, Z. H. Jiang¹, B. Rao¹, Q. M. Hu⁴, Z. Huang¹, M. X. Huang¹, D. Li¹, H. Liu⁵, K. J. Zhao⁶, M. Jiang⁶, Y. J. Shi⁷, H. Zhou¹, Z. F. Lin¹, D. W. Huang¹, K. X. Yu¹, X. W. Hu¹, Y. Pan¹, G. Zhuang^{1,8}, and K. W. Gentle⁹

The J-TEXT Team

¹International Joint Research Laboratory of Magnetic Confinement Fusion and Plasma Physics (IFPP), Huazhong University of Science and Technology, Hubei, People's Republic of China

²Forschungszentrum Jülich, Jülich, Germany

³Institute of Plasma Physics, Chinese Academy of Sciences, Hefei, Anhui, People's Republic of China

⁴Princeton Plasma Physics Laboratory (PPPL), Princeton, NJ 08540, USA

⁵Southwest Jiaotong University, Chengdu, Sichuan, People's Republic of China

⁶Southwestern Institute of Physics, Chengdu, Sichuan, People's Republic of China

⁷Seoul National University, Seoul, Republic of Korea

⁸University of Science and Technology of China, Hefei, Anhui, People's Republic of China

⁹Institute for Fusion Studies (IFS), University of Texas at Austin, Austin, TX 78712, USA

Corresponding Author: N. C. Wang, wangnc@hust.edu.cn

Recent J-TEXT research has highlighted the significance of the role that nonaxisymmetric magnetic perturbations, so called 3D magnetic perturbation (MP) fields, play in fundamentally 2D concept, i.e., tokamak. In this paper, the J-TEXT results achieved over the last two years, especially on the impacts of 3D MP fields on magnetic topology, plasma disruptions, MHD instabilities, and plasma turbulence transport, will be presented.

On J-TEXT, the resonant MPs (RMPs) system, capable of providing either a static (DC) or a high frequency (up to 6 kHz) rotating (AC) nonaxisymmetric MP field, has been upgraded by adding a new set of 12 in-vessel saddle coils, and the total number of in-vessel RMP coils increases from 12 to 24 (3 rows \times 8 columns). The new capabilities advance J-TEXT to the forefront of international magnetic fusion facilities, and allow a flexible study of 3D effects in a tokamak. Both density and plasma rotation dependences of the $m/n = 2/1$ locked mode threshold, $B_{r,(2,1)c}$, have been investigated systematically on J-TEXT. Recent experimental results showed the $B_{r,(2,1)c}$ scales linearly on the toroidal rotation, and depends weakly on plasma density, n_e . The fast rotating RMP field has been successfully applied for avoidance of mode locking and the prevention of plasma disruption. Remarkably, the rotating tearing mode was completely suppressed by the electrode biasing (EB) in addition to the RMP field.

The impacts of 3D magnetic topology on the turbulences have been investigated on J-TEXT. It is found that the fluctuations of electron density, electron temperature, and plasma potential can be significantly modulated by the island structure, and a larger fluctuation level appears at the X-point of islands. The suppression of runaway electrons (REs) during disruptions is essential to the operation of ITER, and it has been reached by utilizing the 3D magnetic perturbations on J-TEXT. The NIMROD simulation indicates that the strong stochastic in the whole plasma cross-section expel out the runaway seed and results in runaway free disruptions on J-TEXT. This may provide an alternative mechanism of runaway suppression for large-scale tokamak and ITER.

Fusion Energy Development Applications Utilizing the Spherical Tokamak and Associated Research Needs and Tools

J. E. Menard¹, F. Alladio², N. N. Bakharev³, R. J. Fonck⁴, Z. Gao⁵, M. Gryaznevich⁶, V. K. Gusev³, K. Hanada⁷, J. R. Harrison⁸, Y.-S. Hwang⁹, D. Kingham⁶, B. Lipschultz¹⁰, B. Lloyd⁸, R. Majeski¹, M. Ono¹, Y. Ono¹¹, M. L. Reinke¹², Y. Takase¹¹, and H. R. Wilson¹⁰

¹Princeton Plasma Physics Laboratory (PPPL), Princeton, NJ 08540, USA

²ENEA, Istituto Confucio, Sapienza – Università di Roma, 00185 Rome, Italy

³Ioffe Institute, St. Petersburg, Russian Federation

⁴University of Wisconsin-Madison, Madison, WI 53706, USA

⁵Tsinghua University, Haidian, Beijing, People's Republic of China

⁶Tokamak Energy Ltd, Abingdon, UK

⁷Research Institute for Applied Mechanics (RIAM), Kyushu University, Kasuga, Japan

⁸Culham Centre for Fusion Energy (CCFE), Culham Science Centre, Abingdon, UK

⁹Seoul National University, Seoul, Republic of Korea

¹⁰University of York, Heslington, UK

¹¹University of Tokyo, Tokyo, Japan

¹²Oak Ridge National Laboratory (ORNL), Oak Ridge, TN 37831, USA

Corresponding Author: J. E. Menard, jmenard@pppl.gov

The spectrum of scientific and technological gaps that must be closed to achieve practical fusion energy using magnetically confined plasmas has been extensively documented. A common barrier to narrowing or closing these gaps is the scale and cost of fusion facilities needed to address the gaps. The low-aspect-ratio “spherical torus/tokamak” (ST) is being explored world-wide as a potentially attractive configuration for closing scientific gaps and demonstrating technical achievements on a path toward a demonstration power plant and as a more compact and/or modular fusion power source in its own right. The international fusion community is presently assessing the suitability of the ST for applications to advance fusion energy development including: developing solutions for the plasma-material-interface (PMI) challenge, fusion-fission hybrid systems, developing fusion components capable of withstanding high fusion neutron flux and fluence including breeding blankets, demonstrating electricity break-even from a pure fusion system, and electricity production at industrial levels in modular and/or larger-scale fusion power plants. This range of fusion energy development applications utilizing the ST will be described, common application-driven research needs discussed, upcoming and recently achieved ST facility capabilities and relevant highlights described, and near-term prioritized ST research directions supporting longer-term fusion energy development applications presented.

Design, Development and Recent Experiments at the CIMPLE-PSI Device

M. Kakati¹, T. Sarmah¹, N. Aomoa¹, J. Ghosh², and G. De Temmerman³

¹*CIMPLE-PSI Laboratory, Centre of Plasma Physics – Institute for Plasma Research (CPP-IPR), Nazirakhat, Assam, India*

²*Institute for Plasma Research (IPR), Bhat, Gandhinagar, India*

³*International Thermonuclear Experimental Reactor (ITER), Cadarache Centre, 13108 St. Paul lez Durance, France*

Corresponding Author: M. Kakati, mayur@cppipr.res.in

It is important to understand how the plasma with unparalleled heat ($\sim 10 \text{ MW/m}^2$) and ion ($\sim 10^{24}/\text{m}^2\text{s}^1$) flux will interact with the tungsten walls in the ITER tokamak, more specifically at the divertor region of the fusion machine. Several linear magnetized plasma devices have been developed worldwide that reproduced ITER divertor like extreme conditions for studies on relevant plasma surface interaction (PSI) issues under simulated plasma conditions. The “CPP-IPR Magnetized Linear Divertor Plasma Experiment for Plasma Surface Interaction” or CIMPLE-PSI is one of the few Tokamak divertor simulator devices that successfully reproduces both ITER-like ion and heat flux values, whose design, development and recent commissioning will be presented in this paper. A segmented plasma torch produced high-density plasma jet collimated with a maximum 0.45 T axial magnetic field propagates at few Pascal chamber pressure that is maintained by four numbers of roots vacuum pumps with $14\,000 \text{ m}^3/\text{h}$ pumping capacity that interacts with a remotely placed tungsten target under controlled experimental conditions. The paper will report detailed diagnostics of the plasma jet through optical emission spectroscopic techniques (1.33 m McPherson spectrometer), a retractable Langmuir probe and water calorimeters while operating the plasma with helium and hydrogen mixture of gases. During recent PSI experiments in this device under irradiation of pure helium plasma (exposed for 1800 s under 0.3 T magnetic field, target biased to -45 V), we had witnessed (FESEM, HRTEM) formation of surface nanotendrils in profuse amounts, recent characterization results from which also will be presented here.

Overview of Diagnostics Upgrade and Experiment Progress on KTX

W. Liu¹, G. Zhuang¹, H. Li¹, J. Xie¹, T. Lan¹, A. Liu¹, S. Wan¹, H. Wang¹, J. Zheng¹, X. Wen¹, H. Zhou¹, W. You¹, W. Bai¹, C. Tu¹, M. Tan¹, B. Luo¹, Z. Li¹, H. Xu¹, T. Deng¹, J. Zhu¹, S. Zhang¹, Y. Adil¹, J. Hu¹, B. J. Xiao², H. Wang², Z. Luo², H. Wang², B. Shen², P. Fu², L. Yang², Y. Song², Q. Yang², J. Zheng², H. Xu², P. Zhang², C. Xiao^{1,2,3}, and W. Ding^{1,4}

¹University of Science and Technology of China, Hefei, Anhui, People's Republic of China

²Institute of Plasma Physics, Chinese Academy of Sciences, Hefei, Anhui, People's Republic of China

³University of Saskatchewan, Saskatoon, SK S7N-5C9, Canada

⁴University of California Los Angeles, CA 90095, USA

Corresponding Author: W. Liu, [wdliu@ustc.edu.cn](mailto:wdliau@ustc.edu.cn)

The Keda torus experiment (KTX) is a new built middle-size reversed field pinch (RFP) device at the University of Science and Technology of China. After the long time conditioning, the favourable wall condition is achieved for implementing experiment on KTX. At present, the maximum plasma current can reach 200 kA, the discharge length is beyond 20 ms and the duration of typical reversed field pinch state is 2.0 ms. The diagnostics on KTX has been greatly developed: 1) Total number of DAQ channel has been upgraded to 960; 2) Terahertz interferometer has been upgraded to 7 chords to obtain density and current profiles; 3) Thomson scattering with 3 J laser is undergoing commissioning; 4) 3D Langmuir probe system has been developed for the electromagnetic turbulence measurement; 5) 3D double-foil soft X-ray diagnostics are mounted on two poloidal sections for 3D MHD research; 6) Edge capacitive probe has been installed for the radial electrical field measurement; 7) Multichannel spectrograph system has been built for detecting impurities of carbon and oxygen. After the wall condition improvement and diagnostics upgrade, many early research such as the 3D RFP physics and electromagnetic turbulence, etc., have been conducted on KTX. The forward scattering is observed by the interferometer system which shows the potential for turbulence research with wider spectrum after improving the beam size and acceptance angle of the diagnostic beam through plasma. The research on MHD activities related with 3D RFP physics on KTX is intensely carried out with the capability upgrade of magnetic field measurement, soft X-ray tomography and high-speed visible imaging system. The electromagnetic turbulence is tentatively investigated on KTX. The 3D spectra characters of electromagnetic turbulence are firstly measured with classical two-point technique by the 3D Langmuir probe arrays, particularly in the small wavenumber range, providing the new prospect of electromagnetic turbulence in RFP plasmas. The confinement improvement of turbulence suppression is achieved in biasing electrode experiment. The resistive MHD modelling of QSH state using NIMROD is setup in the KTX regimes. In the next step, higher performance plasma of KTX with larger plasma current, higher temperature and longer energy confinement time is expected with the capacity upgrade in the second phase.

Formation of Hot, Stable, Long-Lived Field-Reversed Configuration Plasmas on the C-2W Device

H. Gota¹, M. W. Binderbauer¹, T. Tajima^{1,2}, S. Putvinski¹, M. Tuszewski¹, B. H. Deng¹, S. Dettrick¹, D. Gupta¹, S. Korepanov¹, R. Magee¹, T. Roche¹, J. Romero¹, A. I. Smirnov¹, Y. Song¹, V. Sokolov¹, L. Steinhauer¹, M. C. Thompson¹, E. Trask¹, A. Van Drie¹, X. Yang¹, P. Yushmanov¹, K. Zhai¹, L. Schmitz^{1,3}, Z. Lin², A. Ivanov⁴, and T. Asai⁵

The TAE Team

¹TAE Technologies, Inc., Foothill Ranch, CA 92688, USA

²University of California Irvine, CA 92697, USA

³University of California Los Angeles, CA 90095, USA

⁴Budker Institute of Nuclear Physics (BINP), Novosibirsk, Russian Federation

⁵Nihon University, Tokyo, Japan

Corresponding Author: H. Gota, hgota@tae.com

TAE's research has been devoted to producing a high temperature, stable, long-lived field-reversed configuration (FRC) plasma state by neutral-beam injection (NBI) and edge biasing/control. C-2U experiments have demonstrated drastic improvements in particle and energy confinement properties of FRC's, and the plasma performance obtained via ~ 10 MW NBI has achieved plasma sustainment of up to 5 ms and plasma lifetimes of 10+ ms [1]. The emerging confinement scaling, whereby electron energy confinement time is proportional to a positive power of the electron temperature T_e , is very attractive for higher energy plasma confinement; accordingly, exploration of the observed scaling law at $10\times$ higher T_e is one of the key research objectives.

TAE's new experimental device, C-2W (also called "Norman"; the world's largest compact-toroid device), has been constructed with the following key subsystem upgrades from C-2U: i) higher injected power (up to ~ 21 MW), optimum and adjustable energies (15–40 keV), and extended pulse duration (up to ~ 30 ms) of the NBI system; ii) installation of inner divertors with upgraded edge-biasing electrode systems, which allow for higher biasing voltage and longer pulse operation (30+ ms); iii) increased overall stored energy in the FRC formation pulsed-power system; iv) fast external equilibrium/mirror-coil current ramp-up capability for plasma ramp-up and control; v) installation of trim/saddle coils for active feedback control of the FRC plasma; and vi) enhanced overall diagnostic suite. A remarkable side note is the fact that TAE spent only ~ 1 year to construct the C-2W device and produce its first plasma. C-2W experiments have already produced a dramatically improved initial FRC state after translation and merging. As anticipated by design and also in our simulations, the merged initial FRC state exhibits much higher plasma temperatures ($T_e > 250$ eV; total electron and ion temperature > 1.5 keV) and more trapped flux, providing a very attractive target for effective NBI. Edge biasing/control experiments have also demonstrated stabilization of the FRC, thereby improving plasma confinement and prolonging FRC lifetime (up to ~ 10 ms), in which overall plasma performance is already equivalent to or better than that obtained in C-2U.

References

[1] H. Gota *et al.*, Nucl. Fus., **57**, 116021 (2017).

Activity of Indian High Heat Flux Test Facility

S. M. Belsare¹, S. S. Khirwadkar¹, R. Swamy¹, K. S. Bhope¹, S. Tripathi¹, T. Patel¹,
P. K. Mokaria¹, N. Patel¹, M. Mehta¹, and K. Galodiya¹

¹*Institute for Plasma Research (IPR), Bhat, Gandhinagar, India*

Corresponding Author: S. M. Belsare, belsare@ipr.res.in

Plasma facing components (PFCs) of ITER-like tokamak are expected to subject high heat loads up to 10 MW/m² during the tokamak operation in steady state condition. Selection of plasma facing materials/components required extensive qualification and testing for tokamak application. The High Heat Flux Test Facility (HHFTF) plays an important role for the qualification and estimation of the life of the component under defined heat load condition.

HHFTF with heat flux generated by an electron beam system having 200 kW power and 45 kV maximum acceleration voltage is in full-fledged operation since 2016. HHFTF is dedicated for high heat flux testing of numerous materials and plasma facing components (small and medium sized) for several thousand thermal cycles at different heat loads. The facility is equipped with high vacuum pumping systems with pressure regulation, high pressure high temperature water circulation loop and several diagnostics devices such as pyrometers, IR-cameras, video cameras, flow, pressure and temperature sensors.

This paper describes the main capabilities of the HHFTF and gives a glimpse of various tests performed on plasma facing materials and components.

EX: Magnetic Confinement Experiments

EX

Strongly Nonlinear Energetic Particle Dynamics in ASDEX-Upgrade Scenarios with Core Impurity Accumulation

P. Lauber¹, B. Geiger¹, G. Papp¹, G. I. Pokol², G. Por², A. Biancalani¹, X. Wang¹, Z. Lu¹, P. Z. Pölöskei^{1,2}, A. Bottino¹, F. Palermo¹, G. D. Conway¹, V. Igoshine¹, M. Maraschek¹, T. Hayward-Schneider¹, L. Guimaraes³, and I. Novikau¹

The ASDEX-Upgrade Team

¹Max-Planck-Institut für Plasmaphysik, Garching, Germany

²NTI, University of Technology and Economics (BME), Budapest, Hungary

³Instituto Superior Técnico (IST), 1049-001 Lisbon, Portugal

Corresponding Author: P. Lauber, pwl@ipp.mpg.de

In 2017 a new scenario on ASDEX-Upgrade for the dedicated investigation of energetic particle (EP) physics has been developed. This scenario is unique in two aspects: firstly, the neutral beam (NB) induced fast-ion β is comparable to the background plasma β , and secondly, the ratio of the fast ion energy to the thermal background is of the order 100. At ASDEX-Upgrade we reach this previously unexplored regime by NB off-axis heating only and by letting impurities accumulate in the core. Due to strong radiation losses the background temperatures and pressures of both ions and electrons stay low, despite 2.5–5 MW NB heating. In the stable flat-top phase an unprecedented number of various EP-driven instabilities (despite $\nu_{EP}/\nu_{\text{Alfvén}} \approx 0.4 \ll 1$) is simultaneously observed: EP-driven geodesic acoustic modes (EGAMs), β -induced Alfvén eigenmodes (BAEs), reversed shear Alfvén eigenmodes (RSAEs) and toroidal Alfvén eigenmodes (TAEs), that are modulated by transient $q = 2$ sawtooth-like crashes, NTMs and ELMs. The physics reasons for these strong mode activity are discussed.

During the stable flat-top phase meaningful EP distribution function measurements (FIDA) and analysis (TRANSP/FIDASIM) can be performed. First results indicate that the EP profiles differ significantly from neoclassical predictions. Bicoherence analysis using an advanced toolset for nonstationary processes reveals that nonlinear coupling processes between different frequency bands exist. In addition, TAE bursts are observed to trigger the onset of EGAMs which indicates coupling of these modes via the velocity space (EP avalanches). Linear and nonlinear tools (HAGIS/LIGKA, ORB5, XHMGC) are used for modelling mode onset and nonlinear phases. These experiments facilitate the experimental study of the interaction of AEs, zonal modes and turbulence and thus serve as an ideal validation opportunity for various nonlinear analytical and numerical models. In addition, the observed onset of EP avalanches can be quantified. The investigation and understanding of these — so far not accessible — physics elements is a prerequisite for a reliable prediction of the self-organization of a burning plasma.

Reduced Energetic Particle Transport Models Enable Comprehensive Time-Dependent Tokamak Simulations

M. Podestà¹, W. W. Heidbrink², L. Bardoczi³, C. S. Collins⁴, V. Duarte¹, N. Gorelenkov¹, G. J. Kramer¹, E. D. Fredrickson¹, M. Gorelenkova¹, D. Kim¹, F. M. Poli¹, and M. A. Van Zeeland⁴

¹Princeton Plasma Physics Laboratory (PPPL), Princeton, NJ 08540, USA

²University of California Irvine, CA 92697, USA

³Oak Ridge Associated Universities (ORAU), Oak Ridge, TN 37831, USA

⁴General Atomics, San Diego, CA 92186, USA

Corresponding Author: M. Podestà, mpodesta@pppl.gov

The inclusion of the reduced-physics energetic particle (EP) “kick model” for EP transport in TRANSP has resulted in a dramatic improvement of interpretive and predictive capabilities for time-dependent tokamak simulations including the effects of EP transport by instabilities. The kick model has recovered the measured toroidal Alfvén eigenmode (TAE) spectrum on NSTX-U and has reproduced details of the fast ion diagnostic data measured on DIII-D for EP modes and tearing modes. Being able to predict the occurrence and effect of those instabilities is one of the grand challenges for fusion and a necessary step to mitigate their negative effects. The kick model has proven the potential of phase-space resolved EP simulations to unravel details of EP transport for detailed theory/experiment comparison and for scenario planning based on optimization of NBI parameters. Work is also ongoing to complement the kick model approach with the RBQ1D model based on the resonance-broadening quasi-linear theory to develop a self-consistent, numerically efficient predictive EP transport model. On NSTX-U, the kick model successfully reproduces the stability of co- and counter-propagating TAEs driven unstable by NB injection. The model successfully reproduces the transition from a co-TAE dominated scenario to one with coexisting co- and counter-TAEs. Based on the analysis, strategies for mitigating the instabilities are developed through TRANSP by varying the NB injection parameters. The phase space resolution implemented in the model is also crucial for its successful validation against fast ion diagnostics data from fast ion D- α (FIDA) and neutral particle analysers (NPA). For DIII-D discharges with strong Alfvénic activity, the amplitude of the instabilities used in the simulation is first adjusted to match the measured neutron rate. The inferred FIDA and NPA signals based on the simulation are then compared with the experimental data for validation, showing excellent agreement. Initial analysis via the RBQ1D model gives similar results, indicating its potential for predictive simulations. Enhancements to TRANSP via the inclusion of reduced EP transport models are playing an important role in scenario development including realistic treatment of fast ion transport by instabilities, e.g., to optimize the scenario by tailoring NB injection power and voltage.

EX

Impact of ECH/ECCD on Fast-Ion-Driven MHD Instabilities in Helical Plasmas

S. Yamamoto¹, K. Nagaoka², Á. Cappa³, K. Nagasaki¹, S. Kobayashi¹, E. Ascasíbar³, F. Castejón³, A. Ishizawa⁵, M. Isobe², S. Kado¹, A. V. Melnikov⁴, T. Minami¹, T. Mizuuchi¹, Y. Nakamura⁴, K. Ogawa², S. Ohshima², H. Okada¹, M. Osakabe², and G. Weir⁶

¹*Institute of Advanced Energy, Kyoto University, Nishikyo-ku, Kyoto 615-8540, Japan*

²*National Institute for Fusion Science (NIFS), Toki, Gifu, Japan*

³*Laboratorio Nacional de Fusión (LNF),*

Centro de Investigaciones Energéticas, Medioambientales y Tecnológicas (CIEMAT), Madrid, Spain

⁴*National Research Centre "Kurchatov Institute", Moscow, Russian Federation*

⁵*Graduate School of Energy Science, Kyoto University, Nishikyo-ku, Kyoto 615-8540, Japan*

⁶*Max-Planck-Institut für Plasmaphysik, Greifswald, Germany*

Corresponding Author: S. Yamamoto, yamamoto.satoshi.6n@kyoto-u.ac.jp

We discuss the effect of electron cyclotron heating (ECH) and current drive (ECCD) on fast particle (FP)-driven MHD instabilities in stellarator/heliotron (S/H) plasmas obtained in LHD, Heliotron J and TJ-II. We demonstrate that FP-driven MHD instabilities including energetic particle modes (EPMs) and Alfvén eigenmodes (AEs) can be controlled by means of magnetic shear s modified by EC-driven plasma current. EPMs can be controlled by changing continuum damping rate, which is the main damping mechanism of the EPM and depends on s . AEs are significantly affected by the change of structure of the shear Alfvén continuum which can be modified by s . We also find that ECH (non-ECCD) can impact FP-driven MHD instabilities. Candidates to explain the ECH effect on FP-driven MHD instabilities are the variation in the fast ion profile and/or the trapped electron collisional damping.

EX

Excitation Mechanism of the Energetic Particle Driven Resistive Interchange Mode and Strategy to Control the Mode in Large Helical Device

S. Ohdachi^{1,2}, T. Bando², K. Nagaoka¹, H. Takahashi^{1,2}, Y. Suzuki^{1,2}, K. Y. Watanabe¹, X. D. Du³, K. Toi¹, M. Osakabe^{1,2}, and T. Morisaki^{1,2}

Rapporteur by: S. Yamamoto

¹National Institute for Fusion Science (NIFS), Toki, Gifu, Japan

²Department of Fusion Science, Graduate University for Advanced Studies (SOKENDAI), Toki, Gifu, Japan

³University of California Irvine, CA 92697, USA

^{*}The LHD Experiment Group

Corresponding Author: S. Ohdachi, ohdachi@nifs.ac.jp

The helically-trapped energetic-particle (EP) driven resistive interchange mode (EIC) observed in the Large Helical Device (LHD) causes large amount loss of EPs. It is destabilized when the precession motion of the helically trapped EP resonates with the pressure driven mode. A velocity modulation caused by the toroidicity of the magnetic field produces this resonance. Strategy and the initial results to suppress the EIC mode based on the knowledge of the EP orbit effects, by the ECH heating and by the RMP application, are presented.

EPs having perpendicular velocity components are trapped in the weak magnetic field region of the LHD and making precession motion helically. The rotation frequency of this precession motion is slow enough to interact with the pressure driven MHD modes. If the energy transfer from the EP to the mode is estimated by evaluating the correlation of the fluctuating component of the precession motion and the MHD mode, a resonance is found when the MHD mode rotates poloidally -1.2 times of the poloidal component of the helically trapped EP motion. This resonance discussed here is consistent with the following observations found in the hydrogen/deuterium experimental campaign: 1) MHD mode rotates in the electron diamagnetic drift direction while the EP moves in the ion diamagnetic drift direction; 2) The mode frequency is almost the same with the precession frequency of the initial velocity of the NB-injected EPs. The EIC modes are successfully suppressed by the ECH injection and RMP application. The physical mechanism of the stabilization will be discussed.

EX

Impact of ELM Control in JET Experiments on H-Mode Terminations with/without Current Ramp-Down and Implications for ITER

E. de la Luna¹, A. Loarte², F. G. Rimini³, P. C. de Vries², F. Köchl³, C. Reux⁴, P. J. Lomas³, and E. R. Solano¹

The JET Contributors

¹*Centro de Investigaciones Energéticas, Medioambientales y Tecnológicas (CIEMAT), Madrid, Spain*

²*International Thermonuclear Experimental Reactor (ITER),*

Cadarache Centre, 13108 St. Paul lez Durance, France

³*Culham Centre for Fusion Energy (CCFE), Culham Science Centre, Abingdon, UK*

⁴*Institut de Recherche sur la Fusion par confinement Magnétique (IRFM), Commissariat à l'énergie atomique (CEA/Cadarache), 13108 St. Paul lez Durance, France*

Corresponding Author: E. de la Luna, elena.delaluna@ciemat.es

EX An important aspect of ITER operation will be the termination of the high confinement H-mode phase (I_p ramp-down phase) in a controlled and safe way. Previous ramp-down studies in JET and other devices focussed on aspects related to flux consumption and vertical stability control. In this work the emphasis is on aspects related to W accumulation and its control, which can be particularly challenging in a Be/W wall environment, such as JET or ITER. The dynamics of a slow H-mode ramp-down (to mimic the power ramp-down scenario foreseen for ITER) have been systematically studied in JET during both the I_p flat-top and I_p ramp-down phases, in order to explore the conditions under which W accumulation develops and how it can be controlled using external actuators that are known to affect the impurity transport, such as central electron heating (ICRH in JET) or ELM control (vertical kicks and pellet injection).

The use of vertical kicks for ELM control has proven to be an effective method to avoid W accumulation during the H-mode termination phase in JET-ILW. With ELM control the long ELM free phases, typically observed as the plasma approaches the H-L transition, can be avoided, allowing the impurity content of the plasma to be significantly reduced. As a result, the plasma remains in type-I ELMy H-mode for a longer period, leading to a slower decrease of the plasma energy, which can mitigate the radial control requirements in ITER. It is found that ELM control with vertical kicks provides not only impurity control but also density control, which is also a key aspect in the ITER ramp-down scenario. Attempts to use pellet pacing for ELM control has resulted, so far, in terminations with low radiation levels but poor density control and further investigation is required to assess the effectiveness of this ELM control approach. In addition to the ELM control studies, other mechanisms affecting the plasma transport properties during H-mode termination, such as central electron heating (ICRH), NBI momentum and particle sources and plasma shape variations (reduced elongation maintaining $q_{95} \sim \text{constant}$) during the I_p ramp-down, were also investigated. The full set of experimental observations, as well as the more recent modelling results obtained with the JINTRAC suite of codes will be presented and the implications for ITER discussed.

Viability of Wide Pedestal QH-Mode for Burning Plasma Operation

D. R. Ernst¹, K. H. Burrell², X. Chen², K. K. Barada³, C. C. Petty², T. L. Rhodes³, C. Chrystal², C. Paz-Soldan², T. M. Wilks¹, B. A. Grierson⁴, M. E. Austin⁵, T. Carlstrom², J. Chen³, G. R. McKee⁶, T. H. Osborne², C. Sung³, D. Truong⁶, and L. Zeng³

The DIII-D Team

¹*Massachusetts Institute of Technology (MIT), Cambridge, MA 02139, USA*

²*General Atomics, San Diego, CA 92186, USA*

³*University of California Los Angeles, CA 90095, USA*

⁴*Princeton Plasma Physics Laboratory (PPPL), Princeton, NJ 08540, USA*

⁵*University of Texas at Austin, Austin, TX 78712, USA*

⁶*University of Wisconsin-Madison, Madison, WI 53706, USA*

Corresponding Author: D. R. Ernst, dernst@psfc.mit.edu

Wide pedestal QH-mode is a new steady ELM-free regime obtained in DIII-D, exhibiting a transport-limited pedestal regulated by broadband turbulence, with improved confinement relative to QH-Mode under the same conditions, attaining $\beta_N \sim 2.3$ and $H_{98}(y, 2) \sim 1.6$, which increase with power. Toward compatibility with burning plasma conditions, the need for neutral beam torque to initiate and sustain wide pedestal QH-Mode has been completely eliminated. Further, the regime has now been sustained for several confinement times with dominant electron heating, at very low torque, without ELMs or core MHD. Recent experiments show that in wide pedestal QH-Mode, both pedestal and core confinement uniquely improve when electron cyclotron heating (ECH) augments or replaces neutral beam injection (NBI). This is promising for burning plasma operation where α -particles heat electrons. Adding 0.8 MW ECH to 3.8 MW NBI power more than doubles pedestal confinement, increasing pedestal pressure by 50%. Wide pedestal QH-Mode has now been sustained for several confinement times with up to 77% ECH power (3 MW ECH to 0.9 MW NBI), limited by the available ECH power. High electron temperatures exceeding 12 keV are attained suggesting an internal transport barrier (ITB), which is verified using modulated ECH and ECH location scans to measure electron temperature profile stiffness. A deep well forms in the inner core toroidal rotation profile during intense ECH, characteristic of ITBs. The electron transport stiffness has been similarly studied in QH-Mode in the outer core, showing the electron temperature gradient lies close to a critical gradient. Separately, the regime has been maintained with ITER-relevant shape. These and other new developments support wide pedestal QH-Mode regime as a viable solution to avoid ELMs and associated divertor damage in a zero-torque, high-confinement, electron heated scenario at ITER collisionality.

Work supported in part by the U.S. Department of Energy under DE-FC02-08ER54966, DE-SC0014264, DE-FC02-04ER54698, FG02-08ER54984, DE-FG02-08ER54999, DE-AC02-09CH11466 and FG03-97ER54415.

Advances in the Understanding of the I-Mode Confinement Regime: Access, Stationarity, Edge/SOL Transport and Divertor Impact

T. Happel¹, S. J. Freethy^{1,2}, P. Hennequin³, P. Manz¹, D. Prisiazhniuk¹, F. Ryter¹, D. Silvagni¹, D. Brida¹, M. G. Dunne¹, T. Eich¹, M. Faitsch¹, L. Gil⁴, M. Griener¹, L. Guimaraes⁴, A. Merle⁵, D. Nille¹, J. R. Pinzón^{1,6}, B. Sieglin¹, U. Stroth¹, H. J. Sun¹, and E. Viezzer⁷

The ASDEX-Upgrade Team and EUROfusion-MST1 Team

¹Max-Planck-Institut für Plasmaphysik, Garching, Germany

²Plasma Science & Fusion Center, MIT, Cambridge, MA 02139, USA

³Laboratoire de Physique des Plasmas (LPP), CNRS/École Polytechnique, 91128 Palaiseau, France

⁴Institute of Plasmas and Nuclear Fusion (IPNF), Association EURATOM/IST, Lisbon, Portugal

⁵Swiss Plasma Center (SPC), École polytechnique fédérale de Lausanne (EPFL), 1015 Lausanne, Switzerland

⁶Technische Universität München, Garching, Germany

⁷Universidad de Sevilla, Seville, Spain

Corresponding Author: T. Happel, tim.happel@ipp.mpg.de

The I-mode is an improved confinement regime of tokamak plasmas where an edge transport barrier is observed only in the heat transport but not in the particle transport. This is in contrast to H-mode confinement, which is characterized by transport barriers for both heat and particles. The I-mode does not exhibit any edge localized modes. Since the particle confinement is low, the I-mode does not suffer from high impurity content. In I-mode, the edge turbulence spectrum is dominated by an instability called the weakly coherent mode (WCM). After substantial I-mode research by the fusion community in the last years, the mechanism which creates a transport barrier in only one of the transport channels is still not understood.

An overview of recent I-mode studies on ASDEX-Upgrade is given, including L-I and I-H power thresholds, pedestal and confinement properties, extending previous studies to higher Greenwald fractions up to 0.7. The confinement improvement in I-mode is accompanied by a deepening of the edge radial electric field well and a reduction of turbulence with respect to L-mode. New investigations with poloidal correlation reflectometry and correlation electron cyclotron emission diagnostics detect the WCM in the L-mode phase before I-mode starts, showing that the WCM is not exclusive to the I-mode. A newly installed thermal Helium beam allows a precise radial determination of maximum impact of the WCM. A striking feature of I-mode edge turbulence is a reduction of low-amplitude density fluctuations, concomitant with the appearance of strongly intermittent high-amplitude density bursts in the plasma edge inside the separatrix. These density turbulence bursts are linked to the WCM. After their generation, they are expelled from the plasma and appear later in the divertor, observed by bolometry, infrared thermography and probes.

Moreover, stationary I-modes have been obtained recently with neutral beam injection heating. The stationarity allows the characterization of scrape-off layer (SOL) fall-off lengths of density and temperature. While the former are similar to L-mode plasmas, the latter are comparable to H-mode plasmas, indicating that I-mode properties are also found in the SOL. Infrared thermography data yields information on the scrape-off layer power fall-off length and divertor loads, and implications for future devices are discussed.

High Fusion Performance in Super H-Mode Experiments on Alcator C-Mod and DIII-D

P. B. Snyder¹, J. W. Hughes², T. H. Osborne¹, C. Paz-Soldan¹, W. Solomon¹, D. Eldon¹, T. E. Evans¹, T. Golfinopoulos², R. J. Groebner¹, A. E. Hubbard², M. Knolker³, B. LaBombard², F. M. Laggner³, O. Meneghini¹, S. Mordijck⁴, S. Scott³, H. R. Wilson⁵, and Y. B. Zhu⁶

¹General Atomics, San Diego, CA 92186, USA

²Plasma Science & Fusion Center, MIT, Cambridge, MA 02139, USA

³Princeton Plasma Physics Laboratory (PPPL), Princeton, NJ 08540, USA

⁴College of William & Mary, Williamsburg, VA 23185, USA

⁵University of York, Heslington, UK

⁶University of California Irvine, CA 92697, USA

Corresponding Author: P. B. Snyder, snyder@fusion.gat.com

The “Super H-mode” regime is predicted to enable pedestal height and fusion performance substantially higher than for standard H-mode operation. This regime exists due to a bifurcation of the pedestal pressure, as a function of density, that occurs in strongly shaped plasmas above a critical density. Experiments on Alcator C-Mod and DIII-D have achieved access to the super H-Mode regime, and obtained very high pedestal pressure, including the highest pedestal pressure ever achieved on a tokamak ($P_{\text{ped}} \sim 80$ kPa) in C-Mod experiments operating near the ITER magnetic field. DIII-D Super H experiments have demonstrated high performance, including the highest stored energy in the present configuration of DIII-D ($W \sim 2.2\text{--}3.1$ MJ), while utilizing only about half of the available heating power ($P_{\text{heat}} \sim 6\text{--}12$ MW). These DIII-D experiments have achieved the highest value of peak fusion gain, $Q_{\text{DT,equiv}} \sim 0.5$, ever achieved on a medium scale ($R < 2$ m) tokamak. Sustained, stationary high performance operation has been achieved utilizing $n = 3$ magnetic perturbations for density and impurity control. Super H-Mode access is predicted for ITER and expected, based on both theoretical prediction and observed normalized performance, to enable ITER to achieve its performance goals ($Q = 10$) at $I_p < 15$ MA, and to enable more compact, cost effective DEMO designs. We present extensive comparisons of Super H theory to experiments on C-Mod and DIII-D, predictions for Super H access on JET, JT-60SA and ITER, and coupled core-pedestal predictions of fusion performance on existing and future devices.

Work supported in part by the U.S. Department of Energy under DE-FG03-95ER54309, DE-FC02-99ER54512, DE-FC02-04ER54698, and DE-FC02-06ER54873.

Plasma Shape and Fuelling Dependence on the Small ELM Regime in TCV and AUG

B. Labit¹, T. Eich², G. F. Harrer³, M. Bernert², H. De Oliveira¹, M. G. Dunne², L. Frassinetti⁴, P. Hennequin⁵, R. Maurizio¹, A. Merle¹, H. Meyer⁶, P. Molina¹, U. Sheikh¹, S. Saarelma⁷, J. Stober², and E. Wolfrum²

The TCV, AUG, and EUROfusion MST1 Teams

¹Swiss Plasma Center (SPC), École polytechnique fédérale de Lausanne (EPFL), 1015 Lausanne, Switzerland

²Max-Planck-Institut für Plasmaphysik, Garching, Germany

³Technische Universität Wien, 1040 Vienna, Austria

⁴KTH Royal Institute of Technology, Stockholm, Sweden

⁵Laboratoire de Physique des Plasmas (LPP), CNRS/École Polytechnique, 91128 Palaiseau, France

⁶United Kingdom Atomic Energy Authority, Culham Science Centre, Abingdon, UK

⁷Culham Centre for Fusion Energy (CCFE), Culham Science Centre, Abingdon, UK

Corresponding Author: B. Labit, benoit.labit@epfl.ch

A series of experiments has been conducted at AUG and TCV to disentangle the role of fuelling, plasma triangularity and closeness to a double null (DN) configuration for the onset of the small ELM regime. At AUG, the role of the SOL density has been revisited. Indeed, it turns out that a large density SOL is not a sufficient condition to achieve the type-II (small) ELM regime. This has been demonstrated with a constant gas fuelled plasma close to DN which has been progressively shifted down, relaxing therefore the closeness to DN at constant. As the plasma is moved down, type-I ELMs are progressively restored, finally being the unique ELM regime. It is observed that not only the pedestal top profiles are unchanged, but also the SOL profiles remained unaffected by transition from type-II to type-I ELMs. We conclude that the separatrix density is not the unique key parameter and it is hypothesized that the local magnetic shear, modified by the closeness to DN, could play an important role. A small ELM regime with good confinement has been achieved at TCV, a full carbon machine featuring an open divertor. A systematic scan in the fuelling rate has been done for both medium and high triangularity shapes. For the latter case, a configuration close to a DN configuration, the stored energy and the pedestal top pressure increase by 5% and 30% respectively compared to the medium triangularity case. For both shapes, as the D₂ fuelling is increased, the type-I ELM frequency decreases and small ELMs are observed in between large ones. Finally for the high triangularity, at the maximum fuelling rate, the large ELMs are fully suppressed and only the small ELMs remain. As observed in JET and AUG, the pedestal pressure degrades with increasing fuelling, up to 40% for the high triangularity scenario, although the stored energy remains almost unchanged. It is also observed that, for both shapes, the density at the separatrix increases with the fuelling rate, reaching $n_{e,sep}/n_G \sim 0.3$ at $n_{e,av}/n_G \sim 0.75$. The small ELM regime at TCV is associated with a coherent mode at about 30 kHz seen by the magnetic probes located at the outboard midplane. The outer target heat loads from IR tomography are reduced by more than a factor of 5 when transiting towards the small ELM regime.

Integrated Operation of Steady-State Long Pulse H-Mode in EAST

X. Z. Gong¹, B. N. Wan¹, J. G. Li¹, J. P. Qian¹, E. Li¹, F. K. Liu¹, Y. P. Zhao¹, M. Wang¹, H. D. Xu¹, X. J. Wang¹, A. M. Garofalo², A. Ekedahl³, S. Y. Ding¹, J. Huang¹, L. Zhang¹, B. Zhang¹, Q. Zang¹, H. Q. Liu¹, L. Zeng¹, B. Lyu¹, S. Y. Lin¹, B. Shen¹, L. M. Shao¹, B. J. Xiao¹, J. S. Hu¹, C. D. Hu¹, L. Q. Hu¹, L. Wang¹, Y. W. Sun¹, G. S. Xu¹, Y. F. Liang¹, and N. Xiang¹

The EAST Team

¹*Institute of Plasma Physics, Chinese Academy of Sciences, Hefei, Anhui, People's Republic of China*

²*General Atomics, San Diego, CA 92186, USA*

³*Institut de Recherche sur la Fusion par confinement Magnétique (IRFM), Commissariat à l'énergie atomique (CEA/Cadarache), 13108 St. Paul lez Durance, France*

Corresponding Author: X. Z. Gong, xz_gong@ipp.ac.cn

Recent EAST experiment has successfully demonstrated long-pulse steady-state scenario with a good plasma performance through the integrated operation since the last IAEA in 2016. A discharge with a duration over 100 s has been obtained with multi-RF power heating and current drive. Plasma parameters are as follows, plasma current $I_p = 0.4$ MA, poloidal $\beta_p \sim 1.2$, toroidal magnetic field $B_t = 2.5$ T, elongation $\kappa = 1.6$, the safety factor at the 95% normalized poloidal flux surface $q_{95} \sim 6.6$. The zero-loop voltage and pulse length (~ 250 times the current relaxation time) indicate the really steady state condition. Small ELMs were obtained in this long pulse H-mode discharge which facilitates the RF power coupling in the H-mode phase. In the operation, the optimization of X-point, plasma shape, the outer gap and local gas puffing near LHW antenna were investigated to maintain RF power coupling and particle exhaust and to avoid formation of hot spot on the 4.6 GHz LHW antenna. Global parameters of B_t and line averaged electron density were optimized for higher current drive efficiency of LHW and on-axis deposition of ECH. A peaked electron temperature profile was observed with a weak ITB at $\rho \sim 0.4$. No obvious MHD instabilities were found in the whole discharge. The maximum tungsten divertor temperature monitored by the IR camera shows the temperature raises quickly in several seconds and reaches a stable value $\sim 500^\circ\text{C}$. As a key element, wall conditioning was addressed before long pulse plasma operation. Several difficulties are reported in the development of this 100 s long pulse discharge. To achieve the next goal (≥ 400 s long-pulse H-mode operations with $\sim 50\%$ bootstrap current fraction), 0D predictions have been carried out. The modelling suggests that steady-state high performance will require not only increased injected power, but also significantly improved energy confinement quality. The recent long pulse H-mode has demonstrated several key elements and will increase a confidence in achieving high performance, steady state discharges with more key elements in integrated control on EAST.

This work was supported by the National Magnetic Confinement Fusion Program of China No. 2015GB102000, No. 2015GB110005 and No. 2015GB103000.

Developing Steady State ELM-Absent H-Mode Scenarios with Advanced Divertor Configuration in EAST Tokamak

G. Calabrò¹, B. J. Xiao^{2,3}, J. G. Li², Z. P. Luo², Q. P. Yuan², L. Wang², K. Wu^{1,2}, R. Albanese⁴, R. Ambrosino⁴, F. Crisanti⁵, X. Z. Gong¹, Y. Huang¹, H. Q. Liu¹, R. Lombroni¹, S. Minucci¹, J. P. Qian¹, T. Zhang¹, and N. Vianello⁶

The EAST Team

¹University of Tuscia, Largo dell'Università snc, 01100 Viterbo, Italy

²Institute of Plasma Physics, Chinese Academy of Sciences, Hefei, Anhui, People's Republic of China

³School of Nuclear Science and Technology, University of Science and Technology of China, Hefei, Anhui, People's Republic of China

⁴ENEA C. R. Frascati, Dipartimento FSN, Frascati, Italy

⁵Consorzio CREATE, Università degli Studi di Napoli Federico II, 80138 Napoli, Italy

⁶Consorzio RFX, Associazione EURATOM-ENEA sulla Fusione, Padova, Italy

Corresponding Author: G. Calabrò, giuseppe.calabro@unitus.it

The divertor properties of a two nearby magnetic poloidal nulls (2-NDN) configuration have been recently investigated in steady state ($V_{loop} < 0$) H-mode plasmas, ($H_{98} = 1$), edge localized modes (ELM) absent, on EAST tokamak. Due to the location of poloidal field (PF) coils and target plates in EAST, the secondary null could be moved around from the primary one to form a magnetic configuration that features either a contracting or flaring geometry near the plate. An increase of the connection length by $\sim 30\%$ and flux expansion in the outer strike point (SP) region by a factor of ~ 3 with respect the single null (SN) case, in all the upper 2-NDN discharges have been achieved. A reduction of peak heat loads, of the same order of flux expansion increase, on the upper full W divertor targets, both in L-mode and H-mode discharges, has been observed consistently with theory predictions and predictive 2D edge simulations. In all the 2-NDN steady-state discharge the ELMs activity was quiescent, indicating a possible nonlinear interaction between the downstream magnetic topology and the upstream kinetic gradients. Another potential explanation of the quiescent ELMs could be linked with the role of electrostatic edge coherent mode (ECM) which resides in the pedestal region and whom topological structure could be affected by variation of the local connection length. The ECM contribution to ELMs behaviour on 2-NDN scenario is presently under investigation.

Integration of the High- β_N Hybrid Scenario to a High Performance Pedestal, Stable Zero Torque Operation and a Divertor Solution

F. Turco¹, T. H. Osborne², T. W. Petrie², C. C. Petty², T. C. Luce³, B. A. Grierson⁴, and G. Navratil¹

¹*Columbia University, New York, NY 10027, USA*

²*General Atomics, San Diego, CA 92186, USA*

³*International Thermonuclear Experimental Reactor (ITER),
Cadarache Centre, 13108 St. Paul lez Durance, France*

⁴*Princeton Plasma Physics Laboratory (PPPL), Princeton, NJ 08540, USA*

Corresponding Author: F. Turco, turcof@fusion.gat.com

DIII-D experiments have demonstrated the expansion of the high- β_N hybrid scenario to the high density levels necessary for radiating divertor operation, leading to pedestal enhancement, and showed how the choice of injected impurity impacts the effectiveness of a radiating mantle solution, as well as the impurity transport to the core and the divertor. The scenario was made robust to systematic changes in EC power deposition location and current drive magnitude or heating injection, and was extended to zero beam torque, where the plasmas are passively stable with and without EC power. Coupling a high-performance core to an acceptable heat flux divertor is a crucial step for ITER and any fusion reactor. This work presents results on all the necessary ingredients, implemented in the high- β_N hybrid scenario: high density, on- and off-axis electron heating and current drive, pedestal enhancement, puff-and-pump and radiating mantle techniques and impurity transport. Experiments in 2017 confirmed ELITE simulations which predicted that a near double null configuration and reactor-relevant $q_{95} > 5.5$ are required for the pedestal enhancement with density. The impact of impurities used for the radiating mantle on the core of the plasmas, as well as their transport in the edge and divertor will be discussed.

EX

Optimization of JET-DT and ITER Operation by Developing an Understanding of the Role of Low- Z Impurity on the H-Mode Pedestal

C. Giroud¹, N. Aiba², F. Militello¹, C. D. Challis¹, A. Chankin³, B. Lomanowski⁴, D. R. Hatch⁵, J. R. Harrison¹, J. C. Hillesheim¹, D. Frigione⁶, D. Moulton¹, S. Pamela¹, F. I. Parra⁷, J. Parisi⁷, I. Pusztai⁸, D. I. Réfy⁹, S. Saarelma¹, C. Stavrou⁴, B. Tál⁹, E. Belonohy¹, S. Brezinsek¹⁰, S. Buller⁸, M. Barnes⁷, C. Bowman¹¹, E. Delabie¹², A. Field¹, J. M. Fontdecaba¹³, A. Huber¹⁰, A. G. Meigs¹, S. Menmuir¹, and J. Simpson¹

The JET Contributors

¹Culham Centre for Fusion Energy (CCFE), Culham Science Centre, Abingdon, UK

²Japan Atomic Energy Agency (JAEA), Naka, Japan

³Max-Planck-Institut für Plasmaphysik, Garching, Germany

⁴Aalto University, Espoo, Finland

⁵Institute for Fusion Studies (IFS), University of Texas at Austin, Austin, TX 78712, USA

⁶Agenzia nazionale per le nuove tecnologie, l'energia e lo sviluppo economico sostenibile (ENEA), Rome, Italy

⁷Rudolf Peierls Centre for Theoretical Physics, University of Oxford, Oxford, UK

⁸Chalmers University of Technology, Göteborg, Sweden

⁹Wigner Research Center, Association EURATOM, Budapest, Hungary

¹⁰Forschungszentrum Jülich, Jülich, Germany

¹¹University of York, Heslington, UK

¹²Oak Ridge National Laboratory (ORNL), Oak Ridge, TN 37831, USA

¹³Centro de Investigaciones Energéticas, Medioambientales y Tecnológicas (CIEMAT), Madrid, Spain

Corresponding Author: C. Giroud, carine.giroud@ccfe.ac.uk

Impurity seeding via Ne or N injection will be mandatory in ITER $Q=10$ reference scenario to reduce inter-ELM divertor power load to within limits. The challenge is achieving the requirements of $H_{98}(y, 2)=1$, $\beta_N=1.8$, $n/n_{GW}=0.85$, $\delta=0.4$, with a high radiative divertor. These conditions require a high pedestal temperature, leading the pedestal to play a key role in this challenging integration. Unravelling the mechanism that, in the absence of C in the plasma, leads to a decrease in the pedestal temperature is critical in predicting the pedestal pressure in ITER. It is important to learn how to use the extrinsic impurity to optimize the pedestal temperature in high radiative scenarios. This paper aims at: 1) reviewing our understanding of the effect of C, N and Ne-seeding on the pedestal pressure and temperature; 2) assessing whether the peeling ballooning stability limits the pedestal pressure; and 3) determining which instabilities are causing heat and particle transport. In JET-ILW the limitation on the pedestal temperature is alleviated with the injection of N or C in low and high- β_N plasmas. Seeding Ne can result in opposite behaviour on the pedestal density depending on the collisionality ν_e^* and β_N , but in all cases seeding Ne does not lead to a temperature increase, unlike N or C. A detailed analysis of the differences in the electron and ion pedestal profiles in high- β_N plasmas indicates that the difference between C and Ne-seeding can be down to the value of collisionality ν_e^* , but also the $E \times B$ shear considering the difference in $\nabla T_{i, \alpha_{\max}}$ and $\nabla \Omega_{tor, \alpha_{\max}}$ at the position of the maximum normalized pressure gradient. Similarly, seeding C_2D_4 in the low- β_N plasmas increases $\nabla T_{i, \alpha_{\max}}$ and $\nabla \Omega_{tor, \alpha_{\max}}$. Detailed analysis with the GENE code will clarify which instability is at the origin of the difference in the pedestal temperature. The peeling ballooning stability has been assessed with MINERVA-DI code. The plasmas considered have the operational points (OP) of the high and low- β_N plasmas within 20% of the stability boundary.

Increasing the Density in W7-X: Benefits and Limitations

G. Fuchert¹, K. J. Brunner¹, K. Rahbarnia¹, T. Stange¹, D. Zhang¹, J. Baldzuhn¹, C. D. Beidler¹, S. A. Bozhakov¹, R. Burhenn¹, H. Damm¹, A. Dinklage¹, M. Hirsch¹, Y. O. Kazakov², J. Knauer¹, Y. Feng¹, A. Langenberg¹, H. P. Laqua¹, S. Lazerson³, N. Pablant³, E. Pasch¹, T. Sunn Pedersen¹, E. R. Scott¹, F. Warmer¹, and R. C. Wolf¹

The W7-X Team

¹Max-Planck-Institut für Plasmaphysik, Greifswald, Germany

²Laboratory for Plasma Physics, ERM/KMS, Brussels, Belgium

³Princeton Plasma Physics Laboratory (PPPL), Princeton, NJ 08540, USA

Corresponding Author: G. Fuchert, golo.fuchert@ipp.mpg.de

As the first comprehensively optimized stellarator, Wendelstein 7-X (W7-X) is an essential experiment to study high density operation in this kind of device. This contribution presents first experiments on the density dependence of the energy confinement in W7-X and limitations of the achievable density. Theoretical predictions and empirical scaling laws for the energy confinement time in stellarators (e.g., the ISS04) predict a positive correlation between the plasma density and the energy confinement time. However, this might not be valid for plasma operation close to operational limits. Hence, the energy confinement time scaling and the presence of operational limits have to be studied as an intertwined system. The experimental exploitation of W7-X has only started, however, the gradual completion of the machine capabilities is an ideal opportunity to map out the configuration space and to identify key issues on the route to high-performance long-pulse operation.

In the first two experimental campaigns, featuring a limiter and a test divertor configuration, the energy confinement time has been analyzed. A positive density dependence has been found and the scaling coefficient is close to the expectation from ISS04. During these experiments, however, radiative collapses have been observed. Such a radiative density limit is predicted by simplified analytical models. Such a model has been applied to W7-X in order to estimate a critical density and in purely gas-fuelled hydrogen plasmas, no stable plasma operation has been achieved above this density. It has been observed that the critical density also depends on the magnetic configuration, which directly relates this issue to scenario development. Furthermore, first experiments with pellet-fuelling showed densities well above the critical density, which indicates the importance of profile and fuelling effects. These experiments confirm that an increasing density is indeed beneficial for the energy confinement, at least in the currently accessible density range. It remains to be shown that this trend extrapolates to the high-performance plasmas for which W7-X was designed. The experiments have also shown, however, that high-density operation involves a careful scenario development, as fuelling issues and radiative instabilities limit the currently accessible operational space of W7-X in its current state of completion.

Scenario Development for DT Operation at JET

L. Garzotti¹, C. D. Challis¹, R. Dumont², D. Frigione³, J. P. Graves⁴, E. A. Lerche⁵, J. Mailloux¹, M. J. Mantsinen⁶, F. G. Rimini¹, F. J. Casson¹, A. Czarnecka⁷, R. Felton¹, J. Garcia², C. Giroud¹, E. Joffrin², H.-T. Kim⁸, N. Krawczyk⁸, M. Lennholm⁹, P. J. Lomas¹, C. Lowry⁹, L. Meneses¹⁰, I. M. Ferreira Nunes¹⁰, M. Romanelli¹, S. Sharapov¹, S. Silburn¹, M. Tsalas¹¹, D. F. Valcarcel¹, A. C. C. Sips⁹, L. Frassinetti⁸, and E. Stefanikova⁸

The JET Contributors

¹United Kingdom Atomic Energy Authority, Culham Science Centre, Abingdon, UK

²Commissariat à l'énergie atomique (CEA), 91400 Gif-sur-Yvette, France

³Agenzia nazionale per le nuove tecnologie, l'energia e lo sviluppo economico sostenibile (ENEA), Rome, Italy

⁴Swiss Plasma Center (SPC), École polytechnique fédérale de Lausanne (EPFL), 1015 Lausanne, Switzerland

⁵Laboratory for Plasma Physics, ERM/KMS, Brussels, Belgium

⁶Centro Nacional de Supercomputación (BSC), Barcelona, Spain

⁷Institute of Plasma Physics and Laser Microfusion (IPPLM), Warsaw, Poland

⁸KTH Royal Institute of Technology, Stockholm, Sweden

⁹EUROfusion/JET, Culham Science Centre, Abingdon, Oxfordshire, OX14 3DB, UK

¹⁰Instituto Superior Técnico (IST), 1049-001 Lisbon, Portugal

¹¹FOM Institute DIFFER, Association EURATOM-FOM, Nieuwegein, Netherlands

Corresponding Author: L. Garzotti, luca.garzotti@ccfe.ac.uk

EX

The JET exploitation plan foresees DT operations in 2019–20. With respect to the first DT campaign in 1998, when JET was equipped with a C wall, the experiments will be conducted in presence of a Be-W ITER-like wall and will benefit from an extended and improved set of diagnostics and higher available additional power. Among the challenges presented by operations with the new wall there are a general deterioration of the pedestal confinement, the risk of heavy impurity accumulation in the core, and the requirement to protect the W divertor from excessive heat loads. Therefore, an intense activity of scenario development has been undertaken at JET during the last three years to overcome these difficulties and to achieve a stationary scenario of the duration of 5 s featuring $H_{98} > 0.9$, $W_{th} \approx 10\text{--}12$ MJ towards the lowest values of ρ^* and ν^* achievable on JET.

Two complementary scenarios are being developed to approach the problem of developing a scenario suitable for high-performance DT operation. The baseline scenario ($\beta_N \sim 1.8$ and $H_{98} \sim 1.0$) concentrates mainly on pushing the operation towards the high current and field limits with a relaxed current profile, whereas the hybrid scenario ($\beta_N \sim 2\text{--}3$ and $H_{98} > 1.0$) exploits the advantages of operating at high normalized β with a shaped current profile above unity. Encouraging results were achieved for the baseline scenario at 3 MA/2.8 T and for the hybrid scenario at reduced plasma current (2.2–2.5 MA/2.8–2.9 T). High-performance plasmas with $H_{98} \sim 0.9$ producing $\sim 3 \times 10^{16}$ neutrons/s were obtained for > 5 energy confinement times (~ 1.5 s). A third scenario, has also been developed for α -particle studies. This scenario aims at maintaining high plasma performance for 1–2 s to generate a significant population of α -particles for the α -particle studies and deliberately omits ICRH heating to avoid creating RF driven fast particles, which could mask the effect of the fusion-generated α -particles. In these pulses ICRH induced TAEs were observed after the NBI switch-off compatibly with the beam fast ion slowing-down time.

The results of all scenarios have been the object of an extensive activity of code validation and modelling and extrapolated to the target DT scenarios.

Implications of JET-ILW L-H Transition Studies for ITER

J. C. Hillesheim¹, E. Delabie², E. R. Solano³, C. F. Maggi¹, H. Meyer⁴, E. Belonohy^{4,1},
I. S. Carvalho⁵, E. de la Luna³, A. Drenik⁶, M. Gelfusa⁷, C. Giroud¹, J. Hobirk⁶,
A. E. Hubbard⁸, A. Kappatou⁶, H.-T. Kim⁹, A. Huber¹⁰, E. A. Lerche¹¹, B. Lomanowski¹²,
M. Mansinen^{13,14}, S. Menmuir¹, I. M. Ferreira Nunes⁵, E. Peluso⁷, F. G. Rimini¹,
P. A. Schneider⁶, M. Stamp¹, and G. Verdoolaege¹⁵

The JET Contributors

¹Culham Centre for Fusion Energy (CCFE), Culham Science Centre, Abingdon, UK

²Oak Ridge National Laboratory (ORNL), Oak Ridge, TN 37831, USA

³Centro de Investigaciones Energéticas, Medioambientales y Tecnológicas (CIEMAT), Madrid, Spain

⁴EUROfusion/JET, Culham Science Centre, Abingdon, Oxfordshire, OX14 3DB, UK

⁵Instituto Superior Técnico (IST), 1049-001 Lisbon, Portugal

⁶Max-Planck-Institut für Plasmaphysik, Garching, Germany

⁷Università di Tor Vergata, 00173 Rome, Italy

⁸Plasma Science & Fusion Center, MIT, Cambridge, MA 02139, USA

⁹EUROfusion Programme Management Unit Culham, Culham Science Centre, Abingdon, UK

¹⁰Forschungszentrum Jülich, Jülich, Germany

¹¹Laboratory for Plasma Physics, ERM/KMS, Brussels, Belgium

¹²Aalto University, Espoo, Finland

¹³Centro Nacional de Supercomputación (BSC), Barcelona, Spain

¹⁴Catalan Institution for Research and Advanced Studies (ICREA), Barcelona, Spain

¹⁵Ghent University, 9000 Ghent, Belgium

Corresponding Author: J. C. Hillesheim, jon.hillesheim@ukaea.uk

Unravelling the conditions that permit access to H-mode continues to be an unresolved physics issue for tokamaks, and accurate extrapolations are important for planning ITER operations and DEMO design constraints. Experiments have been performed in JET, with the ITER-like W/Be wall, to increase the confidence of predictions for the L-H transition power threshold in ITER. These studies have broadly confirmed established dependencies of P_{L-H} , reduced uncertainties in extrapolations, and highlighted the largest remaining sources of uncertainty. We have also obtained unexpected results with direct relevance for lowering P_{L-H} during the nonactive phase of ITER operation.

A database has been compiled of JET-ILW P_{L-H} measurements spanning a range of plasma magnetic geometries, density and toroidal magnetic field values, hydrogen isotopes, ion species mixtures, effects from impurity seeding, and differences in heating and momentum sources. Regression analysis of the database shows in comparison to past scaling studies and to JET-C results, P_{L-H} is lower for matched density and magnetic field; however, the exponents for density and magnetic field are larger, resulting in possibly reduced threshold at low magnetic field operation in ITER, but increased values at full field operation. The single largest uncertainty in extrapolating to ITER is the effect of the divertor configuration, a factor of two difference in JET alone.

Continued...

The minimum of the density dependence of P_{L-H} also moves to about a 30% higher value in H than D. The dependence of P_{L-H} was also studied in mixed species plasmas. It was found that most of the variation in H-D mixtures was at less than 20% or more than 80% H concentration, with little variation in between.

Fuelling ^4He into H plasmas was also performed, resulting in a $\sim 25\%$ reduction of the threshold with up to about 10% He concentration. This reduction in L-H threshold in H-He mixtures may have application for the nonactive phase of ITER operations. Detailed hydrogen and helium concentration analysis, transport simulations, and ICRH power deposition calculations have been performed to constrain interpretation of the mixed ion species effects. We will summarize results across all JET-ILW P_{L-H} data and the implications of the conclusions for ITER.

L-H Transition Trigger Physics in ITER-Similar Plasmas with and without Applied $n = 3$ Magnetic Perturbations

L. Schmitz¹, Z. Yan², R. Wilcox³, M. Kriete², T. L. Rhodes¹, G. R. McKee², C. Paz-Soldan⁴, A. Marinoni⁵, P. Gohil⁴, L. Zeng¹, and C. C. Petty⁴

¹University of California Los Angeles, CA 90095, USA

²University of Wisconsin-Madison, Madison, WI 53706, USA

³Oak Ridge National Laboratory (ORNL), Oak Ridge, TN 37831, USA

⁴General Atomics, San Diego, CA 92186, USA

⁵Plasma Science & Fusion Center, MIT, Cambridge, MA 02139, USA

Corresponding Author: L. Schmitz, lschmitz@ucla.edu

Quantitative proof is presented that the ion polarization current [1] dominates the evolution of the radial electric field E_r across the L-H transition, and needs to be properly taken into account in Ohm's law. This is an important step towards developing a physics-based reduced L-H transition model, which in addition needs to include at a minimum the poloidal momentum balance, and evolution equations for the turbulence intensity and the pressure gradient [2]. The observed isotope dependence of the threshold power P_{L-H} in ITER-similar H, He and D plasmas [3] can then be qualitatively understood: in D and He, where the Reynolds stress [2–4] dominates the neoclassical bulk viscosity and thermal ion orbit loss, P_{L-H} is relatively low. In hydrogen plasmas, where the Reynolds stress is marginal and comparable to the neoclassical bulk viscosity and thermal orbit loss current, P_{L-H} is much higher. The observed increased transition time to full turbulence suppression in hydrogen plasmas can also be quantitatively understood using this model. Resonant magnetic perturbations (RMP) may have to be applied before the L-H transition in ITER to safely suppress the first ELM. In ITER-similar plasmas in DIII-D the increase of P_{L-H} with $n = 3$ RMP is most pronounced with ECH, with P_{L-H} increasing with decreasing plasma collisionality ($P_{L-H} \sim (\nu^*)^{-0.3}$). Two-fluid modelling with the M3D-C1 code [5] shows that the normalized L-mode radial density gradient a/L_n is toroidally modulated and periodically increased on the outboard midplane with applied RMP. Nonaxisymmetric modifications with RMP include increased local long-wavelength turbulence (measured via BES) and reduction of the E_r well and $E \times B$ shear. We conjecture that the increase in threshold power with RMP results from locally enhanced instability drive (however without simultaneously increased Reynolds stress) and reduced $E \times B$ shear.

Work supported by the U.S. Department of Energy under DE-FG02-08ER54984, DE-FG02-08ER 54999, DE-AC05-00OR22725, and DE-FC02-04ER54698.

References

- [1] K. Itoh, Plasma Phys. Contr. F., **36**, A307–A318 (1994).
- [2] K. Miki, *et al.*, Phys. Plasmas, **19**, 092306 (2012).
- [3] Z. Yan *et al.*, Nucl. Fus., **57**, 126015 (2017).
- [4] L. Schmitz, IAEA FEC–2016, Kyoto, Japan, EX/P3-11, (2016).
- [5] R. S. Wilcox *et al.*, Nucl. Fus., **57**, 116003 (2017).

Transport Barriers in DIII-D High- β_p Plasmas and Development of Candidate Steady State Scenarios for ITER

J. T. McClenaghan¹, A. M. Garofalo², G. M. Staebler², L. L. Lao², D. B. Weisberg², J. Huang³, S. Y. Ding³, X. Gong³, J. Qian³, Q. Ren³, and C. T. Holcomb⁴

¹*Oak Ridge Associated Universities (ORAU), Oak Ridge, TN 37831, USA*

²*General Atomics, San Diego, CA 92186, USA*

³*Institute of Plasma Physics, Chinese Academy of Sciences, Hefei, Anhui, People's Republic of China*

⁴*Lawrence Livermore National Laboratory (LLNL), Livermore, CA 94550, USA*

Corresponding Author: J. T. McClenaghan, mcclenaghanj@fusion.gat.com

EX Shafranov shift stabilizes turbulence and creates a bifurcation in kinetic ballooning mode (KBM) transport that enables high performance ITB plasmas to be sustained at reactor relevant q_{95} . On DIII-D, the internal transport barrier (ITB), high- $\beta_N \sim 3$, and very high normalized confinement $H_{98}(y, 2) \sim 1.6$ of the high- β_p scenario has been achieved at $q_{95} \sim 6.5$. This is projected to meet the ITER steady-state goal of $Q = 5$. The ITB is maintained at lower β_p with a strong reverse shear, confirming predictions that negative central shear can lower the β_p threshold for the ITB. There are two observed confinement states in the high β_p scenario: H-mode confinement state with a high edge pedestal, and an enhanced confinement state with a low pedestal and an ITB. At large radius ($\rho = 0.8$), the enhanced ITB confinement state has a much lower predicted turbulent ion energy transport than the H-mode confinement state. Simulating intermediate states, a large electromagnetic "mountain" of increased transport is found due to a KBM. Transient perturbations such as edge localized modes (ELMs) may trigger the transition between states by temporarily reducing the KBM drive. It has been observed that when there are no large type-I ELMs, and there is no transition to enhanced confinement otherwise observed with lower $n = 3$ perturbation. Quasi-linear gyro-Landau fluid predictive modelling of ITER suggests that only a modest reverse shear is required to achieve the ITB formation necessary for $Q = 5$ when electromagnetic physics including the KBM is incorporated.

Core Density Peaking Experiments in JET, DIII-D and C-Mod in Various Operational Scenarios Driven by Fuelling or Transport

T. Tala¹, J. W. Hughes², S. Mordijck³, H. Nordman⁴, A. Salmi¹, C. Bourdelle⁵, J. Citrin⁶, C. Agatha⁷, C. Giroud⁸, J. C. Hillesheim⁸, A. E. Hubbard², C. F. Maggi⁸, P. Mantica⁹, M. Maslov⁸, L. Meneses¹⁰, S. Menmuir⁸, V. Naulin¹¹, M. Oberparleiter⁴, A. C. C. Sips¹², A. Skyman⁴, D. Tegnered⁴, M. Tsalias¹³, E. A. Tolman², and H. Weisen¹⁴

The JET Contributors

¹VTT Technical Research Centre of Finland Ltd., Espoo, Finland

²Plasma Science & Fusion Center, MIT, Cambridge, MA 02139, USA

³College of William & Mary, Williamsburg, VA 23185, USA

⁴Chalmers University of Technology, Göteborg, Sweden

⁵Institut de Recherche sur la Fusion par confinement Magnétique (IRFM), Commissariat à l'énergie atomique (CEA/Cadarache), 13108 St. Paul lez Durance, France

⁶FOM Institute DIFFER, Association EURATOM-FOM, Nieuwegein, Netherlands

⁷Institute of Plasma Physics and Laser Microfusion (IPPLM), Warsaw, Poland

⁸Culham Centre for Fusion Energy (CCFE), Culham Science Centre, Abingdon, UK

⁹Istituto di Fisica del Plasma (IFP), Consiglio Nazionale delle Ricerche (CNR), 20125 Milan, Italy

¹⁰Institute of Plasmas and Nuclear Fusion (IPNF), Instituto Superior Técnico (IST), 1049-001 Lisbon, Portugal

¹¹Technical University of Denmark (DTU), Lyngby, Denmark

¹²European Commission, Brussels, Belgium

¹³International Thermonuclear Experimental Reactor (ITER), Cadarache Centre, 13108 St. Paul lez Durance, France

¹⁴Swiss Plasma Center (SPC), École polytechnique fédérale de Lausanne (EPFL), 1015 Lausanne, Switzerland

Corresponding Author: T. Tala, tuomas.tala@vtt.fi

Core density profile peaking has been extensively studied by performing several dimensionally matched collisionality scans in various plasma operation scenarios on JET as well as by executing a 3-point collisionality scan on DIII-D and a 2-point collisionality scan in I-mode on C-Mod.

In L-mode, D and V are large in all cases even if the NBI power is much smaller than in the H-mode cases. However in H-mode, D and V are both small, and therefore, NBI fuelling plays an important role in contributing to density peaking. These small D and V here represent electron particle transport, but there is evidence now from JET that the ion particle D_i and V_i can be an order of magnitude larger.

Gyrokinetic GENE simulations were performed to infer the peaking factor of background ions. Peaked density profiles are obtained only for L-mode while H-modes discharges show flat or hollow density profiles at $\rho = 0.6$. TGLF and QuaLiKiz transport simulations confirm the dominant role of NBI fuelling in producing peaked ne profiles in JET H-mode plasmas.

Continued...

A similar 3-point collisionality scan to JET was performed on DIII-D. Density peaking increased with collisionality very similarly to JET. The perturbative analysis from the gas puff modulation data confirms the significant role of NBI fuelling in each case.

The dependence of density peaking on collisionality was studied in I-mode and L-mode on C-Mod by applying gas puff modulation. The steady-state n_e data indicates no dependence on collisionality in neither I- nor L-mode, consistent with JET but in contrast to H-mode data in C-Mod.

The results from the scans on various tokamaks and modelling all indicate that in H-mode the NBI fuelling is a significant contributor to density peaking. The consequences of this on ITER fuelling will be discussed.

This work has been carried out within the framework of the EUROfusion Consortium and has received funding from the Euratom research and training programme 2014-2018 under grant agreement No. 633053. The views and opinions expressed herein do not necessarily reflect those of the European Commission. This material is based upon work supported by the U.S. Department of Energy under awards DE-FC02-04ER54698, DE-FC02-99ER54512, DE-SC0007880 using Alcator C-Mod, a DOE Office of Science User Facility.

Transport Characteristics of Deuterium and Hydrogen Plasmas with Ion Internal Transport Barrier in LHD

K. Nagaoka^{1,2}, H. Takahashi^{1,3}, M. Nakata^{1,3}, K. Tanaka^{1,4}, K. Mukai^{1,3}, M. Yokoyama^{1,3}, S. Murakami⁵, H. Nakano^{1,3}, K. Ida^{1,3}, M. Yoshinuma^{1,3}, S. Ohdachi^{1,3}, T. Bando³, M. Nunami^{1,3}, R. Seki^{1,3}, H. Yamaguchi¹, M. Osakabe^{1,3}, and T. Morisaki^{1,3}

The LHD Experiment Group

¹National Institute for Fusion Science (NIFS), Toki, Gifu, Japan

²Graduate School of Science, Nagoya University, Nagoya, Japan

³Department of Fusion Science, Graduate University for Advanced Studies (SOKENDAI), Toki, Gifu, Japan

⁴Interdisciplinary Graduate School of Engineering Sciences, Kyushu University, Kasuga, Japan

⁵Department of Nuclear Engineering, Kyoto University, Nishikyo-ku, Kyoto 615-8540, Japan

Corresponding Author: K. Nagaoka, nagaoka@nifs.ac.jp

A remarkable achievement of $T_{i0} = 10$ keV with $Z_{\text{eff}} = 2$ was obtained in Large Helical Device (LHD). In order to clarify transport characteristics in ion internal transport barrier (ion ITB) formation with isotope effect, a dataset of pure deuterium (D) ($n_D/n_e > 0.85$) and pure hydrogen (H) ($n_H/n_e > 0.85$) plasmas for high-ion-temperature (high- T_i) regime were analyzed, and two mechanisms of transport improvement were characterized. A significant reduction of ion heat transport in D plasmas was observed in comparison between D and H plasmas, indicating non-gyroBohm mass dependence. The dependence of the heat transport on temperature ratio (T_e/T_i) and normalized T_i -gradient ($R/L_{T_i} = -(R/T_i)(dT_i/dr)$) was investigated in the core region, in which gyrokinetic simulations with GKV code predicts the destabilization of ITG modes. The T_e/T_i dependence shows ITG-like property, while a significant deviation from the ITG-like property is found in the R/L_{T_i} dependence. Moreover, the density fluctuation is well correlated with the heat transport dependence on T_e/T_i and R/L_{T_i} , indicating suppression of ITG mode in large R/L_{T_i} regime and resultant ion ITB formation. The similarity of instabilities found by GKV indicates that both ITG suppression and isotope effect contribute to production of high- T_i plasmas ($T_{i0} \sim 10$ keV) with multiple-ion conditions.

EX

Predicting the Toroidal Rotation Profile for ITER

C. Chrystal¹, B. A. Grierson², S. R. Haskey², J. S. deGrassie¹, G. M. Staebler¹, T. Tala³, and A. Salmi³

¹General Atomics, San Diego, CA 92186, USA

²Princeton Plasma Physics Laboratory (PPPL), Princeton, NJ 08540, USA

³VTT Technical Research Centre of Finland Ltd., Espoo, Finland

Corresponding Author: C. Chrystal, chrystal@fusion.gat.com

EX Toroidal rotation in ITER is predicted with a combination of intrinsic and NBI sources and gyrofluid modelling of momentum transport, and it is found to play a significant role in enhancing DT fusion performance. In a large tokamak such as ITER, intrinsic sources of rotation as well as rotation drive from applied 3D fields will become more significant due to a relatively low amount of neutral beam torque. The predicted intrinsic rotation at the top of the pedestal in ITER is 10 krad/s, and the core rotation driven by NBI is predicted to be ~ 20 krad/s. The predicted rotation for ITER is large enough that the TGLF transport model predicts significant turbulence stabilization, leading to improved confinement and an increase in the predicted fusion gain Q from 5 to 8 when rotation effects are included and the core density is assumed to be flat. Q is further increased to 11 when TGLF is also used to self consistently determine the core density. The predicted intrinsic rotation is derived from dimensionless parameter scan experiments that measured the dependence of intrinsic torque on ρ^* . Confidence in this prediction has been increased with experiments that investigated important uncertainties in the intrinsic torque measurements: the role of fast-ions on the measurement of intrinsic torque, and the effect of neutrals on momentum transport in the pedestal. Intrinsic rotation measured in a ρ^* scan yielded a consistent dependence on ρ^* , and intrinsic rotation was not found to be affected by significant changes in divertor closure when other important parameters were held constant. In addition, it was found that intrinsic rotation undergoes no significant change at the onset of detachment. These results increase confidence in the prediction of the intrinsic rotation in ITER. The dependence of intrinsic rotation on ρ^* found in this work appear to be inconsistent with completely independent database studies of intrinsic rotation. However, careful analysis shows a common dependency on ion temperature that underlies the similar predictions from these different methods.

Work supported in part by the U.S. Department of Energy under DE-FC02-04ER54698 and DE-AC02-09CH11466, and carried out within the framework of the EUROfusion Consortium and has received funding from the Euratom research and training programme 2014-2018 under Grant Agreement No. 633053.

Advances in Runaway Electron Control and Model Validation for ITER

C. Paz-Soldan¹, N. W. Eidietis¹, E. M. Hollmann², A. Lvovskiy³, C. Cooper³, J. Herfindal⁴, R. A. Moyer², D. Shiraki⁴, K. E. Thome³, P. Aleynikov⁵, D. P. Brennan⁶, L. Carbajal⁴, D. del-Castillo-Negrete⁴, O. Embréus⁷, T. Fülöp⁷, M. L. Hoppe⁷, C. Liu⁸, P. Parks¹, and D. A. Spong⁴

¹General Atomics, San Diego, CA 92186, USA

²University of California San Diego, CA 92093, USA

³Oak Ridge Associated Universities (ORAU), Oak Ridge, TN 37831, USA

⁴Oak Ridge National Laboratory (ORNL), Oak Ridge, TN 37831, USA

⁵Max-Planck-Institut für Plasmaphysik, Garching, Germany

⁶Princeton University, Princeton, NJ 08544, USA

⁷Chalmers University of Technology, Göteborg, Sweden

⁸Princeton Plasma Physics Laboratory (PPPL), Princeton, NJ 08540, USA

Corresponding Author: C. Paz-Soldan, paz-soldan@fusion.gat.com

Measurements and modelling of runaway electron (RE) dissipation in DIII-D has resolved key experimental discrepancies and validated predictions for ITER, improving confidence that RE mitigation and avoidance can be predictively optimized without risking first-wall integrity. Energy-resolved measurements of hard X-ray (HXR) flux with a unique γ -ray imaging (GRI) system demonstrate that anomalous dissipation of RE beams is strongest for low energy RE populations. Modelling including the self-consistent interaction of the RE population with RE-driven kinetic instabilities reproduces the enhanced dissipation and finds strong wave-particle interactions with the low energy RE population.

Novel spatio-temporally resolved HXR measurements using the GRI system have also validated RE distribution function (f_e) dependencies and observed the effect of phase-space attractors that pile up REs at a given energy. Increasing synchrotron damping shifts the high-energy f_e towards lower energy, though quantitatively observed synchrotron effects are larger than predicted. Increasing collisional damping shifts the full f_e to lower energy. Validation of f_e in both phase space and real space is further advanced by new synchrotron and bremsstrahlung emission synthetic diagnostics. These tools reproduce experimental images and can validate different pitch-angle distribution models.

Considering RE seed formation and final loss, a new method to experimentally estimate the RE seed current from pellet ablation rates reveals that the hot-tail generation mechanism significantly overestimates RE seed production, while the Dreicer mechanism is insufficient to explain the observed seed. Model predictions of first wall Joule heating during the RE final loss are consistent with experiment at high ion charge (Z). Discrepancies are found at low Z , however, indicating some RE dissipation processes remain poorly understood.

The above measurements and comparison with theory substantially improves confidence that model-based optimization of RE avoidance and mitigation can be achieved. This is essential to fully exploit ITER while avoiding RE-induced damage to the first-wall.

Work supported by the U.S. Department of Energy under DE-AC05-06OR23100, DE-FC02-04ER54698, DE-AC02-09CH11466, and DE-FG02-04ER54761.

Test of the ITER-Like RMP Configurations for ELM-Crash-Suppression on KSTAR

Y. In¹, Y. M. Jeon², J.-K. Park³, A. Loarte⁴, J.-W. Ahn⁵, H. H. Lee², K. Kim², G. Y. Park²,
J. H. Lee², M. W. Kim¹, and H. K. Park¹

The 3D Physics Task Force in KSTAR

¹*Ulsan National Institute of Science and Technology (UNIST), Ulsan, Republic of Korea*

²*National Fusion Research Institute (NFRI), Daejeon, Republic of Korea*

³*Princeton Plasma Physics Laboratory (PPPL), Princeton, NJ 08540, USA*

⁴*International Thermonuclear Experimental Reactor (ITER),*

Cadarache Centre, 13108 St. Paul lez Durance, France

⁵*Oak Ridge National Laboratory (ORNL), Oak Ridge, TN 37831, USA*

Corresponding Author: Y. In, inyongkyoon@unist.ac.kr

KSTAR has demonstrated a divertor heat flux broadening during edge-localized-mode (ELM)-crash-suppression using ITER-like 3-row resonant magnetic perturbation (RMP) configurations for the first time. Over the last couple of years, we have established a robust methodology to fully suppress ELM-crashes using low- n RMPs. To address the ITER relevant ELM control, a systematic exploration of various RMP configurations at lower q_{95} plasmas led us to accomplish RMP-driven, ELM suppression down to $q_{95} = 3.3$ [1]. As long as the mode-locking at low q_{95} is avoided and a quick recovery of the wall conditioning (e.g., cryo-pumping or divertor gas-puffing) is secured, the access to the targeted q_{95} (~ 3) for ITER is foreseen to be feasible in KSTAR. Taking full advantage of 3-row in-vessel control coils (IVCC) in KSTAR, rather than 2-rows in other devices, a series of intentionally misaligned RMP configurations have been investigated for ELM-crash-suppression. The ITER-like 3-row RMPs were found to have broadened the divertor heat flux in the vicinity of outer strike point, while the 2-row has rarely affected the near scrape-off-layer (SOL) heat flux despite a little broadened profile change in the far-SOL area [2]. Since the main focus of divertor heat flux dispersal would be the redistribution of the peaked near-SOL heat flux, such contrasting 3D heat flux broadening must be similarly attributable to the choice of 3-rows in ITER, instead of 2-rows. Since such broadening characteristics could be completely different in partially detached plasmas in ITER [3], KSTAR has conducted an investigation of whether RMP-driven, ELM-crash-suppression would be compatible with detached plasmas. Although a fully detached plasma under RMP has not been obtained yet, we were able to greatly reduce heat flux at $q_{95} = 3.8$ using $n = 2$ RMPs in high density plasmas [4]. Overall, the new lessons we have learned would be directly relevant to the successful ITER RMP research, while resolving any uncertainty associated with 3-row RMPs that could be further exploited in KSTAR.

References

- [1] Y. In *et al.*, APS-DPP invited talk “Tamed Stability and Transport using Controlled Nonaxisymmetric Fields in KSTAR” (2017).
- [2] A. Loarte, Y. In *et al.*, In Preparation (2018).
- [3] R. Pitts, private communications (2018).
- [4] J. W. Ahn *et al.*, APS-DPP (2017).

Dynamic ELM and Divertor Control Using Mixed Toroidal Harmonic Resonant Magnetic Perturbations in DIII-D and EAST

Y. Sun¹, C. Paz-Soldan², R. Nazikian³, S. Gu^{1,4}, M. Jia^{1,4}, H. H. Wang¹, Y. Q. Liu², T. Abrams², I. O. Bykov⁵, L. Cui³, T. E. Evans², A. M. Garofalo², W. Guo¹, X. Gong¹, C. J. Lasnier⁶, M. A. Makowski⁶, S. Munaretto², D. M. Orlov⁵, and T. Shi¹

¹*Institute of Plasma Physics, Chinese Academy of Sciences, Hefei, Anhui, People's Republic of China*

²*General Atomics, San Diego, CA 92186, USA*

³*Princeton Plasma Physics Laboratory (PPPL), Princeton, NJ 08540, USA*

⁴*University of Science and Technology of China, Hefei, Anhui, People's Republic of China*

⁵*University of California San Diego, CA 92093, USA*

⁶*Lawrence Livermore National Laboratory (LLNL), Livermore, CA 94550, USA*

Corresponding Author: Y. Sun, ywsun@ipp.ac.cn

Mixed toroidal harmonic resonant magnetic perturbations (RMPs) have been used on both EAST and DIII-D to reduce the threshold for edge localized modes (ELMs) suppression and to spread the divertor heat flux. Experiments using mixed toroidal harmonic RMPs have validated predictions that divertor heat and particle flux can be dynamically controlled while maintaining ELM suppression in DIII-D. Theoretical modelling has reproduced the linear and nonlinear response observed on magnetic sensors during ELM mitigation and suppression. Mixed $n = 2$ and 3 toroidal harmonic RMP significantly lower the threshold current for ELM suppression compared to the single $n = 3$ RMP. Rotating RMP has been demonstrated recently in EAST as a promising method in controlling the steady state particle and heat flux on the divertor, when the transient power loads induced by ELMs have been eliminated by RMPs. It is observed that the particle flux patterns on the divertor targets change synchronously with rotating RMP fields as predicted by the modelled magnetic footprint patterns by TOP2D. ELM suppression over one full cycle of a rotating $n = 2$ RMP that was mixed with a static $n = 3$ RMP field has been achieved in DIII-D. Strong changes in the three-dimensional heat and particle flux footprint in the divertor were observed during the application of the mixed toroidal harmonic RMPs, which also agrees well with modelling. Plasma response during ELM suppression using mixed toroidal harmonic RMPs shows that small $n = 2$ field help to penetrate $n = 3$ mode which eventually leading to ELM suppression. Plasma response measured by magnetic sensors shows linear relation in the mitigation stage in DIII-D, while a nonlinear jump of plasma response is observed during the transition from mitigation to suppression of ELM in DIII-D. MHD simulation with the MARS-F code shows good agreement during ELM mitigation in both mode structure and phase, while it has a phase shift to the observed response during ELM suppression in DIII-D, which is similar to that in EAST. These results expand physics understanding and potential effectiveness of the technique for reliably controlling ELMs and divertor power/particle loading distributions in future burning plasma devices such as ITER.

Work supported by the U.S. Department of Energy under DE-FC02-04ER54698 and NNSF of China under 11475224.

Experimental Conditions for Suppressing Edge Localized Modes by Magnetic Perturbations in ASDEX-Upgrade

W. Suttrop¹, A. Kirk², V. Bobkov¹, M. Cavedon¹, M. G. Dunne¹, R. M. McDermott¹, H. Meyer², R. Nazikian³, C. Paz-Soldan⁴, D. A. Ryan², E. Viezzer^{1,5}, and M. Willensdorfer¹

The ASDEX-Upgrade Team and EUROfusion-MST1 Team

¹Max-Planck-Institut für Plasmaphysik, Garching, Germany

²Culham Centre for Fusion Energy (CCFE), Culham Science Centre, Abingdon, UK

³Princeton Plasma Physics Laboratory (PPPL), Princeton, NJ 08540, USA

⁴General Atomics, San Diego, CA 92186, USA

⁵Universidad de Sevilla, Seville, Spain

Corresponding Author: W. Suttrop, wolfgang.suttrop@ipp.mpg.de

Full suppression of edge localized modes (ELMs) by magnetic perturbations (MP) in high-confinement mode (H-mode) plasmas has been obtained in ASDEX-Upgrade (AUG) in a shape-match experiment with DIII-D [1]. In contrast to previous scenarios where ELMs were mitigated by MP, full ELM suppression in AUG requires stronger shaping. This finding has been attributed to larger pedestal plasma pressure, which in turn leads to stronger amplification of the external MP by marginally stable, edge localized, kink-peeling modes. Recent experiments in AUG aimed to identify critical parameters for accessing ELM suppression: Safety factor, plasma rotation, plasma edge density and collisionality. Edge safety factor scans in the range of $q_{95} = 3.6\text{--}4.2$ showed a window $q_{95} = 3.66\text{--}3.91$ for ELM suppression with $n = 2$ MP.

In the ELM suppression scenario used so far, there is a clear maximum edge density ($3.5 \times 10^{19}/\text{m}^3$) for ELM suppression, which can also be expressed as a collisionality limit. Our present data set is still too sparse to discriminate between these quantities. In H-modes with ELM mitigation or ELM suppression, the pedestal pressure is typically 32% below that of ELMy H-mode with MP switched off and still somewhat below that of phases with MP-mitigated ELMs.

The resonant, field-aligned MP components near the top of the H-mode edge gradient region are believed to be essential for ELM suppression [2] and their strength in turn depends (in two-fluid MHD) on the absence or presence of electron flow across the magnetic field ($\nu_{e,\perp}$) which can induce helical currents that shield the MP. In our experiment we find that the toroidal rotation at the pedestal top, measured by charge exchange recombination spectroscopy on B^{5+} impurities, varies widely, $\nu_{\text{tor}} = 0\text{--}40$ km/s. There is also significant variation of $\nu_{e,\perp}$, despite ELM suppression being maintained. This includes cases with zero-crossing in the pedestal region (weak shielding) and cases where $\nu_{e,\perp}$ (in electron drift direction) in the entire pedestal region is sufficiently strong to shield the resonant plasma response everywhere.

References

- [1] R. Nazikian *et al.*, IAEA FEC-2016, Kyoto, Japan, [PD/1-1](#), (2016).
- [2] W. Wade *et al.*, Nucl. Fus., **55**, 023002 (2015).

ELM Control Physics with Impurity Seeding and LHCD in the HL-2A Tokamak

G. L. Xiao^{1,2}, X. L. Zou³, Y. P. Zhang¹, D. Mazon³, W. L. Zhong¹, X. Y. Bai¹, Z. Y. Cui¹, L. Delpech³, X. T. Ding¹, J. Q. Dong^{1,4}, A. Ekedahl³, B. B. Feng¹, G. Giruzzi³, J. M. Gao¹, M. Goniche³, G. T. Hoang³, A. D. Liu⁵, B. Lu¹, Y. Peysson³, S. D. Song¹, X. M. Song¹, Z. B. Shi¹, P. Sun¹, D. L. Yu¹, M. Xu¹, and X. R. Duan¹

The HL-2A Team

¹Southwestern Institute of Physics, Chengdu, Sichuan, People's Republic of China

²Tsinghua University, Haidian, Beijing, People's Republic of China

³Institut de Recherche sur la Fusion par confinement Magnétique (IRFM),

Commissariat à l'énergie atomique (CEA/Cadarache), 13108 St. Paul lez Durance, France

⁴Zhejiang University, Xihu, Hangzhou, Zhejiang, People's Republic of China

⁵University of Science and Technology of China, Hefei, Anhui, People's Republic of China

Corresponding Author: G. L. Xiao, xiaogl@swip.ac.cn

ELM control is a key issue in the magnetic fusion reactor. Experiments for controlling ELMs have been performed in the HL-2A tokamak with several tools, including lower hybrid current drive (LHCD), laser blow-off (LBO) seeded impurities (Al, Fe, W) and supersonic molecular beam injected (SMBI) impurities (Ar, Ne). A beneficial effect of the pedestal deposited impurity injected by LBO on ELM mitigation/suppression has been demonstrated in a controlled manner. In addition, the dependence of these effects on impurity species and amount has been systematically investigated. Mixture SMBI with impurity was firstly carried out in HL-2A. Experimental results suggest that there exists an optimal impurity ratio for heat load control in H-mode plasmas, and pedestal dynamics can be actively controlled by exciting pedestal instabilities with impurity seeding.

ELM mitigation with LHCD has been also successfully achieved in HL-2A. The divertor peak heat load during an ELM is strongly reduced during the mitigation phase. After the LHCD application, the pedestal velocity shear has undergone a severe decrease, and the radial wavenumber spectrum of the pedestal turbulence is shifted toward the origin. It has been found that the ELM mitigation is not synchronized to LHCD pulse with a significant delay, while it is closely correlated to the enhancement of the pedestal turbulence, indicating that as for impurity injection, the ELM mitigation with LHCD can be directly caused by the enhancement of the pedestal turbulence.

In order to understand the mechanism of the turbulence enhancement during ELM mitigation, a theoretical turbulent heat transport model, based on the regulation of the turbulence amplitude by its radial wavenumber spectral shift caused by external velocity shear, has been developed. This external velocity shear can be from SMBI, impurity injection or LHCD. A critical growth rate γ_0 for the turbulence regulation has been identified in this theoretical model. It has been found that the turbulence enhancement and ELM mitigation occur when the external velocity shear exceeds a threshold value, which directly depends on γ_0 . Qualitatively, ELM mitigation with pedestal turbulence enhancement and radial spectral shift due to the pedestal velocity shear reduction can be simulated with this theoretical model.

Recent Advances in ICRF Heating of Mixture Plasmas: Survey of JET and AUG Experiments and Extrapolation to JET-DT and ITER

Y. O. Kazakov¹

The Jet Contributors, The ASDEX-Upgrade Team, and The EUROfusion MST1 Team

¹*Laboratory for Plasma Physics, ERM/KMS, Brussels, Belgium*

Corresponding Author: Y. O. Kazakov, yevgen.kazakov@rma.ac.be

This contribution summarizes recent theoretical and experimental developments of a novel “three-ion species” heating scheme that have opened new promising avenues for the application of ICRF in fusion plasmas. Following successful proof-of-principle demonstration on the Alcator C-Mod and JET tokamaks [1], this scenario has also been recently established on AUG. A small amount of ^3He ions ($\sim 1\%$ and below) was injected into H-D plasmas to absorb RF power and heat the plasma. In JET experiments, effective plasma heating was observed both at extremely low ^3He concentrations of $\sim 0.1\text{--}0.2\%$ (maximized fast-ion content) and at moderate concentrations of $\sim 1\text{--}1.5\%$. We further enhanced the efficiency for fast-ion generation and plasma heating by changing the configuration of ICRH antennas from dipole to $+\pi/2$ phasing. Heating AUG plasmas with this ICRF scenario requires ^3He ions to be less energetic than in JET. The combination of moderate ^3He concentrations of $\sim 1\%$ and off-axis ^3He resonance was successfully applied to reduce fast-ion energies and thus improve confinement of RF-heated ions in AUG. ICRH modelling with the state-of-the-art codes SCENIC [2] and TORIC-SSFPQL has been used extensively to validate JET and AUG experimental observations.

In a next-step, we also successfully demonstrated effective heating of JET H-D mixtures using the fast injected D-NBI ions as resonant “third” species [3]. The scenario was tuned such that D-NBI ions with injection energy of 100 keV absorbed most of launched RF power and were accelerated with ICRF up to ~ 2 MeV. The observed 10-fold increase in the neutron rate and its temporal evolution were successfully reproduced with the time-dependent TRANSP modelling. The established technique of accelerating NBI ions in mixture plasmas to higher energies can be applied to generate alpha particles in D^3He plasmas and to maximize DT fusion reactivity.

Finally, we conclude with a discussion of the application of these novel ICRF scenarios for future JET-DT and ITER operations [4].

References

- [1] O. Ye *et al.*, *Nature Physics*, **13**, 973–978 (2017).
- [2] J. M. Faustin *et al.*, *Plasma Phys. Contr. F.*, **59**, 084001 (2017).
- [3] J. Ongena, *et al.*, *EPJ Web Conf.*, **157**, 02006 (2017).
- [4] M. Schneider *et al.*, *EPJ Web Conf.*, **157**, 03046 (2017).

Experimental Evidence of Lower Hybrid Wave Scattering in Alcator C-Mod Due to Scrape Off Layer Density Fluctuations

E. H. Martin¹, C. Lau¹, G. M. Wallace², R. T. Mumgaard², S. Shiraiwa², D. L. Green¹, P. T. Bonoli², J. C. Wright², M. V. Umansky³, A. M. Dimits³, and I. Joseph³

The Alcator C-Mod Team

¹Oak Ridge National Laboratory (ORNL), Oak Ridge, TN 37831, USA

²Plasma Science & Fusion Center, MIT, Cambridge, MA 02139, USA

³Lawrence Livermore National Laboratory (LLNL), Livermore, CA 94550, USA

Corresponding Author: E. H. Martin, martineh@ornl.gov

We present new experimental measurements of the lower hybrid (LH) wave electric field vector, E_{LH} , obtained in Alcator C-Mod and provide a direct comparison with 3D full-wave COMSOL simulations using the cold plasma dielectric tensor and reflectometry measured density profiles. Two key results are reported: 1) The direction of E_{LH} was found to have a substantial poloidal component and is in strong disagreement with the nearly radial full-wave simulation result; 2) Adding scrape off layer (SOL) density fluctuations to the density profile implemented in the full-wave simulations can be used to explain the E_{LH} direction discrepancy.

Polarized passive optical emission spectroscopy was implemented to determine E_{LH} . This technique entails measuring two orthogonally polarized D_β spectral line profiles. The spectra are simultaneously fit to the Schrodinger equation containing both magnetic and time periodic electric field operators. The three components of E_{LH} are the only fit variables. The experimental E_{LH} results were compared to axisymmetry 3D full-wave COMSOL simulations via a synthetic diagnostic. Comparing the experimental and simulation results, good agreement was found with regard to the magnitude of E_{LH} both as a function of measurement location and LH power. However, it was found experimentally that E_{LH} contained a poloidal component having a magnitude on the order or greater than that of the radial component. The poloidal component was found to be a strong function of poloidal angle, increasing towards the midplane, and a weak function of toroidal angle, remaining nearly constant. This result strongly disagrees with the nearly radial E_{LH} predicted by the full-wave simulations. SOL density fluctuations based on an experimentally verified 3D BOUT turbulence simulation of a similar Alcator C-Mod discharge were added to the density profile. We found that diffraction and scattering from a realistic turbulence model generates a substantial poloidal component in E_{LH} , significantly closing the gap between the experimental and simulation results. This result indicates that SOL turbulence can have a detrimental effect on LHCD performance if the wavelength is on the order of the turbulence characteristic scale length.

EX

First Divertor Physics Studies in Wendelstein 7-X

T. Sunn Pedersen^{1,2}

The W7-X Team

¹Max-Planck-Institut für Plasmaphysik, Garching, Germany

²University of Greifswald, 17489 Greifswald, Germany

Corresponding Author: T. Sunn Pedersen, tspe@ipp.mpg.de

Wendelstein 7-X (W7-X) went successfully into operation in 2015 [1–4]. With a 30 m³ volume, a superconducting coil system operating at 2.5 T, and steady-state heating capability of up to 10 MW, it was built to demonstrate the benefits of optimized stellarators at parameters approaching those of a fusion power plant. Operation phase 1.2a (OP1.2a), which was performed in the second half of 2017, was the first operation phase with a full complement of plasma-facing components, including 10 passively cooled fine-grain graphite divertor units. These have the same geometry as the water-cooled steady-state carbon-fibre-composite divertor units that will be in operation in the early 2020's (Operation Phase 2, OP2). They allowed the start of a divertor research program, but at pulse lengths limited to about 80 MJ of pulse energy, e.g., 20 s at 4 MW.

The first divertor results in W7-X are very encouraging. For the foreseen magnetic configurations, the convective heat loads were deposited in the divertor, with strike line patterns closely resembling those predicted from edge modelling. Using trim and sweep coils, it was possible to eliminate the lowest order resonant field errors ($n/m = 1/1$), and thereby symmetrize the heat loads onto the divertor units.

High densities were achieved first in helium and then, using the pellet system, in hydrogen (n_{e0} up to $0.9 \times 10^{20}/\text{m}^3$). With the higher hydrogen densities came the most remarkable divertor result of the OP1.2a campaign: Stable and reproducible heat flux detachment. The infrared cameras show a divertor heat flux reduction of an order of magnitude in all 10 divertor modules. During detachment, no degradation of core confinement was seen.

In addition to these results, several other results related to edge- and divertor physics in W7-X will be presented, including enhanced edge radiation by injection of medium- Z impurities, and operation in magnetic configurations mimicking those of long-lived high-performance discharges foreseen for OP2.

References

- [1] T. Klinger *et al.*, Plasma Phys. Contr. F., **59**, 014018 (2017).
- [2] H.-S. Bosch *et al.*, Nucl. Fus., **57**, 116015 (2017).
- [3] R. C. Wolf *et al.*, Nucl. Fus., **57**, 102020 (2017).
- [4] T. Sunn Pedersen *et al.*, Phys. Plasmas, **24**, 055503 (2017).

Demonstration of Power Exhaust Control by Impurity Seeding in the Island Divertor at Wendelstein 7-X

F. Effenberg¹, S. Brezinsek², Y. Feng³, M. W. Jakubowski³, R. König³, M. Krychowiak³, O. Schmitz¹, Y. Suzuki⁴, D. Zhang³, A. Ali³, T. Barbui¹, C. Biedermann³, D. B. Blackwell⁵, R. Burhenn³, G. Cseh⁶, T. Dittmar², P. Drewelow³, M. Endler³, H. Frerichs¹, Y. Gao², J. Geiger³, K. Hammond³, C. Killer³, G. Kocsis⁶, J. D. Lore⁷, H. Niemann³, M. Otte³, A. Puig Sitjes³, L. Rudischhauser³, J. C. Schmitt⁸, T. Sunn Pedersen³, T. Szepesi⁶, U. Wenzel³, and V. Winters¹

The W7-X Team

¹University of Wisconsin-Madison, Madison, WI 53706, USA

²Institute of Energy and Climate Research, Forschungszentrum Jülich, Jülich, Germany

³Max-Planck-Institut für Plasmaphysik, Greifswald, Germany

⁴National Institute for Fusion Science (NIFS), Toki, Gifu, Japan

⁵Australian National University, Canberra, Australia

⁶Wigner Research Center, Association EURATOM, Budapest, Hungary

⁷Oak Ridge National Laboratory (ORNL), Oak Ridge, TN 37831, USA

⁸Auburn University, Auburn, AL 36849, USA

Corresponding Author: F. Effenberg, effenberg@wisc.edu

Effective power exhaust by impurity seeding and its dependence on the gas species used was demonstrated in island divertor configurations for the first time at Wendelstein 7-X (W7-X). A systematic set of experiments has been conducted during the first island divertor campaign which show that switching from Neon (Ne) to nitrogen (N₂) as seeding gases enables switching from global to more localized edge cooling. In case of Ne seeding significant enhancement of edge radiation with slow decay after end of the injection is observed due to the high recycling properties of this noble gas. The N₂ seeded discharges show immediate response of local plasma parameters at the divertor target correlated to the puff duration. Fast T_e recovery and drop of P_{rad} after end of the puff suggest a rather low recycling coefficient for this impurity species. These effects are analyzed by 3D modelling with EMC3-EIRENE for high and low recycling coefficients. The impact of the 3D edge magnetic structure on radiation is investigated experimentally by changing island size and connection lengths with the island control coils in the 5/5 configuration for scenarios with $n_e \sim 1.8 \times 10^{19}/\text{m}^3$ at $P_{\text{ECRH}} \sim 2.9$ MW. A 22 ms Ne puff causes enhancement of P_{rad} by ~ 1.6 MW. Application of full control coil currents, $I_{\text{cc}} = 2.5$ kA, yields a reduction of intrinsic P_{rad} level from ~ 0.7 MW to 0.3 MW and an reduced increase of P_{rad} by 1.1 MW in response to Ne seeding. The change of island geometry results in a faster decay of total impurity radiation measured by an effective time constant $\tau_{P_{\text{rad}}}$.

The presented findings on power exhaust control by impurity seeding in the W7-X island divertor are the basis for implementing radiative cooling as means to protect plasma facing components as performance levels at this new HELIAS stellarator are rising. With increasing performance, equilibrium effects will impact the 3D magnetic structure, which is addressed by equilibrium reconstruction with V3FIT and the 3D MHD code HINT. Investigating the link between the magnetic structure, the appropriate gas species, the injection location and the impurity transport is of critical importance for the goal of HELIAS divertor optimization. The experimental and numerical studies presented here represent a first-time consistent exploration of this field in the new island divertor configuration.

Progress in DIII-D Towards Validating Divertor Power Exhaust Predictions

A. E. Järvinen¹, S. L. Allen¹, J. M. Canik², M. E. Fenstermacher¹, M. Groth³, D. N. Hill⁴,
E. M. Hollmann⁵, C. J. Lasnier¹, A. W. Leonard⁴, J. D. Lore², M. A. Makowski¹,
A. G. McLean¹, G. D. Porter¹, T. D. Rognlien¹, C. M. Samuel¹, J. G. Watkins⁶, and
H. Q. Wang⁷

The DIII-D Team

¹Lawrence Livermore National Laboratory (LLNL), Livermore, CA 94550, USA

²Oak Ridge National Laboratory (ORNL), Oak Ridge, TN 37831, USA

³Aalto University, Espoo, Finland

⁴General Atomics, San Diego, CA 92186, USA

⁵University of California San Diego, CA 92093, USA

⁶Sandia National Laboratories (SNL), Albuquerque, NM 87185, USA

⁷Oak Ridge Associated Universities (ORAU), Oak Ridge, TN 37831, USA

Corresponding Author: A. E. Järvinen, jarvinena@fusion.gat.com

Understanding of divertor heat load and its control in fusion reactors has been critically advanced in DIII-D radiative power exhaust experiments corroborated with state-of-the-art 2D fluid simulations. UEDGE simulations indicate that the nonlinear interaction between the divertor electron temperatures and drifts can drive a bifurcation of the divertor solution between attached and detached branches. This mechanism provides an explanation for the experimentally observed step-like transition from strongly attached to well detached divertor conditions with increasing plasma density, as measured by Thomson scattering in plasmas with the ∇B -drift towards the X-point (forward B_t). Analysis of the new extreme ultraviolet (EUV) spectroscopy shows that in detachment with D_2 -injection in fwd. B_t , the resonant CIV (154.9 nm) line dominates the radiated power and peaks next to the X-point. In contrast, operating with the ∇B -drift away from the X-point (rev. B_t), the radiated power peaks in front of the outer target and is dominated by the deuterium L_α (121.5 nm). Fluid simulations with UEDGE qualitatively reproduce the relative intensity of the emitting lines and regions in both field configurations. However, the simulations predict the radiation to be about a factor of three more localized than measured, indicating an under prediction of the transport mechanisms expanding the radiating volume.

Work supported by the U.S. Department of Energy under DE-FC02-04ER54698 and DE-AC52-07NA27344, and LLNL LDRD project 17-ERD-020.

Erosion, Screening, and Migration of Tungsten in JET Equipped with Tungsten Divertor

S. Brezinsek¹, I. Borodkina¹, D. Borodin², I. Coffey³, C. Guillemaut⁴, K. Heinola⁵, A. Huber², A. Kirschner¹, S. Krat², S. Jachmich⁶, G. Sergienko¹, G. F. Matthews³, M. Mayer⁷, S. Wiesen¹, A. Widdowson⁸, A. Baron-Wiechec⁸, A. G. Meigs⁸, and M. Imrisek⁹

The JET Contributors

¹Forschungszentrum Jülich, Jülich, Germany

²Institute of Energy and Climate Research, Forschungszentrum Jülich, Jülich, Germany

³Culham Centre for Fusion Energy (CCFE), Culham Science Centre, Abingdon, UK

⁴Instituto Superior Técnico (IST), 1049-001 Lisbon, Portugal

⁵University of Helsinki, 00100 Helsinki, Finland

⁶Laboratory for Plasma Physics, ERM/KMS, Brussels, Belgium

⁷Max-Planck-Institut für Plasmaphysik, Garching, Germany

⁸United Kingdom Atomic Energy Authority, Culham Science Centre, Abingdon, UK

⁹Institute of Plasma Physics AS CR v.v.i., Prague, Czech Republic

Corresponding Author: S. Brezinsek, s.brezinsek@fz-juelich.de

Tungsten, W, is the plasma-facing material of the JET-ILW divertor. W erosion by plasma and impurity impact determines the components lifetime as well as can influence the plasma performance by the W influx into the confined region. Certainly, the W screening by the divertor and the W transport into the plasma determines the W core content, but the W source itself impacts the process. Its quantification is essential to understand the interplay between the W impurity and the plasma.

The JET-ILW provides access to a large set of W erosion-determining parameters permitting a detailed description of the source in the divertor closest to the ITER one. a) Effective sputtering yields and fluxes as function of impact energy of intrinsic (Be,C) and extrinsic (Ne,N) impurities as well as hydrogenic isotopes (H,D) are determined. This includes the interplay between intra- and inter-ELM W sources caused by the flux and energy distributions in these phases. The threshold behaviour and the spectroscopic composition analysis provide an insight in the dominating species and phases causing the erosion. b) The interplay between net and gross W erosion source will be elaborated considering prompt redeposition, thus, the return of W to the surface within one Larmor radius, and surface roughness, thus, the difference between smooth bulk-W and rough W-coating components. Both effects impact the balance equation of local W erosion and deposition. c) Postmortem analysis reveals the campaign-integrated net migration path identifying the W transport to remote areas. The transport is related to the plasma regime, e.g., H-mode with attached divertor and high impact energies of impinging species or detached operation, as well as to the magnetic configuration, e.g., corner with geometrical screening of W or ITER-like vertical target. d) The influence of parameters like surface temperature on the erosion, including the role of chemically assisted physical sputtering, is covered. JET-ILW permitted access to net W erosion in one magnetic configuration within a series of 151 subsequent discharges. Comparison of spectroscopy in the intra-ELM and inter-ELM phases with postmortem analysis of marker tiles provided a set of gross and net W erosion. ERO code simulations could reproduce the pattern as well as confirm high prompt W redeposition factors of more than 95% for the intra-ELM phase.

Isotope Effect on Impurity and Bulk Ion Particle Transport in the Large Helical Device

K. Ida^{1,2}, R. Sakamoto^{1,21}, M. Yoshinuma^{1,2}, K. Yamazaki³, and T. Kobayashi^{1,2}

The LHD Experiment Group

¹National Institute for Fusion Science (NIFS), Toki, Gifu, Japan

²Department of Fusion Science, Graduate University for Advanced Studies (SOKENDAI), Toki, Gifu, Japan

³Research Institute for Applied Mechanics (RIAM), Kyushu University, Kasuga, Japan

Corresponding Author: K. Ida, ida@nifs.ac.jp

Isotope effects of the ion particle transport both for carbon impurity and bulk ions are investigated in Large Helical Device (LHD) in a condition decoupled from electron particle transport. Better particle confinement for both impurity and bulk ions are observed in deuterium plasmas than in hydrogen plasmas. The following findings are presented in this paper: 1) Carbon impurity density gradient is negative (peaked profile with inward convection) inside the internal transport barrier (ITB) region in the deuterium (D) plasma, while it is positive (hollow profile with outward convection) in the hydrogen (H) plasma; 2) The decay time of D ion density measured with bulk charge exchange spectroscopy inside the plasma after the D pellet injections is longer than that of H ion density after H pellet injections by a factor of 1.4. The difference in the decay time of H and D in the H-D mixture plasma strongly suggests that there should be a difference in deuterium and tritium (T) particle transport in the D-T mixture plasma in ITER.

EX

3D Structure of Density Fluctuations in T-10 Tokamak and New Approach for Current Profile Estimation

V. A. Vershkov¹, M. A. Buldakov¹, G. F. Subbotin¹, D. A. Shelukhin¹, A. V. Melnikov¹,
L. G. Eliseev¹, F. O. Khabanov¹, M. A. Drabinsky¹, D. S. Sergeev¹, T. B. Myalton¹,
V. M. Trukhin¹, A. V. Gorshkov¹, I. S. Belbas¹, and G. M. Asadulin¹

¹National Research Centre "Kurchatov Institute", Moscow, Russian Federation

Corresponding Author: V. A. Vershkov, v.vershkov@fc.iterru.ru

Previous correlation reflectometry investigations in T-10 tokamak revealed the existence of several density fluctuation types and strong radial and poloidal variation of their amplitudes and correlation properties. This paper presents the new measurements of the 3D spatial distributions of the amplitudes, radial correlation lengths and long range correlations along the field lines of the different turbulence types. Experiments were carried out in OH and ECRH heated discharges. The density fluctuations were measured by correlation reflectometry using ordinary mode probing and new T-10 antenna set with four horn arrays distributed toroidally and poloidally over the tokamak torus. Experiments confirmed previously found strong poloidal amplitude asymmetry of broad band (BB) and quasi-coherent (QC, typically 110–170 kHz) and uniform poloidal distribution of stochastic low frequency (SLF, 0–50 kHz) density fluctuations. Presence of those turbulence types was also proved by measurements with heavy ion beam probe. Radial correlation measurements were made at four poloidal angles to understand the poloidal dependence of the radial correlation length for different fluctuation types. The significant decrease of the radial correlation lengths with towards high magnetic field side was observed for all turbulence types. The long range correlations along the field lines were measured by reflectometers in two cross-section separated by 1/4 of torus. Reflectometers have the same frequency thus provide reflection from the same magnetic surface. Reflection radii are chosen by frequency variation of the launched wave from shot to shot in a series of reproducible discharges. Measurements were carried out at low and high magnetic field side with two currents and simultaneous reverse of toroidal magnetic field and plasma current. Resonance radii were also calculating using 3D tracing of the magnetic field line and demonstrate good agreement with experiments. These results allow to propose the new approach for the current profile estimation in tokamaks.

EX

Explaining Cold-Pulse Dynamics in Tokamak Plasmas Using Local Turbulent Transport Models

P. Rodriguez-Fernandez¹, A. E. White¹, N. T. Howard¹, B. A. Grierson², G. M. Staebler³, J. E. Rice², X. Yuan², N. M. Cao¹, A. J. Creely¹, M. J. Greenwald¹, A. E. Hubbard¹, J. W. Hughes¹, J. H. Irby¹, and F. Sciortino¹

¹Plasma Science & Fusion Center, MIT, Cambridge, MA 02139, USA

²Princeton Plasma Physics Laboratory (PPPL), Princeton, NJ 08540, USA

³General Atomics, San Diego, CA 92186, USA

Corresponding Author: P. Rodriguez-Fernandez, pablorf@mit.edu

This work demonstrates that cold-pulse phenomena in tokamak plasmas can be fully explained by local transport models [1], including the existence of core temperature inversions at low density and disappearance at high density, thus resolving an enigmatic but universal transient transport phenomenon that has challenged the standard local model of transport for more than twenty years [2]. The TRANSP power balance code coupled with the quasi-linear transport model TGLF-SAT1 [3], with a new saturation rule that came about as a consequence of cross-scale coupling physics and that captures the nonlinear upshift of the critical gradient, are shown to fully describe the cold-pulse phenomenology after laser blow-off injections in the Alcator C-Mod tokamak. By means of experimentally-constrained self-consistent modelling of cold-pulse experiments, this work provides the strongest evidence to date that the existence of nonlocal transport phenomena may not be necessary for explaining the behaviour and timescales of cold-pulse experiments in tokamak plasmas.

Work supported by the U.S. Department of Energy Award No. DE-FC02-99ER5451, using Alcator C-Mod, a DOE Office of Science User Facility. P.R.-F. was also supported by U.S. Department of Energy Award No. DE-SC0014264 and a La Caixa Fellowship.

References

- [1] P. Rodriguez-Fernandez *et al.*, accepted Phys. Rev. Lett., (2018).
- [2] K. Ida *et al.*, Nucl. Fus., **55**, 013022 (2015).
- [3] G. M. Staebler *et al.*, Nucl. Fus., **57**, 066046 (2017).

Origin of Harmonics of Drift Tearing Mode in ADITYA Tokamak

H. Raj^{1,2}, J. Ghosh^{1,2}, A. Sen^{1,2}, R. L. Tanna¹, K. A. Jadeja¹, D. Raju¹,
P. K. Chattopadhyay^{1,2}, and R. Pal³

The ADITYA Team

¹*Institute for Plasma Research (IPR), Bhat, Gandhinagar, India*

²*Homi Bhabha National Institute (HBNI), Anushakti Nagar, Mumbai 400094, India*

³*Saha Institute of Nuclear Physics, Kolkata, India*

Corresponding Author: H. Raj, harshita.raj@ipr.res.in

Tearing modes play a pivotal role in determining two of the most critical parameters for tokamak operation, namely plasma confinement and disruption. They have been extensively studied both theoretically and experimentally, as controlling them is foremost priority for every tokamak, including ITER and future large size tokamaks. Coupling of tearing modes with drift wave is a common phenomenon observed in all tokamaks, resulting in drift tearing modes. Multiple drift tearing modes have also been observed in a bunch of experiments. However, these modes have been identified as different modes with different poloidal (m) and toroidal (n) mode numbers. In ADITYA as well as ADITYA Upgrade tokamak, the frequency spectra of the Mirnov signal show multiple frequency bands corresponding to drift tearing modes. Interestingly, the higher frequencies have been precisely found to be integral multiples of the fundamental frequency. Further analysis reveals that these frequencies do not belong to different modes but to harmonics of a single mode. These harmonic frequencies also reflect significantly in the density as well as impurity radiation. We have also found that the occurrence of these harmonics is strongly correlated with the presence of runaways in the plasma. The origin of these harmonics and their operational regime will be explained in this paper. The role of runaway electrons in manifestation of these harmonics is also proposed.

EX

Effect of Multiscale Interaction between an $m/n = 2/1$ Mode and Microinstabilities on Transport of KSTAR Plasmas

M. J. Choi¹, J.-M. Kwon¹, S. H. Ko¹, J. Kim¹, H. K. Park², T. S. Hahm³, M. H. Woo¹, Y. In², G. S. Yun⁴, and K. D. Lee¹

The KSTAR Team

¹National Fusion Research Institute (NFRI), Daejeon, Republic of Korea

²Ulsan National Institute of Science and Technology (UNIST), Ulsan, Republic of Korea

³Seoul National University, Seoul, Republic of Korea

⁴Pohang University of Science and Technology (POSTECH), Pohang, Gyeongbuk 790-784, Republic of Korea

Corresponding Author: M. J. Choi, mjchoi@nfri.re.kr

Tokamak plasmas often encounter nonaxisymmetric magnetic topology due to unavoidable magnetohydrodynamic (MHD) instabilities and/or external magnetic perturbation. Transport with nonaxisymmetric perturbed equilibrium can be very complicated due to various multiscale interactions between a large scale MHD instability and small scale microinstabilities. This paper reports experimental observations and analyses of two distinguishing multiscale interactions. First, a multiscale interaction between the stationary large $m/n = 2/1$ magnetic island and turbulence through profile modification has been identified using simultaneous 2D measurements of electron temperature (T_e) as well as turbulence and their flow profiles. A significant increase of T_e turbulence is only observed near the X-point, while it is not observed both in inside and outside of the magnetic island near the O-point possibly due to the strong flow shear. The increased turbulence and T_e gradient lead to the violent minor disruption of the plasma. In addition, a small amplitude $m/n = 2/1$ mode can generate a modified spectrum of microinstabilities. The Doppler shift analysis of the measured frequencies of the modes revealed the nonlinear mode coupling among the $m/n = 12/6$ main mode, the $m/n = 10/5$ and $m/n = 14/7$ side lobes, and the $m/n = 2/1$ mode. These coupled modes appear to degrade the tokamak plasma confinement significantly without the violent disruption event.

Work supported by the KSTAR research project funded by Korea Ministry of Science and ICT.

Divertor Impurity Seeding Experiments at the COMPASS Tokamak

M. Komm¹, J. Cavalier¹, J. Seidl¹, J. Adamek¹, P. Bilkova¹, P. Bohm¹, A. Devitre²,
M. Dimitrova¹, S. Elmore³, M. Faitsch⁴, P. Hacek^{1,5}, J. Havlicek¹, M. Imrisek^{1,5},
I. Khodunov^{1,6}, J. Krbec^{1,7}, M. Peterka^{1,5}, R. Panek¹, T. Popov⁸, O. Samoylov⁶, M. Tomes^{1,5},
K. Tomova⁶, P. Vondracek^{1,5}, and V. Weinzettl¹

The EUROfusion MST1 Team

¹*Institute of Plasma Physics AS CR v.v.i., Prague, Czech Republic*

²*Universidad de Costa Rica, San Jose, Costa Rica*

³*Culham Centre for Fusion Energy (CCFE), Culham Science Centre, Abingdon, UK*

⁴*Max-Planck-Institut für Plasmaphysik, Garching, Germany*

⁵*Faculty of Mathematics and Physics, Charles University, V Holešovičkách 2, Prague, Czech Republic*

⁶*Ghent University, 9000 Ghent, Belgium*

⁷*FNSPE, Czech Technical University in Prague, Břehová 7, Czech Republic*

⁸*University of Sofia "St. Kliment Ohridski", Sofia 1164, Bulgaria*

Corresponding Author: M. Komm, komm@ipp.cas.cz

Partial detachment is the desired regime for the baseline burning plasma scenario in ITER and next-step devices, as it allows converting the majority of the energy carried by charged particles through the scrape-off-layer (SOL) into isotropic radiation and thus avoids localized heat flux deposition in the divertor region. In order to maintain relevance to ITER and DEMO, a concentrated effort has been initiated at the COMPASS tokamak to achieve detached operation by means of impurity seeding.

Series of experiments with impurity injection in the range of $2\text{--}9 \times 10^{20}$ molecules per second at different locations in the divertor were performed with the aim to cool the plasma and influence the particle and heat transport in the divertor region and provoke partial detachment. Previously reported results [1] were largely extended by injection of nitrogen at the outer divertor target and also by attempts to seed the plasma with neon. The effects on SOL and divertor plasma conditions were monitored by means of horizontal reciprocating probe manipulator located at the outer midplane and by arrays of divertor Langmuir and Ball-pen probes. The radiation in the edge plasma was observed by AXUV bolometers and fast visible cameras.

Experiments in L-mode discharges with nitrogen injected at the outer divertor target have shown that the presence of radiating impurity leads to drop of pressure in the divertor. Depending on the magnitude of the seeding, the upstream pressure can be also affected, suggesting possible penetration of nitrogen into the confined plasma region. The target pressure, however, drops at faster rate than upstream, which allows reaching the regime of partial detachment. Similar results were obtained by the HFS nitrogen injection, however, the change in divertor pressure was more generally more abrupt and was less sensitive to the amount of injected nitrogen.

References

[1] M. Komm *et al.*, Proceedings of the 44th EPS conference, Belfast P1.118, (2017).

Experimental Studies of Pressure and Plasma Current Profiles for Equilibria Calculations During AC Transition in the ISTTOK Tokamak

A. Malaquias¹, M. J. Hole², R. L. Dewar², C. A. Michael², and R. B. Henriques¹

¹*Institute of Plasmas and Nuclear Fusion (IPNF), Instituto Superior Técnico (IST), 1049-001 Lisbon, Portugal*

²*Australian National University, Canberra, Australia*

Corresponding Author: A. Malaquias, artur.malaquias@ipfn.ist.utl.pt

EX In general, the operation of AC discharges in small tokamaks requires the control of a few external parameters such as vertical and horizontal fields, external heating (where available), chamber conditioning and gas puff. The dynamics and type of control used are mostly based on experimental empirical learning, with different combinations of actuators depending on the tokamak device. Experimental studies performed during the AC operation in the ISTTOK tokamak have addressed the influence of several control parameters in the success of the AC transition. Although the link between the different external actuators and plasma discharge evolution could be verified, successful AC transitions above 4 kA plasma current could not be achieved. In order to build a more predictive control of the AC transition it would be useful to develop a first-principle model which interprets the experimental observations. Such a model would need to combine experimental data and calculations on the equilibria and stability in several time stamps of the transition, current profile evolution, ramp-up and runaway generation, drift electrons, and the electro-technical properties of the tokamak during AC operation. The output of such a model would inform the discharge controller how to balance evolution of the external actuators during the AC transition. The present paper presents an initial step towards the development of a deeper understanding of the equilibria and current profile during the AC transition in ISTTOK. The goal of the present study is to identify the topology of flux surfaces based on experimental pressure-like measurements and matched current profiles, the existence (or not) of antiparallel plasma currents during transition and the existence of drifting electrons and their role during current ramp-up. There is also experimental evidence on the presence of fast electrons (possibly a significant run-away fraction) playing an important role during the initial stages of the discharge immediately after the transition. This will be further investigated using collisionless numerical simulations to determine the maximum lifetime of the drift electrons and their response to H-V fields. It is important to use this electron population in combination with gas puff to produce a more efficient Townsend avalanche during the current ramp-up.

Impact of Neon Injection on Electron Density Peaking in JET Hybrid Plasmas

D. Frigione¹, M. Romanelli², C. D. Challis², L. Frassinetti³, J. P. Graves⁴, J. Hobirk⁵,
F. Köchi², M. J. Mantsinen^{6,7}, C. Mazzotta¹, and G. Pucella¹

The JET Contributors

¹Agenzia nazionale per le nuove tecnologie, l'energia e lo sviluppo economico sostenibile (ENEA), Rome, Italy

²Culham Centre for Fusion Energy (CCFE), Culham Science Centre, Abingdon, UK

³KTH Royal Institute of Technology, Stockholm, Sweden

⁴Swiss Plasma Center (SPC), École polytechnique fédérale de Lausanne (EPFL), 1015 Lausanne, Switzerland

⁵Max-Planck-Institut für Plasmaphysik, Garching, Germany

⁶Catalan Institution for Research and Advanced Studies (ICREA), Barcelona, Spain

⁷Centro Nacional de Supercomputación (BSC), Barcelona, Spain

Corresponding Author: D. Frigione, domenico.frigione@enea.it

Impact of low-mid Z impurity injection on plasma transport and confinement has been observed and reported in several tokamak experiments. Understanding particle transport in mixed species plasmas is crucial for reactor relevant conditions where control of DT mixture along with control of He concentration will be necessary. In this paper we present the analysis of experimental electron density profile evolution in JET hybrid scenario discharges with increasing level of Ne seeding. The measured electron flux is compared with fully predictive transport simulations in search for the possible existence of a particle inward pinch proportional to the light impurity concentration as predicted by first principle gyrokinetic simulations.

These seeding experiments, performed for power exhaust mitigation studies, offered the opportunity to study systematically the effect of Ne on density peaking and to compare it with theory predictions. The database includes hybrid discharges at $I_p = 1.4$ MA, $B_t = 1.9$ T, $\beta_N = 2.2$, additionally heated by 16.5 MW of neutral beam injection power (NBI). A few of the above discharges had a small amount (< 1 MW) of ion cyclotron resonance heating (ICRH). The current ramp-up, overshooting the plateau value was used to produce a central $q_0 \approx 1$ broad low-shear region for better confinement and NTM avoidance. Neon was injected at the start of the NBI heating phase and it was already present during the transition to H-mode: when the central density reached its top value (≈ 4 s later) the Ne contribution to the total number of injected electrons ranged from 5% to 40%. Unseeded reference discharges were also performed with the same engineering parameters. In the seeded discharges, the core density profile peaking, defined as the ratio between the central ($\rho = 0.25$) and the pedestal density, increases up to $n_{\text{peak/ped}} \approx 2$ depending on the amount of injected Ne.

Interestingly, in this database, the density peaking did not increased with the average as previously described for unseeded discharges. Fully predictive transport simulations, carried out with JETTO code proved that the introduction of an inward particle pinch proportional to the effective charge and the ion temperature gradient, as predicted by microturbulence theory, was needed to match the data.

Isotope Dependence of Confinement in JET Deuterium and Hydrogen Plasmas

H. Weisen¹, C. F. Maggi², L. Horvath³, F. Auriemma⁴, T. W. Bache², F. J. Casson², A. Chankin⁵, E. Delabie⁶, C. Giroud², D. King², R. Lorenzini⁴, S. Menmuir², and E. Viezzer⁷

The JET Contributors

¹Swiss Plasma Center (SPC), École polytechnique fédérale de Lausanne (EPFL), 1015 Lausanne, Switzerland

²Culham Centre for Fusion Energy (CCFE), Culham Science Centre, Abingdon, UK

³York Plasma Institute, University of York, Heslington, UK

⁴Consorzio RFX, Associazione EURATOM-ENEA sulla Fusione, Padova, Italy

⁵Max-Planck-Institut für Plasmaphysik, Garching, Germany

⁶Oak Ridge National Laboratory (ORNL), Oak Ridge, TN 37831, USA

⁷Universidad de Sevilla, Seville, Spain

Corresponding Author: H. Weisen, henri.weisen@epfl.ch

Heat, particle and momentum confinement in L- and H-mode in deuterium (D), hydrogen (H) and in D-H mixtures have been investigated in JET. In L-mode (3 T/2.5 MA) at fixed density ($2.5 \times 10^{19}/\text{m}^3$) a weak positive scaling of stored energy with ion mass, $\tau_{Eth} \sim A^{0.15}$, is found [1], consistently with multimachine scaling $\tau_{Eth} \sim A^{0.2}$ [2]. Core temperature profiles are stiff with $T_i \sim T_e$, and $R/L_{Te} \sim 8$ at midradius [1].

Flux-driven core transport modelling with TGLF show ITG's to be dominant and predict no isotope scaling as a result of the T_i profile stiffness. A fuelling rate $\sim 30\%$, higher in H than in D, was necessary to achieve the same density as in D, indicating a difference in particle confinement which was confirmed by EDGE2D/EIRENE simulations near the LCFS [1]. In type-I ELMy H-mode (1 T/1 MA, 1.7 T/1.4 MA and 1.7 T/1.7 MA, P_{aux} in the range 3 to 17 MW) it was not possible, except in a couple of cases, to establish the same densities in H as in D, despite gas fuelling rates several times higher in H, showing a strong reduction of particle confinement. The best regression for the thermal stored energy for ELMy H-mode is obtained as $W_{Eth} \propto A^{0.38} P^{0.64} I_p^{0.89} n^{0.5} \Gamma^{0.21}$ where A is the ion mass and Γ the fuelling rate. The mass scaling is twice that of IPB₉₈(y, 2). GENE gyrokinetic calculations in H-modes show ITG's to be dominant in both species. The observed negative dependence of momentum confinement on the gas fuelling rate suggests that edge fuelling leads to a direct deterioration of ion heat transport. Dimensionless identity experiments for H and D pairs provided good matches for the kinetic profiles in L-mode, but not in H-mode. In H-mode the scaled confinement time in D was 30% higher than in hydrogen for the best approximate match. The evidence from these experiments suggests that the isotope scaling in these experiments, as well as the absence of good dimensionless matches in H-mode, have their origin in the pedestal and boundary region, which are sensitive to atomic physics, fuelling and recycling.

References

- [1] C. F. Maggi *et al.*, Plasma Phys. Contr. F., **60**, 014045 (2018).
- [2] ITER Physics Basis, Nucl. Fus., **39**, 2175 (1999).

High Fusion Performance at High T_i/T_e in JET-ILW Baseline Plasmas with High NBI Heating Power and Low Gas Puffing

H.-T. Kim¹, A. C. C. Sips², M. Romanelli³, C. D. Challis³, L. Garzotti³, F. G. Rimini³,
E. A. Lerche^{3,5}, J. Buchanan³, X. Yuan⁴, and S. M. Kaye⁴

EUROfusion/JET, Culham Science Centre, Abingdon, Oxfordshire, OX14 3DB, UK

¹EUROfusion/JET, Culham Science Centre, Abingdon, Oxfordshire, OX14 3DB, UK

²JET Exploitation Unit, Culham Science Centre, Abingdon, UK

³Culham Centre for Fusion Energy (CCFE), Culham Science Centre, Abingdon, UK

⁴Princeton Plasma Physics Laboratory (PPPL), Princeton, NJ 08540, USA

⁵Laboratory for Plasma Physics, ERM/KMS, Brussels, Belgium

Corresponding Author: H.-T. Kim, hyun-tae.kim@euro-fusion.org

This paper presents the transport analysis of high density baseline discharges in the 2016 experimental campaign of the Joint European Torus with the ITER-Like wall (JET-ILW), where a significant increase in the deuterium-deuterium (DD) fusion neutron rate ($\sim 2.8 \times 10^{16}/s$) was achieved with stable high neutral beam injection (NBI) powers of up to 28 MW and low gas puffing.

Increase in T_i exceeding T_e were produced for the first time in baseline discharges despite the high electron density, and this enabled a significant increase in the thermal fusion reaction rate. As a result, the new achieved record in fusion performance was much higher than the previous record in the same heating power baseline discharges where $T_i = T_e$.

In addition to the decreases in collisionality and the increases in ion heating fraction in the discharges with high NBI power, $T_i > T_e$ can also be attributed to positive feedback between the high T_i/T_e ratio and stabilization of the turbulent heat flux resulting from the ion temperature gradient (ITG) driven mode. The high T_i/T_e ratio was correlated with high rotation frequency. Among the discharges with identical beam heating power, higher rotation frequencies were observed when particle fuelling was provided by low gas puffing and pellet injection. This reveals that particle fuelling played a key role for achieving high T_i/T_e , and the improved fusion performance. The impact of particle fuelling on high T_i/T_e has an important implication for the 2019 DT experimental campaign, as it can provide a further increase in the fusion performance with the present heating power capability.

EX

Singlet Breakdown Optimization to a Doublet Plasma Configuration on the TCV Tokamak

B. P. Duval¹, H. Reimerdes¹, J. Sinha¹, S. Coda¹, and J.-M. Moret¹

The TCV Team

¹*Swiss Plasma Center (SPC), École polytechnique fédérale de Lausanne (EPFL), 1015 Lausanne, Switzerland*

Corresponding Author: B. P. Duval, basil.duval@epfl.ch

EX This paper presents a fresh attempt on TCV to optimize plasma breakdown in the break-less ($45\ \mu\Omega$ impedance) vacuum vessel culminating in a double breakdown and the formation of a doublet configuration. A statistical analysis of legacy single pole breakdown and early plasma current ramp failures helped modify vessel current estimators together with PSU command and control issues to obtain reliable plasma initiation ± 30 cm in TCV's 3:1 elongated vacuum vessel. Although precise control of the vacuum null was achieved, control of the high plasma ramp rate proved complex since the highest (~ 10 V) loop voltage was necessary for reliable breakdown and, through trial, the acceptable range of prefill pressures was limited. A double breakdown with simultaneous, separated, magnetic nulls was then achieved. Initial ohmic heating alone was limited by lobe separation instabilities with the upper lobe merging into the lower lobe after ~ 15 ms. Plasma multipole control was attempted using two X2 gyrotrons, aimed at each lobe's core to modify each lobe's resistivity and thus current. A transport barrier in the mantle surrounding the doublet configuration was observed with both lobes seemingly heating independently of the ECH heating location. To date a combined plasma current of 260 kA after 20 ms was obtained for which Thomson density and temperature profiles indicate two clear plasma lobes. Doublets are predicted to offer increased β limits, vertical stability and the potential of a novel solution to divertor exhaust where the entire mantle, surrounding the plasma, may be available for exhaust dissipation.

Turbulence and Radial Electric Field Asymmetries Measured at TJ-II Plasmas

T. Estrada¹, E. Sánchez¹, J. M. García-Regaña¹, E. Ascasíbar¹, Á. Cappa², D. Carralero³, M. Liniers¹, and I. Pastor¹

The TJ-II Team

¹*Centro de Investigaciones Energéticas, Medioambientales y Tecnológicas (CIEMAT), Madrid, Spain*

²*Laboratorio Nacional de Fusión (LNF),*

Centro de Investigaciones Energéticas, Medioambientales y Tecnológicas (CIEMAT), Madrid, Spain

³*Max-Planck-Institut für Plasmaphysik, Garching, Germany*

Corresponding Author: T. Estrada, teresa.estrada@ciemat.es

Dedicated experiments have been carried out for a systematic comparison of turbulence and radial electric field measured at poloidally separated positions in the same flux-surface in the stellarator TJ-II. The rationale behind this study is twofold, verification of the spatial localization of instabilities predicted by the gyrokinetic simulations in stellarators and verification of the electrostatic potential variation on the flux surface as calculated by neo-classical codes and its possible impact on the radial electric field. Poloidal asymmetries in the turbulence wavenumber spectrum and in the E_r profile have been found that depend on density, heating conditions and magnetic configuration. These quantities have been measured using a Doppler reflectometer that covers the radial region from $\rho = 0.6$ to 0.9 , at different perpendicular wave-numbers of the turbulence: $1\text{--}14\text{ cm}^{-1}$, and at two plasma regions poloidally separated.

Different plasma scenarios have been studied with different profile shapes. These include: high power on-axis ECH heated plasmas vs. low power off-axis ECH heated plasmas; ECH vs. NBI heated plasmas; standard vs. high- ι magnetic configurations, and hydrogen vs. deuterium dominated plasmas.

Differences in the turbulence intensity are found when comparing the k -spectra measured at poloidally separated positions in the same flux-surface in ECH heated plasmas in the standard magnetic configuration. However, almost no asymmetries are found in NBI heated plasmas, i.e., higher density, lower electron temperature, where very similar turbulence intensity and spectral shape are measured at both plasma regions. Besides, no significant differences have been found when comparing hydrogen and deuterium dominated plasmas. The asymmetry in the turbulence intensity found in the standard magnetic configuration reverses in the magnetic configuration with high rotation transform. Radial electric field profiles measured at the two plasma regions show pronounced differences in low density plasmas, i.e., plasmas in neoclassical electron root confinement. At higher densities the E_r asymmetry gradually decreases and almost disappears in ion root plasmas.

The detailed comparison of the k -spectra and E_r profiles under different plasma scenarios are presented, providing valuable information for comparison with gyrokinetic and neoclassical simulations.

Validation of Global Gyrokinetic Simulations in Stellarator Configurations

E. Sánchez¹, T. Estrada¹, J. L. Velasco¹, I. Calvo¹, A. Alonso¹, J. M. García-Regaña¹,
R. Kleiber², and J. Riemann²

The TJ-II and W7-X Teams

¹Laboratorio Nacional de Fusión (LNF),

Centro de Investigaciones Energéticas, Medioambientales y Tecnológicas (CIEMAT), Madrid, Spain

²Max-Planck-Institut für Plasmaphysik, Greifswald, Germany

Corresponding Author: E. Sánchez, edi.sanchez@ciemat.es

In this contribution, recent simulations carried out in stellarator configurations with the global gyrokinetic code EUTERPE and the ongoing validation effort are presented.

The linear relaxation of zonal flows (ZFs) has been studied in global simulations in many stellarator configurations. The code has been verified by comparing results with both other gyrokinetic codes and analytical estimations. Furthermore, these calculations were validated against experimental measurements obtained during pellet injection experiments in TJ-II. The oscillatory relaxation of potential measured by the HIBP was compared to simulations including impurity ions, with a good quantitative agreement in the frequency and damping rates. This is the first experimental confirmation of the ZF oscillation in stellarators, accurately described by the linearized gyrokinetic equation.

The electrostatic microinstabilities have been studied numerically in the stellarators TJ-II and W7-X and an effort to validate simulations against experimental turbulence measurements from Doppler reflectometry (DR) has been done. The model validation has been pursued at different levels of detail, including the density fluctuation level, frequency spectra, and the localization of instabilities along the flux surface.

In dedicated experiments in TJ-II, the power and deposition location of the ECRH heating were changed, thus modifying significantly the density and temperature radial profiles. The experimental measurements from the DR system in TJ-II have been compared to simulations. The relevant wave-numbers and the radial variation of experimental density fluctuations spectra are consistent with the range of unstable wave-numbers and the location of maximum instability found in simulations. No dependency of the power spectra with the bulk ion mass is observed experimentally, which is consistent with the kind of unstable modes (electron-driven) found in simulations. A systematic difference is found between the density fluctuation spectra measured by the DR system at poloidally separated positions on the same flux-surface, which is largely affected by the rotational transform. The localization of instabilities in simulations is also influenced by the rotational transform, however, a discrepancy between the location of maximum fluctuation level in simulations and experiments is found so far.

The Concept of Lithium Based Plasma Facing Elements for Steady State Fusion Tokamak-Reactor and its Experimental Validation

A. Vertkov¹, I. Lyublinski^{1,2}, M. Zharkov¹, A. Berlov¹, S. Mirnov^{3,4}, A. Komov³, A. Varava³, A. Zaharenkov³, G. Mazzitelli⁵, and M. Iafrati⁵

¹JSC "Red Star", Moscow, Russian Federation

²National Research Nuclear University "MEPhI", Moscow, Russian Federation

³National Research University "Moscow Power Engineering Institute", Moscow, Russian Federation

⁴SC "SRC RF TRINITY", Moscow, Russian Federation

⁵ENEA C. R. Frascati, Dipartimento FSN, Frascati, Italy

Corresponding Author: A. Vertkov, avvertkov@redstaratom.ru

The modern results on the implementation of the Russian strategy in the development of designs of long-operating plasma facing element for steady state fusion reactors are considered and analyzed on an example of liquid metal limiters of tokamaks T-15 and FTU. The experimental validation of this strategy is presented and results on liquid metal CPS behaviour in tokamak conditions, effective heat removal up to 12 MW/m² with low pressure heat transferring medium (0.2 MPa) on the basis of a gas-water spray are considered. The promising scheme of liquid metal divertor target plate for DEMO reactor is presented and discussed.

EX

Extrapolation of Be Erosion Modelling from JET and PISCES-B to ITER

D. Borodin^{1,2}, J. Romazanov², S. Brezinsek², S. W. Lisgo³, R. A. Pitts³, R. P. Doerner⁴,
D. Nishijima⁴, I. Borodkina^{2,5}, A. Eksaeva², A. Kirschner², and C. Linsmeier²

The JET Contributors

¹EUROfusion/JET, Culham Science Centre, Abingdon, Oxfordshire, OX14 3DB, UK

²Institute of Energy and Climate Research, Forschungszentrum Jülich, Jülich, Germany

³International Thermonuclear Experimental Reactor (ITER),

Cadarache Centre, 13108 St. Paul lez Durance, France

⁴University of California San Diego, CA 92093, USA

⁵National Research Nuclear University "MEPhI", Moscow, Russian Federation

Corresponding Author: D. Borodin, d.borodin@fz-juelich.de

EX Beryllium (Be) erosion data is one of the key issues for ITER including the first wall (FW) life time predictions [1], which undergo a revisit based on the recent studies at the existing devices: tokamak JET equipped with the ITER-like wall (ILW) and linear plasma device PISCES-B. The extrapolation of physical and chemically assisted sputtering data is based on interpretive and predictive numerical modelling by the 3D plasma-surface interaction and impurity transport ERO code. One of the key elements is the proper treatment of the sputtering ion trajectories in the magnetic sheath, determining the angle and energy distributions by impact with the surface, and, thus the effective local sputtering yield. This recent improvement has helped to resolve the discrepancy in the normal incidence part of the factorized physical sputtering yields, which were interpreted using ERO from the JET-ILW and PISCES-B measurements. The uncertainties due to plasma-facing surface temperature and fuel, e.g., deuterium (D) content in the wall are considered. The D content in plasma-wetted areas was shown to be large (the yields based on the assumed 50% D surface content, which are smaller by about a factor 3–4 than for the pure Be, lead to the best agreement with experiments). This means that the most optimistic of ITER life time predictions [1] of 4200 baseline $Q = 10$ yields discharges based on the lowest yields (50% D) is confirmed, though somewhat corrected down due to the improved sheath model. It is important, however, to emphasize that the zero order uncertainty in these FW net erosion predictions originates in the background plasma specification which remains significant for the ITER far-SOL plasma.

The advantages of the new massive-parallel ERO2.0 which allows treating the whole of JET-ILW or ITER volume, and thus providing self-consistent treatment of self-sputtering and magnetic shadowing are an additional motivation for the revisit of [1]. Furthermore, ERO2.0 enables cross-check between diagnostics, e.g., spectroscopic sightlines and filtered images from 2D cameras characterizing Be influx and plasma content, or IR images mimicking heat load distributions. Related predictive simulations of Be impurity light emission can assist in designing (sensitivity and stray light issues) the ITER visual range spectroscopy systems.

References

[1] D. Borodin *et al.*, Phys. Scr., **T145**, 14008 (2011)

Erosion and Deposition in the JET Divertor During the ITER-Like Wall Campaigns

M. Mayer¹, S. Krat^{1,2}, A. Baron-Wiechec³, S. Brezinsek⁴, P. Coad³, Y. Gasparyan², K. Heinola⁵, I. Jepu⁶, J. Likonen⁷, P. Petersson⁸, C. Ruset⁶, G. de Saint-Aubin¹, and A. Widdowson³

The JET Contributors

¹Max-Planck-Institut für Plasmaphysik, Garching, Germany

²National Research Nuclear University "MEPhI", Moscow, Russian Federation

³Culham Centre for Fusion Energy (CCFE), Culham Science Centre, Abingdon, UK

⁴Forschungszentrum Jülich, Jülich, Germany

⁵University of Helsinki, 00100 Helsinki, Finland

⁶National Institute of Laser, Plasma and Radiation Physics (INFLPR), Bucharest, Romania

⁷VTT Technical Research Centre of Finland Ltd., Espoo, Finland

⁸VR, Fusion Plasma Physics, KTH Royal Institute of Technology, Stockholm, Sweden

Corresponding Author: M. Mayer, matej.mayer@ipp.mpg.de

During JET operation with all carbon walls prior to 2010 (JET-C) massive redeposition of previously eroded carbon was observed in the divertor and in remote divertor areas. This massive carbon redeposition was accompanied by a high retention of hydrogen isotopes trapped by codeposition. Extrapolations of these results to ITER predicted very high potential tritium retention, resulting in the decision to remove carbon from the ITER divertor

One aim of the JET ITER-like wall (JET-ILW) project was to study plasma-surface interactions in a carbon-free beryllium/tungsten environment comparable to the ITER material configuration. All divertor tiles were manufactured either from tungsten coated carbon-fibre composite (CFC) material or from bulk tungsten. Erosion and deposition in the JET divertor were studied during the campaigns JET-ILW1 (2011–2012), ILW-2 (2013–2014) and ILW-3 (2015–2016) by using specially prepared divertor marker tiles using W/Mo marker layers, which were analyzed before and after the campaign using elastic backscattering of 3 and 4.5 MeV incident protons and nuclear reaction analysis using 0.8 to 4.5 MeV ³He ions.

The erosion/deposition pattern observed with the JET-ILW configuration shows partly drastic changes compared to the pattern observed with JET-C: The total material deposition rate in the divertor decreased by a factor of 4–9 compared to the deposition rate of carbon in JET-C. This decrease of material deposition in the divertor is accompanied by a decrease of total deuterium retention inside the JET vessel by a factor of about 20.

The erosion/deposition pattern observed during JET ILW-2 was qualitatively comparable to JET ILW-1, the observed D inventory was roughly comparable to the inventory observed during JET ILW-1. The results obtained during JET ILW-2 therefore confirm the positive results observed in JET ILW-1. Early results from JET ILW-3 also indicate agreement; more details will become available in summer 2018.

The Impact of Poloidal Flux Expansion on JET Divertor Radiation Performance

B. Viola¹, G. Artaserse¹, G. Calabrò², I. Lupelli², F. Maviglia³, S. Minucci², G. Rubino¹,
and G. De Tommasi^{4,5}

The JET Contributors

¹ENEA C. R. Frascati, Dipartimento FSN, Frascati, Italy

²Department of Economics, Engineering, Society and Business Organization (DEIm),
University of Tuscia, Largo dell'Università snc, 01100 Viterbo, Italy

³CREATE/ENEA/EURATOM Association, Università di Napoli, Naples, Italy

⁴Università degli Studi di Napoli Federico II, 80138 Napoli, Italy

⁵Consorzio CREATE, Università degli Studi di Napoli Federico II, 80138 Napoli, Italy

Corresponding Author: B. Viola, bruno.viola@enea.it

For a burning plasma device like ITER, radiative power removal by seeded impurities will be inevitable to avoid divertor damage. Increasing divertor radiation by injecting low- Z impurities such as nitrogen, to reduce scrape-off layer heat flux and to cool the divertor plasma to detachment, is put forward as the primary method to achieve this goal. Here, the possibility of increasing the radiative fraction is assessed by using poloidal magnetic flux expansion. Initial ohmic and nitrogen seeded H-mode high flux expansion (HFE) experiments, characterized by the presence of 2-nearby poloidal magnetic field nulls and a contracting geometry near the inner target plate have been recently achieved at JET tokamak.

In this contribution the physics of the dependence of radiative volume and total radiated power on flux expansion variation at JET, equipped with ITER-like wall (ILW), will be addressed. EDGE2D-EIRENE simulations have already shown that the divertor heat fluxes can be reduced with N_2 -injection, qualitatively consistent with experimental observations, by adjusting the impurity injection rate to reproduce the measured divertor radiation. Through EDGE2D-EIRENE code modelling, a detailed analysis of the power balance has been set up to physically investigate the reason of the increase of the radiated power for HFE discharges. An increase of charge exchange losses has been related to an increase of connection length and flux expansion both at X-point at strike points position. Spectroscopy data suggests that there is evidence of a detachment front moving towards the X-point from both the movement of the electron density and the low charge nitrogen charge states as the flux expansion increases. Initial experiments with a second null, on the high field side, forming a configuration with significant distance between the two nulls and a contracting geometry near the target plates have been performed leading to an increase of the main magnetic divertor geometry parameters. In addition, nitrogen seeded H-mode experiments have been set-up showing an increase of the total radiated power of the same factor of the flux expansion increase. Further experiments will be devoted to varying the divertor coils polarities to move the secondary X-point on the low field side region and consequently increase the outer flux expansion both in the X-point and strike point region.

First Mirror Test in JET for ITER: Complete Overview After Three Campaigns in JET with ITER-Like Wall

M. Rubel¹, S. Moon¹, P. Petersson¹, A. Garcia-Carrasco¹, D. Ivanova¹, A. Widdowson², I. Jecu², A. Baron-Wiechec², E. Fortuna-Zalesna³, and S. Jachmich⁴

The JET Contributors

¹KTH Royal Institute of Technology, Stockholm, Sweden

²Culham Centre for Fusion Energy (CCFE), Culham Science Centre, Abingdon, UK

³Warsaw University of Technology, 00-661 Warsaw, Poland

⁴Laboratory for Plasma Physics, ERM/KMS, Brussels, Belgium

Corresponding Author: M. Rubel, rubel@kth.se

Metallic first mirrors are essential plasma-facing components (PFC) in all optical spectroscopy and imaging systems used for plasma diagnosis. First mirror test (FMT) has been carried out at the JET tokamak with the ITER-like wall (JET-ILW). Over 120 test Mo mirrors were exposed in JET during the entire project. The aim is to provide an overview of results obtained for mirrors exposed during: i) the third ILW campaign, ILW3, 2015–2016, 23.6 h plasma; ii) all three campaigns, i.e., ILW 1–3: 2011–2016, 62 h in total; and iii) a comparison to results in JET-C. Examinations were done by optical, electron and ion beam techniques.

The total reflectivity of all mirrors in the main chamber has decreased by 2–3% from the initial value. All of them are coated by a very thin codeposit (5–15 nm) containing D, Be, C and O. This has affected the optically active layer (15–20 nm on Mo) and led to increased diffuse reflectivity. No W and N have been found on the surface. All mirrors from the divertor lost reflectivity by 20–80%. There are significant differences in the surface state dependent on the location and exposure time. Reflectivity loss is connected predominantly with the codeposition of Be and some C species. The thickest layers have been found in the outer divertor: 850 nm after ILW1-3, indicating the average growth rate of 4 pm/s.

The layers thickness is not directly proportional to the exposure time. Nitrogen, tungsten and nickel are on all mirrors from the divertor. The highest N and W contents are in the inner divertor: N reaches $1 \times 10^{17}/\text{cm}^2$, W is up to $3.0 \times 10^{16}/\text{cm}^2$, while the greatest Ni content is in the outer leg: $2.5 \times 10^{17}/\text{cm}^2$. The results obtained for the main chamber mirrors allow some optimism regarding the diagnostics reliability in ITER. Tests done in JET-C and JET-ILW show that the degradation of optical properties in a machine with metal PFC is distinctly smaller than in the carbon surrounding. However, a long-term exposure and off-normal events may change surface properties of the mirrors. Laser- or plasma-induced cleaning techniques of tokamak mirrors have not brought any positive results. There are some indications that single crystal mirrors may be cleaned more efficiently than polycrystalline. Search for engineering solutions for mirror exchange in a reactor should not be abandoned especially for the divertor mirrors.

Influence of Magnetic Field on Plasma Energy Transfer to Material Surfaces in ELM Simulation Experiments with QSPA-M

I. E. Garkusha¹, V. A. Makhlai¹, Y. V. Petrov¹, V. V. Chebotarev¹, D. V. Yelisseyev¹, N. V. Kulik¹, V. V. Staltsov¹, S. S. Herashchenko¹, D. G. Soliyakov¹, M. S. Ladygina¹, and A. K. Marchenko¹

¹*National Science Center, Kharkov Institute of Physics and Technology (KIPT), Kharkov, 61108, Ukraine*

Corresponding Author: I. E. Garkusha, garkusha@ipp.kharkov.ua

Features of plasma energy transfer to the material surfaces during the plasma-surface interaction in presence of strong magnetic field are investigated within recently developed quasi-stationary plasma accelerator QSPA-M. This novel PSI test-bed facility is able to reproduce the ELM impacts, both in terms of heat load and particle flux to the surface, and to provide plasma transportation in external magnetic field, which mimics the divertor conditions. Investigations of energy transfer to the material surface have been performed for varied plasma heat load and external magnetic field value. Calorimetry, optical emission spectroscopy and a high speed imaging were applied for PSI characterization.

For perpendicular plasma incidence, it has been shown that the transient plasma layer is formed in front of the surface by stopped head of plasma stream even for rather small plasma heat loads, which not resulted in surface melting. The plasma density in this near-surface layer is much higher than in the impacting stream. It leads to the arisen screening effect for the energy transfer to the surface. For $B = 0$, the screening layer thickness is less than 2 cm, but it increases up to 10 cm when $B = 0.8$ T. Reducing the size of the target leads to growth of the fraction of plasma energy, which is absorbed by the surface.

For plasma exposures of tilted target surfaces, the thickness of the transient plasma layer is found to be essentially nonuniform. It is maximal for downstream part of the target while the upstream surface area remains completely unprotected. The impacting plasma shifts the screening layer significantly along the surface and also generates an oblique shock wave from the protruding edge. This shock wave together with the available shift of plasma layer along the target provides an additional shielding for the downstream part of the exposed surface.

The important contribution of external magnetic fields to the plasma energy transfer to the material surfaces is also discussed. It has been found that presence of strong external magnetic field leads to decrease of the energy, which is transferred to the exposed surface, due to the growing plasma density in near-surface layer and its increasing thickness.

SOL Transport and Detachment in Alternative Divertor Configurations in TCV L- and H-Mode Plasmas

C. Theiler¹, J. A. Boedo², B. P. Duval¹, N. Fedorczak³, O. Février¹, A. Fil⁴, A. Gallo³, J. R. Harrison⁵, P. Innocente⁶, B. Labit¹, B. Linehan⁷, B. Lipschultz⁴, R. Maurizio¹, B. Mumgaard⁷, H. De Oliveira¹, H. Reimerdes¹, U. Sheikh¹, A. J. Thornton⁵, C. K. Tsui², K. Verhaegh^{4,1}, N. Vianello⁶, W. A. J. Vijvers⁸, and M. Wensing¹

The TCV Team and The EUROfusion MST1 Team

¹Swiss Plasma Center (SPC), École polytechnique fédérale de Lausanne (EPFL), 1015 Lausanne, Switzerland

²University of California San Diego, CA 92093, USA

³Institut de Recherche sur la Fusion par confinement Magnétique (IRFM), Commissariat à l'énergie atomique (CEA/Cadarache), 13108 St. Paul lez Durance, France

⁴York Plasma Institute, University of York, Heslington, UK

⁵Culham Centre for Fusion Energy (CCFE), Culham Science Centre, Abingdon, UK

⁶Consorzio RFX, Associazione EURATOM-ENEA sulla Fusione, Padova, Italy

⁷Plasma Science & Fusion Center, MIT, Cambridge, MA 02139, USA

⁸FOM Institute DIFFER, Association EURATOM-FOM, Nieuwegein, Netherlands

Corresponding Author: C. Theiler, christian.theiler@epfl.ch

The effect of magnetic geometry on scrape-off layer (SOL) transport and detachment behaviour is investigated on the TCV tokamak with the goal of assessing the potential of alternative divertor geometries and for the validation of theoretical models. L-mode experiments reveal that increasing connection length and hence divertor volume by either increasing poloidal flux expansion or divertor leg length have different effects on the boundary plasma. In attached conditions, the SOL heat flux width λ_q inferred from target infrared thermography measurements is weakly dependent on poloidal flux expansion but increases approximately with the square root of the divertor leg length. The divertor spreading factor S shows no clear trend with leg length but decreases with flux expansion. TOKAM3X turbulence simulations of the leg length scan are in qualitative agreement with the experiment and can explain observations by a strongly asymmetric (ballooning) transport at and below the X-point. Evidence for increased transport in the region of low poloidal field is obtained in the Snowflake minus geometry. The presence of an additional X-point in the low-field side SOL increases the effective SOL width by approximately a factor two.

Increasing flux expansion and leg length both result in enhanced divertor radiation levels, with the effect being much larger in the latter case. This behaviour, together with the observed trend in λ_q , is consistent with a substantial drop in the density threshold for divertor detachment with increasing leg length and a weak variation with flux expansion. Novel spectroscopic techniques reveal that the drop in target ion current and access to detachment is caused by a reduction of the divertor ionization source due to power starvation, while volume recombination is only a small contributor. This interpretation is confirmed by SOLPS modelling.

TCV alternative divertor studies are being extended to neutral beam heated H-mode plasmas. The H-mode power threshold is found to vary weakly between standard, X-, and Super-X geometries. In all cases, ELMy H-mode is obtained at intermediate current, while the discharges are ELM-free at high current. Signs of detachment have so far only been observed in the latter case. Ongoing experiments further investigate H-mode detachment in these plasmas and will be extended to Snowflake configurations.

On the Role of Radial Electric Fields on Turbulence Spreading in the Plasma Boundary of Fusion Devices

G. Grenfell^{1,2}, B. P. van Milligen¹, U. Losada¹, W. Ting^{1,3}, B. Liu^{1,4}, C. Silva⁵, M. Spolaore², and C. Hidalgo¹

The TJ-II Team

¹Centro de Investigaciones Energéticas, Medioambientales y Tecnológicas (CIEMAT), Madrid, Spain

²Consorzio RFX, Associazione EURATOM-ENEA sulla Fusione, Padova, Italy

³Southwestern Institute of Physics, Chengdu, Sichuan, People's Republic of China

⁴Southwest Jiaotong University, Chengdu, Sichuan, People's Republic of China

⁵Institute of Plasmas and Nuclear Fusion (IPNF), Instituto Superior Técnico (IST), 1049-001 Lisbon, Portugal

Corresponding Author: G. Grenfell, gustavo.grenfell@igi.cnr.it

Turbulence spreading is the transfer of free turbulent energy from strongly driven (i.e., unstable regions) to weakly driven locations [1]. The net effect of this phenomenon is the radial redistribution of turbulent energy, modifying local plasma features. It has been pointed out that spreading may be important in setting the scrape-off layer (SOL) width. The peak heat load onto the divertor is intimately related to the SOL width, and the understanding of the mechanisms setting this width is fundamental for a reliable prediction of the SOL decay length for ITER. In this work, we report on measurements of turbulence drive and turbulent spreading, as defined by [2], from the near edge to the far SOL region of TJ-II. A 2D Langmuir probe array [3] was used to measure both parameters as well as the profiles of floating potential, plasma density, radial turbulent particle flux, effective radial velocity, potential turbulence correlation time and phase velocity of the fluctuations. The radial electric field in the edge was modified by a biasing electrode, inserted into the edge of the plasma ($\rho \approx 0.85$), delivering a voltage ± 350 V (with respect to the wall), with a square 40 Hz waveform. All the parameters were modulated by the biasing. At -350 V, the velocity shear reached its maximum, resulting in a strong suppression of turbulent transport and the effective radial velocity fluctuations, not only at the shear layer, but also in the far SOL. Moreover, the ion saturation profile steepened at the shear layer location and was reduced in the SOL. The local turbulence drive and turbulence spreading were also impacted by the biasing. The driving term was strongly reduced in the shear layer, and only slightly reduced in the SOL. Turbulence spreading was mainly modified in the SOL when the $E_r \times B$ shear reached values close to the inverse of the turbulence correlation time in the vicinity of the last close flux surface (LCFS). In summary, biasing was found to reduce edge-SOL coupling by decreasing turbulence spreading, thus affecting the ion saturation current profile, which may have an impact on the SOL width.

References

- [1] X. Garbet *et al.*, Nucl. Fus., **34**, 963 (1994).
- [2] P. Manz *et al.*, Phys. Plasmas, **22**, 022308 (2015).
- [3] J. Alonso *et al.*, Nucl. Fus., **52**, 063010 (2012).

Basic Studies of the Interaction of Blobs with Suprathermal Ions and Millimetre-Wave Beams in the TORPEX Device

I. Furno¹, S. Alberti¹, M. Baquero¹, O. Chellai¹, A. Fasoli¹, T. P. Goodman¹, F. Manke¹, and P. Ricci¹

¹Swiss Plasma Center (SPC), École polytechnique fédérale de Lausanne (EPFL), 1015 Lausanne, Switzerland

Corresponding Author: I. Furno, ivo.furno@epfl.ch

The fundamental interactions between turbulent structures or blobs and suprathermal ions, injected by Li^{6+} beams in plasmas created by microwaves at 2.45 GHz with $n_e \sim 10^{15}\text{--}10^{17}/\text{m}^3$ and $T_e \sim 2\text{--}10$ eV, are extensively investigated on the TORPEX toroidal device. Comparisons between fully validated numerical simulations and experimental 3D time-averaged suprathermal ion profiles reveal an entire spectrum of nondiffusive suprathermal ion transport: superdiffusive, diffusive, or subdiffusive, depending on particle energy and turbulence amplitude. Time-resolved 3D measurements of 30 eV and 70 eV ions, exhibiting super- and subdiffusive transport respectively, show that in all cases the ions are subject to bursty displacement events and that intermittency, quantified by the skewness of the time-traces, is present to some degree in all profiles, also for intermediate energies, including in the subdiffusive cases. We develop an analytical model that links the time averaged-profile of the ion current and the profile of the statistical moments of the fluctuations. In fusion devices, externally injected beams in the electron cyclotron (EC) frequency range are employed for heating and current drive, and to stabilize neoclassical tearing modes. EC beams must propagate through the scrape-off layer where blobs may scatter the incoming wave by locally modifying the plasma permittivity. This may lead to a loss of efficiency in EC heating and mode stabilization. To understand the effect of plasma turbulence and its structures on the propagation of millimetre waves (mmw), we measure wave scattering in TORPEX by blobs of size comparable to the wavelength. A low-power beam is launched at 29.7 GHz in the X-mode from the top of the device using a pyramidal horn antenna. The X-mode component of the transmitted power is detected at the bottom using a pyramidal horn antenna and a Schottky diode, whose position can be radially adjusted. A conditional sampling technique averages the effect of several thousand individual blobs. Combining these scattering measurements with first principle full-wave simulations using COMSOL, we show that density fluctuations associated with plasma blobs, with δn_e as small as $\sim 10^{-3}$ of the critical density, can significantly defocus the mmw-beam in the wake of the blobs, resulting in mmw-power fluctuations that increase monotonically with the blob amplitude.

EX

Early Identification of Disruption Paths for Prevention and Avoidance

C. Sozzi¹, E. Alessi¹, A. Pau², A. Fanni², B. Cannas², P. J. Lomas³, M. Baruzzo⁴, T. Bolzonella⁴, M. Bernert⁵, T. C. Blanken⁶, S. Carcangiu², C. Cianfarani⁷, R. Delogu⁴, F. A. A. Felici⁸, D. Ferreira⁹, C. Galperti⁸, M. Gelfusa¹⁰, S. N. Gerasimov³, I. Ivanova-Stanik¹¹, E. Joffrin¹², F. Köchl³, O. Kudlacek⁵, E. A. Lerche¹³, M. Lungaroni¹⁰, M. Maraschek⁵, A. Murari⁴, E. Pawelec¹⁴, E. Peluso¹⁰, G. Rattà¹⁵, F. G. Rimini³, O. Sauter⁸, U. Sheik⁸, G. Sias², P. Sparapani², G. Stakunas¹⁶, J. Vega¹⁵, I. Voitsekhovitch³, and A. A. Teplukhina⁸

The JET Contributors and The EUROfusion MST1 Team

¹Istituto di Fisica del Plasma (IFP), Consiglio Nazionale delle Ricerche (CNR), 20125 Milan, Italy

²Dip. Ing. Elettrica e Elettronica, Università di Cagliari, 09124 Cagliari CA, Italy

³Culham Centre for Fusion Energy (CCFE), Culham Science Centre, Abingdon, UK

⁴Consorzio RFX, Associazione EURATOM-ENEA sulla Fusione, Padova, Italy

⁵Max-Planck-Institut für Plasmaphysik, Garching, Germany

⁶Eindhoven University of Technology, Eindhoven, Netherlands

⁷ENEA C. R. Frascati, Dipartimento FSN, Frascati, Italy

⁸Swiss Plasma Center (SPC), École polytechnique fédérale de Lausanne (EPFL), 1015 Lausanne, Switzerland

⁹Institute of Plasmas and Nuclear Fusion (IPNF), Instituto Superior Técnico (IST), 1049-001 Lisbon, Portugal

¹⁰Università di Tor Vergata, 00173 Rome, Italy

¹¹Institute of Plasma Physics and Laser Microfusion (IPPLM), Warsaw, Poland

¹²Institut de Recherche sur la Fusion par confinement Magnétique (IRFM),

Commissariat à l'énergie atomique (CEA/Cadarache), 13108 St. Paul lez Durance, France

¹³Laboratory for Plasma Physics, ERM/KMS, Brussels, Belgium

¹⁴University of Opole, 45-040 Opole, Poland

¹⁵Laboratorio Nacional de Fusión (LNF),

Centro de Investigaciones Energéticas, Medioambientales y Tecnológicas (CIEMAT), Madrid, Spain

¹⁶Lithuanian Energy Institute, Kaunas 44403, Lithuania

Corresponding Author: C. Sozzi, sozzi@ifp.cnr.it

Disruption prevention in the perspective of high performance, high current, long duration plasma discharges requires a substantial evolution of the schemes applied in most of the present tokamaks. An efficient prevention scheme requires the early identification of the nature of the off-normal behaviour possibly leading to a disruption and the automatic selection of the appropriated countermeasure, either avoidance or mitigation. The development of such comprehensive scheme is being pursued in a coordinate effort. For the purpose of the avoidance, on which this paper is focussed, the disruption can be seen as the result of the interplay of the physical events and of the control system responses to them and to the technical failures. The building blocks of such description should include the integration of several sets of plasma scalar data, plasma profile data, magneto-hydrodynamics indicators and engineering data. Previous work has shown the potential of the generative topographic mapping (GTM) [1] algorithm for identification and discrimination of the disruptive operational space in tokamak devices [2, 3].

Continued...

In this paper it is shown that the magnetic fluctuations associated with rotating MHD modes can be characterized using a set of observables derived from the singular value decomposition applied to the data collected by an array of pick-up coils. They can provide an input to the GTM analysis such that a clustering separating disruptive and nondisruptive timeslices can be found.

A further source of information comes from the analysis of the sequences of events recorded by the machine control system. The analysis of such sequences shows that disruptions and nondisruptive terminations generally follow different paths, i.e., are not populating equally the same sequences. Moreover, the time analysis of the most populated disruptions paths shows that in most of the cases the sequence can be recognized with an advance ranging about from 0.15 s to 1.5 s with respect to the disruption time. Such information is readily available to the control system and can contribute to the early triggering of the avoidance action. Details of such combined analysis and application to different databases of JET, TCV and AUG tokamaks will be discussed in the paper.

References

- [1] C. Bishop, *Neural Comp.*, **10**, (1998).
- [2] A. Pau, Ph.D Thesis, [Techniques for prediction of disruptions on TOKAMAKS](#), (2014).
- [3] B. Cannas, *Plasma Phys. Contr. F.*, **56**, (2014).

Minimizing Power Load Asymmetries During Disruption Mitigation at JET

S. Jachmich^{1,2}, M. Lehnen³, P. Drewelow⁴, U. Kruezi³, I. S. Carvalho⁵, M. Imrisek⁶, V. V. Plyusnin⁵, and C. Reux⁷

The JET Contributors

¹EUROfusion Programme Management Unit Culham, Culham Science Centre, Abingdon, UK

²Laboratory for Plasma Physics, ERM/KMS, Brussels, Belgium

³International Thermonuclear Experimental Reactor (ITER), Cadarache Centre, 13108 St. Paul lez Durance, France

⁴Max-Planck-Institut für Plasmaphysik, Greifswald, Germany

⁵Institute of Plasmas and Nuclear Fusion (IPNF), Instituto Superior Técnico (IST), 1049-001 Lisbon, Portugal

⁶Institute of Plasma Physics AS CR v.v.i., Prague, Czech Republic

⁷Institut de Recherche sur la Fusion par confinement Magnétique (IRFM), Commissariat à l'énergie atomique (CEA/Cadarache), 13108 St. Paul lez Durance, France

Corresponding Author: S. Jachmich, s.jachmich@fz-juelich.de

The high thermal loads caused by a disruption of an ITER baseline scenario pulse potentially stored thermal energy of 350 MJ and magnetic energy inside the vessel of 400 MJ pose a severe threat to the first wall components [1]. Massive gas injection (MGI) into a disrupting plasma has been shown to be capable of reducing the energy deposited onto the plasma facing components by increasing the radiation. However, the uneven distribution of the radiated power following a single local massive gas injection leads to highly localized radiation and hence to significant thermal loads due to the radiation “flash” [2]. In addition, the presence of the $n = 1$ mode during the disruption produces toroidal and poloidal radiation asymmetries. Depending on the phase relationship between the $n = 1$ mode and the MGI-location, this effect can be enhanced or diminished. In order to address this issue, JET has installed three MGI-valves at poloidal and toroidal positions similar to ITER. Single or a combination of two MGI-valves have been fired into a locked error field mode, whose toroidal O-point position was imposed by applying an external $n = 1$ magnetic perturbation field. By measuring the radiated power at two separate toroidal locations and varying the toroidal phase of the perturbation field a toroidal peaking factor TPF, defined as the ratio of the maximum radiation to the average value, could be estimated. For a single injection TPFs in the range of 1.5 up to 1.8 have been found, depending on the type of impurity gas used. Optimizing the time delay between two MGI-valves, which are toroidally at opposite locations, allowed a reduction of the TPF down to 1.2. The measured radiated power asymmetries are sensitive to small variations of the delay between the two MGI valve triggering times in the order of less than a millisecond. In this contribution the experimental findings of radiation asymmetries during mitigated disruptions caused by a seeded error field mode and the comparison with a heuristic model will be presented and the implications for the ITER disruption mitigation system discussed.

References

- [1] M. Lehnen *et al.*, J. Nucl. Mater., **463**, 39 (2015).
- [2] R. Pitts *et al.*, J. Nucl. Mater., **463**, 748 (2015).

Overview of Disruptions with JET-ILW

S. N. Gerasimov¹, P. Abreu², G. Artaserse³, M. Baruzzo⁴, I. S. Carvalho², T. C. Hender¹,
R. B. Henriques², R. Felton¹, U. Kruezi⁵, P. J. Lomas¹, P. McCullen¹, M. Maslov¹,
S. Moradi⁶, F. G. Rimini¹, W. Schippers¹, G. Szepesi¹, M. Tsalas⁵, and L. E. Zakharov^{7,8}

The JET Contributors

³ENEA for EUROfusion, via E. Fermi 45, 00044 Frascati (Roma), Italy

¹Culham Centre for Fusion Energy (CCFE), Culham Science Centre, Abingdon, UK

²Instituto Superior Técnico (IST), 1049-001 Lisbon, Portugal

³ENEA for EUROfusion, via E. Fermi 45, 00044 Frascati (Roma), Italy

⁴Consorzio RFX, Associazione EURATOM-ENEA sulla Fusione, Padova, Italy

⁵International Thermonuclear Experimental Reactor (ITER),
Cadarache Centre, 13108 St. Paul lez Durance, France

⁶Laboratory for Plasma Physics, ERM/KMS, Brussels, Belgium

⁷LiWFusion, P.O. Box 2391, Princeton NJ-08543, USA

⁸University of Helsinki, 00100 Helsinki, Finland

Corresponding Author: S. N. Gerasimov, sergei.gerasimov@ukaea.uk

This paper presents an analysis of disruptions occurring during JET-ILW plasma operations covering the period from #80128 up to #92504. The total number of disruptions was 1951, including 466 MGI (massive gas injection), VDE (vertical displacement event) and error field correction coil experiments, which led to intentional disruptions; hence the average disruption rate is 16.1%. MGI has been routinely used in protection mode both to terminate pulses when the plasma is at risk of disruption, and to mitigate against disruptions, in total 896 shots were ended by MGI. The subset of 913 natural disruptions, which were not affected by special dedicated experiments or MGI protection, was used for analysis of predisruptive plasma behaviour. The predisruptive plasma parameters of the natural disruptions are $I_p = (0.82\text{--}3.14)$ MA, toroidal field $B_t = (0.98\text{--}3.36)$ T, $q_{95} = (1.52\text{--}9.05)$, $i_i = (0.58\text{--}1.86)$, $\beta_p = (0\text{--}1.1)$, volume average plasma density $n_e = (0.2\text{--}8.5)10^{19}/\text{m}^3$, X-point (317 shots) and limiter (596 shots) configurations. Apart from 21 exceptional cases, the MGI was triggered by $n = 1$ locked mode (523 shots) or by the disruption itself, specifically by dI_p/dt (207 shots) or by toroidal loop voltage (145 shots). On JET, only the locked mode was treated as either a precursor or the cause of disruptions. However, long lasting locked modes (≥ 100 ms) do exist prior to disruption in 75% of cases. Though, 10% of nondisruptive pulses have a locked mode which eventually vanished without disruption. The plasma current quench (CQ) may result in 3D equilibria, termed as asymmetrical disruptions, which are accompanied by sideways forces. Unmitigated VDEs generally have significant plasma current toroidal asymmetries. The unmitigated disruptions also have large plasma current asymmetries presumably because there is no plasma vertical position control during CQ. However, MGI is a reliable tool to mitigate 3D effects and accordingly sideways forces. The vessel structure loads depend on the force impulse and force time behaviour or rotation. The toroidal rotation of 3D equilibria is of particular concern because of potential resonance with the natural frequencies of the vessel components in large tokamaks such as ITER. The amplitude-frequency interdependence is important, since a simultaneous increase of amplitude and frequency would potentially create the most challenging load conditions.

Control of NTMs and Integrated Multiactuator Control on TCV

M. Kong¹, T. C. Blanken², F. Carpanese¹, F. A. A. Felici¹, C. Galperti¹, B. Maljaars², A. Merle¹, J.-M. Moret¹, F. Pesamosca¹, E. Poli³, M. Reich³, O. Sauter¹, A. A. Teplukhina¹, and T. Vu¹

The TCV Team and The EUROfusion MST1 Team

¹Swiss Plasma Center (SPC), École polytechnique fédérale de Lausanne (EPFL), 1015 Lausanne, Switzerland

²Eindhoven University of Technology, Eindhoven, Netherlands

³Max-Planck-Institut für Plasmaphysik, Garching, Germany

Corresponding Author: M. Kong, mengdi.kong@epfl.ch

Detailed experiments have been performed on TCV with its flexible electron cyclotron heating/current drive system to investigate reliable and efficient control of NTMs. For example, a novel sinusoidal sweeping technique has been studied in detail and we have shown for the first time that it is efficient for both NTM stabilization and preemption. This method is important for future devices as it relaxes the demand on the accuracy of the mode location estimation and the beam deposition calculation, and circumvents the need for extra diagnostics or many shots for tuning. Comparison between NTM preemption and stabilization has been achieved with sweeping and it shows that preemption can be more than twice as efficient as stabilization in terms of the necessary power. The reliable, efficient and generic control of NTMs allows the development of a controller working for all the scenarios and independent of the specialties of TCV, facilitating the integration with other real-time (RT) algorithms. RT control of NTMs, β and model-estimated q profiles have been achieved simultaneously on TCV for the first time with a generic integrated control framework that consists of a hierarchy of state estimation/prediction, plasma event monitoring, supervision, high-level (HL-) actuator management (AM), generic controllers and low-level (LL-) AM. In an integrated control test, RT diagnostics are used with RT simulations to reconstruct the plasma state. We will show how RT analyses of magnetic signals are used to provide details of the mode, the RAPTOR observer to reconstruct electron temperature and q profiles, the RAPDENS-observer to generate density profiles and RT-TORBEAM to calculate beam depositions. This information is then used by the plasma event monitor to produce a finite-state representation of the plasma state based on user-defined thresholds. The supervisor prioritizes various tasks, activates relevant controllers and interfaces with a generic control layer. In this layer, controllers send requests for each task to the HL-AM that optimizes the actuator allocation and sends back the actuation capability to the controllers and the LL-AM. The LL-AM sends controller commands to the tokamak-specific actuators. Importantly, the control layer has been made tokamak agnostic to facilitate its reuse in other devices and to provide a layer of abstraction for operators.

EX

Runaway Electron Beam Stability and Decay in COMPASS

O. Ficker^{1,2}, J. Mlynář¹, E. Macusova¹, J. Cеровsky^{1,2}, A. Casolari¹, M. Farnik^{1,2}, A. Havranek^{1,3}, H. Ales^{1,3}, M. Hron¹, M. Imrisek^{1,4}, P. Kulhanek^{1,3}, T. Markovic^{1,2}, D. Naydenkova¹, R. Panek¹, M. Tmes^{1,2}, J. Urban¹, M. Vlaine⁵, P. Vondracek^{1,2}, V. Weinzettl¹, J. Decker⁶, G. Papp⁷, Y. Peysson⁸, M. Gobbin⁹, M. Gospodarczyk¹⁰, V. V. Plyusnin¹¹, M. Rabiniski¹², and C. Reux⁸

The COMPASS Team and EUROfusion MST1 Team

¹*Institute of Plasma Physics AS CR v.v.i., Prague, Czech Republic*

²*Faculty of Nuclear Sciences and Physical Engineering,
Czech Technical University, Prague, Czech Republic*

³*Faculty of Electrical Engineering, Czech Technical University, Prague, Czech Republic*

⁴*Faculty of Mathematics and Physics, Czech Technical University, Prague, Czech Republic*

⁵*Institute of Physics, University of Belgrade, Belgrade, Serbia*

⁶*Swiss Plasma Center (SPC), École polytechnique fédérale de Lausanne (EPFL), 1015 Lausanne, Switzerland*

⁷*Max-Planck-Institut für Plasmaphysik, Garching, Germany*

⁸*Institut de Recherche sur la Fusion par confinement Magnétique (IRFM),
Commissariat à l'énergie atomique (CEA/Cadarache), 13108 St. Paul lez Durance, France*

⁹*Consorzio RFX, Associazione EURATOM-ENEA sulla Fusione, Padova, Italy*

¹⁰*Università di Tor Vergata, 00173 Rome, Italy*

¹¹*Institute of Plasmas and Nuclear Fusion (IPNF), Association EURATOM/IST, Lisbon, Portugal*

¹²*National Centre for Nuclear Research (NCB), Świerk, Poland*

Corresponding Author: O. Ficker, ficker@ipp.cas.cz

Runaway electrons (REs) as one of the yet unsolved threats for ITER and future tokamaks are a topic of intensive research at most tokamaks. The experiments performed on COMPASS are complementary to the experiments at JET and MST (Medium-Size Tokamaks), building on the flexibility of the diagnostics set-up and low safety constraints at this smaller ($R_0 = 0.56$ m, $a = 0.23$ m) device. During the past couple of years two different scenarios with the RE beam generation triggered by gas injection have been developed and investigated. The first one is based on Ar or Ne massive gas injection (MGI) into the current ramp-up phase leading to a disruption accompanied by runaway plateau generation, while the second uses smaller amounts of gas in order to get runaway current dominated plasmas.

The successful generation of the beam in the first scenario depends on various parameters, including the toroidal magnetic field. The generated beam is often radially unstable, and the stability seems to be a function of various parameters, including the value of current lost during the CQ. Surprisingly, the current decay rate of the stable beams is rather similar in most discharges. The second scenario is much more quiescent, with no observable fast current quench. This allows to better diagnose the beam phase and also to apply secondary injections or resonant magnetic perturbations (RMP) to assist the decay of the beam. In this regard, interesting results have been achieved using secondary deuterium injection into a runaway electron beam triggered by Ar or Ne injection and also using $n = 1$ error field generated by top and bottom RMP coils. While D dilution is clearly able to almost stop the beam decay, RMPs help to accelerate the beam decay. The effect of RMPs seems to be very different when acting on Ar and Ne background plasmas.

Very interesting effects have been observed also by the high-speed cameras, including filamentation during the application of the RMPs and a slow local variation of the light intensity similar to turbulence during the beam decay.

Plasma and Diagnostics Preparation for α -Particle Studies in JET DT

S. E. Sharapov¹, R. Dumont², J. Mailloux¹, V. Aslanyan³, C. D. Challis¹, J. Ferreira⁴, M. Fitzgerald¹, E. Joffrin¹, T. Johnson⁵, D. King¹, V. G. Kiptily¹, M. J. Mantsinen^{6,7}, F. Nabais⁴, M. Nocente^{8,9}, P. Puglia¹⁰, P. Vallejos⁵, and H. Weisen¹⁰

The JET Contributors

¹Culham Centre for Fusion Energy (CCFE), Culham Science Centre, Abingdon, UK

²Commissariat à l'énergie atomique (CEA), 91400 Gif-sur-Yvette, France

³Plasma Science & Fusion Center, MIT, Cambridge, MA 02139, USA

⁴Instituto Superior Técnico (IST), 1049-001 Lisbon, Portugal

⁵KTH Royal Institute of Technology, Stockholm, Sweden

⁶Centro Nacional de Supercomputación (BSC), Barcelona, Spain

⁷Catalan Institution for Research and Advanced Studies (ICREA), Barcelona, Spain

⁸Università degli Studi di Milano-Bicocca, 20126 Milano, Italy

⁹Istituto di Fisica del Plasma (IFP), Consiglio Nazionale delle Ricerche (CNR), 20125 Milan, Italy

¹⁰Swiss Plasma Center (SPC), École polytechnique fédérale de Lausanne (EPFL), 1015 Lausanne, Switzerland

Corresponding Author: S. E. Sharapov, sergei.sharapov@ccfe.ac.uk

A deuterium-tritium (DT) experimental campaign DTE2 on JET scheduled for 2019–2020, will be done in the Be/W vessel and will address essential operational, technical, diagnostic and scientific issues in support of ITER [1]. In preparation for the campaign, developments were performed on JET aiming at studies of α -particles. For studying AEs driven entirely by α -particles, a scenario similar to the TFTR beam “afterglow” [2] was developed for JET. In DT plasmas, after NBI is switched off, α -particles will be the only energetic ions during the time interval between slowing-down times for NBI-produced ions and α -particles. Detection of α -driven AEs in this time window may help in diagnosing the temporal evolution of the pressure profile and slowing-down time of α -particles. JET advanced tokamak scenarios with $q \approx 1.5$ –2.5 were chosen and discharges have been successfully developed. The transport modelling extrapolated to DT predicted that α -particle $\beta \approx 0.1\%$ could be achieved comparable to that in successful TFTR experiments.

In “hybrid” scenario plasmas with $q_0 \geq 1$, fast ion losses in the MeV energy range were observed during $n = 1$ fishbones driven by a resonant interaction with D beam ions in the energy range ≤ 120 keV [3]. The losses are identified as an expulsion of DD fusion products, 1 MeV tritons and 3 MeV protons. A mode analysis with the MISHKA code combined with the study of nonlinear wave-particle interaction with HAGIS show that the loss of toroidal symmetry strongly affects the confinement of high energy tritons and protons by perturbing their orbits and expelling them in a good agreement with experiment. The extrapolation to the case of α -particles in DTE2 hybrid scenarios with similar fishbones has shown an additional α -particle loss of $\sim 1\%$ [3].

References

- [1] H. Weisen *et al.*, Fus. React. Diag., AIP Conf. Proc. **1612**, 77–86 (2014).
- [2] R. Nazikian *et al.*, Phys. Rev. Lett., **78**, 2976 (1997).
- [3] M. Fitzgerald *et al.*, Submitted to Nucl. Fusion, (2018).

Subdivertor Fuel Isotopic Content Detection Limit for JET and Impact on the Control of ICRH for JET-ILW and JET-DT Operation

C. C. Klepper¹, M. Goniche², S. Vartanian², D. Douai², D. Van Eester³, E. A. Lerche³, E. Delabie¹, U. Kruezi⁴, and I. Iepu⁴

The JET Contributors

¹*Oak Ridge National Laboratory (ORNL), Oak Ridge, TN 37831, USA*

²*Institut de Recherche sur la Fusion par confinement Magnétique (IRFM), Commissariat à l'énergie atomique (CEA/Cadarache), 13108 St. Paul lez Durance, France*

³*Laboratory for Plasma Physics, ERM/KMS, Brussels, Belgium*

⁴*Culham Centre for Fusion Energy (CCFE), Culham Science Centre, Abingdon, UK*

Corresponding Author: C. C. Klepper, kleppercc@ornl.gov

In preparation for JET Deuterium-Tritium Experiments 2 (DTE-2) and to assure readiness to provide fuel cycle-relevant measurements, the subdivertor fuel isotopic ratio detection limit, as determined by Penning optical gas analysis (OGA) [1, 2], was recently researched. Re-evaluation of OGA data from DTE-1 [1] revealed a 1% uncertainty (error bar) at the 1% T/(H+D+T) concentration level. A similar detectability limit (at $\sim 1\%$ concentration) was found for H/(H+D) when evaluating a more recent JET ICRH-specific dataset. This analysis also shows a persistent $\sim 1\%$ systematic offset of the OGA with respect to divertor spectroscopy values. These studies are in support of substantial diagnostic upgrade for DTE-2 aiming to assure this isotopic detectability, as well mitigate gradual deterioration partly caused by coating of viewport windows by the OGA's own Penning discharge.

The importance of resolving isotopic concentrations at the $\sim 1\%$ level during ICRH plasmas was also explored. When $(H/(H+D))$ is reduced from 2% to $< 1\%$, an increase of core plasma T_i and a decrease of T_e are measured [3, 4]. This is consistent with full wave ICRH modelling indicating that when the concentration of the minority species is low enough, 2nd harmonic D absorption becomes dominant over the fundamental H minority absorption; if the plasma density is large enough, it provides collisional bulk ion heating rather than the typical electron heating observed with H minority absorption. The higher background T_i in conjunction with the RF acceleration of the D NBI ions to supra-source energies leads to an increase of the neutron yield by 30% in the case explored. For the same case, the increase of the energy of the fast H tail at small minority concentrations also contributes to sawtooth stabilization. This would imply that the ability to measure, and ultimately control, the fuel isotopic content down $\lesssim 1\%$ concentration level is important for optimizing the performance of a given ICRH scheme in fusion devices. The ability of the OGA technique to act as a global diagnostic of the isotopic mix is of great consequence for ITER, where divertor spectroscopy is unlikely to work, at least for such low concentrations [2].

References

- [1] D. L. Hillis *et al.*, Rev. Sci. Instrum., **70**, 359 (1999).
- [2] C. C. Klepper *et al.*, J. Instrum., **12**, C10012 (2017).
- [3] E. Lerche *et al.*, Nucl. Fus., **56**, 036022 (2016).
- [4] M. Goniche *et al.*, Plasma Phys. Contr. F., **59**, 055001 (2017).

Extension of the Operating Space of High- β_N Fully Noninductive Scenarios on TCV Using Neutral Beam Injection

C. Piron¹, J. Garcia², T. P. Goodman³, M. Agostini¹, M. Fontana³, G. Giruzzi², M. Gobbin¹, A. N. Karpushov³, M. Kong³, A. Merle³, J. Morales², S. Nowak⁴, L. Pigatto¹, O. Sauter³, D. Testa³, M. Vallar¹, and M. Yoshida⁵

The TCV Team and The EUROfusion MST1 Team

¹*Consorzio RFX, Associazione EURATOM-ENEA sulla Fusione, Padova, Italy*

²*Institut de Recherche sur la Fusion par confinement Magnétique (IRFM),*

Commissariat à l'énergie atomique (CEA/Cadarache), 13108 St. Paul lez Durance, France

³*Swiss Plasma Center (SPC), École polytechnique fédérale de Lausanne (EPFL), 1015 Lausanne, Switzerland*

⁴*Istituto di Fisica del Plasma (IFP), Consiglio Nazionale delle Ricerche (CNR), 20125 Milan, Italy*

⁵*National Institutes for Quantum and Radiological Science and Technology (QST), Chiba-shi, Japan*

Corresponding Author: C. Piron, chiara.piron@igi.cnr.it

The fully noninductive sustainment ($V_{\text{loop}} \sim 0$) of high normalized beta (β_N) plasmas is a crucial challenge for the steady-state operation of a tokamak reactor. In order to assess the difficulties associated with such scenarios, steady-state regimes have been explored on TCV using the newly available 1 MW neutral beam injection (NBI) system. Compared to the past [1, 2], plasmas closer to those expected in ITER, i.e., with significant NBI and ECRH current drive, bootstrap current and fast ion fraction, have been investigated. The operating space has been explored by carefully scanning the total auxiliary power, $P_{aux} = P_{EC} + P_{NB}$, the NB power fraction (P_{NB}/P_{aux}) and the radial deposition location of the NB and EC heating and current drive. Values for β_N up to 1.4 and 1.7 at $V_{\text{loop}} \sim 0$ have been reached in L-mode and H-mode plasmas, respectively. Fully noninductive operation was not achieved with NB alone, whose injection could even increase V_{loop} in presence of EC waves. Internal transport barriers, which are expected to maximize the bootstrap current fraction, were not formed in either the electron or the ion channel in the plasmas explored to date; and this despite a significant increase in the toroidal rotation and fast ion (FI) fraction with NBI, which are known to reduce turbulence [3]. The possibility that these plasmas are trapped electron mode (TEM) turbulence dominated is being analyzed in dedicated transport analyses. A strong contribution of bulk and FIs to the total plasma pressure has been experimentally evidenced and confirmed by modelling (ASTRA, NUBEAM). Interpretative simulations further predict that FI charge-exchange reactions are the main loss channel for NB heating efficiency. Similar results were also obtained in inductive L-mode plasmas in a circular limited configuration at TCV [4]. Interpretative transport analysis with TRANSP coupled to NUBEAM is carried out to quantify the role of NBI losses and of the anisotropy in the FI velocity space distribution in the NBCD efficiency. A complete understanding of this evidence is crucial to the development of fully noninductive plasmas

References

- [1] O. Sauter *et al.*, Phys. Rev. Lett., **84**(15), 3322 (2000).
- [2] S. Coda *et al.*, Phys. Plasmas, **12**, 056124 (2005).
- [3] J. Garcia *et al.*, Nucl. Fus., **55**, 053007 (2015).
- [4] B. Geiger *et al.*, Plasma Phys. Contr. F., **509**, 115002 (2017).

The Software and Hardware Architecture of the Real-Time Protection of In-Vessel Components in JET-ILW

V. Huber¹, A. Huber², D. Kinna³, G. Sergienko², I. Balboa³, S. Brezinsek², P. McCullen³, P. J. Lomas³, G. F. Matthews³, P. Mertens², F. G. Rimini³, and K.-D. Zastrow³

The JET Contributors

¹*Supercomputing Centre, Forschungszentrum Jülich, Jülich, Germany*

²*Institute of Energy and Climate Research, Forschungszentrum Jülich, Jülich, Germany*

³*Culham Centre for Fusion Energy (CCFE), Culham Science Centre, Abingdon, UK*

Corresponding Author: V. Huber, valentina.huber@ukaea.uk

The JET ITER-like wall (JET-ILW) combines plasma-facing components (PFC) made of bulk beryllium for main chamber limiter tiles and of bulk tungsten as well as tungsten coated CFC tiles for divertor tiles. The risk of damaging the metallic PFCs caused by beryllium melting or cracking of tungsten owing to thermal fatigue required a new reliable active protection system. To address this issue, a real-time protection system comprising newly installed imaging diagnostics, real time algorithms for hot spot detection and alarm handling strategy has been integrated into the JET protection system.

This contribution describes the design, implementation, and operation of the near infrared (NIR) imaging diagnostic system of the JET-ILW plasma experiment and its integration into the existing JET protection architecture. The imaging system comprises four wide-angle views, four tangential divertor views, and two top views of the divertor. Regions of interest (ROI) on the selected PFCs of different materials are analyzed in real-time and the maximum temperature measured in each ROI is sent to a real-time algorithm called vessel thermal map (VTM) to determine the likely cause of the overheating and to request an appropriate response from the plasma control system. Postpulse data visualization and advance analysis of all types of imaging data is provided by the new software framework JUVIL (JET Users Video Imaging Library). The hot spots formation at the reionization zones due to impact of the reionized neutrals as well as due to RF-induced fast ion losses is recognized as a big threat due to quick surface temperature rise. Because it could trigger the protection system to stop a pulse, it is important to identify the mechanisms and conditions responsible for the formation of such hot spots. To address this issue a new software tool Hotspot Editor has been developed.

Future development of the JET real-time first wall protection is focussed on the DT campaign and the ITER relevant conditions which will cause failure of camera electronics within the Torus hall. To provide the reliable wall protection, two more sensitive logarithmic NIR camera systems equipped with new optical relays to take images and cameras outside of the biological shield have been installed on JET-ILW and calibrated with in-vessel calibration light source.

$E_r \times B$ Shear Effect on Cross Phase Mitigates ELM at High Collisionality

D. F. Kong^{1,2}, X. Q. Xu², P. H. Diamond³, J. G. Chen⁴, C. B. Huang¹, X. Gao¹, and J. G. Li¹

The EAST Team

¹*Institute of Plasma Physics, Chinese Academy of Sciences, Hefei, Anhui, People's Republic of China*

²*Lawrence Livermore National Laboratory (LLNL), Livermore, CA 94550, USA*

³*University of California San Diego, CA 92093, USA*

⁴*Fusion Simulation Center and State Key Laboratory of Nuclear Physics and Technology, School of Physics, Peking University, Beijing 100871, People's Republic of China*

Corresponding Author: D. F. Kong, dfkong@ipp.ac.cn

A nonstationary, effective edge localized modes (ELMs) mitigation/suppression regime has been recently obtained by counter NBI heating at high collisionality on the Experimental Advanced Superconducting Tokamak (EAST). Our results show that counter NBI can significantly enhance the reversed toroidal rotation as well as the $E_r \times B$ flow shear of the pedestal. With the increased $E_r \times B$ flow shear, the ELM sizes can be suppressed by nearly 80%. The increased $E_r \times B$ flow shear can also broaden the power spectrum of the pedestal turbulence and enhance the amplitude of modes with high frequency ($f > 100$ kHz). The bispectrum study indicates that the nonlinear mode coupling of the pedestal turbulence also increases in counter NBI case, which can interrupt the linear growth of the peeling mode, thus leading to the suppression of ELM. When power of counter NBI is high enough, an ELM-free H mode can even be achieved on EAST. During the ELM-free H mode, the line averaged density as well as the amplitude of resistive ballooning mode keeps increasing until the H-L back transition. Those observations may link with the density limit in H mode discharge.

BOUT++ simulations have been applied to study the characteristics of edge-localized mode at fixed high collisionality for different E_r structure. The simulation result reveals that the increased $E_r \times B$ shear suppresses the ELM size and delays the pedestal crash, which is consistent with the observations on EAST. Analysis of the cross-phase spectrum of potential and pressure perturbations indicates that the increased $E_r \times B$ shear can shorten the phase coherence time τ_c and flatten the spectrum of τ_c , which is limited by nonlinear mode interaction. Thus, the peeling-ballooning mode does not get enough time to allow growth to large amplitude, which can be supported by the bispectrum study on EAST that increased $E_r \times B$ flow shear can enhance the nonlinear interaction.

Besides the collisionality, our simulations suggest a new way (E_r shear) to control the ELM size, which is consistent with observed ELM suppression at larger $E_r \times B$ shear in high collisionality plasmas on EAST.

Tungsten Control in NBI-Dominant H-Mode Discharges in EAST Tokamak

L. Zhang¹, S. Morita^{2,3}, X. D. Yang¹, Z. Xu¹, X. Z. Gong¹, M. H. Li¹, Y. M. Duan¹, Y. Y. Li¹,
Y. W. Sun¹, J. Huang¹, F. Ding¹, L. Wang¹, Y. Liu¹, Q. Zang¹, H. Q. Liu¹, G. S. Xu¹,
Z. W. Wu¹, H. Y. Guo^{1,4}, C. D. Hu¹, J. L. Chen¹, L. Q. Hu¹, Y. F. Liang^{1,5}, and X. D. Zhang¹

The EAST Team

¹*Institute of Plasma Physics, Chinese Academy of Sciences, Hefei, Anhui, People's Republic of China*

²*National Institute for Fusion Science (NIFS), Toki, Gifu, Japan*

³*Department of Fusion Science, Graduate University for Advanced Studies (SOKENDAI), Toki, Gifu, Japan*

⁴*General Atomics, San Diego, CA 92186, USA*

⁵*Institute of Energy and Climate Research, Forschungszentrum Jülich, Jülich, Germany*

Corresponding Author: L. Zhang, zhangling@ipp.ac.cn

In EAST tokamak, H-mode discharges have been obtained without a basic change at various heating conditions after installation of tungsten monoblocks at upper divertor. Recently, a reproducible long pulse H-mode operation with sufficient tungsten suppression has succeeded for both electron cyclotron resonance and lower-hybrid wave heated discharges and various experimental approaches are also attempted for the tungsten suppression. In discharges dominantly heated by NBI, however, the long pulse H-mode operation has been often restricted by appearance of the tungsten accumulation. Therefore, an exploration of experimental scenarios capable of avoiding the tungsten accumulation is urgently necessary for achievement of the long pulse H-mode discharge with NBI heated high-performance plasma. In the present work, control of the tungsten accumulation in the H-mode discharge with NBI-dominant heating is studied in EAST by measuring tungsten spectra and those radial profiles in extreme ultraviolet (EUV) range at 2–50 nm.

In order to control the tungsten accumulation in NBI H-mode discharges, experiments have been done by superimposing the LHW heating. One of the experiments is carried out by changing the 4.6 GHz LHW power intermittently injected in the NBI H-mode discharge. When the LHW pulse is switched on, plasma particles immediately start to pump out. The tungsten concentration is largely reduced in the plasma core, while the tungsten concentration in the plasma outer region does not change so much. Similar behaviour is also observed in the radiation loss. In addition, two-dimensional radiation distribution show that the tungsten accumulates at a very narrow region in plasma core ($\rho < 0.2$) during the NBI phase and considerably flattens during the LHW pulse. These results clearly indicate a change in the tungsten transport in the NBI H-mode discharge. A series of experiments are completed by changing the LHW injection power in the NBI H-mode discharge. As a result, a sufficiently reduced tungsten concentration is obtained at $P_{\text{LHW}}/P_{\text{NBI}} \sim 1.0$, e.g., by an order of magnitude. The beneficial role of LHW injection observed for the first time in EAST is very similar to results of on-axis ECRH and ICRH in ASDEX-U and JET. The tungsten transport in the present experiment is being analyzed with a simulation code.

A Promising Grassy ELM Regime for High-Performance Steady-State Operations with Metal Wall in EAST and CFETR

G. S. Xu¹, Q. Q. Yang¹, N. Yan¹, Y. F. Wang¹, X. Q. Xu², H. Y. Guo³, R. Maingi⁴, and B. N. Wan¹

¹*Institute of Plasma Physics, Chinese Academy of Sciences, Hefei, Anhui, People's Republic of China*

²*Lawrence Livermore National Laboratory (LLNL), Livermore, CA 94550, USA*

³*General Atomics, San Diego, CA 92186, USA*

⁴*Princeton Plasma Physics Laboratory (PPPL), Princeton, NJ 08540, USA*

Corresponding Author: G. S. Xu, gsxu@ipp.ac.cn

EX A highly reproducible stationary grassy ELM regime has been achieved in the EAST superconducting tokamak with water-cooled metal wall, exhibiting good energy confinement, $H_{98}(y, 2) \sim 1.1$, strong tungsten impurity exhaust, and compatibility with low rotation, high density and fully noninductive operations. It offers thus a highly promising operational regime in EAST, potentially applicable to future steady-state tokamak fusion reactors, such as the Chinese Fusion Engineering Test Reactor (CFETR). Recent linear and nonlinear simulations using ELITE and BOUT++ codes have uncovered, for the first time, the underlying physics of this grassy ELM regime. Both grassy and type-I ELMs are triggered by the marginally unstable intermediate- n peeling-ballooning modes (PBMs). However, the radial width of the linear mode structures cannot explain the small ELM size. The nonlinear simulations indicate that the pedestal current-profile relaxation is much slower than the pressure-gradient collapse. For the type-I ELMs, the high current density and gradient can still drive the kink/peeling-dominated low- n PBMs unstable even when the pressure gradient is significantly reduced, thus the collapsing front propagates radially inward, leading to large ELMs, as observed by Lithium BES on EAST. In contrast, for grassy ELMs, the pedestal current density and gradient are inherently lower and the operational parameter space can intrinsically improve the pedestal stability against the low- n PBMs. Hence, the instabilities quickly die away when the pressure gradient is just slightly reduced, leading to small ELMs. Some important features of the EAST grassy ELM regime are expected in future steady-state reactor-level plasmas, such as the relatively lower pedestal density gradient, higher SOL density and wider pedestal at high β_p and low rotation. The desired edge density profile can be self-consistently generated by the strong cross-field particle transport driven by the high-frequency grassy ELMs. In particular, the pedestal density gradient in reactor-level plasmas could be even lower, since the plasma temperature and density at the separatrix are high so that the penetration of recycling neutrals into the pedestal is almost negligible. This may facilitate access to the grassy ELM regime in future devices, thus opening a potentially new avenue for next-step steady-state fusion development.

Leak Width in a Multicusp Field Configuration: A Revisit with a Versatile Experimental Device

M. Sharma¹, A. D. Patel¹, N. Subramanian¹, R. Ganesh¹, and P. K. Chattopadhyay¹

¹*Institute for Plasma Research (IPR), Bhat, Gandhinagar, India*

Corresponding Author: M. Sharma, meenakshee.sharma@ipr.res.in

The cusp configuration reduces the plasma losses to boundary by diverging plasma to the narrow regions where the magnetic field lines intersect the wall. The efficiency of multidipole cusp confinement depends on the plasma losses through cusp loss area, widely known as leak width. The multiline cusp plasma device (MPD) used electromagnets for plasma confinement and gives an opportunity to vary the magnetic field strength which controls the plasma loss area. We discuss the scaling of leak width with different magnetic field strength to understand its role in the particle confinement for such configurations.

EX

Effect of the Controlled Density Gradient on Equilibrium and Confinement in a Simple Toroidal Device with Two Plasma Sources

U. Kumar¹, R. Ganesh¹, K. Sathyanarayana¹, Y. C. Saxena¹, S. G. Thatipamula², and D. Raju¹

¹*Institute for Plasma Research (IPR), Bhat, Gandhinagar, India*

²*National Fusion Research Institute (NFRI), Daejeon, Republic of Korea*

Corresponding Author: U. Kumar, umeshks@ipr.res.in

A simple toroidal device (SMT) is a toroidal device in which plasma is confined by the application of toroidal and vertical magnetic field only resulting in absence of a conventional effective rotational transform. Such devices provide a simple and well diagnosable test-bed for studies related to equilibrium, fluctuations and particle confinement for tokamak edge. The device BETA at IPR is one such SMT with a plasma major radius of 45 cm and minor radius of 15 cm and a maximum toroidal field of 0.1 T. Quasi-static equilibrium in an SMT is controlled by the nature of fluctuation and flow [1, 2]. As observed in hot cathode discharges studied earlier [1, 2], density gradient provide fluctuation in the plasma and hence the instabilities [2]. Whereas radial electric field provides poloidal flow. Thus, the conditions are akin to tokamak edge. To understand experimentally the effect of the density gradient, it is desirable to be able to control the local gradient at the outboard side by an additional plasma source. To this end, a new microwave source of frequency 2.4 GHz and power about 0.5 kW has been developed [3]. Hot cathode and microwave sources are used in tandem such that the upper hybrid resonance falls at the outboard density gradient region, which in turn allows us to control the density gradient locally. The details of the experiment will be presented.

References

- [1] T. S. Goud, Thesis, Institute for Plasma Research, Gandhinagar, Gujarat, India (2012).
- [2] U. Kumar *et al.*, Phys. Plasmas, **23**, 102301 (2016).
- [3] U. Kumar *et al.*, In Preparation.

Imaging of SST-1 Plasma with LHCD Power

M. Kumar¹, P. K. Sharma¹, and V. Chaudhary¹

The LHCD Team and SST-1 Team

¹*Institute for Plasma Research (IPR), Bhat, Gandhinagar, India*

Corresponding Author: M. Kumar, mkg.ipr@gmail.com

Plasma imaging is an essential diagnostics system for any tokamak as it can provide vital information on various plasma parameters. These systems are ones of the first diagnostics installed and are fundamental not only at the start-up stage but also in subsequent operations. Such imaging systems generally consists of at least two cameras, one of which is a high speed camera and another one is slow speed camera. The first one provides study of fast processes in plasma and plasma-wall interaction. The second camera ensures video image for general plasma operation monitoring. Generally, imaging systems make it possible to monitor plasma, plasma formation and start-up: break down and ramp-up, study and observation the magnetohydrodynamic (MHD) instability-edge localized modes (ELMS), multifaceted, asymmetric radiation from the edge (MARFE), displacements study dust migration and deposition study, plasma wall interaction, plasma position control.

A tangential viewing optical imaging system is installed on SST-1. Plasma images are transferred through coherent optical imaging fibre and coupled to the CCD camera placed outside the SST-1 machine. The CCD camera used with this system operates at 30 frames/s to acquire plasma images. The data from the CCD camera is transferred through gigabit ethernet cable to an acquisition PC placed in the diagnostics laboratory. The whole system is fully automated for operation and data acquisition of the imaging data.

In this paper we present observations during LHCD power launching in the SST-1 machine. The LHCD pulse was launched into the plasma at various timea with variations in pulse length. Plasma images exhibit change in distribution of visible radiation during the interaction of LHCD with the plasma. This increase in emission may be attributed to enhancements in plasma wall interaction as the plasma moves outwards which results in an increase of plasma wall interaction. A decrease in plasma size is also observed during interactions of LHCD pulse with the plasma.

EX

Advances in Plasma-Wall Interaction Control for H-Mode Operation over 100 s with ITER-like Tungsten Divertor on EAST

L. Wang¹, F. Ding¹, Y. W. Yu¹, L. Zhang¹, R. Ding¹, G. S. Xu¹, Y. Liang^{1,2}, H. Y. Guo^{1,3}, J. S. Hu¹, G.-N. Luo¹, B. J. Xiao¹, J. B. Liu¹, Z. P. Luo¹, W. Feng¹, G. Z. Deng¹, J. C. Xu¹, K. Wu¹, B. Zhang¹, X. L. Zou⁴, Y. W. Sun¹, X. Z. Gong¹, J. Li¹, and B. N. Wan¹

The EAST Team

¹*Institute of Plasma Physics, Chinese Academy of Sciences, Hefei, Anhui, People's Republic of China*

²*Forschungszentrum Jülich, Jülich, Germany*

³*General Atomics, San Diego, CA 92186, USA*

⁴*Institut de Recherche sur la Fusion par confinement Magnétique (IRFM), Commissariat à l'énergie atomique (CEA/Cadarache), 13108 St. Paul lez Durance, France*

Corresponding Author: L. Wang, wliang@ipp.ac.cn

Managing excessively high divertor power and particle fluxes and related plasma-wall interactions (PWI) is one of the most critical issues for the steady-state operation of the EAST superconducting tokamak and future fusion devices, such as ITER and CFETR. A world record long pulse H-mode operation of 101.2 s with $H_{98} = 1.1$ and total power injection of 0.3 GJ has been successfully achieved in EAST with ITER-like top tungsten (W) divertor, which has steady-state power exhaust capability of 10 MW/m². The peak temperature of the W target of $T \approx 500^\circ\text{C}$ and a heat flux $\approx 3 \text{ MW/m}^2$ was maintained stably. Great efforts have been made to simultaneously control peak heat flux and particle/impurity exhaust towards the long pulse of 100 s time scale. Particle exhaust was optimized by preferentially directing the plasma flow toward the outer target with the ion $B \times \nabla B$ drift away from the W divertor and improving divertor pumping with the top cryo-pump. Effective power dispersal was achieved by tailoring the 3D divertor plasma footprint using lower hybrid wave (LHW) through induced edge magnetic topology change and broadened plasma wetted area, thus reducing peak heat flux and W sputtering. Extensive lithium coating was employed to lower edge recycling, low- Z impurity content and W sputtering. In addition, divertor detachment in H-mode for PWI handling was achieved for the first time with a W divertor in EAST. Compared with previous L-mode in EAST, in H-mode the detachment has a higher density threshold with $n_e/n_G \sim 0.65$. Active feedback control of radiative divertor with neon impurity seeding was successfully achieved with $f_{rad} \sim 18\text{--}36\%$, and a slight loss of plasma stored energy $\sim 7\text{--}11\%$, offering a promising technique for steady-state divertor radiation and heat flux control. The upgrade plan and status of EAST bottom divertor from graphite to water-cooled W to accommodate more challenging PWI for steady-state H-mode over 400 s and L-mode operation over 1000 s will also be presented.

Characterization of Particle Growth and Enhancement of Sputtering Yields in a Cogenerated Dusty Plasma

J. Pramanik¹, P. Patra¹, and P. Bandyopadhyay²

¹*Department of Physics, Kharagpur College, Kharagpur, India*

²*Institute for Plasma Research (IPR), Bhat, Gandhinagar, India*

Corresponding Author: J. Pramanik, jotir_moy@yahoo.com

Most of the tokamaks including ITER, a significant part of the plasma-facing component including divertors, limiters, etc is comprised with graphite material. In the fusion plasma environment, the graphite gets bombarded by hydrogen and its isotopes (deuterium and tritium) ions eroding the graphite to a significant extent. Since such carbon particles can retain large amounts of hydrogen, dust contributes to the problem of radioactive tritium inventory inside the fusion machine. Another impact of the dust particles on the fusion device operation is the possible degradation of the discharge performance. Such particles penetrating in the core plasma region can lead to discharge disruption. Thus, in order to perform successful fusion experiments it is important to assess and understand the processes by which dust is formed and by which it interacts with the fusion device and its plasma. Instead of understanding processes that exactly happen inside a fusion reactor, it is always better to match some aspects of graphite-hydrogen interaction in a plasma environment in small laboratory devices, and study the physical processes. To address some of this issues, we have performed an experiment to examine the particle growth and sputtering yields in a DC glow discharge plasma in between the graphite electrodes.

EX

A Transmission Electron Microscopy Investigation of Defects Induced in Tungsten Foils by Au and B Ion Irradiation

P. Sharma¹, S. Akkireddy², P. N. Maya¹, A. Attri¹, P. M. Raole¹, A. K. Tyagi^{2,6}, P. K. Kulriya³, P. K. Bajpai⁴, S. Mishra⁵, T. A. Trivedi⁴, K. B. Khan⁵, and S. P. Deshpande^{2,6}

¹International Thermonuclear Experimental Reactor (ITER), India Centre, Gujarat, India

²Institute for Plasma Research (IPR), Bhat, Gandhinagar, India

³Inter-University Accelerator Centre, Aruna Asaf Ali Marg, New Delhi

⁴Guru Ghasidas Vishwavidyalaya, Bilaspur, (C.G.), Koni, Chhattisgarh 495009, India

⁵Bhabha Atomic Research Centre (BARC), Mumbai, India

⁶Homi Bhabha National Institute (HBNI), Anushakti Nagar, Mumbai 400094, India

Corresponding Author: P. Sharma, prashanttopquark@gmail.com

Tungsten is a promising candidate for first-wall material in fusion reactors and its use as a plasma-facing material is being investigated in both tokamaks as well as laboratory experiments [1, 2]. In fusion environment tungsten will be exposed to neutron, helium and hydrogen isotope implantation along with the heat flux which will lead to material damage. Irradiation by charged particles such as H, D, T, He, Au, W etc., is employed to surrogate the experiment of high energy and high flux neutron irradiation in tungsten.

EX

The present work concerns the study of ion mass in meso-scale defects created in tungsten using transmission electron microscopy (TEM) after irradiated by: 1) high energy heavy mass gold (Au of 80 MeV); and 2) low mass boron (B of 10 MeV) ions with a fluence of $1.3 \times 10^{14}/\text{cm}^2$. Prior to irradiation tungsten foil samples of 100 μm thickness (99.96% pure), procured from Princeton Scientific corp. USA, and were recrystallized at 1838K under 10^{-3} mbar base pressure in 200 mbar Ar+8% H₂ environment. Defects created by Au and B ions irradiation in the recrystallized foil were characterized for the types of defect such as defect clusters, dislocation lines, loops etc., and are quantified in terms of dislocation line length, dislocation loop size and their densities using transmission electron microscopy. The small defect clusters in Au irradiated samples and dislocations segments and dislocation loops were observed in B irradiated samples. Furthermore, the Au ion irradiation has led to the formation of dislocation lines density lesser than that of B irradiated foil.

References

- [1] E. E. Bloom, Nucl. Fus., **30**, 1879–1896 (1990).
- [2] M. Rubel, Trans. Fus. Sci. Tech., **53**, 459–467 (2008).

Modelling Studies of X-Divertor Configuration on SST-1 Tokamak Using SOLPS5.1

M. Himabindu¹, A. K. Tyagi¹, Deepti Sharma¹, Devendra Sharma¹, R. Srinivasan¹, Z. P. Chen², and S. M. Mahajan²

¹*Institute for Plasma Research (IPR), Bhat, Gandhinagar, India*

²*Institute for Fusion Studies (IFS), University of Texas at Austin, Austin, TX 78712, USA*

Corresponding Author: M. Himabindu, mbindu@ipr.res.in

To solve the challenging problem of heat removal in a tokamak based fusion reactor, several advanced divertor configurations have been proposed and studied. We present here the results of our studies of one of the more promising configurations, the X-divertor, conducted for the parameters of the Indian tokamak SST-1. Using the equilibrium code CORSICA, we develop the appropriate magnetic geometry and then study its performance using the scrape-off layer plasma transport code package SOLPS5.1/B2.5-EIRENE. One of the main motivation was to find out if the X-divertor (XD) could boost the heat handling capacity as compared to the standard divertor (SD) configuration for SST-1 that designed to handle 1 MW of total input power. In order to compare the performance XD with the existing SD, we first ensured the core equivalence of both configurations. An additional poloidal field coil was placed behind the divertor target to produce XD configuration. The plasma equilibrium for SD and XD are generated. The divertor index (DI) is varied from 2 to 13. For a plasma operation with $P = 1$ MW input power and plasma edge density $n_e = 1 \times 10^{19}/\text{m}^3$, the peak heat load on the target plates in the X-divertor configuration has reduced by 50% as compared to standard divertor; the heat flux profile near the separatrix was also broadened due to flaring of field lines. The latter increases the plasma-wetted area at the targets. This is a preliminary demonstration that XD will allow SST-1 to operate at higher input power.

EX

Experimental Study of Multiscale Interaction between (Intermediate, Small)-Scale Microturbulence and MHD Modes in EAST Plasmas

P. J. Sun¹, Y. D. Li¹, Y. Ren², X. D. Zhang¹, G. J. Wu¹, L. Q. Xu¹, R. Chen¹, Q. Li³, H. L. Zhao¹, J. Z. Zhang¹, T. H. Shi¹, H. Q. Liu¹, Y. M. Wang¹, B. Lyu¹, L. Q. Hu¹, and J. Li¹

The EAST Team

¹*Institute of Plasma Physics, Chinese Academy of Sciences, Hefei, Anhui, People's Republic of China*

²*Princeton Plasma Physics Laboratory (PPPL), Princeton, NJ 08540, USA*

³*Guangdong University of Technology, Guangzhou 510006, People's Republic of China*

Corresponding Author: P. J. Sun, sunpj@ipp.cas.cn

Understanding plasma transport in phases with significant MHD activities (especially during plasma current ramp-up/down and disruption) in tokamak plasmas is crucial for predicting and thus controlling plasma behaviour for future fusion devices, e.g., ITER. Since microturbulence plays an important role in driving anomalous plasma transport, the interactions between MHD modes and microturbulence is thought to be important in determining anomalous plasma transport [1]. Recent theoretical results in the literature show that microturbulence can nonlinearly interact with macro-instabilities such as kink/tearing mode through nonlinear cascade process or through temperature and/or density profile modulation from macro-instabilities. Due to the huge temporal and spatial scale separation between microturbulence and MHD modes, it is impossible for present-day supercomputers to simulate their nonlinear interactions in a self-consistent way. In this talk, we present evidence of multiscale interactions between (intermediate, small)-scale ($k\rho_i \sim 2-6$) microturbulence and MHD modes in EAST plasmas, including the first experimental identification of nonlinear coupling between microturbulence and an MHD mode during the current ramp-down phase in a set of L-mode plasmas in EAST [2] and the effects of 2/1 classical tearing mode on microturbulence [3] in the core of another set of EAST L-mode plasmas using the EAST CO₂ laser collective scattering diagnostic in forward mode and far-forward mode. We demonstrate the nonlinear coupling between microturbulence and MHD mode with bispectral analysis [4] and envelope method, showing statistically significant bicoherence and modulated turbulent density fluctuation amplitudes correlated with the MHD mode. We also show that microturbulence spectral power is correlated to the 2/1 tearing mode and modulation effects on microturbulence by the 2/1 tearing mode.

Work supported by the National Natural Science Foundation of China with Contracts Nos. 11475222, 11505228, 11735016, 11575238.

References

- [1] P. J. Sun *et al.*, Nucl. Fus., **58**, 016003 (2018).
- [2] P. J. Sun *et al.*, Plasma Phys. Contr. F., **60**, 025019 (2018).
- [3] Y. C. Kim and E. J. Powers, IEEE Trans. Plasma Sci., **PS-7**, 120 (1979).
- [4] Y. Nagashima *et al.*, Phys. Rev. Lett., **95**, 095002 (2005).

Effect of Cathode Geometry on Magnetically Coupled Hollow Cathode Plasma Source

M. P. Bhuva¹, S. K. Karkari¹, and S. Kumar¹

¹*Institute for Plasma Research (IPR), Bhat, Gandhinagar, India*

Corresponding Author: M. P. Bhuva, montubhuva@yahoo.in

A direct current (DC) plasma source consisting of hollow cathode geometry and a constricted anode is presented. The effect of a hollow cathode geometry on radial density distribution of a magnetized plasma column has been studied in a low-pressure (approximately 1.4 Pa) argon discharge. The plasma column is characterized using Langmuir probe and the radial density distribution for two different “inside” profiles of a hollow cathode is discussed. Probe measurement indicates that a conical-profile hollow cathode produces a plasma column with centrally peaked plasma density whereas a cylindrical-profile hollow cathode forms plasma column with off-centred density peak. Thus overall dynamics of perpendicular and oblique cathode sheaths behind the sustenance of magnetized plasma column has been discussed.

EX

Kink Mode Study in EAST High- β_P Plasma

L. Xu¹, Y. Yuan¹, L. Hu¹, and W. Shen¹

¹*Institute of Plasma Physics, Chinese Academy of Sciences, Hefei, Anhui, People's Republic of China*

Corresponding Author: L. Xu, lqxu@ipp.cas.cn

Two types of kink modes, fishbone and long-lived mode are experimentally and numerically studied at EAST tokamak. In high- β_P plasma, sawtooth instability was replaced by a saturated 1/1 internal kink mode which either manifests itself as a periodical burst energetic ion related fishbone or as a long-lived mode which is associated to the core safety factor at $q_0 \sim 1$. The present of those 1/1 internal modes are beneficial for sustaining the hybrid scenario with extended regions of low-magnetic shear profile and $q_0 \sim 1$, because of that they can expel high- Z impurity and can make flux pumping. The mechanism responsible for the flux pumping caused by kink mode was numerically in nonlinear 3D magnetohydrodynamic simulations using the M3D code. Furthermore, M3D+K code hybrid simulation shows a good agreement to the fishbone activity in EAST.

Fast-Ion Studies in High Performance Fully Noninductive Discharges on EAST

J. Huang¹, J. Chang¹, J. Zhang¹, S. Ding¹, H. Du¹, J. Qian¹, X. Gong¹, G. Zhong¹, M. Xiao¹, J. Wang¹, H. Liu¹, B. Lyu¹, Q. Zang¹, and B. N. Wan¹

The EAST Team

¹*Institute of Plasma Physics, Chinese Academy of Sciences, Hefei, Anhui, People's Republic of China*

Corresponding Author: J. Huang, juan.huang@ipp.ac.cn

On the EAST tokamak, 100 s steady-state H-mode ($H_{98}(y, 2) \sim 1.1$) discharge has been achieved by RF-only (LHW+ECRH+ICRH) heating with improvement of the auxiliary heating and current drive systems on actively cooled ITER-like mono-block tungsten divertor. Towards EAST high performance advanced state-steady operation regimes, fast-ion related physical issues become crucial for achieving EAST scientific objectives with both co- I_p and counter- I_p neutral beam injections. Accordingly, EAST several complementary fast-ion measurements have been developed and validated, e.g., fast-ion D- α (FIDA), fast-ion loss detectors (FILDs), neutral particle analysers (NPA), neutron spectrometers and TOFED, etc. In recent experiments, compared with RF-only discharge, NBI and RF plasmas has a higher β_p and $H_{98}(y, 2)$, although the bootstrap current fraction f_{BS} is nearly the same, TRANSP analysis shows that it is mostly due to fast ions, and fast ions do not contribute significantly to f_{BS} . To obtain high performance plasma and improve confinement and transport on EAST, key related parameters (e.g., density, plasma current, beam energy, etc.) need further optimization to reduce the fast ion slowing down time and prompt loss. To investigate fast-ion distribution function and prompt loss, different beam voltage and plasma current are investigated as well. Experimental results show that prompt loss from counter beams is large and can be reduced by reducing beam voltage and increasing plasma current, which is consistent with simulations. The relationship of the fast ion loss and distribution to the different beam settings and plasma parameters will be reported in this paper, which is very helpful to understand energetic particle physics in long pulse H-mode plasmas on EAST and contributes to ITER.

EX

Progress Towards Development of Long Pulse ITER Operation through RF Heated H-Mode Experiments on EAST and HL-2A

A. Ekedahl¹, X. Z. Gong², X. Y. Bai³, L. Delpech¹, B. J. Ding², X. R. Duan³, M. Goniche¹, J. Hillairet¹, G. T. Hoang¹, M. H. Li², Y. C. Li², B. Lu³, D. Mazon¹, D. Moreau¹, Y. Peysson¹, J. P. Qian², S. D. Song³, X. M. Song³, G. Urbanczyk¹, B. N. Wan², G. L. Xiao³, M. Xu³, X. D. Yang², L. Zhang², Y. P. Zhang³, W. L. Zhong³, X. L. Zou¹, R. Cesario⁴, and A. A. Tuccillo⁴

The EAST Team and HL-2A Team

¹*Institut de Recherche sur la Fusion par confinement Magnétique (IRFM),*

Commissariat à l'énergie atomique (CEA/Cadarache), 13108 St. Paul lez Durance, France

²*Institute of Plasma Physics, Chinese Academy of Sciences, Hefei, Anhui, People's Republic of China*

³*Southwestern Institute of Physics, Chengdu, Sichuan, People's Republic of China*

⁴*ENEA C. R. Frascati, Dipartimento FSN, Frascati, Italy*

Corresponding Author: A. Ekedahl, annika.ekedahl@cea.fr

Recent long pulse experiments in EAST have resulted in a new world record of 100 s long H-mode discharge, sustained by the radiofrequency (RF) systems, predominantly lower hybrid current drive (LHCD). In parallel, experiments in HL-2A have demonstrated successful L-H wave coupling in H-mode plasmas with an ITER-relevant passive-active multijunction (PAM) LHCD launcher. These two achievements, obtained as a part of the specific EU-China collaboration, show the viability of LHCD as a successful method for heating and current drive in high performance H-mode plasmas.

Experimental comparison of the two LHCD systems in EAST shows that the current drive efficiency is higher for the 4.6 GHz system than for the 2.45 GHz system. Higher power was therefore systematically used on the 4.6 GHz launcher in the long pulse experiments. Increasing the radial distance between the plasma and the launchers (up to 8 cm) was employed as method to optimizing the density in front of the launchers and to avoiding hot spots during the long H-modes. Lithium evaporation showed to have a beneficial effect on the L-H current drive efficiency. An increase in efficiency from $\eta = 0.8 \times 10^{19} \text{ A/W}\cdot\text{m}^2$ to $1.1 \times 10^{19} \text{ A/W}\cdot\text{m}^2$ was observed when the accumulated Li in the EAST vessel was above 150 g. Good agreement between experimental results and simulations with C3PO/LUKE is obtained for EAST fully noninductive discharges. C3PO/LUKE can well reproduce the experimental values of the internal inductance, as well as the noninductive current profile obtained from equilibrium reconstruction constrained by interfero-polarimetry.

In HL-2A, a 3.7 GHz LHCD system with four klystrons and an ITER-relevant PAM launcher has been successfully brought into operation and used in H-mode experiments. Coupling of L-H waves in ELMy plasmas has thus been demonstrated with an ITER-relevant launcher for the first time. The maximum coupled L-H power has reached 1 MW in L-mode and 0.9 MW in H-mode. H-modes were triggered and sustained with LHCD together with $\sim 700 \text{ kW}$ NBI power. In H-modes with $n_e > 2.5 \times 10^{19}/\text{m}^3$, a reduction in ELM amplitude and increase in ELM frequency were observed for injected L-H power $> 300 \text{ kW}$. The divertor peak heat load released by the ELMs was strongly reduced during this phase, which suggests that the L-H power can be used for controlling ELMs.

Observations of Plasma Stimulated Electrostatic Sideband Emission and Harmonic Distortion: Evidence of Overdense Plasma Generation Inside a Microwave Discharge Ion Source

C. Mallick¹, M. Bandyopadhyay², and R. Kumar¹

¹*Institute for Plasma Research (IPR), Bhat, Gandhinagar, India*

²*International Thermonuclear Experimental Reactor (ITER), India Centre, Gujarat, India*

Corresponding Author: C. Mallick, chinmoy.mallick@ipr.res.in

Microwave discharge ion source (MDIS) is used in many applications including accelerators based neutron generators on suitable target through DD or DT fusion. The electromagnetic (EM) pump wave (ω_0) can propagate beyond cut off plasma density by changing its polarity and/or decomposing into different daughter waves through which it transfer its energy thus producing overdense plasma. The role of the electric field on power coupling through different decay channels during the density jump from underdense to overdense is obtained by theoretical modelling. This is validated with experimentally obtained spectral features in the ion plasma frequency range. In the present experiment, the plasma stimulated emission spectra was measured in the frequency range $0.5\omega_0$ to $3\omega_0$ to understand the different probable energy decay channels role; e.g., electron Bernstein waves (EBWs), ion cyclotron waves (ICWs), lower hybrid oscillations (LHOs), ion Bernstein waves (IBWs) and ion Acoustic Waves (IAWs), etc. The energy decays through different ion-type waves by parametric instability is studied by observing the different side-bands generation around the pump frequency and also the electron cyclotron (EC) harmonic frequencies. The intensity and growth rate of IAWs/ICWs and harmonics (up to 3rd) from parametrically decayed ordinary (O) mode pump wave was used to get an estimate of electric field and localized electron temperature. The density threshold of each electrostatic IAWs/ICWs was measured by stepping pump wave amplitude and external magnetic field. The IAWs lines appear at lower density threshold than the ICWs emission lines. The measured IAWs and ICWs ranges from 317–397 kHz and 410–555 kHz respectively with a density jump from $9.3 \times 10^{16}/\text{m}^3$ to $4.9 \times 10^{17}/\text{m}^3$. At higher density ($> 3.3 \times 10^{17}/\text{m}^3$), the electrostatic ICWs lines dominates the IAWs thereby yielding negligible damping through ion waves.

EX

Radial Characteristics of a Magnetized Plasma Column

S. Das^{1,2}, S. K. Karkari^{1,2}

¹*Institute for Plasma Research (IPR), Bhat, Gandhinagar, India*

²*Homi Bhabha National Institute (HBNI), Anushakti Nagar, Mumbai 400094, India*

Corresponding Author: S. Das, satadal.das@ipr.res.in

The cross-field transport of electrons/ions across magnetic field is fundamentally important as it determines the characteristics of plasma wetted area in the scrape of layer region and particle confinement in magnetically confined plasma devices. The electrically biased objects in the edge region inside tokamaks as well as in linear plasma devices are known to influence the dynamics of charge particles. The external electrodes in the magnetized column can introduce long range electric fields in the plasma column. This leads to either excitation or suppression of the instabilities responsible for such transport.

In this paper we present experimental results on radial plasma characteristics obtained of a cylindrical plasma column produced in a linear device. The magnetized plasma column at one end is terminated with conducting electrodes which are deliberately biased with respect to the plasma. The nature of the long range perturbation during application of electric bias on the electrodes have been investigated using electric probes and its impact on the radial characteristics have been qualitatively explained.

EX

Investigations on Temperature Fluctuations and Energy Transport in ETG Dominated Large Laboratory Plasma

P. Srivastav¹, R. Singh¹, L. M. Awasthi¹, A. K. Sanyasi¹, P. K. Srivastava¹, R. Sugandhi¹, and R. Singh²

¹*Institute for Plasma Research (IPR), Bhat, Gandhinagar, India*

²*International Thermonuclear Experimental Reactor (ITER), India Centre, Gujarat, India*

Corresponding Author: P. Srivastav, prabhakar.srivastav@ipr.res.in

Extensive measurements are carried out on microturbulence because of their possible role in causing anomalous particle and energy transport in fusion devices. Outcome from past investigations suggest that the electron temperature gradient (ETG) driven turbulence is considered presently as a major source of anomalous plasma transport in fusion devices, as transport by ion scale turbulence is largely understood. Direct measurement of ETG is extremely difficult in fusion devices because of its extremely small scale length ($\sim \mu\text{m}$). In this background, efforts were made in large volume plasma device (LVPD), to produce plasma suitable for carrying out investigations on ETG turbulence ($\sim \text{mm}$). Introduction of electron energy filter (EEF) divides LVPD plasma into three distinct regions of source, EEF and target plasmas. In the core region of target plasma ($x \leq 45 \text{ cm}$), unambiguous, identification of ETG turbulence is successfully demonstrated.

Simultaneous measurement of fluctuations in electron temperature (10%–30%), plasma density (5%–10%) and potential (0.5%–2.5%) are carried out. Particle and energy transport are estimated from $\langle \tilde{n}_e \tilde{E}_\theta \rangle$ and $\langle \tilde{T}_e \tilde{E}_\theta \rangle$ correlations. It was observed that electrostatic particle transport agrees well with theoretical estimates while, electromagnetic particle flux satisfies the relationship $\Gamma_{es} \sim 10^{-5} \times \Gamma_{em}$. Strong negative correlation is observed between fluctuations of density and temperature with potential fluctuations, showing correlation coefficients, $C_{\tilde{n}_e, \tilde{\phi}} \sim -0.8$ and $C_{\tilde{T}_e, \tilde{\phi}} \sim -0.7$ respectively. This paper will present results on work carried out for energy transport due to ETG turbulence. Details on adopted diagnostic methods, for accurate measurement of temperature fluctuations will also be presented. A comparison will be made of experimentally derived energy transport with theoretically estimated values.

EX

Preliminary Results of Wall Conditioning Experiments Using High Power ICRH System on SST-1 at Different Toroidal Magnetic Fields

D. Rathi¹, S. V. Kulkarni¹, K. K. Mishra¹, A. D. Varia¹, S. Kumar¹, S. K. Gupta¹, G. Ashok¹, H. M. Jadav¹, Y. S. S. Srinivas¹, R. Joshi¹, B. Kadia¹, K. M. Parmar¹, D. C. Raval¹, D. Raju¹, M. K. Gupta¹, and R. Manchanda¹

The ICRH Team and SST-1 Team

¹*Institute for Plasma Research (IPR), Bhat, Gandhinagar, India*

Corresponding Author: D. Rathi, drathi@ipr.res.in

Proper wall conditioning has turned out to be an essential element for achieving the highest possible plasma performance in present-day fusion devices. The main issues are controlling the generation of plasma impurities, liberated by plasma-surface interactions. Superconducting fusion machines need efficient wall conditioning techniques for routine operation in between shots in the presence of high toroidal magnetic field for wall cleaning to control the in-vessel impurities. Ion cyclotron wall conditioning (ICWC) is fully compatible with steady-state tokamak in presence of magnetic field.

EX

Here we report the preliminary results of ICRF wall conditioning experiments done on Steady State Superconducting Tokamak (SST-1) using the high power ion cyclotron resonance and heating (ICRH) system indigenously developed including MW RF generator, transmission line with matching system, vacuum transmission line (VTL) and fast wave poloidal antenna with Faraday shield.

In the first stage, the experiments are conducted to condition the complete system and antenna by introducing low power RF pulses in the SST-1 machine. It is observed that the conditioning pulse removes gas species from antenna and VTL. In the second stage, the wall conditioning experiments are conducted at 0.2–0.4 T and in third stage the wall conditioning experiments are conducted at 1.5 T in helium gas. The diagnostics used are the visible camera, spectroscopy, residual gas analyser (RGA), etc. More than 600 RF pulses of 150 kW with 0.5 s on time and 0.8 s off time were introduced and significant impurity generation is observed from antenna and vacuum vessel. It is observed that RF conditioning at low pressure releases H₂ and other gas species.

The previous ICWC experiments done on ADITYA tokamak show that in presence of toroidal magnetic field (0.45 T) conditions as well as with 20% helium gas in a hydrogen plasma is found more effective in releasing wall impurities like water and methane as half an order (~ 5) of initial vacuum condition.

The preliminary results on SST-1 show that the ICWC in the presence of magnetic field seems to be effective and can be used an alternative method for vessel wall conditioning. In this paper, the above-mentioned experiments and results will be discussed.

Recent Finding in Fusion Studies Using Table Top and Miniaturized Dense Plasma Focus Devices Operating from Hundred Joules to less than One Joule

L. Soto^{1,2}, C. Pavéz^{1,2}, G. Avaria^{1,2}, J. Moreno^{1,2}, J. Jain², J. Pedreros², A. Sepulveda^{2,3}, B. Bora^{1,2}, and S. Davis^{1,2}

¹Comisión Chilena de Energía Nuclear (CCHEN), Casilla 188-D, Santiago, Chile

²Center for Research and Applications in Plasma Physics and Pulsed Power, P⁴, Santiago, Chile

³Universidad Mayor, Santiago, Chile

Corresponding Author: L. Soto, leopoldo.soto@cchen.cl

In a dense plasma focus (DPF) the plasma is compressed into a hot-warm dense pinch. Since 50 years ago and during the first three decades the dense plasma focus (DPF) was studied as a possible device to produce dense transient plasmas for fusion research. The trend was to produce bigger devices over MJ stored energy and MA current through the plasma pinch, in order to increase the efficiency of fusion neutron production. Unfortunately, the neutron production suffers saturation in devices operating at MA. Alternatively, in our group we have been studying how to scale a dense plasma focus to very low operation energy, keeping the nuclear fusion reactions and neutron emission. Several dense plasma focus devices under a kJ of stored energy (400 J, 50 J, 2 J, and 0.1 J) were designed and constructed in our laboratory. In all of them, nuclear fusion reactions are obtained. In fact, we recently reported the evidence of nuclear fusion in a plasma focus operating in deuterium at only 0.1 J. Despite the limitation that these devices are far from net energy production, these studies have contributed the knowledge that it is possible to scale the plasma focus in a wide range of energies and sizes keeping the same value of ion density, magnetic field, plasma sheath velocity, Alfvén speed and temperature. However, the plasma stability depends on the size and energy of the device.

Recent findings related to nuclear fusion studies are presented, including: a) evidence of nuclear fusion in an ultraminiaturized plasma focus operating at 0.1 J; b) observations of plasma filaments and its role in the neutron emission; c) characterization of the plasma ejected after the pinch in table top and small DPF devices (50 J, 400 J and 900 J) and their use to study the effects on materials relevant to the first wall of fusion reactors; and d) studies of the plasma interaction with a target material on front of the anode using digital optical refractive diagnostics and visible spectroscopy. In addition, how to increase the current in the pinch plasma, increasing the number of fusion nuclear reactions and neutron production, in a regime of enhanced stability is discussed.

Supported by ACT-172101 CONICYT and FONDECYT 1151471 Chile grants.

Model-Predictive Kinetic Control for Steady State Plasma Operation Scenarios on EAST

D. Moreau¹, J. P. Qian², J.-F. Artaud¹, S. Ding², H. F. Du², M. Li², Z. Luo², E. Olofsson³, B. S. Sammulu³, S. Wang⁴, E. Witrant⁴, and Q. Yuan²

¹*Institut de Recherche sur la Fusion par confinement Magnétique (IRFM),*

Commissariat à l'énergie atomique (CEA/Cadarache), 13108 St. Paul lez Durance, France

²*Institute of Plasma Physics, Chinese Academy of Sciences, Hefei, Anhui, People's Republic of China*

³*General Atomics, San Diego, CA 92186, USA*

⁴*University Grenoble Alpes, CNRS, GIPSA-lab, 38000 Grenoble, France*

Corresponding Author: D. Moreau, didier.moreau@cea.fr

Robust model-predictive control (MPC) algorithms based on extremely simple linear data-driven models have been recently developed for plasma kinetic control on EAST. This paper shows, for the first time, that MPC can be performed using a two-time-scale approximation, considering the kinetic plasma dynamics as a singular perturbation of a quasi-static magnetic equilibrium, which itself is governed by the flux diffusion equation. This technique takes advantage of the large ratio between the time scales involved in magnetic and kinetic transport, and is applied here to the simultaneous control of the safety factor profile, $q(x)$, and of the poloidal β parameter, β_p , on EAST. MPC results in a much faster and more robust control than the so-called near-optimal control algorithms that were tested previously [1]. The models are state-space models identified with datasets obtained from fast nonlinear METIS simulations (METIS includes an MHD equilibrium and current diffusion solver, and combines 0D scaling laws and ordinary differential equations). For a given operation scenario, the identified model is augmented with an output disturbance model, which is used to estimate the mismatch between measured and predicted outputs and ensures robustness to model uncertainties. An observer provides, in real-time, an estimate of the system states and disturbances, and the controller predicts the behaviour of the system over a prediction horizon, taking the actuator constraints into account. For plasma parameters typical of the high- β_p steady state operation scenarios on EAST, nonlinear closed-loop simulations show that the desired $q(x)$ profiles and β_p can be obtained in about 2.5 s and 0.5 s, respectively, and with a monotonic approach to their target values. This is essential for avoiding MHD instabilities during the build up of the plasma equilibrium. In these control simulations, the actuators are the LHCD system at 4.6 GHz, the ICRH system, and optionally the plasma surface loop voltage. Various examples are shown, with negative shear or monotonic q -profiles, and with different β_p target waveforms. The actuators adjust in order to reach the various β_p targets while maintaining the q -profile in steady state, with the desired shape (or as close as possible if the $q(x)$ and β_p targets are not achievable).

References

[1] D. Moreau, *et al.*, Nucl. Fus., **55**, 063011 (2015).

Simulation Study of Heat Transport with On-Off Axis ICRH in Thailand Tokamak Using BALDUR Code

J. Promping¹, B. Chatthong², A. Wisitsorasak³, S. Sangaroon⁴, P. Klaywittaphat⁵,
R. Picha¹, and T. Onjun¹

¹*Thailand Institute of Nuclear Technology, Bangkok, Thailand*

²*Department of Physics, Prince of Songkla University, Songkla, Thailand*

³*Department of Physics, King Mongkut University of Technology Thonburi, Bangkok, Thailand*

⁴*Department of Physics, Mahasarakham University, Mahasarakham, Thailand*

⁵*Faculty of Engineering, Thaksin University, Phatthalung, Thailand*

Corresponding Author: J. Promping, jirapornp@tint.or.th

We report on the self-consistent simulations of plasma in a proposed tokamak design of Thailand Tokamak ($R = 65$ cm, $a = 20$ cm, $I_p = 100$ kA, $B_t = 1.5$ T) are carried out using the 1.5D BALDUR integrated predictive modelling code. The simulations are used to investigate plasma transport with on- and off-axis positions of ion cyclotron resonance heating (ICRH) in the range of 0.3–5 MW. The core transport is predicted using the combination of multimode (MMM95) or mixed Bohm/gyro-Bohm (mixed B/gB) anomalous core transport model and NCLASS neoclassical transport models. It is found that the electron temperatures obtained from both simulations are in the range of 0.3–1 keV, which agree with the HT-6M experimental results. When the ICRH is applied, ion and electron thermal transport increase. Consequently, ion and electron temperature and plasma stored energy increase. During ICRH for both MMM95 and mixed B/gB model, the electron temperature at the centre, T_{e0} ranges from 1 to 1.5 keV with on axis and from 1 to 1.9 keV with off axis. The ion temperature at the centre, T_{i0} , ranges from 0.7 to 25 keV with on axis and 50 eV to 7 keV with off axis.

EX

Fluctuation Suppression by the Potential Formation in GAMMA 10/PDX Plasma

M. Yoshikawa¹, J. Kohagura¹, R. Ikezoe¹, M. Sakamoto¹, N. Ezumi¹, R. Minami¹,
M. Ichimura¹, T. Imai¹, K. Nojiri¹, A. Terakado¹, S. Jang¹, and Y. Nakashima¹

¹Plasma Research Center, University of Tsukuba, Tsukuba, Ibaraki, Japan

Corresponding Author: M. Yoshikawa, yosikawa@prc.tsukuba.ac.jp

In the hot ion mode experiments of the tandem mirror GAMMA 10/PDX plasma, the suppression of drift-type fluctuation, which rotate in the direction of the electron diamagnetic drift, has been observed when the axial confinement potential is formed by the electron cyclotron heating (ECH) at the barrier (B) and plug (P) cells. The flute-type fluctuation of which rotation direction is the same as ion diamagnetic rotation direction was also suppressed with application of both B/P-ECH for the first time. The suppression seems to be caused by $E \times B$ drift shear, which is common in magnetically confined fusion plasmas.

Fluctuation study is one of the most important issues in magnetically confined fusion plasmas, because the fluctuations due to the instabilities cause the anomalous transports. The drift-type fluctuation arises due to the existence of density and temperature gradients. The radial electric field E causes an $E \times B$ plasma rotation in the direction of the ion diamagnetic rotation, which may enhance instabilities such as rotational flute modes, and degrade radial confinement. In the tandem mirror GAMMA 10/PDX, the main plasma is produced and heated by ion cyclotron range of frequency (ICRF) waves, and an electrostatic potential for improving an axial confinement is created by applying electron cyclotron resonance heating (ECH) in the end mirrors of barrier/plug (B/P) cells. The plasma confinement is improved not only by a magnetic mirror configuration but also by high potentials at both end mirrors. The typical electron density, electron and ion temperatures are about $2 \times 10^{18}/\text{m}^3$, 0.1 keV and 5 keV, respectively. We often observed flute-type fluctuations and they seem to be related to $E \times B$ drift. In order to clarify the $E \times B$ drift effects on flute-type fluctuations, we optimized the diameters of iris-limiters, fuelling gas pressures, and ICRF heating powers to produce the rotational flute-type fluctuation before B/P-ECH. The central potential quickly increased and the observed fluctuations on the line density and potential were clearly suppressed by the application of B/P-ECH. Potential and density fluctuations suppressions with the application of B/P-ECH were clearly observed at each radial position. Low frequency flute-type fluctuations in the density and potential were suppressed with applying B/P-ECH for the first time.

EX

Effect of Magnetic Field Structure on Electron Internal Transport Barrier and its Role for the Barrier Formation in Heliotron J

T. Minami¹, N. Kenmochi², A. Ishizawa³, K. Nishioka⁴, G. Weir⁵, C. Takahashi¹, S. Kobayashi¹, Y. Nakamura³, H. Okada¹, S. Kado¹, S. Yamamoto¹, S. Ohshima³, S. Konoshima¹, K. Nagasaki¹, and T. Mizuuchi¹

¹*Institute of Advanced Energy, Kyoto University, Nishikyo-ku, Kyoto 615-8540, Japan*

²*Graduate School of Frontier Science, University of Tokyo, Tokyo, Japan*

³*Graduate School of Energy Science, Kyoto University, Nishikyo-ku, Kyoto 615-8540, Japan*

⁴*Theoretical Plasma Physics Laboratory, Nagoya University, Nagoya, Japan*

⁵*Max-Planck-Institut für Plasmaphysik, Greifswald, Germany*

Corresponding Author: T. Minami, minami@iae.kyoto-u.ac.jp

The effects of magnetic field topology on an electron internal transport barrier (eITB) and on its formation in the helical plasma are discussed in this paper. In helical plasmas, the eITB can be formed by generation of the positive radial electric field with electron cyclotron resonance heating due to the electron-root transition that is related to the neoclassical transport through the helical ripple. A hypothesis of the eITB formation is that the barrier is easily formed in larger helical ripple (ε_{eff}) magnetic configuration. In Heliotron J, however, although the high and low bumpiness configurations have higher ε_{eff} compared to the medium bumpiness configuration, the power thresholds to form the eITB in the low and high bumpiness configurations are larger ($\sim 550 \times 10^{-19} \text{ kWm}^3$) than that of the medium bumpiness ($\sim 250 \times 10^{-19} \text{ kWm}^3$). This result shows that the eITB formation is not determined by ε_{eff} alone. Next, we have investigated the effect of the magnetic topology on the eITB formation. The first result is that the correlated behaviours of the eITB foot point and the low-order rational surface location are observed. The former shows a jump at $I_p \sim 0.7 \text{ kA}$ and a subsequent outward shift by the current increase. The estimated 4/7 rational surface appears at the value of $\sim 0.7 \text{ kA}$, then it moves outward with the increase of the bootstrap current. The second result is that the power threshold for the eITB formation is reduced from $265 \times 10^{-19} \text{ kWm}^3$ to $240 \times 10^{-19} \text{ kWm}^3$ when the plasma current increases above $I_p \sim 0.9 \text{ kA}$, of which value is almost the same as the calculated value that is required to form 4/7 rational surface. Because the 4/7 rational surface is a candidate on which the magnetic island can be formed due to the $n = 4$ toroidal periodicity of the vacuum magnetic field, and other low-order rational surfaces have no contribution to these phenomena, the results show the possibility that the formation of the magnetic island can expand the improved confinement region or reduce the power threshold for the eITB formation. The similar mechanism that the magnetic island affects the plasma transport has been also observed in numerical simulation. It is necessary to consider not only neoclassical transport effect but also magnetic island effect on the eITB formation.

EX

The Configuration Dependence of Isotope Effects on Turbulence System in Heliotron J

S. Ohshima¹, H. Okada¹, L. Zang², S. Kobayashi¹, S. Yamamoto¹, K. Nagasaki¹, T. Minami¹, S. Kado¹, N. Kenmochi³, Y. Ohtani⁴, X. Lu⁵, M. Motoshima⁵, R. Matoike⁵, S. Konoshima¹, and T. Mizuuchi¹

¹*Institute of Advanced Energy, Kyoto University, Nishikyo-ku, Kyoto 615-8540, Japan*

²*Southwestern Institute of Physics, Chengdu, Sichuan, People's Republic of China*

³*Graduate School of Frontier Science, University of Tokyo, Tokyo, Japan*

⁴*National Institutes for Quantum and Radiological Science and Technology (QST), Naka Fusion Institute, Naka-shi, Ibaraki-ken, Japan*

⁵*Graduate School of Energy Science, Kyoto University, Nishikyo-ku, Kyoto 615-8540, Japan*

Corresponding Author: S. Ohshima, ohshima@iae.kyoto-u.ac.jp

EX The hydrogen/deuterium (H/D) isotope effects on fluctuations and its configuration dependence are studied in a helical device, Heliotron J. The isotope dependence of a toroidally symmetric fluctuation in low frequency range of $\lesssim 4$ kHz, which is considered as a zonal flow, is observed in low-density ECH plasmas in Heliotron J. The long-range toroidal correlation of the low frequency range become higher on D dominant plasmas in standard configuration of Heliotron J. Interestingly, however, different dependence on isotope ratios, smaller amplitude and coherence in the frequency range, is observed in D plasmas in the magnetic configuration with low-bumpiness. The configuration dependence can be one of factors to explain the difference in isotope effect between tokamaks and helical devices.

Multiple Turbulent Plasma States in the H-Mode Transition on JT-60U

K. Kamiya¹, K. Itoh^{2,3,4}, S.-I. Itoh^{4,5}, M. Honda¹, A. Isayama¹, and N. Oyama¹

¹*National Institutes for Quantum and Radiological Science and Technology (QST), Chiba-shi, Japan*

²*Institute of Science and Technology Research, Chubu University, Kasugai, Aichi, Japan*

³*National Institute for Fusion Science (NIFS), Toki, Gifu, Japan*

⁴*Research Center for Plasma Turbulence, Kyushu University, Kasuga, Japan*

⁵*Research Institute for Applied Mechanics (RIAM), Kyushu University, Kasuga, Japan*

Corresponding Author: K. Kamiya, kamiya.kensaku@qst.go.jp

Multiple turbulent plasma states in the edge transport barriers (ETBs) formation are studied on JT-60U. Following a slow transition, which causes significant reduction in the ion thermal transport in the pedestal towards the neoclassical level with a weak negative E_r value, we found a clear and fast changes in the particle transport in association with the change in the E_r towards a strong negative value at the later H-phase. This observation suggests the existence of multiple types of turbulent fluctuations in the H-mode plasma state, which affects the ion energy and other channels of transport differently.

EX

Characterization of Isotope Effect on Confinement of Dimensionally Similar NBI-Heated Plasmas in LHD

H. Yamada^{1,2,3}, K. Tanaka^{1,4}, T. Tokuzawa¹, R. Seki^{1,2}, C. Suzuki¹, M. Yokoyama^{1,2}, K. Ida^{1,2}, M. Yoshinuma¹, K. Fujii⁵, H. Yamaguchi¹, and S. Murakami⁵

The LHD Experiment Group

¹National Institute for Fusion Science (NIFS), Toki, Gifu, Japan

²Department of Fusion Science, Graduate University for Advanced Studies (SOKENDAI), Toki, Gifu, Japan

³University of Tokyo, Tokyo, Japan

⁴Kyushu University, Kasuga, Japan

⁵Kyoto University, Nishikyo-ku, Kyoto 615-8540, Japan

Corresponding Author: H. Yamada, hyamada@lhd.nifs.ac.jp

Energy confinement and thermal transport has been widely regarded as gyro-Bohm in tokamak as well as stellarator-heliotron for a single kind of ion. However, this gyro-Bohm model predicts confinement degradation in deuterium (D) plasmas because of larger normalized gyro radius than in hydrogen (H) plasmas, which conflicts with major experimental observations. This study aims to quantify a peculiarity in dependence on normalized gyro radius in H and D plasmas in order to address this unresolved issue. The first deuterium plasma campaign in LHD reveals definitive characteristics of isotope effect on NBI-heated plasmas from elaborated experiments. Stationary uneventful plasmas, which are accompanied by neither ITB nor transition, have been assessed here. Thermal energy confinement time gives the regression expression scaling with the isotope mass as $A^{0.15}$, which shows moderate improvement in D plasmas. This positive isotope dependence contradicts with gyro-Bohm and is similar to the recent result from L-mode plasmas in JET-ILW. Operational flexibility of magnetic field, density, and heating power enables adjustment of three major nondimensional parameters, those being normalized gyro radii, collisionality and β , and dimensionally similar plasmas of H and D in all these three parameters can be obtained. Then TASK3D-a/FIT3D is used for analysis of heating power deposition, power balance and local thermal transport. If gyro-Bohm nature predominates in these plasmas, thermal diffusivity normalized by Bohm diffusion should be the same in a pair of dimensionally similar plasmas of H and D. Different characteristics have been found in electron and ion loss channels. Electron heat diffusivity normalized by Bohm diffusion in H is lower than that in D and even lower by a factor of $1/\sqrt{2}$ which means net improvement. This trend is robust and insensitive to parameters such as normalized gyro radii, collisionality, β , density gradient scale length, etc. In contrast, ion thermal diffusivity shows a same characteristics as in the electron channel in low collisionality regime while that in D compared with the case with H degrades with the increase of collisionality. These results have shown definitively that the gyro-Bohm nature is violated in the comparison of H and D plasmas in a large scale stellarator-heliotron.

Isotope Effects on Confinement and Turbulence in ECRH Plasma of LHD

K. Tanaka¹, M. Nakata¹, Y. Ohtani², T. I. Tsujimura¹, H. Takahashi¹, M. Yokoyama¹, and F. Warmer³

The LHD Experiment Group

¹National Institute for Fusion Science (NIFS), Toki, Gifu, Japan

²National Institutes for Quantum and Radiological Science and Technology (QST), Chiba-shi, Japan

³Max-Planck-Institut für Plasmaphysik, Greifswald, Germany

Corresponding Author: K. Tanaka, ktanaka@nifs.ac.jp

The positive isotope effects have been found in ECRH plasma of LHD. The enhancement factor of global energy confinement time (τ_E) to ISS04 scaling in deuterium (D) plasma is about 17% better than in hydrogen (H) plasma. Ion scale density fluctuation level is higher in D plasma. Core fluctuation level in D decreases rapidly with increase of τ_E .

Both tokamak scaling (ITER98y2) and helical scaling (ISS04) follow gyro-Bohm (GB) scaling with the exception of ion mass and ion charge number. While GB scaling predicts enhanced transport in D plasma, many experiments show better confinement (in tokamak) in D or comparable confinement (in medium-sized helical devices). In this paper, we report the first results of the improved confinement due to the isotope effects in ECRH plasma of LHD

In the dataset, the injection power of 77 and 154 GHz gyrotron was 0.6–3.9 MW in D, 0.8–3.8 MW in H, $n_{e \text{ bar}}$ was $0.6\text{--}3.7 \times 10^{19}/\text{m}^3$ in D, $0.3\text{--}3.8 \times 10^{19}/\text{m}^3$ in H. The one path absorption power was $92 \pm 4\%$ of injection power both for H and D plasma. The magnetic axis was 3.6 m with $B_t = 2.75$ T. Confinement time τ_E is systematically higher in D. This is more apparent in the high collisionality regime. The enhancement factors are $\tau_E/\tau_{E \text{ ISS04}} = 1.27 \pm 0.12$ in D and 1.09 ± 0.02 in H plasma. Thus, improvement of τ_E in D to H is 17%.

For fixed injection power, T_e and T_i profiles are almost identical. However, n_e profile is more hollowed in D plasma. The higher n_e in the edge region results in the higher stored energy and better confinement.

Ion scale turbulence was measured by two-dimensional phase contrast imaging. The measured normalized wavenumber was around 0.4. Surprisingly, it is found that the fluctuation level is higher in D, while τ_E is higher in D plasma. However, the fluctuation level reduces with increase of τ_E . This dependence is clearer in D plasma. Recent gyrokinetic study shows stronger collisional stability of TEM in D than in H plasma. Also, hollow density gradient reduces growth rate both of TEM and ITG. The quicker reduction of fluctuation level the core of D qualitatively agrees with collisional dependence of TEM and more hollowed density profiles in D.

EX

Rapid Radial Propagation of Momentum Change and Flow Oscillation Associated with a Pellet Injection

T. Tokuzawa¹, S. Inagaki², N. Tamura¹, R. Sakamoto^{1,3}, K. Ida^{1,3}, T. I. Tsujimura¹, M. Emoto¹, C. Suzuki¹, H. Tsuchiya¹, A. Ejiri⁴, H. Yamada^{1,3,4}, K. Y. Watanabe^{1,5}, K. Oguri⁵, K. Tanaka¹, G. Motojima^{1,3}, and I. Yamada¹

The LHD Experiment Group

¹National Institute for Fusion Science (NIFS), Toki, Gifu, Japan

²Kyushu University, Kasuga, Japan

³Graduate University for Advanced Studies (SOKENDAI), Hayama, Kanagawa, Japan

⁴University of Tokyo, Tokyo, Japan

⁵Nagoya University, Nagoya, Japan

Corresponding Author: T. Tokuzawa, tokuzawa@nifs.ac.jp

We report the discovery of rapid momentum change and oscillatory flow as a result of the pellet injection. Novel diagnostics tools with high spatio-temporal resolution applied to the perpendicular flow velocity and turbulence intensity measurements in LHD experiments show the following results. Just after the pellet injection: 1) the damped oscillating flow velocity and the increasing density fluctuation are observed in a few milliseconds; 2) the propagating flow structure towards the core direction is observed, and its speed is faster than the pellet penetration speed. These results are quite meaningful for understanding the physics of pellet penetration in toroidal plasma.

Just after the pellet injection, the perpendicular flow velocity is oscillating and damping in a few milliseconds. The damped oscillation model can be applied to fit the observation data. The toroidal mode number of this oscillation is estimated to be 0 or 10. We can also measure the turbulence intensity at the same position. The turbulence increases rapidly and then decreases before the end of the damping of the oscillatory flow. The generation and damping of flow itself might be caused by the turbulence. On the other hand, the electron density increases and the electron temperature decreases with finite delay. Therefore, it is found that the change of local density gradient seems likely not to play an important role for the start of this oscillation.

The ballistic propagation of the change of flow structure towards the core direction is observed in the region at $r/a < 0.97$, where the mono-cycle temporal oscillation is observed. In order to measure such a fine velocity profile, a high sampling rate digital storage of 80 GS/s is applied for the frequency comb microwave Doppler reflectometer. The propagation speed increases at the location of $r/a \sim 0.97$ and exceeds 1.5 km/s, which is three times faster than the pellet penetration speed. This indicates that the rapid propagation of information of momentum change is present. Currently, it is also found that the location of the pivot point is not at the rational surface, and the information of momentum change propagates at least $r/a \sim 0.86$ before the start of the electron density rise. Therefore, it is found that the momentum changes rapidly, and this may lead the global change of the radial electric field and affect the bulk plasma transport.

Experimental Analysis of Self-Organized Structure and Transport on Magnetospheric Plasma Device RT-1

M. Nishiura¹, Z. Yoshida¹, N. Kenmochi¹, T. Sugata¹, K. Nakamura¹, S. Katsura¹, K. Shirahata¹, C. A. Michael², and J. Howard²

¹Graduate School of Frontier Science, University of Tokyo, Tokyo, Japan

²Australian National University, Canberra, Australia

Corresponding Author: M. Nishiura, nishiura@ppl.k.u-tokyo.ac.jp

The dipole plasma exhibits strong heterogeneities in field strength, density, temperature, etc., while maintaining the holistic balance. Enquiring into the internal structures, we reveal the fundamental self-organizing mechanisms operating in their simplest realization (as commonly observed in astronomical systems) [1, 2]. Three new findings are reported from the RT-1 experiment: i) Creation of a high-energy electron core (similar to the radiation belts in planetary magnetospheres) is observed for the first time in a laboratory system. High-energy electrons, 3–15 keV, produced by an electron cyclotron heating (ECH), accumulate in a “belt” located in the low density region (high- β value ~ 1 is obtained by increasing the high-energy component up to 70% of the total electrons). ii) The dynamical process of the “inward diffusion” (a spontaneous mechanism of creating density gradient) has been analyzed by perturbing the density by gas injection. iii) By a system of coherence-imaging spectroscopy, the profiles of the ion temperature and flow velocity have been measured. The effect of the ion cyclotron resonance frequency (ICRF) heating [3] has been visualized. These results advance our understanding of transport and self-organization not only in dipole plasmas, but also in general magnetic confinement systems relevant to fusion plasmas.

References

- [1] A. Hasegawa, *Comments Plasma Phys. Contr. F.*, **1**, 147 (1987).
- [2] Z. Yoshida, *Adv. Phys.* **X1**, 2 (2016).
- [3] M. Nishiura *et al.*, *Nucl. Fus.*, **57**, 086038 (2017).

Synergistic Effect of Impurity and Hydrogen Gas Puffs on Plasma Detachment in the GAMMA 10/PDX Tandem Mirror

N. Ezumi¹, T. Iijima¹, M. Sakamoto¹, Y. Nakashima¹, M. Hirata¹, M. Ichimura¹, R. Ikezoe¹, T. Imai¹, T. Kariya¹, I. Katanuma¹, J. Kohagura¹, R. Minami¹, T. Numakura¹, M. Yoshikawa¹, S. Togo¹, M. S. Islam¹, M. M. Islam¹, K. Nojiri¹, A. Terakado¹, S. Jang¹, T. Yokodo¹, Y. Kinoshita¹, T. Mikami¹, S. Yamashita¹, T. Yoshimoto¹, T. Hara¹, A. Hatayama², K. Ichimura³, S. Kado⁴, S. Masuzaki⁵, T. Nakano⁶, N. Ohno⁷, S. Sawada⁸, H. Tanaka⁷, and A. Toneyawa⁹

¹Plasma Research Center, University of Tsukuba, Tsukuba, Ibaraki, Japan

²Faculty of Science and Technology, Keio University, Yokohama, Japan

³Kobe University, Kobe, Japan

⁴Institute of Advanced Energy, Kyoto University, Nishikyo-ku, Kyoto 615-8540, Japan

⁵National Institute for Fusion Science (NIFS), Toki, Gifu, Japan

⁶National Institutes for Quantum and Radiological Science and Technology (QST), Naka Fusion Institute, Naka-shi, Ibaraki-ken, Japan

⁷Graduate school of Engineering, Nagoya University, Nagoya, Japan

⁸Faculty of Engineering, Shinshu University, Nagano, Japan

⁹Graduate school of Science, Tokai University, Tokyo, Japan

Corresponding Author: N. Ezumi, ezumi@prc.tsukuba.ac.jp

In Plasma Research Center, University of Tsukuba, divertor simulation experiments have been conducted at the end region of GAMMA 10/PDX. The high temperature end-loss plasmas of GAMMA10/PDX are a functional tool for simulating edge and divertor plasmas and contribute to developing a deeper understanding of the physics involved in plasma detachment. Our aim is to study detachment phenomena under equivalent conditions for ITER SOL and divertor plasma under high temperature and strong magnetic field. So far, we have performed characterization of plasma detachment from high temperature plasma (ion temperature has achieved a few hundred eV) produced by a large tandem mirror device for various radiator gases.

For ideal detached plasma operation, the amount of impurities is expected to be as low as possible. In this study, we have investigated the synergistic effect of a combination of various impurity gases and hydrogen gas on plasma detachment of high temperature plasma, equivalent to SOL plasma of tokamaks in the GAMMA 10/PDX end region, utilizing an open magnetic field configuration. A small puff of an impurity gas (N_2 , Ne, Ar, Kr, Xe) in combination with a puff of H_2 gas is examined to evaluate their synergistic effect on the formation of detached plasma; the following results are obtained: i) A combination of N_2 and H_2 puffs showed clear decrease of electron density and ion flux; ii) N_2 and H_2 puffs form a strong density gradient along the axial direction; and iii) other noble impurity gases showed insufficient synergistic effect. The new results indicate the possibility of achieving a reliable divertor operation scheme and the importance of investigating molecular processes in further detail. We can contribute to the optimization of detached plasma formation through a deeper understanding of the H_2 and N_2 assisted recombination process.

Core Transport Improvement in Stable Detachment with RMP Application to the Edge Stochastic Layer of LHD

M. Kobayashi¹, S. Masuzaki¹, M. Yokoyama¹, K. Tanaka¹, T. Ido¹, Y. Narushima¹, and I. Yamada¹

¹National Institute for Fusion Science (NIFS), Toki, Gifu, Japan

Corresponding Author: M. Kobayashi, kobayashi.masahiro@nifs.ac.jp

Significant core plasma transport improvement is observed in the detachment divertor operation, which is stabilized by application of resonant magnetic perturbation (RMP) to the edge stochastic layer of LHD. Pressure profile becomes peaked and the heat transport coefficient, χ_{eff} , estimated from transport analysis, reduced in the entire confinement region. The RMP amplitude scan experiments show change of detachment transition density and of resulting χ_{eff} , while attained divertor particle flux reduction and radiated power are independent of the RMP amplitude. The results are new systematic study of RMP effects on detachment as well as on the core plasma transport. It suggests compatibility of good core plasma performance with divertor power load reduction in 3D magnetic field configuration with RMP application.

Compatibility of good core plasma performance with enhanced edge radiation to mitigate the divertor power load is a crucial issue for magnetically confined fusion reactors. It is, however, commonly observed that the core confinement degrades with increasing radiation fraction. It is also not clear yet how RMP affects the core plasma transport during detachment, where no systematic RMP amplitude scan experiments have been performed so far in either tokamaks or stellarators in this respect. In LHD, stable detachment control is realized with RMP application of $m/n = 1/1$ mode, where the core plasma transport is found to improve in the detached phase. The present paper reports, for the first time, analysis of the core transport, edge radiation, and divertor particle/power flux reduction with systematic scan of RMP amplitude (B_r/B_0).

The RMP application creates a magnetic island of $m/n = 1/1$ in the edge stochastic layer, where the impurity radiation is enhanced due to increased volume of cold plasma region. The divertor power and particle flux exhibit $n = 1$ mode pattern in toroidal direction. With RMP application, the radiated power increases at lower density compared to the no-RMP case, and thus it results in earlier detachment transition. There appears a plateau region of radiation against density rise. This leads to a wide density operation range and thus provides a stable detachment control. RMP amplitude scan experiments show clear change of detachment transition density and resulting energy transport coefficients.

EX

Effect of Deuterium Plasmas on Carbon Impurity Transport in the Edge Stochastic Magnetic Field Layer of Large Helical Device

T. Oishi^{1,2}, S. Morita^{1,2}, M. Kobayashi^{1,2}, G. Kawamura¹, Y. Liu², and M. Goto^{1,2}

The LHD Experiment Group

¹National Institute for Fusion Science (NIFS), Toki, Gifu, Japan

²Department of Fusion Science, Graduate University for Advanced Studies (SOKENDAI), Toki, Gifu, Japan

Corresponding Author: T. Oishi, oishi@nifs.ac.jp

EX Stochastization of edge magnetic fields has been extensively studied not only for the ELM mitigation but also for the plasma detachment and the impurity transport. The ergodic layer of Large Helical Device (LHD) consists of stochastic magnetic fields with three-dimensional structure intrinsically formed by helical coils. Reduction of the parallel impurity transport in the ergodic layer, so called “impurity screening”, has been studied in LHD. The theoretical modelling explains that the parallel momentum balance on impurity ions determines the direction and quantity of the impurity flow driving the impurity screening. Recently, the carbon flow in the ergodic layer was measured in hydrogen (H) plasmas with space-resolved vacuum ultraviolet (VUV) spectroscopy and a close relation between the impurity flow and the impurity screening was experimentally verified for the first time by the comparison between the spectroscopic observations and the impurity transport simulation based on a three-dimensional simulation code, EMC3-EIRENE. In the present report, the VUV spectroscopy for carbon impurities is applied to deuterium (D) plasmas to clarify the effect of the bulk ion mass on the impurity transport in the ergodic layer. Doppler profile measurement at the second order of CIV line emission (2×154.820 nm) is attempted in a flat-top phase of discharges using a 3 m normal incidence VUV spectrometer in the edge plasma at a horizontally-elongated plasma position. The flow velocity becomes the maximum value at the position close to the outermost region of the ergodic layer. The direction of the observed flow is same as the friction force in the parallel momentum balance calculated with EMC3-EIRENE code. The flow velocity increases with the electron density in the H plasmas. The result supports a prediction from the simulation that the friction force becomes more dominant in the force balance in higher density regime. It leads to the increase in the impurity flow which can develop the impurity screening. On the other hand, the flow velocity in the D plasma is smaller than that in the H plasma. The difference of the flow values between D and H plasmas is caused by the mass dependence of the thermal velocity of the bulk ions when the friction force term is dominant in the force balance.

Particle Balance Investigation with the Combination of Rate Equations of Hydrogen State and Hydrogen Barrier Model in Long Duration Discharges on All-Metal PFW QUEST

K. Hanada¹, N. Yoshida¹, M. Hasegawa¹, A. Hatayama², K. Okamoto², I. Takagi³, T. Hirata³, Y. Oya⁴, M. Miyamoto⁵, M. Oya⁶, T. Shikama³, A. Kuzmin¹, Z. X. Wang⁶, H. Long⁶, H. Idei¹, Y. Nagashima¹, K. Nakamura¹, O. Watanabe¹, T. Onchi¹, H. Watanabe¹, K. Tokunaga¹, A. Higashijima¹, S. Kawasaki¹, H. Nakashima¹, T. Nagata¹, S. Shimabukuro¹, Y. Takase⁷, S. Murakami⁸, X. Gao⁹, H. Liu¹, J. Qian⁹, R. Raman¹⁰, and M. Ono¹¹

¹Research Institute for Applied Mechanics (RIAM), Kyushu University, Kasuga, Japan

²Keio University, Yokohama, Japan

³Kyoto University, Nishikyo-ku, Kyoto 615-8540, Japan

⁴Shizuoka University, Shizuoka, Japan

⁵Shimane University, Matsue, Shimane, Japan

⁶Interdisciplinary Graduate School of Engineering Sciences (IGSES), Kyushu University, Kasuga, Japan

⁷University of Tokyo, Tokyo, Japan

⁸Department of Nuclear Engineering, Kyoto University, Nishikyo-ku, Kyoto 615-8540, Japan

⁹Institute of Plasma Physics, Chinese Academy of Sciences, Hefei, Anhui, People's Republic of China

¹⁰University of Washington, Seattle, WA 98195, USA

¹¹Princeton Plasma Physics Laboratory (PPPL), Princeton, NJ 08540, USA

Corresponding Author: K. Hanada, hanada@triam.kyushu-u.ac.jp

Out-flux of fuel particles from plasma-facing walls (PFWs) during long duration discharges on all-metal PFW QUEST is in agreement with a prediction of the hydrogen (H) barrier model we proposed. A simple calculation based on the combination of rate equations of H state and the H barrier model predicts a significant impact in the response of plasma density. This result indicates that a proper wall model including the effect of deposition layer that creates H barrier should be developed even in all-metal PFW devices.

EX

Recent Progresses on the RMP Researches Towards Active Control of Tearing Mode in the J-TEXT Tokamak

D. Li¹, Y. H. Ding¹, B. Rao¹, Q. M. Hu², N. C. Wang¹, H. Jin¹, M. Li¹, Q. Yu³, and Y. Liang^{1,4}

The J-TEXT Team

¹International Joint Research Laboratory of Magnetic Confinement Fusion and Plasma Physics (IFPP), Huazhong University of Science and Technology, Hubei, People's Republic of China

²Princeton Plasma Physics Laboratory (PPPL), Princeton, NJ 08540, USA

³Max-Planck-Institut für Plasmaphysik, Garching, Germany

⁴Forschungszentrum Jülich, Jülich, Germany

Corresponding Author: Y. H. Ding, yhding@hust.edu.cn

Controlling the tearing mode (TM) is one of the major topics of fusion research, since TM degrades the plasma confinement and even induces major disruption if it is locked. Previous experimental and theoretical studies showed that the resonant magnetic perturbations (RMPs) influence both the rotation and width of the TM. As a result, the static RMP could apply a net stabilizing and braking effect on a rotating TM, and hence suppress or lock the TM. Based on these effects, three strategies for controlling the TM have been proposed and tested in J-TEXT by applying the pulsed or fast rotating RMPs. This paper will present these recent efforts.

On J-TEXT, the RMP system is capable of providing either a static or a high frequency (up to 6 kHz) rotating RMP field, with dominant 2/1 component. To study the proposed TM control methods, extensive upgrades of the power supply (PS) system for RMP coils were carried out, such as building a pulsed DC PS which could follow the TM frequency with 50% duty cycle, a hopping frequency AC PS, an on-line system for measuring the TM phase and frequency.

The first control strategy is to apply pulsed RMP to the TM only during the accelerating phase region. By nonlinear numerical modelling, it is proved efficient in accelerating the mode rotation and even completely suppresses the mode. The followed experimental attempt with the pulsed RMP at relative low amplitude has demonstrated the acceleration effect. The second control method is to apply a RMP, rotating with varying frequency which is kept slightly higher than that of a TM. Currently, the open loop application of this hopping PS led to the locking of TM at 4, 5 and 6 kHz successively. Further investigation with feedback controlled hopping PS is needed to validate this method.

Thirdly, the fast rotating RMP field has been successfully applied for the avoidance of mode locking and the prevention of plasma disruption. A set of disruptive discharges induced by intrinsic mode locking were performed by reducing the edge safety factor from 3 towards 2. The braking of TM usually lasted for ~ 20 ms and the disruption followed at ~ 10 ms after the mode locked. Triggered by the mode locking warning system, the 3 kHz rotating RMP was applied before the mode locked. The TM was accelerated to 3 kHz and the intrinsic mode locking was avoided. As a result, the disruption was prevented.

Investigation of Magnetic Topology on Spontaneous Transition Phenomena for High- β Plasma of Large Helical Device

Y. Suzuki^{1,2}, S. Sakakibara^{1,2}, K. Y. Watanabe¹, S. Ohdachi^{1,2}, K. Tanaka¹, K. Ida^{1,2}, R. Seki^{1,2}, M. Yokoyama^{1,2}, M. Kobayashi^{1,2}, G. Kawamura^{1,2}, S. Masuzaki^{1,2}, H. Tanaka³, I. Yamada¹, R. Yasuhara¹, J. Morimoto², and T. Morisaki^{1,2}

The LHD Experiment Group

¹National Institute for Fusion Science (NIFS), Toki, Gifu, Japan

²Department of Fusion Science, Graduate University for Advanced Studies (SOKENDAI), Toki, Gifu, Japan

³Nagoya University, Nagoya, Japan

Corresponding Author: Y. Suzuki, suzuki.yasuhiro@nifs.ac.jp

A topological change of the magnetic field structure on a transition phenomenon is investigated in the Large Helical Device (LHD). In the high- β plasma experiment of the LHD, the spontaneous transition phenomenon is sometimes observed. After the transition, the plasma density is increased and then the plasma stored energy is increased. One important observation after the transition is the increasing plasma volume. This indicates following points: i) the magnetic field structure in the plasma edge is changed by a plasma response of the beta-sequences; ii) the effective plasma volume is expanded by the change of the magnetic field; and iii) the plasma stored energy is increased due to the expansion of the plasma volume. To understand how the magnetic field changes due to the plasma response of the β -sequences, the 3D equilibrium is studied for the transition. For a magnetic configuration with the spontaneous transition, the magnetic field is topologically changed by the plasma response of the β sequences. The vacuum magnetic island on edge rational surfaces shrinks and the stochastic magnetic field of the long connection length expands. Therefore, the effective plasma confinement region expands due to the topological change of the magnetic field. To the improvement of the plasma stored energy on the spontaneous transition, the topological change of the magnetic field is a key factor.

EX

Dependence of RMP Penetration Threshold on Plasma Parameters and Ion Species in Helical Plasmas

K. Y. Watanabe¹, S. Sakakibara¹, Y. Narushima¹, S. Ohdachi¹, Y. Suzuki¹, and Y. Takemura¹

The LHD Experiment Group

¹*National Institute for Fusion Science (NIFS), Toki, Gifu, Japan*

Corresponding Author: K. Y. Watanabe, kiyowata@lhd.nifs.ac.jp

We investigate the penetration threshold of the RMP (resonant magnetic perturbation) by the external coils in the LHD (Large Helical Device) for the various configurations. In a configuration of the LHD, it has qualitative similar dependence with that in Ohmic tokamak plasmas. However, the qualitative dependence on the collisionality is opposite to that in a high plasma aspect configuration, which is a quite unique property, and first found in the LHD. Also, we investigate the threshold on the ion species, and find that the threshold of deuterium is quite smaller than that of hydrogen. In the above cases, the RMP penetration thresholds are higher as the poloidal rotation is faster, which is qualitatively consistent with the torque balance model between the electromagnetic and the poloidal neoclassical viscous torque.

EX

Study of Locking Mechanism of Locked-Mode-Like Instability in Helical Plasmas

Y. Takemura¹, K. Y. Watanabe¹, S. Sakakibara¹, Y. Narushima¹, K. Ida¹, M. Yoshinuma¹, H. Tsuchiya¹, T. Tokuzawa¹, and I. Yamada¹

The LHD Experiment Group

¹National Institute for Fusion Science (NIFS), Toki, Gifu, Japan

Corresponding Author: Y. Takemura, takemura.yuki@nifs.ac.jp

The frequency slowing-down mechanism of the locked-mode-like instability without a large magnetic island is investigated for the first time, based on the LHD experimental analysis. The slowing-down frequency is caused by two processes. One is the resonant surface moving to the small $E \times B$ rotation frequency region and the other is the slowing-down $E \times B$ rotation frequency around the resonant surface. Both processes are almost the same as those of the instability with a large magnetic island. The new experimental results presented in this synopsis suggest that the mode frequency slows down even though the precursor does not have a large magnetic island. In addition, the duration of the frequency slowing-down phase becomes longer as the external RMP amplitude becomes smaller. This is because the slowing-down rate of the $E \times B$ rotation frequency around the resonant surface after excitation of the precursor is smaller for a smaller external RMP amplitude. These results also suggest that error fields, which have the same effect as the RMP, should be reduced to obtain sufficient time for controlling the locked-mode-like instability.

EX

Experimental Studies of Plasmoid Reconnection for Closed Flux Current Generated by Coaxial Helicity Injection on HIST

M. Nagata¹, A. Fujita¹, Y. Ibaraki¹, Y. Kikuchi¹, N. Fukumoto¹, and T. Kanki²

¹University of Hyogo, Hyogo 671-2280, Japan

²Japan Coast Guard Academy, Kure, Hiroshima 737-8512, Japan

Corresponding Author: M. Nagata, nagata@eng.u-hyogo.ac.jp

EX The spherical torus (ST) is a leading candidate for an advanced fusion reactor due to its compactness. Transient coaxial helicity injection (T-CHI) is one of CHI schemes, and it is used to generate and ramp-up the plasma current at the initial phase of a discharge. One of the most important issues in T-CHI is whether it can establish a current sufficient for succeeding current drive and heating. Understanding the fast reconnection mechanism for the flux closure during the start-up process is the primary purpose of the T-CHI experiment on Helicity Injected Spherical Torus (HIST: $R = 0.30$ m, $a = 0.24$ m, $A = 1.25$). The fast reconnection driven by plasmoid for the flux closure has been demonstrated by T-CHI in the HIST device. The intensive measurement of internal magnetic structures indicates that two or three plasmoids are generated in an elongated Sweet-Parker current sheet during the T-CHI. Here, we report that in the T-CHI start-up plasmas: i) the observed regular oscillations of magnetic field, electron density and ion flow indicate repetitive generation of small-size plasmoids due to the magnetic reconnection; and ii) one of plasmoids grows up to a large-size, and a doublet-type ST configurations is formed as a result. Consequently, the plasmoid reconnection could be the leading mechanism for the formation of multiple X-point, i.e., the fast flux closure in the T-CHI discharge.

Electron Bernstein Wave Heating and Current Drive with Multielectron Cyclotron Resonances During Noninductive Start-Up on LATE

H. Tanaka¹, Y. Nozawa¹, M. Uchida¹, R. Kajita¹, Y. Omura¹, Y. Sakai¹, H. Shirai¹, J. Ootani¹, K. Goto¹, W. Tsukamoto¹, T. Noguchi¹, X. Guo¹, and T. Maekawa¹

¹Graduate School of Energy Science, Kyoto University, Nishikyo-ku, Kyoto 615-8540, Japan

Corresponding Author: H. Tanaka, h-tanaka@energy.kyoto-u.ac.jp

Electron cyclotron heating and current drive (ECH/ECCD) by electron Bernstein waves (EBWs) with multielectron cyclotron resonances (ECRs) is carried out by injecting microwaves at two frequencies during the noninductive start-up of a spherical tokamak (ST). When the 2nd EBW at 5 GHz is excited in the noninductively produced ST plasma with the 1st EBW at 2.45 GHz, plasma current is driven strongly while the bulk electron parameters such as density are nearly the same. The 2nd EBW is absorbed mainly by high energy tail electrons between the 2nd ECR layer and the upper-hybrid resonance (UHR) layer by Doppler effect and drive the plasma current, while the 1st EBW sustains the bulk electrons.

EX

Energetic-Ion Confinement Studies by Using Comprehensive Neutron Diagnostics in the Large Helical Device

K. Ogawa^{1,2}, M. Isobe^{1,2}, T. Nishitani¹, S. Murakami³, R. Seki^{1,2}, H. Nuga¹, S. Kamio¹, Y. Fujiwara¹, H. Yamaguchi¹, H. Kawase², N. Pu², Y. Saito³, S. Maeta³, and M. Osakabe^{1,2}

The LHD Experiment Group

¹National Institute for Fusion Science (NIFS), Toki, Gifu, Japan

²Department of Fusion Science, Graduate University for Advanced Studies (SOKENDAI), Toki, Gifu, Japan

³Kyoto University, Nishikyo-ku, Kyoto 615-8540, Japan

Corresponding Author: K. Ogawa, kogawa@nifs.ac.jp

Study on neoclassical and anomalous transport of energetic particle (EP) in the Large Helical Device (LHD) has been performed by means of escaping EP diagnostics. By starting deuterium operation of the LHD, confinement study of EPs has remarkably progressed by using newly developed comprehensive neutron diagnostics providing the information of EPs confined in the core region. Time evolution of total neutron emission rate (S_n) following the short pulse neutral beam (NB) injection is reproduced by drift kinetic simulation, indicating that beam ion transport can be described with neoclassical models. The vertical neutron camera (VNC) works successfully, demonstrating that neutron emission profile shifts according to magnetic axis position (R_{ax}). Correlated with helically-trapped EP driven resistive interchange mode (EIC) burst, substantial drop of (S_n) and change of neutron emission profile are observed, indicating the significant loss of helically-trapped beam ion due to the EIC mode. Time-resolved triton burnup study is performed for the first time in stellarator/heliotron so as to understand the α particle confinement. It is found that the triton burnup ratio which largely increases at inward shifted configurations is similar to that measured in tokamak having a similar minor radius with the LHD. We demonstrate the confinement capability of EPs toward a helical reactor and expansion of the energetic-ion physics study in toroidal fusion plasmas.

EX

Fully Noninductive 2nd Harmonic Electron Cyclotron Current Ramp-Up with Focussed Polarized Beams in the QUEST Spherical Tokamak

H. Idei¹, T. Onchi¹, T. Kariya², T. I. Tsujimura³, S. Kubo³, S. Kobayashi³, M. Fukuyama⁴, M. Yunoki⁴, S. Kojima⁴, M. Hasegawa¹, K. Nakamura¹, A. Ejiri⁵, N. Matsumoto⁵, K. K. Mishra^{4,6}, T. Imai², O. Watanabe¹, K. Kuroda¹, K. Hanada¹, Y. Nagashima¹, A. Higashijima¹, K. Nagata¹, R. Yoneda⁴, G. Taylor⁷, N. Bertelli⁷, M. Ono⁷, Y. Takase⁵, A. Fukuyama⁸, and S. Murakami⁸

¹Research Institute for Applied Mechanics (RIAM), Kyushu University, Kasuga, Japan

²Plasma Research Center, University of Tsukuba, Tsukuba, Ibaraki, Japan

³National Institute for Fusion Science (NIFS), Toki, Gifu, Japan

⁴Interdisciplinary Graduate School of Engineering Sciences, Kyushu University, Kasuga, Japan

⁵University of Tokyo, Tokyo, Japan

⁶Institute for Plasma Research (IPR), Bhat, Gandhinagar, India

⁷Princeton Plasma Physics Laboratory (PPPL), Princeton, NJ 08540, USA

⁸Kyoto University, Nishikyo-ku, Kyoto 615-8540, Japan

Corresponding Author: H. Idei, idei@riam.kyushu-u.ac.jp

A transmission line and a launcher system have been newly developed to conduct the second (2nd) harmonic electron cyclotron (EC) plasma ramp-up with an extraordinary mode wave in the QUEST spherical tokamak. The incident elliptical polarizations were controlled with two corrugated (quarter/one-eighth wavelength) polarizers. The launcher system with two quasi-optical mirrors produced a sharply focussed incident beam with a waist size of 0.05 m at the 2nd electron cyclotron resonance layer. The obtained electron density was one order of magnitude higher, compared to the previous experiments with no polarized focussing-beam. As a new record of noninductive plasma ramp-up with EC-waves, a highest plasma current of 86 kA was achieved with a focussed 230 kW 28 GHz-beam. The record plasma current ramp-up efficiency on the incident power in the 2nd harmonic EC scenario was also achieved.

EX

Investigation of Fine Structure Formation of Guide Field Reconnection During Merging Plasma Startup of Spherical Tokamak in TS-3U

H. Tanabe¹, H. Hatano¹, T. Hayashi¹, Q. Cao¹, A. Sawada¹, M. Akimitsu¹, M. Inomoto¹, and Y. Ono¹

¹Graduate School of Frontier Science, University of Tokyo, Tokyo, Japan

Corresponding Author: H. Tanabe, tanabe@ts.t.u-tokyo.ac.jp

We present the latest results of high-resolution 2D imaging measurement of merging/reconnection heating during the central solenoid (CS)-free plasma startup of spherical tokamak using a new ⁹⁶CH 2D ion Doppler tomography diagnostics. In the last decade, magnetic reconnection research made a major progress such as a) achievement of ~ 1 keV plasma heating in MAST both for ions and electrons; b) demonstration of B_{rec}^2 scaling of ion heating ranging $0.01 \text{ keV} < T_i < 1.2 \text{ keV}$ with $0.01 \text{ T} < B_{\text{rec}} < 0.15 \text{ T}$ in many plasma merging experiments based on outflow heating mechanism; and c) elucidation of fundamental heating characteristics: localized electron heating around X-point mostly by current sheet dissipation and global ion heating downstream where kinetic energy of outflow jet dissipates. Namely in the last three years, it was found that reconnection heating forms fine structure under high guide field condition of $B_t > 3B_{\text{rec}}$. From 2017, the formation process of the fine structure has been investigated in TS-3U ($B_t \sim 5B_{\text{rec}}$) with direct measurement of magnetic field profile and high-resolution 2D imaging measurement of ion temperature profile using a new ⁹⁶CH ion Doppler tomography. As a new finding, it was found that ion temperature increases inside the current sheet as well as downstream. The high temperature region around the X-point is affected by Hall current j_{Hall} from the decoupling of ions and electrons, the characteristic heating profile rotates poloidally toward $j_{\text{Hall}} \times B_t$ direction. This characteristic is clearer in high field side (B_t depends on major radius in tokamak configuration) and with higher mass ratio (enhancement of $j_{\text{Hall}} \times B_t$ due to the larger scale length than current sheet width). While at the end of merging, ion heating downstream is surrounded by closed flux surface formed by reconnected field lines and forms another fine structure. The high temperature profile downstream propagates vertically and finally forms poloidally double-ring-like structure under the influence of better toroidal confinement with higher guide field which strongly suppresses perpendicular heat transport ($\chi^{\parallel}/\chi^{\perp} \sim 2$, $\omega_{ci}\tau_{ii})^2 \gg 10$).

This work was supported by JSPS KAKENHI Grant Numbers 15H05750 and 17H04863, and NIFS Collaboration Research Program NIFS16KLER048.

Plasma Current Generation and Ramp-Up by the Lower Hybrid Wave Using Outboard-Launch and Top-Launch Antennas on the TST-2 Spherical Tokamak

A. Ejiri¹, Y. Takase¹, S. Yajima¹, Y. Yoshida¹, H. Yamazaki¹, Y. Tajiri¹, T. Shinya^{1,2}, A. Kitayama¹, N. Tsujii¹, N. Matsumoto¹, A. Sato³, Y. Takei¹, Y. Iida¹, K. Iwasaki¹, Y. Kawamata¹, S. Sakamoto¹, B. Roidl¹, C. P. Moeller³, H. Kasahara⁴, K. Saito⁴, T. Seki⁴, O. Mitarai⁵, and T. Mutoh⁴

¹University of Tokyo, Tokyo, Japan

²National Institutes for Quantum and Radiological Science and Technology (QST), Rokkasho Fusion Institute, Rokkasho-mura, Aomori, Japan

³General Atomics, San Diego, CA 92186, USA

⁴National Institute for Fusion Science (NIFS), Toki, Gifu, Japan

⁵Kyushu University, Kasuga, Japan

Corresponding Author: A. Ejiri, ejiri@k.u-tokyo.ac.jp

Plasma current start-up without a large flux swing by the central solenoid is a critical issue in fusion research. The lower hybrid wave (LHW) is known to be an effective current drive tool in conventional tokamaks, and it is used in the TST-2 spherical tokamak (ST) device. The TST-2 device provides a unique opportunity to compare outboard-launch and top-launch schemes for plasma current generation and ramp-up by LHW. The top-launch scheme is expected to have good core accessibility and thus expected to be superior than the outboard-launch scheme. However, one of operational difficulties for the top-launch scheme is the initial vertical position control. The recent operational optimization enabled achievement of the maximum plasma current of 27 kA, which is higher than that obtained by the outboard-launch scheme. By flipping the polarity of the toroidal field, we can realize a scheme equivalent to the bottom-launch scheme. We found that the achieved plasma currents are similar to those with the normal toroidal field direction. This fact indicates that the losses associated with wave reflections at the boundaries are not significant in these cases.

The plasma current increases with the toroidal field strength, and this dependence is quite reasonable when we consider wave accessibility of LHW. If we want to increase the toroidal field strength further, one difficulty we will face is preionization. Normally we use ECH (2.45 GHz, 5 kW) for preionization, with the fundamental resonance located around the major radius of the top-launch antenna. We will need another preionization tool for higher field experiments. The AC Ohmic operation is one such tool, which requires only about two orders of magnitude smaller flux swing than that for a typical Ohmic discharge. The growth rate of preionization by AC Ohmic operation is rather insensitive to the toroidal field strength. We confirmed that the operation is useful not only for the outboard-launch scheme but also for the top-launch scheme. This fact implies that we obtained a reliable preionization tool which is insensitive to the magnetic field strength.

Scaling Study of Reconnection/Merging Heating of Spherical Tokamak Plasmas for Direct Access to Burning Plasma

Y. Ono¹, M. Akimitsu¹, S. Inoue¹, A. Sawada¹, A. Borade¹, Q. Cao¹, H. Tanabe¹,
C. Z. Cheng², and R. Horiuchi³

¹University of Tokyo, Tokyo, Japan

²National Cheng-Kung University, Taiwan, China

³National Institute for Fusion Science (NIFS), Toki, Gifu, Japan

Corresponding Author: Y. Ono, ono@k.u-tokyo.ac.jp

The high-power reconnection heating of ST plasma has been developed in TS-3U, TS-4U and MAST experiments, leading us to direct access to burning plasma. This unique method is caused by the promising scaling of ion heating energy that increases with square of reconnecting magnetic field B_{rec} . We studied mechanisms for this B_{rec}^2 -scaling of reconnection (ion) heating mainly using TS-3U experiment and PIC simulations and found the following issues: 1) the ion heating energy is as high as $\sim 40\text{--}50\%$ of poloidal magnetic energy of two merging ST plasmas, and 2) is not affected by (guide) toroidal field B_t , in the region of $B_t/B_{\text{rec}} > 1$ under two important conditions: i) compression of current sheet to order of ion gyroradius, and iv) the ST plasmas fully isolated from coils and walls. The sheet compression to ion gyroradius was found to be a key condition to realize the fast reconnection as well as the high power ion heating consistent with the B_{rec}^2 -scaling prediction. Under this condition, the ion heating energy is determined uniquely by $B_{\text{rec}} \sim B_p$ not by B_t in the conventional tokamak operation region: $B_t/B_p > 1$. The merging ST plasmas need to be fully pinched off from the PF coils for the purpose of minimizing the hot ions heated by the reconnection/merging. This promising scaling is expected to realize the burning plasma temperature $T_i > 10$ keV just by increasing B_{rec} over 0.6 T (under the constant electron density $n_e \sim 1.5 \times 10^{19}/\text{m}^3$), leading us to construction of new high- B_{rec} field merging ST devices: TS-U in the University of Tokyo and ST-40 in Tokamak Energy, Inc.

EX

Safety Factor Profile Control with Reduced CS Flux Consumption During Plasma Current Ramp-Up Phase Using Reinforcement Learning Technique

T. Wakatsuki¹, T. Suzuki¹, N. Hayashi¹, N. Oyama¹, S. Ide¹, and Y. Kamada¹

¹*National Institutes for Quantum and Radiological Science and Technology (QST),
Naka Fusion Institute, Naka-shi, Ibaraki-ken, Japan*

Corresponding Author: T. Wakatsuki, wakatsuki.takuma@qst.go.jp

Safety factor profile control via active feedback control of electron temperature profile during a plasma current ramp-up phase of a DEMO reactor is investigated to minimize the magnetic flux consumption of a central solenoid (CS) for wide range of q profiles. It is shown that q profiles with positive, weak and reversed magnetic shear can be obtained with less than half of the empirical estimation of the resistive flux consumption (Ψ_{res}). For the optimization of time dependent feedback gain, we introduced a reinforcement learning technique. This enables to follow a rapid change in the target profile of the electron temperature by changing the feedback gain adaptively. With this adaptive feature of the reinforcement learning, we also confirmed that T_e profile can be controlled in the plasma simulation with various thermal transport property by one control system.

EX

2D and 3D Modelling of JT-60SA for Disruptions and Plasma Start-Up

G. De Tommasi^{1,2}, F. Villone^{1,2}, T. Bolzonella³, D. Corona⁴, N. Cruz⁴, E. Joffrin⁵, M. Mattei^{6,2}, G. Matsunaga⁷, A. Mele^{1,2}, Y. Miyata⁷, A. Pironti^{1,2}, T. Suzuki⁷, and H. Urano⁷

¹Università degli Studi di Napoli Federico II, 80138 Napoli, Italy

²Consorzio CREATE, Università degli Studi di Napoli Federico II, 80138 Napoli, Italy

³Consorzio RFX, Associazione EURATOM-ENEA sulla Fusione, Padova, Italy

⁴Institute of Plasmas and Nuclear Fusion (IPNF), Instituto Superior Técnico (IST), 1049-001 Lisbon, Portugal

⁵Institut de Recherche sur la Fusion par confinement Magnétique (IRFM),

Commissariat à l'énergie atomique (CEA/Cadarache), 13108 St. Paul lez Durance, France

⁶Università degli Studi della Campania "Luigi Vanvitelli", 80131 Aversa, Italy

⁷National Institutes for Quantum and Radiological Science and Technology (QST),

Naka Fusion Institute, Naka-shi, Ibaraki-ken, Japan

Corresponding Author: G. De Tommasi, detommas@unina.it

The JT-60SA is a superconducting tokamak device being built as a joint international project between Japan and Europe in the frame of the broader approach agreement. One of the main goals of JT-60SA is to study practical and reliable plasma control schemes in view of the power plant. Plasma electromagnetic modelling is one of the essential tools for plasma operation in a fusion device and they require detailed models for ensuring an accurate preparation of the magnetic controllers. To achieve this goal, suitable models are needed at different level of details. 2D plasma nonlinear equilibrium codes are used to develop the operational scenarios and to perform breakdown studies. Furthermore, three-dimensional modelling permits the assessment of 3D vessel structures on the plasma behaviour, e.g., during disruptions, as well as to study nonaxisymmetric plasma instabilities. On the other hand, engineering-oriented models are essential for the commissioning of the magnetic diagnostics, and the design of control algorithms.

In this context, a set of alternative modelling tools based on the CREATE 2D equilibrium codes have been developed as additional benchmark for magnetic modelling. These tools have been exploited to perform breakdown studies and to design a preliminary functional architecture of the plasma magnetic control system. Furthermore, several studies of the impact of three-dimensional structures on plasma evolution have been carried out, ranging from pure electromagnetic analysis of the magnetic field produced by the nonaxisymmetric coils, to nonlinear evolution of $n = 0$ instabilities. In this paper, we report on the activities that have been carried out exploiting the CREATE modelling tools. In particular, 2D modelling has been exploited to study the magnetic configurations for the EC assisted breakdown, while 3D tools have been used to evaluate the effect of three-dimensional structures on evolutionary equilibrium of axisymmetric plasmas.

New Approach to the Control of Particle Recycling Using Divertor Pumping in LHD

G. Motojima^{1,2}, S. Masuzaki^{1,2}, T. Morisaki^{1,2}, H. Tanaka³, R. Sakamoto^{1,2}, T. Murase¹, O. Schmitz⁴, M. Kobayashi^{1,2}, M. Shoji¹, M. Tokitani^{1,2}, Y. Tsuchibushi¹, H. Yamada^{1,2}, and Y. Takeiri^{1,2}

The LHD Experiment Group

¹National Institute for Fusion Science (NIFS), Toki, Gifu, Japan

²Department of Fusion Science, Graduate University for Advanced Studies (SOKENDAI), Toki, Gifu, Japan

³Nagoya University, Nagoya, Japan

⁴University of Wisconsin-Madison, Madison, WI 53706, USA

Corresponding Author: G. Motojima, motojima.gen@lhd.nifs.ac.jp

Superior control of particle recycling and of plasma density has been established in the Large Helical Device (LHD) using greatly enhanced active pumping of the closed helical divertor (CHD). In-vessel cryosorption pumping systems inside the CHD in five out of ten inner toroidal divertor sections have been developed and installed step by step in LHD. The total effective pumping speed obtained was $67 \pm 5 \text{ m}^3/\text{s}$ in hydrogen, which is approximately seven times larger than previously obtained. As a result, a low recycling state was observed with the CHD pumping for the first time under the helical divertor configuration in LHD featuring excellent density control even under intense pellet fuelling conditions. A global particle confinement time is used for comparison of operation with and without the CHD pumping. The global particle confinement time was evaluated from the density decay after the fuelling of hydrogen pellet injection or gas puffing in NBI plasmas. A short global particle confinement time after the fuelling was obtained during the CHD pumping, demonstrating the control of the particle balance with active pumping in CHD for the first time in LHD.

EX

Broadband Characterization of High Temperature Blackbody Source with Fourier Transform Michelson Interferometer for ECE Measurements

A. Sinha¹, S. K. Pathak¹, S. Schmuck², and J. Fessey²

¹*Institute for Plasma Research (IPR), Bhat, Gandhinagar, India*

²*Culham Centre for Fusion Energy (CCFE), Culham Science Centre, Abingdon, UK*

Corresponding Author: A. Sinha, abhishek@ipr.res.in

EX In a tokamak electron cyclotron emission (ECE) is measured to determine electron temperature profile and its evolution. Michelson interferometer (MI) diagnostic is capable of measuring the spectrum of the ECE in a wide spectral range (70–500 GHz). Usually MI is calibrated with hot-cold technique. The lab calibration of the MI diagnostics is carried out locally with room temperature and cold source. The absolute calibration of the diagnostics is done with transmission lines, bends, mode converters, etc. During absolute calibration signal is below noise level and very long integration time is required to improve S/N ratio. Hence a high temperature calibration source is required to reduce the integration time. This paper deals with the design, development and characterization of a high temperature blackbody source. This source has been developed by precise machining of cones on a metallic surface and then coating it with silicon carbide paste and electrically heating to a temperature of 873 K. The broadband characterization of this high temperature source has been done with hot–cold technique. Initially, the calibration factor of the system is determined by periodic switching between the room temperature source (RAM material) and the cold source (LN₂ at 77 K). The calibration factor obtained from two sources at known temperatures is used to determine the radiation temperature of the unknown high temperature (hot) blackbody source by Fourier transform MI over a wide frequency range of 70–1000 GHz. The characterization process will be described in the paper in detail. The radiation temperature of the hot source measured during characterization was found to be in the range 737–755 K in entire band. The radiation temperature was about 125 K below the physical temperature of the hot source due to radiation losses. Dips were observed at frequencies 557 GHz and 753 GHz indicating the presence of water absorption lines as expected. The broadband characterization of high temperature blackbody source with MI has been carried out successfully and results have been presented.

Design and Development of 140 GHz D-Band Phase-Locked Heterodyne Interferometer System for Real-Time Density Measurement

U. C. Nagora¹, A. Sinha¹, S. K. Pathak¹, and P. Ivanov²

¹*Institute for Plasma Research (IPR), Bhat, Gandhinagar, India*

²*ELVA-1 Millimetre Wave Division, St. Petersburg, Russian Federation*

Corresponding Author: U. C. Nagora, omesh@ipr.res.in

In a tokamak, an interferometer system measures plasma density using an electromagnetic wave which experiences a phase shift with respect to a reference signal while passing through the plasma column. In millimetre wave spectra, usually homodyne and heterodyne systems are used to determine phase information. One of the limitations of the homodyne scheme was its inability to differentiate the increase or decrease in phase and corresponding plasma density. Hence a heterodyne scheme was required which can detect the increase or decrease of phase with precision and is capable of real-time density measurement with feedback control. This paper deals with the design, development and characterization of a 140 GHz D-Band phase-locked heterodyne interferometer system with real-time density measurement. Here the transmitter and receiver are phase-locked by a reference crystal oscillator of 100 MHz to provide a stable signal and minimize errors in measurement due to phase mismatch. This phase locking provides a highly stabilized intermediate frequency (IF) of 2 GHz. The IF signal is further down converted by IQ mixer to 100 KHz in-phase (I) and quadrature (Q) signals in the form of sine and cosine waves. These signals are used to calculate the absolute phase by the zero crossing method. These signals are digitized by a 12-bit ADC. The controller uses the digitized signals to generate a real-time density signal which can be used for density feedback control. The system has a temporal resolution of $5\mu\text{s}$ and phase error measurement of 0.07 radians. The performance of the microwave and RF electronics has been shown in the paper. The overall performance of the heterodyne phase locked interferometer system with AGC signal has been presented. Laboratory tests results and plasma results after installation of the system on ADITYA tokamak has been presented. Real-time density signals and actual density signal have been measured for various plasma shots and will be presented.

EX

Study of Iron Impurity Behaviour Using VUV Spectroscopy in ADITYA and ADITYA-U Tokamak

S. Patel¹, M. B. Chowdhuri², A. K. Srivastava¹, R. Manchanda², A. Bhattacharya³, and J. Ghosh^{2,3}

¹Birla Institute of Technology, Jaipur Campus, India

²Institute for Plasma Research (IPR), Bhat, Gandhinagar, India

³Indian Institute of Technology Kanpur, Kalyanpur, Uttar Pradesh, India

Corresponding Author: S. Patel, patel.sharvil8@gmail.com

Studies of medium and high- Z impurities behaviour in high temperature tokamak plasmas have become important considering molybdenum and tungsten are being considered as the first wall materials due to the high melting points and capabilities to handle high heat load. These impurity ions are present mainly due to sputtering processes involving plasma facing components in contact with the edge plasma. Presence of such spectrum of impurities leads to enhanced energy loss, fuel dilution and overall degradation of plasma properties. Thus the study of the behaviour of impurities is carried out in ADITYA and ADITYA-U tokamaks. VUV spectra from impurities is regularly monitored using a absolute calibration VUV survey spectrometer having operation in the spectral range of 10–180 nm, which covers the important lines of partially ionized low and medium- Z impurities and also emissions from higher excited states of highly ionized low- Z impurities. Absolute intensity calibration of this system has been carried out using branching ratio and by simulating the VUV spectra and then comparing those with experimental counts. VUV spectral lines at 28.41 nm ($3p^6 3s^2 \ ^1S_0 - 3s 3p \ ^1P_1$) from Fe^{14+} and, 33.54 nm ($2p^6 3s^2 \ ^2S_{1/2} - 2p^6 3p \ ^2P_{3/2}$) and 36.08 nm ($2p^6 3s^2 \ ^2S_{1/2} - 2p^6 3p \ ^2P_{1/2}$) from Fe^{15+} are measured during the current flat-top region of ADITYA and ADITYA-U tokamak plasmas. The behaviour of iron emission has been studied with respect to plasma parameters and its measured penetration into the plasma has been compared with simulated spectral emissions by taking the impurity transport and relevant atomic data generated using ADAS database.

EX

Runaway Electron (RE) Mitigation Using Supersonic Molecular Beam Injection in the ADITYA-U Tokamak

S. Banerjee¹, H. Raj¹, J. Ghosh¹, N. K. Bisai¹, A. K. Singh¹, S. George¹, R. Manchanda¹, M. B. Chowdhuri¹, R. L. Tanna¹, J. V. Raval¹, Y. Paravastu¹, D. Chandra¹, and A. Sen¹

The ADITYA-U Team

¹*Institute for Plasma Research (IPR), Bhat, Gandhinagar, India*

Corresponding Author: S. Banerjee, sbanerje@ipr.res.in

In fusion devices, runaway electrons (REs) with energies ≥ 10 MeV, generated predominantly during plasma disruptions, can penetrate through the low- Z first wall and melt the interface of actively cooled parts. Majority of disruptions display MHD modes, as precursors. Radiation cool-off at the edge is seen to trigger abrupt growth of MHD modes, mode locking and thereby disruptions. The REs are generated due to increase in plasma resistivity following the thermal quench (TQ). REs pose severe threat to the lifetime of the first wall components and increase the machine down time substantially. Hence, mitigation of REs are a must for successful operation. Several RE mitigation techniques have been tried out in different machines, such as massive gas injection, and resonant magnetic perturbations. However, the effect of both these mechanisms are restricted to the very edge of the tokamak and REs primarily generated inside the plasma following the TQ, are not completely affected by these techniques. Enhancing magnetic fluctuations during disruptions is an alternate method and a more penetrative fuelling technique is required to achieve that. Significant RE flux has been found to suppress the magnetic fluctuations and considerable RE current is generated during the disruptions. There is a recent experimental observation of suppression of the RE current during disruptions by the magnetic perturbations, excited by the supersonic molecular beam injection (SMBI). However, a detailed understanding of the underlying dynamics of such a suppression is far from being completely understood. The present campaign on ADITYA-U explores such a phenomenon over a wide range of experimental parameters. An SMBI system has been installed on the low field side with a Laval nozzle of throat diameter 0.5 mm and a fast response solenoid valve. The plenum gas pressure can be varied to adjust the speed/penetration of the beam. A particle flux of 2.6×10^{22} particles/s is achievable at a plenum pressure of 1 MPa. Volume hard X-rays are monitored along a central chord and suitable SMBI is launched based on the spatial location of the REs to mitigate them in real-time. Interaction of SMBI with REs and magnetic fluctuations will be reported. Finally, a 1D code to study the transport dynamics during SMBI has been developed and simulation results in support of the experiments will also be presented.

EX

Neon Gas Seeded Radiative Improved Mode in ADITYA-U Tokamak

M. B. Chowdhuri¹, J. Ghosh¹, R. L. Tanna¹, K. A. Jadeja¹, K. M. Patel¹, R. Manchanda¹, N. Yadav², P. Pandit¹, S. Patel³, G. Shukla⁴, K. Shah⁴, H. Raj¹, L. T. Lachhvani¹, S. N. Pandya¹, S. B. Bhatt¹, N. C. Patel¹, S. Banerjee¹, U. C. Nagora¹, S. K. Pathak¹, P. K. Atrey¹, J. V. Raval¹, Y. S. Joisa¹, M. V. Gopalakrishna¹, K. Tahiliani¹, C. N. Gupta¹, and P. K. Chattopadhyay¹

¹Institute for Plasma Research (IPR), Bhat, Gandhinagar, India

²Gujarat University, Navrangpura, Ahmedabad 380 009, India

³Birla Institute of Technology, Jaipur Campus, Jaipur 302 017, Rajasthan, India

⁴Pandit Deendayal Petroleum University, Raisan, Gandhinagar, 382 007, Gujarat, India

Corresponding Author: M. B. Chowdhuri, malay@ipr.res.in

EX Neon impurity injection into the tokamak plasma has been found to improve the plasma confinement, known as radiative improved (RI) mode in many tokamaks. It is believed that improved confinement in the RI mode is mostly based on the reduction of growth characteristics of the toroidal ion temperature gradient (ITG) mode due to the increase of Z_{eff} and also because of the suppression of turbulence due to increase of $E \times B$ shear rotation in the impurity injected plasma. During the last phase of operation of ADITYA tokamak, neon gas was puffed at the plasma current flat-top region to obtain RI mode [1]. In that experiment, the time for the gas puff to start, time gap between gas puffs, number of gas puffs, amount of gas injection by varying pulse width and voltage level in the gas fuelling system were varied. It was found that line average electron density, n_e and central electron temperature were increased after the neon puff. Substantial change in plasma edge properties was observed with the increase of radiation and reduction of hydrogen recycling, which led to better particle confinement. The energy confinement time, τ_e , is increased by a factor of 2 from 6.3 to 12.5 ms. This is almost the same as the H-mode scaling law of ITER93 ELM-free and 1.4 times the Neo-Alcator scaling for Ohmically heated tokamak plasma. In ADITYA-U tokamak, an experiment with neon gas puff was carried out to obtain the RI mode and understand the physical mechanism. Along with various similar results obtained earlier in ADITYA, many interesting outcomes observed during the experiments in ADITYA-U tokamak will be reported in this presentation.

References

[1] R. L. Tanna *et al.*, Nucl. Fus., **57**, 102008 (2017).

Impurity Screening in High Density ADITYA Tokamak Plasmas

R. Manchanda¹, M. B. Chowdhuri¹, N. Yadava², J. Ghosh^{1,3}, P. Pandit¹, S. Patel³, G. Shukla⁴, K. Shah⁴, S. Banerjee¹, N. Nimavat¹, K. Tahiliani¹, M. V. Gopalakrishna¹, U. C. Nagora¹, P. K. Atrey¹, J. V. Raval¹, Y. S. Joisa¹, K. A. Jadeja¹, and R. L. Tanna¹

The ADITYA Team

¹Institute for Plasma Research (IPR), Bhat, Gandhinagar, India

²Gujarat University, Navrangpura, Ahmedabad 380 009, India

³Birla Institute of Technology, Jaipur Campus, Jaipur 302 017, Rajasthan, India

⁴Pandit Deendayal Petroleum University, Raisan, Gandhinagar, 382 007, Gujarat, India

Corresponding Author: R. Manchanda, mransjana@ipr.res.in

Impurity behaviour has been studied for the high density ADITYA tokamak plasmas. These discharges were operated with higher toroidal magnetic fields and thereby sustained higher plasma current. Higher densities were achieved with the help of multiple gas puffs. High energy confinement times, sometimes higher than the values predicated by Neo-Alcator scaling for Ohmically heated tokamak plasma were achieved for these discharges [1]. In ADITYA tokamak, visible and VUV spectroscopy have been extensively used to study the impurity behaviour. The neutral hydrogen and impurity emissions were routinely monitored by optical fibre, interference filter and PMT based system in the visible range. The spectral line emissions from higher ionized charge state of impurities, such as C^{4+} , and O^{5+} , were recorded by a VUV survey spectrometer operated in the 10–180 nm. This wavelength range covers the important lines of partially ionized low and medium Z impurities, as for example iron and also emissions from higher excited states of highly ionized low- Z impurities, like carbon and oxygen. It has been found that H_{α} , OII, and CIII emissions normalized with density (n_e), and visible continuum normalized with n_e^2 show a gradual decrease with increase in density indicating lower impurity concentration in the high density discharges. This is also corroborated by the observed reduction in radiation power losses with increase in n_e . These results clearly suggest the achievement of improved confinement for ADITYA plasma and are correlated with obtained higher energy confinement times in those discharges. In this presentation, details studies on impurity behaviour for its role into the improved plasma properties in these high densities plasma discharges will be discussed.

References

[1] R. L. Tanna *et al.*, Nucl. Fus., **57**, 102008 (2017).

Radiation Power Loss Study During Gas Puff Induced Disruptions in ADITYA-U Tokamak

K. Tahiliani¹, M. B. Chowdhuri¹, M. V. Gopalakrishna¹, K. A. Jadeja¹, K. M. Patel¹, P. Kumari¹, U. C. Nagora¹, J. V. Raval¹, H. Raj¹, L. T. Lachhvani¹, S. N. Pandya¹, R. Manchanda¹, P. K. Atrey¹, S. K. Pathak¹, R. L. Tanna¹, J. Ghosh¹, and A. Kumar¹

¹*Institute for Plasma Research (IPR), Bhat, Gandhinagar, India*

Corresponding Author: K. Tahiliani, kumud@ipr.res.in

Understanding the density limit in a tokamak is very crucial for projecting the fusion grade tokamak machine. An important role in the disruptions for density limit is played by magnetohydrodynamic (MHD) instabilities associated with the steepening of the current density profile due to the current channel contraction. This shrinkage in the current channel due to increasing densities is related to the plasma edge cooling induced by influx of particles. Thus the disruption associated with density limit not only depends on the magnetohydrodynamic (MHD) physics, but also seems to involve transport and atomic processes as well. The gas puff experiments are carried out in a tokamak to understand the physics of plasma disruptions. We report here the study of radiation power loss in disruptive discharges. In ADITYA tokamak, multiple pulses of hydrogen gas were injected during the current flattop in the plasma discharge. The gas puff lead to an increase of 20–80% in central plasma density and many-fold increase in the radiation power loss from the plasma edge. The nature and distribution of radiation power loss was distinguishable in disruptive discharges and those discharges that had improved confinement, some of which were due to the edge cooling induced fluctuation suppression. Similar experiments are carried out in ADITYA-U tokamak with various gases, in which along with further establishment of the results obtained in ADITYA with thorough data analysis, many interesting outcomes observed during the experiments in ADITYA-U will be reported in this presentation.

EX

Observations of Intrinsic Toroidal Rotation Using X-Ray Crystal Spectrometer in ADITYA-U Tokamak

K. Shah¹, G. Shukla¹, M. B. Chowdhuri², H. Raj³, R. Manchanda², R. L. Tanna²,
K. M. Jadeja², K. Patel², K. B. K. Mayya¹, and J. Ghosh^{2,3}

The ADITYA-U Team

¹*Pandit Deendayal Petroleum University, Raisan, Gandhinagar, 382 007, Gujarat, India*

²*Institute for Plasma Research (IPR), Bhat, Gandhinagar, India*

³*Homi Bhabha National Institute (HBNI), Anushakti Nagar, Mumbai 400094, India*

Corresponding Author: K. Shah, kajal.sphd16@sot.pdpu.ac.in

A soft X-ray crystal spectrometer has been developed to measure toroidal rotation velocity and ion temperature in the core of ADITYA-U tokamak using Doppler shift and Doppler broadening of helium-like argon emission in the X-ray region respectively. The spectrometer uses cylindrically bent Si (111) crystal and two dimension CCD detector to measure resonance spectral line of Ar XVII ($1S_2 \ ^1S_0 - 1S \ 2P \ ^1P_1$) and satellite lines in the wavelength region of 0.394–0.40 nm, viewing the plasma tangentially at an angle of 26° with respect to the toroidal direction in the magnetic axis. Central electron temperature is measured through line ratios and compared with other diagnostics. Neoclassical toroidal rotation has been calculated using theory and compared with observations from the experiment. The effect of variation in edge plasma parameters on the core plasma rotation has also been studied. Detailed discussion on the first results is presented in the paper.

EX

Controlling Plasma Rotation Using Periodic Gas-Puff in ADITYA-U Tokamak

G. Shukla¹, K. Shah¹, M. B. Chowdhuri², H. Raj³, R. Manchanda¹, R. L. Tanna¹, K. M. Jadeja¹, K. Patel¹, K. B. K. Mayya¹, and J. Ghosh^{2,3}

The ADITYA-U Team

¹*Pandit Deendayal Petroleum University, Raisan, Gandhinagar, 382 007, Gujarat, India*

²*Institute for Plasma Research (IPR), Bhat, Gandhinagar, India*

³*Homi Bhabha National Institute (HBNI), Anushakti Nagar, Mumbai 400094, India*

Corresponding Author: G. Shukla, gaaurav.sphd16@soot.pdpu.ac.in

EX Plasma rotation and its shear in the edge and scrape-off-layer (SOL) region plays an important role in determining overall confinement of tokamak plasmas. The sources of spontaneous generation of these rotations are still not fully understood. Furthermore, to answer the questions like whether they modify the electric field profile or electric field profile modifies the rotation and its shear, the radial profiles of toroidal and poloidal plasma rotation have been measured in ADITYA-U [1, 2] in presence and absence of multiple periodic fuel and neon gas-puffs. Further in typical ADITYA-U discharges, effects of plasma density and different MHD modes on plasma rotation are studied. The results are compared with neo-classical estimations. Plasma rotation velocity is deduced from Doppler shift of the observed line emissions in UV and visible wavelength range. Carbon spectral emission lines at 229.69, 227.09 and 529.01 nm from C^{2+} , C^{4+} , and C^{5+} , respectively are used to estimate the rotation velocity. The collection optics, installed on a tangential viewport of the tokamak, contains three lines-of-sight giving a radial profile of rotation velocity. The Doppler shift of the above spectral lines are measured using a high-resolution 1 m $f/8.7$ Czerny-Turner spectrometer equipped with 1800 g/mm grating coupled to a fast CCD detector. The details on the development of the diagnostics with an emphasis on the results obtained from ADITYA-U plasma rotation profile will be discussed.

References

- [1] S. B. Bhatt *et al.*, Indian J. Pure Appl. Phys., **27**, 710 (1989).
- [2] J. Ghosh *et al.*, IAEA FEC-2016, Kyoto, Japan, [FIP/P4-46](#), (2016).

Effect of Externally Applied Radial Electric Field (Biased-Electrode) on Geodesic Acoustic Modes in SINP Tokamak

L. T. Lachhvani¹, J. Ghosh¹, T. Macwan¹, P. K. Chattopadhyay¹, N. Chakrabarty², and R. Pal²

¹*Institute for Plasma Research (IPR), Bhat, Gandhinagar, India*

²*Saha Institute of Nuclear Physics, 1/AF Bidhannagar, Kolkata 700064, India*

Corresponding Author: L. T. Lachhvani, lavkesh@ipr.res.in

Geodesic acoustic modes (GAMs), believed to play an important role in L-H transition in tokamaks, are the high frequency branch of the zonal flows and are characterized by toroidally and poloidally symmetric in potential $\phi(n = 0, m = 0)$ and toroidally symmetric but poloidally asymmetric in density perturbation ($n = 0, m = 1$). The coherent modes in the spectral analysis of floating potential fluctuations measured in the edge plasma region of Saha Institute for Nuclear Physics tokamak (SINP-tokamak) using Langmuir probes are recently identified as geodesic acoustic modes (GAMs) having different characteristics over a wide range of q_{edge} . The mode is radially localized in the edge plasma and have finite radial propagation. These coherent modes are simultaneously observed in density and radial electric field fluctuation spectra as well. The observed mode conclusively exhibits all the characteristics of the continuum GAM in the discharges having q_{edge} values from 3.0 to 6.0 in normal tokamak regime. In this range of q_{edge} , the poloidal and toroidal components of the wave-vector clearly show the $n \sim 0, m \sim 0$ structure of the mode and the frequency of the mode, and its variation with q_{edge} matches quite well with that predicted by theory. In the intermediate range of $q_{\text{edge}} = 2.5\text{--}3$, the mode exhibits the eigenmode GAM like characteristics as the frequency of modes does not depend on the local plasma parameters; however, the structures remained of $n \sim 0, m \sim 0$ type. Decreasing q_{edge} below 2.5, the mode characteristics change significantly with the poloidal wave number becoming finite. Further, these modes are observed to be affected by the externally applied radial electric fields. The radial electric fields are induced by inserting a biased electrode inside the last closed flux surface of SINP-tokamak plasma. Interestingly, it is observed that the radial electric field affect the frequency and amplitude of GAM modes. Frequency range of the typical eigenmode GAM widens, owing to increase in temperature of the plasma due to improved confinement. Amplitude of the mode is observed to increase with bias potential.

EX

Application of TEM to Study the Changes in Subsurface Defects in Tungsten Samples as a Function of Annealing Temperature

S. Akkireddy¹, P. Sharma², P. N. Maya², P. K. Mokaria¹, S. Mishra³, K. B. Khan³,
P. M. Raole², S. S. Mukherjee¹, and S. P. Deshpande²

¹*Institute for Plasma Research (IPR), Bhat, Gandhinagar, India*

²*International Thermonuclear Experimental Reactor (ITER), India Centre, Gujarat, India*

³*Bhabha Atomic Research Centre (BARC), Mumbai, India*

Corresponding Author: S. Akkireddy, asprasad@ipr.res.in

In a nuclear fusion reactor, hot and dense DT plasma is confined using a combination of magnetic fields in a toroidal shaped vacuum vessel. Interaction of this plasma with the vacuum vessel wall materials is one of the very important areas of interest as plasma-wall interactions will decide the operational lifetime of the reactor in terms of plasma as well as material stability. The choice of the wall-material hence becomes an important factor and high atomic number materials such as tungsten, W, and its alloys are currently identified as candidate materials due to their relatively low H-isotope affinity. However, high energy neutrons and α particles produced in the fusion reaction can introduce subsurface defects in tungsten, which may lead to H-isotope trapping through these defective sites.

EX

In order to understand the effect of these defects, it is critical first to identify them. The defects concerned here, such as dislocations, are like bulk features of the materials and cannot be identified using surface characterization equipment such as scanning electron microscope (SEM). Transmission electron microscope (TEM) is one of the very few instruments which can identify these meso-scale subsurface defects. In the work discussed here, we had used a 300 kV TEM to identify these defects in W samples. TEM microscopy of the as received W samples (cold rolled) was carried out. Grains were observed to be elongated and the dislocation density is very high. Later the W samples were subjected to annealing at various temperatures ranging from 773 K to 1838 K. The annealing was carried in a vacuum furnace under a reducing atmosphere of Ar and H₂ mixture. A base pressure of 10⁻⁵ mbar was obtained before the Ar-H₂ mixture was introduced. The effect of annealing temperature on the changes in defect distribution and restructuring was studied using TEM. Defect density is observed to reduce with increase in annealing temperature (below recrystallization temperature), though there is not much change in grain size. However, above recrystallization temperature, the grain size was observed to change from elongated to regular shape while the defect density was reduced. Present work also explains in detail about the sample preparation procedure adopted for preparing the W samples for TEM analysis.

Effect of Multiple Periodic Gas Puff on Neutral Temperature in ADITYA-U Tokamak

N. Yadav¹, H. Raj², R. Dey², J. Ghosh², M. B. Chowdhuri², R. Manchanda², S. Banerjee², N. Nimavat², R. L. Tanna², K. A. Jadeja², K. Pate², and D. Tripathi¹

¹Gujarat University, Navrangpura, Ahmedabad 380 009, India

²Institute for Plasma Research (IPR), Bhat, Gandhinagar, India

Corresponding Author: N. Yadav, nandini7754@gmail.com

The fuel gas injection in measured quantity during the current flat-top region of ADITYA-U tokamak discharges has been observed to modify significantly the edge and scrape-off-layer (SOL) plasma properties. The effect of these gas puffs on the neutral temperature and their penetration in the edge and SOL region has been studied by measuring the Hydrogen Balmer- α emission spectra at 656.28 nm from different lines-of-sight in the edge and SOL region in both high and low field regions of ADITYA-U. The neutral temperature is estimated from the Doppler broadening of the measured H_α spectrum by appropriately removing the contribution from the Zeeman splitting of the spectral lines. A computer simulation code has been developed in-house which generates synthetic chord-averaged H_α emission spectra at different radius of the plasma using the electron temperature, density and the magnetic field strength of that radial location measured with other diagnostics. The code includes all the broadening mechanisms such as Doppler, Zeeman, Stark or pressure broadening for simulating the H_α emission spectrum along with proper convolution of the instrumental width of the measuring system. Depending on the strength of the magnetic field, the code incorporates 7 Zeeman components in case of normal Zeeman splitting, whereas 48 components (18π and 30σ) are included in the case of Paschen-Back Zeeman splitting. The simulated spectra are used to obtain true values of neutral temperatures by iteratively fitting them to the measured spectrum from the edge and SOL region of ADITYA-U tokamak [1]. Furthermore, the developed code has been used to isolate the cold, warm and hot (charge exchange) components of the hydrogen atoms from the measured H_α emission spectra from the edge region of ADITYA-U tokamak.

References

[1] S. Banerjee *et al.*, J. Plasma Fusion Res. Series **9**, 29 (2010).

Design of a NIR Spectrometer for ADITYA-U Tokamak and Initial Results

P. Pandit¹, R. Manchanda¹, R. Dey¹, J. Ghosh¹, M. B. Chowdhuri¹, and S. Banerjee¹

¹*Institute for Plasma Research (IPR), Bhat, Gandhinagar, India*

Corresponding Author: P. Pandit, drpmm15@gmail.com

The hydrogen line series is a sensitive diagnostic of detached divertor. Divertor plasma is characterized by low temperature (1–10 eV) and high density (10^{19} – $10^{20}/\text{m}^3$). The three body recombination dominates the divertor region and is highly sensitive to the divertor plasma T_e and n_e . Based on earlier experiments, NIR (800 nm–2300 nm) spectroscopy system is designed for ADITYA-U tokamak since it can be used for machine protection, plasma control and performance evaluation. Three experiments are proposed here. First is the spectral survey for Paschen H line series and low- Z impurity monitoring. The second one is to provide a validated background emission for divertor Thomson scattering experiments wherein blackbody radiation, bremsstrahlung, recombination and impurity lines contribute largely to the background noise. The third is the measurement of Br9/Pa α intensity ratio as it is a possible T_e sensitive diagnostic.

EX

The signal estimation for the Pa α line for present plasma parameters has been carried out in the edge region of ADITYA-U tokamak. Since the dark current levels of the commercially available detectors in the NIR range is significantly high ($10 \text{ Ke}^-/(\text{ps})$), signal estimation becomes important. Theoretical estimation of the line and bremsstrahlung emission for the Pa α line using the atomic data from the ADAS database has been done. These are found to be $\sim 3 \times 10^8$ and 1.5×10^8 photons/ $(\text{cm}^2 \text{ s})$ for $n_e = 1 \times 10^{12}/\text{cm}^3$, $T_e = 15 \text{ eV}$ and $n_n = 7 \times 10^9/\text{cm}^3$ respectively. The intensity estimates are well above the dark current levels of the detector. In order to observe clearly resolved spectra, the design and selection of the spectroscopic system comprising of the spectrometer, grating, detector and the collection optics plays an important role. This is also discussed in this work. With this system and with proper line of sight collection optics and optimization for maximum throughput, we can provide information on the plasma control, divertor recycling and machine protection. Initial results namely the survey spectrum and the plasma electron density and temperature estimates will be presented for various ADITYA-U plasma shots and a comparison with other existing diagnostics will be presented.

Mass Dependent Impurity Transport Study in ADITYA Tokamak

S. Mishra^{1,3}, A. K. Singh¹, M. B. Chowdhuri², R. Manchanda², S. Banerjee^{2,3}, K. A. Jadeja², K. M. Patel², R. L. Tanna², S. Varshney^{1,2,3}, and J. Ghosh^{2,3}

The ADITYA Team

¹International Thermonuclear Experimental Reactor (ITER), India Centre, Gujarat, India

²Institute for Plasma Research (IPR), Bhat, Gandhinagar, India

³Homi Bhabha National Institute (HBNI), Anushakti Nagar, Mumbai 400094, India

Corresponding Author: S. Mishra, sapna.mishra@iter-india.org

The investigation of impurities and its transport study in tokamak plasma play a vital role in determining the overall plasma performance. It is important to understand the transport of impurities in tokamak plasmas in order to control impurity inside the plasma and its deleterious consequences affecting overall plasma performance. In ADITYA, strong boron-like carbon lines are usually seen in visible range due to the interaction of plasma with graphite limiters. A 1.0 m multitrack spectrometer (Czerny-Turner) capable of simultaneous measurements from eight lines-of-sight has been used for measuring the radial profiles of C^{1+} (657.805 nm, $3s\ 2S_{1/2}-3p\ 2P_{3/2}^{\circ}$ and 658.288 nm, $3s\ 2S_{1/2}-3p\ 2P_{1/2}^{\circ}$). The carbon transport coefficients are determined by modelling the experimentally measured emissivity profiles of C^{1+} , using a one-dimensional empirical impurity transport code, STRAHL. This code has been earlier also used for studying the oxygen impurity transport in ADITYA which reveals a higher values of the diffusion coefficient compared with the neoclassical values in both the high magnetic field edge region (D_{\max} inboard $\sim 30\ m^2/s$) and (D_{\max} outboard $\sim 45\ m^2/s$) in the low magnetic field edge region [1]. Similar studies are carried out for Ne by injecting neon using neon spectral lines in the UV/visible region at the plasma current flat-top.

In this paper, we compared the transport coefficients of all the three impurity species, i.e., carbon, oxygen, neon etc., through the modelling (using STRAHL code) of experimental emissivity profiles recorded in the typical discharges of ADITYA tokamak. The transport coefficients for these species are determined by minimizing the residual error between the measured and calculated emission profiles for all the three species. By comparing the diffusion coefficient of three species, understanding the mass dependency of impurity transport has been attempted in ADITYA tokamak.

References

[1] M. B. Chowdhuri *et al.*, Nucl. Fus., **53**, 023006 (2013).

Plasma Potential Measurements in the Edge Region of ADITYA-U Tokamak Using Reciprocating Laser Heated Emissive Probes

A. Kanik¹, J. Ghosh², P. Pandit², and A. Sarma¹

The ADITYA-U Team

¹VIT University, Vandalur-Kelambakkam road, Chennai, India

²Institute for Plasma Research (IPR), Bhat, Gandhinagar, India

Corresponding Author: A. Kanik, abhakanik@gmail.com

Laser heated emissive probes (LHEP) have several advantages over conventional filament emissive probes and serve as a tool for direct measurement of plasma potential. Measurement of plasma potential or electric field components perpendicular to magnetic field are necessary for the fundamental understanding of plasma parameters, transport mechanisms and space charge distribution in plasmas. Owing to the complexities of tokamak geometries and the high temperature magnetically confined environment, very few attempts have been made for using emissive probes on such complex devices. Here we present a novel design of the LHEP for ADITYA-U tokamak involving a radially movable probe shaft with dual probe tip provision made up of LaB₆. A CW CO₂ laser at 10.6 μm and up to 55 W is continuously focussed on the probe tip, using a specialized forced-air cooled fibre, despite the radial movement. The set-up is designed for direct measurement of radial profiles of the plasma potential in the edge plasma region of ADITYA-U tokamak. Probe is biased with respect to plasma potential and I-V is acquired with high sampling frequency. The obtained I-V is plotted and explored for the estimation of ion density, electron temperature and plasma potential. Experimental results are reported herein and discussed.

EX

Edge Current Density Profile Measurement Using an Array of Miniature Magnetic Probes in ADITYA-U Tokamak

T. Macwan^{1,2}, H. Raj^{1,2}, R. Kumar¹, D. Kumawat^{1,2}, S. Aich^{1,2}, K. A. Jadeja¹, K. M. Patel¹, R. L. Tanna¹, and J. Ghosh¹

The ADITYA-U Team

¹*Institute for Plasma Research (IPR), Bhat, Gandhinagar, India*

²*Homi Bhabha National Institute (HBNI), Anushakti Nagar, Mumbai 400094, India*

Corresponding Author: T. Macwan, tanmay.macwan@ipr.res.in

The current distribution inside the tokamak needs to be known for understanding the magnetohydrodynamic (MHD) stability and transport. However, the measurement of the current density radial profile is not easy. The external magnetic measurements yield only the plasma shape and global current profile parameters such as β_p and I_i in tokamaks. The radial current density profile is reconstructed using simulations codes such as EFIT incorporating the external magnetic measurements and kinetic profile measurements.

The radial profile of current density in the edge and scrape-off-layer (SOL) is measured for ADITYA-U tokamak using a set of miniature magnetic probes which are inserted inside the last closed flux surface (LCFS). These magnetic probes are designed, fabricated, calibrated and installed in ADITYA-U tokamak, a medium sized air core tokamak with a major radius of 0.75 m and a minor radius of 0.25 m. These coils can be translated along the radial direction and rotated along the axis using a multimotion feedthrough. The linear motion provides the radial profile whereas the rotational motion provides the angular profile of the current density. These miniature coils are housed inside a ceramic assembly for thermal and electrical insulation from the plasma. The coils are adequately calibrated for the frequency response using a test setup before inserting into the tokamak. The current density profile in the edge and SOL region of ADITYA-U tokamak has been successfully measured. The results obtained from the probes will be corroborated by those obtained from an array of miniature Rogowski coils planned to be inserted inside the LCFS. Further, the results are justified by comparison with the measurement of plasma position using a pair of Sine-Cosine Rogowski coils installed in the tokamak. The measured profile matches reasonably well with that reconstructed using EFIT code. After thoroughly establishing the measurements, the changes in current density profile in the edge and SOL region due to externally applied radial electric field with biased electrode and during multiple periodic gas puffing have been studied. The details of probe installation and operation along with current density profile modification due to radial electric field application and multiple periodic gas puff application will be presented in this paper.

EX

Development of Multipurpose Soft X-Ray Tomography System for ADITYA-U

J. V. Raval¹, A. K. Chattopadhyay¹, Y. S. Joisa¹, S. Purohit¹, and P. K. Shukla¹

¹*Institute for Plasma Research (IPR), Bhat, Gandhinagar, India*

Corresponding Author: J. V. Raval, ravaljv@ipr.res.in

Study of soft X-ray (SXR) radiation emitted during plasma discharge gives valuable information on magnetohydrodynamic (MHD) activities, e.g., the nature of minor and major disruptions, mode structure, magnetic island, plasma shape, plasma position and chord average electron temperature in tokamak. Intensity of SXR radiation depends mainly on electron temperature, plasma density as well as on plasma impurities, and is routinely measured with SXR photodiode array. SXR tomography is a powerful diagnostic tool that uses line-integrated measurements of SXR radiation and reconstructs two dimensional SXR emissivity profiles. For this purpose, SXR cameras having array of photodiode detectors are required to mount suitably around poloidal plane of the tokamak. Multipurpose SXR tomography (SXRT) system is designed and developed using 16 channel absolute XUV detector array for ADITYA-U to perform above measurements. In this report, discussions are centred on: 1) the determination of minimum number of SXR cameras and detectors to reconstruct emissivity profile for $m = 2$ mode structure which plays a major role for total disruption of plasma; 2) Fourier-Bessel expansion techniques used in SXR tomography software for the reconstruction of two dimensional SXR emission profile; 3) SXRT camera design, electronics and data acquisition system; and 4) first results of experimental campaigns in ADITYA-U.

EX

Ka-Band Reflectometer System for Measuring Radial Electron Density Profile at IPR

J. J. U. Buch¹, S. K. Pathak¹

¹*Institute for Plasma Research (IPR), Bhat, Gandhinagar, India*

Corresponding Author: J. J. U. Buch, jjubuch@ipr.res.in

The determination of electron density and its fluctuations are essential in understanding the physical principles that determine the confinement in tokamaks. ADITYA tokamak at IPR is routinely operated with a peak density of $\sim 3 \times 10^{19}/\text{m}^3$ and a typical magnetic field of 0.75 T. We present and describe the bench test calibration and its results and the designed FMCW reflectometer which is capable of measuring the electron density profile, $n_e(r)$ in the range $0.84\text{--}1.98 \times 10^{19}/\text{m}^3$ with minimal access requirements.

We assume a parabolic density profile and plot the resultant variation in plasma frequency and thus Ka-band from 26.5 to 40 GHz is selected. A Ka-band frequency modulated continuous wave (FMCW) reflectometer has been designed and developed to measure the electron density profile. It is to be operated in O-mode due to its simplicity. The superheterodyne detection scheme in conjunction with quadrature down-conversion is used for unambiguous phase determination. To overcome the deleterious effects of plasma density fluctuations, the implemented reflectometry system is capable of ultrafast sweep over the entire Ka-band in $5 \mu\text{s}$ and has high data acquisition rates of 200 MSps. The voltage controlled oscillator (VCO) used as the frequency source was linearized by nonlinear tuning voltage as input which resulted in only 5% variation in the output beat frequency. Oversized waveguides in the X-band (WR-90) have been used to minimize the waveguide dispersion over the swept frequency range. The complete system is controlled by a master trigger received from the tokamak control room which is fed to a trigger pattern generator which triggers the microwave circuit and the data acquisition system at predetermined times.

The reflectometer has been calibrated in lab and in-situ in tokamak hall using a custom coaxial delay line for circuit delay as well as the waveguide delay for a length of 9.6 m. The dispersion in delay was found by placing metallic mirrors at different locations and finding the internal circuit delay while the dispersion in waveguide is calculated for rectangular waveguides. Multiple (> 25) sweeps were done for each position of the mirror and the results obtained showed very good repeatability.

EX

Experimental Investigation of Power Coupling by RF Antenna into Plasmas in Presence of Magnetized Ions

J. K. Joshi¹, S. K. Karkari¹, and S. Kumar¹

¹*Institute for Plasma Research (IPR), Bhat, Gandhinagar, India*

Corresponding Author: J. K. Joshi, jay.joshi@ipr.res.in

Capacitive discharges are created in the near field regions of ICRF antennas and thus power coupling by these antennas depend on the sheaths around them. Magnetization of ions in the plasma around these antennas also affects the power coupling into the plasma with major implications in ICRF antenna's in tokamaks.

A capacitive discharge is designed to study power coupling in such plasmas in a linear device. A symmetric capacitively coupled helium discharge is created by three cylindrical electrodes placed at specific axial positions in a linear chamber in presence of axial magnetic fields. Axial magnetic field is strong enough to magnetize helium ions with their cyclotron radius smaller than, the cylindrical electrode radius.

In this study, power measurement in conjunction with detail circuit analysis of magnetized capacitive sheaths has been performed to determine the plasma impedance. Plasma impedance can reveal many important aspects of the power coupling into the plasma such as the mode of discharge, power coupling to individual species (ions and electrons) and conditions of electron series resonance all of which are modified extensively in presence of magnetic field. The obtained impedance characteristics along with power measurements are qualitatively discussed to understand the effect of magnetization of ions on the discharge.

EX

A Diagnostic Approach for the Detection of Spatially Distributed Low Energy Confined Runaway Electrons in the ADITYA-U Tokamak by Means of Synchrotron Emission Imaging in the Sub-Millimetre Wavelength Band

S. P. Pandya¹, S. N. Pandya¹, A. E. Shevelev², V. V. Rozhdestvensky², and S. I. Lashkul²

The ADITYA-U Team and The FT-2 Team

¹*Institute for Plasma Research (IPR), Bhat, Gandhinagar, India*

²*Ioffe Institute, St. Petersburg, Russian Federation*

Corresponding Author: S. P. Pandya, psantosh@ipr.res.in

In recent years, the studies of runaway electron (RE) generation and energy dynamics in tokamaks have gained great importance from the theoretical and experimental perspective. The generation of high power RE beams during plasma disruption may damage in-vessel components. Therefore, it is important to study and to suppress REs for the safe operation of the large size tokamaks, such as ITER. This demands improved, robust and sensitive RE diagnostic methods to provide essential observations of confined REs when they are in the early stage of their energy and population growth. The RE-diagnostic data can be utilized for validation of the theoretical models and also to study the efficiency of the RE mitigation techniques. Out of several RE diagnostic methods, observation of the synchrotron radiation emission (SRE) from REs is an established method to detect the confined REs and studied in the several tokamaks using visible and IR cameras where the lower observed energy of the REs was reported typically more than 20 MeV. Signature of REs and supra-thermal electrons in the cyclotron emission range is often reported from several tokamaks where the energy is in the sub-MeV range. Measurements of REs in the intermediate range from 0.5 MeV to 20 MeV has always been performed by HXR and gamma-ray spectrometers. Nonimaging SRE measurements of the low energy REs ($\sim 2\text{--}7$ MeV) have been performed in the FT-2 tokamak in the range of 106–156 GHz. This motivates the design of a diagnostic that can detect SRE from the low energy confined REs in the sub-millimetre band (THz-band). In this paper, a imaging diagnostic approach has been proposed for the first time to capture spatiotemporally resolved SRE patterns of low-energy confined REs in the ADITYA-U tokamak. In order to design the diagnostic, a detailed forward modelling of RE dynamics in momentum space was performed considering the experimental evolution of the plasma parameters. The simulated RE parameters were used to predict SRE signal level at the given detector location and the diagnostics parameters were optimized. Expected spatial distribution of the SRE brightness images as seen by the THz-camera has also been modelled. From the modelling results, it has been established that the proposed design can provide spatiotemporally resolved SRE images of the confined REs in the energy range 1–20 MeV.

EX

Design and Testing of X-Mode Reflectometry System for Coupling Studies of Lower Hybrid Waves in ADITYA-U Tokamak

J. Kumar¹, P. K. Sharma¹, K. Mahant², A. V. Patel², Y. Jain¹, K. K. Ambulkar¹, and C. G. Virani¹

¹*Institute for Plasma Research (IPR), Bhat, Gandhinagar, India*

²*Charotar University of Science and Technology, Changa, Anand, Gujarat, India*

Corresponding Author: J. Kumar, jagabandhu.kumar@ipr.res.in

A new passive active multijunction antenna (PAM) has been designed and is in advance stages of fabrication for ADITYA-U tokamak. The PAM antenna has the ability to couple lower hybrid waves (LHWs) into the plasma's near cut-off densities. The coupling of LHWs depends on plasma density and its profile near the mouth of the antenna. To determine these plasma parameters experimentally, an X-mode reflectometry system has been designed and is under fabrication. The reflectometry system is designed to operate in the frequency range from 26 GHz to 36 GHz and would cover a density range from SOL to $5 \times 10^{18}/\text{m}^3$ with a toroidal magnetic field between 1 T and 1.5 T. The total frequency band is swept in 100 μs to improve density profile reconstruction. The ADITYA reflectometer is built to operate in frequency modulation continuous mode (FW-CM) or at a fix frequency mode for density fluctuation study. The reflectometry consists of two parts, i.e., the transmitter and the receiver. The transmitter mainly consists of microwave source, amplifier, a single sideband modulator (SSBM), frequency multiplier and a horn antenna to launch X-mode in to the plasma. Similarly the receiver consists of horn antenna, amplifier, mixer and demodulator. In the demodulator section, a quadratic demodulation (IQ) is used to extract in-phase and quadrature-phase information from the reflected signal. These measurements provide the density profile information. Finally, an ADC with 12 bit resolution will convert the analog signal into a digital signal which will be processed through a FPGA based data acquisition system. Sectorial E-plane horn antenna is designed using commercial available software for transmitting/receiving microwave signal to/from the plasma and has an input cross-section of 7.112 mm \times 3.556 mm and output cross-section of 7.112 mm \times 63.64 mm. The length of antenna is 120 mm. The analysis of the antenna meets our design requirement of high gain (16 dB), low insertion loss and low VSWR (1.1). As the sectorial E-plane antenna is placed inside the tokamak, the above mentioned gain is significant.

The details of the reflectometry system focussing on the design of sectorial E-plane horn antenna, microwave hardware, test result of different microwave components, along with the density profile reconstruction technique will be presented in this paper.

Design and Development of Passive Charge Exchange Neutral Particle Analyser for ADITYA-U Tokamak

S. Aggarwal¹, P. Santosh¹, and K. Ajay¹

¹*Institute for Plasma Research (IPR), Bhat, Gandhinagar, India*

Corresponding Author: S. Aggarwal, snehlata@ipr.res.in

The passive charge exchange diagnostic is well established technique for measuring coreion temperature of tokamak plasmas. Energetic neutral particles that are formed due to charge exchange of plasma ions with neutral atoms can escape from the plasma. These neutral atoms that are reionized and analyzed can provide information about the energy distribution of plasma ions [1].

A passive charge exchange neutral particle analyser has been designed and indigenously developed for ADITYA-U tokamak. It consists of an H₂ gas-cell based stripping cell, a 45-degree parallel plate electrostatic energy analyser, channel electron multipliers as detectors and an integrated measurement system CEM-IMS as DAQ. The stripping cell, which is made of soft iron, is a 200 mm long narrow tube of 4 mm diameter. The analyser box is made of soft iron (to reduce the stray magnetic field) and houses the 45-degree parallel plate electrostatic energy analyser and detectors. The CEM-IMS is a modular integrated measurement system capable of recording the measurements by remote control via network. CEM-IMS will be used as a pulse counting module to acquire output pulses of channel electron multipliers of charge exchange neutral particle analyser. Energy calibration of the neutral particle analyser has been carried out using a plasma discharge based H⁺ ion source. This paper describes the principle of coreion temperature estimation and the design, development, and calibration of the passive charge exchange neutral particle analyser for ADITYA-U tokamak plasma.

References

[1] T. A. Santosh *et al.*, IPR/TR-56/96, February 1996.

Excitation of Electron Temperature Gradient (ETG) Turbulence and Effect on Plasma Transport in LVPD

L. M. Awasthi¹, P. Srivastav¹, R. Singh¹, A. K. Sanyasi¹, P. K. Srivastava¹, R. Sugandhi¹, S. K. Singh¹, S. K. Mattoo¹, R. Singh¹, and P. K. Kaw¹

¹*Institute for Plasma Research (IPR), Bhat, Gandhinagar, India*

Corresponding Author: L. M. Awasthi, awasthi@ipr.res.in

Understanding electron transport across magnetic field lines in a fusion device is critical. Linear calculations based on numerical and theoretical models reveal that the electron temperature gradient (ETG) mode, which is responsible for the turbulence, is a fast growing instability driven by ∇T_e with growth rate $\gamma_{ETG} \approx \omega_{*T_e} = k_y \rho_e (c_e / L_{Te})$, when $\eta_e = L_n / L_T$ exceeds a threshold value. Here c_e is the electron thermal velocity and L_n, L_{Te} are the density and temperature gradient scale lengths, respectively. ETG is a short wavelength, $k_\perp \rho_e \leq 1 \ll k_\perp \rho_i$, and low frequency mode, ω in the range $\Omega_i < \omega \ll \Omega_e$, where k_\perp is the perpendicular wave vector, ρ_r / Ω_e and ρ_i / Ω_i are the Larmor radii by gyro frequencies of electrons and ions. Electron gyroscale fluctuations have been reported in National Spherical Torus Experiment and their role have been invoked to explain the plasma transport in Tore Supra. However, all signatures of ETG turbulence could not be obtained due to extremely small wavelength, $\rho_e \sim 1 \mu\text{m}$ in the range of $k_\perp \rho_e \sim 1$, in high magnetic fields ($\sim 20 \text{ kG}$) of tokamaks. Further, tokamaks have complex geometries, which restrict measurement and have limited control over the parameters that govern the turbulence. Basic plasma devices (linear or toroidal), on the other hand, provide a simplified geometry and control of magnetic field, thus brings scale length of turbulence well within the measurable limits. This provide a clear incentive to study ETG in basic plasma devices such as Large Volume Plasma Device (LVPD). However, these devices usually have plasma, which is contaminated by the presence of ionizing, hot and nonthermal electrons, a potential sources of instabilities. This renders making a case for ETG difficult.

An unambiguous observation on ETG driven turbulence is reported in LVPD. In the electron energy filter (EEF) modified dressed plasma, the observed ETG turbulence in lower hybrid range of frequencies $f = 1\text{--}80 \text{ kHz}$ is characterized by a broadband with a power law. The mean wave number, $k_\perp \rho_e = (0.1\text{--}0.2)$ satisfies the condition $k_\perp \rho_e \leq 1$.

ADITYA Experimental Results of Core Ion Temperature Measurements on ADITYA Tokamak Using Four Channel Neutral Particle Analyser

K. Ajay¹, S. Aggarwal¹, and S. P. Pandya¹

¹*Institute for Plasma Research (IPR), Bhat, Gandhinagar, India*

Corresponding Author: K. Ajay, ajaykuma@ipr.res.in

Coreion temperature measurements are routinely carried out by the energy analysis of passive charge exchange (CX) neutrals escaping out of the ADITYA-tokamak ($R = 75$ cm, $a = 25$ cm) plasma using a 45-degree parallel plate electrostatic energy analyser. The temporal evolutions of peak ion temperature in the core regime (typically 80 eV to 120 eV for ADITYA circular ohmic plasma) as estimated by analyzing the energetic neutral spectrum obtained on four Channeltrons of multichannel data acquisition system (MEASAR-minus-A measurement system for CEM array, Dr. Sjuts optotechnik GmbH, Germany) for several plasma discharges in ADITYA, provides an estimate for the core neutral hydrogen (H0) density and its evolution with time. Expected neutral density in the core regime has been estimated for several APPS discharges. The charge exchange diagnostic system on ADITYA and data analysis techniques (using numerical algorithms developed) for NPA measurements are also described. Effect of ion cyclotron radio frequency heating (ICRH) on $T_i(0)$ is observed and reported here, which shows additional increase of $T_i(0)$ up to 60% for the set of plasma discharges investigated herein.

EX

Chord Average Density Measurement Using Microwave Interferometry in LVPD

P. K. Srivastava¹, P. Srivastav¹, A. K. Sanyasi¹, R. Sugandhi¹, P. K. Atrey¹, and L. M. Awasthi¹

¹*Institute for Plasma Research (IPR), Bhat, Gandhinagar, India*

Corresponding Author: P. K. Srivastava, pkumar@ipr.res.in

Microwave interferometer diagnostic is designed and installed for carrying out chord-averaged density measurements for plasma density between $\sim 5 \times 10^{10}$ – 6×10^{11} /cm³ respectively in the source and target plasma regions of Large Volume Plasma Device (LVPD). These regions are developed in LVPD by the introduction of large electron energy filter (EEF). This helped in making LVPD plasma suitable for investigating electron temperature gradient (ETG) turbulence, a major source of plasma loss in fusion devices. In order to get hands-on information about plasma density, the concept of microwave interferometry is conceived. Measurements made by this technique will be compared with density obtained using conventional Langmuir probes. Even though, Langmuir probe diagnostic is widely used in most of the low temperature plasma devices but electron temperature estimated by it suffer with certain degree of error because of measurement uncertainty of 10%, which subsequently corrupts estimate of plasma density. This has prompted us to develop a resident diagnostic based on microwave interferometry for density measurement, which can provide suitable calibration to density measurements made by Langmuir probes.

This paper will present results on design details of microwave diagnostic and its application to LVPD plasma. Plasma of different densities will be produced by varying heating current to cathode, for test and validating the diagnostics. A comparison of chord averaged density measured by microwave interferometry with Langmuir probe data will be presented.

Investigations on Growth of Quasi-Longitudinal (QL) Whistlers with Energy Scaling of Energetic Electrons in LVPD

A. K. Sanyasi¹, L. M. Awasthi¹, P. Srivastav¹, P. K. Srivastava¹, R. Sugandhi¹, and D. Sharma¹

¹*Institute for Plasma Research (IPR), Bhat, Gandhinagar, India*

Corresponding Author: A. K. Sanyasi, amulya@ipr.res.in

Whistler waves are driven unstable by the runaway electrons generated in tokamak disruptions with serious consequences on reactor scale tokamaks and by relativistic electrons in space plasmas but with different electron distributions. In LVPD, we report observations on whistlers of quasi-longitudinal (QL) nature. These are highly oblique in nature and have free energy source associated with anisotropic distribution of electrons, beams, loss cones, magnetic mirrors, ring currents, electron temperature anisotropy etc. Presence of large electron energy filter (EEF) in LVPD divides plasma into three distinct regions of source, EEF and target plasmas. The source plasma, which is the focus of present investigations, is a region between the plasma source and the EEF. Transverse magnetic field of EEF ($B_{\text{EEF}} \sim 160$ G) modifies confining axial magnetic field ($B_z \sim 6.2$ G) of LVPD and imaculates [*sic*] magnetic mirror configuration. Reflected energetic electrons from the developed loss cone, results in the first laboratory observation of QL whistlers.

This paper will report on experimental observation of QL whistlers from an asymmetrically localized, thin rectangular slab in source plasma, populated by energetic electrons. The observed whistlers are electromagnetic in nature and exhibits strong coupling of density with potential and magnetic field fluctuations. The turbulence is broadband in nature with frequency ordering between, i.e., in lower hybrid range. The QL-mode propagate highly obliquely ($\approx 87^\circ$) with its perpendicular and parallel wave numbers as $k_\perp \sim 1.4 \text{ cm}^{-1}$ and $k_\parallel \sim 0.06 \text{ cm}^{-1}$ respectively. These observations are in good agreement with theoretical predictions for reflected electron driven QL whistlers. Analytical observations suggest that the growth of the instability has strong dependence on the plasma density and energy of the energetic electrons apart from the population of reflected electrons. Results on instability growth with energy scaling of reflected energetic electrons will be presented.

EX

Fast Wave Induced ICRF Plasma Expansion in ADITYA Torus

K. K. Mishra¹, S. V. Kulkarni¹, R. L. Tanna¹, R. Manchanda¹, N. Ramaiya¹, M. Gupta¹, J. Ghosh¹, A. Varia¹, M. Jadhav¹, R. Joshi¹, B. Kadia¹, K. Parmar¹, M. Parihar¹, Y. S. S. Srinivas¹, S. Kumar¹, D. Rath¹, G. Ashok¹, K. A. Jadeja¹, and S. B. Bhat¹

The ICRH Team and ADITYA Team

¹*Institute for Plasma Research (IPR), Bhat, Gandhinagar, India*

Corresponding Author: K. K. Mishra, kmishra@ipr.res.in

In ADITYA tokamak, ICRF plasma is produced by a single strap poloidal antenna located at LFS by exciting 24.8 MHz with a RF power < 80 kW for the purpose of developing ion cyclotron wall conditioning (ICWC) scenarios. Suitable combination of density (by regulating RF power and fill pressure) and B_t are investigated to allow the fast wave (FW) propagation in the torus volume. Initially at high B_t , the ICWC plasma which was previously localized inside the antenna box is spread along the toroidal field lines. The plasma is radially and poloidally localized only near the antenna location. Below a particular B_t , plasma is expanded into the vessel in radial direction. This plasma expansion is explained by considering the cold ion dispersion of FWs. It is observed that the slow wave branch is nonpropagating for the entire B_t range, whereas, FW starts propagating towards HFS at $B_t < 0.2$ T for the entire plasma volume. This critical B_t reasonably agrees with the experiment. This scenario could be useful in wall conditioning and wall coating in future fusion machines, where plasma uniformity is desirable.

EX

Gas Fuelling Control System of ADITYA Tokamak

N. Patel¹, C. Chavda¹, K. A. Jadeja¹, S. B. Bhatt¹, J. Ghosh¹, K. M. Patel¹, and R. L. Tanna¹

¹*Institute for Plasma Research (IPR), Bhat, Gandhinagar, India*

Corresponding Author: N. Patel, ncpatel@ipr.res.in

In tokamaks, gas fuelling control plays an important role to produce plasma in different operation phases from plasma current initiation till end. Apart from the main gas injection for plasma initiation, several plasma parameters such as density, temperature, and events like recycling, disruption and runaway mitigation, etc., are controlled by injecting the fuel gas in differing amounts and from differing locations in the vacuum vessel at various times in the plasma discharge cycle. This requires a programmable, sophisticated and precise gas feed control system for piloting different gas feed valves located on the machine. In ADITYA tokamak, a customized gas fuelling control system has been developed, installed and made operational meeting all the requirements of the plasma operation and control. This control system consists of customized programmable pulse generator, signal condition electronics, power supply, isolation, etc. Desirable pulses of designated widths and amplitudes with designated time delays are generated using the (National Instruments) LabVIEW-based control panel and fed into the gas-feed valves for gas insertion. This control system is a subsystem of the overall ADITYA tokamak central operational system and is properly tagged with central data acquisition. The novelty of this system lies in its capability to control eight different gas feed valves simultaneously with equal precision. The system has three separate and individually controlled gas fuelling modes according to the plasma operational requirements: 1) continuous gas-feed mode; 2) pulsed prefill mode; and 3) pulsed/continuous gas puffing mode. Different gas feed valves can be set and operated individually in each of the above modes simultaneously. The pulsed modes can be controlled precisely with a response time $< 100 \mu\text{s}$. This is achieved by applying a threshold voltage to gas feed valve with proper electrical isolation. As the gas is absolutely required for every plasma discharge, the control system is designed with redundant protection mechanisms against failure to work in harsh tokamak environment. Design, development, testing and operation of gas fuelling control system of ADITYA tokamak along with the experimental results of the gas fuelling control during plasma operation of ADITYA tokamak is presented in this paper.

EX

Integrated System Electronics and Instrumentation; Operation and Diagnostic for ADITYA-U Tokamak

R. Rajpal¹, C. J. Hansalia¹, P. Edappala¹, P. Kumari¹, P. Gautam¹, M. Shah¹, V. D. Raulji¹, B. Arambhadiya¹, A. Kumar¹, V. K. Panchal¹, and J. Ghosh¹

¹*Institute for Plasma Research (IPR), Bhat, Gandhinagar, India*

Corresponding Author: R. Rajpal, rachana@ipr.res.in

EX The first phase of ADITYA-U operations successfully performed various plasma experiments with repeatable plasma discharges of maximum plasma current of ~ 160 kA and discharge duration ~ 250 ms. The electronics and instrumentation requirement for these experiments are mainly of signal conditioning, embedded digital signal processing and automation. The signal conditioning electronics are developed to measure signal through sensors of different plasma diagnostics. To measure accurately and precisely the signal of nano order in the highly irradiated tokamak environment (including electric and magnetic fields), special care has been taken in terms of design, component selection, signal transmission and EMC/EMI shielding. The signal conditioning design incorporates attenuation, amplification, isolation, filtration, self-test and offset calibration. At present the electronic system caters around the need of hundreds of channels from different ADITYA-U diagnostics. These channels include electronics for electromagnetic, spectroscopy, bolometer, soft X-ray, microwave and ECE radiometer diagnostic.

FPGA and microcontroller based electronics are designed and developed for plasma operation and control applications. Microcontroller based few real-time feedback control applications were successfully implemented in the last campaigns and these experiments are plasma disruption control using electrode-bias and ICR pulse, radial position control, density feedback control and real-time control of gas-feed pulses to reduce wall loading of fuel gas. FPGA based timing system is developed which generates trigger to operate different subsystems and archive data during ADITYA-U plasma discharge.

The automation and instrumentation system is developed for baking of vacuum vessel and pumping lines, TF coil temperature measurement and logging for ADITYA-U. The LabVIEW based SCADA application monitors and control the temperature of PLC based baking system. The paper will describe electronics for plasma diagnostics, instrumentation, embedded control and timing system for plasma operation.

Plasma Column Position Measurements Using Magnetic Diagnostics in ADITYA-U Tokamak

S. Aich^{1,2}, R. Kumar¹, T. Macwan^{1,2}, D. Kumawat^{1,2}, R. L. Tanna¹, D. Raju¹, E. V. Praveenlal¹, M. Shah¹, K. A. Jadeja¹, K. M. Patel¹, C. N. Gupta¹, and J. Ghosh^{1,2}

¹*Institute for Plasma Research (IPR), Bhat, Gandhinagar, India*

²*Homi Bhabha National Institute (HBNI), Anushakti Nagar, Mumbai 400094, India*

Corresponding Author: S. Aich, suman.aich@ipr.res.in

In a tokamak, for real-time control of plasma column movement, both horizontal and vertical, accurate measurements of plasma column location is compulsory. Magnetic pick-up coils, measuring induced voltage due to change in flux-linkage to them, are widely used of the measurement of temporal evolution of plasma column position in a tokamak. Although measurements of induced voltages are relatively easy, estimation of plasma column position from these measurements are not very straightforward and requires accurate calibration of the coils and huge amount of modelling.

In order to measure the plasma column position accurately in ADITYA-U tokamak, several types of magnetic probes are introduced. They include, Mirnov coils, external pick-up coils, Sine-Cosine coils and flux loops. To have a proper calibration factor for these probes which is a necessity for overcoming geometrical imperfections, discrepancies introduced during installations as well as error magnetic fields from eddy currents in vacuum vessel, an in-situ calibration experiment has been carried out. A time varying current has been passed through a rigid copper conductor placed at different radial and vertical locations inside the vacuum vessel. Induced voltages in all the magnetic probes are recorded due to the different temporal profiles of driven current in the conductor. In addition to that, the magnetic pick-ups by these probes due to different poloidal magnetic field coils, which are operated during plasma operations, has also been measured by driving current through those coils in absence of plasma.

Based on these observations several numerical codes have been developed which analyse the raw data from these magnetic probes during plasma shots. After removing all the unwanted flux-linkages to the probes due to vessel eddies and other set of magnetic coils used for plasma operation, the temporal evolution of plasma column's horizontal and vertical movement has been estimated in real-time. The plasma column position measured with these probes matches fairly well with other diagnostics, such as, edge Langmuir probes, fast camera images etc. Finally the real-time measurements of position movement of plasma column during the plasma discharges have fed onto the plasma position control system for real-time control of plasma position in ADITYA-U tokamak.

Thermal Energy Confinement at the Globus-M Spherical Tokamak

G. S. Kurskiev¹, N. N. Bakharev¹, V. V. Bulanin², F. V. Chernyshev¹, V. K. Gusev¹,
N. A. Khromov¹, E. O. Kiselev¹, V. B. Minaev¹, I. V. Miroshnikov¹, E. E. Mukhin¹,
M. I. Patrov¹, A. V. Petrov², Y. V. Petrov¹, N. V. Sakharov¹, P. B. Shchegolev¹,
A. D. Sladkomedova¹, V. V. Solokha¹, A. Y. Telnova¹, V. A. Tokarev¹, S. Y. Tolstyakov¹, and
A. Y. Yashin²

¹Ioffe Institute, St. Petersburg, Russian Federation

²Peter the Great St. Petersburg Polytechnic University, St. Petersburg, Russian Federation

Corresponding Author: G. S. Kurskiev, gleb.kurskiev@gmail.com

The presentation is devoted to the overview of thermal energy confinement time study at the compact spherical tokamak Globus-M. Globus-M has major radius $R = 0.35$ m and minor radius $a = 0.21$ m ($R/a \sim 1.67$). The lower-null magnetic configuration is characterized by moderate elongation $k \sim 1.9$ and triangularity $\delta \sim 0.35$. The present study was performed in both OH and NBI heated H-mode plasma. The regression fit of the database indicates strong τ_E dependence on both plasma current I_p and toroidal magnetic field B_t , while the dependence on density n_e and absorbed power P was similar to the conventional scaling $IPB_{98}(y, 2)$. The electron heat diffusivity is strongly affected by the plasma current and the toroidal magnetic field. The $B_t \tau_E$ dependence on ν^* is found to be similar to NSTX and MAST results, while q dependence is stronger than on MAST, but weaker than in ITER scaling.

The second part of the presentation is devoted to study of the particle and heat transport in regimes with $q_{min} > 1$. Such transient operational modes were investigated using NBI at the current ramp-up phase, that usually causes ITB formation either for particle or for electron heat flux (e-ITB). In the case of internal diffusion barrier it is located in the region $r/a \sim 0.4$, the e-ITB is located at $r/a \sim 0.7$. These advanced regimes are characterized with enhanced energy confinement relative to conventional H-mode.

EX

Plasma Confinement and Pedestal Dynamics Responses to Impurity Seeding in HL-2A H-Mode Plasmas

W. Z. Zhong¹, X. L. Zou², A. S. Liang¹, G. L. Xiao^{1,3}, Z. C. Yang¹, B. B. Feng¹, C. Y. Chen¹, J. M. Gao¹, Y. P. Zhang¹, Z. Y. Cui¹, C. F. Dong¹, P. Sun¹, M. Jiang¹, P. W. Shi¹, J. Wen¹, X. M. Song¹, L. W. Yan¹, J. Q. Dong^{1,4}, X. T. Ding¹, D. L. Yu¹, Z. B. Shi¹, Y. Liu¹, Q. W. Yang¹, M. Xu¹, X. R. Duan¹, and Y. Liu¹

The HL-2A Team

¹*Southwestern Institute of Physics, Chengdu, Sichuan, People's Republic of China*

²*Institut de Recherche sur la Fusion par confinement Magnétique (IRFM),*

Commissariat à l'énergie atomique (CEA/Cadarache), 13108 St. Paul lez Durance, France

³*Department of Engineering Physics, Tsinghua University, Haidian, Beijing, People's Republic of China*

⁴*Institute for Fusion Theory and Simulation,*

Zhejiang University, Xihu, Hangzhou, Zhejiang, People's Republic of China

Corresponding Author: W. Z. Zhong, zhongwl@swip.ac.cn

In HL-2A H-mode plasmas, the confinement and pedestal response to impurity seeding have been recently investigated [1]. It has been observed that a broadband electromagnetic (EM) turbulence can be driven by peaked impurity density profile at the edge plasma region, and governed by double critical gradients of the impurity density [2]. In addition to the spontaneously accumulated impurity, the electromagnetic turbulence and quasi-coherent EM modes can also be excited by externally seeded impurity in HL-2A [3]. The excited pedestal instabilities can play an important role in the regulation of the pedestal turbulent transport. More recently, the SMBI system has been used for gas impurity seeding (Ar, Ne, etc), which is beneficial for forming an edge radiation layer and avoiding impurity core accumulation. With pure impurity injection, it has been observed that the ELM frequency is increased and the H-mode plasma confinement is improved with a broadened and steepened density pedestal. For the D₂ SMBI, it can mitigate ELMs as observed in several devices. Thus, a newly developed SMBI system with mixture impurity gas (D₂+Ne or D₂+Ar) is used in HL-2A. The impurity gas is mixed with plasma work gas D₂ by different ratios. The dedicated experiments show that the ELM behaviour, plasma confinement and pedestal structure are varied with the ratio of the impurity mixture. It has been found that large ELMs are replaced by very small bursts with 30% Ne-SMBI seeding. The SMBI pulse length is 2 ms. The large ELM is suppressed for a period of about 50 ms. Meanwhile, the divertor heat load is significantly reduced. When the ratio changed to 10%, the confinement response is similar to that of the D₂ SMBI. However, when the gas was changed to pure Ne, the ELM frequency was increased and the confinement was enhanced. The results suggest that both the pedestal structure and pedestal stability are modified with the amount of impurity and impurity species. Experimental observations indicate that there is an optimal impurity ratio for heat load control. The results suggest that pedestal dynamics and heat loads can be actively controlled by exciting pedestal instabilities and forming a steady edge radiation layer.

References

- [1] W. L. Zhong *et al.*, Plasma Phys. Contr. F., **59**, 014030 (2017).
- [2] W. L. Zhong *et al.*, Phys. Rev. Lett., **117**, 045001 (2016).
- [3] Y. P. Zhang *et al.*, Nucl. Fus., **58**, 04601 (2018).

Localized Modulation of Turbulence by Magnetic Islands on HL-2A Tokamak

M. Jiang¹, Y. Xu², W. Chen¹, Z. B. Shi¹, W. L. Zhong¹, X. T. Ding¹, X. Q. Ji¹, P. W. Shi¹, J. Q. Li¹, Z. C. Yang¹, B. S. Yuan¹, Y. G. Li¹, Y. Zhou¹, D. L. Yu¹, Y. Liu¹, Q. W. Yang¹, and M. Xu¹

The HL-2A Team

¹Southwest Jiaotong University, Chengdu, Sichuan, People's Republic of China

²Institute of Fusion Science, School of Physical Science and Technology,
Southwest Jiaotong University, Chengdu, Sichuan, People's Republic of China

Corresponding Author: M. Jiang, jiangm@swip.ac.cn

Magnetic islands formed in magnetically confined plasmas have significant influence on plasma profiles and cross-field transport, and can even cause plasma disruption [1, 2]. However, observations of internal transport barriers near the rational magnetic surface suggest the importance of magnetic islands in plasma confinement via increase of flow shear at the island boundary [3, 4]. In recent years the multiscale interaction between large-scale modes and microscale turbulence has been found to play an important role in regulating turbulent transport and eventually form the low to high mode transition [5, 6]. In this paper, modulation on turbulent electron temperature fluctuations and density fluctuations by an $m/n = 1/1$ tearing mode island was observed in the core plasma region of the HL-2A tokamak. High tempo-spatial resolution two-dimensional images of temperature fluctuations show the first evidence that the turbulence modulation occurs only when the island width exceeds a certain threshold value (6.4 cm) and the modulation is localized merely in the inner half area of the island due to significant alteration of local profiles and turbulence drives. Evidence also reveals that for large islands turbulence spreading takes place across the flat temperature of the O-point at the inner half island region, whereas in the outer half area the small temperature gradient drives a low level of temperature fluctuations.

References

- [1] G. Fiksel *et al.*, Phys. Rev. Lett., **75**, 3866 (1995).
- [2] W. Suttrop *et al.*, Nucl. Fus., **37**, 119 (1997).
- [3] K. Ida *et al.*, Phys. Rev. Lett., **88**, 015002 (2002).
- [4] E. Joffrin *et al.*, Nucl. Fus., **43**, 1167 (2003).
- [5] A. Fujisawa *et al.*, Phys. Rev. Lett., **93**, 165002 (2004).
- [6] I. Shesterikov *et al.*, Phys. Rev. Lett., **111**, 055006 (2013).

Pedestal Dynamics in Inter-ELM Phase on HL-2A Tokamak

J. Cheng¹, J. Q. Dong^{1,2}, K. Itoh^{3,4,5}, S.-I. Itoh^{5,6}, L. W. Yan¹, M. Jiang¹, J. Q. Xu¹, K. J. Zhao¹, Z. H. Huang¹, D. L. Yu¹, S. Inagaki^{5,6}, W. L. Zhong¹, M. K. Han⁷, Z. X. Wang⁷, X. Q. Ji¹, Z. B. Shi¹, Y. Liu¹, Q. W. Yang¹, X. T. Ding¹, M. Xu¹, and X. R. Duan¹

¹Southwestern Institute of Physics, Chengdu, Sichuan, People's Republic of China

²Institute for Fusion Theory and Simulation,

Zhejiang University, Xihu, Hangzhou, Zhejiang, People's Republic of China

³Institute of Science and Technology Research, Chubu University, Kasugai, Aichi, Japan

⁴National Institute for Fusion Science (NIFS), Toki, Gifu, Japan

⁵Research Center for Plasma Turbulence, Kyushu University, Kasuga, Japan

⁶Research Institute for Applied Mechanics (RIAM), Kyushu University, Kasuga, Japan

⁷School of Physics and Optoelectronic Technology, Dalian University of Technology, Liaoning, Dalian, Ganjingzi, People's Republic of China

Corresponding Author: J. Cheng, chengj@swip.ac.cn

Streamer, as well as zonal, flow is a very challenging subject since it is expected to have significant effects on confinement in high temperature plasmas. Theoretical simulation predicts that streamers originate from the nonlinear development of turbulence driven by electron and ion temperature gradient. In experiments, few works have reported the streamer observation only up to now, and detailed analysis of the streamer dynamics is still lacking, in spite of its importance in the understanding of plasma confinement in toroidal fusion devices. Here we report the first observation of streamer formation in the HL-2A edge plasmas in inter-ELM phases. The streamer is developed from turbulence via a quasi-coherent mode which interacts with and modulates ambient turbulence, induces an inward particle flux, and plays an essential role in the pedestal dynamics in the inter-ELM phases. Detailed results on the streamer characteristics and its role in triggering the ELM will also be presented.

EX

Effect of LBO-Seeded Impurity on ELMs in the HL-2A Tokamak

Y. P. Zhang¹, D. Mazon², X. L. Zou², W. L. Zhong¹, J. M. Gao¹, K. Zhang¹, P. Sun¹, C. F. Dong¹, Z. Y. Cui¹, Y. Liu¹, Z. B. Shi¹, D. L. Yu¹, J. Cheng¹, M. Jiang¹, J. Q. Xu¹, M. Isobe^{3,4}, G. L. Xiao¹, W. Chen¹, S. D. Song¹, X. Y. Bai¹, P. F. Zhang¹, G. L. Yuan¹, X. Q. Ji¹, Y. G. Li¹, Y. Zhou¹, L. Delpech², A. Ekedahl², G. Giruzzi², T. Hoang², Y. Peysson², X. M. Song¹, X. Y. Song¹, X. Li¹, X. T. Ding¹, J. Q. Dong¹, Q. W. Yang¹, M. Xu¹, X. R. Duan¹, and Y. Liu¹

The HL-2A Team

¹Southwestern Institute of Physics, Chengdu, Sichuan, People's Republic of China

²Institut de Recherche sur la Fusion par confinement Magnétique (IRFM), Commissariat à l'énergie atomique (CEA/Cadarache), 13108 St. Paul lez Durance, France

³National Institute for Fusion Science (NIFS), Toki, Gifu, Japan

⁴Department of Fusion Science, Graduate University for Advanced Studies (SOKENDAI), Toki, Gifu, Japan

Corresponding Author: Y. P. Zhang, zhangyp@swip.ac.cn

Effect of the pedestal deposited impurity on the edge-localized mode (ELM) behaviour has been observed and intensively investigated in the HL-2A tokamak. Impurities have been externally seeded by a newly developed laser blow-off (LBO) system. Both mitigation and suppression of ELMs have been realized by LBO-seeded impurity. Measurements have shown that the LBO-seeded impurity particles are mainly deposited in the pedestal region. During the ELM mitigation phase, the pedestal density fluctuation is significantly increased, indicating that the ELM mitigation may be achieved by the enhancement of the pedestal transport. The transition from ELM mitigation to ELM suppression was triggered when the number of the LBO-seeded impurity exceeds a threshold value. During the ELM suppression phase, a harmonic coherent mode (HCM) is excited by the LBO-seeded impurity, and the pedestal density fluctuation is significantly decreased, the electron density is continuously increased, implying that HCM may reduce the pedestal turbulence, suppress ELMs, increase the pedestal pressure, thus extending the Peeling-Ballooning instability limit. It has been found that the occurrence of the ELM mitigation and ELM suppression closely depends on the LBO laser spot diameter.

EX

Characteristics of Electromagnetic Turbulence on KTX Experiment Device

W. Mao¹, T. Lan¹, H. Li¹, J. Xie¹, A. Liu¹, T. Deng¹, J. Zhu¹, J. Wu¹, W. Ding^{1,3}, C. Xiao^{1,2,4},
G. Zhuang¹, and W. Liu¹

¹*KTX Laboratory and Department of Engineering and Applied Physics,*

University of Science and Technology of China, Hefei, Anhui, People's Republic of China

²*Institute of Plasma Physics, Chinese Academy of Sciences, Hefei, Anhui, People's Republic of China*

³*University of California Los Angeles, CA 90095, USA*

⁴*Plasma Physics Laboratory, University of Saskatchewan, Saskatoon, SK S7N-5C9, Canada*

Corresponding Author: W. Mao, maozhe@ustc.edu.cn

Electrostatic turbulence is the main constrain of confinement improvement on low- β toroidal magnetic confinement devices. With the development of high- β operation scenario, electromagnetic turbulence is expected to become important for development of resistive tearing mode and resistive wall mode. The characteristics of electromagnetic turbulence on KTX are studied in low current tokamak and in reversed field pinch plasma operations. Electron density fluctuations in the core are measured based on forward scattering signal collection with multichannel interferometer system. The edge electric and magnetic field fluctuations are measured using movable multifunctional probe arrays. The 3D spectral characteristics of the electromagnetic turbulence are present in our research. Biased electrode is applied at the edge of plasma for changing the edge electric field profile, and significant suppression of turbulence and reduction of radial particle flux are observed after applying high biasing voltage.

EX

Electric Potential and Turbulence in OH and ECRH Low-Density Plasmas

A. V. Melnikov¹, L. G. Eliseev¹, S. A. Grashin¹, M. A. Drabinsky¹, M. Y. Isaev¹,
P. O. Khabanov¹, N. K. Kharchev¹, L. A. Klyuchnikov¹, V. A. Krupin¹, S. E. Lysenko¹,
D. V. Ryzhakov¹, R. V. Shurygin¹, N. A. Soloviev¹, V. A. Vershkov¹, and V. N. Zenin¹

The T-10 Team

¹National Research Centre "Kurchatov Institute", Moscow, Russian Federation

Corresponding Author: A. V. Melnikov, melnikov_07@yahoo.com

New experimental observations and theoretical description of the plasma potential and radial electric field E_r formation in the T-10 tokamak are presented. The potential was measured by heavy ion beam probe (HIBP) diagnostic from the plasma core to edge with high spatial (< 1 cm) and temporal ($1 \mu\text{s}$) resolution, and by Langmuir probe (LP) at the edge. Low-density OH deuterium plasma ($n_e = 1.0 \times 10^{19}/\text{m}^3$, $T_e < 1.3$ keV, $T_i < 0.6$ keV) is characterized by a negative potential up to $\phi(0.25) = -800$ V. The potential profile is monotonically increasing towards the edge. The off-axis ($\rho_{\text{EC}} = 0.5$) ECRH with power $P_{\text{EC-off}} < 1.7$ MW ($f_{\text{EC}} = 144$ GHz) leads to the formation of a flat T_e profile at 2 keV inside ρ_{EC} . It causes a dramatic raise of the core potential to positive values over the whole observation area, forming nearly zero E_r . Extra nearly on-axis ($\rho = 0.2$) ECRH with $P_{\text{EC-on}} < 0.5$ MW ($f_{\text{EC}} = 129$ GHz) leads to a further increase of T_e up to 3.3 keV, and to potential raise to $\phi(0.25) = +900$ V forming an extended area of positive E_r , from the core to the edge. Also HIBP and LP measure geodesic acoustic modes (GAMs) and broadband ($f < 400$ kHz) turbulence of the potential and density. GAMs with higher frequency satellite are dominating in potential power spectra in OH plasma, GAM amplitude increases during ECRH. Both GAM and satellite have uniform structure with constant frequencies over a wide radial extension, exhibiting the features of global eigenmodes of plasma oscillations. At the edge, a quasi-coherent (QC) electrostatic mode ($f \sim 50$ – 120 kHz) coexists with the GAM. A stochastic low frequency (SLF) mode with frequency < 50 kHz is seen in the plasma density and potential power spectra, density poloidal coherence and cross-phase, exhibiting the poloidal rotation opposite to QC mode. Neoclassical (NC) modelling use various codes, from the simple analytical approach to the orbit code VENUS+ δf . The radial profiles and the main tendencies like potential decrease with density raise and potential raise with T_e increase due to ECRH were reproduced by NC models. The turbulent dynamics in the edge plasma was described by the 4-field nonlinear two-fluid Braginskii model. The link between the potential and confinement is discussed.

Ecton Mechanism of Energy Load on ITER-Grade Tungsten Limiter T-10 Tokamak and Forecast for ITER

L. N. Khimchenko¹, V. P. Budaev^{2,3}, M. M. Tsventoukh⁴, Y. V. Martynenko²,
S. A. Grashin², and A. V. Karpov²

¹International Thermonuclear Experimental Reactor (ITER),
Project Centre "ITER", Moscow, Russian Federation

²National Research Centre "Kurchatov Institute", Moscow, Russian Federation

³National Research University "Moscow Power Engineering Institute", Krasnokazarmennaya 14, Moscow,
Russian Federation

⁴P. N. Lebedev Physical Institute, RAS, Moscow, Russian Federation

Corresponding Author: L. N. Khimchenko, l.khimchenko@iterrf.ru

Extremely high heat loads, both during steady state and transient events, are expected on the tungsten divertor plates of the ITER facility, undertaken at Cadarache, France. In this paper nonambipolar plasma flow toward the surface, due to arcs and sparks, was investigated as mechanism of power exhaust, leading to enhanced heating of plasma facing materials (PFMs) at a very high heat load. This ecton mechanism results in the pulsed-periodic ignition of explosive electron emission events providing high enough electron current from the wall. Unlike standard thermionic emission, such mechanism can dramatically increase electron emission and, as a result, sparks and arcs activity, leads to a surface overheating and melting. Such phenomenon have been observed in experiments on the T-10 tokamak with ITER-grade tungsten (W) poloidal limiter under a powerful plasma electron cyclotron resonance heating (ECRH) and plasma ring shifted inside. In such conditions, the interior tungsten plates of limiter were heated up to temperature exceeded 2000°C, estimated local thermal load were of more than 40 MW/m² on the plate edges, leading to surface melting. Intensive sparking and arcing, deep cracks and edge melting were observed on W tiles. Also, tile surfaces were flooded by recrystallized tungsten. All W tile surfaces are covered by two crater types: deep, (with dimensions from 10 to 100 μm) and acetabuliform type (with dimensions from 0.5–20 μm) arranged in "long chains"— vacuum arcs, and "short chains"— vacuum sparks. The reason for such sub-μs discharges ignition can be plasma-turbulence-driven fluctuations of particle and energy flux to the plasma-modified surface. The report analyzes consequences for ITER of the EEE appearance on the divertor W surface, the sharpening of SOL power width distribution, parallel to the magnetic field -λ_q; the melting of the W leading edges of divertor targets and the recrystallization of the W surface as a result of the superheated liquid metal droplets appearance. Melt tungsten can be subject to $J \times B$ force. EEE can lead to the erosion enhancement of the divertor plates. Microexplosions lead to droplets, which, like dust particles, can effectively deliver impurities to the central region of the plasma.

EX

Nonlinear Evolution of Multihelicity Neoclassical Tearing Modes in HL-2A Low Rotation Plasmas

X. Q. Ji¹, Y. Liu¹, Z. X. Wang², L. Wei², Y. Xu¹, T. F. Sun¹, S. Y. Liang¹, L. W. Yan¹, and Q. W. Yang¹

¹*Southwestern Institute of Physics, Chengdu, Sichuan, People's Republic of China*

²*Dalian University of Technology, Liaoning, Dalian, Ganjingzi, People's Republic of China*

Corresponding Author: X. Q. Ji, jixq@swip.ac.cn

In HL-2A low rotation and relatively low density plasmas, the critical threshold of the intrinsic error field penetration will be decreasing. And the multihelicity islands can be seeded by the nonaxisymmetric error field penetration, and lead to the change of rotation profile, enhanced transport or even disruption. Sheared flow arising from momentum injection can suppress the coupled islands. For understanding the experimental results, numerical modelling will be carried out by means of reduced magnetohydrodynamic simulations. The results provide important evidence for NTMs stability predictions and their nonlinear dynamic in the low flow plasmas, such as ITER.

Peculiar Properties of Disruptions on T-10 Tokamak at Different Edge Safety Factor Values

D. V. Ryzhakov¹, Y. D. Pavlov¹, A. M. Kakurin¹, S. G. Malzev¹, S. V. Akhtyrskiy¹, and M. M. Sokolov¹

¹National Research Centre "Kurchatov Institute", Moscow, Russian Federation

Corresponding Author: D. V. Ryzhakov, ryzhakov_dv@nrcki.ru

One of the main goals of researching global plasma disruptions is to find a way to prevent the formation of runaway electron beams, after the plasma current disruption. A possible solution to this problem is to generate a strong MHD perturbation during current decay. The experimental study of density limit disruption on tokamak T-10, for study dependency a duration of plasma current decay t_{95} (from 100% to 5% of plasma current on quasi-state stage of discharge) from edge safety factor q_a was carried out. As result, it was found that, if value q_a integer or half-integer than duration of plasma current decay is high increase, up to 100–115 ms.

The increased duration of current decay is uniquely relate with q_a , what showed in experiments where changing of the value of toroidal field and plasma current with constant q_a do not lead to changing character and duration of current decay. From the available experimental data it follows that during slow current decay while plasma column move to high field side, one at a time multiple extensions and contractions by minor radius are occur. The moment of time when the plasma column expands is correlated with peaks on the loop voltage and with peaks on the MHD perturbation of poloidal magnetic field. The main character feature of disruption with a slow current decay is absence of hard X-rays. Thus, from available experimental data, we can conclude, that during a slow current decay, high MHD activity lead to prevent the formation of runaway electron beams.

EX

Energetic-Ion Driven Toroidal and Global Alfvén Eigenmodes on HL-2A

P. W. Shi¹, W. Chen¹, Z. B. Shi¹, and X. R. Duan¹

The HL-2A Team

¹*Southwestern Institute of Physics, Chengdu, Sichuan, People's Republic of China*

Corresponding Author: P. W. Shi, shipw@swip.ac.cn

The stationary and nonstationary toroidal Alfvén eigenmodes (TAE) driven by energetic-ion have been observed on HL-2A. The mode frequencies are about 90–200 kHz and toroidal mode numbers for the most unstable mode are $n = 1$ –3. The radial structure of the mode with $n = 2$ confirmed by the Alfvén mode code (AMC) make up of poloidal harmonic $m = 2$ and $m = 3$, which is a typical feature of TAE. The amplitudes measured by the Mirnov coils suggest that they are much stronger in the LFS than the HFS, which reveals a typical ballooning mode structure. In the down-chirping case, the mode frequency quickly sweeps down from the TAE gap centre to the lower frequency gap accumulation point. The internal amplitude can be determined from the frequency sweep speed of TAEs and it will provide input for simulations of potential ion and alpha particle losses due to energetic particle driven modes. The TAEs were found to nonlinearly couple with tearing mode (TM) and result in the appearances of series of Alfvénic modes (AMs). An axisymmetric mode within the ellipticity-induced frequency gap driven by TAEs coupling with TM was found for the first time. The squared bicoherence suggests that two AMs with the same mode number but propagated in different diamagnetic drift directions couple together and lead to the generation of a high frequency mode with $n = 0$. The symmetrical mode with an “antiballooning” feature prove to be global Alfvén eigenmodes (GAE). It is the even GAE with frequency around 240 kHz, which agrees well with experimental observation of 235–240 kHz. The $m = 1$ poloidal harmonic is dominated for the GAE. The experimental results also indicated that nonlinear mode-mode coupling degenerates the confinement of fast ions and it may be one of mechanisms of the energy cascade in energetic-particle turbulence or Alfvén turbulence.

EX

Suppression and Destabilization of Ion Fishbone Activities on HL-2A

W. Chen¹, L. M. Yu¹, X. L. Zhu², M. Jiang¹, P. W. Shi¹, X. Q. Ji¹, Z. B. Shi¹, B. S. Yuan¹, D. L. Yu¹, Y. G. Li¹, Z. C. Yang¹, Y. R. Yang¹, X. T. Ding¹, M. Xu¹, Q. W. Yang¹, Y. Liu¹, L. W. Yan¹, and X. R. Duan¹

The HL-2A Team

¹*Southwestern Institute of Physics, Chengdu, Sichuan, People's Republic of China*

²*School of Physics and Optoelectronic, Dalian University of Technology, Liaoning, Dalian, Ganjingzi, People's Republic of China*

Corresponding Author: W. Chen, chenw@swip.ac.cn

Magnetohydrodynamic (MHD) instabilities in hot plasmas can strongly limit the operational parameter space of a fusion reactor. Their stabilization, suppression and active control have therefore attracted much attention, in particular with regard to expansion of the operational space, enhancing the fusion performance and decreasing the energetic particle losses in both present-day fusion devices and future devices with burning plasmas. Control of multiple instabilities including sawtooth, neoclassical tearing mode (NTM), resistive wall mode (RWM), edge localized mode (ELM), Alfvén eigenmode as well as energetic-particle mode (EPM), has been successfully achieved, to various degrees, by different means such as the radio frequency wave heating and drive, the three-dimensional magnetic perturbations, and so on, in many fusion devices. On the other hand, understanding of both the control and physics of these instabilities, in many cases, is still far from complete, and remains area of active research. The fishbone mode is one of these key instabilities, which is destabilized by a population of energetic particles. In burning plasmas, energetic alpha particles, though being a minority species, carry a large fraction of the plasma kinetic energy, and can potentially drive the fishbone instability. The fishbone has also been proposed as a possible scheme for ash removal and burn control, as well as tungsten-impurities removing from the plasma core on ITER.

In this paper the recent progress of ion fishbone activities will be present on HL-2A. Firstly, it will be reported the stabilization of $m/n = 1/1$ fishbone by ECRH. The stabilization of $m/n = 1/1$ fishbone depends not only on the injected power but also on the radial deposition location of ECRH, and the instability can be completely suppressed when the injected ECRH power exceeds certain threshold. Analysis by the fishbone dispersion relation, including the resistive effect, suggests that the magnetic Reynolds number plays a key role in the mode stabilization. Secondly, it will be introduced the destabilization of $m/n = 2/1$ fishbone. The evolution of $m/n = 2/1$ fishbone is related to mode rotation reverse. The excitation mechanism of $m/n = 2/1$ fishbone will also be discussed, namely the result of the kink or tearing mode interacting with circulating or trapped EPs.

Influence of Electron Cyclotron Resonance Heating on Ion Heat Conductivity in T-10 Plasma

M. R. Nurgaliev¹, V. A. Krupin¹, L. A. Klyuchnikov¹, A. R. Nemets¹, I. A. Zemtsov¹, A. Y. Dnestrovsky¹, A. A. Borschegovskiy¹, A. Y. Kislov¹, T. B. Mylton¹, D. V. Sarychev¹, D. S. Sergeev¹, N. A. Soloviev¹, V. M. Trukhin¹, S. N. Tugarinov¹, and N. Naumenko^{1,2}

¹National Research Centre "Kurchatov Institute", Moscow, Russian Federation

²B.I. Stepanov Institute of Physics, NASB, Minsk, BY-220072, Belarus

Corresponding Author: M. R. Nurgaliev, maxim.nurgaliev@gmail.com

Investigation of ion heat conductivity in plasma with ECR-heating and suppressed saw-teeth and modes $(m, n) = (1, 1)$ and $(2, 1)$ is carried out. Off-axis heating (localization radius is $\rho = r/a \approx 0.5$) and combined heating (on-axis ECRH together with off-axis) are considered. It is shown for the ohmic stage that ion heat conductivity is on a neoclassical level in the central zone $\rho \leq 0.5$ – 0.6 but it is clearly anomalous outside these radii. Off-axis heating does not lead to any notable changes of the heat conductivity profile. In the regime with combined heating additional ≈ 0.5 MW on-axis ECR-power results in ion heat conductivity magnification up to ≈ 1.5 times and ≈ 1 MW on-axis ECR-power causes the increase up to ≈ 2 times.

EX

Physics and Engineering Design for Chinese First Quasi-Axisymmetric Stellarator (CFQS)

Y. Xu¹, H. Liu^{1,4}, C. Tang^{1,4}, A. Shimizu², M. Isobe^{2,3}, S. Okamura², X. Zhang¹, B. Liu¹, J. Huang¹, X. Wang¹, H. Liu¹, D. Yin⁵, and Y. Wan⁵

The CFQS Team

¹*Institute of Fusion Science, School of Physical Science and Technology, Southwest Jiaotong University, Chengdu, Sichuan, People's Republic of China*

²*National Institute for Fusion Science (NIFS), Toki, Gifu, Japan*

³*Department of Fusion Science, Graduate University for Advanced Studies (SOKENDAI), Toki, Gifu, Japan*

⁴*Sichuan University, Chengdu, Sichuan, People's Republic of China*

⁵*Hefei Keye Electro Physical Equipment Manufacturing Co., Ltd, Hefei, 230000, People's Republic of China*

Corresponding Author: Y. Xu, xuyuhong@swjtu.edu.cn

The Chinese First Quasi-axisymmetric Stellarator (CFQS) is a joint project of international collaboration. It is designed and fabricated by the Southwest Jiaotong University (SWJTU) in China and the National Institute for Fusion Science (NIFS) in Japan. The target parameters of CFQS are as follows: toroidal periodic number $N = 2$, major radius $R = 1.0$ m, aspect ratio $R/a = 4.0$ and magnetic field strength $B = 1.0$ T.

Via the scan of major radius (1.0 m–1.5 m) and aspect ratio (3–5), the target parameters of CFQS configuration are determined by comprehensively considering physics and engineering constrains. The toroidal periodic number $N = 2$ is selected, which guarantees to form the tokamak-like configuration. A low aspect ratio is one of the important features of the CFQS design because of the advantage of compactness and economy, which could be used in future commercial reactors. From the core region to the edge, the vacuum rotational transform is designed between $2/6$ and $2/5$ which is advantageous to avoid low-order rational surfaces. In addition, the presence of a magnetic well is capable to stabilize the MHD and reduce the island widths.

In order to achieve the target magnetic configuration, a modular coil system is necessary to be designed to reproduce the plasma boundary. According to the Neumann boundary condition, the accuracy of the magnetic configuration induced by the coil system depends on the normal component of the magnetic field on the plasma boundary. Via the minimization of the normal component of the magnetic field on the plasma boundary, the modular coil geometry is optimized. Meanwhile, the engineering constraints are also taken into account, which are the minimum interval between adjacent coils and the maximum curvature. This optimization process is accomplished by the NESCOIL code.

The Mercier stability, ballooning stability and neoclassical transport were also calculated to evaluate the property of the CFQS configuration. The MHD equilibrium of the configuration is almost stable up to $\beta = 1\%$. The neoclassical transport in the CFQS is expected to be less than that in $1/\nu$ regime in the W7-X.

EX

Stability and Confinement Studies in the Gas Dynamic Trap

V. V. Prikhodko¹, P. A. Bagryansky^{1,3}, E. D. Gospodchikov^{1,2,4}, A. A. Lizunov¹,
Z. E. Konshin^{1,3}, O. A. Korobeynikova^{1,3}, Y. V. Kovalenko¹, V. V. Maximov^{1,3},
S. V. Murakhtin^{1,3}, E. I. Pinzhenin¹, V. Y. Savkin¹, A. G. Shalashov^{1,2,4}, E. I. Soldatkina¹,
A. L. Solomakhin^{1,3}, and D. V. Yakovlev¹

¹*Budker Institute of Nuclear Physics (BINP), Novosibirsk, Russian Federation*

²*Institute of Applied Physics (IAP), Russian Academy of Sciences (RAS), Nizhny Novgorod, Russian Federation*

³*Novosibirsk State University, Novosibirsk, Russian Federation*

⁴*Lobachevsky State University of Nizhny Novgorod, 23 Gagarina ave., Nizhny Novgorod, Russian Federation*

Corresponding Author: V. V. Prikhodko, v.v.prikhodko@inp.nsk.su

Interest in magnetic mirrors declined in the 1980's because of three key problems: magnet complexity, microinstabilities, and low plasma temperature. However, researches on the Gas Dynamic Trap (GDT) device at the Budker Institute of Nuclear Physics demonstrated the possibility to overcome these difficulties. Confinement of plasma with high energy density have been performed on GDT device with simple circular coils. "Vortex confinement" has been implemented to suppress the radial losses induced by flute-like MHD instability inherent to axially symmetric devices. This technique allowed reaching local plasma β close to 0.6. The auxiliary microwave heating on electron cyclotron resonance (ECR) frequencies raised the electron temperature up to 0.9 keV near the device axis. The Alfvén ion-cyclotron (AIC) instability has been observed, but not affected to the plasma power balance. The proposed report is dedicated to the following three topics. The first is optimization of the "vortex confinement" in presence of ECR heating. Introducing the additional "vortex" layer inside the existing one allows extending high-temperature phase behind the atomic beams turn off time. The second is definition of critical parameters for the divertor. It was shown that the critical wall position corresponds to expansion ratio of magnetic field $K_{crit} \sim 40$. This value is in a reasonable agreement with a simple theoretical model and remains constant in the range of electron temperature 25–700 eV. The neutral gas in the divertor does not affected the discharge until its density exceeded an order of magnitude the plasma density. The third is a study of unstable modes. In addition to AIC, the new type of oscillations are observed at the range of tens of ion-cyclotron frequencies. It was preliminary identified as drift-cyclotron loss-cone instability.

EX

Plasma Transport in Linear and Helical Multiple-Mirror Systems

A. V. Burdakov¹, V. I. Batkin¹, A. D. Beklemishev¹, V. B. Bobylev¹, V. S. Burmasov¹,
N. G. Vasilyeva¹, I. A. Ivanov¹, A. A. Inzhevatkina¹, K. N. Kuklin¹, K. I. Mekler¹,
S. V. Polosatkin¹, V. V. Postupaev¹, A. F. Rovenskikh¹, E. N. Sidorov¹, A. V. Sudnikov¹, and
V. F. Sklyarov¹

¹*Budker Institute of Nuclear Physics (BINP), Novosibirsk, Russian Federation*

Corresponding Author: A. V. Burdakov, a.v.burdakov@mail.ru

The challenge of creating an open trap with reactor-grade plasma is achievable if such a trap will use specialized sections of the magnetic system for suppression of particle and energy losses along the magnetic field. Currently, two new experimental devices are under construction in the Budker Institute for physics studies of plasma confinement in magnetic systems with multiple-mirror configurations. The linear topology of the traps enables an early start of experiments with plasma before the completion of the magnetic and vacuum systems. In the paper, we will report experimental results on the transport of a low-temperature start plasma flow through a section with a multiple-mirror magnetic field as well as the direct comparison with the case of solenoidal magnetic field. In the final configuration of GOL-NB, that plasma stream will be used as the target for the capture of heating neutral beams. In 2017, new SMOLA helical multiple-mirror trap achieved the first plasma. In this trap, plasma rotation is used for the creation of moving magnetic mirrors in the rotating reference frame. An active plasma pumping by the moving magnetic mirrors can deliver an exponential dependence of the confinement efficiency on the system length. Modification of the plasma flow profile at helical mirror confinement was demonstrated in the experiment. Main results from the first experimental campaign will be discussed.

EX

Real-Time Control System of Neoclassical Tearing Modes in the HL-2A Tokamak

L. W. Yan¹, X. Q. Ji¹, S. D. Song¹, F. Xia¹, Y. Xu¹, J. R. Ye¹, M. Jiang¹, W. J. Chen¹, T. F. Sun¹, S. Y. Liang¹, F. Ling¹, R. R. Ma¹, M. Huang¹, H. P. Qu¹, X. M. Song¹, D. L. Yu¹, Z. B. Shi¹, Y. Liu¹, Q. W. Yang¹, M. Xu¹, X. R. Duan¹, and Y. Liu¹

¹*Southwestern Institute of Physics, Chengdu, Sichuan, People's Republic of China*

Corresponding Author: L. W. Yan, lwyan@swip.ac.cn

The stability and performance of tokamak plasmas are routinely limited by various magnetohydrodynamic (MHD) instabilities, such as neoclassical tearing modes (NTMs). This paper presents a rather simple method to control the NTMs in real-time (RT) on a tokamak, including the control principle of feedback approach for RT suppression and stabilization for the NTMs. The control system combines Mirnov, electron cyclotron emission (ECE) and soft X-ray (SXR) diagnostics used for determining the NTM positions. A methodology for fast detection of 2/1 or 3/2 NTM positions with 129×129 grid reconstruction within 0.6 ms is elucidated. The forty poloidal angles for steering ECRH/ECCD launcher are used to establish the alignment of antenna mirrors with the centre of the NTM and to ensure launcher emission intersecting with the rational surface of a magnetic island. Pilot experiments demonstrate the RT control capability to track the conventional tearing modes (CTMs) on HL-2A tokamak. The 2/1 CTMs have been suppressed or stabilized by the ECRH power deposited on site or with steerable launcher. The total time to scan fully poloidal cross section is ~ 200 ms with spatial resolution of ~ 5 mm. The magnetic island is determined by an ECE diagnostic system of 60 channels with spatial resolution about 10 mm. So far, we are improving the NTM control system. The total time will be decreased to ~ 50 ms from ~ 200 ms, which is enough to control any NTM. Further dedicated studies on reliability of the actual NTM control scheme and minimum power requirements will be demonstrated in the spring's experimental campaign in 2018.

EX

Development of the $q = 1$ Advanced Tokamak Scenarios in HL-2A

Y. Liu¹, W. Deng¹, D. L. Yu¹, Z.-B. Shi¹, X.-G. Wang¹, X.-Q. Wang¹, J. Chen¹, Y. B. Dong¹, J. Y. Cao¹, W. L. Zhong¹, J. M. Gao¹, X. Q. Ji¹, Y.-P. Zhang¹, M. Jiang¹, Y.-G. Li¹, Q. W. Yang¹, and X. R. Duan¹

The HL-2A Team

¹*Southwestern Institute of Physics, Chengdu, Sichuan, People's Republic of China*

Corresponding Author: Y. Liu, yiliu@swip.ac.cn

Advanced tokamak scenario with central q close to 1 has been achieved on the HL-2A tokamak. An ITB has been observed during the nonlinear evolution of a saturated long-lived internal mode (LLM) or fishbone activities in HL-2A discharges as the q -profile formed a very broad low-shear region with $q_{\min} \sim 1$. Such steep ion temperature-gradient zone locates around $r/a = 0.5$ – 0.6 with $T_i > T_e$. The observed normalized ion temperature gradient (R/L_{T_i}) is of 10.6, which exceeded the value for a level without ITB of ~ 6.5 . Here, R is the major radius and L_{T_i} is the scale length of the T_i gradient defined by $L_{T_i} = aT_i/(dT_i/d\rho)$. When the barrier forms, the turbulence is significantly reduced around ITB foot ($r/a = 0.6$), as measured by reflectometry. The simultaneous excitation of the ITB and the bursting internal mode can only occur if the q -profile in the core remains flat in the plasma central region. This confirms the role played by the central internal kink instabilities in the production of ITBs in reversed or weak shear plasmas.

It was found that q_{\min} reaching an integer value ($q_{\min} = 1$) throughout the ITB period, and there is a correlation between the emergence of the ITB formation and the evolution of central magnetic shear due to the perturbation of $m/n = 1/1$ LLM or fishbone activity. A possible explanation for the LLM or fishbone being able to trigger or sustain ITBs is that the interaction between MHD instabilities and fast ion leads to a redistribution of the resonant fast ion. Based on this assumption, dedicated experiment have attempted to reproduce the stationary advanced scenario with q_0 close to 1 by applying extra ECRH for enhancement of the fishbone activities. With strong fishbone activities enhanced by application of ECRH, this scenario does exhibit a clear prolonged ITB during the stationary phase of the discharge, extending the domain of existence of ITB from 10 confinement times to 20 confinement times, and the confinement enhancement factors over ITER89P L-mode scaling, from $H^{\text{ITER89-P}} = 1.7$ to a new level of $H^{\text{ITER89-P}} = 2.1$.

First Plasma Scenario Development for HL-2M

X. M. Song¹, J. X. Li¹, J. A. Leuer², J. H. Zhang¹, and X. Song¹

¹*Southwestern Institute of Physics, Chengdu, Sichuan, People's Republic of China*

²*General Atomics, San Diego, CA 92186, USA*

Corresponding Author: X. M. Song, songxm@swip.ac.cn

HL-2M tokamak is now under construction in China as a modification to the HL-2A facility, with nominal parameters as follows: $I_p = 1.5\text{--}3.0$ MA, $B = 2.2$ T, major radius $R = 1.78$ m, minor radius $a = 0.65$ m, elongation $\kappa = 1.6\text{--}1.8$, and triangularity > 0.5 . It is a real challenge to build a new machine in the fusion community, and HL-2M suffers from a long delay for the first plasma. In order to fulfil the requirement of engineering and government qualification of the machine in a short time, two first plasma scenarios for HL-2M are designed with a powerful plasma scenario design tool based on Matlab.

The two scenarios, one for circular limited configuration and one for larger aspect ratio and lower elongation divertor configuration, are compatible with the magnetic diagnostic system and power supply system, which are not fully equipped and well tested. The PF current and voltage waveform for these two scenarios have been calculated with the plasma scenario design tool through a plasma resistive model which can estimate the resistive flux consumption. The key parameters for these two scenarios are as follows: toroidal field 1.4 T, plasma current 200 kA with 1000 μs flattop. For the sake of simplicity and safety in first plasma campaign, only small parts of PF coils are used in the plasma discharge, no initial magnetization is exploited, no PF current zero-crossing is allowed, no vertical displacement event is allowed. To facilitate obtaining the plasma, two gyrotrons of 68 GHz with 500 kW each are exploited for preionization and assisted startup. The vacuum vessel baking temperature will reach 300°C degree during machine conditioning.

In this paper, the geometric parameters of PF and CS, together with that of TF coils and vacuum vessel (VV). Also presented are an original Matlab-based tool for tokamak modelling and plasma scenario development. With this tool, the current waveforms and voltage waveforms of CS and PF coils are calculated by a given plasma resistance model. The parameters of CS and PF coils presented here can provide reference for later plasma scenario design for HL-2M; the ideas for simple and safe first plasma scenarios can apply to other new machine in its first plasma campaign.

This work is supported by the Chinese National Fusion Project for ITER under grant No. 2015 GB105004.

DIII-D Shaping Demonstrates Correlation of Intrinsic Momentum with Energy

J. S. deGrassie¹, T. L. Rhodes², J. A. Boedo³, B. A. Grierson⁴, C. Chrystal¹, T. H. Osborne¹, S. R. Haskey⁴, and A. Ashourvan⁴

¹General Atomics, San Diego, CA 92186, USA

²University of California Los Angeles, CA 90095, USA

³University of California San Diego, CA 92093, USA

⁴Princeton Plasma Physics Laboratory (PPPL), Princeton, NJ 08540, USA

Corresponding Author: J. S. deGrassie, degrassie@fusion.gat.com

Scaling of intrinsic rotation in DIII-D H-mode plasmas demonstrates a strong correlation with the ion temperature (T_i) and stored plasma thermal energy, indicating a coupling between the turbulent intrinsic momentum flux and the turbulent energy flux [1]. The empirical scaling [1] of intrinsic rotation with plasma stored energy has been recently explored by novel experiments on DIII-D that utilize relatively small variations in the plasma shape, namely the triangularity, to modify the intrinsic rotation. Shape variation modifies the turbulent transport, rather than via changes in the auxiliary heating power. These H-modes are heated by ECH with no external torque input. Balanced torque blips from neutral beams [1] measure the ion flow velocity and T_i . Higher energy and intrinsic angular momentum are correlated with higher triangularity. The measured results follow the recently established DIII-D empirical scaling [1]. Turbulent density fluctuations in the pedestal region show a significantly higher level in the lower triangularity, lower confinement phases, possibly the source of greater transport. Changing triangularity is more subtle than the up/down symmetry change experiments in TCV [2]. In DIII-D, we postulate that $E \times B$ shear likely provides the dominant symmetry breaking necessary for a net turbulent momentum stress, rather than the shaping, per se.

This material is based upon work supported by the U.S. Department of Energy under Award Numbers DE-FC02-04ER54698, DE-FG02-08ER54984, DE-FG02-07ER54917, and DE-AC02-09CH11466.

References

- [1] J. S. deGrassie *et al.*, Phys. Plasmas, **23**, 082501 (2016).
- [2] Y. Camenen *et al.*, Phys. Plasmas, **16**, 062501 (2009).

ELMs Onset Triggered by Mode Coupling Near Rational Surfaces in the Pedestal

A. Diallo¹, J. Dominski¹, K. K. Barada², L. Zeng², M. Knolker¹, G. Canal³, G. R. McKee⁴, and R. J. La Haye³

¹Princeton Plasma Physics Laboratory (PPPL), Princeton, NJ 08540, USA

²University of California Los Angeles, CA 90095, USA

³General Atomics, San Diego, CA 92186, USA

⁴University of Wisconsin-Madison, Madison, WI 53706, USA

Corresponding Author: A. Diallo, adiallo@pppl.gov

EX Investigations of pedestal evolution between edge-localized-modes (ELMs) in DIII-D provide strong evidence that coupling of modes located near rational surfaces close to the separatrix leads to the onset of an ELM. While the peeling ballooning model is the leading candidate for the ELM phenomenology, the triggering mechanism is not yet understood and remains one of the most outstanding challenges of both theoretical and experimental fusion science. In this work, the physical mechanism of the triggering of ELMs is studied on the DIII-D tokamak. We extract the dynamics of the most dominant modes localized in the pedestal during multiple inter-ELM periods. We observe a transition from a regime dominated at the beginning of the inter-ELM period by a single mode located near $q = 5$ towards a more balanced organization between this mode and two secondary modes located near the $q = 6$ surface just before the ELM onset. This redistribution suggests a transfer of energy which provides strong evidence that these secondary modes are triggering the ELM onset, because they are strongly coupled to the region extending to the separatrix. The radial expansion to the separatrix provides a channel for the expulsion of energy and particle, which is the ELM. The locality of these modes is determined through the spatial coupling between j_{\parallel} and δn_e . While pedestal width growth has long been the leading explanation of the ELM onset, the results presented describe a different mechanism for ELM onset. In our explanation, the pedestal temperature and density gradients are clamped over multiple transport time scales and it is posited that the inter-ELM fluctuations play a key role in the ELM onset. As shown above, the onset results from modes coupling between the $q = 5$ and $q = 6$ rational surfaces during the ELM cycle. We propose that such coupling opens up a channel from the pedestal top to the separatrix through which the energy to trigger the ELM is released.

Work supported by the U.S. Department of Energy under contracts DE-AC02-09CH11466, DE-FC02-04ER5469, DE-FG02-08ER54984 and DE-FC02-04ER54698.

Rotation Profile Hollowing in DIII-D Low-Torque Electron-Heated H-Mode Plasmas

B. A. Grierson¹, D. R. Ernst², C. Chrystal³, T. Tala⁴, T. L. Rhodes⁵, G. R. McKee⁶,
S. R. Haskey¹, L. Bardoczi⁷, and A. Salmi⁴

¹Princeton Plasma Physics Laboratory (PPPL), Princeton, NJ 08540, USA

²Massachusetts Institute of Technology (MIT), Cambridge, MA 02139, USA

³General Atomics, San Diego, CA 92186, USA

⁴VTT Technical Research Centre of Finland Ltd., Espoo, Finland

⁵University of California Los Angeles, CA 90095, USA

⁶University of Wisconsin-Madison, Madison, WI 53706, USA

⁷Oak Ridge Associated Universities (ORAU), Oak Ridge, TN 37831, USA

Corresponding Author: B. A. Grierson, bgriers@pppl.gov

Recent experiments in the DIII-D tokamak obtained low torque MHD-free H-mode discharges approaching ITER baseline conditions revealing midradius rotation profile hollowing associated with turbulent transport. This indicates that hollowing of toroidal rotation profiles that occurs prior to onset of large-scale MHD observed in low torque ITER Baseline conditions is not due to pre-existing MHD mode drag, but a natural consequence of the turbulent momentum flux. Low torque ($T \sim 0.6$ Nm) plasmas in the ITER similar shape with $q_{95} \sim 4.3$, $\beta_N \sim 1.2$ – 1.6 and electron cyclotron heating (ECH) power between 0–3.4 MW deposited between $\rho = 0.3$ – 0.7 are studied for ion and electron heating effects on momentum transport. Turbulent density fluctuations are measured with Doppler backscattering (DBS) for intermediate- k ($k_\theta \rho_s \sim 1$ – 5) and beam emission spectroscopy (BES) for low- k ($k_\theta \rho_s < 1$). Contrasting times in a discharge with a core tearing mode with a later phase after the tearing mode has disappeared, the role of the mode on rotation profile hollowing can be determined. In the presence of the mode, the rotation profile is flat or moderately peaked. However, after the tearing mode disappears, the profile takes on a nonmonotonic, localized “well” or hollowness, with a positive local rotation gradient. We interpret this phenomenon as the tearing mode reducing the turbulent transport near the island by shunting the thermal flux, flattening the profiles and reducing the turbulent residual stress. When the tearing mode disappears, turbulence increases and the turbulent residual stress is able to drive the nonmonotonic rotation profile. Fluctuations in the region of the nonmonotonic rotation reveal both low- k ion temperature gradient (ITG) as well as intermediate- k trapped electron mode (TEM) scale fluctuations. The theoretical impact of the linearly unstable modes and turbulent transport mechanisms on the rotation hollowing is still being investigated.

Work supported in part by the U.S. Department of Energy under DE-FC02-04ER54698, DE-SC0014264 and DE-AC02-09CH11466, and carried out within the framework of the EUROfusion Consortium and has received funding from the Euratom research and training programme 2014–2018 under Grant Agreement No. 633053.

The Universality of Inter-ELM Pedestal Fluctuations in AUG and DIII-D: Impacting the Edge Profile Structure by Clamping of the Gradients

F. M. Laggner¹, E. Kolemen¹, A. Diallo², R. J. Groebner³, E. Wolfrum⁴, K. K. Barada⁵, M. Cavedon⁴, B. A. Grierson², G. F. Harrer⁶, F. Mink⁴, T. H. Osborne³, and P. B. Snyder³

The ASDEX-Upgrade Team and DIII-D Team

¹*Princeton University, Princeton, NJ 08544, USA*

²*Princeton Plasma Physics Laboratory (PPPL), Princeton, NJ 08540, USA*

³*General Atomics, San Diego, CA 92186, USA*

⁴*Max-Planck-Institut für Plasmaphysik, Garching, Germany*

⁵*University of California Los Angeles, CA 90095, USA*

⁶*Technische Universität Wien, 1040 Vienna, Austria*

Corresponding Author: F. M. Laggner, flaggner@princeton.edu

For wide ranges of operational parameters and in machines with different wall materials, the inter-ELM pedestal profile evolution was robustly linked to characteristic fluctuations, indicating that universal instabilities dominate the pedestal structure and its dynamics in between edge localized modes (ELMs). The presented results substantially advance the comprehension of the underlying instabilities that determine the pedestal structure because ion and electron density as well as temperature gradients were found to become clamped in different phases of the ELM cycle. The general behaviour of the inter-ELM fluctuations supports that similar mechanisms determine the pedestal of future fusion devices, and stresses the necessity that predictive models need to incorporate a robust mechanism, which describes the clamping of individual profile gradients across wide ranges of pedestal parameters.

The inter-ELM fluctuations exhibit a similar sequence of their onsets in ASDEX-Upgrade and DIII-D. This gives strong evidence that their origin is the same, although both machines usually operate in different parameter regimes. Generally, low fluctuation amplitudes are found during the initial recovery of the maximum electron density gradient. After this phase, maximum electron density gradient saturates. The electron temperature pedestal evolves further and the saturation of maximum electron temperature gradient correlates with the onset of high frequency fluctuations.

Fast vertical plasma oscillations were utilized as a tool to probe the pedestal fluctuations as well as the pedestal stability. Such oscillations perturb the edge current. To make them an effective ELM pacing method, the pedestal must evolve close to its gradient saturation. This state of saturated gradients is stable, but marginal to the stability limit. If a perturbation, e.g., of the edge current, is applied, it is highly probable that an ELM crash is triggered.

This work has been carried out within the framework of the EUROfusion Consortium and has received funding from the Euratom research and training programme 2014–2018 under grant agreement No. 633053. The views and opinions expressed herein do not necessarily reflect those of the European Commission. Work supported by the U.S. Department of Energy under DE-FC02-04ER54698, DE-SC0015878 and DE-SC0015480.

Particle Transport from the Bottom Up

S. Mordijck¹, L. Zeng², T. L. Rhodes², L. Schmitz², J. W. Hughes³, T. Tala⁴, A. Salmi⁴,
Y. Baranov⁵, C. C. Petty⁶, R. J. Groebner⁶, and A. L. Moser⁶

The DIII-D and C-Mod Teams, and The JET Contributors

¹College of William & Mary, Williamsburg, VA 23185, USA

²University of California Los Angeles, CA 90095, USA

³Plasma Science & Fusion Center, MIT, Cambridge, MA 02139, USA

⁴VTT Technical Research Centre of Finland Ltd., Espoo, Finland

⁵Culham Centre for Fusion Energy (CCFE), Culham Science Centre, Abingdon, UK

⁶General Atomics, San Diego, CA 92186, USA

Corresponding Author: S. Mordijck, smordijck@wm.edu

Exploration of particle transport behaviour in multiple devices shows the importance of turbulence in determining particle confinement and the density profile. Behaviour on CMOD indicates that as plasma parameters approach ITER, the pedestal and SOL become increasingly opaque. H-mode experiments with density pedestals approaching $4 \times 10^{20}/\text{m}^3$, heated with the maximum auxiliary power available, find that increasing deuterium puffing by a factor of ~ 2 doubles the SOL density while having $< 10\%$ effect on pedestal density and core particle inventory. This suggests that high opacity pushes the neutral fuelling profile into the SOL, leaving the pedestal density profile to be determined by plasma transport and an inward pinch. Similarly, studies on JET and DIII-D show that the inward pinch plays a crucial role in explaining the time dependent density changes when additional gas fuelling is injected. Interestingly, neutral particle fuelling does not play a direct role in pedestal density increases since COCONUT (core/edge integrated) modelling shows that the particle source inside the separatrix reduces when gas fuelling increases because of higher SOL opacity. Where fuelling and opacity play an important role at the plasma edge, in the core particle confinement is strongly affected by changes in turbulence. For example, during strong electron heating in low density H-mode plasmas on DIII-D a strong decrease in particle confinement is observed. This is linked to an increase in ITG drive from $\rho \sim 0.6$ to $\rho \sim 0.8$, which causes an increase in density fluctuations at all scales and results in a density pump-out. We find that where the temperature profiles are fairly insensitive to changes in $E \times B$ shear, particle confinement is directly linked to increases and decreases in $E \times B$ shear. In the core, we observe that the role of NBI fuelling on the density profile cannot be neglected in current machines and that local gradients are directly linked to the turbulence frequency. These results indicate that in burning plasma conditions, opaque SOLs may not result in the collapse of the density pedestal owing to the inward particle pinch at the edge, and that a larger $E \times B$ shear will be beneficial to higher particle confinement.

Work supported by the U.S. Department of Energy under DE-SC0007880, DE-FG02-08ER-54984, DE-AC05-06OR23100, DE-FC02-04ER54698, and DE-SC0012469.

High Confinement in Negative Triangularity Discharges in DIII-D

M. E. Austin¹, A. Marinoni², M. L. Walker³, M. W. Brookman³, J. S. deGrassie³, A. W. Hyatt³, G. R. McKee⁴, C. C. Petty³, T. L. Rhodes⁵, S. P. Smith³, C. Sung⁵, and K. E. Thome⁶

The DIII-D Team

¹*Institute for Fusion Studies (IFS), University of Texas at Austin, Austin, TX 78712, USA*

²*Plasma Science & Fusion Center, MIT, Cambridge, MA 02139, USA*

³*General Atomics, San Diego, CA 92186, USA*

⁴*University of Wisconsin-Madison, Madison, WI 53706, USA*

⁵*University of California Los Angeles, CA 90095, USA*

⁶*Oak Ridge Associated Universities (ORAU), Oak Ridge, TN 37831, USA*

Corresponding Author: M. E. Austin, max.austin@utexas.edu

Discharges with negative triangularity ($-\delta$) shape have been created in DIII-D with H-mode-like confinement ($H_{98}(y, 2) = 1.2$) and high normalized β ($\beta_N = 2.6$) with L-mode-like edge pressure profiles and no ELMs. These inner-wall-limited plasmas with $\delta = -0.4$ had the same global performance as a positive triangularity ($\delta = +0.4$) ELMy H-mode discharge with the same I_p , elongation, and area. For negative delta shots where up to 11 MW of NB heating and 3 MW of ECH heating were applied, the plasma attained high toroidal β of 1.9% while staying in L-mode and without disrupting. Preliminary fluctuation data shows negative δ plasmas have lower levels of density and electron temperature fluctuations, typically reduced by 20%, in the outer region of the plasma, $0.7 < r/a < 1.0$, compared to equivalent positive δ discharges. This reduction of turbulence is consistent with gyrokinetic simulations and is attributed to a modification of the toroidal precession drift of trapped electrons exerted by the negative triangularity. Correspondingly, transport analysis indicates reduced ion and electron diffusivities for negative δ compared to the positive delta cases. Also, the positive triangularity discharges had 30–50% lower neutron rates as the identically heated negative triangularity ones, due primarily to impurity retention and deuterium dilution. These results show that negative triangularity is a viable candidate for reactor scenarios with its high confinement, ELM-mitigated characteristics plus a more economical and effective option for divertor placement.

Work supported by the U.S. Department of Energy under DE-FG02-97ER54415, DE-FG02-94ER54235, DE-FG02-08ER54999, DE-FG02-08ER54984 and DE-FC02-04ER54698.

Rotation-Induced Electrostatic-Potentials and Density Asymmetries in NSTX

L. F. Delgado-Aparicio¹, R. E. Bell¹, G. J. Kramer¹, M. Podestà¹, B. P. LeBlanc¹, A. Diallo¹, S. P. Gerhardt¹, H. Yamazaki^{1,2}, Y. Takase², and M. Ono¹

¹Princeton Plasma Physics Laboratory (PPPL), Princeton, NJ 08540, USA

²Graduate School of Frontier Science, University of Tokyo, Tokyo, Japan

Corresponding Author: L. F. Delgado-Aparicio, ldelgado@pppl.gov

The computation of rotation-induced electrostatic potentials is currently being used to study the associated two-dimensional distribution of impurity density asymmetries in NSTX and NSTX-U plasmas. The main effect of toroidal rotation on heavy impurities is their radial displacement to the outer plasma, which result in a nonuniform distribution around a magnetic flux-surface. Due to the different effect of centrifugal forces on electrons, main ions and low- to high- Z impurity density, an electrostatic potential is generated to satisfy quasineutrality. This calculation relies on flux-surface quantities like electron and ion temperature, $T_{e,i}$, and rotation frequency, ω_ϕ , and finds the 2D electron, deuterium and carbon density profiles self-consistently assuming the presence of a poloidal variation due to centrifugal forces. The few assumptions considered include a zero electron mass, a deuterium plasma, a trace impurity with charge Z given by coronal equilibrium and equilibrated ion temperatures (e.g., $T_D = T_C = T_Z$). The iterative solution for the electrostatic potential from the measured carbon density and central toroidal rotation using NSTX data are routinely obtained and compared with the values derived using the ideal formalism which assumes that the main low- Z intrinsic impurity (e.g., Carbon) is in the trace limit $\alpha_C \equiv 36n_C/n_e \ll 1$; realistic values of the low- Z impurity strength factor can exceed one. While the carbon asymmetry is nearly three times stronger than the ideal description, the depth of the potential well in the high field side can reach -110 to -280 V for core rotation between 180 – 360 km/s. This computation is being used to increase our understanding of medium- and high- Z asymmetries and the reduction of Z -peaking, to examine the effect of electrostatic potentials possibly changing the heat and particle transport, the reduction of the underlying turbulence due to $E \times B$, radiation asymmetries before tearing mode onsets, as well as to aid the design of new diagnostics for NSTX-U (e.g., ME-SXR, XICS, Bolometers, etc). The presence of O, Ne, Ar, Fe, Mo and W are considered at the trace limit with very small changes to quasineutrality and Z_{eff} .

Work supported by the U.S. Department of Energy, Office of Fusion Energy Sciences under contract number DE-AC02-09CH11466.

Extending the Boundary Heat Flux Width Database to 1.3 Tesla Poloidal Magnetic Field in the Alcator C-Mod Tokamak

D. Brunner¹, B. LaBombard¹, A. Q. Kuang¹, J. L. Terry¹, J. W. Hughes¹, A. E. Hubbard¹, M. L. Reinke², S. M. Wolfe¹, and M. V. Umansky³

The Alcator C-Mod Team

¹Plasma Science & Fusion Center, MIT, Cambridge, MA 02139, USA

²Oak Ridge National Laboratory (ORNL), Oak Ridge, TN 37831, USA

³Lawrence Livermore National Laboratory (LLNL), Livermore, CA 94550, USA

Corresponding Author: D. Brunner, brunner@mit.edu

The boundary heat flux width (λ_q) is an important part of the power exhaust challenge in magnetic confinement fusion reactors. Understanding what sets λ_q has largely been an empirical science [1], however, physics understanding is progressing [3–6]. A database of λ_q in H-mode indicated that the poloidal magnetic field (B_p) was the only significant parameter associated with the heat flux width: $\lambda_q \sim B_p^{-1.19}$ [1]. The maximum B_p in the database was ~ 0.8 T, whereas ITER at 15 MA will be ~ 1.2 T.

C-Mod has been the only diverted tokamak capable of operating at reactor-relevant B_p , now with measurements up to 1.3 T. These new measurements in EDA H-mode clearly follow the inverse scaling of λ_q with B_p to values exceeding ITER-level. The heuristic drift (HD) model [4, 5] has done a remarkable job of reproducing the trend and the magnitude of λ_q in the database. The new high-field data from C-Mod are consistent with the HD model. Perhaps more importantly, the new data provide a benchmark for first principles models [6, 7], one of which projects [6] to ~ 10 times larger λ_q than the empirical B_p scaling for ITER. In addition, we have assembled a database of λ_q consisting of over 300 shots that span nearly the entire operating space of Alcator C-Mod (L-, H- and I-modes) under attached divertor conditions. As in earlier studies [8], λ_q at fixed B_p exhibit significant scatter that appears related to the core plasma confinement. We are presently exploring correlations of λ_q with global and pedestal parameters; we will report on the latest results at this meeting. The database now includes a composite of measurements made by surface thermocouples and Langmuir probes. Improved spatial resolution and heat flux dynamic range over IR thermography allows for more accurate fits of λ_q and resolving the role of transport into the private flux region. We find that the assumption of symmetric spreading of heat flux [1] is not appropriate under many conditions.

References

- [1] T. Eich *et al.*, Nucl. Fus., **53**, 093031 (2013).
- [2] R. J. Goldston *et al.*, Nucl. Fus., **52**, 013009 (2012).
- [3] R. J. Goldston, J. Nucl. Mater., **463**, 397–400 (2015).
- [4] C. S. Chang *et al.*, Nucl. Fus., **57**, 116023 (2017).
- [5] B. Chen *et al.*, submitted to Phys. Plasmas.
- [6] B. LaBombard *et al.*, Phys. Plasmas, **18**, 056104 (2011).

Development and First Experimental Tests of a Small Angle Slot Divertor on DIII-D

H. Y. Guo¹, H. Wang¹, J. G. Watkins², L. Casali¹, B. Covele¹, A. L. Moser¹, T. H. Osborne¹, M. W. Shafer³, L. Holland¹, A. W. Hyatt¹, A. Kellman¹, L. L. Lao¹, A. W. Leonard¹, C. Murphy¹, C. F. Sang⁴, P. C. Stangeby⁵, T. S. Taylor¹, and D. M. Thomas¹

The DIII-D Team

¹General Atomics, San Diego, CA 92186, USA

²Sandia National Laboratories (SNL), Albuquerque, NM 87185, USA

³Oak Ridge National Laboratory (ORNL), Oak Ridge, TN 37831, USA

⁴Dalian University of Technology, Liaoning, Dalian, Ganjingzi, People's Republic of China

⁵University of Toronto, Toronto, ON M5S-1A1, Canada

Corresponding Author: H. Y. Guo, guohy@fusion.gat.com

A small angle slot (SAS) divertor has been installed on the DIII-D tokamak to further evaluate the role of divertor closure in achieving efficient heat dispersal for steady-state tokamaks. Initial experiments have shown a significant reduction of the electron temperature (T_e) across the divertor target and access to dissipative divertor operation at lower H-mode operational densities while maintaining high core plasma confinement. The SAS configuration features a small (glancing) angle target and a narrow slot progressively flaring out from the strike point to amplify both neutral and impurity dissipation of power in the divertor. Experiments with closely matched H-mode discharges in DIII-D have demonstrated that SAS achieves dissipative divertor conditions with $T_e < 10$ eV at a lower main plasma density than in an open (horizontal) divertor configuration, based on target Langmuir probe measurements. In addition, SAS can extend plasma cooling into the far scrape-off layer (SOL), in contrast to the vertical target configuration which usually achieves partial detachment with low T_e in the near SOL only. SAS also achieves improved confinement with a confinement enhancement factor $H_{98}(y, 2) \sim 25\%$ higher than the open divertor at the onset of detachment. SAS also widens the high performance H-mode operating window through detachment onset at lower density and X-point MARFE formation at higher density. Detailed transport and pedestal stability analyses find that the confinement improvement with SAS are associated with higher pedestal temperature and pressure, which are primarily due to an increased pedestal width, consistent with previous divertor closure experiments on DIII-D. These results were obtained with the ion ∇B drift away from the SAS divertor. Further research will be conducted to establish the role of drifts in a closed slot divertor and results will also be presented.

Work supported by the U.S. Department of Energy under DE-FC02-04ER54698, DE-AC04-94AL85000 and DE-AC05-00OR22725, and GA corporate funding.

High Performance Double-Null Plasmas Under Radiating Divertor and Mantle Scenarios on DIII-D

T. W. Petrie¹, B. A. Grierson², T. H. Osborne¹, P. Petty¹, F. Turco³, S. L. Allen⁴,
M. E. Fenstermacher⁴, J. R. Ferron¹, H. Guo¹, R. J. La Haye¹, C. J. Lasnier⁴, A. W. Leonard¹,
A. G. McLean⁴, B. S. Victor⁴, and J. G. Watkins⁵

¹General Atomics, San Diego, CA 92186, USA

²Princeton Plasma Physics Laboratory (PPPL), Princeton, NJ 08540, USA

³Columbia University, New York, NY 10027, USA

⁴Lawrence Livermore National Laboratory (LLNL), Livermore, CA 94550, USA

⁵Sandia National Laboratories (SNL), Livermore, CA 94551, USA

Corresponding Author: T. W. Petrie, petrie@fusion.gat.com

Enhanced radiation has been used to reduce divertor heat flux in high power, high performance (AT) double null divertor (DND) and near-DND plasmas in DIII-D, while at the same time maintaining acceptable energy confinement and particle control. Effective radiating mantle operation in high power AT plasma depended strongly on the location of electron cyclotron (EC) heating deposition, on impurity selection and its effect on triggering inimical MHD activity, and on the location where seed impurities are injected. Predictions by ELITE for ways to improve confinement and fuelling in these high performance plasmas have been experimentally verified. The plasmas discussed here are characterized by: $H_{98} = 1.4\text{--}1.7$, $\beta_N = 3\text{--}4$, $q_{95} \approx 6$, neutral beam plus EC power input P_{in} up to 15 MW, with EC providing up to 3.5 MW, $dR_{sep} = 6\text{--}25$ mm. When the radial location of the ECH deposition was near the magnetic axis (e.g., $\rho_{ech} = 0.20$), the radial profiles of both the injected impurity (e.g., neon) and carbon were mostly flat, while ECH deposition farther out (i.e., $\rho_{ech} = 0.45$) produced profiles that were peaked. Analysis with the STRAHL transport code indicates a stronger inwardly-directed pinch for neon in the $\rho_{ech} = 0.45$ case, while analysis for $\rho_{ech} = 0.20$ indicates screening of neon from the central plasma. Using higher- Z seed impurities to form a radiating mantle increases deleterious MHD activity when applied to these AT DND plasmas. For example, when argon seeds were injected into these AT plasmas, the argon seeds triggered more deleterious MHD activity than the neon seed injection. Impurity selection, injection location, the ion ∇B drift direction, and details of scrape-off layer shaping strongly are shown to dictate where injected impurities can be most effectively pumped in DND and near-DND configurations. Finally, we show that conditions leading to improved performance in high power high performance regimes, which were predicted by ELITE code analysis, are largely supported by recent DIII-D experiments.

These studies represent a continuing effort to experimentally identify potential issues related to adapting radiating mantle/divertor methods to high-powered AT DND plasmas.

Work supported in part by the U.S. Department of Energy under DE-FC02-04ER54698, DE-AC05-00OR22725, DE-AC04-94AL85000, DE-AC52-07NA27344, and DE-FG02-07ER54917.

Parallel Energy Transport in Detached DIII-D Divertor Plasmas

A. W. Leonard¹, J. D. Lore², J. M. Canik², S. A. Allen³, A. G. McLean³, J. A. Boedo⁴,
H. Q. Wang⁵, M. Groth⁶, and J. D. Watkins⁷

¹General Atomics, San Diego, CA 92186, USA

²Oak Ridge National Laboratory (ORNL), Oak Ridge, TN 37831, USA

³Lawrence Livermore National Laboratory (LLNL), Livermore, CA 94550, USA

⁴University of California San Diego, CA 92093, USA

⁵Oak Ridge Associated Universities (ORAU), Oak Ridge, TN 37831, USA

⁶Aalto University, Espoo, Finland

⁷Sandia National Laboratories (SNL), Albuquerque, NM 87185, USA

Corresponding Author: A. W. Leonard, leonard@fusion.gat.com

A comparison of experiment and modelling of detached divertor plasmas in DIII-D is examined in the context of parallel energy transport due to electron conduction and plasma convection in order to validate and improve models used for divertor design. Power balance analysis is carried out to determine parallel heat flux and energy dissipation as a function of distance from the divertor target. The relative fractions of conductive and convective heat flux are determined from Thomson scattering measurements of the divertor parallel T_e gradient. Modelling with the fluid code SOLPS is found to underestimate divertor heat flux radiative dissipation due to two effects: 1) lower values of parallel convection than inferred from experiment, and 2) lower impurity radiation than measured experimentally at similar values of T_e . Resolution of these discrepancies is expected to improve accuracy and confidence for predictive modelling of divertor operation in future devices.

Work supported by the U.S. Department of Energy under DE-FC02-04ER54698, DE-AC52-07NA27344, DE-FG02-07ER54917, DE-AC05-00OR22725, DE-AC02-09CH11466, and DE-AC04-94AL85000.

Inter vs. Intra-ELM Tungsten Erosion and Transport from the Divertor in DIII-D High-Performance H-Mode Discharges

T. Abrams¹, A. G. McLean², C. J. Lasnier², H. Q. Wang³, J. Guterl³, E. A. Unterberg⁴, A. R. Briesemeister⁴, D. L. Rudakov⁵, D. C. Donovan⁶, and G. S. Xu⁷

¹General Atomics, San Diego, CA 92186, USA

²Lawrence Livermore National Laboratory (LLNL), Livermore, CA 94550, USA

³Oak Ridge Associated Universities (ORAU), Oak Ridge, TN 37831, USA

⁴Oak Ridge National Laboratory (ORNL), Oak Ridge, TN 37831, USA

⁵University of California San Diego, CA 92093, USA

⁶University of Tennessee, Knoxville, TN 37996, USA

⁷University of Science and Technology of China, Hefei, Anhui, People's Republic of China

Corresponding Author: T. Abrams, abramst@fusion.gat.com

Measured intra-ELM (during ELMs) tungsten erosion profiles in the DIII-D divertor, acquired via W-I spectroscopy with high temporal and spatial resolution, are consistent with OEDGE+SDTrim.SP modelling including measured ion saturation currents and ion impact energies. If pedestal temperature rather than divertor conditions are used as input, quantitative agreement is observed, for the first time, between the Fundamenski-Moulton “free-streaming” (FMFS) model predictions of how W source scales with ELM deposited energy density when broadening of the divertor heat flux footprint and enhanced target electron densities (e.g., via increased neutral recycling) are taken into account. Consistency is observed between this new FMFS-SDTrim.SP model and experimental measurements of intra-ELM W sourcing across a range of ELM frequencies/sizes, except for ELMs with very low energy density. An interpretive model for the time evolution of the W physical sputtering rate during ELMs was also developed including impurity and main ion sputtering. This model reveals that both D and C contribute substantially to W sourcing during ELMs in the DIII-D divertor because the average ion impact energy increases from below to substantially above the energy threshold for D→W sputtering. The measured W sputtering profiles are well matched to this model with a 2% C²⁺ fraction, a factor of 2 higher than in the inter-ELM (between ELMs) phase. This work represents unique progress towards a predictive model to link pedestal conditions to the ELM-induced divertor W impurity source. Such models can be utilized in ITER and beyond to develop and optimize mitigation strategies for minimizing high-Z accumulation in the core.

Work supported by the U.S. Department of Energy under DE-FC02-04ER54698.

The Effect of RMP ELM Control for ITER on Pedestal Pressure Compared to EPED No-RMP Predictions

M. E. Fenstermacher¹, O. Meneghini², B. Zywicki³, R. J. Groebner², and C. Rea⁴

The DIII-D Team

¹*Lawrence Livermore National Laboratory (LLNL), Livermore, CA 94550, USA*

²*General Atomics, San Diego, CA 92186, USA*

³*University of Michigan, Ann Arbor, MI 48109, USA*

⁴*Massachusetts Institute of Technology (MIT), Cambridge, MA 02139, USA*

Corresponding Author: M. E. Fenstermacher, fenstermacher@fusion.gat.com

The ITER baseline and alternate scenarios use 3D resonant magnetic perturbation (RMP) fields to control ELMs, and therefore ITER operating scenario (IOS) analysis needs to include the effect of the 3D fields on the pedestal pressure and overall device performance. In IOS analysis, the pedestal pressure, for a given pedestal density, will be predicted with the EPED code. Neural net techniques (NN-EPED) have already been applied to databases of EPED computational results to decrease the time needed to make a pedestal pressure prediction by about a factor of 10^9 . A new neural network (NN-RMP), trained on measured pedestal data from RMP ELM control discharges in DIII-D, determines the effect of RMP application on the pedestal pressure compared to EPED pressure predictions. Consistent with random forest statistical analysis of the parameters most important to the effect of RMP on pedestal pressure, the NN-RMP shows a strong dependence of the reduction in achieved pressure versus EPED predictions on applied RMP amplitude, but also on pedestal toroidal rotation and either toroidal field (B_t) or plasma current (I_p). The dependence on pedestal rotation is indicative of the dependence on RMP penetration and bifurcation physics. The dependence on either B_t or I_p , with other geometry parameters fixed, is indicative of the sensitivity to edge safety factor (q_{95}) seen in many DIII-D RMP ELM control discharges. The NN-RMP predicted pedestal height is up to 20–25% lower than EPED predictions for the cases with strongest ELM mitigation or ELM suppression. For ITER operating scenario analysis, this work provides a tool to adjust the EPED-predicted ITER pedestal pressure for the use of RMP fields to mitigate or suppress ELMs.

Work supported in part by the U.S. Department of Energy under DE-FC02-04ER54698, LLNL DE-AC52-07NA27344 and the Science Undergraduate Laboratory Internship (SULI) programme and under DE-FC02-04ER549698.

EX

Quantification of Radiating Species in the DIII-D Divertor in the Transition to Detachment Using Extreme Ultraviolet Spectroscopy

A. G. McLean¹, S. L. Allen¹, J. A. Boedo², A. R. Briesemeister³, M. E. Fenstermacher¹, M. Groth⁴, A. E. Järvinen¹, C. J. Lasnier¹, A. W. Leonard⁵, A. L. Moser⁵, G. D. Porter¹, T. D. Rognlien¹, C. M. Samuell¹, V. A. Soukhanovskii¹, D. M. Thomas⁵, H. Wang³, and J. G. Watkins⁶

The DIII-D Team

¹*Lawrence Livermore National Laboratory (LLNL), Livermore, CA 94550, USA*

²*University of California San Diego, CA 92093, USA*

³*Oak Ridge National Laboratory (ORNL), Oak Ridge, TN 37831, USA*

⁴*Aalto University, Espoo, Finland*

⁵*General Atomics, San Diego, CA 92186, USA*

⁶*Sandia National Laboratories (SNL), Albuquerque, NM 87185, USA*

Corresponding Author: A. G. McLean, mclean@fusion.gat.com

EX
Experimental observations of extreme ultraviolet resonance emissions in the divertor of DIII-D are used to quantitatively account for radiated power from molecular, atomic and ionized plasma constituents through the transition to detachment. Deuterium emission is found to be the primary emitter near the target scrape-off layer regions while the main impurity in DIII-D, carbon, is found to dominate the X-point region up the divertor legs. In an attached divertor, C emissions peak inboard of the strike point, while with a detached target, their emission region elongates radially. A relative lack of observed Lyman–Werner bands suggests that radiated power from molecules is minimal even with $T_{e,OSP} = 1\text{--}2\text{ eV}$. Species-resolved measurements are necessary to understand a shortfall in radiated power as modelled with 2D fluid codes on multiple tokamaks. The spectrometer fielded for this purpose is a SPRED (Survey, Poor Resolution, Extended Domain) observing the 10–170 nm region. A broad grating provides views of CII, III, and IV resonance emission lines as well as the D Lyman- α line, together accounting for $> 80\%$ of the power radiated in the divertor. The divertor SPRED (DivSPRED) is mounted with a vertical line of sight into the machine coincident with boundary diagnostics including divertor Thomson scattering.

Work supported by the U.S. Department of Energy under DE-AC52-07NA27344, DE-FG02-07ER54917, DE-FC02-04ER54698, DE-AC05-00OR22725, DE-AC02-09CH11466, and DE-AC04-94AL85000, and LLNL LDRD project 17-ERD-020.

Measurements of High-Z Divertor Impurity Sourcing and Divertor Leakage Using Isotopic Tungsten Tracer Sources in DIII-D

E. A. Unterberg¹, T. Abrams², J. L. Barton³, A. R. Briesemeister¹, D. C. Donovan⁴, J. D. Elder⁵, H. Y. Guo², D. L. Rudakov⁶, P. C. Stangeby⁵, D. M. Thomas², B. S. Victor⁷, and W. R. Wampler³

¹*Oak Ridge National Laboratory (ORNL), Oak Ridge, TN 37831, USA*

²*General Atomics, San Diego, CA 92186, USA*

³*Sandia National Laboratories (SNL), Albuquerque, NM 87185, USA*

⁴*University of Tennessee, Knoxville, TN 37996, USA*

⁵*University of Toronto, Toronto, ON M5S-1A1, Canada*

⁶*University of California San Diego, CA 92093, USA*

⁷*Lawrence Livermore National Laboratory (LLNL), Livermore, CA 94550, USA*

Corresponding Author: E. A. Unterberg, unterberge@fusion.gat.com

DIII-D carried out experiments using novel, isotopic tungsten (W) tracer sources in the outer divertor and has characterized how the W leakage from this region depends on both the exact source location and ELM behaviour. The W sources are toroidally-symmetric and poloidally-localized to two regions: 1) the outer strike point (OSP), a natural-W source, and 2) the far-target, i.e., 3–5 heat flux widths from the OSP, a ¹⁸²W source. With the use of a dual-faced collector probe (CP) in the main SOL near the outside midplane (OMP), it is found that the far-target W source has the smallest upstream deposition efficiency on the CP, i.e., divertor leakage, with high input power and small ELMs; conversely the far-target divertor leakage is highest with large ELMs. Additionally, without ELMs, it is also found that large deposition asymmetries on the opposite CP faces are consistent with model predictions of W accumulation in the near-SOL at the tokamak crown region. This unique experimental setup, together with source (W-I) and core spectroscopic measurements, provide information on the transport link between different W source locations within the divertor and the W content of the plasma outside the divertor, i.e., divertor leakage. These studies are elucidating the physics driving high-Z divertor impurity sourcing and leakage, both with and without ELMs, and are shedding light on this the weakest link, to date, in the chain connecting wall impurity sources to core impurity levels in MFE devices, like ITER.

Work supported by the U.S. Department of Energy under DE-FC02-04ER54698.

Favourable Impact of RMP ELM Suppression on Divertor Heat Fluxes at ITER-like Conditions

D. M. Orlov¹, R. A. Moyer¹, I. O. Bykov¹, T. E. Evans², A. M. Teklu³, J. Lee⁴, A. Loarte⁵, M. E. Fenstermacher⁶, C. J. Lasnier⁶, J. G. Watkins⁷, H. Wang⁸, and A. W. Leonard²

¹University of California San Diego, CA 92093, USA

²General Atomics, San Diego, CA 92186, USA

³Oregon State University, Corvallis, OR 97331, USA

⁴University of California Los Angeles, CA 90095, USA

⁵International Thermonuclear Experimental Reactor (ITER),
Cadarache Centre, 13108 St. Paul lez Durance, France

⁶Lawrence Livermore National Laboratory (LLNL), Livermore, CA 94550, USA

⁷Sandia National Laboratories (SNL), Albuquerque, NM 87185, USA

⁸Oak Ridge Associated Universities (ORAU), Oak Ridge, TN 37831, USA

Corresponding Author: D. M. Orlov, orlov@fusion.gat.com

RMP ELM suppression experiments at ITER-like conditions (shape, collisionality, RMP spectrum) in DIII-D show little splitting of the heat flux to the divertor targets, despite robust splitting in the particle flux. This lack of divertor heat flux splitting is a potentially important result for ITER because splitting of the divertor heat flux into multiple lobes displaced from the primary strike point could complicate heat flux handling during RMP ELM suppression in ITER and other tokamaks with tight divertor baffling. In DIII-D, strike point splitting is routinely observed in the divertor particle flux during RMP operation. The observed splitting is consistent with the toroidal mode number n of the perturbation, but the measured separation of the divertor particle flux lobes exceeds predictions of a vacuum model by factors of 3–5. Similar splitting in the heat flux profile would have serious consequences for heat flux handling during RMP ELM suppression in ITER. However, there is little impact of these particle flux lobes on the measured divertor heat flux. The large particle flux lobe separations present a challenge for plasma response modelling, because the predicted response using linear, resistive MHD simulations is dominantly a screening response, which should reduce the divertor lobe splitting below the vacuum model predictions.

Current ramps, which were limited in amplitude for a subset of RMP coils to be consistent with force limits on the RMP coils in ITER, were used to modify the divertor lobes from an $n = 3$ to an $n = 2$ pattern. The particle flux lobes changed during the RMP current ramps, but the heat flux profile was not affected, consistent with the lack of heat flux lobe structure. Possible synergistic effects of impurity gas injection and RMP current ramps were also examined using neon and argon gas injection into the RMP suppressed phase. Both gases produced stable radiating mantles between $0.95 \leq \Psi_N \leq 1$, a 60% radiated power fraction, and significantly reduced heat flux to both strike points while ELM suppression was maintained. These results show that RMP ELM suppression in ITER-like conditions is compatible with an impurity radiation-enhanced boundary.

Work supported by the U.S. Department of Energy under DE-FG02-07ER54917, DE-FG02-05ER54809, DE-FC02-04ER54698, DE-SC0012706, DE-AC52-07NA27344, DE-NA0003525, and DE-AC04-94AL85000.

Enhancement of Helium Exhaust During Suppression of Edge Localized Modes by Resonant Magnetic Perturbation Fields at DIII-D

E. T. Hinson¹, A. R. Briesemeister², B. A. Grierson³, C. S. Collins⁴, C. Paz-Soldan⁴, D. M. Thomas⁴, E. A. Unterberg², H. Frerichs¹, I. O. Bykov⁵, M. Wade⁴, O. Schmitz¹, R. A. Moyer⁵, T. E. Evans⁴, and T. Abrams⁴

¹University of Wisconsin-Madison, Madison, WI 53706, USA

²Oak Ridge National Laboratory (ORNL), Oak Ridge, TN 37831, USA

³Princeton Plasma Physics Laboratory (PPPL), Princeton, NJ 08540, USA

⁴General Atomics, San Diego, CA 92186, USA

⁵University of California San Diego, CA 92093, USA

Corresponding Author: E. T. Hinson, hinsone@fusion.gat.com

It is shown for the first time that global exhaust of helium, measured by effective helium particle confinement time ($\tau_{p^*,He}$), is improved during edge localized mode (ELM) suppression by resonant magnetic field perturbations (RMP) in high confinement (H-mode) ITER-shaped tokamak plasmas at DIII-D. An up to 40% reduction of $\tau_{p^*,He}$ during RMP-ELM suppression compared to ELMing H-mode discharges without RMP fields was measured using He test pulses in the upper outboard midplane. The ratio $\tau_{p^*,He}/\tau_E$ is reduced from 13 to 11 during RMP ELM suppression, showing that the improvement in He removal from the system exceeds the impact of RMP fields on energy confinement, bringing this ratio closer to the canonical threshold for a fusion reactor of $\tau_{p^*,He}/\tau_E < 10$. To understand the cause of this important observation, we assess the changes to He confinement and exhaust in a three-reservoir model consisting of the core, plasma edge/SOL, and neutral reservoirs. Global He exhaust from the system depends on the exhaust from the confined plasma domain into the SOL and the neutral reservoir, where neutralized He is eventually removed by the pump. However, pumping efficiency (removal rate) for He is low, and it recycles many times before being pumped. Therefore, retaining He in the plasma peripheral regions (SOL and neutral domain) without plasma back-fuelling is vital for the He exhaust cycle.

Penning gauge measurements of He and D₂ neutral pressures in the pump plenum show the He partial pressure increases substantially more than that of D₂ during RMP-ELM suppression, compared with the ELMing H-mode. This selective increase in He concentration suggests a preferential enhancement of He exhaust into the neutral domain, rather than a simple link to main species “pumpout”, and provides substantial evidence of strong He retention in the plasma periphery during RMP ELM suppression, which is a necessary condition to improve removal of He from the system. The He density in the edge confined region measured by charge exchange recombination spectroscopy shows an enhanced decay rate during RMP ELM suppression. These first-time findings are important for ITER, where application of RMP fields is planned for ELM control, as they suggest application of RMP ELM suppression could replace the impurity exhaust produced by the ELM events.

EX

Access Requirements for Stationary ELM-Suppressed Pedestals in DIII-D and C-Mod Plasmas

T. M. Wilks¹, J. W. Hughes¹, A. M. Garofalo², P. H. Diamond³, Z. B. Guo³,
A. E. Hubbard¹, K. H. Burrell², and X. Chen²

The DIII-D and C-Mod Teams

¹*Plasma Science & Fusion Center, MIT, Cambridge, MA 02139, USA*

²*General Atomics, San Diego, CA 92186, USA*

³*University of California San Diego, CA 92093, USA*

Corresponding Author: T. M. Wilks, twilks@psfc.mit.edu

Analysis of pedestal characteristics for quiescent H-mode (QH) and I-mode plasmas from recent experiments on DIII-D and C-Mod exhibit a growing understanding of the access requirements necessary to obtain edge fluctuations or MHD that drive edge particle transport needed to remain ELM-free. In DIII-D QH-mode plasmas, critical values of $E \times B$ shear are required in experiment in order to suppress the transition from QH-mode to ELMy H-mode. The experimental shear values for QH-modes ranging between $q_{95} \sim 3\text{--}5$ and $\delta \sim 0.36\text{--}0.68$ are compared with theory to show good agreement with the predicted scaling parameters of $c_s/\sqrt{L_p \Delta x}$, where c_s is the ion acoustic velocity, L_p the pressure gradient scale length, and Δx is the radial width of the mode. The scaling of the critical shearing rate agrees with experiment, but the absolute magnitude of the limit is overpredicted by theory by two orders of magnitude. Through a normalized predictive scaling, the model demonstrates dynamic transitions into and out of QH-mode qualitatively within a single plasma discharge.

C-Mod I-mode plasmas, which lack an edge particle barrier and exhibit characteristic edge fluctuations over a broad range of B_ϕ , meet upper limits in performance determined by H-mode access. The maximum radial electric field well in I-mode increases with magnetic field strength, suggesting the expanded window for I-mode at high field is linked to a critical value of E_r/B required to induce an H-mode transition. C-Mod I-mode pedestals are analyzed over varied magnetic fields (2.8–5.8 T) and auxiliary power (1.5–4.6 MW) to show consistent edge fluctuation behaviour. Density fluctuations associated with the weakly coherent mode are observed to span the pedestal region, extending out to the separatrix, while the fluctuation associated with the geodesic acoustic mode is observed on the profile reflectometer near the foot of the T_e pedestal. Trends in the edge E_r , $E \times B$ shear, and rotation in I-mode show little correlation with the behaviour of the edge fluctuations, suggesting an alternate driver for destabilization of the WCM and GAM, as compared to the QH-modes analyzed for DIII-D with an EHO.

Machine Learning for Disruption Warning on Alcator C-Mod, DIII-D, and EAST Tokamaks

R. S. Granetz¹, C. Rea¹, K. Montes¹, N. W. Eidietis², O. Meneghini², D. L. Chen³, B. Shen³, and B. J. Xiao³

¹Plasma Science & Fusion Center, MIT, Cambridge, MA 02139, USA

²General Atomics, San Diego, CA 92186, USA

³Institute of Plasma Physics, Chinese Academy of Sciences, Hefei, Anhui, People's Republic of China

Corresponding Author: R. S. Granetz, granetz@mit.edu

We find that disruption prediction using machine learning (ML), trained on large databases containing only plasma parameters that are available in real-time on C-Mod, DIII-D, and EAST, differ substantially in performance among the three machines, implying that a universal real-time disruption warning algorithm may be problematic. This could have important implications for disruption prediction and avoidance on ITER, for which development of a training database of disruptions may be infeasible. Whether or not disruption prediction can be improved by incorporating additional real-time measurements, or with more sophisticated AI methods, is unclear.

The database for each tokamak contains parameters sampled at $\sim 10^6$ times throughout $\sim 10^4$ discharges, disruptive and nondisruptive, over the last 3–4 years of operation. We find that a number of parameters (e.g., $P_{\text{rad}}/P_{\text{input}}$, ℓ_i , n/n_G , $B_{n=1}/B_t$) exhibit changes as a disruption is approached on one or more of these tokamaks. However, the details of these precursor behaviours are markedly different on each machine.

We use a shallow ML method known as “random forests”, applied to a binary classification scheme. We define the two classes as “close to a disruption” and “far from a disruption or from a nondisruptive shot”. The threshold time that divides “close” from “far” is determined by optimizing the classification prediction accuracy for each machine. We find that the timescales of disruption warning behaviour are very different for the different machines, and that the fraction of correctly predicted disruption samples varies considerably, ranging from 74% for DIII-D, to just 35% for C-Mod. For C-Mod in particular, it is difficult to predict upcoming disruptions more than just a few milliseconds in advance.

This work supported in part by: U.S. Department of Energy Grants DE-FC02-99ER54512, DE-SC0010720, DE-SC0010492, DE-FC02-04ER54698, DE-SC0014264; National Natural Science Foundation of China Grants 11475002, 11775262, 11475224, 11575247, 11475225, 11775266 and 11505235; and National Magnetic Confinement Fusion Science Program of China Grants 2014GB103000 and 2015GB102004.

Fast ITER-Relevant Low-Disruptivity Ramp-Downs in DIII-D and EAST

J. L. Barr¹, N. W. Eidietis¹, D. A. Humphreys¹, T. C. Luce², J. P. Qian³, B. S. Sammuli¹, and B. J. Xiao³

¹General Atomics, San Diego, CA 92186, USA

²International Thermonuclear Experimental Reactor (ITER),
Cadarache Centre, 13108 St. Paul lez Durance, France

³Institute of Plasma Physics, Chinese Academy of Sciences, Hefei, Anhui, People's Republic of China

Corresponding Author: J. L. Barr, barrj@fusion.gat.com

Recent experiments on DIII-D and EAST are developing the techniques and scientific understanding that ITER and future devices will need for safe, low-disruptivity shutdown. ITER needs options for reliable termination both in normal operation as well as in response to an off-normal event, where speed to soft landing is paramount. A large survey of ramp-down techniques in a variety of DIII-D plasma conditions shows disruptivity in fast (I_p ramp-rates of 2-3 MA/s), diverted ramp-downs is similar or improved compared to historical, limited ramp-downs with I_p ramp-rates typically ≤ 1 MA/s. The survey used the ramp-down phase of over 370 DIII-D discharges to develop improved soft-landing techniques scalable to ITER. The disruptivity is shown to be minimized by keeping neutral beam injection (NBI) power on for the duration of ramp-down, and at modest power levels roughly comparable to the average radiated power during shutdown. Experiments on ITER Baseline Scenario (IBS) plasmas have tested the limits of the planned ITER ramp-down as well as faster yet "full-bore" ramp-downs, in which the flat-top ITER shape is maintained through ramp-down. Disruptivity statistics for this scenario have been measured to inform ITER operation, and fast (2 MA/s), full-bore ramp-downs reduced the disruptivity to 25% from the historical rate of 58% using DIII-D's standard 1 MA/s, limited ramp-down method. The planned, shape-evolving (dropping elongation) ramp-down of the 15 MA ITER $Q = 10$ scenario has been experimentally simulated at speeds scaling to the fastest ramp-down time of which ITER is expected to be capable (~ 60 s [1]), and the scenario is found to be capable of maintaining the required $l_i < 1$ during the H-mode phase of ramp-down while the elongation is reduced. Experiments on the EAST tokamak have likewise identified robust, fast, diverted ramp-down techniques using sustained lower hybrid (LH) power for the duration of ramp-down. Surveys of plasma current ramp-rate and L-H power were conducted in the ramp-down phase of EAST discharges to complement the ramp-down survey performed on DIII-D. By continuing application of 2 MW of L-H heating power, the fastest ramp-down yet on EAST of 0.5 MA/s has been demonstrated.

Work supported in part by the U.S. Department of Energy under DE-FC02-04ER54698 and DE-SC0010685.

References

[1] A. C. C Sips *et al.*, Phys. Plasmas, **22**, 021804 (2015).

Implementing a Finite-State Off-Normal and Fault Response System for Robust Disruption Avoidance in Tokamaks

N. W. Eidietis¹, W. Choi², S. H. Hahn³, D. A. Humphreys¹, B. S. Sammul¹, and M. L. Walker¹

¹General Atomics, San Diego, CA 92186, USA

²Columbia University, New York, NY 10027, USA

³National Fusion Research Institute (NFRI), Daejeon, Republic of Korea

Corresponding Author: N. W. Eidietis, eidietis@fusion.gat.com

A finite-state off-normal and fault response (ONFR) system is presented that provides the required supervisory logic for robust disruption avoidance and machine protection in tokamaks. Robust event handling is critical for ITER and future large tokamaks, where plasma parameters will necessarily approach stability limits and many systems will operate near their engineering limits. The ONFR system presented provides four critical features of a robust event handling system: sequential responses to cascading events, event recovery, simultaneous handling of multiple events and actuator prioritization. This system has been deployed during live experiments on DIII-D and KSTAR. In the most complex demonstration on DIII-D, the ONFR algorithm asynchronously applies “catch and subdue” electron cyclotron current drive (ECCD) injection scheme to suppress a virulent 2/1 neoclassical tearing mode, subsequently shuts down ECCD for machine protection when the plasma becomes overdense, and enables rotating 3D field entrainment of the ensuing locked mode with synchronized ECCD deposition on the locked mode O-point to allow a safe ramp-down, all in the same discharge without user intervention.

Work supported in part by the U.S. Department of Energy, Office of Science, Office of Fusion Energy Sciences, using the DIII-D National Fusion Facility, under Award DE-FC02-04ER54698. Work on KSTAR was supported by the Korean Ministry of Science and ICT under the KSTAR project and DOE Award DE-SC0010685.

Injection of Multiple Shattered Pellets for Disruption Mitigation in DIII-D

J. Herfindal¹, D. Shiraki¹, L. R. Baylor¹, N. W. Eidietis², E. M. Hollmann³, C. J. Lasnier⁴, and R. A. Moyer³

¹*Oak Ridge National Laboratory (ORNL), Oak Ridge, TN 37831, USA*

²*General Atomics, San Diego, CA 92186, USA*

³*University of California San Diego, CA 92093, USA*

⁴*Lawrence Livermore National Laboratory (LLNL), Livermore, CA 94550, USA*

Corresponding Author: J. Herfindal, herfindaljl@ornl.gov

EX Experiments on DIII-D have injected multiple shattered pellets at different toroidal locations for the first time, as is planned for the ITER disruption mitigation system. Systematically varying the relative timing of the two pellets suggests that simultaneously injected pellets may impact the assimilation of each other, altering the resulting disruption characteristics compared to that due to a single pellet injecting similar neon quantities. Thermal quench (TQ) radiation fractions measured near the injection are reduced with the dual pellets contrary to TQ radiation fractions measured away from the injection ports which do not have a clear difference between single or dual pellet injections. This asymmetric reduction in radiation fraction indicates an overall reduction in the global radiation fraction and that possible radiation asymmetries may be reduced with dual pellet injection. Global disruption mitigation properties, such as the current quench duration, is found to increase when the pellets enter the plasma simultaneously compared to single shattered pellet injections with similar neon quantities. The similar reduction in mitigation of current quench loads is consistent with the observed reduction in TQ mitigation. The time between initial pellet injection and thermal quench onset (plasma cooling duration) is shorter when both pellets are injected simultaneously compared to a single pellet. The faster shutdown with two pellets could be due to the “head start” in the toroidal and poloidal spreading of impurities due to injecting the pellets at different toroidal locations — effectively cooling multiple flux tubes simultaneously. The lower cooling duration may also limit the amount of the neon delivered by the shattered pellet into the plasma prior to the end of the TQ since the shattered pellet plume takes on the order of a few milliseconds to be completely in the plasma. These results suggest that changes in the spatial distribution of the initial impurity injection can impact the evolution of the fast shutdown, indicating that 0D treatments of disruption mitigation metrics are not fully sufficient. This asymmetric reduction in radiation fraction indicates an overall reduction in the global radiation fraction and that possible radiation asymmetries may be reduced with dual pellet injection.

Observation of Multiple Helicity Mode-Resonant Locking Leading to a Disruption on DIII-D

M. W. Shafer¹, X. D. Du², T. E. Evans³, S. Ohdachi⁴, Y. Suzuki⁴, Q. Hu⁵, and J. H. Harris¹

¹*Oak Ridge National Laboratory (ORNL), Oak Ridge, TN 37831, USA*

²*University of California Irvine, CA 92697, USA*

³*General Atomics, San Diego, CA 92186, USA*

⁴*National Institute for Fusion Science (NIFS), Toki, Gifu, Japan*

⁵*Princeton Plasma Physics Laboratory (PPPL), Princeton, NJ 08540, USA*

Corresponding Author: M. W. Shafer, shafermw@ornl.gov

Experimental evidence of the formation of multiple helicity island chains during the mode locking phase preceding plasma disruption is providing a clear picture for the understanding of locked-mode triggered disruptions. This emerging picture uses measurements from a new dual soft X-ray (SXR) tangential imaging system that measures localized internal perturbations in combination with local temperature profile flattening. In mode locking experiments with low- β ($\beta_N \sim 0.5$), inner-wall limited L-mode discharges, a low-order rational surface (2/1) locks and reduces the plasma rotation across the edge region allowing higher order island chains (3/1, 4/1) to form. These signatures are measured by SXR imaging that show the presence of resonant perturbations that have been reproduced consistently with synthetic modelling and local temperature flattening measured by Thomson scattering. The edge 4/1 island cools rapidly by extending into the boundary region. On a slower time scale over 300 ms, both the 2/1 and 3/1 islands widen. This growth leads to eventual island overlap and enhanced stochastic transport that allows a cold boundary region or cold pulse to penetrate into the core resulting in a rapid loss in thermal energy and plasma collapse. The observed growth of multiple island chains and evolution of edge cooling are successfully reproduced by a nonlinear simulation (TM1 code) using a single fluid model without radiation effects. In this picture, the formation and slow widening of multiple helicity island chains leads to a locked mode disruption.

Work supported by the U.S. Department of Energy under DE-AC05-00OR22725, DE-FC02-04ER54698, DE-AC02-09CH11466, and JSPS KAKENHI Grant Number JP26249144.

EX

Critical Processes of Tearing Mode Entrainment in the Presence of a Static Error Field

M. Okabayashi¹, S. Inoue², T. Strait³, Z. Taylor³, J. S. deGrassie³, J. M. Hanson⁴,
R. J. La Haye³, N. Logan¹, and A. Wingen⁵

¹Princeton Plasma Physics Laboratory (PPPL), Princeton, NJ 08540, USA

²National Institutes for Quantum and Radiological Science and Technology (QST),

Naka Fusion Institute, Naka-shi, Ibaraki-ken, Japan

³General Atomics, San Diego, CA 92186, USA

⁴Columbia University, New York, NY 10027, USA

⁵Oak Ridge National Laboratory (ORNL), Oak Ridge, TN 37831, USA

Corresponding Author: M. Okabayashi, mokabaya@pppl.gov

EX DIII-D experiments on control of locked tearing modes are in good qualitative agreement with predictions of a nonlinear reduced MHD code (AEOLUS-IT) [1, 2]. Robust avoidance of locked tearing modes that may cause disruptions is a prerequisite for successful ITER operation. We have tested model predictions that entrainment of a locked mode by a rotating 3D field screens out the error field that caused the initial locking. The plasma condition was the ITER base line scenario target with low safety factor discharges. The simulation is nonlinear, but highlights the fundamental process by simplifying the physics to a zero β , single helicity case with $m/n = 2/1$, using only the vorticity equation and Ohm's law without any additional transport properties. Experiment and simulation both show coupling between the locked mode and a stable kink around the rational surface, and the screening that follows a bifurcation event in which the mode becomes locked to the rotating applied field. Experiments in DIII-D have illuminated some of the critical physical processes in the interaction of a locked tearing mode with a rotating 3D field, including torque balance bifurcation and entrainment in the presence of a static error field. Time evolution of local mode structure near $q = 2$ rational surface including the perturbed rotation profile using charge exchange recombination (CER) has been very useful for the comparisons. Predictive understanding of mode evolution is crucial to the design of locked mode control schemes that will help to avoid disruptions in present and future devices, and the nonlinear reduced MHD model AEOLUS-IT is in good qualitative agreement with experimental observations. Such models will enable design of experiments on locked mode control and other nonlinear MHD processes in present devices, and extrapolation of these studies to large-scale experiments such as in ITER.

Work supported in part by the U.S. Department of Energy under DE-AC02-09CH11466, DE-FC02-04ER54698, DE-FG02-04ER54761.

References

- [1] S. Inoue *et al.*, Nucl. Fus., **57**, 116020-10 (2017).
- [2] S. Inoue *et al.*, Plasma Phys. Contr. F., **60**, 025003 (2018).

Disruption Event Characterization and Forecasting in Tokamaks

S. A. Sabbagh¹, J. W. Berkery¹, Y. S. Park¹, J. H. Ahn¹, Y. Jiang¹, J. D. Riquezes¹, J. M. Bialek¹, R. E. Bell², M. D. Boyer², S. P. Gerhardt², B. P. LeBlanc², C. E. Myers², S. H. Hahn³, Y. M. Jeon³, J. Kim³, J. Ko³, W. H. Ko³, J. Lee³, Y.-K. Oh³, and S. W. Yoon³

¹Columbia University, New York, NY 10027, USA

²Princeton Plasma Physics Laboratory (PPPL), Princeton, NJ 08540, USA

³National Fusion Research Institute (NFRI), Daejeon, Republic of Korea

Corresponding Author: S. A. Sabbagh, sabbagh@pppl.gov

Disruption prediction and avoidance is a critical need for next-step tokamaks such as ITER, as disruptions can place significant thermal heat loads and electromagnetic forces on the device and can potentially lead to damage from runaway electrons. Meeting these challenging goals with the high reliability required for ITER and future tokamaks requires multiple approaches, including an understanding of the connection between events leading to disruptions, and the ability to forecast such events. The Disruption Event Characterization and Forecasting Code (DECAF) is used to fully automate analysis of tokamak data to determine chains of events that lead to disruptions and to forecast their evolution. Disruption event chains related to global MHD instabilities, tearing modes, and many other off-normal events are identified. In an NSTX database exhibiting global MHD modes, resistive wall mode (RWM) and loss of boundary control events are found in all cases and vertical displacement events are found in over 90% of cases. Analysis shows 61% of RWM events occur within 20 conducting wall current diffusion times of the disruption. The remainders occurring earlier in time indicate minor disruptions. Insights are gained on the connection of mode activity to other events, including high Greenwald density fraction. Maximum amplitude of toroidal mode number $n = 1$ magnetic perturbations reached during disruptions and scaling with key parameters, important for ITER, are evaluated. Automated analysis of rotating tearing modes produce physical event chains leading to disruptions through mode slowing and subsequent locking. Analysis of NSTX and NSTX-U plasmas shows that the duration between mode bifurcation and locking varies with plasma conditions and can be shorter than the duration between mode locking and disruption onset. Global MHD instabilities such as external kink/ballooning modes or RWMs give the least amount of warning time before disruption. Kinetic RWM theory has shown high success in determining experimental mode marginal stability. A time-dependent reduced physics model of kinetic stabilization was created to forecast instability-induced disruptions. The initial model predicts instability 84% of the time for experimentally unstable cases with a relatively low false positive rate.

Work supported by U.S. Department of Energy grants DE-FG02-99ER54524, DE-SC0016614, and DE-AC02-09CH11466.

EX

Observation of Efficient Lower Hybrid Current Drive at High Density on Alcator C-Mod

S. G. Baek¹, G. M. Wallace¹, P. T. Bonoli¹, D. Brunner¹, I. C. Faust¹, A. E. Hubbard¹, J. W. Hughes¹, B. LaBombard¹, R. T. Mumgaard¹, R. R. Parker¹, M. Porkolab¹, S. Scott¹, S. Shiraiwa¹, J. L. Terry¹, and S. J. Wukitch¹

¹Plasma Science & Fusion Center, MIT, Cambridge, MA 02139, USA

Corresponding Author: S. G. Baek, sgbaek@psfc.mit.edu

Efficient lower hybrid current drive (LHCD) at high plasma density has been demonstrated on Alcator C-Mod for the first time with the reduction in the Greenwald fraction by raising the plasma current. In order to attain steady-state advanced tokamak operation, efficient off-axis current drive is required. LHCD is highly desirable because it has the highest efficiency of all technologies presently available. However, the LHCD experiment on C-Mod has shown a loss of anomalous current drive efficiency above $\bar{n}_{crit} \approx 1 \times 10^{20} / \text{m}^3$, which prohibited an access to advanced tokamak operation [1]. Parasitic wave interactions in the edge/SOL region may account for the density limit behaviour [2–4] because the scrape-off-layer density profile becomes broadened with an increased level of blobby transport with the increase in the Greenwald fraction [5].

EX

In the most recent C-Mod experiments, the operating plasma current was raised to 1.4 MA in order to minimize the SOL width at $\bar{n}_{crit} \approx 1.4 \times 10^{20} / \text{m}^3$. The injected L-H power (600 kW) produced a loop voltage drop of 0.2 V, consistent with engineering efficiency found at low densities. The nonthermal Bremsstrahlung emission rate was increased by more than two orders of magnitude compared to the lower current case. Parasitic interactions of wave with the SOL plasma are largely suppressed, indicated by the spectrum measurement.

The new experimental results indicate that efficient current drive at a reactor density can be attained with proper management of the edge/SOL plasma. They support a proposal to place L-H launchers at the high-field-side (HFS) of the tokamak in a double null configuration [6]. In this case, the density shoulders and blobby transport phenomena are absent in the HFS SOL. Efficient current drive may be attained even at high Greenwald fraction by avoiding parasitic edge/SOL wave interactions.

Work supported by the U.S. Department of Energy, Contract No. DE-FC02-99ER54512 on Alcator C-Mod, a Department of Energy Office of Science user facility.

References

- [1] G. M. Wallace *et al.*, Phys. Plasmas, **17**, 082508 (2010).
- [2] S. G. Baek *et al.*, Nucl. Fus., **55**, 043009 (2015).
- [3] I. C. Faust *et al.*, Phys. Plasmas, **23**, 056115 (2016).
- [4] S. Shiraiwa *et al.*, AIP **1689**, 030016 (2015).
- [5] B. LaBombard *et al.*, Phys. Plasmas, **15**, 056106 (2008).
- [6] B. LaBombard *et al.*, Nucl. Fus., **55**, 053020 (2015).

High-Frequency Energetic Particle Driven Instabilities and their Implications for Burning Plasmas

K. E. Thome¹, S. Tang², N. A. Crocker², X. D. Du³, W. W. Heidbrink³, D. C. Pace⁴,
C. Paz-Soldan⁴, R. I. Pinsker⁴, D. A. Spong⁵, M. E. Austin⁶, C. S. Collins⁴,
C. A. del Castillo⁷, A. Lvovskiy¹, M. A. Van Zeeland⁴, and Y. B. Zhu³

¹Oak Ridge Associated Universities (ORAU), Oak Ridge, TN 37831, USA

²University of California Los Angeles, CA 90095, USA

³University of California Irvine, CA 92697, USA

⁴General Atomics, San Diego, CA 92186, USA

⁵Oak Ridge National Laboratory (ORNL), Oak Ridge, TN 37831, USA

⁶Institute for Fusion Studies (IFS), University of Texas at Austin, Austin, TX 78712, USA

⁷Stony Brook University, Stony Brook, NY 11794, USA

Corresponding Author: K. E. Thome, thomek@fusion.gat.com

Three high-frequency modes observed in the DIII-D tokamak have been identified as energetic particle instabilities driven unstable by anisotropic fast ions and runaway electrons. These modes could serve as control tools of the energetic particle distribution in fusion-relevant plasmas: 1) Whistler waves with $\omega \gg \omega_{ci}$, excited by multi-MeV runaway electrons in a low-density ($n_e \sim 10^{19}/\text{m}^3$) plasma, have been observed for the first time in a tokamak [1]. The waves occur in multiple discrete frequency bands in the 100–200 MHz range, with the measured whistler frequencies scaling with magnetic field strength and electron density, as expected from the whistler dispersion relation. Whistler activity correlates with runaway intensity (hard X-ray emission level), and a nonlinear interaction between the whistler instability and the runaway electron distribution function is observed. 2) Ion cyclotron emission (ICE) is readily excited across a wide region of operational space by kinetic instabilities at harmonics of the main ion ω_{ci} . ICE is strongest in neutral-beam-heated plasmas with a clear dependence on beam geometry, with the highest emission levels with countercurrent beams. This instability responds promptly to transient MHD events, including ELMs, fishbones and sawteeth. 3) Measurements of Doppler-shifted cyclotron resonant compressional Alfvén eigenmodes (CAEs) below ω_{ci} are consistent with many aspects of CAE theory, including an onset frequency strongly correlated with magnetic field and the observation of frequency splitting. CAEs are excited on DIII-D when the beam ions are near-Alfvénic, with onset frequencies of $\sim 0.6f_{ci}$. Consistent with recent hybrid MHD (HYM) simulations [2], a clear threshold behaviour of the CAE instability is observed as the neutral beam density is varied at fixed energy. These high-frequency modes can potentially serve as much-needed control tools of the energetic particle distribution in fusion-relevant plasmas: Whistlers as a runaway relativistic electron control during a plasma disruption, and ICE and CAEs as passive, noninvasive measurement of the fast-ion activity that could be used to optimize performance.

Work supported in part by the U.S. Department of Energy under DE-FC02-04ER54698.

References

- [1] D. A. Spong *et al.*, submitted to Phys. Rev. Lett., (2017).
- [2] E. Belova *et al.*, Phys. Plasmas, **24**, 042505 (2017).

Fast Wave Experiments in LAPD in Support of Fusion

B. Van Compernelle¹, M. Martin¹, T. A. Carter¹, W. Gekelman¹, P. Pribyl¹, D. Van Eester², K. Crombé², R. J. Perkins³, C. Lau⁴, E. H. Martin⁴, J. B. O. Caughman⁴, S. K. P. Tripathi¹, and S. Vincena¹

¹University of California Los Angeles, CA 90095, USA

²Laboratory for Plasma Physics, ERM/KMS, Brussels, Belgium

³Princeton Plasma Physics Laboratory (PPPL), Princeton, NJ 08540, USA

⁴Oak Ridge National Laboratory (ORNL), Oak Ridge, TN 37831, USA

Corresponding Author: B. Van Compernelle, bvcomper@physics.ucla.edu

Recent work on ICRF physics at the Large Plasma Device (LAPD) at UCLA has focussed on deleterious near-field antenna effects, such as RF rectification, sputtering, convective cells and power lost to the plasma edge. Plasma parameters in LAPD are similar to the scrape-off layer of current fusion devices. The machine has a 17 m long, 60 cm diameter magnetized plasma column with typical plasma parameters $n_e \sim 10^{12}$ – 10^{13} /cm³, $T_e \sim 1$ – 10 eV and $B_0 \sim 1000$ G. A new high-power (~ 150 kW) RF system and fast wave antenna have been developed for LAPD, enabling the generation of large amplitude fast waves.

Evidence of rectified RF sheaths is seen in large increases ($\sim 10T_e$) in the plasma potential on field lines connected to the antenna, and in copper deposition on plasma facing components due to sputtering at the antenna. The rectified potential scales linearly with antenna current. The rectified RF sheaths set up convective cells of local $E \times B$ flows, measured indirectly by potential measurements, and measured directly with Mach probes. At high antenna powers, substantial modifications of the density profile were observed after the RF antenna is powered up. The density rearrangement is asymmetric with a decrease in plasma density near the top of the antenna and an increase near the bottom. The plasma density profile initially exhibits transient low frequency oscillations (~ 10 kHz) and settles into a quasi-steady state profile for the remainder of the RF pulse. RF antenna current is constant during the pulse. The amplitude of the fast wave fields in the core plasma is modulated at the same low frequency, suggesting fast wave coupling is affected by the density rearrangement.

At low antenna powers, the parasitic coupling to slow waves in the low density region in front of the antenna is being studied. Detailed wave field measurements show coupling to both the short wavelength slow wave and the long wavelength fast wave if the density at the antenna is low enough. Coupling to lower hybrid waves was demonstrated for a range of normalized frequencies, from $1 < f/f_{ci} < 30$.

Performed at the Basic Plasma Science Facility, supported by the National Science Foundation and the U.S. Department of Energy.

Global Alfvén Eigenmode Stability Dependence on Fast-Ion Distribution Function

E. D. Fredrickson¹, M. Podestà¹

The NSTX Group

¹*Princeton Plasma Physics Laboratory (PPPL), Princeton, NJ 08540, USA*

Corresponding Author: E. D. Fredrickson, efredrickson@pppl.gov

Global Alfvén eigenmodes (GAE) have been extensively studied on NSTX and with analytic and numerical modelling. Multiple GAE with a range of toroidal mode numbers are commonly observed in NSTX plasmas heated with neutral beams. Recently, analytic and numerical modelling has been used to very successfully model the suppression of GAE experimentally observed with the injection of high pitch ($V_{\parallel}/V \approx 1$) resonant fast ions. In this paper we show that the scaling of the GAE frequency and toroidal mode numbers with toroidal field is qualitatively consistent with the analytic theory describing the Doppler-shifted ion cyclotron resonance (DCR) drive for the GAE. The GAE in NSTX and NSTX-U are excited through an ion cyclotron resonance with comoving beam ions. The GAE propagate in the opposite, or counter, direction at frequencies down-shifted from the ion cyclotron frequency by the motion of the beam ions, that is, in the moving frame of the beam ions, the GAE frequency is up-shifted to the ion-cyclotron frequency. An analytic model of this resonant drive is presented in [1]. An important result from this work is the prediction that resonant fast ions with $k_{\perp}\rho < 1.9$ would be stabilizing ($1.9 < k_{\perp}\rho < 3.9$ would provide drive). In this paper we use a simple dispersion relation for GAE combined with the DCR analytic theory to predict both the range of toroidal mode numbers and frequencies of unstable GAE. We find that this prediction is reasonably consistent with the observed experimental scaling.

References

[1] N. N. Gorelenkov *et al.*, Nucl. Fus., **43**, 228 (2003).

Investigation of Fast Particle Redistribution Induced by Sawtooth Instability in NSTX-U

D. Kim¹, D. Liu², M. Podestà¹, G. Hao², and F. M. Poli¹

¹*Princeton Plasma Physics Laboratory (PPPL), Princeton, NJ 08540, USA*

²*University of California Irvine, CA 92697, USA*

Corresponding Author: D. Kim, dkim@pppl.gov

The effects of sawtooth on fast ion transport have been studied in reproducible, 2 s long sawtooth L-mode discharges during the 2016 experimental campaign on National Spherical Torus Experiment Upgrade (NSTX-U). Experimental observations through solid state neutral particle analyser (SSNPA) and fast-ion D $_{\alpha}$ (FIDA) diagnostics show that passing particles within the measured energy range are strongly redistributed from the plasma core to the edge, whereas trapped particles are weakly affected. The effect of sawteeth is clearly seen as a significant reduction of the signal from passing particles inside the sawtooth inversion radius and a corresponding increase at outer radii. Modelling with the standard sawtooth models available in the TRANSP code reproduces the experimental neutron rate drops with the properly chosen model's parameters. However, the FIDA simulation using the plasma profiles and fast ion distribution from the TRANSP simulation does not agree with the experimental measurement. A likely cause of the disagreement between experiments and simulations is that the sawtooth model in TRANSP does not take into account the different effect of sawtooth crash on fast ions with different orbit type and energy. Therefore a more comprehensive and improved model for quantitative simulations needs to be developed to interpret sawtooth discharges more reliably including the characteristics of fast ion such as energy, toroidal angular momentum and pitch angle that affect the redistribution of fast ions in phase and real spaces. As a first step of the development of the improved sawtooth model, simulations using the Hamiltonian guiding centre code ORBIT have been carried out. The simulation results confirm the experimental observation that fast ions are redistributed by sawtooth crash both in phase and real space depending on their orbit type and energy. In real space, passing particles in the core region are expelled outside the $q = 1$ surface while trapped particles do not experience significant effects from sawtooth crash. The initial interpretative TRANSP simulation using the so-called kick model based on the ORBIT modelling result shows improvement of fast ion redistribution before and after a sawtooth crash but the neutron rate still has discrepancy compared to the experimental measurement.

EX

Advancing Local Helicity Injection for Nonsolenoidal Tokamak Startup

M. W. Bongard¹, G. M. Bodner¹, M. G. Burke¹, R. J. Fonck¹, J. L. Pachicano¹, J. M. Perry¹, C. Pierrren¹, J. A. Reusch¹, A. T. Rhodes¹, N. J. Richner¹, C. Rodriguez Sanchez¹, C. E. Schaefer¹, and J. D. Weberski¹

¹University of Wisconsin-Madison, Madison, WI 53706, USA

Corresponding Author: M. W. Bongard, mbongard@wisc.edu

Robust nonsolenoidal startup methods may simplify the cost and complexity of next-step burning plasma devices, and especially STs, by removing the need for a solenoid. Experiments on the $A \sim 1$ Pegasus ST are advancing the physics and technology basis of local helicity injection (LHI). LHI creates high- I_p tokamak plasmas without a solenoid by injecting helicity with small current sources in the plasma edge. Its hardware can be withdrawn before a fusion plasma enters a nuclear burn phase. Flexible injector placement offers tradeoffs between physics and engineering goals. They are tested with LHI systems on the low-field-side (LFS) and the high-field-side (HFS) of Pegasus, producing plasmas predominantly driven by nonsolenoidal induction and DC helicity drive ($V_{\text{LHI}} \propto B_{\text{inj}} A_{\text{inj}} V_{\text{inj}}$), respectively. Record LHI plasmas with $I_p = 0.2$ MA, $T_e > 100$ eV, $n_e \sim 10^{19}/\text{m}^3$, and $Z_{\text{eff}} < 2.5$ are attained. A predictive 0D power-balance model describes experimental $I_p(t)$ and partitions the active current drive sources. It uses improved inductance models that have been extended to $A \sim 1$. The analysis confirms the dominance of induction in LFS LHI and DC helicity drive in HFS LHI. Model projections for NSTX-U suggest MA-class LHI startup may be feasible with a modest LFS system. An advanced port-mounted LHI system is being deployed on Pegasus to test this path. Studies of HFS scenarios find favourable, positive scalings of I_p with V_{LHI} and T_e with B_t . If they hold at higher B_t , LHI may directly offer useful targets for RF and NBI current drive. High-frequency MHD activity plays a strong role in LHI current drive, in addition to $n = 1$ modes previously found in NIMROD simulation and experiment. A new regime of reduced MHD activity was discovered where the $n = 1$ activity is suppressed. In this regime, high-frequency activity increases, LHI CD efficiency improves, and long-pulse plasmas are sustained with $V_{\text{IND}} \sim 0$. LHI facilitates access to the favourable low- A ST regime with nonsolenoidal sustainment, high κ , low ℓ_i , and high β_t . Low B_t LHI operation has led to record $\beta_t = 100\%$, high β_N , and a minimum- $|B|$ well that may positively affect turbulence, transport, and fast particle confinement. Discharges at highest β_t disrupt at the ideal no-wall MHD limit.

EX

Development of a High-Flux Fusion Neutron Source Using Recent Advances in Technology

C. B. Forest¹, J. Anderson¹, J. Egedal¹, V. V. Mirnov¹, E. Peterson¹, J. S. Sarff¹, J. Wallace¹, R. Waleffe¹, R. W. Harvey², Y. V. Petrov², B. N. Sorbom³, J. Minervini³, D. G. Whyte³, and T. Simonen⁴

¹*University of Wisconsin-Madison, Madison, WI 53706, USA*

²*CompX, Del Mar, CA 92014, USA*

³*Massachusetts Institute of Technology (MIT), Cambridge, MA 02139, USA*

⁴*University of California Berkeley, CA 94720, USA*

Corresponding Author: C. B. Forest, cbforest@wisc.edu

EX We report an overview of theoretical and experimental work at the University of Wisconsin leading to a fusion neutron source based on the gas dynamic trap concept. The design considers the implications of several recent physics and technological advances and uses: 1) off-the-shelf MRI magnets for an inexpensive central cell, 2) state-of-the-art small and planar high field REBCO magnet for plugs, 3) state-of-the-art gyrotrons to allow high density operation, 4) sloshing ions to localize neutron yield away from sensitive high field magnets at edge, 5) radio-frequency heating at the fast-ion turning points to enhance neutron yield, and 6) a liquid lithium expanding divertor for heat removal, electron thermal barrier and MHD stability—lithium seems essential for pumping neutrals, minimize sputtering by ion bombardment, and minimize secondary electron emission to allow the electron thermal barrier to form. Equilibrium, stability, and plasma heating have been modelled using a Grad-Shafranov solver for the mirror including fast ion pressure coupled to the CQL3D/Genray suite of codes. Initial results were extremely promising: 5 MW of neutral beam injection power and 5 MW of rf heating at 15 MHz generated 10^{15} neutrons/s in DD. In addition, progress on the construction of a prototype GDT using REBCO mirror coils a lithium divertor solution will be reported.

First Simulations of Turbulent Transport in the Field-Reversed Configuration

C. K. Lau¹, D. P. Fulton¹, J. Bao², Z. Lin², T. Tajima^{1,2}, and L. Schmitz^{1,3}

The TAE Team

¹TAE Technologies, Inc., Foothill Ranch, CA 92688, USA

²University of California Irvine, CA 92697, USA

³University of California Los Angeles, CA 90095, USA

Corresponding Author: C. K. Lau, clau@tae.com

Experimental progress by TAE Technologies has led to successful suppression of MHD instabilities in field-reversed configuration (FRC) plasmas using C-2U and C-2W devices. Resultant particle and energy confinement times are on the order of several milliseconds, governed by microturbulence driven transport processes. Understanding these mechanisms is essential towards improved confinement and a viable FRC fusion reactor.

Experimental measurements of low frequency density fluctuations in C-2 have shown that fluctuations of the FRC core and SOL exhibit distinct qualities. In the SOL, fluctuations are highest in amplitude at ion-scale lengths and exponentially decrease towards electron-scale lengths. In the core, fluctuations are overall lower in amplitude with a dip in the ion-scale lengths and a slight peak in electron-scale lengths. Using the Gyrokinetic Toroidal Code (GTC), local linear simulations of drift-wave instabilities have found qualitatively similar trends. The SOL is linearly unstable for a wide range of length scales and pressure gradients. On the other hand, the core is shown to be robustly stable due to the stabilizing FRC traits of short field-line connection lengths, radially increasing magnetic field strength, and the large finite Larmor radius (FLR) of ions.

To address microturbulence in a global FRC magnetic geometry that spans the separatrix, "A New Code" (ANC), a particle-in-cell code closely related to GTC, has been developed. Nonlocal cross-separatrix simulations show fluctuations spreading from the SOL to the core with fluctuations in the core saturating at levels an order of magnitude lower than in the SOL, consistent with experimental measurements. Turbulence simulations, domain limited to the SOL, show saturation without zonal flow is achieved at levels around $e\phi/T_e \sim \mathcal{O}(10^{-2})$, and an inverse spectral cascade is observed.

Recent calculations have been extended to more realistically simulate cross-separatrix turbulence. Initial global turbulence simulations show the evolution of the fluctuation spectrum to be comparable to the experimental measurements. In this paper, global turbulence simulations will be compared with experimental results from C-2 and C-2U. The effects of sheared flows, zonal flow, and kinetic electrons and ions on turbulent transport physics will also be reported.

EX

Dynamic Neutral Beam Injection as a Mechanism for Plasma Control and an Actuator for Instability Drive

M. D. Boyer¹, M. E. Austin², W. Hu³, W. W. Heidbrink⁴, C. T. Holcomb⁵, D. C. Pace⁶, B. J. Crowley⁶, K. G. Erickson¹, J. R. Ferron⁶, **B. A. Grierson**¹, S. R. Haskey¹, D. A. Humphreys⁶, C. Pawley⁶, C. C. Petty⁶, J. Rauch⁶, J. T. Scoville⁶, K. E. Thome⁷, M. A. Van Zeeland⁶, and B. S. Victor⁵

¹Princeton Plasma Physics Laboratory (PPPL), Princeton, NJ 08540, USA

²University of Texas at Austin, Austin, TX 78712, USA

³Institute of Plasma Physics, Chinese Academy of Sciences, Hefei, Anhui, People's Republic of China

⁴University of California Irvine, CA 92697, USA

⁵Lawrence Livermore National Laboratory (LLNL), Livermore, CA 94550, USA

⁶General Atomics, San Diego, CA 92186, USA

⁷Oak Ridge Associated Universities (ORAU), Oak Ridge, TN 37831, USA

Corresponding Author: M. D. Boyer, mboyer@pppl.gov

A novel capability has been added to the DIII-D neutral beam injection system, enabling in-shot variation of beam energy and current for the first time [1]. This new capability is now being explored as a tool for integrated control and optimization of equilibrium profiles and Alfvén eigenmode (AE) activity. The capability provides an alternative to the typically used pulse-width-modulation approach to controlling beam injection, and enables continuous variation of torque in the zero-torque regime. The capability also enables optimizing current drive and heating by injecting at lower energy during current ramp and at higher energy later in discharges. The first feedback algorithm making use of the new actuation approach has been experimentally tested, demonstrating stored energy and rotation control while addressing many of the challenges specific to using beam energy and current variation as an actuator. These challenges include constraints on the magnitude of beam voltage and current, slew rate limits on voltage changes, and lag between requested and achieved beam parameters. A real-time optimization-based control algorithm was developed that determines the voltage, current, and duty cycle required at steady state to maintain the optimal stored energy and rotation values, while accounting for the limits on voltage and current. The algorithm compensates the slow response of the voltage through fast adjustments of the current to more quickly track the required power and torque. The power and torque requests are augmented with a feedback term to improve energy and rotation target tracking. In a related experiment, a real-time ECE signal was used to detect AE mode activity and vary the NBI power through beam modulation based on feedback on the mode amplitude. This demonstration of AE mode control also showed that the ratio of the measured neutron rate to the classical predicted value, an indication of the effect of the AE mode on fast ion confinement, was changed through the variation of AE mode amplitude. The results of these two experiments motivate further development to integrate the new actuation and feedback approaches to control equilibrium parameters, including rotation and q , along with AE mode activity.

Work supported by the U.S. Department of Energy Contract No. DE-AC02-09CH11466 and DE-FC02-04ER54698.

References

[1] J. Rauch *et al.*, Fusion Sci. Tech., **72**, 3 (2017).

Physics-Model-Based Real-Time Optimization for the Development of Steady-State Scenarios at DIII-D

E. Schuster¹, W. P. Wehner¹, A. Pajares¹, J. R. Ferron², M. L. Walker², D. A. Humphreys², B. G. Penaflor², R. D. Johnson², and C. T. Holcomb³

¹*Lehigh University, Bethlehem, PA 18015, USA*

²*General Atomics, San Diego, CA 92186, USA*

³*Lawrence Livermore National Laboratory (LLNL), Livermore, CA 94550, USA*

Corresponding Author: E. Schuster, schuster@lehigh.edu

Recent and ongoing experiments on DIII-D demonstrate the potential of model-based real-time optimization for the realization of advanced steady-state scenarios by tightly regulating the q profile and β_N (or the plasma energy W) simultaneously. A primary goal for the DIII-D research programme over the next five years is to develop the physics basis for a high- q ($q_{\min} > 2$), high- β_N , steady-state scenario (fully relaxed plasma state where the current is entirely noninductive) that can serve as the basis for future steady-state burning plasmas. Various approaches are being considered to maximize both the bootstrap current and the noninductive current-drive contributions, so that fully noninductive ($f_{NI} = 1$) discharges can be obtained for several resistive current diffusion times. It is anticipated that the upcoming upgrades to DIII-D, including an additional off-axis neutral beam injection (NBI) system, will provide sufficient auxiliary current drive to maintain fully noninductive plasmas at high β_N . However, much work is still necessary to investigate MHD stability, adequate confinement, and early achievement and sustainment of the steady-state condition. The capability of combined q -profile and β_N control to enable access to and repeatability of steady-state scenarios for $q_{\min} > 1.4$ discharges has been assessed in DIII-D experiments. To steer the plasma to the desired state, a model predictive control approach to both q -profile and β_N regulation numerically solves successive optimization problems in real-time over a receding time horizon by exploiting efficient quadratic programming techniques. A key advantage of this control approach is that it allows for explicit incorporation of plasma-state/actuator constraints to prevent the controller from driving the plasma outside of stability/performance limits and obtain, as closely as possible, steady state conditions. Experimental results demonstrate the effectiveness of the real-time optimization scheme to consistently achieve the desired scenarios at predefined times and suggest that control-oriented model-based scenario planning in combination with real-time optimization can play a crucial role in exploring stability limits of advanced steady-state scenarios.

EX

Error Field Impact on Mode Locking and Divertor Heat Flux in NSTX-U

N. M. Ferraro¹, J.-K. Park¹, C. E. Myers², M. L. Reinke³, S. P. Gerhardt¹, J. E. Menard¹, and A. Brooks¹

¹Princeton Plasma Physics Laboratory (PPPL), Princeton, NJ 08540, USA

²Sandia National Laboratories (SNL), Albuquerque, NM 87185, USA

³Oak Ridge National Laboratory (ORNL), Oak Ridge, TN 37831, USA

Corresponding Author: N. M. Ferraro, nferraro@pppl.gov

Results from the 2016 NSTX-U campaign and the subsequent recovery effort have led to significant new insights regarding error fields in the NSTX-U experiment in particular, and in spherical tokamak configurations in general. During the experimental campaign, many L-mode discharges were found to be locked from the $q = 2$ surface outward, indicating the presence of error fields. At the conclusion of the run campaign, extensive metrology was conducted on the primary vertical field ("PF5") coils, and the centre stack assembly, which includes the central solenoid and the centre rod of the toroidal field ("TF") coils. Error field models based on these measurements indicate that misalignment of the TF rod, while small, produces the largest error field among the sources considered. Plasma response modelling with IPEC and M3D-C1 finds that the TF error field remains the dominant source of resonant braking, despite the fact that the TF error field spectrum couples relatively weakly to the plasma, due to the large current in the TF rod and the proximity of the rod to the plasma. The plasma response to the TF error field is expected to depend significantly on the presence of a $q = 1$ surface, since the TF error field is dominantly $m/n = 1/1$. This is qualitatively consistent with results of several "compass" scans performed during the NSTX-U run campaign, which found that the optimal error field correction before and after the formation of the $q = 1$ surface differed significantly. Interestingly, these discharges typically disrupted via locking of the $1/1$ surface, since the $2/1$ surface was often locked ab initio. It is found that certain characteristics of the TF error field present new challenges for error field correction. Specifically, the error field spectrum differs significantly from that of coils on the low-field side (such as the NSTX-U RMP coils), and does not resonate strongly with the dominant kink mode, thus potentially requiring a multimode correction. Finally, to mitigate heat fluxes using poloidal flux expansion, the pitch angle at the divertor plates must be small ($\sim 1^\circ$). It is shown that large error fields may result in unacceptable local perturbation to the pitch angle. Tolerances for coil alignments in the NSTX-U restart are derived based on both heat flux considerations and core resonant fields independently.

First Analysis of the Updated ITPA Global H-Mode Confinement Database

G. Verdoolaege^{1,2}, S. M. Kaye³, C. Angioni⁴, M. Maslov⁵, M. Romanelli⁵, F. Ryter⁴, and K. Thomsen⁴

The ASDEX-Upgrade Team, EUROfusion MST1 Team, and JET Contributors

¹*Ghent University, 9000 Ghent, Belgium*

²*Laboratory for Plasma Physics, ERM/KMS, Brussels, Belgium*

³*Princeton Plasma Physics Laboratory (PPPL), Princeton, NJ 08540, USA*

⁴*Max-Planck-Institut für Plasmaphysik, Garching, Germany*

⁵*United Kingdom Atomic Energy Authority, Culham Science Centre, Abingdon, UK*

Corresponding Author: G. Verdoolaege, geert.verdoolaege@ugent.be

We report on an ongoing task within the ITPA concerning a revision of the global H-mode energy confinement scaling in tokamaks, known as $IPB_{98}(y, 2)$. The objectives of the task are to update the database with data closer to ITER baseline and hybrid conditions, to expand the parameter range and include new data from devices with reactor-relevant metallic walls, to explore predictor variables and possibly decouple core and pedestal scaling, and to employ advanced regression techniques with an emphasis on the robustness of the scaling.

In this work, first results are presented of a description of the most recent version of the global H-mode confinement database, following addition in 2017 of new data from JET with the ITER-like wall and ASDEX-Upgrade with its tungsten wall. The so-called “standard set”, based on ITER-relevant selection criteria, presently contains 5718 entries from 18 machines. Considerable reduction of the linear correlation between the predictor variables has been observed, in comparison with the database used for the IPB_{98} scaling. Correlation coefficients above 0.5 remain between plasma current and major radius (0.74), current and loss power (0.65), and accordingly between major radius and loss power (0.60).

In pursuing the analysis of the updated database, the classic power-law dependence is assumed and regression analysis is being performed using ordinary least squares, a robust Bayesian technique and robust geodesic least squares. Examination of individual device scalings, both for low- Z and high- Z walls, has given insight into similarities and differences among these individual datasets, and this may lead to the resolution of some of the recently observed discrepancies between IPB_{98} and single-machine scans.

A significant part of the ongoing analysis effort will concentrate on exploring hidden variables not represented in the IPB_{98} scaling, in light of recent insight into the physics governing energy transport in tokamaks. This might resolve issues related to collinearity of predictor variables and may eventually contribute to a multimachine scaling that better reflects the underlying physical dependences. This would also benefit interpretation of the scaling in terms of dimensionless variables. For similar reasons, the power-law form of the scaling may need to be re-evaluated in future work.

Time Resolved Triton Burnup Measurements Using the Scintillating Fibre Detector on KSTAR

J. Jo¹, J. Kim², M. S. Cheon², M. Isobe^{3,4}, K. Ogawa^{3,4}, T. Nishitani³, I. Murata⁵, S. Park², Y. In², K.-J. Chung¹, and Y.-S. Hwang¹

¹*Seoul National University, Seoul, Republic of Korea*

²*National Fusion Research Institute (NFRI), Daejeon, Republic of Korea*

³*National Institute for Fusion Science (NIFS), Toki, Gifu, Japan*

⁴*Department of Fusion Science, Graduate University for Advanced Studies (SOKENDAI), Toki, Gifu, Japan*

⁵*Division of Sustainable Energy and Environmental Engineering, Osaka University, Osaka, Japan*

Corresponding Author: J. Jo, wh1223@snu.ac.kr

EX For the purpose of fusion triton confinement study on KSTAR, square shaped scintillating fibre detector has been installed and tested during the 2017 KSTAR campaign. It is composed of scintillating fibre bundles which are immersed in the lead matrix. A total of 1056 scintillating fibres whose cross-sectional area is 1 mm² are immersed. The scintillation light is detected by Hamamatsu R878 photomultiplier tube (PMT) and its anode signal is digitized and processed by CAEN DT5751. From the DD neutron calibration experiments in National Fusion Research Institute (NFRI) and DT neutron calibration experiments in the Intense 14 MeV Neutron Source Facility, OKTAVIAN, of Osaka University, the appropriate discrimination level for 14 MeV neutron signal is determined. The operation results in the various plasma conditions are described. In the resonant magnetic perturbation driven edge localized mode (ELM) control experiment case, it is observed that as the RMP applied, ELM mitigated and the amount of burned up triton increased. Each observed results are analyzed by considering possible orbits and slowing down characteristics of fusion triton.

Intrinsic Toroidal Rotation for Ohmic L-Mode Plasmas in KSTAR

S. G. Lee¹, J. W. Yoo¹, J. Seol¹, and H. H. Lee¹

The KSTAR Team

¹*National Fusion Research Institute (NFRI), Daejeon, Republic of Korea*

Corresponding Author: S. G. Lee, sglee@nfri.re.kr

The toroidal rotation from pure ohmic discharges without any external momentum sources is one of the most fundamental types of self-generated intrinsic rotation for magnetic fusion research. There have been reported a wide range of magnitudes, directions and abrupt reversals for ohmic toroidal rotation studies, no clear physical mechanisms are concluded to explain these intrinsic ohmic rotation behaviours. Although the origin of the intrinsic ohmic rotation still needs intensive studies, the long-standing question for the direction of the ohmic rotation could be speculated from precise experimental evidences measured from cross validated diagnostics since KSTAR equips two main diagnostics. The core ohmic toroidal rotation has been measured mostly in the countercurrent direction with normal operation conditions and the corresponding scaling is reported from KSTAR. Recently, we expanded the ohmic rotation scaling to the cocurrent direction for the first time utilizing lower electron density regimes. In this presentation, we will investigate the critical clue for the ohmic rotation direction and extended scaling to the cocurrent direction.

EX

The Effect of Electron Cyclotron Heating on Thermal and Fast-Ions Transport in High- β -Poloidal Discharges at KSTAR

S.-W. Yoon¹, Y. M. Jeon¹, H. S. Kim¹, J. S. Kang¹, T. Rhee¹, J. M. Park², and Y.-K. Oh¹

The KSTAR Team

¹National Fusion Research Institute (NFRI), Daejeon, Republic of Korea

²General Atomics, San Diego, CA 92186, USA

Corresponding Author: S.-W. Yoon, swyoon@nfri.re.kr

For the realization of the fusion reactor, solving issues for high- β steady-state operation is one of the essential research topics for the present superconducting tokamaks and as a candidate of steady-state scenarios, characteristics of, so called, “high- β -poloidal” discharges is analyzed in depth for the capability of fully noninductive operation with high bootstrap current fraction. Through the scans of plasma current ($I_p \sim 0.4\text{--}0.6$ MA), toroidal field ($B_t \sim 1.8\text{--}2.7$ MA), additional heating ($P_{\text{NBI+ECH}} \sim 3\text{--}5$ MW), and plasma density (n_e), the access conditions are identified for each parameters for the discharges. Interestingly, it is revealed experimentally the discharge characteristics is rather sensitive on the position of EC deposition layer in the core region. Only in a narrow range of the deposition layer, high- β -poloidal regime with $H_{98} \sim 2.1$ is accessible and sustained, while low- β -poloidal regime with $H_{98} \sim 1.6$ exists either without ECH or with outside deposition of the narrow layer. The difference confinement is investigated with MHD activities and the confinement degradation is strongly correlated with high frequency (> 100 kHz) oscillations which are identified as Alfvén eigenmodes (AEs) and also with DD reduction of neutron rate which suggests the large decrease of fast ion pressure. Therefore, the thermal and fast-ion confinement are analyzed with TRANSP with the measured kinetic profiles and total β from EFIT magnetic reconstruction. To model the fast-ion transport, ad-hoc diffusion coefficient of fast ions (D_{fast}) is introduced and determined by detailed comparison of the results of TRANSP and EFIT and the validity of the derived value of D_{fast} is also confirmed in parallel by neutron rate measurements. In addition, the linear stability of AEs are also examined with MEGA for the onset condition and toroidal mode numbers. According to the analysis, the difference of total confinement (i.e., $H_{98} = 2.1$ and 1.6 respectively) is mainly due to the increased transport of fast ions (i.e., $D_{\text{fast}} = 0.4$ and 1.2 respectively), while there is minor effect from the thermal transport channel (i.e., $H_{98} = 1.1$ and 1.0 , respectively). Finally, based on the present analysis, the performance enhancement of the high- β -poloidal discharge is predicted for the case with more heating power ($P_{\text{NBI+ECH}} \sim 10$ MW) which is envisaged in two years.

Characteristics of Asymmetric (Low-Field-Side and High-Field Side) Divertor Detachment in KSTAR L-Mode Plasmas

J.-S. Park¹, R. A. Pitts², M. Groth³, J. G. Bak⁴, S. G. Thatipamula⁴, S.-H. Hong⁴, and W. Choe¹

¹Korea Advanced Institute of Science and Technology (KAIST), Daejeon, Republic of Korea

²International Thermonuclear Experimental Reactor (ITER),
Cadarache Centre, 13108 St. Paul lez Durance, France

³Aalto University, Espoo, Finland

⁴National Fusion Research Institute (NFRI), Daejeon, Republic of Korea

Corresponding Author: J.-S. Park, jaesunpark@kaist.ac.kr

A divertor detachment experiment in low confinement mode and $B \times \nabla B$ into the divertor was performed in KSTAR to investigate various divertor operation regimes. The low field side (LFS) target parallel particle flux Γ_{\parallel} started roll-over first ($n_e = 2.0\text{--}2.5 \times 10^{19}/\text{m}^3$), and then the high field side (HFS) target Γ_{\parallel} began roll-over at the higher upstream electron density ($n_e = 2.5\text{--}3.0 \times 10^{19}/\text{m}^3$). The observed detachment pattern is similar to the one in TCV [1] and opposite to JET and ASDEX-U [2].

Numerical simulations using the SOLPS-ITER code [3] with different electron density values were performed to identify the physics behind the detachment behaviour observed in the experiment. The simulation result is qualitatively consistent with the experiment in terms of the roll-over pattern of the total particle fluxes on the targets. Pressure and power losses were decomposed into source terms including the kinetic neutral reactions. The dominant pressure and power loss mechanisms were identified in each SOL rings. In the high recycling condition (electron density at the separatrix, outer midplane $(n_e)_{sep}^{OMP} \geq 1.49 \times 10^{19}/\text{m}^3$), volumetric reactions govern power and pressure losses along the flux tube, however the dominant reaction type depends on the radial position of the SOL ring. According to the recycled neutral deuterium particle trajectory observed in the code, D_2 molecules accumulate behind the divertor structure through a gap near the LFS target. The gap acts as a strong neutral particle source near the LFS target, resulting in a 2–10 times larger D_2 density at the LFS than at the HFS target. The simulations predict that this asymmetric neutral particle distribution causes divertor asymmetry. The accumulated D_2 enhances detachment, which is related to the strong correlation between the target D_2 density n_{D_2t} and the target electron temperature [4]. This correlation results from additional power and pressure losses by the molecular related reactions, such as dissociation and charge exchange.

References

- [1] R. A. Pitts *et al.*, J. Nucl. Mater., **290**, 940 (2001).
- [2] A. Loarte *et al.*, Nucl. Fus., **38**, 331 (1998).
- [3] S. Wiesen *et al.*, J. Nucl. Mater., **463**, 480 (2001).
- [4] P. C. Stangeby and C. Sang, Nucl. Fus., **57**, 056007 (2017).

ELM Suppression and Internal Transport Barrier Formation by Krypton Seeding in KSTAR Plasmas

J. J. Jang¹, J. Hong¹, I. Song¹, C. R. Seon², J. Kim², J. S. Kang², K. Kim², B. J. Peterson³, J.-S. Park¹, S.-H. Hong², T. M. Jeon¹, and W. Choe¹

¹Korea Advanced Institute of Science and Technology (KAIST), Daejeon, Republic of Korea

²National Fusion Research Institute (NFRI), Daejeon, Republic of Korea

³National Institute for Fusion Science (NIFS), Toki, Gifu, Japan

Corresponding Author: J. J. Jang, jjh4368@kaist.ac.kr

Impurity seeding with noble gases, such as krypton (Kr), is regarded as a promising way to mitigate divertor heat loads. In this study, ELMs were successfully suppressed by Kr injection in the KSTAR divertor region and the relation between ELM behaviour and Kr amount was studied in KSTAR plasmas with 0.5 MA plasma current and 2.5 T toroidal field. After achieving an intermediate level of Kr seeding, ELM crashes were briefly suppressed and grassy ELMs occurred with slight reduction of line-integrated electron density, core electron temperature and stored energy, while there was no effect on ELMs for a low level of Kr. The ELM suppression time became longer at a higher level of Kr injection.

Detailed analysis including peeling-ballooning stability is on-going to understand the ELM suppression mechanisms with Kr profiles and ECH. At a certain level of Kr injection, an internal transport barrier (ITB) was formed after ELM mitigation and was maintained until the termination of the plasma. Core electron temperature, stored energy and D α signal gradually decrease after Kr injection at 6.0 s. After a sudden increase of core electron temperature at 10 s, electron and ion temperatures and toroidal rotation profiles show strong central peaking, which are the commonly observed feature of an ITB. Both electron and ion heat diffusivities at the plasma core, obtained by TRANSP calculation, also drop significantly after ITB formation, which suggests the reduction of core thermal transport or improvement of core thermal confinement. Two-dimensional radiation profiles obtained by the imaging bolometer diagnostic show off-axis Kr accumulation after ITB formation, while Kr was accumulated mainly in the plasma core before the ITB. Detailed analysis of Kr impurity transport is on-going to investigate the role of Kr impurity on ITB formation.

EX

Experimental Observation and Modelling of High-Z Impurity Transport by Tungsten Powder Injection in KSTAR Plasmas

I. Song¹, C. R. Seon², D.-H. Kwon³, J. Hong¹, R. Guirlet⁴, Y. H. An², S.-H. Hong², and W. Choe¹

¹Korea Advanced Institute of Science and Technology (KAIST), Daejeon, Republic of Korea

²National Fusion Research Institute (NFRI), Daejeon, Republic of Korea

³Korea Atomic Energy Research Institute (KAERI), Daejeon, Republic of Korea

⁴Institut de Recherche sur la Fusion par confinement Magnétique (IRFM), Commissariat à l'énergie atomique (CEA/Cadarache), 13108 St. Paul lez Durance, France

Corresponding Author: I. Song, inwoosong@kaist.ac.kr

In fusion plasmas with electron temperature of several keV, most of the tungsten (W) particles are in W^{27+} to W^{45+} ionic states, which emit line radiations of a few nm wavelength in the EUV range. Thus, a compact ($63 \times 44 \times 18 \text{ cm}^3$) advanced EUV spectrometer system (CAES) was recently developed [1] to simultaneously measure spectrally-resolved tungsten emission and spatially-resolved W density profile. Since the 2016 KSTAR campaign, a few mg of W powder of $12 \mu\text{m}$ typical size was injected to the plasma by a portable compact ($60 \times 30 \text{ mm}^2$) gun-type particle injector [2] which can inject any kind of metal powder. During the experiments, spatiotemporally varying W spectra were successfully obtained by CAES with 2.7 cm and 67 ms of spatial and time resolutions. In conjunction with these experimental setups, a spectral model for high-Z impurity transport has been developed based on coronal approximation. The Flexible Atomic Code (FAC) is used to calculate the PEC of W^{10+} to W^{48+} . The modelled line emissions are compared with the measured data in order to find proper diffusion coefficients and convection velocities from the radial continuity equation. In addition, the radiation power loss relation and the force balance equation with a centrifugal force effect are included to find the two-dimensional global density profile of high-Z impurities and a relation between the toroidal rotation speed and poloidal asymmetry. These schemes are possible by using the infrared imaging video bolometer (IRVB) diagnostics in KSTAR, through which we observed a poloidally asymmetric distribution of tungsten emission due to the centrifugal force effect in the past KSTAR campaigns. Code validations were performed by comparing with the results from SANCO [3], showing a good agreement within 10% error of the intensity of Ar^{15+} 35.3 nm line emission. It is also clearly seen that more spectral lines appear in the modelled structure than in the measured spectrum, which is possibly an indication that a refined description of the W atomic structure must be included in our calculation.

References

- [1] I. Song *et al.*, Rev. Sci. Instrum., **88**, 093509 (2017).
- [2] H. Y. Lee *et al.*, Rev. Sci. Instrum., **85**, 11D862 (2014).
- [3] J. Hong *et al.*, Nucl. Fus., **57**, 036028 (2017).

Observation of Heat Load on the Castellated Tungsten Block by Back-Scattered Particles from Intentionally Misaligned Protruding Edge

S.-H. Hong¹, H. Lee¹, K. Kim¹, H. Kim¹, H. Choi¹, and H. C. Kim¹

¹National Fusion Research Institute (NFRI), Daejeon, Republic of Korea

Corresponding Author: S.-H. Hong, sukhhong@nfri.re.kr

KSTAR has been involved in studying leading-edge heat loads since 2014 by using series of multipurpose, brazed W blocks (W-Cu-CuCrZr). They are mounted and assembled into two adjacent, inertially cooled graphite tiles installed in the outer divertor target region of KSTAR, within the field of view of an infrared (IR) thermography system installed in an upper lateral port and to which special modifications have been made for this study to increase the spatial resolution to ~ 0.4 mm/pixel on the block surface. The blocks are arranged in different groups, with toroidal gaps of 0.5 mm addressing a specific issue: a variety of leading edge heights (0.3, 0.6, 1.0, and 2.0 mm), from the ITER worst case to heights even beyond the extreme value tested on JET. Adjustment of the outer divertor strike point position is used to deposit power on the different blocks in different discharges, but with emphasis in these first studies on studying power loading as a function of leading edge height. The measured power flux density on flat regions of the surrounding graphite tiles is used to obtain the parallel power flux, q_{\parallel} impinging on the various W blocks.

Experiments have been performed in L-mode and type-I ELMing H-mode, but owing to the low power flux densities in L-mode, the inter-ELM H-mode exposures provide the best IR data. Discharges are run at $I_p = 600$ kA, $B_t = 2$ T, $P_{\text{NBI}} = 3.5$ MW, leading to a hot attached divertor with typical pulse lengths of ~ 10 s and total field line incidence angles of 2–3 at the strike point (cf. 2.5 on ITER). During the experiment, an interesting feature was observed: there was clear evidence of heat load on the castellated tungsten block by back-scattered particles from the intentionally misaligned protruding edge. The line profiles show three different peaks corresponding to one from the protruding edge and two others from the edge and surface of block in front of the protruding one. The deconvoluted heat flux profile and corresponding intensity ratio of each peak show that up to 46% of IR intensity was originated from the block in front of the protruding one: around 44% from the edge and 2% from the surface. The peak intensity of back scattered profile depends strongly on the strike point location, which indicates the contribution of energetic ions during ELM.

Effects of Lithium Coating of Chamber Wall on the STOR-M Tokamak Discharges

C. Xiao¹, A. Rohollahi^{1,2}, A. Mossman², S. Elgriw¹, J. Adegun¹, H. Bsharat¹, and I. Voldiner¹

¹Plasma Physics Laboratory, University of Saskatchewan, Saskatoon, SK S7N-5C9, Canada

²General Fusion Inc., Burnaby, BC V3N-4T5, Canada

Corresponding Author: C. Xiao, chijin.xiao@usask.ca

In a recent experimental campaign in the STOR-M tokamak ($R/a = 0.46$ cm/0.12 cm, $B_t = 0.65$ T, $I_p = 22$ kA), approximately 100 mg of lithium per load has been evaporated from a heated lithium reservoir and coated on the stainless-steel inner wall to study its effects on the tokamak discharge. The evaporators were designed, developed and supplied by General Fusion Inc. Although four evaporators are available, only one evaporator has been used at present time. Coating of lithium on the surface visible by the evaporator through line-of-sight is expected and rest of the surface may be coated during the discharge through sputtering and redistribution of coated lithium due to plasma-wall interaction. It has been found that the partial pressure of impurities such as H_2O , CO and CO_2 reduces significantly immediately after coating, possibly due to gettering effect of lithium coating. During the discharge, the total pressure is also reduced, indicating reduced recycling of gas from the wall. Line emission intensity of selected impurity ions (C_{III} , O_V and C_{VI}) clearly reduces. Correspondingly, the peak plasma current increases by 20% and discharge duration increases significantly. The line averaged electron density reduces by more than 50% due to reduced fuel recycling. The loop voltage reduces by approximately 1/3 due to reduced impurity. An increase in hard X-ray radiation has also been observed, suggesting an enhanced generation of supra-thermal runaway electrons at lowered electron density. The density reduction can be restored by refuelling via compact torus injection.

EX

R&D for Reliable Disruption Mitigation in ITER

M. Lehnen¹, D. J. Campbell¹, D. Hu¹, U. Kruezi¹, T. C. Luce¹, S. Maruyama¹, J. A. Snipes¹, and R. Sweeney¹

¹*International Thermonuclear Experimental Reactor (ITER),
Cadarache Centre, 13108 St. Paul lez Durance, France*

Corresponding Author: M. Lehnen, michael.lehnen@iter.org

The disruption mitigation system (DMS) is a key plant system to ensure the reliable and successful operation of ITER from the first experimental campaign onwards. The DMS baseline concept and design is based on present knowledge on disruption mitigation, which, nevertheless, remains subject to significant gaps in understanding, especially as concerns runaway electron (RE) formation and mitigation. This paper outlines the challenges of implementing a highly reliable DMS for ITER, presents recent progress towards the consolidation of the baseline system and develops a strategy and plan for achieving the required level of disruption mitigation to satisfy ITER's operational needs.

The baseline DMS is based on shattered pellet injection (SPI) technology. This technology delivers the material to the tokamak vessel by accelerating large cryogenic pellets that are broken into smaller fragments at the end of the delivery tube. A total of 25 pellets of different sizes can be injected to mitigate the thermal and electromagnetic loads while preventing the formation of runaway electrons. Additionally, as a second layer of defence, the DMS is supposed to provide sufficiently fast energy dissipation should a runaway beam form accidentally.

The most important challenge for disruption mitigation in ITER will be to ensure that runaway electron formation is excluded during the mitigation action up to the nominal plasma current. Designing a DMS that fulfils this essential requirement requires much better understanding of the generation of runaway electron seed populations during the MHD driven thermal quench. Another constraint is the need to ensure that the line radiation is homogeneous enough to prevent first wall melting during the mitigated thermal quench. The required R&D work on the technology side comprises the integration of the baseline DMS into the ITER physical environment, the optimization of the pellet injection and shattering processes with special focus on the fragment ablation and penetration process and the optimum fragment size distribution, the assessment of the requirements for material injection for optimized effectiveness and operability in the ITER environment and the plasma parameter range. The latter will have a strong focus on the efficiency of multiple pellet injection and their relative timing and jitter.

Bifurcation of Perpendicular Rotation and Field Penetration at the Transition to RMP-Induced ELM-Crash Suppression

J. Lee¹, Y.-M. Jeon¹, Y. In², G. Y. Park¹, M. J. Choi¹, W. Lee¹, G. Yun³, M. Kim², J.-H. Lee¹, W.-H. Ko¹, and H. K. Park²

The KSTAR Team

¹*National Fusion Research Institute (NFRI), Daejeon, Republic of Korea*

²*Ulsan National Institute of Science and Technology (UNIST), Ulsan, Republic of Korea*

³*Pohang University of Science and Technology (POSTECH), Pohang, Gyeongbuk 790-784, Republic of Korea*

Corresponding Author: J. Lee, jaehyun@nfri.re.kr

The bifurcation of perpendicular rotation (ν_{\perp}) at the transition of ELM-crash suppression has been measured using electron cyclotron emission imaging (ECEI) system on KSTAR. The ECEI revealed that the ELM crashes are suppressed along with a rapid reduction of ν_{\perp} , which synchronizes with the transition into and out of the ELM-crash suppression. The ν_{\perp} bifurcation is mainly attributed to the rapid change of $E \times B$ velocity and the ν_{\perp} magnitude is maintained the smallest near the q_{95} rational flux surface during the ELM-crash suppression. The plasma response to the RMP, normalized by ν_{\perp} changes, is strongest in the vicinity of q_{95} rational flux surface during the ELM-crash suppression.

EX

Evolution of Locked Mode Under the Existence of Nonaxisymmetric Fields in KSTAR

J. Kim¹, M. J. Choi¹, A. Y. Aydemir¹, Y. In², H. Han¹, J.-K. Park³, J. Lee¹, J. G. Bak¹, W. H. Ko¹, and Y.-K. Oh¹

The KSTAR Team

¹National Fusion Research Institute (NFRI), Daejeon, Republic of Korea

²Ulsan National Institute of Science and Technology (UNIST), Ulsan, Republic of Korea

³Princeton Plasma Physics Laboratory (PPPL), Princeton, NJ 08540, USA

Corresponding Author: J. Kim, jayhyunkim@nfri.re.kr

Since the 2013 KSTAR campaign, we have investigated the effect of nonaxisymmetric (NA) fields on the evolution of magnetohydrodynamic (MHD) instabilities by using the error field (EF) correction coils. Locking and EF penetration were induced by the torque imbalance between the intrinsic rotation and external magnetic braking. Further increase of the $n = 1$ EF resulted in minor and major disruptions. As anticipated by the magnetic braking effect, the stronger $n = 2$ NA field case exhibited earlier EF penetration and locking. On the contrary to the locking phenomena, subsequent minor and major disruptions were delayed and even avoided by the stronger $n = 2$ NA field. Analysis of the $n = 1$ locked mode amplitude revealed that the $n = 2$ NA field started to hinder the growth of $n = 1$ locked mode when the mode amplitude reached certain level in Ohmic discharges. The starting level of the hindrance appears to rely on the $n = 2$ NA field strength. More interestingly, the fast growth was recovered just before minor disruption. Nevertheless, the pure $n = 1$ EF case without $n = 2$ NA field did not show clear change of the growth rate after locking and just exhibited gradual increase of the locked mode towards the minor disruption. A kinematic model of tearing-kink interaction is in qualitative agreement with the experimental observations. In neutral beam (NB) heated L-mode discharges, the overall effect of $n = 2$ NA field appears similar to that in the Ohmic discharges. However, the detailed evolution towards major disruption was somewhat different. With $n = 2$ NA field, initial minor disruptions were much weaker than those in the reference discharge without $n = 2$ NA field. To reach a comparable level of minor disruptions in the reference discharge, we needed stronger $n = 1$ EF in the discharge of $n = 2$ NA field. Electron cyclotron emission imaging (ECEI) showed different patterns of minor disruption depending on the existence of $n = 2$ NA field. As in the Ohmic discharge, the resulting major disruption was delayed in the NB heated L-mode discharge as well. A series of experimental results in various discharge conditions show the possibility of using NA fields to control or delay the plasma disruption process.

Experimental Observations of the Plasma Shape Effect on the RMP-ELM Coupling for Optimization of the KSTAR ELM-Crash Control

Y. M. Jeon¹, Y. In^{1,2}, J.-K. Park³, K. M. Kim¹, J. H. Kim¹, J.-W. Ahn⁴, G. Y. Park¹, H. S. Han¹, S.-W. Yoon¹, Y.-K. Oh¹, and H. K. Park^{1,2}

The KSTAR Team

¹National Fusion Research Institute (NFRI), Daejeon, Republic of Korea

²Ulsan National Institute of Science and Technology (UNIST), Ulsan, Republic of Korea

³Princeton Plasma Physics Laboratory (PPPL), Princeton, NJ 08540, USA

⁴Oak Ridge National Laboratory (ORNL), Oak Ridge, TN 37831, USA

Corresponding Author: Y. M. Jeon, ymjeon@nfri.re.kr

Reliable and robust resonant magnetic perturbation (RMP) on the edge-localized-mode (ELM) crash control is crucial for the success of ITER and beyond. In recent KSTAR experiments, a critical dependence of RMP-ELM coupling on the plasma shape was found to be as important as much as q_{95} . In application of the low- n RMP fields, small variations in the lower triangularity by controlled $R_{X,lower}$ (radial position of lower X-point) made significant changes on RMP coupling, suggesting a narrow window for the ELM-crash suppression. For the shape effects found in 2016, such R_X window for the RMP induced ELM-crash suppression was surprisingly narrow ($\delta_{lower} = 0.74 \pm 0.04$ and $R_{X,lower} = 144 \pm 2$ cm), while the other shape parameters, such as Z_X , seem to have weak effects. Also it was found that the same shape valid for the $n = 1$ RMP was not effective for the $n = 2$ RMP induced ELM-crash suppression. In 2017, further study revealed that such a strict condition of triangularity ($R_{X,lower}$) can be relaxed by allowing for an additional small up-down asymmetry on the plasma shape. Applying this new optimized plasma shape led us to make substantial improvements on reliability and robustness of the RMP induced ELM-crash control. As a result, the $n = 1$ RMP induced ELM-crash suppression were successfully demonstrated in a wide range of q_{95} even with a fixed RMP spectra, achieving a record-long sustainment of ELM suppression more than ~ 30 s. Similarly, the $n = 2$ RMP-induced ELM-crash suppression was achieved with the same shape (universality) at ITER-relevant low $q_{95} = 3.3\text{--}3.5$. Furthermore, we found a singular response to the shape change for the RMP-plasma coupling, with a support of ideal MHD modelling.

EX

Stability, Transport, and Active MHD Mode Control Analysis of KSTAR High Performance Plasmas Supporting Disruption Avoidance

Y.-S. Park¹, S. A. Sabbagh¹, J. H. Ahn¹, J. W. Berkery¹, Y. Jiang¹, J. M. Bialek¹, J. Kim², H. S. Han², S. H. Hahn², Y. M. Jeon², W. H. Ko², B. H. Park², S. W. Yoon², Y. K. In², J. G. Bak², M. D. Boyer³, M. J. Choi², N. M. Ferraro³, A. H. Glasser⁴, S. C. Jardin³, J. G. Kwak², J. S. Ko², H. H. Lee², J. H. Lee², C. E. Myers³, Y.-K. Oh², J. K. Park³, F. M. Poli³, J. D. Riquezes¹, S. Scott³, L. Terzolo², G. S. Yun⁵, S. Wang², Z. Wang³, and H. K. Park^{2,6}

¹Columbia University, New York, NY 10027, USA

²National Fusion Research Institute (NFRI), Daejeon, Republic of Korea

³Princeton Plasma Physics Laboratory (PPPL), Princeton, NJ 08540, USA

⁴Fusion Theory and Computation, Inc., Kingston, WA 98346, USA

⁵Pohang University of Science and Technology (POSTECH), Pohang, Gyeongbuk 790-784, Republic of Korea

⁶Ulsan National Institute of Science and Technology (UNIST), Ulsan, Republic of Korea

Corresponding Author: Y.-S. Park, ypark@pppl.gov

H-mode plasma operation in KSTAR has surpassed the $n = 1$ ideal MHD no-wall β limit computed to occur at $\beta_N = 2.5$ with $l_i = 0.7$. High- β_N operation produced β_N of 3.3 sustained for 3 s, limited by tearing instabilities rather than resistive wall modes (RWMs). High fidelity kinetic equilibrium reconstructions have been developed to include Thomson scattering and charge exchange spectroscopy data, and allowance for fast particle pressure following an approach used in NSTX. In addition, motional Stark effect data are used to produce reliable evaluation of the safety factor, q , profile. The reconstructed equilibria can exhibit significant variation of the q -profile dependent upon the broadness of the bootstrap current profile as computed by TRANSP analysis. Correlations of these differences with observed MHD instabilities are examined to determine favoured scenarios for instability avoidance. TRANSP analysis indicates that the noninductive current fraction has exceeded 50%, and can reach up to 75% while its profile can vary significantly. The stability of the $m/n = 2/1$ tearing mode that limited the high β_N operation is computed by using the resistive DCON code and by the M3D-C1 code with the kinetic EFIT as input. For equilibria at high- $\beta_N > 3$, the tearing stability index, Δ' , is more unstable compared to that of equilibria at reduced β_N , indicating that the neoclassical components of tearing stability need to be invoked to produce consistency with experiment. MISK code analysis which examines global MHD stability modified by kinetic effects shows significant passive kinetic stabilization of the RWM. In preparation for plasma operation at higher β utilizing the new second NBI system, three sets of magnetic field sensors will be used for RWM feedback control. To accurately determine the dominant n -component produced by RWMs, an algorithm has been developed that includes magnetic sensor compensation of the prompt applied field and the field from the induced current on the passive conductors. Developed mode identification using the compensated magnetic signals well measures the toroidal phase of a slowly rotating $n = 1$ MHD mode. This analysis on stability, transport, and control provides the required foundation for disruption prediction and avoidance research on KSTAR.

Work supported by U.S. Department of Energy Grant DE-SC0016614 and DE-FG02-99ER-54524.

Effects of Reconnection Downstream Conditions on Electron Parallel Acceleration during Merging Start-Up of Spherical Tokamak

M. Inomoto¹, T. Ushiki¹, X. Guo¹, T. Sugawara¹, K. Kondo¹, T. Mihara¹, Y. Minami², Y. Inai¹, R. Yanai², Y. Takahata², H. Tanabe¹, Y. Ono¹, A. Sanpei³, and S. Kamio⁴

¹Graduate School of Frontier Science, University of Tokyo, Tokyo, Japan

²Graduate School of Engineering, University of Tokyo, Tokyo, Japan

³Kyoto Institute of Technology, Kyoto, Japan

⁴National Institute for Fusion Science (NIFS), Toki, Gifu, Japan

Corresponding Author: M. Inomoto, inomoto@k.u-tokyo.ac.jp

The axial merging method is one of the candidates to provide centre-solenoid-free start-up of high- β spherical tokamak (ST) plasma, in which two initially formed STs merge through magnetic reconnection in the presence of the guide (toroidal) magnetic field, which is perpendicular to the reconnection (poloidal) magnetic field. Magnetic reconnection between two STs is capable of heating the electrons in the vicinity of the reconnection point, however, its mechanism has not been identified in laboratory experiments yet. During ST merging start-up, electrons are effectively accelerated near the reconnection point where the reconnection electric field is approximately parallel to the magnetic field and will provide the local electron heating. In order to observe the spatial distribution of generated energetic electrons, the SXR (> 100 eV) emission profile was observed by a fast imaging system equipped on the UTST device.

High-intensity SXR emission was observed particularly in the early reconnection phase when the SXR emission profile spread widely in the inboard-side downstream region. Since the reconnection electric field had only toroidal component in the ST merging case, and large parallel component of the electric field in the inboard-side downstream region served to accelerate electrons along the field lines. In the middle merging phase, the SXR emission was clearly localized on two separatrix arms, which correspond to the magnetic field lines on which the electrons toroidally accelerated at the reconnection point will move. Though high toroidal reconnection electric field was still induced in the downstream region, its parallel component was cancelled by the charge separation mostly due to the electrons' motion.

A test particle calculation was carried out based on the experimentally measured magnetic and electric fields. Here, we assume that the parallel electric field in the downstream region is cancelled in the middle merging phase. The energetic electrons are generated in wide area of the downstream region in the early merging phase, possibly accounting for the broad electron heating. Then, the acceleration occurs only on the reconnection separatrix in the middle merging phase, indicating the localized electron heating near the reconnection point.

Conversion of Electrostatic Bernstein Waves in the SCR-1 Stellarator Using a Full Wave Code

V. I. Vargas-Blanco¹, A. Köhn², R. Solano-Piedra¹, E. Meneses³, D. Jiménez³, A. Garro-Vargas³, F. Coto-Vílchez¹, M. A. Rojas-Quesada¹, D. López-Rodríguez¹, J. Sánchez Castro¹, J. Asenjo¹, and J. Mora¹

¹Plasma Laboratory for Fusion Energy and Applications, Instituto Tecnológico de Costa Rica, Cartago, Costa Rica

²Institut für Grenzflächenverfahrenstechnik und Plasmatechnologie (IGVP), Univ. Stuttgart, Germany

³Advanced Computing Laboratory, Costa Rica National High Technology Center, CENAT, San José, Costa Rica

Corresponding Author: V. I. Vargas-Blanco, ivargas@itcr.ac.cr

The small modular SCR-1 Stellarator ($R = 247.7$ mm, $R/a = 6.2$, $\iota_a = 0.264$) has an ECRH system of 2.45 GHz (5 kW) with an average magnetic field of 41.99 mT [1]. Few studies on conversion of electrostatic Bernstein waves under these conditions have been performed in stellarators [2, 3]. This work presents the results of converting electrostatic Bernstein waves in the SCR-1 stellarator using the full wave code IPF-FDMC [3], taking the 3D magnetic field obtained by VMEC code as input and the experimental electron density profile obtained using a Langmuir probe. New microwave heating scenarios that take the SCR-1's vacuum vessel into account in order to improve the O-X conversion due to reflection of the incoming radiation from the ECRH system are presented. The percentage of single pass O-X mode conversion is around 3%. The design of an antenna with its characteristics and locations according to the SCR-1 viewports is explained. Other important aspects of this work are focussed on the BS-SOLCTRA (Biot-Savart Solver for Compute and Trace Magnetic Fields) code, developed by our research group, and its way to convert it into a parallel and high-performance computing platform. This code allows calculations of the 3D vacuum magnetic field and the visualization of the magnetic flux surfaces at SCR-1. Similarly, the results of the comparison of the flux surfaces measured with an electron beam and different kinds of fluorescent rods with computed flux surfaces by means of the BS-SOLCTRA code are shown. Finally, magnetic and energy diagnostics have been developed with special requirements based on the SCR-1 geometry so the design, data analysis tools and measurement technique are introduced.

References

- [1] V. I. Vargas *et al.*, J. Phys.: Conf. Ser. **591**, 012016 (2015).
- [2] R. Ikeda *et al.*, Phys. Plasmas, **15**, 7 (2008).
- [3] A. Köhn *et al.*, Plasma Phys. Contr. F., **55**, 1 (2013).

Power Coupling of Lower Hybrid Fast Wave in VEST

S.-H. Kim¹, J.-G. Jo², H.-W. Lee³, J.-I. Wang², B.-K. Jung¹, B.-J. Lee³, S.-H. Jeong¹, and Y.-S. Hwang²

¹Korea Atomic Energy Research Institute (KAERI), Daejeon, Republic of Korea

²Seoul National University, Seoul, Republic of Korea

³Kwangjuon University, Seoul, Republic of Korea

Corresponding Author: S.-H. Kim, shkim95@kaeri.re.kr

An efficient heating and current drive in the central or off-axis region of tokamak plasma should be developed for the steady state operation of a tokamak fusion reactor. A fast wave within lower hybrid resonance frequency range (LHFW) could be a scheme for the current drive in a high-density, high-temperature reactor grade plasmas [1, 2]. A proof-of-principle experiment was planned for the LHFW H&CD concept in VEST [3], and a LHFW RF system has been successfully developed and installed in VEST through collaboration between KAERI, KWU, SNU, and KAPRA [4, 5]. The klystron RF power is 10 kW with centre frequency of 500 MHz and bandwidth of 20 MHz. The $N_{||}$ spectrum of the comb-line type travelling wave antenna ranges from 3 to 5 corresponding to the operating frequency. Recently, RF commissioning was started and 10 kW RF power was transmitted to the comb-line antenna in the vacuum after intensive RF vacuum conditioning. About 3.5 kW RF power was transmitted to antenna with plasma and 50–60% of input power was coupled to the plasma. The target plasma was generated with Ohmic power of about 60 kW. The peak plasma current was about 30 kA and the edge electron density varies from LHSW to LHFW launching density with the current evolution. The coupled RF power abruptly increased with the launching densities of LHWs. The driven plasma current by LHFW seems to be less than 1 kA compared to pure Ohmic plasmas. The reproducibility and higher power experiments are progressing. The low driven current may be because that the plasma density window in front of antenna for LHFW propagation into core region is very narrow due to the low toroidal magnetic field of 0.1 T. In addition, the electron temperature and RF power is not as high as for efficient current drive of LHFW. More progressing and detailed experimental results will be presented with analysis based on theory and numerical simulation in the conference.

References

- [1] S.-H. Kim *et al.*, Fusion Eng. Des., **109-111**, 707-711 (2016).
- [2] S.-H. Kim *et al.*, EPJ Web of Conferences, **157**, 03023 (2017).
- [3] K. J. Chung *et al.*, Plasma Sci. Technol., **15**, 244 (2013).
- [4] S.-H. Kim *et al.*, 2017 International Spherical Tokamak Workshop (2017).
- [5] H.-W. Lee *et al.*, Submitted to Fusion Eng. Des., (2017).

Collisional Merging of a Field-Reversed Configuration in the FAT-CM Device

T. Asai¹, J. Sekiguchi¹, T. Takahashi¹, J. Ishiwata¹, N. Ono¹, F. Tanaka¹, A. Hosozawa¹, D. Kobayashi¹, S. Okada¹, H. Gota², T. Roche², S. Dettrick², Y. Mok², M. W. Binderbauer², T. Tajima^{2,3}, M. Inomoto⁴, and T. Takahashi⁵

¹*Nihon University, Tokyo, Japan*

²*TAE Technologies, Inc., Foothill Ranch, CA 92688, USA*

³*University of California Irvine, CA 92697, USA*

⁴*Graduate School of Frontier Science, University of Tokyo, Tokyo, Japan*

⁵*Graduate School of Engineering, Gunma University, Maebashi, Gunma, Japan*

Corresponding Author: T. Asai, asai.tomohiko@nihon-u.ac.jp

Experiments investigating the collisional merging of field-reversed configurations (FRCs) at super-Alfvénic velocity have been successfully initiated in the FAT-CM device at Nihon University. Drastic increase of the excluded-flux leading to the improved confinement performance of FRC has been observed. This process has an important role to realize FRC based high- β reactor core to capture high-energy beam ions and it has been clearly observed by magnetic diagnostics of excluded flux and internal probe array. The experimental results are compared with 2D MHD simulation results computed for the typical condition of the FAT-CM experiments. In order to investigate the collisional merging process of a FRC at super-Alfvénic velocity, the FAT device has recently been upgraded to FAT-CM, consisting of two field-reversed theta-pinch (FRTP) formation sections and the central confinement section. Collisional merging of the two separately translated FRCs causes a conversion of the kinetic energy to mostly thermal ion energy, which contrasts with the spheromak merging dominated by magnetic energy, resulting in an increase of the ion pressure that drastically expands the FRC volume. The confinement chamber of FAT-CM device is made of stainless steel (inner bore is 0.78 m) serving as a flux conserver in the timescale of the translation and merging process. Quasi-static confinement coils (inner diameter of 1.03 m) are placed along the confinement region. Initial FRCs are formed by the FRTP method in two formation sections. The initial FRCs are accelerated by the gradient of the external guide magnetic field and then injected into the confinement chamber. The translated FRCs collide in the middle of the confinement chamber at the relative velocity in the range of 300–400 km/s. By the collisional merging, radial expansion of the plasma is clearly observed and the plasma size, in the quasi-equilibrium phase, increase more than twofold compared with the single translation case. The averaged electron density of the merged FRC is $\sim 2.5 \times 10^{20}/\text{m}^3$, which is ten times higher than the previous experiments performed in C-2U device at TAE. The shape of the simulated FRC agrees with experimental results. This also indicates a successful merging of the FRCs, and resulting in the radial expansion and excluded-flux increase due to the collisional merging, as observed in experiments.

Solenoid-Free Start-Up Utilizing Outer PF Coils with the Help of EBW Preionization and Change of External Inductance in VEST

H. Y. Lee¹, Y. G. Kim¹, S. C. Kim¹, J. G. Jo¹, S. C. Hong¹, Y.-S. Na¹, and Y.-S. Hwang¹

¹*Seoul National University, Seoul, Republic of Korea*

Corresponding Author: H. Y. Lee, brbbebbero@snu.ac.kr

Solenoid free start-up scenario is the way to utilize loop voltage from the evolution of equilibrium field using outer PF coils. Also, it can be expected to be as an attractive start-up scheme in the fusion machines with low aspect ratio since flux from external inductance change can be utilized. The solenoid free start-up experiments using outer PF coils have been conducted in various devices, but the results show the failure of closed flux surface (CFS) formation or low plasma current with sufficient ECH power. With decreasing vertical field, the experiments for formation of CFS shows that improved preionization with EBW enhances the initiated plasma current by lowering plasma resistivity. The CFS is formed successfully when the poloidal field from plasma current exceeds the vacuum vertical field and the quantitative condition for CFS formation has been derived in the consideration of preionization plasma resistivity. The preionization plasma with low resistivity is necessary for CFS formation. The enhanced particle confinement along mirror ratio in TPC is helpful for lowering resistivity of preionization plasma near outboard and EBW collisionless heating makes possible to have lower resistivity of preionization plasma due to the existence of 2nd or 3rd harmonics near outboard. After the successful CFS formation, the plasma current has been demonstrated to be ramped-up with loop voltage from outer PF coils with help of reduced external inductance. The plasma current evolution has been presented with 0D power balance modelling with consideration about force balance along plasma current. The initial plasma current evolution has difficulty due to the size of CFS that causes resistive dissipation. Also, the induction voltage from outer PF coils has limitation that it is not easy to change rapidly due to eddy current from vessel wall and causes increase of vertical field that affects to CFS formation and equilibrium. The solenoid free start-up using outer PF coils must consider the distribution between flux from external inductance and resistive dissipation. The solenoid free start-up scheme utilizing outer PF coils has been suggested considering the condition of CFS formation including the location and minor radius of CFS and resistivity of preionization plasma.

EX

Internal Structure of MHD Fluctuations for Various Current Density Profiles during Current Rise Phase of Ohmic Discharge in VEST

J.-H. Yang¹, S. Kim¹, and Y.-S. Hwang¹

The VEST Team

¹*Seoul National University, Seoul, Republic of Korea*

Corresponding Author: J.-H. Yang, yangban@snu.ac.kr

During the current rise phase of tokamak discharges, evolving current density profiles are associated with the MHD fluctuations that are often held responsible for the confinement degradation, or even disruption, early in the discharge. Moreover, VEST, (Versatile Experiment Spherical Torus) for the NBI heated advanced tokamak regime, adopts the fast current ramp up Ohmic discharge, where the study of the reversed shear q profile and the suppression of this “current rise” fluctuations is needed. Here, we present the internal structure of this fluctuation in accordance to the equilibrium current profiles during the current rise phase of VEST, using data from both the external and the internal magnetic diagnostics.

EX

The internal magnetic probe array, upgraded from the previous model, have been used to both constrain the newly developed EFIT-like equilibrium reconstruction and measure the internal magnetic fluctuation. Because VEST hosts a relatively low temperature plasma, the plasma degradation by the introduction of the internal magnetic probe array into the plasma is less than 10%. The mode number is identified by the toroidal and poloidal Mirnov coil array signals analyzed by the method based on singular value decomposition. During a typical Ohmic discharge in VEST, shot #18452, the plasma current is ramped up very fast with $dI_p/dt < 20$ MA/s and a hollow current profile and a weak shear safety factor profile are formed. In the spectrogram of the outboard midplane Mirnov coil, the modes $n = 1$ and $n = 2$ are observed, spanning modes (2, 1), (3, 1) and (3, 2). As the rate of plasma current rise is slowed down to $dI_p/dt < 10$ MA/s, as in shot #18390, the skin current is diffused in to form a more broad current profile and a positive shear safety factor profile. Here, the mode (2, 1) is suppressed and the mode onset is delayed. We conjecture that this change in the mode structure is related to the attainment of a maximum plasma current of 100 kA in shot #18390, a 25% increase from shot #18452, which is driven with the same loop voltage.

From the internal structure of the instability, it is found that the two peaks of the internal fluctuation amplitude $|\delta B_z|$ are localized around a relevant rational q surface in agreement with the mode structure measured by the external magnetic diagnostics.

Advances in Modelling of Plasma Pedestal Behaviour and ELM Control in ITER Reference Plasma Scenarios

A. Loarte¹, A. R. Polevoi¹, S. D. Pinches¹, T. Weyens¹, Y. Q. Liu², L. Li³,
G. T. A. Huijsmans^{4,5}, J. Artola⁶, D. van Vugt⁵, F. Liu⁷, R. Sanchez⁸,
J.-M. Reynolds-Barredo⁸, V. Tribaldos⁸, S. Y. Medvedev⁹, A. A. Ivanov⁹, and S. Futatani¹⁰

¹International Thermonuclear Experimental Reactor (ITER),
Cadarache Centre, 13108 St. Paul lez Durance, France

²General Atomics, San Diego, CA 92186, USA

³Donghua University, Shanghai 201620, People's Republic of China

⁴Institut de Recherche sur la Fusion par confinement Magnétique (IRFM),
Commissariat à l'énergie atomique (CEA/Cadarache), 13108 St. Paul lez Durance, France

⁵Eindhoven University of Technology, Eindhoven, Netherlands

⁶Physique des Interactions Ioniques et Moléculaires (PIIM), CNRS, Aix-Marseille Université, France

⁷Université Côte d'Azur, Laboratoire J.A. Dieudonné UMR n.7351 CNRS UNS 06108 Nice, France

⁸Universidad Carlos III de Madrid, Madrid, Spain

⁹Keldysh Institute of Applied Mathematics, RAS, Moscow, Russian Federation

¹⁰Centro Nacional de Supercomputación (BSC), Barcelona, Spain

Corresponding Author: A. Loarte, alberto.loarte@iter.org

The achievement of ITER fusion performance is based upon plasma operational scenarios in which the plasma is in the high confinement regime (H-mode) during the burning phase. The fusion power production level is predicted to strongly depend on the values of the pedestal plasma temperature and density on the inner side of the edge transport barrier (ETB). Similarly, the steep edge density and temperature gradients in the ETB are expected to trigger edge localized modes (ELMs) with large associated transient loads on plasma facing components that can severely reduce their lifetime in ITER.

Although an intensive experimental R&D programme in ITER Members' fusion facilities is presently addressing edge plasma stability issues and ELM control, significant uncertainties remain regarding the empirical extrapolation of the experimental results to ITER. Indeed the edge transport barrier plasma properties of ITER plasmas differ significantly from those in present experiments highlighting the need for a modelling based upon extrapolation of results from present experiments to ITER.

In order to provide a firmer physics base to evaluate the edge plasma properties in ITER H-mode plasmas, the ITER Scientist Fellow Network pedestal group has been created. The group is formed by fellow modelling experts from the ITER Members' and ITER Organization staff and carries out a coordinated work programme together with a wider network of collaborators and addresses a range of issues covering edge MHD stability and transport in ITER plasmas, power, particle and impurity fluxes during ELMs, triggering of ELMs by active schemes such as pellet pacing and vertical oscillations and the application of 3D fields for ELM control and their effects on edge stability, transport and rotation.

The paper describes the significant progress in many of these areas that has been achieved through the coordinated work of the group.

Implementation of 3D Effects of the ITER Plasma-Facing Components in a 2D Real-Time Model-Based Approach for Wall Heat Flux Control on ITER

H. Anand¹, R. A. Pitts¹, J. A. Snipes¹, P. C. de Vries¹, L. Zabeo¹, Y. Gribov¹, S. Coda², C. Galperti², L. Kos³, M. Brank³, and G. Simic³

¹*International Thermonuclear Experimental Reactor (ITER), Cadarache Centre, 13108 St. Paul lez Durance, France*

²*Swiss Plasma Center (SPC), École polytechnique fédérale de Lausanne (EPFL), 1015 Lausanne, Switzerland*

³*University of Ljubljana, 1000 Ljubljana, Slovenia*

Corresponding Author: H. Anand, himank.anand@iter.org

A real-time (RT) first wall (FW) heat load control system will be required at a very early stage of ITER plasma operations. The long pulse nature of the device imposes active cooling of all plasma-facing components (PFCs) and thus strict control of surface power flux density at all times. Plasma current ramp-up in limiter configuration on the beryllium FW panels (FWP) is foreseen for all ITER discharges, with a preference for the inner wall surfaces. Limiter phase heat flux densities on the shaped FWP in the vicinity of plasma contact are expected to approach the maximum design values and hence the deposited heat flux must be monitored and carefully controlled. Development of a physics-based and control oriented model, based on real-time (RT) equilibrium reconstruction for implementation into the ITER plasma control system has thus already begun. The model-based approach in the simplest case, describes the heat flux deposited on PFCs as a poloidal flux function with two parameters to be specified by the modeller: the power exhausted across the plasma boundary, P_{SOL} and scrape-off layer (SOL) width, λ_q . A modular, flexible and expandable Matlab/Simulink architecture for the 2D model based approach has been successfully developed, implemented, and verified with DINA scenario data on the Plasma Control System Simulation Platform (PCSSP). An additional module containing weighting factors has also been implemented in the 2D RT model based approach to include the true 3D geometry of the FWP. This is an essential modification if a more realistic value for the true maximum heat flux is to be correctly predicted. Integration of the 3D effect into the algorithm is performed by offline determination of the heat load distribution on the full 3D poloidal sector using a new utility, SMITER, developed at the ITER Organization, in which the SMARDDA field line tracing code has been embedded in a GUI interface permitting import and appropriate meshing of full CAD descriptions of the FW geometry. For each equilibrium, weighting factors associated with the position in the poloidal plane and magnitudes of the peak heat flux are extracted for implementation into the 2D model based approach. The improved RT model is also being experimentally tested and validated on the TCV tokamak using infrared measurements of the central column surface power flux density.

EX

Optimizing the ITER 15 MA DT Baseline Scenario by Exploiting a Self-Consistent Free-Boundary Core-Edge-SOL Workflow in IMAS

F. Köchrl¹, S. D. Pinches², F. J. Casson¹, G. Corrigan¹, Y. Gribov², D. Harting¹, A. A. Kavin³, R. R. Khayrutdinov⁴, S.-H. Kim², P. J. Knight¹, S. V. Kononov⁴, A. Loarte², V. E. Lukash⁴, S. Y. Medvedev⁵, and A. R. Polevoi²

¹*Culham Centre for Fusion Energy (CCFE), Culham Science Centre, Abingdon, UK*

²*International Thermonuclear Experimental Reactor (ITER), Cadarache Centre, 13108 St. Paul lez Durance, France*

³*D. V. Efremov Institute of Electrophysical Apparatus (JSC-NIIEFA), St. Petersburg, Russian Federation*

⁴*National Research Centre "Kurchatov Institute", Moscow, Russian Federation*

⁵*Keldysh Institute of Applied Mathematics, RAS, Moscow, Russian Federation*

Corresponding Author: F. Köchrl, florian.koechl@ccfe.ac.uk

The ability to describe the essential physics and technology elements needed to robustly simulate the operation of ITER is critical to being able to model the plasma scenarios that will run in ITER. The Integrated Modelling & Analysis Suite (IMAS) is used to simulate the 15 MA DT baseline scenario operation, including a description of the plasma evolution from its core up to the plasma facing components respecting the principal engineering limitations of the poloidal field coil system.

The free boundary equilibrium code DINA has been combined with the JINTRAC suite of codes exploiting their full core+edge+SOL+MHD modelling capabilities in an IMAS workflow in open loop coupling. For the first time, the 15 MA/5.3 T DT ITER baseline scenario has been assessed for the entire evolution from the early ramp-up phase (from X-point formation) until the late ramp-down phase (X-point to limiter transition) by means of integrated simulations with consideration of core+edge+SOL transport model assumptions recently validated at JET with time-dependent free boundary plasma geometry and with the pedestal pressure being determined by continuous self-consistent edge MHD stability analysis.

The paper will describe the new IMAS modelling workflow for the fast execution of highly integrated DINA+JINTRAC simulations as well as the results of the ITER 15 MA DT baseline scenario optimization study. Conclusions will be drawn regarding the available operational space and control capabilities as well as observed differences with respect to results obtained in previous modelling studies with less sophisticated workflows and a reduced level of integration.

EX

Robust Burn Control in ITER Under Deuterium-Tritium Concentration Variations in the Fuelling Lines

A. Pajares¹, E. Schuster¹

¹*Lehigh University, Bethlehem, PA 18015, USA*

Corresponding Author: A. Pajares, andres.pajares@lehigh.edu

EX Tight regulation of the burn condition in ITER has been proven possible even under time-dependent variations in the fuel concentration by the use of robustification techniques. One of the most fundamental control problems arising in ITER and future burning-plasma tokamaks is the regulation of the plasma temperature and density to produce a determined amount of fusion power while avoiding possible thermal instabilities. Such problem, known as burn control, will require the development of controllers that integrate all the available actuators in the tokamak. Moreover, the complex dynamics of the burning plasma and the uncertain nature of some of its magnitudes suggest that nonlinear, robust burn controllers will be necessary. Available actuators in the burn control problem are auxiliary power modulation, fuelling rate modulation, and impurity injection. Also, recent experiments in the DIII-D tokamak have shown that in-vessel coil-current modulation can be used for burn control purposes. The in-vessel coils generate nonaxisymmetric magnetic fields that have the capability to decrease the plasma-energy confinement time, which allows for regulating the plasma energy during positive energy perturbations. In this work, in-vessel coil-current modulation is included in the control scheme, and it is used in conjunction with the other previously mentioned actuators to design a nonlinear burn controller which is robust to variations in the deuterium-tritium concentration of the fuelling lines. Furthermore, fuelling rate modulation is not only used to control the plasma density, but also to control the plasma energy if necessary by means of isotopic fuel tailoring. Isotopic fuel tailoring is a particular way of fuelling the burning plasma which allows for reducing the fusion power produced and, therefore, also gives the opportunity to decrease the plasma energy when needed. The model-based nonlinear controller is synthesized from a zero-dimensional model of the burning-plasma dynamics. A nonlinear simulation study is used to illustrate the successful controller performance in an ITER-like scenario in which unknown variations of the deuterium-tritium concentration of the fuelling lines are emulated.

The ITER Plasma Current Termination Phase: Physics Constraints on Control

F. M. Poli¹, P. C. de Vries², Y. Gribov², A. A. Kavin⁶, S.-H. Kim², F. Köchl³, V. Leonov⁴, V. E. Lukash⁴, A. R. Polevoi², R. R. Khayrutdinov⁴, A. A. Teplukhina⁵, and I. Voitsekhovitch³

¹Princeton Plasma Physics Laboratory (PPPL), Princeton, NJ 08540, USA

²International Thermonuclear Experimental Reactor (ITER), Cadarache Centre, 13108 St. Paul lez Durance, France

³Culham Centre for Fusion Energy (CCFE), Culham Science Centre, Abingdon, UK

⁴National Research Centre "Kurchatov Institute", Moscow, Russian Federation

⁵Swiss Plasma Center (SPC), École polytechnique fédérale de Lausanne (EPFL), 1015 Lausanne, Switzerland

⁶D. V. Efremov Institute of Electrophysical Apparatus (JSC-NIIEFA), St. Petersburg, Russian Federation

Corresponding Author: F. M. Poli, fpoli@pppl.gov

Following recent characterization of the plasma termination phase from a multimachine database [1], the ITER termination phase is being analyzed, to define uncertainties due to physics assumptions and to deficiencies in the modelling. Considerable modelling and development has been done on ITER termination scenarios, focussing on specific aspects: magnetic control with transport assumptions [2], or particle exhaust control with assumptions on magnetic control [3]. Because of the high nonlinearity in the plasma response, only time-dependent self-consistent simulations can show whether the proposed termination scheme is robust. None of the available time-dependent equilibrium and transport solvers has a complete and extensive physics scope. However, taken together, these codes offer a wide range of complementary physics models that can be used to identify robust operational ranges for the ITER plasma termination phase. We know from experiments and from extensive vertical stability analysis with DINA that the plasma cross-section and elongation on ITER need to be reduced with current, while at the same time guiding the plasma downward [2]. However, when physics-based models are used for the heating and current drive sources, it is found that the reduction rate of the plasma cross-section in H-mode and the vertical displacement are constrained by the ability of maintaining RF core heating for impurity control and tracking the $q = 2$ surface for NTM control. Based on these preliminary results, the joint modelling activity is looking into: a) level of impurities and their dynamics, b) impurity seeding, c) density decay rate, and d) external power stepping-down. The latter, in particular, needs to be adjusted taking into account fast ion stability, fast ion acceleration by IC waves, core heating for impurity control and stabilization of NTMs in H-mode, and stabilization of ELMs. The goal is to define new limits on the ramp-down schemes that combine long-term known magnetic control constraints for ITER with new constraints imposed by physics-based models, whose availability in time-dependent simulations is progressively becoming available.

References

- [1] P. C. de Vries *et al.*, Nucl. Fus., **58**, 026019 (2018).
- [2] Y. Gribov *et al.*, Nucl. Fus., **55**, 073021 (2015).
- [3] F. Koechl *et al.*, Nucl. Fus., **57**, 086023 (2017).

Energy Confinement and Performance of Pure Helium Plasmas and Helium Seeded Deuterium Plasmas

A. Kappatou¹, P. Manas¹, C. Angioni¹, E. A. Lerche², A. C. C. Sips^{3,4}, T. Pütterich¹, M. G. Dunne¹, R. Neu^{1,5}, C. Giroud⁶, H.-T. Kim⁶, F. Ryter¹, P. A. Schneider¹, C. D. Challis⁶, J. Hobirk¹, I. F. Ferreira Nunes⁷, M. Tsalas⁸, R. M. McDermott¹, K. Cave-Ayland⁶, D. F. Valcarcel⁶, S. Potzel¹, R. Dux¹, L. Frassinetti⁹, E. Delabie¹⁰, S. Saarelma⁶, S. Menmuir⁶, M. Bernert¹, A. Lebschy^{1,5}, and E. Viezzer¹¹

The ASDEX-Upgrade Team, EUROfusion MST1 Team, and JET Contributors

¹Max-Planck-Institut für Plasmaphysik, Garching, Germany

²Laboratory for Plasma Physics, ERM/KMS, Brussels, Belgium

³JET Exploitation Unit, Culham Science Centre, Abingdon, UK

⁴European Commission, Brussels, Belgium

⁵Technische Universität München, Garching, Germany

⁶Culham Centre for Fusion Energy (CCFE), Culham Science Centre, Abingdon, UK

⁷Institute of Plasmas and Nuclear Fusion (IPNF), Instituto Superior Técnico (IST), 1049-001 Lisbon, Portugal

⁸International Thermonuclear Experimental Reactor (ITER),

Cadarache Centre, 13108 St. Paul lez Durance, France

⁹KTH Royal Institute of Technology, Stockholm, Sweden

¹⁰Oak Ridge National Laboratory (ORNL), Oak Ridge, TN 37831, USA

¹¹Universidad de Sevilla, Seville, Spain

Corresponding Author: A. Kappatou, athina.kappatou@ipp.mpg.de

The presence of fusion-produced helium is fundamentally connected to the performance of a fusion reactor. Not only will He ash dilute the fusion fuel if not removed promptly, but the presence of He in a D plasma is reported to negatively affect the plasma confinement [1]. Furthermore, He plasmas are a choice for the ITER non-nuclear phase, but the energy confinement in such plasmas is consistently observed to be $\sim 30\%$ lower than in D plasmas [2, 3].

The negative impact on the performance observed with reactor relevant concentrations of He in D plasmas is demonstrated and compared in baseline scenario plasmas in JET and in plasmas with and without N-seeding in ASDEX-Upgrade (AUG). In both devices, a significant reduction of the plasma stored energy (and normalized confinement factor $H_{98}(y, 2)$) is observed with increasing He concentration. Helium impacts the edge and core plasma profiles in a phenomenologically similar way in the two machines, and also affects the ELM behaviour, and the produced neutrons. However, both the core and edge contribute to the loss of stored energy at AUG, while the core alone is responsible for the loss of stored energy at JET. In both JET and AUG, after applied short He puffs, the confinement is observed to recover at the same rate as the He concentration decays.

Continued...

Additionally, the confinement of pure He plasmas at AUG is studied, demonstrating plasma conditions where confinement in He is the same as in D plasmas. Pairs of L- and H-mode plasmas in He and D have been produced, in which a large variation of the electron to ion heating fraction is obtained using the ECRH and the NBI systems. Two regimes are identified. With strong ECRH and low electron density, the confinement in He is equivalent to that in D. With strong NBI heating, there is a significant degradation of the confinement in He ($\sim 70\%$ of the corresponding D plasma). These observations are theoretically explained. In the core, the stronger impact of zonal flows in ITG turbulence as compared to TEM turbulence breaks the gyro-Bohm scaling in the strong NBI case. At the edge, thermal coupling and the destabilization of ETG modes in He prevent the increase of the ion and electron temperatures.

References

- [1] R. Neu *et al.*, Proc. 35th EPS Conf., (2008).
- [2] F. Ryter *et al.*, Nucl. Fus., **49**, 62003 (2009).
- [3] D. C. McDonald *et al.*, Plasma Phys. Contr. F., **46**, 519 (2004).

Impact of Impurity Seeding on Pedestal Structure in ASDEX-Upgrade and Alcator C-Mod

M. G. Dunne¹, M. L. Reinke², L. Frassinetti³, F. Reimold⁴, J. W. Hughes⁵, B. Lipschultz⁶,
M. Wischmeier¹, and E. Wolftrum¹

The Alcator C-Mod, The ASDEX-Upgrade, and MST1 Teams

¹Max-Planck-Institut für Plasmaphysik, Garching, Germany

²Oak Ridge National Laboratory (ORNL), Oak Ridge, TN 37831, USA

³KTH Royal Institute of Technology, Stockholm, Sweden

⁴Max-Planck-Institut für Plasmaphysik, Greifswald, Germany

⁵Plasma Science & Fusion Center, MIT, Cambridge, MA 02139, USA

⁶York Plasma Institute, University of York, Heslington, UK

Corresponding Author: M. G. Dunne, mike.dunne@ipp.mpg.de

Pedestal data from ASDEX-Upgrade (AUG) and Alcator C-Mod are presented. Scans of impurity content have been performed in both machines, reaching states where the outer divertor is partially or fully detached. The impact of impurity seeding on pedestal structure is compared. In the analyzed scenarios, nitrogen seeding increases the achievable pedestal top pressure in AUG, while excessive seeding leads to a decrease of the pedestal pressure in C-Mod as the outer divertor progresses to a fully detached state. Both of these effects are associated with a shift of the peak edge density gradient location; an inward shift (AUG) allows a higher pedestal pressure, while an outward shift (C-Mod) decreases the stability limit.

The origins of these shifts are analyzed in both machines, paying particular attention to the role of the SOL and the radiation associated with impurity seeding. Data from AUG highlight the importance of high density structures in the high-field side SOL in influencing the peak density gradient location, while the degradation in the C-Mod scans is independent of such a structure. This implies that mitigating these high density structures does not guarantee optimal pedestal and global confinement. Additional scans from AUG altering the heating power, seeded impurity and magnetic geometry (lower single null and quasi-double null) are also presented, demonstrating the dominating effects that the SOL can have on the pedestal. Pedestal modelling using the SOL boundary conditions from experiments is also presented, helping to form an understanding of the leading processes affecting pedestal stability.

Heat Transport Driven by the ITG and TEM Instabilities in the ASDEX-Upgrade Tokamak

F. Ryter¹, C. Angioni¹, M. G. Dunne¹, R. Fischer¹, B. Kurzan¹, A. Lebschy¹, R. M. McDermott¹, W. Suttrop¹, G. Tardini¹, E. Viezzer², and M. Willensdorfer¹

The ASDEX-Upgrade Team

¹Max-Planck-Institut für Plasmaphysik, Garching, Germany

²Universidad de Sevilla, Seville, Spain

Corresponding Author: F. Ryter, ryter@ipp.mpg.de

Turbulence-driven ion heat transport in tokamak H-modes is driven by the ion temperature gradient (ITG) instability, while electron heat transport is driven by the ITG, trapped electron mode (TEM) and/or electron temperature gradient (ETG) instabilities. These three instabilities appear above their respective threshold in normalized temperature gradient (R/LT) and drive transport. We present results on the role of these contributions to heat transport in the ASDEX Upgrade tokamak.

We performed dedicated experiments with neutral beam injection (NBI) which heats both electrons and ions and electron cyclotron resonant heating (ECRH) which heats the electrons. From modulating of the electron temperature with ECRH we deduce the electron heat pulse diffusivity (χ^{HP}) which reflects the stiffness directly and is complementary to the power balance diffusivity (χ^{PB}).

The predicted dependences of the ITG-driven ion heat transport on T_i/T_e and $E \times B$ rotational shear are found: the ITG is clearly more stable for high values of T_i/T_e and/or rotational shear. The ITG threshold itself could not be assessed experimentally with accuracy yet and experiments are foreseen in the near future to improve this situation.

The electron heat flux is partly driven by the ITG, but when increasing the electron heat flux with ECRH above the flux driven by the ITG, the TEM and/or ETG instabilities become unstable which is particularly visible in the modulation data. Indeed, a moderate increase of χ^{PB} and a stronger increase of χ^{HP} above $R/LT_e = 5$ indicates unambiguously that an electron instability (TEM or ETG) develops above this threshold. The stiffness is close to that found in ASDEX-Upgrade for TEM-driven electron heat transport. Below the threshold, χ^{HP} and χ^{PB} exhibit about the same value of $1.5 \text{ m}^2/\text{s}$. This rather high value is attributed to the ITG-driven electron heat transport, in agreement with $\chi^{\text{HP}} \approx \chi^{\text{PB}}$ which reflects the fact that the ITG does not depend on ∇T_e . So far, we have found no indication of an ETG contribution predicted to exhibit a stronger stiffness.

Transport modelling and comparisons of the experimental results with gyrokinetic calculations will be presented for both the ITG and TEM/ETG studies.

EX

The ITER Baseline Scenario Investigated at ASDEX-Upgrade

T. Pütterich¹, O. Sauter², V. Bobkov¹, M. Cavedon¹, M. G. Dunne¹, L. Guimarães³, A. Kappatou¹, P. T. Lang¹, M. J. Mantsinen^{4,5}, R. M. McDermott¹, J. Schweinzer¹, J. Stober¹, W. Suttrop¹, and M. Willensdorfer¹

The EUROfusion MST1 Team and The ASDEX-Upgrade Team

¹Max-Planck-Institut für Plasmaphysik, Garching, Germany

²Swiss Plasma Center (SPC), École polytechnique fédérale de Lausanne (EPFL), 1015 Lausanne, Switzerland

³Institute of Plasmas and Nuclear Fusion (IPNF), Instituto Superior Técnico (IST), 1049-001 Lisbon, Portugal

⁴Centro Nacional de Supercomputación (BSC), Barcelona, Spain

⁵Catalan Institution for Research and Advanced Studies (ICREA), Barcelona, Spain

Corresponding Author: T. Pütterich, thomas.puetterich@ipp.mpg.de

At ASDEX-Upgrade experiments have been performed, in which important features of the ITER baseline (ITER BL) scenario are matched or imitated. A crucial property of the ITER BL scenario is the combination of $q_{95} = 3$ with strong plasma shaping, which leads to ELM frequencies (f_{ELM}) as low as 10 Hz, while the ELMs are very large.

One consequence of the low f_{ELM} is that access to ITER-relevant collisionalities has been hindered as a strong deuterium (D) gas puff is required to control the W concentration. The large D gas puff is also suspected [1] to diminish the energy confinement leading to $H_{98}(y, 2)$ -factors in the range of 0.85 at the relevant $\beta_N = 1.8$, while the Greenwald fraction (f_{GW}) is at relevant levels (~ 0.85). In order to achieve the desired performance, strategies for confinement improvement are investigated, such as increasing $q_{95} = 3$ while decreasing the D gas puff or applying N-seeding. However, these routes do not seem to be able to recover sufficient confinement.

While exploring strategies to go towards low ν^* in the ITER BL scenario, the use of MP-coils yielded a breakthrough allowing for an almost match of ITER collisionalities, i.e., $\nu^*/\nu_{\text{ITER}}^* \approx 3$, and for a clear decoupling of ion and electron heat fluxes. The low collisionalities were obtained by density pump-out of more than a factor of 2, while the confinement is almost not diminished. When extrapolating β_N of such a phase heated with NBI and ICRH to ITER relevant values, sufficient confinement is expected. At the same time ELMs are either very small or even suppressed in some cases.

However, when MP-coils are applied to the high density ITER BL scenario matching f_{GW} instead of ν^* , only a small pump-out effect ($\sim 10\%$) and almost no effect on the ELM size is observed. The density dependence of the MP-coil effectiveness is consistent with [2]. In order to mitigate ELMs at high density, pellet pace making, strong gas puffing or a slight shape or position change proved to be more efficient than the application of MP coils. It is remarkable that corresponding high density discharges in helium behave very similarly, with respect to the negligible MP coil effect and the accomplishment of small ELMs at large neutral helium density.

References

- [1] J. Schweinzer *et al.*, Nucl. Fus., **56**, (2016).
- [2] N. Leutholt *et al.*, Plasma Phys. Contr. F., **59**, (2017).

ELM-Induced Energy and Momentum Transport in ASDEX-Upgrade

E. Viezzzer¹, M. Cavedon², E. Fable², F. M. Laggnier³, R. M. McDermott², A. Kappatou², C. Angioni², P. Cano-Megias¹, D. Cruz-Zabala¹, R. Dux², G. F. Harrer⁴, U. Plank², T. Pütterich², F. Ryter², and E. Wolfrum²

The EUROfusion MST1 Team and The ASDEX-Upgrade Team

¹Universidad de Sevilla, Seville, Spain

²Max-Planck-Institut für Plasmaphysik, Garching, Germany

³Princeton University, Princeton, NJ 08544, USA

⁴Technische Universität Wien, 1040 Vienna, Austria

Corresponding Author: E. Viezzzer, eviezzzer@us.es

Heat and momentum transport play a key role in achieving high confinement in fusion plasmas. Recent advances in the diagnostic capabilities at AUG now allow us to measure the edge profiles on a sub-ms to ms time-scale and with a spatial resolution of less than 5 mm, making it ideal to study the profile recovery after an ELM crash. Here, we present the dynamic behaviour of the energy and momentum transport during edge localized mode cycles at the plasma edge of AUG by combining a comprehensive set of pedestal measurements with interpretive and predictive modelling.

The main ion temperature and toroidal rotation profiles were measured in helium plasmas with unprecedented temporal resolution of 250 μ s. A local increase of T_i close to the separatrix is observed at the ELM onset, thus reducing the gradient in the pedestal, similar to the behaviour in D plasmas [1]. Shortly after the initial separatrix increase, the whole profile drops and then the pedestal starts to build up again. The pre-ELM profile is fully recovered 3–4 ms after the ELM crash. Transport analysis of the ion energy reveals that the ion heat transport is at the neoclassical level before the ELM crash in the region where the edge ion temperature gradient is maximal. Further inwards, the ion heat transport is about a factor of 4–5 above the neoclassical level. The dynamics of the edge ion heat transport during the pedestal build-up after the crash is also consistent with neoclassical theory [2].

Helium plasmas provide the unique opportunity to measure both main ion and impurity flows simultaneously. Compared to the impurity (here nitrogen) toroidal rotation, which exhibits a local minimum at the plasma edge during the inter-ELM phase [3], the edge main ion toroidal rotation has a much less pronounced dip and is rather flat. During the ELM the main ion toroidal rotation in the pedestal drops by about 5–10 km/s. This is in contrast to the behaviour of the impurity toroidal rotation, which shows a flattening of the toroidal dip feature [1]. TRANSP simulations and predictive modelling with ASTRA solving the toroidal momentum balance including diffusion, pinch and external sources are used to quantify how much momentum is transported during the ELM and will be presented.

References

- [1] M. Cavedon *et al.*, Plasma Phys. Contr. F., **59**, 105007 (2017).
- [2] E. Viezzzer *et al.*, Nucl. Fus., **58**, 026031 (2018).
- [3] T. Pütterich *et al.*, Phys. Rev. Lett., **102**, (2009).

From RFX-Mod to RFX-Mod2: Perspectives of the Reversed Field Pinch Configuration

L. Marrelli¹

The RFX-Mod Team

¹*Consorzio RFX, Associazione EURATOM-ENEA sulla Fusione, Padova, Italy*

Corresponding Author: L. Marrelli, lionello.marrelli@igi.cnr.it

EX In this contribution the main achievements of the RFX-Mod reversed field pinch (RFP) are summarized as the basis for a substantial upgrade of the device. The RFX-Mod active MHD control system successfully controlled MHD instabilities such as resistive wall modes and mitigated localized plasma wall interaction by avoiding tearing modes wall-locking. This allowed producing the highest RFP plasma current in the world, up to 2 MA. At high current the RFP plasma, as predicted by the theory, has been observed to self-organize in a global helical shape, where one tearing mode dominates the spectrum. In such regimes secondary tearing modes still play a role, influencing both internal transport and recycling, impurity content and density limit, through the non axi-symmetric distortion of the plasma edge. Passive and active boundary structures surrounding the plasma have a significant effect on tearing modes: the RFXLocking code has been developed to describe such an interaction in RFX-Mod and to investigate RFX-Mod limitations, thus indicating possible improvements of the device. A further reduction of secondary modes is only possible by reducing the plasma-stabilizing shell distance and lowering the resistivity of the first conducting wall surrounding the plasma. Both these requirements are met in the design of the upgraded device (dubbed RFX-Mod2) by removing the present vacuum vessel and modifying the support structure to ensure vacuum tightness. This is expected to reduce the edge magnetic deformation, thus improving PWI and confinement. Nonlinear visco-resistive MHD simulations with a boundary layout that mimics RFX-Mod2 are reported, in order to better quantify the reduction of the nonlinearly saturated amplitude of tearing modes. Some technological issues raised by the implementation of the new magnetic boundary are also discussed

Challenges and Solutions in the Design of RFX-Mod2, a Multiconfiguration Magnetic Confinement Experimental Device

R. Cavazzana¹

The RFX-Mod Team

¹*Consorzio RFX, Associazione EURATOM-ENEA sulla Fusione, Padova, Italy*

Corresponding Author: R. Cavazzana, roberto.cavazzana@igi.cnr.it

The RFX toroidal device (major radius $R = 2.0$ m, plasma minor radius $a = 0.457$ m, shell minor radius $b = 0.535$ m; in operation 1992–1999) was designed to be operated in reversed field pinch (RFP) configuration with a plasma current up to 2 MA. RFX-Mod ($R = 2.0$ m, $a = 0.459$ m, $b = 0.512$ m; in operation 2004–2015) was then equipped with 192 independently driven full coverage saddle coils to achieve the full control of RWM modes and a significant mitigation of tearing modes. The mode and plasma equilibrium control innovations allowed effectively reaching the 2 MA current goal and led to the experimental confirmation of the single helical axis equilibrium of the RFP. Operation in ultralow- q (Ulq) pinch gave new insights on fundamental plasma properties. Experiments performed in circular and shaped tokamak configurations led to the first active stabilization at $q(a) \leq 2$ and recently an H-mode by electrode biasing. Such results suggested the two future main goals of RFX-Mod2 ($R = 2.0$ m, $a = 0.490$ m, $b = 0.512$ m), the upgrade of RFX-Mod: improvement of the RFP confinement and knowledge expansion on a broad spectrum of plasma physics in regimes otherwise not accessible on other devices.

The key ingredient of the new design is the enhancement of the shell-plasma proximity ($b/a = 1.04$), expected to provide a significant reduction of the amplitude of RFP tearing modes. This reduction would lead to the positive cascade effects of magnetic chaos mitigation with confinement improvement, reduced plasma wall interaction and better mode control capability. This choice implied challenging major modifications on the components of the machine close to the plasma: removal of the present vacuum vessel and placement of the existing conducting shell in vacuum as close as possible to the plasma; the vacuum barrier would be then provided by the properly modified toroidal support structure. Innovative solutions have been conceived to fulfil vacuum and electrical requirements of the in-vessel components.

Furthermore a number of corollary modifications are foreseen, aimed at widening the operational space in terms of controlled density, magnetic field topology and the diagnostic capability, in all three different magnetic configurations in the foreseen range of plasma currents: 100 kA–2 MA RFP, 40–180 kA tokamak, 20–800 kA Ulq.

High Density and High Performance Operation with Pellet Injection in W7-X

S. A. Bozhenkov¹, J. Baldzuhn¹, Y. O. Kazakov², H. P. Laqua¹, C. Brandt¹, K. J. Brunner¹, H. Damm¹, G. Fuchert¹, M. Hirsch¹, U. Höfel¹, M. W. Jakubowski¹, J. Knauer¹, G. Kocsis⁴, R. König¹, A. Langenberg¹, S. Lazerson³, K. J. McCarthy⁵, E. Pasch¹, N. Pablant³, N. Panadero Alvarez⁵, K. Rahbarnia¹, J. C. Schmitt⁶, H. Thomsen¹, G. A. Wurden⁷, D. Zhang¹, T. Sunn Pedersen¹, and R. C. Wolf¹

The W7-X Team

¹Max-Planck-Institut für Plasmaphysik, Greifswald, Germany

²Laboratory for Plasma Physics, ERM/KMS, Brussels, Belgium

³Princeton Plasma Physics Laboratory (PPPL), Princeton, NJ 08540, USA

⁴Wigner Research Center, Association EURATOM, Budapest, Hungary

⁵Centro de Investigaciones Energéticas, Medioambientales y Tecnológicas (CIEMAT), Madrid, Spain

⁶Auburn University, Auburn, AL 36849, USA

⁷Los Alamos National Laboratory (LANL), Los Alamos, NM 87545, USA

Corresponding Author: S. A. Bozhenkov, sergey.bozhenkov@ipp.mpg.de

EX In this contribution we present details of recent W7-X pellet injection experiments and discuss properties of the achieved plasmas. Hydrogen pellet injections allowed raising the electron density above $1.2 \times 10^{20}/\text{m}^3$ and to establish: i) operation above the cut-off for the X2 polarization of the 140 GHz electron cyclotron resonance heating (ECRH); ii) stable divertor heat flux detachment; iii) plasmas with the diamagnetic energy above 1 MJ. In the latter case, a series of pellets raised the electron density to almost $10^{20}/\text{m}^3$ in a hydrogen discharge heated by X2 ECRH with the total power stepped from 2.7 MW to 5 MW. These electron densities are sufficiently high for electron and ion temperatures to equilibrate and to cause a change in the radial electric field. In the reheat phase after the pellet injection, ion temperatures above 3.5 keV could be reached with the ECRH only and a significant plasma pressure is achieved. The volume averaged $\langle \beta \rangle$ is about 1%, whereas the peak value β_0 is about 3.5%. The diamagnetic energy of about 1.1 MJ corresponds to confinement times above 0.2 s. In the middle of the high energy phase, a sudden crash by about 150 kJ is observed by a number of diagnostics, with an inversion radius present in the ECE and soft X-ray signals. These β values allow for the first time the analysis of the MHD stability and the validation of the Shafranov shift optimization. High central β values are also required for the improved confinement of fast ions.

A further improvement of the plasma performance can be achieved by a further increase of the electron density, which requires ECRH heating in the O2 polarization, as the electron densities are already close to the X2 cut-off. To use the full available ECRH power of 7 MW in the O2 polarization a scenario with a switch of the polarization during the discharge has to be implemented. Such a scenario was successfully tested with initially helium target plasma, because of an easier density control. The hydrogen pellet injection was used to raise the density above the X2 cut-off and to maintain it at this high level for more than half a second. In the second half of the campaign such a scenario will be attempted for hydrogen target plasmas.

Plasma Dynamics and Transport Studies in Wendelstein 7-X

O. Grulke¹

The W7-X Team

¹*Max-Planck-Institut für Plasmaphysik, Greifswald, Germany*

Corresponding Author: O. Grulke, grulke@ipp.mpg.de

A primary goal of Wendelstein 7-X (W7-X) operation is to demonstrate stationary, long pulse discharges at fusion-relevant plasma densities and temperatures. Studies on the behaviour and the control of impurity ions originating from plasma-wall-interaction with the divertor and other plasma facing components is a crucial issue potentially leading to a thermal collapse and dilution of the fuel. W7-X had been equipped with a bolometer diagnostic, the VUV/EUV survey spectrometer system HEXOS, a soft X-ray camera array and a pulse height analysis system as well as two imaging Johann X-ray spectrometers. To distinguish between diffusive and convective impurity transport, a laser blow-off system as transient impurity source was installed at W7-X. In order to characterize the transport properties, the experimental results are compared to the transport code STRAHL. Since W7-X is optimized with respect to neoclassical transport, it is expected that turbulence transport plays a significant role in the regulation of radial particle and heat transport in the core and edge plasma. Fully-nonlinear gyrokinetic simulations in the three-dimensional W7-X magnetic field geometry indicate that turbulence is dominated by ion temperature gradient driven modes with an amplitude pattern which forms relatively narrow poloidal stripes on the W7-X flux surface. Key diagnostics are a phase-contrast imaging diagnostic (PCI) measuring core plasma density fluctuations, radial and poloidal correlation ECE systems for the diagnostics of electron temperature fluctuations, and a set of correlation and Doppler reflectometry systems, which provide edge poloidal flows and density fluctuations. The experimental programme has focussed on the comparison to gyrokinetic GENE simulations. Closely related to the plasma profiles is the question of the stability of the plasma state. In magnetic configurations with co-ECCD (i.e., the bootstrap current and the driven current are coaligned), sudden drops in core temperature (measured by the ECE diagnostic), diamagnetic energy, Mirnov diagnostic and X-ray cameras have been observed. The ECCD-induced crashes repeat on a time scale of several ms to seconds, depending on the amplitude of the driven current. Combined data analysis supported by modelling activity has been started to improve the understanding of the mechanism(s) behind these events.

EX

IST Contributions to the ASDEX-Upgrade Edge and Divertor Physics Using Microwave Reflectometry

C. Silva¹, D. Aguiam¹, M. Bernert², G. D. Conway², L. Gil¹, B. Gonçalves¹, L. Guimarães¹, T. Happel², S. Heuraux³, P. Manz², M. E. Manso¹, V. Nikolaeva¹, J. J. Santos¹, E. Seliunin¹, A. Silva¹, F. da Silva¹, U. Stroth², J. Vicente¹, and E. Wolfrum²

The ASDEX-Upgrade Team and EUROfusion-MST1 Team

¹*Institute of Plasmas and Nuclear Fusion (IPNF), Instituto Superior Técnico (IST), 1049-001 Lisbon, Portugal*

²*Max-Planck-Institut für Plasmaphysik, Garching, Germany*

³*Institut Jean Lamour, Université de Lorraine, CNRS, Nancy, France*

Corresponding Author: C. Silva, csilva@ipfn.ist.utl.pt

Information of the plasma density is essential for the study and operation of magnetically confined fusion devices. Microwave reflectometry appears as an attractive diagnostics due to its high temporal and spatial resolution and its application to profile as well as fluctuation measurements.

The microwave reflectometry systems developed by IST for ASDEX-Upgrade consist of: i) multiband frequency modulated continuous wave (FMCW) O-mode reflectometer with the unique capability of providing simultaneous profile and fluctuations measurements on the high-field side (HFS) and low-field side (LFS), making it the ideal diagnostic for poloidal asymmetry studies; ii) fast frequency hopping O-mode reflectometer used to obtain more detailed information on density fluctuations at the LFS; and iii) A multichannel X-mode reflectometry diagnostic recently installed to measure the edge density profile in front of the ICRF antenna.

This contribution presents an overview of the scientific results obtained on ASDEX-Upgrade where the different reflectometry systems are used in a complementary way in order to address some of the key issues under investigation in this device. Experimental results will be presented on topics such as: i) Influence of the high-field side density front on the midplane density profiles; ii) Edge turbulence in different states of divertor detachment; iii) Edge instabilities across the L-H transition and in H-mode; iv) Understanding density profiles in front of the ICRH antenna; v) Synthetic reflectometry diagnostic; and vi) Real-time plasma position control. The experimental results obtained demonstrate that the IST reflectometry systems provide a valuable contribution to a better understanding of important physics issues such as pedestal instabilities, SOL turbulence, dynamics of the density profiles and connection between midplane and divertor conditions. Different upgrades are under development that will provide uniquely flexible diagnostics for combined profile and fluctuations measurements particularly relevant for edge instabilities and turbulence studies.

Characterization of Advanced Concepts for First Wall Materials by Plasma Exposure in the Linear Plasma Device PSI-2

B. A. Unterberg¹, J. W. Coenen¹, S. Antusch², C. Broeckmann³, H. Gietl⁴, F. Klein¹, A. Kreter¹, R. Krug¹, C. Linsmeier¹, Y. Mao¹, A. Litnovsky¹, Y. Martynova¹, S. Möller¹, R. Neu⁴, G. Pintsuk¹, M. Rasinski¹, M. Rieth², J. Schmitz¹, H. Riesch⁴, M. Wirtz¹, and T. Wegener¹

¹Forschungszentrum Jülich, Jülich, Germany

²Karlsruhe Institute of Technology (KIT), Karlsruhe, Germany

³Lehrstuhl für Werkstoffanwendungen im Maschinenbau, RWTH Aachen, 52062 Aachen, Germany

⁴Max-Planck-Institut für Plasmaphysik, Garching, Germany

Corresponding Author: B. A. Unterberg, b.unterberg@fz-juelich.de

Tungsten is envisaged as plasma-facing material in fusion reactors because of its small tritium retention and low erosion rate as well as its high melting point and high thermal conductivity. However, its intrinsic and operation-induced brittleness and the unacceptably high oxidation rate at high temperatures pose challenges for manufacturing, component lifetime and safety. The development of new advanced material concepts such as new tungsten alloys and composites produced via powder injection molding, self-passivating tungsten alloys produced via field assisted sintering technology and fibre reinforced tungsten composites produced by powder metallurgy or chemical vapour deposition, may help to overcome these issues.

To support a fast route for production of plasma facing components, the characterization of these advanced materials under fusion relevant loading conditions is needed. Plasma exposure in linear plasma devices under synergistic particle and transient heat loads offers the opportunity to investigate the plasma compatibility of the new material concepts at an early stage of development.

In this contribution, we report on first experiments in the linear plasma device PSI-2 to assess erosion rates, fuel retention and damage thresholds of advanced tungsten based alloys and composites in deuterium and mixed deuterium-helium and argon/neon plasmas. Under these conditions, advanced material concepts based on tungsten do not show significantly degraded plasma compatibility with respect to reference tungsten material.

SOL Transport and Filamentary Dynamics in High Density Tokamak Regimes

N. Vianello¹, D. Carralero^{2,3}, C. K. Tsui^{5,4}, V. Naulin⁶, M. Agostini¹, J. A. Boedo⁵, B. Labit⁴, C. Theiler⁴, D. Aguiar⁷, S. Allan⁸, M. Bernert², S. Costea⁹, I. Cziegler¹⁰, H. De Oliveira⁴, J. Galdon-Quiroga¹¹, G. Grenfell¹, A. Hakola¹², C. Ionita⁹, H. Isliker¹³, A. N. Karpushov⁴, J. Kovacic¹⁴, B. Lipschultz¹⁰, R. Maurizio⁴, K. G. McClements⁸, F. Militello⁸, J. Olsen⁶, J. J. Rasmussen⁶, T. Ravensbergen¹⁵, H. Reimerdes⁴, B. Schneider⁹, R. Schrittwieser⁹, M. Spolaore¹, K. Verhaegh¹⁰, J. Vicente⁷, N. R. Walkden⁸, W. Zhang², and E. Wolfrum²

The ASDEX-Upgrade, TCV-, and EUROfusion MST1 Teams

¹Consorzio RFX, Associazione EURATOM-ENEA sulla Fusione, Padova, Italy

²Max-Planck-Institut für Plasmaphysik, Garching, Germany

³Centro de Investigaciones Energéticas, Medioambientales y Tecnológicas (CIEMAT), Madrid, Spain

⁴Swiss Plasma Center (SPC), École polytechnique fédérale de Lausanne (EPFL), 1015 Lausanne, Switzerland

⁵University of California San Diego, CA 92093, USA

⁶Technical University of Denmark (DTU), Copenhagen, Denmark

⁷Institute of Plasmas and Nuclear Fusion (IPNF), Instituto Superior Técnico (IST), 1049-001 Lisbon, Portugal

⁸Culham Centre for Fusion Energy (CCFE), Culham Science Centre, Abingdon, UK

⁹Institute for Ion Physics and Applied Physics, University of Innsbruck, Innsbruck, Austria

¹⁰York Plasma Institute, University of York, Heslington, UK

¹¹Universidad de Sevilla, Seville, Spain

¹²VTT Technical Research Centre of Finland Ltd., Espoo, Finland

¹³Aristotle University of Thessaloniki, Thessaloniki 541 24, Greece

¹⁴Jozef Stefan Institute, 1000 Ljubljana, Slovenia

¹⁵FOM Institute DIFFER, Association EURATOM-FOM, Nieuwegein, Netherlands

Corresponding Author: N. Vianello, nicola.vianello@igi.cnr.it

Addressing the role of scrape off layer filamentary transport is a subject of intense studies in fusion science. Intermittent structures dominate transport in L-Mode and strongly contribute to particle and energy losses in H-mode. The role of convective radial losses has become even more important due to its contribution to the shoulder formation in L-Mode, describing the progressive flattening of the density scrape off layer profile at high density [1–3]. Investigation of this process revealed the strong relationship between divertor conditions and the upstream profiles, mediated by filaments dynamics which varies according to the downstream conditions. Preliminary investigations suggested that similar mechanisms occur in H-Mode [1] and that filaments contribute the SOL transport in H-mode density limit (HDL) as well [4]. The present contribution will report on results obtained on ASDEX-Upgrade and TCV tokamaks, to address the role of filamentary transport in high density regimes both in L- and H-Mode. The combined results enlarge the operational space, from a device with a closed divertor, metallic first wall and cryogenic pumping system to a carbon machine with a completely open divertor. The mechanism of shoulder formation and the role of filaments have been tested against variation of plasma current, magnetic configuration (single and double null plasmas), and divertor neutral densities, through modification of cryopump efficiency. At constant magnetic field the density decay length increases with filament-size independently of the plasma current for both machines in L-mode, consistently with the fact that upstream profiles and divertor neutral pressure exhibit the same trend with normalized Greenwald fraction.

Continued...

In H-Mode fuelling is insufficient to cause flattening of SOL profiles in the inter-ELM phases since large neutral pressure is needed. Consistently inter-ELM blob size in AUG are found larger whenever the cryopumps is switched off. The resulting picture suggests a complex relationship between divertor and upstream profiles, where filaments are modified by divertor conditions as well as by neutral particles interaction.

References

- [1] D. Carralero *et al.*, Nucl. Fus., **57**, 056044 (2017).
- [2] F. Militello *et al.*, Nucl. Fus., **56**, 016006 (2016).
- [3] N. Vianello *et al.*, Nucl. Fus., **57**, 116014 (2017).
- [4] M. Bernert *et al.*, Plasma Phys. Contr. F., **57**, 014038 (2014).

Helical Plasma-Wall Interaction in the RFX-Mod: Effects of High- n Mode Locking

P. Scarin¹, M. Agostini¹, G. Spizzo¹, and P. Zanca¹

The RFX-Mod Team

¹*Consorzio RFX, Associazione EURATOM-ENEA sulla Fusione, Padova, Italy*

Corresponding Author: P. Scarin, paolo.scarin@igi.cnr.it

The edge of toroidally confined plasmas can be characterized by the presence of magnetic perturbations (MP) with helicity m/n , with m and n the poloidal and toroidal mode numbers, respectively. In the reversed field pinch (RFP) RFX-Mod device ($R = 2$ m, $a = 0.46$ m), in high-current discharges ($I_p > 1$ MA, $n/n_G < 0.3$), an almost monochromatic magnetic spectrum spontaneously develops, with $m/n = 1/7$ the dominant mode rotating at a toroidal frequency of ~ 20 Hz. This mode produces a helical equilibrium called quasi-single helicity (QSH). In this new equilibrium, which stands apart from the standard, chaotic RFP state, also the shape of the edge plasma is influenced, with a helical $1/7$ plasma wall interaction (PWI). Were the QSH perfectly monochromatic, the edge would show a helical scrape-off layer (SOL) with good confinement properties, as shown in previous works on RFX. Unfortunately, the QSH is disturbed by the presence of high toroidal harmonics with $7 < n < 20$ ("secondary modes"). These secondary modes, with amplitude one order of magnitude smaller than the dominant $n = 7$ one, interact each other with a constructive interference, called mode or phase locking: the result is a local radial magnetic deformation Δ_{sec} that can be comparable to the dominant one, $\Delta_{1/7}$, due to the $1/7$ mode. From the point of view of particle transport, the presence of the phase locking translates in a localized decrease ("hole") in the helical pattern of the connection length to the wall: L_{cw} . This happens because magnetic field lines, in the vicinity of the locking, are deformed in large poloidal lobes (homoclinic tangles) hitting the plasma-facing components (PFCs), a mechanism similar to the toroidal "fingers" observed in tokamak divertors during RMP application.

A smoother magnetic boundary is expected in the upgraded RFX-Mod, where the magnetic deformation decreases by a factor 2–3. Initial estimates show that the local "hole" of L_{cw} should be strongly reduced by halving the secondary mode amplitude: this is a promising perspective for the RFP helical state performance.

EX

The Effects of Magnetic Topology on the SOL Island Structure and Turbulence Transport in the First Divertor Plasma Operation of W7-X

S. C. Liu^{1,2}, Y. Liang^{1,2}, P. Drews², C. Killer³, G. S. Xu¹, H. Q. Wang¹, X. Q. Wu¹, A. Knieps², X. Han^{1,2}, D. Höschen², A. Krämer-Flecken², D. Nicolai², G. Satheeswaran², A. Alonso³, J. Q. Cai^{1,2}, A. Charl², J. Cosfeld², G. Fuchert³, Y. Gao², J. Geiger³, O. Grulke³, M. Henkel², M. Hirsch³, U. Höfel³, M. W. Jakubowski³, R. König³, O. Neubauer², E. Pasch³, K. Rahbarnia³, M. Rack², N. Sandri², S. Sereda², B. Schweer², E. H. Wang^{1,2}, Y. L. Wei², G. Weir³, T. Windisch³, and S. Xu^{1,2}

The W7-X Team

¹*Institute of Plasma Physics, Chinese Academy of Sciences, Hefei, Anhui, People's Republic of China*

²*Institute of Energy and Climate Research, Forschungszentrum Jülich, Jülich, Germany*

³*Max-Planck-Institut für Plasmaphysik, Greifswald, Germany*

Corresponding Author: S. C. Liu, lshch@ipp.ac.cn

Wendelstein 7-X (W7-X) was operated successfully with the first divertor plasma in the operation phase 1.2a (OP1.2a). A new combined probe head, which consists of Langmuir probe pins, Mach probe, ion sensitive probe (ISP), differential coil and a triaxial pick-up coil, is able to measure the edge plasma profiles (T_e , n_e , ϕ_f , $M_{||}$), magnetic field, poloidal and radial turbulence structures. The plasma parameters in three magnetic configurations (KJM, EJM, FTM) are measured by the new combined probe head, which are in good agreement with the island structure calculated by field line tracer. In configuration of EJM, the floating potential has a negative value around the radial region from 6.065 m to 6.071 m, where the island centre is located at $R = 6.068$ m and $R_{LCFS} = 6.035$ m along the path of probe. Within this region, the electron pressure reveals a platform, the parallel Mach number exhibits a symmetric profile, and the radial particle flux driven by turbulence reduces to a relatively low level. However, outside this region the particle flux is extremely high on both sides. The high particle flux is dominated by the broadband turbulence between 80 to 120 kHz, while the inner radial region with low particle flux is driven by the turbulence below 25 kHz. It should be noticed that the high turbulent particle flux is located in the region with large gradient of electron density, indicating that the transport could be driven by the instability caused by density gradient. Additionally, a large positive floating potential is observed in all the three configurations, which has strong dependence on line integrated density. The mechanism of this positive floating potential has been studied with a simple model, suggesting a large gradient of parallel electron density between upstream and divertor region. In this work, the turbulence modes and their propagations are compared for these three magnetic configurations.

EX

3D Heat and Particle Fluxes in Wendelstein 7-X

M. W. Jakubowski^{1,2}, P. Drewelow¹, Y. Gao³, K. Hammond¹, M. Endler¹, S. Masuzaki⁴,
H. Niemann¹, A. Ali¹, S. Brezinsek³, F. Effenberg⁵, C. Killer¹, M. Kobayashi⁴,
M. Krychowiak¹, R. König¹, S. Lazerson⁶, T. Morisaki⁴, M. Otte¹, A. Puig Sitjes¹,
L. Rudischhauser¹, P. Sinha¹, O. Schmitz⁵, T. Sunn Pedersen¹, M. Ślęczka², and
G. A. Wurden⁷

The W7-X Team

¹Max-Planck-Institut für Plasmaphysik, Greifswald, Germany

²University of Szczecin, Szczecin, Poland

³Forschungszentrum Jülich, Jülich, Germany

⁴National Institute for Fusion Science (NIFS), Toki, Gifu, Japan

⁵University of Wisconsin-Madison, Madison, WI 53706, USA

⁶Princeton Plasma Physics Laboratory (PPPL), Princeton, NJ 08540, USA

⁷Los Alamos National Laboratory (LANL), Los Alamos, NM 87545, USA

Corresponding Author: M. W. Jakubowski, marcin.jakubowski@ipp.mpg.de

Many present and future large magnetic fusion experiments need to consider the 3D topology of the heat and particle exhaust either due to application of external magnetic perturbations to mitigate type-I ELMs or because it is typically inherent to the magnetic configuration of the device (e.g., LHD or W7-X). In both cases, the scrape-off layer forms heterogeneous 3D structures of field lines with different connection lengths. A key question to future and present devices is in how far the presence of the 3D boundary affects the plasma-wall interaction when toroidal symmetry is no longer preserved. W7-X in its recent campaign with an uncooled fine-grain graphite divertor investigated for the first time in full detail a concept of an island divertor, which uses intrinsic large, low resonance island chains at the plasma edge to form heat and particle exhaust channels. The measured strike line width is up to 10 cm with its 3D geometry strongly depending on the magnetic configuration. Similar findings are observed at LHD, which is typical for any device with a stochastic boundary independent if it is a tokamak or a stellarator.

In steady state operation, assumptions that power loads follow the periodicity of the device cannot be made, therefore 10 high-resolution infrared/visible systems are installed to monitor the heat and particle fluxes over the whole divertor surface. We have developed new methods to characterize the local and global heat and particle loads based on recent experimental observations, e.g., by projecting the measured heat flux onto the geometry of the islands forming island divertor. The energy of particles deposited at the strike line varies strongly with plasma density as shown by floating potential. At very low densities a strong negative potential (< -60 V) has been measured by divertor Langmuir probes, whereas at higher densities it goes even slightly positive. In addition, the electron temperatures at the strike line vary strongly depending on the plasma parameters from below 5 eV during divertor heat flux detachment to ~ 100 eV at very low plasma collisionalities.

The data from LHD, W7-AS and W7-X shows that the measured heat and particle flux patterns are rather sensitive to magnetic configuration, changes in finite plasma β and arising toroidal currents.

Strategy and Optimization of Wall Conditioning at the Wendelstein 7-X Stellarator

R. Brakel¹, S. Brezinsek², A. Dinklage¹, J. Fellinger¹, A. Gorjaev^{3,4}, H. Grote¹, R. König¹, H. P. Laqua¹, T. Stange¹, O. Volzke¹, and T. Wauters³

The W7-X Team

¹Max-Planck-Institut für Plasmaphysik, Greifswald, Germany

²Institute of Energy and Climate Research, Forschungszentrum Jülich, Jülich, Germany

³Laboratory for Plasma Physics, ERM/KMS, Brussels, Belgium

⁴Ghent University, 9000 Ghent, Belgium

Corresponding Author: R. Brakel, rudolf.brakel@ipp.mpg.de

Wall conditioning in fusion devices is prerequisite to provide controlled boundary conditions for operation and to achieve high performance plasmas. Major issues are to achieve low outgassing, low particle recycling and a low impurity level. Implementation and optimization of a systematic wall conditioning strategy was a major issue during the second operation campaign at the superconducting Wendelstein 7-X stellarator. W7-X was equipped with a graphite divertor and a first wall of stainless steel and graphite surfaces. Initial conditions for the campaign were provided by baking at 150°C which removed water and higher hydrocarbons. Intense hydrogen glow discharge cleaning (GDC) reduced residual impurities, such as CO and CH₄. Final He-GDC removed hydrogen from the surfaces. Generally, the length of He-GDC was minimized to reduce sputtering at metal surfaces and redistribution of sputtered material.

Since the magnetic field is continuously activated, GDC cannot be applied between plasma discharges but only before or after the experimental time-of-day, when the field is deactivated. Instead, microwave based methods using ECRH are used and continuously optimized for conditioning between plasma discharges. This comprises pulse trains of intermittent short ECRH discharges with pumping intervals as well as single ECRH discharges at low density, both being operated in He. Following this strategy stationary plasma discharges have been achieved lasting, for example, 25 s at 3 MW heating power and constant density of $3 \times 10^{19}/\text{m}^3$. The pulse length was only limited by the admitted heating energy.

The progress of wall conditioning was monitored throughout the campaign by the normalized outgassing after plasma discharges. It decreased with accumulated discharge time by two orders of magnitude. In the next campaign boronization will be available which is expected to further reduce the impurity level and particle recycling.

Characterization of the W7-X Scrape-Off Layer Using the Multipurpose Manipulator

C. Killer¹, O. Grulke¹, P. Drews², A. Knieps², S. Liu², M. Henkel², J. Cai², D. Nicolai², and G. Satheeswaran²

The W7-X Team

¹Max-Planck-Institut für Plasmaphysik, Greifswald, Germany

²Institute of Energy and Climate Research, Forschungszentrum Jülich, Jülich, Germany

Corresponding Author: C. Killer, carsten.killer@ipp.mpg.de

Wendelstein 7-X (W7-X) recently concluded its first operation phase (OP1.2a) featuring an island divertor. In this concept, the heat and particle exhaust to the divertors is governed by intrinsic 3D magnetic islands at the plasma edge. In order to establish high performance plasmas with safe divertor operation, a comprehensive understanding of the island divertor physics is required, for which in turn thorough studies of the plasma properties and dynamics within the islands are essential. The multipurpose manipulator (MPM), a carrier system for probe heads mounted at the outboard midplane of W7-X, is a key diagnostic for the characterization the W7-X scrape-off layer. Being a multiuser platform, it served various scientific aspects during OP1.2a, including different electric and magnetic probes, plasma-surface interaction studies, hydrogen fuelling and impurity injection.

Characterization of the SOL by the MPM mostly relies on the use of reciprocating electric probes which can perform radial fast plunges through a magnetic island up the last closed flux surface. The fundamental quantities inferred from probe measurements (e.g., radial profiles of density, electron temperature, plasma flows, electric fields and potentials) already allow inferring conclusions on the magnitude and spatial distribution of parallel heat and particle transport to the divertor. Employing, in addition, spatially distributed arrays of probes, we obtained insight into the dynamics and propagation of turbulent fluctuations and the associated (perpendicular) fluctuation-induced transport.

Typical fundamental plasma parameters that have been obtained using the MPM are electron temperatures up to 100 eV and densities up to $1 \times 10^{19}/\text{m}^3$ with a strong dependence on operation (e.g., heating power) and core plasma parameters (e.g., density). Furthermore, the complex magnetic field topology in the large configuration space of W7-X is found to play an important role for the edge plasma profiles. Hence, cross-checks with other SOL diagnostics are used for both validation of results as well as identification of local effects (e.g., due to the island structure).

Measurement and Modelling of Magnetic Configurations to Mimic Overload Scenarios in the W7-X Stellarator

J. D. Lore¹, H. Hölbe², J. Boscary³, P. Drewelow², F. Effenberg⁴, H. Frerichs⁴, J. Geiger², J. H. Harris¹, M. W. Jakubowski², S. Lazerson⁵, A. LeViness⁶, A. Lumsdaine¹, H. Niemann², J. C. Schmitt⁷, and G. A. Wurden⁸

The W7-X Team

¹Oak Ridge National Laboratory (ORNL), Oak Ridge, TN 37831, USA

²Max-Planck-Institut für Plasmaphysik, Greifswald, Germany

³Max-Planck-Institut für Plasmaphysik, Garching, Germany

⁴University of Wisconsin-Madison, Madison, WI 53706, USA

⁵Princeton Plasma Physics Laboratory (PPPL), Princeton, NJ 08540, USA

⁶University of Greifswald, Greifswald, Germany

⁷Auburn University, Auburn, AL 36849, USA

⁸Los Alamos National Laboratory (LANL), Los Alamos, NM 87545, USA

Corresponding Author: J. D. Lore, lorejd@ornl.gov

Experiments were performed in short pulse operation (OP1.2) on the Wendelstein 7-X (W7-X) stellarator using a set of five magnetic configurations that were designed to mimic the topology and resultant divertor fluxes of a high-power long-pulse scenario that is predicted to cause component overload. These experiments demonstrated the capability of edge transport simulations to accurately predict the location and relative magnitude of wetted areas on divertor and baffle components, as well as the ability to mimic the effects of otherwise inaccessible operational conditions (toroidal current, significant β) using the magnetic coil set. The overload scenario is predicted to occur in the actively cooled divertor operational phase (OP2) of W7-X, in configurations where the toroidal current is evolution (over ~ 100 s) causes the edges of the primary divertor components along the pumping gap to receive a load in excess of the 5 MW/m² rating. The pulse length and energy input limitations of the nonactively-cooled operational phases of W7-X prohibit direct access to the overload scenario. To validate the predictions of the heat flux patterns and magnitude, and to establish baseline measurements for comparison before two scraper element components are installed, a set of five configurations were designed to mimic the effects of finite plasma β and toroidal current on the magnetic topology and flux patterns. The mimic configurations correspond to five values of the OP2 net toroidal current as it evolves from 0 to 43 kA, including the peak overload case of 224 kA. Measurements of the divertor heat fluxes, H $_{\alpha}$ emission, and neutral pressure were obtained in each configuration with 2 MW of input power and hydrogen and helium as working gasses. In the steady-state and peak overload mimic configurations, density and power scans were performed. The heat flux patterns are well described by predictions from both field-line diffusion and higher fidelity EMC3-EIRENE simulations, indicating that the approach of mimicking inaccessible OP2 configurations is successful and that rapid diffusion-type calculations are valid for approximating fluxes. These results improve confidence in the predictions for advanced operation of W7-X, and more broadly, in the ability to predict the heat flux patterns in stellarator divertors.

Impact of the 3D Geometry from Nonaxisymmetric Magnetic Perturbations on the Local Edge Stability in ASDEX-Upgrade

M. Willensdorfer¹, T. B. Cote², C. C. Hegna², W. Suttrop¹, F. Orain¹, S. S. Denk¹,
M. G. Dunne¹, R. Fischer¹, L. Giannone¹, C. J. Ham³, A. Kirk³, D. A. Ryan³,
E. Strumberger¹, N. Wang⁴, and H. Zohm¹

The EUROfusion MST1 Team and The ASDEX-Upgrade Team

¹Max-Planck-Institut für Plasmaphysik, Garching, Germany

²University of Wisconsin-Madison, Madison, WI 53706, USA

³Culham Centre for Fusion Energy (CCFE), Culham Science Centre, Abingdon, UK

⁴AET, SEEE, Huazhong University of Science and Technology, Hubei, People's Republic of China

Corresponding Author: M. Willensdorfer, mwillens@ipp.mpg.de

One method to mitigate or even suppress the repetitive impulsive energy loss due to edge localized modes (ELMs) is the application of externally applied nonaxisymmetric magnetic perturbation (MP)-fields.

In high confinement mode (H-mode) plasma, these externally applied MP-fields excite marginally stable ideal kink modes at the edge, which amplify the MPs. These kink modes cause a helically symmetric displacement of the plasma boundary, which amounts to ≈ 1 cm in ASDEX-Upgrade [1]. Their amplitude correlate with the mitigation as well as suppression of ELMs and the consequent reduction of the pedestal pressure (density pump-out). Toroidally localized diagnostics with high radial resolution in combination with toroidally rotating $n = 2$ MP-fields are used to characterize the 3D boundary displacement. The amplitude, the toroidal phase and the dependence on applied poloidal mode spectrum of the displacements are in good agreement with 3D single fluid ideal magnetohydrodynamic (MHD) code predictions (MARS-F, VMEC). So far, we have no indication that resistive MHD modes (tearing modes) induced by mode penetration from the external MPs play a role.

The induced 3D MHD geometry does not only lead to significant displacements of the plasma boundary, but it also changes the local stability at the edge. We observe ideal MHD modes with ballooning structure only at certain field-lines (helical position) within the 3D geometry in the H-mode edge barrier region [2]. Infinite- n ballooning stability analysis using a 3D equilibrium from VMEC demonstrates that the local reduction of the magnetic shear causes strongest instability at exactly the same field lines. Perturbations of the local parallel current profile and the additional torsion due to the 3D geometric shape of the magnetic surface are responsible for the changes in local magnetic shear. Additionally, not only the ballooning modes, but also the dynamics of the ELM crashes are influenced by the 3D MHD geometry.

References

- [1] M. Willensdorfer *et al.*, Nucl. Fus., **57**, 116047 (2017).
- [2] M. Willensdorfer *et al.*, Phys. Rev. Lett., **119**, 085002 (2017).

Seeding of Tearing Modes by Internal Crash Events in ASDEX-Upgrade and DIII-D Tokamaks

V. Igochine¹, A. Gude¹, S. Günter¹, J. M. Hanson², K. Lackner¹, C. Paz-Soldan³,
E. J. Strait³, and H. Zohm¹

The ASDEX-Upgrade Team and the DIII-D Team

¹*Max-Planck-Institut für Plasmaphysik, Garching, Germany*

²*Columbia University, New York, NY 10027, USA*

³*General Atomics, San Diego, CA 92186, USA*

Corresponding Author: V. Igochine, valentin.igochine@ipp.mpg.de

Tearing mode formation after internal crash events like sawteeth or fishbones is one of the most important MHD processes that result in a big island structure and associated confinement degradation in tokamaks. This type of tearing mode formation is considered to be the most important for future fusion reactors like ITER, because large internal events provide strong magnetic perturbations and are thus able to trigger the mode already at very small normalized pressure values. The process implies magnetic reconnection at the rational surface, which has been investigated in great detail in the ASDEX Upgrade and DIII-D tokamaks. In this paper we show that such an internal crash event leads to an ideal kink mode which transforms into a tearing mode on a much longer timescale than the crash itself. Thus, the common belief of fast formation of a big island during the crash has to be revised.

EX

Role of the Pressure Position on the Pedestal Stability in AUG, JET-ILW and TCV in Deuterium and Hydrogen Plasmas and Implications for ITER

L. Frassinetti¹, M. G. Dunne², U. Sheikh³, C. F. Maggi⁴, L. Horvath⁵, S. Saarelma⁴, S. Pamela⁴, C. Roach⁴, E. Stefanikova¹, E. de la Luna⁶, E. Wolfrum², M. Bernert², P. Blanchard³, B. Labit³, A. Merle³, L. Guimaraes⁷, S. Coda³, H. Meyer⁴, and J. C. Hillesheim⁴

The ASDEX-Upgrade, JET Contributors, TCV-, and EUROfusion MST1 Teams

¹KTH Royal Institute of Technology, Stockholm, Sweden

²Max-Planck-Institut für Plasmaphysik, Garching, Germany

³Swiss Plasma Center (SPC), École polytechnique fédérale de Lausanne (EPFL), 1015 Lausanne, Switzerland

⁴Culham Centre for Fusion Energy (CCFE), Culham Science Centre, Abingdon, UK

⁵York Plasma Institute, University of York, Heslington, UK

⁶Centro de Investigaciones Energéticas, Medioambientales y Tecnológicas (CIEMAT), Madrid, Spain

⁷Institute of Plasmas and Nuclear Fusion (IPNF), Instituto Superior Técnico (IST), 1049-001 Lisbon, Portugal

Corresponding Author: L. Frassinetti, lorenzo.frassinetti@ee.kth.se

The role of the pedestal pressure position (p_e^{pos}) in the pedestal stability has been recently highlighted in deuterium (D) plasmas in AUG [1], where it was shown that an outward shift of the pressure can lead to a reduction in pedestal pressure height (p_e^{ped}). The work emphasized the role of scrape-off layer conditions and possibly separatrix density (n_e^{sep}) in the global confinement. Instead, the role of p_e^{pos} in JET-ILW has been, so far, elusive [2]. To achieve reliable pedestal predictions for ITER it is necessary to clarify several points:

- Do AUG and JET behave in a similar way in terms of the pressure position?
- Does the pressure position play a role in the pedestal stability in JET?
- Is the variation of p_e^{pos} a general behaviour or is unique to metal wall machines?
- What is the role of n_e^{sep} ?
- Does the isotope species influence these mechanisms?

These questions are addressed in five steps: by i) investigating the behaviour of the pedestal structure in gas and power scans of unseeded plasmas in AUG, JET-ILW and TCV; ii) by studying the corresponding physics mechanisms using the P-B model; and iii) by comparing the results with the self-consistent EUROPED code [3]. Further insight into the physics mechanisms are obtained by: iv) nonlinear resistive MHD simulations with JOEREK; and v) microinstability analysis with GS2. When the pedestal is P-B limited, similar behaviours are observed in all three devices. The increasing fuelling leads to the pedestal degradation. This is explained by the outward shift of the pedestal position, as verified with EUROPED. A preliminary modelling suggests that the ITER pedestal can be affected by 7–8%. However, this might be an underestimation, as also n_e^{sep} plays an important role [1]. EPED overestimates by 25% the experimental p_e^{ped} in the high n_e^{sep} case. The reason for the discrepancy is investigated with JOEREK, to assess the role of resistivity, nonlinear MHD and diamagnetic effects and with GS2, to assess the role of microinstabilities.

References

- [1] M. Dunne, Plasma Phys. Contr. F., **59**, 014017 (2017).
- [2] E. Stefanikova, accepted in Nucl. Fusion.
- [3] S. Saarelma, Plasma Phys. Contr. F., **60**, 014042 (2018).

Ion Cyclotron Range of Frequency Power: Progress in Operation and Understanding for Experiments with Metallic Walls

J.-M. Noterdaeme^{1,2}, V. Bobkov¹, H. Faugel¹, H. Fuenfgelder¹, A. Kostic^{2,1}, R. Ochoukov¹, I. Shesterikov¹, G. Suárez López^{1,3}, W. Tierens¹, M. Usoltceva^{2,1}, W. Zhang^{1,4,5}, K. Crombé^{2,6}, Y. O. Kasakov⁶, R. Ragona^{6,2}, A. Messiaen⁶, R. Maggiora⁷, D. Milanesio⁷, D. Van Eester⁶, L. Colas⁸, S. Heuraux⁹, A. Silva⁹, D. Aguiam⁹, A. Kappatou¹, R. Bilato¹, M. Weiland¹, J. M. Faustin¹⁰, M. J. Mantsinen^{11,12}, and J. Ongena⁵

The ASDEX-Upgrade Team and EUROfusion-MST1 Team

¹Max-Planck-Institut für Plasmaphysik, Garching, Germany

²Ghent University, 9000 Ghent, Belgium

³Ludwig-Maximilian-University of Munich, D-80539 Munich, Germany

⁴Institute of Plasma Physics, Chinese Academy of Sciences, Hefei, Anhui, People's Republic of China

⁵Laboratory for Plasma Physics, ERM/KMS, Brussels, Belgium

⁶Politecnico di Torino, Turin, Italy

⁷Institut de Recherche sur la Fusion par confinement Magnétique (IRFM),

Commissariat à l'énergie atomique (CEA/Cadarache), 13108 St. Paul lez Durance, France

⁸Institut Jean Lamour, Université de Lorraine, CNRS, Nancy, France

⁹Institute of Plasmas and Nuclear Fusion (IPNF), Instituto Superior Técnico (IST), 1049-001 Lisbon, Portugal

¹⁰Max-Planck-Institut für Plasmaphysik, Greifswald, Germany

¹¹Centro Nacional de Supercomputación (BSC), Barcelona, Spain

¹²Catalan Institution for Research and Advanced Studies (ICREA)

Corresponding Author: J.-M. Noterdaeme, noterdaeme@ipp.mpg.de

Significant progress in applying ICRF power to ASDEX-Upgrade (AUG) has been achieved in the last years; this progress has been associated with a similar progress in our understanding and capability to model the relevant processes. The two main challenges of the ICRF system (power coupling and impurity production) have been tackled successfully. First, the outer midplane gas injection techniques that improve the coupling of the fast wave to the confined plasma by increasing the density in front of ICRF antenna have been well established experimentally and consistently modelled numerically. With midplane gas puffing, the local edge density increase in front of the antenna leads to a shift of the fast wave cut-off position closer to the antenna by 2 cm. The results were confirmed with the new density measurements in front of the antenna. The ICRF coupling increases by 120% (25% for top gas puffing). Second, with the installation of the 3-strap antennas in AUG, it was clearly demonstrated that the ICRF-specific tungsten (W) sputtering can be successfully mitigated with a proper antenna design. The reduction of W sputtering with the 3-strap antennas has been achieved by minimizing the RF currents on the antenna surfaces that are exposed to the scrape-off-layer (SOL) plasma. The strap power balance measurements confirm that the local RF currents, rectified DC currents and W sputtering yield at the antenna side limiters experience a clear minimum close to a phasing between the central and the outer straps of 180° and a power balance ratio $P_{\text{cen}}/P_{\text{out}}$ of 2. For this optimal choice, the local source of sputtered W at the limiters is reduced by a factor between 1.5 and 6, depending on the location. This is understood, modelled and confirms the hypothesis of sheath rectification as the source of the sputtered W. Furthermore, the new 3-ion ICRF heating scenario, which can produce very energetic particles, has been successfully reproduced in AUG.

Continued...

The progress in operation, as well as in understanding and modelling capability is strongly supported by improved ICRF diagnostic coverage including density measurements directly in front of the antenna by reflectometry, advanced RF coupling characterization, measurements of antenna limiter currents, B-dot probes, ion cyclotron emission (ICE) measurements as well as by the dedicated test arrangement IShTAR.

Fast-Ion Confinement in Low Collisionality Discharges at ASDEX-Upgrade and TCV

B. Geiger¹, A. N. Karpushov², R. Akers³, A. Bock¹, M. G. Dunne¹, B. P. Duval², M. Fontana², L. Giannone¹, J. Hobirk¹, C. Hopf¹, A. S. Jacobsen¹, D. Keeling³, P. Lauber¹, C. Marini², P. Z. Pölöskei¹, M. Salewski⁴, O. Sauter², P. A. Schneider¹, A. Snicker⁵, A. J. van Vuuren¹, G. J. Wilkie⁶, and M. Willensdorfer¹

The TCV, ASDEX-Upgrade, and EUROfusion MST1 Teams

¹Max-Planck-Institut für Plasmaphysik, Garching, Germany

²Swiss Plasma Center (SPC), École polytechnique fédérale de Lausanne (EPFL), 1015 Lausanne, Switzerland

³Culham Centre for Fusion Energy (CCFE), Culham Science Centre, Abingdon, UK

⁴Plasma Physics and Fusion Energy (PPFE), Technical University of Denmark (DTU), Lyngby, Denmark

⁵Aalto University, Espoo, Finland

⁶Chalmers University of Technology, Göteborg, Sweden

Corresponding Author: B. Geiger, benedikt.geiger@ipp.mpg.de

Previous fast-ion studies show that resonant magnetic perturbations (RMPs), charge-exchange losses, turbulence and magnetohydrodynamic (MHD) activity can degrade the fast-particle confinement in fusion devices. However, a detailed and quantitative assessment has not yet been possible, mainly due to limitations in fast-ion diagnostic capabilities.

In recent years, a comprehensive suite of fast-ion diagnostics and analysis tools has been developed at the ASDEX-Upgrade and TCV tokamaks for a combined quantitative analysis. Measurements of the loop voltage, diamagnetic flux, plasma stored energy and the current profile yield indirect information on the fast ions and can be compared with neoclassical TRANSP predictions. In addition, direct fast-particle measurements from fast-ion D_α (FIDA) spectroscopy, neutral particle analysers (NPAs) and neutron detectors are investigated using tomographic reconstructions and synthetic diagnostics.

In MHD-quiescent NBI heated low collisionality plasmas at TCV, the combined analysis of all indirect and direct measurements shows that charge exchange losses, as modelled by TRANSP, play a significant role (up to 30% of the injected power). Moreover, when additionally applying 2 MW of ECRH, a second transport channel is necessary to explain the data. This transport channel might be explained by turbulence-induced fast-ion redistribution, which could be expected due to the low fast-ion energies (23 keV) and high electron temperatures (3 keV) present at TCV. Simulations using the gyrokinetic GS2 code are ongoing and will test this hypothesis.

In advanced tokamak scenarios at ASDEX-Upgrade with off-axis NBI heating, counter ECCD and RMP-induced density pump for low collisionalities, the current profile measurements do well agree with the neoclassical simulations. However, significant discrepancies are observed for fast ions close to the plasma edge. This is not the case in standard discharge scenario. The discrepancy could in part be explained by charge exchange losses and by RMP-induced losses predicted by the 3D fast-ion code LOCUST using MHD equilibria from VMEC. However, additional fast-ion losses are still necessary to match the experimental data, possibly explained by the presence of reversed shear Alfvén Eigenmodes (AEs) after $q = 2$ sawtooth-like crashes and of NBI driven toroidicity induced AEs near the plasma edge.

Quantification of Neutral Beam Driven Current and the Effect of Radial Fast-Ion Transport in ASDEX-Upgrade

D. Rittich¹, C. Hopf¹, B. Geiger¹, A. Bock¹, R. Fischer¹, F. Ryter¹, and J. Stober¹

The ASDEX-Upgrade Team

¹Max-Planck-Institut für Plasmaphysik, Garching, Germany

Corresponding Author: D. Rittich, david.rittich@ipp.mpg.de

The neutral beam (NB) driven current, like the other intrinsic and driven current contributions to the total plasma current, is not directly measurable. Therefore, two strategies are used to investigate neutral beam current drive (NBCD). First, for quantitative investigations of the total NB driven current the measured total plasma current is compared with the sum of the calculated contributions. Second, changes in the measured plasma current profile due to changes in the neutral beam injection are examined.

An issue for the quantitative approach is the large uncertainty in the reconstruction of the inductive current. This hampers quantitative conclusions on the current composition. Therefore, quantitative investigations of the noninductive contributions were done in discharges with maximized neutral beam driven and bootstrap current fraction, leading to an almost vanishing inductive current. A pressure-measurement based correction of the fast ion content, confirmed independently by fast-ion $D\alpha$ measurements, together with the improved bootstrap current formula of [1] leads to a quantitative decomposition of the plasma current that is consistent with the estimates of the small inductive contribution.

The investigation of the reaction of the total plasma current profile to switching between on- and off-axis neutral beams aimed at revisiting a contradiction that had been found earlier: while the radial profiles of the fast NB ions seemed to behave neoclassically, the current profile appeared to deviate from the neoclassical expectations. In the new discharges the radial fast ion distribution and the radial current profile were measured simultaneously. After improvements to the diagnostics and TRANSP modelling, both diagnostics are now in agreement with each other and the small deviations from the neoclassical theory are of the order of radial transport expected due to microturbulence. Furthermore, reexamination of the old experiments yields results consistent with the new experiments.

References

[1] R. Hager *et al.*, Phys. Plasmas, **23**, 4 (2016).

Impact of an Edge Resonant Transport Layer on Fast-Ion Confinement in the ASDEX-Upgrade Tokamak

J. Galdon-Quiroga¹, M. García Muñoz¹, S. Sharapov², L. Sanchis-Sanchez¹, L. Chen³, M. G. Dunne⁴, J. Gonzalez-Martin¹, M. Hölzl⁴, A. S. Jacobsen⁴, K. G. McClements², M. Nocente⁵, F. Orain⁴, J. F. Rivero-Rodriguez¹, D. A. Ryan², M. Salewski⁶, P. A. Schneider⁴, A. Snicker⁷, W. Suttrop⁴, Y. Todo⁸, M. A. Van Zeeland⁹, E. Viezzer¹, M. Willensdorfer⁴, D. Zarzoso¹⁰, and F. Zonca^{3,11}

The ASDEX-Upgrade Team and EUROfusion-MST1 Team

¹Universidad de Sevilla, Seville, Spain

²Culham Centre for Fusion Energy (CCFE), Culham Science Centre, Abingdon, UK

³Institute for Fusion Theory and Simulation,

Zhejiang University, Xihu, Hangzhou, Zhejiang, People's Republic of China

⁴Max-Planck-Institut für Plasmaphysik, Garching, Germany

⁵Dipartimento di Fisica, Università degli Studi di Milano-Bicocca, 20126 Milano, Italy

⁶Technical University of Denmark (DTU), Lyngby, Denmark

⁷Aalto University, Espoo, Finland

⁸National Institute for Fusion Science (NIFS), Toki, Gifu, Japan

⁹General Atomics, San Diego, CA 92186, USA

¹⁰Physique des Interactions Ioniques et Moléculaires (PIIM), CNRS, Aix-Marseille Université, France

¹¹ENEA C. R. Frascati, Dipartimento FSN, Frascati, Italy

Corresponding Author: J. Galdon-Quiroga, jgaldon@us.es

An edge resonant transport layer has been found to explain many aspects of fast ion confinement under symmetry breaking 3D edge perturbations, such as edge localized modes (ELMs) and externally applied magnetic perturbations (MPs). Experimental measurements in the ASDEX-Upgrade (AUG) tokamak show that fast ion losses in the presence of symmetry breaking 3D fields strongly depend on the poloidal spectra of the applied MPs. This fast ion transport is explained in terms of a resonant interaction between the perturbative fields and the particle orbital frequencies, which leads to the build up of an edge resonant transport layer (ERTL) in the vicinity of the separatrix. Full orbit simulations including the plasma response have been performed to characterize the ERTL by means of the variation in the particle toroidal canonical momentum. The combination of the poloidal spectra of the applied MPs and the relative phase of the particles with respect to the perturbation determines the radial direction of the fast ion transport, therefore degrading or improving the fast ion confinement. Consequently, an appropriate arrangement of the heating systems and externally applied 3D fields provides an excellent tool to tailor the fast ion distribution, thus modifying the drive and damping of electromagnetic instabilities through local wave particle interactions. In this regard, proof of principle experiments have been conducted in AUG, where NBI driven toroidal Alfvén eigenmodes (TAEs) were excited and suppressed on command using this technique.

The importance of the ERTL is extended to ELM induced fast ion losses, during which acceleration of beam ions has been recently observed in AUG. Multiple velocity space structures are observed to vary with the beam source and q_{95} values. This suggests that the acceleration results again from a resonant interaction between the beam ions and parallel electric fields arising during ELM filament eruption.

Continued...

The experimental results presented here may shed light on the physics underlying fast ion confinement in the presence of both self generated and imposed edge 3D perturbations. In the case of externally applied MPs, experiments have demonstrated the possibility of actuating on limited phase space volumes of the fast ion distribution to actively control TAEs, which is of great interest for future burning plasma experiments like ITER.

Preparing the ICRH System for the Wendelstein 7-X Stellarator

J. Ongena¹, M. Berte¹, V. Borsuk², D. Castaño-Bardawil³, S. A. Bozhenkov⁴, K. Crombé¹, P. Despontin¹, A. Dinklage⁴, F. Durodié¹, J. M. Faustin⁴, A. Mauel³, A. Messiaen¹, D. A. Hartmann⁴, K. P. Hollfeld³, G. Jouniaux¹, J. P. Kallmeyer⁴, Y. O. Kazakov¹, A. Krämer-Flecken², A. Krivska¹, H. P. Laqua⁴, F. Louche¹, A. Lysoivan¹, O. Neubauer², D. Nicolai², G. Offermanns³, R. Philips¹, G. Satheeswaran², R. Schick², B. Schweer¹, I. Stepanov¹, M. Vervier¹, M. Van Schoor¹, T. Wauters¹, and R. C. Wolf⁴

The TEC and W7-X Teams

¹Laboratory for Plasma Physics, ERM/KMS, Brussels, Belgium

²Institute of Energy and Climate Research, Forschungszentrum Jülich, Jülich, Germany

³Zentralinstitut für Engineering, Elektronik und Analytik – Engineering und Technologie, (ZEA-1), Forschungszentrum Jülich, Jülich, Germany

⁴Max-Planck-Institut für Plasmaphysik, Greifswald, Germany

Corresponding Author: J. Ongena, j.ongena@fz-juelich.de

An important aim of W7-X is to demonstrate fast ion confinement at volume averaged β values up to 5% for which W7-X was optimized. These high- β values correspond to plasma densities above $10^{20}/\text{m}^3$. Mimicking the behaviour of α -particles in a future stellarator requires the presence of energetic ions with energies in the range ~ 100 keV in the core of W7-X high density plasmas. This is a challenging task, but such a population can be created using ion cyclotron resonance heating (ICRH) using various heating schemes, including the newly demonstrated 3-ion heating scenario.

The ICRH system under construction for W7-X aims in its final configuration at delivering RF power levels up to ~ 1.5 MW in the frequency range 25–38 MHz with pulse lengths up to 10 s. The antenna consists of two straps and is foreseen with a prematching system to limit voltages in the feeding transmission lines and matching system. The shape of the antenna is carefully matched to the 3D shape of the last closed magnetic surface (LCMS) of the standard magnetic field configuration on W7-X.

At the standard magnetic field of 2.5 T, fast (~ 100 –200 keV) H, D, ^3He and ^4He particles can be generated in high density ($n_e > 10^{20}/\text{m}^3$) W7-X plasmas for studies of fast ion confinement in the optimized stellarator magnetic topology of W7-X using various heating scenarios: minority heating of H, 2nd harmonic heating of D or ^4He , and using the 3-ion scenario to generate fast ^3He in H-D or H- ^4He mixture plasmas.

A purposely-built test stand in the Institute for Energy and Climate Research/ Plasma Physics (IEK-4, Forschungszentrum Jülich, Germany) is being assembled to check the main properties of the ICRH antenna before installation in W7-X. Checks of the vacuum compatibility, voltage standoff and functionality of the radial positioning system are underway. We will provide a detailed description of the test stand, obtained results and conclusions for the use of the ICRH system at W7-X, and in as far as possible also first results obtained on W7-X.

On a Path to Steady-State High-Performance Operation in W7-X: Heating, Current Drive and Fuelling Experiments with High Power ECRH

H. P. Laqua¹, J. Baldzuhn¹, S. A. Bozhnikov¹, H. Braune¹, K. J. Brunner¹, Y. O. Kazakov², S. Marsen¹, D. Moseev¹, T. Stange¹, R. C. Wolf¹, and M. Zanini¹

The W7-X Team

¹*Max-Planck-Institut für Plasmaphysik, Greifswald, Germany*

²*Laboratory for Plasma Physics, ERM/KMS, Brussels, Belgium*

Corresponding Author: H. P. Laqua, laqua@ipp.mpg.de

The ECRH system at W7-X demonstrated already all requirements, which are necessary for a high-performance steady state operation. Besides the reliable plasma start-up and routine ECRH wall conditioning, stationary discharges up to 30 s have been achieved, which were only limited by the maximum test divertor energy load. The long discharges were also used to demonstrate current control and bootstrap current compensation by ECCD. In combination with pellet injection (PI), highest performance with a plasma energy above 1 MJ has been achieved with the X2-mode ECRH at a plasma density of $0.8 \times 10^{20}/\text{m}^3$ and an ion temperature of 3.8 keV. With the O2-mode ECRH combined with PI high-performance plasmas at densities above the X2-cutoff and up to $1.4 \times 10^{20}/\text{m}^3$ have been achieved, which is already close to the envisaged future steady-state high-performance plasma scenario.

EX

The LTX- β Research Programme and First Results

R. Majeski¹, R. E. Bell¹, J. M. Bialek², T. M. Biewer³, D. P. Boyle¹, L. Buzi⁴, J. M. Canik³, D. C. Donovan⁵, M. A. Dorf⁶, D. B. Elliott³, C. Hansen⁷, P. E. Hughes¹, T. Jarboe⁷, R. Kaita¹, B. E. Koel⁴, T. Kozub¹, S. Kubota⁸, R. Lunsford¹, A. Maan⁵, E. Merino¹, A. Nelsen¹, M. L. Reinke³, T. L. Rhodes⁸, T. D. Rognlien⁶, F. Scotti⁶, V. A. Soukhanovskii⁶, L. E. Zakharov⁹, and X. Zhang¹

¹Princeton Plasma Physics Laboratory (PPPL), Princeton, NJ 08540, USA

²Columbia University, New York, NY 10027, USA

³Oak Ridge National Laboratory (ORNL), Oak Ridge, TN 37831, USA

⁴Princeton University, Princeton, NJ 08544, USA

⁵University of Tennessee, Knoxville, TN 37996, USA

⁶Lawrence Livermore National Laboratory (LLNL), Livermore, CA 94550, USA

⁷University of Washington, Seattle, WA 98195, USA

⁸University of California Los Angeles, CA 90095, USA

⁹LiWall Fusion, Princeton, NJ, USA

Corresponding Author: R. Majeski, rmajeski@pppl.gov

The research programme for LTX- β , the upgrade to the Lithium Tokamak Experiment, combines lithium walls to produce gradient-free temperature profiles and stabilize ion and electron temperature gradient-driven modes, with approaches to stabilization of density gradient-driven modes, such as the trapped electron mode (TEM). Candidate stabilization mechanisms for the TEM include sheared flow stabilization, which will be tested on LTX- β using neutral beam induced rotation. The goal is to reduce anomalous transport in a low aspect ratio tokamak. The upgrade will approximately double the toroidal field of LTX- β (to 3.4 kG) and plasma current (to 150–175 kA), compared to LTX. Upgrades to the diagnostic set are in the areas of equilibrium, core transport, scrape-off layer (SOL) physics, and plasma-material interactions. Neutral beam injection at 20 kV, 30 A will be added in spring 2018, using a neutral beam system provided by Tri-Alpha Energy. A 9.3 GHz, 50 kW, short-pulse (5–10 ms) magnetron will be available later in 2018 for electron heat pulse propagation experiments. New lithium evaporation sources allow between-shot recoating of the walls.

LTX- β is a collaborative effort, with major participation from both Oak Ridge and Lawrence Livermore National Laboratories (ORNL and LLNL), as well as the University of California at Los Angeles (UCLA). ORNL and the University of Tennessee will focus on spectroscopic improvements, and edge plasma/plasma-material interaction (PMI) analysis. LLNL plans research in the areas of SOL transport and plasma-surface interactions with lithium and tin. UCLA is upgrading the LTX profile reflectometer for high radial wavenumber backscattering. The 1 mm UCLA interferometer system will also be upgraded to probe low perpendicular wavenumber density fluctuations. The LTX- β research programme will be discussed, and initial operation of the upgraded device will be described.

Work supported by the U.S. Department of Energy, contracts DE-AC02-09CH11466, DE-AC05-00OR22725, and DE-AC52-07NA27344.

Plasma Termination by Excess Fuel and Impurities in TJ-II, LHD and W7-X

A. Dinklage¹, H. Yamada², J. Baldzuhn¹, B. Buttenschön¹, H. Damm³, P. Drewelow¹, G. Fuchert¹, K. J. McCarthy⁴, H. Kasahara², J. Miyazawa², G. Motojima², T. Oishi², T. Sunn Pedersen¹, R. Sakamoto², C. Suzuki², N. Tamura², T. Wegner¹, R. C. Wolf¹, and D. Zhang¹

The W7-X and TJ-II Teams and The LHD Experiment Group

¹Max-Planck-Institut für Plasmaphysik, Greifswald, Germany

²National Institute for Fusion Science (NIFS), Toki, Gifu, Japan

³Ernst-Moritz-Arndt Universität, 17489 Greifswald, Germany

⁴Centro de Investigaciones Energéticas, Medioambientales y Tecnológicas (CIEMAT), Madrid, Spain

Corresponding Author: A. Dinklage, dinklage@ipp.mpg.de

EX Plasma termination by excess fuelling or impurity interaction is a safety relevant event in potential fusion reactors. Sudden termination of plasma operation is an aspect that enters material requirements in terms of released energies, localization and respective time-scales of the plasma terminating event. In tokamaks, such events may lead to disruptions or thermal quenches. While disruptions are not expected in (currentless) stellarator/heliotron operation, thermal quenches are certainly to be illuminated for reactor scale stellarators and heliotrons as well. This report is a study on plasma termination in TJ-II, W7-X and LHD. The confinement in W7-X and LHD allows one to study long-mean-free-path collisionality conditions in the plasma core.

Evidence for stellarator/heliotron specific behaviour is given by the spatio-temporal evolution of the electron temperature. After the injection of two fuelling pellets into an LHD discharge, the second pellet induces a cooling of the plasma centre leading to a temperature hole after about 100 ms (τ_E). It is concluded that the stationary confining field has a beneficial impact. In TJ-II, the peaking of TESPEL particle deposition closer to the centre facilitates plasma recovery. For W7-X, plasma termination due to massive LBO tungsten injection shows energy decay by cooling of the plasma. The electron temperature decays on the time scale of energy confinement (~ 100 ms), while the plasma density remains almost constant (even slightly increasing). The plasma is finally terminated along with a strong increase of radiation representatively shown here as increase of impurity lines due to wall material (iron). Similar evolution of temperature and density is observed after iron impurities terminating ICRH long pulse experiments on LHD.

The systematic comparison of plasma terminating events by cryogenic pellets, induced impurity injection or changes of the heating gives evidence that the observed termination takes place on a time scale corresponding to the energy confinement time. Close to marginal termination, the beneficial effect of stellarator confinement of the vacuum field leads to transient plasmas that are cold in the centre but may recover after typically 1 s. The findings indicate the benign impact on transient loads in case of plasma termination in stellarators and heliotrons.

TH: Magnetic Confinement Theory and Modelling

TH

Simulations of Energetic Particle Driven Instabilities and Fast Particle Redistribution in EAST Tokamak

W. Shen¹, Y. Pei^{1,2}, Y. Xu¹, G. Y. Fu^{3,4}, F. Wang⁵, N. Xiang¹, Y. Hu¹, Y. Todo⁶, W. Guo¹, L. Ye¹, X. Xiao¹, S. Wang², D. Zhou¹, L. Xu¹, G. Li¹, J. Huang¹, C. Liu¹, and S. Zhu²

¹*Institute of Plasma Physics, Chinese Academy of Sciences, Hefei, Anhui, People's Republic of China*

²*University of Science and Technology of China, Hefei, Anhui, People's Republic of China*

³*Institute for Fusion Theory and Simulation (IFTS),*

Zhejiang University, Xihu, Hangzhou, Zhejiang, People's Republic of China

⁴*Princeton Plasma Physics Laboratory (PPPL), Princeton, NJ 08540, USA*

⁵*Dalian University of Technology, Liaoning, Dalian, Ganjingzi, People's Republic of China*

⁶*National Institute for Fusion Science (NIFS), Toki, Gifu, Japan*

Corresponding Author: W. Shen, shenwei@ipp.ac.cn

Instabilities driven by energetic particles including fishbones and Alfvén eigenmodes, together with fast particle loss and redistribution due to resonant magnetic perturbations (RMPs), have been investigated numerically with codes M3D-K, MEGA, and GYCAVA in EAST tokamak. Firstly, hybrid simulations with the global kinetic-magnetohydrodynamic (MHD) code M3D-K have been carried out to investigate the beam-driven fishbone in EAST experiment. The results are consistent with the experimental measurement with respect to mode frequency and mode structure. Nonlinear simulations show that the frequency of the fishbone chirps up and down with corresponding hole-clump structures in phase space, consistent with the Berk-Breizman theory. In addition to the low frequency fishbone, a high-frequency β -induced Alfvén eigenmode (BAE) is excited during the nonlinear evolution. Secondly, two kinetic-MHD codes, namely MEGA and M3D-K, have been applied to study fast ion driven toroidal Alfvén eigenmodes (TAEs) in EAST tokamak. Parameter scans show that the frequency and growth rate of TAEs simulated by the two codes agree well with each other. The analysis of the resonant interaction between the TAE and fast ions shows that the TAE exchanges energy with the cocurrent passing particles with parallel velocity $|v_{\parallel}| \approx V_{A0}/3$ or $|v_{\parallel}| \approx V_{A0}/5$, where V_{A0} is the Alfvén speed on the magnetic axis. Moreover, the TAE destabilized by the counter-current passing ions has much smaller growth rate than that driven by the cocurrent ion. Thirdly, the effects of RMPs on the loss and redistribution of passing ions are investigated numerically by the orbit following code GYCAVA for EAST tokamak. The loss fraction and the loss region of passing ions increase with the amplitude of RMPs. For the energetic passing ions, the extra loss induced by RMPs can be comparable to the loss induced by the magnetic drift. The extra loss of passing ions induced by RMPs is related to the drift island structure induced by RMPs and the magnetic drift, and the stochasticity induced by overlap of magnetic islands. The dependence of the loss fraction and loss region on the toroidal mode number of RMPs is related to the safety factor. Finally, the pitch angle and energy of particle can impact the loss of energetic passing ions. These results would provide guidance for future EAST experiments.

Critical Fast Ion Distribution in Phase Space for the Synchronized Sudden Growth of Multiple Alfvén Eigenmodes and the Global Transport of Fast Ions

Y. Todo^{1,2}

¹National Institute for Fusion Science (NIFS), Toki, Gifu, Japan

²Department of Fusion Science, Graduate University for Advanced Studies (SOKENDAI), Toki, Gifu, Japan

Corresponding Author: Y. Todo, todo@nifs.ac.jp

Alfvén eigenmodes (AEs) driven by fast ions in tokamak plasmas and the fast ion distribution formed with the AEs, neutral beam injection (NBI), and collisions are investigated with hybrid simulations for energetic particles and a magnetohydrodynamic (MHD) fluid [1]. The multiphase simulation [2], which is a combination of classical simulation and hybrid simulation, was applied for various beam deposition power (P_{NBI}) and slowing-down time (τ_s). In the classical simulation, energetic particle orbits are followed in the equilibrium magnetic field with NBI and collisions while the MHD perturbations are turned off. The physical parameters other than P_{NBI} and t_s are similar to those of a TFTR experiment [3]. For $P_{\text{NBI}} = 10$ MW and $\tau_s = 100$ ms, which are similar to the TFTR experiment, the AE bursts take place with a time interval 2.7 ms and the maximum amplitude of radial MHD velocity normalized by the Alfvén velocity $v_r/v_A = 3 \times 10^{-3}$, which are close to the TFTR experiment. With increasing volume-averaged classical fast ion pressure, the fast ion confinement degrades monotonically due to the transport by the AEs. The fast ion pressure profile resiliency, where the increase in fast ion pressure profile is saturated, is found for the cases with the AE bursts. In this work, we have clarified the physical process of the AE burst in toroidal plasmas. Before the AE bursts occur, multiple AEs become unstable, and grow to low amplitude. The low-amplitude AEs gradually and locally flatten the fast ion distribution in phase space leading to the formation of a stepwise distribution. The stepwise distribution is a “critical distribution” where the further beam injection leads to the higher AE amplitude, the broadening of the locally flattened regions, and their overlap. This resonance overlap of the multiple AEs [4] brings about the AE burst, the global transport of fast ions, and the saturation of the distribution.

References

- [1] Y. Todo, *New J. Phys.*, **18**, 115005 (2016).
- [2] Y. Todo *et al.*, *Nucl. Fus.*, **54**, 104012 (2014).
- [3] K. L. Wong *et al.*, *Phys. Rev. Lett.*, **66**, 1874 (1991).
- [4] H. L. Berk *et al.*, *Phys. Plasmas*, **2**, 3007 (1995).

A Gyrokinetic Discovery of Fast L-H Bifurcation Physics in a Realistic, Diverted, Tokamak Edge Geometry

S.-H. Ku¹, C.-S. Chang¹, R. M. Churchill¹, I. Cziegler², M. J. Greenwald³, R. Hager¹, J. W. Hughes³, and G. R. Tynan²

¹Princeton Plasma Physics Laboratory (PPPL), Princeton, NJ 08540, USA

²University of California San Diego, CA 92093, USA

³Plasma Science & Fusion Center, MIT, Cambridge, MA 02139, USA

Corresponding Author: S.-H. Ku, sku@pppl.gov

Despite over 30 years of routine H-mode operation in all the major tokamaks, there has not been a fundamental understanding at the kinetic level on how the H-mode turbulence bifurcation occurs. This is a concern over ITER's achievability of the H-mode operation with available heating power when the Δp -driven neoclassical $E \times B$ shearing rate is expected to be weak due to smallness of $\rho_* = \rho_i/a$. The answer to this concern relies on a more fundamental physics question: Will a neoclassically driven mean $E \times B$ shearing (Δp -driven or X-point orbit-loss driven) be essential for the L-H turbulence bifurcation, besides the Reynolds-force driven $E \times B$ shearing? Experimental observations appear to diverge on the cause and dynamics of L-H bifurcation.

From the edge gyrokinetic code XGC1, we find that a neoclassical-driven $E \times B$ -shearing is essential to quench the turbulence irreversibly, and works together with the Reynolds-stress driven $E \times B$ -shearing. New XGC1 study also shows that, in ITER, the weak Δp -driven $E \times B$ shearing can be compensated by the X-point orbit-loss driven $E \times B$ -shearing and toroidal flow if the edge T_i is high enough. The physics found in the XGC1 simulations reconciles a few different L-H bifurcation dynamics observed in experiments: They are not mutually exclusive but can work together, depending upon plasma conditions. These different mechanisms include not only the source of the sheared $E \times B$ flow (turbulent or neoclassical), but also the role of different shearing physics: 1) shearing of the turbulence eddies to smaller structure and higher frequency, leading to dissipation at high wave numbers, or 2) quenching of the turbulence via an eddy tilting-stretching-absorption process via Reynolds work through a conservative absorption process from the turbulence kinetic energy to the plasma $E \times B$ flow energy.

It is also observed that both ion and electron directional modes are involved in the bifurcation process, with a highly different dynamics from each other. Both modes exist before the bifurcation. The electron modes disappear immediately during the bifurcation process, but the ion modes remain until the end of the bifurcation process undergoing the dissipative $E \times B$ shearing action. Experimental observations of two directional modes exist just before the bifurcation process starts.

Gyrokinetic Analysis and Simulations of Pedestals

M. T. Kotschenreuther¹, X. Liu¹, D. R. Hatch¹, S. M. Mahajan¹, A. Diallo², R. J. Groebner³,
J. W. Hughes⁴, C. F. Maggi⁵, S. Saarelma⁵, V. Parail⁵, and F. Köchl⁵

The DIII-D and C-Mod Teams, and The JET Contributors

¹*Institute for Fusion Studies (IFS), University of Texas at Austin, Austin, TX 78712, USA*

²*Princeton Plasma Physics Laboratory (PPPL), Princeton, NJ 08540, USA*

³*General Atomics, San Diego, CA 92186, USA*

⁴*Plasma Science & Fusion Center, MIT, Cambridge, MA 02139, USA*

⁵*Culham Centre for Fusion Energy (CCFE), Culham Science Centre, Abingdon, UK*

Corresponding Author: M. T. Kotschenreuther, mtk@austin.utexas.edu

Major progress has been made in understanding the pedestal transport in several areas. For the first time, the instabilities that dominate energy transport in present experimental pedestals are determined, using identifying ratios of the transport they produce in different channels — their “transport fingerprint”. These are derived from the drift kinetic equation for pedestal parameters, and corroborated by gyrokinetic simulations using GENE [1]. For the typical case where the electron density sources are relatively small compared to the energy sources, MHD-like modes (such as KBM) cannot dominate pedestal energy transport. The analysis is applied to experimental observations from multiple devices, and also, in detail to two DIII-D pedestals, considering transport in multiple channels, measured fluctuations and pedestal equilibrium reconstructions. Microtearing modes (MTM) and electron temperature gradient (ETG) modes dominate energy transport, rather than KBM. Multiple disparate experimental observations can be explained and unified using this analysis, including, surprisingly, density transport from applied resonant magnetic perturbations (RMP). Gyrokinetic simulations of velocity shear suppression of ITG for pedestal equilibria, using GENE [1], find excellent agreement, in detail, with the decorrelation theory of Zhang and Mahajan [2]. This physics-based theory can thus be exploited to estimate/predict turbulent transport in new regimes. In a controlled ρ^* scan (velocity shear $\sim \rho^*$), the suppressed heat flux from ITG modes scales much more poorly than gyro-Bohm, so that it may become relatively large at the low ρ^* of burning plasmas, unlike present experiments. Hence, a detailed examination of the properties of ITG/TEM modes in pedestals and ITBs with high β_{pol} has been undertaken. Unlike core modes, pedestal electrostatic modes are slab-like: destabilization results from parallel resonances, not curvature. Consequently, the density gradients are stabilizing in pedestals, and so is high β_{pol} , impurities and impurity gradients. Routes to optimize confinement in fusion relevant tokamaks, for both for inductive and steady state operations, are discussed.

References

- [1] F. Jenko *et al.*, Phys. Plasmas, 7, 1904 (2000).
- [2] Y. Z. Zhang and S. M. Mahajan, Phys. Fluids B, 5, 2000 (1993).

First Principles and Integrated Modelling Achievements Towards Trustful Fusion Power Predictions for JET and ITER

J. Garcia¹, L. Garzotti², M. Nocente³, A. Bañón Navarro⁴, Y. Baranov², F. J. Casson², C. D. Challis², J. Citrin⁵, R. Dumont¹, D. Gallart⁶, T. Görler⁴, A. Ho⁵, J. Joly¹, K. Kirov², J. Mailloux², M. J. Mantsinen^{6,7}, J. Morales¹, and S. Saarelma²

The JET Contributors

¹*Institut de Recherche sur la Fusion par confinement Magnétique (IRFM), Commissariat à l'énergie atomique (CEA/Cadarache), 13108 St. Paul lez Durance, France*

²*Culham Centre for Fusion Energy (CCFE), Culham Science Centre, Abingdon, UK*

³*Università degli Studi di Milano-Bicocca, 20126 Milano, Italy*

⁴*Max-Planck-Institut für Plasmaphysik, Garching, Germany*

⁵*FOM Institute DIFFER, Association EURATOM-FOM, Nieuwegein, Netherlands*

⁶*Centro Nacional de Supercomputación (BSC), Barcelona, Spain*

⁷*Catalan Institution for Research and Advanced Studies (ICREA), Barcelona, Spain*

Corresponding Author: J. Garcia, jeronimo.garcia@cea.fr

Predictability of burning plasmas is a key issue for designing and building credible future fusion devices. The integration of several physics aspects is mandatory for an accurate extrapolation from present day plasmas, mainly with deuterium (D) as the main ion species, to conditions in which the ion mixture will be dominated by deuterium-tritium (DT). In this framework, an important effort of physics understanding and guidance is being carried out in parallel to the JET experimental campaigns in H, D and T by performing analyses and modelling towards an optimization of the JET-DT neutron yield and fusion born alpha particle physics.

Analyses performed for both baseline and hybrid regimes have shown that reproducibility of heat and particle transport in D plasmas with quasi-linear models as TGLF and Qualikiz is acceptable, showing that in general low density is preferable in the hybrid regime in order to boost the neutron rate generation. This is due to the higher penetration of the NBI beams at low density but as well because in the ion cyclotron resonance heating (ICRH) schemes usually used, H minority, the 2nd harmonic accelerates the central D beams boosting the fusion reactivity and as well reducing turbulence driven by the so called ion temperature gradient (ITG) modes.

For heat and particle transport, quasi-linear models tend to deviate more in H than in D which makes the prediction for T and DT campaigns less satisfactory. Therefore, the comparison of those models against gyrokinetic simulations has been started which has led to a significant improved understanding of the so called isotope effect which can be reproduced in particular circumstances. Gyrokinetic simulations performed with the GENE code show that the fast ion fraction, the $E \times B$ shearing rate or the electromagnetic effects, can lead to deviations from the expected gyro-Bohm (GB) scaling.

Extrapolations to JET-DT from recent experiments using the maximum power available have been performed including some of the most sophisticated codes and a broad selection of models. There is a general agreement that 11–15 MW of fusion power can be expected in DT for the hybrid and baseline scenarios. On the other hand, in high- β , torque and fast ion fraction conditions, isotope effects could be favourable leading to higher fusion yield. This is in line with the fusion power aimed for such campaign.

Predictive Multichannel Flux-Driven Modelling to Optimize ICRH Tungsten Control in JET

F. J. Casson¹, H. Patten², C. Bourdelle³, S. Breton³, J. Citrin⁴, F. Köch¹, C. Angioni⁵, Y. Baranov¹, R. Bilato⁵, E. A. Belli⁶, C. D. Challis¹, G. Corrigan¹, A. Czarnecka⁷, O. Ficker^{8,9}, L. Garzotti¹, M. Goniche³, J. P. Graves², T. Johnson¹⁰, K. Kirov¹, P. J. Knight¹, E. A. Lerche¹¹, M. J. Mantsinen^{12,13}, J. Mlynár⁸, M. Sertoli⁵, and M. Valisa¹⁴

The JET Contributors

¹Culham Centre for Fusion Energy (CCFE), Culham Science Centre, Abingdon, UK

²Swiss Plasma Center (SPC), École polytechnique fédérale de Lausanne (EPFL), 1015 Lausanne, Switzerland

³Institut de Recherche sur la Fusion par confinement Magnétique (IRFM), Commissariat à l'énergie atomique (CEA/Cadarache), 13108 St. Paul lez Durance, France

⁴FOM Institute DIFFER, Association EURATOM-FOM, Nieuwegein, Netherlands

⁵Max-Planck-Institut für Plasmaphysik, Garching, Germany

⁶General Atomics, San Diego, CA 92186, USA

⁷Institute of Plasma Physics and Laser Microfusion (IPPLM), Warsaw, Poland

⁸Institute of Plasma Physics AS CR v.v.i., Prague, Czech Republic

⁹Faculty of Nuclear Sciences and Physical Engineering, Czech Technical University, Prague, Czech Republic

¹⁰KTH Royal Institute of Technology, Stockholm, Sweden

¹¹Laboratory for Plasma Physics, ERM/KMS, Brussels, Belgium

¹²Catalan Institution for Research and Advanced Studies (ICREA), Barcelona, Spain

¹³Centro Nacional de Supercomputación (BSC), Barcelona, Spain

¹⁴Consorzio RFX, Associazione EURATOM-ENEA sulla Fusione, Padova, Italy

Corresponding Author: F. J. Casson, francis.casson@ukaea.uk

The evolution of the JET high performance hybrid scenario, including central accumulation of the tungsten (W) impurity, is reproduced with predictive multichannel integrated modelling over multiple confinement times using first-principle based models. Eight transport channels (T_i , T_e , n_D , n_{Be} , n_{Ni} , n_W , V_{tor} , j) are modelled predictively with self-consistent predictions for sources, radiation, and magnetic equilibrium, yielding a predictive system with multiple nonlinearities which can reproduce observed radiative temperature collapse after several confinement times. The mechanism responsible for W accumulation is inward neoclassical convection driven by the main ion density gradients and enhanced by poloidal asymmetries due to centrifugal acceleration. The slow timescale of bulk density evolution sets the timescale for central W accumulation. Prediction of this phenomenon requires a turbulent transport model capable of accurately predicting particle and momentum transport (QuaLiKiz) and a neoclassical transport model including the effects of poloidal asymmetries (NEO) coupled to an integrated plasma simulator (JINTRAC). The modelling capability is applied to optimize the available actuators to prevent W accumulation, and to extrapolate in power and pulse length. Central NBI heating is preferred for high performance, but comes at the price of central deposition of particles and torque which pose the risk of W accumulation. Several benefits of ICRH to mitigate W accumulation are examined: The primary mechanism for ICRH to control W in JET are via its impact on the bulk profiles and turbulent diffusion, which are insensitive to details of the ICRH scheme.

Continued...

High power density near the axis is found to be best to maximize the beneficial effects of ICRH against W, but changing the minority species or its concentration does not significantly change the W behaviour. With attention to the location of the ICRH resonance and MHD stability, high performance hybrid scenario discharges of 5 s at maximum power should be possible in the coming campaign, and a controlled and steady fusion performance in the subsequent JET DT campaign. This work demonstrates the integration of multiple first-principle models into a powerful multichannel predictive tool for the core plasma, able to guide JET scenario development to its objectives of higher performance and longer pulses.

Runaway Electron Mitigation in ITER Disruptions by Injection of High-Z Impurities

J. R. Martín Solís¹, E. M. Hollmann², M. Lehnen³, and A. Loarte³

¹Universidad Carlos III de Madrid, Madrid, Spain

²University of California San Diego, CA 92093, USA

³International Thermonuclear Experimental Reactor (ITER),
Cadarache Centre, 13108 St. Paul lez Durance, France

Corresponding Author: J. R. Martín Solís, solis@fis.uc3m.es

Large amounts of MeV runaway electrons (REs) can be generated during disruptions, posing a serious threat for future large tokamak devices like ITER. Thus, it is an urgent task to develop robust and confident systems for their control and mitigation. The injection of high-Z impurities by MGI or SPI constitute one of the most promising schemes. Here, with the aim of evaluating the suitability of the injection of high-Z impurities for RE control and mitigation in ITER, the effect of injecting high-Z impurities on the RE dynamics during different phases of the disruption (before the thermal quench (TQ), during the current quench (CQ) and during the RE current plateau) is studied. First, mitigation by Ar or Ne injection before the TQ is considered with the aim of controlling the primary generation of REs during the TQ. The impurities are found to have a strong effect, leading to very low RE current generation for the shortest CQ times compatible with acceptable forces on the ITER vessel and in-vessel components in the case of Ne injection, while for the longest CQs high RE currents can be found. Mixed Ar+deuterium (D) or Ne+D injection before the TQ can be effective in controlling the generation of the RE current if a sufficient amount of Ar/Ne and D is assimilated in the plasma. If the formation of a primary RE seed cannot be avoided, impurities can be injected during the CQ with the aim of reducing the avalanche RE multiplication. The efficiency of this scheme versus the time at which the impurities are injected and the amount of assimilated impurities (and/or D) is analyzed. Finally, if a RE plateau current is formed at the end of the CQ, impurities can be injected with the aim of yielding the dissipation of the RE current before a strong interaction with the PFCs can take place. A simplified approach to the RE beam dissipation including the effect of the collisions with the plasma particles and impurities, and the electron synchrotron and bremsstrahlung radiation, is applied. It is suggested that injection of a few $\text{kPa}\cdot\text{m}^3$ of Ar could be enough for RE electron mitigation before the characteristic time for the vertical instability growth in ITER. The effect of the RE scraping-off during the decay of the current and the consequences on the amount of impurities that should be injected for an efficient RE dissipation is also analyzed.

TH

Self-Consistent Runaway Beam Formation in 3D Magnetic Fields During Radiation-Driven Disruptions

A. Matsuyama¹, N. Aiba¹, A. Isayama², and M. Yagi¹

¹National Institutes for Quantum and Radiological Science and Technology (QST),
Rokkasho Fusion Institute, Rokkasho-mura, Aomori, Japan

²National Institutes for Quantum and Radiological Science and Technology (QST),
Naka Fusion Institute, Naka-shi, Ibaraki-ken, Japan

Corresponding Author: A. Matsuyama, matsuyama.akinobu@qst.go.jp

We report new simulations that predict 3D spatial profiles of runaway electrons (REs) throughout the whole evolution of disruption plasmas using a nonlinear reduced MHD code including a runaway beam model. Both the RE generation mechanisms relevant to mitigated disruption scenario for DT activation phase in ITER and the convective transport of REs due to disruptive MHD instabilities during thermal quench (TQ), such as reconnection, magnetic islands, and their overlapping, are taking into account. In our approach, REs are expressed as the advection of beam density with the zero-orbit width model, and electron runaway is taken into account as source models that account for the parametric dependence of runaway rates in the velocity space for Dreicer generation, hot-tail generation, and intrinsic high-energy electron sources (due to tritium decay and the Compton scattering of γ -rays). The range of the validity is checked via the comparison to Fokker-Planck and orbit-following simulations. The developed simulation code EXTREM is a powerful tool for studying the physical mechanisms of RE generation in the presence of disruptive MHD instabilities and those of subsequent avalanche growth. We here perform a long-term simulation of radiation-driven disruption over the avalanche timescale for the ITER 15 MA parameter with noble gas and deuterium injection. During TQ MHD instabilities, overlapping of multi- n tearing modes and subsequent $m/n = 1/1$ mode, where the latter causes the disruption of the central electron temperature profile, are shown to play a dominant role in mixing of REs in partially-destroyed magnetic fields. The resultant seed current profile localized in the region with the safety factor around unity is inherited by the avalanche growth, and the final RE profile and the net RE generation becomes significantly different from those predicted by the conventional 1D modelling without MHD effects. The sensitivity of the results for different initial q profiles and the impurity injection condition is investigated. In particular, the effectiveness of Ar/Ne+deuterium mixture injection for RE suppression is addressed over the parameter ranges relevant to disruption mitigation scenarios in ITER.

Pitch Angle Dynamics and Synchrotron Emission of Runaway Electrons in Quiescent and Disrupted DIII-D Plasmas

L. Carbajal¹, D. del-Castillo-Negrete¹, C. Paz-Soldan², E. M. Hollmann³, R. A. Moyer³, and C. J. Lasnier⁴

¹Oak Ridge National Laboratory (ORNL), Oak Ridge, TN 37831, USA

²General Atomics, San Diego, CA 92186, USA

³University of California San Diego, CA 92093, USA

⁴Lawrence Livermore National Laboratory (LLNL), Livermore, CA 94550, USA

Corresponding Author: L. Carbajal, carbajalgoml@ornl.gov

We present the validation of theoretical models for the pitch-angle probability distribution function (PDF) of runaway electrons (RE), through simulations of synchrotron radiation (SR) in DIII-D quiescent [1] and disrupted [2] plasmas for which the energy PDF is known from measurements but the pitch-angle PDF is poorly understood. SR of RE in magnetically confinement fusion plasmas is important because it provides a limiting mechanism of the maximum energy that RE can reach, and because it can be used as a diagnostic to infer parameters of the RE energy and pitch-angle PDFs. Recent studies using the SR synthetic diagnostic [3, 4] showed that SR depends on the RE energy, and more strongly on their pitch-angle PDF. Our simulations of RE in quiescent plasmas recover the typical visible SR in DIII-D when the spreading in the initial RE pitch-angle is less than the predicted by simplified theory that only consider the balance of electric field pinching in pitch angle and collisional pitch-angle scattering. We also present results of simulated infrared SR of RE in DIII-D disrupted plasmas after following their dynamics for tens of ms to find a better estimate for their pitch-angle PDF that takes into account the full-orbit dynamics of RE [5], SR energy losses, the acceleration of the electric field, the magnetic field geometry, and collisions with the background plasma and impurities through the use of experimental impurity density profiles.

Research sponsored by the Office of Fusion Energy Sciences of the U.S. Department of Energy at Oak Ridge National Laboratory, managed by UT-Battelle, LLC, for the U.S. Department of Energy under contract DE-AC05-00OR22725, and by the Laboratory Directed Research and Development Program of Oak Ridge National Laboratory. Research sponsored by the Office of Fusion Energy Sciences of the U.S. Department of Energy under contracts DE-FC02-04ER54698, DE-FG02-07ER54917. This research used resources of the National Energy Research Scientific Computing Center, a DOE Office of Science User Facility supported by the Office of Science of the U.S. U.S. Department of Energy under Contract No. DE-AC02-05CH11231.

References

- [1] C. Paz-Soldan *et al.*, Phys. Rev. Lett., **118**, 255002 (2017).
- [2] E. M. Hollmann *et al.*, Phys. Plasmas, **22**, 56108 (2015).
- [3] L. Carbajal *et al.*, Plasma Phys. Contr. F., **59**, 124001 (2017).
- [4] D. del-Castillo-Negrete *et al.*, Phys. Plasmas, Accepted (2018).
- [5] L. Carbajal *et al.*, Phys. Plasmas, **24**, 042512 (2017).

Asymmetric Wall Force Reduction in ITER and JET Disruptions

H. Strauss¹, S. Jachmich², E. Joffrin³, V. Riccardo⁴, R. Paccagnella⁵, and J. Breslau⁴

The JET Contributors

¹HRS Fusion, West Orange, NJ 07052, USA

²EURATOM/UKAEA Fusion Association, Culham Science Centre, Abingdon, UK

³Institut de Recherche sur la Fusion par confinement Magnétique (IRFM),
Commissariat à l'énergie atomique (CEA/Cadarache), 13108 St. Paul lez Durance, France

⁴Princeton Plasma Physics Laboratory (PPPL), Princeton, NJ 08540, USA

⁵Consorzio RFX, Associazione EURATOM-ENEA sulla Fusione, Padova, Italy

Corresponding Author: H. Strauss, hank@hrsfusion.com

It has been thought that asymmetric vertical displacement event (AVDE) disruptions in ITER might produce large electro-mechanical forces on the walls and other conducting structures surrounding the plasma. It is shown that ITER AVDE disruptions should produce a small asymmetric wall force, comparable to JET. This is demonstrated in simulations [1, 2] with the M3D 3D MHD code [3] and confirmed in JET experiments [4] in which the current was quenched with massive gas injection (MGI). In ITER the current quench (CQ) time, τ_{CQ} , is less than or equal to the resistive wall penetration time, τ_{wall} . JET is in a different parameter regime, with $\tau_{CQ} > \tau_{wall}$. JET simulations were validated by comparison [1] to JET shot 71985 data and were in good agreement. The wall time was then artificially increased, keeping τ_{CQ} fixed, and it was found that the wall force decreased. The reduction of the asymmetric wall force was also found in experimental data [4] of JET MGI mitigated disruption shots. Further simulations [2] were carried out of ITER AVDEs. The asymmetric wall force was calculated for a wide range of CQ times. For $\tau_{CQ} < \tau_{wall}$, the force was not much larger than in JET. A fast CQ may cause production of runaway electrons (REs). The effect of replacing part of the current with REs on MHD behaviour will be discussed. Simulations using a modified version of M3D with a fluid RE model [5] will be presented.

Work supported by the U.S. Department of Energy and Euratom research and training programme 2014-2018 under grant agreement No. 633053, within the EUROfusion Consortium. Views and opinions herein do not necessarily reflect those of the European Commission.

References

- [1] H. Strauss *et al.*, Phys. Plasmas, **24**, 102512 (2017).
- [2] H. Strauss, Phys. Plasmas, **25**, 020702 (2018).
- [3] W. Park *et al.*, Phys. Plasmas, **6**, 1796 (1999).
- [4] S. Jachmich *et al.*, 43rd EPS Conf. Plasma Physics, (2016).
- [5] H. Cai and G. Fu, Nucl. Fus., **55**, 022001 (2015).

A Nonlinear 2-Fluid Study of the Effect of Pellet Injection on ELM Dynamics

D. Chandra¹, A. Thyagaraja², and A. Sen¹

¹*Institute for Plasma Research (IPR), Bhat, Gandhinagar, India*

²*University of Bristol, Bristol, BS8 1TH, UK*

Corresponding Author: D. Chandra, debasischandra@gmail.com

We report on nonlinear simulation studies of the dynamical behaviour of ELMs under the influence of repetitive injection of pellets using the nonlinear 2-fluid code CUTIE. ELMs are excited by introducing a particle source in the confinement region and a particle sink in the edge region. High density pellets are injected repeatedly near the edge with different duty cycles, where a duty cycle refers to the ratio of “on” time and “off” time of localized density perturbations. A combination of various duty cycles and different densities of the pellets have been used and comparative studies of the time series in edge density and temperature perturbations both in the absence and presence of pellets have been made. We find that the pellets significantly influence both the frequency and amplitude of the ELMs and the results are sensitive to the duty cycle and the density of the pellets. For pellets with density that are twice the normal edge density and injected with a duty cycle of 1:2, the ELMs are generated on an average at a faster rate (about twice the rate of normal ELMs) and with reduced amplitudes ($\sim 50\%$ of the average height of ELMs without pellets). These changes lead to significant improvements in the plasma β indicative of an improvement in the energy confinement due to pellet injection. Furthermore, advanced spectral analysis of the data shows that in the presence of pellets there is an inward shift in the radial location of the ELMs and a spectral shift of the mode energy towards longer wavelengths. The shifts in the fluctuation spectrum with pellets are opposite to those of earlier RMP results in that pellets induce an inverse cascade while RMPs lead to a direct cascade of the energy. Both mechanisms however lead to an overall improvement in the plasma β .

TH

Modelling Third Field Operation in the ITER Prefusion Power Operation Phase

M. Schneider¹, A. R. Polevoi¹, S. H. Kim¹, A. Loarte¹, J.-F. Artaud², B. Beaumont¹, R. Bilato³, D. Boilson¹, D. J. Campbell¹, P. Dumortier⁴, D. Farina⁵, L. Figini⁵, A. Fukuyama⁶, J. Garcia², L. Garzotti⁷, Y. Gribov¹, N. Hayashi⁸, M. Henderson¹, T. Johnson⁹, R. R. Khayrutdinov¹⁰, A. A. Kavin¹¹, F. Köchl⁷, T. Kurki-Suonio¹², A. Kuyanov¹⁰, P. Lamalle¹, E. A. Lerche^{4,7}, T. C. Luce¹, V. E. Lukash¹⁰, A. Messiaen⁴, S. D. Pinches¹, F. M. Poli¹³, K. Särkimäki¹², M. Singh¹⁴, A. Snicker¹², D. Van Eester⁴, and I. Voitsekhovitch⁷

¹International Thermonuclear Experimental Reactor (ITER),
Cadarahe Centre, 13108 St. Paul lez Durance, France

²Institut de Recherche sur la Fusion par confinement Magnétique (IRFM),
Commissariat à l'énergie atomique (CEA/Cadarahe), 13108 St. Paul lez Durance, France

³Max-Planck-Institut für Plasmaphysik, Garching, Germany

⁴Laboratory for Plasma Physics, ERM/KMS, Brussels, Belgium

⁵Istituto di Fisica del Plasma (IFP), Consiglio Nazionale delle Ricerche (CNR), 20125 Milan, Italy

⁶Kyoto University, Nishikyo-ku, Kyoto 615-8540, Japan

⁷Culham Centre for Fusion Energy (CCFE), Culham Science Centre, Abingdon, UK

⁸National Institutes for Quantum and Radiological Science and Technology (QST),
Naka Fusion Institute, Naka-shi, Ibaraki-ken, Japan

⁹KTH Royal Institute of Technology, Stockholm, Sweden

¹⁰National Research Centre "Kurchatov Institute", Moscow, Russian Federation

¹¹D. V. Efremov Institute of Electrophysical Apparatus (JSC-NIIEFA), St. Petersburg, Russian Federation
¹²Aalto University, Espoo, Finland

¹³Princeton Plasma Physics Laboratory (PPPL), Princeton, NJ 08540, USA

¹⁴International Thermonuclear Experimental Reactor (ITER), India Centre, Gujarat, India

Corresponding Author: M. Schneider, mireille.schneider@iter.org

The ITER low activation phase consists of H and He plasmas, split into prefusion power operation phases 1 and 2 (PFPO-1 and PFPO-2). The PFPO-1 phase will include 20 MW of electron cyclotron resonance heating (ECRH) and possibly 10 MW of ion cyclotron radio frequency heating (ICRH), while the PFPO-2 phase will include the full heating and current drive (H&CD) capabilities, i.e., 73 MW of H&CD power. The L-H power threshold displays a density optimum for ITER $q_{95} = 3$ operation at $n/n_G \sim 0.4$, where n_G is the Greenwald density. At half field for $n/n_G \sim 0.4$ in PFPO-1, H-mode access is predicted to be unlikely in PFPO-1 in H and marginal in He. Accessing H-mode allows the determination of the heating power required to operate ITER in H-mode and to commission/demonstrate ELM control schemes, both of which are key to the research plan. Hence, operating 5 MA/1.8 T ($q_{95} = 3$) plasmas is foreseen, since it makes the H-mode access more likely in PFPO-1. Scenarios have been developed for both PFPO-1 and PFPO-2 phases.

H-mode scenarios at 1.8 T and low density are developed according to the limited power installed in PFPO-1, providing the density upper limit, and to the fact that low density and dominant ECRH can lead to low edge ion power flow preventing H-mode access. Hence it is important to qualify which key elements can be addressed in such plasmas to determine whether the required resources to implement the 1.8 T research programme are worthwhile.

Continued...

Integrated simulations of ITER 5 MA/1.8 T plasmas have been carried out with various 1.5D transport integrated modelling suites of codes by the ITPA topical group on integrated operation scenarios (ITPA-IOS) in collaboration with the IO and with support from the ITPA Transport and Confinement and Energetic Particles groups. The present contribution reports the results of self-consistent transport and H&CD analyses to assess the efficiency of EC and IC heating in 5 MA/1.8 T plasmas in L and H-modes. With a view to study H-modes at 1.8 T in PFPO-2, the possibility to heat these plasmas with NBI has been assessed as well. These issues are assessed by the application of a range of integrated modelling suites, used in association with either simplified H&CD models or more sophisticated codes for ECRH, ICRH and NBI modelling.

Predictions of α -Particle and Neutral-Beam Heating and Transport in ITER Scenarios

E. M. Bass¹, R. E. Waltz²

¹University of California San Diego, CA 92093, USA

²General Atomics, San Diego, CA 92186, USA

Corresponding Author: E. M. Bass, basseem@fusion.gat.com

We present predictions of the ITER fusion- α and neutral-beam-injection (NBI) ion density and power-deposition profiles using a stiff transport critical gradient model (CGM) for Alfvén eigenmode (AE) transport in various ITER scenarios. In a burning plasma such as planned in ITER, deposited heat from fusion-born 3.5 MeV α -particles provides most of the power needed to sustain fusion. Under current plans, high-energy (1 MeV) neutral beam injected (NBI) ions will provide much of the remaining steady-state power. Both processes rely on energetic ions slowing down through collisions with electrons, depositing most of their energy into central plasma heat before being lost. Moreover, edge loss of inadequately slowed EPs poses a risk to plasma-facing components, particularly if such losses are concentrated in intermittent bursts. Looking principally at AE transport, the greatest identified risk, we will show that lower current and reversed-shear ITER scenarios show a decrease in EP confinement. We also show that increasing the NBI fraction of auxiliary heating degrades confinement for both the alpha particles and beam ions. The time-averaged EP profile prediction tools developed for this study have been verified against first-principles nonlinear simulations [1, 2] and validated against a beam-heated DIII-D discharge [3]. A new fast computation of the critical gradient [4] eases integration into whole device modelling (WDM) frameworks. Also, a new quasi-linear time-dependent transport model is used to investigate transport intermittency.

Work supported by the U.S. Department of Energy under Grants DE-FG02-95ER54309 (theory), DE-FC02-08ER54977 (SciDAC-GSEP project), and DE-SC0018108 (SciDAC-ISEP project).

References

- [1] E. M. Bass and R. E. Waltz, *Phys. Plasmas*, **17**, 112319 (2010).
- [2] E. M. Bass and R. E. Waltz, *Phys. Plasmas*, **24**, 122302 (2017).
- [3] R. E. Waltz, *et al.*, *Nucl. Fus.*, **55**, 123012 (2015).
- [4] H. Sheng *et al.*, *Phys. Plasmas*, **24**, 072305 (2017).

Real-Time Simulation of the NBI Fast-Ion Distribution

M. Weiland¹, R. Bilato¹, R. Dux¹, B. Geiger¹, A. Lebschy¹, F. A. A. Felici², R. Fischer¹, W. W. Heidbrink³, W. Hu⁴, D. Rittich¹, M. Scheffer², B. Sieglin¹, and M. A. Van Zeeland⁵

The ASDEX-Upgrade Team and EUROfusion-MST1 Team

¹Max-Planck-Institut für Plasmaphysik, Garching, Germany

²Eindhoven University of Technology, Eindhoven, Netherlands

³University of California Irvine, CA 92697, USA

⁴Institute of Plasma Physics, Chinese Academy of Sciences, Hefei, Anhui, People's Republic of China

⁵General Atomics, San Diego, CA 92186, USA

Corresponding Author: M. Weiland, markus.weiland@ipp.mpg.de

Knowledge of the fast-ion distribution arising from neutral beam injection (NBI) is important for transport analysis and magnetic equilibrium reconstruction. For sophisticated plasma control, which will be essential for the success of future fusion devices, it is very beneficial to know this distribution function already in real-time during the discharge. Then, the relevant quantities (e.g., heating profiles, current-drive etc.) can be fed to real-time transport and equilibrium codes like RAPTOR, which estimate kinetic and current density profiles in real-time. Beyond real-time applications, such fast models are essential for optimization problems, e.g., reactor design studies or discharge planning.

Several sophisticated models exist, that can calculate this beam ion distribution in good agreement with experimental data, such as the Monte Carlo code NUBEAM. The high accuracy of these codes has, however, to be paid with relatively intensive numerical efforts, which compromises their use in real-time applications. In this contribution, we present the novel code RABBIT (Rapid Analytically Based Beam Injection Tool). RABBIT currently takes ≈ 25 ms per time step, which is roughly a factor of 1000 faster than the NUBEAM code. The approximations needed to arrive at this goal are discussed. Benchmarks are carried out with the more accurate but also much slower NUBEAM code, indicating a good agreement.

Several applications of the model on different machines are carried out. RABBIT is run in real-time in the discharge control system of ASDEX-Upgrade to improve active plasma control. In addition, RABBIT is being used for accurate equilibrium reconstructions (with the IDE code) in between shots. This facilitates the development of advanced scenarios, where a fine-tuning of the q -profile is desired.

On DIII-D, RABBIT is foreseen to be used in experiments with the goal to demonstrate real-time control of Alfvén eigenmodes (AE). Here, the neutron rate prediction from RABBIT is compared to the measured neutron rate to detect appreciable fast-ion transport. In conjunction with direct AE detection with ECE diagnostics, when detrimental conditions are observed, countermeasures to stabilize AEs can be activated during the discharge. This could be of great importance for future fusion reactors, where strong AE activity is expected.

Predicting Scrape-Off Layer Profiles and Filamentary Transport for Reactor Relevant Devices

F. Militello¹, R. Akers¹, L. Appel¹, B. Cannas⁴, S. Carcangiu⁴, B. D. Dudson², A. Fanni⁴, T. Farley^{1,3}, A. Kirk¹, J. R. Harrison¹, B. Lipschultz^{1,2}, A. Montisci⁴, T. Nicholas^{1,2}, J. T. Omotani¹, F. Pisano⁴, F. Riva¹, G. Sias⁴, N. R. Walkden¹, and A. Wynn^{1,2}

The MAST and JET Teams

¹Culham Centre for Fusion Energy (CCFE), Culham Science Centre, Abingdon, UK

²York Plasma Institute, University of York, Heslington, UK

³Department of Electrical Engineering and Electronics, University of Liverpool, Liverpool, UK

⁴Department of Electrical and Electronic Engineering, Università di Cagliari, 09124 Cagliari CA, Italy

Corresponding Author: F. Militello, fulvio.militello@ukaea.uk

This paper discusses a statistical framework that relates the fundamental physics of scrape-off layer (SOL) L-mode and inter-ELM filaments with the profiles they generate in magnetic confinement devices. This work reviews the theoretical and numerical work recently carried out at CCFE in support of the statistical framework and compares it with experimental measurements obtained with innovative techniques on MAST and JET. The emphasis will be on extrapolating the knowledge gained to future machines like ITER and to advanced divertor solutions. With a semianalytic treatment using minimal computational resources, the framework predicts and interprets the experimental profiles and of the turbulence statistics on the basis of simple properties of the filaments, such as their radial motion and their draining towards the divertor. Filaments are described as independent events and modelled with a wave function of amplitude and width statistically distributed according to experimental observations and evolving according to fluid equations. The framework predicts that radially accelerating filaments, less efficient parallel exhaust (e.g., due to interaction with neutrals) and also a statistical distribution of the radial velocities can contribute to induce flatter profiles in the far SOL and therefore enhance plasma-wall interactions. It also suggests that profile broadening at high fuelling rates, potentially harmful for ITER, can be caused by interactions with neutrals in the divertor or at the wall or by a significant radial acceleration of the filaments. The results of the framework are backed up by systematic experimental comparison with measurements taken on JET and MAST using Langmuir probes and fast visual cameras. Advanced machine learning algorithms were developed and deployed, including Bayesian analysis of time traces and convolutional neural networks applied to filament identification in images. In all the cases treated, the theoretical prediction matched the experimental data within uncertainty. In addition, 3D simulation in realistic geometry were performed with the 3D SOL turbulence code STORM, with the aim of assessing the validity of the framework assumptions. The mechanisms governing the interaction of pairs of filaments and the dynamics of high- β , inter-ELM like, filaments were investigated and employed to improve the statistical framework.

Study of Passively Stable, Fully-Detached Divertor Plasma Regimes Attained in Innovative Long-Legged Divertor Configurations

M. V. Umansky¹, B. LaBombard², D. Brunner², T. Golfinopoulos², A. Q. Kuang²,
M. E. Rensink¹, J. L. Terry², M. Wigram³, and D. G. Whyte²

¹Lawrence Livermore National Laboratory (LLNL), Livermore, CA 94550, USA

²Plasma Science & Fusion Center, MIT, Cambridge, MA 02139, USA

³York Plasma Institute, University of York, Heslington, UK

Corresponding Author: M. V. Umansky, umansky1@llnl.gov

Passively-stable fully detached divertor regimes have been found in numerical modelling of divertor configurations with radially or vertically extended, tightly baffled, outer divertor legs, with or without a secondary X-point in the leg volume [1]. Simulations carried out with the tokamak edge transport code UEDGE [2] using the base parameters of the ADX tokamak design [3] show that long-legged divertors provide up to an order-of-magnitude increase in the peak power-handling capability compared to conventional divertors, and a fully detached plasma state can be passively maintained over a wide range of parameters. In the simulations, the radial transport in the scrape-off layer is set to reproduce profiles observed in the experiment, which includes “shoulders” indicative of main-chamber recycling phenomena [4]. In the UEDGE model used here, strong radial transport is assumed to occur in the outer divertor leg as well, leading to plasma predominantly recycling on the divertor leg outer sidewall. Analysis of simulations shows that the detachment front location is set by the balance between the power entering the divertor leg and the losses to the walls of the divertor channel. Therefore, for a fixed level of power exhaust, the location of the detachment front is insensitive to the divertor leg length—as long as the leg length exceeds the front location. The key physics for attaining the passively stable, fully detached regime involves an interplay of strong convective plasma transport to the divertor leg outer sidewall, confinement of neutral gas in the divertor volume, geometric effects possibly including a secondary X-point, and atomic radiation. In response to variation of model assumptions (magnitude of anomalous radial transport, impurity radiation, neutral transport model, geometry of plasma-facing components), the overall divertor plasma behaviour remains qualitatively similar: a stable fully detached regime is maintained, lending confidence in the modelling results.

Work supported by U.S. Department of Energy contract DE-AC52-07NA27344 and cooperative agreement DE-SC0014264.

References

- [1] M. V. Umansky *et al.*, Phys. Plasmas, **24**, 056112 (2017).
- [2] B. LaBombard *et al.*, Nucl. Fus., **55**, 053020 (2015).
- [3] T. D. Rognlien *et al.*, J. Nuc. Mat., **196**, 347–123 (1992).
- [4] B. LaBombard *et al.*, Nucl. Fus., **40**, 2041 (2000).

Gyrokinetic XGC1 Simulation Study of Magnetic Island Effects on Neoclassical and Turbulence Physics in a KSTAR Plasma

J.-M. Kwon¹, S. Ku², C.-S. Chang², M. J. Choi¹, R. Hager², E. S. Yoon³, H. H. Lee¹, and H. S. Kim¹

¹National Fusion Research Institute (NFRI), Daejeon, Republic of Korea

²Princeton Plasma Physics Laboratory (PPPL), Princeton, NJ 08540, USA

³Rensselaer Polytechnic Institute, Troy, NY 12180, USA

Corresponding Author: J.-M. Kwon, jmkwon74@nfri.re.kr

We perform gyrokinetic simulations to study the effects of a stationary magnetic island on neoclassical and turbulence physics. A KSTAR L-plasma condition is employed for the simulations. Through the simulations, we aim to understand the underlying physical mechanisms of poloidal flows and fluctuations around a stationary (2, 1) magnetic island, which were observed in a recent KSTAR experiment using 2D ECEI diagnostics [1]. From the simulations, it is found that the magnetic island can significantly enhance the equilibrium $E \times B$ flow. The corresponding flow shearing is strong enough to suppress a substantial portion of ambient microinstabilities, particularly ∇T_e -driven trapped electron modes. This implies that the enhanced $E \times B$ flow can sustain a quasi-internal transport barrier for T_e in an inner region neighbouring the magnetic island. The enhanced $E \times B$ flow has a (2, 1) mode structure, which shows a finite phase difference with the mode structure of the magnetic island. It is shown that the flow shear and fluctuation suppression patterns the simulations imply are consistent with the ECEI observations on the KSTAR experiment.

References

[1] M. J. Choi *et al.*, Nucl. Fus., **57**, 126058 (2017).

Benchmarking of Full-*f* Global Gyrokinetic Modelling Results against the FT-2 Tokamak Doppler Reflectometry Data Using Synthetic Diagnostics

A. B. Altukhov¹, A. D. Gurchenko¹, E. Z. Gusakov¹, M. A. Irzak¹, O. L. Krutkin¹,
P. Niskala², L. A. Esipov¹, T. P. Kiviniemi², and S. Leerink²

¹*Ioffe Institute, St. Petersburg, Russian Federation*

²*Aalto University, Espoo, Finland*

Corresponding Author: A. B. Altukhov, a.altuhov@mail.ioffe.ru

The fast linear (Born approximation) version of the X-mode Doppler reflectometry (DR) synthetic diagnostics is developed in the framework of the ELMFIRE global gyrokinetic modelling of the FT-2 tokamak ohmic discharge. The DR signal frequency spectra and the dependence of their frequency shift and shape on the probing antenna position are computed and shown to be similar to those measured in the high magnetic field side probing DR experiment at the FT-2 tokamak thus demonstrating a correct reproduction of the electric field behaviour in the FT-2 tokamak by the ELMFIRE GK code. However, the computed and measured dependences of the DR signal power on the antenna position characterizing the “poloidal correlation lengths” appear to be different presumably due to underestimation of the small-scale TEM turbulence component in the measurement region by the code. The fluctuation poloidal velocities and the geodesic acoustic mode (GAM) amplitudes are determined using DR experiment and synthetic diagnostics and shown to be close within a 20% accuracy, whereas the GAM frequency spectra demonstrate clear differences. In the case of multifrequency probing the cross-correlation function of radial correlation DR obtained in the experiment is shown to be a factor of four narrower than the computed one due to the phase modulation of the DR signal by long-scale turbulent density fluctuations. A comparison to the alternative version of the DR synthetic diagnostics based on the nonlinear full-wave modelling is also performed. It is shown that in spite of a better description of the radial correlation DR data nonlinear synthetic diagnostics fails to reproduce the DR frequency spectra as opposed to linear version of the synthetic diagnostic. The nonlinear effects in the DR spectra formation are shown to be responsible for this under conditions of small scale turbulence level underestimation by the GK code.

TH

New Results in Stellarator Optimization

M. Drevlak¹, C. D. Beidler¹, J. Geiger¹, P. Helander¹, S. Henneberg¹, C. Nührenberg¹, and Y. Turkin¹

¹*Max-Planck-Institut für Plasmaphysik, Greifswald, Germany*

Corresponding Author: M. Drevlak, drevlak@ipp.mpg.de

The ROSE code was written for the optimization of stellarator equilibria. It uses VMEC for the equilibrium calculation and several different optimizing algorithms for adjusting the boundary coefficients of the plasma. Some of the most important capabilities include optimization for simple coils, the ability to simultaneously optimize vacuum and finite- β field, direct analysis of particle drift orbits and direct shaping of the magnetic field structure. ROSE was used to optimize quasi-isodynamic, quasi-axially symmetric and quasi-helically symmetric stellarator configurations.

Numerical Diagnostic to Investigate Poloidal Asymmetry in Three-Dimensional Magnetic Configurations

N. Kasuya¹, M. Nunami², K. Tanaka², C. A. Michael³, S. Toda¹, and M. Yagi⁴

¹Research Institute for Applied Mechanics (RIAM), Kyushu University, Kasuga, Japan

²National Institute for Fusion Science (NIFS), Toki, Gifu, Japan

³Plasma Research Laboratory, Australian National University, Canberra, Australia

⁴National Institutes for Quantum and Radiological Science and Technology (QST), Rokkasho Fusion Institute, Rokkasho-mura, Aomori, Japan

Corresponding Author: N. Kasuya, kasuya@riam.kyushu-u.ac.jp

Some experimental observations show poloidal asymmetry in the turbulence measurements, which can affect the plasma transport, so detailed spatial structures must be clarified. In Large Helical Device (LHD), an up-down asymmetry has been observed by the PCI diagnostic. Complicated configurations make it difficult to capture the entire structures of fluctuations in helical plasmas, so 3D turbulence simulations are necessary for understanding the mechanism. We are developing the Turbulence Diagnostic Simulator (TDS), and carry out the numerical diagnostics in helical plasmas for understanding the plasma turbulence. In this case, the gyrokinetic simulation code GKV-X provides turbulent fluctuations in 3D configurations, and then, the TDS calculates its line-integration along the line of sight (LS) as in phase contrast imaging (PCI) to give numerical observation signals. There is a problem to resolve the local values from the line-integrated signal. The pitch angle of the magnetic field is used to help the identification of the local spectrum. A finite resolution in the local wavenumber spectrum deteriorates the reconstruction. The ITG modes have a characteristic wavelength and frequency, and difference in the spectrum can be distinguished at different radial positions, considering the spatial resolution. Characteristics of turbulence can be estimated by this analysis. The results of the TDS application indicate three factors to induce the poloidal asymmetry; 3D magnetic configuration with the realistic LS, effect of signal processing techniques, and inherent inhomogeneity of the turbulence itself. The original data includes only small up-down asymmetry, because this is given from a single flux-tube data. The effect from the 3D configuration generates the asymmetry, and tends to be enhanced by signal processing, but is not comparable with the experimental results. Artificial reduction of the fluctuation amplitude in the bottom half of the region can give the comparable asymmetry. This result indicates an inherent asymmetry of the turbulence. This asymmetry may be attributed to the dependence on the field line label, which is being confirmed by the GKV-X code.

Effect of Magnetic Shear and the Finite Banana-Orbit Width on the Neoclassical Toroidal Viscosity in Perturbed Tokamaks

S. Satake^{1,2}, J. L. Velasco³, I. Calvo³, S. Matsuoka⁴, and M. Honda⁵

¹National Institute for Fusion Science (NIFS), Toki, Gifu, Japan

²Graduate School for Advanced Studies, 322-6, Oroshi-cho, Toki-city, 509-5292, Japan

³Laboratorio Nacional de Fusión (LNF),

Centro de Investigaciones Energéticas, Medioambientales y Tecnológicas (CIEMAT), Madrid, Spain

⁴Japan Atomic Energy Agency (JAEA), Naka, Japan

⁵National Institutes for Quantum and Radiological Science and Technology (QST),
Naka Fusion Institute, Naka-shi, Ibaraki-ken, Japan

Corresponding Author: S. Satake, satake@nifs.ac.jp

The effect of magnetic perturbations on the rotation profile in tokamak has been studied both experimentally and theoretically, since the prediction and control of the plasma rotation is one of the key issues for the stable operation. The NTV torque caused by magnetic perturbations is evaluated by adopting either a local or global drift-kinetic models. In the local models, the finiteness of the drift orbit width is neglected, and the magnetic-shear dependence of the precession frequency ω_B has been omitted. However, recent studies have found that the NTV evaluated from the global simulations, which keep the finite-orbit-width (FOW) effect and the magnetic-shear effect, are different from what the local models predict. Therefore, understanding the reason of this discrepancy in the NTV calculations is important.

Here, by comparing global and local simulations, the FOW effect and the magnetic-shear effect are investigated. To study these two effects separately, we prepared two local simulation models, one neglects the magnetic-shear effect while the other keeps it in the evaluation of ω_B .

For electrons, it is found that the NTV profiles from the global and local codes are similar. Strong resonance of drift motions with the perturbed field occurs if $\omega_B \simeq 0$, which causes the strong NTV in low-collisionality regimes. Frequency ω_B depends on the magnetic moment and the local shear. The resonant condition in the velocity space approaches to the trapped-passing boundary as the local magnetic shear becomes more positive. In the positive-shear case, the resonant orbits are easily disturbed by small collisions and therefore the NTV evaluated by the global model tends to be smaller than that by the local one. Opposite tendency can be seen in the negative-shear case. For ions, it is found that the difference in NTV between local and global simulation becomes significant and is caused not only by the magnetic-shear effect but also by the FOW effect. In the global calculation, trapped particles see the spatial variation of the magnetic perturbations along the perturbed drift motions, while the local model assumes that a trapped particle bounces along an unperturbed field line. The nonlocal effect causes a significant difference in the ion NTV and in the rotation profile predicted from global and local simulations.

Steady States for Nonaxisymmetric Rotating Toroidal Plasmas

L. E. Sugiyama¹

¹*Massachusetts Institute of Technology (MIT), Cambridge, MA 02139, USA*

Corresponding Author: L. E. Sugiyama, sugiyama@mit.edu

Small applied nonaxisymmetric magnetic fields have been demonstrated to have strong and complex effects on otherwise axisymmetric toroidal fusion plasmas. Their importance raises the question of the best “steady state” plasma configuration to use for their analysis. A steady state that is valid on fast time scales of a few Alfvén times is needed to invert and interpret experimental measurements and as an initial state to study slower-developing plasma instabilities and plasma processes. It should possess a magnetic flux function Ψ with $B \cdot \nabla \Psi = 0$ and a well-confined boundary surface that confines the magnetic field lines. It contains free functions and parameters that must be taken from observations or outside models. The simplest choice is ideal MHD. Axisymmetric and helical MHD plasmas with zero plasma flow possess a good flux function, the plasma pressure, which in axisymmetry is equivalent to the poloidal magnetic flux ψ . Axisymmetric states with plasma rotation have two functions, ψ and the centrifugally shifted plasma mass density, which represent electron and ion surfaces, respectively. The shifted density modifies the mapping of experimental density to magnetic flux surfaces and allows larger density gradients at the large- R boundary of the torus. Magnetic nonaxisymmetry due to external fields couples the two functions. In single-fluid MHD, the coupling can be shown to impose strong and probably unrealistic constraints on the allowable variation of the rotation and density relative to the magnetic field. Two-fluid models decouple the electron and ion motions and allow greater freedom that removes the restrictions. They also have other properties that reflect experimental observations. The proposed solutions will be studied for experimental cases with rotation and nonaxisymmetry, by numerical simulation with the nonlinear extended MHD code M3D [1, 2], using the real nonaxisymmetric fields. The results will also be compared to the nonlinear evolution.

Work partially supported by the U.S. Department of Energy OFES contract DE-SC0007883.

References

- [1] W. Park *et al.*, Phys. Plasmas, **6**, 1796 (1999).
- [2] L. E. Sugiyama and W. Park, Phys. Plasmas, **7**, 4644 (2000).

Plasma-Surface Related 3D Modelling Results for Wendelstein 7-X and EAST

F. Schluck¹, M. Rack¹, Y. Feng^{2,3}, S. Xu¹, W. Zhlobenko¹, J. Cosfeld¹, and D. Reiter¹

The W7-X Team

¹Forschungszentrum Jülich, Jülich, Germany

²Max-Planck-Institut für Plasmaphysik, Greifswald, Germany

³Max-Planck-Institut für Plasmaphysik, Garching, Germany

Corresponding Author: F. Schluck, f.schluck@fz-juelich.de

Present-day fusion devices are operated with a multitude of diagnostics in different locations, with which important insight in plasma profiles is obtained. However, since the detected signals only represent a spatially small part of the machine, the experiment natively exhibits blind spots, in particular in the 3D edge plasma region, where flux surface averaging reductions are inappropriate. Theory, and especially numerical simulation, may bridge over these unknown areas in order to complete the complex physical picture of the nature of the plasma profile.

The fluid plasma edge Monte Carlo code (EMC3) [1] coupled to the kinetic (neutral) transport code EIRENE [2, 3] is a commonly used fully dimensional plasma edge simulation code for treating such complex magnetic configurations. EMC3 bases on a Monte Carlo algorithm for a reduced set of Braginskii equations formulated in a Fokker-Planck scheme, while EIRENE solves extended Boltzmann equations in full phase-space directly.

Because of its intrinsically 3D structure, one of the main applications of EMC3-EIRENE is the simulation of scrape-off layer physics for the stellarator Wendelstein 7-X. However, also in tokamaks 3D effects may play an important role, e.g., when using resonant magnetic perturbations to suppress the formation of ELMs.

With this contribution, we present recent results obtained with EMC3-EIRENE. After the study of the divertor manipulator concept and design [4], we stress the importance of kinetic treatment of certain minority ions at the example of helium operation in Wendelstein 7-X [5]. Subsequently, we apply the 3D resolved virtual diagnostics module of EIRENE, capable of simulating a fully synthetic helium beam diagnostic and present results on effective charge state distribution modelling. The same computational tools are then applied to intrinsically 3D lower-hybrid wave induced magnetic perturbation modelling on EAST. We close with a discussion and outlook of the physical impact the enhanced kinetic ion transport description in EIRENE has on both, stellarator and tokamak simulations.

References

- [1] Y. Feng *et al.*, J. Nucl. Mater., **266–269**, 812 (1999).
- [2] EIRENE: <http://www.eirene.de>, from 2nd Feb. 2018.
- [3] D. Reiter *et al.*, Fusion Sci. Tech., **47**, (2), 172 (2005).
- [4] M. Rack *et al.*, Plasma Sci. Technol, accepted (2018).
- [5] M. Rack *et al.*, Nucl. Fus., **57**, 056011 (2017).

Influence of Neutral-Plasma Interactions on 3D Scrape-Off Layer Filaments

D. Schwörer^{1,2}, N. R. Walkden², B. D.udson³, F. Militello², H. Leggate¹, and M. M. Turner¹

¹Dublin City University, Ireland

²Culham Centre for Fusion Energy (CCFE), Culham Science Centre, Abingdon, UK

³University of York, Heslington, UK

Corresponding Author: D. Schwörer, schword2@mail.dcu.ie

Filaments are field aligned, nonlinear density perturbations, which have been observed in most plasmas. In tokamaks they can carry a significant amount of particles and heat from the last closed flux surface to the far scrape-off layer (SOL). This highly nondiffusive transport mechanism can cause a significant heat load onto first wall materials. It is important to understand the motion of filaments, particularly in regard to the design of future fusion devices. Recent experiments on several machines have shown that the plasma density of the SOL can have a significant influence on the dynamics of filaments.

We have carried out nonlinear, 3D-seeded filament simulations, with the focus on neutral-plasma interactions, using the BOUT++ library. The model is an extension of the STORM code, which is a two fluid model, including thermal electrons. In order to study the influence of neutrals, 1D background profiles are computed. By varying particle and heat influx, different profiles are generated. The filaments of critical size showed an increasing radial velocity with increasing upstream temperature, as expected from scaling laws. The filament further showed a decreasing radial velocity with increasing plasma density. In these conditions, the neutrals interaction resulted in a reduced radial velocity. It was further observed that the filaments radial velocity had a strong dependency on the target temperature, resulting in an increasing radial motion for an increasing target temperature.

As higher neutral densities could affect the strong sheath currents, studying the neutrals filament interaction at higher densities is of interest. In the current study the density was further increased, as the previous simulations showed an increasing influence of the neutrals on the filaments with increasing background plasma density and temperature on the filament. The purely diffusive neutral model in STORM was extended to enable the modelling of higher density conditions towards detachment. This has been validated against other neutral simulation codes.

This work has been carried out within the framework of the EUROfusion Consortium and has received funding from the Euratom research and training programme 2014–2018 under grant agreement No. 633053.

Comparative Modelling of Plasma Boundary Corrugation due to the Application of 3D Fields with ELM Control Coils in Various ITER Scenarios

L. Li¹, Y. Liu², A. Loarte³, S. D. Pinches³, A. R. Polevoi³, and F. C. Zhong¹

¹*Donghua University, Shanghai 201620, People's Republic of China*

²*General Atomics, San Diego, CA 92186, USA*

³*International Thermonuclear Experimental Reactor (ITER), Cadarache Centre, 13108 St. Paul lez Durance, France*

Corresponding Author: L. Li, lili8068@dhru.edu.cn

The plasma response to the 3D external resonant magnetic perturbation (RMP) fields, applied for controlling type-I edge localized modes (ELMs) in ITER, is systematically computed in terms of the normal displacement of the plasma surface, in other words the 3D corrugation of the plasma boundary. Five representative ITER H-mode plasma scenarios, ranging from an initial hydrogen plasma discharge in pre-nuclear phase to the $Q = 10$ nuclear phase DT operation. The plasma surface corrugation, computed using the MARS-F code, is used as a basis to understand the capability and robustness of the type-I ELM control in these ITER scenarios. A key aspect of this study is to assess effects of variation and uncertainty of pedestal plasma rotation on the plasma response. For each plasma scenario, a set of the toroidal rotation — both amplitude and radial profile — is generated by the transport code ASTRA, assuming different Prandtl numbers as well as different ratios of the toroidal momentum to thermal confinement times. Toroidal modelling results show that: i) the plasma response is similar for the two DT scenarios with 15 MA/5.3 T plasmas but with different fusion gain factors ($Q = 5$ versus $Q = 10$); ii) the other plasma scenarios, with similar rotation profiles, have different plasma boundary corrugation; and iii) the effect on ELM control performance by utilizing 2 or 3 rows of coils, with the coil phasing optimization, varies depending on the availability of the ELM control coil power supplies. The plasma response database, generated in this study, can also be used for further studies such as the divertor footprint and heat load, or energetic particle losses due to RMP.

Predict-First Analysis and Experimental Validation of MHD Equilibrium, Stability, and Plasma Response to 3D Magnetic Perturbations

B. C. Lyons¹, O. Meneghini¹, C. Paz-Soldan¹, L. L. Lao¹, D. B. Weisberg¹, P. B. Snyder¹, N. M. Ferraro², E. A. Belli¹, T. E. Evans¹, M. W. Shafer³, G. Y. Park⁴, W. Guo⁵, and G. Q. Li⁵

¹General Atomics, San Diego, CA 92186, USA

²Princeton Plasma Physics Laboratory (PPPL), Princeton, NJ 08540, USA

³Oak Ridge National Laboratory (ORNL), Oak Ridge, TN 37831, USA

⁴National Fusion Research Institute (NFRI), Daejeon, Republic of Korea

⁵Institute of Plasma Physics, Chinese Academy of Sciences, Hefei, Anhui, People's Republic of China

Corresponding Author: B. C. Lyons, lyonsbc@fusion.gat.com

An integrated-modelling workflow has been developed to predict equilibria and response to 3D magnetic perturbations in tokamak experiments. Starting from an equilibrium reconstruction from a past experiment, the workflow couples together the EFIT Grad-Shafranov solver, EPED model for pedestal stability, and NEO drift-kinetic-equation solver (for bootstrap current calculations) in order to generate equilibria with self-consistent pedestal structures as the plasma shape and various scalar parameters (e.g., normalized beta, pedestal density, q_{95}) are changed. These equilibria are then analyzed using automated M3D-C1 to compute the MHD plasma response to 3D magnetic perturbations. The workflow was created in conjunction with a DIII-D experiment studying the effect of triangularity on plasma response, showing excellent agreement between the analysis of the workflow's equilibria and equilibria reconstructed from the experiment. Various versions of the workflow demonstrated that the details of the edge current profile were not important for these cases, while q_{95} and the details of the global pressure profile had a significant impact on the results. A predict-first study was then carried out for a DIII-D experiment examining how plasma response varies between single- and double-null shapes. The predicted equilibria were used to guide experimental planning and the predicted response was found to agree well with the perturbed magnetic field measured on the high-field-side midplane. Applications of this workflow to KSTAR and EAST experiments will also be explored. This work forms the basis of predictive scenario development across current and future devices (e.g., ITER), allowing for higher-fidelity predictions of MHD stability and 3D plasma response.

Work supported by the U.S. Department of Energy under DE-FG02-95ER54309 and DE-FC02-04ER54698, along with NFRI, Republic of Korea.

Transport Induced by Energetic Geodesic Acoustic Modes

D. Zarzoso¹, D. del-Castillo-Negrete², S. Benkadda¹, X. Garbet³, Y. Sarazin³,
V. Grandgirard³, and M. Sasaki^{4,5}

¹*Physique des Interactions Ioniques et Moléculaires (PIIM), CNRS, Aix-Marseille Université, France*

²*Oak Ridge National Laboratory (ORNL), Oak Ridge, TN 37831, USA*

³*Institut de Recherche sur la Fusion par confinement Magnétique (IRFM),*

Commissariat à l'énergie atomique (CEA/Cadarache), 13108 St. Paul lez Durance, France

⁴*Research Institute for Applied Mechanics (RIAM), Kyushu University, Kasuga, Japan*

⁵*Research Center for Plasma Turbulence (RCPT), Kyushu University, Kasuga, Japan*

Corresponding Author: D. Zarzoso, david.zarzoso-fernandez@univ-amu.fr

Energetic particles naturally exist in a tokamak due to either fusion reactions or external heating such as ICRH or NBI. These energetic particles need to be well-confined in order to transfer their energy to thermal particles and achieve this way a regime with self-sustained fusion reactions. However, energetic particles excite modes that tend to deconfine the particles themselves. This is the reason why energetic particle mode excitation and saturation need to be understood and controlled. We focus our analysis on a special class of energetic particle modes, called energetic geodesic acoustic modes (EGAMs). In this work, we present highly resolved full- f global gyrokinetic 2-species simulations using GYSELA code that evidence the formation of chain of islands in phase space during the nonlinear saturation of EGAMs. Those islands appear at the predicted positions using linear and nonlinear wave-particle interaction theory. By means of a test-particle tracing method we solve the particle equations of motion using the self-consistent electrostatic potential obtained from 2-species GYSELA simulations and show that, even for weak fractions of energetic particles the EGAM island can interact with the trapping/de-trapping region characteristic of toroidal devices. In particular, counter-passing particles can be trapped and eventually deconfined, in agreement with experiments and with previous full-orbit particle simulations. Also, the nature of the transport induced by the energetic modes has been analyzed. For this purpose, statistical analysis of 20000 counter-passing particles around the EGAM resonance has been performed. The variance of the particle displacement in phase space shows a superballistic transport. When the EGAM saturates the losses increase following also a power law and the transport becomes subdiffusive.

Burning Plasma Simulation with α -Particle Heating

U. Maurya¹, D. Banerjee², and R. Srinivasan¹

¹*Institute for Plasma Research (IPR), Bhat, Gandhinagar, India*

²*University of Science and Technology of China, Hefei, Anhui, People's Republic of China*

Corresponding Author: U. Maurya, udaya.maurya@ipr.res.in

To achieve self-sustained ignited operation in a high energy tokamak, it is important to understand and maximize the energy confinement time, which falls in the domain of transport theory. To analyze and understand dynamics of plasma in tokamak, performing a one-dimensional transport simulation is still one of the best approaches. In our work we focus on burning plasma simulation and study the α -particle heating in high energy tokamaks like ITER. Transport simulations can be performed by solving 1D transport equations using codes such as LCPFCT (Laboratory for Computational Physics Flux-Corrected Transport) [1], which is used to solve 1D generalized coupled continuity, momentum and energy equations along with Maxwell's equations. The transport equations are solved in flux coordinates by coupling with 2D tokamak equilibrium. In this model, the effects of fusion reactions, coulomb collisional losses, radiation losses, α -heating, auxiliary heating and neo-classical Ware pinch are included. This will predict the performance of tokamak based fusion reactor for obtaining the steady state operation. This model is being developed and will be bench marked with published results. This will be use to predict the performance of SST2-like [2] and ITER-like [3] cases and results will be presented in this paper.

References

- [1] J. P. Boris *et al.*, NRL Memorandum Report 93-7192 (1993).
- [2] R. Srinivasan *et al.*, Fusion Eng. Des., **112**, 240 (2016).
- [3] K. Ikeda *et al.*, Nucl. Fus., **47**, (2007).

Simulation of Toroidicity-Induced Alfvén Eigenmode Excited by Energetic Ions in HL-2A Tokamak Plasmas

H. He¹, J. Cheng², J. Q. Dong¹, W. Zhang², C. Zhang², J. Zhu³, G. Z. Hao¹, and Z. Lin⁴

¹Southwestern Institute of Physics, Chengdu, Sichuan, People's Republic of China

¹Institute of Physics, Chinese Academy of Sciences, Beijing 100190, People's Republic of China

¹Sichuan University of Arts and Science, Dazhou, People's Republic of China

¹University of California Irvine, CA 92697, USA

Corresponding Author: H. He, hehd@swip.ac.cn

The toroidicity-induced Alfvén eigenmode (TAE) excited by energetic ions was first simulated by using GTC code based on HL-2A experimental configuration. The simulation results show that the fraction of energetic (fast) ions in HL-2A experiments is about 3%. The TAE eigenmode frequency is around 211 kHz and is inversely proportional to the square root of electron density, which is quantitatively in agreement with the experimental observation. The real frequency of TAE modes increases with both temperature of energetic ions (beam energy) and toroidal mode numbers increasing thanks to the toroidal precession resonance is dominant, but almost keeps constant when the density of energetic ions changes. The growth rates of TAE modes increase with increasing density as well as density gradient of fast ions. The amplitude of the vector potential A_{\parallel} exponentially increases with time for linear TAE mode. Besides, the low- n (toroidal mode number) TAE modes, such as $n = 1$ can also be driven by energetic ions when off-axis heating with higher beam energy is employed during HL-2A NBI experiment. The half width of radial mode structures for low- n modes is usually wider than those for high- n modes. The perpendicular wave vector of the TAE modes and Larmor radius of ions satisfy the relation $|k_{\perp} \rho_{Li}|^2 \ll 1$. At the same time, the polarization of the TAE mode shows that the perturbed parallel electric field is zero. Thus, the TAE mode is close to an ideal MHD mode.

Global Gyrokinetic Multimodel Simulations of ITG and Alfvénic Modes for Tokamaks and the First Operational Phase of Wendelstein 7-X

R. Kleiber¹, M. Borchardt¹, R. Hatzky², A. Könies¹, O. Mishchenko¹, J. Riemann¹, and C. Slaby¹

¹*Max-Planck-Institut für Plasmaphysik, Greifswald, Germany*

²*Max-Planck-Institut für Plasmaphysik, Garching, Germany*

Corresponding Author: R. Kleiber, ralf.kleiber@ipp.mpg.de

Results from a hybrid approach (CKA-EUTERPE code) which couples an MHD code with a gyrokinetic code are presented. Although perturbative, it offers a relatively fast way to investigate the destabilization of Alfvén modes by fast particles. TAE saturation amplitudes and their scaling with growth rate and collisionality were investigated in a tokamak as well as in Wendelstein 7-X. Full volume linear electrostatic gyrokinetic simulations for an OP1.1 Wendelstein 7-X scenario showed modes driven by the strong electron temperature gradient with negligible influence from trapped particles. Using a Fourier solver approach, long-time fully kinetic runs of damped GAEs and TAEs could be performed. Super-resolution methods allowed accurately resolution of the the continuous Alfvén spectrum.

Reconstruction of MHD Modes for Energetic Particle Dynamics Studies in Toroidal Equilibria with Arbitrary q Profiles

P. Garcia-Martinez¹, R. Farengo², H. Ferrari^{1,2}, P. Montes^{1,2}, C. Clauser^{1,2}, M.-C. Firpo³, and A. Lifschitz⁴

¹CONICET, Centro Atómico Bariloche (CNEA), RN 8400, Argentina

²Centro Atómico Bariloche (CNEA) and Instituto Balseiro, RN 8400, Bariloche, Argentina

³Laboratoire de Physique des Plasmas (LPP), CNRS/École Polytechnique, 91128 Palaiseau, France

⁴Laboratoire d'Optique Appliquée (LOA), ENSTA-Paris Tech/CNRS/École Polytechnique, 91128 Palaiseau, France

Corresponding Author: P. Garcia-Martinez, pablogm@cab.cnea.gov.ar

The interaction of energetic particles with MHD modes of different types is a major concern for the next generation of experiments involving burning plasmas. This issue arises in different contexts such as particle redistribution due to current driven instabilities (involving or not magnetic reconnection), activation of Alfvén eigenmodes (AE) due to wave-particle interaction or loss of confinement caused by neoclassical tearing modes (NTM). The physics involved in these processes is varied and complex. However, the construction of adequate models to study particle redistribution is usually simplified by assuming that the modes affect the particle dynamics through the perturbation of the equilibrium fields. Thus, the knowledge of the total field, equilibrium plus perturbation, produced in each case enables the calculation of the particle redistribution. In previous works, a model employing a fixed equilibrium and internal modes reconstructed from experimental data was developed and successfully applied to study α -particle redistribution in the presence of kink modes and sawteeth with partial reconnection. To be able to tackle a larger number of problems, in this work, we extend the method to allow for the use of MHD equilibria with arbitrary safety factor (q) profiles. Again, external data either from experiments or simulations may be incorporated to estimate the structure of the modes. The resulting model is flexible and can be employed to study the effect of MHD modes on test particles in a variety of situations. As a first example, the redistribution of energetic particles caused by the sawtooth crash is considered. Several scenarios are investigated including full and partial reconnection in usual tokamak equilibria as well as configurations with an extended region of low magnetic shear at the plasma core.

Nonlinear Decay and Plasma Heating by Toroidal Alfvén Eigenmodes

Z. Qiu¹, L. Chen^{1,2}, F. Zonca^{3,1}, and W. Chen⁴

¹*Institute for Fusion Theory and Simulation,*

Zhejiang University, Xihu, Hangzhou, Zhejiang, People's Republic of China

²*University of California Irvine, CA 92697, USA*

³*ENEA C. R. Frascati, Dipartimento FSN, Frascati, Italy*

⁴*Southwestern Institute of Physics, Chengdu, Sichuan, People's Republic of China*

Corresponding Author: Z. Qiu, zqiu@zju.edu.cn

Gyrokinetic theory of nonlinear mode coupling as a mechanism for toroidal Alfvén eigenmode (TAE) saturation and thermal plasma heating in the fusion plasma related parameter regime is presented, including: 1) parametric decay of TAE into lower kinetic TAE (LKTAE) and geodesic acoustic mode (GAM); and 2) enhanced TAE coupling to shear Alfvén wave (SAW) continuum via ion induced scattering. Nonlinear decay of TAE into a GAM and a LKTAE with the same toroidal/poloidal mode number is investigated due to its crucial implications on TAE nonlinear saturation, improved confinement, as well as energetic particle (EP) power channelling, including fusion- α power density to bulk thermal plasma heating. The parametric dispersion relation is derived and analyzed, and the parameter range for this process to occur and dominate over other mechanisms is discussed. The nonlinearly generated LKTAE and GAM can be dissipated via electron and ion Landau damping, respectively, leading to anomalous EP slowing down and channelling of EP power to thermal ion heating. The thermal plasma heating rates are also estimated. Furthermore, the nonlinearly generated GAM, as the finite frequency zonal flow, could contribute to regulating drift wave turbulence and consequently, improved confinement. The TAE frequency cascading via nonlinear ion induced scattering and saturation due to enhanced coupling to SAW continuum is also investigated. The wave-kinetic equation for the TAE spectrum evolution in the continuum limit is derived using nonlinear gyrokinetic theory, which is then solved to obtain the saturation spectrum of TAE, yielding a lower fluctuation level than previous drift-kinetic theoretical estimates, as a consequence of the enhanced nonlinear couplings in the short wavelength limit. The bulk ion heating rate from nonlinear ion Landau damping is also calculated. Our theory shows that, for TAE saturation in the parameter range of practical interest, several processes with comparable scattering cross sections can be equally important.

Analysis of Energetic Particle Driven Toroidal Alfvén Eigenmodes in CFETR Baseline Scenario

Y. Hou¹, P. Zhu^{1,2,3}, C. C. Kim⁴, and Z. Zou¹

The CFETR Physics Team

¹CAS Key Laboratory of Geospace Environment and Department of Engineering and Applied Physics, University of Science and Technology of China, Hefei, Anhui, People's Republic of China

²KTX Laboratory and Department of Engineering and Applied Physics, University of Science and Technology of China, Hefei, Anhui, People's Republic of China

³University of Wisconsin-Madison, Madison, WI 53706, USA

⁴SLS2 Consulting, San Diego, CA 92107, USA

Corresponding Author: Y. Hou, arvayhou@ustc.edu.cn

For burning plasmas in fusion reactors, energetic particles (EP) generated from plasma heating and the DT reaction can destabilize Alfvén eigenmodes (AE). Alfvén eigenmodes can conversely induce transport and loss of energetic particles. It is one of the crucial issues to study the interaction between EPs and AEs for CFETR (China Fusion Engineering Test Reactor). Eigenanalysis of AEs in CFETR baseline scenario is taken by using AWEAC (Alfvén Wave Eigenanalysis Code), a developing code similar to NOVA/NOVA-k but dealing with asymmetric configuration of tokamaks. Linear simulations of TAEs driven by EPs are performed using the hybrid-kinetic MHD module in the NIMROD code. This HK-MHD module includes the kinetic effects of EPs through the coupling between a δf particle-in-cell (PIC) model for EPs and the 3D MHD model for the bulk plasma. The CFETR equilibrium used is obtained from the EFIT code based on self-consistent core-pedestal coupled OMFIT workflow. The “slowing down” distribution is used to model the equilibrium distribution of energetic ions from α -particles produced by fusion. The frequency of TAEs generated by EPs in NIMROD simulation are consistent with the eigen-analysis results from AWEAC, which are within the range 40–100 kHz. For TAEs/EPs driven by α -particle from DT fusion, the growth rate increases with both the toroidal mode number and EP β fraction. Global 2D twist structures of TAEs/EPs in CFETR baseline scenario, especially RSAE (reverse shear Alfvén eigenmode) structure for some cases, are obtained for the first time using NIMROD. These results may be helpful for the future design of CFETR operations.

This work is supported by the National Magnetic Confinement Fusion Science Program of China grant Nos. 2014GB124002 and 2015GB101004, and by the Natural Science Foundation of China grant No. 11205194. One of the authors P. Zhu also acknowledges the supports from U.S. Department of Energy grant Nos. DE-FG02-86ER53218 and DE-FC02-08ER54975. This research used the computing resources from the Supercomputing Center of University of Science and Technology of China, the National Energy Research Scientific Computing Center in US, and local clusters in USTC, such as HPC, Lenovo, Inspur, and HWC.

The Combined Effect of Neoclassical Tearing Modes and ELM Control Coils on Fast-Ions: Validation in AUG and Extrapolation for ITER

A. Snicker¹, A. S. Jacobsen², and M. García Muñoz³

The ASDEX-Upgrade Team

¹*Aalto University, Espoo, Finland*

²*Max-Planck-Institut für Plasmaphysik, Garching, Germany*

³*Universidad de Sevilla, Seville, Spain*

Corresponding Author: A. Snicker, antti.snicker@aalto.fi

This contribution aims to broaden the understanding of the interplay between the internal and external 3D perturbations on the fast ions in tokamak plasmas. At first, we used simulations using the ASCOT suite of codes to analyze an ASDEX-Upgrade discharge showing clear sign of the interplay between a (3, 2) neoclassical tearing mode (NTM) and external RMP coils on the fast ion loss detector (FILD) signal of neutral beam ion losses. At this context, also a code-code benchmark with the LOCUST code is presented. The same set of analysis tools is then used to predict both the α -particle and neutral beam ion losses in the ITER 15 MA standard H-mode scenario in the presence of (2, 1) and/or (3, 2) NTM and ELM control coils (ECC).

Magnetically confined fusion relies on the fusion-born α -particles being well confined, thus providing significant plasma heating and keeping the first-wall intact. Recent numerical simulations indeed show that this is the case for most planned ITER scenarios. However, these simulations were carried out assuming that the transport is fully neoclassical, and that the plasma is MHD-quiescent. Both of these assumptions should be relaxed before making the final verdict on the fast-ion confinement in ITER. In this contribution we partly relax the MHD-quiescence condition by adding NTMs in our simulations.

Although a significant (up to 100%) increase in the total power losses for ITER was observed, so far no direct risk for the first wall was found. In this study both the NTM and the RMP perturbation was assumed to be static, thus maximizing the interaction between the two. Without further increased transport, by for example toroidal Alfvén waves or turbulence, the fast ion power loads stay within the engineering limits.

Self-Consistent Gyrokinetic Description of the Interaction between Alfvén Modes and Turbulence

A. Biancalani¹, A. Bottino¹, A. Di Siena¹, T. Görler¹, Ö. Gürcan², F. Jenko^{1,3}, E. Lanti⁴, G. Merlo³, O. Mishchenko⁵, P. Morel², I. Novikau¹, N. Ohana⁴, Z. Qiu⁶, and L. Villard⁴

¹Max-Planck-Institut für Plasmaphysik, Garching, Germany

²Laboratoire de Physique des Plasmas (LPP), CNRS/École Polytechnique, 91128 Palaiseau, France

³University of Texas at Austin, Austin, TX 78712, USA

⁴Swiss Plasma Center (SPC), École polytechnique fédérale de Lausanne (EPFL), 1015 Lausanne, Switzerland

⁵Max-Planck-Institut für Plasmaphysik, Greifswald, Germany

⁶Institute for Fusion Theory and Simulation,

Zhejiang University, Xihu, Hangzhou, Zhejiang, People's Republic of China

Corresponding Author: A. Biancalani, biancalani@ipp.mpg.de

It is getting increasingly clear that many tokamak plasma phenomena which have traditionally been investigated separately, are actually intrinsically linked. One outstanding example along these lines—which is investigated in the present contribution—is the the interaction between Alfvén modes (AM), turbulence, and zonal structures (ZS), like zonal flows and geodesic acoustic modes. Recently, a strong interest was raised in the fusion community by the possibility of generating ZS via nonlinear interaction with global modes like Alfvén instabilities. In this work, the interaction of AM, turbulence and ZS is studied with the code ORB5. This model treats ions and electrons respectively as gyrokinetic and drift-kinetic. ORB5 is a nonlinear global particle-in-cell code, developed for turbulence studies [1] and extended to its electromagnetic multispecies version [2] for the investigation of Alfvén dynamics [3]. Recently, the importance of the kinetic electron effects in the ZS dynamics has also been emphasized with ORB5 [4]. ORB5 has also accomplished a verification/benchmark phase for AMs and has been used for the study of the nonlinear wave-particle interaction [5]. The competition between the different excitation mechanisms of ZS is the main focus of this work. When an EP population is added to the electromagnetic turbulence, the perturbed saturated field is observed to be modified by the presence of AMs. The effect of the different players are described separately, and in particular: wave-particle nonlinearity, wave-wave nonlinearity, effect of turbulence on AMs, effect of AMs on turbulence, for example via ZS generation, and bulk plasma ω_* effects on the AM growth rate and saturation. Comparisons with analytical theory and other models like the gyrokinetic Eulerian code GENE [6, 7] are also done.

References

- [1] S. Jolliet *et al.*, Comput. Phys. Comm., **177**, 409 (2007).
- [2] A. Bottino *et al.*, Plasma Phys. Contr. F., **53**, 124027 (2011).
- [3] A. Biancalani *et al.*, IAEA FEC–2016, Kyoto, Japan, [TH/4-2](#), (2016).
- [4] I. Novikau *et al.*, Phys. Plasmas, **24**, 122117 (2017).
- [5] M. D. J. Cole *et al.*, Phys. Plasmas, **24**, 022508 (2017).
- [6] F. Jenko *et al.*, Phys. Plasmas, **7**, 1904 (2000).
- [7] T. Goerler *et al.*, J. Comput. Phys., **230**, 7053 (2011).

Comparison of Energetic Particle Radial Transport between Single- n and Multiple- n Simulations of Alfvénic Modes

G. Vlad¹, S. Briguglio¹, G. Fogaccia¹, V. Fusco¹, C. Di Troia¹, E. Giovannozzi¹, X. Wang², and F. Zonca^{1,3}

¹ENEA C. R. Frascati, Dipartimento FSN, Frascati, Italy

²Max-Planck-Institut für Plasmaphysik, Garching, Germany

³Institute for Fusion Theory and Simulation,

Zhejiang University, Xihu, Hangzhou, Zhejiang, People's Republic of China

Corresponding Author: G. Vlad, gregorio.vlad@enea.it

The results of a set of simulations of Alfvén modes driven by an energetic particle population are presented, with the specific aim of comparing energetic particle radial transport between single- n and multiple- n simulations. The hybrid reduced $\mathcal{O}(\epsilon_0^3)$ MHD gyrokinetic code HMGC is used, retaining both fluid (wave-wave) and energetic particles nonlinearities. The code HMGC retains self-consistently, in the time evolution, the wave spatial structures as modified by the energetic particle (EP) term.

A model equilibrium has been considered, rather than a specific experimental device, with the aim of studying how the dynamics of the EP driven Alfvénic modes changes when considering single- n or multiple- n simulations, while keeping all the other parameters fixed. A circular, shifted magnetic surface, static equilibrium has been considered, characterized by a large aspect ratio ($\epsilon_0 = 0.1$) and a parabolic safety factor profile with $q_0 = 1.1$ and $q_a = 1.9$ being, respectively, the on-axis and edge safety factor. A bulk ion density profile $n_i(r) \propto (q_0/q(r))^2$ has also been assumed, in order to have the toroidal gap radially aligned, for all the mode considered. Regarding the EPs, an isotropic Maxwellian distribution function has been considered.

Simulations with toroidal mode numbers $1 \leq n \leq 15$ have been considered. A variety of modes are observed (TAEs, upper and lower KTAEs, EPMs) during the linear growth phase. All the strongly unstable modes ($4 \leq n \leq 12$) exhibit pronounced (both up and down) frequency chirping at saturation. Nevertheless, no appreciable global modification of the energetic particle density profile is observed at saturation for the unstable modes.

On the contrary, multiple- n simulations, with the same Fourier toroidal mode spectrum of the set of single- n simulations, exhibit an appreciable broadening of the energetic particle radial density profile at saturation, thus showing an enhanced radial transport with respect to the single- n simulations. Moreover, the subdominant modes are strongly modified by the nonlinear coupling, which results both from the MHD and from the energetic particle terms. The present nonlinear simulations show that all the toroidal modes saturate almost simultaneously, after inducing an enhanced energetic particle radial transport. No evidence of the so-called “domino” effect is observed.

Simulations of Two Types of Energetic Particle Driven Geodesic Acoustic Modes and the Energy Channelling in the Large Helical Device Plasmas

H. Wang¹, Y. Todo^{1,2}, M. Osakabe^{1,2}, T. Ido¹, and Y. Suzuki^{1,2}

¹National Institute for Fusion Science (NIFS), Toki, Gifu, Japan

²Department of Fusion Science, Graduate University for Advanced Studies (SOKENDAI), Toki, Gifu, Japan

Corresponding Author: H. Wang, wanghao@nifs.ac.jp

Energetic particle driven geodesic acoustic modes (EGAMs) in the Large Helical Device (LHD) plasmas are investigated using MEGA code. MEGA is a hybrid simulation code for energetic particles (EPs) interacting with a magnetohydrodynamic (MHD) fluid. In the present work, both the conventional and extended models of MEGA are employed. In the conventional model, only the EPs are described by the kinetic equations, while in the extended model not only the EPs but also the thermal ions are described by them. The simulations are conducted based on realistic parameters. The energy of neutral beam injection (NBI) is 170 keV. A Gaussian-type pitch angle distribution is assumed to model the NBI energetic ions. Using MEGA with a conventional model, it is found that the transition between low frequency EGAM and high frequency EGAM is decided by the slope of EP velocity distribution. Also, the phase difference between the bulk pressure perturbation δP_{bulk} and EP pressure perturbation δP_{EP} are analyzed. For the low frequency EGAMs, δP_{bulk} and δP_{EP} are in antiphase. They cancel each other out, which reduces the restoring force of the oscillation leading to the low frequency. While for the high frequency EGAMs, δP_{bulk} and δP_{EP} are in the same phase. They enhance each other, and thus the frequencies are higher. Using MEGA with an extended model, the low frequency EGAMs are reproduced. The mode structure, mode number, and mode frequency are not only consistent with the results of conventional MEGA model but also consistent with theory and experiment. Also, the energy transfer of various species is analyzed and the bulk ion heating during the EGAM activity is observed. The ions obtain energy when the EPs lose energy, and this indicates that an energy channel is established by EGAM. The EGAM channelling is reproduced by simulation for the first time. From $t = 0$ to $t = 0.36$ ms, the energy transferred from EP is 63 J. About half of this energy (51%) is transferred to bulk ions (34%) and electrons (17%), while another half is dissipated. The heating power of bulk ions around $t = 0.1$ ms is 3.4 kW/m^3 which is close to the value 4 kW/m^3 evaluated from the experiments.

Comprehensive Magnetohydrodynamic Hybrid Simulations of Fast Ion Losses due to the Fast Ion Driven Instabilities in the Large Helical Device

R. Seki^{1,2}, Y. Todo^{1,2}, Y. Suzuki^{1,2}, K. Ogawa^{1,2}, M. Isobe^{1,2}, and M. Osakabe^{1,2}

¹National Institute for Fusion Science (NIFS), Toki, Gifu, Japan

²Department of Fusion Science, Graduate University for Advanced Studies (SOKENDAI), Toki, Gifu, Japan

Corresponding Author: R. Seki, seki.ryohsuke@lhd.nifs.ac.jp

In the LHD, the fast ion confinement has been investigated by using three tangentially injected neutral beams (NBs) with 180 keV fast ions and/or two perpendicularly injected NBs with 40–80 keV fast ions. The Alfvén eigenmodes (AEs) are observed during the tangential-NB injections. The fast ion driven instabilities enhance the fast ion losses. It is important to identify the instabilities and clarify the properties of the lost fast ions due to the instabilities.

A hybrid simulation code for nonlinear magnetohydrodynamics (MHD) and energetic-particle dynamics, MEGA, has been developed to simulate recurrent bursts of fast ion driven instabilities including the energetic-particle source, collisions and losses. In order to identify the instabilities and to clarify the process of the fast ion losses in the LHD experiments, MEGA is applied to the LHD plasmas, where fast ion driven instabilities and lost fast ion properties are investigated by using tangential-NBs, with the realistic conditions close to the experiments. In a plasma with tangential-injected neutral beams (NBs), the Alfvén eigenmode (AE) bursts with $m/n = 2/1$ occur recurrently. As a result, the stored fast ion energy is saturated at a lower level than that of a classical slowing down calculation where the magnetohydrodynamic (MHD) perturbations are neglected. Fast ion losses occur during the AE bursts. The fast ion losses brought about by the AE bursts are proportional to the square of AE amplitude, which reproduces well the LHD experiment. This indicates the emergence of stochasticity in the fast ion loss process. The fast ions deposited well inside the plasma up to the magnetic axis are significantly lost for the counter-injected fast ions. We present the first self-consistent simulations that reproduce and clarify the fast ion loss properties in the LHD experiments.

TH

Advanced Energetic Ion and Impurity Ion Physics in 2D and 3D Magnetically Confined Plasmas

J. P. Graves¹, W. A. Cooper¹, A. Fasoli¹, J. M. Faustin², A. Kleiner¹, S. Lanthaler¹, E. Neto¹, H. Patten¹, D. Pfefferlé³, M. Raghunathan¹, and C. Sommariva¹

¹Swiss Plasma Center (SPC), École polytechnique fédérale de Lausanne (EPFL), 1015 Lausanne, Switzerland

²Max-Planck-Institut für Plasmaphysik, Greifswald, Germany

³University of Western Australia, WA 6009, Australia

Corresponding Author: J. P. Graves, jonathan.graves@epfl.ch

The VENUS-LEVIS code [1] has been optimized for full orbit and guiding centre simulations in fully 3D electromagnetic fields. Curvilinear flux coordinate systems are deployed, with analytic (Fourier) representation of the fields for accurate simulation over slowing down time scales of fast particles and heavy impurities. An important recent application includes the viability of ICRH [2] and synergetic NBI-ICRH in Wendelstein 7-X. Optimization of fast ion generation and core heating is identified via variation of magnetic configuration, and methods of heating and associated properties (e.g., 3-ion species heating, minority heating, ICRH heating of NBI minority ions etc). Higher harmonic ICRH is a recent upgrade of the SCENIC ICRH package [3] that will permit various heating scenarios to be validated in advance of experiments. Recent updates to the VENUS-LEVIS code include higher order drift effects [4], and advanced switching between full orbit and higher order drift orbit approximation during particle motion, as required in order to maintain accuracy and numerical efficiency. Applied for example to the current European DEMO design it is found that the magnetic ripple associated with 16 toroidal field coils has a weak affect on the radial transport of α -particles, increasing the power flux due solely to prompt losses by a factor of about two. In addition, higher order guiding centre modelling has facilitated implementation of a 5 1/2D ICRH modelling scheme into SCENIC, which has many advantages over the standard quasi-linear operator approach. The VENUS-LEVIS code has also been updated [5] to include strong toroidal plasma rotation and the neoclassical effect of collisions in the frame of the diamagnetic flows of thermal ions in three dimensions. This upgrade has been applied to the transport of tungsten in JET hybrid scenarios susceptible to $m = n = 1$ continuous modes. Neoclassical collisional transport effects in 3D rotating magnetic fields can cause strong core accumulation of tungsten.

References

- [1] D. Pfefferlé *et al.*, *Compt. Phys. Commun.*, **185**, 3127 (2014).
- [2] J. Faustin *et al.*, *Nucl. Fus.*, **56**, 092006 (2016).
- [3] M. Jucker *et al.*, *Comp. Phys. Commun.*, **182**, 912 (2011).
- [4] S. Lanthaler *et al.*, *Plasma Phys. Contr. F.*, **59**, 044014, (2017).
- [5] M. Raghunathan *et al.*, *Plasma Phys. Contr. F.*, **59**, 124002, (2018).

Simulations of the Sawtooth-Induced Redistribution of Fast Ions in JET and ITER

Y. V. Yakovenko^{1,2}, V. V. Lutsenko¹, B. S. Lepiavko¹, Y. I. Kolesnichenko¹, V. G. Kiptily³, L. Giacomelli⁴, and T. Craciunescu⁵

The JET Contributors

¹Kiev Institute for Nuclear Research, Kiev, Ukraine

²National University of Kyiv Mohyla Academy, Kiev 04070, Ukraine

³Culham Centre for Fusion Energy (CCFE), Culham Science Centre, Abingdon, UK

⁴Università degli Studi di Milano–Bicocca, 20126 Milano, Italy

⁵National Institute of Laser, Plasma and Radiation Physics (INFLPR), Bucharest, Romania

Corresponding Author: Y. V. Yakovenko, yyakovenko58@gmail.com

Simulation results of the sawtooth-induced redistribution of fast ions in JET and ITER with the code OFSEF are presented. The dependence of the redistribution on the particle parameters (energy and pitch angle) is studied. The redistribution of the trapped and marginally passing particles is found to exhibit barrier-like behaviour at the separatrix between the trapped and passing particles: the particles with high energies cannot pass the radial coordinate corresponding to the separatrix. The algorithm and structure of the rapid code developed on the basis of the OFSEF calculations are discussed. Simulations of the sawtooth effect on fusion α -particles in ITER are carried out; they show that when the shape of the q -profile is nonparabolic (which is expected, for example, in the hybrid mode), the postcrash radial profile of the α -particle distribution function can change significantly. Determining the parameters of a sawtooth crash — the sawtooth mixing radius and the sawtooth crash duration — from observations of the electron cyclotron emission in the equatorial plane of a tokamak is discussed; examples for JET sawtooth crashes are presented. Results of simulations of the sawtooth effect on the neutron emission in several recent JET discharges are presented. In most JET discharges, neutrons are mainly born by deuterons of the NBI (neutral beam injection) beam consisting mainly of passing particles with energies ~ 100 keV. However, in discharges with the third-harmonic ICRH (ion cyclotron resonance heating), a significant fraction of neutrons is produced by the ICRH tail of trapped deuterons in the MeV energy range, which provides an opportunity to verify the theory predictions.

TH

Numerical Simulations of GAE Stabilization in NSTX-U

E. V. Belova¹, E. D. Fredrickson¹, and N. A. Crocker²

The NSTX-U Team

¹*Princeton Plasma Physics Laboratory (PPPL), Princeton, NJ 08540, USA*

²*University of California Los Angeles, CA 90095, USA*

Corresponding Author: E. V. Belova, ebelova@pppl.gov

Simulations of confinement-limiting Alfvén eigenmodes in the subcyclotron frequency range show a robust physical stabilizing mechanism via modest off-axis beam injection, in agreement with experimental observations from National Spherical Torus Experiment (NSTX-U). Experimental results from NSTX-U have demonstrated that neutral beam injection from the new beam sources with large tangency radii deposit beam ions with large pitch, which can very effectively stabilize all unstable global Alfvén eigenmodes (GAEs). Beam-driven GAEs have been linked to enhanced electron transport in NSTX, and the ability to control these modes will have significant implications for NSTX-U, ITER, and other fusion devices where super-Alfvénic fast ions might be present. Nonlinear simulations using the HYM code have been performed to study the excitation and stabilization of GAEs in the NSTX-U right before and shortly after the additional off-axis beam injection. The simulations reproduce experimental finding, namely it is shown that off-axis neutral beam injection reliably and strongly suppresses all unstable GAEs. Before additional beam injection, the simulations show unstable counter-rotating GAEs with toroidal mode numbers and frequencies that match the experimentally observed modes. Additional off-axis beam injection has been modelled by adding beam ions with large pitch, and varying density. The complete stabilization occurs at less than 10% of the total beam ion inventory.

Verification and Validation of Integrated Simulation of Energetic Particles in Toroidal Plasmas

Z. Lin¹, J. Bao¹, S. Taimourzadeh¹, G. Dong², Y. Q. Liu³, R. C. He³, and Z. Liu³

¹University of California Irvine, CA 92697, USA

²Princeton University, Princeton, NJ 08544, USA

³Fusion Simulation Center, Peking University, Beijing 100871, People's Republic of China

Corresponding Author: Z. Lin, zhihongl@uci.edu

Energetic particle (EP) pressure gradients in fusion plasmas can readily excite mesoscale EP instabilities such as the Alfvén eigenmodes (AEs) and energetic particle modes that drive large EP transport, which can degrade overall plasma confinement and threaten the machine's integrity. EP could strongly influence thermal plasma dynamics including the microturbulence and macroscopic magnetohydrodynamic (MHD) modes. In return, microturbulence and MHD modes can affect EP confinement. We have developed first-principles capability for global integrated simulation of nonlinear interactions of multiple kinetic-MHD processes by treating both EP and thermal plasmas on the same footing. Verification and validation have been carried out for the gyrokinetic toroidal code (GTC) simulations of EP interactions with thermal plasmas in a DIII-D NBI-heated plasma.

GTC kinetic-MHD simulations of EP interactions with thermal plasmas focus on the DIII-D discharge #159243, which is a NBI-heated plasma with many small-amplitude reversed shear Alfvén eigenmodes (RSAE) and toroidal Alfvén eigenmodes (TAE), significant flattening of the EP profile, and large amplitude microturbulence. GTC linear simulations using EFIT equilibrium and experimental profiles find that the most unstable AE is RSAE with significant growth rate for toroidal mode number $n = 3-6$. The most unstable RSAE is $n = 4$ and has a radial domain of $\rho = 0.3-0.6$ (square-root of normalized toroidal flux function). These results are in good agreement with other gyrokinetic and gyrokinetic MHD-hybrid codes, as well as experimental data. Consistent with experimental observation, GTC simulations also find that weaker TAE exist at the outer radial domain of $\rho = 0.6-0.9$. The most unstable TAE mode is $n = 5$. Finally, GTC simulations find strong drift-wave instability excited by thermal plasma pressure gradients in the core. The most unstable ion temperature gradient (ITG)-like mode is $n = 20$. The linear ITG-like mode amplitude peak at $\rho = 0.3$, but large fluctuations nonlinearly spread to the whole radial domain. These results indicate that RSAE and TAE in this DIII-D experiment could interact nonlinear with each other and with the microturbulence.

Analysis of Electron Cyclotron Wave Assisted Plasma Start-Up in SST-1

A. K. Singh¹, I. Bandyopadhyay¹, S. Banerjee^{2,3}, R. Srinivasan², and P. V. Subhash^{1,3}

¹International Thermonuclear Experimental Reactor (ITER), India Centre, Gujarat, India

²Institute for Plasma Research (IPR), Bhat, Gandhinagar, India

³Homi Bhabha National Institute (HBNI), Anushakti Nagar, Mumbai 400094, India

Corresponding Author: A. K. Singh, amit.singh@iter-india.org

In superconducting tokamaks, the electric field generated by the central solenoid (CS) for plasma start-up is generally less than that for non-superconducting tokamaks due to the requirement of a robust vacuum vessel and cryostat without insulating break. Moreover, with the CS made of NbTi conductor, there is limitation to maximum dI/dt in the coil to avoid stress limits, resulting in limited loop voltage. To ensure reliable start-up, electron cyclotron wave (ECW) assisted preionization has been applied in several superconducting tokamaks. We initiated the study of start-up in SST-1 with a 0D model and show that ~ 100 kW of ECW power must be absorbed for start-up for an initial hydrogen atom density $N_H(t=0) \sim 4 \times 10^{18}/\text{m}^3$, an error field $B_{\text{err}} = 1$ mT, carbon and oxygen impurity fractions $n_C/n_e = n_O/n_e = 0.5\%$, and an EC beam radius of ~ 5 cm. These findings agree well with the temporal evolution of discharges. However, the 0D model is not sufficient for investigating the physical processes as it lacks radial variation of electron density and temperature, transport, and localization of the ECW power. In this paper a 1D model that includes radial transport to study ECW assisted start-up is reported. The 1D model comprises of five equations, viz., energy and particle transport for electrons and hydrogen ions and a toroidal current equation. Electrons are assumed to be heated by ECW and Ohmic power and lose energy via several processes. Ions are heated only by the equipartition energy transferred from electrons and lose energy by charge exchange between hydrogen atoms and ions. We consider cylindrical symmetry, on-axis ECW power absorption and the Bohm diffusion. Reaction rate coefficients are calculated using the average ion model. The present study indicates that with increasing initial hydrogen atom density, greater ECW power is required for start-up. This result is attributed to the power loss from ionization and equipartition. The required ECW power thus depends weakly on direct power loss caused by B_{err} and radiation loss by impurities. These results imply that controlling the initial hydrogen atom density, suppressing B_{err} , and reducing the impurity density are all useful for reliable start-up. Comprehensive analysis of start-up and the physical processes those dominate the radial distribution of parameters, as the discharge evolves, will be reported.

Simulations on the Particle and Heat Fluxes for the RF Heating H-Mode on EAST

T. Y. Xia¹, B. Gui¹, Y. B. Wu^{1,2,3}, and Y. Q. Huang^{1,4}

¹*Institute of Plasma Physics, Chinese Academy of Sciences, Hefei, Anhui, People's Republic of China*

²*Donghua University, Shanghai 201620, People's Republic of China*

³*Anqing Normal University, Anqing 246133, People's Republic of China*

⁴*University of Science and Technology of China, Hefei, Anhui, People's Republic of China*

Corresponding Author: T. Y. Xia, xiaty@ipp.ac.cn

In order to understand and control the heat flux issue for the future tokamaks, the particle and heat fluxes of the EAST RF heating H-mode have been simulated by the 6-field 2-fluid model in BOUT++ framework [1]. The simulated particle fluxes induced by the edge coherent turbulence on the outer divertor targets are comparable with the measurements of the width and peak amplitudes by the divertor probes. Based on this simulation, the EAST ELMy H-mode discharges with different plasma current I_p and geometries are applied to study the scaling law of SOL width. The Eich's Scaling is well reproduced by the simulations [2]. However, the simulated SOL width is only half of the EAST measurements, because there is no RF heating scheme in the simulations, which is effective to change the boundary topology and increases the flux expansion [3]. In order to prove the topology change effects of LHW in SOL region, a modelled helical current filament (HCF) in SOL, which has the same amplitude to the experiments, is added as the force-free form into the 6-field 2-fluid module. The RF sheath boundary condition is also considered in the self-consistent calculation of the radial electric field. The radial magnetic field induced by this HCF could be much smaller than the perturbed field, but it is able to force the perturbations with the same toroidal mode number to grow up at the start of the linear phase. This forced mode is effective to compete with the spontaneous fluctuations and change the linear properties, which leads to the obvious suppression of the divertor heat flux and the broadening of SOL width. The preliminary results shows that the HCF is able to increase the SOL width by $\sim 25\%$, and the peak parallel heat flux towards divertor target is decreased by 32%. The broadening of the particle flux by HCF clearly shows the secondary striate filaments on divertor target, which is similar to the splitting of the strike point found by the divertor probes.

References

- [1] T. Y. Xia and X. Q. Xu, Nucl. Fus., **55**, 113030 (2015).
- [2] T. Y. Xia *et al.*, Nucl. Fus., **57**, 116016 (2017).
- [3] Y. F. Liang *et al.*, Phys. Rev. Lett., **110**, 235002 (2013).

Beam Ion Performance and Power Loads in the ITER Prefusion Power Operating Scenarios (PFPO) with Reduced Field and Current

T. Kurki-Suonio¹, K. Särkimäki¹, A. Snicker¹, and M. Schneider²

¹Aalto University, Espoo, Finland

²International Thermonuclear Experimental Reactor (ITER),
Cadarache Centre, 13108 St. Paul lez Durance, France

Corresponding Author: T. Kurki-Suonio, taina.kurki-suonio@aalto.fi

The ITER Prefusion Power Operating (PFPO) phase will include half-field/half-current (2.65 T, 7.5 MA) and one-third field (1.8 T, 5 MA) operating scenarios, which ought to allow H-mode access even with limited heating [1]. While PFPO-1 relies only on ECRH and ICRH to achieve the H-mode, in PFPO-2 also the neutral beams will be applied. In the PFPO phases, the plasma will consist of either hydrogen or helium, and will operate at about half of the Greenwald density. Beam operation at low densities requires lower acceleration voltages due to shine-through constraints, so that the maximum beam energy in PFPO is limited to below 870 keV for He plasma.

The goal of this contribution is to determine power loads, due to both charged and neutral particles, to the ITER first wall from neutral beam heating in both the one-third and half-field scenarios, as well as determine the overall beam performance (heating, current-drive and torque to the plasma) using the full beam capabilities envisaged for both scenarios. The ASCOT suite of codes was used for this purpose since it allows including the effect of ferritic inserts which, due to the lowered field values, can not work in the manner they were designed for. Since the prefusion phase will also serve as a relatively benign environment for testing various ITER subsystems, notably ELM mitigation methods, we shall also address the effect of ELM control coils (ECC) on fast ion containment.

In the absence of the ECC's, the beam ions are found to be very well confined. For instance, in the half-field scenario, using the full beam power of 33 MW, power losses are less than 0.1%, with peak power of 130 kW/m². Shine-through, on the other, is non-negligible: even in the flat-top phase of the discharge the shine-through was 1.8% of the 870 keV beam power, with a corresponding peak power of 680 kW/m². Additional simulations were carried out to determine the electron density resulting in a peak power load of less than 1 MW/m². By varying electron density while keeping the plasma quasineutral and the plasma composition constant, the critical density was found to be approximately $4 \times 10^{19}/\text{m}^3$.

References

[1] M. Schneider *et al.*, TH/6-1, This Conference.

ECRH and Mode Conversion in Overdense W7-X Plasmas

P. Aleynikov¹, N. B. Marushchenko¹

¹Max-Planck-Institut für Plasmaphysik, Greifswald, Germany

Corresponding Author: P. Aleynikov, pavel.aleynikov@ipp.mpg.de

Electron cyclotron resonance heating (ECRH) is the main plasma heating mechanism in Wendelstein 7-X (W7-X) Stellarator. It is provided by 10 gyrotrons at 140 GHz (corresponding to the second harmonic cyclotron resonance at 2.5 T) with the power of 1 MW each. The X- and the O-modes were successfully used in a wide range of operation scenarios: X-mode for low and moderate densities (up to the cutoff at $1.2 \times 10^{20}/\text{m}^3$), and O2-mode for higher densities (up to $\sim 2 \times 10^{20}/\text{m}^3$). Possible operation at yet higher densities would involve double mode-conversion from O- to slow X- and to Bernstein-mode, i.e., an OXB-scenario. The physics of O-X conversion is outside of applicability of the routinely used geometrical optics approximation (WKB-theory) and should be considered within a full-wave approach.

In this work, the wave physics of O-X conversion in overdense W7-X plasma is investigated. The results are also applicable to the inverse problem of electron Bernstein emission (EBE) diagnostics. The work discusses: a) Possibilities for the realization of this mode conversion scenario within the capabilities of the existing ECRH system in W7-X; b) Development of the “optimal” O- to X- conversion scenario within the constraints set by the 3D plasma equilibrium. A feasible heating scenario with $> 85\%$ efficiency is identified. c) The effect of turbulence on the conversion efficiency is assessed.

For this study, a new 3D, cold-plasma full-wave code has been developed. The code utilizes the finite difference time domain (FDTD) technique. The computational domain is “minimized” around the WKB-trajectory of the reference ray, and is matched to the surrounding plasma by using the so-called “convolutional perfectly matched layers (CPML) boundary condition”. The background magnetic field is recovered from the precomputed 3D equilibrium data. The code takes advantage of massive parallel computations with graphics processing units (GPUs), which allows for up to 100 times faster calculations than on a single-CPU. This feature allows for efficient parametric optimization studies over a broad range of possible experimental conditions.

TH

Global PIC Simulation of RF Waves in Toroidal Geometry

A. Kuley¹, J. Bao², Z. Lin², S. Sharma³, and A. Sen³

¹Indian Institute of Science, Bangalore, India

²University of California Irvine, CA 92697, USA

³Institute for Plasma Research (IPR), Bhat, Gandhinagar, India

Corresponding Author: A. Kuley, akuley@iisc.ac.in

We report on nonlinear PIC simulations of wave-wave and wave particle phenomena relevant for RF heating and current drive schemes in tokamaks. For this we have developed a new nonlinear kinetic simulation model based on the global toroidal code GTC. In this model, the ions are considered as fully kinetic particles obeying the Vlasov equation and the electrons are treated as guiding centres that are evolved by the drift kinetic equation. We have benchmarked this numerical model to verify the linear physics of normal modes, conversion of slow and fast waves and its propagation in the core region of the tokamak using Boozer coordinates. In the nonlinear simulation of ion Bernstein wave (IBW) in a tokamak, parametric decay instability is observed where a large amplitude pump wave decays into an IBW sideband and an ion cyclotron quasimode (ICQM). The ICQM induces an ion perpendicular heating, with a heating rate proportional to the pump wave intensity. Finally, in the electromagnetic lower hybrid wave simulation, nonlinear wave trapping of electrons is verified and plasma current is nonlinearly driven in the core region. However, in many experiments, parametric decay instability is usually observed in the scrape-off layer (SOL). We have upgraded GTC to enable global toroidal simulations that couple the core and SOL across the separatrix by using cylindrical coordinates with field-aligned particle-grid interpolations. Using this new tokamak geometry model, we have implemented the fully kinetic particle pusher to capture the high frequency (ion cyclotron frequency and beyond), and the particle dynamics of guiding centre associated with the low frequency waves. To verify the new simulation model, we have carried out simulations to study ion orbit loss at the edge of the tokamak plasma with single null magnetic separatrix for DIII-D tokamak. The ion loss conditions are examined as a function of pitch angle for cases both with and without an electric field.

Mode Converted Electrostatic Nonlinear Ion-Ion Hybrid Mode in Tokamak Plasma

J. K. Atul¹, L. Gupta², and P. K. Chattopadhyay¹

¹*Institute for Plasma Research (IPR), Bhat, Gandhinagar, India*

²*ENEA C. R. Frascati, Dipartimento FSN, Frascati, Italy*

Corresponding Author: J. K. Atul, jkatulphysics@gmail.com

Mode conversion (MC) process proves to be of prime importance in fusion as well as in magnetospheric plasma [1–3]. However, the presence of multiple ion species, even with small concentrations, can lead to the appearance of new and modified resonance, cutoff, and crossover frequencies [4]. Nonlinear effects such as pump self-induced filamentation and parametric decays further complicate the MC physics and associated heating processes [5–8]. It is generally seen that intense localized electric fields of the soliton form are generated due to the density changes (density cavities) caused by the dominant ponderomotive forces acting on the charged species. It turns out that the nonlinear fate of the mode converted electrostatic wave beyond the MC layer is still an open question. With this motivation, we investigate such a nonlinear state of the mode converted electrostatic ion-ion hybrid wave in the vicinity of the MC layer. In context with it, an exact nonlinear solution of the ion-ion hybrid mode is estimated under the influence of adiabatic perturbations in a two-ion species magnetized plasma. The dominant nonlinearity arises through the ion ponderomotive force term thereby modulating the plasma density profile. The nonlinear equation which has Korteweg De Vries [KdV] soliton as its solution, represents the nonlinear stage of a purely growing mode. It turns out that these solitons exist only if the wave frequency is lower than the Buschbaum frequency and if the concentration of the lighter ions is less than the heavier one. The resultant ponderomotive expulsion of plasma is discussed in terms of intense localized electric fields and associated density cavities. The application of the theoretical model is discussed in terms of proton and tritium minority concentration ratios in deuterium plasma.

References

- [1] J. Wesson, *TOKAMAKS*, ch. 5, (2004).
- [2] Y. O. Kazakov *et al.*, *Plasma Phys. Contr. F.*, **52**, 115006 (2010).
- [3] Y. O. Kazakov *et al.*, *Phys. Rev. Lett.*, **111**, 125002 (2013).
- [4] S. J. Buchsbaum, *Phys. Rev. Lett.*, **5**, 495 (1960).
- [5] G. Morales *et al.*, *Phys. Rev. Lett.*, **35**, 930 (1975).
- [6] S. G. Tagare *et al.*, *Phys. Fluids*, **25**, 11, 2012–2018 (1982).
- [7] M. Toida, *et al.*, *J. Phys. Soc. Japan*, **76**, 104502–104502 (2007).
- [8] M. Toida, *et al.*, *Phys. Plasmas*, **18**, 062303 (2011).

Particle Simulation Studies on Ion Effective Heating through Merging Plasmas

S. Usami¹, R. Horiuchi^{1,2}, H. Ohtani^{1,2}, Y. Ono³, M. Inomoto³, and H. Tanabe³

¹National Institute for Fusion Science (NIFS), Toki, Gifu, Japan

²Department of Fusion Science, Graduate University for Advanced Studies (SOKENDAI), Toki, Gifu, Japan

³University of Tokyo, Tokyo, Japan

Corresponding Author: S. Usami, usami.shunsuke@nifs.ac.jp

The merging of spherical tokamaks (STs) attract the attention as a candidate of future fusion reactors. In plasma merging experiments of STs, through magnetic reconnection, two torus plasmas are merged into a single torus plasmas with higher β . In experiments, it is reported that electrons are significantly heated in the vicinity of the X-point, while ions are mainly heated in the downstream [1]. The comprehension of the heating mechanism can lead to a higher-performance for realizing economical ST reactors. In this paper, we show a new mechanism of ion heating.

We investigate the ion heating mechanism by means of particle simulations, which mimic merging plasmas in a ST. Plasmas are pushed by the driving electric field imposed at the upstream boundary in order to express pushed plasmas by the poloidal field coil current in experiments. The initial condition is one-dimensional equilibrium with a uniform toroidal (guide) magnetic field.

Our simulations demonstrate that the ion temperature perpendicular to the magnetic field grows mainly in the downstream as in experiments. It is further found that ring-like velocity distributions are formed at local points in the downstream. That is, ions are effectively heated [2]. The formation process of the ring-like distribution is as follows. Ions behave as nonadiabatic upon crossing the separatrix, since the period of time during which they pass through the separatrix is shorter than the gyroperiod. The entry speed of the ions is much less than the outflow speed. The ions rotate around the toroidal magnetic field while $E \times B$ drifting in the downstream. The ion orbit in the velocity space is a circle. The ring-like velocity distribution is formed by such ions with different phases of the gyromotion.

It is found that the profile of the ion temperature by our simulation fits well to that by a TS-3 experiment [1]. Furthermore, the dependence of the ion temperature on the toroidal magnetic field is investigated. Our simulations show that the ion temperature decreases as the toroidal field is stronger, but the dependence becomes small for the high toroidal field. This tendency is consistent with that in TS-3 experiments [3].

References

- [1] Y. Ono *et al.*, Plasma Phys. Contr. F., **54**, 124039 (2012).
- [2] S. Usami *et al.*, Phys. Plasmas, **24**, 092101 (2017).
- [3] Y. Ono *et al.*, Phys. Plasmas, **18**, 111213 (2011).

Anomalous Absorption and Emission in ECRH Experiments due to Parametric Excitation of Localized UH Waves

E. Z. Gusakov¹, A. Y. Popov¹, and A. N. Saveliev¹

¹*Ioffe Institute, St. Petersburg, Russian Federation*

Corresponding Author: E. Z. Gusakov, evgeniy.gusakov@mail.ioffe.ru

The extraordinary pump wave two-plasmon decay instability TPDI is analyzed under conditions when only one of the parametrically driven upper hybrid (UH) waves is trapped in the vicinity of the density profile local maximum. It is shown that under these conditions the excitation of absolute TPDI is possible due to a finite width of the microwave pump beam. Its threshold and growth rate are determined. The pump depletion and the secondary decay instability of the localized UH wave are considered as the most likely moderators of primary TPDI and clarify their role in its saturation. We also estimate the pump power fraction gained anomalously throughout the two-UH-plasmon decay. The general consideration is accompanied in the paper by the numerical analysis performed for the experimental conditions typical of the off-axis X2-mode ECRH experiments at TEXTOR. Based on the proposed model the radiance temperature of electromagnetic waves emitted in the high-field-side direction at the frequency close to half the pump frequency is estimated. It is also shown that the nonlinear coupling of the daughter UH waves with the pump could lead to the measurable level of the plasma emission at the 3/2 harmonic of the pump, as it happens in the laser driven inertial fusion experiments.

The parametric excitation of trapped UH waves in the O1-mode ECRH experiments is discussed as well. The threshold in this case is shown to be higher (several hundred kW depending on the plasma parameters) than for the X2-mode scenario whereas the growth rate is large enough (in the range of $10^7/\text{s}$) to expect the nonlinear saturation of the instability.

TH

Modelling of Electron Cyclotron Resonance Heating and Current Drive in the T-15-MD Tokamak with GENRAY and CQL3D Codes

P. V. Minashin¹, A. B. Kukushkin^{1,2}, and R. W. Harvey³

¹National Research Centre "Kurchatov Institute", Moscow, Russian Federation

²National Research Nuclear University "MEPhI", Moscow, Russian Federation

³CompX, Del Mar, CA 92014, USA

Corresponding Author: P. V. Minashin, minashin_pv@gnrcki.ru

The T-15-MD tokamak is planned as a normal magnetic-coil tokamak with a flexible ITER-like configuration of the poloidal magnetic field. The main goal of the tokamak T-15-MD is the achievement of long pulse, noninductive current drive regimes for a high-aspect-ratio divertor plasma configurations.

The simulations of the ECRH and ECCD in T-15-MD tokamak are carried out with the ray-tracing code GENRAY and the kinetic Fokker-Planck code CQL3D for two formerly predicted regimes of tokamak operation, namely hybrid scenario with 12 MW auxiliary heating and 2 MA total plasma current, including inductive (Ohmic) current, and the steady-state scenario with 18 MW auxiliary heating and 1 MA fully noninductive current. The results for 2D distribution of the ECRH power density and ECCD efficiency in the tokamak poloidal cross-section on the flat-top stage of discharge are presented for various injections angles and EC wave modes. It is shown that for the ECCD in the hybrid scenario the injection of the X2-wave from the LFS is more effective than injection of the X1-wave from the HFS.

Theoretical and Computational Studies on the Scattering of Radiofrequency Waves by Fluctuations

A. K. Ram¹, Z. C. Ioannidis², K. Hizanidis³, F. Bairaktaris³, A. Papadopoulos³, S.-I. Valvis³, A. Zisis⁴, and I. G. Tigelis⁴

¹*Plasma Science & Fusion Center, MIT, Cambridge, MA 02139, USA*

²*Karlsruhe Institute of Technology (KIT), Karlsruhe, Germany*

³*National Technical University of Athens, Greece*

⁴*National and Kapodistrian University of Athens, Greece*

Corresponding Author: A. K. Ram, abhay@mit.edu

The practical and economic viability of tokamak fusion reactors depends, in a significant way, on the efficiency of radiofrequency (RF) waves to deliver energy and momentum to the plasma in the core of the reactor. Among the various attributes of RF waves is their ability to heat magnetically confined plasmas, induce plasma currents in an effort to achieve steady state, and modify the current profile so as to control plasma instabilities like the neoclassical tearing modes. The RF electromagnetic waves, excited by antenna structures placed near the wall of a tokamak, have to propagate through the turbulent plasma in the scrape-off layer (SOL) along their path to the core plasma. While the propagation and damping of RF waves in the core is reasonably well understood, the same is not true for RF wave propagation through the SOL. In present day fusion devices, the radial width of the SOL is of the order of a few centimetres. In ITER and in future fusion reactors this width will be of the order of tens of centimetres. Any deleterious effects on RF waves due to plasma turbulence in the SOL could impact the efficient delivery of RF energy and momentum into the core. This paper is on a multipronged approach towards quantifying the effect of SOL plasma on RF waves. The SOL is composed of coherent filamentary structures and incoherent fluctuations. For coherent structures, a full-wave theoretical model has been developed and is used to benchmark computational codes. These codes are subsequently used to study the effect of a general distribution of filaments. For incoherent fluctuations, the theoretical modelling makes use of the Kirchhoff technique. This technique is based on physical optics and the wave fields at any point on a spatially varying surface are approximated to be the same as the fields on a tangent plane at that point. The results from the theoretical analysis are compared with full-wave numerical simulations for incoherent fluctuations. The final part of these studies is to construct the effective permittivity of a turbulent plasma that is a mix of coherent and incoherent fluctuations. Towards this end, the “effective medium approximation” is used to construct the permittivity of the plasma that will be used in full-wave studies of scattering. This cumulative research reveals new and important physical insights into the scattering of RF waves.

The Impact of the Hydrogen Species on the HHFW Performance with Possible New NSTX-U Scenarios

N. Bertelli¹, J. E. Jaeger², R. W. Harvey³, Y. V. Petrov³, E. J. Valeo¹, R. J. Perkins¹,
J. C. Hosea¹, and E.-H. Kim¹

¹Princeton Plasma Physics Laboratory (PPPL), Princeton, NJ 08540, USA

²XCEL Engineering Inc., Oak Ridge, TN 37830, USA

³CompX, Del Mar, CA 92014, USA

Corresponding Author: N. Bertelli, nbertell@pppl.gov

The main goal of the NSTX-U is to operate at $B = 1$ T. With this magnetic field, the 1st and 2nd harmonics of hydrogen (H) are located at the high-field side and in the core plasma, respectively. As a consequence, part of the high-harmonic fast-wave (HHFW) injected power can be absorbed by the H population. This condition might open up new HHFW scenarios, which in turn can be relevant for the initial ITER ICRH experiments. Therefore, it is important to investigate the impact of the H species on HHFW performance in NSTX-U plasmas. First of all, the injected power absorbed by the H species can affect the electron and/or the fast-ion heating with respect to the “standard” HHFW performance in NSTX. Second, the presence of the H species might have some positive effects: the presence of the 2nd cyclotron harmonic of hydrogen in the core plasma can cause a localized H power absorption, which in turn might modify the ion temperature. On the other side, due to the high-energy (non-Maxwellian) tail of the H distribution function (caused by the acceleration of H species by HHFW), part of the H absorbed power could transfer to electron heating via collisions, providing an additional core electron heating to the “standard” HHFW performance.

In this work, we analyze in detail all these possible scenarios by the use of the full wave code AORSA combined with the Fokker–Planck code CQL3D. Initial AORSA simulations have been performed for NSTX-U $B = 1$ T plasma with different H concentrations (from 2% to 10%) with and without NBI. For $f = 30$ MHz and $B = 1$ T, unlike an on-axis power deposition for electrons and fast ions, a localized H absorption around the 2nd cyclotron H harmonic is observed by AORSA. For larger n_ϕ the electron damping is dominant. However, for $n_\phi = 5$ and 10% H concentration, up to 30% and 60% of the total power can be absorbed by H with and without NBI, respectively. A more comprehensive numerical analysis will be presented including also the non-Maxwellian effects in the H and fast ions species by making use of the Fokker–Planck code CQL3D. Furthermore, a magnetic field scan will be performed in order to cover all possible scenarios. H majority plasma will be also considered and compared with D plasma. Finally, the case of 15 MHz wave frequency will also be explored because it would open up the possibility to try ICRH minority heating in NSTX-U with $B = 1$ T.

Sandpile Modelling of Pellet Pacing in Fusion Plasmas

C. A. Bowie¹, M. J. Hole¹

¹Australian National University, Canberra, Australia

Corresponding Author: C. A. Bowie, craig.bowie@anu.edu.au

Sandpile models have been used to provide simple phenomenological models without incorporating the detailed features of a fully featured model. The Chapman sandpile model [1] has been used as an analogue for the behaviour of a plasma edge, with mass loss events (MLEs) being used as analogues for (and anagrams of) ELMs. Here we modify the Chapman sandpile model to form comparisons with pellet pacing, which is used to reduce or eliminate ELMs. We use two different versions of the Chapman model, one in which the system is allowed to relax following an avalanche before further sand (dx) is added (classic model), and one in which further sand is added while an avalanche is propagating (running model). For this purpose, we modify the models in two different ways. First, we increase the amount of sand added at each time step, so that we move from the low driving model typically used in sandpile modelling to a high driving model. Second, we add "bursts" of sand at intervals which are synchronized to MLEs in the sandpile, by way of comparison with pellet injection in a fusion plasma. We then analyse the behaviour of the sandpile in these new models, focussing on changes in the total system size, and on the maximum MLE size (by way of analogy with maximum ELM size). We observe that at low dx , potential energy (E_p) varies with dx in the running model, while E_p remains constant in the classic model. Probability distribution functions of waiting times between MLEs are identical for common values of dx/Z_c , as dx and the critical gradient, Z_c , are varied. Waiting times are observed to scale inversely with fuelling in the classic model, consistent with the observation that E_p is unchanged, such that MLEs depend on the amount of sand in the system, and not on the rate at which the sand builds up. Analysis of $E_p/E_{p\text{ Max}}$ against dx/Z_c for increasing dx shows that step changes occur, often at integer ratios. An heuristic explanation is suggested for this behaviour. At very high driving, the final state of the running model can be determined analytically given the value at cell $n = 1$. At extremely high driving, E_p increases with dx in the classic model, as the cells at the edge do not exceed the critical gradient, while those at the core do exceed the critical gradient.

References

[1] S. C. Chapman *et al.*, Phys. Rev. Lett., **86**, 2814 (2001).

Numerical Relaxation of a 3D MHD Taylor–Woltjer State Subject to Abrupt Expansion

R. Mukherjee¹, R. Ganesh¹

¹*Institute for Plasma Research (IPR), Bhat, Gandhinagar, India*

Corresponding Author: R. Mukherjee, rupakmukherjee01@gmail.com

Since the advent of Taylor–Woltjer theory [1, 2], it has been widely believed that situations with perfectly conducting boundaries and near ideal conditions, the final state of MHD system would be force-free Taylor–Woltjer states defined as $\nabla B = \alpha B$ with α as a constant and B is the magnetic field defined over a volume V . These states are of fundamental importance in fusion plasmas [3]. More recently, several new MHD models have been proposed — for example reduced multiregion relaxed MHD [4] and arbitrary scale relaxation model to Taylor–Woltjer state [5], to mention a few.

In the present work, we use a 3D compressible MHD solver in Cartesian geometry which can handle conducting or periodic as well as mixed boundary conditions to investigate numerically the arbitrary scale relaxation model proposed by [5]. For this purpose, we consider two volumes V_{init} and V_{final} . We load the 3D MHD solver in the limit of zero compressibility with a Taylor–Woltjer state $B_{\text{init}}(x, y, z, t=0)$ and let it again a numerical evolve with conducting boundaries at V_{init} to make sure that we have obtained a numerically steady Taylor–Woltjer state for volume V_{init} . Followed by this procedure, we “suddenly” relax the boundaries to a new volume V_{final} , such that $V_{\text{init}} < V_{\text{final}}$ and evaluate whether or not the system attains quasi-steady state. Details of the numerical method used, the protocol followed, the expansion technique and the novelty of this numerical experiment and details of our results will be presented.

References

- [1] J. B. Taylor, Phys. Rev. Lett., **33**, 1139 (1974).
- [2] L. Woltjer, Proc. Nat. Acad. Sci U.S.A., **44**, 489 (1958).
- [3] J. B. Taylor, Rev. Mod. Phys. **58**, 741, (1986).
- [4] S. R. Hudson *et al.*, Phys. Plasmas, **19**, 112502 (2012).
- [5] H. Qin *et al.*, Phys. Rev. Lett., **109**, 235001 (2012).

ADITYA Up-Gradation Equilibrium Study

D. Sharma¹, R. Srinivasan¹, J. Ghosh¹, and P. K. Chattopadhyay¹

The ADITYA Team

¹*Institute for Plasma Research (IPR), Bhat, Gandhinagar, India*

Corresponding Author: D. Sharma, deepti@ipr.res.in

The ADITYA tokamak device is used to produce circular plasma for few hundreds of milliseconds. The edge physics study in this device is led to significant contributions. The upgrade of this device is focussed to address issues relevant to heat removal capability at the plasma edge. This requires constructing plasma equilibrium with divertor configuration. In this regard, additional pairs of coils at the inboard and outboard are used to construct plasma equilibrium. The inboard pair mainly creates the divertor configuration while the outboard pair provides flexibility in increasing the size of the plasma. This study has shown that plasma equilibrium with double null configurations can be produced for plasma current up to 100 kA and with plasma poloidal- β of 0.3. The limit on the plasma parameter is due to restriction on the allowable divertor coil current which is limited to 150 kAt. The radial distance of divertor null point is kept at least 3 cm away from the circular shaped vacuum vessel so that the divertor configuration can be ensured.

Gyrokinetic Modelling with an Extended Magnetic Equilibrium Including the Edge Region of Large Helical Device

T. Moritaka¹, R. Hager², M. D. J. Cole², S. Satake¹, C.-S. Chang², S. Lazerson², S.-H. Ku², S. Matsuoka³, and S. Ishiguro¹

¹National Institute for Fusion Science (NIFS), Toki, Gifu, Japan

²Princeton Plasma Physics Laboratory (PPPL), Princeton, NJ 08540, USA

³Japan Atomic Energy Agency (JAEA), Naka, Japan

Corresponding Author: T. Moritaka, moritaka.toseo@nifs.ac.jp

We investigate radial electric field structure in Large Helical Device and its impact on high-energy particle loss at the material wall. We employ global gyrokinetic particle-in-cell code for whole-device simulation, X-point Gyrokinetic Code (XGC), which is currently being extended to nonaxisymmetric geometries. The whole-device modelling of fusion plasma is needed to understand edge plasma phenomena strongly coupled to neoclassical and turbulent physics in the core region such as H-mode transition, divertor heat load, X-point particle loss and so on.

As the first step, we have demonstrated two typical processes in LHD within the same framework of XGC: i) GAM oscillation and its damping in a density profile or an electric field perturbation; and ii) long-time motion of high-energy particles and particle loss at the material wall. Our results are in agreement with previous simulation studies using separate codes. One is transport simulation limited in the core region and the other is particle tracing simulation without electric field perturbation. We have also investigated particle loss under the effects of ambipolar radial electric field, which is observed after GAM oscillation. The electric field affects the particle loss in two different ways in accordance with the particle energy: i) confinement due to the inward electric field for high energy range; and ii) additional particle loss due to the disturbance of particle orbit for intermediate energy range. The electric field also affects the strike point of high-energy particle in divertors.

The present scheme including i) combined use of cylindrical and field-aligned triangle meshes, and, ii) extension of VMEC equilibrium using a virtual casing method, would be promising for whole device gyrokinetic modelling of stellarators without artificial boundary at the last closed flux surface.

Effects of Magnetic Perturbations on Magnetic Field Stochastication During Edge Pedestal Collapse

J. Kim¹, S. S. Kim¹, and H. Jhang¹

¹National Fusion Research Institute (NFRI), Daejeon, Republic of Korea

Corresponding Author: J. Kim, yegakjh@nfri.re.kr

Edge localized modes (ELMs) are quasi-periodic relaxation of tokamak pedestal, releasing a large heat flux on divertor places. Although ELMs are thought to be triggered by MHD peeling-ballooning instability, the nonlinear relaxation process is not fully understood. MHD filaments can carry out heat to scrape of layers (SOL) without reconnection [1]. On the contrary, a magnetic topology change due to magnetic reconnection may drive heat and particle out of plasmas. But a reconnection mechanism is not clear in the peeling-ballooning dominated plasmas. Nonlinear generation of tearing-parity fluctuations out of ballooning modes was proposed by [2] as a candidate for the reconnection mechanism, further leading to stochastic magnetic field regions.

In this work, we investigate how the pedestal collapse scenario is modified in the presence of resonant magnetic perturbations (RMPs), using resistive reduced MHD simulations. It is found that RMPs tends to inhibit the growth of the primary/secondary tearing fluctuations, indicating possible modification of a pedestal relaxation process. The growth reduction for the secondary mode correlates with larger pressure and larger magnetic perturbation strength. The detailed nonlinear analysis will be presented with the evaluation of degree of pedestal energy loss in the presence of magnetic perturbations.

References

- [1] H. Wilson and S. Cowley, *Phys. Rev. Lett.*, **92**, 175006 (2004).
- [2] T. Rhee *et al.*, *Nucl. Fus.*, **55**, 032004 (2015).

Roles of RMP-Induced Changes of Radial Electric Fields in ELM Suppression

L. Shi¹, S. Taimourzadeh¹, Z. Lin¹, N. M. Ferraro², R. Nazikian², H. Y. Wang³, and J. Y. Fu³

¹University of California Irvine, CA 92697, USA

²Princeton Plasma Physics Laboratory (PPPL), Princeton, NJ 08540, USA

³Fusion Simulation Center, Peking University, Haidian, Beijing, People's Republic of China

Corresponding Author: L. Shi, leis9@uci.edu

Resonant magnetic perturbations (RMPs) can be used to mitigate or fully suppress the harmful edge localized modes (ELMs). In DIII-D, the ELM suppression is observed to be correlated with the enhanced particle and heat transport near the pedestal top. Initial simulations using Gyrokinetic Toroidal Code (GTC) show that the kink responses to the 3D RMP have little effect on the growth rate of electromagnetic kinetic-ballooning mode and on the turbulent transport and zonal flow damping in electrostatic turbulence [1]. On the other hand, fast RMP modulation experiments in DIII-D tokamak show that the turbulent poloidal velocity changes in phase with the modulated RMP current, suggesting that the RMP may modify the local radial electric field E_r .

Here we report from GTC simulations that reduced $E_r \times B$ shearing rate due to the RMP leads to the much stronger drift-wave instability in the outer edge and outward turbulence spreading, resulting in a larger turbulent transport on the pedestal top in the DIII-D experiments. Simulation results are consistent with experimental observations of increased turbulence and transport near the pedestal top during RMP-induced ELM suppression. Furthermore, GTC simulations of neoclassical transport show that the electron flutter motion due to the RMP islands introduces a radial particle flux that is not strong enough to directly provide the measured enhancement in the transport, but may contribute to the observed change in the radial electric field. Finally, electrostatic turbulence simulations with adiabatic electrons show no significant increase of the saturated ion heat conductivity in the presence of RMP-induced islands. However, electron response to zonal flow in the presence of magnetic islands and stochastic fields can drastically increase zonal flow dielectric constant for long wavelength fluctuations. Zonal flow generation can then be reduced and the microturbulence can be enhanced greatly.

References

[1] I. Holod *et al.*, Nucl. Fus., **57**, 016005 (2017).

Endogenous Magnetic Reconnection and Associated Processes of Relevance to Fusion Burning Plasmas

B. Coppi¹, B. Basu¹, L. E. Sugiyama¹, P. Buratti², A. Cardinali², and R. Gatto³

¹Massachusetts Institute of Technology (MIT), Cambridge, MA 02139, USA

²Agenzia nazionale per le nuove tecnologie, l'energia e lo sviluppo economico sostenibile (ENEA), Rome, Italy

³Sapienza – Università di Roma, 00185 Rome, Italy

Corresponding Author: B. Coppi, coppi@mit.edu

The main characteristic of an endogenous magnetic reconnection process is that its driving factor lays within the layer where a drastic change of magnetic field topology occurs. This kind of process is shown to take place when a significant electron temperature gradient is present in a magnetically confined plasma and when the evolving electron temperature fluctuations are anisotropic [1]. Then [2] two classes of reconnecting modes are identified. The localized class of mode involve a reconnected field \tilde{B}_x of odd parity (as a function of the radial variable), characteristic phase velocities and growth rates differently from the commonly considered reconnecting modes associated with a finite effective resistivity. The width of the reconnection layer remains significant even when large macroscopic distances are considered. In view of the fact that there are plasmas in the Universe with considerable electron thermal energy contents, the features of the considered modes can be relied upon in order to produce generation or conversion of magnetic energy and high energy particle populations through a sequence of mode-particle resonances [3]. With their excitation, these modes acquire momentum in the direction of the main magnetic field component and the main body of the plasma column should recoil in the opposite direction [4].

Endogenous modes associated with a finite electron temperature gradient are shown to be sustained by the electron temperature heating rate due to the charged reaction products in a fusion burning plasma [5]. In this case, the longitudinal thermal conductivity on selected rational magnetic surfaces [5] is decreased, relative to its collisional value, by the effects of reconnection.

The best agreement between theory and experiments concerning the onset of magnetic reconnection is (probably) represented by the theory of the resistive internal kink mode [6]. This is reconsidered for regimes where the effects of local temperature gradients are important.

Work supported by the U.S. Department of Energy.

References

- [1] B. Coppi and B. Basu, Phys. Lett. A, **382**, 400 (2018).
- [2] B. Coppi, Phys. Fluids, **8**, 2273 (1965).
- [3] B. Coppi *et al.*, Nucl. Fus., **57**, 7 (2017).
- [4] B. Coppi, Nucl. Fus., **42**, 1 (2002).
- [5] B. Coppi *et al.*, Nucl. Fus., **55**, 053011 (2015).
- [6] B. Coppi *et al.*, Fiz. Plazmy, **2**, 961 (1976).

Gyrokinetic-MHD Coupled Simulation of RMP Plasma Interaction Reproduces Density Pump-Out Seen in the Tokamak Edge

R. Hager¹, C.-S. Chang¹, N. M. Ferraro¹, and R. Nazikian¹

¹Princeton Plasma Physics Laboratory (PPPL), Princeton, NJ 08540, USA

Corresponding Author: R. Hager, rhager@pppl.gov

The gyrokinetic neoclassical particle-in-cell code XGCa coupled to the MHD code M3D-C1 is applied to study the particle and heat flux caused by external 3D magnetic perturbations in a DIII-D H-mode plasma. Despite the existence of KAM surfaces in the pedestal, our simulations, which so far are limited to the 0.5 to 1 ms directly after the RMP field is switched on, show the beginning of density pump-out at the pedestal top as well as a steepening and narrowing electron temperature pedestal around the separatrix similar to observations in the DIII-D tokamak [1].

The RMP field is known to enhance particle transport leading to density pump-out and to be able to suppress edge localized modes (ELMs) in tokamak plasma. Pump-out occurs with or without ELM suppression [2], and understanding its physics basis is important for developing predictive understanding.

Due to the short time scales studied so far with XGCa, core heat and torque sources, and turbulent transport can be neglected. Only an electron heat sink on the separatrix and in the scrape-off layer is added to model radiative cooling. The increased, RMP induced particle and energy fluxes observed in our study — despite the presence of KAM surfaces in the M3D-C1 computed screened RMP field — are mostly of convective nature as can be seen from the weak change in the electron temperature compared to the particle density at the pedestal top.

While these XGCa simulations already reproduce essential experimental findings such as the beginning density pump-out and the convective nature of the RMP induced energy flux, several enhancements are being investigated. Those enhancements include initializing the simulation with experimental toroidal rotation profiles, adding NBI torque source, replacing the simple SOL heat sink by an actual model for impurity radiation, and adding a turbulent transport model, and core heat and torque sources. Self-consistent, kinetic calculation of the screened RMP field with an XGCa-internal solver for Ampère's law and comparison to the M3D-C1 screened RMP field is investigated as well.

Supported by the U.S. Department of Energy via contracts DE-AC02-09CH11466, DE-FC02-04ER54698. Computing time provided by ALCF (DE-AC02-06CH11357) and NERSC (DE-AC02-05CH11231) through ALCC, INCITE, and ERCAP.

References

- [1] L. Cui *et al.*, Nucl. Fus., **17**, 116030 (2017).
- [2] R. Nazikian *et al.*, Phys. Rev. Lett., **114**, 105002 (2015).

Effects of Microtearing Modes on the Evolution of Electron Temperature Profiles in High Collisionality NSTX Discharges

T. Rafiq¹, S. M. Kaye², W. Guttenfelder², A. Kritiz¹, E. Schuster¹, J. Weiland³, and
F. M. Poli¹

¹Lehigh University, Bethlehem, PA 18015, USA

²Princeton Plasma Physics Laboratory (PPPL), Princeton, NJ 08540, USA

³EURATOM-VR Association and Chalmers University of Technology, Göteborg, Sweden

Corresponding Author: T. Rafiq, trafiqfusion@gmail.com

A goal of this research project is to describe the evolution of the electron temperature profiles in high collisionality NSTX H-mode discharges. In these discharges the ion thermal transport is generally near neoclassical levels. However, it is found that the electron thermal transport is anomalous and can limit the overall global energy confinement scaling. Gyrokinetic simulations indicate that microtearing modes (MTMs) are a source of significant electron thermal transport in these discharges. In order to understand the effect MTMs have on transport and, consequently, on the evolution of electron temperature in NSTX discharges, a reduced transport model for MTMs has been developed. The dependence of the MTM real frequency and growth rate on plasma parameters, appropriate for high collisionality NSTX discharges, is obtained employing the new MTM transport model. The dependencies on plasma parameters are compared and found to be consistent with MTM results previously obtained using the gyrokinetic GYRO code. The MTM real frequency, growth rate, magnetic fluctuations and resulting electron thermal transport are examined for high collisionality NSTX discharges in systematic scans over plasma parameters. The electron temperature gradient along with the collision frequency and plasma- β are found to be sufficient for the microtearing modes to become unstable. In earlier studies it was found that the version of the multimode (MM) transport model, that did not include the effect of MTMs, provided a suitable description of the electron temperature profiles in high collisionality standard tokamak discharges. That version of the MM model included contributions to electron thermal transport from the ion temperature gradient, trapped electrons, kinetic ballooning, peeling ballooning, collisionless and collision-dominated MHD modes, and electron temperature gradient modes. When the MM model, that includes transport associated with MTMs, is installed in the TRANSP code and is utilized in studying electron thermal transport in high collisionality NSTX discharges, it is found that agreement with the experimental electron temperature profile is significantly improved. Future research will involve improving the electron thermal transport model for low collisionality NSTX discharges.

Work Supported by the U.S. Department of Energy, DE-SC0013977, DE-FG02-92ER54141, and DE-AC02-09CH11466.

Electromagnetic Analysis of APPEL Linear Device Magnets

Y. Patil¹, P. Dutta¹, R. Srinivasan¹, and S. K. Karkari¹

¹*Institute for Plasma Research (IPR), Bhat, Gandhinagar, India*

Corresponding Author: Y. Patil, ypatil@ipr.res.in

The APPEL (Applied Plasma Physics Experiments in Linear Device) is an experimental system designed to carry out basic plasma physics experiments as well as serve as a test-bed for experimenting various plasma facing components interaction with strongly magnetized plasma. This versatile device consists of 16 large electromagnet coils weighing up to 700 kg each, which are made from CTC (continuously transposed conductors), wound in double pancake configuration. Each electromagnet coil is made by sandwiching two double pancakes between 10 mm thick stainless steel plates to obtain 100 turns/magnet. The individual coil has 52 cm internal diameter and outer diameter is around 110 cm. The stainless steel plates provide the necessary strength to the magnet while its surface acts as radiator to dissipate heat. The individual electromagnet can be operated continuously to produce peak axial magnetic field in excess of 0.1 T by passing 750 A for 600 s. All 16 magnets in linear configuration produce peak magnetic field in excess of 0.5 T by passing 750 A for 600 s. In this set-up different magnetic field profile can be generated by optimizing the current using two high current DC power supplies as well as configuration of the coils. The paper presents the electromagnets field simulation performed by finite element analysis (FEA) using Comsol Multiphysics and ANSYS to obtain tailored magnetic field profile in linear, magnetic cusp and mirror configurations achieved in APPEL device. In-house magnetic field measurements carried out for the APPEL magnet and experimental validation of the FEA results. The heat loads and stresses on the coils have been calculated for steady state operation of the APPEL device.

The Effect of Pressure Anisotropy on Ballooning Modes in Tokamak Plasmas

M. J. Hole¹, A. Johnston¹, Z. Q. Qu¹, H. Hezabeh¹, and A. Barnes²

¹*Australian National University, Canberra, Australia*

²*Monash University, Clayton Victoria 3800, Australia*

Corresponding Author: M. J. Hole, matthew.hole@anu.edu.au

Edge localized modes (ELMs) are thought to be caused by a spectrum of magnetohydrodynamic instabilities, including the ballooning mode. While ballooning modes have been studied extensively both theoretically and experimentally, the focus of the vast majority of this research has been on isotropic plasmas. The prevalence of pressure anisotropy in modern tokamaks thus motivates further study of these modes. This paper presents a numerical analysis of ballooning modes in anisotropic equilibria. The investigation was conducted using the newly-developed codes HELENA+ATF and MISHKA-A, which adds anisotropic physics to equilibria and stability analysis. We have examined the impact of anisotropy on the stability of an $n = 30$ ballooning mode, confirming results conform to previous calculations in the isotropic limit. Growth rates of ballooning modes in equilibria with different levels of anisotropy were then calculated using the stability code MISHKA-A. The key finding is that the level of anisotropy had a significant impact on ballooning mode growth rates. For $T_{\perp} > T_{\parallel}$, typical of ICRH heating, the growth rate increases, while for $T_{\perp} < T_{\parallel}$, typical of neutral beam heating, the growth rate decreases. For levels of anisotropy observed in JET and MAST plasmas, we expect the impact on growth rates for realistic configurations to be significant. An important conclusion is the possibility that higher ELM-free performance might be achieved by increasing p_{\parallel}/p_{\perp} in the pedestal region.

TH

Centrifugal Force Driven Low Frequency Modes in Spherical Tokamak

G. Z. Hao¹, W. W. Heidbrink², Y. Q. Liu³, S. X. Yang⁴, E. D. Fredrickson⁵, M. Podestà⁵, and N. A. Crocker⁶

¹Southwestern Institute of Physics, Chengdu, Sichuan, People's Republic of China

²University of California Irvine, CA 92697, USA

³General Atomics, San Diego, CA 92186, USA

⁴Dalian University of Technology, Liaoning, Dalian, Ganjingzi, People's Republic of China

⁵Princeton Plasma Physics Laboratory (PPPL), Princeton, NJ 08540, USA

⁶University of California Los Angeles, CA 90095, USA

Corresponding Author: G. Z. Hao, haogz@swip.ac.cn

There is a longstanding issue on the physical nature of a low frequency (< 50 kHz) MHD instability observed at the early phase of the discharges of a spherical tokamak (ST) — the National Spherical Torus Experiment (NSTX) [1]. This work provides evidence that low frequency modes in spherical tokamaks are often driven by the rapid plasma flow. The centrifugal force associated with toroidal plasma flow is identified as the key physics mechanism for generating this instability located in the plasma core region. Positive mode identification between toroidal modelling and experiments is achieved for the mode frequency, the mode internal structure, as well as the threshold flow value for the mode onset. The threshold flow value weakly depends on the precise value of safety factor and the mode is located around the location of sharp density gradient. More important, since the achievable rotation value on NSTX is comparable with that for future component test facilities (CTF) based on ST [2], the presented results in this work are helpful for the conceptual design of ST-CTF to avoid the instability driven by fast plasma flow.

References

[1] M. Ono *et al.*, Nucl. Fus., **40**, 557 (2000).

[2] Y.-K. M. Peng *et al.*, Plasma Phys. Contr. F., **47**, B263. (2005).

Nonlinear MHD Simulations of Quiescent H-Mode in ASDEX-Upgrade and ITER

F. Liu¹, G. T. A. Huijsmans², M. Hölzl³, E. Viezzer³, M. G. Dunne³, A. Loarte⁴, and S. Pamela⁵

The ASDEX-Upgrade Team and EUROfusion-MST1 Team

¹Lab. J.A. Dieudonné, Université Côte d'Azur, Nice, France

²Commissariat à l'énergie atomique (CEA/Cadarache), 13108 St. Paul lez Durance, France

³Max-Planck-Institut für Plasmaphysik, Garching, Germany

⁴International Thermonuclear Experimental Reactor (ITER),

Cadarache Centre, 13108 St. Paul lez Durance, France

⁵Culham Centre for Fusion Energy (CCFE), Culham Science Centre, Abingdon, UK

Corresponding Author: F. Liu, feng.liu@iter.org

Both nonlinear simulations and experiments of DIII-D QH-mode plasmas show that $E \times B$ rotation plays an essential role for obtaining the QH-mode. However, the mechanism for the QH-mode onset and its saturation, the influence of other rotation flows such as neoclassical flow, diamagnetic flow as well as the influence of resistive wall still remains unclear due to the complexity of the physics of edge plasma nonlinear MHD stability. Hence, understanding the physics mechanisms leading to the saturation of the EHO in QH-mode plasmas and the role of plasma rotation in EHO behaviour is an important issue to support experiments in ASDEX-Upgrade to access the QH-mode regime and to assess whether the QH-mode could be a viable alternative regime for an ITER high Q scenario.

In this work nonlinear MHD simulations of ASDEX-Upgrade QH-mode plasma #17686 have been performed with the nonlinear MHD code JOEKE for the first time. The low- n kink-peeling modes (KPMs) have been found unstable and grow to a saturated level in the edge of the ASDEX-Upgrade QH-mode plasma. This leads to a helical structure on the plasma density, which is associated with the 3D localization of the KPM at the separatrix in the toroidal and poloidal direction. The influence of neoclassic rotation, $E \times B$ rotation and diamagnetic rotation on QH-modes have been investigated to understand the physics mechanisms leading to the QH-mode behaviour and to support the achievement of QH-mode plasmas in the ASDEX-Upgrade device.

The simulations for ITER $Q = 10$ scenario have been extended to include $n = 0-5$ modes and $n = 0-10$ modes and including a resistive wall. The results show that the inclusion of a resistive wall has a significant influence on the nonlinear evolution of KPMs in ITER plasma while this effect is found to be small in QH-mode simulations of DIII-D plasmas. The simulations show $E \times B$ rotation/shear plays an important role for ITER high Q plasmas to enter and remain in the QH-mode regime. The results of these simulations will be evaluated in the paper to determine whether this regime is an option for high fusion performance operation at the specific characteristics of ITER plasmas.

NTM Excitation by Sawtooth Crashes and the Suppression of Their Onset by Resonant Magnetic Perturbation

Q. Yu¹, S. Günter¹, K. Lackner¹, E. Strumberger¹, and V. Igoshine¹

¹Max-Planck-Institut für Plasmaphysik, Garching, Germany

Corresponding Author: Q. Yu, qiy@ipp.mpg.de

Neoclassical tearing modes (NTMs) can degrade plasma confinement or even lead to disruptions in existing tokamak discharges. To understand their triggering mechanism by sawtooth crashes and the effect of error fields or externally applied resonant magnetic perturbations (RMPs) on their onset remain to be important for ITER or a fusion power plant. In this paper these two issues are studied numerically based on the two-fluid equations, using ASDEX-Upgrade experimental parameters as input.

Triggering of NTMs by sawtooth crash: Numerical calculations have been carried out to study the triggering of NTMs by sawtooth crashes. In toroidal geometry, the nonlinear harmonics of the $m/n = 1/1$ mode, the $2/2$ component, can have a large amplitude during the sawtooth crash and possibly drive a $3/2$ seed island via toroidal mode coupling, where $m(n)$ is the poloidal (toroidal) mode number. As expected, it is found that the onset of the $3/2$ NTM is most effective for large sawtooth amplitudes, high plasma β value and low relative frequency between these two modes. The $3/2$ magnetic perturbations first have the feature of an ideal mode across the $q = 3/2$ surface and show a tearing character only later in time. The latter is in very good agreement with experiments. The observed immediate increase of the $3/2$ magnetic signal after a sawtooth thus represents an ideal magnetic perturbation rather than a magnetic island.

Effect of RMPs on NTMs: In several tokamak experiments a stabilization of rotating magnetic islands by static RMPs of moderate amplitude have been observed. This is consistent with our numerical results showing that a magnetic island can be suppressed by a static RMP of the same helicity in a certain range of RMP amplitude, if the local perpendicular electron fluid velocity at the resonant surface is sufficiently large. Due to the electron diamagnetic drift, the mode stabilization effect by RMPs is much stronger in the two-fluid case than in the single fluid case. The mechanism only works for moderate RMP amplitudes. In case of a too-large RMP amplitude, the island growth is supported by the RMPs, resulting in a large locked magnetic island.

Simulation of the Internal Kink Mode in Visco-Resistive Regimes

J. Mendonca¹, D. Chandra¹, A. Sen¹, and A. Thyagaraja²

¹*Institute for Plasma Research (IPR), Bhat, Gandhinagar, India*

²*University of Bristol, Bristol, BS8 1TH, UK*

Corresponding Author: D. Chandra, debasischandra@gmail.com

The $m/n = 1/1$ internal kink instability plays an important role in the dynamics of a tokamak discharge and is responsible for the occurrence of sawtooth oscillations. Many experimental observations show that plasma rotation can strongly influence the stability properties of sawtooth oscillations. Past theoretical flow studies to understand such stabilization have been done in the low viscosity regimes. Viscosity can be high in tokamaks due to enhancements from turbulent effects. We investigate the stability of the $1/1$ mode in the presence of sheared flows over a range of viscosity regimes using the CUTIE code for both RMHD and two-fluid models. Initially, we use the RMHD version of CUTIE and systematically examine the effects of several kinds of sheared flows on the $1/1$ mode, namely axial, poloidal and combinations of both types of flows in the linear and the nonlinear regimes. In the absence of flow and for low Prandtl numbers we observe that the growth rate scalings with resistivity and viscosity agree with past theoretical results. However, as we increase the viscosity further, the growth rate scaling changes significantly. It shows that high viscosity can strongly influence the linear growth rate of the modes. We find that in the presence of an axial flow, the stabilizing influence of viscosity is enhanced and can lead to a complete stabilization of the $m = 1$ visco-resistive mode at high Prandtl numbers. In the nonlinear regime, for axial flows, the saturation level of the mode decreases at a higher viscosity compared to the case of no flow but slightly increases at lower viscosity. Similar results are found for the poloidal flow case. In the case of helical flows at high viscosity, there is a significant change in the nonlinear saturation level depending on the flow helicity. We have continued the above studies into the two-fluid regime and found diamagnetic drift stabilization of the $1/1$ mode i.e., the growth rate of the $1/1$ mode reduces with an increase in the density gradient. The nonlinear evolution of the mode in the presence of imposed shear flows also shows distinct differences from the RMHD results due to the presence of two-fluid effects.

TH

A Power-Balance Model of Density Limit in Fusion Plasmas

P. Zanca¹, F. Sattin¹, and D. F. Escande²

The JET Contributors, TCV-Team, and EUROfusion MST1 Team

¹*Consorzio RFX, Associazione EURATOM-ENEA sulla Fusione, Padova, Italy*

²*Physique des Interactions Ioniques et Moléculaires (PIIM), CNRS, Aix-Marseille Université, France*

Corresponding Author: P. Zanca, paolo.zanca@igi.cnr.it

A density limit (DL), causing either a disruption or a soft termination of the discharge, is generally found in magnetic confinement fusion devices. Some empirical scaling laws have been proposed to order the maximum achievable densities. The Sudo density, $n_{\text{Sudo}} \propto \sqrt{PB_\phi}$, with P the heating power, is generally applied to the stellarator. The Greenwald density, $n_G = I_p/(\pi a^2)$, represents a reference for the ohmic tokamak and the reversed field pinch (RFP): a remarkable feature given the differences of these two configurations both in terms of magnetic profiles and transport properties. Additionally heated tokamak experiments in L-mode suggest scaling laws of the form $P^{(0.3-0.5)} I_p^{(0.5-1)}$. The H-mode tokamak DL, identified by a back transition to L-mode and therefore non disruptive in general, seems to be more device dependent. We present a basic power-balance model, providing a unified interpretation of DL in the stellarator, in the L-mode tokamak and in the RFP. In fact, scaling laws resembling the above empirical trends, but richer in their parametric dependence, are derived as special cases of a more fundamental relation, which delimits the thermal equilibrium states having realistic temperature profile (i.e., with low temperature only at the edge) in the presence of radiation losses due to light impurities and edge neutrals. This equation is just the detachment condition that has been discussed within the stellarator framework. Our analysis shows that it can be applied to any magnetic configuration. In particular, by combining this equation with on-axis Ohm's law and Spitzer's resistivity, a Greenwald-like scaling law is obtained, having a tenuous dependence on thermal transport: this explains why the DL does not change appreciably passing from the ohmic tokamak to the RFP. Nonetheless, this scaling departs from the pure Greenwald limit, due to further dependences on the impurity content as well as on the heating power. We show that it describes better than the pure Greenwald limit high density disrupted L-mode experiments performed at TCV and JET.

Resistive Wall Mode Physics and Control Challenges in JT-60SA High- β_N Scenarios

L. Pigatto^{1,2}, T. Bolzonella¹, Y. Q. Liu³, G. Marchiori¹, S. Mastrostefano⁴, G. Matsunaga⁵, M. Takechi⁵, and F. Villone⁶

¹*Consorzio RFX, Associazione EURATOM-ENEA sulla Fusione, Padova, Italy*

²*Università degli studi di Padova, Via VIII Febbraio, 35122 Padova, Italy*

³*General Atomics, San Diego, CA 92186, USA*

⁴*DEIM, Università della Tuscia, Largo dell'Università, 01100 Viterbo, Italy*

⁵*National Institutes for Quantum and Radiological Science and Technology (QST), Naka Fusion Institute, Naka-shi, Ibaraki-ken, Japan*

⁶*CREATE/ENEA/EURATOM Association, Università di Napoli, Naples, Italy*

Corresponding Author: L. Pigatto, leonardo.pigatto@igi.cnr.it

The superconducting tokamak JT-60SA is being built in Naka (Japan) under the Broader Approach Satellite Tokamak Programme jointly by Europe and Japan, and under the Japanese national programme. JT-60SA has an important supporting mission for the development of fusion energy: designed to achieve long pulses (100 s) and break-even equivalent plasmas, challenging high- β operation beyond the no-wall limit. It will help in both the exploitation of ITER and in the definition of an optimized DEMO design. The device will be equipped with off-axis negative-NBI at 0.5 MeV beam energy, allowing current profile tailoring for advanced tokamak scenarios with fully noninductive current drive. The focus of the work is set on high β_N scenarios, in which kink-like instabilities (e.g., one or more RWMs) are potentially unstable and possibly lead to disruptions. In the framework of a joint European-Japanese collaboration, coordinated effort on MHD stability and control modelling is ongoing for the safe realization and exploitation of high- β_N plasmas. These scenarios offer a great opportunity to test and verify present models of RWM physics. The drift-kinetic damping model in particular will be considered in the present work, with a stability study in Scenario 5.1 — like plasmas carried out with MARS-F/K. The challenge of active control is also addressed, taking advantage of the set of RWM control coils that JT-60SA will have. A dynamic simulator, based on the CarMa code, has been developed for feedback control modelling. A demonstration of this tool is given in one of the aforementioned plasmas, showing potential applications, results and latest developments.

Nonlinear Dynamics of Tearing Mode Driven by Static and Rotating External 3D Fields

S. Inoue¹, M. Okabayashi², Z. Taylor³, E. J. Strait³, J. Shiraishi¹, M. Takechi¹,
G. Matsunaga¹, A. Isayama¹, and S. Ide¹

¹*National Institutes for Quantum and Radiological Science and Technology (QST),
Naka Fusion Institute, Naka-shi, Ibaraki-ken, Japan*

²*Princeton Plasma Physics Laboratory (PPPL), Princeton, NJ 08540, USA*

³*General Atomics, San Diego, CA 92186, USA*

Corresponding Author: S. Inoue, inoue.shizuo@qst.go.jp

The interaction of a locked tearing mode with a nonaxisymmetric control field is found to be in good qualitative agreement with predictions of a nonlinear resistive MHD model [1, 2]. Locked tearing mode islands often lead to disruptions in tokamaks. However, experiments have shown that unlocking and rotation of the island by a rotating control field (CF) can postpone or prevent a disruption [3]. The dynamics of this control has been modelled with the “AEOLUS-IT” code [1, 2] in both tearing stable and unstable plasmas. In the tearing stable plasma, a static error field (EF) drives the island growth, which is successfully stabilized by the CF. Even in tearing unstable plasmas, the CF is predicted to reduce the nonlinearly saturated island size. Model predictions of two distinct regimes of plasma response, characterized as standing-wave and travelling-wave, are in good qualitative agreement with DIII-D observations. These results are an important step toward predictive understanding of this new approach to tearing mode control and disruption avoidance.

References

- [1] S. Inoue *et al.*, Nucl. Fus., **57**, 116020 (2017).
- [2] S. Inoue *et al.*, Plasma Phys. Contr. F., **60**, 025003 (2018).
- [3] M. Okabayashi *et al.*, Nucl. Fus., **57**, 016035 (2017).

Ion Kinetic Effects on MHD Instabilities in High- β LHD Plasmas

M. Sato¹, Y. Todo¹

¹*National Institute for Fusion Science (NIFS), Toki, Gifu, Japan*

Corresponding Author: M. Sato, sato.masahiko@nifs.ac.jp

For the high- β plasmas in the inward shifted Large Helical Device (LHD) configurations, the plasma peripheral region is theoretically MHD unstable region since there is always a magnetic hill in the plasma peripheral region. However, high- β plasmas with about 5% of the volume-averaged β value are stably obtained in the LHD experiments. This implies that the nonlinear saturation level of the MHD instabilities does not significantly affect the plasma confinement. On the other hand, the previous MHD simulation study showed that resistive ballooning modes are unstable in the plasma peripheral region and the central pressure is significantly decreases since the influence of the instabilities expands to the core region. In order to resolve the discrepancy between the experimental results and the simulation results, numerical analyses based on the kinetic MHD model have been carried out in this study.

In the kinetic MHD model used here, the drift kinetic description is used for ions and the fluid model is used for the electron. The plasma density, the velocity parallel to the magnetic field and the ion's pressure are evaluated from the velocity moment of the ion's distribution function. The MHD equilibrium is constructed by the HINT code without assumption of the existence of nested magnetic surfaces. The central β value is assumed to be 7.5%.

It is found that the linear growth rates of the resistive ballooning modes obtained from the kinetic MHD model are smaller than the linear growth rates obtained from the MHD model. In the radial mode structure of the pressure obtained from the kinetic MHD model, the amplitude of the ion pressure is about half of the amplitude of the electron pressure due to the ion's finite orbit width (FOW) effects. For the saturated state of the MHD instabilities, although the central pressure decreases for both the MHD model and the kinetic MHD model, the decrease of the central pressure for the kinetic MHD model is smaller than that of the central pressure for the MHD model. Since the MHD instabilities are the resistive modes, the stabilizing effects of the ion kinetic effects is expected to be stronger for the experimental high magnetic Reynolds number so that the core crush may be suppressed.

TH

Comparative Simulations of the Plasma Response to RMPs During ELM-Crash Mitigated and Suppressed Phases in KSTAR

G. Y. Park¹, J. H. Lee¹, Y. In^{1,2}, Y. M. Jeon¹, W. H. Ko¹, B. C. Lyons³, and C.-S. Chang⁴

¹National Fusion Research Institute (NFRI), Daejeon, Republic of Korea

²Ulsan National Institute of Science and Technology (UNIST), Ulsan, Republic of Korea

³General Atomics, San Diego, CA 92186, USA

⁴Princeton Plasma Physics Laboratory (PPPL), Princeton, NJ 08540, USA

Corresponding Author: G. Y. Park, gypark@nfri.re.kr

Control of the edge localized modes (ELMs) is one of the most critical issues for a ITER and the future tokamak fusion reactors. In order to develop a *predictive* model of the access to ELM-crash suppressed states, it is essential to understand first the underlying physics mechanism of ELM-crash-suppression. This paper reports comparative simulation results for particular KSTAR experimental shot, where both of the ELM mitigated and suppressed phases were observed sequentially and separated distinctly in time with low- n resonant magnetic perturbations (RMPs) in KSTAR. We have observed that toroidal (ω_t) and $E \times B$ ($\omega_{E \times B}$) rotation frequencies are increased, while electron pressure gradient and the associated electron diamagnetic rotation frequency (ω_{*e}) reduced near the pedestal top through the transition from mitigation to suppression of ELMs. This results in a small outward shift in the zero-crossing of the electron perpendicular rotation ($\omega_{\perp e} \sim 0$) and $\omega_{\perp e}$ becomes even smaller inside the pedestal. Correspondingly, two-fluid linear plasma response modelling with the resistive MHD code M3D-C1 [1] indicates that resonant tearing response is increased significantly near the pedestal top, which is well correlated to the observed onset of ELM-crash suppression. This result is similar to the recent ECEI observation of perpendicular flow changes at the onset of ELM-crash suppression in KSTAR [2]. It remains unclear how the RMP-driven transport (with associated kinetic effects) bring out such changes to the rotation profiles and we plan to study that with XGC0 [3] and XGC1 [4] codes. Detailed results will be presented.

References

- [1] N. M. Ferraro, Phys. Plasmas, **19**, 056105 (2012).
- [2] J. H. Lee *et al.*, APS-DPP (2017).
- [3] G. Y. Park *et al.*, Phys. Plasmas, **17**, 102503 (2010).
- [4] C. S. Chang *et al.*, Phys. Plasmas, **16**, 056108 (2009).

Plasma Equilibrium Reconstruction of JET Discharges Using the IMAS Modelling Infrastructure

R. Coelho¹, W. Zwingmann¹, B. Faugeras³, E. Giovannozzi³, P. McCarthy⁴, E. P. Suchkov⁵, F. S. Zaitsev⁵, J. Hollocombe⁶, N. Hawkes⁶, G. Szepesi⁶, and D. Terranova⁷

The JET Contributors and The EUROfusion-IM Team

¹*Institute of Plasmas and Nuclear Fusion (IPNF), Instituto Superior Técnico (IST), 1049-001 Lisbon, Portugal*

²*CNRS Laboratory J. A. Dieudonné, Université Nice Sophia Antipolis, Nice, France*

³*ENEA for EUROfusion, via E. Fermi 45, 00044 Frascati (Roma), Italy*

⁴*University College Cork, Cork, Republic of Ireland*

⁵*Comenius University, Bratislava, Slovakia*

⁶*Culham Centre for Fusion Energy (CCFE), Culham Science Centre, Abingdon, UK*

⁷*Consorzio RFX, Associazione EURATOM-ENEA sulla Fusione, Padova, Italy*

Corresponding Author: R. Coelho, rcoelho@ipfn.ist.utl.pt

The reconstruction of tokamak plasma equilibrium is a fundamental step in the understanding of fusion plasma physics since it sets the starting point for all subsequent plasma modelling applications and experimental data interpretation. The verification and validation of the numerical codes used to reconstruct plasma equilibrium, using as many available input experimental data, e.g., magnetic field or flux measurements, density and temperature diagnostics and polarimetry diagnostics, is essential both for physics model interpretation and when qualifying and extrapolating for ITER. In the framework of the EUROfusion Work Package on Code Development for Integrated Modelling, a scientific Kepler [1] workflow for the reconstruction of Tokamak plasma equilibrium was prototyped, using the ITER Integrated Modelling and Analysis Suite (IMAS) [2, 3]. The workflow can seamlessly use any sort of data from tokamak experiments and call reconstruction codes such as EQUAL [4], CLISTE [5], EQUINOX [6] and SDSS [7], all using the same physics and engineering data ontology and methods for accessing the data. In this work, we address plasma equilibrium reconstructions on dedicated JET plasma discharges, performing a code benchmark using, at first, magnetic data only and subsequently considering also other constraints such as polarimetry (Stokes vector based or motional Stark effect). First results with magnetic only give good qualitative and quantitative agreement between the codes.

References

- [1] <https://kepler-project.org>
- [2] S. D. Pinches *et al.*, IAEA FEC–2016, Kyoto, Japan, [TH/P2-14](#), (2016).
- [3] F. Imbeaux, *et al.*, Nucl. Fus., **55**, 123006 (2015).
- [4] W. Zwingmann, Nucl. Fus., **43**, 842 (2003).
- [5] P. J. McCarthy, Phys. Plasmas, **6**, 3554 (1999).
- [6] B. Faugeras *et al.*, Plasma Phys. Contr. F., **56**, 114010 (2014).
- [7] R. Coelho *et al.*, Fusion Sci. Tech., **69**, 611 (2016).

Nonlinearly Saturated Ideal Magnetohydrodynamic Equilibrium States with Periodicity-Breaking in Stellarators

W. A. Cooper^{1,3}, D. López-Bruna², M. A. Ochando², F. Castejón², J. P. Graves³, A. Kleiner³, S. Lanthaler³, H. Patten³, M. Raghunathan³, and J. M. Faustin⁴

¹Swiss Alps Fusion Energy (SAFE), CH-1864 Vers l'Eglise, Switzerland

²Laboratorio Nacional de Fusión (LNF),

Centro de Investigaciones Energéticas, Medioambientales y Tecnológicas (CIEMAT), Madrid, Spain

³Swiss Plasma Center (SPC), École polytechnique fédérale de Lausanne (EPFL), 1015 Lausanne, Switzerland

⁴Max-Planck-Institut für Plasmaphysik, Greifswald, Germany

Corresponding Author: W. A. Cooper, wilfred.cooper@epfl.ch

The relaxation of the constraint of periodicity imposed by the external confining magnetic field coils in a nominally 4-field period Helias Advanced Stellarator configuration produces weak periodicity-breaking deformations of the plasma. The corrugations are driven by the interaction of the pressure gradient with the magnetic field line curvature and correspond to saturated ideal magnetohydrodynamic interchanges with a mode structure dominated by nonresonant $m = 1$, $n = \pm 1$ Fourier components. Very similar low order mode number oscillations are observed in the 4-field period TJ-II Heliac stellarator. The conditions of quasi-isodynamicity of the Helias reactor system investigated are not significantly altered by the periodicity-breaking distortions.

Role of NTV Particle Flux in Density Pumpout during ELM Control by RMP

Y. Liu¹, L. Li², R. Nazikian³, C. Paz-Soldan¹, A. Kirk⁴, A. Loarte⁵, P. Piovesan⁶, Y. Sun⁷, and W. Suttrop⁸

¹General Atomics, San Diego, CA 92186, USA

²Donghua University, Shanghai 201620, People's Republic of China

³Princeton Plasma Physics Laboratory (PPPL), Princeton, NJ 08540, USA

⁴Culham Centre for Fusion Energy (CCFE), Culham Science Centre, Abingdon, UK

⁵International Thermonuclear Experimental Reactor (ITER),
Cadarache Centre, 13108 St. Paul lez Durance, France

⁶Consorzio RFX, Associazione EURATOM-ENEA sulla Fusione, Padova, Italy

⁷Institute of Plasma Physics, Chinese Academy of Sciences, Hefei, Anhui, People's Republic of China

⁸Max-Planck-Institut für Plasmaphysik, Garching, Germany

Corresponding Author: Y. Liu, liuy@fusion.gat.com

Edge localized modes (ELMs) release large bursts of heat and particle flux to the plasma facing components in tokamaks, potentially causing significant material erosion in future devices such as ITER. Externally applied 3D resonant magnetic perturbations (RMP) have been experimentally demonstrated to be effective in tailoring these ELM bursts. A significant yet not well understood phenomenon is the density pumpout effect caused by the RMP field. Understanding physics mechanisms associated with density pumpout is critical to: i) understand the ELM control itself; ii) understand RMP induced plasma performance degradation; and, iii) provide guidance to ELM control design in ITER.

This contribution reports toroidal modelling results of RMP induced density pumpout, based on a self-consistent quasi-linear model implemented into the MARS-Q code. The model combines the resistive plasma response to 3D fields, with the axi-symmetric toroidal momentum and radial particle transport equations. In particular, the radial particle flux includes contributions from that associated with neoclassical toroidal viscosity (NTV). We found that the resonant NTV particle flux, which is significantly enhanced due to Landau resonance between the applied perturbation and the precessional drifts of trapped thermal particles, provides a significant outward particle flux near the pedestal top, where the $E \times B$ rotation velocity is small or even crossing zero. Initial value simulations, lasting longer than the momentum and particle confinement times, demonstrate the important role of the NTV particle flux in causing a large fraction of density pumpout.

Work supported by the U.S. Department of Energy, Office of Science under Contracts DE-FG02-95ER54309 and DEFC02-04ER54698.

Negative Triangularity Effects on Tokamak MHD Stability

L. J. Zheng¹, M. T. Kotschenreuther¹, F. L. Waelbroeck¹, M. E. Austin¹, W. L. Rowan¹,
P. Valanju¹, and X. Liu¹

¹*Institute for Fusion Studies (IFS), University of Texas at Austin, Austin, TX 78712, USA*

Corresponding Author: L. J. Zheng, lzheng@mail.utexas.edu

Recently, discharges with negative triangularity were created in the DIII-D tokamak. These discharges exhibited the H-mode-level confinement features with L-mode-like edge behaviour without ELMs [1]. This led us to extensively examine the MHD stability of negative triangularity tokamaks. Using the numerically reconstructed experimental equilibrium, our computation confirmed the stability of the β_N of 2.6 achieved in DIII-D experiments against low- n MHD kink modes. In parameter variations outside the experimental values, we surprisingly found that the negative triangularity configuration can actually achieve even higher β_N than the positive triangularity case in certain cases. We used the VMEC equilibrium code to construct the equilibria, with the bootstrap current included from the Sauter formula. The stability was investigated using the AEGIS code, supplemented by the DCON code. Indeed, our calculations show that the negative triangularity configuration with low bootstrap current fraction and usual equilibrium profiles is usually not good for MHD stability. However, we found that the negative triangularity configuration leads to a lower safety factor value especially near the edge. That motivates us to reduce the Ohmic current and increase bootstrap current fraction. Surprisingly, it is found that some higher bootstrap fraction, high poloidal β , negative triangularity cases can have much higher β_N limit than 4 Li, while the positive triangularity case is limited by 4 Li as usual. We found that the negative triangularity favours the peak pressure profiles; while the positive triangularity the broad pressure profiles. This leads us to conclude that the negative triangularity tokamak can be more attractive than the positive triangularity case for steady-state confinement in the advanced tokamak scenario from the point of view of low- n MHD stability.

References

[1] M. E. Austin *et al.*, Bull. Am. Phys. Soc., **62**, (2017).

Equilibrium Pressure-Driven Current in the Presence of a Small Magnetic Island: Singular Behaviour and Symmetry Effects

A. Reiman¹, D. Radhakrishnan²

¹*Princeton Plasma Physics Laboratory (PPPL), Princeton, NJ 08540, USA*

²*New York University, New York, NY 10012, USA*

Corresponding Author: A. Reiman, reiman@pppl.gov

A small magnetic island has only a small effect on the ambient pressure gradient, so that the pressure is not constant on the flux surfaces in and near the island. The length scale determining which islands may be regarded as “small” in this context is determined by the ratio of perpendicular to parallel transport. We numerically explore the effect of such a small island on the MHD equilibrium current, assuming that the island is sufficiently large that the MHD perpendicular force balance equation retains its validity. This current plays an important role in determining the stability of the island. We show that the effect of a small island on the equilibrium current density can be significant. The pressure-driven current has, in general, a logarithmic (integrable) singularity at the X-line. In an MHD equilibrium that is invariant under combined reflection in the poloidal and toroidal angles (sometimes called “stellarator symmetry”), there is a cancellation, and the singular component of the pressure-driven current vanishes. Conventional models of magnetic islands used in analytical calculations have this symmetry property. Tokamaks with a single null divertor do not. In 3D MHD equilibrium solutions that are constrained to have simply nested flux surfaces, the pressure-driven current has a (nonintegrable) $1/x$ singularity near rational surfaces, where x is the distance from the rational surface. We have numerically investigated the pressure driven current near a small magnetic island in a cylindrical magnetic field with perturbed circular flux surfaces. The perturbation consists of two components, one that modulates the toroidal magnetic field strength without breaking the flux surfaces, and a second that introduces a resonant radial component of the magnetic field at the rational surface but has little effect on the toroidal field. The relative phase between the two perturbations is varied. The Pfirsch–Schlüter current near the X-line is found to be much larger when both perturbations are present and the relative phase between the two breaks the stellarator symmetry than it is when these conditions are not satisfied. The solution near the X-line agrees with the asymptotic limit calculated in a previously published paper.

Work supported by the U.S. Department of Energy contract DE-AC02-09CH11466 and by the DOE SULI program.

Advances on the High Field Ultralow Aspect Ratio Tokamak

C. Ribeiro¹

¹*Laboratório de Física de Plasmas e Fusão, Instituto de Matemática, Estatística e Física,
Universidade Federal do Rio Grande, Rio Grande do Sul, Brazil*

Corresponding Author: C. Ribeiro, celso_ribeiro@hotmail.com

Spherical tokamaks (STs) offer a potential more economical approach for attain fusion energy and has been also proposed as a neutron source for fusion materials studies. Therefore, it is important to explore the limit of ST's compactness in order to address the potential benefits for both tasks. This is the objective of the medium-size high-field ultralow aspect ratio tokamak (HF-ULART) proposal, which aims to explore very high β under the minimum toroidal field as a target plasma, and then explore higher pressures values using the combined minor and major radius adiabatic compression (AC) technique. This might be one of potential economical pathways scenario for at least an ultracompact pulsed neutron source based on the ST concept. The major characteristics of the target plasma are: $R_o = 0.51$ m, $a = 0.47$ m, aspect ratio $A = 1.1$, $k = 2$, $\delta \sim 0.8$, $B(R_o) = 0.1$ T (0.4 T max), $I_p = 0.5$ MA (2 MA, max), $n_e(0) \sim 1 \times 10^{20}/\text{m}^3$, $T_e(0) \sim 1$ keV, and discharge duration of ~ 100 ms. The vessel is spherical, made of SS, and insulated from the expected natural diverted (ND) plasma by thin (few cm) tungsten (W) semispherical limiters. The central stack is made of cooper cover by a thin (~ 2 mm) W sleeve. No internal PF coils or solenoid is envisaged. This helps the compactness due to the close plasma-vessel fitting, and possibly provides wall stabilization as previously envisaged in the RULART proposal, while also potentializes easier H-mode (small edge neutral source volume), which has already been observed in the ULART Pegasus device operating in ohmic ND plasmas, using inboard gas fuelling. The initial source for heating is provided by I_p generated from RF in combination with transient coaxial/local helicity injection techniques, as both have been successfully demonstrated in STs. By applying the AC technique over a high- β plasma, i.e., $I_p = 0.5$ MA, $B(R_o) = 0.1$ T, $R_o = 0.51$ m, $a = 0.47$ m, $A = 1.1$, $k = 2$, $\delta \sim 0.8$, $q_\psi(\text{Peng}) = 22$, $T_e/T_i = 263/486$ eV, $n_e(0) \sim 0.15 \times 10^{20}/\text{m}^3$, lead to final following values: $I_p = 1.0$ MA, $B(R_o) = 0.61$ T, $R_o = 0.33$ m, $a = 0.28$ m, $A = 1.2$, $k = 1.6$, $\delta \sim 0.1$, $q_\psi(\text{Peng}) = 12$, $T_e/T_i = 1.9/3.4$ keV, $n_e(0) \sim 2.8 \times 10^{20}/\text{m}^3$. Other preliminary analysis will be also presented. They include the time scales of the AC to respect the expected energy confinement time, the neutron yield and standard MHD stability calculations, and some fixed and free-boundary equilibrium simulations by VMEC and FIESTA codes, respectively.

Transport Simulation of EAST Long Pulse Discharge and High- β_N Discharge with Integrated Modelling

G. Q. Li¹, M. Q. Wu^{1,2}, K. Li^{1,2}, J. L. Chen¹, V. S. Chan², X. Gao¹, C. K. Pan¹, Q. L. Ren¹, W. Shen¹, S. Y. Ding¹, Y. M. Duan¹, X. Z. Gong¹, X. Jian³, Y. Y. Li¹, H. Lian^{1,2}, H. Q. Liu¹, B. Lyu¹, J. P. Qian¹, Q. Zang¹, and X. Zhu^{1,2}

¹*Institute of Plasma Physics, Chinese Academy of Sciences, Hefei, Anhui, People's Republic of China*

²*University of Science and Technology of China, Hefei, Anhui, People's Republic of China*

³*School of Electrical and Electronic Engineering, Huazhong University of Science and Technology, Hubei, People's Republic of China*

Corresponding Author: G. Q. Li, ligq@ipp.ac.cn

In the past two years, two major scenarios were developed on the EAST tokamak, the long pulse steady state scenario and the high- β_N scenario. For the steady state scenario, 100 s long pulse discharge was achieved with only radio frequency heating and current drive (CD) and it has improved confinement with $H_{98} \sim 1.1$. For the high- β_N scenario, a $\beta_N \sim 2.0$ was sustained for ~ 2 s, with an internal transport barrier (ITB) in all channels. Under OMFIT framework, a workflow was developed to simulate the two scenarios on EAST. The workflow integrated the equilibrium code EFIT, transport code TGYRO for energy transport, transport code ONETWO for current evolution and radiation, heating and CD code GENARY/TORAY/NUBEAM for driven current and energy sources. For long pulse discharge, the integrated modelling well reproduced the experimental electron and ion temperature profiles and current (or q) profiles. This validated our integrated modelling workflow and validated the TGLF transport model for the scenario possessing dominant electron heating and low torque. The modelling also gives the physical picture of the improved confinement induced by the on-axis ECH: the on-axis ECH increased the central electron temperature, make the LHCD power deposit to inner region and make the current profile more peaked, which suppress the high- k microinstabilities at the core region and improve the confinement. The integrated modelling workflow also was used for the high- β_N discharge of EAST. However, it could not reproduce the experimental temperature profiles. The reason is that the fishbone instability appears in the discharge, which could redistribute the fast ion and affect the energy transport. An heuristic model was developed to include the effects of fishbone instability, then the temperature profiles simulated by our integrated modelling qualitatively agreed with the experiments.

Theory of Turbulence Driven Intrinsic Rotation and Current

L. Wang¹, S. Peng¹, W. He¹, and P. H. Diamond²

¹*International Joint Research Laboratory of Magnetic Confinement Fusion and Plasma Physics (IFPP), Huazhong University of Science and Technology, Hubei, People's Republic of China*

²*University of California San Diego, CA 92093, USA*

Corresponding Author: L. Wang, luwang@hust.edu.cn

We present new results in the theory of turbulence driven intrinsic rotation and current. Both the intrinsic rotation and the intrinsic current driven by microturbulence are important for ITER. The former is critical for ITER due to its important role in suppressing MHD instabilities, since neutral beam injection may not provide enough external rotation drive in ITER. The latter is important because the noninductive current drive is essential for steady state operation of tokamak reactor. This paper presents a novel mechanism for the origin of intrinsic rotation, which is referred as turbulent acceleration [1]. We emphasize that the turbulent acceleration does not contradict momentum conservation law [2]. The possible relevance of the turbulent acceleration to some experimental observations is also discussed [3, 4]. Inspired by the investigation of intrinsic rotation (which is related to ion momentum) driven by turbulence, we also present the intrinsic current (which is related to electron momentum) driven by turbulence [5].

References

- [1] L. Wang and P. H. Diamond, *Phys. Rev. Lett.*, **110**, 265006 (2013).
- [2] S. Peng and L. Wang, *Phys. Plasmas*, **24**, 012304 (2017).
- [3] L. Wang *et al.*, *Phys. Plasmas*, **23**, 042309 (2016).
- [4] S. Peng *et al.*, *Nucl. Fus.*, **57**, 036003 (2017).
- [5] W. He *et al.*, In Preparation, To be submitted to *Nucl. Fus.*

En Route to High-Performance Discharges: Insights and Guidance from High-Realism Gyrokinetics

T. Görler¹, A. Di Siena¹, H. Doerk¹, T. Happel¹, S. J. Freethy^{1,2}, I.-G. Farcas³,
A. Bañón Navarro¹, R. Bilato¹, A. Bock¹, J. Citrin⁴, G. D. Conway¹, A. J. Creely²,
P. Hennequin⁵, F. Jenko¹, T. Johnson⁶, C. Lechte⁷, T. Neckel³, E. Poli¹, M. Schneider⁸,
E. Sonnendrücker¹, J. Stober¹, and A. E. White²

The ASDEX-Upgrade Team and JET Contributors

¹Max-Planck-Institut für Plasmaphysik, Garching, Germany

²Massachusetts Institute of Technology (MIT), Cambridge, MA 02139, USA

³Technische Universität München, Garching, Germany

⁴FOM Institute DIFFER, Association EURATOM-FOM, Nieuwegein, Netherlands

⁵Laboratoire de Physique des Plasmas (LPP), CNRS/École Polytechnique, 91128 Palaiseau, France

⁶KTH Royal Institute of Technology, Stockholm, Sweden

⁷Institut für Grenzflächenverfahrenstechnik und Plasmatechnologie (IGVP), Univ. Stuttgart, Germany

⁸International Thermonuclear Experimental Reactor (ITER),
Cadarache Centre, 13108 St. Paul lez Durance, France

Corresponding Author: T. Görler, tobias.goerler@ipp.mpg.de

Although remarkable progress in ab initio nonlinear gyrokinetic plasma core turbulence studies has been seen in the last decade, some important open issues remain, e.g., in view of high performance discharges where magnetic fluctuations tend to reduce the turbulence levels and where the presence of fast ions may provide further significant stabilization enhancements. This effect was shown to lead to a significant reduction of ion temperature profile stiffness in JET [1] and was required to explain DIII-D quiescent H-modes [2] as well as noninductive ASDEX-Upgrade (AUG) discharges [3]. Several questions immediately arise in this context: Are these — mainly local flux-tube simulation based — results modified by nonlocal effects in steep-gradient regimes? Can fast ion populations be used to control turbulent transport in burning plasmas? All of these questions culminate into this one: To which degree is core gyrokinetics able to reproduce observations from present-day experiments and predict future devices?

In order to address this crucial task, comprehensive state-of-the-art validation studies with AUG fluctuations measurements will be presented as examples. Furthermore, studies for simplified equilibria [4] and high- β AUG discharges will be shown confirming that the level of stabilization and threshold values for transitions between electromagnetic microinstabilities like ion temperature gradient (ITG) driven and kinetic ballooning modes (KBM), may very well be affected by nonlocal effects. In addition, light will be shed on the improvements that can be expected by considering fast ion effects in electrostatic and electromagnetic simulations. Employing the gyrokinetic code GENE [5], a wave-fast ion resonance mechanism was found to be critical in describing corresponding JET discharges [6]. While irrelevant to fusion-generated α -particles which just act as diluting particles, it can be shown that cleverly tailored fast ion temperature (gradient) profiles may still offer pathways towards optimized plasma scenarios with substantial turbulence reduction. The predictions are further improved by studying the impact of more realistic fast ion models than the often employed equivalent Maxwellian backgrounds.

Continued...

References

- [1] J. Citrin *et al.*, Phys. Rev. Lett., **111**, 155001 (2013).
- [2] C. Holland *et al.*, Nucl. Fus., **52**, 114007 (2012).
- [3] H. Doerk *et al.*, Nucl. Fus., **58**, 016044 (2018).
- [4] T. Görler *et al.*, Phys. Plasmas, **23**, 072503 (2016).
- [5] F. Jenko *et al.*, Phys. Plasmas, **7**, 1904 (2000).
- [6] A. Di Siena *et al.*, Nucl. Fus., **58**, 054002 (2018).

Application of the Semi-Implicit Numerical Method on the Radial Impurity Transport Equation and Determination of O^{4+} Emissivity with Two Separate PEC Databases

A. Bhattacharya¹, J. Ghosh², M. B. Chowdhuri², and P. Munshi¹

¹Indian Institute of Technology Kanpur, Kalyanpur, Kanpur-208016, Uttar Pradesh, India

²Institute for Plasma Research (IPR), Bhat, Gandhinagar, India

Corresponding Author: A. Bhattacharya, amritab@iitk.ac.in

The radial impurity transport equation describes the distribution of impurity ion species with different charge states perpendicular to magnetic surfaces of tokamak plasma. The impurity transport equation for each ion with ionization state Z is a second order, coupled, parabolic partial differential equation described in terms of number densities of charge states Z , $Z - 1$ and $Z + 1$. A semiimplicit numerical method has been applied over radial impurity transport equation to obtain the number densities of oxygen ions in present case. The numerical method applied suggests segregating the terms of the transport equation into implicit and explicit forms thereby adhering to a single time treatment (either implicit or explicit) for each of its constituent term. A forward in time and central in space (FTCS) scheme of discretization have been applied first. The terms associated with diffusivity and ionization and recombination terms of charge state Z are next rendered implicit; terms associated with convective velocity, ionization of charge state $Z - 1$ and recombination of charge state $Z + 1$ remain explicit. The system studied is the ADITYA tokamak ($r_o = 0.25$ m, $R = 0.75$ m, $B_t = 0.75$ T) installed at the Institute for Plasma Research, Gandhinagar, India. Plasma in ADITYA is circular in cross-section being confined within limiter. The number density of O^{4+} ions determined using semi-implicit numerical method is used further to obtain radial emissivity profile of (650.024 nm) transition of O^{4+} ion and compare it with experiment data. The emissivity values of 650.024 nm characteristic line of Be-like O^{4+} ion, in visible-spectral region, have been obtained by measuring the brightness in high magnetic field (inboard) and low magnetic field (outboard) regions of ADITYA tokamak and applying an Abel-like matrix inversion on it. Present study compares the emissivity calculated with number density of O^{4+} ion obtained using semi-implicit method with O^{4+} emissivity obtained experimentally using two databases of photon emissivity coefficients (PECs) namely the ADAS (Atomic Data and Analysis Structure) and NIFS (National Institute of Fusion Science) database. The PECs in two databases differ due to a difference in the atomic processes considered while calculating them. This difference thereby influences the radial emissivity profiles of O^{4+} ion studied in present case.

Progress in the ITER Integrated Modelling Programme and the ITER Scenario Database

S. D. Pinches¹, J.-F. Artaud², F. J. Casson³, G. Corrigan³, M. F. M. De Bock¹, D. Harting³, J. Hollocombe³, M. Hosokawa¹, A. A. Ivanov⁴, R. R. Khayrutdinov⁵, S. H. Kim¹, P. J. Knight³, M. Kočan¹, F. Köchl³, S. V. Konovalov⁵, A. Loarte¹, V. E. Lukash⁵, S. Y. Medvedev⁴, D. Muir³, M. G. O'Mullane⁶, A. R. Polevoi¹, J. J. Rasmussen⁷, M. Salewski⁷, O. Sauter⁸, M. Schneider¹, A. Sirinelli¹, and M. Walsh¹

¹International Thermonuclear Experimental Reactor (ITER),

Cadarache Centre, 13108 St. Paul lez Durance, France

²Institut de Recherche sur la Fusion par confinement Magnétique (IRFM),

Commissariat à l'énergie atomique (CEA/Cadarache), 13108 St. Paul lez Durance, France

³Culham Centre for Fusion Energy (CCFE), Culham Science Centre, Abingdon, UK

⁴Keldysh Institute of Applied Mathematics, RAS, Moscow, Russian Federation

⁵National Research Centre "Kurchatov Institute", Moscow, Russian Federation

⁶University of Strathclyde, Glasgow, UK

⁷Technical University of Denmark (DTU), Lyngby, Denmark

⁸Swiss Plasma Center (SPC), École polytechnique fédérale de Lausanne (EPFL), 1015 Lausanne, Switzerland

Corresponding Author: S. D. Pinches, simon.pinches@iter.org

The ITER Integrated Modelling & Analysis Suite (IMAS) is the software infrastructure that is being developed using expertise from across the research facilities within the ITER Members to meet the needs of the ITER Integrated Modelling Programme. It builds around a standardized representation of data described by a Data Dictionary that is both machine independent and extensible. Machine independence is important for allowing tools and workflows developed in IMAS to be tested on existing devices, whilst extensibility allows the Data Dictionary to grow and evolve over time as more and more use cases are addressed. In addition to providing all the tools for the scientific exploitation of ITER once operations start, IMAS also has a role to play during the construction phase by providing simulation data to support systems design, in particular for diagnostics, heating, fuelling and control systems.

Recently an IMAS database of ITER simulations has started to be developed and populated to help manage the exchange of physics data with ITER collaborators and domestic agencies. The database is being populated through a combination of translating existing data and running new simulations. The scenario simulation codes used to initially populate the database are ASTRA, CORSICA, DINA, JINTRAC, and METIS. Additional data structures consistently describing other aspects of these scenarios, for example the fast ion distribution functions, are being added to the database upon request to facilitate the design of specific systems. The scenarios for all stages of the ITER Research Plan are represented in the database and are at least populated with a description of the plasma equilibrium and profiles in the core of the plasma.

This database is accessible by all ITER contributors through the IMAS Access Layer, either for visualization or as input to IMAS-adapted workflows and simulation codes. Subsequently generated data can be stored in the database subject to acceptance criteria and provenance requirements being met. The capabilities of the final implementation of the database, including strict acceptance and validation procedures and full provenance tracking for all entries will be discussed in the paper.

Kinetic Simulation Studies on Multi-Ion-Species Plasma Transport in Helical Systems

M. Nunami^{1,2}, M. Nakata^{1,2}, M. Sato¹, S. Toda¹, H. Sugama^{1,2}, H. Yamaguchi¹, and M. Yokoyama^{1,2}

¹*National Institute for Fusion Science (NIFS), Toki, Gifu, Japan*

²*Department of Fusion Science, Graduate University for Advanced Studies (SOKENDAI), Toki, Gifu, Japan*

Corresponding Author: M. Nunami, nunami.masanori@nifs.ac.jp

The first comprehensive analyses of kinetic simulations for anomalous and neoclassical transport of steady state multi-ion-species plasmas including impurity ions in helical systems are performed by gyrokinetic and drift-kinetic approaches. To design fusion reactors, the transport phenomena of plasma particles and heat need to be quantitatively predicted, and numerical simulation approaches based on the kinetic frameworks are powerful for that purpose. Recently, it becomes able to validate the kinetic simulation results against the experimental observations for the plasma temperature and density profiles with the experimental errors taken into account. Furthermore, studies on the transport of the multi-ion-species plasma are strongly demanded for predicting the performances of the burning plasma in the ITER, future reactors, and also stellarators such as the Large Helical Device (LHD).

In high ion temperature plasmas with hollow impurity density profiles heated by neutral beam injection (NBI), we find that the turbulent contribution of the carbon impurity particle flux remains to be directed inward radially within the allowable ranges of the plasma temperature and density profiles, while the neoclassical ion fluxes can change due to the generated radial electric field (E_r) and the external momentum sources. Even for the case of the negative E_r , the neoclassical carbon flux can be directed outward when the inward-directed current is imposed sufficiently by the co-injected heating beam.

These findings contribute deeper understandings of the hollow profiles in the LHD impurity hole plasmas in terms of fully kinetic framework.

TH

Gyrokinetic Modelling of Turbulent Particle Fluxes towards Efficient Predictions of Density Profiles

E. Narita¹, M. Honda¹, M. Nakata², M. Yoshida¹, H. Takenaga¹, and N. Hayashi¹

¹*National Institutes for Quantum and Radiological Science and Technology (QST),*

Naka Fusion Institute, Naka-shi, Ibaraki-ken, Japan

²*National Institute for Fusion Science (NIFS), Toki, Gifu, Japan*

Corresponding Author: E. Narita, narita.emi@qst.go.jp

A novel quasi-linear particle transport model is constructed by joint analyses with gyrokinetic calculations and JT-60U experimental data. The new model deals with the diagonal (diffusion) and off-diagonal (pinch) transport mechanisms individually. Besides the decomposition, realistic particle sources from neutral-beam fuelling are taken into account, which have not been discussed in earlier studies. Taking advantage of the features offered by the model, i) the contribution from each transport mechanism to particle fluxes is quantitatively clarified, and ii) a framework is developed, which enables us to predict the particle fluxes accurately and quickly, taking a neural-network-based approach. Moreover, iii) a scaling formula is derived, considering linear zonal flows to understand mechanisms which determine the particle fluxes.

Nonlinear Gyrokinetic Analysis of Linear Ohmic Confinement to Saturated Ohmic Confinement Transition

L. Qi¹, J.-M. Kwon¹, T. S. Hahm², H. Jhang¹, and S. Yi¹

¹National Fusion Research Institute (NFRI), Daejeon, Republic of Korea

²Seoul National University, Seoul, Republic of Korea

Corresponding Author: L. Qi, qileister@nfri.re.kr

One of the long lived conundrums in ohmically heated plasmas is that the energy confinement time τ_E shows a transition from a linear regime proportional to the density (LOC) to a saturation regime (SOC) weakly dependent on the density. In the viewpoint of the first principle nonlinear global gyrokinetic simulations, we here present an investigation of LOC to SOC transition for the first time. In this study, by varying a single parameter plasma density, the confinement time estimated by $\tau \propto 1/\chi_{\text{eff}}$ shows a transition from a linearly increasing regime to a saturation regime as the plasma density increases. The effective transport diffusivity is defined as

$$\chi_{\text{eff}} \equiv \frac{n_e \chi_e \nabla T_e + n_i \chi_i \nabla T_i}{n_e \nabla T_e + n_i \nabla T_i},$$

where $n_{e,i}$, $T_{e,i}$ and $\chi_{e,i}$ are density, temperature and heat diffusivity for electron (e) and ion (i). The above nonlinear result follows the trend from the mixing length quasi-linear estimation for the heat transport. A transition of trapped electron dominant heat transport from TEM to ion dominant heat transport from ITG is observed when the LOC to SOC transition occurs. In the simulations, the Coulomb collision operator for ion-ion collision and the pitch-angle scattering operator for electron-ion collision are included. The physical effects of the collisions in the LOC to SOC transition can be understood by analyzing the phase space dynamics. Physics of intrinsic rotation reversal [1, 2] and $E \times B$ staircase [3], both of which were found to have close relations with LOC-SOC transition, will be discussed.

References

- [1] J. E. Rice *et al.*, Phys. Rev. Lett., **107**, 265001 (2011).
- [2] Y. J. Shi *et al.*, Nucl. Fus., **57**, 066040 (2017).
- [3] G. Horning *et al.*, Nucl. Fus., **57**, 014006 (2017).

Flux-Surface Averaged Radial Transport in Toroidal Plasmas with Magnetic Islands

D. López-Bruna¹, B. Momo², I. Predebon², A. López-Fraguas¹, F. Auriemma², and Y. Suzuki³

¹*Laboratorio Nacional de Fusión (LNF),*

Centro de Investigaciones Energéticas, Medioambientales y Tecnológicas (CIEMAT), Madrid, Spain

²*Consorzio RFX, Associazione EURATOM-ENEA sulla Fusione, Padova, Italy*

³*National Institute for Fusion Science (NIFS), Toki, Gifu, Japan*

Corresponding Author: D. López-Bruna, daniel.lopezbruna@ciemat.es

In toroidal magnetic confinement fusion research, 1D transport models rely on one radial coordinate that labels nested toroidal flux surfaces. The presence of magnetic islands in the magnetic geometry does not impede making 1D transport calculations if the island regions are excluded and then, if necessary, treated separately. In this work we show a simple way to modify the flux-surface coordinate and corresponding metric coefficients when an island region is excluded. Comparison with the metrics obtained from Poincaré plots are shown, as well as applications to two types of plasma: Helic (TJ-II, CIEMAT, Spain), where the geometrical effects alone cannot explain the experimental results when islands move throughout minor radius; and Heliotron (LHD, NIFS, Japan), where we estimate the effect of possible heat losses in flux-gradient relations.

Transport of Collisional Impurities with Flux-Surface Density Variation in Stellarator Plasmas

S. Buller¹, H. M Smith², P. Helander², S. L. Newton³, and I. Pusztai¹

¹*Chalmers University of Technology, Göteborg, Sweden*

²*Max-Planck-Institut für Plasmaphysik, Greifswald, Germany*

³*Culham Centre for Fusion Energy (CCFE), Culham Science Centre, Abingdon, UK*

Corresponding Author: S. Buller, bstefan@chalmers.se

Highly charged impurities both dilute plasmas and lead to radiation losses, and thus cannot be allowed to accumulate in the core of a magnetic confinement fusion reactor. For stellarators, the outlook has been particularly pessimistic, as early theories predicted that impurities would unavoidably be transported inwards in the core.

However, recent theoretical work has shown that strong temperature gradients can transport impurities outward, in the reactor-relevant scenario of a weakly collisional bulk ion species and a collisional impurity species. In this work, we extend these results to allow for variations of the impurity density on the flux surface in response to an externally applied electrostatic potential, due to, for example, the presence of anisotropic fast particles.

Specifically, we consider the radial transport of a collisional but trace ($Z^2 n_z \ll n_i$) impurity species which varies in response to Φ . We calculate the neoclassical transport of the impurities, and find that localized impurity densities can have a large effect on the radial flux — even producing sign change — compared to the homogeneous n_z case. Tentative results show that this effect may be highly relevant for understanding the lack of impurities in “impurity hole” shots in LHD, but less relevant for carbon transport in W7-X due to the smaller Φ -variations in the latter. However, the effect becomes more important at higher impurity-charge, and can thus be expected to be relevant for tungsten transport also in W7-X.

TH

Towards a Predictive Modelling Capacity for DT Plasmas: European Transport Simulator (ETS) Verification and Validation

P. Strand¹, J. Ferreira², A. Figueiredo², P. Huynh⁶, T. Jonsson⁴, E. A. Lerche³,
D. Van Eester³, D. Yadykin¹, F. J. Casson¹⁰, R. Coelho², D. Coster⁵, G. L. Falchetto⁶,
I. Ivanova-Stanik⁹, D. Kalupin⁷, S. Moradi³, M. Poradziński⁹, P. Siren⁸, E. Tholerus⁴,
J. Varje⁸, and M. Romanelli¹⁰

The JET Contributors and The EUROfusion-IM Team

¹Chalmers University of Technology, Göteborg, Sweden

²Institute of Plasmas and Nuclear Fusion (IPNF), Instituto Superior Técnico (IST), 1049-001 Lisbon, Portugal

³Laboratory for Plasma Physics, ERM/KMS, Brussels, Belgium

⁴KTH Royal Institute of Technology, Stockholm, Sweden

⁵Max-Planck-Institut für Plasmaphysik, Garching, Germany

⁶Institut de Recherche sur la Fusion par confinement Magnétique (IRFM),
Commissariat à l'énergie atomique (CEA/Cadarache), 13108 St. Paul lez Durance, France

⁷EUROfusion Programme Management Unit Garching, Boltzmannstraße 2, 85748 Garching Germany

⁸Aalto University, Espoo, Finland

⁹Institute of Plasma Physics and Laser Microfusion (IPPLM), Warsaw, Poland

¹⁰Culham Centre for Fusion Energy (CCFE), Culham Science Centre, Abingdon, UK

Corresponding Author: P. Strand, par.strand@chalmers.se

The European Transport Simulator (ETS) [1] has been developed under the EUROfusion Integrated Modelling (EU-IM) effort [2] to meet the requirements for scenario development of burning plasmas. The ETS focusses both on interpretive and predictive modelling and is now being deployed for broader exploitation, e.g., on the JET computing infrastructure for close integration and use in support of JET campaigns. Recently, developments have been undertaken to enhance the ETS modelling capabilities for DT plasmas in view of the upcoming experiments.

A coherent inclusion of fast particle physics effects as well as a consistent approach for multispecies plasmas have been implemented. Major features are the capability for separate modelling of the different hydrogen isotope channels as well as light and heavy impurities — in all their charge states — and a set of advanced heating and current drive modules, which, for example, allows for ICRH heating effects on majority ions. ETS is also used in modelling runaway electron scenarios and NTMs. Here we describe the extensions to the ETS workflow undertaken to enhance the modelling capabilities for DT plasmas and discuss a detailed verification and validation activity.

The ETS also sports a set of transport models (TGLF, Qualikiz, EDWM) capable of resolving and providing transport for hydrogenic isotopes as well as light and heavy impurities. Results with these models as well as a discussion on approaches attempting to resolve inherent mass scaling issues will be shown.

References

- [1] D. Kalupin *et al.*, Nucl. Fus., **53**, 123007 (2013).
- [2] G. L. Falchetto *et al.*, Nucl. Fus., **54**, 043018 (2014).

Ion and Electron Temperature Predictions Based on Thailand Tokamak Plasmas Using CRONOS Code

B. Chatthong¹, T. Makmool¹, J. Promping², S. Sangaroon³, A. Wisitsorarak⁴, and T. Onjun²

¹*Department of Physics, Prince of Songkla University, Songkla, Thailand*

²*Thailand Institute of Nuclear Technology, Bangkok, Thailand*

³*Department of Physics, Mahasarakham University, Mahasarakham, Thailand*

⁴*Department of Physics, King Mongkut University of Technology Thonburi, Bangkok, Thailand*

Corresponding Author: B. Chatthong, boonyarit.ch@psu.ac.th

This work uses CRONOS integrated predictive modelling code to simulate ion and electron temperatures of plasma scenarios based on a future Thailand tokamak. This small tokamak is planned to be installed at Thailand Institute of Nuclear Technology (TINT), under the collaboration of the Center for Plasma and Nuclear Fusion Technology (CPaF). The plasma transport includes both neoclassical, via NCLASS module, and anomalous transports, via Mixed Bohm/gyro-Bohm module. The boundary condition for the thermal transport equation is set at the top of the pedestal where pedestal temperature is calculated based on scaling law. No external heating is given in these simulations so the plasmas remain only in L-mode. A simple electron density profile is given for all simulations with central value around $10^{-19}/\text{m}^3$. Effects of both plasma current and toroidal magnetic field on ion and electron temperatures are investigated. It is found that central electron temperature ranges from 200 to 410 eV, whereas ion temperature ranges from 120 to 170 eV. Evidently, both temperatures are more sensitive on the change of plasma current than that of toroidal magnetic field.

TH

Neural-Network Accelerated Coupled Core-Pedestal Simulations with Self-Consistent Transport of Impurities

O. Meneghini¹, G. Snoep², S. P. Smith¹, A. Tema³, B. A. Grierson⁴, E. A. Belli¹, J. Candy¹, P. B. Snyder¹, G. M. Staebler¹, S. Mordijck⁵, and J. Citrin⁶

¹General Atomics, San Diego, CA 92186, USA

²Eindhoven University of Technology, Eindhoven, Netherlands

³Politecnico di Torino, Turin, Italy

⁴Princeton Plasma Physics Laboratory (PPPL), Princeton, NJ 08540, USA

⁵College of William & Mary, Williamsburg, VA 23185, USA

⁶Dutch Institute for Fundamental Energy Research, Eindhoven, Netherlands

Corresponding Author: O. Meneghini, meneghini@fusion.gat.com

An integrated modelling workflow capable of finding the steady-state solution with self-consistent core transport, pedestal structure, current profile, and plasma equilibrium physics has been developed, validated against several DIII-D discharges, and used to perform predictions for a 15 MA DT ITER baseline scenario. Key features of the proposed core-pedestal coupled workflow are its ability to self-consistently account for the transport of impurities in the plasma, as well as its use of machine learning accelerated models for the pedestal structure, the neoclassical bootstrap current, and for the turbulent and neoclassical transport physics. Self-consistent coupling of physics-based models (or their machine-learning accelerated counterparts) is of great importance since it reduces the number of free parameters and assumptions that are used in the simulations, thus greatly improving the reliability of our numerical forecasts. The results presented in this paper provide supporting evidence that neural network based reduced models are indeed capable of breaking the speed-accuracy trade-off that is expected of traditional numerical physics models, and can provide the missing link towards whole device modelling simulations that are physically accurate, robust, and extremely efficient to run.

Work supported in part by the U.S. Department of Energy under Contract Nos. DE-SC0017992 (AToM), DE-FG02-95ER54309 (GA theory), DE-FC02-06ER54873 (ESL), and DE-FC02-04ER-54698 (DIII-D). This research used resources of the National Energy Research Scientific Computing Center (NERSC), a DOE Office of Science User Facility supported by the Office of Science of the U.S. Department of Energy under Contract No. DE-AC02-05CH11231.

Self-Driven Current Generation in Turbulent Fusion Plasmas

W. X. Wang¹, E. Startsev¹, S. Ethier¹, J. Chen¹, C. H. Ma¹, T. S. Hahm², and M. G. Yoo²

¹*Princeton Plasma Physics Laboratory (PPPL), Princeton, NJ 08540, USA*

²*Seoul National University, Seoul, Republic of Korea*

Corresponding Author: W. X. Wang, wwang@pppl.gov

Plasma self-generated current (e.g., the bootstrap current) contributes to the generation of poloidal magnetic field for plasma confinement in tokamaks, and also strongly affects key MHD instabilities. It is found that plasma turbulence may strongly influence self-driven current generation. This could have a radical impact on various aspects of tokamak physics. Our simulation study employs a global gyrokinetic model coupling self-consistent neoclassical and turbulent dynamics with focus on mean electron current. Distinct phases in electron current generation are illustrated in our initial value simulation. In the early phase before turbulence develops, the electron bootstrap current is established in a time scale of a few electron collision times, which closely agrees with the neoclassical prediction. The second phase follows when turbulence begins to saturate, during which turbulent fluctuations are found to strongly affect electron current. The profile structure, amplitude and phase space structures of electron current density are all significantly modified relative to the neoclassical bootstrap current by the presence of turbulence. Both electron parallel acceleration and parallel residual stress drive due to turbulence are shown to play important roles in turbulence-induced current generation. The former can change the total plasma self-generated current though turbulence-induced momentum exchange between electrons and ions, and the latter merely modifies the current density profile while keeping the total current unchanged. The current density profile is modified in a way that correlates with the fluctuation intensity gradient through its effect on k_{\parallel} -symmetry breaking in fluctuation spectrum. Turbulence is shown to reduce (enhance) plasma self-generated current in low (high) collisionality regime, and the reduction of total electron current relative to the neoclassical bootstrap current increases as collisionality decreases. The implication of this result to the fully noninductive current operation in steady state burning plasma regime could be important and should be investigated. Finally, a significant noninductive current is observed in flat pressure region, which is a nonlocal effect and results from turbulence-spreading-induced current diffusion.

Work supported by the U.S. Department of Energy Contract DE-AC02-09-CH11466.

Scalings of Ion Temperature Gradient Turbulence and Transport

P. W. Terry¹, M. J. Pueschel², G. G. Whelan¹, B. J. Faber¹, C. C. Hegna¹, P.-Y. Li¹, and V. V. Mirnov¹

¹*University of Wisconsin-Madison, Madison, WI 53706, USA*

²*Institute for Fusion Studies (IFS), University of Texas at Austin, Austin, TX 78712, USA*

Corresponding Author: P. W. Terry, pwterry@wisc.edu

TH
An analytic saturation theory for toroidal ion temperature gradient turbulence is derived from a well-known fluid model, providing the saturated levels of the unstable fluctuation, a nearly conjugate stable mode, and the zonal flow, along with their dependencies on the model parameters. The theory utilizes the eigenmode decomposition of the dynamical equations, applies statistical closure, and introduces an ordering expansion to isolate and analyze zonal-flow-catalyzed energy transfer. This is the dominant energy transfer channel, carrying energy from the instability, through a zonal flow to the dissipated stable mode via nearly resonant wavenumber triads. Solution of closed energy balance equations for the critical sources and sinks yields a turbulence level that is proportional to the ratio of the zonal flow damping rate and the inverse of the triplet correlation time of the zonal-flow catalyzed wavenumber triplet interaction. The zonal flow energy is proportional to the ratio of the growth rate and the inverse correlation time. The analytic solutions for saturation level and scalings are applied to the ion heat flux, showing that it has a factor given by the standard prediction of quasi-linear theory, and correction factors that include the inverse of the triplet correlation time a reduction due to the stable mode. This form, which holds for both zero and finite plasma β , is used to model the β scan of modified cyclone-base-case gyrokinetic ITG turbulence in simulations with GENE. Standard quasi-linear theory does not fall off sufficiently fast with β to match the nonlinear flux. Inclusion of the correlation time factor, which increases strongly with β at low perpendicular wavenumber, produces a modified quasi-linear prediction that agrees well with the nonlinear flux.

Total- f Gyrokinetic Turbulent-Neoclassical Simulation of Global Impurity Transport and its Effect on the Main-Plasma Confinement

J. Dominski¹, C.-S. Chang¹, R. Hager¹, K. Kim², S.-H. Ku¹, and E. S. Yoon³

¹Princeton Plasma Physics Laboratory (PPPL), Princeton, NJ 08540, USA

²Korea Advanced Institute of Science and Technology (KAIST), Daejeon, Republic of Korea

³Rensselaer Polytechnic Institute, Troy, NY 12180, USA

Corresponding Author: J. Dominski, jdominsk@pppl.gov

First-principles-based multiscale neoclassical-and-turbulent understanding of the impurity transport and its effect on the main plasma confinement is one of the most important subjects in magnetic fusion research. Seeding of impurity particles was found to improve the plasma confinement in the so-called “RI-mode” of operation [1]. More recently tungsten (W) impurities have been found to degrade the pedestal confinement of JET ILW H-mode plasma while a seeding of nitrogen (N) impurities reduces the degradation [2]. In the present study, the total- f gyrokinetic code XGC1 [3] is used to understand the impurity transport in the whole-volume plasma and its effect on the main plasma confinement.

Recent total- f simulation by XGC1 [4] showed that carbon (C) impurity can improve the main-ion confinement by reducing the ITG turbulence amplitude. In the presence of C^{+6} impurities, the self-organized deuteron temperature and its gradient were found to increase by up to 20% at all radial positions under the same central heating condition. This confinement enhancement was found to be caused by a stabilization effect due to both the impurity-wave interaction and the enhanced mean $E \times B$ shearing rate, rather than by the main-ion dilution effect. Another important finding is that the central peaking of impurity density in the saturated state is not as severe as what has been known from neoclassical theories. The neoclassical impurity inward-pinch is heavily opposed by the outward turbulent transport to yield only a mild impurity-density peaking in the saturated state. In these simulations, gyrokinetic deuteron and carbon ions with $Z_{\text{eff}} \simeq 1.75$ have been utilized with adiabatic electrons.

On-going research on the tungsten-nitrogen impurity transport and its impact on the H-mode pedestal in JET plasmas in realistic divertor geometry will also be presented. Starting with the impact of W-impurity on the neoclassical $E \times B$ shearing profile in a JET pedestal. Transport of the W and N particles into the central core will be included in the discussion. For whole-volume simulations, we will use new core-edge coupling technique developed in the High-fidelity Whole-Device-Modelling programme of the Exascale Computing Project.

References

- [1] R. R. Weynants *et al.*, Nucl. Fus., **39**, 1637 (1999).
- [2] X. Litaudon *et al.*, Nucl. Fus., **57**, 102001 (2017).
- [3] C. S. Chang *et al.*, Phys. Rev. Lett., **118**, 175001 (2017).
- [4] K. Kim *et al.*, Phys. Plasmas, **24**, 062302 (2017).

Confinement in Stellarators with the Global Gyrokinetic Code XGC

M. D. J. Cole¹, T. Moritaka², C.-S. Chang¹, R. Hager¹, S.-H. Ku¹, and S. Lazerson¹

¹Princeton Plasma Physics Laboratory (PPPL), Princeton, NJ 08540, USA

²National Institute for Fusion Science (NIFS), Toki, Gifu, Japan

Corresponding Author: M. D. J. Cole, mcole@pppl.gov

Whole-volume gyrokinetic simulations of stellarators are necessary to address a number of important physics and engineering issues, including energetic particle confinement optimization and turbulent transport prediction. In recent work, a whole-volume stellarator version of the global gyrokinetic particle-in-cell (PIC) code XGC [1] is under development. A 3D interpolation of equilibrium magnetic field to the last closed flux surface, calculated using the VMEC MHD equilibrium code, has been implemented, along with a 3D mesh for calculating the evolution of the electrostatic potential.

The 3D version of XGC has been successfully benchmarked with the NBI code BEAMS3D [2] and the core 3D gyrokinetic code EUTERPE [3] for energetic particle orbit tracing in Wendelstein 7-X (W7-X) geometry. It has been used to investigate collisionless α -particle confinement in potential stellarator reactor designs. The new tool permits direct comparison for α -particle loss between quasi-axisymmetric and quasi-isodynamic designs.

Furthermore, microturbulence has been observed in the outer portion of the core, and in the edge, of the W7-AS stellarator [4], and is likely to dominate in this region of Wendelstein 7-X or any stellarator reactor. Developments to the XGC code will permit 3D global simulation of ion-scale turbulence in stellarators, which has so far not been achieved. By simulating first the linear stage of the ion temperature gradient-driven (ITG) instability, and then nonlinear turbulence, XGC will be applied to better understand the global behaviour of turbulence in the Wendelstein 7-X stellarator.

References

- [1] S.-H. Ku *et al.*, Nucl. Fus., **49**, 115021 (2009).
- [2] M. McMillan and S. A. Lazerson, Plasma Phys. Contr. F., **56**, 095019 (2014).
- [3] V. Kornilov and R. Kleiber, Phys. Plasmas, **11**, 3196 (2004).
- [4] M. Hirsch *et al.*, Plasma Phys. Contr. F., **50**, 053001 (2008).

Physics of Fast Component of Deuterium Gas Jet Injection in Magnetized Plasmas

Z. H. Wang¹, Y. F. Shi¹, D. L. Yu¹, M. Xu¹, X. R. Duan¹, Y. L. Zhou¹, A. P. Sun¹, J. Q. Dong¹, J. Q. Li¹, S. L. Hu¹, L. Nie¹, R. Ke¹, C. Y. Chen¹, and L. H. Yao¹

¹*Southwestern Institute of Physics, Chengdu, Sichuan, People's Republic of China*

Corresponding Author: Z. H. Wang, zhwang@swip.ac.cn

Plasma fuelling with higher efficiency and deeper injection is crucial to enable fusion power performance requirements at high density for next generation devices such as ITER. Compared to pellet injection fuelling method, it penetrates shallower for the fuelling methods of supersonic molecular beam injection (SMBI) and gas puffing (GP). SMBI is one method of deuterium gas jet injection. Fast component (FC) of deuterium gas jet injection has been widely observed in the HL-2A experiment for several years but never been simulated and well understood. It is the first time that simulations of FC with trans-neut module of BOUT++ code are well validated with the HL-2A experimental measurements, in this paper. Simulation results are consistent with the experiment. The real HL-2A experimental profiles of plasma density and temperature are applied as the initial profiles in the simulation. Both the spatial and temporal evolution of D_α intensity is calculated self-consistently in the simulation by using the Atomic Data and Analysis Structure (ADAS) database. The mechanism of FC is revealed. The plasma blocking effect on the FC penetration is also simulated and validated.

Dynamics of Neon Ions after Neon Gas Seeding and Puffing into Tokamak Plasma

N. K. Bisai¹, H. Raj¹, S. Banerjee¹, M. B. Chowdhuri¹, R. Dey¹, R. L. Tanna¹,
R. Manchanda¹, K. A. Jadeja¹, and J. Ghosh¹

The ADITYA Team

¹*Institute for Plasma Research (IPR), Bhat, Gandhinagar, India*

Corresponding Author: N. K. Bisai, nirmal@ipr.res.in

High- Z impurity seeding or puffing is an important topic as it is capable to provide radiative improvement of confinement and disruption mitigation in future tokamaks. Here, in this work, numerically and experimentally, we investigate the effect of low density 1% Ne gas ($Z = 10$, $A = 20$) seeding and also massive gas puffing. Two dimensional electrostatic interchange turbulence simulation has been done in the edge and SOL regions. The Ne ion density is found maximum in the edge region, which indicates inward motion of the ions. The polarization drift and turbulent eddies play a significant role for the inward motion. The numerical results have been compared with the results obtained from the Ne seeding experiments on the ADITYA. This experiment indicates several Ne lines of higher charged states. As Ne VII has an ionization potential of 157.9 eV, hence, a Ne penetration up to at least ~ 0.84 is achieved. Reduction of radially outward flux by the Ne gas has been observed from the numerical simulations and also from the ADITYA experiments. In this work, these results will be compared. Simulation of massive neon gas puff has been done. Substantial cooling and modification of the plasma pressure gradient have been found.

HL

Numerical Simulation of High Neutron Rate JET-ILW DD Pulses in View of Extension to DT Experiments

G. Telesca¹, I. Ivanova-Stanik¹, R. Zagórski¹, S. Brezinsek², P. J. Carvalho³, A. Czarnecka¹,
C. Giroud⁴, A. Huber², E. A. Lerche⁵, and S. Wiesen²

The JET Contributors

¹*Institute of Plasma Physics and Laser Microfusion (IPPLM), Warsaw, Poland*

²*Institute of Energy and Climate Research, Forschungszentrum Jülich, Jülich, Germany*

³*Institute of Plasmas and Nuclear Fusion (IPNF), Instituto Superior Técnico (IST), 1049-001 Lisbon, Portugal*

⁴*Culham Centre for Fusion Energy (CCFE), Culham Science Centre, Abingdon, UK*

⁵*Laboratory for Plasma Physics, ERM/KMS, Brussels, Belgium*

Corresponding Author: G. Telesca, g.telesca@fz-juelich.de

This paper is focussed on the simulation of JET ELMy H-mode pulses pertaining to the baseline scenario with medium-high electron density, n_e , and auxiliary power, P_{aux} , in excess of 30 MW. The auxiliary heating is provided mostly by NBI, while ICRF heating does not exceed 5 MW. We have considered two pulses ($I_p = 3$ MA, $B_t = 2.8$ T) at $n_e = 6.5\text{--}7 \times 10^{19}/\text{m}^3$ which show very high neutron rates and are characterized by $T_i/T_e > 1$ with $T_e(0)$ about 7 KeV. The density was provided either by pellet injection or by gas puffing. The thermal stored energy is 8.1–8.7 MJ, the temperature at the plate, $T_{e,\text{pl}}$, is 25–35 eV and the total power to the target is 15–17 MW. These pulses are slightly Ne seeded (c_{Ne} about 0.2%) with radiated power fraction, $f_{\text{rad}} = 0.40$. Once the simulations of the experimental pulses have been established, extrapolation to DT plasmas has been done, keeping unchanged the code inputs. We have used the COREDIV code, self-consistent with respect to the core-SOL as well as to impurities-main plasma. In spite of some simplifications, the exchange of information between the core (1D) and the SOL (2D) module renders this code quite useful when, as in the case of the JET ILW, the interaction SOL-core is crucial.

Extrapolation to DT plasmas depends on the assumptions for $\tau_{\text{He}}^*/\tau_E$ and for the impurity species considered. Although the DT simulations are ongoing, some comments can be made at this stage. Keeping in the DT simulations n_e and P_{aux} at the same level as in the corresponding experimental pulses the resulting P_α is between 0.7 and 1.1 MW, depending on the assumptions made, with practically unchanged $T_{e,\text{pl}}$ and power to the target. Increasing P_{aux} to 41 MW, P_α increases only slightly while the power to the plate is 27 MW with $T_{e,\text{pl}} = 70$ eV. Recalling that in our simulations only P_α arising from thermal reactions is accounted for, these preliminary results indicate that strike point sweeping might not be sufficient to control the heat load to target plates at peak plasma performance for 5 s and additional impurity seeding might be necessary. As next step, I_p will be increased to 4 MA, keeping unchanged either n_e or n_e/n_{GW} .

Parametric Study of the Impurity Profile in the Thailand Tokamak

S. Sangaroon¹, J. Promping², A. Wisitsorasak³, B. Chatthong⁴, R. Picha², and T. Onjun²

¹*Department of Physics, Mahasarakham University, Mahasarakham, Thailand*

²*Thailand Institute of Nuclear Technology, Bangkok, Thailand*

³*Department of Physics, King Mongkut University of Technology Thonburi, Bangkok, Thailand*

⁴*Department of Physics, Prince of Songkla University, Songkla, Thailand*

Corresponding Author: S. Sangaroon, siriyaporn.s@msu.ac.th

A small tokamak is planned to be installed in Thailand at Thailand Institute of Nuclear Technology (TINT), Ongkarak campus in Nakorn Nayok, under the collaboration of the Center for Plasma and Nuclear Fusion Technology (CPaF). One of the great challenges subject in operating this tokamak is to gain better understanding of the impurities behaviour because the impurities are responsible for the large power losses. Therefore, the studies of impurity behaviours are conducted for the commissioning stage of Thailand tokamak. In this work, the spatial density distribution over all ionization states of helium, carbon, and oxygen have been calculated using the assumption of steady-state plasma under the relevant plasma scenarios that will be operated using Thailand tokamak. Additionally, the prescribed transport coefficients of charge number on neoclassical convection velocity and simplified turbulent transport coefficient effect are taken into account of this model. The quantification of Z_{eff} has been carried out to characterize the impurity content of plasma. Finally, the impurity radiated power have been extracted using ADAS database of the global spectral line and continuum radiative coefficient. Due to the low charge number (Z) of interested impurities, the obtained power loss occurs mostly in the region near the plasma edge. It is found that when the plasma current is increased, the radiated power peak shifts toward the plasma edge. The calculation in this work provides significant contribution in commissioning and operating the Thailand tokamak to be available in various applications.

Analysis and Modelling of NTMs Dynamics in JET Discharges Using the European Transport Simulator (ETS) and Integrated Modelling Tools

S. Nowak¹, O. Sauter², D. Yadykin³, E. Alessi¹, M. Baruzzo⁴, D. Brunetti¹, P. Buratti⁵, R. Coelho⁶, A. Czarnecka⁷, G. L. Falchetto⁸, J. Ferreira⁶, V. Fusco⁵, E. Giovannozzi⁵, J. P. Graves², P. Huynh⁸, M. Imrisek⁹, E. Joffrin⁴, D. Kalupin¹⁰, N. Krawczyk⁷, E. Lazzaro¹, J. Mailloux⁴, C. Marchetto¹, A. Merle², I. G. Miron¹¹, F. M. Poli¹², G. Pucella⁵, M. Romanelli⁴, I. Ivanova-Stanik⁷, P. Strand³, G. Vlad⁵, and R. Zagórski⁷

The JET Contributors and The EUROfusion-IM Team

¹*Istituto di Fisica del Plasma (IFP), Consiglio Nazionale delle Ricerche (CNR), 20125 Milan, Italy*

²*Swiss Plasma Center (SPC), École polytechnique fédérale de Lausanne (EPFL), 1015 Lausanne, Switzerland*

³*Chalmers University of Technology, Göteborg, Sweden*

⁴*Culham Centre for Fusion Energy (CCFE), Culham Science Centre, Abingdon, UK*

⁵*ENEA C. R. Frascati, Dipartimento FSN, Frascati, Italy*

⁶*Institute of Plasmas and Nuclear Fusion (IPNF), Instituto Superior Técnico (IST), 1049-001 Lisbon, Portugal*

⁷*Institute of Plasma Physics and Laser Microfusion (IPPLM), Warsaw, Poland*

⁸*Institut de Recherche sur la Fusion par confinement Magnétique (IRFM),*

Commissariat à l'énergie atomique (CEA/Cadarache), 13108 St. Paul lez Durance, France

⁹*Institute of Plasma Physics AS CR v.v.i., Prague, Czech Republic*

¹⁰*EUROfusion Programme Management Unit Garching, Boltzmannstraße 2, 85748 Garching Germany*

¹¹*National Institute of Laser, Plasma and Radiation Physics (INFLPR), Bucharest, Romania*

¹²*Princeton Plasma Physics Laboratory (PPPL), Princeton, NJ 08540, USA*

Corresponding Author: S. Nowak, nowak@ifp.cnr.it

Stability of JET baseline and hybrid scenarios from previous and present experimental campaign is investigated in the framework of the JET1 task on MHD analysis and modelling in support of scenario development. Modelling of neoclassical tearing modes (NTMs) onset and their effect on heavy impurity transport is performed via the European Transport Simulator (ETS), encompassing an NTM module and MHD stability calculation. The present study is aimed to predict plasma stability conditions avoiding the appearance of NTMs which limit the plasma performance and duration in DT scenarios. In addition, the high energy confinement in hybrid discharges can be deteriorated if impurities accumulate towards the plasma centre. The NTM module implemented in the ETS describes the NTM dynamics by a set of equations for the mode width, through a generalized Rutherford equation and frequency. Investigation and validation of the mode trigger models can be performed with this module as well as the analysis of the effects of NTM on electron, ion and impurity transport. Enhanced perpendicular diffusion coefficients around the mode location is modelled by adding a Gaussian perturbation. In JET discharges, this modification has been considered for electron transport coefficient and similarly used to model the enhancement of tungsten diffusion coefficient initially observed around the mode location. ETS simulator is appropriate since it can compute the evolution of impurities in all their ionization states.

Continued...

A first validation of MHD stability models was performed comparing the mode stability parameter using four different codes: NTM module in ETS, Delta Prime Calculation Code, 3D quasi-analytic code and TRANSP. Full MHD code MARS is also used for comparison of linear growth rate evaluation of the mode with the stability parameter index calculated by the other codes. MARS is part of the Equilibrium & MHD Stability Workflow and the analysis will make use of the outputs produced by the ETS at some time snapshots. All the results obtained from the MHD analysis via these (transport) codes provide a new modelling investigation of the plasma stability for JET baseline and hybrid discharges. A detailed discussion of the calculations will be reported.

Study of Evolution of Trapped Particle Undamped Coherent Structures: An Important Agent in Intermittent Plasma Turbulence and Anomalous Transport

D. Mandal¹, D. Sharma¹, and H. Schamel²

¹*Institute for Plasma Research (IPR), Bhat, Gandhinagar, India*

²*University of Bayreuth, 95440 Bayreuth, Germany*

Corresponding Author: D. Mandal, debuipr@gmail.com

The physics of particle and energy transport in collisionless plasmas presents substantial challenge because of largely linear threshold based plasma turbulence are replaced by their nonlinear counterparts capable of operating at smaller amplitudes. An outstanding property for collisionless plasmas is the essential nonlinear character of coherent structures supported by them at small amplitude. A supplementary mode spectrum of stable coherent structure plays an important role in intermittent plasma turbulence and anomalous transport. In the present work, these additional undamped structures are considered, in a 1D, collisionless plasma as a paradigm of intermittent plasma turbulence and anomalous transport and are investigated based on the result of a kinetic simulation of the plasma. The computational analysis explores initial phase-space perturbation in a current-driven plasma within the linear threshold limit for accessing the regime uncovered under the linear approximation. These coherent structures are described by a continuum of electron and ion hole modes governed by a multiparametric nonlinear dispersion relation (NDR) [1]. On the basis of both the simulation results and the three level comprehensive description, namely fluid, linear Vlasov and nonlinear Vlasov descriptions, the importance of trapped particle nonlinearity and the invalidity of the linear threshold limit for $v_{\text{phase}} \ll v_{\text{th}}$ are presented. The formulation describing the evolution merges the discrete and continuum limits by resolving the inevitable resonant region and shows that coherent electrostatic equilibria are generally controlled by kinetic particle trapping and are hence fundamentally nonlinear. The analytical results are characterized with respect to the evolution observed in the kinetic simulations and quantitative analysis of the associated coherent structure parameters.

References

[1] H. Schamel *et al.*, *Phys. Plasmas*, **24**, 032109 (2017).

Simulation Study of Electrostatic Potential Generated by NBI and its Effect on the Neoclassical Transport of Carbon Impurity Ions in LHD

H. Yamaguchi¹, S. Murakami²

¹National Institute for Fusion Science (NIFS), Toki, Gifu, Japan

²Department of Nuclear Engineering, Kyoto University, Nishikyo-ku, Kyoto 615-8540, Japan

Corresponding Author: H. Yamaguchi, yamaguchi.hiroyuki@nifs.ac.jp

Electrostatic potential Φ_{NBI} generated by the neutral-beam-injection (NBI) to the plasma, and its effect on the neoclassical transport of carbon impurity ions in the Large Helical Device (LHD) are investigated for the first time by means of the global drift-kinetic simulations. The ripple-trapped beam ions of the perpendicular NBI (40 keV) have been found to generate Φ_{NBI} in the order of $0.01\text{--}0.02T_e$ when $n_e = 3 \times 10^{19}/\text{m}^3$, $T_e = T_i = 3$ keV, and the injection power is 5 MW. The global neoclassical transport simulations taking into account Φ_{NBI} have shown that the diffusion coefficient of C^{6+} impurity ions decreased by 14% and the radially inward convection velocity decreased by 22% in the presence of Φ_{NBI} of the 5 MW injection. These new findings suggest that Φ_{NBI} may have a non-negligible impact on the neoclassical impurity transport in LHD, especially in the impurity-hole plasma with high-power NBI heating.

Weak Turbulence Transport with Background Flows Using Mapping Techniques Including Finite Larmor Radius Effects

J. J. Martinell¹, N. Kryukov¹, and D. del-Castillo-Negrete²

¹*Instituto de Ciencias Nucleares, UNAM, A. Postal 70-543, Mexico*

²*Oak Ridge National Laboratory (ORNL), Oak Ridge, TN 37831, USA*

Corresponding Author: J. J. Martinell, martinel@nucleares.unam.mx

Electrostatic drift waves produce transport by the $E \times B$ motion of a particle guiding centre (GC) which can be studied from a Hamiltonian description where the electrostatic potential plays the role of the Hamiltonian. Here, the fluctuating potential is considered to be an infinite spectrum of waves, characteristic of weak turbulence, in two-dimensions. This is studied using a map that presents regular and chaotic regions. With an ensemble of particles transport is studied statistically. Finite Larmor radius (FLR) of the particles is included by taking the gyroaverage over one orbit. The main effect is to reduce the wave amplitude that produces a given level of chaos, so fast particles are better confined. The transport is diffusive and the particle distribution functions (PDF) are Gaussian. Then a thermal distribution of Larmor radii was taken which produces the PDFs to become non-Gaussian with long tails while the transport stays diffusive. This behaviour is explained theoretically and it is shown that it agrees with the numerical results.

When a sheared flow is included the transport is described by a symplectic mapping when the shear is monotonic. The result is that the poloidal flow has the effect of increasing the poloidal transport so that the variance of the distribution has cubic dependence with time. This superballistic scaling means that the particles have an acceleration when the flow is present. This is due to a growth of the particle step size as time increases related to the diffusive spreading in the radial direction. Thus, the waves acting in two dimensions promote particles to take energy from the perpendicular direction of the flow to the parallel direction. The PDF does not deviate much from a Gaussian. Inclusion of FLR effects keeps these results. When there is a thermal distribution of Larmor radii the PDF is no longer Gaussian as in the case without flow. The radial transport is still diffusive but it is enhanced over the values with no flow. The radial transport is still diffusive but it is enhanced over the values with no flow. The self-similarity function is Gaussian for small thermal gyroradius but a long-tailed exponential distribution for large gyroradius. Then, the flow is taken to have nonmonotonic radial shear. The map is double-valued and nontwist. The associated transport barriers are studied as well as the FLR effects.

TH

Poloidal Flows, Asymmetries and Multiscale Organization in Interplaying Core-Edge-SOL Turbulent Plasmas

G. Dif-Pradalier¹, E. Caschera¹, P. Ghendrih¹, Y. Asahi^{1,2}, F. Clairet¹, P. Donnel¹, X. Garbet¹, C. Gillot^{1,3}, V. Grandgirard¹, G. Latu¹, A. Medvedeva⁴, Y. Sarazin¹, Ö. Gürcan⁵, P. Hennequin⁵, P. Morel⁵, L. Vermare⁵, C. Fukuda⁶, J.-M. Reynolds-Barredo⁶, R. Sanchez⁶, and D. Zarzoso⁷

¹*Institut de Recherche sur la Fusion par confinement Magnétique (IRFM), Commissariat à l'énergie atomique (CEA/Cadarache), 13108 St. Paul lez Durance, France*

²*Japan Atomic Energy Agency (JAEA), Naka, Japan*

³*École des Ponts ParisTech, Champs-sur-Marne, France*

⁴*Max-Planck-Institut für Plasmaphysik, Garching, Germany*

⁵*Laboratoire de Physique des Plasmas (LPP), CNRS/École Polytechnique, 91128 Palaiseau, France*

⁶*Universidad Carlos III de Madrid, Madrid, Spain*

⁷*Physique des Interactions Ioniques et Moléculaires (PIIM), CNRS, Aix-Marseille Université, France*

Corresponding Author: G. Dif-Pradalier, guilhem.dif-pradalier@cea.fr

A central challenge in the years to come is to start providing a unified view of magnetized plasma turbulence in regimes of experimental relevance—with near-critical parameters and flux-driven self-organization—when multiple scales and disparate regions of the plasma self-consistently interplay.

We here present a comprehensive discussion of turbulence properties when confined core, edge and scrape-off-layer (SOL) regions interplay, based on well-diagnosed ToreSupra discharges and flux-driven gyrokinetic computations recently extended to modelling the outer edge and SOL regions where commonly assumed separations of scales tend to break down. Various regimes of electrostatic turbulence: ion temperature gradient (ITG) and trapped electron mode (TEM) are investigated in near-critical flux-driven regimes. Advanced statistical properties of transport, rotation and poloidal asymmetries are analyzed and detailed confrontation with high-precision reflectometry is presented, through the use of dedicated synthetic diagnostics.

Integrated Modelling of Core, Edge Pedestal and Scrape-Off-Layer for High- β_N Steady-State Scenarios on DIII-D

R. J. Buttery¹, J. M. Park², D. L. Green², K. Kim³, J. Candy¹, J. M. Canik², J. R. Ferron¹, C. T. Holcomb⁴, J. D. Lore², O. Meneghini¹, S. P. Smith¹, and P. B. Snyder¹

¹General Atomics, San Diego, CA 92186, USA

²Oak Ridge National Laboratory (ORNL), Oak Ridge, TN 37831, USA

³Oak Ridge Associated Universities (ORAU), Oak Ridge, TN 37831, USA

⁴Lawrence Livermore National Laboratory (LLNL), Livermore, CA 94550, USA

Corresponding Author: R. J. Buttery, buttery@fusion.gat.com

A new theory-based integrated modelling of core, edge pedestal, and scrape-off-layer (CESOL) has been developed, validated and used to project core to boundary solutions for an upgrade to DIII-D that will develop the plasma physics path to a steady state fusion reactor. It also represents a significant step towards a whole device modelling (WDM). The simulation reproduces DIII-D high- β_N discharge measured profiles across regions from the magnetic axis to the divertor. CESOL consists of three independent, compound Integrated Plasma Simulator (IPS) workflows: IPS-FASTRAN (1D core transport), IPS-EPED (edge pedestal), and IPS-C2 (2D SOL plasma/neutral transport). In the core region FASTRAN computes all transport channels with TGLF and is self-consistent with an EPED edge pedestal. The total particle and energy fluxes are matched at the separatrix between the FASTRAN+EPED and C2 workflows in an iterative steady-state solution procedure. This specific coupling aims to determine the density and temperature at the separatrix, which are used to update the input to EPED and close the strong nonlinear dependency among the core, edge pedestal, and SOL regions. Projections for DIII-D upgrades indicate that fully noninductive solutions will be able to probe critical stability, transport and energetic particle limits with reactor relevant broad current profiles ($q_{\min} > 2$) and β_N up to ~ 5 at low collisionality and a range of rotations. The use of ultrahigh harmonic “helicon fast wave” or high field side LHCD extends scenarios to high density, low rotation and increased T_e/T_i , reducing divertor heat flux by more than a factor of 2 with increased bootstrap current fraction, $f_{BS} \sim 0.7$. Helicon and LHCD also extend profile range, stability and β_N potential at low and high rotation. These techniques will be combined with new closed pumped upper and lower divertors, materials testing facilities, and 3D upgrades to develop integrated core-edge steady state solutions on DIII-D relevant to future fusion reactors.

Work supported by the U.S. Department of Energy under DE-AC05-00OR22725, DE-FC02-04ER54698, DE-AC52-07NA27344, DE-FG02-95ER54309, and DE-SC0012656.

Simulation Study of the Impurity Radiation in the Quasi-Snowflake Divertor with Ne Seeding for CFETR

M. Y. Ye¹, Y. F. Zhou¹, S. F. Mao¹, and Z. P. Luo²

¹University of Science and Technology of China, Hefei, Anhui, People's Republic of China

²Institute of Plasma Physics, Chinese Academy of Sciences, Hefei, Anhui, People's Republic of China

Corresponding Author: M. Y. Ye, yemy@ustc.edu.cn

It is crucial to exhaust the huge power come from core plasma in future fusion reactor. For a fusion reactor of 1–2 GW fusion power, considering the auxiliary heating power and core radiation, ~ 200 MW will enter into the scrape-off layer (SOL) and exhausted in the divertor. To find an effective way to exhaust the heat power for future fusion reactor, snowflake divertor (SFD) [1] is thought as a possible candidate. China Fusion Engineering Test Reactor (CFETR) is proposed to bridge gaps between ITER and DEMO. In our previous SOLPS simulation work [2], by assuming carbon as the radiation impurity, a reduction in the peak heat flux is shown for the quasi-snowflake (QSF) divertor in CFETR, in comparison with the lower-single-null (LSN) divertor. In order to avoid the fuel retention issue and increase the lifetime of the plasma-facing materials, tungsten wall would be preferred for CFETR, which implies that there will be no intrinsic radiative impurity like carbon. Therefore, radiative impurities, such as neon and/or argon, are indispensable to be seeded. In this work, the radiative SFD with neon seeding are studied by SOLPS simulation. The relation between radiation power, plasma density and effective charge are established for both QSF and LSN divertor. The comparison will give an evaluation of the ability of heat exhaust and compatibility with core plasma for the QSF divertor. Furthermore, the influence of the puffing location on the impurity radiation is also studied, which is considered helpful to find the appropriate impurity seeding scheme.

References

- [1] D. D. Ryutov, *Phys. Plasmas*, **14**, 064502 (2007).
- [2] S. F. Mao *et al.*, *J. Nucl. Mater.*, **463**, 1233 (2015).

Synthetic Edge and SOL Diagnostics: A Bridge between Experiments and Theory

A. H. Nielsen¹, V. Naulin¹, J. J. Rasmussen¹, J. Olsen¹, A. S. Thrysoe¹, T. Eich², G. I. Pokol³, O. Asztalos³, R. Coelho⁴, D. I. Réfy⁵, B. Tál⁵, G. H. Hu⁶, and Y. Ning⁶

The EUROfusion MST1 and IM Teams

¹Technical University of Denmark (DTU), Lyngby, Denmark

²Max-Planck-Institut für Plasmaphysik, Garching, Germany

³Institute of Nuclear Techniques (INT), University of Technology and Economics (BME), Budapest, Hungary

⁴Instituto Superior Técnico (IST), 1049-001 Lisbon, Portugal

⁵Wigner Research Center, Association EURATOM, Budapest, Hungary

⁶Institute of Plasma Physics, Chinese Academy of Sciences, Hefei, Anhui, People's Republic of China

Corresponding Author: A. H. Nielsen, ahnie@fysik.dtu.dk

The scrape-off-Layer (SOL) plasma and its coupling with the edge dictate the performance of a discharge to a high degree — especially as all plasma has to go through the SOL, which is the main exhaust channel for the hot plasma. The understanding of the SOL plasma is a key topic in contemporary fusion research.

This contribution provides an overview of the modelling efforts of the plasma dynamics in the SOL coupled with the edge. We employ fully dynamical fluid models, e.g., the HESEL code. HESEL simulates density, ion and electron pressure evolution together with the evolution of the generalized vorticity [1, 2] and assumes that the SOL is mainly fuelled at the outboard midplane. Parallel losses, including sheath couplings at the material surfaces, have been parameterized in the SOL. HESEL includes a neutral gas module to model the influence of neutrals on the plasma performance in the SOL and outer edge in their interplay with the intermittent SOL turbulence [3].

For interaction with experiments, HESEL is equipped with synthetic diagnostic tools as probe arrays, Li-beam spectroscopy, and gas puff imaging. Running HESEL in a Kepler workflow, developed within the EUROfusion Integrated Modelling framework [4, 5], allows direct and automated access to experimental data and discharge parameters. A workflow for generating synthetic Li beam data, where fluctuation data from HESEL are passed to the RENATE code [6] will be discussed.

Using the synthetic probe arrays to measuring the electron and ion heat advection and conduction, we obtain the upstream power fall-off length for a broad range of plasma parameters and by applying nonlinear fitting procedures we derive the scaling of the fall-off length with different key parameters. The obtained results are in agreement with recent experimental observations from L-mode AUG data [7].

References

- [1] J. Madsen *et al.*, Phys. Plasmas, **23**, 032306 (2016).
- [2] A. H. Nielsen *et al.*, Plasma Phys. Contr. F., **59**, 025012 (2017).
- [3] A. S. Thrysoe *et al.*, Plasma Phys. Contr. F., **58**, 4, 44010 (2016).
- [4] F. Imbeaux *et al.*, Comput. Phys. Commun., **181**(6), 987–998 (2010).
- [5] G. L. Falchetto *et al.*, IAEA FEC–2016, Kyoto, Japan, TH/P2-13, (2016).
- [6] D. Guszejnov *et al.*, Rev. Sci. Instrum., **83**, 113 (2012).
- [7] B. Sieglin *et al.*, Plasma Phys. Contr. F., **58** 055015 (2016).

The Physics Basis for a Solution to the Power and Particle Exhaust Problem of a Next Step Device

M. Wischmeier¹

The EUROfusion MST1 and ASDEX-Upgrade Teams, and JET Contributors

¹Max-Planck-Institut für Plasmaphysik, Garching, Germany

Corresponding Author: M. Wischmeier, marco.wischmeier@ipp.mpg.de

This contribution presents an overview how research in power and particle exhaust studies relevant to next step devices have advanced our quantitative understanding. For a future fusion reactor, such as the European DEMO, a dissipative power fraction, f_{diss} , of 90%–97% would simplify the engineering demands on plasma facing components, PFCs. A quantitative understanding of the impact of f_{diss} on confinement is being developed. It is, e.g., unclear if ITER could operate with a higher degree of detachment than the currently envisaged and achieve its fusion performance.

Seeding of impurities will be mandatory to accommodate the engineering limits of the PFCs. Here, the quantitative understanding of the enrichment of the seed impurities in the divertor is of the essence. The interaction of the plasma with the PFCs together with the volumetric dissipative processes leads to a complex physical system. Based on example cases it is shown how a significant improvement of our qualitative and quantitative understanding of detachment physics has been achieved. The combination of experiments in devices with full metal PFCs, improved diagnostic capabilities and the use of numerical tools with a comprehensive set of physical models provided a major step forward in interpreting experimental data. A steady improvement lead to the identification of missing elements in the models, most prominently the interaction of the numerically expensive drift terms with enhanced far SOL transport. Thus our uncertainty about the highest achievable f_{diss} of the SOL narrows down to the largest extent to a quantitative obscurity about the nature of perpendicular SOL transport. While selected positive example cases of a successful numerical validation against experimental data exist they remain an exception.

The certainty with which we can apply our models to interpret experimental data and thus allow for a more general quantitative statement is just starting to be looked at and will need more attention in the future. In view of the complexity of numerical modelling with fluid transport codes, reduced models are being investigated on the basis of experimental data or numerical simulation results. Validated reduced models of various levels of complexity may then be used in system codes to determine the performance of future devices and to specify their design.

The Scrape-Off Layer Plasma Transport Physics Simulation Activity for Indian Tokamaks ADITYA and SST-1

D. Sharma¹, B. P. Sahoo¹, R. Srinivasan¹, R. Jha¹, J. Ghosh¹, A. K. Tyagi¹, M. Himabindu¹, X. Bonnin², and Y. Feng^{2,3}

¹*Institute for Plasma Research (IPR), Bhat, Gandhinagar, India*

²*Max-Planck-Institut für Plasmaphysik, Greifswald, Germany*

³*Max-Planck-Institut für Plasmaphysik, Garching, Germany*

Corresponding Author: D. Sharma, devendra@ipr.res.in

The computational modelling activity of plasma transport in the scrape-off layer (SOL) region of Indian tokamaks ADITYA and SST-1 has explored a range of aspects of SOL plasma transport in both the devices. While 2D computations using SOLPS have predictively addressed aspects of the phase-I of divertor plasma operation of the tokamak SST-1, complete 3D EMC3-EIRENE computer simulations are applied to the 3D SOL plasma transport in tokamak ADITYA operating for over last three decades. The ADITYA studies are extended to predict operation scenario of its upgrade version and draw conclusions with respect to experience of SOL physics in its original setup.

The phase-I divertor operation scenario of the tokamak SST-1 examined by SOLPS suit of codes recovers access to sheath- and conduction-limited divertor regimes where a transition could be achieved in the edge density scan, affected by the gas puff intensity, beyond $1.5 \times 10^{19}/\text{m}^3$. A need is indicated to optimize the operating scenario with tolerable target heat loads and low enough density for an effective LHCD operation. The analysis provided estimates of the relative power loading of the inboard and outboard targets for cases with and without control by a localized gas-puff.

The ADITYA SOL simulations explored the inherently 3D SOL generated by a toroidally localized ring-like limiter in its circular plasma, complementing the localized probe measurements on device SOL. Since the radial diamagnetic drift enters flow continuity with the $E \times B$ and PS flows, it generates a finite flow vorticity, influencing degree of SOL turbulence, cross field diffusivity and the key pedestal parameter $D_{\text{edge}} = D_{\text{SOL}}$. More recent ADITYA Upgrade relevant setups indicate strongly changed connection length distribution, impacting the total recycling flux and modifying parallel and perpendicular plasma fluxes indicating smaller total recycling flux in upgrade for equivalent edge densities in the original setup. A mechanism identified causing excess main chamber recycling relates to observations in ALCATOR C where despite a regular density variation, a radially diverging main chamber plasma flux causes loss of neutral particle control, even for ITER like conditions. The presentation will highlight the characterization of results from the activity for both ADITYA and SST-1 tokamaks.

Comparative Analysis of the SOL Properties for the Various Magnetic Configurations Proposed for the DEMO Divertor

V. Pericoli Ridolfini¹, R. Ambrosino², S. Mastrostefano³, P. Chmielewski¹,
M. Poradziński¹, and R. Zagórski¹

¹*Institute of Plasma Physics and Laser Microfusion (IPPLM), Warsaw, Poland*

²*Consorzio CREATE, Università degli Studi di Napoli Federico II, 80138 Napoli, Italy*

³*University of Tuscia, Largo dell'Università snc, 01100 Viterbo, Italy*

Corresponding Author: V. Pericoli Ridolfini, vincenzo.pericoli@ifpilm.pl

TH
The mitigating properties of the divertor advanced magnetic configurations on the target heat load have been analyzed with the 2D edge code TECXY for the European DEMO. Particular emphasis is put on the snowflake minus, for which several variants have been proposed just to study this particular effect, where the distance between the two X-points, the primary and secondary ones, is varied. In such a way the magnetic topology in the outboard part of the divertor is varied and regions with low poloidal field and then much longer connection length are created with different extension and localization with respect to the primary X-point. The scenario considered is a low density one, without any added impurity in order to keep at a negligible level the effect of radiative volume losses and then to ascribe any possible change to the transport properties of each configuration. A significant widening of the power flow channel in term of the poloidal flux coordinate, i.e., independent of any expansion effect, is found and correspondingly a drop of the peak power load. The mitigation effect increases for these configurations that more affect the region in close touch with the main separatrix. The possible causes for this effect are discussed in the paper. However some manipulation is required to make the real magnetic topology compatible with the constraints of TECXY, which allows for only two targets. Even if the modifications affect only the more external flux tubes that have less weight in the power transport, the results clearly claim for confirmation by other more complex codes.

Electron Impact Excitation of W^{40+} to W^{43+} Ions: Cross Section and Polarization

N. Shukla¹, T. Das², and R. Srivastava¹

¹Indian Institute of Technology Roorkee, Roorkee-247667, India

²University of Engineering & Management, Kolkata-700160, India

Corresponding Author: N. Shukla, neelu.dph2016@iitr.ac.in

Tungsten has been planned to be used in the divertor region of ITER as it has the highest heat load capacity, highest melting point and more other favourable physical properties among the metals. Distinct ionic states of tungsten are predicted to be present from divertor to core of the ITER device. Thus, to understand the radiation emissions coming from the divertor region plasma, a detailed and complete set of atomic data of electron impact excitation cross sections of various ionized tungsten ions in the wide energy range is required. In fact, such data are prime input in the plasma modelling. In addition to electron impact excitation there is also probability of photon emissions from the decay of these electron excited states. Hence it may be important to study the linear polarization of photons emitted from these excited states to add to the understand the diagnostics of the ITER plasma.

Recently [1] measured spectral lines in the range 12–20 nm and [2] measured spectral line in the range 4–8 nm coming from the charged states of tungsten ions produced in the electron beam ion trap (EBIT) facility at the Gaithersburg and Livermore respectively. In the light of these experiments, we have identified some lines in Se-like W^{40+} to Ga-like W^{43+} tungsten ions and calculated the electron impact excitation cross sections for the corresponding fine structure transitions. We found that there are no theoretical or experimental data of cross section and polarization are available in the literature for such lines. In order to describe the electron impact excitation, process we used fully relativistic distorted wave theory. Using these cross sections and density matrix theory, we further calculated polarization of the emitted photons as a result of decay of the electron from excited states. The detailed results of the cross sections and polarizations for various transitions in different ions will be presented in the conference.

References

- [1] Y. Ralchenko *et al.*, J. Phys. B, **40**, 3861 (2007).
- [2] S. B. Utter *et al.*, Can. J. Phys., **80**, 1503 (2002).

Plasma Transport in Toroidally Discontinuous Limiter Generated 3D SOL Configurations of ADITYA Tokamak

B. P. Sahoo¹, D. Sharma¹, R. Jha¹, and Y. Feng²

¹*Institute for Plasma Research (IPR), Bhat, Gandhinagar, India*

²*Max-Planck-Institut für Plasmaphysik, Greifswald, Germany*

Corresponding Author: B. P. Sahoo, bibhuprasad@ipr.res.in

The coupled plasma-neutral transport characteristics in the scrape-off layer (SOL) produced by toroidally discontinuous limiter are essentially 3D and show strong deviation from the usual uniform SOL approximations. In a recently performed second-phase of EMC3-EIRENE plasma transport simulations for the limiter generated SOL of both original ADITYA and ADITYA Upgrade configurations, a number of aspects related to 3D effects in SOL are addressed. The simulated flux balance for the update relevant block-limiter case indicates that with a reduced total recycling flux for equivalent edge plasma conditions, and with the reduction in chamber wall directed cross field particle fluxes, a wider regime of relatively stable plasma conditions might be accessible for the block-limiter configuration. Although a recycling source localized on the limiter surface is used in the present simulations for the simplicity, the mechanism of main chamber recycling process is essentially captured by the present 3D study where the ionization can be significantly higher in the closed field line sections of the SOL having both higher plasma and neutral density at the downstream toroidal locations. This combination of locally enhanced ionization and longer connection lengths is seen responsible for a radially growing perpendicular flux and convex radial density profiles. This effect, found to be dominant in the original ring-limiter configuration, is however seen to yield usual concave radial density profiles in the block-limiter case, indicating that for equivalent wall conditions, the localized wall recycling can be expected less intense in the block-limiter case. In studies on ALCATOR-C-MOD this effects in a 2D divertor SOL setup was observed leading to an enhanced recycling in main chamber and indicated the possibility of an alternate density limit, capable of restricting essential reactor relevant studies in a moderate size device. The present study captures the effect in toroidally discontinuous limiter generated 3D SOL of ADITYA tokamak and highlights the capacity of the 3D EMC3-EIRENE simulation to analyze it in the large scale reactor relevant conditions.

Self-Consistent Modelling of a Liquid Metal Pool-Type Divertor

R. Zanino¹, G. F. Nallo¹, A. Iovenitti¹, G. Mazzitelli², L. Savoldi¹, and F. Subba¹

¹*Dipartimento Energia, Politecnico di Torino, Turin, Italy*

²*ENEA C. R. Frascati, Frascati, Italy*

Corresponding Author: R. Zanino, roberto.zanino@polito.it

The steady-state power exhaust problem in future fusion reactors (e.g. DEMO) is considered as a major challenge along the path towards fusion electricity. Dedicated work packages are being devoted to this problem within EUROfusion and a dedicated facility (the Italian Divertor Tokamak Test: IDTT) is being designed in Italy. Among the possible solutions for this problem, a liquid metal (LM) divertor has been proposed. The particularly attractive feature of this solution is the absence of damage to the wall, even in the case of high heat fluxes, thanks to the high latent heat of evaporation and to the liquid nature of the wall, which can be constantly replenished. In this work a closed, LM divertor with pool-type configuration is proposed for a reference single-null (SN) scenario, for both the EU DEMO and the IDTT. The assessment of the divertor performance is achieved by means of a newly developed model which self-consistently accounts for the most relevant physics, including plasma-vapour interactions. Self-consistency is achieved by coupling three modules: a 0D thermodynamic module for the LM/vapour system (benchmarked against 2D CFD calculations performed in OpenFOAM), a 1D module for the SOL plasma and a 2D FEM module for the divertor walls. The resulting model is applied to the comparison between Li and Sn as possible LM choices, in terms of mitigation of the parallel heat flux to the target and of contamination of the main/core plasma. An assessment of the representativity of the IDTT in view of the EU DEMO in terms of the performance of a closed box divertor using Li is finally performed.

TH

SOL/Divertor Plasma Simulation of Diverging Magnetic Field Configurations for Advanced Divertors

S. Togo¹, T. Takizuka², D. Reiser³, K. Imano², Y. Li⁴, Y. Ogawa⁴, M. Sakamoto¹, N. Ezumi¹, K. Nojiri¹, and Y. Nakashima¹

¹Plasma Research Center, University of Tsukuba, Tsukuba, Ibaraki, Japan

²Graduate School of Engineering, Osaka University, Osaka, Japan

³Institute of Energy and Climate Research, Forschungszentrum Jülich, Jülich, Germany

⁴Graduate School of Frontier Science, University of Tokyo, Tokyo, Japan

Corresponding Author: S. Togo, togo@prc.tsukuba.ac.jp

Handling heat loads onto divertor plates is one of the crucial issues. Advanced divertors expand the flux tube of a divertor plasma and reduce the heat load onto the divertor plate. A Super-X divertor (SXD) sets the outer target plate at a further position in major radius than an ordinary divertor (OD) leading to a largely diverging magnetic field (DMF). In order to simulate supersonic plasma flows caused by DMFs without giving any boundary conditions at the target plate, we have developed a plasma fluid model incorporating the anisotropic ion pressure (AIP). The parallel-momentum equation becomes hyperbolic with the AIP. Thus, the plasma flow velocity is calculated from the upstream side without using the downstream boundary condition and supersonic plasma flows in DMFs are consistently simulated with the AIP model even if the actual effect of AIP is small due to high collisionality. By a direct comparison between a conventional fluid model and the AIP model in a DMF configuration with no radial transport, it is demonstrated that a quite smooth and natural profile of supersonic flow velocity which is also observed in the magnetic-nozzle experiment is reproduced with the AIP model while an unphysical profile of plasma flow velocity is obtained with the conventional fluid model. An SXD is also simulated with the AIP model by adding another DMF region to an OD. The plasma flow velocity is increasing in the additional DMF region which might be an advantage for the retention of impurities in the divertor region by the friction force while the plasma density becomes lower which might be a disadvantage for the formation of detached plasmas. The AIP model, therefore, is beneficial to analyze the performance of advanced divertors such as an SXD from the viewpoint of impurity retentions and detached-plasma formations.

Ion Inertial Effects on 3D Filament Dynamics

H. Hasegawa^{1,2}, S. Ishiguro^{1,2}

¹*National Institute for Fusion Science (NIFS), Toki, Gifu, Japan*

²*Department of Fusion Science, Graduate University for Advanced Studies (SOKENDAI), Toki, Gifu, Japan*

Corresponding Author: H. Hasegawa, hasegawa.hiroki@nifs.ac.jp

The ion inertial effects on the sheath-limited filament dynamics have been investigated with the 3D electrostatic particle-in-cell (PIC) simulations. We have shown that the radial propagation speed of a sheath-limited filament becomes slightly slower in deuterium-tritium (DT) plasmas than in light hydrogen (H) plasmas because of the gyro-motion effect. The filament (blob) radial propagation speed is the fundamental and important factor for the boundary layer transport. However, the isotope effects on filament dynamics including the radial propagation speed had not been focussed on in previous studies. On the other hand, our previous work showed that the minor heavy ions decelerate the blob by the formation of the dipolar density distribution of minor heavy ions in a blob due to the polarization drift. Nevertheless, according to the traditional static estimation of the sheath-limited filament transport, it is expected that the sheath effect makes the radial propagation speed in DT plasmas faster than that in H plasmas. Thus, in this study, the ion inertial effects on the sheath-limited filament dynamics have been investigated with the 3D-PIC simulations in order to evaluate the isotope influences in the polarization drift effect and the sheath effect. The simulations have revealed that the sheath effect is cancelled out by the polarization drift effect. Therefore, the radial propagation speed in DT plasmas ought to be roughly the same as that in H plasma. However, in the simulations, it has been observed that the radial propagation speed in DT plasmas is slightly slower than that in H plasma. This fact is thought to arise from the gyro-motion effect which induces the poloidal symmetry breaking, the poloidal movement of blob, and the deceleration of radial propagation.

TH

Velocity Profile and Modulation Frequency of Ions in a Magnetized Plasma Sheath Using Kinetic Trajectory Simulation Method

R. Khanal¹, B. R. Adhikari¹

¹*Tribhuvan University, Kirtipur, Kathmandu, Nepal*

Corresponding Author: R. Khanal, plasmanepal@hotmail.com

In all bounded plasmas, the plasma sheath plays an important role for stability as well as in determining the particle fluxes and energies reaching the wall. Velocity variation as well as modulation frequency of ions in a magnetized plasma sheath have been studied for different obliqueness as well as field strength. Due to sharp gradients of physical parameters in the sheath region, fluid theory encounters singularities and we have used the kinetic trajectory simulation model, where the characteristic equations of motion are solved iteratively unless a self-consistent state is achieved for given particle distributions at boundaries. Variation of ion velocities, their mean values, maximum amplitude, damping factor as well as frequency of oscillation are studied for constant magnetic field at different obliqueness as well as for different magnetic fields considering the same obliqueness. The kinetic approach is expected to give better understanding of velocity profiles and hence is of interest in divertor type tokamaks, where the field lines outside the last-closed-flux-surfaces strike the wall at different angles.

Exact Conservative Solutions of Fluid Models for the Scrape-Off Layer as the Ancestors of Blobs?

J. P. S. Bizarro¹, R. Vilela Mendes¹, and L. Venâncio¹

¹*Institute of Plasmas and Nuclear Fusion (IPNF), Instituto Superior Técnico (IST), 1049-001 Lisbon, Portugal*

Corresponding Author: J. P. S. Bizarro, bizarro@ipfn.tecnico.ulisboa.pt

Exact solutions have been obtained for the conservative part of a standard two-fluid (density plus vorticity) model of the scrape-off layer (SOL) which are of the travelling-wave type and describe transport of large-, machine-scale structures across the plasma cross-section (radially and/or poloidally). These conservative solutions can be of various forms and shapes, either extended or localized, moving either outwards (as actual high-density blobs) or inwards (as plasma holes with densities lower than the background's), being conjectured that they are the ancestors of the propagating coherent structures, known as blobs, often seen in experiments and numerical simulations of SOL turbulence. These solutions have added value per se, not only because they are actual solutions of the conservative interchange model of the SOL, but also because they allow some analytical control over numerical implementations of the model as they provide benchmarks, or standards, against which the latter can be verified. In fact, and as it will be shown, they have been used to verify different numerical schemes to solve the equations of SOL turbulence, namely, an explicit 4th order Runge–Kutta and a new semi-implicit method which, contrary to the Runge–Kutta scheme, guarantees stability without the need for very fine meshes and the consequent computational cost. Once confidence has been gained regarding the numerical implementation of the model, nonconservative terms (such as diffusion, sources, and parallel losses) have been added to check what happens to the conservative structures (whether they are merely distorted or end up by disappearing).

TH

Simulation of Beryllium Erosion and Surface Damage Under ITER-Like Transient Plasma Heat Loads

I. B. Kupriyanov¹, G. N. Nikolaev¹, E. V. Basaleev¹, N. Porezanov¹, L. A. Kurbatova¹, V. L. Podkovyrov², A. D. Muzichenko², A. M. Zhitlukhin², and V. Safronov³

¹*A.A. Bochvar High-Technology Research Institute of Inorganic Materials, "VNIINM", Moscow, Russian Federation*

²*SRC RF TRINITI, Moscow, Russian Federation*

³*International Thermonuclear Experimental Reactor (ITER), Project Centre "ITER", Moscow, Russian Federation*

Corresponding Author: I. B. Kupriyanov, igkupr@gmail.com

The first wall panels of the ITER main chamber will be completely armoured with beryllium. The primary reasons for the selection of beryllium as an armour material for the ITER first wall are its low- Z , high oxygen gettering characteristics and high thermal conductivity. During plasma operation in ITER, beryllium, besides low cyclic heat loads (normal events) will suffer high transient heat loads, such as ELMs, disruptions, VDE, etc., (off normal events). These transient loads cause rapid heating of the beryllium surface and can result in significant changes in surface and near-surface regions, such as material loss, melting, cracking, evaporation and formation of beryllium dust as well as hydrogen isotopes retention both in the armour and in the dust. It is expected that the erosion of beryllium under transient plasma loads such as ELMs and disruptions will have significant impact on lifetime of the ITER first wall.

This paper presents the main results of numerous experiments carried out during some last years at QSPA-Be facility in Bochvar Institute. QSPA-Be facility represents a single-stage coaxial quasi-stationary plasma accelerator with its own magnetic field. It is capable to provide plasma (hydrogen or deuterium) and radiation heat loads on target surface relevant to ITER ELMs and mitigated disruptions. Special Be and Be/CuCrZr mock-ups were tested by hydrogen/deuterium plasma streams (5 cm in diameter) with pulse duration of 0.5 ms in a heat loads range of 0.2–2.2 MJ/m² and maximum quantities of plasma pulses up to 100–250 shots. The angle between plasma stream direction and mock-ups surface was 30°. During the experiments, the mock-up temperature has been maintained in the range of RT–500°C. Two beryllium ITER grades: TGP-56FW (RF, Bochvar Institute) and S-65C (USA, Materion Brush) were studied in these experiments. Influences of plasma heat loads, surface temperature and quantities of plasma pulses on the Be erosion and surface damage are presented. The experimental data obtained are used for validation of appropriate numerical models and for the estimation of lifetime of the Be armour.

Assessment of Alternative Divertor Configurations as an Exhaust Solution for DEMO

H. Reimerdes¹, R. Ambrosino², P. Innocente³, R. Albanese², H. Bufferand⁴, A. Castaldo², P. Chmielewski⁵, G. Ciraolo⁴, D. Coster⁶, S. Ha⁷, R. Kemp⁷, V. P. Loschiavo², T. Lunt⁶, S. Merriman⁷, V. Pericoli Ridolfini^{3,5}, M. Siccino⁶, F. Subba⁸, and R. Zagórski⁵

¹Swiss Plasma Center (SPC), École polytechnique fédérale de Lausanne (EPFL), 1015 Lausanne, Switzerland

²Consorzio CREATE, Università degli Studi di Napoli Federico II, 80138 Napoli, Italy

³Consorzio RFX, Associazione EURATOM-ENEA sulla Fusione, Padova, Italy

⁴Institut de Recherche sur la Fusion par confinement Magnétique (IRFM), Commissariat à l'énergie atomique (CEA/Cadarache), 13108 St. Paul lez Durance, France

⁵Institute of Plasma Physics and Laser Microfusion (IPPLM), Warsaw, Poland

⁶Max-Planck-Institut für Plasmaphysik, Garching, Germany

⁷Culham Centre for Fusion Energy (CCFE), Culham Science Centre, Abingdon, UK

⁸Dipartimento Energia, Politecnico di Torino, Turin, Italy

Corresponding Author: H. Reimerdes, holger.reimerdes@epfl.ch

The European roadmap for fusion energy has identified plasma exhaust as a major challenge towards the realization of magnetic confinement fusion. To mitigate the risk that the baseline scenario with a single null divertor (SND) and a high radiation fraction adopted for ITER will not extrapolate to a DEMO reactor, the EUROfusion consortium is assessing potential benefits and engineering challenges of alternative divertor configurations.

A range of alternative configurations that could be readily adopted in a DEMO design have been identified. They include the X divertor (XD), the Super-X divertor (SXD) and the Snowflake divertor (SFD). The flux flaring towards the divertor target of the XD is found to be limited by the minimum grazing angle at the target. The characteristic increase of the target radius in the SXD is a trade-off with the increased TF coil volume, but ultimately limited by forces onto coils. Engineering constraints also limit XD and SXD characteristics to the outer divertor leg with a solution for the inner leg requiring up-down symmetric configurations.

Boundary models with varying degrees of complexity have been used to predict the beneficial effect of the alternative configurations on exhaust performance. Desired effects are an easier access to detachment, reluctance of the detachment front to move along the divertor leg and an increase of the divertor radiation without excessive core confinement degradation. Based on the extended 2-point model and achievable geometric variations the SOL radiation required for the onset of detachment decreases in the SXD and SFD with the tolerable residual power $\propto (1 - f_{\text{rad}})$ being 30–40% larger than in the SND. Additional improvements are expected from the ability to increase f_{rad} without adverse effects on the core performance and through SOL broadening as postulated for the SFD. A systematic study of the alternative configurations and the SND reference using the divertor transport code TECXY confirms that the SFD detaches at a lower f_{rad} , but also shows that the potential gain is modest. The main expected advantage of the XD and similarly of the SXD is an increased reluctance of the detachment front to move towards the X-point. To that end the detachment dynamics are assessed with the SOLPS and SOLEDGE2D-EIRENE codes, which use more sophisticated models of the target geometry and neutral particles.

Performance Assessment of Tightly-Baffled Long-Leg Divertor Geometries in the ARC Reactor Concept

M. Wigram¹, B. LaBombard², M. V. Umansky³, A. Q. Kuang², T. Golfopoulos²,
D. Brunner², J. L. Terry², M. E. Rensink³, and D. G. Whyte²

¹University of York, Heslington, UK

²Plasma Science & Fusion Center, MIT, Cambridge, MA 02139, USA

³Lawrence Livermore National Laboratory (LLNL), Livermore, CA 94550, USA

Corresponding Author: M. Wigram, mrkw500@york.ac.uk

A means to handle the extreme power exhaust from tokamak-based fusion power reactors remains to be demonstrated. Advanced divertor configurations have been proposed as potential solutions, including double-nulls, long-legs and magnetic field flaring with secondary X-points. Modelling of tightly-baffled, long-leg divertor geometries in the divertor test tokamak concept ADX has shown the potential to access passively stable, fully detached divertor regimes over a broad range of parameters [1]. The question remains as to how these advanced divertor configurations may perform in a reactor setting. To explore this, we have performed numerical simulations of these configurations in the context of the ARC reactor concept [2]. The ARC design has been recently updated to include a tightly-baffled, long-leg divertor with an X-point target [3]. ARC provides an appropriate reactor test scenario for advanced divertor configurations, with a projected SOL heat flux width of 0.4 mm and total power exhaust requirement of 105 MW.

Using the divertor geometry and magnetic equilibrium from the updated ARC design, simulations of the ARC edge plasma and divertor are carried out with UEDGE [4]. The anticipated radial plasma profiles at the outer midplane are specified and power exhaust from the core is scanned over a wide range. Anomalous radial transport in the scrape off layer and divertor legs is modelled by a combination of radial diffusion and advection consistent with experimental observations, which also provide guidance for power sharing between the inner and outer divertor legs. Initial studies employing a Super-X Divertor configuration and 0.5% fixed-fraction neon impurity radiation have shown that a stable detached divertor regime exists for power exhaust in the range of 80 to 108 MW [5]. Simulations are presently being extended to study the performance of the X-point target geometry in ARC and to explore the sensitivity of the solutions to modelling assumptions and input parameters. The latest results from these studies will also be presented.

References

- [1] M. V. Umansky *et al.*, Phys. Plasmas, **24**, 056112 (2017).
- [2] B. Sorbom *et al.*, Fusion Eng. Des., **100**, 378 (2015).
- [3] A. Q. Kuang *et al.*, 59th Annual Meeting of the APS DPP, C04.6, 66 (2017).
- [4] T. D. Rognlien *et al.*, J. Nuc. Mat., **196**, 347 (1992).
- [5] M. Wigram *et al.*, PET 2017 conference, submitted to CtPP.

Simulations of Tokamak Boundary Plasma Turbulent Transport

X. Q. Xu¹, B. Chen^{1,2}, J. G. Chen^{1,3}, Z. Y. Li^{1,3}, N. M. Li^{1,4}, T. F. Tang^{1,4}, Y. M. Wang^{1,5},
T. Y. Xia^{1,5}, M. Porkolab⁶, E. Edlund⁶, B. LaBombard⁶, and J. W. Hughes⁶

¹Lawrence Livermore National Laboratory (LLNL), Livermore, CA 94550, USA

²University of Science and Technology of China, Hefei, Anhui, People's Republic of China

³Peking University, Beijing 100871, People's Republic of China

⁴Dalian University of Technology, Liaoning, Dalian, Ganjingzi, People's Republic of China

⁵Institute of Plasma Physics, Chinese Academy of Sciences, Hefei, Anhui, People's Republic of China

⁶Plasma Science & Fusion Center, MIT, Cambridge, MA 02139, USA

Corresponding Author: X. Q. Xu, xu2@llnl.gov

The BOUT++ code has been used to simulate edge plasma electromagnetic (EM) turbulent transport and to study the role of EM turbulence in setting the scrape-off layer (SOL) widths. More than a dozen tokamak discharges from C-Mod, DIII-D, EAST, ITER, and CFETR have been simulated with encouraging success. The simulation results reproduce the measured pedestal turbulence characteristics and the SOL widths. The principal results are: 1) the blobby turbulence originates in the pedestal peak pressure gradient region inside the magnetic separatrix and nonlinearly spreads across the separatrix. The electromagnetic fluctuations provide anomalous transport, which causes particle and heat to be turbulently transported radially down their gradients across the separatrix into the SOL. The electromagnetic fluctuations show the characteristics of both quasi-coherent modes (QCMs) and broadband turbulence. 2) For simulations of C-Mod EDA H-mode plasmas, the mode spectra are in agreement with the phase contrast imaging data; radial location of the mode is generally consistent with measurements localizing QCMs to the pedestal/separatrix region. For simulations of EAST H-mode plasmas, the mode spectra are in agreement with the probe, interferometer, and POINT diagnostics. A series of simulations also shows that the edge bootstrap current plays a critical role to shift the most unstable mode to lower toroidal mode number, narrow the mode spectrum and enhance radial transport. Therefore, it is suggested to control the peeling modes and associated transport by introducing edge current drive to cancel bootstrap current, for example, by means of lower hybrid waves. This may lead to suppression/mitigation of type-I ELMs and facilitate access to the grassy ELM regime, thus opening a potentially new avenue for steady-state operations in ITER, CFETR and beyond.

Wide Divertor Heat-Flux Width in ITER from Self-Organization between the Neoclassical and Turbulent Transports across the Separatrix Surface

C.-S. Chang¹, R. M. Churchill¹, R. Hager¹, S.-H. Ku¹, R. Maingi¹, J. E. Menard¹, A. Loarte², R. A. Pitts², V. Parail³, M. Romanelli³, and F. Köchl⁴

¹Princeton Plasma Physics Laboratory (PPPL), Princeton, NJ 08540, USA

²International Thermonuclear Experimental Reactor (ITER),

Cadarache Centre, 13108 St. Paul lez Durance, France

³Culham Centre for Fusion Energy (CCFE), Culham Science Centre, Abingdon, UK

⁴Atominstytut, Technische Universität Wien, Stadionallee 2, 1020 Vienna, Austria

Corresponding Author: C.-S. Chang, cschang@pppl.gov

A serious concern for ITER operation is the ability for the divertor to withstand the steady plasma exhaust heat that will be deposited on the divertor surface along a narrow toroidal strip. A simple, data-based regression from experimental measurements in present devices shows we would have $\lambda_q \lesssim 1$ mm for ITER operation at $I_p = 15$ MA. However, it is questionable if such a simple extrapolation is valid as there may be differences in fundamental edge physics between ITER plasmas and those in present devices. Therefore, any extrapolation from present experiments to ITER needs to have a solid physics basis, which is one of the goals of the gyrokinetic edge code XGC1. Prediction for λ_q by XGC1 has been validated on several representative C-Mod, DIII-D, NSTX, and JET plasma conditions. However, when the same code is applied to a model ITER plasma at $I_p = 15$ MA, surprisingly, $\lambda_q \approx 6$ mm is obtained [1, 2]. Another abnormality is noticed from high current, high triangularity NSTX-U model plasma simulations. A substantial new understanding has been obtained after the 2016 IAEA-FEC for physics behind the enhanced divertor heat-flux width. XGC1 data reveals an interesting competition effect between the neoclassical and turbulent transports. In the “conventional” tokamaks that obey the Eich scaling [3], a “blob-type” edge turbulence exists across the magnetic separatrix $\Psi_N > 0.97$. On the other hand, in ITER, a “streamer-type turbulence” extends to $\Psi_N > 0.97$ due to the small ρ_i/a effect. The streamer-type turbulence is much more efficient in the radial transport across the magnetic separatrix surface, with the pressure and potential perturbation being highly off-phase, than the blob-type turbulence is. We note here that even with ρ_i/a , the X-point orbit loss and a strong spontaneous corotation in the edge plasma supports a reasonably strong pedestal in ITER that is $\sim 2\times$ wider than the MHD predicted width.

Work predominantly funded by U.S. Department of Energy and ITER. Computing resources provided by OLCF and NERSC.

References

- [1] C. S. Chang *et al.*, IAEA-FEC 2016, TH/2-1.
- [2] C. S. Chang *et al.*, Nucl. Fus., **57**, 116023 (2017) .
- [3] T. Eich *et al.*, Nucl. Fus., **53**, 093031 (2013).

Continuum Gyrokinetic Simulations of NSTX SOL Turbulence with Sheath-Limited Model Geometries

A. Hakim¹, E. L. Shi², T. Bernard³, M. Francisquez⁴, F. Jenko^{5,3}, G. W. Hammett¹, Q. Pan⁶, T. Stoltzfus-Dueck¹, and D. Told⁵

¹*Princeton Plasma Physics Laboratory (PPPL), Princeton, NJ 08540, USA*

²*Princeton University, Princeton, NJ 08544, USA*

³*University of Texas at Austin, Austin, TX 78712, USA*

⁴*Dartmouth College, Hanover, NH 03755, USA*

⁵*Max-Planck-Institut für Plasmaphysik, Garching, Germany*

⁶*Plasma Science & Fusion Center, MIT, Cambridge, MA 02139, USA*

Corresponding Author: A. Hakim, ahakim@pppl.gov

We describe results obtained from Gkeyll, a full- f continuum gyrokinetic code, designed to study turbulence in the edge region of fusion devices. The edge region is computationally very challenging, requiring robust algorithms that can handle large amplitude fluctuations and stable interactions with sheath boundary conditions. Results of turbulence in a scrape-off layer (SOL) for NSTX-type parameters with a model magnetic geometry have been obtained. Key physics of SOL turbulence, such as drive by toroidal bad curvature and steep gradients and interactions with a model sheath boundary condition are included. This allows us to perform parameter scans and physics studies, such as the physics of heat flux width on the divertor plate, and the amplitude and intermittency of SOL turbulence. Initial results find that the heat flux narrows as the connection length is made shorter (the poloidal field becomes stronger). We have begun studies on the effect of recycling on the edge to better understand low-recycling lithium cases. To validate the code, we have studied turbulence in the straight-field LAPD device at UCLA and the helical Helimak device at the University of Texas. We will also describe the extension of the GENE gyrokinetic code to be full- f , and initial GENE simulations for LAPD.

TH

Simulation of Cross-Separatrix Edge Plasma Transport with the Continuum Gyrokinetic Code COGENT

M. A. Dorf¹, M. Dorr¹, D. Ghosh¹, J. Hittinger¹, M. V. Umansky¹, J. Angus¹, and A. Pankin²

¹*Lawrence Livermore National Laboratory (LLNL), Livermore, CA 94550, USA*

²*Lehigh University, Bethlehem, PA 18015, USA*

Corresponding Author: M. A. Dorf, mdorf@lbl.gov

Axisymmetric (4D) simulations using the finite-volume code COGENT are performed to explore the role of ion kinetic effects in tokamak edge plasmas. The simulation model solves the long wavelength limit of the full- f gyrokinetic equation for ion species coupled to the 2D quasi-neutrality equation for electrostatic potential variations, where a fluid model is used for an electron response. The ion-ion collisions are described by the nonlinear Fokker-Planck operator and the effects of anomalous transport are included via a radial diffusion model. Coupling to the 2D fluid code UEDGE is explored in order to improve the electron and neutral models used in COGENT. Illustrative simulations are performed for the parameters of the DIII-D tokamak and compared with the experimental data.

The development of 5D COGENT for edge plasma turbulence modelling is also reported. To that end, the slab-geometry 5D version has been developed and successfully verified in simulations of the collisionless drift-wave instability that involve gyrokinetic equations for both ion and electron species coupled to the long-wavelength limit of the 3D gyro-Poisson equation. Recent work is focussed on extending the 5D code to include the effects of a tokamak edge magnetic geometry.

Multiphysics Modelling of the Long-Term Evolution of Plasma-Exposed Surfaces

J. M. Canik¹, A. Lasa², S. Blondel², M. Cianciosa¹, D. Curreli³, J. Drobný³, W. Elwasif¹, D. L. Green², T. K. Younkin², B. D. Wirth², R. P. Doerner⁴, D. Nishijim⁴, and M. Baldwin⁴

¹Oak Ridge National Laboratory (ORNL), Oak Ridge, TN 37831, USA

²University of Tennessee, Knoxville, TN 37996, USA

³University of Illinois, Urbana-Champaign, IL 61820, USA

⁴University of California San Diego, CA 92093, USA

Corresponding Author: J. M. Canik, canikjm@ornl.gov

We report on a new simulation capability for predicting plasma-surface interactions, including the evolution of the plasma-facing component (PFC) surface layer that is continually modified by contact with the fusion plasma. This involves a wide range of physical phenomena: our current model includes components for: a) the scrape-off layer plasma including fuel ions and extrinsic impurities (using SOLPS [1]); b) transport and redeposition of eroded wall material (using the newly developed Monte Carlo code GITR); c) the implantation of plasma ions into the material and subsequent wall erosion (using F-TRIDYN, and extension of TRIDYN [2]); and, d) the dynamics of the subsurface (Xolotl, a new continuum cluster dynamics code). These components are being integrated to yield predictive capability for the changes in surface morphology, fuel recycling and tritium retention, and how these are impacted by material erosion and redeposition, initially targeting tungsten exposed to mixed hydrogenic and helium plasmas. Initial simulations have focussed on a recent set of experiments at the PISCES linear facility, where tungsten was exposed to helium plasmas with fluxes of $0.5\text{--}4 \times 10^{22}/\text{m}^2\cdot\text{s}$ for durations of 5000–10 000 s, with incident energies of ~ 250 eV controlled through biasing. Initial simulations have demonstrated the effect of including bubble bursting and sputtering on the subsurface evolution, as well as validation against erosion and migration measurements in PISCES. Integrated simulations for ITER-like parameters in a toroidal geometry will be presented.

Work supported by the U.S. Department of Energy under DE-AC05-00OR22725.

References

- [1] W. Miller *et al.*, *Comp. Phys. Comm.*, **51**, 355 (1988).
- [2] R. Schneider *et al.*, *Contrib. Plasma Phys.*, **46**, 3 (2006).

Pressure Balance in a Low Collisionality Tokamak Scrape-Off Layer

R. M. Churchill¹, C.-S. Chang¹, R. Hager¹, S.-H. Ku¹, R. Maingi¹, D. P. Stotler¹, and H. Qin¹

¹Princeton Plasma Physics Laboratory (PPPL), Princeton, NJ 08540, USA

Corresponding Author: R. M. Churchill, rchurchi@pppl.gov

Understanding the physics governing the scrape-off layer is necessary in order to reliably predict critical quantities for both the machine and its operation, such as the heat flux width at the divertor, the plasma-wall interaction, inevitable material migration, the effect of divertor condition on the pedestal profile, and so on. Among the most basic predictable quantities is how the SOL density and temperature change from an upstream location as one approaches the divertor target.

Recent simulation results [1, 2], using the axisymmetric gyrokinetic code XGCa, showed several noteworthy features for a low-collisionality discharge of the DIII-D tokamak. Comparisons of the electron pressure variation in the divertor region between simulation and experiment showed good agreement [1] (measurements were made with the divertor Thomson system). However, the simplified fluid form for total parallel momentum was not conserved in the near-SOL [2], which implies kinetic effects are needed to properly predict the total pressure variation in the near-SOL. However, even taking care to include neutral friction and viscosity resulting from a Chew-Goldberger-Low (CGL) form of the pressure tensor (i.e., only the dominant diagonal terms) does not resolve the imbalance.

Here, additional pressure tensor terms are added to the momentum equation, to determine their effect in the momentum balance in the scrape-off layer. This is similar to “pressure tensor unfolding” [3], but utilizing the full distribution function from XGCa to calculate the, presumably, higher-order pressure tensor terms. We find that certain off-diagonal ion pressure tensor components indeed have a non-negligible parallel variation, suggesting the need to include them in the full fluid parallel momentum balance equation.

Further simulations with higher ion collisionality are explored to study the effect of ion collisionality versus proximity to the separatrix on the momentum equation in the SOL.

Work supported by the U.S. Department of Energy under DE-AC02-09CH11466, DE-AC05-00OR22725, and DE-FC02-04ER54698.

References

- [1] R. M. Churchill *et al.*, Nucl. Mat. Eng., **12**, 978–983. (2017).
- [2] R. M. Churchill *et al.*, Nucl. Fus., **57**, 46029 (2017).
- [3] A. V. Chankin and P. C. Stangeby, Nucl. Fus., **46**, 975–993 (2006).

Highly Collisional Two-Fluid and Gyrokinetic Simulations of Tokamak Edge Turbulence and the Transition between Kinetic and Fluid Regime

K. Hallatschek¹

¹*Max-Planck-Institut für Plasmaphysik, Garching, Germany*

Corresponding Author: K. Hallatschek, klaus.hallatschek@ipp.mpg.de

Gyrokinetic and nonlocal fluid codes have complementary limitations in the tokamak edge. To arrive at a common basis, the gyrokinetic code CGYRO and the nonlocal two-fluid code NLET have both been applied to identical parameters sets ranging from resistive ballooning turbulence — approaching the collisional fluid limit — relevant to the edge of a tokamak, up to high-gradient kinetic ITG modes at higher temperatures in the core-edge transitional regime, yielding comparable results. As a nontrivial, novel result, linear growth rate and nonlinear transport agree between the codes in the fluid limit of high collision numbers ($\nu_e \sim 500\text{--}10000\,c_i/R$), not least, because the kinetic code employs the Sugama collision operator with momentum and energy conservation, Galilean invariance and exact self-adjointness property.

Effect of Poloidal Density Asymmetries on Shear Flows and Radial Electric Field at the Plasma Edge

A. Y. Aydemir¹, Y. In², H. H. Lee¹, B. H. Park¹, and J. Seol¹

¹*National Fusion Research Institute (NFRI), Daejeon, Republic of Korea*

²*Ulsan National Institute of Science and Technology (UNIST), Ulsan, Republic of Korea*

Corresponding Author: A. Y. Aydemir, aydemir@nfri.re.kr

In the simplest magnetohydrodynamic (MHD) description of the plasma equilibrium, rapid transport along the field lines leads to a state where the plasma density and temperature are constant on flux surfaces, exhibiting symmetry in both the poloidal and toroidal directions. This idealization, however, breaks down at the plasma edge where both the magnetic topology and various perpendicular transport processes introduce at least a poloidal asymmetry. We show that the mass flows and radial electric field driven by edge poloidal density asymmetries can be used as a highly effective control mechanism for the edge and thus the global confinement in tokamaks. The underlying physics can be demonstrated entirely within a simple magnetohydrodynamic equilibrium model with an appropriate flow damping mechanism. As an example, strong dependence of the low to high (L-H) transition power threshold on the magnetic topology, an experimental observation still poorly understood, can be easily explained within this framework. Similar arguments also indicate that some of the ITER fuelling ports are misplaced from an operational point of view and may lead to higher input power requirements.

Multiscale Interaction between Ballooning Mode and Electron-Scale Turbulence and the Mesoscale Structure Formation in the Edge Pedestal

R. Singh¹, H. Jhang¹, and M. Mou²

¹National Fusion Research Institute (NFRI), Daejeon, Republic of Korea

²Sichuan University, Chengdu, Sichuan, People's Republic of China

Corresponding Author: R. Singh, rsingh129@gmail.com

Recent MHD simulations [1, 2] have demonstrated that one of the important ingredients giving rise to the ELM [3] crash is the hyper-resistivity in Ohm's law. In this paper, we address three key issues: i) the source for the hyper-dissipations (e.g., hyper-resistivity and hyper-viscosity); ii) high- k ballooning mode (BM) driven by hyper-dissipation near marginally stable BM boundary; iii) the possible nonlinear saturation mechanism of the high- k BM. We present a simple self-consistent theoretical model for hyper-resistivity ballooning modes (HRBM) accounting for the multiscale interaction between the long scale BM and the short scale ETG mode above a BM threshold. Here, the coupling between the BM and the ETG turbulence has been identified as a primary mechanism for the generation of the long scale hyper-resistivity (η_H) [4] and hyper-viscosity (μ_H) in BM dynamics. Based on the linear theory, the physics of HRBM mode has been elucidated, as well as the parameter space where it is important. It is shown that the growth rate of HRBM increases with the increasing poloidal wave vector (k_θ) whereas standard BM growth decreases with k_θ . Another long standing problem is how KBM (here particularly HRBM) saturation occurs so rapidly. The possibility of long scale zonal fields [e.g., mesoscale poloidal magnetic fields (zonal current) and radial magnetic fields (streamers)] are examined in this study. Further their potential impact on thermal transport and an ELM crash are also considered.

References

- [1] X. Q. Xu *et al.*, Phys. Rev. Lett., **105**, 175005 (2010).
- [2] T. Rhee *et al.*, Nucl. Fus., **55**, 032004 (2015).
- [3] P. B. Snyder *et al.*, Phys. Plasmas, **9**, 2037 (2002).
- [4] R. Singh *et al.*, IAEA FEC-2014, St. Petersburg, Russian Federation, TH/P1-15.

Correlation Analysis Based Magnetic Kubo Number Estimation during Pedestal Collapse in BOUT++ Simulation

J. Kim¹, W. Lee¹, H. Jhang², S. S. Kim², H. H. Kaang², and Y.-C. Ghim¹

¹Korea Advanced Institute of Science and Technology (KAIST), Daejeon, Republic of Korea

²National Fusion Research Institute (NFI), Daejeon, Republic of Korea

Corresponding Author: J. Kim, ijwkim@kaist.ac.kr

We perform a correlation analysis to explore how the magnetic Kubo number evolves during and after an abrupt edge pedestal collapse generating stochastic magnetic fields in the simulation. During abrupt edge pedestal collapse caused by type-I ELM (edge localized mode), the stochastic magnetic field is thought to be a possible way to induce significant cross-field diffusion. We analyze the results obtained by the numerical simulations performed within BOUT++ framework solving a set of three-field reduced magnetohydrodynamics equations for toroidally confined plasmas. We set the equilibrium pressure gradient to be much higher than the stability limit of the initially seeded ballooning mode. The magnetic Kubo number in our simulation is found not to exceed unity. This result indicates that the quasi-linear Gaussian diffusion model, not percolation theory, is adequate to explain the cross-field diffusion. Radial correlation length of pressure fluctuations is highly correlated with radial width of the stochastic magnetic fields; while time evolution of poloidal correlation length of pressure fluctuations behaves like that of Chirikov parameter and Kubo number.

Studies of the Gas Puff Effect on Edge Plasma of ADITYA Tokamak Using Coupled DEGAS2-UEDGE Code

R. Dey¹, H. Raj¹, M. B. Chowdhuri¹, J. Ghosh¹, K. A. Jadeja¹, K. M. Patel¹, N. C. Patel¹, R. L. Tanna¹, R. Manchanda¹, S. Banerjee¹, R. Srinivasan¹, D. Sharma¹, U. C. Nagora¹, P. K. Atrey¹, J. V. Raval¹, Y. S. Joisa¹, P. K. Chattopadhyay¹, D. P. Stotler², and T. D. Rognlien³

¹*Institute for Plasma Research (IPR), Bhat, Gandhinagar, India*

²*Princeton Plasma Physics Laboratory (PPPL), Princeton, NJ 08540, USA*

³*Lawrence Livermore National Laboratory (LLNL), Livermore, CA 94550, USA*

Corresponding Author: R. Dey, ritu.dey@ipr.res.in

Fuel neutral penetration and dynamics in the edge and scrape of layer (SOL) plasma region of tokamaks shape the plasma properties in these regions which play an important role in determining the core plasma confinement. Experiments in ADITYA and ADITYA-U tokamaks have shown that fuelling by periodic multiple gas puffs led to improved core plasma properties [1]. These experimental results warrants a detailed understanding of the edge and SOL plasmas during and after the gas puffs to understand the physics behind improvement of plasma properties. Modelling of edge and SOL plasmas of ADITYA and ADITYA-U tokamaks has been carried out using the coupled UEDGE and DEGAS2 code. Neutral hydrogen penetration into the ADITYA [2] and ADITYA-U plasmas has been obtained using the neutral particle transport code, DEGAS2 during the gas-puff. The modifications in plasma parameters in the SOL and edge regions due to these neutrals have been modelled using the UEDGE code, which is a 2D edge-plasma transport code. Both these codes are coupled to obtain the dynamics of edge and SOL plasmas during and after the gas-puffs of different magnitudes. The ADITYA tokamak is operated with a poloidal ring limiter located at one toroidal location, whereas the ADITYA-U tokamak is operated with a toroidal belt limiter on the high field side. Geometries of both limiter configurations are successfully integrated with both the codes, which are run for many discharges with different operational parameters. The coupled code has successfully reproduced the measured temporal evolution of H_α emission and the variations in density and temperature in the edge and SOL regions due to the gas puff. It has been observed that the gas puffs significantly modify the density and temperature profiles in the SOL and edge regions of ADITYA and ADITYA-U. The results show that the periodic gas-puffs of proper magnitudes can be used to control the SOL and edge plasma parameters in order to obtain improved core properties.

References

- [1] R. L. Tanna *et al.*, Nucl. Fus., **57**, 102008 (2017).
- [2] R. Dey *et al.*, Nucl. Fus., **57**, 086003 (2017).

Predictive Simulations of Core-Edge Plasma for Tokamak Plasma Using BALDUR Code

A. Wisitsorasak¹, S. Sangaroon³, B. Chatthong⁴, T. Onjun², and J. Promping²

¹Department of Physics, King Mongkut University of Technology Thonburi, Bangkok, Thailand

²Thailand Institute of Nuclear Technology, Bangkok, Thailand

³Department of Physics, Mahasarakham University, Mahasarakham, Thailand

⁴Department of Physics, Prince of Songkla University, Songkla, Thailand

Corresponding Author: A. Wisitsorasak, apiwat.wis@kmutt.ac.th

Core-Edge simulations of the low confinement mode (L-mode) plasma are carried out using 1.5D BALDUR integrated predictive modelling code. In each simulation, the plasma current, temperatures, and density profiles for both core and SOL regions are self-consistently evolved. The plasma profiles in the SOL region are simulated by integrating the fluid equations, including sources, both along with and perpendicular to the field lines. The transport coefficients in the SOL region are determined by either one of three transport models: i) neoclassical transport; ii) constant transport coefficients; and, iii) anomalous transport. The solutions in the SOL subsequently provide as the boundary conditions of the core plasma region. The core plasma transport model is described using a combination of anomalous transport by multimode-model version 1995 (MMM95) and neoclassical transport provided by NCLASS module. By comparing with 38 L-mode discharges from TFTR, DIII-D, and JET, it is found that the mean standard deviations of the plasma profiles with SOL transport modelled by the anomalous transport are 19% for the electron density, 21% for the electron temperature, and 26% for the ion temperature, while the simulation results using the SOL transport modelled with a fixed constant or the neoclassical transport show higher deviation. Furthermore, the BADLUR code is used to predict the plasma profiles near the edge of the HT-6M tokamak based on the previous developed model. When the plasma current is kept constant and the average density is varied between 1×10^{19} – $9 \times 10^{19}/\text{m}^3$, the simulations show that power loaded to the limiter is about 30–550 kW and the total ion flux to the SOL region is about 2×10^{19} – $20 \times 10^{19}/\text{s}$. Note that no auxiliary heating is provided. The temperature at the separatrix is found to be about 5–7 eV.

Gyrokinetic Neoclassical Study of the Effect of the X-Point Height on $E \times B$ Flow Structure in an H-Mode Edge Plasma

J. Chowdhury¹, R. Hager¹, S.-H. Ku¹, and C.-S. Chang¹

¹Princeton Plasma Physics Laboratory (PPPL), Princeton, NJ 08540, USA

Corresponding Author: J. Chowdhury, jchowdhu@pppl.gov

The X-point height relative to the divertor plates may cause difference in the neutral particle penetration into pedestal and have impact on the pedestal physics in H-mode. In the present work, we utilize the total- f global gyrokinetic neoclassical code XGCa to study the X-point height effect on the $E \times B$ flow profile in a JET-like H-mode pedestal in a realistic JET-like divertor geometry and with neutral particle recycling. The vacuum pump is not modelled in the results presented here. Effect of plasma turbulence on the E_r -well depth is not considered either. The main result is that the neoclassical E_r profile is sensitive to the vertical X-point location, while the plasma profile change is only minimal. The findings here imply that, even though the change in the plasma profile may not be easily noticeable in the experiment, the hidden change in the $E \times B$ profile could cause a difference in the pedestal physics such as the ELM stability and turbulent/neoclassical transport. The change in the $E \times B$ rotation, without much change in the plasma profiles, is balanced by the change in the toroidal flow speed. The vertical X-point movement, as a result of this E_r profile change, can sensitively affect high- Z impurity transport and its accumulation in the pedestal.

Nonlinear Interaction of Runaway Electrons with Resistive MHD Modes in an ITER VDE

V. K. Bandaru¹, M. Hölzl¹, G. Papp¹, P. Aleynikov², G. T. A. Huijsmans^{3,4}, and F. J. Artola⁵

¹Max-Planck-Institut für Plasmaphysik, Garching, Germany

²Max-Planck-Institut für Plasmaphysik, Greifswald, Germany

³International Thermonuclear Experimental Reactor (ITER),
Cadarache Centre, 13108 St. Paul lez Durance, France

⁴Eindhoven University of Technology, Eindhoven, Netherlands

⁵Physique des Interactions Ioniques et Moléculaires (PIIM), CNRS, Aix-Marseille Université, France

Corresponding Author: V. K. Bandaru, skb@ipp.mpg.de

Uncontrolled termination of postdisruption runaway electron (RE) current can cause deep localized melting of the first wall and this poses a serious challenge to the successful operation of fusion grade tokamaks, including ITER. Since the deconfinement of REs depends on the timescale of flux surface reformation and the plasma stability itself is affected by the runaway current, the interaction between REs and MHD is highly nonlinear and has important consequences. This is the motivation of the present work, that complements the tracer particle approach for REs. The final goal is the self-consistent modelling of REs in a disrupted plasma through nonlinear MHD simulations of disruption.

In this contribution, we present results that focus on the interaction of resistive MHD modes with runaway electron growth. This is modelled by extending the nonlinear MHD code JOREK by including a fluid model for the evolution of runaway electron density. Runaway generation due to Dreicer as well as the avalanche sources are included (with an option for initializing an arbitrary RE seed profile), with advection contributions from parallel runaway velocity and an $E \times B$ drift. The first studies shown here are based on pseudothermal quenches that are obtained by artificially increasing the perpendicular thermal conductivity k_{\perp} of the plasma in equilibrium, which in turn triggers the generation of REs.

The JOREK model with REs is applied to analyse the interaction of the (1, 1) resistive internal kink with runaway electrons, given that the resistive kink is naturally destabilized due to the peakedness of the RE current profile that can lead to the central safety factor q_0 dropping below unity. A numerical study of this problem was carried out recently using the spectral MHD code EXTREM, where several simplifying assumptions were made, such as an independent thermal decay, decoupling RE current from perpendicular $E \times B$ dynamics and the neglect of parallel fluid velocity V_{\parallel} . In our study, an attempt is made towards a more comprehensive treatment of the problem. The effect of the mode growth on the RE seed redistribution and the final RE profiles will be discussed in addition to the influence of REs on the mode excitation and dynamics. The effects of prediisruption q_0 and the thermal quench rates will be studied.

Simulations of Plasma Disruptions in ITER due to Material Ingress

I. Bandyopadhyay¹, A. K. Singh¹

¹*International Thermonuclear Experimental Reactor (ITER), India Centre, Gujarat, India*

Corresponding Author: I. Bandyopadhyay, indranil@iter-india.org

Plasma major disruptions (MDs), vertical displacement events (VDEs) and associated runaway electron currents in ITER are a major cause of concern in ITER operations. Major R&D efforts, both experimental and well as through theory and modelling, are underway across the fusion community to understand these events and find suitable amelioration techniques. In the past we have presented detailed predictive simulations of MDs and VDEs in ITER using TSC and benchmarked the results with DINA simulations. Detailed benchmarking TSC modelling with multimachine experimental disruptive and VDE shots were carried out to understand and improve the halo current model used in the code to have better match with experiments, which were reported earlier.

However, in the earlier predictive simulations of MDs and VDEs for ITER that were carried out using TSC and DINA, the detailed particle and heat transport were neglected and the thermal crash was modelled by artificially specifying the plasma pressure drop in a given time scale (typically 1 ms), specifying the precrash and postcrash final electron temperature by hand to suit a given plasma current quench time. Thus in the fast current quench cases, postthermal quench $T_e = 6.5$ eV and in slow current quench cases $T_e = 50$ eV were specified a priori. Also in these simulations, the generation of the runaway electrons and their effect on the disruption evolution and especially halo currents were generally ignored. In this paper, we present TSC simulations of plasma disruptions initiated by material ingress, mainly in the form of pieces of beryllium chunk falling into the plasma from the top dome. A spherical piece of Be of radius 1 cm is dropped from the top imitating that of a knocked-off piece of the Be blanket top dome. The detailed impurity and thermal transport is calculated self-consistently along with the evolution of thermal plasma current, halo current and runaway electron current. The impurity transport of the Be ingress and its ablation in the plasma is treated with the pellet injection model in TSC. As expected the piece of Be acts like a very slow pellet and ablates in the outer periphery of the plasma leading to edge cooling and gradual shrinking of the plasma current, finally leading to disruption. Details of this simulation with interplay between plasma current runaway and halo currents will be presented in this paper.

Nonlinear 3D Simulations of Vertical Displacement Events in Tokamaks

I. Krebs¹, K. Bunkers², J. Chen¹, N. W. Eidietis³, N. M. Ferraro¹, S. C. Jardin¹, L. L. Lao³, D. Pfefferlé⁴, G. Rubinacci⁵, E. S. Seo⁶, M. S. Shephard⁶, C. Sovinec², H. Strauss⁷, and F. Villone⁵

¹Princeton Plasma Physics Laboratory (PPPL), Princeton, NJ 08540, USA

²University of Wisconsin-Madison, Madison, WI 53706, USA

³General Atomics, San Diego, CA 92186, USA

⁴University of Western Australia, WA 6009, Australia

⁵CREATE, DIETI, Università degli Studi di Napoli Federico II, 80138 Napoli, Italy

⁶Rensselaer Polytechnic Institute, Troy, NY 12180, USA

⁷HRS Fusion, West Orange, NJ 07052, USA

Corresponding Author: I. Krebs, ikrebs@pppl.gov

Vertical displacement events (VDEs) where the plasma moves rapidly towards the wall can cause large electromagnetic forces on the vessel structures with possible damaging effects for large tokamaks. Nonaxisymmetric modes developing during the VDE can lead to asymmetric, sometimes rotating forces on the vessel which can be even more severe. Large-scale 3D simulations play a crucial role on the path towards assessing and preventing the damaging effects of VDEs on vessel components in future large tokamaks like ITER.

We use the high-order finite element code M3D-C¹ [1] to perform 2D and 3D nonlinear MHD simulations of VDEs in tokamaks including a resistive wall model [2]. In order to develop predictive capabilities, the simulation results are benchmarked with other codes as well as validated against existing experimental measurements.

Both 2D and 3D nonlinear MHD simulations of VDEs are based on and validated against discharges in NSTX [3] as well as DIII-D. The results of a set of axisymmetric VDE calculations based on NSTX discharge #132859 show the sensitivities of the early VDE evolution to different parameters, in particular the halo resistivity. The 3D simulations show how nonaxisymmetric modes arise in the late VDE phase and lead to a stochastization of the magnetic field lines which allows for an efficient release of thermal energy into the wall. The thermal quench is followed by a fast decay of the plasma current and rise of the wall current.

A detailed benchmarking activity between the M3D-C¹ code and the 3D nonlinear MHD code NIMROD [4] based on an NSTX discharge is being performed. The comparison of axisymmetric VDE calculations is focussed on the early VDE growth and the wall forces. We plan to extend this benchmark to 3D simulations with a 2D wall. In addition, an axisymmetric benchmark between the M3D-C¹ code and the CarMaONL code [5] based on a standard ITER scenario using a simplified 2D model of the ITER first wall is in progress.

References

- [1] S. C. Jardin *et al.*, Comput. Sci. Discov., **5**, 014002 (2012).
- [2] N. M. Ferraro *et al.*, Phys. Plasmas, **23**, 056114 (2016).
- [3] D. Pfefferlé *et al.*, Submitted to Phys. Plasmas (2018).
- [4] C. R. Sovinec *et al.*, J. Comput. Phys., **195**, 355 (2004).
- [5] F. Villone *et al.*, Plasma Phys. Contr. F., **55**, 095008 (2013).

Nonlinear Interplay between Edge Localized Infernal Mode and Plasma Flow

G. Q. Dong¹, Y. Q. Liu^{2,1}, Y. Liu¹, S. Wang¹, N. Zhang¹, G. Z. Hao¹, and G. L. Xia¹

¹*Southwestern Institute of Physics, Chengdu, Sichuan, People's Republic of China*

²*General Atomics, San Diego, CA 92186, USA*

Corresponding Author: G. Q. Dong, donggq@swip.ac.cn

Quiescent H-mode (QH-mode) was first discovered in DIII-D as an ELM-free H-mode regime, which is usually accompanied by the presence of edge harmonic oscillations (EHOs). EHOs are believed to provide necessary transport to eliminate ELMs by dynamics of the plasma itself. The saturated kink-peeling mode has been suggested as a possible candidate for EHO. In this work, we consider another instability — the edge localized infernal mode (ELIM) — as a possible candidate for plasmas where the large edge bootstrap current causes local flattening of the plasma edge safety factor, or even the magnetic shear reversal in the pedestal region. An ELIM is a low- n (for n the toroidal mode number) instability similar to the conventional infernal mode, but being localized at the plasma edge where safety factor is locally flattened. Finite plasma pressure in the pedestal region drives this mode. A saturated ELIM, due to nonlinear interaction with toroidal plasma edge flow, can be responsible for EHO.

Our investigation is divided into three stages: i) linear stability, or the ELIM onset condition, at a given plasma flow; ii) comparison of various toroidal torques, generated by a linear mode instability; and, iii) nonlinear interplay between an ELIM and the toroidal plasma flow.

TH

Nonlinear Turbulent Parallel Momentum Transport due to Blobs

Y. Li^{1,2}, J. Li¹, and Z. Gao²

¹*Southwestern Institute of Physics, Chengdu, Sichuan, People's Republic of China*

²*Tsinghua University, Haidian, Beijing, People's Republic of China*

Corresponding Author: Y. Li, leeyang@swip.ac.cn

Meso-scale size structures including the blobs in the edge plasma can not only transport particle and heat out, but may also contribute to the plasma poloidal/toroidal rotation, namely, the momentum transport. Turbulent parallel momentum stress can be divided into three components, which are the diffusive, convective and residual parts. In the presented work, the triplet nonlinear term is derived by using EDQNM method in 3D Hasegawa–Wakatani system. It is shown that the triplet nonlinear term is comparable to the quasi-linear terms, i.e., the first two terms of quasi-linear stress, in strong turbulence regime such as blobs. If the radial scale length of large edge coherent structure is bigger than its poloidal scale length, nonlinear residual stress can provide opposite torque with respect to the quasi-linear ones and negative nonlinear diffusivity. These effects introduce inward momentum flux so that the rotation in edge region is possibly reversed and momentum is convected into core region. Moreover, it is found that nonlinear coupling for vorticity is the dominating mechanism in parallel momentum transport.

Modelling Runaway Electrons Dynamics in Tokamak Plasmas: Progresses and Challenges

Y. Peysson¹, G. Anastassiou², J.-F. Artaud¹, A. Budai³, A. Brizard⁴, J. Decker⁵, O. Embréus⁶, B. Erdos³, O. Ficker⁷, T. Fülöp⁶, R. S. Granetz⁸, L. Hesslow⁶, E. Hirvijoki⁶, K. Hizanidis², M. L. Hoppe⁶, Y. Kominis², T. Kurki-Suonio⁹, P. Lauber³, M. Lehnen¹⁰, R. Lohner³, J. Mlynář⁷, E. Nardon¹, S. Newton⁶, E. Nilsson¹, G. Papp¹¹, R. Paprock⁷, G. I. Pokol³, C. Reux¹, F. Saint-Laurent¹, K. Särkimäki⁹, A. E. Shevelev¹², C. Sommariva¹, A. Stahl⁶, R. A. Tinguely⁸, M. Vlainic¹³, G. J. Wilkie⁶, and P. Zestanakis²

¹Institut de Recherche sur la Fusion par confinement Magnétique (IRFM), Commissariat à l'énergie atomique (CEA/Cadarache), 13108 St. Paul lez Durance, France

²National Technical University of Athens, Zografou, Athens 15773, Greece

³INT, Budapest University of Technology and Economics, Budapest, Hungary

⁴Saint Michael's College, Colchester, VT 05439, USA

⁵Swiss Plasma Center (SPC), École polytechnique fédérale de Lausanne (EPFL), 1015 Lausanne, Switzerland

⁶Chalmers University of Technology, Göteborg, Sweden

⁷Institute of Plasma Physics AS CR v.v.i., Prague, Czech Republic

⁸Plasma Science & Fusion Center, MIT, Cambridge, MA 02139, USA

⁹Aalto University, Espoo, Finland

¹⁰International Thermonuclear Experimental Reactor (ITER), Cadarache Centre, 13108 St. Paul lez Durance, France

¹¹Max-Planck-Institut für Plasmaphysik, Garching, Germany

¹²Ioffe Institute, St. Petersburg, Russian Federation

¹³Ghent University, 9000 Ghent, Belgium

Corresponding Author: Y. Peysson, yves.peysson@cea.fr

The sudden termination of a plasma discharge known as a major disruption is a well-identified difficulty from the beginning of tokamak research, which remains still today particularly problematic for the design of a reliable fusion reactor. The key questions are principally related to the growth rate of relativistic electron population, closely linked to the level of the critical electrical field for an electron to run-away, and the upper energy limit that it can reach. Recently, very important achievements have been obtained in this domain. The introduction of the synchrotron radiation reaction force in kinetic calculations is shown to limit the upper energy of the runaway beam to 20–30 MeV consistent with observations [1]. Refined studies have also included the effect of bremsstrahlung radiation [2]. The calculation of the runaway avalanche growth rate has been improved by considering accurately the magnetic field inhomogeneity [3] and the screening effect of partially ionized impurities [4]. With the development of a synthetic diagnostic for the synchrotron radiation [5], numerical tools have reached the required level to perform realistic kinetic simulations of the runaway electron population for assessing effective control capabilities of existing techniques for ITER. A review of the progresses and challenges is performed.

References

- [1] J. Decker *et al.*, Plasma Phys. Contr. F., **58**, 025016 (2016).
- [2] O. Embréus *et al.*, New J. Phys., **18**, 093023 (2016).
- [3] E. Nilsson *et al.*, Plasma Phys. Contr. F., **57**, 095006 (2015).
- [4] L. Hesslow *et al.*, Phys. Rev. Lett., **118**, 255001 (2017).
- [5] M. Hoppe *et al.*, Nucl. Fus., **58**, 026032 (2018).

Runaway Electron Modelling in the ETS Self-Consistent Core Transport Simulator

G. I. Pokol¹, A. Hadar¹, B. Erdos¹, G. Papp², M. Aradi³, T. Jonsson⁴, Y. Peysson⁵, J. Decker⁶, M. L. Hoppe⁷, T. Fülöp⁷, D. Coster², D. Kalupin⁸, P. Strand⁷, and J. Ferreira⁹

The EUROfusion-IM Team

¹NTI, University of Technology and Economics (BME), Budapest, Hungary

²Max-Planck-Institut für Plasmaphysik, Garching, Germany

³Graz University of Technology, Fusion@ÖAW, Graz, Austria

⁴KTH Royal Institute of Technology, Stockholm, Sweden

⁵Institut de Recherche sur la Fusion par confinement Magnétique (IRFM),

Commissariat à l'énergie atomique (CEA/Cadarache), 13108 St. Paul lez Durance, France

⁶Swiss Plasma Center (SPC), École polytechnique fédérale de Lausanne (EPFL), 1015 Lausanne, Switzerland

⁷Chalmers University of Technology, Göteborg, Sweden

⁸EUROfusion Programme Management Unit Garching, Boltzmannstraße 2, 85748 Garching Germany

⁹Institute of Plasmas and Nuclear Fusion (IPNF), Instituto Superior Técnico (IST), 1049-001 Lisbon, Portugal

Corresponding Author: G. I. Pokol, pokol@reak.bme.hu

Relativistic runaway electrons are of major concern in tokamaks. Some nice tools have been developed in the recent decades, but we still miss a self-consistent simulation tool that could simultaneously capture all aspects of this phenomenon. The EUROfusion Code Development for integrated modelling project (WPCD) facilitates integration of different plasma simulation tools this by providing an Integrated Modelling framework (EU-IM) [1], and a standard data structure for communication that enables relatively easy integration of different physics codes. A three-level modelling approach was adopted to runaway electron simulation within the EU-IM [2]. Recently, a number of runaway electron modelling actors have been integrated into this framework. The first level of modelling (runaway indicator) is limited to the indication if runaway electron generation is possible or likely. The second level (runaway fluid) adopts a similar approach to the GO code [3], using analytical formulas to estimate changes in the runaway electron current density. The third level is based on the solution of the electron kinetics. One such code is LUKE [4] that can handle the toroidicity-induced effects by solving the bounce-averaged Fokker-Planck equation. Another approach is used in NORSE [5], which features full nonlinear collision operator that makes it capable of simulating major changes in the electron distribution, like slide-away. These runaway-electron modelling codes have been integrated into the EU-IM infrastructure, and into the European Transport Simulator (ETS) [6], which is a fully capable 1.5D core transport simulator. ETS with runaway fluid could be benchmarked to the GO code implementing similar physics [2]. Coherent integration of kinetic solvers requires more effort on the coupling, especially regarding the definition of the boundary between runaway and thermal populations, and on consistent calculation of resistivity. Some of these issues are discussed in detail providing some proposed solutions.

References

- [1] G. L. Falchetto *et al.*, Nucl. Fus., **54**, 043018 (2014).
- [2] G. I. Pokol *et al.*, ECA, **41F**, P2.178 (2017).
- [3] G. Papp *et al.*, Nucl. Fus., **53**, 123017 (2013).
- [4] Y. Peysson and J. Decker, Fusion Sci. Tech., **65**, 22 (2014).
- [5] A. Stahl *et al.*, Comput. Phys. Comm., **212**, 269 (2017).
- [6] D. Kalupin *et al.*, Nucl. Fus., **53**, 123007 (2013).

Energy Loss and Pitch Angle Scattering of Runaway Electrons due to Kinetic Instabilities

C. Liu¹, E. Hirvijoki¹, G. Y. Fu^{1,2}, D. P. Brennan³, A. Bhattacharjee^{1,3}, and C. Paz-Soldan⁴

¹*Princeton Plasma Physics Laboratory (PPPL), Princeton, NJ 08540, USA*

²*Zhejiang University, Xihu, Hangzhou, Zhejiang, People's Republic of China*

³*Princeton University, Princeton, NJ 08544, USA*

⁴*General Atomics, San Diego, CA 92186, USA*

Corresponding Author: C. Liu, cliu@pppl.gov

The effects of kinetic instabilities on the dynamics of runaway electrons in momentum space is investigated using a newly-developed simulation model, and the anomalous dissipation and the fast pitch angle scattering of runaway electrons in low energy are explained. The interaction of runaway electron avalanche and the kinetic instabilities are studied self-consistently using a quasi-linear model. Results show that excited whistler waves can cause runaway electrons to be scattered to large pitch angle and form vortices in momentum space, creating a new energy loss channel, which explains the higher-than-expected critical electric field and the loss of runaway electron population in low energy regime identified experimentally. This finding also explains the fast growth of electron cyclotron emission (ECE) signals observed in experiments.

Interactions of Runaway Electrons with Alfvén and Whistler Waves

D. A. Spong¹, D. P. Brennan², D. del-Castillo-Negrete¹, L. Carbajal Gomez¹, E. F. Jaeger³, C. Lau¹, C. Liu², C. S. Collins⁴, X. D. Du⁵, W. W. Heidbrink⁵, A. Lvovskiy⁶, R. A. Moyer⁷, C. Paz-Soldan⁴, K. E. Thome⁶, and M. A. Van Zeeland⁴

¹Oak Ridge National Laboratory (ORNL), Oak Ridge, TN 37831, USA

²Princeton University, Princeton, NJ 08544, USA

³XCEL Engineering Inc., Oak Ridge, TN 37830, USA

⁴General Atomics, San Diego, CA 92186, USA

⁵University of California Irvine, CA 92697, USA

⁶Oak Ridge Associated Universities (ORAU), Oak Ridge, TN 37831, USA

⁷University of California San Diego, CA 92093, USA

Corresponding Author: D. A. Spong, spongda@ornl.gov

Runaway electrons are of significant interest in tokamaks due to their potential for damage to plasma facing components. Runaways are of particular concern following disruptions when the plasma undergoes a thermal quench and a subsequent current quench; these lead to large loop voltages that can rapidly create runaways. Due to the risks of performing intense runaway experiments, the generation of runaways and the rate at which they can be suppressed is a crucial issue for modelling. Comparison of electric field thresholds from a range of tokamaks with theoretical predictions has shown that the observed thresholds have generally been higher than predictions [1]. This discrepancy can exist for a variety of reasons, but runaway-driven instabilities and scattering from plasma waves are mechanisms not taken into account in the existing predictions. In this paper, examples of both resonant and nonresonant runaway interactions with Alfvén and whistler waves are analyzed and compared with recent DIII-D experiments [2]. The analysis is based on relativistic Monte Carlo models that include runaway/partially ionized impurity collisions, synchrotron radiation, and wave mode structures. The mode structures are calculated using the TAEFL/FAR3D gyrofluid models (for Alfvén instabilities) and the AORSA all-orders full-wave RF model (for whistler instabilities). In addition to an improved understanding of runaway generation, this can also lead to new methods for runaway control.

References

- [1] R. S. Granetz *et al.*, Phys. Plasmas, **21**, 072506 (2014).
- [2] D. A. Spong *et al.*, submitted to Phys. Rev. Lett., (2018).

Time-Dependent Runaway Simulations: Ampère–Faraday Equations Implemented in CQL3D

R. W. Harvey¹, Y. V. Petrov¹, C. B. Forest², L. L. Lao³, and P. B. Parks³

¹CompX, Del Mar, CA 92014, USA

²University of Wisconsin-Madison, Madison, WI 53706, USA

³General Atomics, San Diego, CA 92186, USA

Corresponding Author: R. W. Harvey, rwharvey@compxco.com

The runaway electron distributions driven by a large toroidal electric field E_{tor} induced by the drop in the temperature profile due to disruption or pellets are comprehensively simulated by the 3D Fokker–Planck solver CQL3D [1], recently coupled to the Ampère–Faraday (A-F) equations. The evolution of the toroidal current in a plasma occurs on a resistive time scale τ_r , which is typically of the order of seconds in present tokamaks. From the Faraday EM equation, E_{tor} is proportional to the time derivative of the poloidal magnetic field, which, from the Ampère equation is proportional to the toroidal current. Thus, E_{tor} rapidly increases due to rapid temperature drops, to prevent change in the toroidal current faster than t_r . In simulations with KPRAD [2] of neon pellet injection into a DIII-D shot, T_e drops from 2 keV to 10 eV in 0.1 ms and Z_{eff} increases from 1 to 4, giving that E_{tor} increases $3500\times$ to 0.8 V/cm. As described in [3], this places much of the tail electron distribution beyond the Dreicer runaway velocity, giving so-called “hot-tail runaways” which for a time are the dominant source of runaways, more so than the knockon source. In this prior calculation, performed for a single flux surface, the toroidal current density is held constant on the basis that τ_r is large. Most of the initial current can be converted to runaway current which is then dangerous, particularly for ITER. The A-F model recently implemented in CQL3D, taking into account the time-development of the full-plasma-width E_{tor} on time-scales of order t_r , applies an iterative technique for the E_{tor} previously developed for a different application [4], maintaining the implicit-in-time evolution of CQL3D. The degree of runaway current formation is reduced in A-F augmented CQL3D, but the basic mechanism of “hot-tail runaways” [3] remains a dominant contribution to the runaway electrons at early times after the T_e drop.

Work supported by the U.S. Department of Energy, grants ER54744, DE-SC0016452 (GA SCREAM), and DE-FG02-95ER54309 (GA Theory).

References

- [1] R. W. Harvey and M. McCoy, “The CQL3D Fokker Planck Code”, www.compxco.com/cql3d.html.
- [2] D. G. Whyte *et al.*, Proc. 24th EPS Conf., Berchtesgaden, Germany (1997).
- [3] R. W. Harvey *et al.*, Phys. Plasmas, **7**, 4590 (2000).
- [4] K. Kupfer *et al.*, Phys. Plasmas, **3**, 3644 (1996).

Integrated Simulation of Runaway Electrons: A Backward Monte Carlo Approach for a Fluid-Kinetic Self-Consistent Coupling

D. del-Castillo-Negrete¹, J. D. Lore¹, G. Zhang¹, S. Seal¹, L. Carbajal¹, and D. A. Spong¹

¹Oak Ridge National Laboratory (ORNL), Oak Ridge, TN 37831, USA

Corresponding Author: D. del-Castillo-Negrete, delcastillod@ornl.gov

The dynamics of runaway electrons (RE) is a complex process and, although significant progress has been made in the understanding of individual isolated pieces of the puzzle, a predictive capability calls for an Integrated Simulation (IS) effort. In this presentation we report on recent progress on this problem. The goal is to use the BMC method [1] to couple a kinetic description of the RE population to a fluid description of the background plasma and the self-consistent evolution of the electric field. In addition, the IS includes a synchrotron emission (SE) synthetic diagnostic [2] for model validation. The main novel aspects of our contribution are the use of a probabilistic coupling based on the BMC method, the incorporation of the often-ignored configuration space dependent dynamics, and the use of a flux surface averaged transport model along with a Grad-Shafranov 2D equilibrium. At the heart of our IS effort is the recently developed Kinetic Orbit Runaway electron Code (KORC) that computes relativistic RE orbits using either full-orbit 6D (KORC-FO) or guiding centre (gyro-averaged) descriptions (KORC-GC) incorporating the full geometry of the magnetic field, the spatial dependence of the electric field, and synchrotron radiation damping. Collisions are incorporated using a Monte Carlo method with plasma temperature, plasma density and impurities dependent collision frequencies [3, 4, 5]. To account for the spatio-temporal variations of plasma parameters in KORC, we developed a fluid code that solves the time-dependent flux surface averaged transport equations [6]. Disruption mitigation is simulated by introducing an impurity neutral gas pellet. The kinetic information computed with KORC is feed back to the plasma state and electric field solvers using the BMC method that computes the RE production rate. As an application of the IS framework we study RE generation during rapid plasma shutdown by impurity injection in DIII-D and ITER-like plasmas.

References

- [1] G. Zhang *et al.*, Phys. Plasmas, **24**, 092511 (2017).
- [2] L. Carbajal *et al.*, Plasma Phys. Contr. F., **59**, 124001 (2017).
- [3] L. Carbajal *et al.*, Phys. Plasmas, **24**, 042512 (2017).
- [4] D. del-Castillo-Negrete *et al.*, Phys. Plasmas, accepted (2018).
- [5] D. A. Spong *et al.*, Submitted to Nuclear Fusion (2018).
- [6] J. Lore *et al.*, CP11.098 APS DPP Meeting (2017).

FIP: Fusion Engineering, Integration and Power Plant Design

Completion of the First TF Coil Structure of ITER

M. Nakahira¹, M. Iguchi¹, T. Sakurai¹, H. Ozeki¹, E. Fujiwara¹, K. Takano¹, Y. S. Hong¹, M. Ino¹, M. Nishino¹, N. Koizumi¹, N. Sawa², D. Hara², T. Inagaki², S. Y. Kim³, J. H. Choi³, S. S. Hwang³, and C. Luongo⁴

¹National Institutes for Quantum and Radiological Science and Technology (QST),

Naka Fusion Institute, Naka-shi, Ibaraki-ken, Japan

²Mitsubishi Heavy Industries, LTD, Kobe Shipyard & Machinery Works

³Hyundai Heavy Industries, Ulsan, Republic of Korea

⁴International Thermonuclear Experimental Reactor (ITER),

Cadarache Centre, 13108 St. Paul lez Durance, France

Corresponding Author: M. Nakahira, nakahira.masataka@qst.go.jp

This paper reports the completion of the first Toroidal Field Coil Structure (TFCS) of ITER of which Japan Domestic Agency (JADA) takes 100% share on procurement responsibility. The major technical challenges of the TFCS of ITER are: i) new material development for high ductility under 4 K cryogenic temperature; ii) application of partial penetration welding (PPW); iii) welding deformation control; iv) special ultrasonic test (UT) development considering attenuation by weldment of austenitic stainless steel; and, v) fitting of large (16 m × 9 m) complex D-shape structure for closure welding (CW) within tight tolerance of a range of 0.5 mm. Developed solutions for these challenges lead us to the successful completion of the first TF coil structure.

ITER TFCS requires both high strength and high ductility at cryogenic 4 K temperature. For this, special austenitic stainless steel was newly developed. This developed material is used at inboard straight leg which supports most severe electromagnetic force of 600 MN. JADA also developed a new method to keep fracture toughness requirement finding strong correlation between fracture toughness and Md30.

The PPW is applied to attachments with fracture mechanics assessment using data of crack propagation under cryogenic temperature. JADA developed new UT method to apply for PPW joints, which is to obtain the position of tip of discontinuity with its continuous length and then to assess the area of deviation from nominal position compared with maximum allowable defect area obtained by fracture mechanics.

The mechanical property at cryogenic temperature was checked for fracture toughness as well as yield strength of welded joints. The welding deformation was controlled by special welding process to keep balance of angular distortion. The attenuation of UT beam in the weld is compensated by transfer correction factor obtained by welding test piece made with actual material and weld metal. The TFCS was finally machined on its closure welding root that has a range of 0.5 mm gap and misalignment tolerance between two welding edges. For this, quite precise control was performed such as temperature control/compensation or setting of the machining position target based on as-machined data of the other parts. As a result of fitting test, CW roots were fit and the first TFCS of the ITER was successfully completed.

Completion of 1st ITER Gyrotron Manufacturing and 1 MW Test Result

Y. Oda¹, R. Ikeda¹, T. Nakai¹, K. Kajiwara¹, T. Kobayashi¹, K. Takahashi¹, K. Sakamoto¹, S. Moriyama¹, C. Darbos², and M. Henderson²

¹*National Institutes for Quantum and Radiological Science and Technology (QST),
Naka Fusion Institute, Naka-shi, Ibaraki-ken, Japan*

²*International Thermonuclear Experimental Reactor (ITER),
Cadarache Centre, 13108 St. Paul lez Durance, France*

Corresponding Author: Y. Oda, oda.yasuhisa@qst.go.jp

This paper presents a summary of recent progress pertaining to the manufacturing and inspection of ITER gyrotrons and their operation system in QST. Major achievements are as follows: i) The final design of ITER gyrotron was accomplished and manufacturing of two ITER gyrotrons was finished. Then their factory acceptance test (FAT) in QST has started with ITER relevant high voltage power supply configuration. The 1st ITER gyrotron has achieved 1 MW output power for 10 s pulse and 200 kW operation for 300 s which suggests thermally stable condition and sufficient cooling performance for 1 MW long pulse operation; ii) The coupling function of gyrotron power into the transmission line (TL) waveguide was improved and calculation result of coupling efficiency was increased as high as 96.9% for the fundamental mode purity in waveguide inlet which could produce the sufficient LP01 mode purity in whole EC H&CD system. These results lead to success of ITER EC H&CD system construction toward first plasma.

Outcome of R&D Programme for ITER ICRF Power Source System

R. G. Trivedi¹, A. Mukherjee¹, R. Singh¹, K. Rajnish¹, D. G. Soni¹, S. Verma¹, G. Suthar¹, A. Jha¹, A. P. Subbarao¹, M. Patel¹, R. Anand¹, R. Agarwal¹, K. Mohan¹, J. V. S. Harikrishna¹, H. Machchhar¹, P. Vasava¹, H. Patel¹, H. Dalicha¹, U. K. Baruah¹, A. Patel¹, N. P. Singh¹, N. S. Goswami¹, K. R. Mehta¹, D. V. Upadhyay¹, H. Dhola¹, A. E. White², D. Francois², J. Sainz², and K. Kozard²

Rapporteured by: Y. Oda

¹ITER-India, Institute for Plasma Research (IPR), Bhat, Gandhinagar, India

²Continental Electronics Corporation, Dallas, TX 75227, USA

Corresponding Author: R. G. Trivedi, rgtrivedi@iter-india.org

As a part of in-kind contribution, India is responsible to deliver nine RF sources (1 prototype and 8 production series) to ITER, each having power handling capability of 2.5 MW/CW at VSWR 2:1 in the frequency range 35–65 MHz or 3.0 MW/CW at VSWR 1.5:1 in the frequency range 40–55 MHz, along with other stringent requirements. As there is no such amplifier chain able to meet the output power specifications as per ITER need, the RF source consists of two parallel three-stage amplifier chains, with a combiner circuit on the output side. This kind of RF source is unique in terms of its stringent specifications. A voluntary R&D programme by India has been initiated for establishing the high power technology prior to prototype and series production, using Diacode and Tetrode tubes. In this program, single chain experimentation at 1.5 MW for 2000 s is conducted for the frequency range 35–65 MHz up to VSWR 2:1, with any phase of reflection coefficient. The main objective for the R&D test is to confirm the system performance for the power, duration and frequency range as per ITER need and to check the reliability of both the tube and the amplifier with matched as well as with mismatched load (up to VSWR 2:1), which essentially simulates the plasma load condition.

To support the R&D program, a dedicated high power test facility has been developed at ITER-India to test RF amplifiers based on both the technologies. For Diacode based system, high power ITER relevant tests completed in 2016 and reported elsewhere [1]. Over the past two years, assembly and integration of R&D RF source using Tetrode technology at Indian test facility is completed with validation of all the relevant subsystems/systems as standalone mode. The high power RF test using Tetrode based RF amplifier achieved 1.7 MW of power for 3600 s duration at 36 MHz. For other ITER operating frequencies, the system was operated at 1.5 MW/2000 s successfully. This paper reports commissioning of RF amplifier using Tetrode technology with various operating scenarios, dissipation limit, safety system and challenges faced during high power operation at Indian test facility and describes the final outcome of R&D activity.

References

[1] A. Mukherjee *et al.*, IAEA FEC–2016, Kyoto, Japan, [FIP/1-5](#), (2016).

Recent Progress in the Development of the European 1 MW, 170 GHz CW Gyrotron for ITER

G. Gantenbein¹, F. Albajar², S. Alberti³, K. A. Avramidis¹, W. Bin⁴, A. Bruschi⁴, J. Chelis⁵, F. Fanale⁴, F. Legrand⁷, V. Hermann⁷, J.-P. Hogge³, S. Illy¹, Z. C. Ioannidis¹, J. Jin¹, J. Jelonnek¹, W. Kasperek⁶, G. P. Latsas⁵, C. Lechte⁶, M. Lontano⁴, I. G. Pagonakis¹, T. Rzesnicki¹, P. Sanchez², C. Schlatter³, M. Schmid¹, I. G. Tigelis⁵, M. Thumm¹, M. Q. Tran³, A. Zein¹, and A. Zisis⁵

Rapporteured by: Y. Oda

¹Karlsruhe Institute of Technology (KIT), Karlsruhe, Germany

²F4E: Fusion for Energy, ITER EU Centre, 08019 Barcelona, Spain

³Swiss Plasma Center (SPC), École polytechnique fédérale de Lausanne (EPFL), 1015 Lausanne, Switzerland

⁴Istituto di Fisica del Plasma (IFP), Consiglio Nazionale delle Ricerche (CNR), 20125 Milan, Italy

⁵National and Kapodistrian University of Athens, Greece

⁶Thales Electron Devices S.A., Velizy, France

⁷Institut für Grenzflächenverfahrenstechnik und Plasmatechnologie (IGVP), Univ. Stuttgart, Germany

Corresponding Author: G. Gantenbein, gerd.gantenbein@kit.edu

The European 1 MW, 170 GHz industrial prototype CW gyrotron for ECRH&CD on ITER is a conventional (hollow-cavity) gyrotron, which is being developed by the European Gyrotron Consortium (EGYC) in cooperation with the industrial partner Thales Electron Devices (TED), under the coordination of the European Joint Undertaking for ITER and the Development of Fusion Energy (F4E). The CW industrial prototype was extensively tested in the short-pulse regime (with pulse length up to 10 ms) and operated under long-pulse conditions with pulse lengths of up to 180 s, which is the limit at the high-voltage (HV) power supply currently available at KIT. In this contribution we report on the performance of the tube during the long-pulse operation at the KIT test facility, details regarding the operating points are presented and the long-pulse phase of the experiments with pulses up to 180 s is analyzed.

Technologies for Realization of Large Size RF Sources for –ve Neutral Beam Systems for ITER: Challenges, Experience and Path Ahead

J. Joshi^{1,2}, A. K. Chakraborty¹, H. Patel¹, M. Singh¹, M. Bandyopadhyay^{1,2}, E. Pfaff³, J. Schäfer³, C. Eckardt³, A. Metz³, and M. Gelfert⁴

¹ITER-India, Institute for Plasma Research (IPR), Bhat, Gandhinagar, India

²Homi Bhabha National Institute (HBNI), Anushakti Nagar, Mumbai 400094, India

³PVA Industrial Vacuum Systems GmbH, Wettenberg, Germany

⁴RI Research Instruments GmbH, Bergisch Gladbach, Germany

Corresponding Author: J. Joshi, jaydeep.joshi@iter-india.org

Technologies for manufacturing of small and medium size ion sources (up to four RF drivers) for positive and negative neutral beam systems have been evolved over last many decades and such ion sources are being successfully operated at various experimental facilities across the world. However, as the need arises for the larger size ion sources (eight drivers) for ITER diagnostics and heating neutral beam systems, several existing manufacturing technologies and considerations have to be upgraded and re-evaluated to qualify them for: 1) highest vacuum quality class; and 2) nuclear environment. Diagnostic Neutral Beam (DNB) source is the first candidate in a family of such big size ion sources, being manufactured according to the ITER specification with “re-evaluated” manufacturing technologies and it throws light on many unforeseen challenges as manufacturing progresses. The nature of challenges are mainly related to usage of the material with radioprotection requirement (i.e., restricted contents of Co wt%0.05, Nb wt%0.01 and Ta wt%0.01), special requirements on weld joint configuration to enable full penetration with 100% volumetric inspectability, dissimilar material welding technologies, machining process development to meet stringent dimensional accuracies (in the range of 10–50 μm) of individual “angled” grid segment to achieve overall alignment of ± 0.2 mm, electro-deposition of copper with thickness > 3 mm over the angled surfaces with control over distortion, vacuum brazing, restricted usage of silver for brazing and plating purpose, development of electrical isolators with customized electrostatic shield, threaded connection between metal and alumina load carrying capacity of 10 kN with electrical isolation of 140 kV in vacuum.

The paper shall present experience gathered in the development of the above mentioned manufacturing technologies, the methodology adopted for mitigating the practical limitations, prototyping to establish and qualify the manufacturing procedure, evaluating the nonconformities, assessment of deviation proposals, in compliance with ITER specifications. In summary, the experience generated during the manufacturing of DNB Beam source, presented here, is aimed to help in generating the recipe manufacturing and providing the “re-evaluated” technical specifications for upcoming ITER neutral beam sources.

Progress in the ITER Neutral Beam Test Facility

V. Toigo¹, D. Boilson², T. Bonicelli³, A. K. Chakraborty⁴, M. Kashiwagi⁵, C. Rotti², and P. Sonato¹

Rapporteured by: J. Joshi

¹*Consorzio RFX, Associazione EURATOM-ENEA sulla Fusione, Padova, Italy*

²*International Thermonuclear Experimental Reactor (ITER),
Cadarache Centre, 13108 St. Paul lez Durance, France*

³*F4E: Fusion for Energy, ITER EU Centre, 08019 Barcelona, Spain*

⁴*Institute for Plasma Research (IPR), Bhat, Gandhinagar, India*

⁵*National Institutes for Quantum and Radiological Science and Technology (QST),
Naka Fusion Institute, Naka-shi, Ibaraki-ken, Japan*

**NBTF Team and Contributing Staff of IO2, F4E3, QST5, IPR4*

Corresponding Author: V. Toigo, vanni.toigo@igi.cnr.it

The ITER Heating Neutral Beam (HNB) injectors, one of the tools necessary both to achieve burning conditions and to control plasma instabilities, are characterized by such demanding parameters as to require the construction of a test facility dedicated to their development and optimization. This facility, called NBTF, is in an advanced state of realization in Padua, Italy, with the direct contribution of the Italian government, through the Consorzio RFX as the host entity, IO, the in kind contributions of three DA's (F4E, JADA, INDA) and the technical and scientific support of various European laboratories and universities.

The NBTF hosts two experiments: SPIDER and MITICA. The former is devoted to the optimization of the HNB and DNB ion sources and to the achievement of the required source performances. It is based on the RF negative ion source concept developed at IPP Garching. MITICA is the full size prototype of the ITER HNB, with an ion source identical to the one used in SPIDER.

The construction and installation of SPIDER plant systems was successfully completed with their integration into the facility, followed by integrated commissioning with control (CODAS), protection and safety systems. The mechanical components of the ion source have been installed inside the vessel and connected to the plants. Finally, the integrated commissioning of the whole system ended positively and the first experimental phase began. The realization of the MITICA project is well advanced, although the completion of the system and its entry into operation is expected in 2022 due to the long procurement times of the in-vessel mechanical components. In particular, the power supply designed to operate at 1 MV are in an advanced phase of realization, all the high voltage components have been installed and the complex insulation test phase has begun in 2018. Furthermore, all the other auxiliary plant systems are being installed and/or are undergoing testing. This paper gives an overview of the progress of the NBTF realization with particular emphasis on issues discovered during this phase of activities and to the adopted solutions in order to minimize the impact on the schedule while maintaining the goals of the facilities. Finally, the first results obtained with SPIDER experimentation and with the 1 MV insulation tests on the MITICA HV components will be presented.

Demonstration of 1 MV Vacuum Insulation for the Vacuum Insulated Beam Source in the ITER NB System

A. Kojima¹, H. Tobar¹, N. Umeda¹, M. Kashiwagi¹, J. Hiratsuka¹, M. Ichikawa¹, N. Shibata¹, Y. Yamashita¹, M. Dairaku¹, H. Yamanaka¹, K. Y. Watanabe¹, Y. Yamano², and L. R. Grisham³

Rapporteured by: J. Joshi

¹*National Institutes for Quantum and Radiological Science and Technology (QST),
Naka Fusion Institute, Naka-shi, Ibaraki-ken, Japan*

²*Saitama University, Saitama, Saitama-ken 338-8570, Japan*

³*Princeton Plasma Physics Laboratory (PPPL), Princeton, NJ 08540, USA*

Corresponding Author: A. Kojima, kojima.atsushi@qst.go.jp

For the ITER neutral beam (NB) system, a measure to achieve the 1 MV vacuum insulation of the beam source have been developed. For this purpose, a design basis for 1 MV vacuum insulation has been developed by integrating previous empirical scaling for plane and coaxial electrodes and new scaling for area with locally-concentrated electric field. Consequently, as the measure, the beam source is surrounded by more than three intermediate electrostatic shields instead of single gap to sustain 1 MV. Effectiveness of the shields designed by the design basis was experimentally verified by using a part of the beam source. The voltage holding capability has been significantly improved from 0.7 MV to 1 MV. This result ensures the 1 MV vacuum insulated beam source in the ITER NB system.

Diagnostic Mirrors for ITER: Research in a Frame of International Tokamak Physics Activity

A. Litnovsky¹, V. S. Voitsenya², R. Reichle³, M. Walsh³, A. G. Razdobarin⁴, A. Dmitriev⁴, N. A. Babinov⁴, L. Marot⁵, L. Moser⁵, R. Yan⁶, M. Rubel⁷, S. Moon⁷, S. G. Oh⁸, P. Shigin³, A. Krimmer¹, V. Kotov¹, and P. Mertens¹

The Specialists Working Group on First Mirrors, ITPA Topical Diagnostics Group

¹*Institute of Energy and Climate Research, Forschungszentrum Jülich, Jülich, Germany*

²*National Science Center, Kharkov Institute of Physics and Technology (KIPT), Kharkov, 61108, Ukraine*

³*International Thermonuclear Experimental Reactor (ITER),*

Cadarache Centre, 13108 St. Paul lez Durance, France

⁴*Ioffe Institute, St. Petersburg, Russian Federation*

⁵*Universität Basel, 4056 Basel, Switzerland*

⁶*Institute of Plasma Physics, Chinese Academy of Sciences, Hefei, Anhui, People's Republic of China*

⁷*KTH Royal Institute of Technology, Stockholm, Sweden*

⁸*Ajou University, Suwon 16499, Republic of Korea*

Corresponding Author: A. Litnovsky, a.litnovsky@fz-juelich.de

Mirrors will be used as first plasma-viewing elements in optical and laser-based diagnostics in ITER. Deterioration of the mirror performance due to, e.g., sputtering of the mirror surface by plasma particles or deposition of plasma impurities will hamper the entire performance of the affected diagnostic. The Specialists Working Group on First Mirrors (FM SWG) in the Topical Group on Diagnostics of the International Tokamak Physics Activity (ITPA) plays a crucial role in finding solutions for diagnostic first mirrors. Sound progress was achieved during the past decade. Single crystal (SC) rhodium (Rh) mirrors became available. These SC Rh and molybdenum (Mo) mirrors survived in conditions corresponding to ~ 200 cleaning cycles without a degradation of reflectivity. These results are important for a mirror cleaning system, based on sputtering of contaminants by plasma. Efforts are invested to the physics understanding of a cleaning discharge. Ion energy distribution and flux in radiofrequency (RF) discharge have been studied. Repetitive cleaning was tested on several mirror materials. Experiments were comprised of contamination and cleaning cycles. The reflectivity of SC Mo mirrors was preserved after 34 cycles. First in-situ cleaning was conducted in EAST with a mock-up mirror of ITER Edge Thomson Scattering using RF plasma. Contaminants from the mock-up mirror were removed. Mirror contamination can also be suppressed by a protecting diagnostic duct. A deposition mitigation duct system was exposed in KSTAR. The real-time measurement of deposition in the diagnostic duct was pioneered during this experiment. Results evidenced the dominating effect of the wall conditioning and baking on contamination inside the duct. A baffled cassette with mirrors was exposed in the main wall of JET ILW for 23.6 plasma hours. No significant degradation of reflectivity was measured on mirrors in the ducts. Predictive modelling was advanced. A model for the particle transport, deposition and erosion inside the port-plug was used in selecting an optical layout of the ITER core charge-exchange recombination spectroscopy diagnostic. These achievements contributed to the focussing of the first mirror research, accelerating the diagnostic development. Predictive modelling requires more efforts to be invested. Ensuring the progress in the remaining crucial areas will be a focus of the future work of the FM SWG.

Integration of Thomson Scattering and Laser-Induced Fluorescence in ITER Divertor: Engineering and Performance Analysis

E. E. Mukhin¹, G. S. Kurskiev¹, A. V. Gorbunov², D. S. Samsonov¹, S. Y. Tolstyakov¹, A. G. Razdobarin¹, N. A. Babinov¹, A. N. Bazhenov¹, E. B. Berik³, I. M. Bukreev¹, P. V. Chernakov⁴, Al. P. Chernakov⁴, An. P. Chernakov⁴, A. M. Dmitriev¹, D. I. Elets¹, M. M. Kochergin⁷, A. N. Koval¹, A. S. Kukushkin^{2,5}, M. G. Levashova², A. E. Litvinov¹, V. S. Lisitsa², S. V. Masyukevich¹, A. N. Mokeev⁶, V. A. Solovei¹, V. V. Solokha¹, I. B. Tereschenko¹, L. A. Varshavchik¹, K. Y. Vukolov², P. Andrew⁷, M. Kempenaars⁷, G. Vayakis⁷, and M. Walsh⁷

¹*Ioffe Institute, St. Petersburg, Russian Federation*

²*National Research Centre "Kurchatov Institute", Moscow, Russian Federation*

³*ESTLA Ltd., Riia 185, 51014 Tartu, Estonia*

⁴*Spectral-Tech ZAO, St. Petersburg, Russian Federation*

⁵*National Research Nuclear University "MEPhI", Moscow, Russian Federation*

⁶*International Thermonuclear Experimental Reactor (ITER),*

Project Centre "ITER", Moscow, Russian Federation

⁷*International Thermonuclear Experimental Reactor (ITER),*

Cadarache Centre, 13108 St. Paul lez Durance, France

Corresponding Author: E. E. Mukhin, e.mukhin@mail.ioffe.ru

This paper describes the benefits and challenges of divertor Thomson scattering 55.C4 (DTS) and laser-induced fluorescence 55.EA (LIF) integration into divertor port #8 of ITER. A main challenge for the DTS system is to measure extremely low electron temperatures in the vicinity of the divertor plates. The cool dense divertor plasma leads to pronounced collective effects and significant distortions of the TS spectra. Therefore, standard TS signal processing, valid for light scattering on a swarm of free electrons, is already invalid. To examine the real DTS performance, we apply a special simulation technique based on synthetic experiments. The estimated measurement accuracies of electron temperature and density are quite better than the specified technical requirements, in spite of the pronounced collective effects. On the contrary, in the case of low electron density, when the classical TS spectrum is expected, the diagnostics performance degrades significantly, though still satisfying the technical requirements. Currently, the LIF diagnostic measures He atom density using a collisional-radiative model (CRM) which gives a relation between the fluorescence and plasma parameters. Required for CRM electron parameters are taken from DTS diagnostics. The temporal forms of the He fluorescence are dependent on electron parameters and the pumping laser pulse characteristics. Therefore, LIF can measure electron density in the range of 10^{18} – $10^{20}/\text{m}^3$ analyzing the temporal behaviour of He fluorescence with the He CRM. This technique helps expand the measurable range of electron density. The main advantage of this LIF measurements is that calibration of the collection system spectral and/or absolute sensitivity is not required, contrary to the DTS approach. Both DTS and LIF are laser aided diagnostics; hence, it seems attractive to develop universal laser and probing optics, which is the most sophisticated and expensive part of any ITER optical diagnostics. The engineering solutions discussed and challenges of the DTS and LIF integration includes collinear combination of DTS and LIF lasers, laser mirrors, collection mirrors, etc. Although the proposed solutions are considered in terms of ITER divertor compatibility, their use in currently operating magnetic confinement devices is also under discussion.

Current Design and R&D Progress of CN HCCB TBS

X. Wang¹, K. Feng¹, Y. Chen¹, L. Zhang¹, Y. Feng¹, X. Wu¹, H. Liao¹, X. Ye¹, F. Zhao¹, Q. Cao¹, F. Wang¹, B. Gong¹, Q. Wang¹, B. Zhou¹, C. Pan¹, M. Xu¹, X. Duan¹, M. Wang², K. He², D. Luo³, and Y. Yao³

The Chinese HCCB TBM Team

¹Southwestern Institute of Physics, Chengdu, Sichuan, People's Republic of China

²China International Nuclear Fusion Energy Program Execution Center, Beijing 100862, People's Republic of China

³China Academy of Engineering Physics, Mianyang, People's Republic of China

Corresponding Author: X. Wang, wangxy@swip.ac.cn

As the testing mockup of tritium breeding blanket for DEMO, Chinese Helium Coolant Ceramic Breeder (HCCB) Test Blanket System (TBS) are under developing by China and will be tested in ITER to verify the key tritium breeding blanket technologies. After the approval of conceptual design by ITER Organization in 2015, the design optimization and more R&D activities for HCCB TBS have been under implementation for preliminary design phase.

As the structural material of TBM module, eight tons RAFM steel (CLF-1) plates and forgings have been fabricated and a certification of 3.2 requested by EU Pressure Equipment Directive 97/23/EC (PED) has been obtained for CLF-1 steel. The fabrication techniques for the functional materials, beryllium pebble and Li_4SiO_4 pebble, have also been developed and the properties have tested. The new manufacture facility for Li_4SiO_4 pebble is under construction and the manufacture facility for beryllium pebble was upgraded to achieve production rate 10 kg/batch.

Recently the TBM-set design was significantly optimized and the whole integration method of TBM and the fabrication procedure plan has been updated. The results show that the total heat deposition in TBM was similar with conceptual design, while the tritium production ratio was slightly higher. The fabrication technology of TBM is under development. Following the fabrication procedure plan of TBM, semiprototype of TBM is under fabrication to verify the final integration plan.

Ancillary systems have been optimized considering the review comments, safety and interface requirements. Accordingly the process flow diagram (PFD) and pipe and instrumentation diagram (PID) have been updated, but still some interface issues with ITER facility have been identified and have to be solved. The system performance has been assessed to optimize the operation control plan and equipment requirements. Several test platforms for breeding blanket technology development have been constructed and started experiments to test components, processes and get the operation data. At same time, the safety assessment of HCCB-TBS has been updated and it shows that HCCB TBS has not overtemperature issues for all accident cases. Considering the limited inventories and multiple confinement barriers, no major safety consequences had been identified through accident assessments.

Progress in Developing ITER and DEMO First Wall Technologies at SWIP

J. Chen¹, X. Liu¹, P. Wang¹, J. Wang¹, L. Cai¹, F. Jin¹, X. Zhu¹, Q. Li¹, P. Huang¹, Z. Wei¹, Y. Chen¹, M. Xu¹, and X. Duan¹

¹Southwestern Institute of Physics, Chengdu, Sichuan, People's Republic of China

Corresponding Author: J. Chen, chenjm@swip.ac.cn

The ITER enhanced heat flux (EHF) FW panel utilizes a Be/CuCrZr/316L(N) joint structure with hypervapotron (HVT) cooling channel in the CuCrZr heat sink to withstand cyclic surface heat flux up to 4.7 MW/m². For Chinese CFETR and DEMO, the heat load will be much lower and a simple W/RAFM steel joint with cooling channels in the steel will be used. For all of them, reliable material bonding joint is one of the essential requirements. It is found that the thermal fatigue life of the ITER EHF FW structure could be increased by more than one order if a bottom groove is added to the HVT channel. A hot iso-static pressing (HIP) joining technology has been successfully developed for bonding Be tiles onto the CuCrZr alloy heat sink with a Ti/Cu interlayer. Full-size EHF FW fingers were manufactured with a success rate of ~ 90%. Analyses show six interlayers with Cu-Ti intermetallic phases formed at the interface during the HIP process. Thinning the Cu4Ti layer could lead to a defect-free Be/Cu interface. An ITER EHF FW semiprototype with six Be/CuCrZr/316L(N) fingers was successfully manufactured in 2015. Two finger pairs were subjected to thermal fatigue test at 4.7 MW/m² for 7500 cycles and 5.9 MW/m² for 1500 cycles under active water cooling in 2016. The finger pairs remain perfect without any damage. A post-test dimensional examination showed merely 20 μm deformation at maximum. The vacuum tightness of their HVT cooling channels were kept as good as before the test. Several manufacture routes are under investigation for W/RAFM steel joints. The key is to use a low activation interlayer to accommodate the thermal stress between them. A defect-free joint was made by brazing at 1270°C with Fe-Cr-B-Si amorphous filler material and pure V as accommodation layer. The property of the CLF-1 RAFM steel was fully recovered by a PWHT. In developing the fast CVD W coating on CLF-1 steel, a CVD TiN coating was firstly applied on the steel acting as a tritium permeation barrier. Good bonding performance is presented and neither obvious defect nor detachment is found at the working temperature of 550°C. For the HIP joining, a couple of joints have been made by HIP at 740°C using pure Cr, V and Fe interlayer. Further tests will be done at higher HIP temperature with fast cooling of > 20°C/min to enable the recovery of the microstructure and properties of the CLF-1 steel.

Technologies for Plasma-Facing Wall Protection in EU DEMO

T. R. Barrett¹, W. Arter¹, B. Chuilon¹, M. Kovari¹, F. Maviglia², M. L. Richiusa¹,
E. Rosa Adame¹, R. Tivey¹, and Z. Vizvary¹

¹Culham Centre for Fusion Energy (CCFE), Culham Science Centre, Abingdon, UK

²EUROfusion Consortium, Power Plant Physics & Technology (PPPT), Boltzmannstraße 2, Garching, Germany

Corresponding Author: T. R. Barrett, tom.barrett@ukaea.uk

The plasma-facing wall of the main chamber in DEMO will be unlike any current tokamak. The blanket first wall (FW) is to be actively-cooled reduced-activation steel (Eurofer) under a thin plasma-facing tungsten armour. To help control cost, modest misalignment of this wall must be tolerable at least with respect to a relatively quiescent divertor plasma flat-top equilibrium. However, with present knowledge it is not possible to exclude normal or off-normal plasma transient phases, and during some of these transients the blanket FW will not be sufficient in terms of the engineering heat flux limit of the plasma-facing technology. Particularly challenging are transients during which the plasma is limited, for example during plasma start-up or vertical displacement events (VDEs). In EU-DEMO we propose discrete limiters, with large gaps between them, which serve to protect the blanket FW from these plasma transients. In this work, two proposed protection components are presented: an equatorial port limiter which receives power during the start-up phase, and an upper wall “dump” panel which is intended to sacrificially protect the blanket system in the event of an upward-VDE.

The plasma-facing component (PFC) engineering designs, although an evolution of the ITER W/CuCrZr divertor monoblock technology, are tailored according to their respective transient loading requirements. For the start-up limiter designed for 30–60 s ramp-up phase, we show by thermal-structural finite element analyses that the heat sink properties of tungsten can be exploited to improve the component heat flux limit. This equatorial limiter features a water-cooled Eurofer plug behind the PFCs for neutron shielding and connection to the stainless steel port plug. The manufacturing and assembly proposal for the limiter is described and the effect of the limiter on reactor tritium breeding ratio is shown. In the case of the upper dump PFC, the huge amount of energy deposited during the VDE could lead to extensive melt damage of the tungsten armour. However, the PFC described here has features to deliberately channel the heat flux to the sides and rear of the coolant pipe, and we show by transient engineering analyses that this technique can markedly increase the heat load at which structural failure of the coolant pipe occurs, reducing the likelihood of a loss of coolant accident.

Active Conditioning of ASDEX-Upgrade Tungsten PFCs through Boron Particulate Injection

R. Lunsford¹, V. Rohde², A. Bortolon¹, R. Dux², A. Herrmann², A. Kallenbach², R. M. McDermott², R. Maingi¹, D. K. Mansfield¹, A. Nagy¹, R. Neu², and E. Wolfrum²

The ASDEX-Upgrade Team

¹Princeton Plasma Physics Laboratory (PPPL), Princeton, NJ 08540, USA

²Max-Planck-Institut für Plasmaphysik, Garching, Germany

Corresponding Author: R. Lunsford, rlunsfor@pppl.gov

The injection of boron (B) and boron nitride (BN) powders into ASDEX-Upgrade (AUG) H-mode discharges have shown the ability to effectively control tungsten influx in low density/collisionality operational regimes, similar to conventional boronization methods. A newly designed impurity powder dropper was installed onto AUG with 5 μm diameter BN powder, and 50 μm B powder (99%+ purity) loaded into separate dropper assemblies. The sub-mm powder particles are gravitationally accelerated into the upper edge of a lower single null H-mode plasma. Discharges with $I_p = 800$ kA, $n_e = 6 \times 10^{19}/\text{m}^3$, $P_{\text{NBI}} = 10$ MW, and a conformal boundary shape were used for the conditioning sequences. These were followed by different discharges to evaluate the effects of the conditioning. The first experiment was performed with five BN conditioning discharges, in which injected B was varied from $\sim 4 \times 10^{18}$ atoms/dischARGE to $\sim 4 \times 10^{20}$ atoms/dischARGE. Visible spectroscopy measurements at the outer limiter showed increases in both boron and nitrogen signal levels, well as elevated boron levels in the divertor and an increase in P_{RAD} by greater than a factor of 2. Globally the BN injection also improved energy confinement by 10–20%, similar to gaseous N_2 injection. Discharges with increasing B injection rates were also performed. Injecting, 9.2×10^{21} atoms of pure B resulted in minimal impact on plasma performance and up to 50% increase in radiated power. To test the conditioning effect of B powder, a sequence of discharges with magnetic perturbations for ELM suppression were conducted afterwards. Historically these discharges are very sensitive to wall conditions. However, following the B conditioning discharges, all three attempts to run low density discharges with ELMs suppressed by magnetic perturbations were successful. These preliminary results suggest that the application of B containing powders can be used to both improve plasma performance in real-time, and improve wall conditions. Furthermore the injection system is capable of injecting a wide number of impurities (B, BN, B_4C , Li, C, Sn, Mo, W, ...) for a range of studies. Similar systems are being installed on the EAST and DIII-D devices. Results from these and forthcoming studies on AUG, and possibly other devices, will be reported.

The U.S. authors supported by U.S. Department of Energy contract DE-AC02-09CH11466.

Advances in Predictive Thermo-Mechanical Modelling for the JET Divertor Experimental Interpretation, Improved Protection, and Reliable Operation

D. Iglesias¹, W. Arter¹, I. Balboa¹, P. Bunting¹, C. D. Challis¹, J. W. Coenen², Y. Corre³, S. Esquembri⁴, S. Jachmich^{5,6}, K. Krieger⁷, G. F. Matthews¹, R. A. Pitts⁸, V. Riccardo⁹, M. L. Richiusa¹, M. Porton¹, F. G. Rimini¹, S. Silburn¹, V. Thompson¹, R. Otin¹, D. F. Valcarcel¹, L. Vitton-Mea¹⁰, Z. Vizvary¹, and J. Williams¹

The JET Contributors

¹Culham Centre for Fusion Energy (CCFE), Culham Science Centre, Abingdon, UK

²Institute of Energy and Climate Research, Forschungszentrum Jülich, Jülich, Germany

³Institut de Recherche sur la Fusion par confinement Magnétique (IRFM), Commissariat à l'énergie atomique (CEA/Cadarache), 13108 St. Paul lez Durance, France

⁴UPM-I2A2, Universidad Politécnica de Madrid (UPM), Madrid, Spain

⁵EUROfusion Programme Management Unit Culham, Culham Science Centre, Abingdon, UK

⁶Laboratory for Plasma Physics, ERM/KMS, Brussels, Belgium

⁷Max-Planck-Institut für Plasmaphysik, Garching, Germany

⁸International Thermonuclear Experimental Reactor (ITER), Cadarache Centre, 13108 St. Paul lez Durance, France

⁹Princeton Plasma Physics Laboratory (PPPL), Princeton, NJ 08540, USA

¹⁰École Nationale Supérieure de Physique, Électronique et Matériaux (Phelma), Institut Polytechnique de Grenoble Alpes, France

Corresponding Author: D. Iglesias, daniel.iglesias@ukaea.uk

The JET targets are the in-vessel components which receive the largest sustained thermal load. Operating instructions limit the energy and maximum surface temperature allowed for each shot, while IR cameras are used for protection during each discharge. Surface delamination and radial cracks have been observed in the outboard tungsten-coated CFC tiles, while bulk tungsten special lamellae were intentionally melted in dedicated experiments. These different types of damage were not reproducible using existing models and tools. Several analysis and development activities have been performed during the last campaigns for their improvement, covering from the prediction of the plasma parallel heat flux density to the transient thermo-mechanical behaviour of the tiles. The parallel heat flux density is reconstructed from the surface temperature measurements (acquired by the experimental IR cameras) using inverse analysis techniques. New inverse algorithms have been developed for a realistic representation of the tile geometry and coating thickness. A set of geometrical and loading projection corrections have been introduced which explain a reduction of the measured parallel heat flux density of up to 1/3 when compared to previous estimations.

Once the corrected parallel heat flux has been characterized, predictive analysis can be run for ensuring that the maximum temperature and stress remain within the allowable limits. The integrity assessment of the tiles uses a profile of the heat load defined by an engineering footprint, which has been correlated to several plasma parameters. The engineering footprint averages the inter-ELM, ELM transients, and associated strike point movements, leading to a wider footprint compared to that obtained using typical inter-ELM scaling laws. This has turned out to be critical for replicating the deformation effects of the tiles.

Continued...

The observed failure modes can now be reproduced—and therefore avoided—by means of coupled-field 3D thermo-mechanical models. All these improvements have been implemented in integrated analysis tools which can predict the behaviour of the divertor tiles in a power consistent manner. This development carried out at JET supports the experimental understanding, enhances the real-time protection systems, improves the evaluation of the operating instructions, and is also transferable to ITER.

Overview of the DEMO Design-Staged Approach in Europe

G. Federici¹, C. Bachmann¹, C. Baylard¹, S. Ciattaglia¹, F. Cisondi¹, E. Diegele¹, H. Ebert², T. Franke¹, C. Gliss¹, T. Härtl¹, G. Keech¹, R. Kembleton³, F. Maviglia¹, B. Meszaros¹, M. Siccino¹, C. Vorpahl¹, and H. Walden¹

¹EUROfusion Programme Management Unit Garching, Boltzmannstraße 2, 85748 Garching Germany

²Framatome GmbH, DTIMM-G, Paul-Gossen-Straße 100, 91052 Erlangen, Germany

³Culham Centre for Fusion Energy (CCFE), Culham Science Centre, Abingdon, UK

Corresponding Author: G. Federici, gianfranco.federici@euro-fusion.org

This paper describes the status of the DEMO design activities performed in Europe and discusses the impact of some of the key requirements (such as electrical output, tritium self-sufficiency), the main constraints, e.g., those deriving from the tokamak-side and the Balance-of-Plant (BoP) and Power Conversion System (PCS), on the systems design solutions and on the overall plant architecture. The paper focusses on the main DEMO technical and design integration issues, e.g., those where there are either gaps with ITER because of the inherent differences in the design approach and/or technologies adopted (such as for the protection of the first wall, possibly divertor configuration, tritium-fuel cycle, etc.), or because of the difference of plant requirements (for example, tritium-breeding and extraction, thermal power extraction and conversion to electricity, remote maintenance schemes for high plant availability). The design of the breeding blanket and the selection of its coolant are examples that bear a strong impact on integration, maintenance, and safety because of the interfaces with all key nuclear systems: i.e., the BoP and PCS, tritium recovery and purification systems, and so on.

Work continues to be focussed on the design of a pulsed baseline DEMO plant concept that integrates all the major DEMO subsystems to understand integration risks and resolve design interface issues. Considerations are also given to a design based on latter-stage ITER scenario and able to operate in a short pulse mode (e.g., 1 hr) for nominal extrapolated performance ($H_{98} = 1.0$) and capable of moving to steady-state operation while maintaining the same fusion power and net electrical production in the case of a better confinement being feasible. However, this option requires a much higher confidence in physics extrapolation and highly reliable and efficient current-drive and control systems, which need to be deployed by day one and still need to be developed. The definition and analysis of the physics scenarios for the concept design and identification of the physics basis development needs are described elsewhere.

Incorporating lessons learned from the ITER design and construction, building of relationships with industry and embedding industry experience in the design are needed to ensure early attention is given to industrial feasibility, costs, nuclear safety and licensing aspects.

Development of Physics and Engineering Designs for Japan's DEMO Concept

Y. Sakamoto¹

The Joint Special Design Team for Fusion DEMO

¹*National Institutes for Quantum and Radiological Science and Technology (QST),
Fusion Energy Research Development Directorate, Rokkasho, Aomori-ken 039-3212, Japan*

Corresponding Author: Y. Sakamoto, sakamoto.yoshiteru@qst.go.jp

Recent design progress of Japan's DEMO is presented regarding the engineering and physics conceptual design of a steady-state DEMO with a major radius of 8 m class and fusion power of 1.5 GW level. The design concept of divertor is similar to that of ITER. By considering the neutron irradiation environment, a Cu-alloy cooling pipe is used only in the large heat flux region, while a RAFM steel cooling pipe in the small heat flux region. The divertor cassette design is developed for reducing the fast neutron flux to protect the vacuum vessel and for replacement of the power exhaust units with the tungsten mono-block and Cu-alloy pipes. The breeding blanket concept based on JA ITER-TBM is developed to increase the pressure-tightness of the modules by considering safety assessment of in-box LOCA. Regarding the TF coil design, assessment of the error field indicates that the tolerance can be mitigated by ~ 2.5 times as large as ITER's with correction coil current of several 100 kAt/coil. The concept of remote maintenance for the blanket segments is developed such as the stable transfer mechanism in the vertical, radial and toroidal directions. The rad-wastes generated by the maintenance can be disposed of in shallow land burial after 10-year storage. The concept of primary cooling water system is developed for effective use of thermal power removed from not only blanket but also divertor, where thermal power removed from the divertor is used for preheating the blanket coolant, and a bypass line is installed to control the coolant flow for reducing the pressure drop. As for the physics design, one of the major issues is the compatibility between the operational density and the divertor detachment. The evaluation of the lower boundary of operational density to be compatible with the capability of the heat removal and suppression of tungsten erosion indicates that the partial detachment with the acceptable peak heat load is obtained at the operational density, and that the net erosion is almost suppressed. Furthermore, the plasma operation scenario is developed and indicates the importance of off-axis ECCD for controlling the internal transport barriers. It is concluded that the DEMO concept considerably mitigates power handling issues compared with the previous compact DEMO, SlimCS, although some challenging design issues remain to be resolved.

Novel Radiofrequency Current Drive Systems for Fusion Plasma Sustainment on DIII-D

G. M. Wallace¹, R. C. O'Neill², P. T. Bonoli¹, M. W. Brookman², J. S. deGrassie², J. Doody¹, J. R. Ferron², B. Fishler¹, W. Helou³, C. T. Holcomb⁴, R. Leccacorvi¹, M. LeSher², C. P. Moeller², C. Murphy², A. Nagy⁵, R. I. Pinsker², S. Shiraiwa¹, M. Smiley², J. F. Tooker², H. Torreblanca², R. Vieira¹, and S. J. Wukitch¹

¹Plasma Science & Fusion Center, MIT, Cambridge, MA 02139, USA

²General Atomics, San Diego, CA 92186, USA

³Institut de Recherche sur la Fusion par confinement Magnétique (IRFM), Commissariat à l'énergie atomique (CEA/Cadarache), 13108 St. Paul lez Durance, France

⁴Lawrence Livermore National Laboratory (LLNL), Livermore, CA 94550, USA

⁵Princeton Plasma Physics Laboratory (PPPL), Princeton, NJ 08540, USA

Corresponding Author: G. M. Wallace, wallaceg@mit.edu

The DIII-D National Fusion Facility is advancing the science and technology of steady-state fusion plasma sustainment through the implementation of two first-of-a-kind radio frequency current drive systems: the “helicon” or fast wave in the lower hybrid range of frequencies (LHRF), and high field side (HFS) launch of the lower hybrid slow wave.

Using existing DIII-D discharges, we have identified high performance scenarios that are predicted to have excellent wave penetration, strong single pass absorption and high current drive efficiency. Simulations predict this will raise ideal β_N limits in DIII-D and permit access to higher density advanced tokamak regimes. The higher B -field on the HFS improves wave accessibility and allows for use of lower $n_{||}$, resulting in higher current drive efficiency for LHRF slow waves and damping at $r/a \sim 0.6$ – 0.8 on the first pass. The 476 MHz helicon has better accessibility at lower B -field and higher density than the 4.6 GHz slow wave due to the lower frequency that can be used for the fast wave.

Calculations show that HFS launch of slow waves in the LHRF can lead to a physics current drive efficiency of 0.17×10^{20} A/W·m² at $r/a \sim 0.6$ – 0.8 in DIII-D and 0.4×10^{20} in a high B -field reactor. HFS LHRF represents an integrated solution that both improves core wave physics and mitigates PMI/coupling issues. An innovative, compact HFS LHRF antenna design has been developed combining a slotted waveguide poloidal splitter (used on C-Mod) and multijunction toroidal splitter (used on Tore Supra, EAST). Models show good coupling properties for predicted edge density profiles.

Current drive by helicons is predicted to be significantly more efficient than either off-axis neutral beam current drive or conventional ECCD in high-density, high electron- β regimes. A 12-module helicon antenna was developed and tested in DIII-D and demonstrated sufficient coupling at < 0.4 kW. A ~ 1 MW proof-of-principle experiment using helicon waves at 476 MHz launched with a novel “comb-line” travelling wave antenna with 30 elements will be performed on DIII-D starting in 2019.

Work supported by the U.S. Department of Energy, Office of Science, Office of Fusion Energy Sciences, using User Facility DIII-D, under Award Number DE-FC02-04ER54698 and by U.S. Department of Energy Contract No. DE-FC02-01ER54648 under Scientific Discovery through Advanced Computing.

Impact of High Field & High Confinement on L-Mode-Edge Negative Triangularity Tokamak (NTT) Reactor

M. Kikuchi^{1,2,3}, T. Takizuka⁴, S. Y. Medvedev⁵, T. Ando⁶, D. Chen⁷, J. X. Li³, O. Sauter⁸, L. Villard⁸, M. E. Austin⁹, Y. Kishimoto¹⁰, and K. Imadera¹⁰

¹National Institutes for Quantum and Radiological Science and Technology (QST), Chiba-shi, Japan

²Institute of Laser Engineering, Osaka University, Osaka, Japan

³Southwestern Institute of Physics, Chengdu, Sichuan, People's Republic of China

⁴Graduate School of Engineering, Osaka University, Osaka, Japan

⁵Keldysh Institute of Applied Mathematics, RAS, Moscow, Russian Federation

⁶Formerly of Japan Atomic Energy Agency (JAEA), Naka, Japan

⁷Institute of Nuclear Energy Safety Technology, CAS, Anhui, People's Republic of China

⁸Swiss Plasma Center (SPC), École polytechnique fédérale de Lausanne (EPFL), 1015 Lausanne, Switzerland

⁹Institute for Fusion Studies (IFS), University of Texas at Austin, Austin, TX 78712, USA

¹⁰Institute of Advanced Energy, Kyoto University, Nishikyo-ku, Kyoto 615-8540, Japan

Corresponding Author: M. Kikuchi, kikuchi.mitsuru@qst.go.jp

“NTT” is a unique reactor concept based on “power-handling-first” philosophy by locating a long-leg (~ 2.7 m) divertor at the outboard side with negative triangularity $\delta < 0$ and making flux tube expansion to maximize heat exhaust surfaces (grazing angle $\sim 2^\circ$). Our previous design ($I_p = 21$ MA, $A = R_p/a_p = 3$, $R_p = 9$ m, $H_H = 1.12$, $B_t = 5.86$ T) uses standard magnet design based on the wedge support and maximum field is limited to 13.6 T due to stress limit 800 MPa and large reactor size. It allows adoption of currently available Nb₃Sn superconductor at 4.5 K as well as Bi2122/Pb high- T_c superconductor at 20 K. NTT configuration has technical merits of having space in the inboard except narrowest point to place the blanket piping and auxiliary systems such as pellet injector line and ECH waveguides. Outward placing of the divertor is favourable for pumping conductance. Parameter studies on impact of high- B_t and H_H for $A = 3$ – 3.5 are shown where $H_H I_p A = 69.3$ MA, $n/n_{GW} = 0.85$ and $q_{cy} = 3.5$ are fixed. The reduction of major radius to $R_p = 7$ m is possible with improved confinement ($H_H = 1.5$) while B_{max} is nearly constant. In this case, fusion power is reduced to $P_f = 2$ GW and the neutron wall load stays almost constant $q_n \sim 1.4$ – 1.5 MW/m² while the normalized β , β_N , becomes higher $\beta_N = 2.9$. For fixed $H_H = 1.2$, higher $B_{max} = 16$ T enables to reduce major radius to $R_p = 7$ m. In this case, fusion power P_f and neutron wall load q_n increases while β_N stays almost constant. For $A = 3.5$, we observe similar trend. The plasma volume is smaller ($V_p \sim 1000$ m³) compared with $A = 3$ case ($V_p \sim 1500$ m³). But requirement for B_{max} for fixed $H_H = 1.2$ becomes rather high $B_{max} = 19.5$ T. With improved confinement ($H_H = 1.5$), reduction of major radius to $R_p = 7$ m is possible leading to $I_p = 13.3$ MA, $B_t = 7.53$ T, $n = 0.9 \times 10^{20}$ /m³, $P_f = 1.9$ GW, $B_{max} = 15.5$ T, $P_{CD} = 115$ MW ($\eta_{CD} = 0.5 \times 10^{20}$ A/W·m² is assumed). We made configuration design for this case and the equilibrium calculation. Extended wedge support allows σ_{max} within 800 MPa at 4.5 K. It is concluded that both high magnetic field and high confinement are important for the realization of reasonably compact NTT fusion reactor as future R&D.

Amelioration of Plasma-Material Interactions and Improvement of Plasma Performance with a Flowing Liquid Li Limiter and Li Conditioning on EAST

R. Maingi¹, J. S. Hu², G. Z. Zuo², D. Andruczyk³, J. M. Canik⁴, A. Diallo¹, K. F. Gan⁵, E. Gilson¹, X. Z. Gong², T. K. Gray⁴, M. Huang², R. Lunsford¹, D. K. Mansfield¹, X. C. Meng⁶, T. H. Osborne⁷, D. N. Ruzic³, Z. Sun², K. Tritz⁸, W. Xu², Z. Wang⁹, B. D. Wirth⁹, K. Woller¹⁰, and S. J. Zinkle⁹

The EAST Team

¹Princeton Plasma Physics Laboratory (PPPL), Princeton, NJ 08540, USA

²Institute of Plasma Physics, Chinese Academy of Sciences, Hefei, Anhui, People's Republic of China

³University of Illinois, Urbana-Champaign, IL 61820, USA

⁴Oak Ridge National Laboratory (ORNL), Oak Ridge, TN 37831, USA

⁵University of Tennessee, Knoxville, TN 37996, USA

⁶Department of Applied Physics, Hunan University, Changsha 410082, People's Republic of China

⁷General Atomics, San Diego, CA 92186, USA

⁸Johns Hopkins University, Baltimore, MD 21218, USA

⁹Los Alamos National Laboratory (LANL), Los Alamos, NM 87545, USA

¹⁰Massachusetts Institute of Technology (MIT), Cambridge, MA 02139, USA

Corresponding Author: R. Maingi, rmaingi@pppl.gov

Wall conditioning and ELM control has played a crucial role in enabling access to record long H-mode pulses in EAST. Here we present new results where: 1) a 2nd generation (2G) flowing liquid lithium (Li) limiter was inserted into the EAST midplane and used to mitigate plasma-materials interactions (PMI); 2) Li powder was injected to eliminate ELMs in upper-single null (USN) configuration that used the ITER-like tungsten monoblock divertor; and 3) Li granule injection was used for ELM triggering studies. A 2G flowing liquid Li limiter was inserted into EAST and was found to be compatible with H-modes, even when placed within 1 cm of the separatrix in RF heated discharges. Both the 2G and 1st generation (1G) limiters use a Cu plate for the heat sink, with a thin stainless steel (SS) coating for Li compatibility. The 2G limiter had several design improvements over the 1G limiter, including a thicker SS protective layer, two $j \times B$ pumps instead of one, an improved Li distributor manufacturing process, and surface texturing to improve wetting of the SS face. The fractional surface area that was wetted by the Li was $> 80\%$ in the 2G limiter, versus $\sim 30\%$ in the 1G limiter. The heat flux exhausted by the 2G limiter was up to 4 MW/m^2 . In otherwise similar conditions, there was a shot-by-shot progressive reduction in D_α emission with 2G limiter insertion, culminating in short-lived ELM-free phases for the first time in EAST, with increasing τ_E and transient $H_{H98(y,2)} < 2$. A 3G limiter has been fabricated out of Mo for upcoming tests. Li powder was injected into USN H-modes using ITER-like tungsten monoblock divertor. At constant Li injection rates, the ELM elimination became progressively easier, suggesting a cumulative wall conditioning effect, as also observed with the 2G flowing liquid lithium limiter. Normalized energy confinement $H_{H98(y,2)}$ was maintained at about 1.2, well above the previous ELM elimination with Li injection on the lower carbon divertor with $H_{H98(y,2)} \sim 0.75$. Finally ELM triggering studies with a four-chamber Li granule injector showed a clear size threshold for ELM triggering probability, as qualitatively predicted by theory. The observed threshold was similar to DIII-D experiments. ELM pacing was also observed, but the paced ELM frequency was below the 200 Hz natural ELM frequency in these discharges, preventing ELM heat flux mitigation conclusions.

Experiments on FTU with a Liquid Tin Limiter

G. Mazzitelli¹, M. L. Apicella¹, M. Iafrati¹, and G. Apruzzese¹

Rapporteur by: R. Maingi

¹ENEA C. R. Frascati, Dipartimento FSN, Frascati, Italy

^{*}The FTU Team

Corresponding Author: G. Mazzitelli, giuseppe.mazzitelli@enea.it

In this paper we report experimental results obtained, for the first time in the world, in a tokamak with a liquid tin limiter (TLL). The FTU TLL was realized by using a molybdenum tube covered with capillary porous system (CPS) made by stripes of tungsten felt filled with tin. The TLL can be cooled by flowing air and atomized water inside a copper pipe inserted in the molybdenum tube. To test TLL, a standard FTU discharge was used with a toroidal field $B_t = 5.3$ T, a plasma current $I_p = 0.5$ MA and an electron density $n_e \leq 1.0 \times 10^{20}/\text{m}^3$. The thermal load on the limiter was progressively varied moving up the limiter shot by shot in the scrape-off-layer (SOL), until almost reaching the last closed magnetic surface (LCMS). The most significant results without active cooling, were obtained by increasing the heat load on the TLL by changing the average electron density from 0.6 to $1.0 \times 10^{20}/\text{m}^3$. The thermal load onto the TLL by Langmuir probes increased proportionally with the electron density reaching a value greater than $q_{LP} = 15$ MW/m² for almost 1 s for TLL position close to the LCMS. By looking at the temporal evolution of the IR maximum surface temperature and of the measured Sn XXI line emission monitored by the UV spectroscopy, it was deduced that tin evaporation becomes the dominant tin production mechanism when the maximum surface temperature ($T_{s,max}$) of the limiter exceeds 1300°C up to the upper value of 1700°C reached at the end of the pulse. A maximum heat flux of $q_{max} = 18$ MW/m² resulted in this case by the application of the 3D finite-element code ANSYS to the real design of the limiter and of CPS. A concentration of tin of about 5.0×10^{-4} of the electron density was deduced from the Z_{eff} value. By applying the JETTO code, no significant difference was found in the confinement time with respect to the case of absence of tin limiter and without degradation of the plasma performance. No droplets into plasma and no damages were observed on the TLL after the plasma exposition.

Development of a Lithium Vapour Box Divertor for Controlled Plasma Detachment

R. J. Goldston¹, T. D. Rognlien², E. D. Emdee¹, M. A. Jaworski¹, M. E. Rensink²,
J. A. Schwartz¹, and D. P. Stotler¹

¹Princeton Plasma Physics Laboratory (PPPL), Princeton, NJ 08540, USA

²Lawrence Livermore National Laboratory (LLNL), Livermore, CA 94550, USA

Corresponding Author: R. J. Goldston, rgoldston@pppl.gov

A lithium vapour-box configuration [1] has been proposed to provide volumetric radiative dissipation in the divertor region of tokamak plasmas. While recent experiments have achieved continuous vapour shielding in close proximity to a lithium coated target in Magnum-PSI [2], this approach seeks to provide controlled detachment far from the divertor target, in a lithium vapour cloud maintained through controlled evaporation and kept away from the main plasma through baffling and recondensation.

We performed edge-plasma simulations with the geometry and parameters of the recent FNSF study [3]. A set of calculations are performed with the 2D UEDGE plasma model and a simple diffusive neutral model [4]. To mimic a crude vapour-box, Li vapour is injected near the divertor plate from the private-flux and outer divertor leg regions and is removed assuming a wall albedo of 0.5 on both PF and outer walls, which allows steady state solutions. For a range of Li vapour input, steady-state, detached-plasma solutions are shown where well over 90% of the exhaust power is radiated by Li, resulting in peak surface heat fluxes $\leq 2 \text{ MW/m}^2$ on the divertor plate, outer wall, and private-flux wall. While Li ions dominate in the divertor leg, their density is much less than the DT density at the midplane. Here the key issue is possible dilution of the core DT fuel.

We also developed a simulation of the neutral lithium vapour flow in the divertor using the Stochastic Parallel Rarefied-gas Time-accurate Analyser (SPARTA) Direct Simulation Monte Carlo (DSMC) code [5]. We have simulated the open geometry of the present FNSF design, as well as begun studies using (so far) a single baffle. While the original open geometry allows 75% of the lithium absorption in the plasma to occur in the far SOL, distant from the divertor leg, this is reduced to 5% through the use of a single baffle.

References

- [1] R. J. Goldston *et al.*, Nucl. Mat. Eng., **12**, 1118 (2017).
- [2] P. Rindt, ISLA Conference, Moscow 2017.
- [3] C. E. Kessel *et al.*, Fusion Eng. Des., *In Press*, (2017).
- [4] T. D. Rognlien *et al.*, Fusion Eng. Des., *In Press*, (2017).
- [5] M. A. Gallis *et al.*, AIP Conference Proceedings, **1628**, 27 (2014).

Shattered Pellet Injection Technology Design and Characterization for Disruption Mitigation Experiments

L. R. Baylor¹, S. J. Meitner¹, T. E. Gebhart¹, J. B. O. Caughman¹, and D. Shiraki¹

¹Oak Ridge National Laboratory (ORNL), Oak Ridge, TN 37831, USA

Corresponding Author: L. R. Baylor, baylorlr@ornl.gov

The technology of forming high-Z cryogenic pellets mixed with D₂ that are shattered upon injection into a plasma has been developed at ORNL for mitigating disruptions and has been selected as the basis for the baseline disruption mitigation system on ITER. In these shattered pellet injectors (SPIs), large pellets of neon and argon mixed with D₂ are formed from gas and are shattered upon impact with a bent tube just before entering into disrupting plasmas in order to radiate the plasma energy to mitigate possible damage to in-vessel components [1]. In support of disruption mitigation research for ITER, SPI systems have been designed and fabricated for use on thermal mitigation and runaway electron dissipation experiments on DIII-D and JET. These systems have common features of three barrels of different size pellets that are formed in-situ and collimated into a single injection line. The shatter tubes are bent stainless steel tubes that are mounted inside the vacuum vessel of the tokamak. The large pellets are formed in-situ from the low-pressure gas feed into the barrels that are cooled with liquid helium and held intact ready to fire until needed. Pressurized gas is also used to accelerate these pellets with gaps in the injection lines to remove as much of the gas as is practical to avoid influencing the plasma shutdown.

Solid pellets of argon in particular present a challenge to fire the pellet because of high shear stress, thus mechanical punches have been developed that can apply higher impact to release these pellets. Punches using high pressure gas and solenoid drivers have been developed. Tests of gas punches have revealed that argon can be released and achieve speeds up to 160 m/s for 8 mm size pellets. The slower pellet speeds achieved with a punch have been found to result in larger fragment sizes, which is appealing for deeper penetration in high performance plasmas. Higher speed pellets that are achieved with high pressure gas and high deuterium content in the same shatter tube result in finer particles and higher gas content in the resulting shatter material spray.

This work was supported by ORNL managed by UT-Battelle, LLC for the U.S. Department of Energy under Contract Nos. DE-AC05-00OR22725 and DE-FC02-04ER54698.

References

- [1] N. Commaux, *et al.*, Nucl. Fus., **50**, 112001 (2010).
- [2] L. R. Baylor, *et al.*, Fusion Sci. Tech., **68**, 211 (2015).

Automated Testing of ITER Diagnostics Scientific Instrumentation

S. Simrock¹, L. Abadie¹, R. Barnsley¹, L. Bertalot¹, P. Makijarvi¹, R. Lange¹, M. Park¹, R. Reichle¹, D. Stepanov¹, G. Vayakis¹, A. Wallander¹, P. Petitpas¹, M. Walsh¹, Z. Li², T. Yamamoto³, S. Varshney⁴, J. Choi⁵, E. Mironova⁶, A. Neto⁷, B. DeVan⁸, P. Patil⁹, M. Annigeri⁹, A. Ghatge⁹, D. Makowski¹⁰, P. Perek¹⁰, M. Orlikowski¹⁰, G. Jablonski¹⁰, K. Meyer¹¹, and V. Martin¹²

¹International Thermonuclear Experimental Reactor (ITER),
Cadarache Centre, 13108 St. Paul lez Durance, France

²International Thermonuclear Experimental Reactor (ITER),
Chinese Domestic Agency, People's Republic of China

³Japan Atomic Energy Agency (JAEA), Naka, Japan

⁴International Thermonuclear Experimental Reactor (ITER), India Centre, Gujarat, India

⁵International Thermonuclear Experimental Reactor (ITER), Korea Domestic Agency, Korea, Republic of

⁶International Thermonuclear Experimental Reactor (ITER),
Project Centre "ITER", Moscow, Russian Federation

⁷F4E: Fusion for Energy, ITER EU Centre, 08019 Barcelona, Spain

⁸International Thermonuclear Experimental Reactor (ITER), US Domestic Agency, USA

⁹TCS, Pune 411 057, India

¹⁰DMCS, Lodz University of Technology, Poland

¹¹COSYLAB, 1000 Ljubljana, Slovenia

¹²BERTIN Technologies, Aix-en-Provence, France

Corresponding Author: S. Simrock, stefan.simrock@iter.org

ITER requires extensive diagnostics to meet the demands for machine operation, plasma control, protection, safety and physics studies. Most diagnostics require high performance scientific computing for the processing of complex algorithms for the measurements. The most stringent requirements are found in the more than 50 diagnostics measurement systems in terms of high performance data acquisition, data processing and real-time data streaming from distributed sources to the plasma control system as well as large amounts of raw data streaming to scientific archiving. While most of these requirements have been achieved individually the challenge for ITER will be the integration of these state-of-the-art technologies in a coherent design while maintaining all of the performance aspects simultaneously. The instrumentation and control (I&C) systems for each diagnostic must meet around 500–700 functional and nonfunctional requirements which include also the requirements from the ITER handbooks such as the Plant Control Design Handbook (PCDH), Electrical Engineering Design Handbook (EDH) and the Radiation Compatibility Handbook. While the diagnostics I&C system engineering methodology is well established for requirements management, detailed design, and implementation, the acceptance testing, demonstrating the compliance of the I&C system with the requirements needs further elaboration. This includes the definition of the test scenarios, detailed test procedures, and well-defined pass-fail criteria for each test. Since compliance validation against a large number of requirements can be very time consuming a high degree of automation during testing is desirable. This paper presents the elaboration of the pass/fail criteria, the acceptance testing procedures for diagnostics plant system I&C, and describes the design and implementation for automated testing. First results will illustrate the reduction in testing time for obtaining a detailed compliance evaluation.

Hollow Pellets for Magnetic Fusion

Z. Wang¹, M. Hoffbauer¹, E. M. Hollmann², J. Hu³, R. Maingi⁴, J. E. Menard⁴, X. Q. Xu⁵,
and Y.-M. Wang⁵

¹*Los Alamos National Laboratory (LANL), Los Alamos, NM 87545, USA*

²*University of California San Diego, CA 92093, USA*

³*Institute of Plasma Physics, Chinese Academy of Sciences, Hefei, Anhui, People's Republic of China*

⁴*Princeton Plasma Physics Laboratory (PPPL), Princeton, NJ 08540, USA*

⁵*Lawrence Livermore National Laboratory (LLNL), Livermore, CA 94550, USA*

Corresponding Author: Z. Wang, zwang@lanl.gov

Motivated by edge localized mode (ELM) control in H-mode plasmas, we summarize experimental and theoretical progress in MHD physics of plasma interaction with small pellets ranging from 10's of μm to a few mm in size. Layered spherical structures with a hollow core ("hollow pellets") are attractive in comparison with solid spheres and gas puffing. Theoretical results based on multifluid calculations of pellet-induced cold plasmoid formation and interactions with background plasmas are given. The experimental results include a new dual-spectroscopy technique for imaging of ELMs and fabrication of prototype hollow pellets.

Recent Progress on the Production and Testing of the ITER Central Solenoid Modules

J. Smith¹, N. Norausky¹, D. Priddie¹, K. Schaubel¹, and A. Stephens¹

¹*General Atomics, San Diego, CA 92186, USA*

Corresponding Author: J. Smith, john.smith@ga.com

Several key milestones have been completed recently in the fabrication of the Central Solenoid (CS) modules for ITER. The qualification coil has been completed and tested with many lessons learned that have now been incorporated into the processing of the production modules. Currently four modules are in production with the first module scheduled for completion in 2018 followed by full current testing at 4.5 K. Shipment of the first module to Cadarache is scheduled for 2019, arriving in advance of its need date. The Central Solenoid is a key component of the ITER tokamak providing the inductive voltage to initiate and sustain the plasma current and to position and shape the plasma. The design of the CS has been a collaborative effort between the US ITER Project Office (USIPO), the international ITER Organization (IO) and General Atomics (GA). GA is fabricating seven 110 tonne CS modules (one is a spare). After arrival at the ITER site, the six modules will be stacked in the Assembly Hall, the structure added and transferred in a single lift to the ITER tokamak.

In a dedicated facility in Poway, California, USA, GA is currently fabricating the modules, with each one requiring approximately 22 months start to finish. Following fabrication a series of tests including high voltage testing of the insulation, full current testing of the conductor at 4.5 K and a repeat of the high voltage tests at room temperature are performed. The testing duration is an additional five months for each module and is the programme critical path.

Recently, the qualification coil was completed, electrically tested, and cooled to 4.5 K by supercritical helium. While at 4.5 K, a series of tests were performed which simulated those tests that will be performed on the modules to validate the test methods and equipment. After the tests were completed, the mockup coil was dissected to determine the quality of the resin injection. This paper describes some of the challenges in accomplishing the recent milestones in completing the qualification coil fabrication and testing, the implications on the module production, and the status of the module production.

Dielectric Windows as Front-End Diagnostic Elements in ITER

A. G. Razdobarin¹, N. A. Babinov¹, A. N. Bazhenov¹, I. M. Bukreev¹, A. M. Dmitriev¹, D. A. Kirilenko¹, A. N. Koval¹, G. S. Kurskiev¹, A. E. Litvinov¹, S. V. Masyukevich¹, E. E. Mukhin¹, D. S. Samsonov¹, A. A. Sitnikova¹, V. V. Solokha¹, I. B. Tereschenko¹, S. Y. Tolstyakov¹, L. A. Varshavchik¹, Al. P. Chernakov², D. I. Elets², V. L. Bukhovets³, A. E. Gorodetsky³, A. V. Markin³, A. P. Zakharov³, R. K. Zalavutdinov³, P. Andrew⁴, and M. Kempenaars⁴

¹*Ioffe Institute, St. Petersburg, Russian Federation*

²*Spectral-Tech ZAO, St. Petersburg, Russian Federation*

³*A. N. Frumkin Institute of Physical Chemistry and Electrochemistry, RAS, Moscow, Russian Federation*

⁴*International Thermonuclear Experimental Reactor (ITER),*

Cadarache Centre, 13108 St. Paul lez Durance, France

Corresponding Author: A. G. Razdobarin, aleksey.razdobarin@mail.ioffe.ru

The performance of the frontend elements of optical diagnostics in ITER under long-term operation and with limited access for their maintenance is in the focus of extensive R&D programme involving laboratory study and testing in working tokamaks. The requirements to the frontend element design are driven by high-energy neutron and γ -radiation, intense particle fluxes and thermal loads at the element location on the one hand and necessity to provide periodic or continuous surface recovery on another. The insulating diagnostic window as an alternative to commonly accepted first mirror option is discussed in the presentation. The approach implementation is illustrated for the divertor Thomson scattering (DTS) optical scheme using frontend windows for injection of laser beam and collecting of scattered light. Surface recovery techniques based on plasma cleaning and laser ablation are described with the focus on the performance of the windows under laser and plasma treatment. The windows made from fused silica glass KU-1 and Al_2O_3 were tested. Plasma cleaning experiments have been performed for clean windows and windows coated with Al films. As was shown by the means of optical microscopy, XPS and AFM the dominant mechanism of window optical degradation is surface roughening. The development of surface relief becomes more intensive after deposition and removal of Al. The clear indication of the dependence of surface degradation rate on the initial polishing quality was also obtained for the windows with and without Al deposition. Laser experiments reveal the decrease in laser-induced damage threshold by the factor of ~ 3 for both window materials under continuous tungsten deposition. In the case of Al droplets spraying, damage threshold is about 6 times as low as that of pure KU-1 window. The experiments on the long-term laser cleaning under continuous contamination showed that the evolution of tungsten film stops over the first hundreds of pulses and further exposition has no effect on the film thickness. The steady-state thickness of tungsten deposit in the beam spot was found to be ~ 5 nm for the deposition rate of ~ 10 nm/min and laser (3 ns) energy density of ~ 2 J/cm², forming almost transparent coating in visible and near-IR regions. Radiation-induced effects in silica glass and sapphire and corresponding limitations are also discussed.

Exhaust Behaviour and Mass Balance of Tritium in Large Helical Device

M. Tanaka¹, N. Suzuki¹, and H. Kato¹

¹National Institute for Fusion Science (NIFS), Toki, Gifu, Japan

Corresponding Author: M. Tanaka, tanaka.masahiro@nifs.ac.jp

The control and management of tritium in a fusion test facility is one of the important issues from the viewpoints of radiation safety and public acceptance. As for the tritium control in a fusion test device, understanding of tritium behaviour in the exhaust gas would give us new knowledge into the characteristics of the tritium release and inventory. In the deuterium plasma experiment on the Large Helical Device (LHD) which has a stainless-based first wall, a small amount of tritium is produced by deuterium-deuterium reaction in the core plasma and it can be used as a tracer. A portion of produced tritium is exhausted from the vacuum vessel via the vacuum pumping system. To investigate the tritium behaviour, the tritium in the exhaust gas was monitored by a water bubbler system for discriminating chemical forms and an ionization chamber.

In the exhaust gas from LHD, the chemical forms of tritiated hydrogen gas was more than 95% and the tritiated hydrocarbons was a few %. Since the divertor tiles are made of carbon, a part of the tritium was incorporated into the hydrocarbons by chemical sputtering. The ratio of tritiated hydrocarbon exhaust gas was less than that in JT-60U which has carbon-based first wall. On the other hands, the tritium in the plasma facing component was released by the He and D₂ glow discharge cleaning operation. The tritium release mechanism was supposed to the hydrogen isotope exchange reaction and diffusion limited process.

The tritium exhaust rate was gradually increased with the progress of deuterium experiment. Then, the total amount of exhausted tritium was approximately 35.5% of produced tritium at the end of the plasma experimental campaign. It suggested that two-thirds of produced tritium would be implanted in the first wall. The ratio of exhaust tritium during plasma experiment in LHD was about 1.5 times larger than that of JT-60U. Thus, the metal first wall would reduce the tritium inventory in the fusion machine.

The tritium tracer study in the first deuterium plasma experiment in LHD revealed that i) the tritium on the surface was removed by hydrogen isotope exchange reaction and the tritium release from plasma facing component was diffusion limited process, and ii) the metal wall is one of key factors to control the tritium inventory and to reduce the tritium compounds in exhaust gas.

Progress in Development and Fabrication of the JT-60SA ECH/CD System

T. Kobayashi¹, S. Moriyama¹, K. Takahashi¹, K. Kajiwar¹, Y. Oda¹, R. Ikeda¹,
A. Isayama¹, L. Novello², M. Sawahata¹, M. Terakado¹, S. Hiranai¹, F. Sato¹, K. Wada¹,
J. Hinata¹, and K. Yokokura¹

¹National Institutes for Quantum and Radiological Science and Technology (QST),

Naka Fusion Institute, Naka-shi, Ibaraki-ken, Japan

²F4E: Fusion for Energy, ITER EU Centre, 08019 Barcelona, Spain

Corresponding Author: T. Kobayashi, kobayashi.takayuki@qst.go.jp

Development of the ECH/CD system for JT-60SA has been progressed. Successful results on the JT-60SA gyrotron development for multifrequency, high-power, long-pulse oscillation such as 1 MW/100 s at both 110 and 138 GHz, 1.9 MW/1 s and 1.5 MW/5 s at 110 GHz, 1.3 MW/1.2 s at 138 GHz and 1 MW/1 s at 824 GHz were reported in IAEA FEC in 2014 and 2016. The development of the high-power, long-pulse and multifrequency JT-60SA ECH/CD system is now focussing on the launcher, transmission line (TL), control and power supply. In addition, design, fabrication and testing of a part of these components have been progressed toward start of the first plasma experiment of JT-60SA.

The main results achieved in this time are as follows: i) A full length (~ 7 m) mock-up of the mirror steering structure of the launcher has been successfully tested in vacuum. The required life without maintenance, which is 10^5 cycles for the poloidal steering range of 60° and 10^4 cycles for toroidal beam steering range of 30° , has been achieved. A newly introduced solid lubricant enabled the smooth movement of the steering shaft by reducing the sliding resistance between balls and rail/block of the linear guide used in the steering structure. ii) The temperature rise distribution of aluminium waveguides has been measured at high-power of 0.5 MW. It is in the range from 0.2 to 1.2°C per 1 MJ transmission and acceptable for 1 MW/100 s (100 MJ) transmission required in JT-60SA. iii) The preparation of the JT-60SA ECH/CD system is progressing as planned. For instance, an ECH/CD control system has been designed with a layered and distributed structure to achieve sufficient flexibility for upgrading and for easy optimization depending on the experimental purposes. In addition, fabrication of TL components including waveguides, cooling and vacuum system has been started. Moreover, the new power supplies for two gyrotrons (1 MW/100 s each) have been designed and the fabrication has started by F4E as a part of broader approach activities.

The above discussed progress in the launcher and waveguide developments and in the design and fabrication of the JT-60SA ECH/CD system components significantly contribute to a smooth start of the JT-60SA experiment and improve the plasma performance with high reliability and flexibility.

Preliminary Pipe Stress Analysis of High Pressure, High Temperature Experimental Helium Cooling System

A. K. Verma¹, B. K. Yadav¹, A. Gandhi¹, and E. Rajendra Kumar¹

¹*Institute for Plasma Research (IPR), Bhat, Gandhinagar, India*

Corresponding Author: A. K. Verma, adityakumar@ipr.res.in

Experimental Helium Cooling Loop (EHCL) is a high pressure-high temperature helium gas system. EHCL is similar to the First Wall Helium Cooling System (FWHCS) of LLCB TBM and in this loop first wall mock-ups up to one fourth size of TBM can be tested.

EHCL modelling consists of equipment arrangement, pipe routing, support, cable tray routing, instrumentation arrangement and tube routing. EHCL lab floor dimensions are 18 m × 18 m length and width respectively while the vertical height is 5 m. The lab is divided in three major areas: process area, control room and free space for maintenance activities. The process and control room covers 9 m × 9 m and 14 m × 5 m floor area respectively.

The EHCL is designed to operate with helium gas at 8.0 MPa (gauge) pressure and at 300–400°C temperature. The flow rate varies from 0.2 kg/s to 0.4 kg/s. The selected size for the connection pipes is DN 50. The high temperature pipes in this loop are at 400°C and at 8 MPa pressure, and these pipes are connected to equipment in a limited space. The detailed flexibility analysis was carried out, to ensure safety of the piping system and to maintain the structural integrity under loading conditions (both external and internal), which may occur during the lifetime of the system. SS 316L is used as structural material for piping and equipment.

This poster presents the modelling of EHCL and the results of detailed flexibility analysis of EHCL pipes. To carry out the analysis, the entire piping system of the loop was modelled and the static and dynamic analysis was carried out in CAESAR II software. For the floor response spectra, the floor level in two horizontal and one vertical direction was computed.

As IPR lies in seismic zone-III, and the process loop is planned to be located at ground level at IPR campus, accordingly the FRS was used to find out the induced stress in the process loop. The dynamic effect and weight effects are considered in the design so that the stresses created by the combined loads do not exceed the allowable stresses prescribed by the design codes. Finally the piping layout satisfying the code requirements along with the results are presented in the poster.

Completion of DC 1 MV Power Supply System for ITER Neutral Beam Test Facility

H. Tobari¹, M. Kashiwagi¹, K. Y. Watanabe¹, T. Maejima¹, Y. Yamashita¹, M. Dairaku¹,
Y. Oda¹, S. Sasaki¹, A. Kojima¹, N. Umeda¹, H. Yamanaka¹, N. Shibata¹, S. Oohara²,
T. Suto², and H. Kawakami²

¹*National Institutes for Quantum and Radiological Science and Technology (QST),
Naka Fusion Institute, Naka-shi, Ibaraki-ken, Japan*

²*Hitachi, Ltd., Japan*

Corresponding Author: H. Tobari, tobari.hiroyuki@qst.go.jp

Technologies of DC 1 MV insulation with water and DC 1 MV vacuum insulation have been developed. As the result, manufacturing of DC 1 MV power supply components to produce 1 MeV negative ion beams have been completed for the ITER neutral beam test facility (NBTF). For the transmission line (TL), insulating tubes for hot and cooling water have been developed by clarifying resistivity of high-temperature water and properties of insulation material with water absorption. Based on these results, the integrated configuration of the TL has been established through electrical and thermo-mechanical analyses. For the HV bushing, 1 MV vacuum insulation was achieved based on the empirical scaling for the vacuum insulation. Then, all components have been manufactured and shipped to the NBTF site in 2017. The installation is on-going toward the integration test in 2018. These achievements contribute to push forward with a start of the NBTF operation and a realization of the ITER NB.

Improvement of ITER Equatorial EC Launcher Design for Poloidal Steering Compatibility

K. Kajiwara¹, K. Takahashi¹, G. Abe¹, N. Kobayashi¹, Y. Oda¹, M. Isozaki¹, M. Komatsuzaki², T. Omori³, M. Henderson³, R. Ikeda¹, T. Kobayashi¹, and S. Moriyama¹

¹National Institutes for Quantum and Radiological Science and Technology (QST),
Naka Fusion Institute, Naka-shi, Ibaraki-ken, Japan

²MHK Systems Co. Ltd., 2-21-4-101 Funaishikawa-eki Higashi, Tokai-mura, Naka-gun, Ibaraki 319-1118, Japan

³International Thermonuclear Experimental Reactor (ITER),
Cadarache Centre, 13108 St. Paul lez Durance, France

Corresponding Author: K. Kajiwara, kajiwara.ken@qst.go.jp

This report describes the key development of the ITER equatorial ECH/ECCD launcher (EL) for poloidal steering compatibility. The steering direction of the EL has been changed from toroidal to poloidal in order to enhance the current drive capability. The design modification is being progressed toward the design finalization in 2019.

The concept of upper launcher (UL) steering mechanism of steering-mirror assembly (SMA) is adapted for EL for poloidal steering. However, the redesign of the SMA for EL is needed and the key of the design is the torque balance between the bellows actuator, the coil springs and spiral pipe for mirror. Since the heat load of the steering mirror is larger than that of UL, the pipe diameter of the spiral-cooling water channel must be larger to provide more cooling water, which increases the torque of the spiral pipe. In order to compensate the increased torque, the design change of the coil spring is performed.

Another of the redesign issues is the thermal stress at the blanket shield module (BSM) for poloidal steering configuration. The thermal analysis shows the peak stress of the cooling channel is 820 MPa, which exceeds the allowable stress limit (370 MPa). By separating the first wall from the integrated shield structure, more cooling water channels can be routed close to the surface, which reduces the thermal stress of the cooling channel to around 300 MPa.

The mirror and waveguide unit are attached to the closure plate by rectangular flanges in the poloidal steering configuration. Because the surface pressure at the corner of the rectangular flange is high, it is impossible to keep homogeneous pressure to the rectangular vacuum seal. A simulation of the vacuum seal compression shows the necessary load for the bolts is 67.8 kN, which exceeds the stainless steel bolt limit. In order to solve this problem, the introduction of the Inconel 718 bolt is considered.

The 8 RF beams radiated from 8 waveguides are injected to the large parabolic steering mirror and focussed to plasma. Therefore, injection angles of each beam are slightly different, which gives modified RF absorption profile compared to expected profile. In order to improve this situation, a ray tracing code is integrated with the EL optical system optimization program.

Integrated Modelling of Core and Divertor Plasmas for DEMO-FNS Hybrid Facility

A. Y. Dnestrovsky¹, A. S. Kukushkin^{1,2}, B. V. Kuteev^{1,2}, and V. Y. Sergeev³

¹National Research Centre "Kurchatov Institute", Moscow, Russian Federation

²National Research Nuclear University "MEPhI", Moscow, Russian Federation

³St. Petersburg State Polytechnical University, St. Petersburg, Russian Federation

Corresponding Author: A. Y. Dnestrovsky, dnestrov0@gmail.com

The steady state regime for tokamak based neutron source DEMO-FNS with parameters $R/a = 3.2$ m/1 m, $B_t = 5$ T, $I_p = 4\text{--}5$ MA, $P_{\text{NBI}} = 30$ MW and $P_{\text{ECR}} = 6$ MW is studied using a consistent modelling of the central and divertor plasma. In our formulation, the divertor plasma state is determined by the values of heat flux P_{SOL} and the pressure of the neutrals in the divertor p_n . As boundary conditions for the central plasma we use values of density and temperatures of ions and electrons on the separatrix and the neutral flux through the separatrix toward to the central plasma column. In divertor region all values calculated by the programme SOLPS4.3 for a set of operating points (~ 30 in our case) with different values of P_{SOL} and p_n , and then the calculation results are approximated by analytical formulas. Heat transport in the central plasma is calculated using the ASTRA code and sets the scaling for the confinement time of energy $\text{IPB}_{98}(y, 2)$ with variation of H-factor. The simplified physical model for the description of the pedestal in H-mode inside the separatrix is used, based on the scalings for width and pressure at the pedestal. The density of the plasma (electrons or ions of deuterium and tritium) is modelled taking into account sources of neutrals coming from divertor region, as well as the injection of fast atoms and/or pellet injection. The neon injection is modelled to reduce the heat loads to divertor plates, that would able to radiate up to 60% of input power. The He plasma dilution is taken into account to estimate the maximum permissible helium confinement values.

The simulation determines the window of plasma parameters DEMO-TIN, in which the heat load on divertor plates remain at an acceptable level, and the divertor plasma does not go into "detachment" mode. The dependence of these conditions on the radiation power, the impurity level, fraction of α -particles is investigated.

RFQ Commissioning of Linear IFMIF Prototype Accelerator (LIPAc)

A. Kasugai¹, P. Abbon², T. Akagi¹, L. Antoniazzi³, N. Bazin², P.-Y. Beauvais⁴, L. Bellan³, B. Bolzon², D. Bortolato³, P. Cara⁴, N. Chauvin², S. Chel², M. Comunian³, H. Dzitko⁴, T. Ebisawa¹, E. Fagotti³, D. Gex⁴, R. Gobin², F. Grespan³, R. Heidinger⁴, Y. Hirata¹, R. Ichimiya¹, D. Jimenez-Rey⁵, A. Jokinen⁴, J. Knaster⁶, I. Kirpichev⁵, K. Kondo¹, S. Maebara¹, A. Marqueta⁶, J. Marroncle², P. Mendez⁵, J. Molla⁵, C. de la Morena⁵, M. Montis³, I. Moya⁴, A. Palmieri³, G. Phillips⁴, A. Pisent³, I. Podadera⁵, G. Pruneri⁶, D. Regidor⁵, K. Sakamoto¹, F. Scantamburlo⁶, T. Shinya¹, M. Sugimoto¹, and M. Weber⁵

¹National Institutes for Quantum and Radiological Science and Technology (QST), Rokkasho Fusion Institute, Rokkasho-mura, Aomori, Japan

²Commissariat à l'énergie atomique (CEA/Saclay), 91191 Gif-sur-Yvette, France

³Istituto Nazionale di Fisica Nucleare (INFN), Laboratori Nazionali di Legnaro, Legnaro, Italy

⁴F4E: Fusion for Energy, EUROfusion Consortium, 85748 Garching, Germany

⁵Centro de Investigaciones Energéticas, Medioambientales y Tecnológicas (CIEMAT), Madrid, Spain

⁶International Fusion Materials Irradiation Facility (IFMIF/EVEDA), Rokkasho, Aomori, Japan

Corresponding Author: A. Kasugai, kasugai.atsushi@qst.go.jp

The IFMIF project aiming at material tests for a future fusion DEMO reactor is under the EVEDA phase in the BA Agreement of fusion program between Japan and EU. As the accelerator activity, the installation and commissioning of the Linear IFMIF Prototype Accelerator (LIPAc) is at the second stage of demonstration of the feasibility of the low energy section of an IFMIF deuteron accelerator up to 9 MeV with a beam current of 125 mA, CW. The installation of injector, RFQ, MEBT, D-Plate and LPBD for LIPAc with eight coaxial high-power transmission lines and RF power system was just done in 2017 at Rokkasho, Japan. After that, the RF conditioning of RFQ for beam commissioning is underway. The beam commissioning of RFQ with H^+ / D^+ and the acceleration demonstration up to 5 MeV–125 mA–0.1% duty cycle with D^+ will be done.

Development of the Far-Infrared Laser Polarimetry for Current Profile Measurement on ITER

R. Imazawa¹, T. Ono², T. Hatae¹, and K. Itami¹

¹National Institutes for Quantum and Radiological Science and Technology (QST),
Naka Fusion Institute, Naka-shi, Ibaraki-ken, Japan

²Nippon Advanced Technology Co., Ltd., 3129-45 Muramatsu, Tokai-mura, Ibaraki, 319-1112, Japan

Corresponding Author: R. Imazawa, imazawa.ryota@qst.go.jp

The authors are demonstrating the key technology necessary for the ITER poloidal polarimeter (PoPola) in order to measure the plasma current profile in ITER. The entire optical train of a prototype channel was made to evaluate the performance of the laser alignment system and the stability of the polarization measurement. The PoPola system injects multiple far-infrared (FIR) laser beams into the plasmas (wavelength is 119 μm) and those probing beams are reflected by retro-reflectors (RRs). The polarization state of the FIR laser beams returning to the diagnostic room are measured by means of the rotating waveplate Stokes polarimeter (RWS polarimeter). The RWS polarimeter technique measures both orientation angle (θ) and ellipticity angle (ε) of the polarization state. Changes in θ and ε , which are mainly associated with the Faraday and the Cotton-Mouton effects, provide information of electron density, electron temperature and magnetic field. Equilibrium reconstruction of PoPola measurement data together with other ITER diagnostics data provides the current profile. Since the RWS polarimeter technique does not use interference signal of a probing and a reference beam, it does not need to take care about wave front distortion of laser beams and change of path length difference between the probing and the reference beam. However, the RWS polarimeter technique needs higher power ($\sim 10 \mu\text{W}$) of the laser beam returning to a detector than other polarimeter based on interferometer. Key technologies for getting high power of the returning laser beam are a retro-reflector and a laser beam alignment system. Prototypes of the tungsten RR was made of a tungsten mono-block by machining and the angle between orthogonal mirrors was 89.9167° . Taking into account the thermal expansion during the plasma operation, the achieved manufacturing tolerance is promising. We developed the laser beam alignment method in order to minimize the loss due to shading at the vacuum window and RR. When the laser beam is tilted within ± 1 mrad for the sake of searching the RR centre, the beam position displacement at the vacuum window was 2.0 mm or less. The alignment error above leads to the laser power loss of 4% owing to shading and acceptable.

Overview of ITPA R&D Activities in Support of ITER Diagnostics

D. L. Brower¹, D. Mazon², and G. Vayakis³

The ITPA Topical Group on Diagnostics

¹University of California Los Angeles, CA 90095, USA

²Commissariat à l'énergie atomique (CEA/Cadarache), 13108 St. Paul lez Durance, France

³International Thermonuclear Experimental Reactor (ITER),
Cadarache Centre, 13108 St. Paul lez Durance, France

Corresponding Author: D. L. Brower, brower@ucla.edu

The International Tokamak Physics Activity (ITPA) Topical Group (TG) on Diagnostics has been conducting R&D activities to support improved ITER diagnostic performance. In this paper, highlights of the Topical Group activity are overviewed: mitigation of first mirror degradation in optical systems, mirror cleaning techniques have been progressed; in-vessel stray-light has been investigated to reduce its impact on diagnostics; diagnostics of escaping particles, feasibility test of the activation probe technique has progressed under a multimachine joint experiment. Diagnostic systems are essential for machine protection, reliable machine operation and comprehensive understanding of burning plasma behaviour in ITER. In order to achieve the above aims, more than fifty subsystems will be developed for measurement of plasma and plasma facing components in the harsh ITER environment, e.g., higher neutron/ γ -ray irradiation and lower accessibility/maintainability compared to that of existing fusion devices. ITPA Diagnostics TG has addressed common physics issues in diagnostics development. The TG activity is mainly directed to high priority research areas (HP);

- HP-1: Optimization of the life-time of plasma facing mirrors used in optical systems,
- HP-2: Assessment of impact of in-vessel wall reflections on diagnostic systems,
- HP-3: Develop methods of measuring the energy and density distribution of escaping α 's,
- HP-4: Plasma control system measurement requirements.
- HP-5: Develop diagnostic calibration techniques/strategies compatible with the burning plasma environment;

and Joint Experiments for Diagnostics (JEX-DIAG) under a framework between ITPA and the Implementing Agreement on Cooperation of Tokamak Programmes of the International Energy Agency (IEA);

- JEX-DIAG-2: Environmental tests on first mirrors,
- JEX-DIAG-5: Field test of an activation probe,
- JEX-DIAG-6: Cross comparisons of charge exchange recombination spectroscopy and X-ray imaging crystal spectroscopy,
- JEX-DIAG-7: Distributed monitoring of microwave power density,
- JEX-DIAG-8: Benchmark of wall reflections,
- JEX-DIAG-9: Spectral MSE (MSE-LS) experiments as design driver for ITER,
- JEX-DIAG-10: Minimizing microwave absorption in vacuum windows,
- JEX-DIAG-11: Determination of the runaway electron distribution function by spectral Bremsstrahlung measurements in the γ -ray energy range.

Verification Tests for Remote Participation at ITER REC

S. Clement-Lorenzo¹, J.-F. Artaud², G. De Tommasi^{3,4}, J. Farthing⁵, G. Giruzzi², H. Kubo⁵, N. Hayashi⁵, O. Hemming⁶, A. Hynes⁶, F. Imbeaux², S. Ide⁵, Y. Ishii⁵, G. Manduchi⁷, M. Matsukawa⁵, M. Mattei^{8,4}, A. Mele^{3,4}, Y. Miyata⁵, N. Nakajima^{9,10}, H. Nakanishi¹¹, J. Noe¹², O. Naito⁵, S. Ohira¹⁰, T. Ozeki⁵, A. Rigoni⁷, F. Robin¹², F. Sartori⁴, Y. Sugie⁹, T. Totsuka⁵, H. Urano⁵, V. Vitale¹³, M. Wheatley⁶, and K. Yamanaka¹⁴

¹F4E: Fusion for Energy, ITER EU Centre, 08019 Barcelona, Spain

²Institut de Recherche sur la Fusion par confinement Magnétique (IRFM), Commissariat à l'énergie atomique (CEA/Cadarache), 13108 St. Paul lez Durance, France

³Università degli Studi di Napoli Federico II, 80138 Napoli, Italy

⁴Consorzio CREATE, Università degli Studi di Napoli Federico II, 80138 Napoli, Italy

⁵National Institutes for Quantum and Radiological Science and Technology (QST), Naka Fusion Institute, Naka-shi, Ibaraki-ken, Japan

⁶Culham Centre for Fusion Energy (CCFE), Culham Science Centre, Abingdon, UK

⁷Consorzio RFX, Associazione EURATOM-ENEA sulla Fusione, Padova, Italy

⁸Università degli Studi della Campania "Luigi Vanvitelli", 80131 Aversa, Italy

⁹International Fusion Energy Research Center (IFERC), Rokkasho, Aomori, Japan

¹⁰National Institute for Fusion Science, Rokkasho Research Center, Rokkasho-mura, Aomori 039-3212, Japan

¹¹National Institute for Fusion Science (NIFS), Toki, Gifu, Japan

¹²Commissariat à l'énergie atomique (CEA/Saclay), 91191 Gif-sur-Yvette, France

¹³ENEA C. R. Frascati, Dipartimento FSN, Frascati, Italy

¹⁴National Institute of Informatics (NII), Tokyo, Japan

Corresponding Author: S. Clement-Lorenzo, susana.clement-lorenzo@f4e.europa.eu

The ITER Remote Experimentation Centre (REC) in Rokkasho is a project implemented within the Broader Approach (BA) agreement at IFERC. The long-term objective of the REC is to allow researchers to take part in the experimentation on ITER from a remote location. On a shorter time scale, before ITER will be operated, the REC facility will be used to test technologies for remote participation in collaboration with existing European tokamaks and with JT-60SA, whose first operations are envisaged in 2020. Other than setting up and equipping the REC control room, during the first phase of REC (2013-2017) the project scope included activities aimed at developing and evaluating software tools for fast data transfer, remote participation, data analysis, and plasma simulation. These activities have been carried out by an Extended-Integrated Project Team (E-IPT). Indeed, due to the characteristics of the remote experiment, the collaborations with experts in other institutes providing experimental data, network infrastructure, data transfer protocol, and experiences on intercontinental data transfer and data acquisition were essential for the success of the REC activities. As a consequence, members from different Japanese and European institutions were invited to join in E-IPT; among the various contributors, there are members of the ITER project and of the Satellite Tokamak Programme (STP), members of the NII and the NIFS in Japan, and members of JET and WEST in Europe.

In this paper, we report on the results of the REC verification tests that have been carried out in 2017. These tests were mainly aimed at assessing the functionalities of the REC control room (i.e., the configurability of the room layout, the capabilities of the video wall, etc.), as well as the functionalities of the software tools for remote participation that have been developed during the first BA period. A report on the preliminary remote participation tests carried out in collaboration with the JET tokamak will be also given, together with a description of the tests with both JET and WEST that have been planned for 2018.

Consorzio RFX Contribution to the JT-60SA Project in the Frame of the Broader Approach Agreement

E. Gaio¹, A. Ferro¹, A. Maistrello¹, F. Gasparini¹, and R. Piovan¹

¹*Consorzio RFX, Associazione EURATOM-ENEA sulla Fusione, Padova, Italy*

Corresponding Author: E. Gaio, elena.gaio@igi.cnr.it

The JT-60SA satellite tokamak is now under advanced assembly phase in Naka (Japan). The majority of the new power supplies are provided by Europe, and the Italian National Research Council (CNR), acting through Consorzio RFX, has contributed in particular with two systems: the quench protection circuits (QPC) for the superconducting magnets and the power supply system for RWM control.

The procurement of both the systems has been successfully carried out: the QPCs were delivered to Naka site in autumn 2014; the installation, commissioning and acceptance tests were completed in July 2015, fully in line with the schedule agreed in 2009. The protection system for the superconducting coils is composed of thirteen units: three for the TF circuit and ten for the PF circuits. Their duty is to conduct the coil current in normal operation and commutate it into a dump resistor in case of quench or other faults by means of a DC circuit breaker (CB). The nominal currents to be interrupted and the maximum reapplied voltages are 25.7 kA and 2.8 kV for the TF QPCs and ± 20 kA and ± 5 kV for PF QPCs.

As for the RWM-PS system, we are very close to completion, with the delivery on site and closure of the procurement expected in autumn 2018. This system consists in an input rectifier stage and 18 power amplifiers, one for each coil, capable to supply a peak current of 300 A and an output voltage of 240 V and satisfy strict dynamic requirements in terms of latency and current bandwidth (50 μ s, 3 kHz) thanks to the adoption of new hybrid silicon-silicon carbide (Si-SiC) power semiconductors for the power amplifiers and to the development of a new sophisticated control board, based on the combination of a fast microcontroller and a FPGA running optimized firmware.

A summary of the studies for the development of both the systems, of the main phases of their procurement and relevant results will be presented. The innovative aspects of their design will be highlighted: JT-60SA QPC represents the first application of hybrid mechanical-static technology for protection of superconducting magnets in fusion experiments and RWM-PS is the first PS system in fusion experiments adopting SiC semiconductors. The future work will be also discussed; outcomes from the operation of these systems, useful for ITER and DEMO, are expected.

The Influence of Displacement Damage and Helium on Deuterium Transport and Retention in Tungsten

T. Schwarz-Selinger¹, S. Markelj², J. Bauer¹, A. Manhard¹, and K. Schmid¹

¹Max-Planck-Institut für Plasmaphysik, Garching, Germany

²Jožef Stefan Institute, 1000 Ljubljana, Slovenia

Corresponding Author: T. Schwarz-Selinger, tms@ipp.mpg.de

Among many other favourable properties of tungsten its low intrinsic fuel retention makes it a promising candidate as plasma facing material. However, during operation defects in the tungsten lattice will evolve that will trap hydrogen isotopes. While for present day devices this increased retention is only limited to the near surface it will take place throughout the whole bulk in future nuclear devices as a consequence of the neutron irradiation. There is not yet a microscopic understanding that would allow describing the processes that will prevail in a reactor environment quantitatively, where damage creation and hydrogen retention will mutually influence each other. Present day predictions are only based on extrapolation of data collected from non-nuclear machines. Hence, the influence of hydrogen on defect production, the influence of defects on hydrogen isotopes transport as well the influence of the presence of helium (directly implanted close to the material surface from the plasma as well as produced throughout the bulk by tritium decay and transmutation) is not considered in these extrapolations.

Implantation of different ion species with energies in the MeV range can be used to simulate the displacement damage neutrons will cause. Contrary to neutron irradiation, ion beam irradiation is fast and does not activate the samples. Likewise, the influence of He on transport and retention can be studied by implanting He with MeV-energy deep into the material. In this way surface effects can be separated from bulk effects. These kind of experiments allow dedicated parameter studies under well controlled conditions. In this contribution such benchmark experiments on transport and retention of deuterium in displacement damaged and helium containing tungsten are presented that allow to test and extend present day understanding on a quantitative level. The dependence of deuterium retention on the damage level, the influence of damage rate as well as the influence of the specific ion used to create the displacement damage will be shown. Results from hydrogen isotope exchange experiments are presented that reveal the dynamics of hydrogen transport which is a chain of trapping and detrapping processes. Rate equation modelling without free parameters is used to describe the observed uptake during plasma exposure as well as the release during annealing.

Experimental Measurements of Cryogenic Heat Loads on SST-1 Helium Cryogenic Plant

N. Bairagi¹, V. L. Tanna¹, P. N. Panchal¹, R. N. Panchal¹, D. Sonara¹, R. Patel¹, G. Mahesuria¹, G. L. N. Srikanth¹, A. Garg¹, D. Christian¹, R. Sharma¹, K. Patel¹, H. Nimavat¹, P. Shah¹, G. Purwar¹, J. C. Patel¹, G. K. Singh¹, U. Prasad¹, A. K. Sahu¹, R. Srinivasan¹, and D. Raju¹

¹*Institute for Plasma Research (IPR), Bhat, Gandhinagar, India*

Corresponding Author: N. Bairagi, nbairagi@ipr.res.in

The SST-1 cryostat houses 130 thermal shields cooled using liquid nitrogen, 16 toroidal field (TF) coils, 9 poloidal field (PF) coils and their associated support structures. The superconducting magnets system (SCMS) of the SST-1 consisting of TF and PF coils is designed to cool with forced-flow supercritical helium (SHe) at 4 bar, 4.5 K and a mass flow rate of 300 g/s using helium refrigerator-cum-liquefier (HRL) of 1.3 kW equivalent cold power at 4.5 K. In the last several campaigns, we have observed that the TF and PF coils could not be simultaneously cooled to 4.5 K due to heat loads from SCMS exceeding the installed cryogenic capacity of HRL. In order to cool the TF coils system at desired conditions of 4.5 K, we had to isolate PF coils as well as TF Case hydraulics from HRL at intermediate temperatures of ~ 20 K. In this specific case, the PF coils and TF Case surfaces would be at elevated temperatures in the range of 40 K–50 K. To ascertain overall heat loads from SCMS, its associated supports structure along with the cryogenic distribution system under different cooling scenarios on SST-1 helium cryogenic plant, we have recently conducted a dedicated campaign. In this experiment, we demonstrate cool down of TF magnets in single phase supercritical helium mode to ~ 5 K for the first time. Helium supply pressure, temperature and mass flow rate are measured at the outlet of HRL before it is fed to SCMS while helium return temperature and pressure from SCMS are recorded at return line of HRL. This gives a clear picture of equivalent heat loads on HRL system. The cryogenic heat load is found to be ~ 1286 – 1350 W ($\pm 3\%$) at 5.5 K under single phase flow conditions. In the same campaign we have succeeded to cool all the nine PF coils to ~ 5 K by isolating TF coils from HRL for the first time. In this work, we report the experimental measurement procedure, instrumentation details and heat load data analysis. These results serve useful purpose in assessing the net cooling power requirement for the simultaneous cooling of the TF and PF coils and facilitate long duration plasma experiments in future.

Thermo-Mechanical Experiments On Lithium Titanate Pebble Bed

R. Bright¹, P. Chaudhuri¹, M. N. Makwana¹, S. Gupta¹, M. Panchal¹, A. Shrivastava¹,
E. Rajendra Kumar¹, C. Zhang², and A. Ying²

¹*Institute for Plasma Research (IPR), Bhat, Gandhinagar, India*

²*Fusion Science and Technology Center, University of California Los Angeles, CA 90095, USA*

Corresponding Author: R. Bright, riscob.bright@ipr.res.in

Among the various lithium ceramics, Li_2TiO_3 is one which has been received much attention due to its very excellent properties, such as reasonable lithium atom density, low activation, excellent tritium release performance and chemical stability, etc. Lithium Titanate [Li_2TiO_3] pebbles with the diameter of 1 mm was widely used for the experiments after successful completion of variety of modelling and experiments. In the present study we have prepared lithium titanate from its high pure raw material of lithium carbonate and titanium dioxide by solid state reaction in the stoichiometric ratio. The reaction temperature has been estimated from the thermo-gravimetric and differential thermal analysis (TG-DTA) and the same scenario has been executed for the bulk production using high temperature furnace. The phase and phase stability at different temperature were analyzed by using powder X-ray diffractometer. The pebble preparation has been carried out from this raw material after once again ground them to fine powder and addition of PVA as a binder for the preparation of green pebbles using extruder-spheronizer technique. The green pebbles were sintered at high temperature to attain desired density for further studies. The details of the Li_2TiO_3 powder and pebble fabrication and their characterizations like XRD, density, porosity, crush load, SEM analysis, Young's Modulus and creep will be discussed in the paper.

The Operation, Control, Data Acquisition System of ASDEX Pressure Gauge for Neutral Pressure

K. Patel¹, K. A. Jadeja¹, A. Kumar¹, and J. Ghosh¹

¹*Institute for Plasma Research (IPR), Bhat, Gandhinagar, India*

Corresponding Author: K. Patel, kkpatel@ipr.res.in

The Bayard–Alpert (BA) type hot-cathode ionization gauge is widely used to measure neutral pressure precisely in vacuum system below 10^{-3} Torr pressure. Neutral pressure measurement in magnetic confinement fusion experiments is quite challenging for standard BA type gauge due to higher pressure limitation and its ionization is affected by high magnetic and electrical fields. To overcome above limitations, a special hot-cathode ionization gauge, named ASDEX Pressure Gauge (APG) system has been developed by G. Haas at the Max-Planck-Institute, Germany [1]. The APG system works in high magnetic field up to 6 T and high temperature plasma environment with broad pressure measurement range from 10^{-1} to 10^{-6} mbar with fast response (< 10 ms) and good noise immunity.

For ADITYA Tokamak, a customized system of operation, control and data acquisition for standard APG system has been designed and developed to measure real-time neutral pressure during high-temperature plasma discharges. The developed system can achieve synchronous control of gauge controller using GPIB and data acquisition of ion and emission current of gauge head using PCI based data acquisition module. Initially, the APG calibration with standard BA type hot cathode ionization gauge had been carried out on the test setup of low magnetic field and ultrahigh vacuum system with different gases like H_2 , Ar, He. For APG calibration in various pressure range of different gases, precise gas feed control system has been developed using controller based hardware and LabVIEW software. After successfully testing and calibration, the APG was installed on ADITYA tokamak and calibrated under high magnetic field of ADITYA Tokamak. The developed APG control system has been configured to set the gauge parameter before the plasma discharge and acquired real-time analog signal acquisition using simultaneous sampling by analog to digital convertor (ADC) during plasma discharge. The acquired raw data and processed real-time pressure measurement gives valuable neutral density information to tokamak plasma.

References

[1] G. Haas and H. S. Bosch, *Vacuum*, **51**, 39–46 (1998).

Conceptual Design Study for Heat Exhaust Management in the ARC Fusion Pilot Plant

E. A. Tolman¹, N. M. Cao¹, A. J. Creely¹, C. A. Dennett², J. Hecla², H. Hoffman¹,
A. Q. Kuang¹, M. Major¹, J. Ruiz Ruiz¹, R. A. Tinguely¹, D. Brunner¹, B. LaBombard¹,
B. N. Sorbom¹, D. G. Whyte¹, P. Grover³, and C. Laughman³

¹Plasma Science & Fusion Center, MIT, Cambridge, MA 02139, USA

²Nuclear Science and Engineering Department, Massachusetts Institute of Technology (MIT), Cambridge, MA 02139, USA

³Mitsubishi Electric Research Laboratories, Cambridge MA 02139 USA

Corresponding Author: E. A. Tolman, etolman@mit.edu

The ARC pilot plant conceptual design study [1] is extended to explore options for managing ~ 525 MW of fusion power generated in a compact high field ($B_t = 9.2$ T) tokamak about the size of JET ($R_0 = 3.3$ m). Exploiting ARC's demountable high temperature superconductor toroidal field (TF) magnets, poloidal magnetic field (PF) coils located inside the TF, and vacuum vessel (VV) immersed in molten salt FLiBe blanket, this follow-on study identifies novel robust power exhaust solutions. The superconducting PF coil set is reconfigured to create double-null plasma equilibria that include an X-point target divertor geometry. Modelling shows that such long-leg configurations enhance power handling and can achieve passively-stable detachment fronts that stay in the divertor leg over a wide power window [2, 3]. The VV is modified to include the divertors while retaining original core plasma volume and TF magnet size. The molten salt FLiBe blanket shields all superconductors, functions as an efficient tritium breeder, and, with augmented forced flow loops, serves as a single-phase, low-pressure coolant for the divertor and VV. MCNP neutronics calculations show a tritium breeding ratio of ~ 1.08. The neutron damage rate of the remote divertor targets is ~ 3 times lower than that of the first wall, which is beneficial because high neutron damage often leads to degradation in thermal performance. The demountable TF magnets allow for vertical maintenance schemes and replacement every 1–2 years, increasing tolerance for neutron damage. The divertor has tungsten swirl-tube cooling channels capable of exhausting 12 MW/m^2 of heat flux, which includes a factor of ~ 8 safety margin over anticipated steady state heat loads. Novel diagnostics supporting the heat exhaust mission compatible with the neutron environment are proposed, including the use of Cherenkov radiation emitted in FLiBe to measure fusion reaction rate, microwave interferometry to measure divertor detachment front location, and IR imaging through the FLiBe blanket to monitor divertor "hotspots."

The authors acknowledge support from the MIT Nuclear Science and Engineering Department and the PSFC.

References

- [1] B. N. Sorbom *et al.*, Fusion Eng. Des., **100**, 378–405 (2015).
- [2] M. V. Umansky *et al.*, Phys. Plasmas, **24**, 056112 (2017).
- [3] M. Wigram *et al.*, Conts. to Plasma Phys., (2018).

Progress on Lithium Ceramic Breeder Materials Development, Characterization and R&D Activities in IPR

P. Chaudhuri¹, M. Panchal¹, A. Shrivastava¹, M. N. Makwana¹, and S. Kanjiya¹

¹*Institute for Plasma Research (IPR), Bhat, Gandhinagar, India*

Corresponding Author: P. Chaudhuri, paritosh@ipr.res.in

Several materials have been developed and being investigated for reliable and sustainable breeder candidate material. Lithium meta-titanate (Li_2TiO_3) and Lithium ortho-silicate (Li_4SiO_4) are the prominent among the suitable candidate materials for breeders. India has proposed lithium meta-titanate (Li_2TiO_3) as the tritium breeder materials in the form of pebble bed for LLCB TBM. Li_2TiO_3 powder was prepared by solid state reaction using LiCO_3 and TiO_2 followed by ball-milling and calcination. Li_2TiO_3 pellets and pebbles are prepared from this powder followed by high temperature sintering. Effect of sintering time and temperature on the properties of pebbles has been studied. At every stage of preparation, extensive characterizations are being carried out to meet the desired properties of these materials. The geometry and loading conditions of the breeder blankets makes the analysis complex. For a robust design of blankets requires a thorough understanding of the thermo-mechanical response of the breeder materials at different loading conditions. In this context, the material characterization plays a vital role in determining the breeder response. It is essential to measure the mechanical and thermo-mechanical properties of pebble bed. Experimental set ups have been built indigenously at IPR for the measurement of effective thermal conductivity of pebble bed using steady state-axial heat flow and transient hot wire methods. The effective thermal conductivity (k_{eff}) of pebble beds is an important parameter for the design and analysis for a fusion tritium breeder blanket. The k_{eff} of Li_2TiO_3 pebble bed is measured as a function of average bed temperature from RT to 500°C in different environment (vacuum, helium gas, etc.). Initial results obtained from these experiments will be discussed in this paper. Details of lithium ceramic breeder material development, their characterizations and related R&D activities will be discussed in this paper.

Machine Control System for Large Volume Plasma Device: Current Status and Future Directions

R. Sugandhi¹, P. K. Srivastava¹, P. Srivastav¹, A. K. Sanyasi¹, and L. M. Awasthi¹

¹*Institute for Plasma Research (IPR), Bhat, Gandhinagar, India*

Corresponding Author: R. Sugandhi, ritesh@ipr.res.in

The Large Volume Plasma Device (LVPD) [1] is a cylindrical shaped pulsed plasma device dedicated in carrying investigations relevant to fusion and magneto-spheric plasma. For meeting requirements for its upgrade, efforts are in progress towards enhancing plasma duration ($t_{\text{pulse}} \sim 9\text{--}50$ ms), to cater to the needs of controlled experiments on electron temperature gradient (ETG) turbulence, a major source of plasma loss in fusion devices by suitably varying the density gradient scale length.

The machine control system (MCS) has the responsibility of protected and integrated operation of the device using standardized interface. MCS consists of namely: 1) PXIe based data acquisition system [2], 2) Modbus based process automation system [3, 4], and 3) RAID configured based data handling system. The PXIe based data acquisition system is already implemented and its upgradation for data processing to convert raw signals of various diagnostics to plasma parameters and up gradation of hardware for nonlinear structure study are underway. The Modbus bus has been selected for process automation of the device. Currently, process automation has been carried out for high current filament power supply and radially movable probe positioning system (~ 12 numbers). The efforts are ongoing for extension of the automation for 3-axis probe drive system, camera based surveillance system, axial probe positioning, vacuum production system and different power supplies. A RAID configured server is under procurement for hosting MDS+ based data handling system. LabVIEW has been selected as supervisory data acquisition and control system for development. The novelty of the work lies in integration and handling of heterogeneous I&C controllers under single console. The paper will discuss the results obtained for integration and operation of machine control system.

References

- [1] S. K. Mattoo *et al.*, Phys. Rev. Lett., **108**, 255007 (2012).
- [2] R. Sugandhi *et al.*, 7th Int. Conf. on Cloud Computing, Data Science and Engineering, IEEE Conference Series, **804**, (2017).
- [3] R. Sugandhi *et al.*, Fusion Eng. Des., **112**, 804 (2016).
- [4] R. Sugandhi *et al.*, Fusion Eng. Des., **115**, 49 (2017).

Application of Finite Element Techniques in Simulation of Mechanical Design and Performance Assessment of Different Components of a Neutral Beam Systems

V. N. Muvvala^{1,3}, A. Yadav¹, D. Singh¹, D. Sharma^{2,3}, J. Joshi¹, H. Patel¹, S. Pillai¹, S. Shah^{1,3}, M. Singh¹, M. Bandyopadhyay^{1,3}, and A. K. Chakraborty¹

¹ITER-India, Institute for Plasma Research (IPR), Bhat, Gandhinagar, India

²Institute for Plasma Research (IPR), Bhat, Gandhinagar, India

³Homi Bhabha National Institute (HBNI), Anushakti Nagar, Mumbai 400094, India

Corresponding Author: V. N. Muvvala, mvnraju@iter-india.org

Accelerators, ion dumps and beam transport system for neutral beam application are designed to manage high heat loads in the range of 2–10 MW/m². The performance of these components under various damage criteria are assessed for their thermo-mechanical stability under various operating and faulty conditions. Due to the pulse nature (3 s on / 20 s off with 5 Hz modulation) of beam operation, components often exposed to cyclic thermal loads. Further, the above system is incorporated with large number of flexible elements (e.g., bellows, etc.) to absorb the thermal movements. For systems like accelerator and electrostatic residual ion dumps, there is an additional need of nonmetallic components, like ceramics, which function as electrical isolation as well act as structural elements. To assess diverse nature of such systems with complex loading requirements, finite element analysis tools (e.g., ANSYS, CFX, SYSWELD, etc.) have been employed as part of design evolution and results are verified according to codes and standards (ASME / RCC-MR / EJMA). The experimental validation of effectiveness of these assessment have been also performed by prototype testing and performing the tests on the real manufactured products. It is also important to note that, the tools are also useful to address the in-process manufacturing modification those may arise due to feasibility constraints.

The paper shall present some of the important simulations results on 10 MW/m² capability of heat transfer elements, functional tests on 100 kV post insulators, bellows assessment in water lines, CFD simulations for beam source components, etc.

TRIGA Integral Activation of Mn Foils, Li₂O and LiF as Potential Tritium Production Monitors for Fusion Applications

I. Kodeli¹, V. Radulović¹, G. Veniger¹, D. Kavšek¹, T. Kuc², M. Ciechanowski², and W. Pohorecki²

¹Jožef Stefan Institute, 1000 Ljubljana, Slovenia

²AGH University of Science and Technology, Krakow, Poland

Corresponding Author: I. Kodeli, ivan.kodeli@ijs.si

In the future fusion reactors, such as ITER or DEMO, tritium will be produced by bombardment of lithium atoms with neutrons and several types of special tritium breeder modules (TBM) will be installed in the ITER reactor to demonstrate the self-sufficiency of tritium production. LiF pellets commercially produced as thermo-luminescent detectors (LiF-TLDs) can be used to measure tritium production. The similarities between the sensitivity profiles of the neutron reaction of tritium production in ${}^6\text{Li}(n, t)$ and those of the ${}^{55}\text{Mn}(n, \gamma){}^{56}\text{Mn}$ reaction in the TBMs indicated that the latter reaction could be used as a tritium production monitor, at least for short-term monitoring, the half-life of ${}^{56}\text{Mn}$ being 2.579 h. However, experimental verification and improvements and validation of the Mn cross-sections are needed in order to meet the required accuracy. In the scope of the Fusion for Energy (F4E) project of the European Commission, foils of certified reference materials Al-1%Mn and Al-0.1%Au, as well as TLD(LiF) and Li₂O samples were irradiated in the JSI TRIGA research reactor, both bare, and under Cd and boron-nitride to study the potential use of manganese detectors for monitoring the tritium production in fusion machines. In order to obtain complementary information for data validation purposes, the irradiations were performed in different neutron spectra, i.e., in the central channel, the pneumatic tube in position F24 in the outer “F” ring of the reactor core, in position F19 and in the IC-40 irradiation channel in the graphite reflector. Bare, and under Cd and boron-nitride irradiations were needed for the subtraction of epi-thermal neutron contribution in the ${}^{55}\text{Mn}(n, \gamma){}^{56}\text{Mn}$ reaction. Two series of measurements was performed, in 2014 and 2017. The transport calculations were performed using the Monte Carlo transport code MCNP6.1 with a detailed model of the TRIGA reactor including the irradiation capsules. The uncertainties involved in the measurements and the calculations were carefully evaluated. The principle objective was to study the energy response of the ${}^{55}\text{Mn}(n, \gamma){}^{56}\text{Mn}$ reaction and correlations between the Mn and TLD / Li₂O measurements. Good consistency between the measured and calculated reaction rates, in most cases within the uncertainty bars, was observed and will be reported in the paper.

Seismic Analysis of High Power Amplifier in ITER ICRF Range

R. Anand¹, A. P. Subbarao¹, A. Jha¹, P. Vasava¹, R. G. Trivedi¹, and A. Mukherjee¹

¹ITER-India, Institute for Plasma Research (IPR), Bhat, Gandhinagar, India

Corresponding Author: R. Anand, rohith.anand@iter-india.org

ITER-India is responsible for delivery of 8+1 (production+prototype) RF sources to the ITER project. Each RF source will provide 2.5 MW of RF power at VSWR 2:1 in the frequency range of 35 to 65 MHz. Eight such RF sources will generate total 20 MW of RF power. Two RF chains containing three high power amplifiers (HPA1, HPA2 and HPA3) need to be combined to build an RF source. HPA2 and HPA3 are RF tube-based amplifiers while HPA1 is a solid state power amplifier. This paper covers detailed seismic analysis of high power amplifiers for worst case seismic loading condition.

A SL-2 seismic event has been analyzed to determine potential areas that will require inspection and/or replacement. According to the design basis, a response spectra analysis (RSA) has been performed for the frames and cavity of high power amplifiers which includes the self-weight of all structural members, platform dead weight and reactions from the base. The RSA requires a modal analysis to be performed which is used to determine the rigidity of the support structures. The accelerations of the zero peak acceleration (ZPA) are applied in order to account for all masses. All structures and components must respect the requirement that there must be no failure that would prevent a SIC-1 or SIC-2 component from performing its safety function.

The ANSYS software is used for modal analysis and response spectrum analysis. This paper will also point out the maximum stressed link in structure and modifications may be proposed to achieve the required strength.

ACTYS Code System: Towards Next Generation Nuclear Activation Codes for Fusion Reactors

P. V. Subhash^{1,2}, S. C. Tadepalli¹, P. Kanth³, R. Srinivasan³, and S. P. Deshpande^{1,2}

¹ITER-India, Institute for Plasma Research (IPR), Bhat, Gandhinagar, India

²Homi Bhabha National Institute (HBNI), Anushakti Nagar, Mumbai 400094, India

³Institute for Plasma Research (IPR), Bhat, Gandhinagar, India

Corresponding Author: P. V. Subhash, subhashpv@iter-india.org

Nuclear activation and subsequent radiological response of structural materials within fusion reactors like ITER and beyond need to be studied for operational, safety and radiological waste management reasons. The future fusion machines should be equipped with low radioactive materials optimized for expected neutron environment. Numerical tools with extended capabilities are needed for this kind of analysis. A project named ACTYS-Project is initiated at the IPR to meet the requirements stated above. This effort so far developed more than five state-of-the-art codes and few innovative computational tools for analysis and design of fusion reactors. The details of all the codes and tools will be presented in this paper. ACTYS is the first code within the project. It is a single-point neutron activation code and computes nuclide inventories and other radiological responses within materials when exposed to neutron flux through either continuous, pulse irradiation or mixed. It solves coupled first-order LODEs using Bateman solution for linearized chains. An “exponential convergence” algorithm and “chain weighing” termination technique is developed in-situ for this purpose. These two methods lend ACTYS an added edge over typical linear chain solvers. ACTYS is well validated and the details of the same will be presented. Highly resolved nuclear activation analysis and radiation waste classification are warranted for large-sized fusion machines with a wide variety of materials. To ensure a fast multipoint activation analysis without sacrificing accuracy, inherent changes must be done to single-point activation codes like ACTYS. To this end, a multipoint activation code-named ACTYS-1-GO is developed. Recently, it has been coupled with transport code ATILA by developing a subsidiary module, activation source generator. One of the important features is that nearly 1 million meshes can be computed in less than few hours. A mathematical formulation to account for the contribution of the parent constituents of any irradiated material towards the radiological responses was derived and implemented. The first order derivatives of Bateman linear chain solution with respect to the decay and cross sections constants are generally used for the sensitivity analysis. A simplified and improved set of recursive relations are developed for these derivatives.

Deuterium Depth Profile Measurement in Pre- and Postirradiated Tungsten

A. K. Tyagi^{1,2}, P. N. Maya¹, P. Sharma¹, R. Kumar³, K. Saravanan⁴, V. Karki⁵, M. Singh⁵, A. Mutzke⁶, R. Schneider⁷, C. David⁴, S. Kannan⁵, M. R. Abhang³, S. S. Vala³, A. Attri¹, P. K. Kulriya⁸, P. K. Bajpai⁹, P. M. Raole^{1,3}, and S. P. Deshpande^{1,2}

¹ITER-India, Institute for Plasma Research (IPR), Bhat, Gandhinagar, India

²Homi Bhabha National Institute (HBNI), Anushakti Nagar, Mumbai 400094, India

³Institute for Plasma Research (IPR), Bhat, Gandhinagar, India

⁴Indira Gandhi Center for Atomic Research (IGCAR), Kalpakkam, Tamil Nadu 603102, India

⁵Bhabha Atomic Research Centre (BARC), Mumbai, India

⁶Max-Planck-Institut für Plasmaphysik, Greifswald, Germany

⁷Universität Greifswald, Domstraße 11, 17489 Greifswald, Germany

⁸Inter University Accelerator Centre (IUAC), Aruna Asaf Ali Marg, New Delhi, India

⁹Guru Ghasidas Vishwavidyalaya, Bilaspur, (C.G.), Koni, Chhattisgarh 495009, India

Corresponding Author: A. K. Tyagi, aktyagi@iter-india.org

Tungsten (W) will be used in ITER as a plasma facing material (PFM) in divertor due to its capability to handle high heat flux while having a low hydrogen (H) isotope affinity. However, in presence of fusion neutrons and α -particles, tungsten can accumulate radiation damage, which might significantly enhance its H retention property. In order to investigate the effects of radiation damage on deuterium (D) trapping in tungsten, we have carried out experiments using D beam in pre- and postirradiated polycrystalline tungsten foils. In this paper we present the comparison of D depth profile measurements using elastic recoil detection analysis (ERDA) and secondary ion mass spectroscopy (SIMS) techniques.

Polycrystalline tungsten foil samples of size 8 mm × 8 mm × 0.1 mm foils were mechanically polished and annealed at 1838 K to release the stress and to minimize the defects. These foils were further irradiated with gold ions (80 MeV) and boron ions (10 MeV) to create defects. These samples were then exposed to a D beam of 100 keV energy for a fluence of 5×10^{17} ions/cm². The trapped D was measured using ERDA and SIMS, and the depth profiles were modelled using binary collisions Monte Carlo method by including the surface roughness. The preliminary results show the enhancement in amount of trapped D in pre-damaged tungsten samples in contrast to the undamaged ones. The effect of helium (He) on D trapping in the sample was also analyzed and it was observed that D trapping is reduced in presence of He. The details of the experiments and the analysis will be presented.

Development of a High-Temperature Blackbody Source for ITER ECE Diagnostic

R. Kumar¹, H. B. Pandya^{1,2}, J. Pathak³, S. Danani¹, and V. Kumar^{1,2}

¹ITER-India, Institute for Plasma Research (IPR), Bhat, Gandhinagar, India

²Homi Bhabha National Institute (HBNI), Anushakti Nagar, Mumbai 400094, India

³Maharaja Sayajirao University of Baroda, Vadodara-390002, India

Corresponding Author: R. Kumar, ravinder.kumar@iter-india.org

For the ITER electron cyclotron emission (ECE) diagnostic, there is a requirement of a high-temperature blackbody radiation source operating at atmospheric pressure. This source needs to be operated at high temperature ($\sim 500^{\circ}\text{C}$) having a microwave emissivity > 0.95 in the frequency band 100–500 GHz, and > 0.75 for 500–1000 GHz. Moreover, the radiation surface should have temperature uniformity within $\pm 10^{\circ}\text{C}$. This source will be utilized for characterizing the ITER ECE measuring instruments like Michelson Interferometer and radiometer.

For this purpose, a radiation source has been designed and developed. The radiation source consists of a heater and an emissive surface. The emissive surface is made of silicon carbide (SiC), as it has high thermal conductivity, low thermal coefficient of expansion, excellent machinability, good vacuum compatibility and high emissivity in the mm-wave region. The diameter of the emissive surface is 150 mm. The suitable heating element has been used having high resistivity and good oxidation resistance nature.

This paper deals with the design, analysis, and characterization of the developed high-temperature blackbody radiation source in the frequency range 100 to 1000 GHz. The finite element method based software, “COMSOL”, has been used to analyze and optimize the heating coil design to get desired temperature uniformity of the emissive surface. Experimentally, the temperature uniformity is measured by an IR camera and microwave emissivity is measured by a Michelson interferometer. The operating temperature of 500°C is achieved in the developed source with temperature uniformity within $\pm 10^{\circ}\text{C}$. The short and long-term temperature stability up to $\pm 2^{\circ}\text{C}$ and $\pm 10^{\circ}\text{C}$ respectively has also been achieved. Further, the microwave emissivity of ~ 0.8 – 0.9 has been observed over wideband 100–1000 GHz. The above measured values are in compliance with ITER requirement.

Alignment and Calibration Schemes for ITER CXRS-Pedestal Diagnostic

G. L. Vyas¹, M. F. M. De Bock², M. Von Hellermann², R. Manchanda³, Z. Alexander⁴, and V. Kumar^{1,5}

¹ITER-India, Institute for Plasma Research (IPR), Bhat, Gandhinagar, India

²International Thermonuclear Experimental Reactor (ITER),
Cadarache Centre, 13108 St. Paul lez Durance, France

³Institute for Plasma Research (IPR), Bhat, Gandhinagar, India

⁴RFDA Project Center ITER, 123098 Moscow, Russian Federation

⁵Homi Bhabha National Institute (HBNI), Anushakti Nagar, Mumbai 400094, India

Corresponding Author: G. L. Vyas, gheesa.vyas@iter-india.org

Charge exchange recombination spectroscopy (CXRS) diagnostic shall provide the key measurement for ITER advance plasma control and physics studies. ITER CXRS-pedestal has a primary role of edge ion temperature, plasma rotation (toroidal and poloidal velocity) and impurity density measurements in the pedestal region ($r/a = 0.85-1.0$). Meeting the measurement requirements for these parameters in ITER is more challenging than the present tokamaks due to restricted access for diagnostics components in addition to the harsh environment of ITER.

Some of these challenges are like the calibration offset that limits the velocity measurement accuracy requirement. As well as precise alignment required because of the lower angle between the line of sight with a toroidal plane that introduces additional error in the measurement. Therefore, to meet the measurement requirements in ITER, robust calibration and alignment schemes are being developed. CXRS-pedestal shall cover broad wavelength range, the emission of (He, Be, Ne, Ar, C) recombining lines (460–532 nm) and beam emission spectroscopy (BES) H_{α} (656.3 nm) spectral line simultaneously, compatible with the spatial resolution of 20 mm (that demands a fine alignment) with 5 Hz DNB modulation: 100 ms exposure with DNB ON, 100 ms background exposure. Statistical and systematic errors including atomic modelling along with low light signal due to strong attenuation of the diagnostic neutral beams require better light transmission path and high throughput spectrometer detection system. To access this requirement, preliminary performance assessment carried out using simulation of spectra (SOS) code to see the dependency of the measurement accuracy on SNR.

In this contribution, details of the design and development of the ITER CXRS-pedestal diagnostic system in view of alignment and calibration in the suitable transmission system, this includes the optimum light transmission path analysis using ZEMAX ray tracing tool. This will ensure the required alignment for accurate measurement from the DNB and plasma cross-section area of the pedestal region. The various calibration and alignment schemes are studied and shall be developed to test the performance in the ITER-India Lab to meet the ITER requirement.

Thermal Analysis of Protection Important Components of ITER XRCS-Survey Diagnostic System

S. Varshney^{1,2}, S. Kumar¹, S. Mishra¹, P. V. Subhash^{1,2}, V. Kumar^{1,2}, G. Julio³, P. Bernascolle³, M. Ivantsivskiy⁴, V. Udintsev³, R. Barnsley³, and M. Walsh³

¹ITER-India, Institute for Plasma Research (IPR), Bhat, Gandhinagar, India

²Homi Bhabha National Institute (HBNI), Anushakti Nagar, Mumbai 400094, India

³International Thermonuclear Experimental Reactor (ITER),

Cadarache Centre, 13108 St. Paul lez Durance, France

⁴Budker Institute of Nuclear Physics (BINP), Novosibirsk, Russian Federation

Corresponding Author: S. Varshney, sanjeev@iter-india.org

In ITER, an important aspect of qualifying the components to the mandatory regulatory requirements, the system developers have a challenge to first design the components fulfilling guidelines of the ITER recommended French nuclear code RCC-MR (2007) and later on demonstrate to the regulator. It is even more involving for systems that are extending primary vacuum to the interspace and port-cell as these zones are accessible by a human. The paper addresses such requirements in the thermal design of the X-Ray Crystal Spectroscopy-Survey (XRCS-Survey) system, which is a first plasma diagnostic.

The XRCS-Survey is a broadband (0.1–10 nm) X-ray crystal spectrometer for real-time monitoring of absolute concentration and in-flux of the plasma impurities. For measurements, the transport of X-ray emission is done using a nearly 10 m long sight-tube directly connecting the spectrometer to the closure plate of the port-plug. The sight-tube components, classified as Protection Important Components due to their function in confinement of radioactive tritium and dust, are subjected to various thermal loads while machine operations. These loads are mostly due to baking to achieve ultra-high vacuum inside the ITER vacuum vessel. Furthermore, the components are also subjected to the neutron and γ radiation of DT fusion.

For reliable performance and safe operation of XRCS-Survey diagnostic, a preliminary engineering design and ANSYS analysis of the XRCS-Survey sight-tube components have been performed, with and without radiation shielding, in order to analyze the behavior of components under baking heat loads, operational heat loads and also accidental fire heat loads.

The paper presents an optimized design layout for the sight-tube of the XRCS Survey and results of the thermal analysis; defining temperature limits to observe compliance with safety criterion defined by ITER regulatory guidelines on PIC (class SIC-1) components as well as providing inputs to the structural integrity analysis of the system.

Preliminary Design of IN-DA Diagnostic Plant Instrumentation & Control

S. Jha¹, S. Varshney^{1,2}, S. Danani¹, S. Kumar¹, R. Rajpal³, H. B. Pandya¹, S. Simrock⁴, P. Patil⁴, M. Walsh⁴, and V. Kumar^{1,2}

¹ITER-India, Institute for Plasma Research (IPR), Bhat, Gandhinagar, India

²Homi Bhabha National Institute (HBNI), Anushakti Nagar, Mumbai 400094, India

³Institute for Plasma Research (IPR), Bhat, Gandhinagar, India

⁴International Thermonuclear Experimental Reactor (ITER),
Cadarache Centre, 13108 St. Paul lez Durance, France

Corresponding Author: S. Jha, shivakant.jha@iter-india.org

In ITER, plant Instrumentation and Control (I&C) components are exposed to harsh environments. Hence I&C for plant system is one of the most challenging requirements to fulfil the ITER demands. IN-DA is responsible for the delivery of several diagnostics systems including: 1) X-Ray Crystal Spectroscopy (XRCS) edge and survey to measure the plasma impurity for machine protection and basic control as well as well measure the profile of plasma parameters for advanced control; 2) Electron Cyclotron Emission (ECE), to provide temperature profile, fluctuation and the power due to emission in 70–1000 GHz for ITER plasma; 3) UP#09 for housing the diagnostics in the port plug and integration with rest of its system; and, 4) CXRS-pedestal to provide the ion velocity and temperature of plasma for advanced control and physics studies. Out of these, the XRCS diagnostics and UP#09 are classified as protection important components (PIC) and hence need special attention to achieve safety functions.

ITER plant I&C systems are being developed according to industrial systems engineering standards, and compliant with the standards, specifications and interfaces defined in the Plant Control Design Handbook (PCDH) and its satellite documents. Enterprise Architect (EA) is the tool is to be used for diagnostic I&C documentation. EA helps to trace high-level specifications for the analysis, design, implementation, test and maintenance models using unified modelling language (UML), SysML and other open standards. I&C deliverable documents are being developed according to the ITER diagnostic guidelines.

This paper describes the detailed preliminary design of plant I&C for diagnostics system: a) Operation procedures, b) functional analysis including variable definition, c) hardware architecture and signal, d) cubicle configuration, and e) the plant system operating state machine (PSOS) for automation including the mapping to Common Operation States (COS).

Design Validation of ITER XRCS Survey Spectrometer with Nuclear Code RCC-MR

S. Kumar¹, S. Varshney^{1,2}, S. Mishra^{1,2}, P. V. Subhash^{1,2}, V. Kumar^{1,2}, J. Guirao³, P. Bernascolle³, M. Ivantsivskiy⁴, V. Udintsev³, R. Barnsley³, J. Elbez-Uzan¹, and M. Walsh³

¹ITER-India, Institute for Plasma Research (IPR), Bhat, Gandhinagar, India

²Homi Bhabha National Institute (HBNI), Anushakti Nagar, Mumbai 400094, India

³International Thermonuclear Experimental Reactor (ITER),
Cadarache Centre, 13108 St. Paul lez Durance, France

⁴Budker Institute of Nuclear Physics (BINP), Novosibirsk, Russian Federation

Corresponding Author: S. Kumar, siddharth.kumar@iter-india.org

At ITER, systems are classified into different safety categories as per their function in the machine; protection important components (PIC) need more attention during their design and analysis for better safety margins. The French Nuclear Code RCC-MR (2007) is employed in the design, analysis and manufacture, applicable to the ITER protection important mechanical components. It is always a challenge to the designers to develop and qualify the design for a PIC system under ITER loading conditions. This becomes even more stringent when the system is exposed to high nuclear radiation and performing the confinement function of radioactive tritium as in the case of X-Ray crystal spectroscopy (XRCS) Survey system.

XRCS Survey diagnostics is an ITER PIC system, located in equatorial port-11, which will be used to monitor impurities in the highly ionized state and measure line emission from plasma in the X-ray range 0.1–10 nm. This system is connected with the port plug flange, due to its specific nature and exposed to complex environments of neutron radiation, high heat flux, electromagnetic forces, etc.

To ensure the structural integrity of XRCS Survey from the constant loading (P Type damage), repeated loading (S type damage); we have studied various loads and associated load responses. These loads are broadly categorized in the following three types: i) ITER generic loads, ii) accidental loads, and, iii) radiation loads. Finite element (ANSYS) analysis has been performed and design is validated using the French Nuclear design rules RCC-MR (2007).

This paper describes results obtained from structural damage analysis of XRCS Survey system, and their compliance with relevant design rules given in the French Nuclear code RCC-MR validating the design.

In-Vessel Inspection System: Design Progress of High Vacuum and Temperature Compatible Remote Handling for Fusion Purposes

M. Manuelraj¹, K. K. Gotewal¹, P. Dutta¹, N. Rastogi¹, R. R. K. Tiwari¹, and J. P. Chauhan¹

¹*Institute for Plasma Research (IPR), Bhat, Gandhinagar, India*

Corresponding Author: M. Manuelraj, manoah@ipr.res.in

The plasma facing components (PFCs) in a tokamak are subjected to high heat flux and high temperature during plasma operation, which causes erosion of the first wall. There is also hot spot formation on the PFC due to physical phenomenon like thermal electron emission. In addition to the aforementioned phenomenon, events such as edge localized mode (ELM) and vertical displacement event (VDE) are serious concerns for the fatigue damage of the PFCs. Therefore, health monitoring of the PFCs is an essential requirement in any tokamak, which is met by periodic inspection of the PFCs. The periodic inspection can be performed during the tokamak shutdown period or during plasma operation. The latter is most desirable as it allows quick and frequent in-service inspection of the PFCs between the plasma shots without breaking the vacuum.

The work presented in this paper covers the conceptual design of in-vessel inspection system (IVIS) and storage chamber to carry out in-service visual inspection of SST-1 like tokamak under vacuum in between the plasma shots. The designed IVIS manipulator is ~ 2 m long with 04-degrees of freedom, comprising of three rotary joints and one linear motion for deployment within the tokamak. The manipulator is designed to handle a cantilevered payload of ~ 1 kg with a positional accuracy of < 2 mm. IVIS is initially stowed in a 4 m long ultrahigh vacuum (UHV) storage chamber isolated from the VV by a UHV gate valve. During (one quarter, i.e., +90°) viewing, the gate valve will open so that IVIS can be deployed inside the VV, complete the viewing procedure and return back to its initial position outside the VV. Issues like choices of the structural materials to minimize the out-gassing under vacuum and high temperature during conditioning are discussed with feasible solutions. Improvements to enhance IVIS operation under temperature and vacuum conditions for SST-1 like machine are reviewed. Results for theoretical calculations, kinematic and structural integrity analyses are presented in detail along with ways to optimize the design.

Preliminary Development on a Conceptual First Wall for DEMO

L. Cai¹, X. Liu¹, Y. Lian¹, X. Zeng¹, J. Song², and J. Chen¹

¹Southwestern Institute of Physics, Chengdu, Sichuan, People's Republic of China

²Xiamen Tungsten Company, Xiamen, People's Republic of China

Corresponding Author: L. Cai, cailz@swip.ac.cn

For a DEMO reactor, the first candidate material for plasma facing material (PFM) is tungsten (W) and current available structure material is reduced activation ferritic-martensitic (RAFM). Tungsten coating material is promising to be applied on first wall. Since chemical vapour deposition tungsten (CVD-W) has a higher density, less porosity and better thermal shock resistance, thick CVD-W coating is used as the plasma facing material here. Southwestern Institute of Physics (SWIP) has developed a new RAFM material, which is called CLF-1. The new conceptual first wall for DEMO in this work is designed and developed with CVD-W and CLF-1.

Due to different thermal expansion coefficients of tungsten and steel, CVD-W will detach from CLF-1 steel under heat load and plasma exposure if it is coated onto the CLF-1 directly. As a result, an interlayer must be applied to mitigate the stress between CVD-W and CLF-1. Furthermore, the tungsten will generate cracks under steady state and transient heat loads in reactors and crack in the tungsten will allow tritium to penetrate into the substrate rapidly. Tritium accumulation is a critical parameter for reactors which is very important for safety and steady state operations.

The new conceptual first wall consists of CVD-W, CLF-1 and an interlayer between them. The interlayer is required to have good bonding property and tritium prevention, which is crucial for controlling the inventory buildup and maximizing the fuel efficiency. SiC and TiN applied as the interlayer between W and CLF-1 in the first wall are investigated. In order to figure out the influence of fabrication technology, layer thickness and coating rate, a series of material samples are fabricated and tested. The SiC interlayer on the CLF-1 substrate is made by three means of coating technologies including physical vapour deposition (PVD), chemical vapour deposition (CVD) and chemical vapour infiltration (CVI) while TiN interlayer is obtained by CVD. On the top of the interlayer SiC or TiN, a CVD-W layer with the thickness of 1 mm is coated with the rate of 0.5 mm/h at the temperature of 450–550°C.

The material analysis and mechanical tests on those samples present that SiC by CVI and TiN by CVD and TiN by CVD have sufficient adhesiveness as an interlayer between W and CLF-1, which show good bonding property and no obvious detachment or delamination is found.

Installation and Initial Run of 96 kV 7.2 MW Acceleration Grid Power Supplies

N. P. Singh¹, H. Dhola¹, A. Patel¹, S. Gajjar¹, B. Raval¹, A. Thakar¹, D. V. Upadhyay¹, N. S. Goswami¹, K. R. Mehta¹, V. Gupta¹, R. Dave¹, and U. K. Baruah¹

¹ITER-India, Institute for Plasma Research (IPR), Bhat, Gandhinagar, India

Corresponding Author: N. P. Singh, npsingh@iter-india.org

Acceleration grid power supplies (AGPS) provides 8 MW power at -96 kV to the beam source of DNB (diagnostic neutral beam) and SPIDER (source for production of ion of deuterium extracted from RF plasma) for acceleration of negative ions with specific modulation. High voltage power supplies (HVPS) based on PSM (pulse step modulation) topology has already demonstrated its ability for broadcast transmitters, accelerators of RF source, neutral beam injectors. PSM based 96 kV/75 A AGPSs have been developed to feed the acceleration grid of beam sources.

Design redundancy $\sim 15\%$ allows for tolerating SPS modules failure without leaving the ongoing campaign. The AGPS is designed to turn off in a time much lower than $100\ \mu\text{s}$ to minimize the energy (20 J) delivered to the arc in case of short circuit or breakdown. AGPS is mainly composed of multisecondary transformers (3 nos., 2.8 MVA each), switched power supply (SPS) modules (150 nos., 60 kW each), FPGA/real-time based controller and other auxiliaries including passive protection devices; factory tested in witness of IO. Novel, state-of-the-art technologies for HV insulation such as multiple bushings integrated on large resin insulators and building feedthroughs have been developed.

To ensure described functionalities a single AGPS is controlled by 9 powerful synchronous FPGAs managed by real-time controller which support high performance requirement of PSM based HVPS like low ripple, high resolution, programmable rise time, fast dynamics, full depth modulation, fast switching off and fast (a few milliseconds) re-application in case of breakdowns.

Deliveries of AGPSs are sequenced to allow early operational drills at ITER-India lab while other unit is being installed at NBTF site. Present article describes operational drills including protection functions, insulation test and specified behaviour of AGPS on dummy load at ITER-India lab. This allows for offering DNB-AGPS for extended factory acceptance testing.

R&D Status of Indian Test Facility for ITER DNB Characterization

M. J. Singh¹, A. K. Chakraborty¹, M. Bandyopadhyay^{1,3}, J. Joshi¹, H. Patel¹, S. Shah¹,
A. Gahlaut², A. Yadav¹, D. Parmar¹, D. Sharma¹, D. Singh¹, H. Tyagi², K. Joshi¹,
K. B. Pandya², M. V. Nagaraju¹, M. Bhuyan¹, M. Patel¹, R. K. Yadav¹, S. Pillai¹, D. Boilson⁴,
J. Chareyre⁴, B. Schunke⁴, and C. Rotti⁴

¹ITER-India, Institute for Plasma Research (IPR), Bhat, Gandhinagar, India

²Institute for Plasma Research (IPR), Bhat, Gandhinagar, India

³Homi Bhabha National Institute (HBNI), Anushakti Nagar, Mumbai 400094, India

⁴International Thermonuclear Experimental Reactor (ITER),
Cadarache Centre, 13108 St. Paul lez Durance, France

Corresponding Author: M. J. Singh, mahendrajit@iter-india.org

Indian Test Facility (INTF) is a R&D facility under development at IPR, Gandhinagar, as a part of the neutral beam development from negative ion source (NNBI) program. The major advantage of the INTF, besides developing the beams from large ion sources, is to characterize and benchmark the ITER diagnostic neutral beam (DNB) to the desired specifications over transport lengths of ~ 21 m, a unique feature of this test bed. Such a study will enable establishing the expected power to be delivered by DNB into the ITER plasma, an important parameter to estimate the S/N ratio expected from the He ash measurements by CXRS in ITER plasmas. The INTF beam line has a one-to-one correspondence with the DNB in ITER in terms of the components, their placement and the intercomponent distances. However, the 9 m long 4.5 m diameter vacuum vessel with a top openable lid and with double O-ring seals for the vacuum is different from the rectangular vessels envisaged at ITER. The other difference is the 12 modular cryopumps providing the same pumping surface as the single panel ITER cryopumps. In addition, the beam characterization at 21 m is planned with a second calorimeter housed in the vacuum vessel connected to the end of the duct. The data acquisition and control system is developed using ITER CODAC platform and integrates around 800 channels from all plant systems for enabling safe remote operations. Extensive physics and thermomechanical calculations for various types of operational heat loads and loads due to various accidental scenarios have been performed to finalize the component design. Adequate choice of materials, manufacturing and jointing processes compatible to ITER safety standards has been made in order to make the components adhere to the safety and quality classification thereby ensuring that the components survive the ITER life time while operating in harsh nuclear environments. The components are currently in various phases of manufacturing and the first operations INTF are anticipated in Q4 of 2019. The experiments on INTF are supported by single driver test bed, ROBIN, and the two driver TWIN source. The paper will describe the R&D status of different components and auxiliary systems of Indian Test Facility (INTF), the envisaged experimental programme of operation and some results from operational test beds.

Design and Development of Safety Control System of Indian Test Facility (IN-TF) for ITER DNB

H. Tyagi¹, R. K. Yadav¹, K. Patel², J. Joshi¹, M. Bandyopadhyay^{1,3}, M. Singh¹, and A. K. Chakraborty¹

¹ITER-India, Institute for Plasma Research (IPR), Bhat, Gandhinagar, India

²Institute for Plasma Research (IPR), Bhat, Gandhinagar, India

³Homi Bhabha National Institute (HBNI), Anushakti Nagar, Mumbai 400094, India

Corresponding Author: H. Tyagi, htyagi@iter-india.org

Indian Test Facility (IN-TF) [1] is being built in IPR to characterize diagnostic neutral beam [2] in cooperation with ITER Organization. INTF is a complex system which consists of several plant systems like beam source, gas feed, vacuum, cryogenics and mechanical systems. To ensure successful operation INTF, integrated operation involving all the constituent plant systems is required. The experimental phases involve application of HV power supplies and high-power RF power (~ 800 KW) which will produce considerable amount of power (~ 6 MW) within the facility for longer durations. Hence the entire facility will be exposed high heat fluxes and RF radiation.

For ensuring occupational safety for working personnel, it is of prime importance that a mature safety control system [3] be developed and commissioned for INTF. The design of safety control system (SCS) is based on ITER PCDH guidelines and industrial standards for programmable safety systems (IEC 61511 and IEC 61508). The process of detailed design includes identification of safety instrumented functions (SIF), sensor selection and prototype development. The control hardware includes fault tolerant Siemens PLC with distributed interface on Profisafe protocol and safety software which is developed using Siemens safety programming environment. The SCS has to interface with the conventional INTF Control system (which is based on CODAC core system) for noncritical data exchange. The SCS also dictates the overall mode of INTF operations.

This paper describes the design methodology involved in arriving at final design with details of application of safety standards for identifying the safety integrity levels (SIL) of SIFs and details of software level interface. The overall integrated system configuration and test results are also discussed.

References

- [1] M. J. Singh, *Fusion Eng. Des.*, **86**, 732–735 (2011).
- [2] A. Chakraborty, *IEEE Trans. Plasma Sci.*, **38**, (2010).
- [3] H. Tyagi, *Fusion Eng. Des.*, **112**, 766–770 (2016).

Study of Corrosion Properties ITER In-Wall Shield (IWS) Fasteners and Structural Integrity of IWS

A. Maheshwari¹, H. A. Pathak¹, and S. Dani¹

¹ITER-India, Institute for Plasma Research (IPR), Bhat, Gandhinagar, India

Corresponding Author: A. Maheshwari, abha.maheshwari@iter-india.org

In-wall shield (IWS) blocks will be inserted between the inner and outer shells of the ITER vacuum vessel. These blocks comprise of number of plates of stainless steel stacked together using fasteners of XM-19 and M30 size. Plates are tightened with pretension of 107 kN to withstand EM force of 18.3 kN during ITER operation. These bolts are spot welded with blocks to lock any type of rotation. There are approximate 1500 such bolts exposed to vacuum in one vessel sector with approximate surface area of 70.5 m². Hence, the surface condition of these fasteners play an important role while leak testing the VV. XM-19 material is very corrosive resistant but, if the fasteners are exposed to normal or humid environment for a long time its surface may oxidize and accumulate corrosion which may further impact the ITER operation in three ways: a) reduced structural integrity of blocks; b) gas load due to outgassing; and, c) generation of corrosion products in cooling water system. This corrosion has been assessed by: a) measuring the corrosion rate (CR) of XM-19 fasteners (exposed in natural environment), and, b) XM-19 washer exposed to water with ITER operating temperature and pressure. This study is carried out using scanning electron microscope (SEM) and electrochemical polarization technique. For SEM analysis, samples were polished and corrosion depth was measured and accordingly CR was calculated. In electrochemical polarization technique, samples were induced with corrosion at room temperature and high temperature in water medium. Pt electrode was used as cathode and Ag-AgCl₃ as reference electrode. CR was calculated with the help of corrosion current. Tafel curves of corroded samples show that, reverse polarization path do not intersect the forward path and indicate no tendency of pitting corrosion. Maximum corrosion observed by using Tafel curve is 0.1067 mpy. Outgassing rate of naturally corroded XM-19 bolt was measured 6.06×10^{-8} Pa m³/(s m²) which is less than the acceptable limit for IWS. Total corrosion product for one vessel sector was calculated with the help of CR and surface area in one vessel sector and found 3.20 kg/year. It can be removed by appropriate filters. Study shows that corrosion and outgassing properties of corroded XM-19 fasteners are acceptable for ITER IWS. Detailed experimental set up and results of corrosion study will be presented in this paper.

Nuclear Performance Analysis and Optimization Study of Indian Solid Breeder Blanket for DEMO

D. Aggarwal¹, M. Z. Youssef²

¹*Institute for Plasma Research (IPR), Bhat, Gandhinagar, India*

²*University of California Los Angeles, CA 90095, USA*

Corresponding Author: D. Aggarwal, deepakagg@ipr.res.in

The tritium breeding blanket is the essential part of a fusion reactor which provides the tritium fuel self-sufficiency to the reactor. India under its breeding blanket R&D programme for DEMO is focussing on the development of two breeding blanket concepts, viz., lead-lithium cooled ceramic breeder (LLCB) and helium cooled ceramic breeder (HCCB). The study presented in this paper focusses on the neutronic design analysis and optimization of HCCB blanket which is having an edge on configuration and is one of the variants of helium cooled solid breeder blanket concepts proposed by several other countries. Indian HCCB blanket aims at utilizing the low energy neutrons at the rear part of the blanket and has RAFMS as the structural material, lithium titanate (Li_2TiO_3) as tritium breeder with beryllium (Be) as neutron multiplier. The aim of the optimization is to minimize the radial blanket thickness, while ensuring tritium self-sufficiency and provide data for further neutronic design and thermal-hydraulic layout of HCCB blanket. Several parametric studies have been performed considering different ^6Li enrichment, varying composition of Be and Li_2TiO_3 in the breeder blanket and radial length of the breeder zone, as well as different arrangements of Be and Li_2TiO_3 layers in the blanket. The cases provided tritium self-sufficiency and sufficient shielding of the TF-coils have been identified.

Neutronic calculations are performed using the 1D discrete ordinate code ANISN with FENDL-2.1 nuclear cross section data library to assess the overall nuclear performance of HCSB blanket. The inboard and outboard blanket thicknesses of 40 cm and 60 cm respectively can give $\text{TBR} > 1.3$, with 60% ^6Li enrichment which is assumed to be sufficient to cover potential tritium losses and uncertainties. It is found that optimal multiplier to breeder material volume fraction ratio obtained is around 3:1. The results also demonstrated that Be packing fraction has more profound impact on the TBR as compared ^6Li enrichment and packing fraction of Li_2TiO_3 . Other improvements on the TBR are seen by introducing a 10 mm breeder layer before multiplier layer behind the first wall.

Design and Development of the Articulated Robotic Inspection Arm (ARIA) for Fusion Machine

K. K. Gotewal¹, M. Manuelraj¹, N. Rastogi¹, P. Dutta¹, and R. R. K. Tiwari¹

¹*Institute for Plasma Research (IPR), Bhat, Gandhinagar, India*

Corresponding Author: K. K. Gotewal, kgotewal@ipr.res.in

Remote handling (RH) systems for maintenance and inspection of in-vessel components have been addressed in great detail for fusion machines around the world. Maintaining high availability of fusion machine and minimizing the maintenance time require robust and dependable RH systems. Such RH systems, being electro-mechanical in nature, requires research and development in various areas such as structural design, kinematic and dynamic modelling, efficient real-time control, and virtual reality (VR) based monitoring. Adding to the aforesaid requirements is criticality of investment protection of the sophisticated in-vessel components and their size and weight scales. The articulated robotic inspection arm (ARIA) has been indigenously developed at IPR, India, as a proof-of-concept for in-vessel maintenance.

The paper presents, in detail, the design and development of the ARIA and associated VR based monitoring and control system. ARIA is a 6-degree-of-freedom manipulator with a cantilevered payload capacity of ~ 25 kg at 2 m distance. ARIA is controlled using a VR based user interface that immerses the ARIA model into the working environment. The effective 1:1 scale mapping of the VR model with the manipulator hardware makes provision for task planning and executing of the control commands from a remote location. The theoretical calculations with structural analysis of components like links, shafts, couplers, lugs and bearings are elaborately discussed. Results for payload sensitivity analysis during dynamic behaviour are also presented. The system is optimized and developed to incorporate efficient commercially available servo actuators, bearings and gear-boxes, to maintain a high degree of accuracy and repeatability. Experimental validation and test results on a mock-up facility show that the system can be controlled with an end-effector positional accuracy within 2 mm. The design and integration methodology, presented here, lays foundation to develop efficient RH systems with greater reach and payload capacity for future fusion machines.

Baking System of ADITYA Upgrade Tokamak

K. M. Patel¹, K. A. Jadeja¹, B. A. Arambhadiya¹, V. D. Raulji¹, J. Ghosh¹, R. L. Tanna¹, S. B. Bhatt¹, Y. C. Saxena¹, M. B. Kalal¹, K. S. Acharya¹, B. R. Doshi¹, M. K. Gupta¹, and S. Jaiswal¹

The ADITYA-U Team

¹*Institute for Plasma Research (IPR), Bhat, Gandhinagar, India*

Corresponding Author: K. M. Patel, kaushal@ipr.res.in

In tokamaks, baking of vacuum vessel and first wall components is a prerequisite in order to obtain impurity-free plasmas. Baking is performed to remove impurities, viz., H₂, H₂O and hydrocarbons from the vessel and first wall components. ADITYA tokamak has been upgraded ADITYA-U tokamak to achieve shaped plasmas. The ADITYA-U is equipped with a comprehensive baking system for heating the SS vacuum vessel, pumping systems, associated diagnostics along with the graphite limiter and divertor tiles up to 150°C. The DC glow discharge cleaning is also carried out in presence of baking to achieve better wall conditioning for high performance plasma operation. Due to space limitation between vessel and Toroidal field coils at the high-field side, 1.5 mm thick silicon heaters have been designed and procured. In-situ installation of heaters has been quite challenging due to structural complexity. For efficient heat insulation, 6 mm thick silicon jacket designed, fabricated and installed according to vessel profile. A detail analysis carried out in ANSYS for its optimum performance and to examine its effect on vessel, especially on the several weld joints. Whole baking system consists of ~ 80 heaters installed on different sectors of the vessel, pumps and diagnostics. The heaters are controlled in closed-loop by in-house developed programmable logic controller (PLC) based automatic control system. It comprises of three main phases, temperature ramp-up, constant heating and ramp-down to room temperature. All these phases are individually controlled as required. The entire baking system has been tested thoroughly for its automatic operations for long hours (~ 48 h), integration, ruggedness, reliability, small form factor. The detailed hardware concept, software design and prototype testing and its regular operation in presence and absence of GDC will be discussed. Partial pressure of impurities is monitored in every baking cycle which decides the controls of the baking temperature and duration automatically. Further, the potency of lithiumization carried out before, during and after baking has been compared for the first time in ADITYA-U by estimating the lithium lifetime on the walls with plasma operation. The improved wall conditioning with baking and its effect on plasma operation along with technical challenges faced during installation will be presented in this paper.

Dynamic Simulation of Loss of Insulation Vacuum Event for ITER Cryodistribution System

S. Muralidhara¹, H. Vaghela¹, P. Patel¹, V. Shukla¹, and K. Choukekar¹

¹ITER-India, Institute for Plasma Research (IPR), Bhat, Gandhinagar, India

Corresponding Author: S. Muralidhara, srinivasa.muralidhara@iter-india.org

The auxiliary cold boxes (ACBs) of the ITER cryodistribution system has multiple cryogenic process volumes as well as interfaces with cryolines with isolated vacuum spaces. The cryogenic process volumes inside a single vacuum space have different temperature level, 4 K and 80 K as well as different operating pressure, 0.5 MPa and 1.8 MPa. The cryogenic process volumes including interfacing cryolines are protected with safety relief valves (SRVs). In the event of loss of insulation vacuum (LIV) of any particular vacuum space, the incidental heat load of the order of $\sim 6.5 \text{ kW/m}^2$ results in rapid pressurization of the cryogenic process volume and pressure must be relieved through SRV. As per the safety requirements of the ITER, the maximum helium inventory inside the tokamak building is restricted and therefore a common relief header is necessary for collecting the release of helium through SRV and carrying it outside the tokamak building. The sizing of the SRVs is performed for the various scenarios as per applicable standard; however, due to the long length of relief header, the required information regarding back pressure on the SRVs is not known in advance. The back pressure is an important parameter to be considered for the sizing and selection of SRV and is a function of geometric condition of relief header, process condition of relieving process volume and relieving mass flow rate. Estimation of back pressure considering steady state condition and maximum mass flowrate through SRV may results in a conservative and unrealistic value of back pressure. Dynamic simulation of the safety relief event along with the complete model of process volume, correct boundary conditions as well as geometric detail of relief header is developed and analyzed based on pressure flow solver model in Aspen HYSYS®. Results are presented for the most demanding scenario, viz., LIV event of the largest cryoline and comparison made with the two approaches of back pressure prediction, one with steady state and the other with dynamic simulation model. Results obtained from the dynamic simulation of the entire safety relief system gave useful results at various locations; moreover, the back pressure on SRV is almost half of the back pressure resulting from the steady state approach. Certainly, the dynamic simulation provided valuable input for the overall system configuration.

Visual Servo of Tokamak Relevant Remote Handling Systems Using Neural Network Architecture

P. Dutta¹, N. Rastogi¹, R. R. K. Tiwari¹, J. P. Chauhan¹, M. Manuelraj¹, and K. K. Gotewal¹

¹*Institute for Plasma Research (IPR), Bhat, Gandhinagar, India*

Corresponding Author: P. Dutta, pramitd@ipr.res.in

Tokamak inspection and maintenance requires different remote handling (RH) systems such as long reach planar manipulators, multi-DOF hyper-redundant arms, etc. As no structural support can be provided inside the tokamak, these RH systems are usually cantilevered and have a number of articulations to traverse the toroidal geometry of the tokamak. The kinematic configuration is thus different for conventional manipulators. Due to long cantilevered length, heavy payload handling, structural deformations, gearbox backlash and control system inaccuracies the final pose of the end effector may vary from the desired pose when only a servo feedback loop is used. Such inaccuracies can only be eliminated by using visual servo (VS) technique, where the inverse kinematics and trajectory planning are done based on visual feedback from cameras mounted on the RH system. The paper gives a fresh approach to visual servo for tokamak RH systems using artificial neural networks (NN) architecture. A multilayered feed-forward NN is trained using the joint angle vector as input and the corresponding feature vector(s) of markers in a sample tile as output. The trained NN can thus predict the joint configurations for given features vectors. This eliminates the requirement of closed-form inverse kinematic solution of the manipulator and camera calibration. The NN architecture and proposed controller are validated and presented using simulation on 5DOF remote handling manipulator. Real-time implementation methodology for NN based controller are also discussed.

The Influence of Fe-Ion Irradiation on the Microstructure of Reduced Activation Ferritic-Martensitic Steel Eurofer 97

S. V. Rogozhkin^{1,2}, A. A. Nikitin^{1,2}, A. A. Khomich¹, A. A. Lukyanchuk¹, O. A. Raznitsyn¹, A. S. Shutov¹, A. O. Ovchinnikova¹, P. A. Fedin¹, T. V. Kulevoy¹, A. L. Vasiliev¹, M. Y. Presnyakov¹, A. Möslang³, and P. Vladimirov³

¹National Research Centre "Kurchatov Institute", Moscow, Russian Federation

²National Research Nuclear University "MEPhI", Moscow, Russian Federation

³Karlsruhe Institute of Technology (KIT), Karlsruhe, Germany

Corresponding Author: S. V. Rogozhkin, sergey.rogozhkin@itep.ru

The reduced-activation ferritic-martensitic steel Eurofer 97 is the European benchmark structural material for in-vessel components of fusion reactor. Experimental data on neutron irradiated Eurofer 97 material have shown a decrease in plasticity and radiation hardening at irradiation temperatures about 300°C. Formation of dislocation loops and α' pre-precipitates is considered as the main reason of this phenomenon. In this work, Eurofer 97 steel was irradiated with Fe ions up to 10^{16} ions/cm² at 250, 300 and 400°C. The irradiated samples were characterized by TEM and APT. TEM study of ion irradiated samples revealed nucleation of dislocation loops. The pair-correlation analysis of APT data detected an initial stage of solid solution decomposition. The hardening of ion irradiated Eurofer 97 was calculated with DBH model taking into account radiation-induced dislocation loops to comparison with the change of yield stress for neutron irradiated Eurofer 97. According to obtained results it can be supposed that the formation of dislocation loops plays the main role in the low temperature radiation hardening of Eurofer 97 at the dose level up to ~ 10 dpa.

Electromagnetic Particle Injector (EPI) as a Fast Time Response Disruption Mitigation Concept

R. Raman¹, W.-S. Lay¹, T. R. Jarboe¹, J. Sachdev², R. Lunsford², R. Nazikian²,
J. E. Menard², and M. Ono²

¹University of Washington, Seattle, WA 98195, USA

²Princeton Plasma Physics Laboratory (PPPL), Princeton, NJ 08540, USA

Corresponding Author: R. Raman, raman@aa.washington.edu

The electromagnetic particle injector (EPI) has the potential for delivering the radiative payload to the plasma centre on a 3–4 ms time scale, much faster, and deeper, than what can be achieved using present methods. Predicting and controlling disruptions is an important and urgent issue for ITER. While a primary focus is the early prediction and avoidance of conditions favourable to a disruption, it is understood that some disruptions may be inescapable. For these cases, a fast time response method is essential to protect the ITER facility. Experimental tests on a prototype system have been able to verify the predicted rapid response capability of the EPI system by accelerating a 3.2 g sabot to 150 m/s in 1.5 ms.

The primary advantage of the EPI concept over present systems is its ability to meet short warning time scales while accurately delivering a radiative payload composed of acceptable low-*Z* materials such as Be, B or BN. This is done at velocities of ≥ 1 km/s required to achieve core penetration in high power ITER discharges, thus providing thermal and runaway current mitigation. This capability will provide the means for initiating a controlled plasma termination that originates at the plasma centre, rather than from the outer periphery. This added capability, in addition to the fast time-response capability, should provide greater flexibility in controlling tokamak disruptions.

Work is supported by the U.S. Department of Energy Contracts: DE-AC02-09CH11466 DE-FG02-99ER54519 AM08, and DE-SC0006757.

FIP

Preliminary Results of Prototype Martin–Puplett Interferometer and Transmission Line Developed for ITER ECE Diagnostic

H. B. Pandya^{1,2}, R. Kumar¹, S. Danani¹, P. Vaghashiya¹, V. K. Srivastva^{1,2}, D. Naylor^{3,4}, B. Gom⁴, S. Gunganti⁴, and T. Fulton⁴

¹ITER-India, Institute for Plasma Research (IPR), Bhat, Gandhinagar, India

²Homi Bhabha National Institute (HBNI), Anushakti Nagar, Mumbai 400094, India

³University of Lethbridge, Lethbridge, AB T1K-3M4, Canada

⁴Blue Sky Spectroscopy Inc., Suite 9-740 4th Avenue South, Lethbridge, AB T1J-0N9, Canada

Corresponding Author: H. B. Pandya, hitesh@ipr.res.in

The ECE Diagnostic system in ITER will be used to determine the electron temperature profile evolution, the high frequency fluctuation of the plasma electron temperature, the characterization of runaway electrons and the radiated power in the electron cyclotron frequency range (70–1000 GHz). These measurements will be used for advanced real-time plasma control (e.g., steering the electron cyclotron heating beams) and the ITER plasma physics studies.

In view of the ITER requirements, an ultrawide band (70–1000 GHz) transmission line coupled to a fast scanning, broadband spectrometer are required to estimate the ECE radiated power loss and to study the behaviour of runaway electrons. Typically, the transmission lines and spectrometers are not operated in vacuum and there are consequently significant losses at certain frequencies due to water vapour line absorption over this large frequency range. To avoid these losses, both the transmission line and the spectrometer must be operated in vacuum. Further, producing an efficient high-étendue long-wavelength spectrometer with extremely high scan speeds in vacuum is a major challenge. Also long distance (~ 43 m) transmission of very low in-situ calibration source power (few nW level) with an ultrawide frequency range is another challenge for the transmission line development. For the purpose, a prototype polarizing Martin–Puplett interferometer has been developed to operate in a low vacuum with high throughput and excellent time resolution of 10 ms with scanning length of 15 mm, and this coupled with a prototype transmission line as developed for use in vacuum.

An experimental set up has been established at ITER-India lab to test the performance of various prototype subsystems of the ECE diagnostic. The experimental set up consists of the high temperature blackbody source in this frequency range, transmission line and the Martin–Puplett interferometer with data acquisition system. This paper describes the experimental set up and preliminary results of subsystems developed for ECE diagnostic.

Performance of the Plasma Source and Heating Concept for the Prototype-Material Plasma Exposure Experiment (Proto-MPEX)

J. Rapp¹, C. J. Beers^{1,2}, T. M. Biewer¹, T. S. Bigelow¹, J. F. Caneses¹, J. B. O. Caughman¹, D. C. Donovan², R. H. Goulding¹, A. Lumsdaine¹, N. Kafle¹, G.-N. Luo³, L. W. Owen¹, P. Piotrowicz^{1,4}, H. B. Ray^{1,2}, and M. Showers^{1,2}

The MPEX Team

¹*Oak Ridge National Laboratory (ORNL), Oak Ridge, TN 37831, USA*

²*University of Tennessee, Knoxville, TN 37996, USA*

³*Institute of Plasma Physics, Chinese Academy of Sciences, Hefei, Anhui, People's Republic of China*

⁴*University of Illinois, Urbana-Champaign, IL 61820, USA*

Corresponding Author: J. Rapp, rappj@ornl.gov

The material plasma exposure experiment (MPEX) is a planned linear plasma device to address plasma-material interactions for future fusion reactors. Its concept does foresee the capability to expose a priori neutron irradiated material samples to fusion reactor grade divertor plasmas. This new capability will be unique world-wide addressing important research needs in the area of fusion nuclear science. It will be an evolution to current operating steady-state linear plasma devices, which are limited either in the plasma fluxes they can deliver to the material targets or by the plasma temperatures (for ions and electrons) they can reach in front of the material targets. The concept of MPEX does foresee a combination of a high-power helicon plasma source with microwave electron heating and ion cyclotron resonance heating. This source and heating concept is being tested on the prototype-material plasma exposure experiment (Proto-MPEX). With 100 kW helicon power, a plasma density of $8 \times 10^{19}/\text{m}^3$ was achieved, which is about a factor 2 more than required for MPEX. Electron heating was pursued with a 28 GHz gyrotron. A maximum power of 50 kW was delivered to the plasma, which is produced by the helicon. At this frequency, the plasma is overdense in the plasma centre ($>10^{19}/\text{m}^3$). Maximum electron temperatures of 20 eV have been achieved under those overdense plasma conditions with electron Bernstein wave (EBW) heating. This is almost the electron temperature required for MPEX (25–30 eV). Ion cyclotron heating (ICH) was performed in the frequency range of 6–12 MHz with a low power ICH antenna able to launch about 25–30 kW of power. Without ICH, the ion temperature is about 2–4 eV. With ICH ion temperatures of 8–12 eV were measured. The ion fluxes to the target are about $5 \times 10^{23}/\text{m}^2\text{s}$. The plasmas produced by the helicon antenna have been modelled extensively with a fluid plasma code, coupled to a Monte Carlo neutral code (B2-EIRENE). The plasma transport can be well explained by this fluid approach and a radial diffusion coefficient consistent with Bohm-like transport. The transport of auxiliary heated plasmas (ECH/EBW and ICH) is currently being investigated and experimental results of this investigation will be presented.

Exploring Deuterium Beam Operation and Behaviour of Coextracted Electron in Negative-Ion-Based Neutral Beam Injector

K. Ikeda¹

The LHD-NBI Team

¹National Institute for Fusion Science (NIFS), Toki, Gifu, Japan

Corresponding Author: K. Ikeda, ikeda.katsunori@lhd.nifs.ac.jp

Deuterium beam operation of the negative-ion-based neutral beam injector (N-NBI) was initiated in the Large Helical Device (LHD) in 2017. Both hydrogen (H) and deuterium (D) neutral beams were generated by changing the operation gas using the same accelerator. Comparison of the beam properties such as the extracted negative ion current and the coextracted electron current, obtained with H₂ and D₂ gases, will clarify the production and extraction mechanism of the negative ions. Remarkable results are as follows: i) 46 A deuterium negative ion current (I_{D^-}) has been extracted with the averaged negative ion current density of 190 A/m² by two negative ion sources in the injector; ii) The current ratio of coextracted electrons to negative ions (I_e/I_{D^-}) was 0.39 using 0.43 Pa source gas pressure. Although the configuration of the ion source is not optimized for D, the observed current of D⁻ ions reached 82% of the LHD requirement and those results were comparable to the ITER-NBI specification ($I_{D^-} = 40$ A with the current density of 200 A/m² at 0.3 Pa); iii) Linear dependence of the minimum value of the I_e/I_{D^-} on the arc-discharge power is found, and is stronger in the D⁻ operation than I_e/I_{H^-} in the H⁻ operation. The degradations of the negative ion current and the increase in the coextracted electrons are probably caused by decrease of the surface production rate of D⁻ ions which strongly depends on the incident D⁰ atom velocity to the plasma grid (PG) surface. In addition, caesium (Cs) sputtering became enhanced in the deuterium discharge. This Cs behaviour suggests that larger energy transfer by the deuterium ions impinging onto the PG surface removes the Cs layer required for surface production of the negative ions. These features could be a technical issue in D⁻ beam operation in future NBI where a higher power and a longer pulse duration are required.

Thermal-Hydraulics and Structural Analyses of LLCB TBM Set

D. Sharma¹, S. Ranjithkumar¹, P. Chaudhuri¹, and E. Rajendra Kumar¹

¹*Institute for Plasma Research (IPR), Bhat, Gandhinagar, India*

Corresponding Author: D. Sharma, deepaks@ipr.res.in

India is developing lead-lithium cooled ceramic breeder (LLCB) test blanket module (TBM) for testing in ITER for the validation of fusion blanket design tools, tritium breeding performance and high grade heat extraction capability relevant to Indian DEMO. The LLCB-TBM will be tested from the first phase of ITER operation (H-H phase) in one half of the ITER port #2. LLCB-TBM set consists of TBM and its shield along with supports and piping. The LLCB-TBM consists of U-shaped helium-cooled first wall (FW) with back plate enclosing internal components covered by top and bottom plates. The TBM internals consist of four ceramic breeder canisters (Li_2TiO_3) in the form of pebble bed with PbLi flowing around these canisters to cool the internal structure. The TBM is supported at TBM shield by supports. The back side of shield is welded to TBM set flange, which is bolted to the ITER port plug frame. TBM shield made of SS-316L (N)-IG located behind the TBM is composed of steel and water with a combination of 50:50 to shield neutrons. It consists of two symmetrical parts that have grooves to accommodate pipes. The neutronic heat generated inside shield structure is extracted by water flowing inside the shield.

The detailed thermal-hydraulics of TBM set has been performed based on the heat flux on FW and neutronic heat generation on TBM set. The temperature distribution obtained from thermal analysis has been used for thermo-structural analysis. CFD analysis of helium flow inside the FW channels and manifolds has been carried out to estimate temperature, pressure drop and heat transfer coefficient. The distribution of flow inside the different flow circuits of FW from manifolds and water flow in TBM shield will also be described in this paper. Structural analysis has been performed on TBM set based on load combinations as per ITER load specifications. RCC-MR 2007 code has been used for the structural assessment for the prevention of p-type and s-type damages and calculation of safety margins. The structural analysis results of different components of TBM set which include TBM, back plate, supports, process pipes and TBM shield will be discussed in detail in this paper.

Development of High Power Gyrotrons for Advanced Fusion Devices and DEMO

T. Kariya¹, R. Minami¹, T. Imai¹, T. Numakura¹, M. Okada¹, Y. Endo¹, Y. Nakashima¹, H. Idei², T. Onchi², K. Hanada², T. Shimozuma³, Y. Yoshimura³, H. Takahashi³, H. Igami³, T. I. Tsujimura³, S. Ito³, S. Kobayashi³, S. Kubo³, K. Sakamoto⁴, Y. Oda⁴, R. Ikeda⁴, K. Kajiwara⁴, K. Takahashi⁴, T. Kobayashi⁴, S. Moriyama⁴, M. Ono⁵, K. Nagasaki⁶, T. Eguchi⁷, Y. Kawakami⁷, and Y. Mitsunaka⁷

¹Plasma Research Center, University of Tsukuba, Tsukuba, Ibaraki, Japan

²Research Institute for Applied Mechanics (RIAM), Kyushu University, Kasuga, Japan

³National Institute for Fusion Science (NIFS), Toki, Gifu, Japan

⁴National Institutes for Quantum and Radiological Science and Technology (QST), Naka Fusion Institute, Naka-shi, Ibaraki-ken, Japan

⁵Princeton Plasma Physics Laboratory (PPPL), Princeton, NJ 08540, USA

⁶Institute of Advanced Energy, Kyoto University, Nishikyo-ku, Kyoto 615-8540, Japan

⁷Toshiba Electron Tubes and Devices Co., Tochigi, Ltd

Corresponding Author: T. Kariya, kariya@prc.tsukuba.ac.jp

Megawatt (MW) gyrotrons with a wide frequency range from 14 to 300 GHz are being developed in a collaborative ECH study for advanced fusion devices and a DEMO. 1) Detailed designs of a 14 GHz 1 MW gyrotron has been started for actual fabrication. For a 14 GHz RF beam with high divergence, a calculated transmission efficiency of 85% to the corrugated waveguide coupling position was initially obtained by minimizing the RF transmission path. 2) In the experimental tests of a new 28/35 GHz dual-frequency gyrotron, the cooling characteristics of an optimal-structure double-disk sapphire window was evaluated. We confirmed that operating at 0.4 MW with a continuous wave (CW) at 28 GHz is possible, which is two times the output power reported in previous studies. 3) A 77/51 GHz dual-frequency gyrotron with an output of over 1 MW is presented. 4) In an experiment with a 300 GHz gyrotron, the influence of the reflected wave from the window was reduced by tilting the output window, and mode competition in the cavity was suppressed. An output power of 0.62 MW with a pulse width of 1 ms, which is the new record in this frequency, was obtained.

Performance Evaluation of 1.3 kW at 4.5 K Helium Refrigerator/Liquefier (HRL) at IPR

R. N. Panchal¹, P. N. Panchal¹, R. Patel¹, G. Mahesuria¹, D. Sonara¹, G. L. N. Srikanth¹, A. Garg¹, N. Bairagi¹, D. Christian¹, R. Sharma¹, K. Patel¹, P. Shah¹, H. Nimavat¹, G. Purwar¹, J. C. Patel¹, V. L. Tanna¹, A. K. Sahu¹, and D. Raju¹

¹*Institute for Plasma Research (IPR), Bhat, Gandhinagar, India*

Corresponding Author: R. N. Panchal, rpanchal@ipr.res.in

At IPR, 1350 W at 4.5 K helium cryoplant is dedicated to facilitate the cooling requirements of SST-1 machine. Since 2004, helium refrigerator/liquefier (HRL) (Make: M/S. Air Liquide, France) is operational in mixed mode equivalent to 650 W (refrigeration power) and 200 ℓ/h (liquefaction capacity) at 4.5 K. The HRL can be operated in two phase (1.3–1.5 bar at 4.5–4.7 K) as well as single phase supercritical helium (at 4 bar and 4.5 K with nominal mass flow rate of 300 g/s) modes of operation. The refrigeration capacity of the HRL is 650 W at 4.5 K used to make TF and PF coils superconducting whereas the remaining capacity of 200 ℓ/h is utilized for powering the vapour cooled current leads system of SST-1 at rated current of 10 kA.

To ensure the availability of the HRL and its best performance as per the needs of long duration SST-1 experiments, we carry out preventive maintenance of the different cryogenic components and subsystems as per defined schedule. These activities result in increasing the life span of the HRL as well as ensure its maximum availability during SST-1 operation. M/S. Air Liquide envisaged to carry out every five years preventive maintenance of the HRL for all the subsystems and components. After major maintenance, it is desirable to have performance test on the HRL. We have carried out major preventive maintenance of the HRL and measure the HRL capacity during 2009–2010.

Recently, we have further carried out the maintenance ourselves and carried out the performance test. The equivalent cold power of HRL found to be 1160 W (in pure refrigeration mode), 10.7 g/s (in pure liquefaction mode) and 1300 W equivalent (in mixed mode) at 4.5 K. These values match with our last experimental measurements during HRL maintenance performed in 2010 and as expected considering the operational hours of HRL after thirteen years of operation. These results are quite satisfactory from the HRL performance point of view. The HRL capacity strictly depends on the different modes of operations. In this paper, we report the performance evaluation of cold capacity of HRL at IPR since its commissioning to till date.

Survey on Hot Isostatic Pressing Technique for Development of Tokamak Components

G. Vadolia¹, K. P. Singh¹, B. R. Doshi¹, and M. K. Gupta¹

¹*Institute for Plasma Research (IPR), Bhat, Gandhinagar, India*

Corresponding Author: G. Vadolia, gautamv@ipr.res.in

Hot isostatic press (HIP) equipment is basically an electric furnace which is contained in a pressure vessel. In HIP, the component is subjected to elevated temperature (generally over 1000°C) and pressure (generally over 1000 bar) which results in fully isotropic material properties. As per 2012 estimate, approximately 1000 HIP systems have been installed worldwide. Around half of these HIP installations were for R&D applications. HIP is used to eliminate pores (and remove casting defects), consolidation of powder and diffusion bonding of dissimilar metals or alloys. The components are often of net shape or near net shape. HIP eliminates inspectability issues, enables new alloy system and enhances weldability. HIP improves fatigue properties, creep properties, ductility and impact strength. It provides an alternate supply route for long lead-time components. Hot isostatic pressing of austenitic stainless steel powders for pressure retaining applications is reported in The American Society of Mechanical Engineers (ASME) proceedings.

The technology has developed over the last 20 years and HIP can now produce twice as much product using the same type of machine as they could twenty years ago. The capability of producing full-dense near net-shape product can be utilized for multilayered plasma facing components fabrication. Joining of various dissimilar materials is possible, such as tungsten to copper, copper to copper alloy, SS to CuCrZr material, etc., using HIP. The fabricated joints are reported to be satisfactory. Many fusion components are also fabricated through powder metallurgy route using HIP technique.

In this paper, we have performed a survey on applications of HIP in various R&D in fusion community. Some offshore applications, interesting applications in science projects and application for additive manufactured components, etc., shall also be discussed.

Design and Development of 500 kV, 100 mA DC High Voltage Power Supply for Particle Accelerators at IPR

A. D. Mankani¹, S. Amal¹, U. Thakker¹, S. Kumar¹, P. Christian¹, A. K. Chakraborty¹, and U. K. Baruah¹

¹*Institute for Plasma Research (IPR), Bhat, Gandhinagar, India*

Corresponding Author: A. D. Mankani, ashok@ipr.res.in

At IPR neutral beam injection (NBI) facility to heat and drive the plasma current in tokamak is been built by accelerating the positive or negative ion beam of energy around 100 keV. Under the current R&D plan the projection is to develop the technology for future MV-range DC power source facility to accelerate ion beam of energy near 1 MeV and power of the order of few MW. To meet this objective a compact 500 kV, 100 mA DC upgradable to 1000 kV power supply is being designed and developed as a first step. This power supply shall also be used for several other applications within IPR related to particle accelerator.

The 500 kV, 100 mA, 50 kW DC particle accelerator power supply is being designed using a symmetrical Cockcroft–Walton (CW) voltage multiplier topology owing to its design simplicity and economical construction. Other advantages of such cascade generators are: a) low voltage rating of components; b) balanced voltage with respect to ground; c) gradual build-up of voltage; and, d) modular construction. The use of a high-frequency power source gives an added advantage of low stored energy, less ripple, better regulation and faster response. A 415 V, 50 Hz 3-phase AC input source is converted into single phase high frequency (i.e., 20 kHz) source using IGBT based full H bridge inverter power supply rated for 100 kVA, 400 V (rms). The high frequency power supply charges the symmetrical CW voltage multiplier through a high voltage high frequency (HVHF) step-up centre-tap ferrite core transformer rated for 80 kVA, 400 V / 25kV–0–25 kV (rms). The output voltage and current of the voltage multiplier unit are controlled by controlling the output voltage of the front end inverter operating in close loop control.

This paper will present the design and simulation results of 500 kV, 100 mA DC power supply modelled in MATLAB Simscape toolbox. The paper will explain the optimization and sensitivity study performed in selecting and sizing of various active and passive components of the CW voltage multiplier, inverter and step-up transformer taking into account the possible operational difficulties and future expansion. Both steady state and transient study results will be explained. This paper will briefly cover the engineering assembly design aspects of voltage multiplier unit in general and of a 250 kV prototype voltage multiplier developed.

Surface Characterization of Li Coatings and their Interaction with Plasmas for Fusion Applications via Ion Beam Analysis Techniques

F. Bedoya¹, K. Woller², and D. G. Whyte¹

¹Plasma Science & Fusion Center, MIT, Cambridge, MA 02139, USA

²Massachusetts Institute of Technology (MIT), Cambridge, MA 02139, USA

Corresponding Author: F. Bedoya, bedoya@mit.edu

Conditioning of plasma facing components (PFC) is a common practice to improve the plasma performance in both tokamaks and stellarators. The evaporation of thin Li films on the PFC and first wall has given positive results in multiple machines (CDX-U, LTX, TFTR, NSTX, EAST). Reduced recycling and impurity concentration in the plasma are commonly associated with Li. As a consequence, improved energy confinement times and increased stored energy have been observed, in addition to the reduction of edge localized modes (ELMs) frequency.

As a consequence, multiple studies have been dedicated to investigate the surface properties of Li and its interaction with species that are common in fusion environments e.g., H, D, O. As the plasma material interactions (PMI) occur near the surface of the PFC (top 10–100 nm), methods with such probing depths, such as ion beam analysis (IBA) techniques, are a remarkable resource to characterize these materials and the effect that plasmas have on them.

The dynamics of ion implantation and sputtering of surfaces (DIONISOS) is an in-situ PMI facility, designed to expose samples to plasmas and interrogate their surfaces using IBA. The experiment is equipped with a helicon plasma source that can produce discharges with fluxes near $10^{21}/\text{m}^2\text{s}$ and electron temperatures close to 6 eV. DIONISOS is attached to an ion accelerator, allowing execution of elastic recoil detection (ERD), Rutherford backscattering spectroscopy (RBS), and nuclear reactions analysis (NRA). Recently, the facility has been equipped with a Li evaporation system for in-situ deposition of thin films on the substrates. The combination of modification and analysis tools available in DIONISOS, makes it ideal to study the dynamic and multivariable relationship of Li and plasmas.

This work includes real-time ERD and RBS data collected during deposition and erosion of thin Li films applied on different substrates. Various substrates have been used for characterization of the deposited films preparing to study the interaction of Li with materials relevant to fusion applications. In the same way, several experimental parameters have been optimized for better quantification of the relevant species.

Contribution of Fusion Energy to Low-Carbon Development under the Paris Agreement and Accompanying Uncertainties

K. Gi¹, F. Sano¹, K. Akimoto¹, R. Hiwatari², and K. Tobita²

¹Research Institute of Innovative Technology for the Earth (RITE), Kyoto, Japan

²Joint Special Design Team for Fusion DEMO, National Institutes for Quantum and Radiological Science and Technology (QST), Rokkasho Fusion Institute, Rokkasho-mura, Aomori, Japan

Corresponding Author: K. Gi, kgi@rite.or.jp

The Paris Agreement requires deep reduction of greenhouse gas emissions. The world is toward rapid transition not only for climate change mitigation but also for sustainable development. Fusion energy has outstanding characteristics of plentiful resources, no nuclear runaway and zero-carbon emission, and its development has made remarkable progress thanks to large and committed investment for more than 50 years. However, long-term strategies for fusion energy development will become critically important in order to promote future DEMO projects by another large-scale investment and gain social acceptance. In this study, we assessed potential contribution of fusion energy to low-carbon development which is prescribed in the Paris Agreement under the combination of uncertainties of future socioeconomic development, the 2°C target and future commercial fusion power plants.

We analyzed global energy systems up to 2100 in consideration of uncertainties by combining socioeconomic scenarios, global CO₂ emission pathways, and fusion power plants by using a global energy systems model: DNE21+. We used three shared socioeconomic pathways (SSPs) to express the uncertainty of future socioeconomic development. Assumptions and parameters for DNE21+ were harmonized with the SSP narratives. Four global CO₂ emission pathways were used to simulate the uncertainty of the long-term targets of the Paris Agreement. For the uncertainty of fusion energy development, we set three scenarios, i.e., no fusion, conventional R&D and advanced R&D which have different assumptions on parameters of fusion power plants. The parameters were set by considering potential and achievable cost reduction and performance improvement on the extension of DEMO concept design.

Global negative CO₂ emission in 2100 by drastic decarbonization of energy systems is required in order to achieve the 2°C target, and fusion power plants will be installed in the latter half of the 21st century mainly in the countries which have limited potentials of zero-emission energy sources such as Japan, Korea and Turkey. If inexpensive power plants could be developed by enhanced R&D and advanced design in DEMO projects, fusion power plants will also be deployed in the EU28, India and China. This study could be implicated in long-term strategy planning for fusion energy development.

Dispersion Strengthened Copper Alloys Produced by Mechanical Alloying and Hot Isostatic Pressing for Divertor Application

H. Noto¹, B. Huang¹, Y. Hishinuma¹, and T. Muroga¹

¹*National Institute for Fusion Science (NIFS), Toki, Gifu, Japan*

Corresponding Author: H. Noto, noto.hiyoyuki@nifs.ac.jp

The realization of advanced fusion reactors rests with improvement of cooling capacity of divertors, and enhancing the mechanical properties of Cu alloys is one of the critical issues for that improvement. This paper reports development of dispersion strengthened Cu alloys using ball-milling, encapsulation, and hot isostatic pressing (HIP) facilities. Cu-Al, Zr and Y alloys have been produced so far. The new facilities installed in NIFS made it possible to control oxygen level of the products. In the case of Cu-Y, CuO was added in the middle of the milling for supplying oxygen. These processes resulted in formation of fine microstructures, oxide dispersion, and significant strengthening of Cu alloys.

Neutron Flux Distributions in the LHD Torus Hall Evaluated by an Imaging Plate Technique in the First Campaign of Deuterium Plasma Experiment

M. Kobayashi¹, T. Tanaka², T. Nishitani¹, K. Ogawa^{1,3}, M. Isobe^{1,3}, G. Motojima^{1,3}, A. Kato¹, T. Saze¹, S. Yoshihashi², and M. Osakabe^{1,3}

The LHD Experiment Group

¹National Institute for Fusion Science (NIFS), Toki, Gifu, Japan

²Department of Fusion Science, Graduate University for Advanced Studies (SOKENDAI), Toki, Gifu, Japan

³Nagoya University, Nagoya, Japan

Corresponding Author: M. Kobayashi, kobayashi.makoto@nifs.ac.jp

In the Large Helical Device, deuterium plasma experiments began in March 2017 and completed in August 2017. In this experimental campaign, about 4×10^{18} neutrons were generated and activated components in the torus hall. The concentration of radioactive isotopes in the components in the torus hall must be evaluated to estimate the radiation dose for workers and to plan the decommissioning of LHD.

For this purpose, the global flux distributions for thermal, epithermal and fast neutrons in the torus hall of large fusion devices were experimentally evaluated for the first time in LHD using the activation foil method measured by the imaging plate (IP) and high-purity germanium detector (HPGe). The thermal neutron flux distribution was concentrated within about 15 m from the centre of LHD. In particular, the highest flux was observed at the west region underneath the LHD where an unborated polyethylene blocks. The borated polyethylene blocks, which works as the decelerator of fast neutron and the absorber of thermal neutron, were placed on the floor underneath the LHD except the west region. It turned out that the thermal neutron was effectively absorbed by borated polyethylene blocks placed beneath the LHD. This should reduce the radioactivity of the floor and is beneficial to maintain good environment for radiation workers. The almost uniform distribution of fast neutron was observed just underneath the LHD. The flux of fast neutron near the LHD was about one order of magnitude higher than that of thermal neutron. The region with high fast-neutron flux was narrower compared to that of thermal neutron due to the quick energy loss process for fast neutron.

The neutron flux distribution measurement with rough energy discrimination based on the threshold energy of neutron activation foil allows us to estimate the spatial radiation dose rate as well as the radioactivity in components in the torus hall. Therefore, the neutron flux distribution obtained here is conducive to developing the radiation safety in the deuterium plasma experiments comprehensively and to planning the future decommissioning of the LHD.

A Multiparameter Optimization Technique Considering Temporal and Spatial Variation in Nuclear Response of Materials in Fusion Devices

P. Kanth¹, S. C. Tadepalli², and P. V. Subhash^{2,3}

¹*Institute for Plasma Research (IPR), Bhat, Gandhinagar, India*

²*ITER-India, Institute for Plasma Research (IPR), Bhat, Gandhinagar, India*

³*Homi Bhabha National Institute (HBNI), Anushakti Nagar, Mumbai 400094, India*

Corresponding Author: P. Kanth, priti.kanth@ipr.res.in

Structural materials present in and around any fusion device will face stringent conditions due to the high-energy, high-intensity neutron flux emitted from the fusion plasma. This will have significant life-limiting impacts on the reactor components of both experimental and commercial fusion devices. The neutrons interact with the material initiating nuclear reaction leading to the production of radioactive isotopes, gas molecules and related defects. These gases, particularly helium, can cause swelling and embrittlement of the material. Furthermore, the radioactive isotopes produce would cause heating in the material. These isotopes may have long lives which would contribute towards the radwaste produced in the fusion devices. Hence designing of low activation materials for fusion devices is warranted.

At ITER-India, IPR, a number of computational tools are being developed to estimate the nuclear response of materials and to optimize accordingly. ACTYS-1-GO, a multipoint neutron activation code which can calculate radiological responses of materials located at various positions in a fusion reactor efficiently is developed. Also, a mathematical framework is developed for accessing the relationship of radiological quantity with the initial elements present in the material. Such framework helps in identifying and minimizing the fraction of most dangerous elements and isotopes from the material composition. In the present study both the methodologies are efficiently coupled for a complete material optimization. Quantities responsible for various radiological effects (like activity, dose, heat, and radwaste) and related defects in the material are considered and their contributing elements are optimized accordingly. Also, since a single material faces a gradient of neutron flux over its entire volume, all such optimization is carried out over the entire range of neutron flux faced by that material. This provides a comprehensive picture of the response of the material to neutron irradiation, enabling the assessment of structural integrity of components in a fusion device.

Design Progress of Advanced Fusion Neutron Source for JA/DEMO Fusion Reactor

K. Ochiai¹, S. Sato¹, H. Kondo¹, M. Ohta¹, M. Oyaizu¹, M. Nakamura¹, S. Kwon¹, C. Park¹,
H. Tanigawa¹, T. Nozawa¹, M. Teduka¹, and H. Suzuki¹

¹National Institutes for Quantum and Radiological Science and Technology (QST),
Department of Fusion Reactor Materials Research, Rokkasho-mura, Aomori, Japan

Corresponding Author: K. Ochiai, ochiai.kentaro@qst.go.jp

Based on results from the IFMIF/EVEDA project in the Broader Approach (BA) activities, a conceptual design of the Advanced Fusion Neutron Source (A-FNS) in Rokkasho aiming at obtaining material irradiation data up to 20 dpa for a fusion DEMO reactor is presented in this paper. The A-FNS is composed of an accelerator facility with a 40 MeV and 125 mA deuteron beam, a test facility and a postirradiation examination facility. A particular attention in the design is paid on an integration of the test facilities by adopting a newly designed test specimen module for A-FNS. Recently, the nuclear analysis of test module has been progressed to optimize the irradiation of test pieces and then it was clarified that our original module enabled the test pieces to be irradiated uniformly.

Neutronic Analysis of IFMIF-DONES Test Cell Cooling System

G. Stankunas¹, A. Tidikas¹, and U. Fischer²

¹*Lithuanian Energy Institute, Laboratory of Nuclear Installation Safety,
Breslaujos str. 3, LT-44403 Kaunas, Lithuania*

²*Karlsruhe Institute of Technology, Institute for Neutron Physics and Reactor Technology,
Eggenstein-Leopoldshafen, Germany*

Corresponding Author: G. Stankunas, gediminas.stankunas@lei.lt

IFMIF-DONES (International Fusion Materials Irradiation Facility — DEMO-Oriented Neutron Source) is an accelerator based d-Li neutron source which aims at the qualification of materials at the irradiation conditions of a DEMO fusion power reactor as being developed in the frame of EUROfusion's Power Plant and Technology (PPPT) programme. The high-intensity neutron radiation produced in the liquid lithium target results in a strong activation of the test cell (TC) with the high flux test module (HFTM), housing the irradiation specimens, the TC steel liner and the water-cooled concrete walls. The activation and decay heat generation of the cooling pipes need to be assessed for maintenance, decommissioning and waste management purposes and the related safety analyses.

This paper presents the analyses performed within the ENS (early neutron source) project of EUROfusion/PPPT for providing up-to-date estimates of the activity inventories and the decay heat generation in the DONES TC facility. To this end, a series of coupled McDeLicious transport and FISPACT inventory calculations were performed using the 2017 DONES TC model and nuclear cross-section data from the FENDL-3.1 data library. Activity inventories and decay heat data were assessed for the water pipes assumed for cooling the walls.

FIP

The paper discusses the results obtained for the activity and the decay heat as a function of the decay time after radiation and also addresses the issue of the radiation dose loads which are to be expected due to the activated components and systems including the cooling water system.

The DEMO Fuel Cycle: Novel Technologies for Tritium Inventory Reduction

C. Day¹, G. Federici², B. Butler³, T. Giegerich¹, Y. Hörstensmeyer¹, and B. Ploeckl⁴

¹Karlsruhe Institute of Technology (KIT), Karlsruhe, Germany

²EUROfusion Programme Management Unit Garching, Boltzmannstraße 2, 85748 Garching Germany

³Culham Centre for Fusion Energy (CCFE), Culham Science Centre, Abingdon, UK

⁴Max-Planck-Institut für Plasmaphysik, Garching, Germany

Corresponding Author: C. Day, christian.day@kit.edu

In the framework of the EUROfusion Programme, the EU is preparing the conceptual design of the fuel cycle for a pulsed fusion DEMO. Over the last years, a completely novel and most innovative fuel cycle architecture has been developed, driven by the need to reduce the tritium inventory to an absolute minimum.

To achieve this goal, batchwise processes used in the fusion fuel cycle so far were replaced by continuous processes wherever possible. This includes the change from discontinuous cryopumping to mercury-based continuous vacuum pumping with zero demand on cryoplant power, and the introduction of thermal cycling ab- and adsorption processes for isotope separation in the tritium plant instead of large cryogenic distillation columns with tritiated liquid hold-ups. To further reduce inventory, the well-known approach to route all exhaust gas through the tritium plant has been abandoned in favour of a three-loop architecture. There, superpermeable metal foils are introduced in the divertor ports to separate a pure DT stream which is then immediately recycled to feed the pellet injection systems. Continuous reinjection of the exhaust gas can artificially increase the wall recycling coefficient and hence increase the burn-up fraction resulting in reduced gas throughputs needed to maintain a stable plasma operation at acceptable fuel dilution. To increase the core fuelling efficiency, optimization potentials in the design of the high field side guiding tube systems are being exploited. The tritium accountancy system under development will rely on modern, real-time and online tritium instrumentation. Finally, a unified fuel cycle simulator is under development on a commercial software platform in order to identify optimization potentials within the fuel cycle, to allow impact studies, and on a long term to support the development of tailored control and operational strategies.

The paper presents the first integrated and consolidated design point of the fuel cycle based on the 2017 European DEMO baseline. It is shown how the DEMO requirements are picked up and affect system level performance. Examples are given for integration issues and how they were solved. Finally, a roadmap is delineated which illustrates the remaining R&D efforts needed to achieve at a validated and complete conceptual design until the mid-2020s.

Multiphysics Approach to Plasma Neutron Source Modelling at the Tokamak JET

Ž. Štancar¹, M. Gorelenkova², S. Conroy³, P. Sauvau⁴, J. Buchanan⁵, H. Weisen⁶, and L. Snoj¹

The JET Contributors

¹*Jožef Stefan Institute, 1000 Ljubljana, Slovenia*

²*Princeton Plasma Physics Laboratory (PPPL), Princeton, NJ 08540, USA*

³*Uppsala University, Uppsala, Sweden*

⁴*Universidad Nacional de Educación a Distancia, 28040 Madrid, Spain*

⁵*Culham Centre for Fusion Energy (CCFE), Culham Science Centre, Abingdon, UK*

⁶*Swiss Plasma Center (SPC), École polytechnique fédérale de Lausanne (EPFL), 1015 Lausanne, Switzerland*

Corresponding Author: Ž. Štancar, ziga.stancar@ijs.si

The work presented in the paper is focussed on the development of a multiphysics methodology for the creation of a realistic plasma neutron source for Monte Carlo neutron transport calculations. We begin with a description of the plasma neutron sources used in fusion neutronics so far, systems based on the assumption that the plasma is in thermal equilibrium, the neutrons being emitted isotropically and their spectrum approximated with a Maxwellian distribution. The plasma shape and neutron emissivity profiles are analyzed, exhibiting major discrepancies from the current JET ITER-like wall plasma state. The analysis serves as motivation for the development of a more adequate description of JET plasma neutron emission. The methodology is based on the use of the state-of-the-art plasma transport code TRANSP and the neutron spectrum computation code DRESS. The diagnostic data of a baseline DD discharge of the JET tokamak is used as input for the TRANSP/NUBEAM ion orbit code, which evaluates the beam-target fusion reactions that govern neutron production. These simulations are the basis for the evaluation of the neutron spectra, which are performed with the DRESS code. In the next step the generation of a Monte Carlo neutron source description is discussed, where the data on plasma state relevant to neutron emission is processed, meaning that the probability density functions for specific quantities are computed. The script assigned for the preprocessing is designed to serve as a tool for the analysis of neutron emission, outputting both the measured and simulated neutron rates, offering insight not only into the essentials for neutronics but also discharge specific plasma physics. A subroutine based on the source code characteristics of the advanced Monte Carlo neutron transport code MCNP is described. Within the routine the prepared plasma data is used to obtain fundamental source neutron information, i.e., location of birth, angle of emission and energy. The performance of the subroutine is analyzed and found to be comparable to MCNP generic and much simpler source descriptions. The paper is concluded with a comparison of the response of several neutron detector systems at JET (KN1, KN2) as calculated with the MCNP Monte Carlo neutron transport code, using the generic and newly developed neutron source generators.

The Potential for Retention of Spin Polarization to Raise Fusion Reactivity

S. P. Smith¹, A. M. Sandorfi², D. C. Pace¹, L. R. Baylor³, M. Wade¹, G. W. Miller⁴, A. Deur², J. Liu⁵, M. M. Lowry², S. Tafti⁵, X. Wei², and X. Zheng²

¹General Atomics, San Diego, CA 92186, USA

²Thomas Jefferson National Accelerator Facility (JLab), Newport News, VA 23606, USA

³Oak Ridge National Laboratory (ORNL), Oak Ridge, TN 37831, USA

⁴Department of Radiology and Medical Imaging, University of Virginia, Charlottesville, VA 22908, USA

⁵Department of Physics, University of Virginia, Charlottesville, VA 22908, USA

Corresponding Author: S. P. Smith, smithsp@fusion.gat.com

Spin polarized fusion (SPF), which increases the DT fusion cross section by 50% and is predicted to yield power gains of 75% in an ITER $Q = 10$ plasma (without SPF), could be demonstrated in the DIII-D tokamak, using recent technological advances. The cross section (i.e., probability) for thermal DT fusion is not only temperature dependent, but also depends on the spin orientation of the nuclei, increasing the DT fusion cross section by up to 50%. A self consistent transport calculation predicts up to a 75% increase in fusion power in that ITER scenario. A test of the survivability of spin polarized DT fuel through to the fusion reaction can be obtained by injecting spin polarized D and ^3He pellets into the DIII-D tokamak. The DT fusion reaction $\text{D} + \text{T} \rightarrow \alpha + n$ is isospin equivalent to the reaction $\text{D} + ^3\text{He} \rightarrow \alpha + p$. Simulation synthetic diagnostic data of the resultant energetic proton fluxes, such as could be measured with a fast ion loss detector, calculated for polarized material with currently available levels of polarization, show that there can be up to a 30% change between the anti-parallel and parallel alignment configurations at several locations near the vessel walls. Spin polarized D is routinely produced in the nuclear physics community. The purity fraction is currently $\sim 40\%$. D-pellet polarization will have a depolarization decay time of about a year at liquid helium temperatures, which would be sufficient to produce the pellets in Virginia, USA, and then transport them to DIII-D for the proposed polarization survival experiment. We have recently shown that highly ($\sim 65\%$) polarized ^3He can retain essentially all of its polarization during diffusion through a polymer shell to make a ^3He pellet for injection in the proposed polarization survival experiment. Because the depolarization time for these ^3He filled pellets at liquid nitrogen temperatures is only a few hours, a device for producing ^3He would be built onsite at DIII-D, and then the pellets filled shortly before injection into DIII-D. Polarization retention in the proposed D^3He experiment would be a breakthrough for fusion.

Work supported by General Atomics Internal Research and Development funds, a grant from the University of Virginia Research and Initiative Fund, and the U.S. Department of Energy through grants DE-FC02-04ER54698 and DE-AC05-06OR23177.

Artificial Neural Network for Yield Strength Prediction of Irradiated RAFM Steels

A. Abhishek¹, H. T. Iyer¹

¹*Institute for Plasma Research (IPR), Bhat, Gandhinagar, India*

Corresponding Author: A. Abhishek, agraj@ipr.res.in

Structural materials to be used in proposed fusion reactor will be exposed to hostile neutron environmental conditions. These steels will interact with high-energy neutrons. The interaction is expected to degrade structural material properties causing loss of ductility, increase of yield strength and DBTT temperature. An artificial neural network (ANN) with back-propagation (BPN) technique is used in this work to develop a numerical model which predicts the change in yield strength of irradiated steels at various irradiation condition. More than 15 000 material related parameters such as composition, temperature and yield strengths are obtained from literature. These experimental results are used to generate more than 100 networks after proper training, testing and validation. A statistically validated neural network is used to predict the change in yield strength of RAFM steel in the range of 290 K–900 K and 0–80 dpa. For instance, at 673 K and 300 K of test temperature and irradiation temperature, the yield is first found to increase and then remain constant after 50 dpa. Again at the same test temperature and higher irradiation temperature of 700 K, the yield strength is first found to increase until 25–30 dpa and then decreases thereafter. In the work we plan to present such kind of behaviour at different temperatures and dpa conditions.

Modification in LHCD DAC System to Incorporate Measurement of RF Power

R. Joshi¹, C. G. Virani¹, K. K. Ambulkar¹, and P. K. Sharma¹

¹*Institute for Plasma Research (IPR), Bhat, Gandhinagar, India*

Corresponding Author: R. Joshi, rjoshi@ipr.res.in

The lower hybrid current drive (LHCD) system has four klystrons, each rated for 0.5 MW, CW power at 3.7 GHz, which are employed to launch the lower hybrid waves into plasma. VME and PXI based data acquisition and control (DAC) system has already been implemented for the operation of LHCD System. VME based DAC system has been modified to incorporate measurement of RF power signals.

The VGD4 acquisition card was integrated for the measurement of power from 96 signals of LHCD system. However, because of random data acquisition problem, this card is replaced by IP330 analog input cards. IP330 analog cards have been included and integrated with existing system to measure 128 power measurement signals requirement with the subsystem. Carrier boards have been replaced with new version of device driver to integrate IP modules of AI, AO and timer card. Existing device driver programme have been modified to add additional functionality for data acquisition and time synchronization. Adaptor classes have been developed to integrate with RTOS application environment for low context switching and higher performance. NTFS has been used to handle long chunk of data during experimental shots. User interface is modified on Linux host machine to monitor and acquire for additional signals. The system has been validated during the SST-1 campaigns. Developed DAC software is modular, hierarchical and scalable in nature. To achieve the data storage with calibration and plotting, MDSPlus has been integrated for data visualization and management of after shot analysis. In this paper, the design, implementation and results obtained with IP330 cards are reported and discussed.

Thermal Performance Analysis of Al_2O_3 –Water Nanofluid as a Coolant in Nuclear Applications

S. S. Mukherjee¹, P. C. Mishra¹, P. Chaudhuri², and H. Bhattacharjee³

¹Kalinga Institute of Industrial Technology (KIIT), Bhubaneswar, Odhisa, India

²Institute for Plasma Research (IPR), Bhat, Gandhinagar, India

³St. Mary's Technical Campus, Kolkata, West Bengal, India

Corresponding Author: S. S. Mukherjee, [sayantan2210@gmail.com](mailto:sayantant2210@gmail.com)

The thermal performance of plasma facing components in a fusion reactor receiving high heat fluxes could be enhanced significantly by using nanofluids, which are suspensions of 0.001–10% nanoparticles of <100 nm size. Nanofluids show a promising heat transfer enhancement compared to the base fluid. Water-based nanofluids have the potential to deliver much improved high heat flux cooling while retaining all the advantages of water. The exciting prospect of nanofluids has motivated this investigation into their suitability as coolants of a fusion reactor.

This paper intends to present a theoretical investigation on energetic feasibility of Al_2O_3 –water nanofluid as coolant streaming inside a smooth horizontal tube. Existing experimental results are utilized to compute the thermo-physical properties, heat transfer coefficient and pumping power of nanofluid. The heat transfer coefficient ratio, i.e., the ratio between heat transfer coefficients of nanofluid to the same of base fluid has been calculated from the existing correlations at constant Reynolds number. The derived mathematical model of heat transfer coefficient ratio was validated with data available in existing literature. The pumping power ratio which is the ratio of pumping power required for nanofluid flow to the same required for basefluid flow has been estimated. The effective increase in heat transfer coefficient makes nanofluid more promising than water for ultrafast cooling in nuclear applications. However, the effective increase in pumping power due to dispersion of nanoparticles in its base fluid makes it unfavourable for efficient heat transfer applications.

RGA Analysis and Surface Analysis of SST-1 Graphite Tiles in High Temperature Vacuum Baking

A. Arumugam¹, R. Gattu¹, P. Dave², A. Zala², D. C. Raval¹, and Z. Khan¹

¹*Institute for Plasma Research (IPR), Bhat, Gandhinagar, India*

²*Facilitation Centre for Industrial Plasma Technologies (FCIPT),
Institute for Plasma Research (IPR), Bhat, Gandhinagar, India*

Corresponding Author: A. Arumugam, arun@ipr.res.in

Steady state Superconducting Tokamak (SST-1) is a large aspect ratio tokamak with a major radius of 1.1 m and minor radius of 0.20 m. The plasma facing components (PFC) are one of the major subsystems of SST-1. PFCs of SST-1 consist of divertors, passive stabilizers, baffles and poloidal limiters. PFCs are designed and fabricated to be ultrahigh vacuum (UHV) compatible and high temperature compatible for steady-state plasma operation. All PFCs are made up of graphite tiles mechanically attached to the copper alloy substrate. Graphite is chosen as a first wall armour material in SST-1 tokamak because of its high thermal shock resistance and low atomic number. Graphite, because of its porous nature, absorbs water vapour and other gasses when exposed to atmosphere. Generally, graphite tiles are given a high temperature bake-out treatment prior to installation inside the tokamak to reduce the in-situ wall conditioning period. There are about 3800 graphite tiles of different sizes to be fitted on 132 base PFC copper modules. All 3800 graphite tiles were given a high temperature bake-out at 1000°C to remove entrapped gasses, under high vacuum in a vacuum furnace before installation into the SST-1 vacuum vessel. A residual gas analyser (RGA) was used to measure the outgassing at various temperatures during the entire vacuum baking process. RGA works on the principle of quadrupole mass spectrometer. RGA is used to detect and analyse the residual gases during vacuum pumping and high temperature baking of graphite tiles. Surface analysis of graphite tiles have been carried-out using scanning electron microscope (SEM) and X-ray diffraction analysis (XRD) before and after baking. Elemental analysis was also carried-out before and after baking to qualify the graphite samples. This paper will discuss the residual gas analysis and surface analysis of SST-1 graphite tiles in high temperature vacuum baking process.

Studies on High Temperature Vacuum Brazing of Tungsten to Tungsten Alloy Materials for DEMO Divertor Application

K. P. Singh¹, A. Patel¹, K. S. Bhope¹, and S. S. Khirwadkar¹

¹*Institute for Plasma Research (IPR), Bhat, Gandhinagar, India*

Corresponding Author: K. P. Singh, kpsingh@ipr.res.in

This work summarizes the experimental studies on joining of tungsten based refractory materials at high temperature using vacuum brazing process. The objective of the joining of these refractory materials is to develop the joining technique for fabricating helium cooled divertor target relevant to DEMO fusion reactor. These so called “divertor fingers” are expected to handle the incident heat flux of 10 MW/m^2 , to be cooled by multiple helium jet at high pressure ($\sim 10 \text{ MPa}$) and high temperature ($\sim 600^\circ\text{C}$) helium gas environment. For joining of W (tungsten) to WL10 alloy (tungsten + 1% lanthanum oxide), high temperature vacuum brazing has been performed at temperatures above 1000°C using selective brazing fillers using Gleeble-3800 thermo-mechanical simulator at IPR. For pre-qualification of the brazed joints, the brazed specimens are subjected to 500 thermal cycles at 950°C to 800°C using Gleeble-3800 system. The brazed joints are characterized by non-destructive testing (NDT), ultrasonic testing (UT), microstructural and mechanical characterization. The experimental methodology and results of the characterization will be presented in the paper.

Deuteron Beam Commissioning of the Linear IFMIF Prototype Accelerator Source and LEBT

N. Chauvin¹, T. Akagi², L. Bellan³, P.-Y. Beauvais⁴, B. Bolzon¹, P. Cara⁴, S. Chel¹, M. Comunian³, H. Dzitko⁴, E. Fagotti³, F. Gérardin¹, R. Gobin¹, F. Harrault¹, R. Heidinger⁴, R. Ichimiya², A. Ihara², A. Kasugai², T. Kitano², J. Knaster⁵, M. Komata², K. Kondo², A. Marqueta⁵, K. Nishiyama⁵, Y. Okumura⁵, A. Pisent³, G. Pruneri⁵, K. Sakamoto², F. Scantamburlo⁵, F. Sénéé¹, T. Shinya², and M. Sugimoto²

¹*Institut de recherche sur les lois fondamentales de l'Univers (IRFU), Commissariat à l'énergie atomique (CEA/Saclay), 91191 Gif-sur-Yvette, France*

²*National Institutes for Quantum and Radiological Science and Technology (QST), Rokkasho Fusion Institute, Rokkasho-mura, Aomori, Japan*

³*Istituto Nazionale di Fisica Nucleare (INFN), Laboratori Nazionali di Legnaro, Legnaro, Italy*

⁴*F4E: Fusion for Energy, EUROfusion Consortium, 85748 Garching, Germany*

⁵*International Fusion Materials Irradiation Facility (IFMIF/EVEDA), Rokkasho, Aomori, Japan*

Corresponding Author: N. Chauvin, nicolas.chauvin@cea.fr

The Linear IFMIF Prototype Accelerator aims to operate in Rokkasho Fusion Institute a 125 mA CW deuteron beam at 9 MeV in order to prove the technical feasibility of the IFMIF accelerators concept. A 2.45 GHz ECR ion source developed by CEA-Saclay is designed to deliver 140 mA 100 keV CW D⁺ beam. The low energy beam transfer line (LEBT) relies on a dual solenoid focussing system to transport and match the beam into the next accelerating section which is a radiofrequency quadrupole (RFQ). At the end of the LEBT, the normalized RMS emittance has to be lower than 0.3π mm·mrad in order to reach the optimal beam transmission through the RFQ.

This contribution will present the different commissioning phases of LIPAC ion source and LEBT. The experimental results that have been obtained will be reported. In particular beam emittance measurements as a function of ion source extraction voltage gaps, total extracted current from the source and solenoid tunings will be showed. In order to model as well as possible the beam transport through LEBT, intensive beam dynamics simulations that take into account space charge compensation have been performed using a self-consistent particle-in-cell code. Simulation results will be discussed and compared to experimental data.

Overview of the Methods Developed for Fission Plants Safety Relevant to the Safety of Fusion Facilities

D. Panayotov¹

¹F4E: Fusion for Energy, ITER EU Centre, 08019 Barcelona, Spain

Corresponding Author: D. Panayotov, dobromir.panayotov@f4e.europa.eu

Safety studies for fusion facilities are commonly conducted using codes originally developed for fission reactor accident analysis and adapted to model the fusion-relevant phenomena. Nevertheless there are many “fission developed” methods still not considered in fusion safety assessment which could offer significant advantages in fusion power commercialization. Along with solving the safety and licensing critical for the fusion power commercialization, will be the ability to reduce the cost and increase the efficiency of power production. Among other means, these were achieved in fission power by limiting or even avoiding conservatism in the safety assessment, by improving the methods and by use of state-of-the-art tools. There are many reasons for looking into fission similar to the nuclear regulatory environment, the very same nuclear safety principles and regulatory limits apply, use of mature and proven methods already accepted by the regulators, etc. The paper will address the following topics:

- Experimental programmes, test matrixes and databases;
- Computer code development, verification and validation;
- Computer code assessments;
- Conservative or best estimate (BE) methodology;
- Uncertainty estimation methods;
- Phenomena identification and ranking tables (PIRT).

The parallel between the fission and fusion safety approaches and accident analyses methodologies will be drawn. For each of the above topics a brief presentation of the fission historical development followed by an overview of published adaptations of methods and their applications to fusion safety will be reported. The presentation will draw in particular on availability of qualified tools for accidents analyses, use of PIRT, the verification and validation of computer codes by means of separate and integral effect tests and establishing benchmark problems as well on code assessment and development of multiphysics, multi-fluids integrated code systems. These efforts should be aimed at developing a systematic safety demonstration defined by an integrated fusion safety assessment methodology.

Status of Studies of Pulsed Heat Load Influence on Tungsten at BETA Facility and Station of SR Scattering “Plasma” in BINP

A. S. Arakcheev^{1,2,3}, A. V. Burdakov^{1,2,3}, I. V. Kandaurov^{1,2}, V. V. Kurkuchekov¹, V. A. Popov^{1,2}, L. I. Shekhtman¹, M. R. Sharafutdinov⁴, B. P. Tolochko^{1,4}, Y. A. Trunev¹, A. A. Vasilyev^{1,2}, and L. N. Vyacheslavov^{1,2}

¹*Budker Institute of Nuclear Physics (BINP), Novosibirsk, Russian Federation*

²*Novosibirsk State University, Novosibirsk, Russian Federation*

³*Novosibirsk State Technical University, Novosibirsk, Russian Federation*

⁴*Institute of Solid State Chemistry and Mechanochemistry,
Russian Academy of Sciences (RAS), 1 Novosibirsk, Russian Federation*

Corresponding Author: A. S. Arakcheev, asarakcheev@gmail.com

Experiments simulating the pulsed heat loads expected in the ITER divertor were carried out at the BETA facility in the Budker Institute. Using a pulsed electron beam with a duration of 0.2–0.3 ms and heat load with a heat flux factor $HFF \approx 30 \text{ MJ/m}^2 \sqrt{s}$ below the melting point of tungsten were obtained. A distinctive feature of BETA is the ability to study the processes of tungsten erosion in-situ during the heating and immediately after it in the cooling stage. This ability is provided by optical diagnostic methods, using the thermal radiation of the surface and illumination by a continuous laser. The obtained data make it possible to study the dynamics of the temperature distribution on the target surface and the development of its erosion in time. The image of the target surface in its own thermal radiation shows that even under a homogeneous electron beam, having a Gaussian profile with a full width at a half maximum of about 17 mm, hot spots are visible with a temperature much higher than the temperature of the surrounding area. Analysis with SEM and microsections shows that overheating is associated with a decrease in heat removal from these surface areas due to cracks caused by pulsed heating. The method of laser illumination reveals a two-stage process of erosion of the polished tungsten surface after the first heat load. Initially, the surface roughness begins to increase, reaching a maximum at the end of the heating pulse, and then decreases within a few milliseconds upon cooling to a value 2–3 times higher than the initial level of roughness. The second stage of surface modification, corresponding to surface cracking, occurs spontaneously and rapidly develops for a time of the order of $10 \mu s$ on a sample already cooled to room temperature. The delay in the initiation of surface cracking exceeded the time required for the transition from the plastic to the brittle state by 3–4 orders of magnitude.

Synchrotron radiation scattering station “Plasma” develops diagnostics of deformations and stresses in the material under the pulse heat load using the diffraction dynamics. This diagnostic has three principal features: measurements with time resolution, measurements inside the material and measurements with the depth resolution. Currently, the measurement of the dynamics of the shape of the diffraction peak is demonstrated.

Global Supply of Tritium for Fusion R&D

M. Coleman^{1,2}, M. Kovari¹

¹*Culham Centre for Fusion Energy (CCFE), Culham Science Centre, Abingdon, UK*

²*EUROfusion Consortium, Boltzmannstraße 2, Garching, Germany*

Corresponding Author: M. Coleman, matti.coleman@ukaea.uk

The tritium start-up inventory required by a tritium self-sufficient DEMO-class fusion reactor is subject to a wide margin of uncertainty, with estimates in the literature varying from less than 1 kg to almost 20 kg for a ~ 2 GW fusion reactor. If ITER is successful, it is conceivable that multiple DEMO-class devices may be developed in parallel; the European DEMO machine, the Chinese Fusion Engineering Test Reactor and others could require several kilograms of tritium each in the 2050s. Tritium production from heavy water (D_2O) CANDU reactors in Canada presently meets the entire fusion R&D demand of tritium. Ontario Power Generation (OPG) plans to supply ITER with all of the tritium required for its exploitation. Yet OPG may only be able to supply up to 8 kg for a DEMO reactor in the mid-2050s, following the delay to the ITER DT operations (now scheduled in 2036), owing to the progressive phasing out of Canadian CANDU reactors in the 2030s and the natural decay of stocks. There is a risk that commercially available tritium stockpiles in the 2050s are insufficient to meet the fusion demand.

Herein, we present several data-based scenarios of tritium production from heavy water reactors (HWRs) and fusion tritium consumption with varying degrees of optimism. At present, only Canada and the Republic of Korea actively extract tritium from their HWRs in tritium extraction facilities (TEFs), and Romania plans to build one. Based on the assumption that only these countries contribute to the global supply of commercially available tritium, results range from 0 kg to 30.5 kg of T available in 2055, depending on the scenario considered.

Alternative methods for tritium production are discussed; DD fusion start-up with a breeding blanket, modifications to CANDU reactors and other HWRs, and production of tritium in commercial light water reactors using tritium-producing burnable absorber rods.

Tritium production in HWRs remains the best source of tritium for fusion R&D. If Canada, the Republic of Korea, and Romania supply the fusion community with their HWR tritium, there is a reasonable chance that 10 kg of T would be available for fusion R&D in 2055.

We call attention to the dependency of the fusion community on events outside its control, most critically the refurbishment of existing HWRs and TEFs, and the construction of new ones in several countries.

The Advanced Tokamak Path to a Compact Net Electric Pilot Plant

J. M. Park¹, R. J. Buttery², J. T. McClenaghan³, D. B. Weisberg², J. M. Canik¹, J. R. Ferron², A. M. Garofalo², C. T. Holcomb⁴, J. A. Leuer², and P. B. Snyder²

The ATOM Team

¹*Oak Ridge National Laboratory (ORNL), Oak Ridge, TN 37831, USA*

²*General Atomics, San Diego, CA 92186, USA*

³*Oak Ridge Associated Universities (ORAU), Oak Ridge, TN 37831, USA*

⁴*Lawrence Livermore National Laboratory (LLNL), Livermore, CA 94550, USA*

Corresponding Author: J. M. Park, parkjm@fusion.gat.com

Physics based simulations using a new integrated 1.5D core-edge approach for a whole device modelling capability project a compact net electric fusion pilot plant is possible at modest scale based on the advanced tokamak concept, and identify the key parameters for its optimization. These first-of-a-kind reactor simulations provide new insights compared with previous “systems code” projections by self-consistently applying transport, pedestal and current drive physics models to converge fully noninductive stationary solutions without any significant free parameters. The approach provides new insights into reactor optimization with increasing plasma density, pressure and toroidal field found to lower auxiliary heating and current drive demands, and thus required fusion performance and recirculating power. Solutions at the ~ 4 m major radius scale are identified with margins and trade-offs possible in achievable parameters. Remaining current drive is projected from neutral beam and helicon ultrahigh harmonic fast wave, though other advanced current drive approaches presently being developed may also be useful. The resulting low recirculating power and double null configuration leads to a divertor heat flux challenge that is comparable to ITER. Neutron wall loadings also appear tolerable. Strong H-mode access (factor > 2 margin over transition scaling) is maintained with ~ 30 – 60% core radiation. The approach would benefit from high temperature demountable superconductors to provide performance margin at elevated field, and to aid in a nuclear testing mission. However, solutions are possible with conventional superconductors. An advanced load sharing and reactive bucking approach in the main field and solenoid coils has been developed and would facilitate handling of mechanical stresses. Nevertheless, the prospect of an affordable test device which could close the loop on net-electricity production is compelling, motivating research to prove the techniques projected here.

Work supported by the U.S. Department of Energy under DE-AC05-00OR22725 and DE-FC02-04ER54698.

Neutron Irradiation Impact on ITER Grade Insulating Material

S. Shah^{1,4}, S. Kumar², S. S. Vala^{2,4}, R. Kumar², M. R. Abhangi², S. Prasad³,
M. Bandyopadhyay^{1,4}, and A. K. Chakraborty¹

¹ITER-India, Institute for Plasma Research (IPR), Bhat, Gandhinagar, India

²Institute for Plasma Research (IPR), Bhat, Gandhinagar, India

³Facilitation Centre for Industrial Plasma Technologies (FCIPT),

Institute for Plasma Research (IPR), Bhat, Gandhinagar, India

⁴Homi Bhabha National Institute (HBNI), Anushakti Nagar, Mumbai 400094, India

Corresponding Author: S. Shah, sshah@iter-india.org

Study is performed to assess the irradiation impact on ITER grade ceramic which is widely being used for high voltage insulation in neutral beam injectors of ITER. Production proof samples of required sizes of high purity alumina were prepared and ultrasonically cleaned and are irradiated by two neutron sources. In-situ and ex-situ characterizations were performed to study irradiation impact on material properties and to ensure its structural and electrical compatibility. Insulation resistance was observed to improve with time from 250 GΩ to 3.3 TΩ and leakage current was in correlation with Curie-von Schweindler law. However, spontaneous reduction of IR at the time of irradiation was observed which was due to radiation induced conductivity. Further, the impact of irradiation on the structure was studied by X-ray diffraction analysis. The result reveals decrease in crystalline behaviour after irradiation. Surface morphology of pristine and irradiated samples was studied by scanning electron microscopy and atomic force microscopy. SEM of low energy neutron irradiated sample showed defect cluster formation on ceramic surface which was also cross-checked by increased surface roughness postirradiation by AFM.

It is observed that surface morphology is affected mainly due to low energy neutrons whereas electrical and structural properties are affected by high energy neutrons. To understand material performance for similar conditions of operational reactor, the study is initiated to create neutron equivalent defects in the material using ion beams and see the changes in material properties. This study will help in defining material grade for fusion based applications. Analytical assessment of nuclear activation along with experimental outcome shall be presented.

Conceptual Design of Neutron Activation System for IN-LLCB TBM

S. Tiwari¹, A. Kumar¹, V. Chaudhari¹, D. Sharma¹, A. N. Mistry¹, H. L. Swami¹,
C. Danani¹, and E. Rajendra Kumar¹

¹*Institute for Plasma Research (IPR), Bhat, Gandhinagar, India*

Corresponding Author: S. Tiwari, shailja@ipr.res.in

Neutron activation system (NAS) is the primary neutron diagnostics for Indian Lead-Lithium Ceramic Breeder (LLCB) Test Blanket Module (TBM) in ITER. The main objective of NAS is to measure spatial distribution of neutron flux and energy spectra and in-situ measurement of tritium production rate inside the TBM. These measurements will be utilized for validation of neutron transport tools (software codes) and tritium breeding predictions used for breeding blanket systems design.

NAS for LLCB TBM mainly consists of transfer station, capsule loader, transfer lines, foil gamma activity measurement system and irradiation ends. The irradiation of capsules consisting of foils is positioned inside the LLCB TBM at midplane location. The conceptual design of TBM along with NAS irradiation piping has been developed and its engineering design is in progress. All the components of NAS will be kept inside tritium building level L-2 of ITER building. The capsules are pneumatically transferred to irradiation end of piping located inside the TBM. After irradiation, the capsules are transferred back to counting station for foil activation measurement. This paper will present the conceptual design of NAS system along with preliminary engineering analysis and sequence of operations.

Energy Differential and Displacement Damage Cross Section of DT Neutron Induced Reactions on Fusion Reactor Materials (Fe, Cr & W)

M. Rajput^{1,2}, S. S. Vala^{1,2}, P. V. Subhash^{2,3}, and R. Srinivasan^{1,2}

¹*Institute for Plasma Research (IPR), Bhat, Gandhinagar, India*

²*Homi Bhabha National Institute (HBNI), Anushakti Nagar, Mumbai 400094, India*

³*ITER-India, Institute for Plasma Research (IPR), Bhat, Gandhinagar, India*

Corresponding Author: M. Rajput, mayank.rajput@ipr.res.in

Displacement per atom (dpa) in fusion reactor materials are essential designing parameters to ensure the reliable functioning and structural integrity of fusion reactor components. All probable reaction channels such as (n, n') , $(n, 2n)$, (n, p) , (n, α) and (n, d) are open for the interactions of DT neutrons of 14.14 MeV energy with the fusion reactor material. Evaluation of dpa requires energy spectra of recoil nuclei for each reaction channel. The iron, chromium, and tungsten are important materials widely proposed for structural and first wall components of the reactor. TALYS 1.8 and Empire3.2 codes have been used to calculate cross-section data and recoil spectra for each reaction channel. In the cross-section and spectra calculations, contribution from all possible reaction mechanism such as direct, pre-equilibrium, compound and multiple emission reaction mechanisms have been considered. Prediction of σ_{dpa} requires energy differential cross section (EDX) of recoil nuclei from each reaction channel. EDX of emitted charged particles have been predicted and compared with the existing evaluated and experimental data from IAEA data libraries to select the best fitted nuclear models and parameters. Energy spectra of recoil nuclei also considered as primary knock-on atoms for each reaction channel, have been predicted using the appropriate nuclear models and parameters in TALYS code for incident neutrons up to 15 MeV energy. PKA data have been used in NRT (Norgett, Robinson, and Torren), BCA (binary collision approximation), BCA+MD (molecular dynamics) and kinetic Monte Carlo methods. Predicted σ_{dpa} is compared with the existing database of σ_{dpa} , prepared using the NJOY code. EDX data of each reaction channels are calculated for all stable isotope of Fe (^{54}Fe , ^{56}Fe , ^{57}Fe , ^{58}Fe), Cr (^{50}Cr , ^{52}Cr , ^{53}Cr , ^{54}Cr), and W (^{182}W , ^{183}W , ^{184}W , ^{186}W) and used for the prediction of σ_{dpa} for natural elements. For the experiments of DDX measurement of charged particles, neutron flux is measured with the diamond detector (efficiency = 0.00109% for DT neutrons). The efficiency of diamond detector has been measured with the alpha counting method using silicon surface barrier detector. Experiments for the DDX measurements are being carried out for natural iron and chromium.

Application of ANSYS FLUENT MHD Code for Liquid Metal MHD Studies

A. Patel¹, R. Bhattacharyay¹

¹*Institute for Plasma Research (IPR), Bhat, Gandhinagar, India*

Corresponding Author: A. Patel, anita@ipr.res.in

Magnetohydrodynamic (MHD) phenomena play an important role in governing liquid metal flow characteristics under strong transverse magnetic field and have, therefore, gained the attention of the fusion community for the design of liquid breeder blankets. In presence of plasma confining toroidal magnetic field, the flow of electrically conducting liquid metal (Li/PbLi), typically used for coolant and/or tritium carrier, is greatly affected due to the flow-opposing Lorentz force, which arises due to the interaction between the magnetic field and current induced in the liquid metal. For the successful design and development of liquid breeder blankets, detailed MHD analysis is highly desirable to understand various effects of MHD, such as change in velocity profile, pressure drop, heat transfer, and so on.

The liquid metal MHD studies are being carried out using both analytical and numerical approaches. The analytical solutions, derived under 2D fully developed flow approximations, are limited to the simple flow geometries and hence they are not applicable for the analysis of complex blanket flow configuration, which consists of bends, transition zone, multichannel flow, etc. Numerical simulation techniques are, therefore, used extensively to perform MHD analysis in such complex flow configuration and various MHD codes, either newly developed or commercially available are being reported. The MHD code, however, needs to be benchmarked extensively and validated before its application to complex flow configuration in liquid breeder blanket. In the present work, three MHD benchmark problems of [1] have been successfully analyzed using ANSYS FLUENT MHD code and results are compared with available literature data. The selected problems are: i) 2D fully developed laminar steady MHD flow; ii) 3D laminar, steady developing MHD flow in a nonuniform magnetic field; and, iii) MHD flow with heat transfer (buoyant convection). The results have provided more confidence in using FLUENT as a promising MHD analysis tool for fusion application. The numerical model, analysis, methodology and simulation results of each benchmark problem will be discussed in detail.

References

[1] S. Smolentsev *et al.*, Fusion Eng. Des., **100**, 65–72 (2015).

Structural and Vibrational Properties of Lead-Lithium Alloys: A First Principles Study

S. G. Khambholja¹, A. Abhishek²

¹*Bhailalbhai and Bhikhabhai Institute of Technology (BBIT), Vallabh Vidyanagar, Gujarat, India*

²*Institute for Plasma Research (IPR), Bhat, Gandhinagar, India*

Corresponding Author: S. G. Khambholja, physik.shyam@gmail.com

Lead-Lithium (PbLi) alloy in its eutectic composition is one of the promising candidates to be used as liquid blanket in fusion reactor. Helium cooled lead-lithium (EU-HCLL), dual cooled lead-lithium (US-HCLL), Indian LLCB are some of the concepts being explored worldwide for future fusion reactor. In this scenario, the characterization of PbLi alloy becomes important to gainfully understand its underlying physical and structural behaviour. In the present paper, we report the results of our computer experiments on structural and vibrational properties of PbLi. Present work is performed using plane wave pseudopotential density functional theory within generalized gradient approximation (GGA). Calculations of various structural properties at ambient condition ($T, P = 0$) are performed using Quantum ESPRESSO package. Further, phonon frequencies along major symmetry directions are also calculated using density functional perturbation theory. Three independent elastic constants are also calculated for both the compensating structures namely rhombohedral and CsCl type. Calculations of the equation-of-state at elevated temperatures suggest that PbLi is a soft material undergoing large volume change with pressure. Further, some thermodynamic properties at elevated temperatures are also reported.

Structural Analysis for Strength and Fatigue Life of Half Coupling Weldment for Large Cooling Water Pipes

K. S. Bhatt¹, S. S. Sandhu¹, T. K. Sharma¹, S. B. Padasalagi¹, A. P. Singh¹, and M. Jadhav¹

¹ITER-India, Institute for Plasma Research (IPR), Bhat, Gandhinagar, India

Corresponding Author: K. S. Bhatt, kunal.bhatt@iter-india.org

The ITER cooling water system consists of large piping network to remove the heat load of about 950 MW through various branched connections. Many of the branches are connected to main pipes by half-coupling full-penetration weld joints. There the requirement is to have full penetration for all the joints, however, quality classification (QC-2), recommends only 10% testing of the total weldment. In view of this it is expected that there can be some joints with little or no penetration. The above requirement demands for the structural strength and fatigue life is assessment to ascertain that components is not failing even if there is no weld penetration. The design by analysis approach is considered for structural and fatigue life assessment, for maximum expected loads combination case. The weld joint is structurally qualified using ASME code. Fatigue life of weld joint is calculated using both ASME Section VIII Div.2 and RCC-MR RR3261.12. The maximum stress and fatigue life observed for full penetration is 92 MPa and 315 766 cycles as per ASME and 200 000 cycles as per RCC-MR. Whereas, in no penetration the stress is 188 MPa and fatigue life is 137 210 cycles as per ASME and 1500 cycles as per RCC-MR. It is concluded in the paper that weld joint is safe for both the case in most severe load case combination.

Performance of 14-MeV Neutron Generator at IPR

S. S. Vala^{1,2}, M. R. Abhangi^{1,2}, R. Kumar¹, S. Tiwari¹, and M. Bandyopadhyay^{1,2}

¹*Institute for Plasma Research (IPR), Bhat, Gandhinagar, India*

²*Homi Bhabha National Institute (HBNI), Anushakti Nagar, Mumbai 400094, India*

Corresponding Author: S. S. Vala, sudhir@ipr.res.in

The Fusion Neutronics laboratory at IPR, Gandhinagar, India, has indigenously developed an accelerator based 14-MeV neutron generator for fusion neutronics studies for material development under the Indian fusion program. This neutron generator is producing neutron yield of 10^{10} n/s and it will be further upgraded to 10^{12} n/s. It consists of a 2.45 GHz ECR ion source, 300 kV linear accelerator, beam diagnostic system, TMP based vacuum system, solid tritium target and a control system. Various neutron detection techniques like foil activation, associated α -particle detector, and ^3He proportional counter have been set up in the system to measure the neutron yield independently and online neutron yield. Results of all independent diagnostics were compared. Monte Carlo technique was used to get reaction rate for foil activation. This paper describes the experimental setup and performance of the 14-MeV neutron generator including its neutron diagnostic to highlights its stability for continuous operation.

Tritium Handling and Recovery System for Accelerator Based 14-MeV Neutron Generator

D. Dubey¹, S. S. Vala², and S. P. Deshpande^{1,2}

¹*ITER-India, Institute for Plasma Research (IPR), Bhat, Gandhinagar, India*

²*Institute for Plasma Research (IPR), Bhat, Gandhinagar, India*

Corresponding Author: D. Dubey, deepti.dubey@iter-india.org

An accelerator based 14 MeV neutron source is under development to study the fusion neutronics for Indian fusion programmes. The neutrons are generated by impinging 10 mA deuterium beam accelerated up to 340 keV energy over a 140 Ci tritium target. Being a system handling tritium radioactive material, a recovery system is to be designed to minimize airborne tritium effluent releases to well below the permitted limit. In addition, the system should minimize tritium exposure to staff by maintaining low levels of tritium in the rotating tritium target holder (RTTH). The paper presents the first estimated value of tritium escaping into the exhaust of the accelerator system. A mathematical model is developed to estimate the amount of tritium sputtered from the target. The calculated result is then successfully simulated using SRIM software, and validated using the experimental results available. According to [1], tritium release from the target at maximum power has been evaluated to be 37 GBq/h experimentally. As per our calculation method and the simulated results, the tritium release is calculated to be 40 GBq/h which is in very close conformance with the claimed value. Based on this primary calculated data a conceptual design of the tritium handling and recovery system (THRS) is also presented. There are a number of technologies available for THR like, metal membrane reactors, cryogenic adsorption on molecular sieve beds, getter beds, cryogenic freezing, high temperature electrolysis, and catalytic oxidation. Today globally, getter bed technology for the tritium separation is in frequent practice. This paper also elaborates the specific selection criteria for development of recovery system. Followed by determining the significance of the selection criteria using pairwise comparison (Pugh matrix) approach for weighting the criteria accordingly, and selecting the appropriate technology.

References

[1] M. Martone, J. Nucl. Mater., **212–215**, 1661–1664 (1994).

Extent of Tritium Contamination of Helium Circuit in a Fusion Reactor: Probable Scenarios

V. Shukla¹, V. J. Lakhera²

¹ITER-India, Institute for Plasma Research (IPR), Bhat, Gandhinagar, India

²Mechanical Engineering Department, Nirma University, Gujarat, India

Corresponding Author: V. Shukla, vinit.shukla@iter-india.org

In the presently available fusion reactors, cryogenic helium is an integral part for cooling the magnets in order to achieve superconductivity. Some of the fusion reactors use tritium as a nuclear fuel along with deuterium, in which a part of tritium is proposed to be bred through lithium blanket covering the first wall of plasma. Since fusion reactors have very small burn up efficiencies (~ 0.3 to 2% only), a very small amount of fuel is consumed and majority of the unburnt fuel must be pumped out and reprocessed for subsequent cycles. Due to the magnetic and neutronic environment prevailing inside the fusion reactor, for the evacuation of the vacuum vessel, cryopumps are the suitable choice as compared to other available options. Cryopumps provide cooled surface of charcoal as an adsorber bed to trap the gaseous molecules. The adsorber beds are cooled down to 5 K with the help of cryogenic liquid helium being supplied from a cooling plant with an intermediate cold box in order to provide better controllability. The contamination of cryogenic helium with tritium arises in the cryopumps and may be extended to the cryoplant. Thus there are possible scenarios where the hand-shaking of tritium with cryogenic helium is possible thereby posing a threat to cryogenic plant safety depending on the extent of tritium contamination of cryogenic fluid and hence is required to be analyzed while designing the system. The tritium impact on cryoplant design in the presently available tokamaks (such as ITER, etc.) has not been taken into consideration in the design as the amount of tritium permeated through stainless steel to cryogenic helium, through cryopumps, is not substantial. But, for future fusion reactors where the amount of tritium to be handled would be substantial, the threat can not be evaded. This opens a new area of research in the context of design of cryoplants for future fusion reactors.

The present study throws light on the possible scenario and mechanism of tritium diffusion along with the extent of contamination and its validation through available experimental data. This study will also be helpful for design of the cryo-plants for future fusion commercial reactors.

Novel Method for Determination of Tritium Depth Profiles in Metallic Samples

E. Pajuste¹, G. Kizane¹, and I. Igaune²

¹*Institute of Chemical Physics, University of Latvia, Riga, LV 1004, Latvia*

²*Faculty of Chemistry, University of Latvia, Riga, LV 1004, Latvia*

Corresponding Author: E. Pajuste, elina.pajuste@lu.lv

A novel method for determining the depth profile of tritium in metallic samples has been demonstrated. Tritium accumulation in the fusion reactor materials is considered as a radiological issue due to its radioactivity. Therefore, tritium behaviour prediction and estimation of its overall retention in fusion devices is of high importance. The proposed method in this study allows measuring the depth profile of tritium in the metallic samples after exposure to tritium containing plasma, tritium gas or after irradiation with neutrons resulting in tritium formation.

In the method, successive layers of metal are removed using an appropriate etching agent in the controlled regime and the amount of evolved gases is measured by means of chromatography (gas composition and release rate) and proportional gas flow detector (tritium). Results on the tritium profile in neutron irradiated, plasma exposed and tritium gas loaded beryllium have already been reported. Possible applications of the method for other metallic samples have been tested within this research.

Effect of Magnetic Field on the Corrosion Behaviour of Indian RAFMS in Liquid PbLi

P. Chakraborty¹, V. Singh¹, P. Trivedi¹, S. Malhotra¹, K. Singh¹, V. Kain¹, and R. Tewari¹

¹*Bhabha Atomic Research Centre (BARC), Mumbai, India*

Corresponding Author: P. Chakraborty, poulamic@barc.gov.in

In the present study, the effect of magnetic field on the corrosion of Indian reduced activation ferritic martensitic steel (IN RAFMS) in flowing lead lithium eutectic (PbLi) has been studied in an electromagnetic pump driven loop (EMPPIL-M). The corrosion rate in the presence of 0.5 kG magnetic field at a temperature of 773 K has been found to be 1.3 times higher than that observed in the absence of magnetic field. The surface of the IN RAFMS sample located inside the magnetic field showed nonuniform corrosion and formation of distinct surface features which were revealed through optical and secondary electron (SE) micrographs. The PbLi attack in the presence of magnetic field was not only confined to the prior austenite and lath boundaries as in the absence of magnetic field; but also happened in the intralath regions causing formation of subgrains. The change in PbLi flow profile due to magnetohydrodynamic effect is expected to play a major role in the formation of surface features, nonuniformity in surface attack and increased corrosion rates in the presence of magnetic field. The detailed discussion on the results obtained from analysis of the exposed samples through various characterization techniques (stereomicroscope, optical profilometry, secondary electron microscopy-energy dispersive spectroscopy [SEM-EDS], etc.) will be presented in this paper.

Er₂O₃ Coating by Multilayer Metallic Sputtering and Intermediate Oxidation Approach

P. A. Rayjada¹, N. P. Vaghela¹, and A. Sircar¹

¹*Institute for Plasma Research (IPR), Bhat, Gandhinagar, India*

Corresponding Author: P. A. Rayjada, pratipal@ipr.res.in

Erbia (Er₂O₃) is a leading candidate for hydrogen isotope barrier and electrical insulation coating applications in some subsystems of advanced nuclear fusion research reactor designs. Due to the harsh environment of the reactor, structural and microstructural stability of the coatings at elevated temperature is critical. The polymorphs of erbia are reported in cubic, monoclinic and hexagonal phases depending on the ambience of the formation. Cubic is the most stable phase among these as it does not transform up to 2327°C. Hence, it is important to choose and tune the deposition process so as to obtain cubic phase Er₂O₃ coatings with dense packed and compact microstructure.

Our previous study conclusively showed that reactive sputter deposition leads either to a coating with monoclinic phase and compact microstructure or to cubic phase and cracked/bulged microstructure, depending on the process temperature. Also inferred from the study was that metallic Erbium deposition converts into cubic phase upon postoxidation. Hence, a novel approach of depositing thin multilayers (~ 40 nm) of Erbium with intermediate in-situ oxidation has been adopted in this work. The structural phases and microstructure of the deposited films are studied using X-ray diffraction (XRD), grazing incidence diffraction (GID) and scanning electron microscope (SEM). The variation in these properties is correlated with the variation in process parameters such as layer thickness, oxidation duration, temperature, postannealing, etc. The detailed results of this study in comparison to those of reactive sputter deposition will be presented in this paper.

Development of HINEG and its Experimental Campaigns

Y. Wu¹, Y. Wang¹, C. Liu¹, Z. Wang¹, T. Li¹, and J. Jiang¹

The FDS Team

¹*Institute of Nuclear Energy Safety Technology, CAS, Anhui, People's Republic of China*

Corresponding Author: Y. Wu, yican.wu@fds.org.cn

A high intensity DT fusion neutron generator is an important experimental platform for research and development (R&D) of nuclear energy and nuclear technology applications. The high intensity DT fusion neutron generator (HINEG) facility has been developed by the INEST (CAS)/FDS team to perform research on fusion nuclear technology and safety including validation of neutronics theory and software, neutronics performance of blanket and reactor, materials irradiation damage mechanism, etc. Also, the application of HINEG can be extended to neutron radiography, neutron radiotherapy, and so on. The R&D of HINEG includes three phases: HINEG-I has been finished, and successfully produced DT fusion neutrons with yield up to 6.4×10^{12} n/s. Meanwhile, HINEG-I has been operated to drive the lead-based zero power critical/subcritical reactor CLEAR-0. HINEG-II aims at a high neutron yield of 10^{15} – 10^{16} n/s and the R&D for key components is on-going. HINEG-III is designed as a volumetric fusion neutron source with neutron yield of 10^{18} n/s, which is based on the gas dynamic trap.

Recently, a series of experiments have been carried out on HINEG facility by FDS team, such as neutronics performances of fusion reactor blanket, biological effects of neutron irradiation, fast neutron radiography, and so on. A dual function lithium-lead (DFLL) test blanket module (TBM) has been developed by FDS team to demonstrate the technologies of the liquid Li-Pb breeder blanket. The neutronics experiment of DFLL-TBM mockup was carried out to validate the tritium breeding and shielding performances. The comparison of experiment results and corresponding calculation performed using SuperMC and FENDL3.1 library was obtained, and a good agreement was observed between the experimental and calculated values. This presentation will introduce the R&D activities as well as the experimental campaigns of HINEG.

Radiation Properties of the Metal Structural Materials during Low-Temperature Damaging Irradiation

V. M. Chernov¹

¹A.A. Bochvar High-Technology Research Institute of Inorganic Materials, "VNIINM",
Moscow, Russian Federation

Corresponding Author: V. M. Chernov, vmchernov@bochvar.ru

The structure and physical-mechanical properties of the metal structural materials (SM) with BCC (ferrite-martensitic steels, alloys of vanadium, etc.) and FCC (austenitic steels, etc.) crystal lattices in the conditions of "before-after-during" low-temperature irradiation were analyzed. The qualitative and quantitative distinctions of the states and properties of SM "before-after" (an equilibrium state) and "during" (essentially nonequilibrium state) irradiation occur. Depending on the rigidity of the stress-deformed state, type of a crystal lattice, the low-temperature yield strength and mobility of dislocations there can be different modes of the plastic deformations with the brittle fracture by rupture or shear (cold brittleness). The conditions for occurrence of the cold brittleness are the formation of the critical cracks of rupture and shear, generating dislocations, high low-temperature yield strength, high starting stress for movement of dislocations and low level of viscous braking of the dislocations in the dynamic area of their mobility on the fronts of a cracks of rupture and shear. The speeds of propagation of a critical crack and deformation shear strip are determined by the dynamic mobility of the dislocations on their fronts. The conditions for occurrence of the cold brittleness can be implemented in BCC SM, defining their temperature ranges of the cold brittleness, and are not implemented in FCC SM (the cold brittleness is absent).

"Before-after" irradiation in BCC SM the cold brittleness manifests itself by the modes of the plastic deformation with a brittle fracture during an avalanche propagation of a critical crack (rupture cold brittleness) or with a brittle shear during formation and avalanche propagation of the deformation shear strips (shear cold brittleness). "During" low-temperature irradiation in BCC SM the state of irradiation cold brittleness with a brittle fracture by rupture or shear is not formed (absent).

Possibilities and difficulties are discussed for development of the physical models and computer simulation of the radiation structures, defects and physical-mechanical properties of SM.

Effect of Simulated Postweld Heat Treatment on the Microstructure and Mechanical Properties of IN-RAFM Steel

C. S. Sasmal¹, S. Sam¹, H. M. Taylor¹, J. P. Chauhan¹, and P. Chaudhuri¹

¹*Institute for Plasma Research (IPR), Bhat, Gandhinagar, India*

Corresponding Author: C. S. Sasmal, chandra@ipr.res.in

Indigenously developed India specific reduced activation ferritic-martensitic (IN-RAFM) steels are currently considered as a structural material for the Indian lead lithium cooled ceramic breeder test blanket module (IN-LLCB TBM). Advanced ferritic-martensitic steels offer the opportunity for improvements in fusion reactor performance, operational lifetime and reliability, superior neutron radiation damage resistance, higher thermodynamic efficiency and reduced construction costs. Typically RAFM steels are normalized at high temperature, i.e., 980°C for 30 minutes followed by low temperature tempering for longer duration, i.e., 760°C for 90 minutes. The resulting microstructure determines the mechanical properties of the steel. These microstructures are designed to produce an optimum combination of strength and toughness at high temperature. However, situations may arise in practice, particularly during welding operations for example, whereby the RAFM steel may receive an additional heat treatment which briefly exceeds the Ac1 and possibly the Ac3 temperature before stabilizing at the tempering temperature. To restore the properties of the weld joints, postweld heat treatment (PWHT) is applied to the steel at 750°C for 2 hours followed by furnace cooling. During PWHT, the base or parent metal of the RAFM steel weld joints also undergo heat treatment process. In this present investigation, the consequence of PWHT effect on base metal of IN-RAFM steel is studied. Simulated postweld heat treatments (SPWHT) have been applied to IN-RAFM steel in a muffle furnace at 750°C and 770°C for 2 hours followed by cooling inside the furnace. Hardness measurements were carried out on the heat treated sample and was found to be ~ 210 HVN which is comparable with base metal hardness properties. Advanced electron microscopy has been carried out to investigate the effect of the SPWHT excursions on subsequent microstructural evolution. Tensile tests have been carried out on SPWHT specimens at various temperatures from room temperature to 600°C. Tensile properties of SPWHT specimen at room temperature is ~ 650 MPa and at 550°C is ~ 320 MPa. Impact toughness up to -100°C are also being evaluated in this present investigation. The results discuss the effect of SPWHT on mechanical properties of RAFM steel during high temperature service.

Ion Irradiation Induced Modifications in Tungsten Foils

A. Attri¹, P. N. Maya¹, P. Sharma¹, A. Zala², P. Kikani², A. Lakhani³, R. Jha²,
M. R. Abhang², S. S. Vala², A. K. Tyagi¹, P. K. Kulriya⁴, K. Mal⁴, P. K. Bajpai⁵,
T. A. Trivedi⁵, P. M. Raole¹, and S. P. Deshpande¹

¹ITER-India, Institute for Plasma Research (IPR), Bhat, Gandhinagar, India

²Institute for Plasma Research (IPR), Bhat, Gandhinagar, India

³IUC-DAE Consortium for Scientific Research, Indore 452001, India

⁴Inter University Accelerator Centre (IUAC), Aruna Asaf Ali Marg, New Delhi, India

⁵Guru Ghasidas Vishwavidyalaya, Bilaspur, (C.G.), Koni, Chhattisgarh 495009, India

Corresponding Author: A. Attri, asha-pdf@iter-india.org

The ion-solid interaction has fundamental importance and is a subject of evolving understanding for years. Energetic ions of energies eV to MeV are responsible for the kinetics in solids by transferring energy via elastic or inelastic interaction depending on the nature of the material. Tungsten is prime material to be used in future fusion devices because of its thermal and mechanical properties. In lieu of neutron irradiation, ion irradiation of tungsten is an active area of research.

To explore the surface morphological effects, energetic ions of various masses were bombarded on polycrystalline tungsten. Polycrystalline tungsten foils were procured from Princeton Scientific Corporation, USA as a starting material for our study. Tungsten foils of 0.1 mm thickness were mechanically polished and annealed at two different temperature (1373 and 1838 K) to minimize any pre-existing defects. These foils were further irradiated with Au ions of 80 MeV energy. Further sequential irradiation with helium/deuterium ions of energy 250/100 keV were done on the same set of Au irradiated tungsten foils. Pre- and postirradiation surface morphological studies were done with high resolution scanning electron microscope (FESEM). FESEM studies revealed the bubble formation and other surface morphological changes of tungsten foils due to gaseous ion irradiation. In D irradiated tungsten, bubble formation is more located at grain boundaries and in case of sequential irradiation with He preirradiated with heavy ions, it is noticed that bubbles were seen at the foil surface. Statistical analysis is continuing and results will be presented during the meeting. Ion-irradiation in tungsten induces different and distinguishable modifications within the bulk and on the surface. Four-probe DC resistivity measurements were performed in a temperature range of 10 K to 300 K to study the overall defects in tungsten foils before and after irradiation. The correlation between residual resistivity ratio (RRR) and the defects in the samples will be presented.

Tungsten Fuzz Formation on the Nitrided Tungsten Surface

A. Miniyazov¹, I. Tazhibayeva¹, M. Skakov¹, Y. Koyanbayev¹, T. Kulsartov¹,
T. Tulenbergenov¹, D. Ganovichev¹, and I. Sokolov¹

¹*Institute of Atomic Energy, National Nuclear Center, Kurchatov, Kazakhstan*

Corresponding Author: A. Miniyazov, armanminiyazov@gmail.com

The research goals are to determine the effect of nitrogen plasma on tungsten and to perform comparative analysis of the formation of tungsten fuzz on the helium plasma interaction on the initial surface of tungsten and on the surface of tungsten, previously subjected to nitriding. The experiments were carried out on an imitation stand with a plasma-beam installation. The device provides the following parameters of the plasma flow: the diameter of the plasma flow in front of the target up to 30 mm; the intensity of the magnetic field produced on the axis of the plasma-beam discharge chamber is 0.1 T; the plasma density in the beam is up to $10^{18}/\text{m}^3$; the maximum current in the plasma is 1 A; the electron temperature range of the plasma is 5–15 eV.

All stages of the experiments contained studies of the surface of tungsten using optical and SE microscopy, elemental and X-ray analysis, and determination of the hardness of the surface of tungsten samples.

As a result of the series of experiments on nitridation of tungsten, an optimal nitriding regime was determined that lead to the formation of tungsten nitrides on the surface of the irradiated sample. A series of irradiation experiments were realized on the initial tungsten surface with helium plasma in the plasma-beam discharge regime. On the surface of the samples, a coating was found of tungsten fuzz. Experiments have been carried out on the irradiation of tungsten with a helium plasma with a previously nitrided surface. The results of the investigations showed that tungsten fuzz forms on the nitrided surface of tungsten, as well as on the initial surface. On the initial surface of tungsten, the structure of the fuzz is more uniform than on nitrided samples.

To conclude, the conducted experiments showed that nitridation of the tungsten surface does not play an important role in the formation of the tungsten nanostructure as a result of irradiation of tungsten with helium plasma.

Neutronics Experiment for Design Validation of Indian TBM Shield Module

H. L. Swami¹, M. R. Abhangi¹, S. Sharma^{1,2}, S. Tiwari¹, A. N. Mistry¹, S. S. Vala¹,
C. Danani¹, V. Vasava¹, V. Mehta¹, V. Chaudhari¹, and P. Chaudhuri¹

¹*Institute for Plasma Research (IPR), Bhat, Gandhinagar, India*

²*Pandit Deendayal Petroleum University, Raisan, Gandhinagar, 382 007, Gujarat, India*

Corresponding Author: H. L. Swami, hswami@ipr.res.in

The testing of the breeding blanket systems is one of the vital objectives of ITER. It will generate significant information for the DEMO fusion reactor. ITER has assigned the three equatorial ports for testing of six blanket systems. In those six, there is a test blanket system (TBS) of India which is lead-lithium ceramic breeder (LLCB) blanket system and it will be integrated into one-half of ITER equatorial port#2. Being a part of ITER, TBS has to follow all safety and design guidelines of ITER. In order to follow the safety guideline of radiation dose limits in ITER ports interspaces, a shield module, made of stainless steel and water channels, is associated with the test blanket module (TBM) to limit the direct radiations in port interspace areas. The conceptual design of Indian TBM shield module has been assessed by neutronic simulation using MCNP. The shield module is having the classification of radiation protection important component due to the function of radiation exposure control which leads to ensure the design of the component. A neutronic experiment is designed and performed to validate and verify the design of shield module. The design of the experiment is made by considering the two references; one is the neutron spectra on the front surface of TBM shield under ITER environment and second is the neutron attenuation in shield module under ITER conditions. The experiment is designed considering the irradiation of mock-up under 14 MeV neutron source facility of IPR. The neutron source is having the yield of 10^{10} n/s. The neutron spectra of the front surface of the shield mock-up have been optimized to achieve the reference spectra of TBM shield module. The neutron spectra and flux are measured using the activation foils detectors. The C/E ratio is obtained from the comparison of measured and simulated neutronic responses. The neutronic simulation is performed using MCNP5 and FENDL-2.1 cross section data. The unfolding code SAND-II-SNL is employed to obtain the neutron spectra from activation foil measurements. This experiment will also support in preparation of neutron spectra measurement for Indian TBM system and improvement of nuclear simulations. The paper will cover the detailed neutronic design, details of irradiation, neutron spectra measurements and outcome of the experiment.

Study on Production and Extraction of Negative Ion Impurity Ions in a Caesiated Negative Ion Source

P. Bharathi¹, M. Bhuyan², A. J. Deka^{1,3}, M. Bandyopadhyay^{1,2,3}, K. B. Pandya¹, R. K. Yadav², H. Tyagi², A. Gahlaut¹, and A. K. Chakraborty^{1,2}

¹*Institute for Plasma Research (IPR), Bhat, Gandhinagar, India*

²*ITER-India, Institute for Plasma Research (IPR), Bhat, Gandhinagar, India*

³*Homi Bhabha National Institute (HBNI), Anushakti Nagar, Mumbai 400094, India*

Corresponding Author: P. Bharathi, bharathi@ipr.res.in

The detection of a peak corresponding to a hydrogen bearing impurity species (mostly due to water vapour: H₂O) was reported many times in the past while performing the Doppler shift spectroscopy (DSS) diagnostics in several neutral beam injectors based on positive ion sources. However, for the experiments based on negative ion sources, we are reporting the detection of this peak for the first time. This peak always appeared in DSS spectrum when the background pressure at the observation location is $\sim 1 \times 10^{-4}$ mbar and disappeared when the pressure at the observed location is $\sim 1 \times 10^{-5}$ mbar. For the present experiments, the negative ions of H₂O can be formed by dissociative attachment of (H₂O⁻)* leading to the formation of H⁻, O⁻ and OH⁻ fragments. The dissociative attachment seems to be the cause of the formation of this negative ion species due to favourable conditions such as 5–10 eV in driver region for vibrational excitation and 1–2 eV near plasma grid. A detailed study on this peak using the DSS spectrum and the pressure traces obtained using a residual gas analyser was carried out in ROBIN (RF Operated Beam source in India for Negative Ion research) test stand. Estimates of impurity content have been made using intensity ratio of fast hydrogen peak and hydrogen peak originating from the negative ion impurity. The extracted current of hydrogen neutrals originating from these impurities are estimated. To obtain this value, the Balmer- α excitation cross-section at low energies (~ 1.5 keV) were reviewed and few approximations were made since the published data is available only for the higher-energy ranges for such processes. These approximations are outlined in this paper. There is some evidence that the amount of impurity present in the ion source affects the ratio of the main species.

3 MW Dual-Output High Voltage Power Supply Operation: Results for Accuracy, Stability and Protection Test

A. Patel¹, D. V. Upadhyay¹, K. R. Mehta¹, H. Dhola¹, N. S. Goswami¹, N. P. Singh¹,
B. Raval¹, R. Dave¹, S. Gajjar¹, V. Gupta¹, A. Thakar¹, K. Rajnish¹, D. G. Soni¹, S. Verma¹,
R. Singh¹, R. G. Trivedi¹, A. Mukherjee¹, and U. K. Baruah¹

¹ITER-India, Institute for Plasma Research (IPR), Bhat, Gandhinagar, India

Corresponding Author: A. Patel, ampatel@ipr.res.in

High temperatures inside tokamak for fusion research is achieved from auxiliary heating systems like neutral beam injectors (NBI), or RF heating devices, viz., ion cyclotron (IC), electron cyclotron and lower hybrid systems where the high voltage power supply (HVPS) is an essential requirement. ITER requires 20 MW of ICRF for heating and driving plasma current. A cascaded chain of amplifier is a practical solution due to limiting level of power with available vacuum tubes. Each amplifier chain has to provide 1.5 MW power in frequency range of 35–65 MHz for 3600 s. The system must be capable to operate both at matched and mismatched load condition (VSWR 2) [1].

HVPS based on pulse step modulation (PSM) topology has already demonstrated its ability for broadcast transmitters, accelerators using radiofrequency (RF) source and neutral beam injectors. A novel concept of tapping two outputs from single PSM based HVPS is attempted for the first time. A PSM-based HVPS is developed with dual output to feed driver and end stages of a high power RF amplifier [2].

The developed dual output HVPS is capable of providing 14–18 kV, 250 kW to driver stage and 16–27 kV, 2800 kW to end stage of a RF amplifier chain, simultaneously [3]. Present article covers the validation of dual output HVPS for integrated operation with RF Amplifier system. It includes wire burn test conducted at the output of HVPS, demonstrating tight synchronization among both stages. Test set up, gauge/length for fuse wire to meet the critical energy limit qualifications is presented. HVPS performance parameters, viz., ripple, regulation and stability over extended duration of 3600 seconds are presented for various scenario of RF amplifier operation. Implemented scheme for protection against overvoltage and overcurrent is also discussed.

References

- [1] A. Mukherjee *et al.*, IAEA FEC–2016, Kyoto, Japan, [FIP/1-5](#), (2016).
- [2] A. Patel *et al.*, International Power Modulator and High Voltage Conference (IPMHVC-2016), San-Francisco, July 5-9, (2016).
- [3] A. Patel *et al.*, Fusion Eng. Des., **126**, 59–66 (2018).

Evaluation of Beam Properties of a Negative Hydrogen Source by Doppler Shift Spectroscopy

A. J. Deka¹, P. Bharathi¹, K. B. Pandya¹, M. Bandyopadhyay^{1,2,3}, M. Bhuyan³, R. K. Yadav³, H. Tyagi³, A. Gahlaut¹, and A. K. Chakraborty^{1,3}

¹*Institute for Plasma Research (IPR), Bhat, Gandhinagar, India*

²*Homi Bhabha National Institute (HBNI), Anushakti Nagar, Mumbai 400094, India*

³*ITER-India, Institute for Plasma Research (IPR), Bhat, Gandhinagar, India*

Corresponding Author: A. J. Deka, arnabdeka@hotmail.com

ROBIN (RF Operated Beam source in India for Negative Ion research) is a negative H⁻ ion source, which is operational in IPR, Gandhinagar. For measurement of various beam parameters such as beam energy, beam divergence, beam homogeneity and the stripping losses, Doppler shifted spectroscopy diagnostics was established on ROBIN. The beam properties are studied by varying the source pressure (0.3–0.6 Pa), RF power (30–60 kW), decreasing tank pressure ($70\text{--}5 \times 10^{-5}$ mbar), the total applied voltage in the range of 7–24 kV has been carried out. The beam divergence and stripping losses are estimated from the line profiles analysis of the observed Doppler shift spectrum. The homogeneity of the beam in the vertical direction has been evaluated by using eight lines-of-sight located at two symmetrical locations in the ROBIN test vessel. The effect of space charge compensation on beam divergence has also been studied by varying the test stand pressure. The observed beam divergence is found to be lower at lower applied voltages and started increasing monotonically with an increase in voltage. The beam divergence is found to be decreasing with increase in RF power. The stripping losses are higher at lower voltages and start decreasing with increase in applied voltage. The beam is more uniform in the upper portion in comparison with the lower portion. In this present work, the parametric evaluation of the beam properties is presented in detail and results are discussed.

Thermohydraulic Analysis of Forced Flow Helium Cooled Cryopanel of Cryopump Using Venecia Code

S. S. Mukherjee¹, V. Gupta¹, R. Gangradey¹, J. S. Mishra¹, P. Nayak¹, P. N. Panchal¹, S. Das¹, and J. Agarwal¹

¹*Institute for Plasma Research (IPR), Bhat, Gandhinagar, India*

Corresponding Author: S. S. Mukherjee, samiran@ipr.res.in

Cryoadsorption cryopump with large pumping speeds application has been developed at IPR. These pumps are cooled with liquid helium for cryopumping panels below 5 K to adsorb hydrogen and helium gases and with gaseous helium for thermal shields at around 80 K during fusion reactor relevant applications. The panels are coated with activated carbon as sorbent. Sorbent with micropores adsorbs gases and the pores become saturated after certain duration of pumping operation. During regeneration by increasing the panel temperature adsorbed gases get removed. A cycle of operation is thus followed comprising, cool down from 80 K to ~ 4 K and warm up from ~ 4 K to 80 K during the normal operation cycle of the cryopump. Cryopanel and shielding panels are mostly hydroformed quilted stainless steel panels with sheet thickness of 1.5 mm. Hydroformed panel of size 1000 mm \times 200 mm (l \times w) with the same sheet thickness connected by inlet and outlet tubes are used as 4 K cryopanel. Thermohydraulic analyses are carried out in Venecia software developed by Alphysica for the 24 panel cryopump for different cooling schemes. To investigate the necessary mass flow rates and cool down time, optimized selection of the cryopanel arrangements, flow paths and manifolds is required. Results of cool-down time, mass flow requirement and temperature and velocity profile will be presented for different cooling and regeneration schemes.

Pellet Fuelling Prospects and Injector System for ADITYA-U Tokamak

J. S. Mishra¹, R. Gangradey¹, S. S. Mukherjee¹, P. N. Panchal¹, P. Nayak¹, J. Agarwal¹, V. Gupta¹, and S. Das¹

¹*Institute for Plasma Research (IPR), Bhat, Gandhinagar, India*

Corresponding Author: J. S. Mishra, jsmishra@ipr.res.in

High density plasma operation with centrally peaked profile is one of the key aspects in achieving break-even condition in magnetically confined fusion devices. In this prospect an efficient fuelling method capable of supplying particles into the core of the plasma is desired. Till date, cryogenically solidified pellets of hydrogen isotopes have been proved as an efficient method of replenishing the spent fuel in fusion devices. Apart from fuelling, pellet injection is also useful for plasma confinement improvement, ELM (edge localized mode) pacing, plasma disruption mitigation (which can damage the tokamak first wall) using shattered pellets are other important application. The use of pellet injection technique is actively considered for ITER plasma and for future DEMO relevant studies.

IPR, India, has initiated the development of a pellet injection system. A study related to pellet injection in ADITYA-U is planned and desired pellet parameter is estimated by applying standard theoretical models such as neutral gas shielding models (NGS). While designing the pellet injection system, the targeted plasma electron temperature considered is few hundreds eV to 2 keV. For ADITYA the pellet size and speed are chosen to be ~ 1.5 mm and < 800 m/s, respectively. Considering estimated design parameters a single barrel hydrogen pellet injection system is developed for pellet injection related studies. The injector is based on pipe gun concept, where, a pellet formed in-situ in the gun barrel is accelerated to high speed using high-pressure light propellant gas. This system uses a cryogen free, closed loop compact cryocooler, which provides operational reliability to the pellet freezing process. Pellet formation study is successfully demonstrated using the designed injector. In test bench setup pellet size of < 1.8 mm and velocity of < 900 m/s has been demonstrated. A programmable logic controller based control system is integrated to the tokamak to operate the injector remotely during plasma operation. The pellet parameters are characterized using standard diagnostic such as fast imaging camera and light gate system. This injector will be employed for experiment in ADITYA-U tokamak. The design of the pellet injector and its future prospect for application in ADITYA-U tokamak will be presented.

Performance of Transmission Line System at 42.0 ± 0.2 GHz for an Indigenous Gyrotron System

P. Bhatt¹, A. Patel¹, K. Mahant¹, K. Sathyanarayana¹, and S. V. Kulkarni¹

¹*Institute for Plasma Research (IPR), Bhat, Gandhinagar, India*

Corresponding Author: P. Bhatt, pujitabhatt@gmail.com

In high microwave power applications like gyrotron, transmission line system, calorimetric dummy load, etc, requires design, modelling, simulation and evaluation of transmission line system before fabrication of the same is undertaken. Under the aegis of Department of Science and Technology (DST), a multi-institutional programme for the development of a gyrotron operating at 42.0 ± 0.2 GHz/200 kW/3 s in TE₀₃ mode has been undertaken. It is currently in an advance stage of test and commissioning at IPR. It is desired for plasma applications that the output mode of gyrotron in TE₀₃ mode is to be converted to HE₁₁ mode for efficient coupling to plasma. The HE₁₁ mode (TEM₀₀ mode), has an electric field distribution very close to that of an ideal Gaussian mode. This Gaussian-like mode is preferred for high-power transmission through overmoded corrugated waveguides, which gives insertion loss lower than that of any other modes. The proposed design of transmission line system converts unpolarized TE₀₃ mode into polarized HE₁₁ mode.

The ripples walled mode converters are designed for converting TE₀₃ to TE₀₁ in two steps. TE₀₁ mode is converted to TM₁₁ by bending a smooth waveguide at an angle of 34.94° . Finally TM₁₁ mode is converted to HE₁₁ mode. Miter bend for TE₀₁ mode and HE₁₁ mode are also designed. The designed corrugated waveguide operates at 42.0 ± 0.2 GHz. The final design of all the components are verified using simulation studies carried out in CST-MWS. Performance optimization has been carried out prior to fabrication process. At of now, fabrication of many of the mode converters has been completed and miter bends are under mechanical fabrication process. As a part of a design, transmission line system is mechanically compatible to high vacuum and 1 bar pressurization.

The system includes two design approaches whose performances are compared in terms of insertion loss, bandwidth and cost effective manufacturing. Both the proposed design approaches of transmission line system have total insertion loss of 1.3 to 1.5 dB. The bandwidth of first design approach is wider as compared to second. Flexibility of manufacturing process of transmission line system is an advantage of second approach. The salient point of design and simulation studies of transmission line system are discussed and highlighted in the manuscript.

Development and Qualification of Passive Active Multijunction (PAM) Launcher for LHCD System of ADITYA-Upgrade Tokamak

Y. M. Jain^{1,2}, P. K. Sharma^{1,2}, K. K. Ambulkar¹, P. R. Parmar¹, J. Kumar¹, and H. V. Dixit¹

¹*Institute for Plasma Research (IPR), Bhat, Gandhinagar, India*

²*Homi Bhabha National Institute (HBNI), Anushakti Nagar, Mumbai 400094, India*

³*Birla Institute of Technology and Science, Pilani-Hyderabad Campus, Hyderabad, Telangana, India*

Corresponding Author: Y. M. Jain, yogesh.jain@ipr.res.in

A passive active multijunction (PAM) antenna is designed and developed and would be commissioned on the ADITYA-U tokamak. The PAM antenna has many advantages over the grill antenna such as exhibiting a lower reflection coefficient at the plasma densities close to its corresponding cut-off density. The PAM antenna along with its transmission line components are designed to deliver RF power up to 250 kW for 1 s and its design is validated using COMSOL Multiphysics and CST studio. This paper describes the fabrication protocols of each component of the PAM launcher and its transmission line components along with its low power test methodology.

Effect of Sorbent Selection and Geometrical Arrangement of Cryopanel on Pumping Speed of Cryopump

R. Gangradey¹, S. S. Mukherjee¹, J. S. Mishra¹, P. N. Panchal¹, P. Nayak¹, J. Agarwal¹, V. Gupta¹, and S. Das¹

¹*Institute for Plasma Research (IPR), Bhat, Gandhinagar, India*

Corresponding Author: R. Gangradey, ranjana@ipr.res.in

Vacuum is an inherent part of any fusion machine. The requirement of providing large pumping speed is growing as fusion science is progressing towards high temperature, high density, and large confinement machines. In its domestic programme of development of technologies for fusion grade machines, IPR developed the sorbent-based cryopumps. Using coconut shell charcoal pumping speed of 2 $\ell/\text{cm}^2\text{s}$ for helium and 5 $\ell/\text{cm}^2\text{s}$ for hydrogen is demonstrated. Different sorbents are under study for their pumping speed performance, for example carbon cloth and flocked carbon panels. Experimental study of pumping speed is being carried for different geometrical configurations of panel arrangements. MOLFLOW+ is used for simulating the pumping speed. Initial experiments are being carried out at 80 K and compared with MOLFLOW+ results. This paper discusses in detail simulation and experimental results of developed pumps

Advanced Capabilities of Multifunctional Calculation Programme SuperMC3.2 for Complex Nuclear System

L. Hu¹, L. Hao¹, J. Song¹, P. Long¹, B. Wu¹, S. Yu¹, G. Sun¹, P. He¹, J. Zou¹, Q. Gan¹,
L. Wang¹, B. Li¹, and Y. Wu¹

The FDS Team

¹*Institute of Nuclear Energy Safety Technology, CAS, Anhui, People's Republic of China*

Corresponding Author: L. Hu, liqin.hu@fds.org.cn

Super Multifunctional Calculation Programme for Nuclear Design and Safety Evaluation, SuperMC, is a full-function neutronics simulation software system including inner-coupled calculations among efficient radiation transport, depletion, activation and shutdown dose. Its advanced capabilities include CAD/image-based accurate modelling for complex irregular geometry, intelligent data analysis based on multi-D/multistyle visualization and network collaborative nuclear analysis on cloud computing platform. Besides, several advanced radiation transport methods such as global weight window generator (GWWG) were proposed to solve the key problems for radiation protection in fusion system, such as deep penetration problem, sky scattering problem.

SuperMC has been verified and validated by more than 2000 benchmark models and experiments including HCPB mock-up experiments in SINBAD, IAEA-Activation Calculation Benchmark (ACB), FNG-ITER SDR experiment and so on. And it was also applied in the neutronics analysis of ITER, DEMO, etc.

Development of Technology for Fabrication of Prototype Ion Extraction Grid for Fusion Research

M. R. Jana¹, P. Ram Sankar²

¹*Institute for Plasma Research (IPR), Bhat, Gandhinagar, India*

²*Raja Ramanna Centre for Advanced Technology (RRCAT), Indore, India*

Corresponding Author: M. R. Jana, muktijana@gmail.com

Steady state Superconducting Tokamak (SST-1) has a provision for positive hydrogen ion based neutral beam injector (NBI) to raise the tokamak plasma ion temperature ~ 1 keV with neutral hydrogen beam (H^0) power of 0.5 MW at 30 kV. The heart of NBI system is ion extractor system which consists of three grids each made up of OFHC copper. The beamlets originating from the extractor system are focussed horizontally at 5.4 mm and vertically at 7 mm to reduce power dissipation at beam line components. The required beam divergence is $< 1^\circ$. For long pulse operation, active water cooling is provided by an inlaid dense network of 22 wavy semicircular ($r = 1.10 \pm 0.05$ mm) cooling channels in the space available between the apertures. The required flatness of the copper plate is 100 μm and positioning tolerance of aperture is ± 60 μm . All these stringent requirements dictates that fabrication of extractor grid is very complex process as it involves several critical technology, e.g., i) joining of SS-304L stub rod with OFHC copper grid plate; ii) precision CNC, etc., machining on large-size OFHC copper plate for making shaped apertures, and, iii) copper electroforming for fabrication of embedded cooling channels inside thin OFHC copper plate. None of these technologies are available in India. This paper describes the work done on prototype activities to gain experience in each of the above-mentioned technology areas. Friction welding (FW) is developed for joining of dissimilar metals of SS-304L rod with OFHC copper plate with joining strength of 264 MPa. Then FW on actual size of OFHC copper plate is successfully done. Critical tolerances required for CNC machining for drilling and shaping of apertures and milling in thickness of OFHC copper grid plate of size 180×90 mm² with 19 holes and 4 semicircular cooling channel. Copper electro-deposition of 2.5 mm thickness is done on the above-mentioned prototype grid sample using technique of periodic reversal process where 20 s electro-deposition was followed by a 4 s reversal. Test specimens were also electro-deposited along with the prototype grid plate for testing of mechanical properties and conductivity. The conductivity was $101 \pm 1\%$ IACS with microhardness values 56 to 61 HV5. All these experiences shall be useful for manufacturing of large size ion extractor grid in India.

Development of RF Based Capacitively-Coupled Plasma System for Deposition of Tungsten Nanolayers on Graphite

S. S. Chauhan¹, U. Sharma¹, J. Sharma², A. K. Sanyasi³, J. Ghosh³, N. Yadav⁴,
K. K. Choudhary⁵, and S. K. Ghosh⁶

¹Department of Physics, Shri Vaishnav Institute of Technology and Science, Indore, India

²Department of Physics, M.B. Khalsa College, Indore, India

³Institute for Plasma Research (IPR), Bhat, Gandhinagar, India

⁴Gujarat University, Navrangpura, Ahmedabad 380 009, India

⁵Indian Military Academy, Uttarakhand, India

⁶Department of Physics, Vikram University, Ujjain, India

Corresponding Author: S. S. Chauhan, druttamsharma1971@gmail.com

Based on the current trends in thermonuclear fusion research, it is quite likely that future fusion machines, DEMO and beyond, will be operating with tungsten and alloys based on tungsten as the plasma facing material on their walls and targets to dissipate the thermal as well as particle loads under extreme conditions. Tungsten is being preferred because of its superior thermo-mechanical properties as well as for its low tritium retention. However, use of pure tungsten as a structural material itself will substantially increase the manufacturing cost and overall system mass and also it is difficult to machine. Hence, tungsten coatings on light substrate such as graphite are preferred which essentially reduce the cost and structural weight considerably. In this article, we report the development of a RF based capacitively coupled plasma reactor for tungsten coating on graphite tiles using plasma assisted chemical vapour deposition at SVITS, India. Tungsten nanolayers have been successfully deposited on graphite test pieces by reducing the heavy tungsten hexafluoride gas in hydrogen. Characterization and postanalysis of the tungsten coated tiles has been carried out to study the presence of tungsten, thickness of the coating, thermal fatigue, etc.

Real-Time Feedback Control System for Plasma Position Stabilization in ADITYA-U Tokamak

R. Kumar¹, P. Gautam¹, S. Gupta¹, T. Macwan^{1,2}, E. V. Praveenlal¹, M. Shah¹, K. S. Shah¹, M. N. Makwana¹, V. Balakrishnan¹, C. N. Gupta¹, R. L. Tanna¹, S. Aich^{1,2}, D. Kumawat¹, K. Sathyanarayana¹, and J. Ghosh^{1,2}

The ADITYA-U Team

¹*Institute for Plasma Research (IPR), Bhat, Gandhinagar, India*

²*Homi Bhabha National Institute (HBNI), Anushakti Nagar, Mumbai 400094, India*

Corresponding Author: R. Kumar, rohith.kumar@ipr.res.in

The ADITYA-U tokamak ($R_0 = 0.75$ m, $a = 0.25$ m) is designed to have shaped plasmas in both single and double null divertor configurations. It is quite well known that sustaining a shaped plasma in tokamak requires very good plasma column position control, both horizontal and vertical. A proportional-integral-derivative (PID) based control system has been designed and operated to achieve horizontal and vertical plasma positions control in ADITYA-U tokamak. In this control system, the transfer function model of control power supply and different position diagnostics has been incorporated such that whole system fulfils the stability criteria of the whole control system. In order to incorporate effect of change in radius of plasma column and the vessel eddy current on the position measurements, new adaptive techniques are incorporated to achieve plasma position regulation with minimum error. Detailed comparisons have been carried out between the results obtained with the conventional PID approach and adaptive method approach. Furthermore, the system has been trained to take appropriate actions during the disruption or plasma failure in the tokamak. The complete system has been rigorously tested with sample signals before implementing to the ADITYA-U plasma discharges. The control system is integrated to the composite plasma control system of ADITYA-U. The complete design, installation, operation, training of the system along with all the relevant testing will be presented in the paper.

Design and Simulation Studies of Calorimetric Dummy Load for Gyrotron System

A. Patel¹, M. Shah¹, C. Prajapati¹, K. Sathyanarayana², and P. Chaudhuri²

¹CHARUSAT Space Research and Technology Center, CHARUSAT University, Gujarat, India

²Institute for Plasma Research (IPR), Bhat, Gandhinagar, India

Corresponding Author: A. Patel, axatpatel.me@charusat.ac.in

High microwave power is generally measured and characterized by calorimetric dummy loads, which are designed to suit the exiting modes of the gyrotron/HPM. The output mode of the gyrotron is converted to a Gaussian mode-HE₁₁ mode after passing through a series of mode converters. The objective of this study is to design and fabricate a calorimetric dummy load with efficient cooling medium which absorb maximum power of 200 kW at 42.0 ± 0.2 GHz frequency applied for 3 s, suited for microwave power propagating in HE₁₁ mode. There is rigorous requirement of proper cooling channel or cooling medium over the dummy load system for the dissipation of heat in the quickest manner. As an effect of high microwave energy (maximum heat), internal heat buildup in the dummy load system which could results in a catastrophic failure or decrease in the life span of the dummy load. This research envisaged the thermal effect of microwave energy on a reflecting structure incorporated to transfer microwave energy to heat absorber media concatenating the effect of heat conduction via multiflow path technique. In this manuscript, CFD analysis using ANSYS has been carried out to find the temperature contour, velocity contour, and pressure contour for water passing through the helical tubes and thermal analysis has also been carried out for reflecting medium and microwave absorber material inside the enclosure. Details of these analyses results and their optimizations will be discussed in this paper.

Overview of the NSTX-U Recovery Project Physics and Engineering Design

S. P. Gerhardt¹, J. E. Menard¹, C. Neumeyer¹, R. Feder¹, N. Atnafu¹, N. Allen¹, M. Awad¹, A. Basile¹, W. Blanchard¹, A. Brooks¹, A. Brereton¹, R. Burke¹, D. Cai¹, F. Cai¹, C. Ciummo¹, M. Cropper¹, M. D'Agostino¹, N. Dean¹, J. Dellas¹, D. Downing¹, L. Dudek¹, R. Ellis¹, K. G. Erickson¹, N. M. Ferraro¹, C. Freeman¹, A. Gao¹, T. K. Gray², N. Greenough¹, J. Guttenfelder¹, F. Hoffmann¹, M. A. Jaworski¹, F. Jones¹, M. Kalish¹, A. Khodak¹, A. Jariwala¹, J. Klabacha¹, M. Kumar¹, B. Linn¹, D. Loesser¹, M. Mardenfeld¹, J.-K. Park¹, J. Petrella¹, W. Que¹, S. Raftopoulos¹, M. L. Reinke², H. Schneider¹, M. Smith¹, B. Stratton¹, M. Sibilia¹, T. Stevenson¹, G. Tchilinguirian¹, P. Titus¹, M. Viola¹, W. Wang¹, I. Zatz¹, G. Zimmer¹, Y. Zhai¹, and H. Zhang¹

¹Princeton Plasma Physics Laboratory (PPPL), Princeton, NJ 08540, USA

²Oak Ridge National Laboratory (ORNL), Oak Ridge, TN 37831, USA

Corresponding Author: S. P. Gerhardt, sgerhardt@pppl.gov

The NSTX-U device began operation in 2016, producing 10 weeks of commissioning and scientific operations. However, a number of technical issues, including the failure of a key divertor coil, resulted in the suspension of operations. A comprehensive extent of condition review was initiated at the request of the Department of Energy; this paper will summarize the result of that process, focussing on the design and implementation improvements that are in progress in order to resume operation and increase reliability. Many elements of the physics design have been revisited as part of the recovery, although most key NSTX-U mission goals remain. New requirements for the divertor heat fluxes have been defined, based on recent SOL heat flux width models. New halo currents loads have been determined based on combining data from NSTX, NSTX-U, MAST, and conventional aspect ratio devices. New error field analysis has been conducted, with the goal of optimizing both the global MHD stability and minimizing PFC heat flux asymmetries for scenarios with large poloidal flux expansion. New divertor coil current requirements have been defined, based on the tolerable heat fluxes and current drive for the various potential equilibria. Numerous design improvements are being included as part of the recovery effort, with a primary goal of supporting flexible operations at $B_t = 1$ T, $I_p = 2$ MA, $P_{inj} = 10$ MW, and $t_{pulse} = 5$ s. New designs of graphite plasma-facing components utilize castellations to reduce the mechanical stresses, allowing tiles to reach surface temperature limits, $\sim 1600^\circ\text{C}$, driven by sublimation. Improved divertor coil designs simplify fabrication and facilitate turn-to-turn testing. Modifications to the NSTX-U vacuum chamber will eliminate one the ceramic insulators necessary for coaxial helicity injection (CHI), increasing system reliability at the expense of the CHI research capability. The physics and engineering R&D activities that support recovery will be summarized, along with highlights of the new design.

Work supported by the U.S. Department of Energy Contract D-AC02-09CH11466 and DE-AC05-00OR22725.

Novel Approach of Pulsed-Glow Discharge Wall Conditioning in ADITYA Upgrade Tokamak

K. A. Jadeja¹, J. Ghosh¹, K. Patel¹, K. M. Patel¹, B. G. Arambhadiya¹, K. S. Acharya¹, R. L. Tanna¹, S. B. Bhatt¹, M. B. Chowdhuri¹, R. Manchanda¹, M. Shah¹, S. Ghosh², V. P. Kella¹, R. Kumar¹, S. Aich¹, D. Kumawat¹, M. B. Kalal¹, R. Rajpal¹, C. N. Gupta¹, and P. K. Chattopadhyay¹

The ADITYA-U Team

¹*Institute for Plasma Research (IPR), Bhat, Gandhinagar, India*

²*University of California San Diego, CA 92093, USA*

Corresponding Author: K. A. Jadeja, kumarpal@ipr.res.in

In ADITYA-Upgrade, glow discharge wall conditioning (GDC) is performed for long hours after the tokamak plasma operation using H gas to control oxygen and carbon containing impurities. This leads to high retention of H gas on graphite limiter and the stainless steel (SS) vessel. Subsequently, high H outgassing rate requires increased pumping time and high H recycling during plasma discharges affect the plasma performance in respect to H fuelling control of the plasma. Intermittent He GDC for shorter duration can be used to decrease the H retention mainly in graphite. However, the removal of He from the limiter and wall is more difficult than H due to its properties of nonreactive, hard-to-trap, vacuum pumping limitation, etc. A new approach involving pulsed glow discharge wall conditioning (P-GDC) has been introduced in ADITYA-U tokamak to reduce the residual H concentration in the SS vessel and graphite limiters. It has been observed earlier with continuous GDC that the impurity removal rate is usually high in initial few seconds of GDC operation. The initial high reaction rate is due to the reaction of working gas ions with loosely bound outer-most monolayers species. The removal rate then decreases exponentially as hard bonded O and C containing impurities come out slowly. Moreover, the released impurity gases are re-implanted in the wall materials partially deeper in presence of continuous GDC that they have been in its absence. Thus overall impurity removal rate decreases exponentially with time in presence of continuous gas GDC. Initiation of the glow discharge needs filling of H gas at high pressure $\sim 10^{-2}$ mbar and ~ 1 kV voltage in ADITYA-Upgrade. In case of pulsed GDC the gas needs to be injected in pulsed mode and the discharge needs to be initiated during every gas. Therefore in P-GDC, to facilitate the fast initiation of discharge, a source of free electrons has been introduced in the vessel. A fast feedback pulsed gas-fuelling control system and electrons emission system has been developed to initiate glow discharge in each gas-feed pulse at various operating pressure of 10^{-4} mbar and above. The different P-GDC experiments have been carried out with H, He, and Ar as working gases and the results are compared with traditional continuous GDC. The design, development, operation and results of pulsed GDC has been described in this paper in details.

New Fusion Facilities at UKAEA: FTF and H3AT

E. Surrey¹, D. P. Brennan¹, I. T. Chapman¹, and C. Walters¹

¹United Kingdom Atomic Energy Authority, Culham Science Centre, Abingdon, UK

Corresponding Author: E. Surrey, elizabeth.surrey@ukaea.uk

The UK Government has invested ~ 100 M€ to create two new UKAEA centres for fusion research: Hydrogen-3 Advanced Technology (H3AT) and the Fusion Technology Facilities (FTF) both opening in 2020–21. FTF and H3AT will foster close cooperation with industry, academia and other international laboratories to develop and transfer knowledge between partners, offering opportunities to undertake R&D to reduce risk for ITER and to make significant contributions to the EU DEMO and international fusion programmes. The FTF offers a complete development life cycle for materials and components in three facilities. The Materials Technology Laboratory develops and qualifies materials using small sample testing techniques to reduce costs and offer in-service testing. The Joining and Advanced Manufacturing Laboratory specializes in material joining and manufacturing technologies for fusion including additive manufacture and laser welding. It has a dedicated small sample test facility, HIVE, capable of providing up to 20 MW/m² over 20×20 mm². The Module Test Facility provides fusion relevant testing environments, with heat flux up to 2 MW/m² (and higher localized flux) and DEMO relevant water cooling loop for metre-scale components. H3AT provides space for active and inactive experiments with tritium-grade ventilation and glove boxes complete with pressure control and purging systems offer user-ready specialist facilities for a range of R&D activities. In addition to providing a supply of tritium, H3AT offers a flexible gas mixing capability, removing the need for gas mixture preparation for experiments. A flexible gas analytical system is networked to the experimental stations that are also served with vacuum systems, tritium recovery and detritiation facilities. This paper will describe the new facilities in terms of their technical capabilities and the progress to their realization.

A Concept of Self-Cooled Breeding Blanket with Advanced Molten Salt FLiNaK for High-Efficiency and Long-Life Operation

**J. Yagi¹, T. Tanaka^{2,3}, G. Yamazaki³, K. Kumagai³, T. Watanabe², A. Sagara^{2,3},
T. Nagasaka^{2,3}, and T. Muroga^{2,3}**

¹*Institute of Advanced Energy, Kyoto University, Nishikyo-ku, Kyoto 615-8540, Japan*

²*National Institute for Fusion Science (NIFS), Toki, Gifu, Japan*

³*Department of Fusion Science, Graduate University for Advanced Studies (SOKENDAI), Toki, Gifu, Japan*

Corresponding Author: J. Yagi, j-yagi@iae.kyoto-u.ac.jp

An advanced molten salt (AMS), in which powders of hydrogen-soluble and chemically reactive metals such as titanium are mixed, is investigated as a potential self-cooled breeding blanket material. It is shown that hydrogen isotope uptake in a vanadium plate in molten salt FLiNaK is suppressed by the addition of Ti powders into the salt. In addition, the corrosion of candidate structural materials in FLiNaK with HF is also suppressed by the addition of titanium powders. Considering these result, tritium formed in the molten salt in fusion blanket will be trapped by the Ti powders, not being trapped by the structure materials (vanadium alloy) and not corroding the structure materials. Neutronics and tritium mass balance calculations are also performed and it is showed that FLiNaK based Be-free blanket is feasible.

Development of a Plasma Scenario for the EU-DEMO: Current Activities and Perspectives

M. Siccinio^{1,2}, E. Fable², F. Janky², R. Ambrosino³, W. Biel⁴, M. Cavedon², T. Franke^{1,2}, T. Görler², T. Härtl^{1,2}, R. Kembleton^{1,5}, Y. Liu⁶, M. Mattei⁷, F. Maviglia^{1,3}, G. Pautasso², L. Pigatto⁸, S. Saarelma⁵, O. Sauter⁹, F. Subba¹⁰, M. Q. Tran⁹, E. Viezzer¹¹, and H. Zohm²

¹EUROfusion Consortium, 85748 Garching, Germany

²Max-Planck-Institut für Plasmaphysik, Garching, Germany

³Consorzio CREATE, Università degli Studi di Napoli Federico II, 80138 Napoli, Italy

⁴Forschungszentrum Jülich, Jülich, Germany

⁵Culham Centre for Fusion Energy (CCFE), Culham Science Centre, Abingdon, UK

⁶General Atomics, San Diego, CA 92186, USA

⁷Consorzio CREATE, Università degli Studi della Campania "Luigi Vanvitelli", 80131 Aversa, Italy

⁸Consorzio RFX, Associazione EURATOM-ENEA sulla Fusione, Padova, Italy

⁹Swiss Plasma Center (SPC), École polytechnique fédérale de Lausanne (EPFL), 1015 Lausanne, Switzerland

¹⁰NEMO group, Politecnico di Torino, Turin, Italy

¹¹Universidad de Sevilla, Seville, Spain

Corresponding Author: M. Siccinio, mattia.siccinio@euro-fusion.org

In order for the first fusion reactor DEMO to accomplish its mission, it is necessary to identify a plasma scenario which is at the same time performing in terms of fusion power generation and sufficiently stable to ensure the integrity and availability of the machine components for a long time. In the present work, the activities undertaken for this purpose by EUROfusion PMU are summarized.

In the course of the current preconceptual design analysis phase for the European DEMO, it is necessary to define scenarios by considering from the early phases their compatibility with the performance of the available diagnostics, of the actuators for plasma control and with the response of the heating and current drive systems. A coupling between the 1D transport code ASTRA and the control software Simulink has been performed, providing a tool able to simulate the plasma behaviour while accounting for the constraints linked to the detectability of the signals and the delay and power limitations of the actuators responses. In our work, the DEMO-related results of such a tool are presented. In parallel, the numerous ongoing activities concerning the open issues which require to be addressed before the scenario could be considered complete and robust enough (e.g., plasma ramp-up and -down definition, identification of disruption precursors, ELM mitigation etc.) are also illustrated.

The reference scenario which is considered for the EU-DEMO is the so called "DEMO 1", i.e., a pulsed scenario based on conservative physics assumptions and analogous, at least from a macroscopic level, to the ITER 15 MA. However, other, alternative scenarios are investigated in parallel. The main alternative concept developed is the so called Flexi-DEMO, which relies on more advanced scenarios as compared to DEMO 1, with a large fraction of auxiliary current drive and a tailoring of the safety factor profile which aims at maximizing the bootstrap current fraction to achieve a steady-state discharge. Furthermore, the possibility of extrapolating other, more speculative scenarios to a reactor condition is also considered inside our activities.

Implications of Uncertainties on the European DEMO Design

H. Lux¹, M. Morgan^{1,2}, M. Siccino^{3,4}, W. Biel⁵, G. Federici⁴, R. Kembleton^{1,6},
W. A. Morris¹, E. Patelli², and H. Zohm³

¹Culham Centre for Fusion Energy (CCFE), Culham Science Centre, Abingdon, UK

²Institute for Risk and Uncertainty, University of Liverpool, Liverpool, UK

³Max-Planck-Institut für Plasmaphysik, Garching, Germany

⁴EUROfusion Programme Management Unit Garching, Boltzmannstraße 2, 85748 Garching Germany

⁴Institute of Energy and Climate Research, Forschungszentrum Jülich, Jülich, Germany

⁴EUROfusion Programme Management Unit Culham, Culham Science Centre, Abingdon, UK

Corresponding Author: H. Lux, hanni.lux@ukaea.uk

During the preconceptual design phase of fusion devices such as the European demonstration fusion power plant (DEMO), systems codes provide a fast evaluation of optimal design points and highlight high impact areas. However, determining or evaluating a design point at such an early stage comes with uncertainties in many of the design parameters. These uncertainties are both associated with the physics as well as the engineering basis of the European DEMO design.

This work applies an uncertainty quantification analysis to the 2017 pulsed European DEMO design using the PROCESS systems code. It assumes that DEMO will be built as suggested by the baseline and explores what implications the currently known physics and engineering uncertainties have on the expected performance parameters (net electric output and pulse length), while optimizing the fusion gain Q or the pulse length. It furthermore compares the analysis of the conservative DEMO baseline design to the more advanced Flexi-DEMO option.

A more detailed single parameter analysis is clearly identifying high impact parameters. This is confirming previous investigations as well as revealing new areas that warrant deeper investigation.

Development of DEMO-FNS Fuelling Systems and Modelling Hydrogen Isotopes Distribution via “FC-FNS” Simulation Code

S. S. Ananyev¹, A. V. Spitsyn¹, and B. V. Kuteev¹

¹National Research Centre “Kurchatov Institute”, Moscow, Russian Federation

Corresponding Author: S. S. Ananyev, ananyev_ss@nrcki.ru

In the NRC “Kurchatov Institute”, the fuelling systems (FS) concept for the DEMO-FNS facility, incorporating components maintaining plasma parameters, tritium processing and breeding, is being developed. The FS computer model provides calculation functions using the computer code “FC-FNS”. It calculates gas flows, tritium inventories and losses in FS for steady-state operation mode.

Within the DEMO-FNS design development the device parameters were better specified and “FC-FNS” code was upgraded accordingly. In 2016–2018, the structural diagram of the fuel cycle was expanded to include systems for fuel mixture deprotonation, cooling the divertor and first wall, tritium extraction from lithium circulating in the vacuum vessel. The code functionality was expanded to take into account the new systems and operating modes. The updated version simulates the balance of all three hydrogen isotopes (H, D, T). The values of tritium inventory in main systems (blanket, storage, processing and separation) calculated on the basis of the particle balance can be compared with those obtained using solution of differential equations describing the dynamics of tritium inventories.

Due to the fact that the neutral beam injection (NBI) system is included in the FS, its gas supply configuration and integration in the facility FS are being considered. Calculations showed that in a neutral injection system it is inappropriate to use D:T= 1:1 gas mixture. The scenario is optimal in which a tritium-containing gas mixture is pumped out to the facility’s FS when a specified tritium fraction (5%) is reached. The total tritium inventory in FS can be reduced to 1.5–2 times compared with 1:1 case.

Previously, the particles balance was set on the assumption that the injection systems must compensate the particles loss from plasma due to burnout and removal of hydrogen isotopes from the plasma. The new code version includes the possibility to simulate the gas inlet to the vacuum chamber associated with control of the edge plasma parameters, ELMs control, etc. Tritium losses in the FS reach 30–50 g due to its decay and about 20 g due to diffusion through the structural materials in addition to the burnout of 1.7 kg per year in plasma. Tritium inventories in structural materials reach up to 90 g per year. In this case, the total amount of tritium in the FS will be up to 1000 g.

Development of Capacitively-Coupled Comb-Line Antennas for Current Drive in Tokamaks

Y. Takase¹, C. P. Moeller², A. Ejiri¹, T. Shinya^{1,3}, Y. Tajiri¹, Y. Takei¹, N. Tsujii¹, S. Yajima¹, and H. Yamazaki¹

¹University of Tokyo, Tokyo, Japan

²General Atomics, San Diego, CA 92186, USA

³National Institutes for Quantum and Radiological Science and Technology (QST), Rokkasho Fusion Institute, Rokkasho-mura, Aomori, Japan

Corresponding Author: Y. Takase, takase@k.u-tokyo.ac.jp

The capacitively-coupled comb-line (CCC) antenna has been developed for current drive by the lower hybrid wave (LHW) on the TST-2 spherical tokamak. In order to excite a highly directional wave required for efficient current drive, an antenna array consisting of many elements is necessary, but it is impractical to feed each of these elements independently in a device with limited accessibility. The comb-line antenna was developed to satisfy the requirements of high directionality, low reflectivity, and simple feeding. Since the comb-line antenna makes use of mutual coupling between neighbouring elements, only the first and the last elements are connected to external feedlines. Each element is an LC resonant circuit, coupled to neighbouring elements by mutual capacitance, and exhibits a passband characteristic. The copper capacitive elements are shaped so that the RF electric field extends well into the plasma. The inductive elements are covered so neighbouring elements do not couple inductively to each other and the RF magnetic field does not extend into the plasma. A Faraday shield is not necessary. RF powers and power densities of the order of 100 kW and 1 MW/m² can be achieved easily in small antennas of the order of 0.1 m², because of the inherently low standing-wave ratio. The two CCC antennas installed in TST-2 (outboard-launch and top-launch) excite toroidal refractive index (n_ϕ) spectra peaked around 5 with full width at half maxima of around 2. Wave excitation calculation using COMSOL Multiphysics shows that the excited power of the $n_\phi = 5$ LHW component increases rapidly when the plasma cutoff density layer (where $n_e = 5 \times 10^{14}/\text{m}^3$) becomes closer than 27 mm from the antenna surface, in agreement with experiment. Experimentally, the density profile in front of the antenna can be controlled by adjusting the side limiter location or antenna-plasma distance, and should be optimized for antenna-plasma coupling, since too high coupling results in a broadened and less directional n_ϕ spectrum, and too low coupling results in a less efficient power coupling, which necessitates recirculation of the transmitted power. Using these antennas, successful ST plasma start-up and I_p ramp-up to over 25 kA (about 1/4 of the nominal I_p for OH operation) have been achieved with RF power of less than 100 kW in about 40 ms.

Progresses at CEA on EU DEMO Reactor Cryomagnetic System Design Activities and Associated R&D

L. Zani¹, F. Bonne², D. Ciazynski¹, P. Decool¹, G. Gros¹, P. Hertout¹, C. Hoa², B. Lacroix¹, V. Lamaison¹, Q. Le Coz¹, N. Misaria³, S. Nicolle¹, F. Nunio³, J.-M. Poncet², A. Torre¹, and R. Vallcorba³

¹*Institut de Recherche sur la Fusion par confinement Magnétique (IRFM), Commissariat à l'énergie atomique (CEA/Cadarache), 13108 St. Paul lez Durance, France*

²*Institut Nanosciences et Cryogénie (INAC), Commissariat à l'énergie atomique (CEA/Grenoble), 38054 Grenoble, France*

³*Institut de recherche sur les lois fondamentales de l'Univers (IRFU), Commissariat à l'énergie atomique (CEA/Saclay), 91191 Gif-sur-Yvette, France*

Corresponding Author: L. Zani, louis.zani@cea.fr

The EU DEMO reactor is expected to be among the first applications of fusion for electricity generation in the near future and the design of its magnet system is of central importance as driving power plant performance, budget and production efficiency. In this purpose activities were led by CEA in the framework of EUROfusion to contribute to the EU DEMO magnet system design. It encompassed design activities (dimensioning and development of associated modelling tools) with R&D (design and tests of mock-ups).

The CEA design activity was mainly oriented towards toroidal field (TF) coils system to propose a conceptual option (pancake-wound, no radial plates) established with a semianalytical CEA tool that considers the interdependent electromagnetic and mechanical behaviours. Then the proposed design is consolidated by detailed analyses:

- Thermo-hydraulics evaluation by coupling THEA, TRAPS and CAST3M software respectively for thermo-hydraulics, electromagnetic and thermal items. The outcomes obtained in normal and off-normal regimes are exposed and discussed in the paper.
- Mechanics evaluation with the most stressed zones identified and their criticality evaluated, in particular in the insulation zones. Design optimization is conducted on jacket corner radii and shape of the TF structures (casing and OIS). Finally analyses are led on the thermo-mechanic hotspot criterion.

Further to the TF system, the poloidal field (PF) coils and the central solenoid (CS) design were addressed by the same methodology, the outcomes will be expose and discussed. Besides design activities, TF is also studied through manufacturing considerations with organization of the winding stations manufacturing.

The DEMO cryoplant design was also addressed considering the loads to be absorbed and its process structure. The CEA proposal and the factors of merit considered will be presented and discussed. On another side, CEA also conducted R&D activities, mostly regarding the TF system with:

- Hydraulic tests at variable void fraction to explore its impact on helium friction.
- A full-scale TF conductor sample design and manufacture. The activity also included non-destructive examinations by tomography. Finally perspectives will be discussed regarding dimensioning with tools developed at CEA and the R&D activities to be extended.

Design Optimization of Helium Cooling Systems for Indian LLCB TBM

B. K. Yadav¹, A. Gandhi¹, K. T. Sandeep¹, D. Sharma¹, A. Saraswat¹, and P. Chaudhuri¹

¹*Institute for Plasma Research (IPR), Bhat, Gandhinagar, India*

Corresponding Author: B. K. Yadav, byadav@ipr.res.in

India is developing the lead-lithium cooled ceramic breeder as the blanket concept to be tested in ITER. In the Indian Lithium cooled Ceramic Breeder (LLCB) Test Blanket Module (TBM), PbLi eutectic alloy is used as multiplier, breeder, and coolant for the CB zones, and Li₂TiO₃ ceramic breeder (CB) is used as a tritium breeding material. The outer box structure is made of India specific reduced activation ferritic martensitic steel (IN-RAFMS) cooled by high pressure (8.0 MPa) and high temperature (300–500°C) helium gas named as first wall helium cooling system (FWHCS). The PbLi flow velocity is kept moderate enough such that its self-generated heat and the heat transferred from the ceramic breeder bed is extracted effectively. The PbLi system is cooled by another high-pressure helium system named as lead-lithium helium cooling system (LLHCS). Eventually, the two helium systems transfer the heat to the component cooling water system (CCWS) of ITER. In the conceptual design of LLCB TBM and its ancillary systems, two independent helium circuits were considered for extracting heat separately from the FW and the PbLi system. These helium systems are thermally and hydraulically independent to each other and they have their own components for operation and control. However, after detailed study, it is found that installation and assembly of all these components along with coolant purification system in the allocated space of the tokamak cooling water system (TCWS) vault annex is very difficult and the existing system to be optimized to fit into the space. Accordingly, studies were carried to reduce the number of components and their sizing and schemes to combine the two independent helium systems. In parallel, studies were also conducted to optimize the helium flow requirements for cooling the TBM FW. In the optimized configuration, a single helium system is proposed catering the cooling requirements of FW and PbLi system and the main components and piping of the optimized configurations of helium system are modelled in the modified version of RELAP/MOD4.0 and transient analysis is carried out. This paper discusses the results of the optimization studies and process parameters and features of the circuit diagram of the combined helium system. Thermo-hydraulic analysis results with the chosen optimized process parameters of the first wall are also presented.

Progress in Design of DEMO-FNS Hybrid Facility

Y. S. Shpanskiy¹

The DEMO-FNS Project Team

¹National Research Centre "Kurchatov Institute", Moscow, Russian Federation

Corresponding Author: Y. S. Shpanskiy, shpanski@mail.ru

Further development of a fusion-fission hybrid facility based on superconducting tokamak DEMO-FNS continues in Russia for integrated commissioning of steady-state and nuclear fusion technologies at the power level up to 40 MW fusion and 400 MW fission reactions. This facility is considered as the main source of technological and nuclear science information in the national programme for development of controlled fusion and plasma technologies until 2035 that is being currently developed and submitted to the authorities for approval. The facility DEMO-FNS exploits a conventional tokamak (CT) with major radius $R = 3.2$ m, minor radius $a = 1.0$ m, elongation 2.7, triangularity 0.5. The design is aimed at reaching steady state operation of the plant with the neutron wall loading of ~ 0.2 MW/m², the lifetime neutron fluence of ~ 2 MWA/m², with the surface area of the active cores and tritium breeding blanket ~ 100 m².

This report summarizes works performed in 2017–2018. The design goals of 2017 were concentrated on development of new simulation tools and plasma scenario, improving characteristics of enabling systems, implementing upgraded and new systems like first wall, divertor, active core, tritium breeding blanket, NBI, fuelling and pumping, heat transfer, remote handling in the integrated device design. NBI system with six injectors, five of which operate in 2 hour-cycle with sequential recuperation and one which can be used for repair and maintenance procedures. Total power of 500 keV deuterium beams is 36 MW. Optimization of beam transport ducts allowed reduction of their cross section to 0.4×0.8 m². Core plasma modelling showed that neutron yield is maximal if the tritium/deuterium density ratio is 1.5–2.3. For active core with $k_{\text{eff}} = 0.95$ (hybrid plant case) the neutron damage of FW-materials in dpa is comparable for fusion and fission neutron sources. Advantages of supercritical CO₂ as a coolant for active cores, TBB, FW and divertor were evaluated. This coolant is attractive due to acceptable pressure (~ 75 bar) and temperature (up to $\sim 500^\circ\text{C}$) ranges, low activation level in neutron environment, saving the hard neutron spectra, and compatibility with lithium technologies better than water coolant. Selection of prospective concepts is being made for hybrid fuel cycle and blankets capable to support development of nuclear power in RF with thermal and fast nuclear reactors.

SST-1 Cryogenic Requirements and the Way Forward

V. L. Tanna¹, A. K. Sahu¹, C. Chakrapani¹, P. N. Panchal¹, R. N. Panchal¹, R. J. Patel¹, G. Mahesuria¹, D. Sonara¹, N. Bairagi¹, U. Prasad¹, B. R. Doshi¹, R. Srinivasan¹, and D. Raju¹

¹*Institute for Plasma Research (IPR), Bhat, Gandhinagar, India*

Corresponding Author: V. L. Tanna, vipul@ipr.res.in

The SST-1 Machine consists of sixteen TF and nine PF superconducting coils. The cryostable operation of these coils demand the operation temperature of 4.5 K. This technical requirement is met by 1350 W at 4.5 K helium cryogenic system and is operational since 2003. The SST-1 cryogenics systems include helium, as well as nitrogen, cryosystems along with its storage, distribution and recovery systems facilitated to the SST-1 cooling requirements. The cryosystem mainly comprises of helium cryogenic system and liquid nitrogen management system.

Recent operational experience on SST-1 cryosystem has revealed that there is higher heat loads than the installed cryocapacity observed while carrying out simultaneous cooling of the TF and PF coils of the SST-1. It was able to cool down the TF coils along with the current leads and PF3 coils without current leads. Higher pressure drops observed are attributed to higher heat loads in the PF coils. It has been observed that the higher pressure demand of at least 40 g/s at 2.7–2.8 bar at 4.5 K with stand-alone cooling of PF coils. That will finally cause the higher pressure demand of at least 40 g/s at 2.7–2.8 bar at 4.5 K. In order to provide simultaneous cooling of the TF and PF coils, we have addressed several short term and long term plans by which we will be able to cool the SST-1 coils as follows:

- i) Cryogenic heat load minimization within the SST-1 by identifying the possible sources of heat loads and the feasibility to minimize them;
- ii) Introduction of efficient design of the current leads as “cold capacity saver”;
- iii) PF3 (U/L) coils operation with the VF coils to get elongated plasma in SST-1 by using NBI cryoplant of capacity 140 W at 4.5 K (short term). However, other PF coils will be cooled down to its best achieved low temperatures using existing 1350 W at 4.5 K helium plant.
- iv) Full-fledged PF coils operation with the TF coils by additional similar capacity helium plant (1500 W at 4.5 K); or,
- v) Designing a cold process using helium compressor or blower (when the heat load mitigation is achieved) and array of heat exchangers precooled by readily available liquid helium (long term).

In this paper, a brief review of the installed cryo-subsystems as well as the plans of simultaneous cool down of the TF and PF coils of SST-1 will be discussed.

Thermal-Hydraulic Characteristics Study of Superconducting Magnets of SST-1

U. Prasad¹, V. L. Tanna¹, P. Varmora¹, B. Parghi¹, C. Chakrapani¹, A. K. Sahu¹, B. Sarkar¹, D. Raju¹, and R. Srinivasan¹

¹*Institute for Plasma Research (IPR), Bhat, Gandhinagar, India*

Corresponding Author: U. Prasad, upendra@ipr.res.in

Steady-state Superconducting Tokamak (SST-1) magnet system consists of NbTi/Cu based CICC (cable-in-conduit conductor) wound toroidal (TF) and poloidal (PF) coils. The TF coils are wound in double pancakes (DP), whereas the PF coils are in DP as well as a layered winding scheme. These coils are cooled down up to 5 K using forced flow circulation of helium. The void fraction of helium within the square CICC (14.8 mm × 14.8 mm, 1.5 mm thick) is about 40%. There are 192 parallel hydraulic paths in the TF coils of lengths about 48 m each. The hydraulic path lengths of PF coils vary from 67–130 m.

Experience from several SST-1 cool down campaigns revealed that the PF coils have much higher hydraulic resistance, a factor of three as compared to its ideal expected value with reference to the TF coils. In order to improve the understanding on this issue, cool down trial of PF coils of similar hydraulic path lengths have been attempted with better control by dividing them in separate groups. The specific experimental campaign carried out to study the thermo-hydraulic behaviour of the SST-1 coils and to investigate the cause of the higher hydraulic resistances within the PF coils. The experiment conducted to measure the hydraulic resistance at room temperature and at subsequent possible lower temperatures. This dedicated experiment revealed that even at lower temperature of 5 K, the pressure drop within the PF coils winding packs are almost three times higher than the ideally expected values. Due to these facts, the simultaneous cooling down of the TF coils and PF coils has not been possible as the cryogenic plant has limited pressure head available in the range of 0.5–0.6 bar. Thermal hydraulic analyses of TF and PF coils have also been attempted to understand the pressure drop experimental data. In this paper, we report the thermal hydraulic behaviour of the TF and PF coils and its comparison with theoretical analysis.

Pump Characterization of 80 K Liquid Nitrogen Booster System for SST-1

G. Mahesuria¹, R. Patel¹, G. L. N. Srikanth¹, K. Patel¹, P. Shah¹, and V. L. Tanna¹

¹*Institute for Plasma Research (IPR), Bhat, Gandhinagar, India*

Corresponding Author: G. Mahesuria, gaurang@ipr.res.in

The Steady state superconducting Tokamak (SST-1) is medium size tokamak, which requires liquid nitrogen (LN₂) cooled 80 K bubble shields for reducing direct static heat load from room temperature to superconducting magnets system (SCMS). A dedicated liquid nitrogen booster system has been installed and commissioned to deliver 0.7 MPa, 80 K single-phase flow for uniform temperature distribution among all the 80 K shields of the SST-1 machine. The boosting system has been driven by three centrifugal cold pumps at liquid nitrogen services. These pumps have been tested at steady state mode around 0.5 MPa/80 K at the inlet and 0.7 MPa/80 K at discharge. These pumps can handle a pressure head in the range of 1.3–3.5 bar at the rated speed of 5500–7000 rpm respectively, over cryogenic stability. Each of the three pumps was characterized at their rated speed by evaluating various differential pressure and mass flow rates. The active current, apparent current and the actual voltages have been measured onset from the frequency controller. Based on these measurements, the efficiency of each pump have been deduced using the rated parameters and the efficiencies were obtained to be in the range of 32–45%, which is found to be at satisfactory level as guaranteed.

Overview of Recent Gyrotron R&D towards DEMO within EUROfusion Work Package Heating and Current Drive

K. A. Avramidis¹, G. Aiello¹, S. Alberti², P. T. Brücker¹, A. Bruschi³, I. Chelis⁴, T. Franke⁵, G. Gantenbein¹, S. Garavaglia³, J. Genoud², M. George¹, G. Granucci³, G. Grossetti¹, J.-P. Hogge², S. Illy¹, Z. C. Ioannidis¹, J. Jelonck¹, J. Jin¹, P. C. Kalaria¹, G. P. Latsas⁴, A. Marek¹, I. G. Pagonakis¹, D. V. Peponis⁴, S. Ruess¹, T. Ruess¹, T. Rzesnicki¹, T. Scherer¹, M. Schmid¹, D. Strauss¹, M. Thumm¹, I. G. Tigelis⁴, M. Q. Tran², C. Wu¹, A. Zein¹, and A. Zisis⁴

¹Karlsruhe Institute of Technology (KIT), Karlsruhe, Germany

²Swiss Plasma Center (SPC), École polytechnique fédérale de Lausanne (EPFL), 1015 Lausanne, Switzerland

³Istituto di Fisica del Plasma (IFP), Consiglio Nazionale delle Ricerche (CNR), 20125 Milan, Italy

⁴National Centre for Scientific Research "Demokritos" (NCSR),

National and Kapodistrian University of Athens, Greece

⁵EUROfusion Consortium, 85748 Garching, Germany

Corresponding Author: K. A. Avramidis, konstantinos.avramidis@kit.edu

Within the work package "Heating and Current Drive" (WPHCD), coordinated by the Power Plant Physics and Technology Department of EUROfusion, detailed studies are ongoing, which cover three different systems for plasma heating and current drive. These are, namely, systems using electron cyclotron waves, ion cyclotron waves, and neutral beam injection. The studies are in line with the European Fusion Roadmap towards a demonstration power plant (DEMO). The work breakdown structure of WPHCD, launched in 2014, includes branches dedicated to the conceptual design of the electron cyclotron system, as well to R&D focussed mainly on the microwave source, the gyrotron. Gyrotron R&D is a necessary step to bridge the gap between today's state-of-the-art gyrotrons and future gyrotrons for DEMO. Significant challenges are posed by the need for dual frequency (170/204 GHz) operation and/or frequency step-tunability of gyrotrons at a 2 MW power level, as well as by the requirements for significantly higher efficiency (> 60%) and level of reliability-availability--maintainability-inspectability (RAMI). Gyrotron R&D within WPHCD is addressing those challenges by exploring innovative, promising approaches. In addition, and in order to keep the R&D relevant with respect to possible baseline changes and to alternative reactor configurations towards a future power plant, efficient MW-class gyrotron operation at higher (~ 240 GHz) frequencies is also investigated. This paper gives an overview of the recent progress of gyrotron R&D within WPHCD, driven by the aforementioned challenges and conducted along the following lines: i) Experimental verification of coaxial gyrotron technology at longer pulses and design of a 2 MW 170/204/(238) GHz coaxial gyrotron; ii) investigations on multistage depressed collector concepts to increase the overall gyrotron efficiency; iii) development of large broadband diamond windows to allow for frequency step-tunability in steps of 2-3 GHz over a range of ~ 20 GHz; and, iv) advances on performance and reliability of gyrotron components to increase the RAMI level. Instrumental to the gyrotron R&D is the new Fusion Long Pulse Gyrotron Lab (FULGOR) at Karlsruhe Institute of Technology, a test stand able to support the development of continuous wave gyrotrons with a power of up to 4 MW at frequencies up to 240 GHz.

Assessment and Optimization of the Cavity Thermal Performance for the European Continuous Wave Gyrotrons

L. Savoldi¹, F. Albajar², S. Alberti⁶, K. A. Avramidis⁴, A. Bertinetti¹, F. Cau², F. Cismondi⁵, G. Gantenbein⁴, J.-P. Hogge⁶, Z. C. Ioannidis⁴, P. C. Kalaria⁴, A. Leggieri³, F. Legrand³, I. G. Pagonakis⁴, S. Ruess⁴, T. Rzesnicki⁴, and R. Zanino¹

¹NEMO group, Politecnico di Torino, Turin, Italy

²F4E: Fusion for Energy, ITER EU Centre, 08019 Barcelona, Spain

³Thales Electron Devices S.A., Velizy, France

⁴Karlsruhe Institute of Technology (KIT), Karlsruhe, Germany

²EUROfusion Consortium, 85748 Garching, Germany

⁶Swiss Plasma Center (SPC), École polytechnique fédérale de Lausanne (EPFL), 1015 Lausanne, Switzerland

Corresponding Author: L. Savoldi, laura.savoldi@polito.it

The large Ohmic load ($\sim 20 \text{ MW/m}^2$) of the wall of the resonant cavity of high-power gyrotrons, designed for tokamaks and stellarators for EC resonance heating and current drive to deliver a microwave power of the order of MW per unit, constitutes one of the major technological limiting factors, despite the small extension of the surface on which it is deposited. Even before reaching the material strength limits, the thermal deformation of the cavity is responsible for the gyrotron frequency shift with respect to its nominal operating condition.

The proper modelling of the gyrotron cavity during long-pulse operation, including the assessment of its cooling capability, is mandatory for predicting the gyrotron performance as well as for the interpretation of experimental results. In Europe, the multiphysics tool for the integrated simulation of the cavity (MUCCA) was developed in the last couple of years to compute the operating conditions of the gyrotron cavity accounting self-consistently for its thermal-hydraulic, thermo-mechanical and electrodynamic behaviour. Since the validation of the numerical tool against data collected from the tests of the European 170 GHz 1 MW CW prototype gyrotron tested at KIT, which is cooled with forced-flow subcooled water passing through a porous highly-conductive copper matrix, is giving encouraging results, MUCCA is being applied to push the design of the cavity cooling to more effective solutions.

In the paper, we present and discuss first the improvement of the cooling strategy of the cavity, aiming at decreasing the bell-shaped deformation by increasing the axial length of the porous region around the cavity. This solution has been implemented in the dual frequency 84/126 GHz, 1 MW, 2 s gyrotron, built for the upgrade of the TCV tokamak at SPC, EPFL, Lausanne and ready to be commissioned in the next months. Then, the ongoing design of a new cavity equipped with mini-channels is introduced, and the trade-off between increased cooling capability and increased pressure drop will be discussed. Finally, the status of the analysis of new cooling concept for the cavity, allowed by the presence of an insert inside the resonator in the so-called "co-axial" KIT gyrotron, is presented.

Operational Results and Troubleshooting in Current Feeder System for SST-1

A. Garg¹, H. Nimavat¹, P. Shah¹, K. Patel¹, D. Sonara¹, G. L. N. Srikanth¹, N. Bairagi¹, D. Christian¹, R. Patel¹, G. Mahesuria¹, R. N. Panchal¹, P. N. Panchal¹, R. Sharma¹, G. Purwar¹, J. C. Patel¹, and V. L. Tanna¹

¹*Institute for Plasma Research (IPR), Bhat, Gandhinagar, India*

Corresponding Author: A. Garg, agarg@ipr.res.in

Current feeder system (CFS) plays vital role in the superconducting (SC) fusion device, SST-1 (Steady state Superconducting Tokamak). As long pulse operation of the tokamak and fusion reactors require high magnetic field to confine and shape the plasma, which is fulfilled through the superconducting magnets operating at high current ratings. CFS serves as an interface between the power supply bus bars exposed at room temperature and SC magnets at 4.5 K temperature. This complex system has been designed to energize all the superconducting coils namely toroidal field (TF) and poloidal field (PF) of SST-1 maximum up to 10 kA rated current. An optimal design of its subsystems may significantly reduce the operational cryogenic cost in long term steady state operation of these coils. Further, reliable operations of vapour cooled current leads (VCCLs), 80 K thermal radiation shield systems, SC (Nb-Ti/Cu) bus bar feeders, high-vacuum systems and associated cryogenic circuits, etc., contribute towards successful and stable operations of CFS during the SST-1 plasma experiments. However, it has performed to excite the total 16 number of TF coils for longer duration in the total twenty-one campaigns so far. The operational performances in terms of cryogenic stability, current carrying capability have been validated in the excitation mode under long duration of steady state as well as in transient states such as current ramp up, ramp down and quench. This paper highlights the recent operational results with major milestone achieved as well as troubleshooting experiences since its successful commissioning in 2012.

Recent Progress in Developing Gamma Spectrometer in ITER

D. B. Gin¹, I. Chugunov¹, A. E. Shevelev¹, E. Khilkevitch¹, I. Polunovskii¹, V. Naidenov¹,
D. Doinikov¹, and M. Iliasova¹

¹*Ioffe Institute, St. Petersburg, Russian Federation*

Corresponding Author: D. B. Gin, pipha@mail.ru

Gamma-spectrometry is used at many tokamaks currently due to its ability to provide unique data on fast ions and runaway electrons in hot plasma [1]. Current report dedicated to the γ -ray spectrometer that will operate as a part of the ITER neutral particles analyser complex — one of the leading diagnostic systems in development progress. Conceptual and preliminary projects were approved after reviewing; preparation of detailed documentation with justifications of solutions for associated challenges - agenda for current works. Earlier development stages were regularly reported, particularly at IAEA FECs 2010–2016 [2]. Current phase of the work included components mockups manufacturing and various tests. Firstly it was studied radiation resistance using fast neutrons from ${}^9\text{Be}(d, n\gamma){}^{10}\text{B}$ reaction induced on SPBPu cyclotron beam. Study demonstrated high performance of the diagnostic port cell components during and after irradiation with the fluence of $1.1 \times 10^{13}/\text{cm}^2$, that corresponds to the whole lifetime of the system on ITER.

Another successfully completed task was the development and test of the approaches for transmitting signals and power lines to the Diagnostic Building while demanding reliable system operation while using long (100 m) cables. Connection schemes were tested together with newly developed DAQ solutions capable in proceeding with 400 s acquisition without data losses. New fast/real-time streaming, preprocessing and compression codes tried proved reliable collection and storage of events lists and raw data, particularly while using DAQ hardware from ITER catalogue. Preliminary studies of processing parameters optimization for high count rate modes typical for active ITER scenarios were carried out as well. Finally, updated MCNP models simulated to reveal possible deviation of the signal and background levels due to the alterations in design and estimated worst case defects in the radiation protection.

The views and opinions expressed herein do not necessarily reflect those of the ITER Organization. This work was supported in part by the RF State Contract No. N.4a.241.9B.17.1001. In MCNP calculations MCAM software was used.

References

- [1] V. G. Kiptily *et al.*, Plasma Phys. Contr. F., **48**(8), R59–R82 (2006).
- [2] D. Gin *et al.*, IAEA FEC–2016, Kyoto, Japan, [FIP/P4-15](#), (2016).

Timing and Synchronization for Integrated Operation of Large Volume Plasma Device

R. Sugandhi¹, P. K. Srivastava¹, P. K. Srivastava¹, A. K. Sanyasi¹, and L. M. Awasthi¹

¹*Institute for Plasma Research (IPR), Bhat, Gandhinagar, India*

Corresponding Author: R. Sugandhi, ritesh@ipr.res.in

The Large Volume Plasma Device (LVPD) [1] is a cylindrical shaped, linear device (length= 3 m, diameter= 2 m) dedicated in carrying out pulsed plasma experiments ($t_{\text{pulse}} \sim 9\text{--}50$ ms) relevant to fusion and magnetospheric plasma. In the recent past, investigations are switched from active wave plasma investigations to understanding of plasma turbulence of whistler and electron temperature gradient (ETG) nature, relevant to magnetospheric and fusion plasmas. In LVPD, efforts are in progress towards enhancing plasma duration from existing 9 ms to 50 ms in order to cater to the need of carrying out controlled experiments on ETG turbulence, a major source of plasma loss in fusion devices by using variation in density gradient scale lengths. For this purpose, a single console based system for LVPD operation using LabVIEW interface is developed, which will provide timing synchronization to the operation of different subsystems and helps in the implementation of a new machine operation and control system (MCS). The timing and synchronization of the heterogeneous I&C modules in terms of centralized clock, trigger, timing and interlocking is critical. The configured MCS consists of: a) PXI based high-end instrumentation system for diagnostics data acquisition [2]; b) Process automation system for multiple I&C controllers for slow process [3, 4]; and, c) data handling system. This paper discusses results of: i) state-of-the-art techniques for timing and synchronization of large physics experiments; ii) centralized timing and synchronization schema; iii) multimodule PXI module clock synchronization on multisegment PXIe bus; and, iv) timing and synchronization requirement of high current pulsed power supplies.

References

- [1] S. K. Mattoo *et al.*, Phys. Rev. Lett., **108**, 255007 (2012).
- [2] R. Sugandhi *et al.*, 7th Int. Conference on Cloud Computing, Data Science and Engineering, IEEE conference series, 804 (2017).
- [3] R. Sugandhi *et al.*, Fusion Eng. Des., **112**, 804 (2016).
- [4] R. Sugandhi *et al.*, Fusion Eng. Des., **115**, 49 (2017).

Design and Thermal Fluid Structure Interaction Analysis of Liquid Nitrogen Cryostat of Cryogenic Molecular Sieve Bed Adsorber for Hydrogen Isotopes Removal System

V. G. Devi¹, A. Sircar¹, and P. Lathiya¹

¹*Institute for Plasma Research (IPR), Bhat, Gandhinagar, India*

Corresponding Author: V. G. Devi, gayathri@ipr.res.in

Efficient design of tritium extraction system (TES) for the fuel cycle of any fusion reactor is very important to maintain the tritium breeding ratio and hence sustain the fusion reaction. Hydrogen isotopes removal system (HIRS) for Indian Tritium Breeder Blanket removes Q₂ (Q=H, D or T) and impurities using cryogenic molecular sieve bed (CMSB) adsorber at 77 K. The CMSB is maintained at liquid nitrogen temperature using a double walled cryostat made from SS-304L.

This paper describes the design and thermal fluid structure interaction (FSI) analysis of cryostat assembly for CMSB of HIRS. The coupled analysis performed in this work involves solving for the fluid domain and transferring the results to ANSYS Thermal-Static Structural set up to determine the stresses and displacement due to combined effects in the system. The mechanical design of the cryostat components is analytically performed using ASME codes. The velocity, pressure drop and time taken to cool the CMSB are determined by solving the fluid and energy equations in ANSYS Fluent Analysis System. The solutions are imported into ANSYS Thermal-Static Structural analysis system and the thermal-structural stresses and deformations are determined considering the temperature, pressure and acceleration loads. The space between inner and outer vessel is maintained at vacuum, which might lead to buckling. So, the critical buckling load multiplier factor is determined. The modal analysis is also performed to determine the fundamental frequency of vibration of the structure. These results would be used in fabricating the complete cryostat system for CMSB of HIRS.

Error Field Experiment and Analysis in SST-1

S. Dutta¹, Y. Paravastu¹, J. Dhongde¹, H. H. Chudasma¹, S. George¹, K. R. Dhanani¹, A. R. Makwana¹, C. Dodiya¹, P. Varmora¹, D. K. Sharma¹, A. K. Singh¹, U. Kumar¹, D. C. Raval¹, U. Prasad¹, Z. Khan¹, R. Srinivasan¹, and D. Raju¹

¹*Institute for Plasma Research (IPR), Bhat, Gandhinagar, India*

Corresponding Author: S. Dutta, sdutta@ipr.res.in

The SST-1 Tokamak has 16 toroidal field (TF) coils and 9 superconducting poloidal field (PF) coils. They have been assembled and the positioning inaccuracy of the coils is measured. The deviations in coil positions will generate error field and this will degrade the plasma performance. The error field produced by the TF coil misalignment can impact the plasma startup and it is necessary to quantify that error. The averaged toroidal field error can be measured and detected using an electron beam source inside tokamak vessel.

In SST-1 tokamak (major radius $R = 1.1$ m and minor radius $a = 0.2$ m), a low voltage electron beam source is mounted on the radial port at the midplane and can be moved to any point between $R = 0.95$ – 1.35 m. Cameras are mounted in radial port as well as top port to capture the deviation of the electron beam lines. The vacuum vessel is filled with helium gas which creates a luminescent trace of the electron beam due to impact excitation, creating a visual toroidal electron beam inside the vacuum vessel when the toroidal field coils are energized. This paper present the experimental observation of beam deviation with respect to various TF currents and then, the estimation of measured error field in SST-1 tokamak.

An attempt is also made to explain the electron beam deviations measured through these experiments. The deviations in R , φ and Z are incorporated into the numerical model of the SST-1 TF coils for the error-field estimation. Effect of other coils on this error field would also be analyzed. Error field profiles in both R and Z direction would be quantified, which would be a useful information for the plasma operation.

Maintenance Experience of 315 kW Electrical Motor of Helium Screw Compressor in 1.3 kW Helium Liquefier

D. Christian¹, G. Purwar¹, G. L. N. Srikanth¹, D. Sonara¹, K. Patel¹, P. Shah¹, J. C. Patel¹, R. N. Panchal¹, P. N. Panchal¹, R. Patel¹, G. Mahesuria¹, H. Nimavat¹, and V. L. Tanna¹

¹*Institute for Plasma Research (IPR), Bhat, Gandhinagar, India*

Corresponding Author: D. Christian, dikens@ipr.res.in

A 1.3 kW helium liquefier (HRL) system is installed and in operational at the cryogenic division of IPR since 2003. The Steady State superconducting Tokamak consists of superconducting magnets which are cooled by the HRL plant. Three 315 kW asynchronous induction motors are used to drive helium screw compressors of the HRL, therefore, it is essential to maintain the electrical motors in working condition for continuous tokamak experiment operation. This paper describes the electrical aspects of operation, maintenance and troubleshooting experiences with the electrical motors, including motor overhauling, motor winding insulation testing, no- and full-load testing, online temperature monitoring and motor cooling arrangements as well as vibration measurements of the compressor, motor and the skid.

Thermo-Structural and Heat Load Analysis of SST-1 Superconducting Coils

A. Tomar¹, R. Srinivasan¹, U. Prasad¹, P. Dutta¹, V. L. Tanna¹, D. Raju¹, B. R. Doshi¹, and H. S. Agravat¹

¹*Institute for Plasma Research (IPR), Bhat, Gandhinagar, India*

Corresponding Author: A. Tomar, arvind.kumar@ipr.res.in

Steady-State Superconducting Tokamak-1 (SST-1) has sixteen toroidal field (TF) and nine superconducting poloidal field (PF) coils. The TF coils are connected in series, whereas, the PF coils are operated individually in pulse mode. TF coils are operating up to 2.5 T in steady state condition but PF coils have hydraulic as well as heat load issues. In order to operate TF coils and PF coils simultaneously, and understand related issues, thermo-structural and heat load analysis have been initiated using ANSYS software. In these analysis, a CATIA model is prepared for SST-1, consisting of superconducting coils, support structure, 80 K cooling system and cryostat. Meshing is done using ANSYS. Initial condition and boundary conditions for temperature, pressure and other constraints in structure are given as inputs from experimental data. Steady state thermal and static structural modules of ANSYS were used for these analyses. Structural analysis of supports, cantilever ring, TF and PF coils, OICS at cryogenic temperatures were carried out. Validation of stresses and thermal contraction results were compared with analytical results, design and experimental results. Using a similar CATIA model, radiative heat loads on PF and TF magnet coils, conduction loads from OICS supports, hydraulic pipes, valves and other instrumentation and on cantilever support ring from ground supports was estimated using ANSYS software. The estimated heat loads due to residual gas conduction, radiation and conduction on various components are compared with analytically calculated and experimental results. Simulated and estimated heat loads are found comparable. Model preparation, meshing, boundary conditions and calculation methodologies will be discussed in this presentation.

Thermal Diffusivity Measurement of Functional & Structural Materials for Fusion Blanket Application

A. Shrivastava¹, C. S. Sasmal¹, N. Singh¹, and P. Chaudhuri¹

¹*Institute for Plasma Research (IPR), Bhat, Gandhinagar, India*

Corresponding Author: A. Shrivastava, aroh@ipr.res.in

Evaluation of thermal profile inside breeding blanket is an important aspect for fusion reactor. Due to thermal neutron flux during steady state operation of future fusion reactor, breeder materials in the blanket will be at elevated temperature up to 900°C. However, during ITER pulse operation with 1800 s pulse length, the maximum estimated temperature is ~ 650°C. India specific reduced activation ferritic martensitic (IN-RAFMS) steel has been considered as the structural material and various functional materials such as lithium titanate (Li_2TiO_3) pebbles as the tritium breeder and molten lead-lithium (PbLi) eutectic alloy as coolant and tritium breeder have been identified. Li_2TiO_3 pebbles of 80–90% density will be kept inside the canisters made of IN-RAFMS. To analyze the thermal profile inside the breeding blanket, several simulations are being performed. Thermal properties as a function of temperature and density are the major parameter to perform these simulations. It is therefore necessary to evaluate the thermal diffusivity and thermal conductivity of Li_2TiO_3 material as a function of temperature and density. The thermal diffusivity of the IN-RAFMS is also measured as a function of temperature from room temperature to 800°C. In the present investigation it is observed that thermal diffusivity of lithium titanate is decreasing from ~ 0.013 cm²/s at RT to ~ 0.006 cm²/s at 800°C. However thermal diffusivity of IN-RAFMS is decreasing from ~ 0.08 cm²/s at RT to ~ 0.035 cm²/s at 700°C which further increase to ~ 0.045 cm²/s at 800°C. In the present studies lead lithium samples are also measured from room temperature to its eutectic temperature. Simultaneous measurement of thermal conductivity and specific heat capacity of Li_2TiO_3 pellet, IN-RAFMS and lead lithium are also discussed in this paper.

Development of a Prototype Collaborative Robot for Fusion Remote Handling Applications

N. Rastogi¹, P. Dutta¹, R. R. K. Tiwari¹, M. Manuelraj¹, K. K. Gotewal¹, and J. P. Chauhan¹

¹*Institute for Plasma Research (IPR), Bhat, Gandhinagar, India*

Corresponding Author: N. Rastogi, naveen@ipr.res.in

Remote handling (RH) systems are highly challenging for application in the maintenance of fusion devices. The challenges include accurate handling of very heavy payloads using long cantilevered robotic arms with a dexterous manipulator. For the flexibility to execute dynamic tasks safely, these manipulators are typically controlled using a “man in the loop” architecture. Haptic systems with real-time force feedback integrated to full 3D virtual reality environment can enable the RH operators to have the sense of virtual presence. These are highly complex systems requiring integration of several technologies with a closed loop control system. One modern approach for handling such application can be by the development of collaborative robot mechanisms. A collaborative robot is a robotic device designed to assist human beings as a guide or assistor in a specific task. It can assist a human operator semiautonomously during the task as if it were a real mechanical tool and improves the manoeuvrability and the efficiency in the teleoperation. The collaborative robot mechanism with human-robot interactions in a shared workspace can be used as a training platform for the operators to check the feasibility and optimize the operation sequences for planning the RH tasks. This can be extremely beneficial to reduce the duration of maintenance cycles and to maximize the availability of the fusion device for plasma operations.

In this work, a concept is developed for a tokamak-relevant collaborative robot mechanism followed by implementation of a prototype system. The system uses back-drivable actuators with force feedback in the closed loop control system. High precision encoders are used to measure the joint movements and mapped in the control system. The system aims for the development of a low friction, efficient system for fusion RH requirements and can act as a training platform for the RH operators.

Design of the TF/PF Bus Bar Layout and its Connections with Current Feeder System of SST-1 Tokamak

B. R. Doshi¹, S. Jayswal¹, P. Santra¹, A. Garg¹, V. L. Tanna¹, K. Vasava¹, M. Gupta¹,
D. Gupta¹, and S. Nair¹

¹*Institute for Plasma Research (IPR), Bhat, Gandhinagar, India*

Corresponding Author: B. R. Doshi, doshi@ipr.res.in

Steady state Superconducting Tokamak (SST-1) is an indigenously built working experimental tokamak at IPR. The primary magnetic configurations and plasma shaping magnetic requirements are provided by superconducting magnet systems (SCMS) comprising of sixteen superconducting D-shaped toroidal field (TF) magnets and nine superconducting poloidal field (PF) magnets together with a pair of resistive PF coils inside the vacuum vessel. The current feeding system of TF & PF magnets consists of power supplies, current carrying bus bar and its connections with current leads at room temperature on one side and other side at 4.5 K with SCMS. Current lead chamber (CLC), which contains the superconducting current leads of toroidal field (TF) and poloidal field (PF) coils inside the vacuum chamber, has to be connected outside the vacuum chamber to the current feeder bus bars at room temperature. These bus bars are required to be supported with the proper support structure without any interference with the nearby components. The design of the bus bar layout along with its support structures to withstand the static and electromagnetic load and bus bar connections with current feeder system will be presented in this paper.

Preventive Measures to Avoid Electrical Arcing Incidences in SST-1 PF Current Leads

S. Roy¹, N. Kumar¹, M. Ghate¹, D. Kanabar¹, U. Prasad¹, and R. Srinivasan¹

¹*Institute for Plasma Research (IPR), Bhat, Gandhinagar, India*

Corresponding Author: S. Roy, swati@ipr.res.in

Steady-State Superconducting Tokamak-1 (SST-1) has 16 toroidal field (TF) and 9 superconducting poloidal field (PF) coils rated for 10 kA DC. The TF coils are connected in series and operated in DC condition, whereas the PF coils are operated independently in pulse mode. The SST-1 current feeder system (CFS) houses nine pairs of PF superconducting current leads and one pair of TF superconducting current leads. The SST-1 CFS had observed arcing incidences during OT discharge in past SST-1 campaigns. Similar arcing incidences have also been observed in other tokamaks devices also like KSTAR, W7-X, and EAST. The conditions which led to the electrical arcing in SST-1 CFS, thereby resulting in severe damages to the PF current leads and helium hydraulic lines will be presented in this paper. As an important preventive measure to avoid such arcing at PF current leads during SST-1 operation, insulation strengthening processes of the PF current leads have been initiated to increase the voltage isolation capability of the PF current leads. In the view of same, development of an insulation scheme using combination of polyimide and GFRP along with DGEBA epoxy resin and its validation at lab scale has been carried out. It involves study of chemical kinetics of resin towards curing cycle, electrical and mechanical characterizations of insulation samples at room temperature as well as at LN₂ temperature. A breakdown voltage of > 25 kV DC has been successfully achieved with ~ 1.2 mm of insulation thickness at lab scale insulation samples. In order to validate the proposed insulation system under specified helium Paschen conditions, a lab scale setup considering SST-1 operational requirements has been developed. The operation, salient features of test setup and results will also be presented in this paper. The progressive development of insulation system and validation from prototype scale to half-dummy current lead scale and thereafter implementation on actual PF current leads will also be presented in this paper.

Model Development and Electromagnetic Analysis of Vertical Displacement Event for CFETR Helium Cooled Solid Blanket

H. Chen¹, Q. Xu¹, and C. Jin¹

¹*University of Science and Technology of China, Hefei, Anhui, People's Republic of China*

Corresponding Author: H. Chen, hlchen1@ustc.edu.cn

As one of typical blanket concepts for Chinese Fusion Engineering Test Reactor (CFETR), a conceptual structure of helium cooled solid breeder (HCSB) blanket was designed by USTC. Considering that electromagnetic load is one of the main concerns for the blanket module, a FEM (finite element method) model of the HCSB was developed and the electromagnetic analysis of the blanket module was implemented using a finite element analysis (FEA) software called MAXWELL. For transient electromagnetic analysis with the vertical displacement event (VDE), a more accurate model where the plasma described by 69 filaments was adopted and the whole fifteen blankets lying in a toroidal-poloidal section were explored. The research of the ferromagnetic effect of RAFM steel was carried out and the magnetic field, induced eddy currents, the magnetic force were computed and analyzed. The analysis results show that ferromagnetic effect broadened the range of magnetic field of the model and strengthened eddy current effects. In addition, the maximum value of the eddy current density was 71.2 MA/m^2 and the maximum magnitude of the electromagnetic forces was 1409.0 kN under the ferromagnetic effect.

Key Considerations in the Power Extraction from Fusion Reactors

P. Prajapati¹, S. B. Padasalagi¹, and S. P. Deshpande¹

¹*Institute for Plasma Research (IPR), Bhat, Gandhinagar, India*

²*Homi Bhabha National Institute (HBNI), Anushakti Nagar, Mumbai 400094, India*

Corresponding Author: P. Prajapati, piyush.prajapati@ipr.res.in

As the demand for energy grows, futuristic energy sources like the DT thermonuclear fusion using the magnetic confinement scheme called tokamak are being researched upon. It is generally presumed that a fusion blanket surrounds the tokamak plasma which absorbs the fusion neutrons, using their energy to convert into heat energy and nuclear transmutation with lithium to regenerate the lost tritium. Since the focus of the fusion community is largely on design, construction, operation and research of fusion devices and plasma performance, the engineering study (in-depth) of how is one going to take the power out from the blankets, through the complex geometry, all the way up to the steam generator (SG) has hardly received any attention. It is almost assumed without any reason that “if we have the heat source, the rest is well known”. To some extent, this state of affairs could also be due a belief that such reactors would be realized only in the far future.

This paper presents an in-depth look at the key considerations for transporting the power from the blankets to the SG. The main purpose of the study is to develop and compare conceptual designs for the above, based on engineering considerations. The problem involves three main steps: a) transport of heat from the blanket-outlet up to the SG; b) heat-exchange within SG; and, c) return of the blanket coolant to the blanket-inlet. Three different coolants seem to have been considered currently by the fusion blanket community: water, helium and lead-lithium eutectic (PbLi). However, it appears that an additional heat-exchanger (HX) will be needed for PbLi (which is most likely to be with helium) before the heat is transferred to SG. From this point of view, both the concepts (PbLi and He cooled) finish in requiring a design of SG based on He-water HX.

Using the current available designs of fusion power plants; to some extent the layout of ITER and the consideration of SG for fission power reactors, we have developed some conceptual designs for extraction of power. A computational tool has been developed to efficiently determine the thermo-hydraulic parameters to be verified by detailed ANSYS calculations.

Development and Experiment of PbLi Facilities for Fusion Nuclear Technology

Q. Huang¹, Z. Meng¹, Z. Zhu¹, W. Huang¹, Z. Xiao¹, D. Zhou¹, and D. Chen¹

The FDS Team

¹Key Laboratory of Neutronics and Radiation Safety,
Institute of Nuclear Energy Safety Technology, CAS, Anhui, People's Republic of China

Corresponding Author: Q. Huang, qunying.huang@fds.org.cn

The liquid lead-lithium (PbLi) blanket concept has become a promising design for fusion DEMO and power plant reactors. To promote the successful application of fusion energy, some R&D activities on the PbLi blanket have been performed, such as structure material corrosion, thermal hydraulics, magnetohydrodynamic (MHD) effect, coolant impurities technology and LOCA/LOFA, etc. Therefore, it is centrally important to develop an experimental facility to perform the out-of-pile experiments and studies on these key issues before the engineering design of fusion reactor.

Series DRAGON PbLi experimental loops have been developed and constructed in China, including the thermal convection PbLi loops DRAGON-I (500°C) and DRAGON-II (700°C), and the multifunctional liquid PbLi experimental loop DRAGON-IV (800°C, 2 T). To perform the integrated experiments under the multiphysical field conditions for DEMO blanket, the dual coolant thermal hydraulic integrated experimental loop DRAGON-V was designed and finished the construction in 2017. It is composed of a lead-lithium loop and a helium gas loop. The maximum flow rate of PbLi and helium gas pressure are 40 kg/s and 10.5 MPa, respectively. The magnetic field is designed up to 5 T. It is a unique test platform for the R&D of thermal hydraulic, material corrosion, purification technology and safety issues of liquid PbLi blanket to provide the necessary database for ITER-TBM and DEMO-TBM.

At present, some experiments have been conducted to investigate the key issues of PbLi technologies, such as corrosion behaviours of candidate structural materials with and without magnetic field, the PbLi alloy fabrication with high-level controlling of the impurities, purification technology of liquid PbLi coolant in the loop, MHD pressure drop test, and the interaction for typical coolants during accidents, etc. The results can support the development of the in-pile key techniques and components and the engineering design for ITER-TBM and DEMO-TBM, and also contribute to the final application of the advanced reactors.

Implementation of the Spherical Tokamak MEDUSA-CR: Stage 1

J. Mora-Meléndez¹, V. I. Vargas-Blanco¹, L. A. Araya-Solano¹, A. M. Rojaz-Loaiza¹,
I. Monge¹, J. F. Rojas¹, N. Piedra-Quesada¹, and J. M. Arias-Brenes¹

¹Plasma Laboratory for Fusion Energy and Applications, Instituto Tecnológico de Costa Rica, Cartago, Costa Rica

Corresponding Author: J. Mora-Meléndez, jamora@itcr.ac.cr

The low aspect ratio Spherical Tokamak (ST) MEDUSA (Madison Education Small Aspect Ratio Tokamak) is currently being recommissioned at the Instituto Tecnológico de Costa Rica, after it was donated by the University of Wisconsin-Madison, USA. The main characteristics of this magnetic confinement device are described as follows: plasma major radius of $R_o < 0.14$ m, plasma minor radius $a < 0.10$ m, plasma vertical elongation 1.2, toroidal field at the geometric centre of the vessel $B_t < 0.5$ T, plasma current $I_p < 40$ kA, $n_e(0) < 2 \times 10^{20}/\text{m}^3$, central electron temperature $T_e(0) < 140$ eV, discharge duration is < 3 ms, top and bottom rail limiters, and natural divertor D-shaped ohmic plasmas [1]. Training students and researchers is the main goal as for ST MEDUSA-CR, to merge knowledge between physics and engineering in order to address relevant concepts for spherical and conventional tokamaks [2].

Currently diverse topics are being addressed in the first engineering stage of the MEDUSA-CR. For the vacuum system design there has been developed a corresponding documentation process of the implementation and testing vacuum, also it is present a new design of the vacuum vessel made of stainless steel. The design of the new injection system, entirely developed to accomplish the spherical tokamak's requirements has been successfully tested. The electric current control of the coils presents a possible upgrade to converting ST MEDUSA-CR to AC mode. Additionally, a MHD equilibrium simulation for the original configuration of the device has been performed using a code named Fiesta; which was facilitated by Geoffrey Cunningham from Culham Centre for Fusion Energy (CCFE) [3, 4].

References

- [1] G. D. Garstka, PhD thesis, University of Wisconsin at Madison, September 1997.
- [2] V. I. Vargas *et al.*, 23rd IAEA Technical Meeting on Research Using Small Fusion Devices (23rd TM RUSFD), March 29–31 2017, Santiago, Chile.
- [3] V. I. Vargas *et al.*, IAEA FEC–2016, Kyoto, Japan, [EX/P4-47](#), (2016).
- [4] V. I. Vargas *et al.*, 16th Latin American Workshop on Plasma Physics (LAWPP), 4–8 September 2017, Mexico City, Mexico.

Early Definition of the Maintenance Plan Is Essential to Achieve an Economic EU DEMO

O. Crofts¹, A. Loving¹, R. Gowland¹, and G. Keech²

¹*Remote Applications in Challenging Environments (RACE), United Kingdom Atomic Energy Authority, Culham Science Centre, Abingdon, UK*

²*EUROfusion Consortium, Power Plant Physics & Technology (PPPT), Boltzmannstraße 2, Garching, Germany*

Corresponding Author: O. Crofts, oliver.crofts@ukaea.uk

The development of fusion as a viable power source is moving from the science driven design of experimental devices to the engineering design considerations required to develop a feasible power plant. An effective maintenance plan is essential because the time in maintenance is potentially very large. To be effective, a maintenance plan must be outlined early in the plant design because it has two key requirements that must be embedded from the outset of the plant layout. First it requires the efficient transport of components and equipment around the plant through corridors, shield doors and contamination control systems using the most appropriate transport system. Second it requires maintenance-oriented strategies to reduce the maintenance burden and to achieve the maintenance in a shorter time, with lower risk of failure and with simpler recovery scenarios. Work is therefore required at the preconcept design stage to define the maintenance plan so that the design driving factors required to enable the plan can be embedded in the plant design from the outset. This paper will describe this work, including the key transport system that has been proposed for the transfer of components and equipment to and from the tokamak using ceiling mounted cranes and dexterous manipulator systems. A qualitative comparison will be made between the proposed system and an alternative cask-based system will be made. The paper will also briefly describe some of the proposed maintenance-oriented strategies and development and testing work that is being carried out to mitigate the technical risks associated with the proposed maintenance plan.

This work has been carried out within the framework of the EUROfusion Consortium and has received funding from the Euratom research and training programme 2014–2018 under grant agreement No. 633053 and from the RCUK Energy Programme, grant number EP/P012450/1. The views and opinions expressed herein do not necessarily reflect those of the European Commission.

The Influence of Toroidal Magnetic Field Growth on Plasma Performance in the Spherical Tokamak Globus-M/-M2

V. B. Minaev¹, V. K. Gusev¹, Y. V. Petrov¹, N. V. Sakharov¹, N. N. Bakharev¹, E. N. Bondarchuk², V. V. Bulanin³, F. V. Chernyshev¹, A. A. Kavin², N. A. Khromov¹, E. O. Kiselev¹, G. S. Kurskiev¹, A. D. Melnik¹, A. B. Mineev², I. V. Miroshnikov¹, A. N. Novokhatsky¹, K. Y. Oshuev¹, M. I. Patrov¹, A. V. Petrov³, P. B. Shchegolev¹, A. E. Shevelev¹, A. D. Sladkomedova¹, V. V. Solokha¹, A. Y. Telnova¹, V. A. Tokarev¹, S. Y. Tolstyakov¹, V. I. Varfolomeev¹, A. Y. Yashin³, and E. G. Zhilin⁴

¹Ioffe Institute, St. Petersburg, Russian Federation

²D. V. Efremov Institute of Electrophysical Apparatus (JSC-NIIEFA), St. Petersburg, Russian Federation

³Peter the Great St. Petersburg Polytechnic University, St. Petersburg, Russian Federation

⁴Ioffe Fusion Technology Ltd., St. Petersburg, Russian Federation

Corresponding Author: V. B. Minaev, vladimir.minaev@mail.ioffe.ru

Globus-M was a compact spherical tokamak with unique features such as plasma column tightly fitted into the vacuum vessel and high NB heating power density. The toroidal magnetic field in it was limited to 0.5 T. Globus-M2 is an upgraded version of Globus-M machine with substantial increase of engineering parameters (the toroidal magnetic field up to 1 T, the plasma current up to 0.5 MA). The goal of the scientific programme is to achieve the improved plasma performance with subfusion temperature value and collisionality much less than unity in compact geometry and to get closer to the operating conditions of the compact fusion neutron sources. The first plasma experiments ought to be started in 2018.

In the final Globus-M experimental campaign the toroidal magnetic field and the plasma current were raised by 25% as compared with routine parameters. As a result an overall improvement in plasma performance was observed. The plasma total stored energy and the energy confinement time grew by about 30% in the discharges with moderate density. DD beam-plasma neutron rate increased significantly at the same heating power. The main reasons for this effect, in order of importance, are electron temperature rise and fast ion confinement improvement. Decrease of first orbit, sawtooth-induced and TAE-induced fast ion losses was recorded. The energy confinement time growth proportionally to the toroidal magnetic field was observed. The energy confinement time and power decay length scalings, acquired in the experiments, are in a reasonable agreement with MAST and NSTX data. The experiments were continued on the Globus-M2 tokamak with substantially increased values of the toroidal magnetic field and the plasma current.

Progress in Design and Fabrication of Current and Helium Feeding System for JT-60SA Superconducting Coils

K. Kizu¹, K. Kamiya¹, H. Murakami¹, K. Natsume¹, K. Usui¹, H. Ichige¹, A. Honda¹, M. Sato¹, K. Fukui¹, Y. Kashiwa¹, K. Tsuchiya¹, K. Kawano¹, and T. Isono¹

The JT-60SA Team

¹*National Institutes for Quantum and Radiological Science and Technology (QST),
Naka Fusion Institute, Naka-shi, Ibaraki-ken, Japan*

Corresponding Author: K. Kizu, kizu.kaname@qst.go.jp

To realize JT-60SA of the largest superconducting tokamak device in the world, the current feeder and helium pipes have been designed so as to have the flexible structure with bend and to be supported with octagonal shape. The control system for feeding current and helium has been also developed to operate 18 toroidal coils, six equilibrium coils and a central solenoid. The engineering solutions developed for JT-60SA can be adopted for future fusion devices. This paper reports the progress in the design and fabrication of the current and helium feeding system to be used in JT-60SA.

Noninvasive Plasma Density Measurement in a 13.56 MHz Magnetized Capacitive Coupled RF Discharge

S. Binwal¹, J. Joshi², S. K. Karkari², and L. Nair¹

¹*Jamia Millia Islamia (A Central University), Jamia Nagar, New Delhi, 110025, India*

²*Institute for Plasma Research (IPR), Bhat, Gandhinagar, India*

Corresponding Author: S. Binwal, binwal.shikha@gmail.com

Capacitive coupled plasmas (CCP) have unique applications in microelectronic industries, besides they are also important in plasma interaction with material surfaces, such as near field region of ICRF antenna infusion devices. Systematic studies of these plasmas are concurrently carried in laboratory plasma devices to develop models to explain the anomalous behaviour of plasma sheath interactions. Plasma diagnostics plays a crucial role in providing necessary input data for the verification of these models. Recently a capacitive coupled discharge with externally imposed transverse magnetic field has been developed. It has been found that the external magnetic field greatly modifies the discharge characteristics, by introducing $E \times B$ drifts adjacent to the discharge plates.

Direct measurement of plasma parameters in CCP discharge is primarily difficult due to very large amplitude oscillation in plasma potential. To certain extent, a triple probe is convenient as it is routinely used in the strongly magnetized edge plasma region in tokamaks. However its application in radiofrequency plasmas needs careful design of electrical feedthrough and measurement of voltage and currents using external circuits. An alternative method to determine the average plasma density can be achieved by looking at the impedance characteristics of the discharge. The discharge impedance is the measure for the plasma conductivity, which in turn determines the plasma density. Recently electrical circuit analysis has been applied to estimate the collisionality in magnetized CCP discharge. In this paper, we show that the plasma density can also be determined using this technique. The obtained results have been compared with a triple Langmuir probe and the results are shown to be in good qualitative agreement.

Advanced Assembly Technology of the Superconducting Coils in JT-60SA Tokamak

Y. Shibama¹, K. Masaki¹, J. Yagyu¹, F. Okano¹, K. Tsuchiya¹, H. Murakami¹, K. Kizu¹, A. Sakasai¹, M. Hanada¹, S. Davis², and V. Tomarchio²

The JT-60SA Team

¹*National Institutes for Quantum and Radiological Science and Technology (QST),
Naka Fusion Institute, Naka-shi, Ibaraki-ken, Japan*

²*F4E: Fusion for Energy, EUROfusion Consortium, 85748 Garching, Germany*

Corresponding Author: Y. Shibama, shibama.yusuke@qst.go.jp

The JT-60SA is a superconducting coil tokamak, which is the project combined with Japanese national project and Japan-EU Satellite Tokamak Programme. The coil system is composed of 18 toroidal field (TF) coils, six equilibrium field (EF) coils and a centre solenoid (CS). The size of the TF coil is 7.5 m high and 4.6 m wide. The EF coil structures are 12 m in the maximum diameter. These large components, which are over 10 m size, must be assembled with high accuracy. In particular, a tolerance of ± 1 mm is required for TF coil assembly. In order to achieve such high accuracy at large components assembly, the following techniques are used: 1) 3D CAD is used for the confirmation of the fabrication tolerances, the designed position and interference at the intermediate assembly route; 2) laser tracking is used for the positioning of the large components to know three dimensional data and to confirm the data in 3D CAD quickly; and, 3) special jigs are used for the positioning of the components. The assembly procedure for the coil system including the final sector of vacuum vessel (VV) and thermal shield (TS) is established considering the above technique.

The full-scale assembly of the JT-60SA started in 2013. In the actual assembly of the TF coil, all operation are proceeding successfully. This advanced technology can be also applied for the next machine, i.e., ITER.

A Toroidal Confinement Facility Study and Eventual Experimental Device to Investigate a Range of Liquid Metal Divertor and First-Wall Concepts

T. Brown¹, J. E. Menard¹, M. A. Jaworski¹, R. Majeski¹, and Y. Zhai¹

¹*Princeton Plasma Physics Laboratory (PPPL), Princeton, NJ 08540, USA*

Corresponding Author: T. Brown, tbrown@pppl.gov

A toroidal confinement facility study and development of a characteristic experimental device was undertaken to investigate a range of liquid metal divertor and first-wall concepts build on past and expected results from liquid metal experiments: the Lithium Tokamak Experiment (LTX), the National Spherical Torus Experiment Upgrade (NSTX-U), and the Experimental Advanced Superconducting Tokamak (EAST). The device configuration is driven by the need to adequately provide the concept details that depicts component features, space allocations, plumbing arrangements, thermal insulation, etc., of liquid metal systems. Of equal importance is to validate that the developed designs are upward compatible to exist within a blanket system of a DEMO or an eventual fusion power plant design. The proposed studies also builds upon recent low-A High Temperature Superconductor (HTS) tokamak pilot plant studies that incorporated a liquid metal divertor for high-heat-flux mitigation as a means of reducing poloidal field coil current and simplifying the magnet layout and maintenance schemes. Tokamak aspect ratios in the range of $A = 1.8$ to 2.5 would be considered based upon recent pilot plant studies indicating this range would be optimal for fusion power production if high-current-density HTS magnets were utilized. This aspect ratio range is subject to change pending the results of the first 1 to 1.5 years of the study. A current snapshot of a 1 m, 2.4 m aspect ratio device configuration is illustrated in the included figure incorporating HTS magnets and a fast flowing liquid metal divertor/FW system.

This paper will provide the design details of the toroidal confinement facility: defining the general arrangement of the device configuration, and detailing the HTS magnet system and all LM system details investigated along with any engineering defined limitations or issues that may be expected when attempting to migrate the designs into the environment of a DEMO operated blanket defined system.

Conceptual Design of a Compact Helical Fusion Reactor FFHR-c1 for the Early Demonstration of a Year-Long Electric Power Generation

T. Goto¹, J. Miyazawa¹, H. Tamura¹, T. Tanaka¹, R. Sakamoto¹, C. Suzuki¹, R. Seki¹, S. Satake¹, M. Nunami¹, M. Yokoyama¹, N. Yanagi¹, and A. Sagara¹

The FFHR Design Group

¹National Institute for Fusion Science (NIFS), Toki, Gifu, Japan

Corresponding Author: T. Goto, goto.takuya@nifs.ac.jp

Conceptual design of a compact LHD-type helical fusion reactor FFHR-c1 has been conducted. This design focusses on a year-long electric power generation with as small a reactor size as possible by adopting the operation with auxiliary heating and innovative ideas for the design of engineering system. This design ensures the path to helical commercial power plants through the examination of confinement scaling and steady-state operation test of engineering components. Though intensive R&Ds are needed, the innovative ideas provide more options and increase the probability of solving critical issues of fusion reactors: accommodation of high heat and particle load on the divertor, construction and maintenance within a reasonable period.

The candidate design point of FFHR-c1 has been identified using the systems code HELIO-SCOPE. A smaller reactor with the same plasma confinement property can be realized by increasing the magnetic field. However, the size reduction is limited by the decrease of the thickness of the neutron shield in the blanket system. In this regard, the adoption of supplementary helical coils can increase the blanket space by $\sim 15\%$. Finally, the design point with the major radius of 10.92 m, the magnetic field on the helical coil winding centre of 7.3 T and the fusion gain $Q \sim 10$, which can achieve positive net electric power with a minimum reactor size, have been selected.

To confirm the feasibility of the core plasma design, integrated physics analysis has been conducted. The magnetic configuration with a high aspect ratio and inward-shifted magnetic axis position was assumed. As a result, $Q \sim 15$ can be achieved within the operation regime that has already been confirmed in the LHD experiment: the Mercier index $D_I < 0.3$ at the $n/m = 1/1$ rational surface and the neoclassical energy loss lower than a half of the total absorbed power.

Although there are some issues to be solved (e.g., design of the helical coils with a current density of $> 40 \text{ A/mm}^2$, achievement of the peak β value of $\sim 3\%$ with an inward-shifted configuration), this comprehensive study has shown the design feasibility of a compact LHD-type helical reactor that can satisfy the requirements on Japanese fusion DEMO: steady-state electricity generation above several hundred MW, tritium fuel self-sufficiency and practical availability.

Negative Ion Beam Source Physics as a Complex System: Identification of Main Processes and Key Interdependence

V. Antoni¹, P. Agostinetti¹, M. Cavenago², G. Chitarin¹, A. De Lorenzi¹, N. A. Ferron¹, S. Longo³, E. Sartori¹, G. Serianni¹, E. Spada¹, S. Suweis⁴, and P. Veltri¹

¹*Consorzio RFX, Associazione EURATOM-ENEA sulla Fusione, Padova, Italy*

²*Istituto Nazionale di Fisica Nucleare (INFN), Laboratori Nazionali di Legnaro, Legnaro, Italy*

³*Dipartimento di Chimica, Università degli studi di Bari Aldo Moro, Bari, Italy*

⁴*Physics and Astronomy Dept. "G. Galilei" & CNISM, INFN, Università di Padova, Padova PD, Italy*

Corresponding Author: V. Antoni, gianluigi.serianni@cnr.it

A key component of ITER is the heating neutral beam injector (NBI) system, expected to be the main source of the input power necessary to reach fusion conditions. The nominal parameters of the ITER NBI (40 A negative H^-/D^- ion beam accelerated to 1 MeV and then neutralized) are so challenging that they require extensive international research and development activities. Reliable operation of NBI for one hour remains an open issue: it results from several processes, mutually interacting in a nonlinear way.

In this contribution, complex network theory is applied to the physical processes (nodes) affecting generation, extraction and acceleration of negative ions in the simpler case of the NIO1 experiment, operating at Consorzio RFX. The number of driver nodes is four; preferential matching identifies multiple sets of driver nodes. The most frequently identified driver nodes are interpreted as the most relevant processes: deflection of H^- in the PG-EG gap depends on meniscus asymmetry, linked due to nonuniform ion flow in the plasma, as experimentally found; gas pressure in the vessel drives the compensation of the beam space charge, allowing the beam to propagate with no divergence increase. Evidence of the latter driver node spurred the investigation of the beam-generated plasma by means of a retarding field energy analyser and numerical simulations.

Two surface phenomena will be discussed in the contribution, as they are very important for the NBI operation and must be included in the complex network. Initial H^- production is enhanced by evaporating caesium over the source wall material. The arrangement of the caesium atoms is correctly simulated by molecular dynamics: the resulting imperfect film is found to be affected by moderate temperature, which allows redistribution of caesium, whereas higher temperatures disorder again the film leading to evaporation. Another key role played by surfaces regards high voltage holding, for which a novel model, based on the assumption of a dielectric layer (oxidized metal), is proposed. When the dielectric strength of the layer is exceeded, quantum mechanical computations provide the current, which acts as a trigger for breakdown.

JET Upgraded Diagnostic Capabilities and Scientific Exploitation in Support of Deuterium-Tritium Operation

J. Figueiredo^{1,2}, A. Murari^{1,3}, C. Perez Von Thun^{1,4}, D. Marocco⁵, M. Tardocchi⁶, F. Belli⁵, M. García Muñoz⁷, A. Silva², T. Craciunescu⁸, P. Blanchard⁹, I. Balboa¹⁰, N. Hawkes¹⁰, I. S. Carvalho², B. Tál¹¹, J. Bernardo^{2,12}, I. Zychor¹³, and V. G. Kiptily¹⁰

The JET Contributors

¹EUROfusion Programme Management Unit Culham, Culham Science Centre, Abingdon, UK

²Institute of Plasmas and Nuclear Fusion (IPNF), Instituto Superior Técnico (IST), 1049-001 Lisbon, Portugal

³Consorzio RFX, Associazione EURATOM-ENEA sulla Fusione, Padova, Italy

⁴Institute of Energy and Climate Research, Forschungszentrum Jülich, Jülich, Germany

⁵ENEA C. R. Frascati, Dipartimento FSN, Frascati, Italy

⁶Istituto di Fisica del Plasma CNR, EURATOM-ENEA-CNR Association, Milano, Italy

⁷Universidad de Sevilla, Seville, Spain

⁸National Institute of Laser, Plasma and Radiation Physics (INFLPR), Bucharest, Romania

⁹Swiss Plasma Center (SPC), École polytechnique fédérale de Lausanne (EPFL), 1015 Lausanne, Switzerland

¹⁰Culham Centre for Fusion Energy (CCFE), Culham Science Centre, Abingdon, UK

¹¹Wigner Research Center, Association EURATOM, Budapest, Hungary

¹²JET Exploitation Unit, Culham Science Centre, Abingdon, UK

¹³National Centre for Nuclear Research (NCBJ), Świerk, Poland

Corresponding Author: J. Figueiredo, joao.figueiredo@euro-fusion.org

JET upcoming deuterium-tritium campaign, DTE2, is scheduled to take place before the end of 2020. From a point of view of diagnostics developments, for many years JET diagnostics have been upgraded in order to provide adequate support for the scientific exploitation of a DT campaign, with particular attention to the experimental and operational conditions expected during DT campaigns. Diagnostic capabilities relevant for burning plasmas conditions have been specifically targeted with the focus mainly on fast ions, instabilities, neutron, γ , ion temperature and operations support. JET diagnostic capabilities and obtained experimental results relevant for the scientific exploitation of the upcoming DT operations are discussed.

This work has been carried out within the framework of the EUROfusion Consortium and has received funding from the Euratom research and training programme 2014–2018 under grant agreement No. 633053. The views and opinions expressed herein do not necessarily reflect those of the European Commission.

Installation and Commissioning of 80 K Liquid Nitrogen Booster System

R. Patel¹, G. Mahesuriya¹, G. L. N. Srikanth¹, D. Christian¹, K. Patel¹, H. Nimavat¹, P. Shah¹, P. N. Panchal¹, R. N. Panchal¹, D. Sonara¹, G. Purwar¹, J. C. Patel¹, and V. L. Tanna¹

¹*Institute for Plasma Research (IPR), Bhat, Gandhinagar, India*

Corresponding Author: R. Patel, rpatel@ipr.res.in

The static heat loads on the 80 K thermal shields of SST-1 will be removed using single phase liquid nitrogen cooling at 0.7 MPa. The single phase liquid nitrogen is obtained using 80 K liquid nitrogen booster system. The booster system is in the form of three storey building with pump cryostat at bottom, subcooler vessel cryostat at middle and pressurized vessel cryostat at upper. Boosting system utilized three centrifugal cold pumps at liquid nitrogen services among them two remain in operation and one remain in cold standby mode as redundant. Preassembly leak tightness test at individual components level were carried out before final integrated installation of booster system. Functional validation of booster system as per defined PFD was carried out after installation at IPR site. The booster system's different operation modes, such as purge, LN₂ filling, first phase cool-down, second phase cool-down, steady state and warm up, were successfully tested along with their process alarms, safety interlocks and failure events. The booster system performance test was conducted using system inbuilt dummy load of 20 kW at 80 K, which is similar to actual heat load on SST-1 thermal shields from ambient. The 80 K booster system installation and commissioning detail is presented in this paper.

High Power Helicon Antenna Design for DIII-D

R. C. O'Neill¹, M. W. Brookman¹, J. S. deGrassie¹, B. Fishler¹, M. LeSher¹, C. P. Moeller¹,
C. Murphy¹, A. Nagy², M. Smiley¹, J. F. Tooker¹, and H. Torreblanca¹

¹General Atomics, San Diego, CA 92186, USA

²Princeton Plasma Physics Laboratory (PPPL), Princeton, NJ 08540, USA

Corresponding Author: R. C. O'Neill, oneill@fusion.gat.com

A new current drive system is being designed and fabricated for the DIII-D tokamak to drive current in high- β discharges, using electromagnetic helicon waves. The high-power helicon antenna (HPHA) is expected to couple 1 MW of power into the DIII-D plasmas at a frequency of 476 MHz without degrading the plasma characteristics or introducing metal impurities. This high-power travelling wave antenna array is expected to have higher efficiency in driving current than other typical tokamak systems. The HPHA is a 30 CuCrZr module array mounted on a series of back plates. The modules inductively couple and resonate with the adjacent module. The two end modules are connected to a dual inner conductor strip-line transmitting RF power to and from four, 15 cm diameter vacuum coaxial feed-throughs located at the two DIII-D upper vessel ports. The modules, pitched 15° to follow the magnetic field lines of the tokamak, are bolted to six water cooled back-plates which are mounted on pedestals welded to the vessel wall. A description of the design and analyses of the HPHA and the RF strip-line feeds with anticipated overall antenna performance is presented.

Work supported by the U.S. Department of Energy under DE-FC02-04ER54698.

Implementation of Synchronous Reference Frame Theory Based Shunt Active Power Filter Using DSP Controller

C. K. Gupta¹, T. A. Trivedi²

¹*Institute for Plasma Research (IPR), Bhat, Gandhinagar, India*

²*Marwadi Education Foundation Group of Institutions, Rajkot, India*

Corresponding Author: C. K. Gupta, ckgupta@ipr.res.in

This paper conceptualizes shunt active power filter (SAPF) using synchronous-reference-frame (SRF) theory to mitigate the harmonics present in the power system. The shunt active power filter injects a suitable compensating current at a point called the “point of common coupling” (PCC) so that the harmonics present in the line are cancelled out and the sinusoidal nature of the current waveforms is restored. A three-phase current-controlled voltage source inverter (VSI) with DC link capacitor across it is used as an active filter. The synchronous reference frame (SRF) algorithm is developed for low voltage laboratory prototype using a TMS320F28335 digital signal processor (Texas instruments “Delfino”). The experimental test results demonstrate that the viability of the control strategy is successful in meeting the IEEE 519–1992 recommended harmonic standard limits.

Operation and Control of 42 GHz Gyrotron System in ECRH

J. Patel¹, N. Rajanbabu¹, H. Patel¹, D. Purohit¹, H. Mistry¹, and B. K. Shukla¹

¹*Institute for Plasma Research (IPR), Bhat, Gandhinagar, India*

Corresponding Author: J. Patel, jatin@ipr.res.in

Electron cyclotron resonance heating (ECRH) is one of the essential RF heating system used for preionization and heating experiments in ADITYA and SST-1 tokamak. The 42 GHz gyrotron system capable of delivering 500 kW RF power for 500 ms has been installed for operation with ADITYA and SST-1 tokamak. Gyrotron operation requires a systematic and sequential controlled operation of different power supplies. High voltage power supplies connected with collector and anode needs more attention for pulsing the gyrotron tube for conditioning as well as for microwave output. As the gyrotron tube is an expensive microwave device, fast interlock circuits are implemented for its protection during any abnormal event. Data acquisition and control systems (DAC) are designed and developed for gyrotron operation considering all safety measures and protection. Gyrotron system can be operated standalone as well as remotely through programmed time base trigger command from central control system. VME based DAC and the other PXIe based DAC have been installed with the gyrotron system and are under operation with SST-1 and ADITYA. Recently VME based DAC has been upgraded with NI Labview based GUI and control interface with new advance features. Also control application software on target VME hardware has also been upgraded for two pulse operation. PXIe based DAC has been designed to operate both 42 GHz and 82.6 GHz gyrotron with a single console application. The essential part of gyrotron operation is pulsing the anode and cathode high voltages simultaneously with preprogrammed delay and rise time with fast active interlocks. Gyrotron operation covers the start up sequence of power supplies, its preinspection and checking of different interlocks, HV pulse interface test, conditioning of gyrotron tube. This paper explains the sequence of steps necessary for gyrotron operation and control. It also showcases the features of DAC systems for gyrotron operation, its software design, adopted methodology and the problems faced during operation and control of gyrotron.

Design and Development of Control Grid Power Supply for RF Amplifier

K. Mohan¹, G. Suthar¹, H. Dalicha¹, R. G. Trivedi¹, and A. Mukherjee¹

¹ITER-India, Institute for Plasma Research (IPR), Bhat, Gandhinagar, India

Corresponding Author: K. Mohan, kartik.mohan@iter-india.org

ITER require 20 MW of RF power to a large variety of plasmas in the ion cyclotron frequency range for heating and driving plasma current. Eight RF sources of 2.5 MW RF power level each collectively will accomplish the above requirement. Each RF source consists of a solid state power amplifier (SSPA), driver, and end-stage, above which driver and end-stage amplifier are a tube (tetrode/diacrode) based which require DC power supplies, viz., anode, filament, screen grid, and control grid DC power supply. The DC power supply has stringent requirements like low stored energy, fast turn off, and low ripple value, etc.

This paper includes a detailed study of zero voltage switching (ZVS) resonant converter based buck converter, understanding with the help of mathematical equations of its various modes, simulation of the design in PSIM software and power supply development. The control grid of RF tube needs a negative biased DC power supply which would be operating in three modes of operation namely, viz., i) cut off mode (-500 V, 10 A); ii) conduction mode with no RF power extraction (-350 V, 7 A); and, iii) conduction mode with RF power extraction (-350 V, 2 A to 7 A). Depending upon the application, it needs to fulfil the requirement of constant voltage variable current when operating in conduction mode with RF application. A 500 V, 10 A modular DC power supply has been developed and tested on resistive load; it has four modules of 125 V, 10 A each in series for obtaining 500 V at the output with 1% peak-to-peak ripple voltage in the output and stored energy well within the limit. The power circuit of each module consists of six pulse rectifier units with DC link capacitor followed by resonant buck converter with switching frequency of the IGBT switch is of the order of 20 kHz. This paper addresses the analysis, design and hardware implementation of CGPS for Diacrode based system.

TCV Heating and Divertor Upgrades

A. Fasoli¹

The TCV Team

¹Swiss Plasma Center (SPC), École polytechnique fédérale de Lausanne (EPFL), 1015 Lausanne, Switzerland

Corresponding Author: A. Fasoli, ambrogio.fasoli@epfl.ch

The range and the reactor relevance of the TCV experiments are being enhanced by two sets of major upgrades. The first set includes the installation of neutral beam injection (NBI) and new electron cyclotron (EC) power sources, to heat the ions and vary the electron to ion temperature ratio, in plasmas with ITER relevant β values. A 15–30 keV, 1 MW, 2 s tangential NBI system is operational on TCV since 2015. A second beam at 1 MW, ~ 50 keV, also tangential but opposite to the first beam, is foreseen to approach β limits, vary the applied momentum input and investigate suprathreshold ion physics. For the EC power, two 0.75 MW gyrotrons at the 2nd harmonic have been installed. The next step consists of two 1 MW dual frequency gyrotrons (2nd and 3rd harmonics), one of which is being commissioned. The heating upgrades will raise the total heating power for high-density plasmas from 1.25 MW to 5.25 MW. The main element of the second set is an in-vessel structure to form a divertor chamber of variable closure, to reach relatively high neutral density and impurity compression and access reactor relevant divertor regimes for conventional or advanced divertor configurations. Graphite gas baffles will be installed to define a divertor and a main chamber region. The first set of baffles consists of 32 tiles on the high-field side (HFS) and 64 tiles on the low-field side (LFS), with geometry chosen on the basis of simulations performed using the SOLPS-ITER and EMC3-EIRENE codes.

FIP The HFS baffles are expected to be effective for a wide range of divertor configurations, including snowflake and super-X divertors, yet keeping the plasma close to the inner wall for passive stabilization. The dimension of the LFS tiles will be varied to modify the divertor closure. Control of the plasma, neutral and impurity densities, and He compression will be achieved by a combination of toroidally distributed gas injection valves, impurity seeding, and cryo-condensation pumps. Significant developments will be undertaken also in plasma diagnostics, to characterize the divertor plasma, measure power and particle deposition at the strike points, and obtain information on the detachment process. The possibility of installing dedicated divertor coils, made of high temperature superconductors, to expand the range of divertor configurations and improve their control, will be discussed.

Design and Simulation of Circular Waveguide Elbows Applicable in High Power Microwave Coupling to Plasma

J. Kumar¹, R. Singh¹, and V. P. Anitha¹

¹*Institute for Plasma Research (IPR), Bhat, Gandhinagar, India*

Corresponding Author: J. Kumar, jitu.kumar87@gmail.com

System for microwave plasma experiments (SYMPLE) is an experimental system set up at IPR, Gandhinagar, India, to investigate the physics of linear and nonlinear interaction of high-power microwave (HPM) with plasma. BWO based HPM source, proposed to be used for these studies, generates pulsed (~ 50 ns) microwave power of ~ 500 MW at 3 GHz frequency in TM_{01} mode. The BWO output power is extracted via an oversized circular waveguide of radius 15 cm. A transmission system is required between the HPM source and the plasma in order to couple the HPM power to plasma and to carry out measurements of forward and reflected microwave power. This transmission system will need a few elbows which can maintain same operating frequency, power level and propagating mode.

Understanding of HPM compatible waveguide elbows assumes further significance due to their applications in modern HPM systems in general. In the design of waveguide elbows, two considerations are of foremost significance. One is the minimization of the return loss as well as maintainability of mode purity in a frequency band as wide as possible and the other is the minimization of the size of the elbow. Various configurations of elbows have been subject to analysis by the solver, CST Microwave Studio, for efficient transmission of power while maintaining the operating frequency and propagating mode. Irrespective of the shape of elbows used, those with gradual bends have been found to perform better compared to 90° elbows, in terms of power loss and frequency/mode shift. Further, of the various configurations studied, Z-shaped, L-shaped, U-shaped and Pi-shaped elbows are found to perform relatively better. Performance of circular waveguide elbows having configurations discussed above has been studied in detail in the present work. Observations show that, at 3 GHz frequency, U-shaped elbow shows good power transmission and reflection but not mode purity while others show either poor or average transmission. Pi-shaped elbows, however, maintains TM_{01} mode but not power. Choice of the elbow configuration for any particular application should therefore depend on the requirement, i.e., having the minimum power loss, or having the frequency or mode retained. A detailed account of the design, simulation and analysis of various elbow configurations is presented in this report.

Development of Solid State Power Amplifier for ICH & CD RF Source

M. Patel¹, A. Jha¹, J. V. S. Harikrishna¹, K. Rajnish¹, R. Singh¹, R. G. Trivedi¹, and A. Mukherjee¹

¹ITER-India, Institute for Plasma Research (IPR), Bhat, Gandhinagar, India

Corresponding Author: M. Patel, manoj.patel@iter-india.org

ITER-India is developing the ion cyclotron heating and current drive (ICH&CD) RF source in the frequencies of 35 to 65 MHz. Three cascaded amplifiers along with low power RF section, AC/DC power supplies and controls will be used for getting MW level RF power from one source. In the present configuration, two tube-based tuned amplifiers, i.e., driver (150 kW) and final (1.7 MW) stage amplifiers are driven by a 10 kW wideband solid-state power amplifier (SSPA). Development of such SSPA with required ± 1.5 dB gain flatness in the above frequency range is very challenging, due to unique design of combiner and output matching circuit. This development is also aiming for achieving compact modular design, higher efficiency, usage of low voltage power supplies and better MTBF value compared with tube based amplifier of similar specification.

Since 8 kW is needed as input power to the driver stage amplifier, the design goal for SSPA is to achieve power level of around 10 kW/CW. Multiple pallet amplifier modules having capability of 1 kW are to be combined to achieve desire output. Pallet amplifier module is designed using LDMOS transistors (MRFE6VP61K25H, NXP Semiconductors, Netherlands), which is capable of delivering 1000 W CW power in the required frequency range with adequate tune matching circuits. For input matching 9:1 ferrite based balun is used. For output circuit, 1:9 impedance transformation and balance to unbalance quarter wave transformer is used. For gate and drain supply voltages, adequate filters are designed and installed. In this paper, detailed design and development of single pallet amplifier module as a part of wideband SSPA will be discussed along with test results. This paper also include integration and testing of four pallet amplifier modules using 4-way power splitter and combiner. Control and monitoring of the SSPA will be discussed in brief. Further, upcoming plan for integration of 16 such pallet modules with controls and monitoring system will be discussed.

RT Amplitude Control Loop: Testing of R&D ICRF Source at High Power

R. Kumar¹, S. Verma¹, D. G. Soni¹, M. Patel¹, A. Jha¹, A. P. Subbarao¹, R. Anand¹, G. Suthar¹, K. Mohan¹, H. Dalicha¹, P. Vasava¹, A. Patel¹, H. Dhola¹, D. V. Upadhyay¹, R. Singh¹, R. G. Trivedi¹, and A. Mukherjee¹

¹ITER-India, Institute for Plasma Research (IPR), Bhat, Gandhinagar, India

Corresponding Author: R. Kumar, kumar.rajnish@iter-india.org

Ion cyclotron heating and current drive (ICH&CD) system is one of the important auxiliary heating and current drive systems for the ITER experiment. A total of 20 MW of IC power is required to couple with ITER plasmas using eight independent RF sources (35–65 MHz) having power handling capability of 2.5 MW at VSWR of 2:1 with other stringent specifications. To finalize the source configuration, an R&D activity has been started and diacode-based amplifier is tested successfully at 1.5 MW for 3600 s, VSWR 2:1 on ITER-India test facility.

One of the critical requirements of IC-RF source is to operate the amplifier at constant power for dynamic load condition of VSWR 2:1 and able to match the requested power within 10 ms time scale. To realize this, amplitude control loop is developed using NI make PXI-7841R and LabVIEW-FPGA module. The output power is controlled by changing the drive reference of solid state power amplifier having in-built amplitude control loop. Further to manage the dynamic load condition, online variation of anode biasing is incorporated in this amplitude control loop. In this control loop, other parameters like screen grid current, anode current and anode dissipation are critically monitored and ensure constant output power by adjusting different biasing voltage in real-time. Putting the reliable and safe operation at highest priority, if any of the operating parameter is changing in uncontrolled manner, source will be forced to operate in power down mode forcing internal reference generated by this amplitude control loop itself. Even if the power down mode is also not able to make operating parameter stable, local protection function initiate RF off sequence for reliable and safe operation of RF source.

In this paper, characteristics and experimental result of amplitude control loop at high power operation (~ 1 MW) on ITER-India test bench will be discussed.

Mechanical Engineering Aspects for Overhauling of Helium Compressor and Heavy Duty Electrical Motors of 1.3 kW Helium Refrigerator/Liquefier System

J. C. Patel¹, K. Patel¹, P. Shah¹, G. L. N. Srikanth¹, D. Christian¹, R. N. Panchal¹, D. Sonara¹, N. Bairagi¹, G. Purwar¹, P. N. Panchal¹, R. Patel¹, G. Mahesuria¹, H. Nimavat¹, R. Sharma¹, A. Garg¹, and V. L. Tanna¹

¹*Institute for Plasma Research (IPR), Bhat, Gandhinagar, India*

Corresponding Author: J. C. Patel, jcpatel@ipr.res.in

The IPR has a 1.3 kW helium refrigerator/liquefier (HRL) cryogenics system, which is in operational state since 2003. The cryogenic HRL plant is used to cool down the magnets of Steady State superconducting Tokamak (SST-1). Three identical Mycom made helium screw-compressors with Fimet made 315 kW electrical motors and oil removal system operate to supply high-pressure helium gas to HRL cold-box and subsystems. Heavy duty electrical motors of rated for 315 kW in an asynchronous induction drive is used to run the helium screw compressors. The compressors along with the electrical motors run continuously for a month long operation. Hence, its reliability and availability is mandatory. Therefore, it is essential to maintain and overhaul the compressor and motors as per their schedule of operation hours to facilitate the reliable operation of the tokamak. In this paper, we will describe the mechanical engineering aspects of overhauling experiences of compressors and motors that include their alignment with compressor, online temperature monitoring and motor cooling arrangements and vibrations measurement of compressor, motor and skid.

A Travelling Wave Array System as Solution for the ICRF Heating of DEMO

R. Ragona^{1,5}, A. Messiaen¹, J.-M. Noterdaeme^{2,5}, J. Ongena¹, D. Van Eester¹, M. Q. Tran³, J.-M. Bernard⁴, J. Hillairet⁴, and M. Van Schoor¹

¹Laboratory for Plasma Physics, ERM/KMS, Brussels, Belgium

²Max-Planck-Institut für Plasmaphysik, Garching, Germany

³Swiss Plasma Center (SPC), École polytechnique fédérale de Lausanne (EPFL), 1015 Lausanne, Switzerland

⁴Institut de Recherche sur la Fusion par confinement Magnétique (IRFM),

Commissariat à l'énergie atomique (CEA/Cadarache), 13108 St. Paul lez Durance, France

⁵Ghent University, 9000 Ghent, Belgium

Corresponding Author: R. Ragona, riccardo.ragona@rma.ac.be

Travelling wave array (TWA) antennas distributed all along the periphery of the tokamak are presently considered as ion cyclotron resonance frequencies (ICRF) heating solution for the DEMO reactor. Compared to the conventional ICRF antenna systems currently in use or designed for future machines like ITER, the TWA consists of antenna sections integrated in the breeding blanket all around the machine, each one fed through a variable coupler in a resonant ring configuration.

Modelling an antenna system for DEMO with 18 quadrupole TWA sections of eight straps shows that a power capability exceeding 60 MW can be obtained in the frequency band of interest using the reference low coupling plasma profile of ITER. The described system optimizes the coupling to the plasma providing a large number of radiating elements, which results in enhanced antenna directivity, and decreasing the antenna power density. This results in a maximum strap voltage amplitude of only 15 kV and maximum interstrap voltage amplitude of 18 kV. The on purpose absence of vertical septa between straps increases the performance of the TWA compared to the classical antenna layouts. The generators remain matched for all loading conditions: the system is totally load resilient. A TWA fed with a resonant ring circuit should allow having almost 100% of the generator power injected in the plasma with associated negligible damping in the dummy load of the variable coupler. The voltage standing wave ratio (VSWR) remains close to 1 for a broad range of loading resistances and frequencies.

The proposed TWA system has been successfully tested on a scaled mock-up loaded by a salty water dummy load. The system tuning procedure is simple and an algorithm is under development. To assess the feasibility of the TWA fed by a resonant ring for a DEMO reactor a test on an existing Tokamak is under study.

Development of Indigenous Electrical Insulation Breaks for Superconducting Magnets of Fusion Devices

R. Sharma¹, V. L. Tanna¹

¹*Institute for Plasma Research (IPR), Bhat, Gandhinagar, India*

Corresponding Author: R. Sharma, rajivs@ipr.res.in

Electrical insulation breaks are very critical component of large-scale fusion devices employing superconducting magnets. The electrical insulation breaks developed for the requirement of the hydraulic upgrade for the superconducting poloidal field coils (SC) of SST-1 fusion machine. The electrical insulation breaks have been installed in the hydraulic, validated and sustained the operational required temperature. It has performed in rigorous environment of many thermal cycling from 300 down to 4.2 K, supporting pressure changes between 1 to 12 bar which induced more thermal stress in electrical insulation breaks. Main function of such insulation break is to supply cold helium to SC magnets and to isolate the magnets electrically from ground potential during the quench. The salient design features include bigger dimension of 1/2" size, break-down voltage to 5 kV, helium leak tightness $\leq 1 \times 10^{-8}$ mbarℓ/s at 4.5 K and needless to mention the cryogenic compatibility and flexibility issues. Success rate is about 75% as it is new attempt with indigenous epoxy resin system. The basic structural materials are SS-316L feed tube separated by a cryogenic grade G10 GFRP insulation material which bonded with cryogenic epoxy resin. The failures causes have been identified, analyses that considered and rectified during indigenous development of electrical insulation breaks. The failure was observed after the repeated 4.2 K cryogenic cycles which doubts the reliability of component and epoxy resin system. The real research and development as well as challenge are to define and develop an adequate cryo compatible epoxy. The electrical insulation breaks and cryogenic epoxy resin are not commercially available items, not reliable, cost factor and failure was noticed after cold thermal cycles. The in-house indigenous developed electrical insulation breaks can be used for future indigenous superconducting magnet fusion machines, electrical isolation and for low temperature experiments purpose (up to 15 kV applications), bonding and sealing of dissimilar materials at cryogenic temperature with very much cost effective. In this paper, the design, development, fabrication, performance test at 300 K, 77 K and 4.2 K of electrical insulation breaks and highlight on development of indigenous cryogenic epoxy resin system will be presented.

Recent Progress of ITER Magnet Supports Package in SWIP

P. Y. Li¹, B. L. Hou¹, S. L. Han¹, Z. C. Sun¹, D. A. Kang¹, T. Zhang¹, R. R. Lou¹, G. Liu¹,
T. F. Yan¹, C. J. Pan¹, and B. Zhang²

¹*Southwestern Institute of Physics, Chengdu, Sichuan, People's Republic of China*

²*China International Nuclear Fusion Energy Program Executive Center (CNDA), Beijing, People's Republic of China*

Corresponding Author: P. Y. Li, lipy@swip.ac.cn

SWIP has assumed the responsibility of the magnet supports package, which includes 18 gravity supports (GS) to support the toroidal field (TF) coil. ITER's GS will be confronted with about 10 000 tonnes of magnet dead weight—or 580 tonnes per support. At the same time, the gravity supports must withstand the electromagnetic forces of operation, seismic loads (if they occur), and thermal gradient deformation, which causes the top of the support to shrink toward the centre of the machine while the bottom remains stable. This contribution will detail the current state of progress towards the production of the supports.

Nuclear Design Issues of a Stellarator Fusion Power Plant with Breeder Blanket in Comparison to Tokamaks

U. Fischer¹, L. V. Boccaccini¹, G. Bongiovi¹, A. Häußler¹, and F. Warmer²

¹*Institut für Neutronenphysik und Reaktortechnik,*

Karlsruhe Institute of Technology (KIT), 76344 Eggenstein-Leopoldshafen, Germany

²*Max-Planck-Institut für Plasmaphysik, Greifswald, Germany*

Corresponding Author: U. Fischer, ulrich.fischer@kit.edu

The European Roadmap to the realization of fusion energy considers the stellarator concept as a possible long-term alternative to a tokamak fusion power plant (FPP). A corresponding R&D programme is conducted by the EUROfusion consortium to advance the stellarator concept with the scientific exploitation of the W7-X experiment. The aim is to optimize the stellarator performance, prove the feasibility for steady-state operation, and, on such a basis, study the prospects of a power producing plant based on the helical-axis advanced stellarator (HELIA) configuration. An important issue towards this goal is the analysis of specific nuclear issues of a HELIA type FPP equipped with a tritium breeding blanket. This work addresses these issues based on the achievements of the blanket development work conducted within EUROfusion's Power Plant Physics and Technology (PPPT) programme on a tokamak fusion power demonstration plant (DEMO) and recent results obtained for HELIA in the neutronics area.

Numerical Investigations towards Manufacturing of High Current Carrying Superconducting CICC

M. Ghate¹, M. Padaliya², S. S. Chauhan¹, P. Raj¹, U. Prasad¹, and R. Srinivasan¹

¹*Institute for Plasma Research (IPR), Bhat, Gandhinagar, India*

²*Silver Oak College of Engineering and Technology, Gujrat, India*

Corresponding Author: M. Ghate, mghate@ipr.res.in

Fusion relevant high field superconducting magnets require large current carrying conductor of the order of tens of kilo-Amperes. High current carrying cable in conduit conductor (CICC) are based on low-temperature NbTi and Nb₃Sn superconductors. The manufacturing of superconducting cable is carried out by twisting required strands into the desired configuration by application of tensile and compressive forces using cabling machine. The selection of tensile and compressive forces is critical as it can lead to deformation of superconducting strands which may lead to degradation of its performance. The long length CICC is manufactured by adopting pulled through technique where the superconducting cable is inserted inside stainless steel jacket tube which further shaped to require size using rotary swaging. The cold working during this process results in the generation of stresses in jacket material as well as in superconducting cable. The effect of critical factors on the distribution of stresses during cabling (such as twist pitch, contact angles, and compression forces) and jacketing (such as the percentage of cold work and feed velocity) of CICC have been simulated using FEA. The contact stress and deformation between two strands of cable and distribution of radial stresses along with a change in thickness for jacket tube have been estimated during this numerical investigation. These kinds of studies are essential to generate and optimize the manufacturing parameters for cabling and jacketing of CICC.

Development of Wideband Amplifier in ITER ICRF Range

A. Jha¹, P. Ajesh¹, J. V. S. Harikrishna¹, H. N. Patel¹, M. Patel¹, R. Anand¹, H. Dalicha¹,
R. G. Trivedi¹, and A. Mukherjee¹

¹ITER-India, Institute for Plasma Research (IPR), Bhat, Gandhinagar, India

Corresponding Author: A. Jha, akhil.jha@iter-india.org

ITER-India is responsible for delivery of 8+1 (production + prototype) RF sources to the ITER project. Each RF source will provide 2.5 MW of RF power at VSWR 2:1 in the frequency range of 35 to 65 MHz. Eight such RF sources will generate a total of 20 MW of RF power. Two RF chains containing three high power amplifiers (HPA1, HPA2 and HPA3) need to be combined to build an RF source. HPA2 and HPP3 are RF tube-based amplifiers while HPA1 is a solid state power amplifier. Development work is ongoing for a tetrode tube-based wide-band HPA1. The aim is to achieve a -1 dB bandwidth over any 5 MHz band in the frequency range 35–65 MHz. To achieve this specification the design of output cavity is based on wideband impedance matching circuit. Two LC circuits connected in series are tuned to achieve a wideband response over the desired frequency band. Input circuit design is based on tunable wide band impedance transformer. The amplifier is designed to operate in grounded grid configuration with CPI 4CW25000B (Richardson Electronics) tube. The rated output power is 10 kW/CW. A detailed calculation is performed to find operating parameters of tetrode tube at rated power. A LabVIEW based code tetrode tube calculator (TTC) is developed to perform load line calculation for tetrode tube. The code requires as input, parameters like DC anode bias, input DC power, anode voltage swing etc. and calculates the parameters like output power, efficiency, output impedance, input impedance etc. The calculated parameters are used as input for cavity design. This paper discusses the tube parametric calculation using TTC code in detail. The detailed design of HPA1 cavity using CST Microwave studio software is discussed.

Development of Various Diagnostics for NNBI Programme in IPR

M. Bandyopadhyay^{1,2,3}, A. J. Deka^{2,3}, D. Mukhopadhyay^{2,3}, P. Singh^{2,3}, D. Borah^{2,3}, H. Tyagi¹, R. K. Yadav¹, M. Bhuyan¹, K. B. Pandya², P. Bharathi², A. K. Chattopadhyay^{2,3}, M. J. Singh¹, and A. K. Chakraborty^{1,2}

¹ITER-India, Institute for Plasma Research (IPR), Bhat, Gandhinagar, India

²Institute for Plasma Research (IPR), Bhat, Gandhinagar, India

³Homi Bhabha National Institute (HBNI), Anushakti Nagar, Mumbai 400094, India

Corresponding Author: M. Bandyopadhyay, mainak@iter-india.org

The characteristics of a negative hydrogen ion (H^-) source and its neutralization mainly determine the performance of a negative ion based neutral beam injector (NNBI) performance. Ion sources possess many technological challenges in terms of production of uniform, extracted and accelerated negative ion beam current and also its transport to the tokamak plasma or the beam dump without damaging the beamline components during its transit. Therefore, for safe operation and also to characterize the beam, it is necessary to monitor the performance of the ion source and the beam. A judicious choice of various diagnostics comprises of optical, electrical, calorimetric and thermal are required. For that, a number of diagnostics are being developed for NNBI R&D program. Indian Test Facility (INTF) is an integral part of this program. Due to having versatility in nature, independent prototype experimental efforts have been carried out to establish different diagnostics. For ion source plasma characterization, optical emission spectroscopy (OES), cavity ring-down spectroscopy (CRDS) and electrical probe (EP) are mainly envisaged apart from different electrical measurements in RF circuit. All are either implemented in ROBIN source in prototype setup. Regarding beam characterization, Doppler shift spectroscopy (DSS), optical emission tomography (TOMO), infrared (IR) thermal imaging on carbon fibre composite (CFC) target plates in addition to thermocouple based calorimetric diagnostics on different beam line components along with electrical measurements in the accelerator power supply circuits and residual ion deflection (RID) circuits are planned. The DSS system with eight lines of sight (LOS) (blue-shifted and red-shifted) is already implemented in ROBIN ion source. An algorithm for TOMO and the corresponding code based on maximum entropy concept is developed to reconstruct the 2D emissivity profile which is obtained from the inversion of the LOS integral of brightness. The code has been tested using mathematical functions representing simulated INTF beam profile. In the paper present status of various diagnostics for ion source and beam characterization, in terms of its designs, characterization algorithms, results either on separate prototype or on associated operational ion source testbed will be presented.

Studies of Ultrasonic and Phased Array Inspection NDT Techniques on High Thick SS-316L Welded Joint Mock-Ups of Fusion Reactor Components Fabrication Applications

R. K. Buddu¹, K. S. Bhope¹, M. Mehta¹, and S. S. Khirwadkar¹

¹*Institute for Plasma Research (IPR), Bhat, Gandhinagar, India*

Corresponding Author: R. K. Buddu, buddu@ipr.res.in

Fusion reactor component manufacturing mainly deals with austenitic stainless steels with different welding techniques and kinds of weld structure joints. Thick steel like 40 mm and 60 mm plates are used mainly in the fabrication of vacuum vessel, divertor and other supporting structures with different weld joining techniques like tungsten inert gas (TIG) welding, narrow groove TIG (NG-TIG) welding, and electron beam welding (EBW). The challenges arise to qualify the acceptance of welds inspection with NDT techniques. X-ray radiography examination shows limitation for thicker steels inspection and liquid dye penetrant tests pose restriction for inside vacuum vessel welded joints due to penetrant chemicals exhibiting outgassing effects. Ultrasonic and phased array examination techniques have shown advantages over conventional techniques for weld inspection in cases of thick plate steel welded structures by providing the size and shape of weld defects (porosity, under cut, cracks, inclusions etc) in critical positions and depth inspection in the welded joints. The present paper reports the examination studies carried out with conventional ultrasonic examinations (A-scan technique), phased array examination techniques on the different weld SS-316L plate mock-ups. Weld mock-up coupons have been fabricated with different welding procedures (TIG, EB, and NG-TIG) and joint preparations such as butt and narrow groove, T-weld joints of 40 mm and 60 mm thick plates of SS-316L. Weld joints of T-type coupons have been fabricated with TIG welding and are examined with the conventional and phased array ultrasonic examinations. Calibration is implemented with known defect size and reference methodology with phased array ultrasonic inspection technique. The phased array examination (PA, angle beam phased array S-scan, 2.25 MHz probe), has shown superiority over the conventional ultrasonic technique by revealing minor size defects with mapped welded regions. However, the detected weld defects are well within the acceptable limits. The welded samples are inspected by X-ray radiography is compared and it is noted that the line defects and porosity conditions are not revealed. The present paper discusses the welding mock-ups tests like calibration tests, NDT techniques methodology and results of the weld defects.

Simulation Studies for Optimization of 60 MHz Rod-Type Radiofrequency Quadrupole Accelerator Design at IPR

R. Bahl¹

¹*Institute for Plasma Research (IPR), Bhat, Gandhinagar, India*

Corresponding Author: R. Bahl, renu@ipr.res.in

A 60 MHz rod-type radiofrequency quadrupole (RFQ) accelerator has been designed for material studies through Ion Irradiation at IPR, Gandhinagar. Ion Irradiation has been preferred for characterization of fusion research material properties due to its inherited advantages of: 1) absence of high residual radioactivity; 2) well defined energy, dose rate and temperature values; and, 3) its potential for well controlled experiments along with the fact that it rarely requires more than several tens of hours to reach damage levels of 1–100 dpa range. RFQ is chosen as the frontend accelerator in almost all accelerators these days as it can accelerate, bunch and focus the beam simultaneously. The accelerated ion beam produced by RFQ and the subsequent reaction of the beam with different targets is used to study: a) radiation enhanced segregation; b) irradiated microstructure; c) radiation hardening; and, d) irradiation assisted stress corrosion cracking in materials. For ion-irradiation, the ion beam generated by an electron cyclotron resonance (ECR) ion (H^+) source coupled to (copper) rod-type RFQ accelerator through a LEPT will be accelerated to 1 MeV at 60 MHz. Usually, high current RFQ are vane-type RFQ's that are designed at higher frequencies of few hundred of MHz due to their advantage of reduced RFQ length for particular energy gain and higher shunt impedance and quality factor. But their machining is very difficult as well as they have disadvantage of presence of detrimental dipole modes. At IPR, it has been decided to use the indigenously developed RF source (35–65 MHz frequency at 1 MW power) and design a rod-type RFQ at 60 MHz RF frequency to obtain the required energy gain. Design considerations involve special emphasis on reduction of beam instabilities by keeping zero-current phase advance $< 90^\circ$ in longitudinal as well as transverse direction, reduction of space charge effects by avoiding the resonance condition along with other considerations. Detailed beam dynamic design of 60 MHz rod-type RFQ for hydrogen beam is carried out and a 4.2 m long RFQ comprising of 97 cells is designed after optimizing various parameters. A resonating frequency of 59.6 MHz has been achieved with 12 posts.

Manufacturing Technologies for UHV Compatible 10 MW/m² High Heat Flux Components for Application in Fusion Devices

H. K. Patel¹, N. Panda², N. Kanoongo², K. Balasubramanian², and A. K. Chakraborty¹

¹ITER-India, Institute for Plasma Research (IPR), Bhat, Gandhinagar, India

²Nonferrous Materials Technology Development Centre (NFTDC), Kanchanbagh, Hyderabad 500058, India

Corresponding Author: H. K. Patel, hitesh.patel@iter-india.org

High heat flux components form the primary interface of thermal management of injectors in the fusion devices. The requirement for such application varies from 1 to 10 MW/m². UHV compatibility is the inherent characteristics of such components also manufacturing processes involves the development of specific material, process qualification of special process like EB welding and component performance validation.

One such component of active thermal management in neutral beam injector is Hypervapotron based heat transfer element (HTE) which is designed to absorb heat flux as high as 10 MW/m². The realization route is through prototype and established on one to one model and evaluating their performance. The development route of the HTEs represents several important areas, like: 1) development of precipitation hardened CuCrZr material characterized for its fatigue life (more than 10⁵ stress controlled cycles), mechanical properties at ambient (UTS > 384 MPa, elongation > 13%) and at operational temperature, i.e., 350°C (UTS > 263 MPa, elongation > 14%), restricted chemical composition range of Cr, Zr, Cd and O₂ to enhance precipitation effect and weldability of the component; 2) similar (CuCrZr to CuCrZr) and dissimilar material (CuCrZr-Ni-SS-316L) joining by advanced technology like EB welding in controlled environment to enhance the localized high heat input over a large weld penetration depth with minimal distortion and thereby overcome the effect of thermal diffusion by typical copper during welding; 3) validation of these weld joints with respect to international codes/standards; and, 4) validation of design through performance testing by simulating the operational scenario. Successful realization of this route establishes HTEs as main baseline components of high heat flux system or neutral beam system. Similar application areas can be identified in various fusion devices.

The paper presents the implementation of this realization route of prototype heat transfer elements including the details of assessment carried out with respect to application.

Development and Validation of Cryostat Finite Element Model with Unique FE Method

T. K. Sharma¹, S. S. Sandhu¹, M. Patel¹, S. B. Padasalagi¹, G. K. Gupta¹, A. K. Bhardwaj¹, and V. More¹

¹ITER-India, Institute for Plasma Research (IPR), Bhat, Gandhinagar, India

Corresponding Author: T. K. Sharma, tarun.sharma@iter-india.org

The ITER Cryostat, the largest stainless steel vacuum pressure chamber ever built which provides the vacuum confinement to components operating in ITER ranging from 4.5 K to 80 K. Cryostat Design Model was qualified [1] by ITER. As a safety important class system, design qualification at every change in its development and installation phases is mandatory. The cryostat system is currently at the manufacturing stage, several deviation request are being reported, e.g., tolerances change, rib modifications, etc. These changes affect the behaviour of the cryostat, and thus need reassessment. The conventional design approach in the finite element method (FEM) needs significant time and effort, as incorporation of changes calls for redevelopment of the full mathematical model.

In this paper a “unique method” of developing FE model for complex systems like cryostat is presented, which typically addresses above need and the method is qualified with results of cryostat engineering model (CEM) [1, 2]. This unique method involves dividing and meshing of the big components into subcomponents, so the full cryostat is divided into 30 subcomponents and mathematical models of these individual components are developed. These subcomponents are integrated using suitable constraint equations to create full FE model [3, 4]. Then the integrity of model is assessed using the modes shapes. This unique method enables to incorporate component level changes without affecting the full FE model, thus saving time and efforts of redevelopment of the mathematical model.

For qualification of the developed FE model, category II loading and selected load combinations are applied. The results obtained are in close approximation with CEM results [1, 2]. As the present need was to address the changes of manufacturing model, so further cryostat manufacturing FE model (CMM) is developed with this unique approach. It is then analyzed for category II loading and selected load combination. This paper gives detailed insight about the developing and qualification of the unique Method and details of the analysis results of CMM.

References

- [1] B. Doshi *et al.*, Fusion Eng. Des., **86**, 1924–1927 (2011).
- [2] C. Liang *et al.*, Fusion Eng. Des., **88**, 42–45 (2013).
- [3] Instructional Material Complementing FEMA 451, Design Example, SI-15-7-53.
- [4] ANSYS Reference Manual.

Characterization of Argon Plasma in a Multiline Cusp Magnetic Field: Towards a Favourable Source for NBI System

A. Patel¹, M. Sharma¹, R. Narayanan¹, R. Ganesh¹, and P. K. Chattopadhyay¹

¹*Institute for Plasma Research (IPR), Bhat, Gandhinagar, India*

Corresponding Author: A. Patel, amitpatel@ipr.res.in

The positive or negative ion sources which form the primary component of neutral beam injection (NBI) in controlled nuclear fusion using magnetic confinement have to meet, simultaneously, several demanding requirements, like high current production, high energy and low-emittance stable H^- ion sources and to confine them, etc. It is very well known that multicusp magnetic fields can confine high dense plasmas and thus the application of multicusp magnetic field geometry has received a great attention in a wide range of systems, viz., ion sources, plasma facing material and diagnostic testing in fusion reactors. Apart from the fusion studies, cusp magnetic fields are rigorously used in plasma etching reactors, ion thrusters, magnetrons and also in plasma wave study experiments.

A versatile multiline cusp plasma device of axial length 1.2 m and diameter 40 cm has been developed in house, by using six electromagnets placed over the periphery of a cylindrical chamber. The magnetic field lines are profiled by using a core material Vacoflux-50. In this paper, by performing simulations in FEMM (field element method magnetic) tools, we first show how to profile the magnetic field lines as per the requirements. Then we characterize the filamentary argon plasma in this variable multiline cusp magnetic field and illustrate the effect of variable magnetic field on mean plasma density, particle confinement time, leak width and size of field free region by changing the magnet current.

A Versatile Multicusp Plasma Device for Confining Contact Ionized Alkali Ions: Source for the Experimental Studies

Z. Shaikh^{1,2}, A. D. Patel², M. Sharma², H. H. Joshi¹, and N. Ramasubramanian²

¹*Department of Physics, Saurashtra University, Rajkot, India*

²*Institute for Plasma Research (IPR), Bhat, Gandhinagar, India*

Corresponding Author: Z. Shaikh, zubin.ipr@gmail.com

The confinement by multicusp magnetic field configuration is being revisited in prospect of developing a negative ion beam source for heating the plasma in fusion devices. For this, an experimental device namely the multicusp plasma device (MPD), has been constructed to study the physics of plasma confinement in a multicusp configuration. In this experiment alkali ions of low ionization potential will be produced by contact ionization and will be confined in the multicusp magnetic field configuration. The caesium ions will be produced by impinging a collimated neutral caesium atom beam on an ionizer consisting of a hot tungsten plate. The temperature of the tungsten plate will be made high enough (~ 2700 K) such that it will also be contributing electrons to the plasma. Hence the design of hot plate ionizer is crucial. For heating the tungsten plate, the hot cathode technique will be used. Thermionic electron emission from the tungsten plate is exponentially proportional to the temperature of the plate. A gradient of very little value in the temperature of the hotplate, might cause a large temperature gradient and hence large potential difference in plasma which will result in drift thus affecting the experiment. So it is desired to keep the hot plate temperature to be uniform within 1%. The tungsten plate is so hot that the direct contact method for the temperature measurements can not be used. To measure the thermal contours of the ionizer hot plate, a noncontact method will be used and characterized.

Evolution and Implementation of Lossless Data Acquisition for Steady State Tokamak

M. Sharma¹, I. Mansuri¹, T. Raval¹, A. L. Sharma¹, and D. Raju¹

¹*Institute for Plasma Research (IPR), Bhat, Gandhinagar, India*

Corresponding Author: M. Sharma, bithi@ipr.res.in

The evolution of data acquisition system (DAS) for steady-state operation of tokamak has been technology driven. Steady-state tokamak demands a data acquisition system which is capable enough to acquire data losslessly from diagnostics. The needs of lossless continuous acquisition have a significant effect on data storage and takes up a greater portion of any data acquisition system. With the expected long discharge duration from the variety of fast and slow diagnostics, the challenge is also to cater the need of a real-time monitoring of signals by multiple locally networked users. So there is strong demand for something that would control the expansion of both these portion by a way of employing compression technique in real-time. With these objectives, the DAS is based on a model where the objects of the systems are integrated with the Central Control System of SST-1 using TCP/IP communication. The DAS software essentially meets the demand of an active remote configuration of hardware digitizers, like PXI system and that of the initialization of acquisition within the local network.

The present work describes the evolution of TCP/IP based DAS software in Labview for configuring, acquiring, and subsequently, pushing the sampled data into network. It presents a model of data acquisition system employing real-time data compression technique based on LZO. It is a data compression library suitable for data compression and decompression in real-time. The algorithm used favours speed over compression ratio. The compression/decompression system has been rigged up based on PXI bus and dual buffer mode architecture is implemented for lossless acquisition. The acquired buffer is compressed in real-time and streamed to network and hard disk for storage. Observed performance of measure on various data type like binary, integer float, types of different type of wave form as well as compression timing overheads. Various software modules for real-time acquiring, online viewing of data on network nodes have been developed in Labview & Lab-Windows/CVI based on client server architecture. The focus will also be on the recent first phase operations of SST-1 in short pulse mode which have provided an excellent opportunity for the essential initial tests and benchmark of the SST-1 Data Acquisition Systems.

Technology Developments for ECRH System

B. K. Shukla¹, R. Babu¹, J. Patel¹, H. Mistry¹, K. G. Parmar¹, H. Patel¹, and D. Purohit¹

¹*Institute for Plasma Research (IPR), Bhat, Gandhinagar, India*

Corresponding Author: B. K. Shukla, shukla@ipr.res.in

The gyrotron based electron cyclotron resonance heating (ECRH) system is used on tokamaks ADITYA-U and SST-1. The ECRH system consists of a high power gyrotron, corrugated waveguide based transmission line and a quasi-optical launcher. The 42 GHz gyrotron delivers 500 kW power for 500 ms duration. This gyrotron operates at ~ -48 kV beam voltage and +18 kV anode voltage. This system draws around 20 A beam current. This is a critical systems associated with high voltage power supply systems. A dedicated protection system is used to protect the gyrotron in an event of fault. An ignitron based crowbar system removes the voltage within 10 μ s and ensures the safe operation of the gyrotron.

In order to operate the system with more reliability, power supplies and protection system are being upgraded indigenously. An advance thyristor-based solid-state crowbar is under development which will replace the ignitron crowbar system. A 20 kV solid-state crowbar has been developed and tested successfully, and subsequently integrated with the existing anode power supply. The prototype crowbar at 30 kV has also been tested successfully. A 50 kV solid-state crowbar has been designed and is under development. An IGBT based solid-state switch has been developed successfully which has been tested up to 18 kV. This can replace the existing anode power supply which has slow rise time. This IGBT based switch facilitates the system for modulation.

An advance launcher has been designed and is currently under procurement. This launcher consists of two mirrors (one focussing and other plane) mounted on a SS flange. The focussing mirror is fixed, however, the plane mirror can be steered in ultrahigh vacuum (UHV) environment. The plane mirror is connected with two mechanisms for necessary movement in two directions. The system is designed to minimize backlash and give precession movement with position indication. This prototype launcher can be used as a real-time feedback launcher with some additional modifications.

The paper discusses the technologies developed indigenously for the safe, reliable and accurate operation of ECRH system on tokamaks.

Concept of a New Approach in Thermographic Measurements for Plasma-Wall Interaction Studies on KTM Tokamak

B. Chektybayev¹, E. Batyrbekov¹, M. Skakov¹, and A. Sadykov¹

¹*Institute of Atomic Energy, National Nuclear Center, Kurchatov, Kazakhstan*

Corresponding Author: B. Chektybayev, chektybaev@nnc.kz

In the paper is described concept of noncontact temperature measuring technique of metallic surface currently being developed for KTM tokamak. Suggested technique is based on using thermographic camera and infrared carbon dioxide laser (CO₂) with 10.6 μm wavelength. The pulsed IR laser radiation is used to observe changes in the emissivity of the body. This information will give possibility to make a correction of the thermal measurements of the thermographic camera.

Preliminary experimental results of measurement technique are shown in the paper and discussed. Plans for implementation and testing of measuring technique are also discussed. The developed technique will be used for an accurate spatial measurement of the heating temperature of the metal surface of the first wall candidate materials under the influence of thermal plasma fluxes on the KTM tokamak.

IFE: Inertial Fusion Experiments and Theory

Two-Colour Mixed Petawatt Laser Designed for Fast Ignition Experiment

Y. Arikawa¹, Z. Hu², Y. Zhao², H. Tu², F. Fan², S. Kojima³, M. Hata¹, Y. Sentoku¹, T. Johzaki⁴, H. Sakagami⁵, S. Sakata¹, Y. Abe¹, S. Lee¹, K. F. F. Law¹, H. Kishimoto¹, H. Morita¹, S. Kambayashi¹, M. Alessio¹, S. Tokita¹, J. Kawanaka¹, N. Miyanaga¹, M. Yoshimura¹, A. Yogo¹, H. Nishimura¹, H. Azechi¹, H. Shiraga¹, M. Nakai¹, S. Fujioka¹, and R. Kodama¹

The LFEX Group

¹*Institute of Laser Engineering, Osaka University, Osaka, Japan*

²*Technical Institute of Physics and Chemistry, Chinese Academy of Science, People's Republic of China*

³*Advanced Research Center for Beam Science, Institute for Chemical Research, Kyoto University, Japan*

⁴*Graduate School of Engineering, Hiroshima University, Higashi-Hiroshima, Japan*

⁵*National Institute for Fusion Science (NIFS), Toki, Gifu, Japan*

Corresponding Author: Y. Arikawa, arikawa-y@ile.osaka-u.ac.jp

Here we report a novel design of a heating laser for the fast ignition, combining fundamental and second harmonics lights. Such a two-colour laser is expected to heat a dense core more efficiently than a laser only with a fundamental light. We chose a LBO (LiB_3O_5) crystal which can convert a focussing beam due to its large acceptance of phase matching angle. We experimentally demonstrated the second harmonic conversion with efficiency of 60% at the maximum. The LBO crystal shows a high damage threshold more than 5 J/cm^2 with a down-scale LFEX beams. A full size ($10 \text{ cm} \times 10 \text{ cm} \times 2 \text{ mm}$) LBO crystal was manufactured completely and is ready to install for the full-scale LFEX operation.

Production of keV-Temperature Plasma Core with Magnetized Fast Isochoric Heating

S. Fujioka¹, S.-H. Lee¹, S. Sakata¹, T. Johzaki², H. Sawada^{1,3}, H. Morita¹, K. Matsuo¹, A. Yao¹, K. F. F. Law¹, H. Kishimoto¹, A. Morace¹, A. Yogo¹, Y. Abe¹, S. Kojima¹, M. Hata¹, N. Iwata¹, A. Sunahara⁴, H. Sakagami⁵, T. Ozaki⁵, K. Mima^{1,6}, T. Taguchi⁷, M. Bailly-Grandvaux⁸, J. J. Santos⁸, T. Shiroto⁹, N. Ohnishi⁹, K. Yamanoi¹, T. Norimatsu¹, K. Tsubakimoto¹, S. Tokita¹, Y. Nakata¹, J. Kawanaka¹, T. Jitsuno¹, N. Miyanaga¹, M. Nakai¹, H. Nishimura¹, H. Shiraga¹, H. Azechi¹, H. Nagatomo¹, Y. Arikawa¹, Y. Sentoku¹, R. Kodama¹, and N. Yoshiki¹

¹*Institute of Laser Engineering, Osaka University, Osaka, Japan*

²*Graduate School of Engineering, Hiroshima University, Higashi-Hiroshima, Japan*

³*University of Nevada, Reno, NV 89557, USA*

⁴*Purdue University, West Lafayette, Indiana, USA*

⁵*National Institute for Fusion Science (NIFS), Toki, Gifu, Japan*

⁶*Graduate School for the Creation of New Photonics Industries, Hamamatsu, Shizuoka, Japan*

⁷*Department of Electrical and Electronics Engineering, Setsunan University, Neyagawa, Osaka, Japan*

⁸*Centre Lasers Intenses et Applications (CELIA), Université Bordeaux I, 33405 Talence, France*

⁹*Department of Aerospace Engineering, Tohoku University, Sendai, Miyagi, Japan*

Corresponding Author: S. Fujioka, sfujioka@ile.osaka-u.ac.jp

The quest for the inertial confinement fusion (ICF) ignition is a grand challenge, as exemplified by extraordinary large laser facilities like National Ignition Facility (NIF) [1, 2]. Although scientific break-even, the energy released by fusion reaction exceeds the energy contains in the compressed fusion fuel, was achieved on NIF [3], the pathway to the ignition is still unclear. Fast isochoric heating, also known as fast ignition, of a precompressed fuel core with a high-intensity laser is an attractive and alternative approach to the ICF ignition [4] that avoids the ignition quench caused by the hot spark mixing with the cold fuel, which is the crucial problem of the currently pursued ignition scheme.

High-intensity laser-plasma interactions efficiently produce relativistic electron beams (REB). However, only a small portion of the REB collides with the core because of its large divergence. Here we have demonstrated enhanced laser-to-core coupling with a magnetized method to confine the REB in a narrow transport region resulting in efficient isochoric heating. The method employs a laser-produced kilo-tesla-level magnetic field [5] that is applied to the transport region from the REB generation point to the core which results in guiding the REB along the magnetic field lines. We have created successfully a 1.6 ± 0.2 keV-temperature plasma core having 1 Gbar of energy density by using the MFI scheme with $7.7 \pm 1.3\%$ of an efficient laser-to-core energy coupling [6]. We should emphasize that our result can be explained by a simple model coupled with the comprehensive plasma diagnostics, while several ICF experiments rely heavily on computer simulations due to difficulties of diagnosing microscale phenomena occurred in the small and complex plasma. The simplicity may secure scalability of this scheme to the ignition. 15% of the laser-to-core coupling is achievable for an ignition-scale high area density core ($0.3\text{--}0.5$ g/cm²) according to the model. The ignition target based on the MFI scheme is being designed by using multiscale and multidimensional simulations.

Continued...

References

- [1] J. Lindl *et al.*, Phys. Plasmas, **11**, 339 (2004).
- [2] J. Lindl *et al.*, Phys. Plasmas, **21**, 020501 (2014).
- [3] O. A. Hurricane *et al.*, Nature **506**, 343 (2014).
- [4] M. Tabak *et al.*, Phys. Plasmas, **1**, 1637 (1994).
- [5] S. Fujioka *et al.*, Sci. Rep. **3**, 1170 (2013).
- [6] S. Sakata *et al.*, ArXiv **172.06029**, (2017).

Liquid DT Layer Approach to Inertial Confinement Fusion

R. E. Olson¹, R. J. Leeper¹, R. R. Peterson¹, B. M. Haines¹, S. A. Yi¹, A. B. Zylstra¹,
P. A. Bradley¹, S. H. Batha¹, and J. L. Kline¹

¹Los Alamos National Laboratory (LANL), Los Alamos, NM 87545, USA

Corresponding Author: R. E. Olson, reolson@lanl.gov

The baseline approach to high-gain ICF involves the implosion of capsules containing a layer of DT ice [1]. DT ice layer designs require a high convergence ratio ($CR > 30$) implosion, with a hot spot that is dynamically created from DT mass originally residing in a thin layer at the inner DT ice surface. Although high CR is desirable in an idealized 1D sense, it amplifies the deleterious effects of realistic features and asymmetries [2]. An alternative ICF concept uses DT liquid layers [3]. DT liquid layers allow for much higher vapour densities than are possible with DT ice layers. The wide range of vapour densities that are possible with DT liquid layers provides flexibility in hot-spot CR ($12 < CR < 25$), which, in turn, will provide a reduced sensitivity to asymmetries and instability growth. Given enough vapour mass, the hot spot can be formed from the mass originally residing in the central vapour region. Recent experiments at the National Ignition Facility (NIF) have demonstrated cryogenic liquid DT layer ICF implosions, along with the associated flexibility in the hot spot CR [4, 5].

There are tradeoffs involved in high CR ice layer and reduced CR liquid layer designs. With reduced CR, hot spot formation is expected to have improved robustness to instabilities and asymmetries [2–5]. In addition, the hot spot pressure (P_r) required for self-heating is reduced if the hot spot radius (R_{hs}) is increased ($P_r \propto R_{hs}^{-1}$). With a reduction in the hot spot P_r requirement, the implosion velocity and fuel adiabat requirements are relaxed. On the other hand, with larger hot spot size, the hot spot energy requirement for self-heating (E_{hs}) is increased ($E_{hs} \propto R_{hs}^2$), and the required capsule absorbed energy is increased. In this presentation, we will summarize the recent liquid layer experiments at the NIF and will discuss the hot spot energy, hot spot pressure, cold fuel adiabat, and capsule-absorbed energy requirements for achieving self-heating and propagating burn using liquid layer capsules with hot spot $CR < 20$.

References

- [1] S. W. Haan *et al.*, Phys. Plasmas, **18**, 051001 (2011).
- [2] B. M. Haines *et al.*, Phys. Plasmas, **24**, 072709 (2017).
- [3] R. E. Olson and R. J. Leeper, Phys. Plasmas, **20**, 092705 (2013).
- [4] R. E. Olson *et al.*, Phys. Rev. Lett., **117**, 245001 (2016).
- [5] A. B. Zylstra *et al.*, In Preparation for Phys. Plasmas, (2018).

Thermo-Mechanical and Atomistic Assessment of First Wall and Optics in Nonprotective Chamber in Inertial Fusion Energy

J. M. Perlado¹, A. Rivera¹, R. González-Arrabal¹, O. Peña¹, D. Garoz^{1,2}, F. Sordo^{1,3}, L. Soto^{4,5}, and M. Panizo¹

¹*Instituto de Fusión Nuclear (IFN), Universidad Politécnica de Madrid (UPM), Madrid, Spain*

²*Mechanics of Material and Structures, Ghent University, 9000 Ghent, Belgium*

³*European Spallation Source (ESS)-Bilbao, Spain*

⁴*Comisión Chilena de Energía Nuclear, Santiago, Chile*

⁵*Center for Research and Applications in Plasma Physics and Pulsed Power, Santiago, Chile*

Corresponding Author: J. M. Perlado, josemanuel.perlado@upm.es

Different inertial fusion energy (IFE) first wall (FW) protections have been proposed in diverse conceptual designs that lead to very different irradiation conditions and macroscopic effects. A review is needed to understand their behaviour. Some years ago a European proposal projected the possibility of nonprotective FWs considering W and nano-tungsten. This work is describing in detail the behaviour of a W and nano-tungsten first wall under pulsed irradiation conditions predicted for the different operational scenarios of that laser fusion project by using advanced engineering modelling tools. Starting with the calculations of the time-dependent pulsed radiation fluxes, assuming 3D geometrical configurations, we estimate the irradiation-induced evolution of first wall temperature as well as, the thermo-mechanical response of the material. Finally, we carry out crack propagation calculations. Results allow us to define operational windows and to identify the main limitations for operation. The atomistic effects of irradiation in the FW are the other key magnitude to determine available lifetime. The role of grain boundaries on the radiation-induced damage and light species behaviour is studied both experimentally and computationally, also under pulsed conditions. Important differences are observed in the density of vacancies between nanostructured and coarse-grained samples as well as the preferential places for H accumulation concluding with the influence of temperature.

Optics damage is a great concern in IFE; a new full conceptual final focussing system based on silica transmission lenses for dry wall chambers was designed assuming pulsed conditions based on a temperature control system by using a heat transfer fluid. Optical response of composite materials containing metal nanoparticles was investigated and optimized. Highly concentrated silver colloidal nanoparticle solutions were produced thanks to fs laser ablation and it was demonstrated that such embedded plasmonic nanoparticles may be viable candidates to reduce damages produced on optics by swift heavy ions due to the change of their shape under irradiation.

Demonstrations of Foam Shell and Infrared Heating Methods for FIREX Targets

A. Iwamoto¹, K. Iwano², T. Norimatsu², K. Yamanoi², S. Fujioka², and R. Kodama²

¹*National Institute for Fusion Science (NIFS), Toki, Gifu, Japan*

²*Institute of Laser Engineering, Osaka University, Osaka, Japan*

Corresponding Author: A. Iwamoto, iwamoto.akifumi@lhd.nifs.ac.jp

We study fuel layering for Fast Ignition Realization Experiment (FIREX) cryogenic targets according to two strategies: a foam shell and infrared (IR) heating. Foam is a porous material and would soak up a liquid fuel uniformly by capillarity. The method has the difficulty to form void-less solid fuel because of the density difference between the liquid and solid phases. We have demonstrated the residual void fraction of $\sim 1\%$ in a foam wedge. ANSYS simulations have represented that the technique would be applicable to a FIREX target. We examine the simulated process using a dummy foam shell target and succeed to form an ice layer with a reduced void fraction. The IR heating technique has originally been developed for central ignition targets, which requires spherical symmetry. We modify it for an axisymmetric FIREX target. We have developed the dedicated layering system with additional temperature control of the cone. To date, the sphericity of a formed ice layer reaches 95%.

Experimental Discharge Characterization of IEC Plasma Device

G. M. Elaragi¹

¹*Plasma Physics and Nuclear Fusion Department, Egyptian Atomic Energy Authority (EAEA), Cairo, Egypt*

Corresponding Author: G. M. Elaragi, elaragi@gmail.com

In this paper, Egyptian first inertial electrostatic confinement fusion (IECF) device, constructed at the Egyptian Atomic Energy Authority (EAEA-IEC), is introduced the characterization of IEC Plasma Device. It consists of 2.8 cm stainless steel cathode, 6.5 cm anode diameter with 10 cm diameter 30 cm high vacuum chamber. The discharge current and voltage of plasma discharge has been recorded using current probe and resistive voltage divider respectively. The X-ray emissions in IEC plasma device were investigated by employing time-resolved detector. The temporal distributions of detected X-rays emission are occurring during the initial 1 μ s. The calculated rate of DD-neutron generation using the same electrode configuration about 10^6 – 10^8 neutrons/second.

H-¹¹B Fusion Reactor with Extreme Laser Pulses for Non-LTE Ignition

H. Hora^{1,2}, S. Eliezer^{3,4}, N. Nissim³, M. J. Hole⁵, and Y. Mori⁶

¹University of New South Wales, Sydney, NSW 2052, Australia

²HB11 Energy, Freshwater, NSW 2096, Australia

³SOREQ Nuclear Research Center (SNRC), Yavne 8180000, Israel

⁴Universidad Politécnica de Madrid (UPM), Madrid, Spain

⁵Australian National University, Canberra, Australia

⁶Graduate School for the Creation of New Photonics Industries,
Hamamatsu, Shizuoka, Japan

Corresponding Author: H. Hora, h.hora@nsw.edu.au

The progress for the design of a reactor for laser boron fusion is following a road map [1] based on the use of extreme deviations from local thermal equilibrium LTE conditions by using just available picosecond laser pulses of more than petawatt PW power. Fusion of hydrogen H with the boron isotope 11 (HB11 fusion) at LTE is extremely difficult. For spherical compression with lasers, densities 100 000 times of the solid state and temperatures above 100 keV are necessary, such that the energy gains are about five orders of magnitudes below the usual DT fusion. The necessary non-LTE ignition condition is possible if the equation of motion is determined by the electric and magnetic fields E and H of the laser such that the gas dynamic pressure is only a small perturbation. The nonlinear (ponderomotive) force calculations of 1978 [2] resulted in ultrahigh accelerations, measured by Sauerbrey [3] as predicted. With the present ps extreme laser pulses, the measured [4] nine orders of magnitude higher energy gains from HB11 can be explained with inclusion of the avalanche reaction due to the generated three 3 MeV α 's at each reaction [5]. Combining these results with the kilotesla magnetic fields [6] for cylindrical trapping of the reaction in solid density HB11 fuel ignited end-on by the petawatt laser pulse, shows how 14 mg of boron produces 300 kWh energy in nearly equal energetic 3 MeV α 's. The reported steps for the design of the reactor follows the parameters [1] for energy generation with no problems of nuclear radiation producing low cost electricity.

References

- [1] H. Hora, *et al.*, Laser and Particle Beams **35**, 730 (2017).
- [2] H. Hora, Physics of Laser Driven Plasmas, Wiley New York (1981).
- [3] R. Sauerbrey, Phys. Plasmas, **3**, 4712 (1996).
- [4] A. Picciotto, *et al.*, Phys. Rev., **X4**, 031030 (2014).
- [5] S. Eliezer, *et al.*, Phys. Plasmas, **23**, 050704 (2016).
- [6] S. Fujioka, *et al.*, Nat. Sci. Rep. **3**, 1170 (2013).

Development of Shell Injection System for the Future IFE Power Plant

Y. Mori¹, A. Iwamoto², K. Ishii¹, Y. Nishimura³, R. Hanayama¹, S. Okihara¹, Y. Kitagawa¹, O. Komeda⁴, T. Hioki⁵, T. Motohiro⁵, A. Sunahara⁶, Y. Sentoku⁷, E. Miura⁸, H. Sakagami², and T. Johzaki⁹

¹Graduate School for the Creation of New Photonics Industries,
Hamamatsu, Shizuoka, Japan

²National Institute for Fusion Science (NIFS), Toki, Gifu, Japan

³Toyota Technical Development Corp., Japan

⁴Advanced Material Engineering Div., TOYOTA Motor Corporation, Japan

⁵Institutes of Innovation for Future Society, Nagoya University, Nagoya, Japan

⁶Purdue University, West Lafayette, IN 47907, USA

⁷Institute of Laser Engineering, Osaka University, Osaka, Japan

⁸National Institute of Advanced Industrial Science and Technology (AIST), Tokyo, Japan

⁹Hiroshima University, Higashi-Hiroshima, Japan

Corresponding Author: Y. Mori, ymori@gpi.ac.jp

A laser-driven inertial fusion energy (IFE) reactor should achieve the fusion of injected fuel pellets, which are continuously delivered into the reaction chamber and engaged by laser beams at 10's Hz. Using a repetitive, 100 fs ultraintense laser HAMA [1], we have demonstrated the engagement of 1-Hz-injected flying pellets involving fusion neutron reaction for the first time [2]. To induce the fusion burn, injected fuel pellets should be imploded to reach a high-density states that beyond 1000 times of solid density and an ignition temperature beyond 5 keV. A spherical shell is most reliable target design to achieve such a high-density state which has been confirmed in several inertial confinement fusion (ICF) facilities.

IFE

We have developed a testbed of shell injection system that delivers a spherical shell of deuterated polystyrene with 500 μm in diameter and 7 μm in thickness. The testbed was placed in a vacuum chamber with pressure below 0.02 MPa. 25 shells are lined up in a horizontal tube and pushed by the horizontal needle to the injection point. The vertical needle dropping speed, which is driven by the free-fall gravity, was carefully tuned not to destroy the shell being stuck each other due to static electricity. We found that shells were distorted by a force of the horizontal needle. When the number of shells exceeded 25, they started to be distorted by the needle force and then lost sphericity to the level less than 88%. The friction of the tube surface is the key of the system. The number of injected shells was also depending on the tip structure of the vertical tube. In the current system, the "cone dip" structure with line contact to the surface of the shell has in the best result for release and injection of the shells resulting injection-success-ratio of 75%.

We demonstrate that: i) repetitive shell injection was possible with the needle speed of 28 cm/s to release the shell one by one without distortion of the shell structures, and, ii) distribution of injected shell after 18 cm free-fall was within 11 mm diameter circle, which is still 10 times larger than that of the bead injection system, and the laser-hit-ratio would be the level of 5%. This specification is enough for the first laser engagement experiment.

References

- [1] Y. Mori *et al.*, Nucl. Fus., **53**, 073011 (2013).
- [2] O. Komeda *et al.*, Sci. Reports **3**, 0730113 (2013).

Mechanical Mockup of IFE Reactor Intended for the Development of Cryogenic Targets Mass Production and Rep-Rate Delivery into the Reaction Chamber

E. R. Koresheva¹, B. V. Kuteev², I. V. Aleksandrova¹, A. A. Akunets¹, I. E. Osipov¹, and A. I. Nikitenko¹

¹P. N. Lebedev Physical Institute, RAS, Moscow, Russian Federation

²National Research Centre "Kurchatov Institute", Moscow, Russian Federation

Corresponding Author: E. R. Koresheva, elena.koresheva@gmail.com

A vital goal of inertial fusion energy (IFE) research is development of high-precision, mass production technologies for cryogenic fuel targets fabrication and their delivery to the reaction chamber at a high rate (10–20 Hz).

At the Lebedev Physical Institute (LPI), a mechanical mockup of an IFE reactor has been proposed for developing the reactor-scaled technologies that are applicable to mass production of the cryogenic targets and their high-rep-rate delivery. The report presents an overview of the researches underlying this approach, including:

- Target mass production. Free-standing cryogenic target production using the FST-technology developed at LPI was demonstrated for cryogenic targets of 1 to 2 mm-diameter with fuel layer up to 100 μm -thick.
- Target rep-rate delivery. A system for high-rep-rate assembly of the sabot and target (sabot is the target carrier during its acceleration). The report discusses the results, both theoretical and experimental, on modelling a friction-free electromagnetic acceleration of the levitating assembly "HTSC-Sabot + Target", where HTSCs are the high temperature superconductors.
- Injected target on-line tracking. The results of computer experiments on Fourier holography for application to injected target on-line diagnostics and tracking are presented.
- Target protection. A system proposed for multiple target protection methods is based on the following principles:
 1. Formation of the cryogenic layer with an isotropic ultrafine fuel structure to reduce the layer sensitivity to the external thermal and mechanical loads.
 2. Use of friction-free delivery of the "HTSC-Sabot + Target" assembly to reduce the heat flux on the target.
 3. Use of conical supports for a target nest in the sabot to reduce the mechanical loads arising during acceleration of the "HTSC-Sabot + Target" assembly.
 4. Use of outer coatings (cryogenic, metal) in the target design to reduce risks of cryogenic layer damage as a result of target heating by thermal radiation of the hot chamber walls.
 5. Co-injection of a target and a protective cover from freezing gases (D_2 , Xe) to reduce risks of cryogenic layer damage as a result of target heating by hot residual gases in the reaction chamber.

This work was supported by the RF State Task of the Lebedev Physical Institute, and by the International Atomic Energy Agency.

Electron Acceleration in Dense Plasmas Heated by Picosecond Relativistic Laser

N. Iwata¹, Y. Sentoku¹, T. Sano¹, and K. Mima²

¹*Institute of Laser Engineering, Osaka University, Osaka, Japan*

²*Graduate School for the Creation of New Photonics Industries, Hamamatsu, Shizuoka, Japan*

Corresponding Author: N. Iwata, iwata-n@ile.osaka-u.ac.jp

Laser light with relativistic intensities and pulse length exceeding picosecond (ps) has been available recently. Fast electrons generated by over-ps laser-matter interactions are found to be enhanced beyond the scaling laws used in the sub-ps regime. Theories for sub-ps interactions cannot be scaled up simply to ps regime due to that meso-scale physics such as ion fluid dynamics and multiple scattering of electrons by intense fields set in.

We develop theoretical models for superthermal electron generation in ps relativistic laser-plasma interactions. Relativistic-intensity lasers are capable to push dense plasma and form a sharp interface by the laser hole boring (HB). We find that due to the continuous laser heating in ps time scale, the pressure balance between plasma and laser light is established being assisted by the sheath electric field, which acts as a surface tension, and then, the HB stops [1]. By solving the pressure balance equation, we derive the limit density for the HB, above which the laser light cannot push beyond. After the HB stops, the hot plasma starts to blowout back towards the laser at the interface where electrons interact with the intense laser multiple times stochastically and gain energy.

Electron acceleration through multiple scattering by laser is also found in a multi-ps laser interaction with thin foil where fast electrons recirculate around [2]. We here study the electron energy distribution based on the relativistic Fokker-Plank equation in momentum- p space. We introduce new diffusion and friction coefficients that represent the stochastic processes in the laser-foil interaction. The steady solution of the Fokker-Plank equation is found to be a power law when the diffusion coefficient is proportional to p . The particle-in-cell simulation shows that the high energy component of the electron distribution becomes a power law during the over-ps interaction. Our finding provides a further insight for complex multi-ps laser plasma interactions.

The new electron acceleration mechanisms we studied here are essential for various applications of ps intense lasers, and also important in terms of laboratory astrophysics being related to the stochastic acceleration of cosmic rays in universe.

References

- [1] N. Iwata *et al.*, Nat. Commun. **9**:623, (2018).
- [2] N. Iwata *et al.*, Phys. Plasmas, **24**, 073111 (2017).

Target Design Study of Fast Ignition for Ignition and Burning Experiments

H. Nagatomo¹, T. Johzaki², T. Asahina¹, A. Hata¹, Y. Sentoku¹, K. Mima³, and H. Sakagami⁴

¹*Institute of Laser Engineering, Osaka University, Osaka, Japan*

²*Hiroshima University, Higashi-Hiroshima, Japan*

³*Graduate School for the Creation of New Photonics Industries, Hamamatsu, Shizuoka, Japan*

⁴*National Institute for Fusion Science (NIFS), Toki, Gifu, Japan*

Corresponding Author: H. Nagatomo, naga@ile.osaka-u.ac.jp

In the fast ignition of laser fusion, a reliable target design is required for an ignition scale target. This paper shows the first optimized target design of an implosion phase of the fast ignition, which is scalable to larger targets.

The fast ignition scheme can be divided into three main processes; the formation of highly compressed fuel core plasma, the generation of high-energy electrons by an intense short pulse laser, and the heating fuel core by the high energy electrons. In the first process, a high-areal-density fuel core should be formed to stop the high-energy electrons. For the demonstration of a self-ignition the areal density should be more than 1.1 g/cm^2 . For the self-ignition and high gain target designs it is necessary to carry out many implosion simulations for the large targets which require large amount of computer resources. We conducted 2D implosion simulation of DT solid spherical target with gold cone target using the optimized laser pulse shape. Finally, we estimated the requirement of the implosion laser energy on the basis of the hydrodynamic similarity rule.

In conclusion, a target can be highly compressed using multistep laser pulse irradiation to a solid spherical target. In the FIREX-I scale implosion ($6.25 \text{ kJ}/0.35 \text{ }\mu\text{m}$), the maximum areal density of DT fuel (ρR_{max}) reaches 0.28 g/cm^2 with a gold guiding-cone according to two-dimensional simulation. Based on the hydrodynamic similarity, we estimate that the requirement of implosion laser energy for ignition scale target ($\rho R_{\text{max}} = 1.1 \text{ g/cm}^2$) is 380 kJ .

In order to optimize the whole process of fast ignition, heating simulation is necessary in the next step. This highly compressed fuel core profiles at the maximum ρR time will be the initial conditions of kinetic simulations for the next processes, where generation of energetic electrons due to the nonlinear relativistic laser plasma interaction, transport and absorption of the energetic electrons processes will be simulated. External magnetic field is effective for improving the heating efficiency because it reduce the divergence angle of the energetic electrons. It will be taken account in next design study.

Progress of a DPSSL Based R&D Facility TERU for IFE Technology and Industrial Applications

T. Watari¹, T. Sekine¹, R. Yoshimura¹, Y. Hatano¹, K. Matsukado¹, N. Akiyama¹, Y. Muramatsu¹, Y. Mizuta¹, Y. Takeuchi¹, H. Kimura¹, Y. Kabeya¹, T. Kurita¹, and Y. Kato¹

¹Hamamatsu Photonics, K.K., Hamamatsu City, Shizuoka, Japan

Corresponding Author: T. Watari, takeshi.watari@lsr.hpk.co.jp

In the most recent study of inertial confinement fusion, the integration experiments to demonstrate ignition burn are planned using kilojoule to megajoule class laser beam lines in the world. These experiments are based on the “single-shot” experiment of which repetition rate is several-shots per day due to limitations of laser cooling time. A dozen shots every second are required to realize the inertial fusion energy (IFE) power plant. We focus on the development of high-energy and high-repetition-rate laser system to assess a continuous supply system of fuel pellets, a control system of the laser injection, and a feedback system linked with radiation measurements. Since 2010, we have initiated a construction of a 100 J class diode-pumped solid-state laser (DPSSL) based facility “TERU” (Trek on fusion Energy Roadmap toward Utopia) for research and development on component technologies and related industrial applications. TERU is the first laser facility for IFE research based on 100 J class DPSSL. Status of the current DPSSL is 50 J at 0.5 Hz. The laser amplifier head was designed to evaluate a high gain with high energy storage in the cryogenically cooled Yb:YAG ceramics. A small-signal-gain (SSG) of the Yb:YAG ceramics amplifier pumped by 400 kW has reached 20 with stored energy of 148 J at cooling temperature of 100 K. This is the highest SSG of the cryogenically cooled Yb:YAG ceramics amplifier storing energy over 100 J. This result becomes a benchmark of the high gain with stored energy performance to design the next kilo-joule-class cryogenically cooled Yb:YAG ceramics amplifier. We also start the laser irradiation experiment to explore the fundamental physics of implosion processes, e.g., plane target acceleration, which could replicate the implosion in laser fusion. In our preliminary experiment, a velocity of the aluminium plane target (a thickness of 20 μm) accelerated with $2.0 \times 10^{12} \text{ W/cm}^2$ laser irradiation was observed by VISAR measurement. The acceleration velocity reached 560 m/s. The acceleration velocity changing target thicknesses is stored as a database with repetitive laser irradiation. Such database will be useful for the target design and benchmark of hydrodynamics codes.

Interpenetration and Stagnation in Collapsing Plasmas

K. F. Al-Shboul¹

¹*Nuclear Engineering Department, Jordan University of Science & Technology, Jordan*

Corresponding Author: K. F. Al-Shboul, kfshboul@just.edu.jo

Future inertial fusion reactors are supposed to work with long pulses or with high repetition rates using repeated pellet implosions. In such extreme environments, the reactor wall materials will be disclosed to short X-ray pulses and fusion generated fragments. This will cause ablation of the wall material in the form of plasma that is expected to collide with each other in the centre of the chamber or interpenetrate to elsewhere within the reactor chamber. In this work, a laboratory experimental setup is devoted to use colliding plasmas scheme to investigate the collision effects similar to plasma facing components in fusion reactors.

Different materials were used for these collapsing plasma experiments for controlling the velocity of plasma plumes. A special experimental setup was built where the laser is focussed into a line-like shape impinged as two perpendicular beams onto a semicircular target. The setup was carefully built to force the seed plasmas to collapse in the centre of the chamber prior to the colliding process. The interpenetration and stagnation layer, if exists, of plasmas of candidate fusion wall materials, viz., carbon and tungsten, and other materials, viz., aluminium, and molybdenum were investigated in this study. While tungsten plumes interpenetrate each other at the colliding interface, carbon colliding plumes formed a strong stagnation layer, which could be a source of nanoparticles and plasma aerosols generation that may hinder fusion high repletion rates.

MPT: Materials Physics and Technology

Influence of Plasma Impurities on the Fuel Retention in Tungsten

A. Kreter¹, D. Nishijima², R. P. Doerner², M. Freisinger¹, C. Linsmeier¹, Y. Martynova¹, S. Möller¹, M. Rasinski¹, M. Reinhart¹, A. Terra¹, Y. Torikai³, and B. A. Unterberg¹

¹*Institute of Energy and Climate Research, Forschungszentrum Jülich, Jülich, Germany*

²*University of California San Diego, CA 92093, USA*

³*Ibaraki University, Mito, Ibaraki, Japan*

Corresponding Author: A. Kreter, a.kreter@fz-juelich.de

The first wall in ITER will be subjected to mixed species fluxes containing hydrogenic isotopes, helium produced in DT reactions and radiator gases such as argon, neon or nitrogen. It is necessary to test how plasma-facing materials perform with respect to hydrogen retention under the mixed species plasma conditions. In this study, the influence of helium, argon, neon and nitrogen as plasma impurities on the deuterium retention in tungsten was investigated in the linear plasma devices PSI-2 and PISCES-A. Tungsten samples were mechanically polished then recrystallized at 2070 K for 1 h before the exposure. The following mixed plasmas were produced: pure D, D+0.03He, D+0.07Ar, D+0.1Ne, D+0.05N and D+0.03He+0.07Ar. The exposure conditions were as follows: incident ion flux of $\sim 10^{21}$ to $10^{22}/\text{m}^2\text{s}$, incident ion fluence of 1×10^{25} to $1 \times 10^{26}/\text{m}^2$, sample temperatures of 500 and 770 K. The incident ion energy was 70 eV, above the W sputtering threshold for Ar and N, but below it for D and He. For Ne, in addition, it was varied between 20 and 70 eV, below and above the W sputtering threshold, respectively. After exposures, samples were analyzed by SEM, TEM, NRA and TDS. The He admixture reduced the D retention by one order of magnitude, while Ar increased it by about 50%. In the D+He+Ar case the effect was similar as for D+Ar. Ar probably sputtered the near-surface layer and thus overrode the He effect. The effect of Ne appeared to be sensitive on the incident ion energy. Ne had an effect similar to Ar increasing the D retention for the ion energies above the sputtering threshold, while for lower energies its effect was less pronounced. Addition of nitrogen increased the D retention by a factor of ~ 10 and ~ 100 for 500 K and 770 K, respectively. In general, the effect of impurities on D retention appears to be sensitive to the properties of the damaged near-surface layer of tungsten. Admixed species, i.e., He, can form a near-surface damaged layer with open porosity, which serves as an escaping channel for D thus decreasing the D retention. However, if the process is dominated by sputtering, as for Ar, such a layer cannot be formed. The N enriched layer, in contrast, serves as a desorption barrier for D increasing its retention.

High-Temperature Creep Properties of NIFS-HEAT-2 High-Purity Low-Activation Vanadium Alloy

T. Nagasaka^{1,2}, T. Muroga^{1,2}, T. Tanaka^{1,2}, A. Sagara^{1,2}, K.-I. Fukumoto³, P. F. Zheng⁴, and R. J. Kurtz⁵

¹National Institute for Fusion Science (NIFS), Toki, Gifu, Japan

²Graduate University for Advanced Studies, Toki, Gifu, Japan

³Research Institute of Nuclear Engineering, University of Fukui, Tsuruga, Japan

⁴Southwestern Institute of Physics, Chengdu, Sichuan, People's Republic of China

⁵Pacific Northwest National Laboratory (PNNL), Richland, WA 99354, USA

Corresponding Author: T. Nagasaka, nagasaka@nifs.ac.jp

The National Institute for Fusion Science (NIFS) developed the NIFS-HEAT in collaboration with Japanese universities. Previous heats exhibited brittle fracture of weld joints and cracking during tubing fabrication at room temperature, due to ductility loss caused by interstitial impurities, such as C, N and O. The total of interstitial impurity level of NH₂ is almost half that of the US heat. As a result, weldability and workability were successfully improved because of enhanced ductility. Although many properties were improved by the purification, possible degradation of high-temperature strength due to purification softening was a concern. Therefore, the present study evaluated the high-temperature creep properties of NH₂, which were expected to be sensitive to impurity levels.

Creep rupture time of NH₂ in the lower applied stress region (≤ 100 MPa) was comparable to the US heat at 800°C, although in the higher stress region, the rupture time was shorter than that for US data. The creep activation energy of the US heat was 320 kJ/mol in average, and consistent with 270 kJ/mol for self-diffusion energy in pure vanadium. This indicates that climb-assisted dislocation motion is the predominant process for creep. NH₂ showed higher activation energy, 640 kJ/mol, suggesting additional deformation process. Since the applied stress in the creep tests, 150 to 200 MPa, was close to the yield stress (195 MPa) of NH₂, thermally activated dislocation glide was thought to be induced and thus enhanced creep.

The creep data were converted by time-temperature equivalence scaling using the Larson-Miller parameter. Some of the parameters for NH₂ are smaller than those for the US heat, however are still superior to fusion-grade steels. As mentioned above, creep properties were not degraded by the purification at stress levels ≤ 100 MPa. This means that the purification requires no change in design stress for blanket, because the thermal stress would be less than this level, assuming the first wall consists of a simple edge-constraint plate with heat flux and wall thickness of less than 1 MW/m² and 5 mm, respectively.

In conclusion, the purification for NH₂ improved many properties, such as weldability and workability, and raised no negative effect on high-temperature creep properties under the projected blanket service stresses.

Model Validation on EAST and DIII-D Experiments towards Understanding of High-Z Material Erosion and Migration in a Mixed Materials Environment

R. Ding¹, H. Xie¹, M. Komm², D. L. Rudakov³, T. Abrams⁴, A. R. Briesemeister⁵, S. Brezinsek⁶, I. O. Bykov³, V. S. Chan⁴, J. Chen¹, R. Dejarnac², F. Ding¹, J. D. Elder⁷, H. Y. Guo⁴, A. Kirschner⁶, P. B. Snyder⁴, P. C. Stangeby⁷, E. A. Unterberg⁵, W. R. Wampler⁸, H. Q. Wang¹, L. Wang¹, and J. G. Watkins⁸

¹*Institute of Plasma Physics, Chinese Academy of Sciences, Hefei, Anhui, People's Republic of China*

²*Institute of Plasma Physics AS CR v.v.i., Prague, Czech Republic*

³*University of California San Diego, CA 92093, USA*

⁴*General Atomics, San Diego, CA 92186, USA*

⁵*Oak Ridge National Laboratory (ORNL), Oak Ridge, TN 37831, USA*

⁶*Forschungszentrum Jülich, Jülich, Germany*

⁷*Institute for Aerospace Studies, University of Toronto, Toronto, ON M5S-1A1, Canada*

⁸*Sandia National Laboratories (SNL), Albuquerque, NM 87185, USA*

Corresponding Author: R. Ding, rding@ipp.ac.cn

The 3D Monte Carlo code ERO taking into account a material mixing surface model has been used to simulate tungsten (W) erosion and migration on EAST with an upper full W divertor and DIII-D with toroidally continuous W rings embedded in the divertor target. Modelling shows that the transport of carbon (C) impurities not only dominates the W sputtering source but also determines the overall erosion and deposition balance in the mixed materials surface. With a self-consistent calculation of C impurity transport and taking into account the re-erosion of W by returned eroded particles, W gross erosion rates measured by WI spectroscopy can be well reproduced by the modelling for both devices. The $E \times B$ drift and lower electron temperature at the radial outboard side lead to a net deposition zone where W and C are accumulated, which is consistent with the measurements with several changeable inserts in a specially designed collector probe at the DiMES system in DIII-D. In the net erosion zone closer to the outer strike point, the W coverage on C is very low and saturated independent of exposure time, agreeing with the measurements by collector probes. Strong sheath effects on material erosion rates have also been observed using external biasing samples. The particle flux and material erosion as a function of biasing voltage have been analyzed by SPICE2 and ERO codes. Both the PIC simulation and the D_α emission measured by a fast camera reveal that with increasing biasing voltage the ion flux decreases at the biased area while increases at the adjacent downstream tile, although the biased sample potential is far below the plasma potential. Detailed modelling shows that the ion flux variation at different area is due to the strong gradient of the electric field in the sheath, which results in different magnitude of the polarization drift above the biased and unbiased surface. The reduced ion flux and incident energy are responsible for more than an order of magnitude reduction of erosion with slight positive voltage biasing in the experiments. The critical role of C impurities and the sheath in determining high-Z material erosion and migration have been revealed. This understanding indicates promising methods for erosion control, which is critical for material lifetime, plasma impurity content, and tritium retention in future fusion reactors.

Evaluation of Tungsten as Divertor Plasma-Facing Material: Results from Ion Irradiation Experiments and Computer Simulations

P. N. Maya¹, P. Sharma¹, P. M. Raole¹, S. S. Vala², A. Satyaprasad², S. S. Mukherjee³,
P. K. Pujari³, P. K. Kulriya⁴, P. K. Bajpai⁵, A. Attri¹, A. K. Tyagi¹, M. Warriar⁶,
P. V. Subhash¹, P. Kikani², P. A. Rayjada², C. David⁷, A. Lakhani⁸, V. Karki³, M. Singh³,
R. Kumar², M. R. Abhangi², K. D. Devi⁴, K. Kedarmal⁴, S. P. Patel⁵, T. A. Trivedi⁵,
K. Saravanan³, S. Kannan³, S. Mishra³, K. B. Khan³, P. Nandi¹, S. S. Khirwadkar¹, and
S. P. Deshpande¹

¹International Thermonuclear Experimental Reactor (ITER), India Centre, Gujarat, India

²Institute for Plasma Research (IPR), Bhat, Gandhinagar, India

³Bhabha Atomic Research Centre (BARC), Mumbai, India

⁴Inter-University Accelerator Center, New Delhi, India

⁵Guru Ghasidas Vishwavidyalaya, Bilaspur, (C.G.), Koni, Chhattisgarh 495009, India

⁶Bhabha Atomic Research Centre (BARC), Visakhapatnam, India

⁷Indira Gandhi Center for Atomic Research, Kalpakkam, TN, India

⁸UGC-DAE Consortium for Scientific Research, Indore, MP, India

Corresponding Author: P. N. Maya, maya.padivattathumana@iter-india.org

Tungsten has emerged as divertor-plasma-facing material in fusion reactors due to its excellent thermal and mechanical properties as well as low tritium affinity. It is therefore essential to understand the behaviour of tungsten in reactor-like conditions from the point of view of radiation damage and fuel retention. There is already a world-wide effort in creating a database of radiation damage and retention by surrogate ion irradiation. In this paper, we present results of experiments and computer simulations of radiation damage and deuterium trapping due to light, medium and heavy ions in poly-crystalline tungsten. The idea is to develop a deeper understanding of the radiation damage, evolution of the defects and their impact on hydrogen-isotope trapping.

Several irradiation experiments have been carried out with ions of Au, W, B, He and D of energies ranging from 100 keV–80 MeV. We have found that for the same fluence (1.3×10^{18} ions/m²) of the impinging ions, the ion-mass plays a critical role in the defect creation and subsequent deuterium trapping. The samples irradiated with 80 MeV Au ions were found to show more D-isotope retention in comparison with 10 MeV boron ions. The range of both the ions were similar. For an order of magnitude higher fluence of boron (1.0×10^{19} ions/m²), the trapped deuterium content was considerably lower than that of Au. The defect density observed Au irradiated sample was several orders of magnitude higher than the B irradiated ones. A similar observation was also confirmed using low temperature resistivity measurements.

In MD simulations, we see that at large energies of the primary knock-on Atom (> 160 keV) the fragmentation of the cascade occurs which may have a direct relation to the experiments of heavy ion irradiation at 80 MeV where we see prominently dense clustering of dislocations and vacancies. Interestingly 10 MeV boron damage seems to produce PKA spectrum somewhat similar to that of 14 MeV neutron which is distinctly different than the defects produced and consequently deuterium trapping from heavy ion irradiation. These results will be presented along with computer simulations and limits to extrapolation damage from surrogate to neutrons will be highlighted.

The European Approach to the Fusion-Like Neutron Source: The IFMIF-DONES Project

A. Ibarra¹, M. Pérez¹, F. Arbeiter², D. Bernardi³, A. García¹, W. Krolas⁴, M. Cappelli⁶, U. Fischer², R. Heidinger⁵, D. Jiménez¹, F. Martín-Fuertes¹, G. Micciché³, F. S. Nitti³, T. Pinna⁶, and K. Tian²

The IFMIF-DONES Team

¹*Centro de Investigaciones Energéticas, Medioambientales y Tecnológicas (CIEMAT), Madrid, Spain*

²*Karlsruhe Institute of Technology (KIT), Karlsruhe, Germany*

³*ENEA/Brasimone, Camugnano BO, Italy*

⁴*Institute of Nuclear Physics, Polish Academy of Sciences, PL-31342 Krakow, Poland*

⁵*F4E: Fusion for Energy, ITER EU Centre, 08019 Barcelona, Spain*

⁶*ENEA C. R. Frascati, Dipartimento FSN, Frascati, Italy*

Corresponding Author: A. Ibarra, angel.ibarra@ciemat.es

The need of a neutron source for the qualification of materials to be used in future fusion power reactors have been recognized in the European (EU) fusion programme since many years. The construction and exploitation of this facility is presently considered to be in the critical path of DEMO. This issue prompted the EU to launch activities for the design and engineering of the IFMIF-DONES (International Fusion Materials Irradiation Facility-DEMO Oriented Neutron Source) facility based on and taking profit from the results obtained in the IFMIF/EVEDA (Engineering Validation and Engineering Design Activities) project, presently conducted in the framework of the EU-Japan bilateral agreement on the broader approach to fusion.

These activities and R&D work for the IFMIF-DONES Plant are presently taking place in the framework of a work package of the EUROfusion Consortium, in direct collaboration with Fusion for Energy Organization. The main objective of these activities is to consolidate the design and the underlying technology basis in order to be ready for IFMIF-DONES construction as early as possible. This paper presents the main engineering results for a generic site obtained during the first years of design work, as indicated in the recently released IFMIF-DONES Preliminary Engineering Design Report, making emphasis on the design evolution from previous phases and on the critical issues to be further developed in the near future. The proposed European site to host the facility (Granada Spain) is briefly introduced as well.

This work has been carried out within the framework of the EUROfusion Consortium and has received funding from the Euratom research and training programme 2014–2018 under grant agreement No. 633053. The views and opinions expressed herein do not necessarily reflect those of the European Commission, Fusion for Energy, or of the authors' home institutions or research funders.

PPC: Plasma Overall Performance and Control

Predictive Integrated Modelling of Plasmas and their Operation Scenarios towards Exploitation of JT-60SA Experiment

N. Hayashi¹, J. Garcia²

The JT-60SA Team

¹*National Institutes for Quantum and Radiological Science and Technology (QST),
Naka Fusion Institute, Naka-shi, Ibaraki-ken, Japan*

²*Institut de Recherche sur la Fusion par confinement Magnétique (IRFM),
Commissariat à l'énergie atomique (CEA/Cadarache), 13108 St. Paul lez Durance, France*

Corresponding Author: N. Hayashi, hayashi.nobuhiko@qst.go.jp

Plasmas and their operation scenarios have been predicted by using integrated modelling codes towards the exploitation of JT-60SA experiment. Through the close collaboration between Japan and EU including the model validation and verification using JT-60U and JET experimental data, the following key results were obtained in various modelling activities. Improved modelling predicted a steady-state high- β ($\beta_N > 4$) plasma with an internal transport barrier (ITB), its controllability to sustain the ITB location and target performance, and its tolerance to the core accumulation of impurity seeded to reduce the divertor heat load below 10 MW/m^2 , with actuator powers within the machine capability. Integrated rotation and pedestal modelling for inductive scenarios revealed that the rotation with the neoclassical toroidal viscosity (NTV) due to the toroidal magnetic field ripple degrades the pedestal height, but it is high enough to achieve target parameters, and error field correction coils in JT-60SA have the potential to control the rotation by changing NTV. The obtained predictions clarified the JT-60SA capability to explore the plasma scenarios indispensable to ITER and DEMO.

Exploring an Alternate Approach to $Q = 10$ in ITER

T. C. Luce^{1,3}, F. Turco¹, J. R. Ferron², J. M. Hanson¹, and A. W. Hyatt²

¹Columbia University, New York, NY 10027, USA

²General Atomics, San Diego, CA 92186, USA

³International Thermonuclear Experimental Reactor (ITER),
Cadarache Centre, 13108 St. Paul lez Durance, France

Corresponding Author: T. C. Luce, tim.luce@iter.org

Stable and robust ITER Baseline Scenario demonstration discharges have been achieved in DIII-D at zero injected input torque (matching the ITER LSN shape including the aspect ratio, $\beta_N = 1.9$ – 2.05 , and $q_{95} = 3$), and repeated under various conditions (I_p , density, wall conditions). However, an alternate route to $Q = 10$ conditions has been explored that starts at higher q_{95} and maximum B_t . Performance to reach 500 MW of fusion power is reached at all torque levels. With co-NBI, the goal is reached by 11 MA equivalent, and the achieved β does not increase above 12.5 MA. At zero torque, 13.5 MA may be sufficient to reach $P_{fus} = 500$ MW. The gain metric β_τ does not improve above 13 MA equivalent (which corresponds to $q_{95} \sim 3.7$), and all torque curves show the same trends for the evolution to saturation. This indicates that this saturation effect, observed previously in DIII-D, is not likely to be due to an $E \times B$ shear effect.

Comparing 15 and 13 MA equivalent cases, three causes for the confinement changes will be assessed: i) differences in dimensionless parameters such as ρ^* , β , ν^* , q ; ii) increase in the sawtooth inversion radius at higher current; and, iii) broadening of the NBI deposition profile. The fusion gain metric β_τ saturates around the 13 MA equivalent mark for all torque values, so the benefits to fusion energy performance of increasing current may not be fully realized. Further study is needed to determine the origin of this.

SEE: Safety, Environmental and Economic Aspects of Fusion

Tritiated Dust: The Impact on Tokamak Operation

C. Grisolia¹, F. Gensdarmes², G. Dougniaux², S. Peillon², E. Bernard¹, A. Autricque¹, G. Pieters³, B. Rousseau³, S. Feuillastre³, S. Garcia-Argote³, O. Carvalho³, V. Mallard⁴, T. Orsiere⁵, C. Uboldi⁵, J. Rose⁶, D. Lambertin⁷, C. Decanis⁸, D. Vrel⁹, and K. Liger¹⁰

¹Institut de Recherche sur la Fusion par confinement Magnétique (IRFM),

Commissariat à l'énergie atomique (CEA/Cadarache), 13108 St. Paul lez Durance, France

²Institut de Radioprotection et de Sûreté Nucléaire (IRSN), PSN-RES, Gif-sur-Yvette, France

³Institut des sciences du vivant Frédéric-Joliot, CEA/Saclay, 91191 Gif-sur-Yvette, France

⁴BIAM, Commissariat à l'énergie atomique (CEA/Cadarache), 13108 St. Paul lez Durance, France

⁵Institut Méditerranéen de Biodiversité et d'Ecologie marine et continentale (IMBE),

Aix-Marseille Université, Marseille, France

⁶L'Institut de recherche pour le développement (IRD), Aix-Marseille Université, Marseille, France

⁷DEN/DE2D/SEAD/LCBC, CEA/Marcoule, 30207 Bagnols-sur-Cèze, France

⁸DEN/DDCC/UADC/BD, CEA/Cadarache, 13108 St. Paul lez Durance, France

⁹Laboratoire des Sciences des Procédés et des Matériaux (LSPM),

Université Paris 13, Sorbonne Paris Cité, 93430 Villetaneuse, France

¹⁰DEN/DTN/SMTA/LIPC, CEA/Cadarache, 13108 St. Paul lez Durance, France

Corresponding Author: C. Grisolia, christian.grisolia@cea.fr

During ITER operation, plasma interacts with the machine plasma facing components (PFCs) through various physical processes and gives birth to particles from nanometer to tens of μm sizes, called “dusts” in the fusion community. Depending on the plasma wall interaction, different dust types will be created from almost spherical particles induced by high heat flux interaction with metal (unipolar arcs, ELMs, disruption) to fractal ones created by accretion in the edge of this high density/long pulse plasma machine. Dust properties, especially their ability to be covered by an oxide insulating layer and their surface topology, deeply affect their tritium inventory. It has been already shown [1] that dust tritium inventory is two to three orders of magnitude higher than massive material. It can be then asserted that tritium inventory can be ranged from some GBq/g for tungsten particles to much higher values for beryllium ones. Due to tritium beta decay, these particles are rapidly positively charged. As an example, a $5\ \mu\text{m}$ diameter single tungsten particle with a tritium inventory of 10 GBq/g will have a charge of 6×10^{-17} Coulomb in 1 hour. Dust physico-chemical properties and radioactive electrical self-charging process have numerous consequences in term of operation and safety and the major goal of this presentation is to highlight them.

The first step of this paper consists to list how the dusts are created in the ITER machine using laboratory and tokamak current results. The properties of the created particles (composition, size and morphology) considering all the physical processes initiated in this framework will be presented. Moreover, we will insist here on the fact that all the particles are covered by an insulating oxide layer that triggers dust adhesion properties as it has been clearly exemplified in [2]. In this paper, experimental investigations on the electric field strength required to overcome the adhesion forces of micron size tungsten metallic dust as well as silver and aluminium oxide in powdery form deposited on a conductive surface are presented.

References

- [1] A. El-Kharbachi *et al.*, Int. J. Hydrogen Energy, **39-20**, 10525 (2014).
- [2] S. Peillon *et al.*, Journal of Electrostatics, **88**, 111–115 (2017).

Waste Implications from Minor Impurities in European DEMO Materials

M. R. Gilbert¹, T. Eade¹, C. Bachmann², U. Fischer³, and N. P. Taylor¹

¹*Culham Centre for Fusion Energy (CCFE), Culham Science Centre, Abingdon, UK*

²*EUROFusion (EFDA), Max-Planck-Institut für Plasmaphysik, Garching, Germany*

³*Karlsruhe Institute of Technology (KIT), Karlsruhe, Germany*

Corresponding Author: M. R. Gilbert, mark.gilbert@ukaea.uk

Waste-production predictions for the future demonstration fusion power plant (DEMO) are necessary to produce an accurate picture of the likely environmental and economic costs of radioactive waste disposal at end-of-life (EOL). Even during the conceptual stage of DEMO design it is important to perform waste assessment so as to avoid potential surprises caused by design flaws that could lead to unacceptable levels of long-term high-level waste. An integrated simulation process combining Monte Carlo neutron transport simulations, high-fidelity inventory calculations, and extensive and reproducible postprocessing algorithms has been used for the evolving European DEMO designs to quantify the time-varying mass inventories in different waste classes for individual regions and components of the reactor vessel, as well as for the reactor as a whole.

Waste categories based on UK regulations reveal that minor impurities contained in certain materials, such as Eurofer, tungsten, and beryllium, can have a significant impact on the waste classification prospects of materials, potentially leading to the production of waste that will remain as intermediate level-waste (or worse) for hundreds of years beyond DEMO EOL.

The computational framework developed for these assessments can be rapidly and continuously applied to the maturing DEMO design, helping to guide design choices to mitigate long-lived waste production and ensure that most waste becomes low-level waste (or better) within a few decades.

SEE

Future Possibility of Carbon Sequestration by Biomass-Fusion Hybrid Systems

S. Konishi¹, S. Takeda¹, H. Nam¹, and K. Tokimatsu²

¹*Institute of Advanced Energy, Kyoto University, Nishikyo-ku, Kyoto 615-8540, Japan*

²*Tokyo Institute of Technology, Tokyo, Japan*

Corresponding Author: S. Konishi, s-konishi@iae.kyoto-u.ac.jp

This paper proposes a new and innovative fusion energy application in the emissions trading market based on the combination with biomass processing. An endothermic biomass conversion reaction of charcoal making process, or dry distillation; $(\text{CH}_{1.6}\text{O}_{0.6}) = \text{C} + 0.4\text{H}_2 + 0.6\text{H}_2\text{O} - 451 \text{ kJ}$ (where biomass is assumed to be woody including a large fraction of lignin) can convert fusion energy obtained as high-grade heat into carbon.

The product solid char is separated and can be stored as it is or sintered. This biomass-fusion hybrid system will provide an innovative carbon sequestration method that originally is recovered from atmosphere by the photosynthesis by plants. What this system provides is the isolation of CO_2 from the earth cycle including fossil combustion, and stabilizes it as solid carbon, and “sells” in the emissions trade market. If the values of the electricity and emission credits are similar to those currently observed, total sales, i.e., chance to return the investment for fusion would be similar. While competition in the clean electricity market in the future is anticipated to be tough, CCS market can provide significantly larger capacity because no other alternative technologies are known other than the underground storage. In this emissions credit market, fusion has fewer competitors that may have limiting siting and environmental constraint.

Because transport, some industrial and residential heat sectors unavoidably release CO_2 , net negative emission by human activity with biomass is inevitable. This new fusion-biomass hybrid can provide net negative emission not only for electricity, but for all kinds of CO_2 sources, and suggests the solution to return the CO_2 concentration to the age before the industrial revolution. This study proposes an innovative option of fusion application that could potentially be larger and more important than electricity generation, and justifies the investment of fusion development that could be recovered from the future market.

Economic Performance of Fusion Power Plant on Future Deregulated Electricity Market

S. Takeda¹, S. Sakurai¹, and S. Konishi²

Rapporteured by: S. Konishi

¹*Graduate School of Advanced Integrated Studies in Human Survivability,
Kyoto University, Nishikyo-ku, Kyoto 615-8540, Japan*

²*Institute of Advanced Energy, Kyoto University, Nishikyo-ku, Kyoto 615-8540, Japan*

Corresponding Author: S. Takeda, shu.takeda@gmail.com

The economic performance of steady-state fusion power plants on future deregulated electricity markets was quantitatively analyzed for the first time with a newly constructed Simplified PJM Market Model. The results showed that: i) discussions based on simple levelized cost of electricity are insufficient for deregulated markets; and, ii) the unplanned outage frequency target should be lowered to 0.3 times/year on deregulated market to achieve economic rationality of fusion power plants.

Conventionally, the development strategies for fusion power plants came from extrapolation of past fission plant installation trends. However, due to the rapid transformations of the markets around the world, the future electricity markets will be significantly different from that of half a century ago. The fusion development strategies shall be revised accordingly: conventional measures such as levelized cost of electricity (LCOE) may no longer be applicable to future fusion power plants.

To quantitatively analyze the economic performance of steady-state fusion power plants on future deregulated electricity markets, Simplified PJM Market Model that incorporates three energy market, imbalance fee and ancillary service market was constructed. A steady-state fusion power plant with 1200 MW electrical output (2801 MW fusion) was assumed. The net present values (NPVs) of 40 years of plant operation were calculated with the discount rate of 1.7%. A sensitivity analyses were conducted for the unplanned outage frequency from 0.001 to 0.00001 times/hours.

The economic performance of a fusion power plant showed higher sensitivity to the unplanned outage frequency on deregulated market. The NPV of fusion plant on deregulated market would be devaluated from +368 million USD to -741 million USD when the unplanned outage frequency rises from 10^{-5} per hour to 10^{-4} per hour, while on conventional market, the devaluation would be only from 370 to 285 million USD.

This study pioneered a vital new area for the economic assessment of fusion power plant: the economic performance on the deregulated electricity market. Results show that discussions based on simple LCOE would be inapplicable to deregulated markets, and the unplanned outage frequency target should be lowered on deregulated market.

SEE

Techno-Economic Analysis of Biodiesel and Hydrogen Production via Fusion-Biomass Hybrid Model

H. Nam¹, S. Konishi¹

Rapporteured by: S. Konishi

¹Graduate School of Energy Science, Kyoto University, Nishikyo-ku, Kyoto 615-8540, Japan

Corresponding Author: H. Nam, namhs0107@gmail.com

This paper aims to investigate techno-economic analysis of fusion-biomass hybrid model based on previously proposed technical and chemical concept. Fusion-biomass hybrid model, which takes no value of waste biomass from municipal, agricultural, and forestry areas as feedstock, produces synthetic gas generated by endothermic pyrolytic gasification using high temperature of fusion heat. Several blanket designs based on LiPb and SiC technology such as dual coolant lithium lead (DCLL) would be available for the heat over 700°C. Its technical extension is possible to perform biomass gasification of ($C_6H_{10}O_5 + H_2O \rightarrow 6H_2 + 6CO - 814 \text{ kJ}$) to produce chemical energy, synthetic gas. Produced synthetic gas can be converted into two different products; diesel and hydrogen. First, synthetic gas that contains hydrogen (H_2) and carbon monoxide (CO) can be converted into diesel which is regarded as "carbon-neutral biofuel" by Fischer-Tropsch process ($2H_2 + CO \rightarrow -CH_2 + H_2O + 160 \text{ kJ}$). The other is to produce hydrogen by water-gas shift reaction process ($CO + H_2O \leftrightarrow H_2 + CO_2 + 32 \text{ kJ}$). Carbon dioxide from water-gas shift reaction can be managed by carbon capture and sequestration technology. Underlying the technical and chemical process of fusion-biomass hybrid model, levelized cost of fuel for diesel and hydrogen is calculated as 0.41 \$/kg and 1.21 \$/kg, respectively. Breakeven price is 0.73 \$/kg for diesel and 2.65 \$/kg for hydrogen under the assumption of 1000 ton/day of fusion-biomass hybrid plant with 30-year lifetime. Sensitivity analysis is performed applying total capital investment, operation and maintenance cost, fuel production amount, operating time and fusion heat cost to understand the correlations between variables and fuel price. In addition to that, net present value after 30-year operation is calculated according to the change in fusion heat cost and fuel price, because technical structure and advancement highly affect fusion heat cost. Fusion-biomass hybrid model benefits in terms of environmental aspect by decreasing both waste biomass and CO_2 emission. This study can provide a guideline in targeting which fuel could be economically justified in the circumstances of variable environmental policy under different market demand and economical situations that would have a significant impacts on the designing of the fusion commercial reactors.

Indexes

Abstracts by Paper Number

EX/1-1.....	160	EX/P1-24.....	219	EX/P3-26.....	272
EX/1-2.....	161	EX/P1-25.....	220	EX/P3-27.....	273
EX/1-3Ra.....	162	EX/P1-26.....	221	EX/P3-3.....	250
EX/1-3Rb.....	163	EX/P1-28.....	222	EX/P3-4.....	251
EX/10-1.....	194	EX/P1-29.....	223	EX/P3-5.....	252
EX/10-2.....	195	EX/P1-3.....	201	EX/P3-6.....	253
EX/10-3.....	196	EX/P1-30.....	224	EX/P3-7.....	254
EX/11-1.....	197	EX/P1-31.....	225	EX/P3-8.....	255
EX/11-2.....	198	EX/P1-4.....	202	EX/P3-9.....	256
EX/2-1.....	164	EX/P1-5.....	203	EX/P4-1.....	274
EX/2-2.....	165	EX/P1-6.....	204	EX/P4-10.....	282
EX/2-3.....	166	EX/P1-9.....	205	EX/P4-11.....	283
EX/2-4.....	167	EX/P2-1.....	226	EX/P4-12.....	284
EX/2-5.....	168	EX/P2-10.....	234	EX/P4-13.....	285
EX/3-1.....	169	EX/P2-11.....	235	EX/P4-14.....	286
EX/3-2.....	170	EX/P2-12.....	236	EX/P4-15.....	287
EX/3-3.....	171	EX/P2-13.....	237	EX/P4-16.....	288
EX/3-4.....	172	EX/P2-14.....	238	EX/P4-17.....	289
EX/3-5.....	173	EX/P2-15.....	239	EX/P4-18.....	290
EX/3-6.....	174	EX/P2-16.....	240	EX/P4-19.....	291
EX/4-1.....	175	EX/P2-17.....	241	EX/P4-2.....	275
EX/4-2.....	177	EX/P2-18.....	242	EX/P4-20.....	292
EX/4-3.....	178	EX/P2-20.....	243	EX/P4-21.....	293
EX/4-4.....	179	EX/P2-22.....	244	EX/P4-22.....	294
EX/5-1.....	181	EX/P2-23.....	245	EX/P4-23.....	295
EX/5-2.....	182	EX/P2-26.....	246	EX/P4-24.....	296
EX/6-1.....	183	EX/P2-27.....	247	EX/P4-25.....	297
EX/7-1.....	184	EX/P2-3.....	227	EX/P4-26.....	298
EX/7-2.....	185	EX/P2-4.....	228	EX/P4-27.....	299
EX/7-3.....	186	EX/P2-5.....	229	EX/P4-28.....	300
EX/7-4.....	187	EX/P2-6.....	230	EX/P4-29.....	301
EX/8-1.....	188	EX/P2-7.....	231	EX/P4-3.....	276
EX/8-2.....	189	EX/P2-8.....	232	EX/P4-30.....	302
EX/9-1.....	190	EX/P2-9.....	233	EX/P4-31.....	303
EX/9-2.....	191	EX/P3-1.....	248	EX/P4-4.....	277
EX/9-3.....	192	EX/P3-10.....	257	EX/P4-5.....	278
EX/9-4.....	193	EX/P3-11.....	258	EX/P4-6.....	279
EX/P1-1.....	199	EX/P3-12.....	259	EX/P4-7.....	280
EX/P1-11.....	206	EX/P3-13.....	260	EX/P4-9.....	281
EX/P1-12.....	207	EX/P3-14.....	261	EX/P5-10.....	310
EX/P1-14.....	208	EX/P3-15.....	262	EX/P5-13.....	311
EX/P1-15.....	209	EX/P3-16.....	263	EX/P5-15.....	312
EX/P1-16.....	210	EX/P3-17.....	264	EX/P5-16.....	313
EX/P1-17.....	211	EX/P3-19.....	265	EX/P5-19.....	314
EX/P1-18.....	212	EX/P3-2.....	249	EX/P5-2.....	304
EX/P1-19.....	213	EX/P3-20.....	266	EX/P5-20.....	315
EX/P1-2.....	200	EX/P3-21.....	267	EX/P5-21.....	316
EX/P1-20.....	214	EX/P3-22.....	268	EX/P5-23.....	317
EX/P1-21.....	215	EX/P3-23.....	269	EX/P5-25.....	318
EX/P1-22.....	216	EX/P3-24.....	270	EX/P5-26.....	319
EX/P1-23.....	218	EX/P3-25.....	271	EX/P5-27.....	320

EX/P5-28.....	321	EX/P7-20.....	376	FIP/2-1.....	578
EX/P5-3.....	305	EX/P7-21.....	377	FIP/2-2.....	579
EX/P5-30.....	322	EX/P7-22.....	378	FIP/2-3.....	580
EX/P5-4.....	306	EX/P7-23.....	379	FIP/2-4.....	581
EX/P5-6.....	307	EX/P7-24.....	380	FIP/3-1.....	583
EX/P5-8.....	308	EX/P7-25.....	381	FIP/3-2.....	584
EX/P5-9.....	309	EX/P7-26.....	382	FIP/3-3.....	585
EX/P6-1.....	323	EX/P7-27.....	383	FIP/3-4.....	586
EX/P6-10.....	331	EX/P7-3.....	360	FIP/3-5Ra.....	587
EX/P6-11.....	332	EX/P7-4.....	361	FIP/3-5Rb.....	588
EX/P6-12.....	333	EX/P7-5.....	362	FIP/3-6.....	589
EX/P6-13.....	334	EX/P7-7.....	363	FIP/P1-1.....	590
EX/P6-14.....	335	EX/P7-8.....	364	FIP/P1-10.....	598
EX/P6-15.....	336	EX/P7-9.....	365	FIP/P1-11.....	599
EX/P6-16.....	337	EX/P8-1.....	384	FIP/P1-12.....	600
EX/P6-17.....	338	EX/P8-11.....	394	FIP/P1-13.....	601
EX/P6-18.....	339	EX/P8-12.....	395	FIP/P1-14.....	602
EX/P6-19.....	340	EX/P8-13.....	396	FIP/P1-15.....	603
EX/P6-2.....	324	EX/P8-14.....	398	FIP/P1-16.....	604
EX/P6-20.....	341	EX/P8-15.....	399	FIP/P1-17.....	605
EX/P6-21.....	342	EX/P8-16.....	400	FIP/P1-18.....	606
EX/P6-22.....	343	EX/P8-17.....	401	FIP/P1-19.....	607
EX/P6-23.....	344	EX/P8-18.....	402	FIP/P1-2.....	591
EX/P6-24.....	345	EX/P8-19.....	403	FIP/P1-20.....	608
EX/P6-25.....	346	EX/P8-2.....	386	FIP/P1-21.....	609
EX/P6-26.....	347	EX/P8-20.....	404	FIP/P1-22.....	610
EX/P6-28.....	348	EX/P8-21.....	405	FIP/P1-24.....	611
EX/P6-29.....	349	EX/P8-22.....	406	FIP/P1-25.....	612
EX/P6-3.....	325	EX/P8-23.....	407	FIP/P1-26.....	613
EX/P6-30.....	350	EX/P8-24.....	409	FIP/P1-27.....	614
EX/P6-32.....	351	EX/P8-25.....	410	FIP/P1-28.....	615
EX/P6-33.....	352	EX/P8-26.....	411	FIP/P1-29.....	616
EX/P6-34.....	353	EX/P8-27.....	413	FIP/P1-3.....	592
EX/P6-36.....	354	EX/P8-28.....	414	FIP/P1-31.....	617
EX/P6-37.....	355	EX/P8-29.....	415	FIP/P1-32.....	618
EX/P6-38.....	356	EX/P8-3.....	387	FIP/P1-33.....	619
EX/P6-39.....	357	EX/P8-30.....	416	FIP/P1-34.....	620
EX/P6-4.....	326	EX/P8-4.....	388	FIP/P1-35.....	621
EX/P6-40.....	358	EX/P8-5.....	389	FIP/P1-36.....	622
EX/P6-5.....	327	EX/P8-6.....	390	FIP/P1-37.....	623
EX/P6-6.....	328	EX/P8-7.....	391	FIP/P1-38.....	624
EX/P6-8.....	329	EX/P8-8.....	392	FIP/P1-39.....	625
EX/P6-9.....	330	EX/P8-9.....	393	FIP/P1-4.....	593
EX/P7-1.....	359			FIP/P1-40.....	626
EX/P7-10.....	366	FIP/1-1.....	568	FIP/P1-41.....	627
EX/P7-11.....	367	FIP/1-2Ra.....	569	FIP/P1-42.....	628
EX/P7-12.....	368	FIP/1-2Rb.....	570	FIP/P1-43.....	629
EX/P7-13.....	369	FIP/1-2Rc.....	571	FIP/P1-44.....	630
EX/P7-14.....	370	FIP/1-3Ra.....	572	FIP/P1-45.....	631
EX/P7-15.....	371	FIP/1-3Rb.....	573	FIP/P1-46.....	632
EX/P7-16.....	372	FIP/1-3Rc.....	574	FIP/P1-47.....	633
EX/P7-17.....	373	FIP/1-4.....	575	FIP/P1-5.....	594
EX/P7-18.....	374	FIP/1-5.....	576	FIP/P1-50.....	634
EX/P7-19.....	375	FIP/1-6.....	577	FIP/P1-51.....	635

FIP/P1-52	636	FIP/P3-57	692	FIP/P8-16	750
FIP/P1-53	637	FIP/P3-58	693	FIP/P8-17	751
FIP/P1-54	638	FIP/P3-6	649	FIP/P8-18	752
FIP/P1-55	639	FIP/P3-62	694	FIP/P8-19	753
FIP/P1-56	640	FIP/P3-63	695	FIP/P8-2	736
FIP/P1-57	641	FIP/P3-64	696	FIP/P8-20	754
FIP/P1-58	642	FIP/P3-65	697	FIP/P8-22	755
FIP/P1-59	643	FIP/P3-66	698	FIP/P8-23	756
FIP/P1-7	595	FIP/P3-7	650	FIP/P8-24	757
FIP/P1-8	596	FIP/P3-8	651	FIP/P8-25	758
FIP/P1-9	597	FIP/P3-9	652	FIP/P8-26	759
FIP/P3-1	644	FIP/P7-1	699	FIP/P8-29	760
FIP/P3-10	653	FIP/P7-10	708	FIP/P8-3	737
FIP/P3-12	654	FIP/P7-12	709	FIP/P8-4	738
FIP/P3-14	655	FIP/P7-13	710	FIP/P8-5	739
FIP/P3-15	656	FIP/P7-14	711	FIP/P8-6	740
FIP/P3-16	657	FIP/P7-15	712	FIP/P8-7	741
FIP/P3-18	658	FIP/P7-16	713	FIP/P8-8	742
FIP/P3-19	659	FIP/P7-17	714	FIP/P8-9	743
FIP/P3-2	645	FIP/P7-19	715		
FIP/P3-20	660	FIP/P7-2	700	IFE/1-1	762
FIP/P3-23	661	FIP/P7-20	716	IFE/1-2	763
FIP/P3-25	662	FIP/P7-21	717	IFE/1-3	765
FIP/P3-26	663	FIP/P7-22	718	IFE/1-4	766
FIP/P3-27	664	FIP/P7-24	719	IFE/1-5	767
FIP/P3-28	665	FIP/P7-25	720	IFE/P4-1	768
FIP/P3-29	666	FIP/P7-26	721	IFE/P4-10	774
FIP/P3-3	646	FIP/P7-27	722	IFE/P4-13	775
FIP/P3-30	667	FIP/P7-28	723	IFE/P4-4	769
FIP/P3-31	668	FIP/P7-29	724	IFE/P4-6	770
FIP/P3-32	669	FIP/P7-3	701	IFE/P4-7	771
FIP/P3-33	670	FIP/P7-30	725	IFE/P4-8	772
FIP/P3-34	671, 672	FIP/P7-33	726	IFE/P4-9	773
FIP/P3-36	673	FIP/P7-34	727		
FIP/P3-38	674	FIP/P7-35	728	MPT/1-1	778
FIP/P3-39	675	FIP/P7-36	729	MPT/2-1	779
FIP/P3-4	647	FIP/P7-37	730	MPT/2-2	780
FIP/P3-40	676	FIP/P7-38	731	MPT/2-3	781
FIP/P3-41	677	FIP/P7-39	732	MPT/2-4	782
FIP/P3-42	678	FIP/P7-4	702		
FIP/P3-44	679	FIP/P7-40	733	O/1-4	116
FIP/P3-45	680	FIP/P7-42	734	O/1-5	117
FIP/P3-46	681	FIP/P7-5	703	O/1-6	119
FIP/P3-47	682	FIP/P7-6	704	O/1-7	120
FIP/P3-48	683	FIP/P7-7	705	OV/1-1	122
FIP/P3-49	684	FIP/P7-8	706	OV/1-2	123
FIP/P3-5	648	FIP/P7-9	707	OV/1-3	124
FIP/P3-50	685	FIP/P8-1	735	OV/1-4	125
FIP/P3-51	686	FIP/P8-10	744	OV/2-1	126
FIP/P3-52	687	FIP/P8-11	745	OV/2-2	127
FIP/P3-53	688	FIP/P8-12	746	OV/2-3	128
FIP/P3-54	689	FIP/P8-13	747	OV/2-4	130
FIP/P3-55	690	FIP/P8-14	748	OV/2-5	131
FIP/P3-56	691	FIP/P8-15	749	OV/3-1	133

OV/3-2.....	134	TH/P1-3	440	TH/P5-5	476
OV/3-3.....	135	TH/P1-4	441	TH/P5-6	477
OV/3-4.....	136	TH/P1-5	442	TH/P5-7	478
OV/4-1.....	137	TH/P1-6	443	TH/P5-8	479
OV/4-2.....	138	TH/P1-7	444	TH/P5-9	480
OV/4-3.....	139	TH/P1-8	445	TH/P6-1	499
OV/4-4.....	140	TH/P2-1	446	TH/P6-10	507
OV/4-5.....	141	TH/P2-10	455	TH/P6-12	508
OV/5-1.....	142	TH/P2-11	456	TH/P6-13	509
OV/5-2.....	143	TH/P2-12	457	TH/P6-14	510
OV/5-3.....	144	TH/P2-14	458	TH/P6-15	511
OV/5-4.....	145	TH/P2-15	459	TH/P6-16	512
OV/5-5Ra	146	TH/P2-16	460	TH/P6-17	513
OV/5-5Rb	147	TH/P2-17	461	TH/P6-19	514
OV/P-1.....	148	TH/P2-2	447	TH/P6-20	515
OV/P-11.....	156	TH/P2-3	448	TH/P6-21	516
OV/P-12.....	157	TH/P2-4	449	TH/P6-22	517
OV/P-2.....	149	TH/P2-5	450	TH/P6-23	518
OV/P-3.....	150	TH/P2-6.....	451	TH/P6-24	519
OV/P-4.....	151	TH/P2-7	452	TH/P6-25	520
OV/P-5.....	152	TH/P2-8	453	TH/P6-26	521
OV/P-6.....	153	TH/P2-9	454	TH/P6-28	523
OV/P-7.....	154	TH/P4-1	462	TH/P6-29	524
OV/P-8.....	155	TH/P4-10	469	TH/P6-30	525
		TH/P4-11	470	TH/P6-4	500
PPC/1-1	784	TH/P4-12	471	TH/P6-5.....	501
PPC/2-1.....	785	TH/P4-13	472	TH/P6-6	503
		TH/P4-2	463	TH/P6-7	504
SEE/1-1	788	TH/P4-5	464	TH/P6-8	505
SEE/2-1	789	TH/P4-6	465	TH/P6-9	506
SEE/3-1Ra	790	TH/P4-7	466	TH/P7-1	526
SEE/3-1Rb	791	TH/P4-8	467	TH/P7-10	535
SEE/3-1Rc.....	792	TH/P4-9	468	TH/P7-11	536
		TH/P5-1	473	TH/P7-12	537
TH/1-1.....	418	TH/P5-10	481	TH/P7-13	538
TH/1-2.....	419	TH/P5-11	482	TH/P7-15	539
TH/2-1.....	420	TH/P5-12	483	TH/P7-17	540
TH/2-2.....	421	TH/P5-13	484	TH/P7-18	541
TH/3-1.....	422	TH/P5-18	485	TH/P7-2	527
TH/3-2.....	423	TH/P5-19	486	TH/P7-20	542
TH/4-1.....	425	TH/P5-21	487	TH/P7-21	543
TH/4-2.....	426	TH/P5-22	488	TH/P7-22	544
TH/4-3.....	427	TH/P5-23	489	TH/P7-23	545
TH/4-4.....	428	TH/P5-24	490	TH/P7-24	546
TH/5-1.....	429	TH/P5-25	491	TH/P7-25	547
TH/6-1.....	430	TH/P5-26	492	TH/P7-26	548
TH/6-2.....	432	TH/P5-27	493	TH/P7-3	528
TH/6-3.....	433	TH/P5-28	494	TH/P7-4	529
TH/7-1.....	434	TH/P5-3	474	TH/P7-5	530
TH/7-2.....	435	TH/P5-30	495	TH/P7-6.....	531
TH/8-1.....	436	TH/P5-31	496	TH/P7-7	532
TH/8-2.....	437	TH/P5-32	497	TH/P7-8	533
TH/P1-1	438	TH/P5-33	498	TH/P7-9	534
TH/P1-2	439	TH/P5-4	475	TH/P8-1	549

TH/P8-10	558	TH/P8-17	564	TH/P8-5	553
TH/P8-12	559	TH/P8-18	565	TH/P8-6	554
TH/P8-13	560	TH/P8-19	566	TH/P8-7	555
TH/P8-14	561	TH/P8-2	550	TH/P8-8	556
TH/P8-15	562	TH/P8-3	551	TH/P8-9	557
TH/P8-16	563	TH/P8-4	552		

Contributions by Indico Submission Number

IAEA-CN-258-002....	699	IAEA-CN-258-062....	646	IAEA-CN-258-119....	520
IAEA-CN-258-003....	591	IAEA-CN-258-063....	249	IAEA-CN-258-120....	264
IAEA-CN-258-004....	771	IAEA-CN-258-064....	181	IAEA-CN-258-121....	574
IAEA-CN-258-005....	304	IAEA-CN-258-065....	767	IAEA-CN-258-122....	583
IAEA-CN-258-006....	341	IAEA-CN-258-066....	269	IAEA-CN-258-123....	394
IAEA-CN-258-007....	576	IAEA-CN-258-067....	251	IAEA-CN-258-125....	506
IAEA-CN-258-008....	768	IAEA-CN-258-068....	162	IAEA-CN-258-127....	584
IAEA-CN-258-009....	700	IAEA-CN-258-069....	258	IAEA-CN-258-128....	163
IAEA-CN-258-011....	701	IAEA-CN-258-070....	639	IAEA-CN-258-129....	732
IAEA-CN-258-012....	512	IAEA-CN-258-071....	256	IAEA-CN-258-130....	255
IAEA-CN-258-014....	196	IAEA-CN-258-072....	419	IAEA-CN-258-131....	774
IAEA-CN-258-015....	459	IAEA-CN-258-074....	152	IAEA-CN-258-132....	135
IAEA-CN-258-016....	508	IAEA-CN-258-075....	133	IAEA-CN-258-133....	376
IAEA-CN-258-018....	212	IAEA-CN-258-076....	772	IAEA-CN-258-134....	595
IAEA-CN-258-020....	519	IAEA-CN-258-077....	254	IAEA-CN-258-135....	507
IAEA-CN-258-022....	428	IAEA-CN-258-078....	265	IAEA-CN-258-136....	596
IAEA-CN-258-023....	346	IAEA-CN-258-079....	207	IAEA-CN-258-137....	784
IAEA-CN-258-024....	330	IAEA-CN-258-080....	568	IAEA-CN-258-138....	136
IAEA-CN-258-025....	558	IAEA-CN-258-081....	450	IAEA-CN-258-139....	597
IAEA-CN-258-026....	171	IAEA-CN-258-082....	762	IAEA-CN-258-140....	457
IAEA-CN-258-027....	592	IAEA-CN-258-083....	426	IAEA-CN-258-141....	489
IAEA-CN-258-029....	587	IAEA-CN-258-085....	763	IAEA-CN-258-142....	598
IAEA-CN-258-031....	727	IAEA-CN-258-087....	594	IAEA-CN-258-143....	648
IAEA-CN-258-032....	637	IAEA-CN-258-088....	731	IAEA-CN-258-144....	210
IAEA-CN-258-033....	532	IAEA-CN-258-089....	505	IAEA-CN-258-145....	439
IAEA-CN-258-034....	644	IAEA-CN-258-090....	270	IAEA-CN-258-146....	400
IAEA-CN-258-035....	451	IAEA-CN-258-091....	373	IAEA-CN-258-148....	789
IAEA-CN-258-036....	593	IAEA-CN-258-092....	262	IAEA-CN-258-150....	599
IAEA-CN-258-037....	573	IAEA-CN-258-093....	490	IAEA-CN-258-151....	556
IAEA-CN-258-038....	322	IAEA-CN-258-094....	468	IAEA-CN-258-153....	488
IAEA-CN-258-039....	257	IAEA-CN-258-095....	259	IAEA-CN-258-154....	586
IAEA-CN-258-040....	702	IAEA-CN-258-096....	194	IAEA-CN-258-155....	509
IAEA-CN-258-041....	266	IAEA-CN-258-097....	252	IAEA-CN-258-156....	440
IAEA-CN-258-042....	380	IAEA-CN-258-098....	792	IAEA-CN-258-157....	600
IAEA-CN-258-045....	248	IAEA-CN-258-099....	263	IAEA-CN-258-158....	358
IAEA-CN-258-046....	645	IAEA-CN-258-100....	537	IAEA-CN-258-160....	268
IAEA-CN-258-047....	271	IAEA-CN-258-101....	773	IAEA-CN-258-161....	539
IAEA-CN-258-048....	728	IAEA-CN-258-102....	640	IAEA-CN-258-162....	434
IAEA-CN-258-049....	729	IAEA-CN-258-103....	647	IAEA-CN-258-163....	601
IAEA-CN-258-050....	494	IAEA-CN-258-104....	438	IAEA-CN-258-164....	429
IAEA-CN-258-051....	730	IAEA-CN-258-105....	189	IAEA-CN-258-165....	396
IAEA-CN-258-052....	638	IAEA-CN-258-106....	569	IAEA-CN-258-166....	414
IAEA-CN-258-053....	316	IAEA-CN-258-107....	253	IAEA-CN-258-167....	526
IAEA-CN-258-054....	536	IAEA-CN-258-108....	449	IAEA-CN-258-168....	575
IAEA-CN-258-055....	195	IAEA-CN-258-110....	546	IAEA-CN-258-169....	224
IAEA-CN-258-056....	770	IAEA-CN-258-111....	273	IAEA-CN-258-171....	733
IAEA-CN-258-057....	469	IAEA-CN-258-112....	444	IAEA-CN-258-172....	564
IAEA-CN-258-058....	310	IAEA-CN-258-113....	399	IAEA-CN-258-173....	491
IAEA-CN-258-059....	437	IAEA-CN-258-114....	473	IAEA-CN-258-174....	476
IAEA-CN-258-060....	203	IAEA-CN-258-115....	261	IAEA-CN-258-175....	267
IAEA-CN-258-061....	495	IAEA-CN-258-118....	791	IAEA-CN-258-176....	649

IAEA-CN-258-177....	524	IAEA-CN-258-238....	225	IAEA-CN-258-299....	561
IAEA-CN-258-178....	602	IAEA-CN-258-240....	542	IAEA-CN-258-300....	420
IAEA-CN-258-179....	456	IAEA-CN-258-241....	219	IAEA-CN-258-302....	320
IAEA-CN-258-180....	250	IAEA-CN-258-242....	170	IAEA-CN-258-303....	497
IAEA-CN-258-181....	405	IAEA-CN-258-243....	391	IAEA-CN-258-304....	544
IAEA-CN-258-182....	698	IAEA-CN-258-244....	463	IAEA-CN-258-306....	185
IAEA-CN-258-183....	435	IAEA-CN-258-245....	327	IAEA-CN-258-307....	236
IAEA-CN-258-184....	550	IAEA-CN-258-246....	240	IAEA-CN-258-308....	183
IAEA-CN-258-185....	779	IAEA-CN-258-248....	606	IAEA-CN-258-309....	315
IAEA-CN-258-186....	487	IAEA-CN-258-249....	345	IAEA-CN-258-310....	708
IAEA-CN-258-188....	398	IAEA-CN-258-250....	736	IAEA-CN-258-311....	654
IAEA-CN-258-189....	782	IAEA-CN-258-252....	641	IAEA-CN-258-313....	292
IAEA-CN-258-191....	734	IAEA-CN-258-253....	430	IAEA-CN-258-314....	369
IAEA-CN-258-192....	571	IAEA-CN-258-254....	237	IAEA-CN-258-316....	655
IAEA-CN-258-194....	529	IAEA-CN-258-255....	706	IAEA-CN-258-317....	607
IAEA-CN-258-196....	413	IAEA-CN-258-256....	198	IAEA-CN-258-318....	368
IAEA-CN-258-197....	188	IAEA-CN-258-257....	211	IAEA-CN-258-319....	160
IAEA-CN-258-198....	324	IAEA-CN-258-259....	562	IAEA-CN-258-320....	741
IAEA-CN-258-199....	603	IAEA-CN-258-260....	205	IAEA-CN-258-321....	206
IAEA-CN-258-200....	455	IAEA-CN-258-261....	166	IAEA-CN-258-322....	742
IAEA-CN-258-201....	164	IAEA-CN-258-262....	737	IAEA-CN-258-324....	306
IAEA-CN-258-202....	123	IAEA-CN-258-263....	652	IAEA-CN-258-325....	656
IAEA-CN-258-203....	565	IAEA-CN-258-264....	190	IAEA-CN-258-326....	541
IAEA-CN-258-204....	200	IAEA-CN-258-265....	214	IAEA-CN-258-327....	743
IAEA-CN-258-205....	650	IAEA-CN-258-266....	570	IAEA-CN-258-328....	744
IAEA-CN-258-206....	703	IAEA-CN-258-267....	738	IAEA-CN-258-329....	209
IAEA-CN-258-207....	351	IAEA-CN-258-268....	739	IAEA-CN-258-330....	395
IAEA-CN-258-208....	332	IAEA-CN-258-269....	404	IAEA-CN-258-331....	411
IAEA-CN-258-209....	182	IAEA-CN-258-270....	299	IAEA-CN-258-332....	681
IAEA-CN-258-211....	323	IAEA-CN-258-271....	422	IAEA-CN-258-333....	745
IAEA-CN-258-212....	343	IAEA-CN-258-272....	168	IAEA-CN-258-334....	139
IAEA-CN-258-214....	704	IAEA-CN-258-273....	186	IAEA-CN-258-335....	608
IAEA-CN-258-215....	318	IAEA-CN-258-274....	790	IAEA-CN-258-336....	232
IAEA-CN-258-216....	134	IAEA-CN-258-275....	707	IAEA-CN-258-337....	609
IAEA-CN-258-217....	441	IAEA-CN-258-276....	141	IAEA-CN-258-339....	657
IAEA-CN-258-218....	313	IAEA-CN-258-277....	387	IAEA-CN-258-343....	658
IAEA-CN-258-219....	409	IAEA-CN-258-278....	416	IAEA-CN-258-344....	179
IAEA-CN-258-220....	148	IAEA-CN-258-279....	486	IAEA-CN-258-345....	709
IAEA-CN-258-221....	778	IAEA-CN-258-280....	389	IAEA-CN-258-346....	175
IAEA-CN-258-222....	246	IAEA-CN-258-283....	740	IAEA-CN-258-347....	172
IAEA-CN-258-223....	651	IAEA-CN-258-284....	342	IAEA-CN-258-349....	485
IAEA-CN-258-224....	465	IAEA-CN-258-285....	218	IAEA-CN-258-350....	407
IAEA-CN-258-226....	272	IAEA-CN-258-287....	406	IAEA-CN-258-351....	127
IAEA-CN-258-227....	769	IAEA-CN-258-288....	403	IAEA-CN-258-352....	402
IAEA-CN-258-228....	735	IAEA-CN-258-289....	216	IAEA-CN-258-353....	453
IAEA-CN-258-229....	359	IAEA-CN-258-290....	653	IAEA-CN-258-354....	161
IAEA-CN-258-230....	604	IAEA-CN-258-291....	481	IAEA-CN-258-355....	143
IAEA-CN-258-231....	401	IAEA-CN-258-292....	472	IAEA-CN-258-356....	535
IAEA-CN-258-232....	126	IAEA-CN-258-293....	220	IAEA-CN-258-357....	388
IAEA-CN-258-233....	201	IAEA-CN-258-294....	514	IAEA-CN-258-359....	521
IAEA-CN-258-234....	705	IAEA-CN-258-295....	383	IAEA-CN-258-361....	348
IAEA-CN-258-235....	501	IAEA-CN-258-296....	191	IAEA-CN-258-362....	433
IAEA-CN-258-236....	425	IAEA-CN-258-297....	340	IAEA-CN-258-363....	659
IAEA-CN-258-237....	605	IAEA-CN-258-298....	516	IAEA-CN-258-364....	660

IAEA-CN-258-365....	710	IAEA-CN-258-428....	533	IAEA-CN-258-490....	421
IAEA-CN-258-366....	530	IAEA-CN-258-429....	661	IAEA-CN-258-491....	538
IAEA-CN-258-367....	580	IAEA-CN-258-430....	199	IAEA-CN-258-492....	173
IAEA-CN-258-368....	169	IAEA-CN-258-431....	150	IAEA-CN-258-493....	713
IAEA-CN-258-369....	423	IAEA-CN-258-432....	353	IAEA-CN-258-494....	375
IAEA-CN-258-370....	202	IAEA-CN-258-433....	326	IAEA-CN-258-498....	551
IAEA-CN-258-371....	223	IAEA-CN-258-434....	319	IAEA-CN-258-499....	554
IAEA-CN-258-372....	585	IAEA-CN-258-435....	466	IAEA-CN-258-500....	314
IAEA-CN-258-373....	432	IAEA-CN-258-437....	610	IAEA-CN-258-502....	208
IAEA-CN-258-374....	566	IAEA-CN-258-438....	518	IAEA-CN-258-503....	308
IAEA-CN-258-375....	334	IAEA-CN-258-440....	364	IAEA-CN-258-504....	477
IAEA-CN-258-376....	192	IAEA-CN-258-441....	154	IAEA-CN-258-505....	780
IAEA-CN-258-377....	547	IAEA-CN-258-442....	363	IAEA-CN-258-507....	563
IAEA-CN-258-378....	415	IAEA-CN-258-443....	748	IAEA-CN-258-508....	372
IAEA-CN-258-379....	344	IAEA-CN-258-444....	365	IAEA-CN-258-509....	572
IAEA-CN-258-380....	350	IAEA-CN-258-445....	436	IAEA-CN-258-510....	156
IAEA-CN-258-381....	527	IAEA-CN-258-446....	785	IAEA-CN-258-511....	226
IAEA-CN-258-382....	339	IAEA-CN-258-447....	418	IAEA-CN-258-512....	496
IAEA-CN-258-383....	590	IAEA-CN-258-448....	452	IAEA-CN-258-513....	355
IAEA-CN-258-384....	311	IAEA-CN-258-449....	228	IAEA-CN-258-515....	231
IAEA-CN-258-385....	471	IAEA-CN-258-451....	510	IAEA-CN-258-516....	467
IAEA-CN-258-386....	479	IAEA-CN-258-453....	611	IAEA-CN-258-517....	241
IAEA-CN-258-387....	335	IAEA-CN-258-454....	193	IAEA-CN-258-518....	362
IAEA-CN-258-389....	493	IAEA-CN-258-455....	337	IAEA-CN-258-519....	347
IAEA-CN-258-390....	331	IAEA-CN-258-456....	392	IAEA-CN-258-520....	229
IAEA-CN-258-391....	328	IAEA-CN-258-457....	137	IAEA-CN-258-521....	663
IAEA-CN-258-392....	445	IAEA-CN-258-458....	749	IAEA-CN-258-522....	559
IAEA-CN-258-393....	361	IAEA-CN-258-459....	578	IAEA-CN-258-524....	277
IAEA-CN-258-394....	333	IAEA-CN-258-460....	128	IAEA-CN-258-526....	751
IAEA-CN-258-395....	338	IAEA-CN-258-461....	662	IAEA-CN-258-527....	448
IAEA-CN-258-396....	460	IAEA-CN-258-466....	545	IAEA-CN-258-528....	714
IAEA-CN-258-397....	178	IAEA-CN-258-467....	187	IAEA-CN-258-529....	752
IAEA-CN-258-398....	167	IAEA-CN-258-468....	612	IAEA-CN-258-530....	484
IAEA-CN-258-399....	543	IAEA-CN-258-469....	235	IAEA-CN-258-531....	615
IAEA-CN-258-403....	528	IAEA-CN-258-470....	147	IAEA-CN-258-532....	525
IAEA-CN-258-404....	410	IAEA-CN-258-471....	499	IAEA-CN-258-534....	234
IAEA-CN-258-405....	242	IAEA-CN-258-472....	138	IAEA-CN-258-535....	616
IAEA-CN-258-406....	588	IAEA-CN-258-473....	613	IAEA-CN-258-536....	244
IAEA-CN-258-407....	746	IAEA-CN-258-474....	711	IAEA-CN-258-537....	553
IAEA-CN-258-408....	305	IAEA-CN-258-475....	245	IAEA-CN-258-541....	307
IAEA-CN-258-409....	443	IAEA-CN-258-476....	482	IAEA-CN-258-542....	321
IAEA-CN-258-410....	184	IAEA-CN-258-477....	750	IAEA-CN-258-543....	753
IAEA-CN-258-413....	642	IAEA-CN-258-478....	329	IAEA-CN-258-544....	336
IAEA-CN-258-415....	560	IAEA-CN-258-479....	712	IAEA-CN-258-545....	664
IAEA-CN-258-416....	500	IAEA-CN-258-480....	131	IAEA-CN-258-546....	243
IAEA-CN-258-417....	747	IAEA-CN-258-481....	775	IAEA-CN-258-547....	287
IAEA-CN-258-418....	766	IAEA-CN-258-482....	379	IAEA-CN-258-549....	665
IAEA-CN-258-419....	213	IAEA-CN-258-483....	480	IAEA-CN-258-550....	666
IAEA-CN-258-420....	483	IAEA-CN-258-484....	614	IAEA-CN-258-551....	125
IAEA-CN-258-422....	765	IAEA-CN-258-485....	384	IAEA-CN-258-552....	667
IAEA-CN-258-424....	577	IAEA-CN-258-486....	367	IAEA-CN-258-553....	227
IAEA-CN-258-425....	356	IAEA-CN-258-487....	349	IAEA-CN-258-554....	668
IAEA-CN-258-426....	239	IAEA-CN-258-488....	461	IAEA-CN-258-555....	370
IAEA-CN-258-427....	325	IAEA-CN-258-489....	579	IAEA-CN-258-556....	581

IAEA-CN-258-558....464	IAEA-CN-258-624....759	IAEA-CN-258-686....722
IAEA-CN-258-559....754	IAEA-CN-258-625....124	IAEA-CN-258-687....293
IAEA-CN-258-560....511	IAEA-CN-258-626....718	IAEA-CN-258-688....723
IAEA-CN-258-561....215	IAEA-CN-258-627....291	IAEA-CN-258-689....275
IAEA-CN-258-563....300	IAEA-CN-258-629....285	IAEA-CN-258-690....130
IAEA-CN-258-564....517	IAEA-CN-258-630....557	IAEA-CN-258-691....632
IAEA-CN-258-565....390	IAEA-CN-258-631....447	IAEA-CN-258-692....280
IAEA-CN-258-566....312	IAEA-CN-258-632....674	IAEA-CN-258-693....633
IAEA-CN-258-567....475	IAEA-CN-258-635....760	IAEA-CN-258-694....309
IAEA-CN-258-568....298	IAEA-CN-258-636....675	IAEA-CN-258-697....691
IAEA-CN-258-569....492	IAEA-CN-258-637....624	IAEA-CN-258-698....286
IAEA-CN-258-570....142	IAEA-CN-258-638....683	IAEA-CN-258-699....692
IAEA-CN-258-571....284	IAEA-CN-258-639....295	IAEA-CN-258-700....458
IAEA-CN-258-573....462	IAEA-CN-258-640....279	IAEA-CN-258-701....155
IAEA-CN-258-574....715	IAEA-CN-258-641....274	IAEA-CN-258-702....247
IAEA-CN-258-578....278	IAEA-CN-258-642....625	IAEA-CN-258-703....146
IAEA-CN-258-579....140	IAEA-CN-258-643....276	IAEA-CN-258-704....693
IAEA-CN-258-580....165	IAEA-CN-258-644....676	IAEA-CN-258-705....549
IAEA-CN-258-582....617	IAEA-CN-258-646....626	IAEA-CN-258-708....724
IAEA-CN-258-583....669	IAEA-CN-258-648....627	IAEA-CN-258-709....357
IAEA-CN-258-584....197	IAEA-CN-258-649....628	IAEA-CN-258-711....515
IAEA-CN-258-585....386	IAEA-CN-258-650....684	IAEA-CN-258-713....122
IAEA-CN-258-586....716	IAEA-CN-258-651....288	IAEA-CN-258-714....289
IAEA-CN-258-588....352	IAEA-CN-258-652....281	IAEA-CN-258-715....317
IAEA-CN-258-589....755	IAEA-CN-258-653....629	IAEA-CN-258-716....149
IAEA-CN-258-590....366	IAEA-CN-258-654....282	IAEA-CN-258-717....503
IAEA-CN-258-591....393	IAEA-CN-258-655....454	IAEA-CN-258-718....781
IAEA-CN-258-592....302	IAEA-CN-258-656....677	IAEA-CN-258-719....260
IAEA-CN-258-593....381	IAEA-CN-258-657....630	IAEA-CN-258-720....303
IAEA-CN-258-594....144	IAEA-CN-258-658....360	IAEA-CN-258-724....694
IAEA-CN-258-595....618	IAEA-CN-258-659....643	IAEA-CN-258-725....634
IAEA-CN-258-596....301	IAEA-CN-258-660....294	IAEA-CN-258-726....635
IAEA-CN-258-597....233	IAEA-CN-258-661....552	IAEA-CN-258-728....636
IAEA-CN-258-598....756	IAEA-CN-258-662....623	IAEA-CN-258-729....382
IAEA-CN-258-600....670	IAEA-CN-258-663....474	IAEA-CN-258-730....725
IAEA-CN-258-602....619	IAEA-CN-258-664....719	IAEA-CN-258-732....589
IAEA-CN-258-603....177	IAEA-CN-258-665....685	IAEA-CN-258-733....695
IAEA-CN-258-604....620	IAEA-CN-258-666....531	IAEA-CN-258-736....696
IAEA-CN-258-605....157	IAEA-CN-258-667....523	IAEA-CN-258-737....374
IAEA-CN-258-606....378	IAEA-CN-258-668....678	IAEA-CN-258-738....679
IAEA-CN-258-607....671	IAEA-CN-258-670....720	IAEA-CN-258-739....151
IAEA-CN-258-608....442	IAEA-CN-258-671....283	IAEA-CN-258-741....504
IAEA-CN-258-610....230	IAEA-CN-258-672....631	IAEA-CN-258-743....478
IAEA-CN-258-611....672	IAEA-CN-258-674....427	IAEA-CN-258-746....682
IAEA-CN-258-612....296	IAEA-CN-258-675....686	IAEA-CN-258-747....153
IAEA-CN-258-614....222	IAEA-CN-258-676....534	IAEA-CN-258-748....680
IAEA-CN-258-615....621	IAEA-CN-258-677....204	IAEA-CN-258-750....371
IAEA-CN-258-616....297	IAEA-CN-258-678....687	IAEA-CN-258-751....290
IAEA-CN-258-617....622	IAEA-CN-258-679....688	IAEA-CN-258-752....470
IAEA-CN-258-618....717	IAEA-CN-258-680....689	IAEA-CN-258-753....354
IAEA-CN-258-619....145	IAEA-CN-258-681....788	IAEA-CN-258-754....498
IAEA-CN-258-620....673	IAEA-CN-258-682....690	IAEA-CN-258-756....377
IAEA-CN-258-621....757	IAEA-CN-258-684....174	IAEA-CN-258-757....555
IAEA-CN-258-622....758	IAEA-CN-258-685....721	IAEA-CN-258-758....540

IAEA-CN-258-759	446	IAEA-CN-258-766	726	IAEA-CN-258-902	120
IAEA-CN-258-761	221	IAEA-CN-258-767	697	IAEA-CN-258-904	116
IAEA-CN-258-763	548	IAEA-CN-258-900	117	IAEA-CN-258-905	238
IAEA-CN-258-764	513	IAEA-CN-258-901	119		

Contributor Index

— A —

Abadie, L. 591
 Abbon, P. 135, 601
 Abe, G. 599
 Abe, Y. 762, 763
 Abhangi, M. R. 617, 664, 670, 679, 681, 781
 Abhijit, S. 10
 Abhishek, A. 29, 654, 668
 Abrams, T. 44, 185, 334, 337, 339, 780
 Abreu, P. 219
 Acharya, K. S. 631, 696
 Adamek, J. 150, 199
 Adegun, J. 367
 Adhikari, B. R. 538
 Adil, Y. 155
 Agarwal, J. 685, 686, 689
 Agarwal, R. 570
 Agatha, C. 179
 Aggarwal, D. 20, 629
 Aggarwal, S. 36, 295, 297
 Agostinetti, P. 733
 Agostini, M. 224, 396, 398
 Agravat, H. S. 717
 Aguiam, D. 394, 396, 407
 Ahn, J.-W. 128, 184, 371
 Ahn, J. H. 347, 372
 Aiba, N. 140, 172, 426
 Aich, S. 36, 144, 289, 303, 693, 696
 Aiello, A. 135
 Aiello, G. 709
 Ajay, K. 36, 295, 297
 Ajesh, P. 750
 Akagi, T. 135, 601, 659
 Akers, R. 409, 434
 Akhtyrskiy, S. V. 313
 Akimitsu, M. 268, 270
 Akimoto, K. 645
 Akiyama, N. 774
 Akkireddy, S. 35, 234, 284
 Aktaa, J. 136
 Akunets, A. A. 771
 Albajar, F. 571, 710
 Albanese, R. 170, 541
 Alberti, S. 215, 571, 709, 710

Aleksandrova, I. V. 771
 Ales, H. 221
 Alessi, E. 216, 521
 Alessio, M. 762
 Alexander, Z. 619
 Aleynikov, P. 37, 183, 465, 556
 Ali, A. 191, 400
 Alladio, F. 153
 Allan, S. 396
 Allen, N. 695
 Allen, S. A. 333
 Allen, S. L. 192, 332, 336
 Alonso, A. 206, 399
 Al-Shboul, K. F. 37, 775
 Altukhov, A. B. 59, 65, 145, 437
 Amal, S. 643
 Ambrosino, R. 170, 532, 541, 699
 Ambulkar, K. K. 294, 655, 688
 An, Y. H. 365
 Anand, H. 52, 380
 Anand, R. 19, 570, 615, 743, 750
 Ananyev, S. S. 53, 701
 Anastassiou, G. 561
 Anderson, J. 354
 Ando, T. 586
 Andrew, P. 576, 594
 Andruczyk, D. 587
 Angioni, C. 359, 384, 387, 389, 423
 Angus, J. 546
 Anitha, V. P. 741
 Annigeri, M. 591
 Antoni, V. 55, 733
 Antoniazzi, L. 135, 601
 Antusch, S. 395
 Aomoa, N. 154
 Apicella, M. L. 588
 Appel, L. 434
 Apruzzese, G. 588
 Aradi, M. 562
 Arakcheev, A. S. 30, 661
 Arambhadiya, B. 144, 302
 Arambhadiya, B. A. 631
 Arambhadiya, B. G. 696
 Araya-Solano, L. A. 725

Arbeiter, F.	782	Bairagi, N.	18, 607, 641, 706, 711, 744
Arias-Brenes, J. M.	725	Bairaktaris, F.	471
Arikawa, Y.	26, 34, 762, 763	Bajpai, P. K.	234, 617, 679, 781
Artaserse, G.	210, 219	Bak, J. G.	363, 370, 372
Artaud, J.-F.	246, 430, 504, 561, 604	Bakharev, N. N. 13, 21, 145, 153, 304, 727	
Arter, W.	579, 581	Balakrishnan, V.	144, 693
Artola, F. J.	556	Balasubramanian, K.	754
Artola, J.	379	Balboa, I.	225, 581, 734
Arumugam, A.	29, 657	Baldwin, M.	547
Asadulin, G. M.	195	Baldzuhn, J.	173, 392, 414, 416
Asahi, Y.	526	Bandaru, V. K.	63, 556
Asahina, T.	773	Bando, T.	163, 181
Asai, T.	52, 156, 376	Bandyopadhyay, I.	63, 122, 462, 557
Ascasibar, E.	12, 21, 139, 162, 205	Bandyopadhyay, M. 62, 241, 572, 613, 626,	
Asenjo, J.	374	627, 664, 670, 682, 684, 751	
Ashok, G.	244, 300	Bandyopadhyay, P.	233
Ashourvan, A.	323	Banerjee, D.	447
Askinazi, L. G.	145	Banerjee, S. 34, 144, 277–279, 285–287, 462,	
Aslanyan, V.	222	518, 553	
Asztalos, O.	529	Bañón Navarro, A.	422, 501
Atnafu, N.	695	Bao, J.	355, 461, 466
Atrey, P. K.	144, 278–280, 298, 553	Baquero, M.	215
Attri, A.	31, 234, 617, 679, 781	Barabaschi, P.	12, 14, 133
Atul, J. K.	37, 467	Barada, K. K.	165, 324, 326
Auriemma, F.	202, 508	Baranov, Y.	327, 422, 423
Austin, M. E.	44, 165, 328, 349, 356, 496,	Barbui, T.	191
586		Bardoczi, L.	161, 325
Autricque, A.	788	Barnes, A.	483
Avaria, G.	245	Barnes, M.	172
Avramidis, K. A.	571, 709, 710	Barnsley, R.	591, 620, 622
Awad, M.	695	Baron-Wiechec, A.	193, 209, 211
Awasthi, L. M. 36, 243, 296, 298, 299, 612,		Barr, J. L.	45, 141, 342
713		Barrett, T. R.	42, 50, 579
Aydemir, A. Y.	63, 370, 550	Barton, J. L.	337
Azechi, H.	762, 763	Baruah, U. K.	122, 570, 625, 643, 683
— B —		Baruzzo, M.	216, 219, 521
Babinov, N. A.	145, 575, 576, 594	Basaleev, E. V.	540
Babu, R.	759	Basile, A.	695
Bache, T. W.	202	Bass, E. M.	57, 59, 432
Bachmann, C.	583, 789	Basu, B.	479
Baek, S. G.	45, 348	Batha, S. H.	131, 765
Bagryansky, P. A.	318	Batkin, V. I.	319
Bahl, R.	62, 753	Batyrbekov, E.	760
Bai, W.	155	Bauer, J.	606
Bai, X. Y.	187, 240, 308	Baylard, C.	583
Bailly-Grandvaux, M.	763	Baylor, L. R.	17, 344, 590, 653

Bazhenov, A. N.	145, 576, 594	Bhope, K. S.	157, 658, 752
Bazin, N.	135, 601	Bhuva, M. P.	23, 237
Beaumont, B.	430	Bhuyan, M.	626, 682, 684, 751
Beauvais, P.-Y.	135, 601, 659	Bialek, J. M.	347, 372, 415
Bedoya, F.	29, 644	Biancalani, A.	24, 160, 454
Beers, C. J.	637	Biedermann, C.	191
Beidler, C. D.	173, 438	Biel, W.	699, 700
Beklemishev, A. D.	319	Biener, J.	131
Belbas, I. S.	195	Biener, M. M.	131
Bell, R. E.	329, 347, 415	Biewer, T. M.	415, 637
Bellan, L.	135, 601, 659	Bigelow, T. S.	637
Belli, E. A.	423, 445, 512	Bigot, B.	10, 12, 123
Belli, F.	734	Bilato, R.	407, 423, 430, 433, 501
Belokurov, A. A.	145	Bilkova, P.	150, 199
Belonohy, E.	172, 175	Bin, W.	571
Belova, E. V.	24, 460	Binderbauer, M. W.	156, 376
Belsare, S. M.	13, 157	Binwal, S.	55, 729
Benedetti, L. R.	131	Bionta, R.	131
Benkadda, S.	446	Bisai, N. K.	47, 277, 518
Bennett, D.	131	Bizarro, J. P. S.	56, 539
Berik, E. B.	576	Blackwell, D. B.	191
Berkery, J. W.	141, 347, 372	Blanchard, P.	406, 734
Berlov, A.	207	Blanchard, W.	695
Bernard, E.	788	Blanken, T. C.	216, 220
Bernard, J.-M.	745	Blondel, S.	547
Bernard, T.	545	Bobkov, V.	186, 388, 407
Bernardi, D.	782	Bobylev, V. B.	319
Bernardo, J.	734	Boccaccini, L. V.	748
Bernascolle, P.	620, 622	Bock, A.	409, 410, 501
Bernert, M.	168, 216, 384, 394, 396, 406	Bodner, G. M.	353
Bertalot, L.	591	Boedo, J. A.	213, 323, 333, 336, 396
Berte, M.	413	Bogar, O.	150
Bertelli, N.	37, 267, 472	Bohm, P.	150, 199
Bertinetti, A.	710	Boilson, D.	430, 573, 626
Berzak-Hopkines, L. F.	131	Bolzon, B.	135, 601, 659
Bhandarkar, S.	131	Bolzonella, T.	216, 272, 489
Bharathi, P.	31, 682, 684, 751	Bond, E.	131
Bhardwaj, A. K.	755	Bondarchuk, E. N.	145, 727
Bhat, S. B.	300	Bongard, M. W.	46, 353
Bhatt, K. S.	30, 669	Bongiovì, G.	748
Bhatt, P.	31, 687	Bonicelli, T.	573
Bhatt, S. B.	144, 278, 301, 631, 696	Bonne, F.	703
Bhattacharjee, A.	563	Bonnin, X.	531
Bhattacharjee, H.	656	Bonoli, P. T.	189, 348, 585
Bhattacharya, A.	46, 276, 503	Bora, B.	245
Bhattacharyay, R.	667	Borade, A.	270

Borah, D.	751	Buchanan, J.	203, 652
Borchardt, M.	449	Budaev, V. P.	311
Borodin, D.	16, 193, 208	Budai, A.	561
Borodkina, I.	193, 208	Buddu, R. K.	62, 752
Borschegovskiy, A. A.	316	Bufferand, H.	541
Borsuk, V.	413	Bukhovets, V. L.	594
Bortolato, D.	135, 601	Bukreev, I. M.	145, 576, 594
Bortolon, A.	580	Bulanin, V. V.	145, 304, 727
Boscary, J.	403	Buldakov, M. A.	195
Bottino, A.	160, 454	Buller, S.	47, 172, 509
Bourdelle, C.	179, 423	Bunkers, K.	558
Bowie, C. A.	40, 473	Bunting, P.	581
Bowman, C.	172	Buratti, P.	479, 521
Boyer, M. D.	347, 356, 372	Burdakov, A. V.	40, 319, 661
Boyle, D. P.	415	Burhenn, R.	173, 191
Bozhenkov, S. A. ...	60, 173, 392, 413, 414	Burke, M. G.	353
Bradley, D.	131	Burke, R.	695
Bradley, P. A.	131, 765	Burmasov, V. S.	319
Brakel, R.	60, 401	Burrell, K. H.	165, 340
Brandt, C.	392	Butler, B.	651
Brank, M.	380	Buttenschön, B.	416
Braun, T.	131	Buttery, R. J.	26, 55, 527, 663
Braune, H.	414	Buzi, L.	415
Brennan, D. P.	183, 563, 564, 697	Bykov, I. O.	185, 338, 339, 780
Brereton, A.	695		
Breslau, J.	428	— C —	
Breton, S.	423	Cagadas, B.	131
Brezinsek, S.	57, 58, 172, 191, 193, 208, 209, 225, 400, 401, 519, 780	Caggiano, J.	131
Brida, D.	166	Cai, D.	695
Briesemeister, A. R.	334, 336, 337, 339, 780	Cai, F.	695
Bright, R.	18, 608	Cai, J.	402
Briguglio, S.	455	Cai, J. Q.	399
Brizard, A.	561	Cai, L.	19, 578, 624
Broeckmann, C.	395	Calabrò, G.	39, 170, 210
Brookman, M. W.	328, 585, 736	Callahan, D. A.	131
Brooks, A.	358, 695	Calvo, I.	206, 440
Brower, D. L.	18, 603	Campbell, D. J.	66, 368, 430
Brown, T.	55, 731	Canal, G.	324
Brücker, P. T.	709	Candy, J.	512, 527
Brunetti, D.	521	Caneses, J. F.	637
Brunner, D.	330, 348, 435, 542, 610	Canik, J. M. ...	56, 192, 333, 415, 527, 547, 587, 663
Brunner, K. J.	173, 392, 414	Cannas, B.	216, 434
Bruschi, A.	571, 709	Cano-Megias, P.	389
Bsharat, H.	367	Cao, J. Y.	321
Buch, J. J. U.	35, 291	Cao, N. M.	196, 610
		Cao, Q.	268, 270, 577

Cappa, Á.....	162, 205
Cappelli, M.....	782
Cara, P.....	135, 601, 659
Carbajal Gomez, L.....	564
Carbajal, L.....	38, 44, 183, 427, 566
Carcangiu, S.....	216, 434
Cardenas, T.....	131
Cardinali, A.....	479
Carlstrom, T.....	165
Carpanese, F.....	220
Carralero, D.....	205, 396
Carter, T. A.....	13, 151, 350
Carvalho, I. S.....	175, 218, 219, 734
Carvalho, O.....	788
Carvalho, P. J.....	519
Casali, L.....	331
Caschera, E.....	526
Casolari, A.....	221
Casson, F. J.....	38, 43, 174, 202, 381, 422, 423, 504, 510
Castaño-Bardawil, D.....	413
Castaldo, A.....	541
Castejón, F.....	162, 494
Castro, C.....	131
Cau, F.....	710
Caughman, J. B. O.....	350, 590, 637
Cavalier, J.....	150, 199
Cavazzana, R.....	59, 391
Cave-Ayland, K.....	384
Cavedon, M.....	186, 326, 388, 389, 699
Cavenago, M.....	733
Cerijan, C.....	131
Cerovsky, J.....	221
Cesario, R.....	240
Chakrabarty, N.....	283
Chakraborty, A. K.....	10, 12, 122, 572, 573, 613, 626, 627, 643, 664, 682, 684, 751, 754
Chakraborty, P.....	30, 674
Chakrapani, C.....	706, 707
Challis, C. D.....	172, 174, 201, 203, 222, 384, 422, 423, 581
Chan, V. S.....	134, 499, 780
Chandra, D.....	41, 49, 59, 277, 429, 487
Chang, C.-S.....	47, 56, 57, 128, 420, 436, 476, 480, 492, 515, 516, 544, 548, 555

Chang, J.....	239
Chankin, A.....	172, 202
Chapman, I. T.....	697
Chareyre, J.....	626
Charl, A.....	399
Chatthong, B.....	47, 247, 511, 520, 554
Chattopadhyay, A. K.....	290, 751
Chattopadhyay, P. K.....	144, 197, 229, 278, 283, 467, 475, 553, 696, 756
Chaturvedi, S.....	10
Chaudhari, V.....	665, 681
Chaudhary, V.....	231
Chaudhuri, P.....	18, 608, 611, 639, 656, 678, 681, 694, 704, 718
Chauhan, J. P.....	623, 633, 678, 719
Chauhan, S. S.....	32, 692, 749
Chauvin, N.....	135, 601, 659
Chavda, C.....	301
Chebotaev, V. V.....	212
Chektybayev, B.....	62, 760
Chel, S.....	135, 601, 659
Chelis, I.....	709
Chelis, J.....	571
Chellai, O.....	215
Chen, B.....	543
Chen, C. Y.....	305, 517
Chen, D.....	54, 586, 724
Chen, D. L.....	341
Chen, H.....	54, 722
Chen, J.....	42, 50, 165, 321, 513, 558, 578, 624, 780
Chen, J. G.....	226, 543
Chen, J. L.....	227, 499
Chen, L.....	411, 451
Chen, R.....	236
Chen, W.....	40, 306, 308, 314, 315, 451
Chen, W. J.....	320
Chen, X.....	165, 340
Chen, Y.....	577, 578
Chen, Z. P.....	152, 235
Chen, Z. Y.....	152
Cheng, C. Z.....	270
Cheng, J.....	39, 307, 308, 448
Cheng, Z. F.....	152
Cheon, M. S.....	360
Chernakov, Al. P.....	145, 576, 594

Chernakov, An. P.	576	Coda, S.	12, 21, 143, 204, 380, 406
Chernakov, P. V.	576	Coelho, R.	41, 493, 510, 521, 529
Chernov, V. M.	31, 49, 677	Coenen, J. W.	395, 581
Chernyshev, F. V.	145, 304, 727	Coffey, I.	193
Child, P. A.	10, 119	Colas, L.	407
Chitarin, G.	733	Cole, M. D. J.	47, 476, 516
Chmielewski, P.	532, 541	Coleman, M.	30, 662
Choe, W.	363–365	Collins, C. S.	161, 339, 349, 564
Choe, W. H.	128	Comunian, M.	135, 601, 659
Choi, H.	366	Conroy, S.	652
Choi, J.	591	Conway, G. D.	160, 394, 501
Choi, J. H.	568	Cooper, C.	183
Choi, M. J.	58, 65, 128, 198, 369, 370, 372, 436	Cooper, W. A.	458, 494
Choi, W.	141, 343	Coppi, B.	479
Choudhary, K. K.	692	Corona, D.	272
Choukekar, K.	632	Corre, Y.	581
Chowdhuri, M. B.	35, 144, 276–282, 285–287, 503, 518, 553, 696	Corrigan, G.	381, 423, 504
Chowdhury, J.	63, 555	Cosfeld, J.	399, 442
Christian, D.	54, 607, 641, 711, 716, 735, 744	Costea, S.	396
Christian, P.	643	Coster, D.	510, 541, 562
Chrystal, C.	38, 43, 165, 182, 323, 325	Cote, T. B.	404
Chu, Y.	128	Coto-Vílchez, F.	374
Chudasma, H. H.	715	Covele, B.	331
Chugunov, I.	712	Craciunescu, T.	459, 734
Chuilon, B.	579	Creely, A. J.	196, 501, 610
Chung, J.	128	Crisanti, F.	170
Chung, K.-J.	360	Crocker, N. A.	349, 460, 484
Churchill, R. M.	56, 420, 544, 548	Crofts, O.	54, 726
Cianciosa, M.	547	Crombé, K.	350, 407, 413
Cianfarani, C.	216	Cropper, M.	695
Ciattaglia, S.	583	Crowley, B. J.	356
Ciazynski, D.	703	Cruz, N.	272
Ciechanowski, M.	614	Cruz-Zabala, D.	389
Ciraolo, G.	541	Cseh, G.	191
Cismondi, F.	583, 710	Cui, L.	185
Citrin, J.	179, 422, 423, 501, 512	Cui, Z. Y.	187, 305, 308
Ciummo, C.	695	Curreli, D.	547
Clairret, F.	526	Czarnecka, A.	174, 423, 519, 521
Clark, D.	131	Cziegler, I.	396, 420
Clauser, C.	450		
Clement, M.	141		
Clement-Lorenzo, S.	18, 604		
Coad, P.	209		

— D —

D'Agostino, M.	695
Dairaku, M.	574, 598
Dalicha, H.	570, 739, 743, 750
Damm, H.	173, 392, 416
Danani, C.	665, 681
Danani, S.	618, 621, 636

Dani, S.	628	DeVan, B.	591
Darbos, C.	569	Devi, K. D.	781
Das, S. 23, 242, 685, 686, 689		Devi, V. G. 54, 714	
Das, T.	533	Devitre, A.	199
da Silva, F.	394	de Vries, P. C. 164, 380, 383	
Daughton, W. S.	131	Dewald, E. L.	131
Dave, P.	657	Dewar, R. L.	200
Dave, R.	625, 683	Dey, R. 63, 285, 286, 518, 553	
David, C.	617, 781	Dhanani, K. R.	715
Davis, S.	245, 730	Dhola, H. 570, 625, 683, 743	
Day, C.	29, 651	Dhongde, J.	715
Dean, N.	695	Diallo, A. 44, 324, 326, 329, 421, 587	
De Bock, M. F. M.	504, 619	Diamond, P. H.	226, 340, 500
Decanis, C.	788	Diegele, E.	136, 583
Decker, J.	221, 561, 562	Dif-Pradalier, G.	526
Decool, P.	703	Dimitrova, M.	150, 199
deGrassie, J. S. 44, 182, 323, 328, 346, 585, 736		Dimits, A. M.	189
Dejarnac, R.	150, 780	Ding, B. J.	127, 240
Deka, A. J.	31, 682, 684, 751	Ding, F.	127, 227, 232, 780
Delabie, E.	172, 175, 202, 223, 384	Ding, R.	49, 50, 232, 780
de la Luna, E. . . 26, 34, 140, 164, 175, 406		Ding, S.	239, 246
de la Morena, C.	135, 601	Ding, S. Y.	127, 169, 178, 499
del Castillo, C. A.	349	Ding, W.	155, 309
del-Castillo-Negrete, D. 64, 183, 427, 446, 525, 564, 566		Ding, X. T.	187, 305-308, 315
Delgado-Aparicio, L. F.	44, 329	Ding, Y. H.	27, 152, 260
Dellas, J.	695	Dinklage, A.	61, 173, 401, 413, 416
Delogu, R.	216	Di Siena, A.	454, 501
De Lorenzi, A.	733	Di Troia, C.	455
Delpech, L.	187, 240, 308	Dittmar, T.	191
Deng, B. H.	156	Divol, L.	131
Deng, G. Z.	232	Dixit, H. V.	688
Deng, T.	155, 309	Dmitriev, A.	575
Deng, W.	321	Dmitriev, A. M.	576, 594
Denk, S. S.	404	Dnestrovsky, A. Y.	18, 316, 600
Dennett, C. A.	610	Dodd, E. S.	131
De Oliveira, H.	168, 213, 396	Dodiya, C.	715
de Saint-Aubin, G.	209	Doerk, H.	501
Deshpande, S. P. . . 10, 117, 122, 234, 284, 616, 617, 671, 679, 723, 781		Doerner, R. P.	208, 547, 778
Despontin, P.	413	Doinikov, D.	712
De Temmerman, G.	154	Dominski, J.	324, 515
De Tommasi, G. . . . 16, 28, 210, 272, 604		Dong, C. F.	305, 308
Dettrick, S.	156, 376	Dong, G.	461
Deur, A.	653	Dong, G. Q.	63, 559
		Dong, J. Q. . . . 187, 305, 307, 308, 448, 517	
		Dong, Y. B.	321
		Donnel, P.	526

Donovan, D. C.	334, 337, 415, 637
Doody, J.	585
Döppner, T.	131
Dorf, M. A.	56, 415, 546
Dorr, M.	546
Doshi, B. R.	54, 631, 642, 706, 717, 720
Douai, D.	223
Dougniaux, G.	788
Downing, D.	695
Drabinsky, M. A.	195, 310
Drenik, A.	175
Drevlak, M.	17, 438
Drewelow, P.	191, 218, 400, 403, 416
Drews, P.	399, 402
Drobny, J.	547
Du, H.	239
Du, H. F.	127, 246
Du, X. D.	163, 345, 349, 564
Duan, X.	577, 578
Duan, X. R.	187, 240, 305, 307, 308, 314, 315, 320, 321, 517
Duan, Y. M.	227, 499
Duarte, V.	161
Dubey, D.	30, 671
Dudek, L.	695
Dudson, B. D.	434, 443
Dumont, R.	174, 222, 422
Dumortier, P.	430
Dunne, M. G.	59, 166, 168, 186, 384, 386–388, 404, 406, 409, 411, 485
Durodié, F.	413
Dutta, P.	20, 482, 623, 630, 633, 717, 719
Dutta, S.	54, 715
Duval, B. P.	16, 204, 213, 409
Dux, R.	384, 389, 433, 580
Dylla-Spears, R.	131
Dzitko, H.	135, 601, 659

— E —

Eade, T.	789
Ebert, H.	583
Ebisawa, T.	135, 601
Eckardt, C.	572
Eckart, M.	131
Edappala, P.	302
Edgell, D.	131
Edlund, E.	543

Edwards, M. J.	131
Effenberg, F.	57, 58, 191, 400, 403
Egedal, J.	354
Eguchi, T.	640
Eich, T.	166, 168, 529
Eidietis, N. W.	45, 141, 183, 341–344, 558
Ejiri, A.	28, 254, 267, 269, 702
Ekedahl, A.	23, 49, 169, 187, 240, 308
Eksaeva, A.	208
Elaragi, G. M.	36, 768
Elbez-Uzan, J.	622
Elder, J. D.	337, 780
Eldon, D.	167
Elets, D. I.	576, 594
Elgriw, S.	367
Eliezer, S.	769
Eliseev, L. G.	195, 310
Elliott, D. B.	415
Ellis, R.	695
Elmore, S.	199
Elwasif, W.	547
Embréus, O.	183, 561
Emdee, E. D.	589
Emoto, M.	254
Endler, M.	191, 400
Endo, Y.	640
Erdos, B.	561, 562
Erickson, K. G.	356, 695
Ernst, D. R.	26, 34, 165, 325
Escande, D. F.	488
Esipov, L. A.	145, 437
Esquembri, S.	581
Estrada, T.	16, 205, 206
Ethier, S.	513
Evans, T. E.	167, 185, 338, 339, 345, 445
Ezumi, N.	27, 248, 256, 536

— F —

Faber, B. J.	514
Fable, E.	389, 699
Fagotti, E.	135, 601, 659
Faitsch, M.	166, 199
Falchetto, G. L.	510, 521
Fan, F.	762
Fanale, F.	571
Fanni, A.	216, 434
Farcas, I.-G.	501

Farengo, R.	450	Fil, A.	213
Farina, D.	430	Firpo, M.-C.	450
Farley, T.	434	Fischer, R.	387, 404, 410, 433
Farnik, M.	221	Fischer, U.	62, 650, 748, 782, 789
Farrell, M.	131	Fishler, B.	585, 736
Farthing, J.	604	Fittinghoff, D. N.	131
Fasoli, A.	61, 215, 458, 740	Fitzgerald, M.	222
Faugel, H.	407	Fogaccia, G.	455
Faugeras, B.	493	Fonck, R. J.	153, 353
Faust, I. C.	348	Fontana, M.	224, 409
Faustin, J. M.	407, 413, 458, 494	Fontdecaba, J. M.	172
Favuzza, P.	135	Forest, C. B.	46, 354, 565
Feder, R.	695	Fortuna-Zalesna, E.	211
Federici, G.	43, 50, 583, 651, 700	Francisquez, M.	545
Fedin, P. A.	634	Francois, D.	570
Fedorczak, N.	213	Franke, T.	583, 699, 709
Felici, F. A. A.	216, 220, 433	Frassinetti, L. . . .	60, 168, 174, 201, 384, 386, 406
Fellinger, J.	401	Fredrickson, E. D.	161, 351, 460, 484
Felton, R.	174, 219	Freeman, C.	695
Feng, B. B.	187, 305	Freethy, S. J.	166, 501
Feng, K.	577	Freisinger, M.	778
Feng, W.	232	Frerichs, H.	191, 339, 403
Feng, Y.	173, 191, 442, 531, 534, 577	Frigione, D.	15, 172, 174, 201
Fenstermacher, M. E. . . .	44, 192, 332, 335, 336, 338	Fu, G. Y.	418, 563
Ferrari, H.	450	Fu, J. Y.	478
Ferraro, N. M. . . .	46, 63, 358, 372, 445, 478, 480, 558, 695	Fu, P.	155
Ferreira Nunes, I. F.	384	Fuchert, G.	33, 39, 173, 392, 399, 416
Ferreira Nunes, I. M.	174, 175	Fuenfgelder, H.	407
Ferreira, D.	216	Fujii, K.	252
Ferreira, J.	222, 510, 521, 562	Fujioka, S.	26, 34, 762, 763, 767
Ferro, A.	605	Fujita, A.	264
Ferron, J. R. . . .	332, 356, 357, 527, 585, 663, 785	Fujiwara, E.	568
Ferron, N. A.	733	Fujiwara, Y.	266
Fessey, J.	274	Fukuda, C.	526
Feuillastre, S.	788	Fukui, K.	728
Février, O.	213	Fukumoto, K.-I.	779
Ficker, O.	16, 150, 221, 423, 561	Fukumoto, N.	264
Field, A.	172	Fukuyama, A.	267, 430
Field, J.	131	Fukuyama, M.	267
Fierro, F.	131	Fülöp, T.	183, 561, 562
Figini, L.	430	Fulton, D. P.	355
Figueiredo, A.	510	Fulton, T.	636
Figueiredo, J.	55, 734	Furno, I.	16, 215
		Fusco, V.	455, 521
		Futatani, S.	140, 379

— G —

- Gaganidze, E. 136
- Gahlaut, A. 626, 682, 684
- Gaio, E. 18, 605
- Gajjar, S. 625, 683
- Galdon-Quiroga, J. 61, 396, 411
- Gallart, D. 422
- Gallo, A. 213
- Galodiya, K. 157
- Galperti, C. 216, 220, 380
- Galvao, R. 66
- Gan, K. F. 587
- Gan, Q. 690
- Gandhi, A. 597, 704
- Ganesh, R. 229, 230, 474, 756
- Gangradey, R. 31, 685, 686, 689
- Ganovichev, D. 680
- Gantenbein, G. 15, 53, 571, 709, 710
- Gao, A. 695
- Gao, J. M. 187, 305, 308, 321
- Gao, X. 226, 259, 499
- Gao, Y. 191, 399, 400
- Gao, Z. 153, 560
- Garavaglia, S. 709
- Garbet, X. 446, 526
- García, A. 782
- Garcia, J. . . . 38, 43, 140, 174, 224, 422, 430, 784
- Garcia-Argote, S. 788
- Garcia-Carrasco, A. 211
- Garcia-Martinez, P. 24, 450
- García Muñoz, M. 411, 453, 734
- García-Regaña, J. M. 205, 206
- Garg, A. 53, 607, 641, 711, 720, 744
- Garkusha, I. E. 16, 212
- Garofalo, A. M. . . . 169, 178, 185, 340, 663
- Garoz, D. 766
- Garro-Vargas, A. 374
- Garzotti, L. 33, 39, 174, 203, 422, 423, 430
- Gasparini, F. 605
- Gasparyan, Y. 209
- Gatto, R. 479
- Gattu, R. 657
- Gatu-Johnson, M. 131
- Gautam, P. 302, 693
- Gebhart, T. E. 590
- Geiger, B. 61, 160, 409, 410, 433
- Geiger, J. 191, 399, 403, 438
- Gekelman, W. 151, 350
- Gelfert, M. 572
- Gelfusa, M. 175, 216
- Genoud, J. 709
- Gensdarmes, F. 788
- Gentle, K. W. 152
- George, M. 709
- George, S. 277, 715
- Gérardin, F. 659
- Gerasimov, S. N. 16, 216, 219
- Gerhardt, S. P. 32, 329, 347, 358, 695
- Gex, D. 135, 601
- Ghate, A. 591
- Ghate, M. 62, 721, 749
- Ghendrih, P. 526
- Ghim, Y.-C. 552
- Ghosh, D. 546
- Ghosh, J. 144, 154, 197, 276–283, 285–289, 300–303, 475, 503, 518, 531, 553, 609, 631, 692, 693, 696
- Ghosh, S. 696
- Ghosh, S. K. 692
- Gi, K. 29, 645
- Giacomelli, L. 459
- Giannone, L. 404, 409
- Giegerich, T. 651
- Gietl, H. 395
- Gil, L. 166, 394
- Gilbert, M. R. 49, 51, 789
- Gillot, C. 526
- Gilson, E. 587
- Gin, D. B. 53, 145, 712
- Giovannozzi, E. 455, 493, 521
- Giroud, C. 33, 39, 172, 174, 175, 179, 202, 384, 519
- Giruzzi, G. 187, 224, 308, 604
- Glasser, A. H. 372
- Gliss, C. 583
- Gobbin, M. 221, 224
- Gobin, R. 135, 601, 659
- Goerler *see* Görler
- Gohil, P. 177
- Goldston, R. J. 43, 50, 589
- Golfinopoulos, T. 167, 435, 542

Gom, B.	636	Grisolia, C.	42, 51, 788
Gonçalves, B.	394	Groebner, R. J.	167, 326, 327, 335, 421
Gong, B.	577	Gros, G.	703
Gong, X.	39, 178, 185, 239	Grossetti, G.	709
Gong, X. Z.33, 127, 169, 170, 227, 232, 240, 499, 587		Grote, H.	401
Goniche, M.	187, 223, 240, 423	Groth, M.	192, 333, 336, 363
González-Arrabal, R.	766	Grover, O.	150
Gonzalez-Martin, J.	411	Grover, P.	610
Goodman, T. P.	215, 224	Grover, R. B.	10, 116
Gopalakrishna, M. V.	144, 278–280	Grulke, O.	60, 393, 399, 402
Gorbunov, A. V.	145, 576	Gryaznevich, M.	153
Gorelenkov, N.	161	Gu, S.	185
Gorelenkova, M.	161, 652	Gude, A.	405
Goriaev, A.	401	Guenter	<i>see</i> Günter
Görler, T.	46, 422, 454, 501, 699	Gui, B.	463
Gorley, M.	136	Guillemaut, C.	193
Gorodetsky, A. E.	594	Guimaraes, L.	160, 166, 388, 394, 406
Gorshkov, A. V.	195	Guirao, J.	622
Gospodarczyk, M.	221	Guirlet, R.	365
Gospodchikov, E. D.	318	Guler, N.	131
Goswami, N. S.	570, 625, 683	Gunganti, S.	636
Gota, H.	13, 156, 376	Günter, S.	41, 405, 486
Gotewal, K. K.	20, 623, 630, 633, 719	Guo, H.	332
Goto, K.	265	Guo, H. Y. 44, 227, 228, 232, 331, 337, 780	
Goto, M.	258	Guo, W.	185, 418, 445
Goto, T.	55, 732	Guo, X.	265, 373
Goulding, R. H.	637	Guo, Z. B.	340
Gowland, R.	726	Gupta, C. K.	61, 737
Grandgirard, V.	446, 526	Gupta, C. N.	144, 278, 303, 693, 696
Granetz, R. S.	45, 141, 341, 561	Gupta, D.	156, 720
Granucci, G.	709	Gupta, G.	122
Grashin, S. A.	310, 311	Gupta, G. K.	755
Graves, J. P.24, 174, 201, 423, 458, 494, 521		Gupta, L.	467
Gray, T. K.	587, 695	Gupta, M.	300, 720
Green, D. L.	189, 527, 547	Gupta, M. K.	244, 631, 642
Greenough, N.	695	Gupta, S.	144, 608, 693
Greenwald, M. J.	196, 420	Gupta, S. K.	244
Grenfell, G.	214, 396	Gupta, V.	625, 683, 685, 686, 689
Grespan, F.	135, 601	Gürcan, Ö.	454, 526
Gribov, Y.	380, 381, 383, 430	Gurchenko, A. D.	145, 437
Griener, M.	166	Gusakov, E. Z.	33, 37, 145, 437, 469
Grierson, B. A. . 44, 46, 165, 171, 182, 196, 323, 325, 326, 332, 339, 356, 512		Gusev, V. K.	145, 153, 304, 727
Grim, G.	131	Guterl, J.	334
Grisham, L. R.	574	Guttenfelder, J.	695
		Guttenfelder, W.	481

— H —

Ha, S.	541	Harvey, R. W.	64, 354, 470, 472, 565
Haan, S.	131	Hasegawa, H.	56, 537
Hacek, P.	150, 199	Hasegawa, M.	259, 267
Hadar, A.	562	Haskey, S. R.	182, 323, 325, 356
Haertl <i>see</i> Härtl		Hata, A.	773
Hager, R. 41, 420, 436, 476, 480, 515, 516, 544, 548, 555		Hata, M.	762, 763
Hahm, T. S.	198, 507, 513	Hatae, T.	602
Hahn, S. H.	343, 347, 372	Hatano, H.	268
Haines, B. M.	131, 765	Hatano, Y.	774
Hakim, A.	56, 545	Hatarik, R.	131
Hakola, A.	396	Hatayama, A.	256, 259
Hallatschek, K.	63, 549	Hatch, D. R.	172, 421
Ham, C. J.	404	Hatzky, R.	449
Hamilton, C. E.	131	Häußler, A.	748
Hammett, G. W.	545	Havlicek, J.	150, 199
Hammond, K.	191, 400	Havranek, A.	150, 221
Hamza, A. V.	131	Hawkes, N.	493, 734
Han, H.	370	Hawryluk, R.	66
Han, H. S.	371, 372	Hayashi, N. 38, 43, 271, 430, 506, 604, 784	
Han, M. K.	307	Hayashi, T.	268
Han, S. H.	128	Hayward-Schneider, T.	160
Han, S. L.	747	He, H.	24, 448
Han, X.	399	He, K.	577
Hanada, K. 27, 153, 259, 267, 640		He, P.	690
Hanada, M.	730	He, R. C.	461
Hanayama, R.	770	He, W.	500
Hansalia, C. J.	302	Hecla, J.	610
Hansen, C.	415	Hegna, C. C.	404, 514
Hanson, J. M. 141, 346, 405, 785		Heidbrink, W. W. 161, 349, 356, 433, 484, 564	
Hao, G.	352	Heidinger, R.	135, 601, 659, 782
Hao, G. Z. 41, 448, 484, 559		Heinola, K.	193, 209
Hao, L.	31, 690	Helander, P.	438, 509
Happel, T. 26, 34, 166, 394, 501		Helou, W.	585
Hara, D.	568	Hemming, O.	604
Hara, T.	256	Hender, T. C.	219
Harikrishna, J. V. S.	570, 742, 750	Henderson, M.	430, 569, 599
Harrault, F.	659	Henkel, M.	399, 402
Harrer, G. F.	168, 326, 389	Henneberg, S.	438
Harris, J. H.	345, 403	Hennequin, P.	166, 168, 501, 526
Harrison, J. R. 13, 147, 153, 172, 213, 434		Henriques, R. B.	200, 219
Harting, D.	381, 504	Herashchenko, S. S.	212
Härtl, T.	583, 699	Herfindal, J.	45, 183, 344
Hartmann, D. A.	413	Hermann, V.	571
Hartouni, E. P.	131	Hernderson, K.	131
		Herrmann, A.	580

Herrmann, H. W.	131	Holland, L.	331
Hertout, P.	703	Hollfeld, K. P.	413
Hesslow, L.	561	Hollmann, E. M. . 183, 192, 344, 425, 427, 592	
Heuraux, S.	394, 407	Hollocombe, J.	493, 504
Hezabeh, H.	483	Hölzl, M.	140, 411, 485, 556
Hidalgo, C.	16, 214	Honda, A.	728
Higashijima, A.	259, 267	Honda, M.	251, 440, 506
Hill, D. N.	192	Hong, J.	364, 365
Hillairet, J.	240, 745	Hong, S.-H.	51, 363–366
Hillesheim, J. C. 33, 39, 172, 175, 179, 406		Hong, S. C.	377
Himabindu, M.	23, 235, 531	Hong, S. H.	128
Hinata, J.	596	Hong, Y. S.	568
Hinkel, D.	131	Hoover, D.	131
Hinson, E. T.	45, 339	Hopf, C.	409, 410
Hioki, T.	770	Hoppe, M. L.	131, 183, 561, 562
Hiranai, S.	596	Hora, H.	36, 769
Hirata, M.	256	Horacek, J.	150
Hirata, T.	259	Horiuchi, R.	270, 468
Hirata, Y.	135, 601	Hörstensmeyer, Y.	651
Hiratsuka, J.	574	Horvath, L.	202, 406
Hirose, T.	136	Höschen, D.	399
Hirsch, M.	173, 392, 399	Hosea, J. C.	472
Hirvijoki, E.	561, 563	Hosokawa, M.	504
Hishinuma, Y.	646	Hosozawa, A.	376
Hittinger, J.	546	Hou, B. L.	747
Hiwatari, R.	645	Hou, Y.	24, 452
Hizanidis, K.	471, 561	Howard, J.	255
Ho, A.	422	Howard, N. T.	196
Ho, D. D.	131	Hron, M.	150, 221
Hoa, C.	703	Hsing, W. W.	131
Hoang, G. T.	187, 240	Hu, C. D.	169, 227
Hoang, T.	308	Hu, D.	368
Hobirk, J.	175, 201, 384, 409	Hu, G. H.	529
Hoefel	see Höfel	Hu, J.	155, 592
Hoelbe	see Hölbe	Hu, J. S.	169, 232, 587
Hoelzl	see Hölzl	Hu, L.	238, 690
Höfel, U.	392, 399	Hu, L. Q.	169, 227, 236
Hoffbauer, M.	592	Hu, Q.	345
Hoffman, H.	610	Hu, Q. M.	152, 260
Hoffmann, F.	695	Hu, S. L.	517
Hogge, J.-P.	571, 709, 710	Hu, W.	356, 433
Hohenburger, M.	131	Hu, X. W.	152
Hölbe, H.	403	Hu, Y.	418
Holcomb, C. T. 141, 178, 356, 357, 527, 585, 663		Hu, Z.	762
Hole, M. J. . . 15, 41, 65, 200, 473, 483, 769		Huang, B.	646

Huang, C. B.	226	Igami, H.	640
Huang, D. W.	152	Igaune, I.	673
Huang, H.	131	Iglesias, D.	42, 50, 581
Huang, J. 23, 127, 169, 178, 227, 239, 317, 418		Igochine, V.	60, 160, 405, 486
Huang, M.	320, 587	Iguchi, M.	568
Huang, M. X.	152	Ihara, A.	659
Huang, P.	578	Iida, Y.	269
Huang, Q.	724	Iijima, T.	256
Huang, W.	724	Ikeda, K.	20, 638
Huang, Y.	170	Ikeda, R.	569, 596, 599, 640
Huang, Y. Q.	463	Ikezoe, R.	248, 256
Huang, Z.	152	Iliasova, M.	712
Huang, Z. H.	307	Illy, S.	571, 709
Hubbard, A. E. ... 167, 175, 179, 196, 330, 340, 348		Imadera, K.	586
Huber, A.	172, 175, 193, 225, 519	Imai, T.	248, 256, 267, 640
Huber, V.	17, 225	Imazawa, R.	18, 602
Hughes, J. W. 167, 179, 196, 327, 330, 340, 348, 386, 420, 421, 543		Imbeaux, F.	604
Hughes, P. E.	415	Imrisek, M. ... 150, 193, 199, 218, 221, 521	
Huijsmans, G. T. A. ... 140, 379, 485, 556		In, Y. ... 49, 58, 128, 184, 198, 360, 369-371, 492, 550	
Humphreys, D. A. 128, 141, 342, 343, 356, 357		In, Y. K.	372
Hurricane, O. A.	131	Inagaki, S.	254, 307
Huynh, P.	510, 521	Inagaki, T.	568
Hwang, S. S.	568	Inai, Y.	373
Hwang, Y.-S. 153, 360, 375, 377, 378		Innocente, P.	213, 541
Hyatt, A. W.	328, 331, 785	Ino, M.	568
Hynes, A.	604	Inomoto, M.	52, 268, 373, 376, 468
— I —		Inoue, S.	41, 270, 346, 490
Iafrati, M.	207, 588	Inoue, T.	66
Ibano, K.	536	Inzhevatkina, A. A.	319
Ibaraki, Y.	264	Ioannidis, Z. C.	471, 571, 709, 710
Ibarra, A.	49, 51, 782	Ionita, C.	396
Ichige, H.	728	Iovenitti, A.	535
Ichikawa, M.	574	Irby, J. H.	196
Ichimiya, R.	135, 601, 659	Irzak, M. A.	145, 437
Ichimura, K.	256	Isaev, M. Y.	310
Ichimura, M.	248, 256	Isayama, A.	251, 426, 490, 596
Ida, K. . 58, 65, 66, 181, 194, 252, 254, 261, 263		Ishiguro, S.	476, 537
Ide, S.	271, 490, 604	Ishii, K.	770
Idei, H.	28, 259, 267, 640	Ishii, Y.	604
Ido, T.	257, 456	Ishiwata, J.	376
Iepu, I.	223	Ishizawa, A.	162, 249
		Islam, M. M.	256
		Islam, M. S.	256
		Islaker, H.	396
		Isobe, M. 162, 266, 308, 317, 360, 457, 647	

Isono, T.	728
Isozaki, M.	599
Itami, K.	602
Ito, S.	640
Itoh, K.	251, 307
Itoh, S.-I.	251, 307
Ivanov, A.	156
Ivanov, A. A.	379, 504
Ivanov, I. A.	319
Ivanov, P.	275
Ivanova, D.	211
Ivanova-Stanik, I.	216, 510, 519, 521
Ivantsivskiy, M.	620, 622
Iwamoto, A.	26, 34, 767, 770
Iwano, K.	767
Iwasaki, K.	269
Iwata, N.	37, 763, 772
Iyer, H. T.	654
Izumi, N.	131

— J —

Jablonski, G.	591
Jachmich, S.	16, 193, 211, 218, 428, 581
Jacobsen, A. S.	409, 411, 453
Jacquemot, S.	26
Jadav, H. M.	244
Jadeja, K. A.	32, 144, 197, 278–280, 285, 287, 289, 300, 301, 303, 518, 553, 609, 631, 696
Jadeja, K. M.	281, 282
Jadhav, M.	300, 669
Jaeger, E. F.	564
Jaeger, J. E.	472
Jain, J.	245
Jain, Y.	294
Jain, Y. M.	31, 688
Jaiswal, S.	631
Jakubowski, M. W.	60, 191, 392, 399, 400, 403
Jana, M. R.	32, 691
Jang, J. J.	51, 364
Jang, S.	248, 256
Janky, F.	699
Jarboe, T.	415
Jarboe, T. R.	635
Jardin, S. C.	372, 558
Jariwala, A.	695

Järvinen, A. E.	57, 58, 192, 336
Jaworski, M. A.	589, 695, 731
Jayswal, S.	720
Jelonnek, J.	571, 709
Jenko, F.	454, 501, 545
Jeon, T. M.	364
Jeon, Y.-M.	369
Jeon, Y. M.	52, 128, 184, 347, 362, 371, 372, 492
Jeong, S.-H.	375
Jepu, I.	209, 211
Jha, A.	62, 570, 615, 742, 743, 750
Jha, R.	531, 534, 679
Jha, S.	19, 621
Jha, S. K.	144
Jhang, H.	477, 507, 551, 552
Ji, X. Q.	40, 306–308, 312, 315, 320, 321
Jia, M.	185
Jian, X.	499
Jiang, J.	31, 676
Jiang, M.	39, 152, 305–308, 315, 320, 321
Jiang, Y.	347, 372
Jiang, Z. H.	152
Jiménez, D.	374, 782
Jimenez-Rey, D.	135, 601
Jin, C.	722
Jin, F.	578
Jin, H.	260
Jin, J.	571, 709
Jitsuno, T.	763
Jo, J.	51, 360
Jo, J.-G.	375
Jo, J. G.	377
Joffrin, E.	10, 12, 124, 174, 216, 222, 272, 428, 521
Johnson, R. D.	357
Johnson, S.	131
Johnson, T.	222, 423, 430, 501
Johnston, A.	483
Johzaki, T.	762, 763, 770, 773
Joisa, Y. S.	144, 278, 279, 290, 553
Jokinen, A.	135, 601
Joly, J.	422
Jones, F.	695
Jones, O. S.	131
Jonsson, T.	510, 562

Joseph, I.	189
Joshi, H. H.	757
Joshi, J. 11, 15, 572–574, 613, 626, 627, 729	
Joshi, J. K.	35, 292
Joshi, K.	626
Joshi, R.	29, 244, 300, 655
Jouniaux, G.	413
Julio, G.	620
Jung, B.-K.	375

— K —

Kaang, H. H.	552
Kabeya, Y.	774
Kadia, B.	244, 300
Kado, S.	162, 249, 250, 256
Kafle, N.	637
Kain, V.	674
Kaita, R.	415
Kajita, R.	265
Kajiwara, K.	18, 569, 596, 599, 640
Kakati, M.	13, 154
Kakurin, A. M.	313
Kalal, M. B.	144, 631, 696
Kalaria, P. C.	709, 710
Kalish, M.	695
Kallenbach, A.	580
Kallmeyer, J. P.	413
Kalupin, D.	510, 521, 562
Kamada, Y.	133, 271
Kambayashi, S.	762
Kamio, S.	266, 373
Kamiya, K.	27, 251, 728
Kanabar, D.	721
Kandaurov, I. V.	661
Kang, D. A.	747
Kang, J. S.	362, 364
Kanik, A.	35, 288
Kanjiya, S.	611
Kanki, T.	264
Kannan, S.	617, 781
Kanoongo, N.	754
Kanth, P.	29, 616, 648
Kappatou, A. ...	59, 175, 384, 388, 389, 407
Kariya, T.	20, 256, 267, 640
Karkari, S. K.	237, 242, 292, 482, 729
Karki, V.	617, 781
Karpov, A. V.	311
Karpushov, A. N.	224, 396, 409
Kasahara, H.	269, 416
Kasakov, Y. O.	407
Kashiwa, Y.	728
Kashiwagi, M.	573, 574, 598
Kasperek, W.	571
Kasugai, A.	18, 135, 601, 659
Kasuya, N.	17, 439
Katanuma, I.	256
Kates-Harbeck, J.	141
Kato, A.	647
Kato, H.	595
Kato, Y.	774
Katoh, Y.	136
Katsura, S.	255
Kavin, A. A.	145, 381, 383, 430, 727
Kavšek, D.	614
Kaw, P. K.	296
Kawakami, H.	598
Kawakami, Y.	640
Kawamata, Y.	269
Kawamura, G.	258, 261
Kawanaka, J.	762, 763
Kawano, K.	728
Kawasaki, S.	259
Kawase, H.	266
Kaye, S. M.	146, 203, 359, 481
Kazakov, Y. O. .	57, 58, 173, 188, 392, 413, 414
Ke, R.	517
Kedarmal, K.	781
Keech, G.	583, 726
Keeling, D.	409
Kella, V. P.	696
Kellman, A.	331
Kembleton, R.	583, 699, 700
Kemp, R.	541
Kempenaars, M.	576, 594
Kenmochi, N.	249, 250, 255
Khabanov, F. O.	195
Khabanov, P. O.	310
Khambholja, S. G.	30, 668
Khan, K. B.	234, 284, 781
Khan, S.	131
Khan, Z.	657, 715
Khanal, R.	56, 538

- Kharchev, N. K. 310
- Khayrutdinov, R. R. 381, 383, 430, 504
- Khilchevitch, E. 712
- Khimchenko, L. N. 40, 311
- Khirwadkar, S. S. 157, 658, 752, 781
- Khodak, A. 695
- Khodunov, I. 199
- Khomich, A. A. 634
- Khromov, N. A. 145, 304, 727
- Kikani, P. 679, 781
- Kikuchi, M. 43, 50, 586
- Kikuchi, Y. 264
- Kilkenny, J. 131
- Killer, C. 60, 191, 399, 400, 402
- Kim, C. C. 452
- Kim, D. 46, 161, 352
- Kim, E.-H. 472
- Kim, H. 366
- Kim, H.-T. 15, 174, 175, 203, 384
- Kim, H. C. 366
- Kim, H. S. 362, 436
- Kim, J. 41, 52, 63, 198, 347, 360, 364, 370,
372, 477, 552
- Kim, J. H. 128, 371
- Kim, K. 184, 364, 366, 515, 527
- Kim, K. M. 371
- Kim, M. 369
- Kim, M. W. 184
- Kim, S. 378
- Kim, S.-H. 52, 375, 381, 383
- Kim, S. C. 377
- Kim, S. H. 430, 504
- Kim, S. S. 477, 552
- Kim, S. Y. 568
- Kim, Y. G. 377
- Kimura, H. 774
- King, D. 202, 222
- Kingham, D. 153
- Kinna, D. 225
- Kinoshita, Y. 256
- Kiptily, V. G. 222, 459, 734
- Kirilenko, D. A. 594
- Kirk, A. 186, 404, 434, 495
- Kirov, K. 422, 423
- Kirpichev, I. 135, 601
- Kirschner, A. 193, 208, 780
- Kiselev, E. O. 145, 304, 727
- Kishimoto, H. 762, 763
- Kishimoto, Y. 65, 586
- Kislov, A. Y. 316
- Kitagawa, Y. 770
- Kitano, T. 659
- Kitayama, A. 269
- Kiviniemi, T. P. 145, 437
- Kizane, G. 673
- Kizu, K. 54, 728, 730
- Klabacha, J. 695
- Klaywittaphat, P. 247
- Kleiber, R. 24, 206, 449
- Klein, F. 395
- Kleiner, A. 458, 494
- Klepper, C. C. 17, 223
- Kline, J. L. 11, 12, 131, 765
- Klinger, T. 12, 21, 137
- Klyuchnikov, L. A. 310, 316
- Knaster, J. 135, 601, 659
- Knauer, J. 173, 392
- Knieps, A. 399, 402
- Knight, P. J. 381, 423, 504
- Knolker, M. 167, 324
- Ko, J. 347
- Ko, J. S. 128, 372
- Ko, S. H. 198
- Ko, W.-H. 369
- Ko, W. H. 128, 347, 370, 372, 492
- Kobayashi, D. 376
- Kobayashi, M. 27, 29, 257, 258, 261, 273,
400, 647
- Kobayashi, N. 599
- Kobayashi, S. 162, 249, 250, 267, 640
- Kobayashi, T. 18, 194, 569, 596, 599, 640
- Kočan, M. 504
- Kochergin, M. M. 576
- Köchl, F. 53, 164, 201, 216, 381, 383, 421,
423, 430, 504, 544
- Kocsis, G. 191, 392
- Kodama, R. 762, 763, 767
- Kodeli, I. 19, 614
- Koechl *see* Köchl
- Koel, B. E. 415
- Koenies *see* Könies
- Koenig *see* König

Kohagura, J.	248, 256	Krbec, J.	150, 199
Köhn, A.	374	Krebs, I.	558
Koizumi, N.	568	Kreter, A.	42, 50, 395, 778
Kojima, A.	15, 574, 598	Krieger, K.	581
Kojima, S.	267, 762, 763	Kriete, M.	177
Kolemen, E.	141, 326	Krikunov, S. V.	145
Kolesnichenko, Y. I.	459	Krimmer, A.	575
Komata, M.	659	Kripner, L.	150
Komatsuzaki, M.	599	Kritz, A.	481
Komeda, O.	770	Krivska, A.	413
Kominis, Y.	561	Krolas, W.	782
Komm, M.	13, 15, 150, 199, 780	Kroll, J.	131
Komov, A.	207	Kruezi, U.	218, 219, 223, 368
Kondo, H.	649	Krug, R.	395
Kondo, K.	135, 373, 601, 659	Krupin, V. A.	310, 316
Kong, C.	131	Krutkin, O. L.	145, 437
Kong, D. F.	22, 226	Krychowiak, M.	191, 400
Kong, M.	16, 220, 224	Kryukov, N.	525
Könies, A.	449	Ku, S.	436
König, R.	191, 392, 399–401	Ku, S.-H. ...	33, 39, 420, 476, 515, 516, 544, 548, 555
Konishi, S.	51, 65, 790–792	Kuang, A. Q.	330, 435, 542, 610
Konoshima, S.	249, 250	Kubo, H.	604
Konovalov, S. V.	381, 504	Kubo, S.	267, 640
Konshin, Z. E.	318	Kubota, S.	415
Korepanov, S.	156	Kuc, T.	614
Koresheva, E. R.	771	Kudlacek, O.	216
Kornee, K.	141	Kuklin, K. N.	319
Kornev, V. A.	145	Kukushkin, A. B.	470
Korobeynikova, O. A.	318	Kukushkin, A. S.	576, 600
Kos, L.	380	Kulevoy, T. V.	634
Kostic, A.	407	Kuley, A.	37, 466
Kotov, V.	575	Kulhanek, P.	221
Kotschenreuther, M. T. ...	33, 39, 421, 496	Kulik, N. V.	212
Kovacic, J.	396	Kulkarni, S. V.	244, 300, 687
Koval, A. N.	145, 576, 594	Kulriya, P. K.	234, 617, 679, 781
Kovalenko, Y. V.	318	Kulsartov, T.	680
Kovari, M.	579, 662	Kumagai, K.	698
Kovarik, K.	150	Kumar, A.	122, 144, 280, 302, 609, 665
Koyanbayev, Y.	680	Kumar, J.	36, 61, 294, 688, 741
Kozard, K.	570	Kumar, M.	22, 144, 231, 695
Kozioziemski, B. J.	131	Kumar, N.	721
Kozub, T.	415	Kumar, R. ...	19, 32, 61, 144, 241, 289, 303, 617, 618, 636, 664, 670, 693, 696, 743, 781
Kramer, G. J.	161, 329	Kumar, S. ...	19, 237, 244, 292, 300, 620–622,
Krämer-Flecken, A.	399, 413		
Krat, S.	193, 209		
Krawczyk, N.	174, 521		

643, 664	
Kumar, U.	22, 230, 715
Kumar, V.	122, 618–622
Kumari, P.	280, 302
Kumawat, D.	144, 289, 303, 693, 696
Kupriyanov, I. B.	56, 540
Kurbatova, L. A.	540
Kurita, T.	774
Kurki-Suonio, T.	37, 430, 464, 561
Kurkuchekov, V. V.	661
Kuroda, K.	267
Kurskiev, G. S.	39, 145, 304, 576, 594, 727
Kurtz, R. J.	779
Kurzan, B.	387
Kuteev, B. V.	37, 66, 600, 701, 771
Kuyanov, A.	430
Kuzmin, A.	259
Kwak, J. G.	128, 372
Kwon, D.-H.	365
Kwon, J.-M.	59, 65, 198, 436, 507
Kwon, J. M.	128
Kwon, S.	649
Kyrala, G. A.	131

— L —

Labit, B.	26, 34, 168, 213, 396, 406
LaBombard, B.	167, 330, 348, 435, 542, 543, 610
Lachhvani, L. T.	35, 278, 280, 283
Lackner, K.	405, 486
Lacroix, B.	703
Ladygina, M. S.	212
Laggner, F. M.	44, 167, 326, 389
La Haye, R. J.	141, 324, 332, 346
Lakhani, A.	679, 781
Lakhera, V. J.	672
Lamaison, V.	703
Lamalle, P.	430
Lambertin, D.	788
Lan, T.	155, 309
Lancot, M.	141
Landen, O. L.	131
Lang, P. T.	388
Lange, R.	591
Langenberg, A.	173, 392
Lanthaler, S.	458, 494
Lanti, E.	454

Lao, L. L.	178, 331, 445, 558, 565
Laqua, H. P.	61, 173, 392, 401, 413, 414
Lasa, A.	547
Lashkul, S. I.	293
Lasnier, C. J.	185, 192, 332, 334, 336, 338, 344, 427
Lathiya, P.	714
Latsas, G. P.	571, 709
Latu, G.	526
Lau, C.	189, 350, 564
Lau, C. K.	355
Lauber, P.	14, 22, 160, 409, 561
Laughman, C.	610
Law, K. F. F.	762, 763
Lay, W.-S.	635
Lazerson, S.	173, 392, 400, 403, 476, 516
Lazzaro, E.	521
Lebedev, S. V.	145
LeBlanc, B. P.	329, 347
Lebschy, A.	384, 387, 433
Leccacorvi, R.	585
Lechte, C.	501, 571
Le Coz, Q.	703
Lee, B.-J.	375
Lee, H.	366
Lee, H.-W.	375
Lee, H. H.	184, 361, 372, 436, 550
Lee, H. Y.	52, 377
Lee, J.	52, 338, 347, 369, 370
Lee, J.-H.	369
Lee, J. H.	128, 184, 372, 492
Lee, K. C.	128
Lee, K. D.	198
Lee, S.	762
Lee, S.-H.	763
Lee, S. G.	51, 361
Lee, W.	128, 369, 552
Leeper, R. J.	26, 34, 131, 765
Leerink, S.	145, 437
Leggate, H.	443
Leggieri, A.	710
Legrand, F.	571, 710
Lehnen, M.	52, 218, 368, 425, 561
Le Masurier, S. J.	66
Lennholm, M.	174
Leonard, A. W.	44, 192, 331–333, 336, 338

Leonov, V.	383	Likonen, J.	209
LePape, S.	131	Lin, S. Y.	169
Lepiavko, B. S.	459	Lin, Z. 25, 41, 46, 156, 355, 448, 461, 466, 478	
Lerche, E. A. 174, 175, 203, 216, 223, 384, 423, 430, 510, 519		Lin, Z. F.	152
LeSher, M.	585, 736	Linehan, B.	213
Leuer, J. A.	322, 663	Ling, F.	320
Levashova, M. G.	576	Liniers, M.	205
LeViness, A.	403	Linn, B.	695
Li, B.	690	Linsmeier, C.	208, 395, 778
Li, D.	152, 260	Lipschultz, B.	153, 213, 386, 396, 434
Li, E.	169	Lisgo, S. W.	208
Li, G.	418	Lisitsa, V. S.	576
Li, G. Q.	46, 127, 445, 499	Litnovsky, A.	11, 15, 395, 575
Li, H.	155, 309	Litvinov, A. E.	576, 594
Li, J.	134, 232, 236, 560	Liu, A.	155, 309
Li, J. G.	169, 170, 226	Liu, A. D.	187
Li, J. Q.	306, 517	Liu, B.	214, 317
Li, J. X.	322, 586	Liu, C.	63, 183, 418, 563, 564, 676
Li, K.	499	Liu, D.	352
Li, L.	17, 379, 444, 495	Liu, F.	41, 379, 485
Li, M.	246, 260	Liu, F. K.	169
Li, M. H.	127, 227, 240	Liu, G.	747
Li, N. M.	543	Liu, H.	152, 239, 259, 317
Li, P.-Y.	514	Liu, H. Q.	127, 169, 170, 227, 236, 499
Li, P. Y.	62, 747	Liu, J.	653
Li, Q.	236, 578	Liu, J. B.	232
Li, T.	676	Liu, S.	402
Li, X.	308	Liu, S. C.	60, 399
Li, Y.	63, 536, 560	Liu, W.	13, 155, 309
Li, Y.-G.	321	Liu, X.	421, 496, 578, 624
Li, Y. C.	240	Liu, Y. 40, 42, 227, 258, 305-308, 312, 315, 320, 321, 444, 495, 559, 699	
Li, Y. D.	236	Liu, Y. Q. 141, 185, 379, 461, 484, 489, 559	
Li, Y. G.	306, 308, 315	Liu, Z.	461
Li, Y. Y.	227, 499	Lizunov, A. A.	318
Li, Z.	155, 591	Lloyd, B.	153
Li, Z. Y.	543	Loarte, A. 52, 128, 164, 184, 338, 379, 381, 425, 430, 444, 485, 495, 504, 544	
Lian, H.	499	Loesser, D.	695
Lian, Y.	624	Logan, N.	141, 346
Liang, A. S.	305	Lohner, R.	561
Liang, S. Y.	312, 320	Lomanowski, B.	172, 175
Liang, Y.	127, 152, 232, 260, 399	Lomas, P. J.	164, 174, 216, 219, 225
Liang, Y. F.	169, 227	Lombroni, R.	170
Liao, H.	577	Long, H.	259
Lifschitz, A.	450		
Liger, K.	788		

Long, P.....	690
Longo, S.....	733
Lontano, M.....	571
Loomis, E.....	131
López-Bruna, D.....	42, 47, 494, 508
López-Fraguas, A.....	508
López-Rodríguez, D.....	374
Lore, J. D.	60, 191, 192, 333, 403, 527, 566
Lorenzini, R.....	202
Losada, U.....	214
Loschiavo, V. P.....	541
Lou, R. R.....	747
Louche, F.....	413
Loving, A.....	726
Lowry, C.....	174
Lowry, M. M.....	653
Lu, B.....	187, 240
Lu, X.....	250
Lu, Z.....	160
Luce, T. C.	57, 59, 141, 171, 342, 368, 430, 785
Lukash, V. E.....	381, 383, 430, 504
Lukyanchuk, A. A.....	634
Lumsdaine, A.....	403, 637
Lungaroni, M.....	216
Lunsford, R.....	42, 50, 415, 580, 587, 635
Lunt, T.....	541
Luo, B.....	155
Luo, D.....	577
Luo, G.-N.....	43, 232, 637
Luo, Z.....	155, 246
Luo, Z. P.....	127, 170, 232, 528
Luongo, C.....	568
Lupelli, I.....	210
Lutsenko, V. V.....	459
Lux, H.....	53, 700
Lvovskiy, A.....	183, 349, 564
Lyons, B. C.....	17, 445, 492
Lysenko, S. E.....	310
Lysssoivan, A.....	413
Lyu, B.....	127, 169, 236, 239, 499
Lyublinski, I.....	207

— M —

Ma, C. H.....	513
Ma, R. R.....	320
Ma, T.....	131

Maan, A.....	415
Machchhar, H.....	570
Mackinnon, A. J.....	131
MacLaren, S.....	131
MacPhee, A. G.....	131
Macusova, E.....	150, 221
Macwan, T.....	35, 144, 283, 289, 303, 693
Maebara, S.....	135, 601
Maejima, T.....	598
Maekawa, T.....	265
Maeta, S.....	266
Magee, R.....	156
Maggi, C. F.....	175, 179, 202, 406, 421
Maggiora, R.....	407
Mahajan, S. M.....	235, 421
Mahant, K.....	294, 687
Maheshwari, A.....	19, 628
Mahesuria, G.....	53, 607, 641, 706, 708, 711, 716, 744
Mahesuriya, G.....	735
Mailloux, J.....	174, 222, 422, 521
Maingi, R.....	11, 43, 50, 228, 544, 548, 580, 587, 588, 592
Maistrello, A.....	605
Majeski, R.....	61, 153, 415, 731
Major, M.....	610
Makhlai, V. A.....	212
Makijarvi, P.....	591
Makmool, T.....	511
Makowski, D.....	591
Makowski, M. A.....	185, 192
Makwana, A. R.....	715
Makwana, M. N.....	144, 608, 611, 693
Mal, K.....	679
Malaquias, A.....	200
Malhotra, S.....	674
Maljaars, B.....	220
Mallard, V.....	788
Mallick, C.....	23, 241
Malzev, S. G.....	313
Manas, P.....	384
Manchanda, R.....	35, 144, 244, 276-282, 285-287, 300, 518, 553, 619, 696
Mandal, D.....	48, 523
Manduchi, G.....	604
Manhard, A.....	606

Mankani, A. D.	20, 643	Masuzaki, S.	256, 257, 261, 273, 400
Manke, F.	215	Masyukevich, S. V.	576, 594
Mansfield, D. K.	580, 587	Matoi, R.	250
Mansinen, M.	175	Matsukado, K.	774
Manso, M. E.	394	Matsukawa, M.	604
Mansuri, I.	758	Matsumoto, N.	267, 269
Mantica, P.	179	Matsunaga, G.	272, 489, 490
Mantsinen, M. J. ...	174, 201, 222, 388, 407, 422, 423	Matsuo, K.	763
Manuelraj, M.	19, 623, 630, 633, 719	Matsuoka, S.	440, 476
Manz, P.	166, 394	Matsuyama, A.	38, 44, 426
Mao, S. F.	528	Mattei, M.	272, 604, 699
Mao, W.	40, 309	Matthews, G. F.	193, 225, 581
Mao, Y.	395	Mattoo, S. K.	296
Maraschek, M.	160, 216	Mauel, A.	413
Marchenko, A. K.	212	Maurizio, R.	168, 213, 396
Marchetto, C.	521	Maurya, U.	24, 447
Marchiori, G.	489	Maviglia, F.	210, 579, 583, 699
Mardenfeld, M.	695	Maximov, V. V.	318
Marek, A.	709	Maya, P. N. 49, 51, 234, 284, 617, 679, 781	
Marini, C.	409	Mayer, M.	16, 193, 209
Marinoni, A.	177, 328	Mayya, K. B. K.	281, 282
Markelj, S.	606	Mazon, D.	187, 240, 308, 603
Markin, A. V.	594	Mazzitelli, G.	50, 207, 535, 588
Markovic, T.	150, 221	Mazzotta, C.	201
Marmar, E. S.	11, 12, 130	McCarthy, K. J.	392, 416
Marocco, D.	734	McCarthy, P.	493
Marot, L.	575	McClements, K. G.	396, 411
Marqueta, A.	135, 601, 659	McClenaghan, J. T.	33, 39, 178, 663
Marrelli, L.	59, 390	McCullen, P.	219, 225
Marroncle, J.	135, 601	McDermott, R. M. 186, 384, 387-389, 580	
Marsen, S.	414	McKee, G. R.	165, 177, 324, 325, 328
Martín Solís, J. R.	38, 44, 425	McLean, A. G.	45, 192, 332-334, 336
Martin, E. H.	189, 350	McNaney, J.	131
Martin, M.	350	Medvedev, S. Y.	379, 381, 504, 586
Martin, V.	591	Medvedeva, A.	526
Martin-Fuertes, F.	782	Meezan, N. B.	131
Martinell, J. J.	48, 525	Mehta, K. R.	570, 625, 683
Martynenko, Y. V.	311	Mehta, M.	157, 752
Martynova, Y.	395, 778	Mehta, V.	681
Marushchenko, N. B.	465	Meigs, A. G.	172, 193
Maruyama, S.	368	Meitner, S. J.	590
Masaki, K.	730	Mekler, K. I.	319
Maslov, M.	179, 219, 359	Mele, A.	272, 604
Masse, L.	131	Melnik, A. D.	145, 727
Mastrostefano, S.	489, 532	Melnikov, A. V.	40, 162, 195, 310
		Menard, J. E. 13, 20, 21, 146, 147, 153, 358,	

544, 592, 635, 695, 731	
Mendez, P.	135, 601
Mendonca, J.	487
Meneghini, O. 47, 167, 335, 341, 445, 512, 527	
Meneses, E.	374
Meneses, L.	174, 179
Meng, X. C.	587
Meng, Z.	724
Menmuir, S.	172, 175, 179, 202, 384
Merino, E.	415
Merle, A.	166, 168, 220, 224, 406, 521
Merlo, G.	454
Merrill, J. F.	131
Merriman, S.	541
Merritt, E. C.	131
Mertens, P.	225, 575
Messiaen, A.	407, 413, 430, 745
Meszaros, B.	583
Metz, A.	572
Meyer, H.	10, 12, 126, 168, 175, 186, 406
Meyer, K.	591
Micciché, G.	135, 782
Michael, C. A.	200, 255, 439
Mihara, T.	373
Mikami, T.	256
Milanesio, D.	407
Militello, F.	57, 59, 172, 396, 434, 443
Miller, G. W.	653
Milovich, J. L.	131
Mima, K.	763, 772, 773
Minaev, V. B.	54, 145, 304, 727
Minami, R.	248, 256, 640
Minami, T.	27, 162, 249, 250
Minami, Y.	373
Minashin, P. V.	37, 470
Mineev, A. B.	145, 727
Minervini, J.	354
Miniyazov, A.	680
Mink, F.	326
Minucci, S.	170, 210
Mirnov, S.	207
Mirnov, V. V.	354, 514
Miron, I. G.	521
Mironova, E.	591
Miroshnikov, I. V.	145, 304, 727
Misaria, N.	703
Mishchenko, O.	449, 454
Mishra, J. S.	31, 685, 686, 689
Mishra, K. K.	36, 244, 267, 300
Mishra, P. C.	656
Mishra, S. 35, 234, 284, 287, 620, 622, 781	
Mistry, A. N.	665, 681
Mistry, H.	738, 759
Mitarai, O.	269
Mitosinkova, K.	150
Mitsunaka, Y.	640
Miura, E.	770
Miyamoto, M.	259
Miyanaga, N.	762, 763
Miyata, Y.	272, 604
Miyazawa, J.	416, 732
Mizuta, Y.	774
Mizuuchi, T.	162, 249, 250
Mlynář, J.	150, 221, 423, 561
Moeller, C. P.	269, 585, 702, 736
Mohan, K.	61, 570, 739, 743
Mok, Y.	376
Mokaria, P. K.	157, 284
Mokeev, A. N.	576
Molina, P.	168
Molla, J.	135, 601
Möller, S.	395, 778
Momo, B.	508
Monge, I.	725
Montes, K.	341
Montes, P.	450
Montgomery, D. S.	131
Montis, M.	135, 601
Montisci, A.	434
Moody, J.	131
Moon, S.	211, 575
Mora, J.	374
Mora-Meléndez, J.	54, 725
Morace, A.	763
Moradi, S.	219, 510
Morales, G.	151
Morales, J.	224, 422
Mordijck, S.	33, 44, 167, 179, 327, 512
More, V.	755
Moreau, D.	23, 240, 246
Morel, P.	454, 526

Moreno, J.	245	Muroga, T.	646, 698, 779
Moret, J.-M.	204, 220	Murphy, C.	331, 585, 736
Morgan, M.	700	Mutoh, T.	269
Mori, Y.	36, 769, 770	Mutzke, A.	617
Morimoto, J.	261	Muvvala, V. N.	19, 613
Morisaki, T. 12, 21, 138, 163, 181, 261, 273, 400		Muzichenko, A. D.	540
Morita, H.	762, 763	Myalton, T. B.	195
Morita, S.	227, 258	Myers, C. E.	141, 347, 358, 372
Moritaka, T.	40, 476, 516	Mylton, T. B.	316
Moriyama, S.	569, 596, 599, 640	— N —	
Morris, W. A.	700		
Moseev, D.	414	Na, Y.-S.	128, 377
Moser, A. L.	327, 331, 336	Nabais, F.	222
Moser, L.	575	Nagaoka, K.	38, 43, 162, 163, 181
Möslang, A.	634	Nagaraju, M. V.	626
Mossman, A.	367	Nagasaka, T.	49, 50, 698, 779
Motohiro, T.	770	Nagasaki, K.	162, 249, 250, 640
Motojima, G.	28, 254, 273, 416, 647	Nagashima, Y.	259, 267
Motoshima, M.	250	Nagata, K.	267
Mou, M.	551	Nagata, M.	28, 264
Moulton, D.	172	Nagata, T.	259
Moya, I.	135, 601	Nagatomo, H.	37, 763, 773
Moyer, R. A. . 183, 338, 339, 344, 427, 564		Nagora, U. C. . 34, 144, 275, 278–280, 553	
Mueller, D.	128	Nagy, A.	580, 585, 736
Muir, D.	504	Naidenov, V.	712
Mukai, K.	181	Nair, L.	729
Mukherjee, A. 122, 570, 615, 683, 739, 742, 743, 750		Nair, S.	720
Mukherjee, R.	40, 474	Naito, O.	604
Mukherjee, S. S. 29, 31, 284, 656, 685, 686, 689, 781		Nakahira, M.	11, 15, 568
Mukhin, E. E. . 11, 15, 145, 304, 576, 594		Nakai, M.	762, 763
Mukhopadhyay, D.	751	Nakai, T.	569
Mumgaard, B.	213	Nakajima, N.	604
Mumgaard, R. T.	189, 348	Nakamura, K.	255, 259, 267
Munaretto, S.	141, 185	Nakamura, M.	649
Munshi, P.	503	Nakamura, Y.	162, 249
Murakami, H.	728, 730	Nakanishi, H.	604
Murakami, S. 181, 252, 259, 266, 267, 524		Nakano, H.	181
Murakhtin, S. V.	318	Nakano, T.	256
Muralidhara, S.	20, 632	Nakashima, H.	259
Muramatsu, Y.	774	Nakashima, Y.	248, 256, 536, 640
Murari, A.	216, 734	Nakata, M.	181, 253, 505, 506
Murase, T.	273	Nakata, Y.	763
Murata, I.	360	Nallo, G. F.	535
		Nam, H.	51, 790, 792
		Nam, Y. B.	128
		Nam, Y. U.	128
		Nandi, P.	781

Narayanan, R.	756
Nardon, E.	561
Narita, E.	46, 506
Narushima, Y.	257, 262, 263
Natsume, K.	728
Naulin, V.	179, 396, 529
Naumenko, N.	316
Navratil, G.	171
Nayak, P.	685, 686, 689
Naydenkova, D.	150, 221
Naylor, D.	636
Nazikian, R.	185, 186, 478, 480, 495, 635
Neckel, T.	501
Nelsen, A.	415
Nemets, A. R.	316
Neto, A.	591
Neto, E.	458
Neu, R.	384, 395, 580
Neubauer, O.	399, 413
Neumeyer, C.	695
Newton, S.	561
Newton, S. L.	509
Nicholas, T.	434
Nicolai, D.	399, 402, 413
Nicollet, S.	703
Nie, L.	517
Nielsen, A. H.	55, 529
Niemann, H.	191, 400, 403
Nikitenko, A. I.	771
Nikitin, A. A.	634
Nikolaev, G. N.	540
Nikolaeva, V.	394
Nikroo, A.	131
Nille, D.	166
Nilsson, E.	561
Nimavat, H.	607, 641, 711, 716, 735, 744
Nimavat, N.	279, 285
Ning, Y.	529
Nishijim, D.	547
Nishijima, D.	208, 778
Nishimura, H.	762, 763
Nishimura, Y.	770
Nishino, M.	568
Nishioka, K.	249
Nishitani, T.	266, 360, 647
Nishiura, M.	27, 255

Nishiyama, K.	659
Niskala, P.	145, 437
Nissim, N.	769
Nitti, F. S.	782
Nocente, M.	222, 411, 422
Noe, J.	604
Noguchi, T.	265
Nojiri, K.	248, 256, 536
Norausky, N.	593
Nordman, H.	179
Norimatsu, T.	763, 767
Noterdaeme, J.-M.	60, 407, 745
Noto, H.	29, 646
Novello, L.	596
Novikau, I.	160, 454
Novokhatsky, A. N.	145, 727
Nowak, S.	47, 224, 521
Nozawa, T.	136, 649
Nozawa, Y.	265
Nuga, H.	266
Nührenberg, C.	438
Numakura, T.	256, 640
Nunami, M.	46, 181, 439, 505, 732
Nunio, F.	703
Nurgaliev, M. R.	40, 316

— O —

Oberparleiter, M.	179
Ochando, M. A.	494
Ochiai, K.	29, 649
Ochoukov, R.	407
Oda, Y.	11, 15, 569–571, 596, 598, 599, 640
Oertel, J.	131
Offermanns, G.	413
Ogawa, K.	28, 162, 266, 360, 457, 647
Ogawa, Y.	536
Oguri, K.	254
Oh, S. G.	575
Oh, Y.-K.	38, 128, 347, 362, 370–372
Ohana, N.	454
Ohdachi, S.	22, 163, 181, 261, 262, 345
Ohira, S.	604
Ohnishi, N.	763
Ohno, N.	256
Ohshima, S.	27, 162, 249, 250
Ohta, M.	649
Ohtani, H.	468

Ohtani, Y.	250, 253	Ozaki, T.	763
Oishi, T.	27, 258, 416	Ozeki, H.	568
Okabayashi, M.	45, 141, 346, 490	Ozeki, T.	604
Okada, H.	162, 249, 250		
Okada, M.	640	— P —	
Okada, S.	376	Pablant, N.	173, 392
Okamoto, K.	259	Paccagnella, R.	428
Okamura, S.	317	Pace, D. C.	349, 356, 653
Okano, F.	730	Pachicano, J. L.	353
Okihara, S.	770	Padaliya, M.	749
Okumura, Y.	659	Padasalagi, S. B.	669, 723, 755
Olofsson, E.	246	Pagonakis, I. G.	571, 709, 710
Olsen, J.	396, 529	Pajares, A.	357, 382
Olson, R. E.	131, 765	Pajuste, E.	30, 673
Omori, T.	599	Pak, A.	131
Omotani, J. T.	434	Pal, R.	197, 283
O'Mullane, M. G.	504	Palaniyappan, S.	131
Omura, Y.	265	Palermo, F.	160
Onchi, T.	259, 267, 640	Palmieri, A.	135, 601
O'Neill, R. C.	61, 585, 736	Pamela, S.	12, 21, 140, 172, 406, 485
Ongena, J.	61, 407, 413, 745	Pan, C.	577
Onjun, T.	247, 511, 520, 554	Pan, C. J.	747
Ono, M.	153, 259, 267, 329, 635, 640	Pan, C. K.	499
Ono, N.	376	Pan, Q.	545
Ono, T.	602	Pan, Y.	152
Ono, Y.	28, 153, 268, 270, 373, 468	Panadero Alvarez, N.	392
Oohara, S.	598	Panayotov, D.	30, 660
Ootani, J.	265	Panchal, M.	608, 611
Orain, F.	404, 411	Panchal, P. N.	607, 641, 685, 686, 689, 706, 711, 716, 735, 744
Orlikowski, M.	591	Panchal, R. N.	20, 607, 641, 706, 711, 716, 735, 744
Orlov, D. M.	45, 185, 338	Panchal, V. K.	144, 302
Orsiere, T.	788	Panda, N.	754
Osakabe, M.	162, 163, 181, 266, 456, 457, 647	Pandit, P.	35, 278, 279, 286, 288
Osborne, T. H.	165, 167, 171, 323, 326, 331, 332, 587	Pandya, H. B.	20, 122, 618, 621, 636
Oshuev, K. Y.	145, 727	Pandya, K. B.	626, 682, 684, 751
Osipov, I. E.	771	Pandya, S. N.	36, 144, 278, 280, 293
Otin, R.	581	Pandya, S. P.	293, 297
Otte, M.	191, 400	Panek, R.	150, 199, 221
Ovchinnikova, A. O.	634	Panizo, M.	766
Owen, L. W.	637	Pankin, A.	546
Oya, M.	259	Papadopoulos, A.	471
Oya, Y.	259	Papp, G.	160, 221, 556, 561, 562
Oyaizu, M.	649	Paprok, R.	561
Oyama, N.	251, 271	Parail, V.	421, 544
		Paravastu, Y.	277, 715

Parghi, B.	707	Patel, R.	61, 607, 641, 708, 711, 716, 735, 744
Parihar, M.	300	Patel, R. J.	706
Parisi, J.	172	Patel, S.	34, 276, 278, 279
Park, B. H.	128, 372, 550	Patel, S. P.	679, 781
Park, C.	649	Patel, T.	157
Park, G. Y.	41, 184, 369, 371, 445, 492	Patelli, E.	700
Park, H. K.	11, 12, 21, 128, 184, 198, 369, 371, 372	Pathak, H. A.	122, 628
Park, J.-K.	141, 184, 358, 370, 371, 695	Pathak, J.	618
Park, J.-S.	51, 363, 364	Pathak, S. K.	144, 274, 275, 278, 280, 291
Park, J. K.	128, 372	Patil, P.	591, 621
Park, J. M.	30, 362, 527, 663	Patil, Y.	41, 482
Park, K. R.	128	Patra, P.	233
Park, M.	591	Patrov, M. I.	145, 304, 727
Park, S.	360	Patten, H.	423, 458, 494
Park, Y.-S.	52, 372	Patterson, B. M.	131
Park, Y. S.	128, 347	Pau, A.	216
Parker, R. R.	348	Pautasso, G.	699
Parks, P.	183	Pavéz, C.	245
Parks, P. B.	565	Pavlo, P.	150
Parmar, D.	626	Pavlov, Y. D.	313
Parmar, K.	300	Pawelec, E.	216
Parmar, K. G.	759	Pawley, C.	356
Parmar, K. M.	244	Paz-Soldan, C.	38, 43, 141, 165, 167, 177, 183, 185, 186, 339, 349, 405, 427, 445, 495, 563, 564
Parmar, P. R.	688	Pedrerros, J.	245
Parra, F. I.	172	Pei, Y.	418
Pasch, E.	173, 392, 399	Peillon, S.	788
Pastor, I.	205	Peluso, E.	175, 216
Pate, K.	285	Peña, O.	766
Patel, A. 30-32, 62, 570, 625, 658, 667, 683, 687, 694, 743, 756		Penafior, B. G.	357
Patel, A. D.	229, 757	Peng, S.	500
Patel, A. V.	294	Peponis, D. V.	709
Patel, H.	570, 572, 613, 626, 738, 759	Perek, P.	591
Patel, H. K.	62, 754	Pérez, M.	782
Patel, H. N.	750	Perez Von Thun, C.	734
Patel, J.	61, 738, 759	Pericoli Ridolfini, V.	55, 532, 541
Patel, J. C. 61, 607, 641, 711, 716, 735, 744		Perkins, R. J.	151, 350, 472
Patel, K.	18, 281, 282, 607, 609, 627, 641, 696, 708, 711, 716, 735, 744	Perlado, J. M.	26, 34, 766
Patel, K. M. 20, 144, 278, 280, 287, 289, 301, 303, 553, 631, 696		Perry, J. M.	353
Patel, M.	61, 570, 626, 742, 743, 750, 755	Perry, T. S.	131
Patel, N.	36, 157, 301	Pesamosca, F.	220
Patel, N. C.	278, 553	Peterka, M.	150, 199
Patel, P.	131, 632	Peterson, B. J.	364
		Peterson, E.	354

Peterson, R. R.....	131, 765	Pohorecki, W.....	614
Pettersson, P.....	209, 211	Pokol, G. I.....	63, 160, 529, 561, 562
Petitpas, P.....	591	Polevoi, A. R. 379, 381, 383, 430, 444, 504	
Petrella, J.....	695	Poli, E.....	220, 501
Petrie, T. W.....	44, 171, 332	Poli, F. M. . 41, 53, 141, 161, 352, 372, 383,	
Petrov, A. V.....	145, 304, 727	430, 481, 521	
Petrov, Y. V. . 145, 212, 304, 354, 472, 565,	727	Polosatkin, S. V.....	319
Petty, C. C. 10, 12, 125, 165, 171, 177, 327,	328, 356	Pölöskei, P. Z.....	160, 409
Petty, P.....	332	Polunovskii, I.....	712
Peysson, Y.63, 187, 221, 240, 308, 561, 562		Poncet, J.-M.....	703
Pfaff, E.....	572	Popov, A. Y.....	145, 469
Pfefferlé, D.....	458, 558	Popov, T.....	199
Philips, R.....	413	Popov, V. A.....	661
Phillips, G.....	135, 601	Por, G.....	160
Piceno, E.....	131	Poradziński, M.....	510, 532
Picha, R.....	247, 520	Porezanov, N.....	540
Piedra-Quesada, N.....	725	Porkolab, M.....	348, 543
Pierren, C.....	353	Porter, G. D.....	192, 336
Pieters, G.....	788	Porton, M.....	581
Pigatto, L.....	41, 224, 489, 699	Postupaev, V. V.....	319
Pillai, S.....	613, 626	Potzel, S.....	384
Pinches, S. D. . 14, 46, 379, 381, 430, 444,	504	Poulos, M. J.....	151
Pinna, T.....	782	Prajapati, C.....	694
Pinsker, R. I.....	349, 585	Prajapati, P.....	54, 723
Pintsuk, G.....	136, 395	Pramanik, J.....	22, 233
Pinzón, J. R.....	166	Prasad, S.....	664
Pinzhenin, E. I.....	318	Prasad, U. 53, 607, 706, 707, 715, 717, 721,	
Piotrowicz, P.....	637	749	
Piovan, R.....	605	Praveenlal, E. V.....	144, 303, 693
Piovesan, P.....	495	Predebon, I.....	508
Piron, C.....	17, 224	Presnyakov, M. Y.....	634
Pironti, A.....	272	Pribyl, P.....	151, 350
Pisano, F.....	434	Priddie, D.....	593
Pisent, A.....	135, 601, 659	Prikhodko, V. V.....	40, 318
Pitts, R. A. . . 128, 208, 363, 380, 544, 581		Prinja, N. K.....	10, 120
Plank, U.....	389	Prisiazhniuk, D.....	166
Ploeckl, B.....	651	Prompting, J.....	23, 247, 511, 520, 554
Plyusnin, V. V.....	218, 221	Pruneri, G.....	135, 601, 659
Podadera, I.....	135, 601	Pu, N.....	266
Podestà, M. 14, 22, 46, 161, 329, 351, 352,	484	Pucella, G.....	13, 148, 201, 521
Podkovyrov, V. L.....	540	Pueschel, M. J.....	151, 514
Podolnik, A.....	150	Puglia, P.....	222
		Puig Sitjes, A.....	191, 400
		Pujari, P. K.....	781
		Purohit, D.....	738, 759
		Purohit, S.....	290

Purwar, G. . . . 607, 641, 711, 716, 735, 744
 Pusztai, I. 172, 509
 Pütterich, T. 59, 384, 388, 389
 Putvinski, S. 156

— Q —

Qi, L. 47, 507
 Qian, J. 178, 239, 259
 Qian, J. P. 127, 169, 170, 240, 246, 342, 499
 Qin, H. 548
 Qiu, Z. 24, 451, 454
 Qu, H. P. 320
 Qu, Z. Q. 483
 Que, W. 695

— R —

Rabinski, M. 221
 Rack, M. 399, 442
 Radha, B. P. 13, 66, 149
 Radhakrishnan, D. 497
 Radulović, V. 614
 Rafiq, T. 481
 Raftopoulos, S. 695
 Raghunathan, M. 458, 494
 Ragona, R. 61, 407, 745
 Rahbarnia, K. 173, 392, 399
 Raj, H. 58, 65, 144, 197, 277, 278, 280–282,
 285, 289, 518, 553
 Raj, P. 749
 Rajanbabu, N. 738
 Rajendra Kumar, E. . . . 597, 608, 639, 665
 Rajnish, K. 570, 683, 742
 Rajpal, R. 36, 302, 621, 696
 Rajput, M. 30, 666
 Raju, D. . 144, 197, 230, 244, 303, 607, 641,
 706, 707, 715, 717, 758
 Ralph, J. E. 131
 Ram Sankar, P. 691
 Ram, A. K. 37, 471
 Ramaiya, N. 300
 Raman, R. 259, 635
 Ramasubramanian, N. . . . 757
 Randolph, R. B. 131
 Ranjan, V. 144
 Ranjithkumar, S. 639
 Rao, B. 152, 260
 Rao, S. L. 122

Raole, P. M. 234, 284, 617, 679, 781
 Rapp, J. 20, 637
 Rasinski, M. 395, 778
 Rasmussen, J. J. 396, 504, 529
 Rastogi, N. 54, 623, 630, 633, 719
 Rath, D. 23, 244, 300
 Rattà, G. 216
 Rauch, J. 356
 Raulji, V. D. 144, 302, 631
 Raval, B. 625, 683
 Raval, D. C. 244, 657, 715
 Raval, J. V. . . . 35, 144, 277–280, 290, 553
 Raval, T. 758
 Ravensbergen, T. 396
 Ray, H. B. 637
 Rayjada, P. A. 30, 675, 781
 Razdobarin, A. G. . 17, 145, 575, 576, 594
 Raznitsyn, O. A. 634
 Razumenko, D. V. 145
 Rea, C. 141, 335, 341
 Réfy, D. I. 172, 529
 Regidor, D. 135, 601
 Reich, M. 220
 Reichle, R. 575, 591
 Reiman, A. 42, 497
 Reimerdes, H. . . . 56, 204, 213, 396, 541
 Reimold, F. 386
 Reinhart, M. 778
 Reinke, M. L. 153, 330, 358, 386, 415, 695
 Reiser, D. 536
 Reiter, D. 442
 Ren, Q. 178
 Ren, Q. L. 499
 Ren, Y. 236
 Renard, B. 135
 Rensink, M. E. 435, 542, 589
 Reusch, J. A. 353
 Reux, C. 164, 218, 221, 561
 Reynolds-Barredo, J.-M. . . . 379, 526
 Rhee, T. 362
 Rhodes, A. T. 353
 Rhodes, T. L. 165, 177, 323, 325, 327, 328,
 415
 Ribeiro, C. 42, 498
 Riccardo, V. 428, 581
 Ricci, P. 215

Rice, J. E.	196	Rudakov, D. L.	334, 337, 780
Rice, N.	131	Rudischhauser, L.	191, 400
Richiusa, M. L.	579, 581	Ruess, S.	709, 710
Richner, N. J.	353	Ruess, T.	709
Riemann, J.	206, 449	Ruiz Ruiz, J.	610
Riesch, H.	395	Ruset, C.	209
Rieth, M.	395	Ruzic, D. N.	587
Rigoni, A.	604	Ryan, D. A.	186, 404, 411
Rimini, F. G. . 164, 174, 175, 203, 216, 219, 225, 581		Rygg, J. R.	131
Riquezes, J. D.	347, 372	Ryter, F. . 59, 166, 359, 384, 387, 389, 410	
Rittich, D.	61, 410, 433	Ryzhakov, D. V.	40, 310, 313
Riva, F.	434	Rzesnicki, T.	571, 709, 710
Rivera, A.	766		
Rivero-Rodriguez, J. F.	411	— S —	
Roach, C.	406	Saarelma, S. . 168, 172, 384, 406, 421, 422, 699	
Robey, H. F.	131	Sabbagh, S. A.	45, 128, 141, 347, 372
Robin, F.	604	Sachdev, J.	635
Roche, T.	156, 376	Sacks, M. R.	131
Rodriguez Sanchez, C.	353	Sadharakiya, D. H.	144
Rodriguez-Fernandez, P.	58, 65, 196	Sadykov, A.	760
Rognlien, T. D.	192, 336, 415, 553, 589	Safronov, V.	540
Rogozhkin, S. V.	20, 634	Sagara, A.	698, 732, 779
Rohde, V.	580	Sahoo, B. P.	56, 531, 534
Rohollahi, A.	367	Sahu, A. K.	607, 641, 706, 707
Roidl, B.	269	Saint-Laurent, F.	561
Rojas, J. F.	725	Sainz, J.	570
Rojas-Quesada, M. A.	374	Saito, K.	269
Rojaz-Loaiza, A. M.	725	Saito, Y.	266
Romanelli, M. 174, 201, 203, 359, 510, 521, 544		Sakagami, H.	762, 763, 770, 773
Romazanov, J.	208	Sakai, Y.	265
Romero, J.	156	Sakakibara, S.	261–263
Rosa Adame, E.	579	Sakamoto, K.	135, 569, 601, 640, 659
Rose, J.	788	Sakamoto, M.	248, 256, 536
Ross, J. S.	131	Sakamoto, R.	194, 254, 273, 416, 732
Rossi, G.	151	Sakamoto, S.	269
Rotti, C.	573, 626	Sakamoto, Y.	43, 50, 584
Rousseau, B.	788	Sakasai, A.	730
Rovenskiikh, A. F.	319	Sakasegawa, H.	136
Rowan, W. L.	496	Sakata, S.	762, 763
Roy, S.	54, 721	Sakharov, N. V.	145, 304, 727
Rozhdestvensky, V. V.	293	Sakurai, S.	791
Rubel, M.	211, 575	Sakurai, T.	568
Rubinacci, G.	558	Salewski, M.	409, 411, 504
Rubino, G.	210	Salmi, A.	179, 182, 325, 327
		Salmonson, J.	131
		Sam, S.	678

Sammuli, B. S.	246, 342, 343
Samoylov, O.	199
Samsonov, D. S.	145, 576, 594
Samuell, C. M.	192, 336
Sánchez, E.	16, 205, 206
Sánchez Castro, J.	374
Sanchez, P.	571
Sanchez, R.	379, 526
Sanchis-Sanchez, L.	411
Sandeep, K. T.	704
Sandhu, S. S.	669, 755
Sandorfi, A. M.	653
Sandri, N.	399
Sang, C. F.	331
Sangaroon, S.	47, 247, 511, 520, 554
Sano, F.	645
Sano, T.	772
Sanpei, A.	373
Santos, J. J.	394, 763
Santosh, P.	295
Santra, P.	720
Sanyasi, A. K. . 36, 243, 296, 298, 299, 612,	692, 713
Saraswat, A.	704
Saravanan, K.	617, 781
Sarazin, Y.	446, 526
Sarff, J. S.	354
Sarkar, B.	707
Särkimäki, K.	430, 464, 561
Sarma, A.	288
Sarmah, T.	154
Sartori, E.	733
Sartori, F.	604
Sarychev, D. V.	316
Sasaki, M.	446
Sasaki, S.	598
Sasmal, C. S.	31, 678, 718
Satake, S.	17, 440, 476, 732
Sater, J. D.	131
Satheeswaran, G.	399, 402, 413
Sathyanarayana, K. 144, 230, 687, 693, 694	
Sato, A.	269
Sato, F.	596
Sato, M.	41, 491, 505, 728
Sato, S.	649
Sattin, F.	488

Satyaprasad, A.	781
Sauppe, J.	131
Sauter, O. 216, 220, 224, 388, 409, 504, 521,	586, 699
Sauvan, P.	652
Saveliev, A. N.	145, 469
Savkin, V. Y.	318
Savoldi, L.	53, 535, 710
Sawa, N.	568
Sawada, A.	268, 270
Sawada, H.	763
Sawada, S.	256
Sawahata, M.	596
Saxena, Y. C.	42, 230, 631
Sayre, D.	131
Saze, T.	647
Scantamburlo, F.	135, 601, 659
Scarin, P.	398
Schaefer, C. E.	353
Schäfer, J.	572
Schamel, H.	523
Schaubel, K.	593
Scheffer, M.	433
Scherer, T.	709
Schick, R.	413
Schippers, W.	219
Schlatter, C.	571
Schluck, F.	17, 442
Schmid, K.	606
Schmid, M.	571, 709
Schmidt, D. W.	131
Schmitt, J. C.	191, 392, 403
Schmitz, J.	395
Schmitz, L. 33, 39, 156, 177, 327, 355	
Schmitz, O.	191, 273, 339, 400
Schmuck, S.	274
Schneider, B.	396
Schneider, H.	695
Schneider, M. . 57, 59, 131, 430, 464, 501,	504
Schneider, P. A.	175, 384, 409, 411
Schneider, R.	617
Schoff, M.	131
Schrittwieser, R.	396
Schunke, B.	626
Schuster, E.	46, 53, 357, 382, 481

Schwartz, J. A.	589	Sharma, D. . 20, 40, 55, 299, 475, 523, 531, 534, 553, 613, 626, 639, 665, 704	
Schwarz-Selinger, T.	18, 606	Sharma, D. K.	715
Schweer, B.	399, 413	Sharma, Deepti	235
Schweinzer, J.	388	Sharma, Devendra	235
Schwörer, D.	17, 443	Sharma, J.	692
Sciortino, F.	196	Sharma, M.	22, 62, 229, 756–758
Scott, E. R.	173	Sharma, P.	23, 234, 284, 617, 679, 781
Scott, S.	167, 348, 372	Sharma, P. K.	231, 294, 655, 688
Scotti, F.	415	Sharma, R.	62, 607, 641, 711, 744, 746
Scoville, J. T.	356	Sharma, S.	466, 681
Seal, S.	566	Sharma, T. K.	62, 669, 755
Seidl, J.	150, 199	Sharma, U.	692
Seki, R.	24, 181, 252, 261, 266, 457, 732	Shchegolev, P. B.	145, 304, 727
Seki, T.	269	Sheik, U.	216
Sekiguchi, J.	376	Sheikh, U.	168, 213, 406
Sekine, T.	774	Shekhtman, L. I.	661
Seliunin, E.	394	Shelukhin, D. A.	195
Sen, A.	197, 277, 429, 466, 487	Shen, B.	155, 169, 341
Sénée, F.	659	Shen, W.	14, 22, 238, 418, 499
Sentoku, Y.	762, 763, 770, 772, 773	Shephard, M. S.	558
Seol, E. S.	558	Shesterikov, I.	407
Seol, J.	361, 550	Shevelev, A. E.	145, 293, 561, 712, 727
Seon, C. R.	364, 365	Shi, E. L.	545
Sepke, S.	131	Shi, L.	478
Sepulveda, A.	245	Shi, P. W.	40, 305, 306, 314, 315
Sereda, S.	399	Shi, T.	185
Sergeev, D. S.	195, 316	Shi, T. H.	236
Sergeev, V. Y.	600	Shi, Y. F.	517
Sergienko, G.	193, 225	Shi, Y. J.	152
Serianni, G.	733	Shi, Z.-B.	321
Sertoli, M.	423	Shi, Z. B.	187, 305–308, 314, 315, 320
Seugling, R.	131	Shibama, Y.	55, 730
Shafer, M. W.	45, 331, 345, 445	Shibata, N.	574, 598
Shah, K.	35, 278, 279, 281, 282	Shigin, P.	575
Shah, K. S.	144, 693	Shikama, T.	259
Shah, M.	144, 302, 303, 693, 694, 696	Shimabukuro, S.	259
Shah, P. . 607, 641, 708, 711, 716, 735, 744		Shimizu, A.	317
Shah, R. C.	131	Shimozuma, T.	640
Shah, S.	30, 613, 626, 664	Shinya, T.	135, 269, 601, 659, 702
Shaikh, Z.	62, 757	Shiraga, H.	762, 763
Shalashov, A. G.	318	Shirahata, K.	255
Shao, L. M.	169	Shirai, H.	133, 265
Sharafutdinov, M. R.	661	Shiraishi, J.	490
Sharapov, S.	174, 411	Shiraiwa, S.	189, 348, 585
Sharapov, S. E.	16, 222	Shiraki, D.	183, 344, 590
Sharma, A. L.	758		

Shiroto, T.	763	Sirinelli, A.	504
Shoji, M.	273	Sitnikova, A. A.	594
Showers, M.	637	Skakov, M.	680, 760
Shpanskiy, Y. S.	53, 705	Sklyarov, V. F.	319
Shrivastava, A.	54, 608, 611, 718	Skyman, A.	179
Shukla, B. K.	62, 144, 738, 759	Slaby, C.	449
Shukla, G.	35, 278, 279, 281, 282	Sladkomedova, A. D.	145, 304, 727
Shukla, N.	55, 533	Ślęczka, M.	400
Shukla, P. K.	290	Smiley, M.	585, 736
Shukla, V.	30, 632, 672	Smirnov, A. I.	145, 156
Shurygin, R. V.	310	Smith, H. M.	509
Shutov, A. S.	634	Smith, J.	17, 593
Sias, G.	216, 434	Smith, M.	695
Sibilia, M.	695	Smith, S.	140
Siccinio, M.	53, 541, 583, 699, 700	Smith, S. P.	29, 328, 512, 527, 653
Sidorov, E. N.	319	Snicker, A.	24, 409, 411, 430, 453, 464
Sieglin, B.	166, 433	Snipes, J. A.	368, 380
Silburn, S.	174, 581	Snoep, G.	512
Silva, A.	394, 407, 734	Snoj, L.	652
Silva, C.	60, 214, 394	Snyder, P. B.	26, 34, 167, 326, 445, 512, 527, 663, 780
Silvagni, D.	166	Sokolov, I.	680
Simic, G.	380	Sokolov, M. M.	313
Simonen, T.	354	Sokolov, V.	156
Simpson, J.	172	Solano, E. R.	164, 175
Simrock, S.	17, 591, 621	Solano-Piedra, R.	374
Singh, A. K.	37, 277, 287, 462, 557, 715	Soldatkina, E. I.	318
Singh, A. P.	669	Solokha, V. V.	145, 304, 576, 594, 727
Singh, D.	613, 626	Solomakhin, A. L.	318
Singh, G. K.	607	Solomon, W.	167
Singh, K.	674	Solovei, V. A.	145, 576
Singh, K. P.	29, 642, 658	Soloviev, N. A.	310, 316
Singh, M.	430, 572, 613, 617, 627, 781	Solyakov, D. G.	212
Singh, M. J.	19, 626, 751	Sommariva, C.	458, 561
Singh, N.	718	Sonara, D.	607, 641, 706, 711, 716, 735, 744
Singh, N. P.	19, 570, 625, 683	Sonato, P.	573
Singh, P.	751	Song, I.	51, 364, 365
Singh, R.	63, 243, 296, 551, 570, 683, 741-743	Song, J.	624, 690
Singh, S. K.	296	Song, S. D.	187, 240, 308, 320
Singh, V.	674	Song, X.	322
Sinha, A.	34, 274, 275	Song, X. M.	40, 187, 240, 305, 308, 320, 322
Sinha, J.	204	Song, X. Y.	308
Sinha, P.	400	Song, Y.	155, 156
Sips, A. C. C.	174, 179, 203, 384	Soni, D. G.	570, 683, 743
Sircar, A.	675, 714	Sonnendrucke, E.	501
Siren, P.	510	Sorbom, B. N.	354, 610

Sordo, F.	766	Strait, E. J.	12, 21, 141, 405, 490
Soto, L.	23, 245, 766	Strait, T.	346
Soukhanovskii, V. A.	336, 415	Strand, P.	47, 510, 521, 562
Sovinec, C.	558	Stratton, B.	695
Sozzi, C.	16, 216	Strauss, D.	709
Spada, E.	733	Strauss, H.	38, 44, 428, 558
Sparapani, P.	216	Stroth, U.	166, 394
Spitsyn, A. V.	701	Strozzi, D. J.	131
Spizzo, G.	398	Strumberger, E.	404, 486
Spolaore, M.	214, 396	Suárez López, G.	407
Spong, D. A.	63, 183, 349, 564, 566	Subba, F.	535, 541, 699
Srikanth, G. L. N.	607, 641, 708, 711, 716, 735, 744	Subbarao, A. P.	570, 615, 743
Srinivas, Y. S. S.	244, 300	Subbotin, G. F.	195
Srinivasan, R.	235, 447, 462, 475, 482, 531, 553, 607, 616, 666, 706, 707, 715, 717, 721, 749	Subhash, P. V.	19, 462, 616, 620, 622, 648, 666, 781
Srivastav, P.	23, 243, 296, 298, 299, 612	Subramanian, N.	229
Srivastava, A. K.	276	Suchkov, E. P.	493
Srivastava, P. K.	36, 243, 296, 298, 299, 612, 713	Sudnikov, A. V.	319
Srivastava, R.	533	Sugama, H.	505
Srivastva, V. K.	636	Sugandhi, R.	18, 54, 243, 296, 298, 299, 612, 713
Stadermann, M.	131	Sugata, T.	255
Staebler, G. M.	178, 182, 196, 512	Sugawara, T.	373
Stahl, A.	561	Sugie, Y.	604
Stakunas, G.	216	Sugimoto, M.	12, 14, 30, 135, 601, 659
Staltsov, V. V.	212	Sugiyama, L. E.	17, 41, 441, 479
Stamp, M.	175	Sun, A. P.	517
Štancar, Ž.	29, 652	Sun, G.	690
Stange, T.	173, 401, 414	Sun, H. J.	166
Stangeby, P. C.	331, 337, 780	Sun, P.	187, 305, 308
Stankunas, G.	29, 650	Sun, P. J.	23, 236
Startsev, E.	513	Sun, T. F.	312, 320
Stavrou, C.	172	Sun, Y.	49, 58, 127, 185, 495
Stefanikova, E.	174, 406	Sun, Y. W.	169, 227, 232
Steinhauer, L.	156	Sun, Z.	587
Stepanov, D.	591	Sun, Z. C.	747
Stepanov, I.	413	Sunahara, A.	763, 770
Stephens, A.	593	Sung, C.	165, 328
Stevenson, T.	695	Sunn Pedersen, T.	57, 58, 173, 190, 191, 392, 400, 416
Stober, J.	168, 388, 410, 501	Surrey, E.	66, 697
Stockel, J.	150	Suthar, G.	570, 739, 743
Stoeffl, W.	131	Suto, T.	598
Stoltzfus-Dueck, T.	545	Suttrop, W.	49, 58, 186, 387, 388, 404, 411, 495
Stotler, D. P.	548, 553, 589	Suweis, S.	733

Suzuki, C.....	252, 254, 416, 732
Suzuki, H.....	649
Suzuki, N.....	595
Suzuki, T.....	271, 272
Suzuki, Y. 27, 163, 191, 261, 262, 345, 456, 457, 508	
Swami, H. L.....	31, 665, 681
Swamy, R.....	157
Sweeney, R.....	368
Szepesi, G.....	219, 493
Szepesi, T.....	191

— T —

Tadepalli, S. C.....	616, 648
Tafti, S.....	653
Taguchi, T.....	763
Tahiliani, K.....	35, 144, 278–280
Tailor, H. M.....	678
Taimourzadeh, S.....	461, 478
Tajima, T.....	156, 355, 376
Tajiri, Y.....	269, 702
Takagi, I.....	259
Takahashi, C.....	249
Takahashi, H.....	163, 181, 253, 640
Takahashi, K.....	569, 596, 599, 640
Takahashi, T.....	376
Takahata, Y.....	373
Takano, K.....	568
Takase, Y. 53, 153, 259, 267, 269, 329, 702	
Takechi, M.....	489, 490
Takeda, S.....	51, 790, 791
Takei, Y.....	269, 702
Takeiri, Y.....	10, 273
Takemura, Y.....	28, 262, 263
Takenaga, H.....	506
Takeuchi, Y.....	774
Takizuka, T.....	536, 586
Tál, B.....	172, 529, 734
Tala, T.....	33, 39, 179, 182, 325, 327
Tamura, H.....	732
Tamura, N.....	254, 416
Tan, M.....	155
Tanabe, H.....	28, 268, 270, 373, 468
Tanaka, F.....	376
Tanaka, H.....	28, 256, 261, 265, 273
Tanaka, K. 27, 181, 252–254, 257, 261, 439	
Tanaka, M.....	17, 595

Tanaka, T.....	647, 698, 732, 779
Tang, C.....	317
Tang, S.....	349
Tang, T. F.....	543
Tanigawa, H.....	12, 14, 136, 649
Tanna, R. L. 13, 21, 144, 197, 277–282, 285, 287, 289, 300, 301, 303, 518, 553, 631, 693, 696	
Tanna, V. L. . . . 53, 607, 641, 706–708, 711, 716, 717, 720, 735, 744, 746	
Tardini, G.....	387
Tardocchi, M.....	734
Taylor, G.....	267
Taylor, N. P.....	141, 789
Taylor, T. S.....	331
Taylor, Z.....	346, 490
Tazhibayeva, I.....	680
Tchilinguirian, G.....	695
Teduka, M.....	649
Tegneder, D.....	179
Teklu, A. M.....	338
Telesca, G.....	47, 519
Telnova, A. Y.....	145, 304, 727
Tema, A.....	512
Teplukhina, A. A.....	216, 220, 383
Terakado, A.....	248, 256
Terakado, M.....	596
Tereschenko, I. B.....	576, 594
Terra, A.....	778
Terranova, D.....	493
Terry, J. L.....	330, 348, 435, 542
Terry, P. W.....	47, 151, 514
Terzolo, L.....	372
Testa, D.....	224
Tewari, R.....	674
Thakar, A.....	625, 683
Thakker, U.....	643
Thatipamula, S. G.....	230, 363
Theiler, C.....	16, 213, 396
Tholerus, E.....	510
Thomas, C.....	131
Thomas, D. M.....	331, 336, 337, 339
Thomas, J.....	144
Thome, K. E. . . 45, 183, 328, 349, 356, 564	
Thompson, M. C.....	156
Thompson, V.....	581

Thomsen, H.....	392	Trask, E.....	156
Thomsen, K.....	359	Tribaldos, V.....	379
Thornton, A. J.....	213	Tripathi, D.....	285
Thrysoe, A. S.....	529	Tripathi, S.....	157
Thumm, M.....	571, 709	Tripathi, S. K. P.....	151, 350
Thyagaraja, A.....	429, 487	Tritz, K.....	587
Tian, K.....	782	Trivedi, P.....	674
Tidikas, A.....	650	Trivedi, R. G...15, 570, 615, 683, 739, 742,	743, 750
Tierens, W.....	407	Trivedi, T. A.....	234, 679, 737, 781
Tigelis, I. G.....	471, 571, 709	Trukhin, V. M.....	195, 316
Ting, W.....	214	Trunev, Y. A.....	661
Tinguely, R. A.....	561, 610	Truong, D.....	165
Tipton, R.....	131	Tsalas, M.....	174, 179, 219, 384
Titus, P.....	695	Tsao, S.-W.....	151
Tivey, R.....	579	Tsubakimoto, K.....	763
Tiwari, R. R. K.....	623, 630, 633, 719	Tsuchibushi, Y.....	273
Tiwari, S.....	30, 665, 670, 681	Tsuchiya, H.....	254, 263
Tobari, H.....	18, 574, 598	Tsuchiya, K.....	728, 730
Tobita, K.....	645	Tsui, C. K.....	213, 396
Toda, S.....	439, 505	Tsujii, N.....	269, 702
Todo, Y.14, 22, 411, 418, 419, 456, 457, 491		Tsujimura, T. I.....	253, 254, 267, 640
Togo, S.....	56, 256, 536	Tsukamoto, W.....	265
Toi, K.....	163	Tsventoukh, M. M.....	311
Toigo, V.....	15, 573	Tu, C.....	155
Tokarev, V. A.....	145, 304, 727	Tu, H.....	762
Tokimatsu, K.....	790	Tuccillo, A. A.....	240
Tokita, S.....	762, 763	Tugarinov, S. N.....	316
Tokitani, M.....	273	Tukachinsky, A. S.....	145
Tokunaga, K.....	259	Tulenbergenov, T.....	31, 680
Tokuzawa, T.....	27, 252, 254, 263	Turco, F.....	33, 39, 141, 171, 332, 785
Told, D.....	545	Turkin, Y.....	438
Tolman, E. A.....	18, 179, 610	Turnbull, A.....	141
Tolochko, B. P.....	661	Turner, M. M.....	443
Tolstyakov, S. Y...145, 304, 576, 594, 727		Tuszewski, M.....	156
Tomar, A.....	54, 717	Tyagi, A. K.19, 234, 235, 531, 617, 679, 781	
Tomarchio, V.....	730	Tyagi, H.....	19, 626, 627, 682, 684, 751
Tomes, M.....	150, 199, 221	Tynan, G. R.....	420
Tomova, K.....	199		
Tonegawa, A.....	256	— U —	
Tooker, J. F.....	585, 736	Ubaldi, C.....	788
Torikai, Y.....	778	Uchida, M.....	265
Torre, A.....	703	Udintsev, V.....	620, 622
Torreblanca, H.....	585, 736	Umansky, M. V. 44, 57, 59, 189, 330, 435,	542, 546
Totsuka, T.....	604	Umeda, N.....	574, 598
Town, R. P. J.....	131	Unterberg, B. A.....	60, 395, 778
Tran, M. Q.....	571, 699, 709, 745		

Unterberg, E. A.	45, 334, 337, 339, 780
Upadhyay, D. V.	570, 625, 683, 743
Urano, H.	140, 272, 604
Urban, J.	150, 221
Urbanczyk, G.	240
Usami, S.	37, 468
Ushigusa, K.	57
Ushiki, T.	373
Usoltceva, M.	407
Usui, K.	728

— V —

Vadolia, G.	20, 642
Vaghashiya, P.	636
Vaghela, H.	122, 632
Vaghela, N. P.	675
Vala, S. S.	30, 617, 664, 666, 670, 671, 679, 681, 781
Valanju, P.	496
Valcarcel, D. F.	174, 384, 581
Valeo, E. J.	472
Valisa, M.	423
Vallar, M.	224
Vallcorba, R.	703
Vallejos, P.	222
Valvis, S.-I.	471
Van Compernelle, B.	45, 151, 350
Van Drie, A.	156
Van Eester, D.	223, 350, 407, 430, 510, 745
van Milligen, B. P.	214
Van Schoor, M.	413, 745
van Vugt, D.	379
van Vuuren, A. J.	409
Van Zeeland, M. A.	161, 349, 356, 411, 433, 564
Varava, A.	207
Varavin, M.	150
Varfolomeev, V. I.	145, 727
Vargas-Blanco, V. I.	52, 374, 725
Varia, A.	300
Varia, A. D.	244
Varia, D. S.	144
Varje, J.	510
Varju, J.	150
Varmora, P.	707, 715
Varshavchik, L. A.	576, 594
Varshney, S.	19, 287, 591, 620–622
Vartanian, S.	223
Vasava, K.	720
Vasava, P.	570, 615, 743
Vasava, V.	681
Vasiliev, A. L.	634
Vasilyev, A. A.	661
Vasilyeva, N. G.	319
Vayakis, G.	576, 591, 603
Vega, J.	216
Velasco, J. L.	206, 440
Veltri, P.	733
Venâncio, L.	539
Veniger, G.	614
Verdoolaege, G.	51, 175, 359
Verhaegh, K.	213, 396
Verma, A. K.	18, 597
Verma, S.	570, 683, 743
Vermare, L.	526
Vershkov, V. A.	58, 65, 195, 310
Vertkov, A.	16, 207
Vervier, M.	413
Vianello, N.	33, 60, 170, 213, 396
Vicente, J.	394, 396
Victor, B. S.	332, 337, 356
Vieira, R.	585
Viezzzer, E.	59, 166, 186, 202, 384, 387, 389, 411, 485, 699
Vijvers, W. A. J.	213
Vilela Mendes, R.	539
Villard, L.	454, 586
Villone, F.	272, 489, 558
Vincena, S.	151, 350
Viola, B.	210
Viola, M.	695
Virani, C. G.	294, 655
Vitale, V.	604
Vitton-Mea, L.	581
Vizvary, Z.	579, 581
Vlad, G.	24, 455, 521
Vladimirov, P.	634
Vlainic, M.	221, 561
Voitsekhovitch, I.	216, 383, 430
Voitsenya, V. S.	575
Voldiner, I.	367
Volegov, P. L.	131
Volzke, O.	401

Von Hellermann, M.	619
Vondracek, P.	150, 199, 221
Vorpahl, C.	583
Vrel, D.	788
Vu, T.	220
Vukolov, K. Y.	576
Vyacheslavov, L. N.	661
Vyas, G. L.	19, 619

— W —

Wada, K.	596
Wade, M.	339, 653
Waelbroeck, F. L.	496
Wakatsuki, T.	28, 271
Walden, H.	583
Waleffe, R.	354
Walkden, N. R.	396, 434, 443
Walker, M. L.	328, 343, 357
Wallace, G. M.	43, 50, 57, 58, 189, 348, 585
Wallace, J.	354
Wallander, A.	591
Walsh, M.	504, 575, 576, 591, 620–622
Walters, C.	32, 131, 697
Waltz, R. E.	432
Wampler, W. R.	337, 780
Wan, B. N.	10, 12, 38, 127, 169, 228, 232, 239, 240
Wan, S.	155
Wan, Y.	317
Wan, Y. X.	134
Wang, E. H.	399
Wang, F.	418, 577
Wang, H.	24, 155, 331, 336, 338, 456
Wang, H. H.	185
Wang, H. Q.	192, 333, 334, 399, 780
Wang, H. Y.	478
Wang, J.	239, 578
Wang, J.-I.	375
Wang, L.	22, 46, 127, 152, 169, 170, 227, 232, 500, 690, 780
Wang, M.	131, 169, 577
Wang, N.	404
Wang, N. C.	13, 152, 260
Wang, P.	578
Wang, Q.	577
Wang, S.	246, 372, 418, 559
Wang, S. J.	128
Wang, W.	695
Wang, W. X.	47, 513
Wang, X.	11, 15, 160, 317, 455, 577
Wang, X.-G.	321
Wang, X.-Q.	321
Wang, X. J.	169
Wang, Y.	676
Wang, Y.-M.	592
Wang, Y. F.	228
Wang, Y. M.	236, 543
Wang, Z.	17, 372, 587, 592, 676
Wang, Z. H.	47, 517
Wang, Z. R.	141
Wang, Z. X.	259, 307, 312
Warmer, F.	173, 253, 748
Warrier, M.	781
Watanabe, H.	259
Watanabe, K. Y.	28, 163, 254, 261–263, 574, 598
Watanabe, O.	259, 267
Watanabe, T.	698
Watari, T.	37, 774
Watkins, J. D.	333
Watkins, J. G.	192, 331, 332, 336, 338, 780
Wauters, T.	401, 413
Weber, M.	135, 601
Weberski, J. D.	353
Wegener, T.	395
Wegner, T.	416
Wehner, W. P.	357
Wei, L.	312
Wei, X.	653
Wei, Y. L.	399
Wei, Z.	578
Weiland, J.	481
Weiland, M.	57, 59, 407, 433
Weinzettl, V.	150, 199, 221
Weir, G.	162, 249, 399
Weisberg, D. B.	178, 445, 663
Weisen, H.	15, 179, 202, 222, 652
Weland, A.	141
Wen, J.	305
Wen, X.	155
Wensing, M.	213
Wenzel, U.	191
Weyens, T.	379

Wheatley, M.	604
Whelan, G. G.	514
White, A. E.	196, 501, 570
Whyte, D. G.	354, 435, 542, 610, 644
Widdowson, A.	193, 209, 211
Wiesen, S.	193, 519
Wigram, M.	56, 435, 542
Wilcox, R.	177
Wilde, C.	131
Wilkie, G. J.	409, 561
Wilks, T. M.	45, 165, 340
Willensdorfer, M. . .	60, 186, 387, 388, 404, 409, 411
Williams, J.	581
Wilson, C.	131
Wilson, H. R.	153, 167
Windisch, T.	399
Wingen, A.	346
Winters, V.	191
Wirth, B. D.	547, 587
Wirtz, M.	395
Wischmeier, M.	55, 386, 530
Wisitorsasak, A. . .	63, 247, 511, 520, 554
Witrant, E.	246
Woerner, E.	131
Wolf, R. C.	173, 392, 413, 414, 416
Wolfe, S. M.	330
Wolfrum, E.	168, 326, 386, 389, 394, 396, 406, 580
Woller, K.	587, 644
Woo, M. H.	198
Wright, J. C.	189
Wu, B.	690
Wu, C.	709
Wu, G. J.	236
Wu, J.	309
Wu, K.	170, 232
Wu, M. Q.	499
Wu, X.	577
Wu, X. Q.	399
Wu, Y.	676, 690
Wu, Y. B.	463
Wu, Z. W.	227
Wukitch, S. J.	348, 585
Wurden, G. A.	392, 400, 403
Wynn, A.	434

— X —

Xia, F.	320
Xia, G. L.	559
Xia, T. Y.	37, 127, 463, 543
Xiang, N.	127, 169, 418
Xiao, B. J.	155, 169, 170, 232, 341, 342
Xiao, C.	52, 155, 309, 367
Xiao, G. L.	49, 58, 187, 240, 305, 308
Xiao, M.	239
Xiao, X.	418
Xiao, Z.	724
Xie, H.	780
Xie, J.	155, 309
Xu, G. S.	22, 127, 169, 227, 228, 232, 334, 399
Xu, H.	155
Xu, H. D.	169
Xu, J. C.	232
Xu, J. Q.	307, 308
Xu, L.	23, 238, 418
Xu, L. Q.	236
Xu, M. 12, 21, 142, 187, 240, 305–308, 315, 320, 517, 577, 578	
Xu, Q.	722
Xu, S.	399, 442
Xu, W.	587
Xu, X. Q.	56, 226, 228, 543, 592
Xu, Y.	40, 306, 312, 317, 320, 418
Xu, Z.	227

— Y —

Yadav, A.	613, 626
Yadav, B. K.	53, 597, 704
Yadav, N.	35, 278, 285, 692
Yadav, R. K.	626, 627, 682, 684, 751
Yadava, N.	279
Yadykin, D.	510, 521
Yagi, J.	32, 698
Yagi, M.	426, 439
Yagyu, J.	730
Yajima, S.	269, 702
Yakovenko, Y. V.	24, 459
Yakovlev, D. V.	318
Yamada, H.	27, 252, 254, 273, 416
Yamada, I.	254, 257, 261, 263
Yamaguchi, H. 48, 181, 252, 266, 505, 524	
Yamamoto, S. . . .	14, 22, 162, 163, 249, 250

Yamamoto, T.	591	Yokoyama, M.181, 252, 253, 257, 261, 505, 732	
Yamanaka, H.	574, 598	Yoneda, R.	267
Yamanaka, K.	604	Yong, L.	14
Yamano, Y.	574	Yoo, J. W.	361
Yamanoi, K.	763, 767	Yoo, M. G.	513
Yamashita, S.	256	Yoon, E. S.	436, 515
Yamashita, Y.	574, 598	Yoon, S.-W.	51, 362, 371
Yamazaki, G.	698	Yoon, S. W.	128, 347, 372
Yamazaki, H.	269, 329, 702	Yoshida, M.	224, 506
Yamazaki, K.	194	Yoshida, N.	259
Yan, L. W.	40, 305, 307, 312, 315, 320	Yoshida, Y.	269
Yan, N.	228	Yoshida, Z.	255
Yan, R.	575	Yoshihashi, S.	647
Yan, T. F.	747	Yoshikawa, M.	27, 248, 256
Yan, Z.	177	Yoshiki, N.	763
Yanagi, N.	732	Yoshimoto, T.	256
Yanai, R.	373	Yoshimura, M.	762
Yang, J.-H.	52, 378	Yoshimura, R.	774
Yang, L.	155	Yoshimura, Y.	640
Yang, Q.	155	Yoshinuma, M.	181, 194, 252, 263
Yang, Q. Q.	228	You, W.	155
Yang, Q. W. . .	305–308, 312, 315, 320, 321	Younkin, T. K.	547
Yang, S. X.	484	Youssef, M. Z.	629
Yang, X.	156	Yoxall, B.	131
Yang, X. D.	227, 240	Yu, D. L. .187, 305–308, 315, 320, 321, 517	
Yang, Y. R.	315	Yu, K. X.	152
Yang, Z. C.	305, 306, 315	Yu, L. M.	315
Yang, Z. J.	152	Yu, Q.	260, 486
Yao, A.	763	Yu, S.	690
Yao, L. H.	517	Yu, Y. W.	232
Yao, Y.	577	Yuan, B. S.	306, 315
Yashin, A. Y.	145, 304, 727	Yuan, G. L.	308
Yasuhara, R.	261	Yuan, Q.	246
Ye, J. R.	320	Yuan, Q. P.	170
Ye, L.	418	Yuan, X.	196, 203
Ye, M. Y.	55, 528	Yuan, Y.	238
Ye, X.	577	Yun, G.	369
Yeamans, C.	131	Yun, G. S.	128, 198, 372
Yelisyeyev, D. V.	212	Yunoki, M.	267
Yi, S.	507	Yushmanov, P.	156
Yi, S. A.	131, 765		
Yin, D.	317	— Z —	
Ying, A.	608	Zabeo, L.	380
Yogo, A.	762, 763	Zacek, F.	150
Yokodo, T.	256	Zagórski, R.	519, 521, 532, 541
Yokokura, K.	596	Zaharenkov, A.	207

Zaitsev, F. S.	493	Zhao, F.	577
Zajac, J.	150	Zhao, H. L.	236
Zakharov, A. P.	594	Zhao, K. J.	152, 307
Zakharov, L. E.	219, 415	Zhao, Y.	762
Zala, A.	657, 679	Zhao, Y. P.	169
Zalavutdinov, R. K.	594	Zharkov, M.	207
Zanca, P.	41, 60, 398, 488	Zheng, J.	155
Zang, L.	250	Zheng, L. J.	42, 496
Zang, Q.	127, 169, 227, 239, 499	Zheng, P. F.	779
Zani, L.	53, 703	Zheng, X.	653
Zanini, M.	414	Zhilin, E. G.	145, 727
Zanino, R.	56, 535, 710	Zhitlukhin, A. M.	540
Zarnstorff, M.	21	Zholobenko, W.	442
Zarzoso, D.	23, 55, 411, 446, 526	Zhong, F. C.	444
Zastrow, K.-D.	225	Zhong, G.	239
Zatz, I.	695	Zhong, W. L.	187, 240, 306-308, 321
Zein, A.	571, 709	Zhong, W. Z.	39, 305
Zemtsov, I. A.	316	Zhou, B.	577
Zeng, L.	127, 165, 169, 177, 324, 327	Zhou, D.	418, 724
Zeng, X.	624	Zhou, H.	152, 155
Zenin, V. N.	310	Zhou, Y.	306, 308
Zestanakis, P.	561	Zhou, Y. F.	528
Zhai, K.	156	Zhou, Y. L.	517
Zhai, Y.	695, 731	Zhu, J.	155, 309, 448
Zhang, B.	169, 232, 747	Zhu, P.	452
Zhang, C.	448, 608	Zhu, S.	418
Zhang, D.	173, 191, 392, 416	Zhu, X.	499, 578
Zhang, G.	566	Zhu, X. L.	315
Zhang, H.	695	Zhu, Y. B.	167, 349
Zhang, J.	239	Zhu, Z.	724
Zhang, J. H.	322	Zhuang, G.	12, 14, 134, 152, 155, 309
Zhang, J. Z.	236	Zhubr, N. A.	145
Zhang, K.	308	Zimmer, G.	695
Zhang, L.	22, 127, 169, 227, 232, 240, 577	Zinkle, S. J.	587
Zhang, N.	559	Zisis, A.	471, 571, 709
Zhang, P.	155	Zohm, H.	404, 405, 699, 700
Zhang, P. F.	308	Zonca, F.	411, 451, 455
Zhang, S.	155	Zou, J.	690
Zhang, T.	127, 170, 747	Zou, X. L.	187, 232, 240, 305, 308
Zhang, W.	396, 407, 448	Zou, Z.	452
Zhang, X.	317, 415	Zuo, G. Z.	587
Zhang, X. D.	227, 236	Zwingmann, W.	493
Zhang, X. J.	127	Zychor, I.	734
Zhang, Y.	127	Zylstra, A. B.	131, 765
Zhang, Y.-P.	321	Zywicki, B.	335
Zhang, Y. P.	40, 187, 240, 305, 308		